

COURSE 1

NONEQUILIBRIUM PHASE TRANSITIONS

Z. RÁCZ

*Institute for Theoretical Physics,
Eötvös University, Budapest, Hungary*



Contents

1	Introduction	3
1.1	Nonequilibrium steady states	4
1.2	Problems with usual thermodynamic concepts	6
2	Phase transitions far from equilibrium	8
2.1	Differences from equilibrium – constructing models with NESS . .	8
2.2	Generation of long-range interactions – nonlocal dynamics	11
2.3	Generation of long-range interactions – dynamical anisotropies . .	13
2.4	Driven lattice gases, surface growth	15
2.5	Flocking behavior	16
3	Where do the power-laws come from?	18
3.1	Self-organized criticality (SOC)	19
3.2	Absorbing state transitions and their connection to SOC	21
4	Distribution functions in nonequilibrium steady states	24
4.1	Power laws and universality of nonequilibrium distributions	24
4.2	Picture gallery of scaling functions	25
4.3	Upper critical dimension of the KPZ equation	28
5	Quantum phase transitions	30
5.1	Spin chains with fluxes	31
5.2	Effective interactions	35
6	Outlook	37

NONEQUILIBRIUM PHASE TRANSITIONS

Z. Rácz

Abstract

Nonequilibrium phase transitions are discussed with emphasis on general features such as the role of detailed balance violation in generating effective (long-range) interactions, the importance of dynamical anisotropies, the connection between various mechanisms generating power-law correlations, and the emergence of universal distribution functions for macroscopic quantities. Quantum spin chains are also discussed in order to demonstrate how to construct steady-states carrying fluxes in quantum systems, and to explain how the fluxes may generate power-law correlations.

1 Introduction

There are many reasons for studying nonequilibrium phase transitions. Let us start by mentioning a few which carry some generality.

First and foremost, equilibrium in nature is more of an exception than the rule, and structural changes (which constitute a significant portion of interesting phenomena) usually take place in nonequilibrium conditions. Thus there is much to be learned about the complex ordering phenomena occurring far from equilibrium.

Second, while very little is understood about the general aspects of nonequilibrium systems, the equilibrium critical phenomena have been much studied and have been shown to display universal features. This universality emerges from large-scale fluctuations in such a robust way that one can expect that similar mechanisms will work in nonequilibrium situations as well. Thus, investigating the similarities and differences of equilibrium and nonequilibrium orderings may help to discover the distinguishing but still robust properties of nonequilibrium systems.

My research partially described in this lecture series has been supported by the Hungarian Academy of Sciences (Grant No. OTKA T029792).

Third, power law correlations are present in many nonequilibrium phenomena and there have been many attempts to explain these correlations through general mechanisms. Closer examination, however, usually reveals a close connection to equilibrium or nonequilibrium critical phenomena.

My lectures were designed to revolve around problems related to the above points. The lectures are built on the theory of equilibrium phase transitions [1, 2], thus I assume knowledge about both static and dynamic critical phenomena at least on the level of familiarity with the basic concepts (symmetry breaking, order parameter, diverging correlation length, order parameter, scaling, universality classes, critical slowing down, dynamical symmetries). I discuss simple examples throughout so that enterprising students could try out their luck implementing their ideas in simple calculations. Due to space restrictions, however, not all of the details discussed in the lectures and afterwards are covered in the written notes. In particular, the picturesque parts of the explanations are often left out since they take up disproportionately large part of the allowed space. Nevertheless, these pictures may be important in both understanding and memorizing what has been taught. Thus I strongly encourage the reader to go through the slides of the lectures, as well. They can be found through the homepage of the school, http://lpmcn.univ-lyon1.fr/houches_ete/lectures/racz/ or at my homepage at <http://poe.elte.hu/~racz/>.

1.1 Nonequilibrium steady states

A general feature that distinguishes a nonequilibrium steady state (NESS) from an equilibrium one is the presence of fluxes of physical quantities such as energy, mass, charge, etc. Thus the study of NESS is, in a sense, a study of the effects of fluxes imposed on the system either by boundary conditions, or by bulk driving fields, or by some combination of them. A well known example is shown in Figure 1.

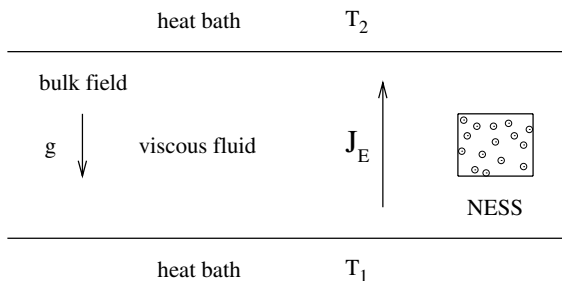


Fig. 1. Setup for Rayleigh-Bénard experiments.

This is the Rayleigh-Bénard experiment [3] in which a horizontal layer of viscous fluid (the system) is heated from below *i.e.* it has two heat baths of temperatures T_1 and T_2 attached (boundary conditions generating an energy flux). The presence of gravity (the bulk drive) is also important (it generates mass and momentum fluxes at large $\delta T = T_1 - T_2 > 0$).

For $T_1 = T_2$ this system relaxes into a quiescent equilibrium state while a small δT will also result in a quiescent state but it is already a NESS since energy flux is flowing through the system. Increasing δT , this steady state displays a nonequilibrium phase transition (Rayleigh-Bénard instability), first to a stationary convective pattern, and then to a series of more complicated structures which have fascinated researchers for the past century [3].

Starting from the Navier-Stokes equations, one can arrive at a mean-field level of understanding of the above phenomena. It is, however, not the level of sophistication one got used to in connection with equilibrium phase transitions. There, we have simple exactly solvable models such as *e.g.* the Ising model which give much insight into the mechanism of ordering and, furthermore, this insight can be used to develop theories which reveal the universal features of equilibrium orderings [1, 2].

The trouble with the Rayleigh-Bénard system is that we do not have a theory even for the NESS. The reason for this is that the fluxes result in steady state distributions, P_n^* , which break the detailed balance condition $w_{n \rightarrow n'} P_n^* = w_{n' \rightarrow n} P_{n'}^*$, where n and n' are two “microstates” and $w_{n \rightarrow n'}$ is the rate of the $n \rightarrow n'$ transition. As a consequence of the breaking of detailed balance, a NESS is characterized not only by the probability distribution, P_n^* , but also by the probability currents in the phase space. Unfortunately, we have not learned yet how to handle the presence of such loops of probability currents.

The main lesson we should learn from the Rayleigh-Bénard example is that, in order to have Ising type models for describing phase transitions in NESS, one should use models which relax to steady states with fluxes present. Such models have been developed during the last 20 years, and most of my lectures are about these stochastic models defined through “microscopic” elementary processes. The first level of description is in terms of master equations which are conceptually simple and allow one to make use of general results (uniqueness of stationary state, etc.) which in turn are helpful in defining dynamics that leads to NESS (Sect. 2). The next level is to describe the same problem in terms of Langevin equations and develop field-theoretic techniques for the solution. Our discussions will include both levels of description and I hope that at the end an understanding will emerge about a few results which grew in importance in the last decade (generation of long-range interactions and effects of dynamical anisotropies (Sect. 2), connection between mechanisms generating power-law correlations

(Sect. 3), and universality of distribution functions for macroscopic quantities (Sect. 4)).

Before starting, however, I would like to insert here a little essay about effective temperatures. This concept is being widely discussed in connection with slowly relaxing systems, the topic of this school. So it may be of interest to present here a view from the perspective of NESS.

1.2 Problems with usual thermodynamic concepts

Systems close to equilibrium may retain many properties of an equilibrium state with the slight complication that the intensive thermodynamic variables (temperature, chemical potential, etc.) become inhomogeneous on long lengthscales and they may slowly vary in time. This type of situations are successfully dealt with using the so called local equilibrium approximation [4], with the name giving away the essence of the approximation. The applicability of the concept of local equilibrium should diminish, however, as a system is driven far from equilibrium. Nevertheless, questions of “how large drive produces a far-enough state” and “couldn’t one try to find a new equilibrium state near-by” are regularly asked and have legitimacy. So I will try to illuminate the problems on the example of the fluctuation-dissipation theorem much discussed nowadays due to attempts of associating effective temperatures with the various stages of relaxation in glasses [5] or with steady states in granular materials [6].

Let us consider a simple system of Ising variables σ with Hamiltonian \mathcal{H}_0 and in equilibrium at temperature $\beta = 1/(k_B T)$. Assuming that there is an external field H coupling linearly to the macroscopic magnetization $M = \sum_i \sigma_i$, one can write the equilibrium distribution function as

$$P_{\text{eq}}(\sigma) = Z^{-1} e^{-\beta \mathcal{H}_0(\sigma) + \beta H M(\sigma)}. \quad (1.1)$$

The average value of the magnetization is given by

$$\langle M \rangle = Z^{-1} \sum_{\sigma} M(\sigma) e^{-\beta \mathcal{H}_0(\sigma) + \beta H M(\sigma)}. \quad (1.2)$$

and the static limit of the fluctuation-dissipation theorem is obtained as

$$\chi_M = \left. \frac{\partial \langle M \rangle}{\partial H} \right|_{H \rightarrow 0} = \beta \langle M^2 \rangle \quad (1.3)$$

where we assumed the system to be in the high-temperature phase ($\langle M \rangle = 0$). Note the simplicity and the accompanying generality of this derivation. It uses only the fact that the external field is linearly coupled to the quantity (M) we are considering.

The fluctuation-dissipation theorem is used in many ways. It helps simplify field-theoretic studies of fluctuations through diagrammatic expansions and it also gives a powerful checking procedure in both experiments and Monte Carlo simulations. Note that equation (1.3) can also be used to define the temperature of the system through $\beta = \chi_M / \langle M^2 \rangle$, and the temperature defined in this way would be the same when using different “ M ”-s and conjugate fields “ H ”.

It is clear that a fluctuation-dissipation theorem generalized to NESS would be extremely useful. Let us now try to imagine how a similar relationship may arise when we drive the above system away from equilibrium (*e.g.* by attaching two heat baths of different temperatures). If the system relaxes to a NESS then there will be steady-state distribution function, (P) but the effective Hamiltonian ($\ln P$) will contain all the interactions allowed by the symmetries of the system. Thus, assuming that the effective Hamiltonian can be expanded in H , one finds in the $H \rightarrow 0$ limit

$$P_{\text{ne}}(\sigma) \sim e^{-a\mathcal{H}_1(\sigma) + bH[M(\sigma) + S_3(\sigma) + \dots]} \quad (1.4)$$

where S_3 is a notation for sums over all three-spin clusters with different couplings for different types of spatial arrangements of the three spins. Furthermore, a , b and all other newly generated couplings depend on the original couplings in \mathcal{H}_0 and on the temperatures of the heat baths.

Now a derivation of the fluctuation-dissipation theorem similar to the equilibrium case yields a more complicated equation

$$\chi_M = \left. \frac{\partial \langle M \rangle}{\partial H} \right|_{H \rightarrow 0} = a [\langle M^2 \rangle + \langle MS_3 \rangle + \dots]. \quad (1.5)$$

There are two ways a simple form for the fluctuation-dissipation theorem may emerge from equation (1.5). One is that a nonlinear field

$$Q = M + S_3 + \dots \quad (1.6)$$

that is conjugate to H can be introduced (and effectively worked with). Then one obtains

$$\chi_Q = a \langle Q^2 \rangle \quad (1.7)$$

and thus a becomes the nonequilibrium β .

The other possibility is that a mean-field type decoupling scheme works well and then

$$\langle MS_3 \rangle = \langle M^2 \rangle f(C_2) \quad (1.8)$$

where $f(C_2)$ is a functional of the two-point correlations (and similar expressions are obtained for $\langle MS_{2n+1} \rangle$). Then equation (1.5) becomes

$$\chi_M = a \mathcal{F}(C_2) \langle M^2 \rangle. \quad (1.9)$$

If the theory provides $\mathcal{F}(C_2)$ then the effective temperature can again be read off from the above generalized fluctuation-dissipation relationship.

There are problems with both lines of reasoning. Apart from the practical difficulties of nonlinear fields and the validity of mean-field type approaches, the main conceptual difficulty is the fact that changing from the magnetization to other fields (*e.g.* energy) the nonequilibrium version of the fluctuation-dissipation theorem leads to different values for the same “temperature” [10]. There are cases where the above schemes generalized to time-dependent processes work both at the theoretical [5, 7, 8] and the experimental levels [9] but there are clear examples when the concept of effective temperature does not apply [10]. Thus the meaning and use of nonequilibrium temperature has not been clarified enough to make a verdict on it.

2 Phase transitions far from equilibrium

As mentioned in the Introduction, nonequilibrium phase changes constitute a large part of interesting natural phenomena and they are studied without worries about wider contexts. From a general perspective, on the other hand, the investigations of nonequilibrium phase transitions [11, 12] can be viewed as an attempt to understand the robust features of NESS. This view is based on the expectation that the universality displayed in critical phase transitions carries over to criticality in NESS as well. If this is true then studies of the similarities to and differences from equilibrium will lead to a better understanding of the role and general consequences of the dynamics generating NESS.

In the following subsections, we shall construct, describe, and discuss models which display nonequilibrium phase transitions. Apart from getting familiar with a few interesting phenomena, the main general conclusion of these discussions should be that dynamical anisotropies often yield dipole-like effective interactions [13–15] and, furthermore, competing non-local dynamics (anomalous diffusion) generates long-range, power-law effective interactions [16]. Along the way, we shall also understand that the detailed-balance violating aspects of local relaxational dynamics do not affect the universality class of the nonequilibrium phase transitions [15, 17].

2.1 Differences from equilibrium – constructing models with NESS

The violation of detailed balance has the consequence that not only the interactions determine the properties of the NESS but the dynamics also plays an important role. In order to understand and characterize the role of dynamics, a series of simple examples will be discussed in the following subsections.

First, let us discuss how to construct a model which yields a NESS in the long-time limit. A simple way is to attach two heat baths to a system, each generating a detailed-balance dynamics but at different temperatures. To see an actual implementation, let us consider how this is done for the one dimensional kinetic Ising model. This type of models have been much studied and a collection of mini-reviews about them can be found in [18].

The state of the system $\{\sigma\} \equiv \{\dots, \sigma_i, \sigma_{i+1}, \dots\}$ is specified by stochastic Ising variables $\sigma_i(t) = \pm 1$ assigned to lattice sites $i = 1, 2, \dots, N$. The interaction is short ranged (nearest neighbor) $-J\sigma_i\sigma_{i+1}$ and periodic boundary conditions ($\sigma_{N+1} = \sigma_1$) are usually assumed. The dynamics of the system is generated by two heat baths (labeled by $\alpha = 1, 2$) at temperatures T_α , meaning that the heat baths try to bring the system to equilibrium at temperature T_α by *e.g.* spin flips and spin exchanges, respectively.

Let us denote the rate of the flip of i th spin ($\sigma_i \rightarrow -\sigma_i$) by $w_i^{(1)}(\{\sigma\})$, and let the rate of the exchanges of spins at sites i and j ($\sigma_i \leftrightarrow \sigma_j$) be $w_{ij}^{(2)}(\{\sigma\})$. Then the dynamics is defined by the following master equation for the probability distribution $P(\{\sigma\}, t)$:

$$\begin{aligned} \partial_t P(\{\sigma\}, t) = & \sum_i \left[w_i^{(1)}(\{\sigma\}_i) P(\{\sigma\}_i, t) - w_i^{(1)}(\{\sigma\}) P(\{\sigma\}, t) \right] \\ & + \sum_{ij} \left[w_{ij}^{(2)}(\{\sigma\}_{ij}) P(\{\sigma\}_{ij}, t) - w_{ij}^{(2)}(\{\sigma\}) P(\{\sigma\}, t) \right] \quad (2.1) \end{aligned}$$

where the states $\{\sigma\}_i$ and $\{\sigma\}_{ij}$ differ from $\{\sigma\}$ by the flip of the i th spin and by the exchange of the i th and j th spins, respectively.

The assumption that the dynamics is generated by heath baths means that the rates satisfy detailed balance at the appropriate temperatures:

$$w_{i(j)}^{(\alpha)}(\{\sigma\}) P_\alpha^{\text{eq}}(\{\sigma\}) = w_{i(j)}^{(\alpha)}(\{\sigma\}_{i(j)}) P_\alpha^{\text{eq}}(\{\sigma\}_{i(j)}), \quad (2.2)$$

where $P_\alpha^{\text{eq}} \sim \exp[-J/T_\alpha \sum_i \sigma_i \sigma_{i+1}]$ is the equilibrium distribution of the Ising model at temperature T_α . Equation (2.2) leaves some freedom in the choice of w^α -s, and one is usually guided by simplicity. The most general spin flip rate that depends only on neighboring spins has the following form [19]

$$w_i^{(1)}(\sigma) = \frac{1}{2\tau_1} \left[1 - \frac{\gamma}{2} \sigma_i (\sigma_{i+1} + \sigma_{i-1}) \right] \left(1 + \delta \sigma_{i+1} \sigma_{i-1} \right). \quad (2.3)$$

Without any other heath baths, equations (2.1) and (2.3) define the Glauber model [19] which relaxes to the equilibrium state of the Ising model at temperature T_1 defined through $\gamma = \tanh(2J/k_B T_1)$. The time-scale for flips is set by τ_1 and δ is restricted to the interval $-1 < \delta < 1$.

The competing dynamical process is the generation of spin exchanges (Kawasaki dynamics [20]) by a second heat bath at a temperature $T_2 \neq T_1$. In the simplest case, the exchanges are between nearest neighbor sites and the rate of exchange satisfying detailed balance (2.2) is given by

$$w_i^{(2)}(\sigma) = \frac{1}{2\tau_2} \left[1 - \frac{\gamma_2}{2} (\sigma_{i-1}\sigma_i + \sigma_{i+1}\sigma_{i+2}) \right]. \quad (2.4)$$

where $\gamma_2 = \tanh(2J/k_B T_2)$ and τ_2 sets the timescale of the exchanges. It is often assumed that the exchanges are random ($T_2 = \infty$) and thus $w_i^{(2)}(\sigma) = 1/(2\tau_2)$.

Equations (2.1), (2.3) and (2.4) define a model which can be shown to have a NESS and one can start to ask questions about the phase transitions in this steady state. The generalizations to higher dimensions, to various combinations competing dynamics (flip – flip, flip – exchange, exchange – exchange), and other types of dynamical steps (resulting *e.g.* from a bulk driving field) should be obvious. Just as it should be obvious that there are not too many exactly solvable models in this field and most of the results are coming from simulations [11, 12].

Before turning to results, let us also introduce a Langevin equation description of competing dynamics. The Langevin approach has been successful in dynamic critical phenomena [2] where the counterparts of the Glauber and Kawasaki models are called Model A and B, correspondingly. This correspondence makes the “two-heat-baths” generalization straightforward. The coarse grained magnetization of the Ising model is replaced by n -component order-parameter field, $S^i(\mathbf{x}, t)$, ($i = 1, \dots, n$) ($n = 1$ is the Ising model, and $n \rightarrow \infty$ is the spherical limit that allows simple analytic calculations as shown below). The system evolves under the combined action of local relaxation (Model A) satisfying detailed balance at temperature T_1 and diffusive dynamics (Model B) at temperature T_2 which yields the following Langevin equation for the Fourier transform $S_{\mathbf{q}}^i(t)$

$$\partial_t S_{\mathbf{q}}^i = -\mathcal{L}_{\mathbf{q}}^{(1)} S_{\mathbf{q}}^i + \eta_1^i(\mathbf{q}, t) - \mathcal{L}_{\mathbf{q}}^{(2)} S_{\mathbf{q}}^i + \eta_2^i(\mathbf{q}, t). \quad (2.5)$$

Here $\mathcal{L}_{\mathbf{q}}^{(\alpha)} S_{\mathbf{q}}^i = \Gamma_{\mathbf{q}}^{(\alpha)} \delta F^{(\alpha)} / \delta S_{-\mathbf{q}}^i$ with $F^{(\alpha)}$ being the free energy at temperature T_α , and the kinetic coefficient $\Gamma_{\mathbf{q}}^{(\alpha)}$ is enforcing the conservation laws. In particular, $\Gamma_{\mathbf{q}}^{(\alpha)} = \Gamma_0^{(\alpha)}$ in Model A without conservation laws, and $\Gamma_{\mathbf{q}}^{(\alpha)} = D^{(\alpha)} \mathbf{q}^2$ for Model B with diffusive dynamics conserving the total magnetization. In case $F^{(\alpha)}$ is the Landau-Ginsburg functional, we have

$$\mathcal{L}_{\mathbf{q}}^{(\alpha)} S_{\mathbf{q}}^i = \Gamma_{\mathbf{q}}^{(\alpha)} \left[(r_0^\alpha + q^2) S_{\mathbf{q}}^i + u \sum_{j=1}^n \int_{\mathbf{q}'} \int_{\mathbf{q}''} S_{\mathbf{q}'}^j S_{\mathbf{q}''}^j S_{\mathbf{q}-\mathbf{q}'-\mathbf{q}''}^i \right] \quad (2.6)$$

where r_0^α is linear in T_α and $u \sim 1/n$ in the $n \rightarrow \infty$ spherical limit. In order to ensure that in case of a single heat bath, the system relaxes to equilibrium satisfying detailed balance, the noise terms in equation (2.5) are Gaussian-Markovian random forces with correlations of the form:

$$\langle \eta_\alpha^i(\mathbf{q}, t) \eta_{\alpha'}^j(\mathbf{q}', t') \rangle = 2\Gamma_{\mathbf{q}}^{(\alpha)} \delta_{\alpha\alpha'} \delta_{ij} \delta(\mathbf{q} + \mathbf{q}') \delta(t - t'). \quad (2.7)$$

Equations (2.5–2.7) define the model for the particular competing dynamics chosen and we are now ready to deduce some features of the NESS generated. Of course, just as in case of kinetic Ising models, the number of possible competing dynamics is infinite and the question is whether conclusions of some generality could be reached.

2.2 Generation of long-range interactions – nonlocal dynamics

The remarkable consequences of competing dynamics can be seen already on the example of $d = 1$ flip-and-exchange model which may produce ordering even though the interactions are of short range. Indeed, if T_1 temperature spin flips are competing with $T_2 = \infty$ spin exchanges of randomly chosen pairs then the system orders below a certain T_{1c} [16].

It turns out that the transition is of mean-field type and this gives a clue to understanding. Indeed, let us imagine that the rate of spin exchanges is large compared to the rate of flips. Then the random exchanges mix the spins in between two flips and the flipping spin sees the “average spins” in its neighborhood – a condition for mean-field to apply.

The mean field result can also be interpreted as the generation of infinite-range effective interactions. This interpretation can be put on more solid base by studying the above model with $T_2 = \infty$ spin exchanges where the probability of exchange at a distance r is decaying with r as $p(r) \sim 1/r^{d+\sigma}$ (the spins exchanges are σ dimensional Levy flights in dimension d). The system orders again below a T_{1c} and the examination of the critical exponents reveals [16] that the transition is in the universality class of long-range interactions decaying with r as $J(r) \sim 1/r^{d+\sigma}$. It is important to note that the above results are nonequilibrium effects which would disappear if the spin exchanges would also be at T_1 .

Let us now see if the same results can be derived from the Langevin equation approach. The spin flips are translated into the Model A part of the dynamics while the Levy flights can be represented [21] by anomalous diffusion with $\Gamma_{\mathbf{q}}^{(2)} = D^{(2)} \mathbf{q}^2$ replaced by $\Gamma_{\mathbf{q}}^{(2)} = D^{(2)} \mathbf{q}^\sigma$ with $0 < \sigma < 2$

being the dimension of the Levy flight. Thus the Langevin equation becomes

$$\begin{aligned} \dot{S}_{\mathbf{q}}^i = & -\Gamma_0(r_0 + q^2)S_{\mathbf{q}}^i - \Gamma_0 u \sum_{j=1}^n \int_{\mathbf{q}'} \int_{\mathbf{q}''} S_{\mathbf{q}'}^j S_{\mathbf{q}''}^j S_{\mathbf{q}-\mathbf{q}'-\mathbf{q}''}^i + \eta_{\mathbf{q}}^i(t) \\ & - Dq^\sigma S_{\mathbf{q}}^i + \bar{\eta}_{\mathbf{q}}^i(t). \end{aligned} \quad (2.8)$$

Note that due to the randomness of the Levy flights ($T_2 = \infty$), the interaction and the nonlinear terms are missing in the Levy flight part (second line) of the equation. As discussed in Section 2.1, the η -s are Gaussian-Markoffian random forces with correlations $\langle \eta_{\mathbf{q}}^i(t) \eta_{\mathbf{q}'}^j(t') \rangle = 2\Gamma_0 \delta_{ij} \delta(\mathbf{q} + \mathbf{q}') \delta(t - t')$ and $\langle \bar{\eta}_{\mathbf{q}}^i(t) \bar{\eta}_{\mathbf{q}'}^j(t') \rangle = 2Dq^\sigma \delta_{ij} \delta(\mathbf{q} + \mathbf{q}') \delta(t - t')$.

In order to see the generation of long range interaction in the above model, let us first make an exact calculation [16] in the spherical limit ($n \rightarrow \infty$) where fluctuations in $u \sum S_{\mathbf{q}}^j(t) S_{\mathbf{q}'}^j(t)$ may be neglected and this quantity may be replaced by

$$u \sum_{j=1}^n \langle S_{\mathbf{q}}^j(t) S_{\mathbf{q}'}^j(t) \rangle = unC(q, t) \delta(\mathbf{q} + \mathbf{q}'), \quad (2.9)$$

where the brackets $\langle \rangle$ denote averaging over both the initial conditions and the noises η and $\bar{\eta}$ (we restrict ourselves to the study of the high-temperature phase where the dynamic structure factor $C(q, t) = \langle S_{\mathbf{q}}^j(t) S_{-\mathbf{q}}^j(t) \rangle$ is independent of j).

The decoupling (2.9) leads to a linear equation of motion and so the self-consistency equation for $C(q, t)$ can be easily derived

$$C(q, t) = 2(\Gamma_0 + Dq^\sigma) \int_0^t dt' e^{-2 \int_0^{t'} \{\Gamma_0[r_0 + q^2 + unC(q, s)] + Dq^\sigma\} ds}. \quad (2.10)$$

Here, the initial condition $C(q, 0) = 0$ was used for simplicity. The $t \rightarrow \infty$ limit does not depend on the initial condition and the equation for the steady state structure factor $C(q) = C(q, t \rightarrow \infty)$ becomes

$$C(q) = \frac{\Gamma_0 + Dq^\sigma}{\Gamma_0(r_0 + q^2 + unS) + Dq^\sigma}, \quad (2.11)$$

where $S = \int d\mathbf{q} C(q)$.

The long-wavelength instabilities are determined by the $q \rightarrow 0$ form of $C(q)$ which for $0 < \sigma < 2$ can be written as

$$C(q) \approx (r_0 + \lambda q^\sigma + unS)^{-1}, \quad (2.12)$$

with $\lambda = D/\Gamma_0$. This form coincides with the long-wavelength limit of the equilibrium structure factor of a spherical model in which the interactions decay with distance as $r^{-d-\sigma}$. Consequently, both the self-consistency

equation for $r = r_0 + unS$ and the critical behavior that follows from it are identical to that of the equilibrium long-range model. Thus we can conclude that the critical properties of the NESS are dominated by an effective long-range potential proportional to $r^{-d-\sigma}$.

The above conclusion should be valid quite generally for finite n as well. Looking at equation (2.8), one can see that the correlations in the effective noise ($\eta_{\text{eff}} = \eta + \bar{\eta}$) have an amplitude $2(\Gamma_0 + Dq^\sigma)$. One expects that the Dq^σ term can be neglected in the long-wavelength limit and thus that the noise $\bar{\eta}$ in the Levy-flight exchanges can be omitted. Without $\bar{\eta}$, however, the system described by equation (2) satisfies detailed balance and has an effective Hamiltonian which, apart from the usual short-range interaction pieces, contains the expected long-range part $\lambda \int d\mathbf{q} q^\sigma \sum_i S^i(\mathbf{q}) S^i(-\mathbf{q})$.

We should note here that $\sigma \rightarrow 2$ corresponds to usual diffusion and that the above arguments changes for $\sigma = 2$ since no long-range interactions are generated any more, and no change in critical behavior occurs. This result is another way of saying that Model A type dynamics is robust against diffusive perturbations which break detailed balance [17]. Note also that if both the competing dynamics are relaxational then, adding up the corresponding deterministic and noise parts in the Langevin equation (2.5), one can easily deduce that the breaking of the detailed balance does not change the universality class of the equilibrium phase transition.

2.3 Generation of long-range interactions – dynamical anisotropies

In order to understand the meaning of dynamical anisotropy, let us consider the two-temperature, diffusive kinetic Ising model [22] on a square lattice. Two heat baths are attached and both of them generate nearest neighbor spin exchanges. Exchanges along one of the axis (called “parallel” direction) satisfy detailed balance at temperature T_{\parallel} while exchanges in the ‘perpendicular’ direction are produced by a heat bath of temperature T_{\perp} . It is important to note that the interactions $J\sigma_i\sigma_j$ are the same along both axes. It is the dynamics that is anisotropic.

For $T_{\perp} = T_{\parallel} = T$, this is the Kawasaki model [20] which relaxes to the equilibrium Ising model at T and, consequently, it displays a continuous transition. Since the dynamics conserves the total magnetization, the ordering for $T < T_c$ appears as a phase separation.

For $T_{\perp} \neq T_{\parallel}$, on the other hand, there is a flow of energy between the \parallel and \perp heat baths and the system relaxes to a NESS. MC simulations [14,22] show that a critical phase transition is present for $T_{\perp} \neq T_{\parallel}$ as well but the phase separation is distinct from that occurring in equilibrium. The interfaces between the domains of up and down spins align with normals along the directions of lower temperatures. Thus the symmetries of the ordered states are different from the symmetry of the equilibrium order

where interfaces with normals along any of axes coexist (isotropic ordering). As a consequence, the universality classes of the \parallel and \perp orderings are found to be distinct from the Ising class [22, 23]. Renormalization group calculations actually show that the universality class of the nonequilibrium ordering is that of a uniaxial ferromagnet with dipolar interactions [24].

A dramatic demonstration of the long-range nature of the interactions generated by anisotropic dynamics comes from the generalization of the above model to $n = 2$ component spins ($2T - XY$ model). One finds that the NESS in this system displays an ordering transition [14], a fact that would be in contradiction with the Mermin-Wagner theorem [25] should the effective interaction be short-ranged.

Let us try now understand the generation of the dipole-like interactions using the Langevin equation approach and considering the spherical limit again. The two-temperature, diffusive Ising model corresponds to competition of two Model B type dynamics along \parallel and \perp axes. Thus the equation of motion is $\dot{S}_{\mathbf{q}}^i(t) = \mathcal{L}_{\parallel}(q)S_{\mathbf{q}}^i + \eta_{\parallel}^i(\mathbf{q}, t) + \mathcal{L}_{\perp}(q)S_{\mathbf{q}}^i + \eta_{\perp}^i(\mathbf{q}, t)$ with the diffusion in the $\alpha = \parallel, \perp$ directions described by the corresponding \mathcal{L}_{α} terms:

$$\mathcal{L}_{\alpha}S_{\mathbf{q}}^i = D_{\alpha}q_{\alpha}^2 \left[(r_0^{\alpha} + q^2) S_{\mathbf{q}}^i + u \sum_{j=1}^n \int_{\mathbf{q}'} \int_{\mathbf{q}''} S_{\mathbf{q}'}^j S_{\mathbf{q}''}^j S_{\mathbf{q}-\mathbf{q}'-\mathbf{q}''}^i \right]. \quad (2.13)$$

where $\mathbf{q} = (q_{\parallel}, q_{\perp})$. Note the isotropy of the interaction (q^2 term) and the different temperatures (r_0^{α}) for diffusion in different directions. The noise correlations follow from detailed balance requirements, $\langle \eta_{\alpha}^i(\mathbf{q}, t) \eta_{\alpha'}^j(\mathbf{q}', t') \rangle = 2D_{\alpha}q_{\alpha}^2 \delta_{\alpha\alpha'} \delta_{ij} \delta(\mathbf{q} + \mathbf{q}') \delta(t - t')$.

Just as in the kinetic Ising model, for $r_0^{\parallel} = r_0^{\perp}$ we have Model B with anisotropic diffusion (not a dynamical anisotropy!) and with an equilibrium steady state, while a NESS is produced for $r_0^{\parallel} \neq r_0^{\perp}$. The nature of the phase transitions in the NESS becomes transparent in the spherical limit ($n \rightarrow \infty$ and $u \sim 1/n$) where the fluctuations in $u \sum S_{\mathbf{q}}^j(t) S_{\mathbf{q}'}^j(t)$ may be neglected. This linearizes the equation of motion and allows to write down a selfconsistency equation for $C(\mathbf{q}) = \langle S_{\mathbf{q}}^j(t) S_{\mathbf{q}'}^j(t) \rangle$. The $t \rightarrow \infty$ limit then yields the steady state structure factor in the following form [14]

$$C(\mathbf{q}) = \frac{q_{\parallel}^2 + a q_{\perp}^2}{q_{\parallel}^2(r_0^{\parallel} + q^2 + S) + a q_{\perp}^2(r_0^{\perp} + q^2 + S)}, \quad (2.14)$$

where $a = D_{\perp}/D_{\parallel}$ and $S = un \int d\mathbf{q} C(\mathbf{q})$.

One can see now the origin of dipole-like effective interactions. Because of the dynamical anisotropy, the $\mathbf{q} \rightarrow 0$ limit of $C(\mathbf{q})$ is different whether first $q_{\parallel} \rightarrow 0$ and then $q_{\perp} \rightarrow 0$ or *vice versa*. This singularity of

the long-wavelength limit translates into such power law correlations in real space which are characteristic of dipole interactions in equilibrium systems. Hence the conclusion [14, 24] that the dynamical anisotropy has generated dipole-like interactions. Note that this is a nonequilibrium effect. The long-wavelength singularity disappears as soon as the heat baths have equal temperatures ($r_0^\parallel = r_0^\perp$).

The dynamical anisotropy is a strong effect and its mechanism of action is rather simple as we have seen above. Accordingly, it is the most viable candidate to change the universality class of equilibrium phase transitions by breaking detailed balance [15].

2.4 Driven lattice gases, surface growth

Models of NESS have a long history but the first one that became the center of attention and was recognized as the “Ising model” of NESS was the driven lattice gas (see [11] and references therein). The model can be understood as a kinetic Ising model with the up-spins being the particles in the lattice gas. Spin exchange dynamics at temperature T represents the particle diffusion and an external bulk field E_x drives the up-spins (particles) along one of the lattice axes (x). In order to have a NESS with particle current one must also use periodic boundary conditions in the field direction.

This model displays a critical phase transition in its NESS and the phase separation that follows at low T is characterized by strong anisotropy: the interfaces align parallel with E_x . Thus one can see some similarities with the two-temperature diffusive model of Section 2.3.

One can easily recognize that dynamical anisotropy is at work here. The driving field can be considered as a second heat bath which generates the essential part of the dynamics along the x direction. There is a difference, however, from the two-temperature model of Section 2.3 in that the drive now has a directionality (the forward-backward symmetry of diffusion is broken). As a result the phase transition is expected to belong to a new (nonequilibrium) universality class distinct from that of the dipole class. This is indeed what has been obtained in renormalization group calculations [11]. Unfortunately, the structure of the long-wavelength singularities in the two systems are similar and thus there are difficulties in observing the differences in numerical work. This problem has generated some debate that is still going on [26]. We believe the debate will not modify the general picture summarized in [11], and it will not change the conclusion about the importance of dynamical anisotropy.

An interesting and important field where even the simplest systems show “effective” critical behavior due to the unbounded long-wavelength fluctuations is the field of surface growth processes. Most of the roughening transitions and transitions between various rough phases are genuine

nonequilibrium phase transitions and have been much studied [27, 28]. Remarkably, however, these transitions have not provided new insight into the general features of nonequilibrium criticality, they merely confirmed that the dynamics and dynamical anisotropy play an important role in determining the universality classes of growth processes.

One of the unsolved problems that continues to fascinate researchers is the phase transition in the Kardar-Parisi-Zhang equation [29]. We shall discuss the problem of growing surfaces including KPZ equation in connection with the nonequilibrium distribution functions in Section 4.

2.5 Flocking behavior

Up to this point, we have considered usual physical systems driven out of equilibrium. Here I would like to give a taste of what awaits one if the studies are extended to the living realm.

Living creatures can also be viewed as units attached to two heat baths. One of them is the internal energy source which on a short time-scale is an infinite bath from which energy can be drawn at a given rate. The other one is the surroundings to which energy is lost by dissipation (friction, heat loss, ...) due to the activity of the unit. This view suggests that a collection of such self-propelled units will show orderings (nonequilibrium phase transitions) depending on the interactions between the units, on their density, on their possible motions and on the dissipation mechanisms. Indeed, collective behavior is often observed in flocks of birds, in schools of fish, in swimming cells, etc. and, as shown below, some of these phenomena can be described in terms of a surprisingly simple model.

Model [30] was introduced to describe the collective motion of self-propelled particles with birds and bacteria being candidates for these particles. We shall use the language of “birds” below.

The basic assumptions of the model are that (i) the birds fly with constant speed $|\vec{v}_i| = 1$ (i is the bird index), and (ii) the birds adjust their direction θ_i in time intervals of $\tau = 1$ to the average direction of other birds within a distance r

$$\theta_i(t + \tau) = \langle \theta(t) \rangle_r + \eta_i \quad (2.15)$$

where η_i is random noise with amplitude η .

Assumption (i) handles the energy in- and outflow by strictly equating them, while assumption (ii) handles the interactions by seemingly reducing them to interactions in the space of velocity directions. This is not quite so, however, since the motion of the birds $\vec{x}_i(t + \tau) = \vec{x}_i(t) + \vec{v}_i(t)\tau$ couples the directional and spatial motions.

The control parameters in the system are r , η and the density of particles ρ . Keeping r and ρ fixed while varying the “temperature” η , one finds

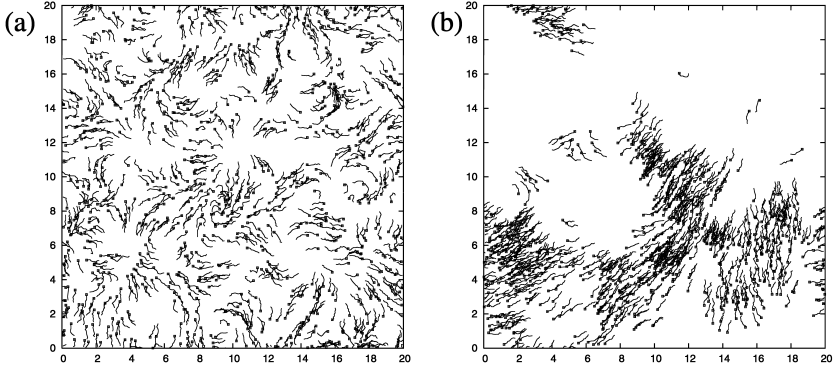


Fig. 2. Flocking: trajectories of 10 000 self-propelled particles in the model described in the text. The parameters are chosen so that the stationary order parameter is $\phi = 0.8$. Each particle is represented by a point marking its current position as well as a continuous line showing its recent (10 time step long) trajectory. **a)** Initial stage of the relaxation, **b)** the stationary regime. Pictures are courtesy of A. Czirók and T. Vicsek.

that the birds are flying randomly for $\eta > \eta_c(r, \rho)$ while collective motion develops below η_c where the birds tend to move in the same direction. An order parameter characterizing this spontaneously symmetry breaking can be chosen *e.g.* $\phi = |\sum_i^N \vec{v}_i|/N$. Figure 2 shows the time evolution deep in the ordered regime ($\phi = 0.8$) starting from a random configuration. One can see that local orientational order develops in the initial stages of relaxation (the state here shows resemblance to the states in classical XY ferromagnet) while the stationary state with almost full orientational order shows large density fluctuations. The structure and the large density fluctuations observed in the ordered state and, furthermore, the measurements of the critical exponents of the transition [30] suggest that the ordering in this system is in a universality so far not encountered.

A remarkable field theory has also been constructed for flocking [31]. It is a generalized Navier-Stokes equation with additional Model A type terms which drive the velocity to $\langle |\vec{v}_i| \rangle = 1$. This theory explains the large density fluctuations present in the ordered state. The investigation of ordering transition is at a higher level of difficulty, however, and has not been completed yet.

Clearly, much remains to be done before we understand flocking and before the model can be compared with experiments quantitatively. Nevertheless, activity is expected in this direction since the model of flocking is not much more complicated than the more standard NESS models discussed

above, and, at the same time, it has close connection with experimentally observable, truly “far-from-equilibrium” phenomena. Hopefully, by designing and understanding similar models, a kind of “universality map” of the collective dynamics of self-driven units can be found.

3 Where do the power-laws come from?

Systems displaying power law behavior in their various characteristics (correlation in space or time, fluctuation power spectra, size-distributions, etc.) are abundant in nature. The most impressive examples are found in biology (*e.g.* the metabolic rate *vs.* mass relationship for living creatures displays scaling over 28 decades [32]) but there are remarkable examples in solid state physics (power spectra of voltage fluctuations when a current is flowing through a resistor [33] – 6 decades of scaling), in geology (the number of earthquakes *vs.* their magnitude [34] – 5 decades) and scaling over 2–3 decades is seen everywhere [see *e.g.* the white-dwarf light emission [35], the flow of sand through an hourglass [36], the number of daily trades in the stock market [37], water flow fluctuations of rivers [38], the spike trains of nerve cells [39], the traffic flow on a highway [40], interface fluctuations [27], dissipation in turbulent systems [41]].

Understanding the (possibly) common origins of scaling in the above phenomena appears to be a highly nontrivial task. Power laws, of course, arise naturally in critical phenomena and we understand them: their origins are in the diverging fluctuations at the critical point. Thus the first question one may ask is the following.

- Can the power laws just be the result of nonequilibrium phase transitions and the associated critical behavior?

In equilibrium systems, however, one must tune a parameter to its critical value in order to observe scale-invariant behavior while nonequilibrium systems appear to be in scale-invariant states without any tuning. Thus the answer to the first question appears to be negative.

The wide variety of the phenomena in the above list suggests that the next question could be as follows.

- Can the scaling merely be a natural outcome of complex dynamics?

After all, we have seen in Section 2.3 that competing dynamics may generate long-range (power-law) interactions which may be at the origin of scaling even away from a critical point. The answer to this question may be a yes but, unfortunately, many of the problems mentioned are not amenable to an analysis in terms of simple competing dynamics and then the following

question remains unanswered:

- What are the ingredients of complex dynamics which determine the existence and the characteristics (*e.g.* exponents) of the power laws?

There is an attempt to answer all the above question in affirmative along a logic that begins with the notion of self-organized criticality (SOC) introduced by Bak *et al.* [42]. According to this notion, systems with complex dynamics tune themselves to a state with a kind of avalanche type dynamics that is underlying a large number of scale-invariant phenomena. The notion of SOC has now been understood in terms of an interplay between local and non-local dynamics [43] which indeed tunes the system [44] to a nonequilibrium (absorbing-state) critical point. Then the problem of SOC is reduced to investigating the absorbing state transitions [45] and the characteristics of power laws can be determined by studying the universality of absorbing state transition. This is an interesting and active field of research and it is worth understanding the main points. Accordingly, I will discuss SOC in the next subsection, and will explain the connection to absorbing state transitions in the following one.

3.1 Self-organized criticality (SOC)

The first model of SOC was introduced to describe sandpiles. Later developments, however, made energy packets from the grains of sand, so the balls in Figure 3 will be grains at the beginning but will be called energy packets later. The dynamics defining the model consists of local and non-local elements. The sites of a (usually) two-dimensional lattice are occupied by grains and the local aspect of their dynamics is in the redistribution of the grains. If a site contains more than z_c grains (*e.g.* $z_c = 4$ on a square lattice) then the site is active and z_c grains are redistributed to the neighboring lattice sites. The redistribution of particles (avalanche) continues until active sites are found. Clearly, an avalanche stops after a while since the redistribution leads to loss of particles at the boundaries (or, in terms of the energy model, dissipation occurs at the boundaries). Once the avalanche stopped, an external supervisor notices it (this is the nonlocal part of the dynamics) and starts to add new particles (energy is injected into the system) until a new avalanche starts.

The above dynamics yields a stationary state in the long-time limit, and the steady state characteristics of avalanches can be measured. Such a characteristics is *e.g.* the number of sites s which become active during the process, and the remarkable feature of this model is that the distribution of s (and of other quantities such as the spatial size and the lifetime of the avalanches) is found to display a power law form

$$P(s) \sim s^{-\tau}. \quad (3.1)$$

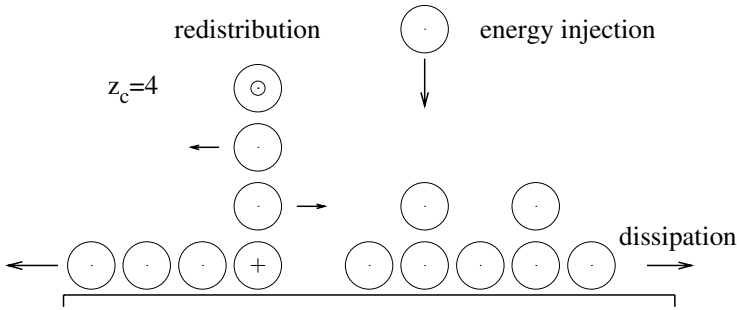


Fig. 3. Sandpile model. Particles (energy packets) are deposited on a two-dimensional substrate (one-dimensional section is shown). Injection stops when a site becomes active, *i.e.* it is occupied by z_c particles. Then redistribution to neighboring sites take place and particles disappear (dissipation of energy) at the edges. The process continues until all active sites are eliminated. Then the particles source is switched on again.

Thus one discovers that although the model does not contain parameters to tune, nevertheless it shows critical behavior (z_c can be changed without changing the criticality of the outcome). This observation generated a large amount of activity and *criticality-without-tuning* was seen in a number of similar models [46]. The resulting notion of *self-organized criticality* grew in importance [47] and, accordingly, new effort was put into understanding how SOC works.

An important feature that was recognized quite early [43] is the existence of a *non-local supervisor* who watches the activity of the avalanches and, upon ceasing of the activity, switches on the source of particles (or of energy). In principle, non-local dynamics can generate long-range correlations in both time and space so the emergence of criticality is not necessary a surprise. Viewing the problem from another angle, the non-local dynamics separates the timescales of the avalanches and of the particle injection. Thus, in practice, there is tuning. Namely, the system is considered in the limit of particle injection rate going to zero (actually, the dissipation is also tuned to zero since the particles disappear only at the boundaries of the system).

The zero injection rate, however, does not have to be a critical point, and the next important development was [44] the demonstration that it is indeed a nonequilibrium (absorbing state) critical point.

3.2 Absorbing state transitions and their connection to SOC

Absorbing state transitions appear in many contexts in nonequilibrium statistical physics [12, 48], and they are studied intensively since they are thought to be one of the truly nonequilibrium phenomena without counterpart in equilibrium systems. In order to understand the basics of it, let us consider a fixed energy sandpile model [49] shown in Figure 4.

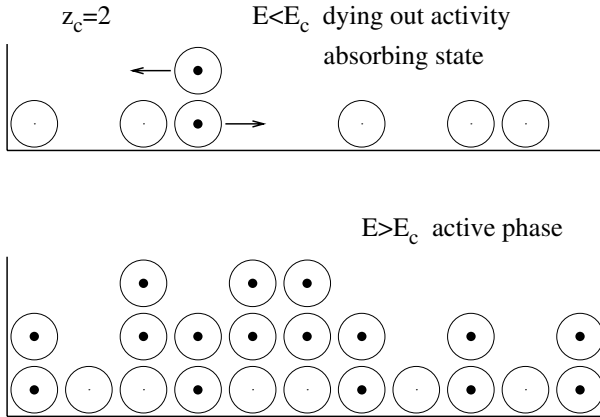


Fig. 4. A one-dimensional fixed energy sandpile model. Dynamics is defined by the energy (particles) being redistributed if a site contains z_c or more units of energy (the units which are redistributed in the next time-step are marked by large dots in their center). The total energy of the system is conserved since the boundaries prevent the loss of energy.

This model differs from the sandpile model by calling the particles energy units, and by the absence of both the injection and the dissipation of energy (particles). Thus the total energy E is conserved and as one can easily see from Figure 4 the behavior of the system is essentially different at small and large values of E . At small $E < E_c$, the activity (redistribution) ceases in the long-time limit and the system falls into a so called *absorbing state*. For large $E > E_c$, on the other hand, there are always active sites and the redistribution continues forever. For $t \rightarrow \infty$, the system settles into a steady state which is called *active state* and the *activity* can be quantified by measuring *e.g.* the number of active sites. One finds then that the absorbing state transition (*i.e.* the absorbing-active state transition) is a critical phase transition with the *activity* changing continuously through the transition point E_c (see Fig. 5).

Once the absorbing state transition is understood, it is easy to make the connection to SOC. Indeed, let us assume that we have the fixed energy

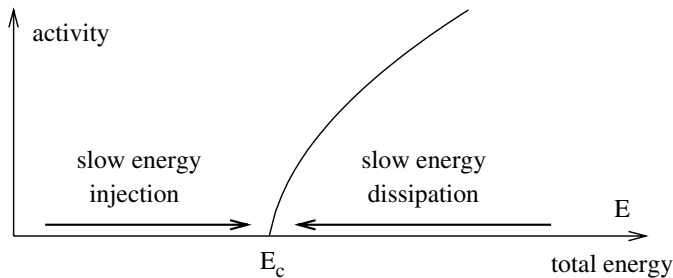


Fig. 5. Activity as a function of the total energy for the fixed energy sandpile model described in Figure 4. The evolution of the system as dissipation at the boundaries or the energy injection is switched on is given by the left and right arrows, respectively.

sandpile in the active state ($E > E_c$) and let us switch on the dissipation at the boundaries. Then the energy decreases slowly (note that the dissipation is proportional to the surface of the sample while E is proportional to the volume). This lowering of energy will continue until E reaches just below E_c when the system falls into the absorbing state and thus the dissipation stops.

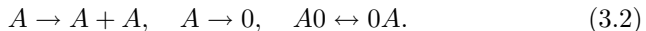
Let us now return to the fixed energy sandpile but this time let us start from an absorbing state ($E < E_c$) and switch on the “external supervisor” who is injecting energy into the system. The supervisor is required to stop the injection if adding of the last energy packet started activity in the system. This process increases the energy E infinitesimally slowly and brings the system near and perhaps slightly past the threshold of activity $E = E_c$.

Now, if both the dissipation at the boundaries and the “external supervisor” are present then the fixed energy sandpile model is nothing else but the sandpile model generating SOC. And we see that SOC emerges because the combined action of the dissipation and the “supervisor” brings the system to the critical point of the absorbing state transition of the fixed energy sandpile model.

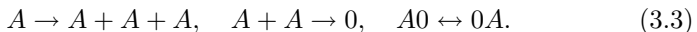
The mechanism unmasked above is rather general and present in many models of self organized criticality [44, 50]. The value of recognizing this mechanism lies in making it possible to describe and calculate scaling properties of SOC by studying “usual” nonequilibrium phase transitions. In particular, one may hope that field-theoretic description of SOC may be obtained through studies of the appropriate absorbing state transitions.

Of course, absorbing state transitions are numerous and it is not obvious which one is in the same universality class as a given system displaying SOC. In general, continuous phase transitions to an absorbing state are in

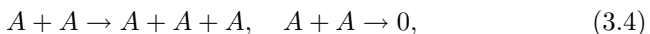
the universality class of *directed percolation* [51–53] that can be described by the following reaction diffusion process



Directed percolation is rather robust to various changes in its rules but the presence of extra symmetries (conservation laws) may change the universality class of an absorbing state transition. A well known example is the *parity conserving process* [54–56] which has the following reaction-diffusion representation



Both of the above processes have been much investigated and the scaling properties have been accurately determined. Furthermore, understanding (if not complete solution) has emerged even on field theoretic level [51,53,56]. Unfortunately, neither of the above processes have been directly related to models of SOC. Accordingly, the present day research is concentrated on absorbing state transitions which have more contact with SOC. An example is the critical point observed in the so called *pair contact process* [57] where particles diffuse only through the birth-death processes given by the reaction scheme



where the first and the second reactions take place with probabilities p and $1 - p$, respectively. A related problem is the epidemic model [58] where the reaction scheme



describes static healthy subjects (A) getting infected by diffusing infectious agents (B) who, in turn, recover with time.

The last two models are close to the fixed energy sandpile models (and thus to SOC) in that both of them have an infinite number of absorbing states and their coarse-grained description involves an order parameter (the active particles) coupled to a static field (the temporarily immobile particles). It has recently been suggested that the similarity may go deeper, *i.e.* they all belong to the same universality class [59]. This conclusion is based on a field-theoretic calculation near dimension $d = 6$ [59] using Langevin equations which were suggested on phenomenological grounds for the processes (3.4) and (3.5) [49,60]. At this point there is still a debate about both the applicability of the Langevin equations and the validity of the results in lower dimensions. Nevertheless, it appears that the approach of SOC through absorbing state transitions may be coming to an interesting and satisfactory conclusion.

Of course, one should not forget that apart from the connection to SOC, absorbing state transitions in general constitute an important problem in the theory of NESS. The field is developing fast and there are many interesting details scattered across the papers. A guide to the models and to the extensive literature about them can be found in recent reviews [48, 61].

4 Distribution functions in nonequilibrium steady states

The simplicity of the description of equilibrium system lies in the existence of the Gibbs distribution *i.e.* in the elimination of the dynamics from the calculation of averages. Although dynamics is clearly important in nonequilibrium steady states, it is not inconceivable that a prescription exist for a nonequilibrium equivalent of the Gibbs distribution which would include the essential features of the dynamics. Such a distribution function may have singularities as shown in simple examples [62, 63] or it may have problems with the additivity of the associated entropies (which is not unexpected in systems with long-range correlations) [64, 65]. Nevertheless, a prescription with well defined restrictions on its applicability would be valuable and the search for nonequilibrium distribution function(s) has been going on for some time.

A phenomenological approach to the above problem is the non-extensive statistical mechanics [64], an approach that takes its name from the nonextensive character of the postulated entropy. This approach has been much developed during the last decade, and not surprisingly, it has its success in connection with systems which have long-range interactions or display (multi)fractal behavior [64].

Below we shall present a alternative approach that is somewhat less general but it is based on the extension of our knowledge of universality of distribution functions in strongly fluctuating systems.

4.1 Power laws and universality of nonequilibrium distributions

Distribution functions of additive quantities such as *e.g.* the total magnetization in the Ising model are Gaussian in usual equilibrium systems. This Gaussianity follows from the central limit theorem that is applicable due to the correlations being short ranged away from critical points. At critical points, however, the power law correlations result in non-Gaussian distributions. The emerging distributions are quite restricted in their possible shapes, however, the reason being that the distribution functions at critical points are scaling functions and their shape is determined by the universality class associated with the given critical point.

The above observation can be used to develop a classification of nonequilibrium distribution functions. Namely, one knows that “effective” criticality (*i.e.* strong fluctuations and power-law correlations) is the norm for nonequilibrium steady states. Of course, the “effective” critical behavior is determined not only by the interactions but by the dynamics as well. Accordingly, one may expect that the scaling functions (and thus the distribution of macroscopic quantities) are determined by the nonequilibrium universality classes. Once we build a gallery of such scaling functions, we can use them in the same way as in the equilibrium case: we can identify symmetries and underlying mechanisms in experimental systems; we may find seemingly different systems belonging to the same universality class, and thus we can discover common underlying processes present in those systems. We can also use these distribution functions to find the critical dimension of a model and the applications are restricted only by imagination. Below we shall show how to calculate these distribution functions in simple systems and present a few applications.

4.2 Picture gallery of scaling functions

The simplest nonequilibrium systems displaying “effective” criticality are the growing surfaces [27, 28]. They are rough quite generally which means that the mean-square fluctuations of the surface diverge with system size. The roughness is defined by

$$w_2 = \frac{1}{A_L} \sum_{\vec{r}} [h(\vec{r}, t) - \bar{h}]^2 \sim L^\chi, \quad (4.1)$$

where A_L is the area of the substrate of characteristic linear dimension L , $\bar{h} = \sum_{\vec{r}} h(\vec{r}, t)/A_L$ is the average height of the surface, and χ is a critical exponent characterizing the given universality class. We shall be interested in the steady-state distribution of $P(w_2)dw_2$ and expect that due to criticality, the diverging scale $\langle w_2 \rangle$ will be the only relevant scale in $P(w_2)$ and, consequently, it can be written in a scaling form

$$P_L(w_2) \approx \frac{1}{\langle w_2 \rangle_L} \Phi \left(\frac{w_2}{\langle w_2 \rangle_L} \right), \quad (4.2)$$

where $\Phi(x)$ is a scaling function characteristic of the universality class the growth process belong to. Below, we show how to calculate Φ for a simple growth process (Edwards-Wilkinson equation [27]) and will demonstrate that the Φ -s are different for growth processes distinct in the sense of distinct universality classes.

Let us begin by discussing the equations for growing surfaces. In general, deposition of particles on a substrate, under the assumption that the

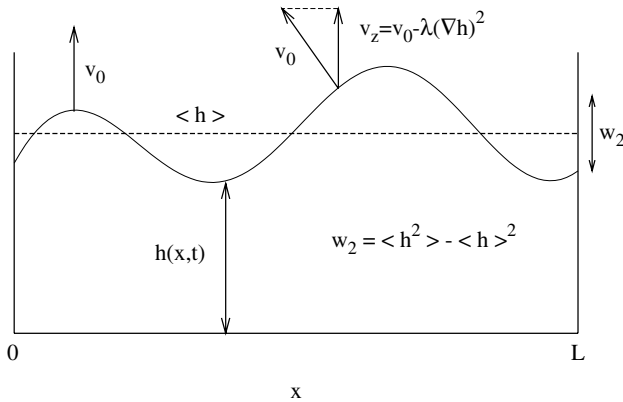


Fig. 6. Surface growth. The height of the surface above the substrate is given by $h(x,t)$ and the width of the surface w_2 is characterized by the mean-square fluctuation. The vertical velocity of the surface in general a function of the local properties of the surface, $v(\partial_x h, \partial_x^2 h, \dots)$.

surface formed is a single valued function $h(x,t)$, can be described by the equation $\partial_t h = v(h)$ where $v(h)$ gives the velocity of advance of the interface perpendicular to the substrate (Fig. 6). The velocity is usually written as $v(h) = v_0 + F(h) + \eta$ where v_0 is the average velocity due to the average rate of deposition, $F(h)$ is related both to the motion of the particles on the surface and to the dependence of the growth on the inclination of the surface. Finally the fluctuations in the above processes are collected in η which is assumed to be a Gaussian white noise in both space and time.

A simple form for $F(h)$ follows from the assumption that particles like to stick at points with large number of neighbors *i.e.* at large ∂_x^2 . Then, $F(h)$ is approximated as $F(h) = \nu \Delta_x^2$ and, in the frame moving with v_0 , one has the Edwards-Wilkinson (EW) model [27] of surface growth

$$\partial_t h(x,t) = \nu \Delta h(x,t) + \eta(x,t). \quad (4.3)$$

This equation can be solved and one finds that the steady-state probability distribution is given by

$$\mathcal{P}[h(x)] = A e^{-\frac{\sigma}{2} \int_0^L (\nabla h)^2 dx} \quad (4.4)$$

where σ is related to ν and to the amplitude of the white noise.

Once $\mathcal{P}[h(x)]$ is known, $P(w_2)$ is formally obtained from

$$P(w_2) = \left\langle \delta \left(w_2 - \left[\overline{h^2} - \overline{h}^2 \right] \right) \right\rangle \quad (4.5)$$

where the average $\langle \rangle$ is over all $h(x)$ with the distribution function $\mathcal{P}[h(x)]$ (note that $\overline{h^n}$ is a spatial average and it is still a fluctuating quantity). In practice, it is more convenient to calculate the generating function

$$G(s) = \int_0^\infty e^{-sw_2} P(w_2) dw_2 = \left\langle e^{-s(\overline{h^2} - \overline{h}^2)} \right\rangle \quad (4.6)$$

with the above expression demonstrating why $P(w_2)$ can be calculated analytically in simple models. Namely, if the partition function with \mathcal{P} can be found then the generating function (4.6) is just the partition function of the model with a quadratic term added and such term usually does not spoil the solvability of the problem. Indeed, *e.g.* in case of the $d = 1$ EW model with periodic boundary conditions, the problem is reduced to the evaluation of the partition function of a $d = 1$ quantum oscillator thus obtaining [66]

$$G(s) = \prod_{n=1}^{\infty} \left(1 + \frac{sL}{\sigma\pi^2 n^2} \right)^{-1}. \quad (4.7)$$

Now one can find the average width diverging $\langle w_2 \rangle = -\partial G(s)/\partial s|_{s=0} = L/(6\sigma)$ in the $L \rightarrow \infty$ limit. Using $\langle w_2 \rangle$ to eliminate L from (4.7), one observes that $G(s)$ is a function of the product $s\langle w_2 \rangle$ only and, consequently the inverse Laplace transform yields $P(w_2)$ in the scaling form (4.2). The calculation of the scaling function $\Phi(x)$ consist of collecting contributions from the poles in $G(s)$ and one obtains

$$\Phi(x) = \frac{\pi^2}{3} \sum_{n=1}^{\infty} (-1)^{n-1} n^2 \exp\left(-\frac{\pi^2}{6} n^2 x\right). \quad (4.8)$$

Figure 7 shows the above function displaying a characteristic shape of exponential decay $\Phi(x) \sim e^{-\pi^2 x/6}$ at large x and essential singularity $\Phi(x) \sim x^{-5/2} e^{-3/(2x)}$ for $x \rightarrow 0$.

In Figure 7 we have also included the results for the so called curvature driven growth process which is also called the Mullins-Herring model of surface growth [27]. This is a model where the rearrangement of deposited particles goes on by surface diffusion and the particle current j_h is towards places where there are many neighboring particles *i.e.* Δh is large. This means that $j_h \sim \nabla \Delta h$ and $F(h) = -\zeta \Delta^2 h$. The resulting equation is called the Mullins-Herring (MH) equation

$$\partial_t h(x, t) = -\zeta \Delta^2 h(x, t) + \eta(x, t). \quad (4.9)$$

The surfaces described by the MH equation belong to a universality class distinct from that of the EW growth. Indeed, the MH equation can be solved easily and one finds that $\langle w_2 \rangle_{\text{MH}} \sim L^2$ in contrast to the EW result

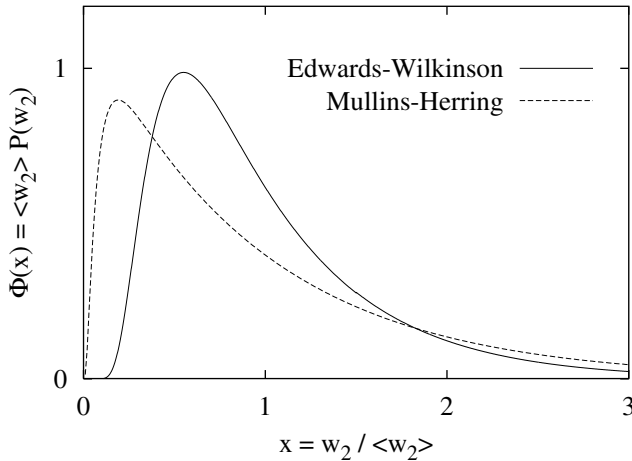


Fig. 7. Comparison of the scaling functions for the EW and MH models.

$\langle w_2 \rangle_{\text{EW}} \sim L$. Accordingly, the scaling function should also be different. A calculation similar to that described above for the EW case verifies this expectation [67] as can be observed in Figure 7.

An important point to remark about the comparisons of the EW and MH curves is that they are well distinguishable. Their maximum, their small x cutoff, and their decay at large x are all sufficiently different so that no ambiguity would arise when analyzing experimental data. Indeed, the $d = 2$ versions of the above Φ -s as well as a number of others characterizing various growth processes have been obtained in [68] and it did not appear to be difficult to pick the scaling function which was corresponding to a given set of experiments [68].

Finding out the universality class of a growth process is one possible application if one has a sufficiently developed gallery of scaling functions. Below we discuss other possibilities for application.

4.3 Upper critical dimension of the KPZ equation

The KPZ equation [29] is the simplest nonlinear model describing growth in terms of a moving interface. It differs from the EW model by taking into account that the surface grows in the direction of its normal provided the incoming particles have no anisotropy in their arrival direction. Then the z component of the velocity of the surface has a correction term proportional to $(\nabla h)^2$ as shown in Figure 6 and the equation in lowest order in the

nonlinearities becomes the so called KPZ equation

$$\partial_t h = \nu \vec{\nabla}^2 h + \lambda \left(\vec{\nabla} h \right)^2 + \eta. \quad (4.10)$$

Here ν and λ are parameters, while $\eta(\vec{r}, t)$ is again a Gaussian white noise. The steady state surfaces generated by (4.10) appear to be rough (critical) in any dimension if the nonequilibrium drive (λ) is large enough. Since equation (4.10) gives account of a number of interesting phenomena (Burgers turbulence, directed polymers in random media, etc.) lots of efforts have been spent on finding and understanding the scaling properties of its solutions [27, 28]. Nevertheless, a number of unsolved issues remain, the question of upper critical dimension (d_u) being the most controversial one. On one hand mode-coupling and other phenomenological theories suggest that $d_u = 4$ [69] while all the numerical work fail to find a finite d_u and the indication is that $d_u = \infty$ [70]. Below I would like to show how the scaling functions of the roughness can shed some light on this controversy [71].

Let us begin with the observation that scaling functions do not change above d_u . Thus if we build $\Phi(x)$ in dimensions $d = 1-5$ and observe that they differ significantly in $d = 4$ and 5 then we can conclude that $d_u > 4$. Since $\Phi(x)$ cannot be exactly calculated for $d \geq 2$ we must evaluate it through simulations with the results displayed in Figure 8.

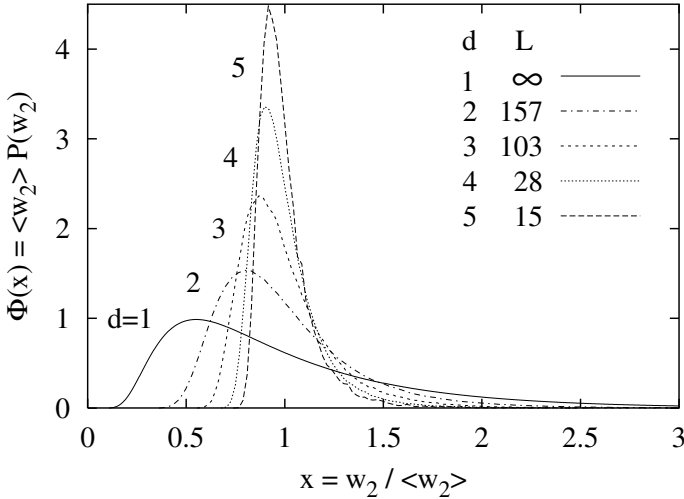


Fig. 8. Roughness distribution for KPZ steady-state surfaces in dimensions $d = 1-5$.

As one can see in Figure 8, the scaling functions change smoothly with d . The $\Phi(x)$ -s get narrower and more centered on $x = 1$ with increasing d , and

there is no break in this behavior at $d = 4$. The equality of the $d = 4$ and 5 scaling functions appears to be excluded.

Of course, our result is coming from numerical work with the same general conclusion as in previous studies. So, why is it more believable? Because one of the main criticism of numerical studies does not apply to it. Namely, no fitting parameters and fitting procedures are used in contrast to the usual determination of critical exponents. One just builds the histograms, calculates the averages to determine the scaling variable and plots the scaled histogram. This is clear and well understood but there is another remarkable feature in these scaling functions the origin of which is less obvious. Namely, the scaling functions in principle should depend on the size of the system,

$$\Phi(x) = \Phi_L(w_2/\langle w_2 \rangle_L). \quad (4.11)$$

What is observed, however, is that the L dependence is practically all in $\langle w_2 \rangle_L$ and L dependence of the shape of Φ (explicit dependence on L) disappears already at small L . These are important points and the KPZ application of the scaling functions was mainly chosen to emphasize them.

It seems that these scaling functions are versatile tools which can be used in computer science [72] as well as in understanding the propagation of chemical fronts [73]. An interesting application was *e.g.* the establishment of a connection between the energy fluctuations in a turbulence experiment and the interface fluctuations in the $d = 2$ Edwards-Wilkinson model [74], and thus prompting a search for an interface interpretation of the dissipative structure in the turbulent system [75]. In another case [76], it helped to make a link between the much studied $1/f$ noise and the extreme value statistics [77]. Since the effective criticality is a real feature of many nonequilibrium system, we expect that many more use will be found for the scaling functions discussed in this section.

5 Quantum phase transitions

Quantum critical points are associated with the change of the symmetry of the ground state of a quantum system as the interactions or an external field (control parameter) are varied. They have been much investigated in recent years with the motivation coming from solid state physics [78]. Namely, the strongly-correlated electron systems often produce power law correlations, and the origin of the observed scale-invariance is suggested to be the presence of a quantum critical point at $T = 0$ provided the effect of the quantum phase transition is felt at finite T as well.

From our point of view, the quantum phase transitions are interesting because they are good candidates for studying the effects of a nonequilibrium drive on well established symmetry-breaking transitions. The advantage of

these systems is that there is no arbitrariness in their dynamics (it is given by quantum mechanics), the one-dimensional systems are simple with examples of exactly solvable models displaying genuine critical phase transitions (see *e.g.* the transverse Ising chains discussed below) and, furthermore, there is much previous work to build on.

The only problem is how to force a quantum system into a non-equilibrium steady state. An obvious way is to attach two heat baths of different temperatures at the two ends of a spin chain. Unfortunately, this makes the problem unsolvable (even numerically) for any reasonable size system [79] and thus it is practically impossible *e.g.* to draw conclusions about the long-range correlations generated in the system. Below we show a way to avoid the problem of heat baths. The idea is that the nonequilibrium steady states always carry some flux (of energy, particle, momentum, etc.). Thus a steady state that is presumably not very far from the one generated by boundary conditions may be constructed by constraining the quantum system to have a flux equal to the one generated by the boundary conditions. For example, in the case of the transverse Ising chain treated below [80], we shall constrain the system to carry an energy current and will investigate the correlations in this constrained state¹.

5.1 Spin chains with fluxes

As a simple model with critical phase transition, we consider the $d = 1$. Ising model in a transverse field h which has the following Hamiltonian:

$$\hat{H}_1 = - \sum_{\ell=1}^N \left(\sigma_{\ell}^x \sigma_{\ell+1}^x + \frac{h}{2} \sigma_{\ell}^z \right). \quad (5.1)$$

Here the spins σ_{ℓ}^{α} ($\alpha = x, y, z$) are represented by $1/2$ times the Pauli matrices located at the sites $\ell = 1, 2, \dots, N$ of a one-dimensional periodic chain ($\sigma_{N+1}^{\alpha} = \sigma_1^{\alpha}$). The transverse field, h , is measured in units of the Ising coupling, J , which is set to $J = 1$ in the following.

This model can be solved exactly [81,82] and it is known that a second order phase transition takes place in the system as h is decreased. The order parameter is the expectation value $\langle \sigma_x \rangle$ *i.e.* $\langle \sigma_x \rangle = 0$ for $h > 1$, while $\langle \sigma_x \rangle \neq 0$ for $h < 1$ and $h_c = 1$ is a critical point. The scaling behavior at and near h_c belongs to the $d = 2$ Ising universality class.

In order to constrain the above system to carry a given energy flux J_E we shall use the Lagrange multiplier method. Namely, we add a term $\lambda \hat{J}_E$

¹It should be noted that this section was not discussed during the main lectures of the course. It was described only in a seminar for interested students.

to the Hamiltonian where \hat{J}_E is the local energy flux operator summed over all sites, and find that value of λ which produces a ground state with the expectation value $\langle \hat{J}_E \rangle = J_E$.

The above scheme requires the knowledge of the local energy current, \hat{J}_ℓ . It can be obtained using the quantum mechanical equation of motion for the energy density $\hat{\varepsilon}_\ell = i/\hbar [\hat{H}_I, \varepsilon_\ell]$, and representing the result as a divergence of the energy current $\hat{\varepsilon}_\ell = J_\ell - J_{\ell+1}$. The calculation yields ($\hbar = 1$ is used in the following)

$$\hat{J}_\ell = \frac{\hbar}{4} \sigma_\ell^y (\sigma_{\ell-1}^x - \sigma_{\ell+1}^x) \quad (5.2)$$

and this allows to construct the “macroscopic” current $\hat{J}_E = \sum_\ell \hat{J}_\ell$. Adding it to \hat{H}_I with a Lagrange multiplier, $-\lambda$,

$$\hat{H} = \hat{H}_I - \lambda \hat{J}_E. \quad (5.3)$$

We obtain the Hamiltonian whose ground states with $\langle \hat{J}_E \rangle = J_E \neq 0$ will give us information about the current carrying states of \hat{H}_I .

In order to avoid confusion, we emphasize that the energy current, \hat{J}_E , is associated with \hat{H}_I and not with the new Hamiltonian, \hat{H} . We also note that \hat{H} is just another equilibrium Hamiltonian, it differs from \hat{H}_I by an extra term which breaks the left-right symmetry of \hat{H}_I . Finding the ground state of \hat{H} , however, gives us the minimum energy state of \hat{H}_I which carries an energy current, $J_E = \langle \hat{J}_E \rangle$. Thus the ground-state properties of \hat{H} provide us with the properties of the nonequilibrium steady states of the transverse Ising model.

It turns out that $[\hat{H}_I, \hat{J}_E] = 0$ and \hat{H} can be diagonalized by the same transformations which diagonalize \hat{H}_I [80], and one arrives to a system of free fermions with a spectrum of excitation energies given by $\omega_q = |\Lambda_q|$ where

$$\Lambda_q = \frac{1}{2} \sqrt{1 + h^2 + 2h \cos q} + \frac{\lambda h}{4} \sin q. \quad (5.4)$$

with the wave numbers restricted to $-\pi \leq q \leq \pi$ in the thermodynamic limit ($N \rightarrow \infty$).

Figure 9 displays the spectrum for $h = 2/3$ and various λ and one can see that the $q \rightarrow -q$ symmetry of the spectrum is broken for $\lambda \neq 0$. Nevertheless, for small λ the ground-state remains that of the transverse Ising model ($\lambda = 0$) since $\Lambda_q \geq 0$ and the occupation number representation of the ground state does not change. Accordingly, no energy current flows ($J_E = 0$) for $\lambda < \lambda_c$. This rigidity of the ground state against the symmetry-breaking field which drives the energy current is a consequence of the facts that the fermionic spectrum of the transverse Ising model has a gap and that the operator \hat{J}_E commutes with \hat{H}_I (similar rigidity is observed in the studies of energy flux through transverse XX chain [83]).

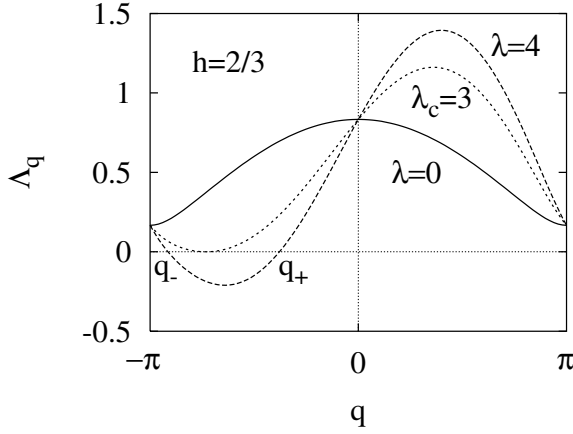


Fig. 9. Spectrum of the transverse Ising model in the presence of a field (λ) which drives the current of energy. The excitation energies are given as $\omega_q = |\Lambda_q|$. Increasing the drive makes the ground-state change at a critical $\lambda = \lambda_c$ ($\lambda_c = 3$ for $h = 2/3$) when negative energy states start to appear and get occupied. The qualitative picture is the same at all transverse fields h .

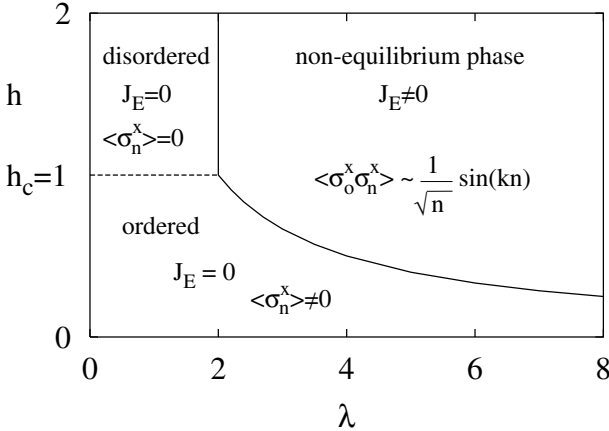


Fig. 10. Phase diagram of the driven transverse Ising model in the $h - \lambda$ plane where h is the transverse field while λ is the effective field which drives the flux of energy. Power-law correlations are present in the nonequilibrium phase ($J_E \neq 0$) and on the Ising critical line in the equilibrium phase ($J_E = 0$, dashed line).

The ground-state properties do change when $\Lambda_q < 0$ in an interval $[q_-, q_+]$ and these q states become occupied. Due to the resulting

asymmetry in the occupation of the q and $-q$ states, the energy current becomes nonzero. The line $\lambda_c(h)$ which separates the region of unchanged transverse Ising behavior from the $J_E \neq 0$ region is obtained from the conditions $\Lambda_q = 0$ and $\partial\Lambda_q/\partial q = 0$, and is displayed on the phase diagram (Fig. 10) as a solid line. Another phase boundary in Figure 10 is shown by dashed line. It separates the magnetically ordered ($h < 1$, $\lambda < 2/h$) and disordered ($h \geq 1$, $\lambda < 2$) transverse Ising regions. Since the ground state is independent of λ for $\lambda < \lambda_c$, one has the same second order transition across the dashed line as at $h = 1$ and $\lambda = 0$ *i.e.* it belongs to the $d = 2$ Ising universality class [82].

Clearly, one can view the region $\lambda < \lambda_c$ as an equilibrium phase while the $\lambda > \lambda_c$ region as a nonequilibrium one since there is a nonzero energy flux through the latter. This flux can actually be calculated easily with the simple result

$$j_E = \langle \hat{J}_E / N \rangle = (4\pi)^{-1} \sqrt{(1 - 4/\lambda^2)(h^2 - 4/\lambda^2)}. \quad (5.5)$$

Apart from the fact that $J_E \neq 0$, the $\lambda > \lambda_c$ region should also be considered as a distinct phase since the long-range magnetic order existing for $h < 1$ breaks down when $J_E \neq 0$ and the magnetic correlations become oscillatory with amplitudes decaying as a power of distance. Indeed, this can be seen by investigating the $\langle \sigma_\ell^x \sigma_{\ell+n}^x \rangle$ correlations which can be expressed through Pfaffians [84] and thus making possible numerical calculations for $n \leq 100$. In the presence of long-range order one should have $\langle \sigma_\ell^x \sigma_{\ell+n}^x \rangle \rightarrow \langle \sigma_\ell^x \rangle^2 \neq 0$ for $n \rightarrow \infty$ while we find that the correlations decay to zero at large distances as

$$\langle \sigma_\ell^x \sigma_{\ell+n}^x \rangle \sim \frac{Q(h, \zeta)}{\sqrt{n}} \cos(kn) \quad (5.6)$$

where the wavenumber, $k = \arccos(2/\lambda h)$. The above result (5.6) is coming from numerics and it is exact in the $\lambda \rightarrow \infty$ limit where the correlations are those of the $d = 1$ XX model [84].

One can observe power-law correlations for $\lambda > \lambda_c$ in other physical quantities as well. For example, the envelopes of both $\langle \sigma_\ell^z \sigma_{\ell+n}^z \rangle$ and $\langle \hat{J}_\ell \hat{J}_{\ell+n} \rangle$ correlations behave as n^{-2} in the large n limit [80]. Thus we arrive at the main conclusion of this section, namely that a simple, exactly soluble quantum system shows power-law correlations in the current carrying state in agreement with the notion that power-law correlations are a ubiquitous feature of nonequilibrium steady states.

Actually, remembering that power-law correlations in quantum models are associated with a gapless excitation spectrum, we can reformulate the transverse Ising model result to see a general connection between the emergence of power-law correlations and the presence of a current. Indeed, let us assume that a system with Hamiltonian \hat{H}_0 has a spectrum with a gap

between the ground-state and the lowest excited state. Furthermore, let \hat{J} be a “macroscopic” current of a conserved quantity such that $[\hat{H}_0, \hat{J}] = 0$. Generally, there is no current in the ground state and adding $-\lambda\hat{J}$ to \hat{H}_0 does not change the $\langle\hat{J}\rangle = 0$ result for small λ . Current can flow only if some excited states mix with the ground state and, consequently, a branch of the excitation spectrum must come down and intersect the ground-state energy in order to have $\langle\hat{J}\rangle \neq 0$. Once this happens, however, the gap disappears and one can expect power-law correlations in the current-carrying state. Admittedly, the above argument is not strict and is just a reformulation (in general terms) of what we learned from the transverse Ising model. We believe, however, that the above picture is robust and suggestive enough to try to find other soluble examples displaying the flux \rightarrow power-law-correlations relationship.

5.2 Effective interactions

When using the Lagrange multiplier method, one assumes that the flux generated by boundary conditions can be replaced by the effective interactions contained in an appropriately chosen global flux \hat{J} . These interactions are generally short ranged since the flux is usually a sum of local terms. The short-range nature of the effective interactions is actually not in contradiction with the power-law correlation being generated since the Lagrange multiplier gets tuned in order to achieve a given flux and, furthermore, the tuning is not quite trivial since λ must be increased past a critical value in order to have *e.g.* a nonzero flux energy. The question nevertheless arises whether adding a flux term in \hat{H} was an adequate description for the nonequilibrium steady state which is expected to display power-law correlations.

In order to investigate the above question one would have to solve the problem with the boundary drive but, as discussed above, an exact solution does not seem to be feasible. Instead, however, one can prepare initial conditions which will lead in the long-time limit to a steady flux. Then the steady state obtained in this natural way can be compared to the one found by the Lagrange multiplier method. This program has been carried out [85] for the XX chain defined by the following Hamiltonian

$$\hat{H}_{XX} = - \sum_{\ell=1}^N (\sigma_{\ell}^x \sigma_{\ell+1}^x + \sigma_{\ell}^y \sigma_{\ell+1}^y + h \sigma_{\ell}^z) . \quad (5.7)$$

In this model, the transverse magnetization $M_z = \sum_i \sigma_i^z$ is conserved and one can investigate the nonequilibrium states which carry a given magnetization flux by using the Lagrange multiplier method [83]. At the same time, the model is simple enough so that one can solve the time dependent

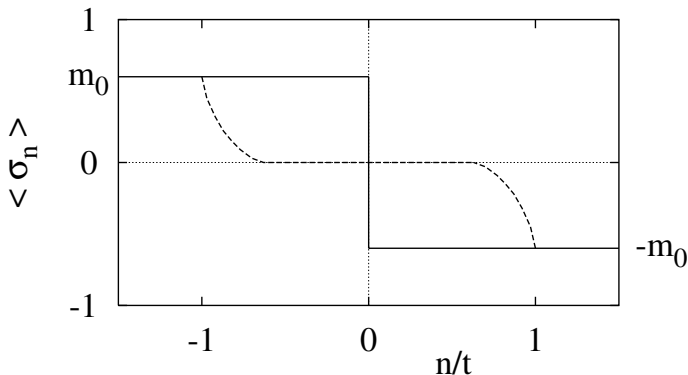


Fig. 11. Time evolution of the magnetization profile starting from a step-like initial conditions shown as solid line. There are two fronts going out to $\pm\infty$. They diminish the magnetization and leave behind a homogeneous $\langle s_n^z \rangle = 0$ state. In the scaling limit $t \rightarrow \infty$, $n/t \rightarrow x$, the magnetization $m(n, t) \approx \Phi(n/t)$ is given by $\Phi(x) = m_0$ for $-1 < x$, $\Phi(x) = m_0 - \pi^{-1} \arccos(x)$ for $-1 < x < -\cos(\pi m_0)$, $\Phi(x) = 0$ for $-\cos(\pi m_0) < x < 0$, and $\Phi(x) = -\Phi(-x)$ for $x > 0$ (dashed line).

problem where a steady magnetization flux is achieved by starting with an inhomogeneous initial state that is the ground state at fixed magnetization but with $m = \langle s_n^z \rangle$ reversed from m_0 for $n \leq 0$ to $-m_0$ for $n > 0$. The time-evolution of this step-like initial state can be followed exactly and the magnetization profile emerging in the long-time limit is shown in Figure 11. The remarkable feature of this magnetization profile is the middle part which is an $m = 0$ homogeneous state carrying a magnetization flux $j(m_0)$. Comparing this state to the one generated by adding the flux term to the Hamiltonian and fixing the Lagrange multiplier to have the same $j(m_0)$, we find that various expectation values such as the energy, the occupation number in fermionic representation are all equal in the two states. Thus the Lagrange multiplier yields a correct description of the states carrying a magnetization flux.

It should be noted, however, that recent calculation with an inhomogeneous initial state of different temperatures (T_1 for $x < 0$ and T_2 for $x > 0$) has yielded a different result for the asymptotic state carrying an *energy* flux [86]. Namely, it was shown that, at least in the neighborhood of $x = 0$ and in the $t \rightarrow \infty$ limit, the properties of the flux-carrying state can be interpreted in terms of the ground state of an effective Hamiltonian

$$\hat{H}_{\text{eff}} = \hat{H}_{XX} + \sum_{n=1}^N \mu_n \sum_{j=1}^N \hat{Q}_j^{(n)}, \quad (5.8)$$

where $Q_j^{(n)}$ is a product of local operators at sites j and $j + n$, and the interaction is of long-range type since $\mu_n \sim 1/n$ [86] (remarkably, the first two operators $\hat{Q}_j^{(1)}$ and $\hat{Q}_j^{(2)}$ are those appearing in the Lagrange multiplier treatment of the energy flux in the XX chain). Although the homogeneity of the asymptotic state was not shown and thus the comparison may be questioned, the above result indicates that the Lagrange multiplier approach may be only a first approximation in describing the flux-carrying states.

In summary, the studies of quantum systems described above strengthen the view that fluxes generate long-range correlations. Furthermore, the quantum systems also give a simple picture of how the emergence of these correlations is related to the closing a gap in the excitation spectrum above the ground state.

6 Outlook

There are topics which are important but were not discussed in these lectures. To mention a few, there is a large body of work on one-dimensional systems displaying nonequilibrium phase transitions, on orderings of granular gases under shear, on pattern formation with phase transitions described by the complex-coefficient Landau-Ginzburg equation, and the list could be continued. My choice of topics mainly reflects my past work and my attempts to develop simple starting points for making inroads into the beautiful but rather difficult field of far from equilibrium phenomena.

Finally, I was asked to provide entertainment for readers by trying to guess the future developments in connection with nonequilibrium orderings. Well, one of the present problem of the field is the lack of simple experimental systems which can be taken far enough from equilibrium and compared to elementary models of NESS. Search for such systems will intensify and I expect that there will be a shift towards biological problems. There the condition of being far from equilibrium is satisfied and there may be surprisingly simple phenomena under the guise of complicated pictures. This line of research may in the future meet up with game theories generalized to take into account spatial structures.

Search for better understanding of the emerging effective interactions will also continue, just as the sorting out of the absorbing-state transitions (surprising connections may be still found there, in addition the existing one to SOC). I also believe that theory of nonequilibrium distributions will be much developed, and limiting distributions such as the ones emerging in extreme statistics will have a much wider use in physics. These are more or less safe bets. And then there is the unpredictable part of future.

I thank the organizers for providing ideal surroundings for delivering these lectures. Thanks are also due to M. Droz and F. van Wijland for helpful discussions and comments on the manuscript.

References

- [1] P.M. Chaikin and T.C. Lubensky, *Principles of Condensed Matter Physics* (Cambridge University Press, 1995); S.-K. Ma, *Mod. Theory Crit. Phenom.* (Benjamin Cummings, Reading, 1976).
- [2] P.C. Hohenberg and B.I. Halperin, *Rev. Mod. Phys.* **49** (1977) 435.
- [3] M.C. Cross and P.C. Hohenberg, *Rev. Mod. Phys.* **65** (1993) 851.
- [4] E.M. Lifshitz and L.P. Pitaevski, *Statistical Physics, Part II* (Butterworth-Heinemann, Oxford, 1995).
- [5] L.F. Cugliandolo, J. Kurchan and L. Peliti, *Phys. Rev. E* **55** (1997) 3898; S. Franz and M.A. Virasoro, *J. Phys. A* **33** (2000) 891.
- [6] A. Barrat, J. Kurchan, V. Loreto and M. Sellitto, *Phys. Rev. Lett.* **85** (2000) 5034.
- [7] L. Berthier and J.-L. Barrat, *Phys. Rev. Lett.* **89** (2002) 095702.
- [8] I.K. Ono, C.S. O'Hern, D.J. Durian *et al.*, *Phys. Rev. Lett.* **89** (2002) 095703.
- [9] L. Bellon, S. Ciliberto, C. Laroche, *Europhys. Lett.* **51** (2000) 551; D. Herisson, M. Ocio, *Phys. Rev. Lett.* **88** (2002) 257202.
- [10] P. Sollich, S. Fielding and P. Mayer [[cond-mat/0111241](#)]; T.M. Nieuwenhuizen, *Phys. Rev. E* **61** (2000) 267.
- [11] B. Schmittmann and R.K.P. Zia, in *Phase Transitions and Critical Phenomena*, edited by C. Domb and J.L. Lebowitz (Academic Press, New York, 1996).
- [12] J. Marro and R. Dickman *Nonequilibrium Phase Transitions in Lattice Models* (Cambridge University Press, 1999).
- [13] B. Schmittmann, *Europhys. Lett.* **24** (1993) 109.
- [14] K.E. Bassler and Z. Rácz, *Phys. Rev. Lett.* **73** (1994) 1320; *Phys. Rev. E* **52** (1995) 9.
- [15] U.C. Täuber, V.K. Akkineni and J.E. Santos, *Phys. Rev. Lett.* **88** (2002) 045702.
- [16] M. Droz, Z. Rácz and P. Tartaglia, *Phys. Rev. A* **41** (1989) 6621; B. Bergersen and Z. Rácz, *Phys. Rev. Lett.* **67** (1991) 3047; H.-J. Xu, B. Bergersen, and Z. Rácz, *Phys. Rev. E* **47** (1993) 1520.
- [17] G. Grinstein, C. Jayaprakash and Y. He, *Phys. Rev. Lett.* **55** (1985) 2527.
- [18] *Nonequilibrium Statistical Mechanics in One Dimension*; edited by V. Privman (Cambridge University Press, 1996).
- [19] R.J. Glauber, *J. Math. Phys.* **4** (1963) 294.
- [20] K. Kawasaki, *Phys. Rev.* **145** (1966) 224.
- [21] B.D. Hughes, M.F. Schlesinger and E. Montroll, *J. Stat. Phys.* **28** (1982) 111.
- [22] P.L. Garrido, J.L. Lebowitz, C. Maes and H. Spohn, *Phys. Rev. A* **42** (1990) 1954.
- [23] B. Schmittmann and R.K.P. Zia, *Phys. Rev. Lett.* **66** (1991) 357.
- [24] B. Schmittmann, *Europhys. Lett.* **24** (1993) 109.
- [25] N.D. Mermin and H. Wagner, *Phys. Rev. Lett.* **17** (1966) 1133.
- [26] P.L. Garrido, F. de los Santos and M.A. Muñoz, *Phys. Rev. E* **57** (1998) 752; B. Schmittmann *et al.*, *Phys. Rev. E* **61** (2000) 5977; A. Achahbar *et al.*, *Phys. Rev. Lett.* **87** (2001) 195702.
- [27] J. Krug and H. Spohn, in *Solids far from Equilibrium*, edited by C. Godrèche (Cambridge University Press, 1991).

- [28] A.-L. Barabási and H.E. Stanley, *Fractal Concepts in Surface Growth* (Cambridge University Press, 1995).
- [29] M. Kardar, G. Parisi and Y.-C. Zhang, *Phys. Rev. Lett.* **56** (1986) 889.
- [30] T. Vicsek, A. Czirók, E. Ben-Jacob, I. Cohen and O. Shochet, *Phys. Rev. Lett.* **75** (1995) 1226.
- [31] J. Toner and Y. Tu, *Phys. Rev. E* **58** (1998) 4828.
- [32] G.B. West, *Physica A* **263** (1999) 104; K. Schmidt-Nielsen, *Why is Animal Size so Important?* (Cambridge University Press, 1984).
- [33] M.B. Weissman, *Rev. Mod. Phys.* **60** (1988) 537.
- [34] D. Sornette, *Critical Phenomena in Natural Sciences* (Springer, Berlin, 2000).
- [35] H.W. Press, *Astrophysics* **7** (1978) 103.
- [36] K.L. Schick and A.A. Verveen, *Nature* **251** (1974) 599.
- [37] F. Lillo and R.N. Mantegna, *Phys. Rev. E* **62** (2000) 6126.
- [38] B.B. Mandelbrot and J.R. Wallis, *Water Res. Res.* **5** (1969) 321.
- [39] M. Yamamoto *et al.*, *Brain Res.* **366** (1986) 279.
- [40] K. Nagel and M. Paczuski, *Phys. Rev. E* **51** (1995) 2909.
- [41] U. Frisch *Turbulence: The Legacy of A.N. Kolmogorov* (Cambridge University Press, 1995).
- [42] P. Bak, C. Tang and K. Wiesenfeld, *Phys. Rev. Lett.* **59** (1987) 381.
- [43] G. Grinstein, in *Scale Invariance, Interfaces and Non-Equilibrium Dynamics*, edited by A. McKane *et al.*, NATO Advanced Study Institute, *Series B: Physics* **344** (Plenum, New York, 1995); D. Sornette, A. Johansen and I. Dornic, *J. Phys. I (France)* **5** (1995) 325; A. Vespignani, S. Zapperi and V. Loreto, *Phys. Rev. Lett.* **77** (1996) 4560.
- [44] A. Vespignani and S. Zapperi, *Phys. Rev. Lett.* **78** (1997) 4793; A. Vespignani, R. Dickman, M.A. Muñoz and S. Zapperi, *Phys. Rev. Lett.* **81** (1998) 5676.
- [45] R. Dickman in *Nonequilibrium Statistical Physics in One Dimension*, edited by V. Privman (Cambridge University Press, 1996).
- [46] H.J. Jensen, *Self Organized Criticality* (Cambridge University Press, 1998).
- [47] P. Bak, *How Nature Works* (Springer, New York, 1999).
- [48] H. Hinrichsen, *Adv. Phys.* **49** (2000) 1.
- [49] R. Dickman, A. Vespignani and S. Zapperi, *Phys. Rev. E* **57** (1998) 5095.
- [50] M. Rossi, M. Pastor-Satorras and A. Vespignani, *Phys. Rev. Lett.* **85** (2000) 1803.
- [51] H.K. Janssen, *Z. Phys. B* **42** (1981) 151.
- [52] P. Grassberger, *Z. Phys. B* **47** (1982) 365.
- [53] J. Cardy and R.L. Sugar, *J. Phys. A* **13** (1980) L423.
- [54] P. Grassberger, F. Krause and T. von der Twer, *J. Phys. A* **17** (1984) L105.
- [55] N. Menyhárd, *J. Phys. A* **27** (1994) 6139; N. Menyhárd and G. Ódor, *J. Phys. A* **29** (1996) 7739.
- [56] J. Cardy and U.W.C. Täuber, *Phys. Rev. Lett.* **77** (1996) 4780.
- [57] I. Jensen, *Phys. Rev. Lett.* **70** (1993) 1465; I. Jensen and R. Dickman, *Phys. Rev. E* **48** (1993) 1710.
- [58] M. Pastor-Satorras and A. Vespignani, *Phys. Rev. E* **62** (2000) 5875.
- [59] F. van Wijland, *Phys. Rev. Lett.* **89** (2002) 190602.
- [60] M.A. Muñoz, G. Grinstein, R. Dickman and R. Livi, *Phys. Rev. Lett.* **76** (1996) 451.
- [61] G. Ódor [[cond-mat/0205644](#)].
- [62] R. Graham and T. Tél, *Phys. Rev. A* **31** (1985) 1109, 3364.

- [63] B. Derrida, J.L. Lebowitz and E.R. Speer, *Phys. Rev. Lett.* **87** (2001) 150601; *J. Stat. Phys.* **107** (2002) 599 [cond-mat/0203161].
- [64] C. Tsallis, *J. Stat. Phys.* **52** (2000) 479, The literature related to the ensuing activity can be tracked at <http://tsallis.cat.cbpf.br/biblio.html>
- [65] C. Beck, *Phys. Rev. Lett.* **87**, 180601 (2001); C. Beck and E.G.D. Cohen [cond-mat/0205097].
- [66] G. Foltin, K. Oerding, Z. Rácz, R.L. Workman and R.K.P. Zia, *Phys. Rev. E* **50** (1994) 639.
- [67] M. Plischke, Z. Rácz and R.K.P. Zia, *Phys. Rev. E* **50** (1994) 3589.
- [68] Z. Rácz and M. Plischke, *Phys. Rev. E* **50** (1994) 3530.
- [69] F. Colaiori and M.A. Moore, *Phys. Rev. Lett.* **86** (2001) 3946, and references therein.
- [70] E. Marinari, A. Pagnani and G. Parisi, *J. Phys. A* **33** (2000) 8181; see also references in [71].
- [71] E. Marinari, A. Pagnani, G. Parisi and Z. Rácz, *Phys. Rev. E* **65** (2002) 026136.
- [72] G. Korniss, Z. Toroczkai, M.A. Novotny and P.A. Rikvold, *Phys. Rev. Lett.* **84** (2000) 1351.
- [73] G. Tripathy and W. van Saarloos, *Phys. Rev. Lett.* **85** (2000) 3556.
- [74] S.T. Bramwell, P.C.W. Holdsworth and J.-F. Pinton, *Nature* **396** (1998) 552.
- [75] V. Aji and N. Goldenfeld, *Phys. Rev. Lett.* **86** (2001) 1007.
- [76] T. Antal, M. Droz, G. Györgyi and Z. Rácz, *Phys. Rev. Lett.* **87** (2001) 240601; *Phys. Rev. E* **65** (2002) 046140.
- [77] E.J. Gumbel, *Statistics of Extremes* (Columbia University Press, 1958).
- [78] S. Sachdev, *Quantum Phase Transitions* (Cambridge University Press, 1999).
- [79] For treating the heath baths attached to the end of spin chains see K. Saito, S. Takesue and S. Miyashita, *Phys. Rev. E* **54** (1996) 2404.
- [80] T. Antal, Z. Rácz and L. Sasvári, *Phys. Rev. Lett.* **78** (1997) 167.
- [81] E. Lieb, T. Schultz and D. Mattis, *Ann. Phys. (N.Y.)* **16** (1961) 407.
- [82] P. Pfeuty, *Ann. Phys. (N.Y.)* **57** (1970) 79.
- [83] T. Antal, Z. Rácz, A. Rákos and G.M. Schütz, *Phys. Rev. E* **57** (1988) 5184.
- [84] E. Baruch and B. McCoy, *Phys. Rev. A* **3** (1971) 786.
- [85] T. Antal, Z. Rácz, A. Rákos and G.M. Schütz, *Phys. Rev. E* **59** (1999) 4912.
- [86] Y. Ogata, *Phys. Rev. E* **66** (2002) 016135.

COURSE 2

MECHANICAL AGING AND NON-LINEAR RHEOLOGY OF CONCENTRATED COLLOIDAL SUSPENSIONS: EXPERIMENTAL FACTS AND SIMPLE MODELS

A. AJDARI

*Physico-Chimie Théorique,
UMR CNRS-ESPCI 7083,
10 rue Vauquelin, 75005 Paris, France*



Contents

1	Introduction	43
1.1	Colloidal glasses?	43
1.2	Model and real colloids: Interactions	44
1.3	Gels or glasses: Various kinds of soft solids?	48
1.4	Wrapping up the introduction	49
2	Experimental facts 1: Soft solids that flow and age	50
2.1	Concentrating colloidal suspensions: From a “viscous liquid” to a “soft-solid” behaviour	50
2.2	Probing the system in its “soft-solid” phase	51
2.3	Mechanical aging	52
3	A class of simple models	54
3.1	A Maxwell model with one scalar internal variable	54
3.2	Relation to other models in the literature	55
3.3	Predictions	57
3.4	Intermediary conclusion	61
4	Experimental facts 2: Soft solids that flow in a strange way	61
4.1	Avalanches and “viscosity bifurcation”	61
4.2	Parallel with flow induced transitions: Heterogeneous “banded” flows	62
4.3	Description within the simple class of models	63
4.4	Intermediary conclusion	66
5	Criticism of the model and perspectives	67
5.1	A classification of the phenomenologies	67
5.2	Successes and failures of these models	68
5.3	Better models: More variables? which collective physics?	69
5.4	Back to facts	71

MECHANICAL AGING AND NON-LINEAR RHEOLOGY OF CONCENTRATED COLLOIDAL SUSPENSIONS: EXPERIMENTAL FACTS AND SIMPLE MODELS

A. Ajdari

Abstract

Many colloidal systems display very non-Newtonian and solid-like behaviour when concentrated, a striking feature being the apparition of a yield stress. After recalling some basics about the interactions between colloidal particles, I present a few experimental facts commonly observed in these systems: aging and non-linear rheology. A simple phenomenological model is then introduced, in which the local state of the system is described by a single scalar parameter, the fluidity. I proceed with comments on heterogeneous flows in some of these systems. These notes are not intended to be a comprehensive review, and the reader is directed to the references for further reading.

1 Introduction

1.1 Colloidal glasses?

In the last years many works [3, 16, 23, 41, 55, 58] have suggested possible cross-interests between (i) research on the glass transition (statistical mechanics, structural glasses, solid polymers), (ii) studies on colloidal “soft” systems. Such cross-interests are based on the two following hopes.

First, colloidal systems could be ideal systems to understand fundamental aspects of the glass transition: they are *tunable* “equivalents” of atomic or molecular systems with controllable interactions, that also sometimes freeze into amorphous disordered phases with solid-like behaviour (“glasses”). The spatial scale is advantageously roughly a thousand times larger than in atomic systems, which could permit easier experimental investigation. In addition, playing with the viscosity of the solvents, one can

Great thanks to Lydéric Bocquet, Michael Cates, Caroline Derc, David Head, François Lequeux and Guillemette Picard, for past and ongoing collaboration on related topics.

hope to tune the temporal scales, allowing an easier span of the huge range of accessible time scales required for the study of the glass transition.

Second, many common colloidal systems (gels, foams, creams, emulsions) are actually used in this soft solid form that may bear similarities with glasses. Mayonnaise for example is a disordered arrangement of oil drops that behave as an amorphous elastic solid under a weak constraint, and flows plastically under larger stress. Some of the mechanical features of these amorphous colloidal systems may be better apprehended if they are considered as glasses.

1.2 Model and real colloids: Interactions

A first step toward the understanding of the behaviour of a colloidal system is the examination of the interactions between its constituents. Without aiming at an exhaustive review, I describe below a set of commonly encountered attractions and repulsions between colloidal particles embedded in a fluid solvent (thorough reviews are provided by textbooks such as [37, 52]). The term “colloid” is often coined to particles of size smaller than a few microns dispersed in a solvent, so that gravity has a limited effect on a *single* particle (the exact limit depending on the experiment or application considered). This allows the dispersion of the particles by simple thermal agitation.

1.2.1 Interactions between model colloids

Attractions and Repulsions. I consider here two identical colloidal spheres of radius R in a solvent, separated by a distance d (Fig. 1). They induce on each other both attractions (A) and repulsions (R):

- A1) the van der Waals attraction, due to the difference in dielectric properties of the solvent and the particles. This leads to a long-range attractive potential $U_{\text{vdw}}(d)$, that, in a simple picture neglecting retarded interactions, behaves as $\sim -Hd/R$ for $d \ll R$ and $\sim -H(d/R)^6$ for $d \gg R$. The Hamaker constant H is roughly proportional to the square of the difference in dielectric constant (or in optical index) and of order $k_{\text{B}}T$. By fine-tuning solvent mixtures it is sometimes possible to diminish the contrast and significantly reduce this attraction;
- A2) depletion forces, that can for example be induced by dissolving in the solvent polymers that do not adsorb on the surface. The dissolved polymer coils behave as impenetrable objects of typical size say b , which are sterically excluded (depleted) from a corona around the colloidal particles of a thickness of order b . Bringing particles together induces overlap of these depletion coronas, and thus increases

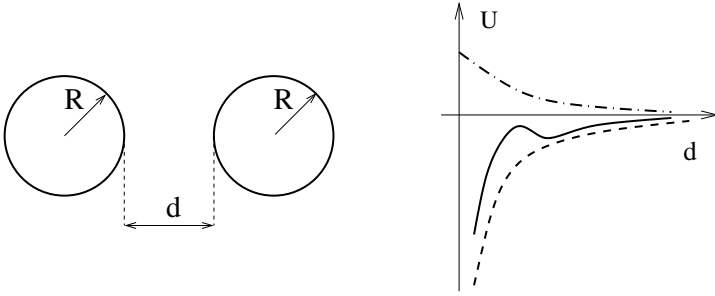


Fig. 1. *Left:* two model spherical colloids. *Right:* typical pair potentials in the DLVO theory: the van der Waals attraction (dashed line) and the electrostatic repulsion (dot-dashed line) result in an overall interaction potential (solid line) with a secondary minimum at a finite distance d .

the volume accessible to the polymers and consequently the configurational entropy of the system. This induces a *short-range “depletion” attraction* of entropic origin. Its range is of order b and its amplitude controlled by the polymer concentration;

- R1) core steric repulsion: the particles cannot interpenetrate which results in a very strong and very short-ranged repulsion (a few Angströms);
- R2) screened electrostatic repulsion: similarly charged particles dispersed in an electrolyte solvent (*e.g.* water) repel each other. Electrostatic effects are screened over the Debye length λ_D (a few nm to a few tens of nm typically), due to the presence of dissociated counter-ions and salt. The resulting repulsion potential $U_{el}(r)$ decreases as $\sim \exp(-d/\lambda_D)$ for large separations. Increasing the ionic strength of the solution (*e.g.* by adding salt) induces a drop of both the amplitude and range λ_D of this repulsion;
- R3) (Steric) protection by polymer layers. A classical way to avoid aggregation of the particles is to sterically “protect” the colloids with a polymer layer of thickness δ (grafted or adsorbed). Such layers swollen by the solvent repel each other for entropic reasons and thus provide a rather strong wall potential at $d \simeq 2\delta$. In addition, the dielectric properties of these layers of low polymer concentration are close to that of the solvent, so that they do not induce unfavorable additional van der Waals attractions.

Resulting pair potentials. In general many interactions act concurrently. The classical DLVO theory describes the behaviour of simple charged

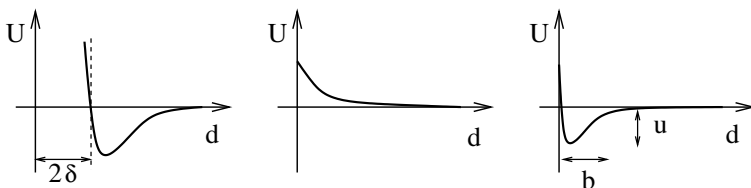


Fig. 2. Examples of pair interaction potentials achievable with model systems.

colloidal spheres in a salty solution under the action of van der Waals attraction and electrostatic repulsions (A1, R1 and R2). The attraction always dominates at very long and very short separations, and the electrostatic repulsion if strong enough can induce a “secondary” potential minimum (see Fig. 1). The overall behaviour of a suspension of such particles then depends on the depth of this minimum and on the amplitude of the barrier that separates it from the “primary” minimum (which corresponds to quasi-contact). If particles reach this quasi-contact state, very short range interactions and chemistry often take over that result in an irreversible binding.

If the attraction wins, for example upon addition of salt to the system, the particles tend to aggregate into big lumps that sediment or cream (gravity is far from negligible for large aggregates), leading to the “destabilization” of the suspension, an effect often fought against (for example in paints, inks, etc.). Protection techniques have often been used to strengthen repulsion (R3) and prevent actual contact.

From a fundamental point of view, playing with the set of interactions mentioned above, one can to some extent tailor the interparticle potential, with control of both amplitude and range (see *e.g.* Figs. 2b–d), and thus prepare in the lab model colloidal systems. In particular the Edinburgh group has managed in the 80s to prepare colloidal suspensions that behave as genuine hard spheres solutions [59]. As such this substantiates the claim that model colloidal systems constitute a rich tool-box for the study of the collective behaviour that leads to crystallization or to the glass transition. The reader is however warned that the mastering of the “tunability” of the interaction requires a significant expertise, especially in the chemistry and surface chemistry involved in the preparation of the particles.

1.2.2 More common colloidal systems

The somewhat naive textbook picture for model colloids given above must rapidly be supplemented by corrections that are often relevant:

Colloidal particles are not always rigid. As such they can elastically deform under internal or external forces, which renders the description of their

interactions more complex. This in particular the case for emulsions and foams, where the dispersed phase (the particles) is liquid or gaseous. When the system is concentrated the particles pushed against one-another tend to facet at the cost of an elastically stored surface energy. In other systems the elementary particles are elastic and compressible in their bulk. This is for example the case for small gel beads [8] or multi-lamellar vesicles (onions) that can expel solvent and deform upon compression [27, 51].

Colloidal particles are not necessarily spherical. Rods or needle-shape objects are rather common, as well as plate-like or disk-like particles. Such objects start to interact and produce collective behaviour at volume fractions much weaker than their spherical counterpart. For example laponite systems are made of disk-like particles of a few nm thickness and about 100 nm in diameter, that deviate from dilute behaviour at very low volume fractions [5].

Colloidal particles are seldom/never uniform. This is in particular true for the surface charge: heterogeneities in surface charge can lead to very anisotropic electrostatic interactions, and even to attractions between particles of same *average* charge. For example, laponite particles are said to have a different charge density on their perimeter and on their faces for some pH and salt values, allowing for the building of “house of cards” structures.

Colloidal particles are seldom/never perfectly smooth, in line with the two previous points. Their roughness can affect their interactions at short distances, control the apparition of capillary bridges in mixed solvents, and render the link between two particles in the primary minimum rigid [52].

Colloidal systems are seldom/never monodisperse. Large variations in size, shape factor, etc. is the rule for many practical systems.

There is rarely a single kind of particle in a colloidal system. One extreme, industrial systems (creams, paints, etc.), are often made of at least 5 or 6 different main ingredients aimed at fulfilling different (and often conflicting) tasks (see the notes of B. Cabane).

Eventually, while we are later in these notes going to discuss physical aging and a mild form of history dependence in these systems, a much more stringent one is that the physico-chemical state of the system, even at small scales, can in general not be anticipated from its sole composition. For example polymers adsorbing on the particles surface can lead to protected colloids if added in a dilute suspension (a complete protecting layer forming around each particle), but can induce bridging and thus promote aggregation if added when the particles are close to one another. Similarly any earlier stage at which the particles have been in contact can induce chemical reactions and irreversible sticking between the particles that will resist later attempts to re-disperse the system.

At this stage, the second point of Section 1.1 appears rather a matter of trust: although clean model colloidal systems can be prepared, many common colloidal systems rely on very varied and uncontrolled interactions. As such it is not clear that such various and complex systems should obey rather universal features. However we will see below that they share some similarity in terms of mechanical behaviour, which suggests that it is worth digging further, if only to clarify in what sense “glassy” dirty colloidal systems differ from “model glasses”.

1.3 Gels or glasses: Various kinds of soft solids?

Eventually let me stress that since the “soft glass/concentrated colloid” analogy has developed, some confusion has invaded the community working on colloidal systems, that is often mirrored in the terminology used to describe the soft solids that these systems form when concentrated. The terms “gel”, “physical gel”, “glass”, “paste”, “jammed system” and others are often used interchangeably, with various authors obviously having different definitions of these terms in mind. There is a great need for a clearer classification (either from the point of view of underlying interactions or resulting behaviour) and for a more systematic terminology, that hopefully the years to come could provide.

Schematically, there are two extreme pictures along which colloidal systems behave when concentrated, corresponding to very different underlying interactions (see Fig. 3).

The first one is that of rigid spheres that stick to one another upon contact, with a rather strong and rigid binding (*e.g.* due to local chemical binding, or because the roughness of the surface prevents any further rotation). Such particles diffusing in solution tend to form fractal aggregates that also diffuse and aggregate, so that if the concentration is large enough, one ends with a (history dependent) network made of rigidly interconnected aggregates. The volume fraction of such a physical “gel” may be rather weak (sometimes only a few percent), with solvent filling the many voids in the aggregates structure (cite see *e.g.* [40] and references therein).

The second image is that of particles that repel through a soft potential (either rigid particles with a repulsive potential of some range or deformable particles with a short range repulsion). As concentration is increased (typically beyond roughly 50 percent), the particles are “pushed” into one another, the energy of the system increases and it is trapped in a metastable situation of disorderedly crowded particles [16, 24]. This is what many authors call a soft glass. In contrast with the previous rigidly connected “gel”, such a “glass” has a positive osmotic pressure and should swell noticeably and unlimitedly upon addition of solvent.

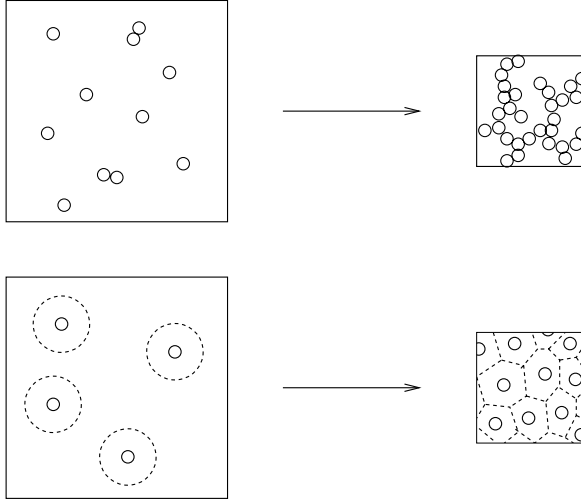


Fig. 3. Two scenarios for the formation of soft solids upon concentration. Top: sticky particles forming aggregates. Bottom: soft repelling particles under osmotic compression (the dashed lines represents the range of the repulsive potential).

Given the discussion in the previous subsection, it should be clear that there is potentially a continuum of colloidal systems that connect these two limiting cases (see for example the studies of the Weitz group in the last decade where the attraction energy is systematically varied [58], and *e.g.* [22, 44] and references therein). In most systems there are both attractions and repulsions, the intensity of which is often comparable (and of order a few k_bT). A systematic “gel or glass” distinction according to the interactions is difficult, since it is not clear that the elementary object at the scale of which such a “gel or glass” distinction should/could be made is the individual colloidal particle rather than some kind of aggregate. Eventually, the rheological properties of such systems are usually probed through dynamical schemes, so that a static picture may not be sufficient to anticipate the response: in some systems the weak aggregation of soft particles can lead to the formation of transient rigid aggregates that can resist a finite force (for a certain amount of time).

1.4 Wrapping up the introduction

To conclude, colloidal systems are very diverse. Model systems can be produced in the lab that may be used to study fundamental issues regarding the glass state and the glass transition. Most practical systems behave

when concentrated as soft and weak solids that can be forced to flow under mechanical constraint. These solids are in general *soft* as their elastic modulus is low (down to a few Pascal in some cases), and *weak* because they flow plastically under weak stresses (also a few Pascal for some systems). The behaviour of these soft-solids is however likely to be somewhat system-dependent, and a systematic classification of their behaviour in relation to their microscopic nature would be welcomed.

The remainder of these notes is devoted to experimental studies and modelisation of these soft and weak solids, with an emphasis (especially in Sect. 2) on systems with little attractions (*i.e.* away from the strong gel picture). I will from now on very non-specifically refer to those as “soft-solids”, rather than using more specific names that could bear undesired meanings (paste, gel, glass, yield stress fluid).

2 Experimental facts 1: Soft solids that flow and age

2.1 Concentrating colloidal suspensions: From a “viscous liquid” to a “soft-solid” behaviour

At low concentrations, colloidal suspensions tend to flow in a Newtonian way under weak stresses. In particular at steady-state the shear stress σ is linear in the shear rate $\dot{\gamma}$: $\sigma = \eta\dot{\gamma}$ where η is the viscosity of the suspension. Often a shear-thinning regime takes over for stronger shear as evidenced by a bending in the stress-shear rate curve. The onset of non-linearities $\dot{\gamma}_{NL}$ is often identified with $1/\tau$ the inverse of the longest relaxation time of structures in the suspension. In a related way, when probed through oscillatory rheology (see definitions in the lectures of M.E. Cates), the system behaves as a viscous liquid $G''(\omega) \gg G'(\omega)$ at frequencies well below $1/\tau$, and as an elastic solid at larger frequencies.

Increasing the volume fraction, the viscosity of the system rises and the range of linear behaviour decreases. At even higher concentrations, the steady-state flow curve looks altogether different. An often encountered situation is schematized in Figure 4: for low shear rates $\dot{\gamma}$, the stress tends to a finite value, the yield stress, often denoted σ_Y [16, 24, 43]. At higher shear rates (in the non linear domain) the behaviour is however not much different from what it looks like at weaker concentrations. It is important to note that what happens at low $\dot{\gamma}$ is not easy to ascertain experimentally. Rheometers allow reliable measurements only down to a finite value of $\dot{\gamma}$, so it is usually impossible to discriminate between a power-law fluid with a weak exponent and an actual finite limit σ_Y . A common engineer’s formula to encompass both is the Hershel-Buckley one: $\sigma \rightarrow \sigma_Y + A\dot{\gamma}^\alpha$ for $\dot{\gamma} \rightarrow 0$.

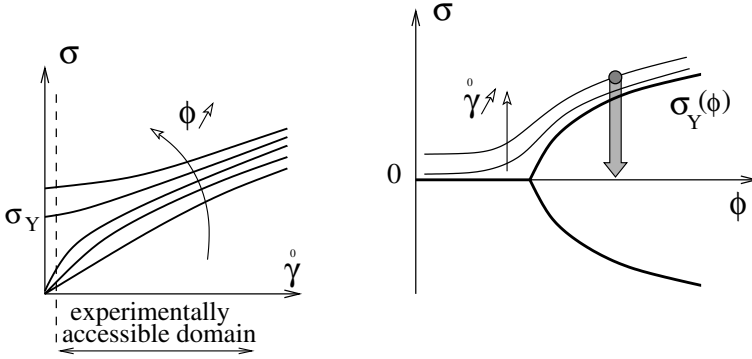


Fig. 4. Sketch of a typical steady-state flow response of a concentrated suspension. Left: steady-state flow curves $\sigma(\dot{\gamma})$ for increasing volume fractions ϕ . Right: steady-state stress as a function of volume fraction ϕ for different imposed shear rates $\dot{\gamma}$ (the thick line corresponds to the limit curve for $\dot{\gamma} \rightarrow 0$, i.e. $\sigma = \sigma_Y(\phi)$). The arrow is a schematic representation of a quench from a mechanically fluidized system into the soft-solid region.

In addition it may also be difficult to guarantee that a steady-state is indeed reached in such conditions¹.

Under oscillatory rheology the response becomes that of a *soft solid* $G' \gg G''$ even at low frequencies. Various frequency dependence of the moduli have been observed: they can both increase with the same weak power-law, stay both roughly constant, or G' can be roughly constant with G'' displaying a shallow minimum at rather low frequencies.

Obviously some kind of transition occurs upon increase of the concentration, bringing the system from a viscous liquid state to a soft-elastic one. The longest relaxation time-scale and the viscosity increase noticeably (diverge?) when the transition is approached. Conversely, effective values for the putative yield stress decrease on the solid side when the concentration is decreased. We will from now on deal only with the soft-solid states.

2.2 Probing the system in its “soft-solid” phase

In the solid phase, the system appears as frozen in some region of phase space given that a finite perturbation is required to have it flow. In most cases however, its local structure is disordered and amorphous (only very clean systems crystallize). It is thus likely that such systems lie in a metastable

¹Note that the existence of a finite yield stress σ_Y does not forbid non-steady flow for a fixed weaker stress: creeping flows with a decreasing $\dot{\gamma}(t)$ are allowed.

state that is noticeably history dependent. Consequently, to study the mechanical properties of these soft-solids, it is first necessary to define reproducible preparation procedures. In analogy with thermal quenches performed for molecular glasses or magnetic spin glasses, a natural way is to prepare the system in a reproducible fluid initial state, so as to “erase” any history dependence, and then to quench it quickly in the soft-solid phase.

Unfortunately, changing the concentration or other physico-chemical parameters homogeneously and rapidly throughout the sample is usually very difficult, and temperature is not always very relevant here (unless in the vicinity of some structural thermodynamic transition, see *e.g.* [51]). An alternative is to take advantage of the flow induced fluidization of the system to perform a mechanical quench [16, 24, 61], which is the route represented by the vertical arrow in Figure 4. A steady or oscillatory shear of strong amplitude is applied for some time to the system, with the hope that this leads to a reproducible initial state. Cessation of flow then quenches the system in the soft-solid phase, with the history of the soft-solid starting at this “initial time” that we will call $t = 0$. The validity of such a mechanical quench should of course be asserted by experimental verification of the reproducibility.

2.3 Mechanical aging

An issue which has recently received attention, fed by ideas and concepts coming from the community working on the glass transition, is that of physical aging. In the present context, we focus here on mechanical aging, *i.e.* the influence of the age t of the system since its quench on its mechanical properties. A measurement usually lasting some time, it is common to introduce the following notations for the time sequence. The quench is at $t = 0$. The system is left at rest until $t = t_w$ (the waiting time), time at which a measurement is started. If the system is not ergodic on experimental time scales, the instantaneous outcome of the measurement at time t depends on the time $t' = t - t_w$ elapsed since the onset of the measurement (as is common), but also in a systematic way on the waiting time t_w .

Recent systematic experiments on microscopically very different colloidal soft-solids have indeed shown a strong dependence of the mechanical relaxation time or time-scale τ of the system, on its “age” t_w (see *e.g.* Fig. 5). Remarkably a clean power law relation is found in many cases $\tau \sim t_w^\mu \tau_0^{1-\mu}$, with τ_0 a system dependent time. The exponent μ is called the *aging exponent* in the glass community [10, 56]. Let us cite a few examples to emphasize the great disparity of systems: such a law has been found through stress relaxation measurement (i) in a solution of PEO-protected spherical silica particles [24] with $\mu \sim 0.5\text{--}0.7$, (ii) in a dense suspensions of onions

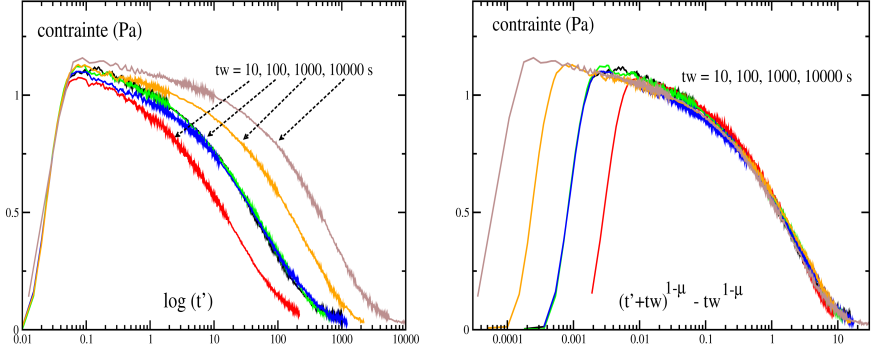


Fig. 5. Experimental stress relaxation measurements after different waiting times (linear-log plot) for a solution of PEO-protected silica particles [26]: (left) as a function of time t' elapsed since onset of the deformation, (right) as a function of the rescaled variable $(t' + t_w)^{1-\mu} - t_w^{1-\mu}$, which is roughly $\simeq t'/t_w^\mu$ at times t' shorter than t_w .

made of surfactant bilayers “doped” with copolymers [51] with $\mu \sim 0.7$ – 0.8 , and through creep measurements (iii) in dense suspensions of swollen micro-beads of polyelectrolyte gel [16] with μ close to 1. For other systems the dependence on the age of the system can be even stronger: the effective oscillatory viscosity of laponite solutions was found in [7] to increase exponentially with t_w which suggests $\tau \sim \exp(t_w/\tau_0)$ (*i.e.* $\mu \rightarrow \infty$).

This demonstrates physical aging through a systematic route in these systems: the dynamics of the system gets slower and slower as time goes on, with less stable arrangements more rapidly disappearing leaving the system in deeper and deeper metastable states. This slow drift can in principle be driven by energy stored in the system, by experimental mechanical agitation or noise, or by genuine thermal agitation. The description of the mechanisms at work in this slow evolution of the system are clearly the clue to a proper and complete understanding of the physics of aging. In the following we bypass this question for the moment and report on a recent attempt to build a simple phenomenological model able to account for the observations quoted in this section. A more explicit and sophisticated but still phenomenological set of equations, the SGR model, is presented in the lectures of M.E. Cates.

3 A class of simple models

3.1 A Maxwell model with one scalar internal variable

Essentially the aim is here to write down the simplest model that accounts for the observations reported above for the “soft-solid state”: (i) there is no obvious intrinsic rheological relaxation time, so that the instantaneous relaxation spectrum ages progressively, (ii) shear is able to fluidize the system and to bring it to a flowing steady-state with a finite instantaneous relaxation spectrum. We implement these features in a model that neglects for the moment heterogeneities.

This can be achieved through a simple adaptation of the Maxwell model, which is the simplest visco-elastic model, with a single time scale τ , corresponding to an elastic element in series with purely viscous one. The resulting equation for a scalar description of shear linking the stress σ to the applied shear rate $\dot{\gamma}$ is then: $\partial_t \sigma = -\sigma/\tau + G_0 \dot{\gamma}$, with G_0 the elastic modulus and $\eta = G_0 \tau$ the viscosity. For the soft-solids that we aim to describe there is no intrinsic time scale, but an instantaneous one that drifts towards infinity spontaneously, unless an applied shear fluidizes the system. We thus chose to take the mechanical relaxation time scale as a variable describing the instantaneous state of the system, the evolution of which is ruled by the competition of spontaneous aging and flow induced fluidization. We use equivalently $a = 1/\tau$, which we call the “fluidity” of the system. The resulting set of equations read:

$$\partial_t \sigma = -a(t)\sigma + G_0 \dot{\gamma} \quad (3.1)$$

$$\partial_t a = -f(a) + g(a, \sigma, \dot{\gamma}) \quad (3.2)$$

where f (spontaneous aging) and g (shear-induced fluidization) are positive functions. Aging requires that under the sole action of f , a tends towards 0 as time goes on. G_0 is taken constant in the simplest picture.

For long waiting times and weak shear the fluidity is expected to be small (the relaxation time is very long), so what will matter is the behaviour of functions f and g in the vicinity of $a \simeq 0$. Using rather formal expansions we write:

$$f(a)_{a \rightarrow 0+} \simeq r_1 a^\alpha + r_2 a^{\alpha+\beta} + \dots \quad (3.3)$$

$$g(a, \sigma, \dot{\gamma})_{a \rightarrow 0+} \simeq u_1 a^{n_1} \sigma^{m_1} \dot{\gamma}^{p_1} + u_2 a^{n_2} \sigma^{m_2} \dot{\gamma}^{p_2} + \dots \quad (3.4)$$

It is expected that g should be even in $(\sigma, \dot{\gamma})$, so that if g is analytic then $m_1 + p_1$ and $m_2 + p_2$ should be even. If g is not analytic, then σ and $\dot{\gamma}$ in the above equation should be replaced by their absolute values.

In our earliest attempts we proposed in an analogy with a Landau description of a transition where a would be the order parameter, to consider

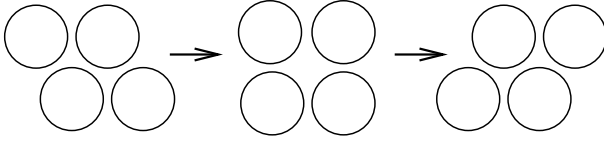


Fig. 6. Elastic deformation and rearrangement under shear of a set of particles.

that r_1 increases with concentration from a negative value in the viscous-liquid state to a positive one in the soft-solid one: $r_1 \sim (\phi - \phi_c)$. We will not pursue this any further here (see [25, 26] for related discussions) and instead focus on the properties of the soft-solid phase, taking r_1 and u_1 as positive constants.

3.2 Relation to other models in the literature

3.2.1 Bond models for gels

Given that it is the simplest approach, the use of a single scalar parameter to describe the state of the system has been pursued in many works.

For example an empirical model for particles that stick to one another describes the instantaneous state of the system by an average number of bonds per particle Λ . This number tends to increase spontaneously, but is reduced by the action of shear breaking some bonds. A set of equations proposed by Coussot *et al.* in [19] is $\partial_t \Lambda = 1/\tau - \Lambda \dot{\gamma}$, complemented with the phenomenological rheological law $\sigma/\dot{\gamma} = \eta = \eta_0(1 + \Lambda^n)$, with τ and A constants, and n an exponent.

Taking the rheological law to be roughly equivalent to the Maxwell equation (3.1) if stress relaxes faster than Λ , this model can be more or less recast into (3.1, 3.2) with $a = (G_0/\eta_0)(1 + \Lambda^n)^{-1}$. In that case, the exponents proposed in (3.3, 3.4) read: $\alpha = 1 + 1/n$, $n_1 = 1$, $m_1 = 0$, $p_1 = 1$.

3.2.2 Activated hopping

In many models for plastic flows of amorphous solids, flow is thought to occur by the elastic distortion of “elements” up to a point where they become unstable to a rearrangement of the local structure (see *e.g.* [21, 55, 57]), rearrangement that yields a reorganization of the stress field on other elements (Fig. 6).

For these plastic events to occur, an activated state must thus be reached, which is usually a conformation of higher energy and lower density (to allow the particles to pass each other). It is often chosen to describe the rates for such events as the exponential of an activation factor \mathcal{E} that is often

conceptualized as $\Delta E/T_{\text{eff}}$ with ΔE the barrier to overcome and T_{eff} the effective temperature in the system [55]. The rheological equation is then $\dot{\gamma} = \dot{\gamma}_{\text{elastic}} + \dot{\gamma}_{\text{plastic}}$, with $\dot{\gamma}_{\text{elastic}} = \partial_t \sigma / G_0$ and in a linearized version $\dot{\gamma}_{\text{plastic}} \simeq \tau_0^{-1} e^{-\mathcal{E}} (\sigma / \sigma_0)$ as in the Eyring model (τ_0 and σ_0 are constants).

This is very similar to our adaptation of the Maxwell model with $a = (\sigma_0 \tau_0)^{-1} e^{-\mathcal{E}}$. If the effective temperature of the system decreases as the system ages, or conversely if the typical barrier for rearrangement increases then this should be described by an evolution equation for \mathcal{E} . This spontaneous evolution itself is likely to occur through activated rearrangements that may or may not be identical to those probed by the shearing. This yields for the spontaneous evolution of \mathcal{E} a law of the kind $\partial_t \mathcal{E} \sim K e^{-n\mathcal{E}}$ with K a constant and n the ratio between the activation factor for these rearrangements and those corresponding to the plastic shear deformation (if those are identical, as *e.g.* in the SGR model [55] then $n = 1$). The above mentioned dynamics for \mathcal{E} corresponds to an exponent $\alpha = 1 + n$ in (3.3).

In a similar description inspired by a “free-volume” picture for activated rearrangements, where $\mathcal{E} = \Delta v / v_{\text{free}}$ and the free-volume v_{free} measures the compaction of the system and controls the statistical likelihood of an activation volume Δv , Lemaitre [39] has recently proposed a model that in its linearized isotropic version boils down to something very close to equations (3.1–3.4) (with additional logarithms) with $\alpha = 1 + n$, $n_1 = 2$, $m_1 = 2$, $p_1 = 0$.

3.2.3 A 4-state model

Eventually let me briefly mention a model that we proposed a few years ago inspired by the same physics than in the previous Section 3.2.1 [23]. In this model each element is supposed to be in one of the four following state of stress $-3, -1, +1$ and $+3$. The dynamics of the system (the evolution of the probability for an element to be in a given state of stress) is ruled by three processes: (i) a positive shear rate $\dot{\gamma}$ tends to shift the elements to states of higher stress, (ii) the states -3 and $+3$ are unstable, so that they rearrange and relax with a decay rate $1/\tau_0$ to either of -1 or $+1$, (iii) these rearrangements trigger a random re-shuffling of the stresses of other elements modeled by an effective diffusion of the stress value at a rate D proportional to the instantaneous number of rearrangements. The dynamics of this system was shown to be similar to (3.1–3.4) in the vicinity of the liquid/soft-solid transition observed, with D proportional to the fluidity a , and $\alpha = 1$, $\beta = 1$, $n_1 = 0$, $m_1 = 0$, $p_1 = 1$.

3.2.4 A concluding remark

In conclusion, the simple class of models described by equations (3.1–3.4) roughly encompass various models in the literature corresponding to specific choices for the phenomenological exponents describing the behaviour of f and g at low fluidity. We will consequently pursue without much restrictions on the latter to examine the behaviours described by these models. In particular, α need not be an integer. Let us however point out that in all the models quoted here $\alpha \geq 1$, which simply states that at long waiting times (low values of a), the instantaneous rate of decrease of a , which reads $r_1 a^{\alpha-1}$, decreases with time (in line with the picture of physical aging). We thus restrict ourselves to $\alpha \geq 1$ in the following.

We will now examine in some detail the predictions of this model, leaving a discussion of its virtues and shortcomings to Section 5.

3.3 Predictions

Let us now briefly span some of the predictions of the model for various mechanical probing. We refer the reader to [25, 26] for a more thorough presentation. In all cases the system has been quenched at $t = 0$, and the measurement starts at t_w .

3.3.1 Mechanical aging

An immediate remark is that during the spontaneous relaxation before the onset of the measurement, a decreases with time. More precisely $a(t) \sim 1/(r_1 t_w)^\mu$ for long times with an aging exponent:

$$\mu = 1/(\alpha - 1). \quad (3.5)$$

This holds for $\alpha > 1$, with for the marginal case $\alpha = 1$, $a(t) \sim \exp(-r_1 t_w)$.

We show below that μ indeed coincides with the definition given in 2.3: the characteristic mechanical time scale of the system τ is the inverse of the fluidity at the onset of this measurement, and $\tau \simeq \tau_0^{1-\mu} t_w^\mu$ (with the microscopic time $\tau_0 = r_1^{-\frac{\mu}{1-\mu}}$).

An important distinction can be obtained by inspection of equations (3.1) to (3.4): if $\alpha > 2$ then a relaxes much slower than the stress σ , whereas if $\alpha < 2$, a relaxes to zero faster which freezes the dynamics and prevents σ to relax down to 0. This distinction matches here the classical one between subaging ($\mu < 1$) and superaging ($\mu > 1$). “Full aging” ($\mu = 1$) here corresponds to the limit case $\alpha = 2$, where the same processes rule the relaxation of a and σ .

Let us now assert these points by examining the linear response to a stress-relaxation measurement performed at t_w : at t_w a weak deformation

of amplitude γ_0 is applied to the system and then maintained fixed. This creates an almost instantaneous stress $\sigma = G_0\gamma_0$ that subsequently relaxes as $\sigma(t) = G(t', t_w)\gamma_0$, where $G(t', t_w)$ is the time-dependent modulus that for an aging system depends on both the age of the system at onset of the deformation t_w and of the time elapsed since onset $t' = t - t_w$.

- For $\alpha > 2$ (*i.e.* sub-aging $\mu < 1$),

$$G(t', t_w) = G_0 \exp \left[-\frac{(t' + t_w)^{1-\mu} - t_w^{1-\mu}}{(1-\mu)\tau_0^{1-\mu}} \right]. \quad (3.6)$$

This kind of scaling variable appears in the description of mean field models for glassy phases in spin-glass systems [10]. For times shorter than the system's age $t' \ll t_w$, $G(t', t_w) \sim \exp[-t'/\tau]$, a simple exponential relaxation with a characteristic time $\tau = \tau_0^{1-\mu} t_w^\mu$. For much longer times $t' \gg t_w$, $G(t', t_w) \sim \exp[-t'^{1-\mu}/((1-\mu)\tau_0^{1-\mu})]$, the stress decreases to 0 as a stretched exponential² with a stretching exponent $1-\mu$ smaller than 1.

- For $\alpha < 2$ (*i.e.* super-aging $\mu > 1$),

$$G(t', t_w) = G_0 \exp \left[-\frac{\frac{1}{t_w^{\mu-1}} - \frac{1}{(t' + t_w)^{\mu-1}}}{(\mu-1)\tau_0^{1-\mu}} \right]. \quad (3.7)$$

At short times $t' \ll t_w$ we have again $G(t', t_w) \sim \exp[-t'/(\tau_0^{1-\mu} t_w^\mu)]$, whereas at longer times $t' \gg t_w$, relaxation proceeds as $G(t', t_w) \rightarrow G_\infty(t_w) = G_0 \exp(-(\tau_0/t_w)^{1-\mu})$, *i.e.* there remains a non-zero residual stress $\sigma_\infty = G_\infty(t_w)\gamma_0$ that increases with t_w .

- For $\alpha = 2$ (full aging $\mu = 1$), The stress decays algebraically:

$$G(t', t_w) \simeq G_0 \left(\frac{t_w}{t' + t_w} \right)^{1/r_1}. \quad (3.8)$$

3.3.2 Non-linear “steady-state” rheology

We now address the most common rheological characterization, namely the steady-state flow curve $\sigma(\dot{\gamma})$. With the equations at hand, such a steady-state is always reached if a fixed $\dot{\gamma}$ is applied, with the history of the system

²Note that the stretched exponential here stems from the non-linear equation, in contrast to the classical picture for glassy systems of a convolution of single exponential processes with a distribution of time scales.

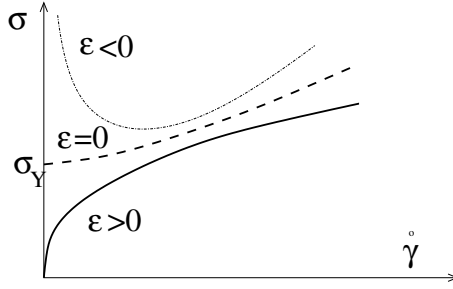


Fig. 7. Steady-state rheology as a function of the exponent $\epsilon = \alpha - n_1 - p_1$. The case $\epsilon < 0$ is unphysical (see text).

erased (aging suppressed). Using (3.1), the fluidity a in this steady state is set by $f(a) = g(a, G_0 \dot{\gamma}/a, \dot{\gamma})$. For low values of $\dot{\gamma}$, the fluidity remains weak so that using the formal expansions (3.3, 3.4), one finds from the competition of spontaneous aging and flow-induced rejuvenation $a \sim \dot{\gamma}^{\frac{\nu-\epsilon}{\nu}}$, which leads to a power law steady-state relation $\sigma(\dot{\gamma} \rightarrow 0) \sim \dot{\gamma}^{\frac{\epsilon}{\nu}}$, where $\nu = \alpha - n_1 + m_1$ and $\epsilon = \alpha - n_1 - p_1$. Note that $\nu - \epsilon = m_1 + p_1$ is likely to be a positive number if shear is to enhance fluidity in (2-4).

So the low shear steady-state behaviour leads us to the following distinction according to $\epsilon = \alpha - n_1 - p_1$ (see Fig. 7):

- for $\epsilon > 0$, at low shear rates the fluid behaves as a power law fluid $\sigma(\dot{\gamma} \rightarrow 0) \sim \dot{\gamma}^{\frac{\epsilon}{\nu}}$ (full line in Fig. 7);
- for $\epsilon = 0$, stress tends to a finite value $\sigma_y = G_0^{\frac{p_1}{\nu}} (r_1/u_1)^{\frac{1}{\nu}}$ (dashed line in Fig. 7);
- $\epsilon < 0$ corresponds to a stress diverging as $\dot{\gamma}$ goes to zero which is unphysical for the local flow rule of a realistic system, which has clearly finite stress limits for yield to occur.

For larger values of the shear, the next terms in the expansion of both f and g start to play a role, modifying the effective stress-strain rate behaviour (see *e.g.* [25]). This can lead to some subtleties for the case $\epsilon = 0$ as we will see later.

3.3.3 More complex topics: Oscillating rheology and transients

This subsection deals with more intricate points that the reader may want to skip in a first reading, if only to secure that it does not become the last reading too...

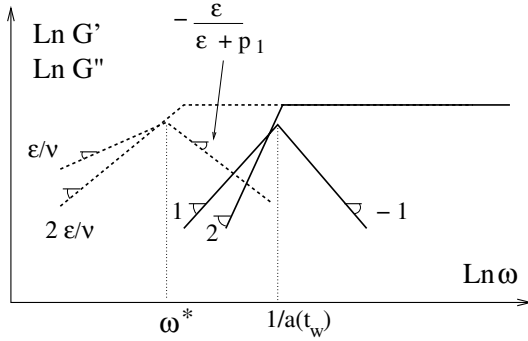


Fig. 8. Oscillatory rheology: $\gamma = \gamma_0 \cos(\omega t)$. Left (dashed lines): effective moduli in the asymptotic long-time regime (non-linear). Right (full lines): linear response at short times ($t - t_w \ll t_w$). As time goes on, the measured moduli drift from the latter to the former. $\omega^* \sim \gamma_0^{\nu/(\nu-\epsilon)}$ depends on the measurement amplitude.

“Steady state” oscillatory rheology. An oscillatory measurement is performed on the pasty phase, *e.g.* a deformation $\gamma = \gamma_0 \cos(\omega t + \psi)$ is applied from t_w on. No matter how small γ_0 , at long times it is this shear that will control the oscillating value of the fluidity through equation (3.2) (this is for example in contrast with the SGR model where the effective temperature is fixed to a finite value, which guarantees an intrinsic linear domain). As a consequence the long-time response is intrinsically non-linear with many harmonics in the stress response.

Although there are consequently no linear moduli $G'(\omega)$ and $G''(\omega)$, we can still discuss the outcome of a rheometer measuring the in-phase and out-of-phase first harmonic of the stress divided by γ_0 , and call these numbers $G'_\infty(\omega, \gamma_0)$ and $G''_\infty(\omega, \gamma_0)$ by extension (the ∞ subscript is to emphasize that these are asymptotic long-time values). A qualitative analysis developed in [25, 26] shows that one expect a frequency dependence reminiscent of the Maxwell model in gross features but with different slopes for $\epsilon > 0$ (see dashed lines in Fig. 8). The cross-over frequency ω^* in this non-linear situation is amplitude dependent and weak if γ_0 is small. Therefore experimental observations may well be restricted to the $\omega > \omega^*$ domain³.

Transients and thresholds for non-linear behaviour. The results mentioned above, both for steady and oscillatory rheology, correspond to the long-time behaviour in measurement processes by which energy is constantly fed into the system (in contrast to stress relaxation measurement – see 3.3.1 –, where a finite perturbation is made on a system of initially non-zero fluidity).

³The case $\epsilon = 0$ yields non-linear constants $G'_\infty(\omega, \gamma_0) = G_0$ and $G''_\infty(\omega, \gamma_0) \sim G_0 \gamma_0^{\frac{\nu}{p_1-1}}$.

However, when the measurement (applied constant shear rate or oscillatory shear) starts at t_w the system initially responds as a Maxwell fluid of characteristic time $1/a(t_w) \sim t_w^\mu$. There is thus in the two experiments a cross-over in time from the linear response at short times to the non-linear “steady” response at long times. The duration of the linear response decreases if the amplitude $\dot{\gamma}$ or γ_0 increases, but also if the waiting time t_w increases [25].

Following the response in time, one thus anticipates in the steady shear experiment an instantaneous viscosity that decreases from $\eta(t_w) \sim 1/a(t_w)$ to its asymptotic value $\eta_\infty \sim \dot{\gamma}^{\frac{\epsilon-\nu}{\nu}}$ for very weak applied shear rate $\dot{\gamma}^4$.

Similarly, if one follows the first harmonic of the stress in an oscillatory experiment, one expects that the hump in G'' slides progressively to lower frequencies before saturating at ω^* with the slopes of the moduli becoming progressively weaker (Fig. 8).

3.4 Intermediary conclusion

The class of models described by the simple equations (3.1–3.4) generates a rich physics not dissimilar to experimental observations quoted in Section 2. For systems under weak shear, the response is dictated by the behaviour for small fluidities of the functions f and g describing spontaneous aging and flow induced rejuvenation in (3.2). If these behaviour are power-law like ($f \simeq r_1 a^\alpha$, $g \simeq u_1 a^{\alpha-\epsilon} \sigma^{\nu-\epsilon} (\dot{\gamma}/a\sigma)^{p_1}$), then (i) physical aging is characterized by the exponent $\mu = (\alpha - 1)^{-1}$ (see 3.3.1) and (ii) the low shear steady-state rheology is that of a power-law fluid for $\epsilon > 0$ and of a yield stress fluid for the smallest acceptable value $\epsilon = 0$. We will see later that this last case deserves more careful attention.

4 Experimental facts 2: Soft solids that flow in a strange way

4.1 Avalanches and “viscosity bifurcation”

The rheological behaviour of colloidal soft-solids is sometimes less smooth than suggested by the flow curves discussed in the previous section. A spectacular manifestation is that of surface avalanches as reported in a recent letter [19]: a plane covered by a layer of soft-solid is progressively inclined with respect to horizontal. For a power-law fluid (*e.g.* flow curve akin to the lower curve in Fig. 7) one expects a progressively increasing downhill

⁴If the measurement is so strong that it “immediately” leads the system into non-linearity, other features can be observed such as a peak (overshoot) in the stress response to a fixed applied $\dot{\gamma}$. The value of this peak drifts with the age of the sample, providing a simple way to assess physical aging in the system (see [26] for a related discussion).

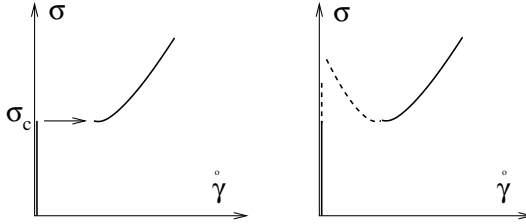


Fig. 9. Scheme for the observed viscosity bifurcation.

sliding as the slope is increased. For a yield-stress fluid (*e.g.* steady flow curve as the middle one in Fig. 7), one expects no flow before the tangential component of the stress reaches the yield stress value σ_Y , and a progressive flow thereafter. What is in contrast sometimes observed, for a wide variety of soft solids of very different chemical nature, is the sudden onset of an “avalanche” for a stress σ_c , with some material spontaneously accelerating [19].

In more conventional rheometry, a related experiment is as follows [19]: for a given reproducible preparation scheme, apply at time t_w a fixed stress σ and subsequently measure the instantaneous flow rate $\dot{\gamma}(t)$ or equivalently an instantaneous viscosity $\eta(t) = \dot{\gamma}(t)/\sigma$. The observation, again for many complex systems of different microscopic nature, is that for σ smaller than a value σ_c , the viscosity $\eta(t)$ tends to infinity with time (in the model terms the fluidity tends to 0, the system freezes), whereas for σ larger than σ_c , the viscosity tends at long times to a finite value. The long time viscosity $\eta(t \rightarrow \infty)$ actually jumps from ∞ to a finite value at σ_c , hence the term “viscosity bifurcation” coined for this jump.

Such a phenomenon suggests a jump between two branches in the steady-state flow diagram (Fig. 9 left), which in a simple picture can be the outcome of an underlying flow curve with a decreasing branch (Fig. 9 right).

4.2 Parallel with flow induced transitions: Heterogeneous “banded” flows

In many complex fluids, non monotonic local flow curves are taken to be often responsible for transitions between a high viscosity branch and a low viscosity one. Such a decreasing branch is notoriously unstable when inertial effects are taken into account. As a result the system can separate into domains (bands) of material corresponding to each of the stable branches. Many studies have recently explored these flow induced transitions and started to shine some light on these complex far from thermal equilibrium problems [2, 11, 28, 29, 45, 46, 49, 50]. The resulting macroscopic flow behaviour, relating the macroscopic stress Σ to the macroscopic or effective

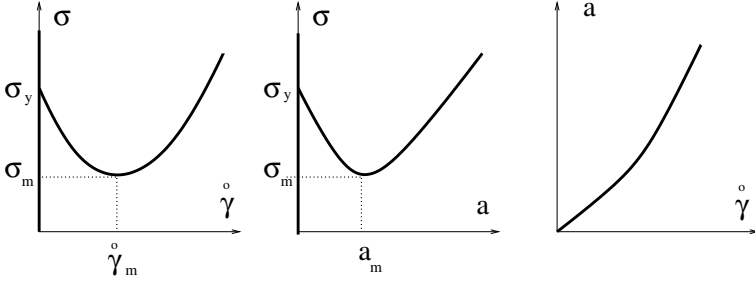


Fig. 10. Steady-state solutions of equations (3.1, 3.2) for $\epsilon = 0$ and a non-monotonic $\sigma(\dot{\gamma})$.

shear rate $\dot{\gamma}$, can be rather complex, with selection rules in the banded regime very sensitive to gradient terms in the equation that decide of the stability of the interfaces between bands [42].

Direct observation of banding in the slow flows of some soft-solids have been reported [17, 20, 21, 48] and also shows up in some numerical simulations [21, 60]. In both experiments and numerical work, boundaries where sometimes shown to affect the banding phenomena. One in principle expects all the complexity revealed by former studies on “flowing” complex fluids to be potentially present here, with in addition the specificities linked to having one of the “phases” being a non-ergodic aging soft-solid.

4.3 Description within the simple class of models

Given this potential complexity it is tempting to investigate such behaviour within our simple model by considering situations where the competition between aging and flow induced fluidization results in a local flow curve similar to Figure 9b. A necessary condition within our model is that $\epsilon = 0$. For example if $n_2 + p_2 > \alpha + \beta$ and if r_2 and u_2 are positive, then $\sigma_{\dot{\gamma} \rightarrow 0^+} \simeq \sigma_y [1 - (..) \dot{\gamma}^{n_2+p_2-\alpha}]$. In such a case, both the $\sigma(a)$ and $\sigma(\dot{\gamma})$ plots present a decreasing section down to a value σ_m , before increasing monotonically again (Fig. 10).

4.3.1 Adapting the model

We have investigated the behaviour of the system in this situation for the simplest geometry where heterogeneity is allowed only in the direction of the velocity gradient (gradient banding): the fields σ , a and $\dot{\gamma}$ vary along a single direction z normal to the two boundaries in relative motion. We then add a diffusion like term for the equation describing the evolution of the local fluidity. I will not enter here the detailed description of the model

(the reader is referred to [47]) but rather focus on a few remarks before presenting the resulting macroscopic behaviour under steady driving, either at fixed stress Σ or at fixed strain rate $\dot{\Gamma}$.

- There is now an absolute need for boundary conditions on the walls, not only for the fluid velocity but also for the internal variables, here the fluidity a . How the wall affects the density, degree of order and mobility of a colloidal fluid in their neighborhood is a difficult question, that will be shown to have important consequences on the overall macroscopic behaviour.
- The choice of a diffusion term in the equation for the evolution of a is debatable, and used here as a simple choice involving gradients. Obviously the corresponding diffusion coefficient D may itself depend on a . As a result the thickness ℓ of the interface between frozen ($a \sim 0$) and fluidized regions (a finite) in a banded flow, is fixed on the frozen side by the competition between $f(a) \sim -r_1 a^\alpha$ and the diffusion term scaling as $D(a)a/\ell^2$, which yields $\ell \sim (D(a)a^{1-\alpha})^{1/2}$ indicating an algebraic decay unless D scales as $a^{\alpha-1}$. Thus in contrast with flow induced transitions between two branches of finite viscosity, the interfaces between bands need not have a finite thickness, and the bands can interact through algebraic effective potentials.

4.3.2 Fixed stress Σ

In the case where the macroscopic stress Σ is maintained at a fixed value, within our model the dynamics of the field $a(z)$ is such that the system evolves toward the local minimum of a Σ dependent functional (very similar to a free-energy in a field theory for wetting).

Essentially there are two effective branches: a frozen branch corresponding to a frozen bulk $a \sim 0$ with layers of finite fluidity close to the wall induced by the boundary conditions, and a fluidized branch with the bulk at a value of a corresponding to the stress Σ on the up-rising part of the local flow curve (Fig. 11a) with layers of possibly weaker fluidity close to the walls. It is important to point out that σ_i and σ_d in Figure 11a depend sensitively on the boundary conditions for a on the wall, as the walls can act as nucleation centers for either of the frozen and fluidized “phases”⁵.

For stress values Σ lower than σ_d only the frozen branch is stable, whereas for values larger than σ_i only the fluidized branch is. For intermediate values of the stress $\sigma_d < \Sigma < \sigma_i$, both branches are possible solutions at long times. *Which branch is selected depends then on the initial*

⁵A finite amount of noise in the dynamics can also trigger this nucleation in the bulk which would result in the narrowing of the hysteresis loop around a value σ^* .

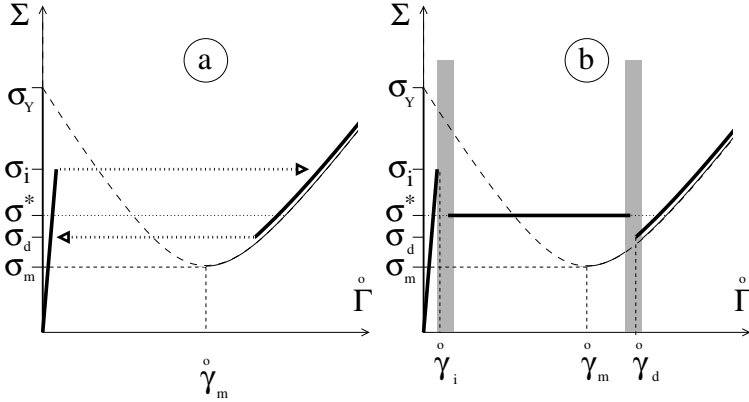


Fig. 11. Flow behaviour (full lines) under steady driving: **a)** at fixed stress Σ , **b)** at fixed average shear rate $\dot{\Gamma}$. The thin lines are the local steady-state solutions of (3.1, 3.2) depicted in Figure 10. Oscillating stress response can be observed in the grey areas.

conditions. For a given preparation scheme of the system, and test under increasingly large applied fixed stresses, one thus anticipate a sudden jump from the frozen to the fluid branch at a given value Σ_c that depends on the preparation scheme (with $\sigma_d < \Sigma_c < \sigma_i$). This is in agreement with the experimental picture for the “viscosity bifurcation” (Sect. 4.1), and further suggests that this value increases with the age of the system, the transition occurring later for a weaker initial fluidity.

If the stress is ramped up and down slowly a hysteresis loop is described as indicated by the arrows in Figure 11a. In an avalanche experiment as reported in 4.1 [19], σ_i would thus play the role of the critical stress σ_c . Other rheological experiments could conclude that the system has an effective yield stress anywhere between σ_d and σ_i .

4.3.3 Fixed shear rate $\dot{\Gamma}$

The case of an imposed macroscopic constant shear rate $\dot{\Gamma}$ (*i.e.* the two bounding plates moved at a constant relative velocity), is much more complex as both the field $a(z, t)$ and $\Sigma(t)$ evolve in a coupled way.

The resulting macroscopic picture is represented in Figure 11b. Basically the two branches described in the previous subsection are still present, but for intermediate shear rates, the system can now stabilize in a banded state at a stress very close to σ^* . In these banded situations the system is essentially divided into a fraction of the system at a fluidity close to 0 and

a fraction at a fluidity close to $a(\sigma^*)$, the proportion between the two being set by the value of $\tilde{\Gamma}$ ⁶.

Actually the physics is sometimes even richer. For some parameters, usually close to the frozen branch – plateau region (left shaded area in Fig. 11b), an oscillating situation is reached for both $a(z, t)$ and Σ : there is thus no steady-state! Looking at the structure of $a(z, t)$, these oscillations correspond to a *localized* oscillation of a in a narrow region, often but not always close to a wall, that alternatively freezes, so that the stress increases beyond σ_Y then fluidizes which induces a release of the stress that drops below σ_m which induces in turn the re-freezing. This localized oscillating fracture, results in a macroscopic stick-slip behaviour.

The overall behaviour is very similar to that observed by Pignon *et al.* [48] on a laponite suspension (an oscillating fracture was observed by direct imaging), and by Varnik *et al.* in their simulations [60]. It should however be noted that in the situation where macroscopic bands are present these works show some evidence of a value of $\dot{\gamma}$ in the flowing band that changes with $\tilde{\Gamma}$ (and thus the size of this flowing region), in contrast to the predictions of the present simple model.

4.3.4 Transients

Of course there are in principle lots of thing that can be analyzed beyond the long-time response to an applied constant stress or shear-rate. Of particular interest could be the analysis of the mechanical aging of a system prepared in a heterogeneous banded state⁷.

4.4 Intermediary conclusion

From experimental observations emerges the picture that for some colloidal soft solids, the structure of slow flows can be complex, both temporally and spatially. To apprehend this complexity various experimental schemes, possibly going beyond the measurement of purely mechanical responses may be necessary. Eventually, experimental, analytic and numerical works emphasize the role of the boundaries, always present in a mechanical measurement.

⁶In the absence of noise, there may be various banding patterns that constitute attainable steady states, corresponding to only imperceptibly different macroscopic stresses. In this banding domain, the transient that lead to one of this or these steady-state solutions essentially consists of two stages. First the fluidity evolves to form domains or bands of frozen ($a \sim 0$) and fluid ($a \sim a(\sigma^*)$) material, then in a second much slower stage these bands coarsen until a steady-state is reached.

⁷For a mechanical quench to study mechanical aging (see 2.2), one should clearly shear the system strongly so that it lies fully on the fluidized branch.

5 Criticism of the model and perspectives

We end with a brief description of the interests and shortcomings of the models described by equations (3.1) and (3.2), before presenting a few comments as to some perspectives.

5.1 A classification of the phenomenologies

We have built a very simple class of models, where the main ingredients of the physics at work is hidden in the functions f and g . Analyzing these models a classification has naturally emerged related to the behaviour of these functions at low fluidity.

- A choice for f determines the value of α and thus of $\mu = (\alpha - 1)^{-1}$.
 - If $\alpha > 2$ the system undergoes spontaneously sub-aging ($\mu < 1$), with the corresponding rescaling of the stress relaxation modulus, in qualitative accordance with some experiments [24, 51].
 - On the contrary $\alpha < 2$ imposes super-aging $\mu > 1$, and stresses that freeze without relaxing to 0. The limit case $\alpha = 1$ corresponds to an exponential temporal increase of the mechanical relaxation time, as observed in [7].
 - The marginal full-aging case $\alpha = 2, \mu = 1$ is consistent with other observations [16, 62].
- The combined choice of f and g sets the value of ϵ ⁸.
 - If $\epsilon > 0$, the steady-state flow curve is that of a “gentle” power-law fluid, that flows homogeneously, and can be confused with a yield-stress fluid only due to experimental difficulties to access the weak $\dot{\gamma}$ domain.
 - If $\epsilon = 0$, the system has a true yield stress, and a Herschel-Buckley behaviour $\sigma(\dot{\gamma} \rightarrow 0) \simeq \sigma_Y + A\dot{\gamma}^n$. If $A \geq 0$ the system again is expected to flow homogeneously, at a steady rate $\dot{\gamma}$ if the stress is larger than σ_Y . However, A can be negative, in which case there is an initial decreasing branch in the flow curve, yielding the viscosity bifurcation, gradient banding and sometimes oscillating phenomenologies described in Section 4⁹.

⁸Once again, a realistic model according to (3.1–3.4) forbids $\epsilon < 0$, as this would mean resistance of the frozen state ($a = 0, \dot{\gamma} = 0$) to an infinite amount of stress.

⁹There is then another important characteristic state ($a_m, \dot{\gamma}_m, \sigma_m$) (see Fig. 10) that may or not be in the range of small fluidities that allow the expansions of (3.3, 3.4).

The classifications according to the signs of $\alpha - 2$ and ϵ are *a priori* not directly related to one another which allows in principle for the existence of various kind of soft-solids from a phenomenological point of view. In both the scalar model of Section 3.2.1 and in the activated model of Lemaitre (3.2.2), the exponents α and ϵ are related by $\alpha - 2 = \epsilon$, so that the two classifications above boil down to a single one. In the 4-state model presented in 3.2.3, $\alpha = 1$ and $\epsilon = 0$ corresponding to a super-aging yield-stress fluid. The SGR model [55], which cannot be mapped onto the simple equations (3.1, 3.2), yields a phenomenology corresponding to full aging ($\alpha = 2$) and a finite yield stress ($\epsilon = 0$).

This diversity of possible behaviour seems indeed to show up in the spectrum of “soft solids”. Very crudely what people often name “gels” typically fall in the super-aging ($\alpha < 2$) and yield-stress behaviour ($\epsilon = 0$) category, whereas “glasses” often display sub-aging or aging behaviour, with a rheology often difficult to discriminate between a power-law behaviour with a weak exponent or a true yield stress-behaviour. I recall however (see Sect. 1) that there is no clear definition of these terms, and that tuning of some parameters (ionic strength, temperature, etc.) can lead continuously from one category to the other.

5.2 Successes and failures of these models

An potential interest of the models encompassed by equations (3.1, 3.2) is their analytical simplicity which could allow to use them to follow or anticipate complex rheological histories.

A more thorough attempt to confront experimental data with a specific set of exponents in equations (3.3, 3.4) was performed for suspensions of protected silica particles [26], with the following set of successes and failures:

Successes: the equations naturally describe mechanical aging with a rescaling variable $S(t', t_w) = \frac{(t' + t_w)^{1-\mu} - t_w^{1-\mu}}{(1-\mu)\tau_0^{1-\mu}}$ naturally showing up in equation (3.6), that is well suited to account for the rescaling of relaxation experiments performed at different waiting times on rather diverse systems [16, 24, 51]. Also many non-linear features of steady and oscillatory rheology are reasonably captured with rather simple forms for f and g . A nice point is that the model also apprehends semi-quantitatively correctly features of transient regimes [26], and as such can be of help to anticipate/interpret experiments.

Failures: the use of a single (although evolving) time scale leads to inadequate scaling functions for the mechanical response. For example equation the modulus in (3.6) is a single exponential of the rescaling variable, whereas experiments in [24, 51] suggest a stretched exponential (in $S(t', t_w)$) (see *e.g.* Fig. 5). In addition, in many systems [9, 26] the value of the elastic plateau,

which is a constant G_0 in the model, actually increases slowly with time as $\log(t_w)$. This usually mild feature can in principle be accounted for by a natural modification of the system of equations if one thinks in terms of activation barriers ($G_0 = G_0(\mathcal{E})$ with \mathcal{E} increasing as $\log(t_w)$ in the description of 3.2.2, see also [62]), but at the cost of an increased complexity. Eventually the description of the vicinity of the fluid/soft-solid transition using only r_1 as a control parameter was shown to be unsatisfactory again because it neglects the variations of G_0 with concentration.

So altogether, the main merit of these models is indeed that their simplicity and tractability permits simple estimates for the outcome of an experiment. They also allow one to make qualitative comments on the influence of heterogeneities in banding flow, in a domain where more accurate/complete models may be practically unusable.

A clear drawback at this stage is the total absence of connection of the phenomenological equations and exponents with microscopic mechanisms of some generality, or with coarse-grained versions of the latter. It is at this level that a possible relation between the microscopic interactions and the macroscopic rheological behaviour is to be made.

In the following we comment briefly on direction for possible extensions of these models, very likely at the cost of simplicity.

5.3 Better models: More variables? which collective physics?

Taking the equations (3.1, 3.2) as a starting point, extensions of the number and type of variables are suggested by experimental observations and theoretical considerations:

- the observation of stretched exponentials response functions [24, 51] (in the rescaled variables) suggests the existence of a spectrum of relaxation time rather than a single one. For homogeneous systems this suggests the use of instantaneous distributions or probability distributions for either the local deformation (as *e.g.* in the SGR) or the local stress (as *e.g.* in [21, 23, 36]), rather than the local averages σ and $\dot{\gamma}$ in the models quoted here;
- recent experimental observations have shown that an applied moderate shear can in some special conditions lead to an actual increase of the apparent mechanical age of the system [61, 62]. To account for such a flow induced “overaging” it is tempting to evoke a set of processes operating in parallel, in line with the previous point;
- in the observations of Cloitre *et al.* [16], a logarithmic recovery of the strain is observed when stress is cut down to 0. Such an evolution is forbidden in the Maxwell model which implicitly takes $\dot{\gamma}(t)$ as the

driving and $\sigma(t)$ as the response. A way out if one insists on avoiding using whole distributions is to introduce at least a single “tensorial” variable in addition to the stress, which keeps the memory of the direction of past flow (a task which the “scalar” fluidity a is unable to perform). I point out that in related models for the plastic flow of amorphous solids, recent developments by Langer *et al.* actually suggest the use of such local variables to describe the instantaneous state of the system (“shear-transformation-zones” models [30, 31, 38, 39]). Of course models involving local distributions of stresses or strains will naturally bear such “tensorial” memory;

- to take into account the banding observed in some cases and the corresponding localization of the deformation, it is necessary to extend whatever is the set of local variables to spatially and temporally dependent fields. Of course this can be performed in the simple fluidity model presented here [47], but should in principle be done for models involving local distributions;
- an eventual point in this list is that the description we have made up to now has neglected the intrinsically tensorial nature of both stress, deformation, and structure or texture factors. There are instances where normal stresses have been shown to play a role in the selection of heterogeneous patterns [54], and situations where the convection of fluctuations or structures by the flow is important require a proper tensorial description (see *e.g.* the recent mode-coupling description of [32]).

As a relevant aside, let me emphasize that the respective role of stress and strain (or strain rate) in constitutive mechanical models is far from clear. Most models actually take one or the other as the driving field, the remaining one acting as a state variable. In an experiment, what is actually imposed is in general boundary conditions on one or the other, with the propagation of these tensorial fields in the bulk ruled by mechanical equilibrium and conservation laws, in addition to the constitutive rule chosen.

At the end of this list one expects thus that a general model should consist in a set of coupled non-linear differential equations (or possibly worse integro-differential), describing a large number of spatially and temporally varying fields, with consequently very diverse possible outcomes even under steady driving [13, 34, 35]. Such models could remain rather phenomenological (as *e.g.* the SGR model) or try to make tighter connections with structural information on the colloidal system (as *e.g.* in models inspired by mode-coupling theories [32]). At a very local scale, one expects very dramatic non-linear events, the “rearrangements”, to be the building elements of a more collective macroscopic response.

It is also possible that for some problems involving heterogeneous flows, it could be physically more meaningful to describe the evolution by focusing on a dynamical description of the interfaces between the “dynamical phases” in contact, rather than carrying a complete description of the fields everywhere in the bulk [1, 12, 33, 45].

5.4 Back to facts

Given the complexity alluded to above in the construction of models, it seems that the most important thing to do now is, guided by concepts and simple models that have emerged in the last years, to build first sets of experimental data on well controlled systems, where one has grasp on the synthesis of the system and experimental means of investigation of their structure under flow beyond the simple mechanical response (see *e.g.* the review [15]). A similar statement holds for numerical simulations [21, 57, 60]. From the discussion above, one should obviously not necessarily expect too much universality but rather try to infer classes of behaviour from the analysis of such sets of data.

I am very grateful to D. Bartolo, L. Bocquet, G. Picard and V. Viasnoff for their critical comments on earlier versions of these notes.

References

- [1] A. Ajdari, *Phys. Rev. E* **58** (1998) 6294.
- [2] J.F. Berret, G. Porte and J.P. Decruppe, *Phys. Rev. E* **55** (1997) 1668.
- [3] L. Berthier, J.L. Barrat and J. Kurchan, *Phys. Rev. E* **61** (2000) 5464-5472.
- [4] L. Bocquet, W. Losert, D. Schalk, T.C. Lubensky and J. Gollub, *Phys. Rev. E* **65**, 011307 (2002).
- [5] D. Bonn, *et al.*, *Europhys. Lett.* **45** (1999) 52.
- [6] D. Bonn, *et al.*, *Langmuir* **15** (1999) 7534.
- [7] D. Bonn, *et al.*, *Phys. Rev. Lett.* **89** (2002) 015701.
- [8] R. Borrega, *et al.*, *Europhys. Lett.* **47** (1999) 729.
- [9] R. Borrega, Thèse de l’Université Paris 6 (2000).
- [10] J.P. Bouchaud, L.F. Cugliandolo, M. Mézard and J. Kurchan, in *Spin Glasses and Random Fields*, edited by A.P. Young (World Scientific, Singapore, 1997); and references therein.
- [11] M.M. Britton and P.T. Callaghan, *J. Rheol.* **41** (1997) 1365.
- [12] S. Butler and P. Harrowell, *Nature* **415** (2002) 1008.
- [13] M.E. Cates, *et al.*, *Phys. Rev. E*, **66** (2002) 025202(R).
- [14] L.B. Chen, B.J. Ackerson and C.F. Zukoski, *J. Rheol.* **38** (1994) 193.
- [15] L. Cipelletti and L. Ramos, *Current Opinion Colloid Interf. Sci.* **7** (2002) 228-234.
- [16] M. Cloitre *et al.*, *Phys. Rev. Lett.* **85** (2000) 4819.
- [17] M. Cloitre and R. Borrega, Preprint (2001).

- [18] P. Coussot, *et al.*, *J. Non-Newt. Fluid Mech.* **46** (1993) 179.
- [19] P. Coussot, *et al.*, *Phys. Rev. Lett.* **88** (2002) 175501.
- [20] P. Coussot, *et al.*, *Phys. Rev. Lett.* **88** (2002) 218301.
- [21] G. Debrégeas, H. Tabuteau and J.-M. di Meglio, *Phys. Rev. Lett.* **87** (2001) 178305 and G. Debregeas, Private Communication (2002).
- [22] E. Del Gado, L. De Arcangelis and A. Coniglio, Preprint (2002) [con-mat/0209478].
- [23] C. Derec, A. Ajdari and F. Lequeux, *Faraday Disc.* **112** (1999) 195.
- [24] C. Derec, A. Ajdari, G. Ducouret and F. Lequeux, *C. R. Acad. Sci. Paris* **1** (2000) 1115.
- [25] C. Derec, A. Ajdari and F. Lequeux, *EJPE* **4** (2001) 355.
- [26] C. Derec, Thèse de l'Université Paris 6 (2001).
- [27] O. Diat and D. Roux, *J. Phys. II France* **3** (1993) 1427.
- [28] O. Diat, D. Roux and F. Nallet, *Phys. Rev. E* **51** (1995) 3296.
- [29] J.K.G. Dhont, *Phys. Rev. E* **60** (1999) 4534.
- [30] L.O. Eastgate, *et al.*, *Phys. Rev. Lett.* **90** (2003) 045506.
- [31] M. Falk and J. Langer, *Phys. Rev. E* **57** (1998) 7192.
- [32] M. Fuchs and M.E. Cates, Preprints (2002) [cond-mat/0210194] and [cond-mat/0207530].
- [33] J.L. Goveas and D. Pine, *Europhys. Lett.* **48** (1999) 706.
- [34] A. Groisman, *et al.*, *Europhys. Lett.* **43** (1998) 165.
- [35] M. Grosso, *et al.*, *Phys. Rev. Lett.* **86** (2001) 3184.
- [36] P. Hébraud and F. Lequeux, *Phys. Rev. Lett.* **81** (1998) 2934-2937.
- [37] J.N. Israelachvili, *Intermolecular and surface forces* (Academic Press, London, 1985).
- [38] J. Langer, *Phys. Rev. E* **64** (2001) 011504.
- [39] A. Lemaitre (2002) Preprint [Condmat 0206417].
- [40] J. Lewis, *J. Am. Ceram. Soc.* **83** (2000) 2341-2359.
- [41] A. Liu and S. Nagel, *Nature* **396** (1998) 21-22.
- [42] C.Y. Lu, P.D. Olmsted and R.C. Ball, *Phys. Rev. Lett.* **84** (2000) 642 and references therein.
- [43] T.G. Mason, J. Bibette and D.A. Weitz, *J. Colloid Interf. Sci.* **179** (1996) 439.
- [44] A. Moussaid, *et al.*, *Science* **296** (2002) 104-106.
- [45] P.D.Olmsted and C.Y. Lu, *Phys. Rev. E* **56** (1997) R55.
- [46] P.D. Olmsted and C.Y. Lu, *Faraday Disc.* **112** (1999) 183.
- [47] G. Picard, *et al.*, *Phys. Rev. E* **66** (2002) 051501.
- [48] F. Pignon, A. Magnin and J.M. Piau, *J. Rheol.* **40** (1996) 573.
- [49] O. Radulescu, P.D. Olmsted and C.Y. Lu, *Rheol. Acta* **38** (1999) 606.
- [50] L. Ramos, F. Molino and G. Porte, *Langmuir* **16** (2000) 5846.
- [51] L. Ramos and L. Cippelliti, *Phys. Rev. Lett.* **87** (2001) 245503.
- [52] W.B. Russel, D.A. Saville and W.R. Schowalter, *Colloidal dispersions* (Cambridge University Press, Cambridge, 1989).
- [53] J.B. Salmon, *et al.*, *Phys. Rev. E* **66** (2002) 031505.
- [54] V. Schmitt, C.M. Marques and F. Lequeux, *Phys. Rev. E* **52** (1995) 4009.
- [55] P. Sollich, F. Lequeux, P. Hébraud and M.E. Cates, *Phys. Rev. Lett.* **78** (1997) 2020; P. Sollich, *Phys. Rev. E* (1998).
- [56] L.C.E. Struick, *Physical aging in amorphous polymers and other materials* (Elsevier, Amsterdam, 1978).

- [57] S. Tewari, *et al.*, *Phys. Rev. E* **60** (1999) 438, and references therein.
- [58] V. Trappe, *et al.*, *Nature* **411** (2001) 772-775.
- [59] W. van Megen and P.N. Pusey, *Phys. Rev. Lett.* **59** (1987) 2083-2086.
- [60] F. Varnik, *et al.* (2002) [[cond-mat/0208485](#)].
- [61] V. Viasnoff and F. Lequeux, *Phys. Rev. Lett.* **89** (2002) 065701.
- [62] V. Viasnoff, *et al.*, Preprint (2002), to appear in *Faraday Discussions*.

COURSE 3

**STRUCTURAL RELAXATION AND RHEOLOGY
OF SOFT CONDENSED MATTER**

M.E. CATES

*School of Physics,
University of Edinburgh,
JCMB Kings Buildings,
Mayfield Road, Edinburgh EH9 3JZ,
U.K.*



Contents

1	Soft condensed matter	79
2	Rheology	81
2.1	Stress tensor	82
2.2	Statistical mechanics of stress	83
2.3	Strain and strain rate	85
3	Linear rheology	87
3.1	Step-strain response	87
3.2	Oscillatory flow	88
3.3	Steady shear	89
3.4	Typical cases	89
3.5	Linear creep measurements	91
3.6	Simple forms for $G(t)$	91
4	Linear viscoelasticity of polymers	92
4.1	Entanglements	92
4.2	Entropic elasticity	93
4.3	Escape from the tube	94
5	Nonlinear rheology of polymers	95
5.1	Typical experiments	95
5.2	Nonlinear relaxation of polymers	96
5.3	Constitutive equation	98
5.4	Why are polymers tractable?	99
6	Dumbing down	99
6.1	Dumbell model	100
6.2	Scalarisation	101
7	What rheologists want	101
8	Rheology of soft glasses	102
8.1	The effective temperature problem	102
8.2	Phenomenology	103
8.3	Bouchaud's trap model	103
9	The SGR model	105
9.1	Features of the model	106
9.2	Constitutive equation for SGR	108
9.3	Tensorial SGR models	109

10 Rheological aging	111
10.1 Step stress and step strain	111
10.2 Oscillatory flows	112
10.3 AOFOT?	112
10.4 Weak long term memory	113
10.5 The G'' problem	114
10.6 Aging scenarios	114
10.7 Nonlinear aging	116
10.8 Ongoing work on aging and rheology	118
11 Shear thickening and jamming	118
11.1 Nonmonotonic flow curves	118
11.2 Shear thickening mechanisms	119
11.3 Jamming SGR model	121
12 Rheological instability and oscillation	121
12.1 A simpler model for rheo-instability	123
13 Rheochaos	124
14 More fundamental approaches	125
15 Conclusion	127

STRUCTURAL RELAXATION AND RHEOLOGY OF SOFT CONDENSED MATTER

M.E. CATES

Abstract

These lectures address the relation between structural dynamics and macroscopic flow behaviour (rheology) in soft condensed matter. After a brief introduction to soft condensed matter, various types of observed rheological behaviour are introduced and classified. I then move on to discuss the flow of entangled polymers. These exhibit slow dynamics, but nevertheless remain close to equilibrium locally at all times. I outline a simple version of the tube model as developed for nonlinear flows by Doi and Edwards in the late 1970s, and also outline an even simpler “dumbbell” model. The success of these polymer models is hard to emulate, especially in systems which are nonergodic at rest. Those include many kinds of pastes, dense emulsions, liquid crystal textures etc., and recent attempts are described to develop rheological constitutive equations for these “soft glasses”. This is followed by a discussion of rheological aging, in which the flow properties of a sample depend on the time since its preparation. I then discuss some simple models of “shear thickening”, which attempt to connect jamming phenomena, seen in colloids and some other materials, with a stress-induced glass transition. Finally, I point to ongoing work on two further topics: chaotic dynamics in the flow of soft materials (rheochaos) and fundamental approaches to glasses under flow (based on mode-coupling theory).

1 Soft condensed matter

Soft condensed matter includes colloids, polymers, emulsions, foams, surfactant solutions, powders, and similar materials. (Domestic examples are respectively paint, engine oil, mayonnaise, shaving cream, shampoo, talc, etc.) In each case, the precise molecular composition of the system has only limited influence on the physical behaviour, which is controlled by structure on the mesoscopic scale (between, say, 1 nm and 1 μm) that can reorganise

under external influence. This gives material properties that are strikingly different from simple fluids or solids. Because whole classes of material behave similarly, their behaviour can best be studied by detailed experiment on *model systems*, prototypical of the given class. The tools of statistical mechanics can powerfully address such simplified cases. Indeed, soft matter experiment frequently offers the best testing ground for very fundamental ideas: for example, colloids represent the closest approach in nature to the hard sphere fluid favoured by theorists.

Most early studies in soft matter physics addressed equilibrium structure, phase behaviour and fluctuation dynamics at equilibrium. These remain a prerequisite for further progress, but attention is now turning to nonequilibrium phenomena, such as nonlinear rheology (the flow response of materials to large imposed stresses). Flow of soft materials is relevant to many industries – chemicals, food, coatings, ceramics etc. At the same time it raises, and offer experimental insight into, some of the most challenging theoretical issues confronting modern statistical physics [1]. This is particularly true in systems which are nonergodic: a central theme of the present school. Very many soft materials are nonergodic, though there are important exceptions such as polymer melts.

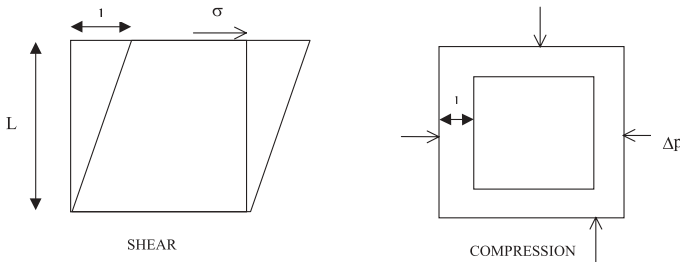


Fig. 1. Shear and compressive strain geometries.

How may we define soft matter? This is best answered mechanically (Fig. 1). Consider a cube of material subject to sudden small shear strain of order l/L with l a displacement and L the linear sample size. This causes a shear stress σ . The shear modulus is $G = \sigma L/l$. Compare this to a compressive distortion, creating an excess pressure Δp ; the strain is again $\sim l/L$, and the compression modulus $K \simeq \Delta p L/l$. Most familiar solids, such as metals, hard plastics, etc., have $G \simeq K \simeq 10^{11}$ Pa. The two quantities are similar, because shear and compression both change bond lengths by similar amounts. In soft condensed matter, one has instead $G \ll K$. Values of G of order 100 Pa are common (for example in polymer gels); figures as low as 1 Pa are not unheard of (for example, among colloidal

crystals). In contrast, compression moduli are usually still of order 10^{10} Pa: this is the value for water or a similar solvent. For example, a polymer gel is mostly solvent, and it resists compression similarly. But since the solvent has no shear modulus, the gel's static resistance to shear has a different origin – in the mesoscopic degrees of freedom associated with the polymer configurations. The characteristic scale for G is of order nkT , where n is the number of such degrees of freedom per unit volume (*e.g.* in colloids, their number density). The small shear moduli of soft condensed matter therefore stems from the fact that n is small (compared to the corresponding density in a metal, say) but not zero.

On the other hand, if you compress a polymer gel or similar soft material *osmotically* (this means placing it within a semipermeable membrane through which solvent can pass, and squeezing on the membrane) then you will measure instead of $K \sim 10^{10}$ a much lower *osmotic* compression modulus, K_{osm} , which is typically similar in magnitude to G .

The distinction between hard and soft materials is partly a matter of time scales. A solvent like water *does* actually resist shear (with a rather large n , of order the inverse molecular volume) but its stress response to a sudden strain relaxes on a time scale too fast to be measured easily, and plays no role in rheological experiments as commonly performed in the laboratory. In contrast, because they have stress relaxation times on laboratory time scales (*e.g.* $10^{-3} - 10^3$ s) many soft materials can exhibit solid-like and fluid-like responses in the same experiment and are thus called “viscoelastic”. The existence of long relaxation times and small shear moduli have a common cause in the presence of large objects (polymers, colloids, emulsion droplets, domains...). Such objects are easily perturbed by flow fields, and there is a complicated feedback between microstructure and flow response. Hence the study of *nonlinear* phenomena is an essential part in understanding the rheological behaviour of soft matter [2].

2 Rheology

Rheology is the measurement and prediction of flow behaviour. The basic experimental tool is a rheometer – a device for applying a controlled stress to a sample and measuring its deformation, or *vice versa*. However, in recent years a variety of rheophysical probes, which allow simultaneous microscopic characterisation or imaging, have been developed [3–5]. For the complex flows that can arise in soft materials, the latter offer important additional information.

One common flow cell used in rheometers is the Couette cell (two concentric cylinders, of radius r and $r+h$ with the inner one rotating). Another is a cone-plate cell where a rotating cone contacts a stationary plate at its

apex, Figure 2, with a small opening angle θ . In the limit of small h/r or small θ , each results in a uniform stress in steady state, so that one can usually expect a simple shear flow of constant velocity gradient. In each case, the shear stress can be measured from the torque, but some cone-and-plate devices can also measure “normal stress differences” (*e.g.* from the upthrust). Normal stress differences play an important part in nonlinear rheology, and we return to them below.

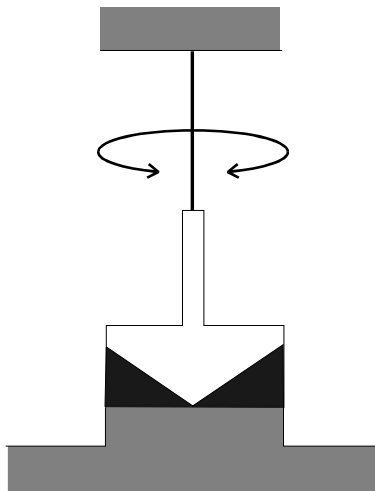


Fig. 2. A cone and plate device; the sample (black) is between the cone (white) and the plate (grey).

Other useful devices allow study of elongational flows in which the velocity gradient direction lies parallel to the velocity itself (unlike in simple shear, where it is at right angles). Two such flows are possible; uniaxial elongation, which is roughly equivalent to yanking on a piece of chewing gum that is clamped between your teeth (a geometry important in making textile fibres), and planar, which is roughly equivalent to blowing up a balloon of bubble gum (a geometry used to create plastic sheets). Although elongational flows are important [6], our main interest in these lectures is to understand the response of soft materials to simple shear flows.

2.1 Stress tensor

We shall use suffix notation, with roman indices, for vectors and tensors; letters $a...w$ can therefore stand for any of the three cartesian directions x, y, z . Greek indices will be reserved for labels of other kinds.

Consider a surface element of area dA with normal vector n_i . Denote by dF_i the force acting on the interior of the surface element caused by what is outside. If n_i is reversed (switching the definitions of interior and exterior), then so is F_i ; this accords with Newton's third law. Writing the usual vectorial area element as $dS_i = n_i dA$, we have

$$dF_i = \sigma_{ij} dS_j \quad (2.1)$$

which defines the stress tensor σ_{ij} . This tensor is symmetric, as can be seen by computing the torque on an infinitesimal cube of material of side l . (The torque about the z axis, say, is $l^2(\sigma_{xy} - \sigma_{yx})$, but since the moment of inertia of this cube is of order l^5 , an asymmetric stress tensor would give infinite angular acceleration, which is unphysical.)

A pure hydrostatic pressure (as arises in fluids at rest) corresponds to a diagonal stress tensor $\sigma_{ij} = -p\delta_{ij}$ (the force is directed inward, hence the sign). More generally, the hydrostatic pressure is *defined via* the trace of the stress tensor, as $p = -\sigma_{ii}/3$. But we have already commented on the largeness of K compared to G , so that very large pressures can arise from very tiny volume changes. Setting K infinite is therefore a good approximation: in this limit, p takes whatever value is needed at every instant to ensure the incompressibility of the material. This means it is not rheologically interesting to study p in its own right. What matters is the (traceless) “deviatoric” stress

$$\sigma_{ij}^{\text{dev}} = \sigma_{ij} + p\delta_{ij} \quad (2.2)$$

which, unlike p , comes mainly from the soft degrees of freedom. It includes all shear stresses, and also two combinations of the diagonal elements that do not change the trace of σ_{ij} (and hence are linearly independent of p). These are usually chosen as the two normal stress differences,

$$N_1 = \sigma_{xx} - \sigma_{yy}; \quad N_2 = \sigma_{yy} - \sigma_{zz}. \quad (2.3)$$

Hence the deviatoric stress has five independent components in all.

2.2 Statistical mechanics of stress

For simplicity we assume pairwise interactions between particles. (The choice of what we define as a particle is clarified later.) The force $f_i^{\alpha\beta}$ exerted by particle α on particle β then depends on their relative coordinate $r_i^{\alpha\beta}$ (measured by convention from α to β). But this pair of particles contributes to the force dF_i acting across a surface element dS_i only if the surface divides one particle from the other. The probability of this happening is $dS_i r_i^{\alpha\beta} / V$ where V is the volume of the system. This is easiest seen for a cubic box of side L with a planar dividing surface of area $A = L^2$ with

normal n_i along a symmetry axis (Fig. 3). The separation of the particles normal to the surface is clearly $\ell = r_i^{\alpha\beta} n_i$, and the probability of their lying one either side of it is then just ℓ/L , which can be written as $A r_i^{\alpha\beta} n_i / V$. The differential form of this argument gives the stated result.

Accordingly, the total force across a surface element dS_i is

$$dF_i = - \sum_{\alpha\beta} \frac{dA}{V} (r_j^{\alpha\beta} n_j) f_i^{\alpha\beta} \quad (2.4)$$

which by definition acts outward (hence the minus sign). Bearing in mind equation (2.1), this gives

$$\sigma_{ij} = -V^{-1} \sum_{\alpha\beta} r_i^{\alpha\beta} f_j^{\alpha\beta}. \quad (2.5)$$

This can also be written $\sigma_{ij} = -\rho^2 \langle r_i f_j \rangle$ where the average is taken over pairs and ρ is the mean particle density.

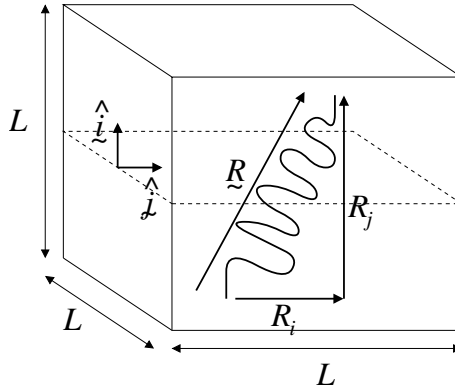


Fig. 3. Contribution from a polymer “subchain” to the stress tensor. The end-points of the chain can be viewed as two particles, with the chain in between supplying a “spring force” between them.

An example is shown in Figure 3, where a polymer “subchain” is shown crossing the surface. At the most microscopic level of description for a polymer, one could choose the individual monomers (repeat units along the chain backbone) as the particles, and their covalent, van-der-Waals, and other direct interactions as the forces, when using equation (2.5). Indeed, this is often done in computer simulation [7,8]. But so long as the force $f_i^{\alpha\beta}$ is suitably redefined as an effective, coarse grained force that includes entropic contributions, we can equally well consider a polymer chain as a sparse string of

“beads” connected by “springs”. (The beads could be every 500th monomer, for example.) This has the advantage that, at a coarse-grained scale, the interaction force $f_i^{\alpha\beta}$ has a universal and simple dependence on $r_i^{\alpha\beta}$, deriving from an “entropic potential” $U(r_i) = (3kT/2b^2)r_i r_i$, where $b^2 \equiv \langle r_i r_i \rangle$. This is a consequence of the well-known gaussian distribution law for random walks, of which the polymer, at this level of description, is an example. The entropic potential is defined so that the probability distribution for the end-to-end vector of the subchain obeys $P(r_i) \propto \exp[-U(r_i)/kT]$; this form identifies U as the free energy.

The force now obeys

$$f_i^{\alpha\beta} = -dU(r_i^{\alpha\beta})/dr_i^{\alpha\beta} = -(3kT/b^2)r_i^{\alpha\beta} \quad (2.6)$$

which gives, using equation (2.5), the polymeric contribution to the stress tensor:

$$\sigma_{ij}^{\text{pol}} = \frac{N_{\text{spr}}}{V} \frac{3kT}{b^2} \langle r_i r_j \rangle \quad (2.7)$$

where the average is over the probability distribution $P(r_i)$ for the end-to-end vectors of our polymeric subchains (or springs); N_{spr}/V is the number of these per unit volume.

In many soft systems, contributions such as the one we just calculated (which derive from the free energy of the mesoscopic degrees of freedom) completely dominate the deviatoric stress. However, there may also be other significant contributions, *e.g.* from local viscous dissipation in the solvent. In this case, although a formula such as equation (2.5) still holds if all the microscopic degrees of freedom are included, it is more convenient to use that only for the mesoscopic ones, and then to add a separate solvent contribution directly to the stress tensor. So long as the solvent is Newtonian, this additional contribution takes a standard form, $\sigma_{ij}^{\text{sol}} = \eta^{\text{sol}}(K_{ij} + K_{ji})$, where K_{ij} is the velocity gradient tensor introduced below.

2.3 Strain and strain rate

Consider a uniform deformation of a material to a strained from an unstrained state (with no assumption of small strain). The position vector r_i of a material point is thereby transformed into a new vector r'_i ; the deformation tensor E_{ij} is defined by

$$r'_i = E_{ij} r_j. \quad (2.8)$$

For small deformations, at least, it is useful to write this as $E_{ij} = \delta_{ij} + e_{ij}$ so that the displacement $u_i = r'_i - r_i$ obeys $u_i = e_{ij} r_j$. Alternatively we may write this as $e_{ij} = \nabla_i u_j$.

Consider now a time-dependent strain, for which $v_i \equiv \dot{u}_i$ defines the fluid velocity, which depends on the position r_i . We define the velocity gradient tensor

$$K_{ij} = \nabla_i v_j = \dot{e}_{ij} \quad (2.9)$$

which is also known as the “rate of strain tensor” or “deformation rate tensor”. If we now consider a small strain increment, $\dot{e}_{ij}\delta t$,

$$r_i(t + \delta t) = (\delta_{ij} + \dot{e}_{ij}\delta t) r_j(t). \quad (2.10)$$

The left hand side of this is, by definition, $E_{ij}(t + \delta t)r_i(0)$ where the time-dependent deformation tensor $E_{ij}(t)$ connects coordinates at time zero with those at time t . Inserting also $r_j(t) = E_{jk}(t)r_k(0)$ we obtain the result

$$\partial E_{ij}/\partial t = \dot{e}_{ik}E_{kj} \quad (2.11)$$

or, equivalently, $\dot{E}_{ij} = K_{ik}E_{kj}$.

We illustrate this with two examples. The first is simple shear, where for definiteness we choose the flow velocity to be along x and its gradient along y . This means that the velocity obeys $v_i = \dot{\gamma}y\delta_{ix}$, where $\dot{\gamma}$ is called the shear rate. Hence the velocity gradient tensor is $K_{ij} = \dot{\gamma}\delta_{ix}\delta_{jy}$, that is, K_{ij} is a matrix with $\dot{\gamma}$ in the xy position and all other entries zero. Solving equation (2.11) for arbitrary $\dot{\gamma}(t)$ then gives

$$E_{ij}^{tt'} = \delta_{ij} + \gamma(t, t')\delta_{ix}\delta_{jy} \quad (2.12)$$

where $E_{ij}^{tt'}$ is defined as the deformation tensor connecting vectors at time t to those at time t' , and $\gamma(t, t') = \int_t^{t'} \dot{\gamma}(t'')dt''$ is the total strain between these two times.

The second example is uniaxial extension (pulling chewing gum), for which we assume stretching along the x direction with a strain rate $\dot{\epsilon}$, accompanied by shrinking in the other two directions at the rate required to conserve volume:

$$K_{ij} = \dot{\epsilon}(\delta_{ix}\delta_{jx} - \delta_{iy}\delta_{jy}/2 - \delta_{iz}\delta_{jz}/2). \quad (2.13)$$

Hence K_{ij} is a diagonal matrix with entries $\dot{\epsilon}, -\dot{\epsilon}/2, -\dot{\epsilon}/2$ down the diagonal. From this one finds that $E_{ij}^{tt'}$ also takes a diagonal form, with $E_{xx} = \exp \epsilon(t, t')$, $E_{yy} = E_{zz} = \exp(-\epsilon(t, t')/2)$, and $\epsilon(t, t') = \int_t^{t'} \dot{\epsilon}(t'')dt''$. Note that for steady strain rate, this flow gives exponential stretching of embedded vectors, as one might expect from equation (2.11). Indeed, a naive inspection (ignoring suffices) of that equation would suggest such separation for any steady flow. This is indeed the generic case, but crucially the exception is simple shear, where the velocity gradient is always at right angles to the velocity itself, and the “compound interest” of deformation building upon deformation does not accrue.

3 Linear rheology

Linear rheology addresses the response of systems to very small stresses. An interesting theoretical question is: how small? The same question can be asked of all other areas of linear response theory, such as susceptibilities in magnetic systems etc. The conventional answer, at least for ergodic systems in thermal equilibrium, is this: the perturbation must be small compared to spontaneous thermal fluctuations. This is correct, but only if interpreted correctly.

What does it mean to say that an applied stress is small compared to the spontaneous thermal fluctuations of stress that are anyway present? A naive interpretation applies this criterion to the whole sample. This leads to nonsense, because the rms. thermal fluctuation in stress σ^T varies with system volume as $V^{-1/2}$, like any other intensive fluctuation. Clearly we do not require the applied stress to obey $\sigma^{\text{app}} \ll \sigma^T$ since otherwise the range of linear response would vanish in the thermodynamic limit; experimentally of course, this range does not vanish, but saturates. Instead, let us define a scale of volume $V^T(\sigma^{\text{app}})$ such that $\sigma^T(V^T) \simeq \sigma^{\text{app}}$. This is the size of subregion for which thermal fluctuations in stress are comparable to the externally applied one. What we now require is for V^T to be thermodynamically large; this means large compared to all relevant length scales such as the size of colloidal or polymeric particles, and (if one is near a phase transition) large compared to the correlation length. This is, in qualitative terms, the condition for linearity.

The above remarks assume Boltzmann equilibrium. What about a non-ergodic system, such as a glass: is there a linear response regime in that case, and if so, what is its extent? This is a far harder question. The only safe answer is: no, there is no such regime in general. However, numerous experiments (rheological and other) do report apparently linear response behaviour in nonergodic systems [1]. On the other hand, the response tends to drift slowly with time – an aging phenomenon to which we return later on. For the moment, let us stick with ergodic materials.

3.1 Step-strain response

Imagine an undeformed block of material which is suddenly subjected, at time t_1 , to a small shear strain γ , as shown in Figure 1. Taking the displacement along x and its gradient along y , we then have for the resulting deformation tensor $E_{ij} = \delta_{ij} + \gamma\delta_{ix}\delta_{jy}$. Suppose we measure the corresponding stress tensor $\sigma_{ij}(t)$. Linearity requires that for $t > t_1$

$$\sigma_{yx} = \sigma_{xy} = G(t, t_1)\gamma \quad (3.1)$$

and that all other deviatoric components of σ_{ij} vanish, at linear order in γ , by symmetry. (For example, $N_1(\gamma) = N_1(-\gamma)$, which requires $N_1 = O(\gamma^2)$.)

In a Boltzmann equilibrium state, the material properties cannot depend on t and t_1 except through their difference, $t - t_1$. This is a statement of *time translational symmetry* (we will relax it later on for nonergodic systems). Hence

$$\sigma_{xy} = G(t - t_1)\gamma \quad (3.2)$$

which defines the linear step-strain response function $G(t)$. This function is zero for $t < 0$; it is discontinuous at $t = 0$, jumping to an initial value which may be very large. This largeness reflects the role of microscopic degrees of freedom (compare our earlier discussion of the viscoelastic response of a solvent such as water); there follows a very rapid decay to a more modest level arising from mesoscopic degrees of freedom. In many cases this level persists for a while, in which case it is useful to identify it as G_0 , the transient elastic modulus. (In models that ignore microscopics, one can identify $G_0 = G(t \rightarrow 0+)$.) On the timescale of mesoscopic relaxations, which are responsible for viscoelasticity, $G(t)$ then falls further. In viscoelastic *liquids* it eventually decays to zero faster than $1/t$. In viscoelastic *solids* it decays to a plateau. Materials where it decays to zero like $1/t$ or slower are in a class of their own; we return to this point later.

Now suppose we apply a time dependent, but small, shear strain $\gamma(t)$. By linearity, we can decompose this into a series of infinitesimal steps of magnitude $\dot{\gamma}(t')dt'$; the response to such a step is $d\sigma_{xy}(t) = G(t - t')\dot{\gamma}(t')dt'$. We may sum these incremental responses, giving the integral

$$\sigma_{xy}(t) = \int_{-\infty}^t G(t - t')\dot{\gamma}(t')dt' \quad (3.3)$$

where, to allow for any displacements that took place before $t = 0$, we have extended the integral into the indefinite past. Hence $G(t)$ is the memory kernel giving the linear stress response to an arbitrary shear rate history.

3.2 Oscillatory flow

The case of an oscillatory flow is often studied. We write $\gamma(t) = \gamma_0 e^{i\omega t}$ (taking the real part whenever appropriate); substituting in equation (3.3) gives after trivial manipulation

$$\sigma_{xy}(t) = \gamma_0 e^{i\omega t} G^*(\omega) \quad (3.4)$$

where $G^*(\omega) \equiv i\omega \int_0^\infty G(t) e^{-i\omega t} dt$; this is called the complex modulus. (Note that the factor $i\omega$ comes from the presence in equation (3.3) of $\dot{\gamma}$ rather than γ ; it means that G^* , like $G(t)$ has the dimensions of a modulus.) The complex modulus, or “viscoelastic spectrum”, is conventionally

written $G^*(\omega) = G'(\omega) + iG''(\omega)$ where the real quantities G' and G'' are respectively the in-phase or elastic response, and the out-of-phase or dissipative response. These are often called the “storage modulus” and the “loss modulus” respectively.

One can also study the steady-state flow response to an oscillatory stress. This defines a frequency-dependent complex compliance $J^*(\omega)$; however, within the linear response regime this is just the reciprocal of $G^*(\omega)$.

3.3 Steady shear

In steady shear $\dot{\gamma}(t)$ is constant; therefore from equation (3.3) one has $\sigma_{xy}(t) = \dot{\gamma} \int_{-\infty}^t G(t-t')dt'$. However, the definition of a fluid’s linear viscosity (sometimes called its zero-shear viscosity) is the ratio of shear stress to strain rate in a steady measurement when both are small; hence the viscosity is

$$\eta = \int_0^\infty G(t)dt = \lim_{\omega \rightarrow 0} [G^*(\omega)/i\omega]. \quad (3.5)$$

This is finite so long as $G(t)$ decays to zero faster than $1/t$ at late times. (Note that an integrable divergence at $t \rightarrow 0$ is acceptable.)

3.4 Typical cases

3.4.1 “Normal” viscoelastic fluids and solids

Most fluids have a “longest relaxation time” τ in the sense that for large enough t , the relaxation modulus $G(t)$ falls off like $\exp[-t/\tau]$. In this case one has at low frequencies $G' \sim \omega^2$ and $G'' \sim \omega$. For many materials, *e.g.* molten polymers, as frequency is raised G' passes through a plateau whereas G'' starts to fall; eventually at high frequencies both rise again. This is shown schematically in Figure 4 where, as is common practice, a double logarithmic scale is used to plot the viscoelastic spectra.

The viscoelastic spectrum for a soft *solid*, such as a crosslinked polymer gel, often looks very similar to the one shown, except that instead of falling towards zero at low frequency, the storage modulus asymptotes to a constant. This reflects the existence of a nonzero asymptote for $G(t \rightarrow \infty)$. But once this is subtracted there is still usually an exponential approach to it, from which a longest relaxation time can be extracted. This fixes the low frequency slope of G'' .

3.4.2 Power law fluids

A peculiar class of viscoelastic materials cannot be classified as either fluid or solid in the above terms. For example, in a critical system, such as a

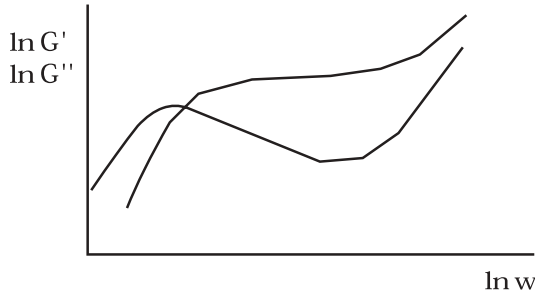


Fig. 4. Artist's impression of the viscoelastic spectrum for a typical polymeric material.

polymer gel at its percolation threshold, one finds $G(t) \sim t^{-y}$ with $y < 1$ a power law index. This translates into $G^*(\omega) \sim (i\omega)^y$, giving two parallel lines for the G', G'' spectra on a log plot. There is no longest relaxation time (unless the power law spectrum is cutoff at low frequencies and reverts to the “normal” behaviour). The peculiar feature of a power law fluid is that its viscosity η (defined by Eq. (3.5)) is infinite while at the same time its elastic modulus (defined by $G(t \rightarrow \infty)$) is zero.

3.4.3 Soft glasses

Many soft nonergodic materials (pastes, foams, etc.) appear to show power-law-fluid behaviour [9]. Others give a slow approach, at late times, towards a finite limit $G(t \rightarrow \infty)$. The resulting spectra can show anomalies: for example, one often finds a plateau in G' at low frequency, but G'' , instead of decaying like ω at low frequencies, also seems to saturate or even appears to be rising at the lowest frequencies measured. The picture strongly resembles the right hand half of Figure 4, and it is sometimes assumed that the measurement window lies to the right of a peak in G'' . If the system were linear and time translational invariant, this would be a persuasive deduction, since it follows from their definitions that G' and G'' are even and odd in frequency respectively. Unless a strange nonanalyticity develops at very low frequency this rules out either a rising or a saturating trend in G'' as ω is lowered: the asymptotic $G'' \sim \omega$ must be recovered. However, for nonergodic (and hence aging) systems the assumptions underlying our definitions of $G(t)$ and $G^*(\omega)$ need closer examination (Sect. 10).

3.5 Linear creep measurements

Suppose, instead of applying a step strain as was used to define $G(t)$ in equation (3.2), we apply a small step in shear stress of magnitude σ_0 and measure the strain response $\gamma(t)$. This defines a compliance function $\gamma(t)/\sigma_0 = J(t)$ which is the functional inverse of $G(t)$ (that is, $\int J(t)G(t - t')dt = \delta(t')$). To see this, one can repeat the derivation of equation (3.4) with stress and strain interchanged, to find that $J^*(\omega) = i\omega \int J(t)e^{-i\omega t}dt$. But clearly $J^*(\omega)G^*(\omega) = 1$ since these quantities measure inverse ratios (stress over strain or *vice versa*) in steady, small amplitude, oscillatory shear.

For a viscoelastic liquid $\gamma(t)$ rises smoothly from zero, and the system eventually asymptotes to a steady flow: $\gamma(t \rightarrow \infty) = \sigma_0(t/\eta + J_e^{(0)})$. The offset $J_e^{(0)}$, measured by extrapolating the asymptote back to the origin, is called the steady-state compliance. It can be written as

$$J_e^{(0)} = \int_0^\infty t G(t) dt / \eta^2 \quad (3.6)$$

and is therefore more sensitive to the late-time part of $G(t)$ than the viscosity $\eta = \int_0^\infty G(t) dt$. For a viscoelastic solid, $\gamma(t)$ again rises smoothly from zero but now plateaus at $\gamma = \sigma_0/G(\infty)$. For a power law fluid, $\gamma(t)$ has neither a linear nor a constant asymptote, but rises forever in a sublinear fashion.

3.6 Simple forms for $G(t)$

The simplest imaginable $G(t)$ takes the form $G(t) = G_0 \exp(-t/\tau_M)$ and is called the linear Maxwell model, after its inventor James Clerk Maxwell. G_0 is a transient elastic modulus and τ_M a relaxation time (in this model, it is the *only* such time) called the Maxwell time. The viscosity is $\eta = G_0\tau_M$; note that a newtonian fluid is recovered by taking $G_0 \rightarrow \infty$ and $\tau_M \rightarrow 0$ at fixed η . In nature, nothing exists that is quite as simple as the Maxwell model, but certain entangled micellar systems (very similar to what you get in some shampoos) come very close (Fig. 5). The viscoelastic spectrum of the Maxwell model is $G^*(\omega) = G_0 i\omega\tau_M / (1 + i\omega\tau_M)$ whose real and imaginary parts closely resemble Figure 5: a symmetric maximum in G'' on log-log through which G' passes as it rises towards a plateau.

In an obvious extension of the Maxwell model one can add several Maxwell-like “modes” to give $G(t) = \sum_i G_i \exp[-t/\tau_i]$. If the modes are well separated, each one will give a smooth step upward (magnitude G_i) in $G'(\omega)$ at around $\omega\tau_i = 1$; there will be a corresponding “loss peak” (like the one in Fig. 4) at the same place. These features are blurred together if the modes are closely spaced, and one can talk of a smooth spectrum of modes, $G(t) = \int_0^\infty P(\tau) \exp[-t/\tau] d\tau$. However, this offers little physical insight, since with suitable $P(\tau)$ one can recover almost any $G(t)$.

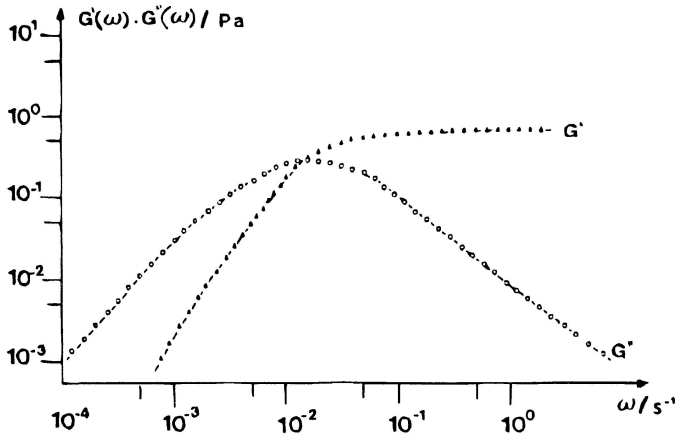


Fig. 5. Linear viscoelastic spectrum for a system of entangled micelles [10]: nature's closest approach to the linear Maxwell model. In the Maxwell model, the peak in G'' is perfectly symmetric and G' crosses through this peak at the maximum – nearly true here.

4 Linear viscoelasticity of polymers

Figure 6 shows a flexible polymer (ignore the dotted lines and open circles for the moment). The chain conformation is a random walk; its end-to-end vector is gaussian distributed. For real polymers there is a subtlety concerning the fact that no two monomers can be in the same place. This causes an isolated chain to expand; its statistics are no longer Gaussian. However, once chains are at high enough density to strongly interpenetrate, their tendency to expand is screened out and Gaussian statistics are recovered at large distances [11]. This is because, although expansion of an isolated coil gives more entropy (the self-avoidance constraint is more easily satisfied in an expanded configuration), in dense systems it does not: the chain has to avoid *all* other monomers, not just its own, and the density of *other* chains monomers it encounters (which dominates the total) is not lowered by swelling. In what follows we consider only concentrated polymer solutions and melts, and so treat chains as Gaussian.

4.1 Entanglements

Although the effect of other chains is to make the statics simpler, it makes the dynamics more complicated. Dense polymers are like an entangled mass of spaghetti, lubricated by Brownian motion. The presence of other chains, shown schematically as circular obstacles in Figure 6, strongly impedes the

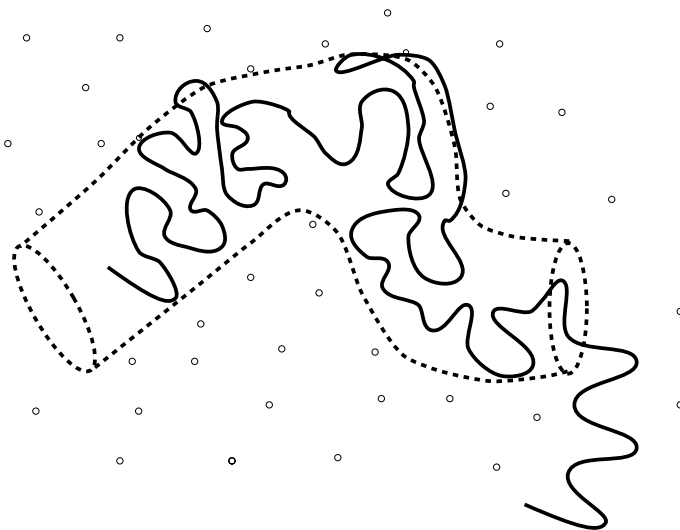


Fig. 6. A polymer chain (heavy line). Surrounding chains present obstacles (circles) that the chain cannot cross. These can be modelled by a tube (dotted), from which this particular chain has partially emerged.

thermal motion of any particular chain. Suppose for a moment that the ends of that chain are held fixed. In this case, the effect of the obstacles can be represented as a tube (also shown in Fig. 6). Because it wraps around a random walk, the tube is also a random walk; its number of steps N and step-length b (comparable to the tube diameter) must obey the usual relation $\langle R^2 \rangle = Nb^2$ where R is the end-to-end distance of both the tube and the chain. This distance can be measured by scattering with selected labelling [12], as can, in effect, the tube diameter (or step length), by looking at fluctuations in chain position on short enough timescales that the chain ends do not move much. However, there is no fundamental theory that can predict b ; in what follows it is a parameter. It is quite large, so that chains smaller than a few hundred monomers do not feel the tube at all.

4.2 Entropic elasticity

Suppose we take a dense polymer system and perform a sudden step-strain with shear strain γ (Fig. 1). The chain will instantaneously deform with the applied strain. Since a deformed random walk is not maximally random, but biased, this causes a drop in its configurational entropy. Quite rapidly, though, degrees of freedom at short scales (within the tube) can relax by Brownian motion. Once this has happened, the only remaining bias is at the

scale of the tube: the residual entropy change ΔS of the chain is effectively that of the tube in which it resides. A calculation [13] of the entropy of deformed random walks gives a resulting free energy change

$$\Delta F = -T\Delta S = \frac{1}{2}G_0\gamma^2 \quad (4.1)$$

where we identify G_0 as the transient elastic modulus; this comes out as $G_0 = 4kTn/5$ where n is the number of tube segments per unit volume. Hence the elastic modulus is close to, but not exactly, kT per tube segment.

4.3 Escape from the tube

What happens next? The chain continues to move by Brownian motion, as does its neighbours. Although the individual constraints (circles in Fig. 6) come and go to some extent, the primary effect is as if the chain remains hemmed in by its tube. Therefore it can diffuse only along the axis of the tube (curvilinear diffusion). The curvilinear diffusion constant D_c is inversely proportional to chain length L [11]. (To see this, note that by the Einstein relation, D_c is kT times a mobility $\tilde{\mu}$. Assuming a local drag between the chain and its surroundings, the force required to pull the chain at a certain speed, whose ratio is $1/\tilde{\mu}$, increases linearly with L , hence the result.)

Curvilinear diffusion allows a chain to escape through the ends of the tube. When it does so, the chain encounters new obstacles and, in effect, creates new tube around itself. However, we assume that this new tube, which is created at random *after* the original strain was applied, is undeformed. This turns out to be a very good approximation, mainly since b is so large: the deformation at the tube scale leads to a local, molecular level alignment that is very small indeed. (Such an alignment might “steer” the emerging chain end so that new tube was correlated the old; but this is negligible.) This causes the stored free energy ΔF to decay away as $\Delta F = G(t)\gamma^2/2$ where

$$G(t) = G_0\mu(t). \quad (4.2)$$

Here we identify $\mu(t)$ as the fraction of the original tube (created at time zero) which is still occupied, by any part of the chain, at time t .

The problem of finding $\mu(t)$ can be recast [11] as the problem of finding the survival probability up to time t of a particle of diffusivity D_c which lives on a line segment $(0, L)$, with absorbing boundary conditions at each end; the particle is placed at random on the line segment at time zero. To understand this, choose a random segment of the initial tube and paint it red; then go into a frame where the *chain* is stationary and the tube is moving. The red tube segment, which started at a random place, diffuses

relative to the chain and is lost when it meets a chain end. This tube segment is our particle, and its survival probability defines $\mu(t)$.

It is remarkable that the tube concept simplifies our dynamics from a complicated many-chain problem, first into a one-chain (+tube) problem, and then into a one-particle problem. The result of this calculation, which is a good revision exercise in eigenfunction analysis [13], is:

$$\mu(t) = \sum_{n=\text{odd}} \frac{8}{n^2\pi^2} \exp[-n^2t/\tau_r] \quad (4.3)$$

where $\tau_r = L^2\pi^{-2}/D_c$. This parameter is called the “reptation time” (“reptate” means to move like a snake through long grass), and sets the basic timescale for escape from the tube. The calculated $\mu(t)$ is dominated by the slowest decaying term – hence it is not that far from the Maxwell model, and resembles the left part of Figure 4. (To understand the upturn at the right hand side of that figure, you need to include intra-tube modes and this is beyond these lectures; see [13].)

From this form of $\mu(t)$ follow several results: for example the viscosity $\eta = \int G(t)dt = G_0\tau_r\pi^2/12$ and the steady-state compliance obeys $J_e^{(0)}G_0 = 6/5$, etc. Thus the tube model gives quantitative inter-relations between observable quantities, and the number of these relations significantly exceeds the number of free parameters in the theory (which can be chosen, in effect, as G_0 and a friction constant $\tilde{D}_c = D_cL$).

The model predicts that, for chains of similar chemistry and fixed volume fraction, $\eta = G_0L^3/(12\tilde{D}_c)$; since G_0 is molecular-weight independent, η varies as L^3 for long chains. The experiments lie closer to $\eta \sim L^{3.4}$, at least for modest L , but with a prefactor such that the observations lie *below* the tube model’s prediction until extremely large L is attained (at which point, in fact, the data bend over towards L^3). This viscosity deficit at intermediate chain lengths has, in recent years, been successfully accounted for by studying more closely the role of intra-tube fluctuation modes and their effects on other chains; see *e.g.* [14] for a recent account.

5 Nonlinear rheology of polymers

Nonlinear rheology addresses the response of a system to finite or large stresses.

5.1 Typical experiments

In the absence of a superposition principle as holds for linear response, the range of independent measurements is much wider. Nonlinear versions exist of the step-strain and step-stress response measurements discussed in

Section 3, and so do oscillatory measurements in which either stress or strain oscillate sinusoidally (though in the nonlinear regime, the induced strain or stress will have a more complicated waveform).

5.1.1 Nonlinear step-strain

We discuss only one such measurement, the nonlinear step strain. In this case a deformation tensor $E_{ij} = \delta_{ij} + \gamma\delta_{ix}\delta_{jy}$ is suddenly applied at time t_1 ; this is just as in Section 3.1 with the important difference that γ need not be small. Analogous to equation (3.1), we define

$$\sigma_{xy} = G(t, t_1; \gamma)\gamma \quad (5.1)$$

where a factor of γ ensures that $G(t, t_1; 0) = G(t, t_1)$ (so the small-strain limit coincides with the linear modulus defined previously). For time translationally invariant systems, $G(t, t_1; \gamma) = G(t - t_1; \gamma)$. A system is called “factorable” if $G(t, t_1; \gamma) = G(t, t_1)h(\gamma)$; this is not the general case, but when observed, usually says something interesting about the system in question.

Whereas at linear order all other deviatoric components of σ_{ij} vanished by symmetry, in the nonlinear regime they do not. In general one can expect to measure finite normal stress differences N_1, N_2 , as defined in equation (2.3). In some systems, including the wormlike micelles of Figure 5, these quantities are much larger in magnitude than the shear stress σ_{xy} .

5.1.2 Flow curve

Another key experiment in the nonlinear shear regime is to measure the “flow curve”, that is, the relationship $\sigma(\dot{\gamma})$ in steady state. For a Newtonian fluid this is a straight line of slope η ; upward curvature is called shear-thickening and downward curvature shear-thinning. For solid-like materials, though not molten polymers, the flow curve can exhibit a nonzero intercept on the vertical axis

$$\lim_{\dot{\gamma} \rightarrow 0} \sigma(\dot{\gamma}) = \sigma_Y > 0 \quad (5.2)$$

where σ_Y is called the yield stress. Flow curves can also exhibit vertical or horizontal discontinuities: these are usually associated with an underlying instability to an inhomogeneous state [15].

5.2 Nonlinear relaxation of polymers

Imagine a dense polymer system to which a *finite* strain is suddenly applied. We are thinking mainly of shear, but can equally consider an arbitrary strain

tensor E_{ij} . As previously discussed, the random walk comprising the tube, which describes the slow degrees of freedom, becomes nonrandom. If we define the tube as a string of vectors bu_i^α (where α labels the tube segment) then the initial u_i^α are random unit vectors. After deformation

$$u_i^\alpha \rightarrow E_{ij}u_j^\alpha \quad (5.3)$$

where it is a simple matter to prove [13] that the average length of the vector has gone up: $\langle E_{ij}u_j^\alpha \rangle_\alpha \equiv \xi > 1$, where the average so defined is over the initial, isotropic distribution. The length increment is of order γ^2 (for the usual reasons of symmetry; strains γ and $-\gamma$ must be equivalent, macroscopically) but for large strains cannot be neglected.

This increase in the length of the tube is rapidly relaxed by motion of the free ends, on a similar timescale to the intra-tube modes mentioned previously. The rapid relaxation is called “retraction”; it effectively kills off a fraction $1 - 1/\xi$ of the tube segments, so that the number of such segments per unit volume falls as $n \rightarrow n/\xi$. Retraction also has the effect of relaxing the magnitude, but not the direction, of the mean spring force in a tube segment back to the equilibrium value. The resulting force (according to Eq. (2.6)) is $f_i^\alpha = (3kT/b)E_{ij}u_j^\alpha/|E_{ij}u_j^\alpha|$, while the corresponding end-to-end vector of the segment is $bE_{ij}u_j^\alpha$. Plugging these results in equation (2.7) gives

$$\sigma_{ij}(t > t_1) = \frac{3nkT}{\xi} \left\langle \frac{E_{ik}u_k^\alpha E_{jl}u_l^\alpha}{E_{im}u_m^\alpha} \right\rangle_\alpha \mu(t - t_1). \quad (5.4)$$

Here the final $\mu(t - t_1)$ is inserted on the grounds that, after retraction is over, the dynamics proceeds exactly as discussed previously for escape of a chain from a tube.

This stress relaxation is of factorable form (now choosing $t_1 = 0$):

$$\sigma_{ij}(t) = 3nkTQ_{ij}(E_{mn})\mu(t). \quad (5.5)$$

Which defines a certain tensor Q_{ij} as a function of the step deformation E_{mn} . Note that computing Q_{ij} involves only some angular integrations over a sphere, since the α average in equation (5.4) is over isotropic unit vectors [13].

Expanding the result in γ for simple shear gives $Q_{xy} = 4\gamma/15 + 0(\gamma^2)$ and this is the reason for the value of the transient modulus G_0 quoted after equation (4.1) above. In finite amplitude shear, Q_{ij} is sublinear in deformation: this is called “strain-softening” and the same physics is responsible for shear-thinning in polymers under steady flow. There are two ways to explain the sublinearity. One is retraction, leading to loss of tube segments. The other is “overalignment”: a randomly oriented ensemble of tube segments will, if strained too far, all point along the flow direction. Hence none

will cross a plane transverse to the flow as required to give a shear stress (Fig. 3). But the second argument is fallacious unless retraction also occurs (the number of chains crossing the given plane is otherwise conserved) and indeed crosslinked polymer networks, where retraction cannot happen because of permanent connections, do not strain-soften.

Details of how well these calculations works in practice can be found in [13]: they are, like many other predictions of the tube model, good to 10 or 15 percent. Note that the factorability stems from the separation of timescales between slow (reptation) modes and the faster ones causing retraction; close experimental examination shows that the factorisation fails at short times.

5.3 Constitutive equation

Alongside shear thinning, polymeric fluids exhibit a number of exotic phenomena under strong flows; these go by the names of rod-climbing, recoil, the tubeless syphon etc. [2]. Because the behaviour of a viscoelastic material cannot be summarised by a few linear or nonlinear tests, the goal of serious theoretical rheology is to obtain for each material studied a *constitutive equation*, that is, a functional relationship between the stress at time t and the deformation applied at all previous times (or *vice versa*). The tube model, in its simplest form (involving a further simplification called the “independent alignment approximation, or IAA”) has the following constitutive equation [13]:

$$\sigma_{ij}^{\text{pol}}(t) = G_0 \int_{-\infty}^t \dot{\mu}(t-t') Q_{ij} \left(E_{mn}^{tt'} \right) dt' \quad (5.6)$$

where $Q_{ij}(E_{mn})$ is as defined in equation (5.5), and $E_{mn}^{tt'}$ denotes the deformation tensor connecting the shape of the sample at time t to that at an earlier time t' . (Recall this is found by solving Eq. (2.11) with initial condition $E_{mn}^{t't'} = \delta_{mn}$, so it is fully determined by the strain rate history.) This is the deformation seen by tube segments that were created at time t' ; $G_0 Q_{ij}$ gives the corresponding stress contribution. The factor $\dot{\mu}(t-t')$ (with $\mu(t)$ obeying Eq. (4.3)) is the probability that a tube segment, still alive at time t , was indeed created at the earlier time t' .

We see that, despite its tensorial complexity, the constitutive equation for the tube model (within the IAA approximation, at least) has a relatively simple structure in terms of an underlying “birth and death” dynamics of tube segments, which are, in effect, the fundamental mesoscopic entities which carry the stress in entangled polymeric materials [13].

5.4 *Why are polymers tractable?*

It is interesting to note that, since the development of the tube model by Doi and Edwards (following a seminal idea by de Gennes, who derived Eq. (4.3)) in the late 1970s, there has been relatively slow progress made in developing similar meso- or microscopic models for the nonlinear rheology of any other class of material. Meanwhile the tube model has evolved a great deal beyond the simplest version outlined above, for example to cover rigid polymers [13]; chains of more complex architectures than the simple linear ones [6]; breakable chains [16], etc. Remarkably, it has done this without ever undermining the basic conception of the model: each new refinement and extension confirms, rather than replaces, the supremacy of the tube.

Why are polymers tractable in this way? First, there is a mean-field character to the problem, in the sense that each chain interacts with very many others. (This is why the effective tube constraint remains dynamically intact even though other chains are reptating out of their own environments just as fast as any chosen test-chain.) Secondly, and crucially, everything stays close to equilibrium locally. This stems from the (as yet unexplained) largeness of the tube diameter b : even under strong strains *e.g.* $\gamma \sim 10$, chains remain flexible, locally gaussian, and weakly perturbed at scales smaller than b . That is the reason why the polymer stress formula equation (2.7) can be applied even for nonlinear flows. Third, the tube concept translates a complicated many-chain problem into a simple one-chain problem (and, at the level of calculating $\mu(t)$, even into a one-body problem). Hence a full nonlinear constitutive model can be obtained by considering only one chain moving under suitable constraints.

Other soft materials are less tractable. For example, in a fluid phases of colloids each particle interacts with a dozen or so neighbours, not thousands. Also, colloids can be driven far from local equilibrium (on the scale of the colloid hard-core interactions) by relatively modest flows. And in many soft materials, including but not limited to colloidal glasses, the system is not ergodic even at rest: no “near-equilibrium” assumption is ever possible. Such difficulties make the construction of constitutive equations for materials other than polymers a particularly challenging task.

6 Dumbing down

“Dumbing down” is a phrase used in academic circles (in the UK, at least) to describe the iterative simplification of educational standards so as to ensure better examination results. In this section I will present a “dumbed-down” version of the polymer constitutive equation (5.6), leading ultimately to a scalar equation describing shear flow. However, by going through the dumbing-down process, one can see (at least in outline) how its steps might

be reversed, and hence how the scalar description that will be developed for soft glasses in Section 8 might be converted into something more respectable.

6.1 Dumbell model

We proceed *via* the dumbell (or strictly dumb-bell) model, which in fact predated the tube model by many years. A polymer dumbell is defined as two beads connected by a Gaussian spring. We forget now about entanglement effects, and imagine each polymer to be represented by a single dumbell, whose end to end vector is R_i . The force in the spring is $f_i = -\lambda R_i$. (Hence $\lambda = 3kT/N_m b_m^2$ where N_m is the number of monomers in the underlying chain and b_m is the bond length; but this does not actually matter once we adopt the dumbell picture.) In thermal equilibrium, it follows that $\langle R_i R_j \rangle = \delta_{ij}/\lambda$ and we can write equation (2.7) as

$$\sigma_{ij}^{\text{pol}} = n_D \lambda \langle R_i R_j \rangle \quad (6.1)$$

where $n_D = N_D/V$ is the number of dumbells per unit volume.

The dumbell model assumes that the two beads undergo independent diffusion subject to (a) the spring force, and (b) the advection of the beads by the fluid in which they are suspended. These ingredients can be combined to give a relatively simple equation of motion for $\langle R_i R_j \rangle$, and hence for σ_{ij}^{pol} , as follows. First, consider diffusion alone. This would give

$$\frac{d}{dt} \langle R_i R_j \rangle = \frac{4kT}{\zeta} \delta_{ij} . \quad (6.2)$$

This equation says that the separation vector evolves through the sum of two independent diffusion processes, each of diffusivity $D = kT/\zeta$, and hence with combined diffusivity $2D$; ζ is the friction factor (or inverse mobility) of a bead.

Next, add the spring force: this gives a diffusive regression towards the equilibrium value of $\langle R_i R_j \rangle = \delta_{ij}/\lambda$:

$$\frac{d}{dt} \langle R_i R_j \rangle = \frac{4kT}{\zeta} (\delta_{ij} - \lambda \langle R_i R_j \rangle) . \quad (6.3)$$

Finally, we allow for advection of beads by the flow; on its own this would give $\dot{R}_i = K_{ij} R_j$, from which it follows that

$$\left[\frac{d}{dt} \langle R_i R_j \rangle \right]_{\text{flow}} = K_{il} \langle R_l R_j \rangle + \langle R_i R_l \rangle K_{jl} . \quad (6.4)$$

Combining these elements yields

$$\frac{d}{dt} \langle R_i R_j \rangle = K_{il} \langle R_l R_j \rangle + \langle R_i R_l \rangle K_{jl} + \frac{4kT}{\zeta} (\delta_{ij} - \lambda \langle R_i R_j \rangle) \quad (6.5)$$

which is equivalent to

$$\frac{d}{dt}\sigma_{ij}^{\text{pol}} = K_{il}\sigma_{lj}^{\text{pol}} + \sigma_{il}^{\text{pol}}K_{jl} + \tau^{-1}\left(G_0\delta_{ij} - \sigma_{ij}^{\text{pol}}\right) \quad (6.6)$$

where $\tau = \zeta/(4kT\lambda)$ is the relaxation time, and $G_0 = N_D\lambda/V$ is the transient modulus, of the system. This is a differential constitutive equation, which can also be cast into an integral form resembling equation (5.6); it is, for historical reasons, often called the “upper convected Maxwell model”.

It is a good exercise to show that, in uniaxial extension, the dumbell model is unstable for $\dot{\epsilon}\tau > 1/2$. The harmonic spring force, in that case, is not enough to restrain the exponential separation of the beads, and the stress diverges. The cure for this is to make the springs stiffer at high extensions so that the particles cannot separate indefinitely. In steady shear ($K_{ij} = \dot{\gamma}\delta_{ix}\delta_{jy}$) this problem does not arise; solving the dumbell model gives sensible results for the polymer shear stress ($\sigma_{xy} = \dot{\gamma}G_0\tau$) and also for the normal stresses ($N_1 = 2G_0(\dot{\gamma}\tau)^2$ and $N_2 = 0$).

6.2 Scalarisation

It is notable, for the dumbell model, that if we introduce a time-dependent simple shearing so that $K_{ij} = \dot{\gamma}(t)\delta_{ix}\delta_{jy}$, the equation for the polymer shear stress $\sigma_{xy}^{\text{pol}} \equiv \sigma(t)$ decouples as

$$\dot{\sigma} = G_0\dot{\gamma}(t) - \sigma/\tau. \quad (6.7)$$

The first term on the right is stretching by the flow and the second is regression towards an equilibrium, isotropic distribution of dumbells. The general solution of this equation is

$$\sigma(t) = \int_{-\infty}^t G(t-t')\dot{\gamma}(t')dt' \quad (6.8)$$

where $G(t) = G_0 \exp(-t/\tau)$. This is simply the linear Maxwell model, although note that within the dumbell picture, it applies for large strain rates as well as small ones. In the present context, it represents an fully dumber-down, scalarised constitutive equation for polymers under nonlinear shear.

7 What rheologists want

For each system, rheologists want a constitutive equation giving the present stress as a functional of the strain rate history:

$$\sigma_{ij}(t) = \mathcal{F}_{ij}[K_{lm}(t' < t)] \quad (7.1)$$

or *vice versa*. The challenge to physicists is to create constitutive equations based on statistical mechanics or other mechanistic foundations, not just made up out of thin air to fit the data. This is a hard problem. The remainder of these lectures addresses the issue for certain types of nonergodic or glassy materials. For the most part we adopt a dumbed-down, scalarised approach but point to places where the full tensorial glory of nonlinear rheology might be restored with suitable further assumptions.

8 Rheology of soft glasses

Many soft materials, including foams, dense emulsions, slurries, pastes, and textured morphologies of liquid crystals, are characterised by the presence of structural disorder on a mesoscopic (nanometre to micron) scale, causing metastability and slow dynamical evolution. Such materials are not ergodic, and can therefore be viewed, in at least one sense, as glasses.

8.1 The effective temperature problem

Rough estimates of the energy scale for mesoscopic rearrangements ΔE in these materials typically give $\Delta E \gg kT$ (often by a factor of hundreds *e.g.*, for rearrangement of bubbles in a foam). And yet, somewhat surprisingly, it appears that such systems are not *completely* frozen but exhibit slow, aging dynamics. It is not yet clear what is the origin of this remaining motion. In many cases (*e.g.* foams) it is impossible to completely prevent “extrinsic” processes such as a gradual coarsening of the structure by coalescence, or drainage under gravity. Gravity also causes slow settlement in colloids, pastes etc. It could be that, so long as these extraneous processes are present, they inject enough noise into the system to excite spontaneous relaxation dynamics for mesoscopic stresses. It could also be that naive estimates of rearrangement energy are too high since they do not account for the full complexity of the free energy landscape. Or it may be that, on preparation of a sample of soft matter (*e.g.*, loading it into a rheometer) enough stored energy is injected into mesoscopic degrees of freedom that, despite the apparently large energy scale, genuinely thermal processes are then sufficient to nucleate a slow downhill evolution in energy over a prolonged aging period. This last scenario resembles the “marginal dynamics” of spin-glasses [17] where a quench to very low temperature leads to aging dynamics characterised by a higher “effective temperature”, close to that of the glass transition. Perhaps different combinations of these three factors apply in different cases.

In any case, empirically it is possible to explain many of the rheological properties of soft glasses by assuming that there is some sort of effective temperature $kT_{\text{eff}} = x$, chosen lie somewhere near a glass transition point.

A tempting but problematic idea is to suppose that the noise associated with x , in a rheological experiment, in fact arises from the imposition of flow itself. This will not do, since x would then vanish in any small-amplitude, linear response regime.

In what follows we shall treat x as a constant that may depend on sample preparation, but does not depend on the stresses and strains to which a material is subjected. As we shall see, this simplified approach leads generically to shear-thinning behaviour. It is easy to modify it at the expense of introducing extra parameters into the model; such changes were recently introduced to describe shear thickening and jamming effects; see Section 11.

8.2 Phenomenology

The rheological phenomenology of many nonergodic soft materials is similar. In shear-thinning materials, data for the steady state flow curve are very often fitted either to (a) the ‘‘Herschel-Bulkley’’ form:

$$\sigma(\dot{\gamma}) - \sigma_Y \sim \dot{\gamma}^p \quad (8.1)$$

where $\sigma_Y > 0$ is a yield stress and $0 < p < 1$; or (b) to the ‘‘power law fluid’’ form which is the same except $\sigma_Y = 0$. A survey of edible soft matter [9] lists a very large number of instances of such fits in the literature. The linear spectra are also often close to either (a) the anomalous class of a flat or rising G'' at low frequencies discussed in Section 3.4.3; or (b) power law fluid behaviour as defined in Section 3.4.2. For nice examples of the former, see work on dense emulsions [18], though in fact there are many other such examples in the literature. Of course, more complicated behaviours (including shear-thickening and various kinds of kink in the flow curve) are also often seen, but the above characteristics are generic enough that we may plausibly seek a common explanation for them in terms of glassy dynamics.

8.3 Bouchaud’s trap model

Possibly the simplest model of glasses was introduced by Bouchaud [19]. By a mathematical trick, this reduces the glass transition to an effective one-body problem. Or rather, Bouchaud identified the existence of a one-body problem that could show a glass transition: which is somewhat amazing, since we all know that glass transitions are intrinsically co-operative. Fortunately, many dynamical properties of this simplified model seem to be fairly faithful to the ‘‘real’’ glass transition, at least in spin-glasses. Its relevance to structural glasses (including soft ones) is less clear, though.

The trap model considers an ensemble of independent particles moving by activated hopping between traps. Each trap is uncorrelated with the next. There is a distribution of barrier heights $\rho(E)$; it is best to think of the tops of all the barriers being at the same height, in which case $\rho(E)$ is also a distribution of trap *depths*. The dynamics chosen is activated hopping with a jump rate out of a trap $\Gamma_0 \exp[-E/x]$ where we have introduced the effective temperature x (discussed above). These dynamics define the equation of motion for a probability distribution $P(E, t)$ of traps occupied:

$$\dot{P}(E, t) = -\Gamma_0 e^{-E/x} P(E, t) + \Gamma(t) \rho(E) \quad (8.2)$$

where the first term on the right is escape from, and the second is jumping into, traps of energy E . Since jumps are uncorrelated, the latter is a product of the total jump rate $\Gamma(t) = \langle \Gamma_0 \exp[-E/x] \rangle_P$ (in an obvious notation) and the prior distribution of trap depths $\rho(E)$.

Bouchaud showed that if we choose $\rho(E) \sim \exp[-E/x_g]$ for large E , then $x = x_g$ represents a glass transition: the system is ergodic for $x > x_g$ and nonergodic for $x < x_g$. This exponential choice of $\rho(E)$ may appear restrictive, but in the present context it should be viewed, not as a further assumption, but as an intrinsic part of the recipe for creating a one-body model of the glass transition.

In what follows, we set $x_g = 1$ which amounts to using the mean trap depth as the scale of energy. In this case one finds that for $x > 1$, the distribution $P(E, t)$ evolves under equation (8.2) to a unique (Boltzmann) equilibrium state, $P_e(E) \sim \rho(E) \exp[E/x]$. The corresponding hop time $\tau = \exp[E/x]/\Gamma_0$ is distributed with a probability (setting $\Gamma_0 = 1$ as the time unit)

$$p(\tau) = (x - 1) \tau^{-x} \quad (8.3)$$

thus leading generically to power law relaxation.

However, the Boltzmann result has $P_e \sim \rho(E) \exp[E/x]$ which cannot extend to $x < 1$ since it ceases to be normalisable. Instead, one finds there is no steady state; the system evolves forever into deeper and deeper traps. This behaviour, in which the system is not localized in phase space but not ergodic either, was called “weak ergodicity breaking” by Bouchaud [19]. It leads naturally to aging behaviour. This is shown in Figure 7 where the evolution of the lifetime distribution $p(\tau)$ is shown above and below the glass transition (following a quench from high temperature). In the first case there is *transient* behaviour: one must wait a long time for the deepest traps to become populated, but the shallow part of the distribution converges rapidly to the equilibrium state and stays there. In the aging case, the shallow traps are continuously depleted as time proceeds and weight shifts forever into deeper and deeper traps.

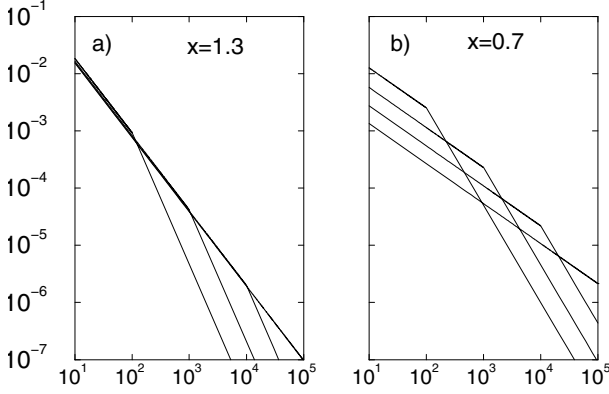


Fig. 7. Evolution of $p(\tau)$ above and below the glass transition in Bouchaud's model [20]. Curves lie in the order of increasing time at the bottom of each figure.

9 The SGR model

To extend Bouchaud's model to rheology [21,22] we need to give it a spatial structure and say how the activated dynamics couples to flow. Instead of particles in traps, we associate the wells with locally harmonic mesoscopic degrees of freedom. The stored elastic energy in each of these “mesoscopic elements” is $kl^2/2$, where k is an elastic constant (presumed uniform for simplicity, and not to be confused with Boltzmann's constant) and l is a local shear strain. We argue that the stored energy can be used to overcome the barrier, whose height is now $E - kl^2/2$; thus we have a jump rate $\Gamma_0 \exp[-(E - kl^2/2)/x]$ which depends on the local state of strain. Jumps can be viewed, with equal validity, as strain-assisted (quasi-)thermal hopping, or as noise-assisted local yield. We assume affine deformation between jump events (identified as local rearrangements) so that $\dot{l} = \dot{\gamma}$ except for when a jump occurs, at which point l is reset to zero and E selected afresh from $\rho(E)$. The model is summarised in Figure 8.

This gives the following equation of motion for the probability distribution of elements with intrinsic barrier heights E and local strains l :

$$\dot{P}(E, l, t) = -\dot{\gamma} \partial P / \partial l - \Gamma_0 e^{-(E - kl^2/2)/x} P(E, l, t) + \Gamma(t) \rho(E) \delta(l) \quad (9.1)$$

where the first term on the right is from the affine deformation of local elements between jumps, and the remaining two terms have the same interpretation as in equation (8.2). To complete the specification of the SGR model we must give an equation for the macroscopic stress; we consider only

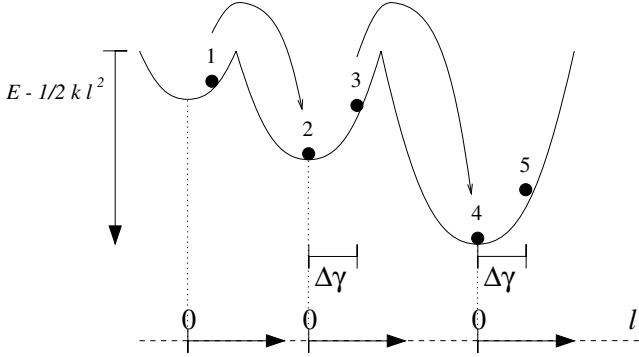


Fig. 8. Dynamics of the SGR model. A representative particle (1) may hop out of its trap by activated hopping ($1 \rightarrow 2$). It enters a new trap in a state of zero local strain $l = 0$; application of strain $\Delta\gamma$ raises its energy ($2 \rightarrow 3$) making a subsequent hop ($3 \rightarrow 4$) more likely. Note that hopping is effectively in infinite dimensions (rather than one, as drawn); there is no correlation in E between one hop and the next. From [20].

shear stress σ , and write

$$\sigma = k\langle l \rangle_P \quad (9.2)$$

which is the macroscopic average of the stresses in mesoscopic elements.

9.1 Features of the model

The physics of the model is dominated by the large- E tail of the trap distribution. For example in steady flow, much of the stress is contributed by mesoscopic elements whose E value (recall that this represents a local yield energy) is far above average. These acquire large mesoscopic strains, which perhaps justifies use of the word “soft” in the name “soft glassy rheology model” or SGR model.

When $\dot{\gamma} = 0$, the model reduces to that of Bouchaud and hence shows weak ergodicity breaking for $x < 1$. However, it is easily established from equation (9.1) that *flow interrupts aging*: ergodicity is restored with a normalisable steady-state distribution $P_{\dot{\gamma}}(E, l)$ whenever one imposes a steady $\dot{\gamma} > 0$. The form found for the E dependence is $P(E) \sim \rho(E) \exp \times [E/x](E/E^*)$ where $E^* \sim x \ln[x^{1/2}/\dot{\gamma}]$. This contrasts with the static case where the same form applies but with E^* , the characteristic depth of wells occupied, a slowly evolving function of time (giving aging behaviour).

Steady-state flow curves $\sigma(\dot{\gamma})$ are readily found from equation (9.1) and shown in Figure 9. One finds $\sigma \sim \dot{\gamma}$ for $x > 2$ (quasi-Newtonian); a power

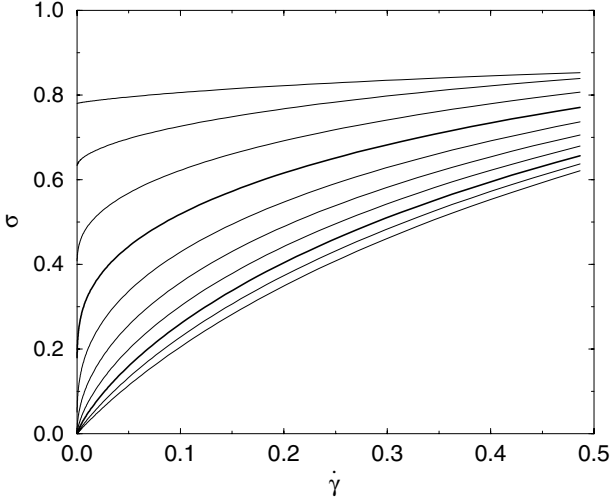


Fig. 9. Flow curves for the SGR model, with x decreasing bottom to top. The bold lines are for $x = 2$ and $x = 1$; the latter shows a yield stress as do all curves with $x < 1$. (Courtesy of D. Head.)

law fluid with $\sigma \sim \dot{\gamma}^{x-1}$ for $1 < x < 2$; and Herschel-Bulkley behaviour (Eq. (8.1) with $p = 1 - x$) for $x < 1$. Note that onset of the glass phase at $x = 1$ coincides with the first appearance of a yield stress (and hence of a static elastic modulus). But the viscosity diverges, as x is decreased, at the higher threshold of $x = 2$. The region in between is the power-law fluid described previously.

Given that each mesoscopic element behaves elastically during its own lifetime, the *linear* rheology (in which the flow is too weak to affect the lifetimes) can be read off from equation (8.3):

$$G(t) = \int p(\tau) e^{-t/\tau} d\tau; \quad G^*(\omega) = \int p(\tau) \frac{i\omega\tau}{1 + i\omega\tau} d\tau \quad (9.3)$$

which yields $G'(\omega) \sim \omega^2$ (respectively $\sim \omega^{x-1}$) for $x > 3$ (resp. $1 < x < 3$), and $G''(\omega) \sim \omega$ (resp. $\sim \omega^{x-1}$) for $x > 2$ (resp. $1 < x < 2$). In other words, the model shows newtonian behaviour at $x > 3$; quasi-Newtonian behaviour except for an anomalous power law in the storage modulus for $2 < x < 3$; and power-law fluid behaviour for $1 < x < 2$. The linear rheology for $x < 1$ (in the glass phase) cannot, however, be addressed without a detailed discussion of aging effects (see Sect. 10 below).

9.2 Constitutive equation for SGR

Regardless of x , the evolution dynamics of equation (9.1) and the stress formula equation (9.2) imply, without further assumption, a definite nonlinear constitutive equation for the model [22]. Since only shear stress was considered, this is a “dumbed down” scalar constitutive equation along the lines of equation (6.8); it gives the shear stress at time t in terms of the preceding shear strain history $\gamma(t' < t)$. To save writing, we now set $k = \Gamma_0 = 1$.

We imagine that at the zero of time the sample is prepared in a known state that has, for simplicity, all mesoscopic elements unstrained (this assumption could be relaxed, but saves writing). This state is characterised by $P(E, l, 0) = P_0(E)\delta(l)$. The constitutive equation then reads

$$\sigma(t) = G_0(z_{t0})\gamma(t) + \int_0^{t'} dt' \Gamma(t') G_1(z_{tt'}) [\gamma(t) - \gamma(t')] . \quad (9.4)$$

Here $G_0(z_{t0})$ is the fraction of elements present originally (at $t = 0$) surviving to time $t > 0$. The factor $\gamma(t)$ (in the chosen units) is the stress they contribute. The integral is over elements created at $t' < t$, with creation rate $\Gamma(t')$ and survival probability $G_1(z_{tt'})$ to time t ; each has been strained through $\gamma(t) - \gamma(t')$ and contributes stress accordingly. Note that this equation has a broadly similar “birth and death” structure to the one for the tube model, equation (5.6). The following equations complete the prescription [22]:

$$1 = G_0(z_{t0}) + \int_0^{t'} dt' \Gamma(t') G_1(z_{tt'}) \quad (9.5)$$

$$z_{tt'} = \int_{t'}^t dt'' \exp [(\gamma(t'') - \gamma(t'))^2 / 2x] \quad (9.6)$$

$$G_0(z) = \left\langle e^{-z/\tau} \right\rangle_{P_0} ; \quad G_1(z) = \left\langle e^{-z/\tau} \right\rangle_{\rho} . \quad (9.7)$$

Equation (9.5) fixes, by normalisation, the jump rate $\Gamma(t')$ required in equation (9.4). Equation (9.6) defines a “effective time interval” z between times t and t' ; this is defined in such a way as to absorb the factor by which the jump rate out of a well is enhanced due to the presence of a strain. In other words, within this model, the nonlinear effect of shear can be viewed as “making the clock tick faster” for any element that has accumulated nonzero value of the local strain l since its creation. Indeed, this is the *only* nonlinearity, which is why equation (9.7) defines the survival functions for each class of element exactly as one would in Bouchaud’s model, except that z replaces t .

As an example of this last point, it is instructive to consider the response to a finite step strain of size γ (for simplicity at $t = 0$). Here one has $\sigma(t) = \gamma G_0(z(t, 0)) = \gamma G_0(\exp[\gamma^2/2x]t)$ where the exponential factor enhances all jump rates equally (recall we have set $k = 1$). This has the interesting consequence that the $\sigma(t)$ curves for large and small stresses actually cross at late times, *i.e.*, $\sigma(t)$ is nonmonotonic in the strain amplitude γ . These predictions [22] so far remain untested by experiment.

9.3 Tensorial SGR models

The structure and interpretation of the scalarised SGR constitutive equation, equation (9.4), allow one easily to construct various tensorial descriptions based on the same underlying physics, but with more specific assumptions about the local elastic and yield behaviour of the mesoscopic elements. We present this here for an entirely schematic SGR-dumbell model, utilizing the ideas of Section 6.1. A somewhat more realistic tensorialisation, specifically adapted to describe the case of foams and dense emulsions, has also been proposed recently [23].

We consider an ensemble of dumbell-like objects, somewhat different from those of Section 6.1. Each dumbell is characterised by an end-to-end vector u_i ; the stress contributed by such dumbells is deemed to be $\sigma_{ij} = nk\langle u_i u_j \rangle_P$ where the average is over some distribution function $P(E, u_i, t)$; n is the density of dumbells and k an elastic constant. SGR-like dynamics is introduced by assuming that each dumbell follows the flow affinely, except that from time to time it makes a jump to a completely new configuration, with a jump rate $\Gamma_0 \exp[-(E - ku_i u_i/2)/x]$. Here E is an energy barrier which is lowered by the stored elastic energy $ku_i u_i/2$. (You can imagine the dumbells as hooked into a network of neighbours, which deforms affinely; but when a particular dumbell becomes too elongated, the connections will break.) After a jump, the dumbell is assigned a new yield energy E drawn from the usual prior $\rho(E) = e^{-E}$. It is also assigned at random a new value of u_i , drawn from the equilibrium distribution at noise temperature x , $p_e(u_i) \sim \exp[-u_i u_i/3x]$ (where we have chosen the root mean square length of the dumbell $\langle u_i u_i \rangle_e$ as the unit of length).

The resulting equation of motion, closely analogous to equation (9.1), is

$$\dot{P}(E, u_i, t) = -K_{jk} u_j \partial P / \partial u_k - \Gamma_0 e^{-(E - ku_i u_i/2)/x} P + \Gamma(t) \rho(E) p_e(u_i) \quad (9.8)$$

with $\Gamma(t) = \Gamma_0 \langle \exp[-(E - ku_i u_i/2)/x] \rangle_P$ the total jump rate. A new feature is the appearance of $p_e(u_i)$ in the last term to replace $\delta(l)$ in the scalar SGR model: this is the closest we can get to the assumption, made there, of “zero strain” in local elements without actually setting u_i to zero (in which case every dumbell would collapse to a point and never be stretched under

the affine flow). The above choice will recover Boltzmann equilibrium for the u_i (at temperature x) in the absence of flow, which is not true of the scalar model: but it is a moot point whether this *should* be recovered, since x is not a true temperature. An alternative choice would be to use $4\pi p_e = \delta((u_i u_i)^{1/2} - 1)$, corresponding to a selection of new dumbbells with random directions on the unit sphere.

Now assume that at time zero a system is prepared by some definite process (*e.g.* a quench) that gives a known initial distribution of dumbbell barrier heights and unit vectors $P(E, u_i) = P_0(E)p_0(u_i)$ (chosen factorable for simplicity). Then, following the same arguments as lead to equation (9.4), the constitutive equation can be written

$$\begin{aligned} \sigma_{lm}(t) = & \left\langle G_0(z_{t0}(u_i)) E_{lk}^{t0} u_k E_{mj}^{t0} u_j \right\rangle_{p_0} \\ & + \int_0^{t'} dt' \left\langle G_1(z_{t0}(u_i)) E_{lk}^{tt'} u_k E_{mj}^{tt'} u_j \right\rangle_{p_e}. \end{aligned} \quad (9.9)$$

Here G_0, G_1 are precisely as defined in equations (9.7); the total jump rate $\Gamma(t)$ is found from

$$1 = \langle G_0(z_{t0}(u_i)) \rangle_{p_0} + \int_0^{t'} dt' \Gamma(t') \langle G_1(z_{tt'}(u_i)) \rangle_{p_e} \quad (9.10)$$

and the “effective time” variable z , which is now explicitly dependent on the end-to-end vector u_i with which an element was created, obeys

$$z_{tt'}(u_i) = \int_{t'}^t dt'' \exp \left[E_{kl}^{tt'} u_l E_{km}^{tt'} u_m / 2x \right]. \quad (9.11)$$

The above constitutive equation involves, as well as a tensorial dependence of the elastic stress and of the yield energy, an extra layer of averaging over the u_i variables describing the end-to-end vectors with which dumbbells were created after their most recent jump. Arguably though, this extra averaging involved ought to be redundant, given that the basic elements of the SGR picture are not individual molecules or particles (as the dumbbell idea tacitly assumes) but mesoscopic elements. One could hope for a reasonably adequate description in which such elements have a distribution of yield energies E but otherwise are taken as isotropic bodies with a well-behaved, deterministic elastic response (possibly nonlinear): no averaging over u_i would be necessary if we replaced our dumbbells with elastic spheres, for example. The general structure of the constitutive equations then would be:

$$\sigma_{lm}(t) = G_0(z_{t0}) Q_{lm}(E_{ij}^{t0}) + \int_0^{t'} dt' \Gamma(t') G_1(z_{tt'}) Q_{lm}(E_{ij}^{tt'}) \quad (9.12)$$

$$z_{tt'} = \int_{t'}^t dt'' \exp \left[R(E_{ij}^{tt'})/x \right] \quad (9.13)$$

with G_0, G_1 and $\Gamma(t)$ obeying equations ((9.7), (9.5)). Here Q_{lm} and R are tensor and scalar functions of E_{ij} that can be freely chosen, in principle; suitable choices for foams and dense emulsions are suggested in [23].

By construction, these tensorial models are guaranteed to behave extremely like the scalar SGR model (with glass transition at $x = 1$, aging and power-law fluid regimes etc.), while at the same time describing nontrivial normal stress effects under shear flow and, for the first time, the behaviour of a soft glassy material in extensional flow. They represent a “smartening up” of the scalar SGR model, and hopefully will make it interesting to a wider range of rheologists.

10 Rheological aging

Let us now turn finally to the problem of describing the rheological behaviour of a material which is nonergodic at rest. For notational and conceptual simplicity we revert to a “scalarised” description in which the flow is described by a shear rate $\dot{\gamma}(t)$ and the stress by a shear stress, $\sigma(t)$. We follow the presentation of [20].

10.1 Step stress and step strain

We start by restating our remarks about the stress response of a system to a step strain, but now making no assumption about time-translational invariance (TTI) of the material properties. Suppose the sample is prepared in some known state at time $t = 0$ and then left unstrained until time $t = t_w$ (the “waiting time”) when a step strain of amplitude γ is applied. Then we may write

$$\sigma(t) = \gamma G(t - t_w, t_w; \gamma) \quad (10.1)$$

where the dependence of G on all three arguments maintains complete generality. If the response is linear, we may set the γ argument to zero; and if it is time translation invariant, we may omit the second time argument. (If it is both of these things, we recover $\sigma = G(t - t_w)\gamma$, in agreement with Eq. (3.1).) Likewise, we can consider a creep measurement (strain response to a step stress of size σ at $t = t_w$) in which

$$\gamma(t) = \sigma J(t - t_w, t_w; \sigma) \quad (10.2)$$

where again the last argument can be suppressed in a linear system; the second time argument suppressed in a TTI system; and both suppressed when both conditions apply.

10.2 Oscillatory flows

Things are messier when we turn to an oscillatory shear test; this is, nonetheless, so important a part of experimental rheology that we cannot ignore it. Again we prepare the sample at time $t = 0$, but now switch on at t_s (the “start time”) an oscillatory strain: $\gamma(t) = \theta(t - t_s)\gamma e^{i\omega t}$ where γ is generally complex (this allows us to choose the point in the phase cycle at which the oscillation begins). Let us assume that the material responds linearly. This may be a dangerous assumption for nonergodic materials, but can be checked simply by varying the amplitude; it is reported experimentally that a linear regime does exist in very many nonergodic soft materials. If so we can represent the oscillation as a superposition of infinitesimal step strains (a decomposition that does not require TTI):

$$\sigma(t) = G^*(\omega, t, t_s)\gamma(t) \quad (10.3)$$

$$G^*(\omega, t, t_s) = i\omega \int_{t_s}^t e^{-i\omega(t-t')} G(t-t', t') dt' + e^{-i\omega(t-t_s)} G(t-t_s, t_s). \quad (10.4)$$

The second term on the right arises from the finite step strain with which, in mid-cycle, the oscillation begins (unless the phase is chosen carefully to make this term vanish). An exactly analagous definition can be used to define a complex compliance $J^*(\omega, t, t_s)$.

10.3 AOFOT?

The linear complex modulus $G^*(\omega, t, t_s)$ (likewise J^*) is seen to have two time arguments, alongside frequency. In a system with TTI, steady state should be reached when both $\omega(t - t_s) \gg 1$ and $\omega t_s \gg 1$; this steady state should then be independent of t_s , so that a well-defined $G^*(\omega)$ is recovered. One can hope for a *partial* simplification along these lines even without TTI. If $\omega(t - t_s) \gg 1$ and $\omega t_s \gg 1$, so that many cycles have been performed, and any transient associated with the initial step has died away, then it is reasonable to hope that the t_s argument is redundant, so that $G^*(\omega, t, t_s) \simeq G^*(\omega, t)$. In other words, one has a fairly stable viscoelastic spectrum, measurable by experiment, but one which retains a relatively slow time evolution or drift, on timescales much longer than the period of oscillation.

If this is the case, and the same applies to J^* , it is reasonable to conjecture that, just as in a TTI system, $G^*(\omega, t)J^*(\omega, t) = 1$. One may also hope that $G^*(\omega, t)$ can be found from the step strain response by fourier transforming on the first (time interval) argument of the latter quantity: $G^*(\omega, t) = i\omega \int_0^\infty e^{-i\omega t'} G(t', t) dt'$, with a similar relation between $J^*(\omega, t)$

and $J(t', t)$. In other words, one can hope that, under favorable conditions, the age dependence (t -dependence) of all four quantities G, G^*, J, J^* is slow enough that, within some window of time near a given age, an effective form of TTI is recovered. In that case, just as with the corresponding four linear response functions in equilibrium systems, “any one fixes the other three” (written “AOFOT” for short).

The crux is then to decide what are the “favorable” conditions under which AOFOT holds. Fielding *et al.* [20] make the conjecture that AOFOT holds, under the conditions on ω, t_s stated above, in systems with *weak long term memory*. As shown in the same paper, AOFOT is rather well obeyed in the SGR model, which does satisfy this criterion. However, a general proof is lacking.

10.4 Weak long term memory

A system is said to show long term memory if (in rheological language) its linear stress relaxation modulus obeys

$$\lim_{t \rightarrow \infty} G(t - t_w, t_w) \neq \lim_{t \rightarrow \infty} \lim_{t_w \rightarrow \infty} G(t - t_w, t_w). \quad (10.5)$$

Following a step strain, the left hand side of the inequality gives the final value of the residual stress after all stresses that can ever relax have done so. But on the right hand side, stresses whose relaxation time diverges with the waiting time t_w also contribute to the residual stress. Hence, if there are relaxation processes whose lifetimes diverge with the system age t_w , the two limits will not be the same.

Long term memory is described as “weak” if, despite equation (10.5) holding,

$$\lim_{t \rightarrow \infty} [G(t - t_0, t_0) - G(t - t_1, t_1)] = 0. \quad (10.6)$$

This quantity is the asymptotic long-time stress response to a small strain that is switched on at time $t = t_0$ and off again at t_1 . If it is zero, then any weak perturbation, maintained for a *finite* interval $t_1 - t_0$, is eventually forgotten. According to this definition, the SGR model exhibits weak long term memory [20].

If equation (10.6) is not obeyed, the long term memory is strong. Conventional rheological study of materials with strong long-term memory is a somewhat difficult task: these systems remember, forever, every detail of what happened to them previously. While it is clear that foams, pastes etc. are capable of remembering for extremely long periods certain *strong* perturbations (such as *e.g.* the intimate mixing process which resulted in a foam being formed originally), we must hope that they do not remember weak ones. Materials with strong long term memory have been dubbed “Funeous matter” (I think by Denis Weaire). This commemorates a fictional

character in a Jorge Luis Borges story called “Funes”, who “was not very capable of thought” because of his inability to forget anything at all [24].

10.5 The G'' problem

In Section 3.4.3, the anomalous behaviour of G'' at low frequencies, in many soft nonergodic materials, was mentioned. In particular, it was explained there that a rising trend in the loss modulus upon lowering frequency is generally not allowed in systems with TTI; seeing such a trend leads one naturally to expect a loss peak at still lower frequencies.

In aging materials, without TTI, this need not be true. The lowest frequency accessible is inversely proportional to the system age: $\omega t \leq 1$. If, in effect, the longest relaxation time τ_r of the material is directly proportional to age (this is called “full aging” and is the behaviour found in the SGR model), then it is impossible to reach the low frequency limit, as usually defined: $\omega \tau_r \ll 1$. Whereas (as mentioned in Sect. 3.4.3) the data for some soft nonergodic materials resembles the right hand half of Figure 4, this does not mean that there actually is a loss peak at lower frequencies; for the left hand half of the figure does not exist, even in principle.

Figure 10 illustrates this effect by showing low frequency viscoelastic response for the SGR model in its glass phase. The complex modulus is defined formally through equation (10.4) but is plotted, for various system ages t , under conditions $\omega(t - t_s) \gg 1$ where the dependence on t_s has faded away. Aging has relatively little effect on G' , but has the effect of moving the G'' curve steadily leftward, while maintaining its slope (which depends on x , not age). This drift is as if there was indeed a loss peak, but one with $\tau_r \sim t$. Such scaling means that, however long one waits to perform the experiment, the peak will not be seen. There is no pot of gold at the end of the rainbow.

It would be wise to suspect nonergodicity, aging and a breakdown of TTI in any experimental system where (a) a flat or rising curve in G'' is seen at low frequency; and (b) there is no *obvious* candidate mechanism for a loss peak at frequencies below those studied. But of course, the real test is to see whether the behaviour, particularly G'' , has a discernable dependence on the age of the sample.

10.6 Aging scenarios

Consider the linear step-strain response function $G(t - t_w, t_w)$. In the simplest scenario, called full aging and exemplified by SGR, one has

$$G(t - t_w, t_w) = \mathcal{G}\left(\frac{t - t_w}{\tau(t_w)}\right) \quad (10.7)$$

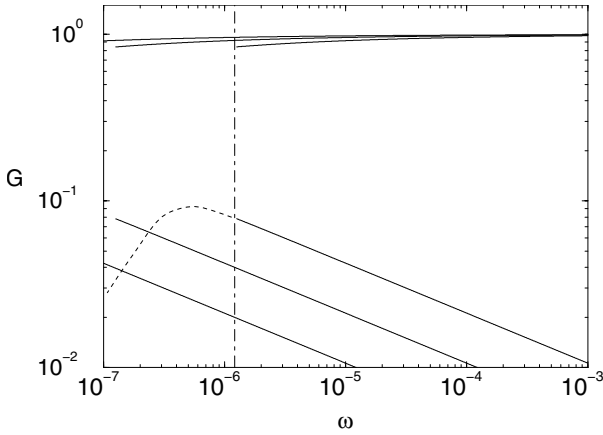


Fig. 10. Viscoelastic spectra of the SGR model for $x = 0.7$; the ages of the sample increase by one decade between each curve and the next, moving leftward. A fictitious loss peak is shown (dashed) for the youngest sample; extending the frequency window to “see the peak” results in aging and hence a different curve. The elastic modulus G_0 is unity. From [20].

with an effective relaxation time proportional to age: $\tau(t_w) \sim t_w$. The expected behaviour is then as in Figure 10. But other scenarios are possible [25], for example that $\tau(t'_w) \sim t_w^\mu$ where $\mu \neq 1$. For $\mu < 1$, the system is called “sub-aging” and, in this case, a loss peak in G'' should eventually appear, if one is patient. The case $\mu > 1$ is called “super-aging” and means that, even if the frequency axis in a $G^*(\omega)$ plot is scaled by the system age t , the loss modulus G'' decreases forever as the system gets older. It is not clear yet which scenario best represents experiment in the linear regime [26–30].

Under relatively general conditions [31] one can show that

$$G(t - t_w, t_w) = \sum_i \mathcal{G}_i [h_i(t)/h_i(t_w)] \quad (10.8)$$

of which the preceding examples are special cases. In fact, a more complicated form of this kind seems to be needed right at the glass transition in SGR, where logarithmic corrections emerge. The results for $G(t - t_w, t_w)$ for noise temperatures x above, at and below the glass transition can be found in [20], and show that equation (10.7) applies asymptotically at late times and large t_w both above and below the transition, but with τ independent of t_w in the first case and linear in t_w in the second. Right at the transition ($x = 1$) neither fit is correct. The corresponding plots of $G^*(\omega, t)$ are shown in Figure 11 where the same effect is observable in the data for $x = 1$.

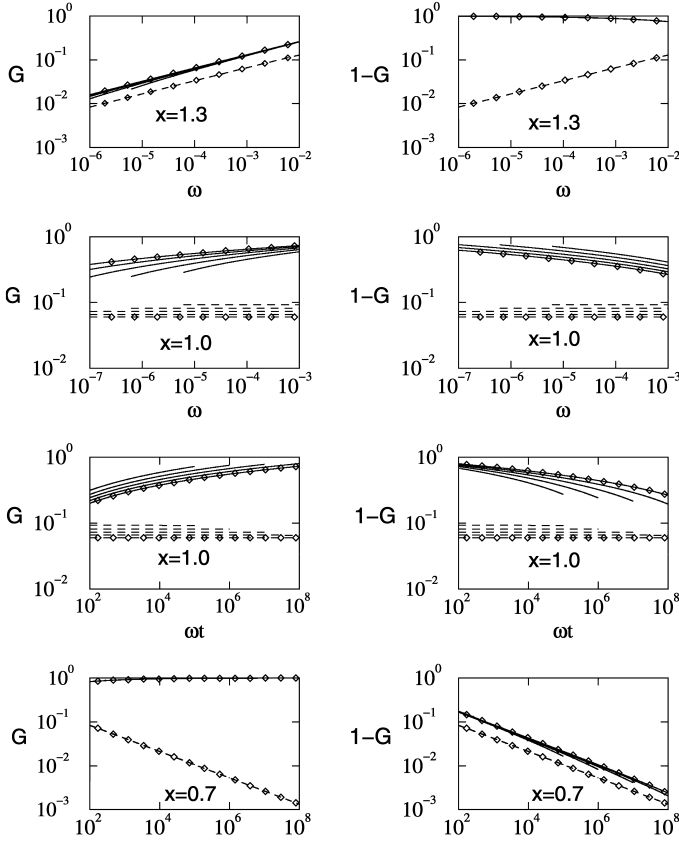


Fig. 11. Relaxation spectra $G'(\omega, t)$ (solid) and $G''(\omega, t)$ (dashed) for systems aged $t_s = 10^{7 \dots 11}$ found for the SGR model at various x . The left column shows G', G'' and the right column $1 - G', G''$; all plots are log-log. The top four panels use scaling that should lead to data collapse in a TTI system, the bottom four use scaling appropriate to full aging. Data for $x = 1$ (the glass point) is shown in both representations (middle four panels) and does not fit either scaling due to logarithmic corrections. (We are using units where $k = \Gamma_0 = G_0 = 1.$) From [20].

10.7 Nonlinear aging

It is interesting to consider the effect of sample age on the nonlinear rheology. For example, one can consider the effect of starting up a steady shear flow at finite strain rate $\dot{\gamma}$ after the sample has been aged at rest (in the absence of any stress) for a period t_w . Measuring the stress as a function of $t - t_w$, or equivalently as a function of strain $\gamma = \dot{\gamma}(t - t_w)$, one gets a

“startup curve” which, within linear response, usually rises smoothly to a plateau from below. For larger $\dot{\gamma}$ there is often an overshoot. Interestingly, within the SGR model [20] the height of this overshoot is found to increase logarithmically with t_w . This reflects a gradual consolidation of the structure as it ages: mesoscopic elements acquire larger and larger yield energies as time proceeds. The reason for the overshoot is that one has to pull the elements over these barriers to initiate a flow; but once flow is initiated, ergodicity is restored so the final, steady-state stress is independent of t_w . These effects can be seen in Figure 12.

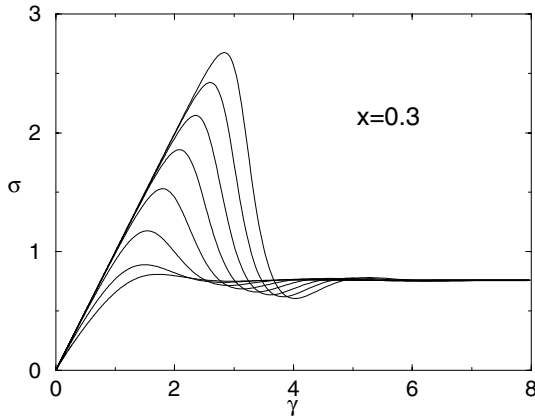


Fig. 12. Stress response in startup of steady shear in SGR model at $\dot{\gamma} = 0.001$. Curves from top to bottom correspond to increasing ages $t_w = 10^2, 10^3 \dots 10^9$. From [20].

Even more interesting is the effect of imposed stress on the aging process itself. We know that if a stress larger than the yield stress is applied, the resulting flow will ergodify the sample and end the aging process. But if a nonzero stress is applied that remains below the yield stress, the result is not obvious. A remarkable feature of the experimental data [27] (see also [26]) which the SGR model can so far not explain, is that the aging exponent μ (as defined following Eq. (10.7)) seems to depend in a nontrivial way on the stress applied during aging, with smaller exponents seen as the yield threshold is approached. Another, equally remarkable feature is that under conditions of finite amplitude *oscillatory* stress, certain aspects of the aging process can be enhanced, rather than impeded, by the application of modest stress [32]. An important conclusion of [32] is that aging cannot be understood in terms of the evolution of a single “effective” relaxation time, but must be considered as the effect of sample age on the entire distribution of relaxation processes (represented within SGR by $P(E, l)$) present in the

system. As well as rejuvenation (the erasure of aging by large amplitude strain), these authors showed that “over-aging”, as they called it, could be accounted for within the SGR modelling framework.

10.8 Ongoing work on aging and rheology

An important aspect of current research concerns the link between the relatively simple aging typified by concentrated pastes, and a somewhat different aging scenario explored in recent work on low density colloidal gels [33–35]. This scenario seems to involve a slow evolution of elastic inhomogeneities within the material, which may couple in some rather subtle way to gravity and other extraneous (possibly nonlinear) driving. This research links to a wider effort to relate the nonergodic properties of low density gels, in which the nonergodicity is caused by attractive forces between particles with energy scales of $5-15kT$, to generic theories of repulsive glasses (such as mode coupling theories) [36,37]. It remains to be seen whether simple models like SGR have much to offer this debate, although the work of [32] certainly suggests a range of new experiments that could be done. In any case, it would be very valuable to have a deeper modelling framework to study the interaction of aging processes with nonlinear rheological perturbations.

One avenue is to interpret the word “rheology” in a particularly liberal way [38] and study the effects of dissipative driving (though not actual flow) on an Ising p -spin model for which the static aging behaviour is relatively well understood [39]. One must of course be careful to consider the extent to which the imposed driving is really a good substitute for shearing; nonetheless, the results, if carefully interpreted, can help address important generic issues such as the existence of a yield stress in nonergodic soft materials [40].

11 Shear thickening and jamming

11.1 Nonmonotonic flow curves

All the materials discussed so far have been shear thinning: the flow curve $\sigma(\dot{\gamma})$ is bent downwards at high shear rates $\dot{\gamma}$ (see Fig. 9). In extreme cases, such as wormlike micelles (Fig. 5), the curve can be nonmonotonic, in which case the decreasing part is mechanically unstable [15]. Assuming that $d\sigma/d\dot{\gamma}$ becomes positive again at high flow rates (and a background solvent viscosity is enough to ensure this), then one can recover a steady state by the shear-banding mechanism [15]. This mechanism is somewhat akin to phase separation (though definitely more complicated!). By arranging layers of fast and slow-flowing material at a common stress (each from a stable part of the curve, having positive slope) with layer normals in the velocity gradient direction, one can satisfy the steady state conditions for

parallel plates moving at fixed relative velocity $L\dot{\gamma}$, where $\dot{\gamma}$, the imposed shear rate, represents a suitably weighted average over the layers. However, there is now an interface between layers, and this could become unstable in its own right; we ignore this here, and also ignore the possibly complex physics which decides the value of the common stress [15]. Assuming this common stress to be unique, the measured flow curve will then consist of two rising branches connected by a horizontal plateau; however, hysteresis is possible so that the plateau value is different depending on whether the flow curve is traversed by raising or lowering the shear rate; genuine bistability of the flow curve may arise in certain ranges of shear rate. These phenomena have been seen in various micellar systems (*e.g.* [41, 42]).

Shear thickening is the opposite tendency, where the flow curve bends upwards. But now it is possible in principle for it to bend over backwards into an S-shape (see Fig. 14 below). Once again, the part of curve with negative slope is unstable. As before, shear banding can restabilize the situation, but now with layers of material of high and low stress (each from a stable part of the curve) coexisting at a common shear rate. The macroscopic stress exerted on a moving rheometer plate is the weighted average across the bands, since these are now oriented with layer normals in the neutral direction. Similar remarks apply to the shape of the effective flow curve, except that this now contains a vertical segment. This corresponds to a scenario called “discontinuous shear thickening” which has been reported experimentally; as in the shear thinning case, an element of bistability and hysteresis appears to be present [43–45].

What happens if we make the shear thickening tendency even stronger? An intriguing possibility, called “full jamming” in [51], is that the flow curve returns to cross the vertical axis (see Fig. 14), creating a window of stress within which the flow rate is strictly zero. There are now some preliminary experimental reports of this [46], and below we outline models that show this behaviour.

Note that in neither the shear thickening nor the shear thinning case does the possible existence of shear bands guarantee a stable, steady flow; it is currently a question for experiment (in any particular system) whether steady banded flows exist or whether the result of steady applied stress or strain rate is an *unsteady* behaviour in the other.

11.2 Shear thickening mechanisms

The mechanism of shear thickening seems related to the so-called “dilatancy” of dry powders. As reported by Reynolds in 1885 [47], dry powders tend to expand in volume as they are being sheared, and can therefore only flow readily if they are in a container that allows expansion. Colloidal suspensions, where shear thickening is best studied, are lubricated by both

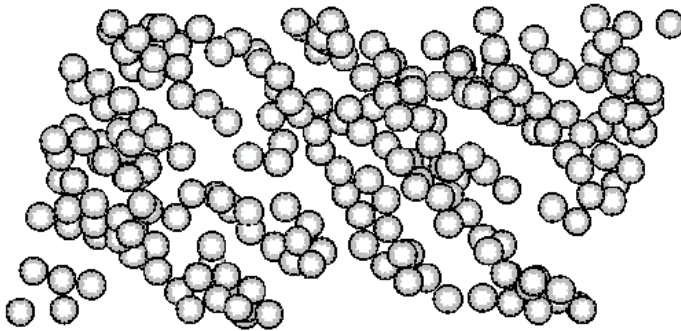


Fig. 13. Snapshot of a sheared 3D simulation of 2000 particles, 54% volume fraction, in simple shear. Only particles separated by less than 10^{-5} particle radii are shown. Courtesy J. Melrose.

Brownian motion and by a solvent; but the fact that the solvent is incompressible effectively confines the colloids to a fixed volume. The volumetric expansion which allows particles to jostle past each other is prevented, and, if the volume fraction is too high, stress-induced jamming can result.

At a more microscopic level, it appears that under shear the particles get jammed into “hydrodynamic clusters” or “force chains” that are roughly linear and aligned at about 45 degrees to the flow direction. This is shown in Figure 13 where the dynamics was simulated without Brownian motion; in its absence, the system becomes jammed up and unable to flow after a finite strain. This is connected with very large lubrication forces [48] and also is sensitive to the microscopic physics of particle-particle contacts [49]. If such behaviour were to arise in a system *with* Brownian motion, then there would be a good case for calling the arrested structure an anisotropic, stress-induced glass [50]. This assumes that, by the time arrest occurs, the thermodynamic forces between particles have taken over from hydrodynamic ones; if arrest is complete, this must be the case (since a static state cannot be maintained by viscous friction alone). But the idea could be questionable if the fully jammed state is subject to creep, which it might, as full jamming requires only that $\dot{\gamma} = 0$ in steady state. Hence, as discussed previously, sublinear creep in response to a steady shear stress is permitted. If particles were to get ever closer to touching at late times, in such a manner that a constant lubrication force were maintained, this could perhaps explain jamming without bringing in the idea of a stress-induced glass. With this caveat, though, it seems worthwhile to explore the link between jamming under shear and the static glass transition under stress.

11.3 Jamming SGR model

The SGR model is exclusively shear thinning, with a monotonic flow curve for all x (Fig. 9). Hence the preceding discussion about shear banding does not apply to it directly. However, at least in the scalar case, one can adapt the model, in a rather *ad-hoc* fashion, to describe shear thickening materials.

The simplest route is to declare that the noise temperature x is a decreasing function of the global shear stress: $x = x(\sigma)$ [51]. This results in the global jamming SGR model (GJSGR). Apart from this modification, all the equations of motion remain unaltered. The motivation for this is based on the idea that in shear thickening materials, stress can force particles into close proximity (*e.g.*, to form threadlike clusters [49] or “force chains” as seen in granular materials [52] and in Fig. 13). This will make local rearrangements more difficult, rather than less, at least for intermediate stresses, and is therefore antagonistic to the basic shear thinning tendency in SGR (which is for stored elastic energy to lower the activation threshold for rearrangement).

Depending on the form of $x(\sigma)$, a range of scenarios can be obtained. We have investigated cases where $x(0) > 1$ and $1 > x(\infty) > 0$, with a fairly abrupt drop at some intermediate stress. If the dependence is too weak (with only a small range for the x variation) the shear thinning SGR model is essentially recovered, but a stronger dependence gives, progressively, continuous and then discontinuous shear thickening. The model also predicts a “full jamming” regime in which a sufficient stress, applied to a material that at rest is an ergodic fluid. This happens so long as $x(\sigma)$ crosses the yield curve $\sigma_Y(x)$, in which case a range of stresses exists within which the static system self-consistently maintains itself at an effective temperature such that the given stress lies below the yield stress. These developments are explored further in [51].

12 Rheological instability and oscillation

An interesting variant of the jamming SGR model is described in [51, 53]. Suppose that instead of declaring the effective temperature x to be a function of the global stress σ , we choose a *local* dependence of x for a given element on its strain l . This defines the local jamming SGR model or LJSGR. An arbitrary dependence of this nature allows one to introduce an equally arbitrary dependence of jump rate on strain, parameterised as $\Gamma(l) = \Gamma_0 \exp[-(E - kl^2/2)/x(l)]$. If x decreases with l (saturating to finite limits at zero and infinite strain), then the jump rate has a maximum at intermediate strains, followed by a minimum, before rising again as $l \rightarrow \infty$.

At first sight one might expect similar effects to be found in the LJSGR model as for GJSGR. Interestingly though, this is not what happens.

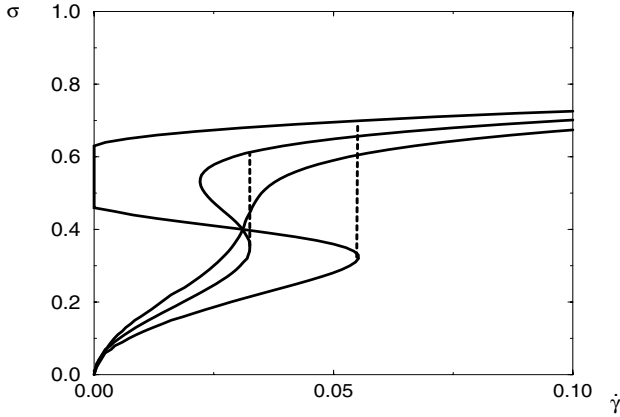


Fig. 14. Flow curves for the jamming SGR model, with various strengths of coupling between the global effective temperature x and the global stress σ . The curves evolve (lower to upper at right) from continuous shear thickening, *via* discontinuous shear thickening, to full jamming. Dashed vertical lines indicate the stability limit on increasing $\dot{\gamma}$. One expects discontinuous shear thickening at this point, or possibly before it. (Courtesy of D. Head.)

Instead [53] the LJSGR flow curve generally remains monotonic, so there is no sign of any shear-banding instability. Despite this, an instability of a different nature can arise at intermediate stresses: if the system is driven at fixed stress, the shear rate can undergo spontaneous oscillation. Note this oscillatory instability survives, in this model, even if the exponential prior $\rho(E)$ for mesoscopic yield energies is changed to a delta function $\rho(E) = \delta(E - E_0)$; in other words, it is not directly linked to the presence of glassiness in the model.

During one cycle of the oscillation, the strain distribution $P(l, t)$ (where there is no E dependence in the simplest variant of the model) changes from being unimodal to bimodal and back again. The period of the cycle corresponds, for most parameter values, to an order unity strain. Starting in the bimodal phase, one can think of two populations, one of “hot” (low l) and one of “cold” (high l) elements. At this stage, $\dot{\gamma}$ is small, but as all the l values of elements drift upwards (advection), the “cold” population is depleted first by strain-induced yield. Other things being equal, this would reduce the stress, but that is held constant, so the strain increases rapidly to compensate; a pulse of yielding occurs after which $P(l, t)$ is unimodal at low l . This distribution is swept up in l by advection, until part of it enters

the cold (high l) region; here a peak develops because of the reduced jump rate, and the cycle begins again [53].

Although this mechanism is somewhat specific to the LJSGR model, it is interesting since, in recent years, a number of soft materials have been found experimentally to exhibit spontaneous oscillations in stress at fixed strain rate, or *vice versa*. These include, under some but not all conditions, both onion phases [54] and wormlike micellar phases [55] of surfactants. However it is certain that in both of these cases the physics of the oscillation is much more complicated than described above: in the onion case the oscillations involve periodic cycling from an ordered to a disordered packing of the onions. For the micelles, slow structural changes may also be involved, entailing the cyclical buildup of a gel network and/or modification to the micellar length distribution (see *e.g.* [56] for a discussion of how these mechanisms might be related to one another).

It is also quite possible that the mechanism for the observed oscillations generically involves shear banding, which does not arise in LJSGR, although closer experimental investigation is needed to establish this conclusively.

12.1 A simpler model for rheo-instability

Despite these uncertainties about the experimental position, it is interesting to look for even simpler generic models capable of showing oscillatory strain rate at fixed stress or *vice versa*. Such models are somewhat in the spirit of the “fluidity” approaches [62] developed further in Ajdari’s lectures at this school.

The simplest such model we have found [57] suppresses all spatial inhomogeneities, and writing a simple integrodifferential constitutive equation as follows:

$$\dot{\sigma} = \dot{\gamma} - R(\sigma) - \lambda \int_{-\infty}^t \sigma(t') M(t - t') dt'. \quad (12.1)$$

Let us take $\dot{\gamma}$ to be constant (steady flow) and consider the resulting stress. In these terms, the first term on the right represents the continuous buildup of elastic stress among mesoscopic elements (whose elastic constant is set to unity as usual). The second term represents instantaneous jumps at a rate $J(\sigma) = R/\sigma$; this represents the local nonlinearity associated in the LJSGR models with $\Gamma(x, l)$. The function $R(\sigma)$ is chosen so that its inverse, $\sigma(R)$, is a sigmoid shape, like the middle flow curve in Figure 14. Hence there is a region where $R'(\sigma) \equiv dR/d\sigma < 0$. The third term (the integral) reflects schematically the presence of some additional memory effects, which here can be thought of as “delayed jumps”. The memory kernel $M(t - t')$ is arbitrary but defined so that $\int M(t) dt = 1$, so that the strength of this term is controlled by λ .

The flow curve of the model now follows trivially from equation (12.1): $\sigma(\dot{\gamma})$ is the solution of $\dot{\gamma} - R(\sigma) - \lambda\sigma = 0$. It follows that the flow curve is everywhere monotonic if λ is chosen large enough that $\lambda + R'(\sigma) > 0$ everywhere. By adding a linear term (albeit delayed) to a sigmoidal flow curve $\sigma(R)$ we have “unwrapped” the kink to give a steady-state curve that is monotonic. Such a flow curve is now stable against shear banding; but interestingly, it need not be stable against oscillation. To illustrate this, we can choose $M(t) = \tau^{-1} \exp(-t/\tau)$. This particular choice allows the integral term in equation (12.1) to be got rid of by differentiating the equation; one obtains

$$\ddot{\sigma} = -\frac{\partial V}{\partial \sigma} - \beta(\sigma)\dot{\sigma}. \quad (12.2)$$

This is the equation of motion of an effective particle that resides in a potential $V(\sigma)$ with position-dependent damping $\beta(\sigma)$. These quantities obey $V'(\sigma) = R(\sigma) + \lambda\sigma - \dot{\gamma}$ and $\beta(\sigma) = R'(\sigma) + 1/\tau$. A state of steady stress (corresponding to the particle at rest) is only possible at $V'(\sigma) = 0$; this recovers the flow curve in the form $R(\sigma) + \lambda\sigma - \dot{\gamma} = 0$ as previously derived. We can now inspect the stability of this solution: clearly if $V''(\sigma) < 0$, the particle is at rest at a potential maximum and is unstable. This corresponds to a simple mechanical instability against small displacement ($d\sigma/d\dot{\gamma} < 0$); this instability is the one responsible for shear banding. However, even when $V''(\sigma)$ is positive, the steady state at $V'(\sigma) = 0$ is *still* unstable unless $\beta(\sigma) > 0$ there. Negative β corresponds locally to an “antidamped” oscillator which is unstable against a small velocity. The latter will grow through antidamping until a limit cycle is reached, whereby positive damping at the extremes of the cycle balance the negative damping around the middle. (This always happens at large enough amplitudes if $R(\sigma)$ is sigmoidal as assumed.) Related phenomena have recently been reported in a somewhat different model by Lemaitre [58].

In summary, equation (12.1) shows spontaneous oscillation if parameters are chosen such that (a) the flow curve is monotonic only by virtue of the delayed term; and (b) the delay time τ is too large. Unless parameter values are chosen rather carefully, this generally requires a delay time τ larger than the Maxwell time $\tau_M = 1/J(\sigma \rightarrow 0)$ with which small stresses would relax in the absence of the integral term in equation (12.1). That is, the system requires some sort of *structural memory* above and beyond the Maxwell time.

13 Rheochaos

In both the onion and the micellar surfactant systems [54, 55], upon varying experimental parameters one can find not only spontaneous oscillation but transition to unsteady flow regimes that seem, at least in some cases, to

exhibit low-dimensional chaotic dynamics. The term “rheological chaos” or simply “rheochaos” has been coined to describe chaotic dynamics in complex fluids under regimes where the Reynolds number, which controls the effects of inertia, is effectively zero. Other examples include the “elastic turbulence” reported in certain polymer solutions close to the entanglement threshold [59]. In contrast to “ordinary” fluid-mechanical chaos, which requires high Reynolds number, this type of chaotic dynamics appears to stem from the combination of nonlinearity and memory that is present in many viscoelastic materials. In fact, one might ask why it is not seen more often. Its exploration represents an interesting area of ongoing research. Chaotic dynamics of a possibly different nature has also been reported and modelled for liquid crystals under flow [60].

One interesting question is whether rheochaos is possible in the absence of spatial heterogeneity: can one have chaotic time evolution while retaining a spatially uniform flow? If so (and experimentally that is far from clear) one might hope for a description based on equation (12.1) or a similarly simplified equation. Equation (12.1) itself does in fact permit chaotic dynamics though not for exponential $M(t)$. The latter results in a second order dynamical system (Eq. (12.2)) whereas chaos can only arise in a third or higher order system [61]. General $M(t)$ represents infinite order, and in that case chaos is certainly possible though we have not found it so far for rheologically sensible (*i.e.*, monotonically decaying) $M(t)$.

The simplest model along these lines that we have found to show chaos instead introduces a delay to the nonlinear ($R(\sigma)$) term in equation (12.1) as well as to the linear term [57]. It is not yet clear whether (and if so, how) such a model is relevant to experiment but one possible interpretation of the resulting equation involves the slow evolution of a structural control parameter (somewhat resembling the “fluidity” parameter of Ajdari *et al.* [62]). This supports the idea that rheochaos is more likely to arise in systems that support structural variables with relaxation times longer than the typical viscoelastic (Maxwell) relaxation time for the rheological stress itself. Such variables could include internal order parameters for the arrangement of particles [54] but might arise, in shear banding systems, from slow evolution of the interfacial position [57, 63].

14 More fundamental approaches

The reader will be aware of a significant decline in predictive power, between the first half of these notes, dealing largely with entangled polymers, and the second half, dealing with nonergodic systems, as described by the SGR model and its relatives. As discussed in Section 5.4, there are good excuses for the much more phenomenological and *ad-hoc* flavour of the work on soft

glasses. An obvious question is whether any scope exists for a deeper theory of rheology in systems that are not ergodic at rest, perhaps comparable with the reptation theory of polymers in terms of quantitative predictive power. But we are not yet seeking a rigorous, “final” theory (any more than reptation is a final theory of polymer dynamics). In this respect, the case of colloidal glasses offers experimental promise as a testing ground for any quantitative theory. Colloidal glasses [64] arise in purely hard-sphere suspensions for which the interactions are fully characterised. Interestingly, their behaviour is accounted for quite well by mode coupling theory (MCT) [65]. In fact, if one makes an ad-hoc (and deeply unjustified!) rescaling of the critical volume fraction at which the glass transition occurs, MCT offers a near-quantitative account of the divergence of structural relaxation times as the glass transition is approached, as probed by light scattering [66]. Sadly though it offers much less information about the aging behaviour etc., that should arise deep within the glass phase.

There are many good reasons not to believe MCT as a “final” theory of hard-sphere colloidal glasses, but increasing reasons to accept it as a provisional one. For example, MCT offered a clear and surprising prediction that adding slight attractions to hard sphere colloids should melt the glass [36], whereas increasing the attraction further should arrest the system again; experiments bear this out [37]. MCT also predicts logarithmic decay of correlations [65] near a higher-order glass transition which resides, in parameter space, close to the “corner” of the re-entrant glass line [36]; this has been seen in simulation [67] and now experiment [68]. Also, MCT offers promising insights into the structure of nonergodic phases at much lower concentrations in attractive colloidal systems (where the bonding energies are high enough to cause long-lived arrested states, but not high enough to be thought of as completely reversible) [70]. Perhaps the status of MCT is best summarised by paraphrasing Churchill [69]: MCT is the *worst* theory of colloidal glasses – apart from all the others that have been tried from time to time.

In that context, it is interesting to develop a rheological modelling framework that builds on MCT. This programme, which involves rather technical calculations, has recently been initiated [71]. Within the approximations made, the theory predicts a yield stress $\sigma_Y > 0$ throughout the glass phase, dropping discontinuously to zero at the glass transition. These predictions, though qualitative, are nontrivial [39, 40] and more detailed experimental studies will be needed to check them. The calculations predict exclusively shear thinning behaviour, but this might be related to a known shortcoming of MCT (which effectively treats all thermodynamic interactions as harmonic in density fluctuations). The shear thickening case can be addressed within a so-called “schematic” MCT approach (which is known to capture

the static nonergodicity transition relatively well) by postulating generic dependencies of the MCT vertex on $\dot{\gamma}$ and σ . This approach, though quite different in spirit, gives flow curves similar to those of the GJSGR model of Figure 14, including a full jamming regime [72]. Although phenomenological, it offers the tantalizing promise that the fundamental programme started in [71] may eventually be able to confirm the link, which so far remains hypothetical, between jamming of colloids under shear and the glass transition.

15 Conclusion

In these lectures I have described two main strands in the theoretical rheology of soft materials. The first, polymer dynamics, is one of the great success stories of late 20th century statistical dynamics. It does, however, exploit several special properties of polymers (ergodicity, local equilibrium even under strong deformation, each chain interacting with many others); this precludes any direct generalisation to nonpolymeric materials. Many other soft materials, if not the majority (at least from the viewpoint of technological applications) are in some form of metastable or arrested state, and this complicates their rheology significantly. Strong departures from equilibrium occur both locally and globally in such materials which include foams, dense emulsions, pastes, particulate gels and the like. Shear thinning, shear thickening, and many more complex and nonintuitive phenomena such as spontaneous oscillation and rheochaos, can be found. Some of these are doubtless related to the slow evolution of material properties with time, which is in turn connected with aging. It is not yet clear to what extent aging is an “intrinsic” aspect of the same dynamics as is responsible for rheology (mesoscopic rearrangement of material) and to what extent aging is controlled by “extrinsic” phenomena such as drainage, sedimentation etc.: the answer may be very different for different types of system. In view of all this, there is little hope yet of robust quantitative theories being developed except in a few simple cases. The latter half of these lectures has therefore concentrated mainly on phenomenological models which seem to capture some generic features of nonergodic soft materials in a qualitative manner. While no attempt was made to do justice to the recent experimental literature, the experimental exploration of these ideas is of course vital to future progress. It may well take several iterations between theory and experiment before a clear picture emerges.

I thank the numerous colleagues who have collaborated on the work described or otherwise assisted in the preparation of these notes.

References

- [1] M.E. Cates and M.R. Evans, *Soft and Fragile Matter: Nonequilibrium Dynamics, Metastability and Flow* (IOP Publishing, Bristol, 2000).
- [2] R.G. Larson, *The Structure and Dynamics of Complex Fluids* (Clarendon Press, Oxford, 1999).
- [3] D.J. Pine, *Light Scattering and Rheology of Complex Fluids Driven far from Equilibrium*, in [1], pp. 9-47.
- [4] D. Roux, *Equilibrium and Flow Properties of Surfactants in Solution*, in [1], pp. 185-204.
- [5] P.T. Callaghan, *Repts. Prog. Phys.* **62** (1999) 599-670.
- [6] T.C.B. McLeish, *Rheology of Linear and Branched Polymers*, in [1], pp. 79-111.
- [7] M.P. Allen and D.J. Tildesley, *Computer Simulation of Liquids*, 2nd Ed. (Oxford Univ. Press, 1989).
- [8] K. Kremer, *Computer Simulations in Soft Matter Science*, in [1], pp. 145-184.
- [9] S.D. Holdsworth, *Trans. Inst. Chem. Eng.* **71** (1993) 139-179.
- [10] H. Rehage and H. Hoffmann, *Mol. Phys.* **74** (1991) 933-973.
- [11] P.-G. de Gennes, *Scaling Concepts in Polymer Physics* (Cornell Univ. Press, Ithaca, 1979).
- [12] J.S. Higgins and H.C. Benoit, *Polymers and Neutron Scattering* (Clarendon Press, Oxford, 1997).
- [13] M. Doi and S.F. Edwards, *The Theory of Polymer Dynamics* (Clarendon Press, Oxford, 1986).
- [14] S.T. Milner, T.C.B. McLeish and A.E. Likhtman, *J. Rheol.* **45** (2001) 539-563.
- [15] P.D. Olmsted, *Curr. Opinion Colloid Interf. Sci.* **4** (1999) 95-100; C.Y.D. Lu, P.D. Olmsted and R.C. Ball, *Phys. Rev. Lett.* **84** (2000) 642-645.
- [16] M.E. Cates and S.J. Candau, *J. Phys. Cond. Matt.* **2** (1990) 6869-6892.
- [17] L.F. Cugliandolo, J. Kurchan and L. Peliti, *Phys. Rev. E* **55** (1997) 3898-3914; see also L.F. Cugliandolo, this volume.
- [18] T.G. Mason, J. Bibette and D.A. Weitz, *Phys. Rev. Lett.* **75** (1995) 2051-2054; *Phys. Rev. Lett.* **75** (1995) 2770-2774; *J. Colloid Interf. Sci.* **179** (1996) 439-449.
- [19] J.-P. Bouchaud, *J. Phys. France I* **2** (1992) 1705-1713.
- [20] S.M. Fielding, P. Sollich and M.E. Cates, *J. Rheol.* **44** (2000) 323-369.
- [21] P. Sollich, F. Lequeux, P. Hebraud and M.E. Cates, *Phys. Rev. Lett.* **78** (1987) 2020-2023.
- [22] P. Sollich, *Phys. Rev. E* **58** (1998) 738-759.
- [23] P. Sollich and M.E. Cates, in preparation.
- [24] J.L. Borges, Funes the Memorious, in *Fictions* (Everyman Publishers) (reprinted, 1993).
- [25] B. Rinn, P. Maas and J.-P. Bouchaud, *Phys. Rev. B* **64** (2001) 104417; *Phys. Rev. Lett.* **84** (2000) 5403-5406.
- [26] C. Derac, A. Ajdari, G. Doucouret and F. Lequeux, *C. R. Acad. Sci. IV* **1** (2000) 1159-1119.
- [27] M. Cloitre, R. Borrega and L. Leibler, *Phys. Rev. Lett.* **85** (2000) 4819-4822.
- [28] D. Bonn, S. Tanase, B. Abou, *et al.*, *Phys. Rev. Lett.* **89** (2002) 015701.
- [29] L. Ramos and L. Cipelletti, *Phys. Rev. Lett.* **87** (2001) 245503.
- [30] R. Hohler, S. Cohen-Addad and A. Asnacios, *Europhys. Lett.* **48** (1999) 93-98.
- [31] L.F. Culiandolo and J. Kurchan, *J. Phys. A* **27** (1994) 5749-5772.

- [32] V. Viasnoff, S. Jurine and F. Lequeux, *Faraday Disc.* **123**, in press; V. Viasnoff and F. Lequeux, *Phys. Rev. Lett.* **89** (2002) 067501.
- [33] W.C.K. Poon, L. Starrs, S.P. Meeker, *et al.*, *Faraday Disc.* **112** (1999) 143-154.
- [34] L. Cipelletti, S. Manley, R.C. Ball and D.A. Weitz, *Phys. Rev. Lett.* **84** (2000) 2275-2278.
- [35] J.-P. Bouchaud and E. Pitard, *Eur. Phys. J. E* **6** (2001) 231-236.
- [36] K. Dawson, G. Foffi, M. Fuchs, *et al.*, *Phys. Rev. E* **63** (2001) 011401.
- [37] K.N. Pham, A.M. Puertas, J. Bergenholtz, *et al.*, *Science* **296** (2002) 104-106.
- [38] J. Kurchan, *Rheology, and How to Stop Aging* [cond-mat/8912347].
- [39] L. Berthier, J.-L. Barrat and J. Kurchan J., *Phys. Rev. E* **61** (2000) 5464-5472.
- [40] L. Berthier, *Yield Stress, Heterogeneities and Activated Processes in Soft Glassy Materials* [cond-mat/0209394].
- [41] J.P. Ducruppe, S. Lerouge and J.-F. Berret, *Phys. Rev. E* **63** (2001) 022501.
- [42] C. Grand, J. Arrault and M.E. Cates, *J. Phys. II France* **7** (1997) 1071-1086.
- [43] O. Hess and S. Hess, *Physica A* **207** (1994) 517-540.
- [44] J. Bender and N.J. Wagner, *J. Rheol.* **40** (1996) 889-916.
- [45] H.M. Laun, *J. Non-Newtonian Fluid Mec.* **54** (1994) 87-108.
- [46] E. Bertrand, J. Bibette and V. Schmitt, *From Shear Thickening to Shear-Induced Jamming*, Preprint (2001).
- [47] O. Reynolds, *Phil. Mag. S5* **20** (1885) 469-481.
- [48] J.F. Brady, *Curr. Opinion Colloid Interf. Sci.* **1** (1996) 472-480.
- [49] R.C. Ball and J.R. Melrose, *Adv. Colloid Interf. Sci.* **59** (1995) 19-30; R.S. Farr, J.R. Melrose and R.C. Ball, *Phys. Rev. E* **55** (1997) 7203-7211.
- [50] A.J. Liu and S.R. Nagel, *Nature* **396** (1998) 21-22.
- [51] D.A. Head, A. Ajdari and M.E. Cates, *Phys. Rev. E* **64** (2001) 061509.
- [52] M.E. Cates, J.P. Wittmer, J.-P. Bouchaud and P. Claudin, *Phys. Rev. Lett.* **81** (1998) 1841-1844.
- [53] D.A. Head, A. Ajdari and M.E. Cates, *Europhys. Lett.* **57** (2002) 120-126.
- [54] A.S. Wunenburger, A. Colin, J. Leng, *et al.*, *Phys. Rev. Lett.* **86** (2001) 1374-1377; J.B. Salmon, A. Colin and D. Roux, *Phys. Rev. E* **66** (2002) 031505.
- [55] R. Bandyopadhyay and A.K. Sood, *Europhys. Lett.* **56** (2001) 447-453; R. Bandyopadhyay, G. Basappa and A.K. Sood, *Phys. Rev. Lett.* **84** (2000) 2022-2025.
- [56] M.E. Cates and S.J. Candau, *Europhys. Lett.* **55** (2001) 887-893.
- [57] M.E. Cates, D.A. Head and A. Ajdari, *Phys. Rev. E* **66** (2002) 025202(R).
- [58] A. Lemaitre, *A Dynamical Approach to Glassy Materials* [cond-mat/0206417].
- [59] A. Groisman and V. Steinberg, *Nature* **405** (2000) 53-55.
- [60] M. Grosso, R. Keunings, S. Crescitelli and P.L. Maffettone, *Phys. Rev. Lett.* **86** (2001) 3184-3187.
- [61] P. Glendinning, *Stability, Instability and Chaos* (Cambridge University Press, 1994).
- [62] C. Derec, A. Ajdari and F. Lequeux, *Eur. Phys. J. E* **4** (2001) 355-361.
- [63] S.M. Fielding and P.D. Olmsted, *Kinetics of the Shear Banding Instability in Startup Flows* [cond-mat/0208599].
- [64] P.N. Pusey, Colloidal Suspensions, in *Liquids, Freezing and Glass Transition*, edited by J.P. Hansen, D. Levesque and J. Zinn-Justin, Les Houches Session LI (North Holland 1991), 763-942.
- [65] W. Goetze, Aspects of Structural Glass Transitions, in *Liquids, Freezing and Glass Transition*, edited by J.P. Hansen, D. Levesque and J. Zinn-Justin, Les Houches Session LI (North Holland 1991), 287-503.

- [66] W. van Meegen, S.M. Underwood and P.N. Pusey, *Phys. Rev. Lett.* **67** (1991) 1586-1589; W. van Meegen and S.M. Underwood, *Phys. Rev. E* **49** (1994) 4206-4220.
- [67] A.M. Puertas, M. Fuchs and M.E. Cates, *Phys. Rev. Lett.* **88** (2002) 098301.
- [68] K.N. Pham, private communication.
- [69] W.S. Churchill, *Democracy is the worst form of Government except all those other forms that have been tried from time to time*, House of Commons, 11 Nov. 1947; cited in Oxford Dictionary of Quotations, 3rd Ed. (Oxford University Press, 1979).
- [70] K. Kroy, *et al.*, work in progress.
- [71] M. Fuchs and M.E. Cates, *Theory of Nonlinear Rheology and Yielding of Dense Colloidal Suspensions* [cond-mat/0204628]; *Faraday Discussion* **123** (2002) (in press) [cond-mat/0207530].
- [72] C. Holmes, M. Fuchs and M.E. Cates, in preparation.

COURSE 4

GRANULAR MEDIA: SOME IDEAS FROM STATISTICAL PHYSICS

J.P. BOUCHAUD

*Service de Physique de l'État
Condensé, CEA, Orme des Merisiers,
91191 Gif-sur-Yvette Cedex, France*



Contents

1	Introduction	133
1.1	Basic phenomenology	133
1.2	Theoretical issues	136
2	The scalar model I: Discrete version	140
2.1	Definition and motivation	140
2.2	Stress distribution and the exponential tail	141
2.3	The “critical” case	143
3	The scalar model II: Continuous limit and perturbation theory	144
3.1	Continuous limit of the scalar model	144
3.2	Calculation of the averaged response and correlation functions	147
3.3	Further results: The un-averaged response function	153
3.4	The scalar model with bias: Edwards’ picture of arches	154
4	Static indeterminacy; elasticity and isostaticity	155
4.1	Elasticity and response functions	155
4.2	Indeterminacy at the grain level and isostaticity	157
4.3	Numerical simulations and Edwards’ assumption	158
5	A stress-only approach to granular media	160
5.1	A vectorial q -model	160
5.2	A constitutive relation between stress components	162
5.3	Some simple situations	163
5.4	Symmetries and constitutive relations	164
5.5	Boundary conditions and “fragility”	166
6	Experimental and numerical determination of the stress response function	167
7	Force chains scattering I: Weak disorder limit	168
7.1	A stochastic wave equation	168
7.2	Calculation of the averaged response function	171
7.3	Generalized wave equations	174
8	Force chains scattering II: Strong disorder limit	177
8.1	Introduction and numerical results	177
8.2	A Boltzmann description of force chain splitting	178
8.3	The role of chain merging	181
9	Statics of granular materials: Concluding remarks and open questions	182
10	Glassy dynamics in granular media: A brief survey	184
10.1	Slow compaction	184
10.2	Self-inhibitory dynamics and dynamical heterogeneities	186
10.3	Granular dynamics and the trap model	190

GRANULAR MEDIA: SOME IDEAS FROM STATISTICAL PHYSICS

J.P. Bouchaud

Abstract

These lecture notes cover the statics and glassy dynamics of granular media. Most of the lectures were in fact devoted to “force propagation” models. We discuss the experimental and theoretical motivations for these approaches, and their conceptual connections with Edwards’ thermodynamical analogy. One of the distinctive feature of granular media (common to many other “jammed” systems) is indeed the large number of metastable states that are macroscopically equivalent. We present in detail the (scalar) q -model and its tensorial generalization, that aim at modelling the existence of force chains and arching effects without introducing any displacement field. The contrast between the hyperbolic equations obtained within this line of thought and elliptic (elastic) equations is emphasized. The role of disorder on these hyperbolic equations is studied in details using perturbative and diagrammatic methods. Recent (strong disorder) force chain network models are reviewed, and compared with the experimental determination of the force “response function” in granular materials. We briefly discuss several issues (such as isostaticity and generic marginality) and open problems. At the end of these notes, we also discuss the basic dynamical properties of *weakly tapped* granular assemblies, and stress the phenomenological analogies with other glassy materials. Simple models that account for slow compaction and dynamical heterogeneities are presented, that are inspired by “free-volume” ideas and Edwards’ assumption. A connection with the theory of fluctuating random surfaces, also noted recently by Castillo *et al.*, is suggested. Finally, we discuss how the “trap model” can be adapted to granular materials, such that more subtle “memory” effects can be accounted for.

1 Introduction

1.1 Basic phenomenology

Although granular materials are made of classical particles of macroscopic size, they exhibit a host of interesting and sometimes counter-intuitive

properties, which are of interest both to the academic community and for industrial applications: enormous amounts of “granular assemblies” are routinely handled (stored, transported, mixed together, etc.). The reason why these systems are still not fully understood yet is that they require a proper statistical treatment of collective effects. Although the physics at the grain level is reasonably well understood, the behaviour of a large assembly of these grains, with strongly non-linear interactions, demand concepts and methods that only recently emerged from the study of disordered systems in statistical mechanics. The main property of granular materials, that leads both to most of the non trivial phenomenology and to most of the theoretical difficulties, is the existence of a *large number of different microscopic metastable states* that are macroscopically equivalent. It turns out, quite interestingly, that this feature (metastability) is common to a wider class of materials in their “jammed” state. This includes glasses, colloids, compressed emulsions and foams, spin-glasses, vortex glasses and other collectively pinned structures, etc.

There is a vast body of experimental results on granular materials that we do not aim to cover here (for reviews, see [56,57,80,81]). We will mainly restrict to *dry* grains in static and weakly driven situations. Correspondingly, we will focus on the statistical properties of the *static states* (and in particular the distribution of stresses) and on the glassy dynamics of *gently “tapped” assemblies*, that slowly evolve from one static state to another. We have therefore excluded from these lectures, because of lack of time, “strongly” driven situations, such as granular flows, avalanches and surface flows, dune formation, etc. This is not to suggest that these problems are less interesting and that collective effects are irrelevant. Quite on the contrary, the dynamics of strongly driven granular systems also displays remarkable effects, such as collisional clustering which generates non trivial spatial structures in granular flows, and invalidates simple hydrodynamical descriptions [16,72,96]. Some recent papers on these matters can be found in references [57,80,98,112,113].

Stress patterns in dry granular media exhibit some rather unusual features when compared to either liquids or elastic solids. For example, the vertical pressure below conical sand-piles does not follow the height of material above a particular point. Depending on the way the pile is prepared, it shows a *minimum* underneath the apex of the pile [29,128,140] when the pile is built from a point source, and a broad, flat maximum when it is built layer by layer from a uniform “rain” of grains. Furthermore, local stress fluctuations are large, sometimes on length scales much larger than the grain size. For example, repeatedly pouring the very same amount of powder in a silo results in fluctuations of the weight supported by the bottom plate of 20% or more [30,141]. Weak perturbations of the packing can sometimes cause

large rearrangements [44,50]. Qualitatively, these features are attributed to the presence of *stress paths* which can focus the stress field into localized regions and also deflect it to cause “arching” (see [49] for early qualitative experiments). More quantitative experiments were performed in [13,29,93], where the local fluctuations of the normal stress deep inside a silo or at the base of a sandpile were measured. It was found that the stress probability distribution is rather broad, decaying exponentially for large stresses. This behaviour was also found in numerical simulations [114], and more recently in other situations [109], such as compressed emulsions [31]. Similarly, standard “triaxial” test experiments used to determine the elastic properties of materials from the (macroscopic) relation between stresses and deformations show highly irreproducible, hysteretic behaviour which only seem to converge towards a well defined curve after a large number of deformation cycles have been imposed to the granular system in order to “anneal” it down to a reproducible state.

The dynamics of slowly driven granular systems also exhibit unusual features when compared to either liquids or solids, and has actually much in common with *glasses*. In particular, the way these systems very slowly compact when vibrated, the unusual dependence of the density on the system history, etc. has strong similarities with the properties of glassy materials. At the phenomenological level, the dynamics of these systems appears to be a succession of hops between different (metastable) equilibrium states. The understanding of static and weakly driven granular assemblies therefore require a proper description of the statistical properties of these “blocked” configurations. We now discuss these issues in the perspective of the present lectures¹.

¹The content of these lecture notes owes a lot to my collaborators on these issues: Mike Cates, Philippe Claudin, Eric Clément, Dov Levine, Josh Socolar, Matthias Otto, Loic Vanel and Joachim Wittmer. Parts of these notes actually are extracted from various papers co-written with them. I have tried to add my own present understanding of the subject, in particular concerning Edwards ensembles, the hyperbolic approach to the statics of granular media, and their glassy dynamics, in particular dynamical heterogeneities. Some ideas are still speculative and are by no means intended to be definitive, but I hope that the theoretical concepts and methods are of sufficiently broad interest to deserve appearing in print in the present Les Houches volume. I wish to express my gratitude to Jean-Louis Barrat and Jorge Kurchan for giving me the opportunity of giving these lectures and for many very inspiring discussions. I thank the participants of the school for interesting comments and ideas, in particular G. Biroli, L. Berthier, E. Bertin, L. Cugliandolo, D. Fisher, A. Lefevre, J. Snoeijer, V. Viasnoff and O. White. I also thank E. Bertin for carefully reading the manuscript, and D. Bonamy, O. Dauchot, F. Daviaud, C. Godrèche, M. Mézard, J.N. Roux, R. da Silveira and E. Vincent for discussions.

1.2 Theoretical issues

1.2.1 Static properties

How can one then describe the statics of granular materials on large length scales? The basic problem stems from the fact that the equilibrium equations for the stress tensor are not sufficient to determine the stress. For example, in two dimensions the stress tensor has three independent components, but there are only two equilibrium equations. Some additional assumptions about the properties of the material must be provided. For example, the assumption that the material is elastic and follows Hooke's law gives extra constraints on the stress tensor and allows one to solve the static problem as soon as some appropriate boundary conditions are given. For granular materials, the standard procedure is to use elastic or elasto-plastic theories from soil mechanics [148]. However, the relation between force chains on short length scales and an elasto-plastic description on large length scales is far from obvious. To our knowledge, no systematic procedure has ever been proposed to go from the mechanics at the grain level to coarse-grained equations that would justify the use of an elasto-plastic framework and estimate the parameters of the theory (effective elastic moduli, etc.). One of the main difficulty is that some indeterminacy exists already at the grain level, since many different configurations of the contact forces are allowed and satisfy local equilibrium. This leads to several conceptual problems: even if an elastic-like description of small perturbations around an arbitrary reference state (such as sound waves, for example) might make sense in general, the description of – say – a conical sandpile using elasto-plasticity theory [33] requires the identification of a (zero stress) reference state from which deformations can be defined, at least for *some* regions of the pile. In the case of a pile of infinitely hard grains (which should be the correct benchmark for an assembly of grains with a Young modulus much larger than the gravity induced stresses) that rests in one particular metastable state (among a large number of macroscopically equivalent ones), switching the gravity back to zero will hardly affect the packing. Each of these metastable states can thus equally well be taken as a reference state; on the other hand, it is precisely the stress pattern in one of these “native” metastable state (*i.e.* obtained when grains come to rest without further tapping) that one wants to predict. One peculiarity of (dry) granular materials is the absence of tensile stresses between the grains; the cohesion of the assembly is therefore induced by the applied stress itself and the zero stress state is ill defined.

Even the description of small perturbations around a given reference state might be problematic. For example, the existence of a (large volume) limiting curve relating incremental stresses and deformations requires, as

already mentioned above, at least some “annealing” procedure to define a reproducible initial state. This limiting curve might not even exist in the absence of friction [44]. Even for moderate deformations, following the so-called consolidation phase, the response to cyclic loads in standard triaxial tests shows some significant irreversibility.

The absence of any obvious deformation field from which the stress tensor may be constructed has motivated an alternative, “stress-only” approach [18, 21, 42, 145]. The basic tenet of these theories is that in equilibrium, some (history dependent) large scale relations between the components of the stress tensor should exist. These relations should be determined by the global statistical features of the particular metastable state in which the packing sits but not on its microscopic details, nor on the particular loading conditions, provided these do not lead to further rearrangements of the packing. Much as random collisions between molecules give rise, on large length scale, to well defined hydrodynamical equations, the hope is that an appropriate coarse-graining of the local force balance equations leads, on large length scales, to the missing “closure” equation that allows to solve for the static equilibrium. (For rather formal attempts in this direction, see [2, 62].) A well known relation of this type arises from the assumption that the material is everywhere on the verge of plastic failure, leading to a Mohr-Coulomb (non-linear) relation between the stress components [106], but we will motivate and discuss simpler relations below, based both on symmetry arguments [18] and on the consideration of simple rules for the transfer of stresses between adjacent grains [41]. The consequence of a fixed relation between the components of the stress tensor is that stresses obey an *hyperbolic* equation, as compared to the *elliptic* equations encountered in elasticity theory. This means that stresses “propagate” or are “transmitted” along lines: as discussed below, the characteristics of this hyperbolic equation are the mathematical transcription of the force chains that are well known to exist in granular materials [35].

1.2.2 Tapping and non thermal ensembles

As mentioned above, many different packings and configurations of the contact forces are compatible with the local equilibrium of each grain for a given macroscopic situation. This is actually intimately related to the fact that stresses in granular media often show large fluctuations; some kind of averaging is therefore needed to obtain reproducible results. In the case of sand-piles, one must repeat the construction of the pile several times, and use a pressure gauge that averages over a sufficiently large number of grains, in order to obtain a satisfactory stress profile that a statistical theory of blocked states should predict. Another possibility is to vibrate the packing such as to make it probe, during its evolution, several equilibrium

states with the same macroscopic geometry. The natural question is then: with which statistical weight the different equilibrium (blocked) states appear in a given experiment? To what extent are these weights dependent on the dynamics that leads to the blocked states? Is the ensemble of “native” (as-built) packings identical to the ensemble of packings obtained under tapping?

The simplest answer, proposed more than ten years ago by Sam Edwards, is to postulate that all blocked states with a given density are equiprobable [60]. This micro-canonical assumption defines what is now called the “Edwards ensemble” [86]; it turns out that several toy models of jammed systems do obey, either exactly or to a good approximation, Edwards’ prescription [5, 45, 52, 127]. This is a first step towards a “thermodynamical” description of out-of-equilibrium, dissipative systems [3, 4, 8, 97]. However, several remarks of various nature should be made here.

- First, the analogy between tapping strength and temperature. In many cases, this is a useful intuitive guide and several experiments discussed in Section 10 do indeed confirm the phenomenological analogies between the two. However, tapping is a long-wavelength excitation, whereas temperature in solid state physics is thought to give rise to very short wavelength fluctuations. Although the long-wavelength excitation probably cascades down, through collisions, to short wavelengths, ideas such as detailed balance and activated processes might be affected by the correlated nature of the noise. In this respect, the non trivial clustering patterns induced by the dissipative collisions might also obliterate simple ideas on the statistics of blocked states.
- One must distinguish at least two types of tapping excitations. One would be very gentle taps, that are insufficient to change the packing *geometry*, but do change the contact forces for each grain. In this case, tapping induces a random walk in “force space”, but for a fixed configuration of the grains. The Edwards hypothesis in this restricted case is to assign a uniform weight for all force configurations that (i) lead to static equilibrium (forces and torques on each grain add up to zero) and (ii) satisfy the Coulomb inequality at each contact. One can also drive the system with an amplitude such that the motion of grains is possible, in which case the dynamics is a random walk both in force space and in packing space. The extended Edwards ensemble in this case is to assign equal weight to any packing and any force configuration such that equilibrium is obeyed and the Coulomb inequality satisfied. In principle, the Edwards prescription could be correct in one case and not in the other, or in both, or in none, or more complicated situations still.

- The Edwards prescription is however ambiguous for continuous variables. In the “gentle” tap case, one is tempted to interpret Edwards’ measure as follows. Let us call \vec{f}_i^α the contact force on the α -th contact of the i -th grain, and \vec{r}_i^α the position of the contact point. We call μ the friction coefficient, and the indices N and T refer to the normal and tangential components of the force. The natural Edwards measure reads:

$$P(\{\vec{f}_i^\alpha\}) = \frac{1}{Z} \prod_i \left[\delta \left(\sum_\alpha \vec{f}_i^\alpha \right) \delta \left(\sum_\alpha \vec{f}_i^\alpha \times \vec{r}_i^\alpha \right) \times \prod_\alpha \Theta(\mu f_{i,N}^\alpha - |f_{i,T}^\alpha|) \right], \quad (1)$$

which is a formal way to impose the constraints on each grain. (Θ is the step function). However, this assumes that the *a priori* measure on the forces is uniform, which is reasonable but not obvious. The usual microcanonical ensemble for particles is constructed similarly: one imposes the total energy of the system using a δ -function on an *a priori* uniform measure on the canonical variables (position and momentum). However, in the latter case, this procedure is justified by the Liouville theorem which selects the relevant canonical variables. In general, however, there is an ambiguity since the assumption of uniformity is not invariant under changes of variables.

It is instructive to discuss the simplest case where the Edwards assumption can be discussed in details, and perhaps tested experimentally or numerically. Consider, as proposed by Ertas and Halsey, a single disk in a wedge [64]. In equilibrium, there are two contact points and therefore four unknowns: $f_{1,N}, f_{1,T}$ and $f_{2,N}, f_{2,T}$, where $f_{\alpha,T} > 0$ means that the force pushes upwards. These forces must lead to equilibrium, which gives three equations. There is therefore one degree of freedom which is not fixed by the equilibrium requirement, and is dynamically selected. It is easy to see that one must have $f_{1,T} = f_{2,T} = f_T$ and $f_{1,N} = f_{2,N} = f_N$. The Edwards measure then reads:

$$P(f_N, f_T) = \frac{1}{Z} \delta \left(f_N \sin \psi + f_T \cos \psi - \frac{1}{2} M g \right) \Theta(\mu f_N - |f_T|), \quad (2)$$

where ψ is (half) the opening angle of the wedge. From this result, one can compute the distribution of the “mobilization” ratio $r = f_T/f_N$, which is found to be parabolic:

$$P(r) \propto (\sin \psi + r \cos \psi)^2 \quad (-\mu \leq r \leq \mu), \quad (3)$$

and, of course, zero outside the allowed interval $[-\mu, \mu]$. One could test this simple predictions by repeatedly tapping spheres made of different materials, and investigate the relevance of the tapping mode and the contact dynamics on the statistical ensemble of forces that one generates. This would be quite a valuable starting point, before speculating on more complex multi-grain situations. We will discuss below some numerical results that indeed suggest some dependence of the statistics of forces on the microscopic dynamics.

The Edwards prescription is in fact at the heart of the simplest “scalar” model for the statistics of forces in granular materials, which was proposed in [46, 93] to account for the empirical exponential tail in the distribution of forces. Although this model represents a highly stylized view of granular systems and cannot be expected to be accurate, it provides both an extremely rich theoretical benchmark and a pedagogical starting point for more elaborate descriptions.

2 The scalar model I: Discrete version

2.1 Definition and motivation

The drastic simplification of the scalar model is to only retain one component of the stress tensor, namely the “weight” $w = \sigma_{zz}$, and correspondingly, to only consider the force balance equation along the vertical axis. Again for simplicity, one can think that the grains reside on the nodes of a two-dimensional lattice, and are labeled by two integers: i in the horizontal direction and j in the vertical direction; j increases as one moves downwards. The equilibrium equation can then be written as:

$$w(i, j) = w_0 + q_+(i-1, j-1)w(i-1, j-1) + q_-(i+1, j-1)w(i+1, j-1) \quad (4)$$

where “ w_0 ” is the weight of each grain, and $q_{\pm}(i, j)$ are “transmission” coefficients giving the fraction of weight which the (i, j) transmits to its right (resp. left) neighbour immediately below, such that $q_+(i, j) + q_-(i, j) = 1$ for all i, j ’s. The case of an ordered pile of identical grains and identical conditions for each contacts corresponds to $q_{\pm} = \frac{1}{2}$. In this case, the equation for the w ’s become identical to the Master equation describing the population of un-biased random walkers in a one space dimension (corresponding to i), evolving in “time” (corresponding to j):

$$w(i, j) = w_0 + \frac{1}{2} [w(i-1, j-1) + w(i+1, j-1)]. \quad (5)$$

The term w_0 is a constant source of particles that are created uniformly in space and in time. We will explore this analogy further below.

Now, grain assemblies are usually not perfectly ordered: grains have various shapes and sizes; there are packing defects and irregularities; even for a perfectly ordered packing of identical grains one can expect that the history has imposed different contact loadings. In the above language, it means that the $q_{\pm}(i, j)$ are not all identical and reflect the above sources of randomness. The idea of Edwards, in this highly simplified framework, can easily be worked out, since each “blocked” state corresponds to a particular choice of – say – $q_+(i, j)$ for all i, j . Provided $q_-(i, j) = 1 - q_+(i, j)$, equilibrium is ensured. The uniform measure on all blocked states, advocated by Edwards, merely translates, in the present case, as a uniform probability distribution for q_+ (or q_-) between 0 and 1. This defines the q model, which was originally written with an arbitrary number N of downward neighbours ($N = 2$ in the example above), and can thus be (in principle) generalized to three dimensions [46, 93]. In this case, there are N coefficients q_{α} , $\alpha = 1, \dots, N$ per grain, and the Edwards measure corresponds to the choosing all the q_{α} independently on each node i, j such that:

$$P(\{q_{\alpha}\}) = \frac{1}{Z} \delta \left(\sum_{\alpha=1}^N q_{\alpha} - 1 \right). \quad (6)$$

Therefore, in the present case, Edwards prescription can be explicitly followed. It may seem *a priori* that this microcanonical assumption is too simple and can only lead to trivial predictions. However, as we discuss below, this is not the case: much as for gases where the microcanonical hypothesis can be used to derive, for example, the Maxwell distribution for the particle velocities, the q -model predicts a non trivial distribution for the local vertical stress.

2.2 Stress distribution and the exponential tail

The case of a uniform distribution of the q 's is interesting because it leads to an exact solution for the local weight distribution $P(w)$ for large heights. Let us assume for the moment that the weights on neighbouring sites become asymptotically independent [46, 129]. Then $P(w)$ obeys the following mean-field equation:

$$P_{j+1}(w) = \int_0^1 dq_1 dq_2 \rho(q_1) \rho(q_2) \times \int_0^\infty dw_1 dw_2 P_j(w_1) P_j(w_2) \delta[w - (w_1 q_1 + w_2 q_2 + w_0)] \quad (7)$$

where $\rho(q)$ is the distribution of q , here taken to be $\rho(q) = 1$. In the limit $j \rightarrow \infty$, the stationary distribution P^* of this equation can be explicitly

constructed and is given by:

$$P^*(w) = \frac{w}{\overline{w}^2} \exp -\frac{w}{\overline{w}} \quad (8)$$

where $2\overline{w} = jw_0$ is the average weight. For $N \neq 2$, the distribution is instead a Gamma distribution of parameter N ; its small w behaviour is w^{N-1} while the large w tail is exponential. Liu *et al.* [46, 93] have argued that this behaviour is generic and survives deviations away from the strict Edwards prescription: for example, the condition for the local weight w to be small is that all the N q 's reaching this site are themselves small; the phase space volume for this is proportional to w^{N-1} if the distribution $\rho(q)$ is regular around $q = 0$. However, if instead $\rho(q) \propto q^{\gamma-1}$ when q is small, one expects $P^*(w)$ to behave for small w as $w^{-\alpha}$, with $\alpha = 1 - N\gamma < 0$.

Similarly, the exponential tail at large w is sensitive to the behaviour of $\rho(q)$ around $q = 1$. In particular, if the maximum value of q is $q_M < 1$, one can study the large w behaviour of $P^*(w)$ by taking the Laplace transform of equation (7). One finds in that case that $P^*(w)$ decays *faster* than an exponential:

$$\log P^*(w) \propto_{w \rightarrow \infty} -w^\beta \quad \beta = \frac{\log N}{\log q_M N}. \quad (9)$$

(Notice that $\beta = 1$ whenever $q_M = 1$, and that $\beta \rightarrow \infty$ when $q_M = 1/N$: this last case corresponds to an ordered lattice with no fluctuations.) In this sense, the exponential tail of $P^*(w)$ is not universal: it requires the possibility that one of the q can be arbitrarily close to 1. This implies that all other q 's originating from that point are close to zero, *i.e.* that there is a non zero probability that one grain is entirely bearing on one of its downward neighbours.

The success of the q -model with a uniform distribution of the q 's is that it provides a simple explanation for the ubiquitous exponential tail for the distribution of forces, observed in many experimental and numerical situations. Note in particular that this exponential tail was observed in a regular packing of grains, suggesting that very strong heterogeneities in fact exist at the contact level. On the other hand, the probability to observe very small w is much underestimated by equation (8): see [13, 29, 41, 114]. This might be due to the fact that *arching* effects are absent in this scalar model. A generalization of the q -model allowing for arching was suggested in [40], which dynamically generates some sites where $q_+ = 1$ and $q_- = 0$ (or *vice versa*). This indeed leads to much higher probability density for small weights. For a more detailed discussion of the relation between the q -model the experimental situations, in particular the role of boundaries, see [130].

2.3 The “critical” case

There is however one special case of particular interest where the results for $P(w)$ are qualitatively different. Suppose that q is a random variable that only takes the values 0 or 1 with probability 1/2. This is called the Takayasu model, which is a model for directed river networks for example: at each site of the lattice a river flowing “south-east” or “south-west” is randomly deflected to the left or to the right. Rivers coalesce upon meeting. The “source” term w_0 here describes a constant density of “springs” that feed the river network. It can also be seen as a model of diffusing and aggregating clusters in a solution with a constant density of “monomers” (that again play the role of the source term). In this case, it turns out [136] that the stationary distribution $P^*(w)$ becomes, for large heights, a power law, $P^*(w) \propto w^{-1-\mu}$, with $\mu = 1/3$ in dimension $d = 2$ (*i.e.* one “spatial” and one “temporal” dimension).

The exponent μ was derived analytically but can also be understood as follows. Since the direction of the “rivers” is, at each step, a random variable, the typical “basin of attraction” of a given site is a parabolic object of height t and width \sqrt{t} . Therefore, on the order of $t^{3/2}$ “springs” at most can contribute to the river flux on a given site; in other words, one expects the distribution $P^*(w)$ to take the scaling form:

$$P^*(w) = \frac{1}{w^{1+\mu}} F\left(\frac{w}{t^{3/2}}\right), \quad (10)$$

where F is a certain function which falls off fast for large arguments. On the other hand, since one must have $\langle w \rangle = w_0 t$ exactly, the exponent μ is fixed:

$$\int_0^{+\infty} dw w P^*(w) = w_0 t = t^{3\mu/2} \int_0^{+\infty} du \frac{F(u)}{u^\mu} \longrightarrow \mu = \frac{1}{3}. \quad (11)$$

(Note that the integral over u is convergent for this value of μ .)

Therefore, this model generates a power-law distribution for the local masses, and was proposed early on as a model of “self-organized criticality”. In fact, the model is critical in the sense that any deviation of $\rho(q)$ from a sum of two equal delta peaks at 0 and 1 leads to an exponential truncation of $P^*(w)$ at large w ’s. Let us add several remarks:

- one can compute higher moments of the local weight, to find $\langle w^q \rangle \sim t^{3q/2-1/2}$ for $q > 1/3$. In particular, $\langle w^2 \rangle \sim t^{5/2}$, a result that we will recover below using direct methods;
- one can also generalize the model to higher (spatial) dimensions, where one finds $\mu = 1/2$ for all $d \geq 3$ (with logarithmic corrections in $d = 3$);

- consider a rectangular sample of width W and height H . What is the order of magnitude of the largest weight encountered at the bottom? For a pure power law distribution such as equation (10) with $t \rightarrow \infty$, the maximum value of w is known to be of order $w_{\max} \sim W^{1/\mu}$. This estimate can obviously only be valid if w_{\max} is found to be much smaller than the truncation imposed by the function F , which is of order $H^{3/2}$. This requires $W \ll H^{3\mu/2} \sim H^{1/2}$. However, in this regime where W is smaller than the diffusion length, the very argument leading to equation (10) breaks down, since the maximum weight now scales like WH , and not as $H^{3/2}$. Extending the argument, we now find that the distribution of weights reads:

$$P^*(w) = \frac{1}{Ww} G\left(\frac{w}{WH}\right), \quad \left(W \ll aH^{1/2}\right). \quad (12)$$

Therefore (a) for $W \gg H^{1/2}$, the maximum value of w is imposed by the cut-off and of order $H^{3/2}$, and not W^3 . Correspondingly, the participation ratio $Y_2 = \sum_{i=1} w_i^2 / (w_0 HW)^2$ that characterizes the “localization” of the weight is of order $H^{1/2}/W \ll 1$. In the case (b) $W \ll H^{1/2}$, on the other hand, the weight is localized on a finite number of sites, and $Y_2 \sim 1$.

3 The scalar model II: Continuous limit and perturbation theory

3.1 Continuous limit of the scalar model

Let us focus on the case $N = 2$ and define v to be such that $q_{\pm}(i, j) = (1 \pm v(i, j))/2$. If v is small, the local weight is smoothly varying, and the discrete equation (4) can then be written in the following differential form:

$$\partial_t w + \partial_x(vw) = \rho + D_0 \partial_{xx} w \quad (13)$$

where $x = ia$ and $t = j\tau$ are the horizontal and (downwards) vertical variables corresponding to indices i and j , and a and τ are of the order of the size of the grains. The vertical coordinate has been called t for its obvious analogy with time in a diffusion problem. ρ is the density of the material (the gravity g is taken to be equal to 1), and D_0 a “diffusion” constant, which depends on the geometry of the lattice on which the discrete model has been defined. This diffusion constant is of the order of magnitude of the size of the grains, a .

In this model and in the following, we shall assume that the density ρ is not fluctuating. Density fluctuations could be easily included; it is however easy to understand that the resulting relative fluctuations of the weight at the bottom of the pile decrease with the height of the pile H as $H^{-1/2}$,

and are thus much smaller than those induced by the randomly fluctuating direction of propagation, encoded by q (or v), which remain of order 1 as $H \rightarrow \infty$.

Two interesting quantities to compute are the average “response” $G(x, t|x_0, t_0)$ to a small density change at point (x_0, t_0) , measured at point (x, t) , and the correlation function of the force field, $C(x, t, x', t') = \langle w(x, t)w(x', t') \rangle_c$, where the averaging is taken over the realizations of the noise $v(x, t)$.

Equation (13) shows that the scalar model of stress propagation is identical to that describing tracer diffusion in a (time dependent) flow $v(x, t)$. This problem has been the subject of many recent works in the context of turbulence [38]; interesting qualitative analogies with that field can be made. In particular, “intermittent” bunching of the tracer field correspond in the present context to patches of large stresses, which may induce anomalous scaling for higher moments of the stress field correlation function.

• Fourier transforms

The limit where $a \rightarrow 0$ is ill defined and leads to a divergence of the perturbation theory for large wave-vectors k . We thus choose to regularize the problem by working within the first Brillouin zone, *i.e.*, we keep all wave vector components within the interval $\mathcal{I} = [-\Lambda, +\Lambda]$, where $\Lambda = \frac{\pi}{a}$. Our Fourier conventions for a given quantity f will then be the following:

$$f(x, t) = \int_{-\Lambda}^{\Lambda} \frac{dk}{2\pi} e^{ikx} f(k, t) \quad (14)$$

$$f(k, t) = \ell_x \sum_{x=-\infty}^{+\infty} e^{-ikx} f(x, t). \quad (15)$$

One has to be particularly careful when computing convolution integrals, such as $\int \frac{dq}{2\pi} f_1(q) f_2(k-q)$ which must be understood with limits $-\Lambda + k, \Lambda$ (resp. $-\Lambda, \Lambda + k$) if $k \geq 0$ (resp. $k \leq 0$). An important example, which will appear in the response function calculations, is:

$$\int_{q, k-q \in \mathcal{I}} \frac{dq}{2\pi} q = \frac{\Lambda k}{2\pi} + \mathcal{O}(k^2). \quad (16)$$

Let us then take the Fourier transform of equation (13) along x , to obtain:

$$(\partial_t + D_0 k^2) w_k = \rho_k + ik \int \frac{dq}{2\pi} w_q v_{k-q}. \quad (17)$$

Our aim is to calculate, in the small- k limit, the average response (or Green) function $G(k, t-t')$ defined as the expectation value of the functional

derivative $\langle \delta w(k, t) / \delta \rho(k, t') \rangle$; and the two points correlation function of w , $C(k, t) = \langle w(k, t) w(-k, t) \rangle$.

- The noiseless Green function

The noiseless (bare) Green function (or “propagator”) G_0 is the solution of the equation where the “velocity” components v_q are identically zero: $(\partial_t + D_0 k^2) G_0(k, t - t') = \delta(t - t')$ which is:

$$G_0(k, t - t') = \theta(t - t') e^{-D_0 k^2 (t - t')}. \quad (18)$$

In real space, the propagator is simply the heat kernel,

$$G_0(x, t - t') = \frac{\theta(t - t')}{\sqrt{4\pi D_0 (t - t')}} e^{-\frac{x^2}{4D_0 (t - t')}}. \quad (19)$$

This shows that in the non-disordered scalar model, the stress “diffuses”, as already noticed above in the discrete formulation of the model, see equation (5).

- Statistics of the noise $v(x, t)$

The noise term v represents the effect of local heterogeneities in the granular packing. The mean value of the noise v is taken to be zero, and its correlation function is chosen for simplicity to be of the factorable form $\langle v(x, t) v(x', t') \rangle = \sigma^2 g_x(x - x') g_t(t - t')$, where g_x and g_t are noise correlation functions along x and t axis. We shall take g_x and g_t to be short-ranged (although this may not be justified: fluctuations in the micro-structure of granular media may turn out to be long-ranged due to *e.g.* the presence of long stress paths or arches), with correlation lengths ℓ_x and ℓ_t . Our aim is to describe the system at a scale L much larger than both the lattice and the correlation lengths: $a, \tau, \ell_x, \ell_t \ll L$. This will allow us to look for solutions in the regime $k, E \rightarrow 0$, where k and E are the conjugate variables for x and t respectively, in Fourier-Laplace space. However, we shall see below that the limit $a, \tau, \ell_x, \ell_t \rightarrow 0$ can be tricky, and must be treated with care: this is because the noise appears in a multiplicative manner in equation (13). For computational purposes, we shall often implicitly assume that the probability distribution of v is Gaussian; this might however introduce artifacts which we try to discuss.

- Ambiguities due to multiplicative noise. Ito *vs.* Stratonovitch

In equation (17), we have omitted to specify the dependence on the variable t . There is actually an ambiguity in the product term $w_q v_{k-q}$. In the

discrete q -model model [93], the q_{\pm} 's emitted from a given site are independent of the value of the weight on that site. In the continuum limit, this corresponds to choosing $w_q(t)$ to be independent of $v_{k-q}(t)$, or else that the v 's must be thought of as slightly posterior to the w 's (*i.e.* the product is read as $w_q(t-0)v_{k-q}(t+0)$). In this case, the average of equation (17) is trivial and coincides with the noiseless limit; hence $G = G_0$. This can be understood directly on the discrete model by noticing that the Green function $G(i, j|0, 0)$ can be expressed as a sum over paths, all starting at site $(0, 0)$, and ending at site (i, j) :

$$G(i, j|0, 0) = \sum_{\text{paths } \mathcal{P}} \prod_{(k, l) \in \mathcal{P}} q_{\pm}(k, l) \quad (20)$$

where the $q_{\pm}(k, l)$ are either $q_+(k, l)$ or $q_-(k, l)$, depending on the path. Since each bond $q_{\pm}(k, l)$ appears only once in the product, the averaging over q is trivial and leads to:

$$G(i, j|0, 0) = \sum_{\text{paths } \mathcal{P}} 2^{-j} \equiv G_0(i, j|0, 0). \quad (21)$$

(Note that this argument fails for the computation of the correlation function C , since paths can “interfere”. We shall return later to this calculation.)

The above choice corresponds to Ito's prescription in stochastic calculus. Another choice (*i.e.* Stratonovitch's prescription) is however possible, which corresponds to the proper continuum time limit in the case where the correlation length ℓ_t is very small, but not smaller than a . In this case, the w 's and the v 's cannot be taken to be independent. This is the choice that we shall make in the following.

3.2 Calculation of the averaged response and correlation functions

Two approaches will be presented. The first one, based on Novikov's theorem, leads to exact differential equations for G and C , which can be fully solved. The second one is a mode-coupling approximation (MCA), based on a re-summation of perturbation theory. It happens that, for this particular model where the noise is Gaussian and short range correlated in time, both approaches give the same results, because perturbation theory is trivial. In other cases, though, where exact solutions are no longer available, the MCA is in general very useful to obtain non perturbative results.

We shall see that the effect of the noise is to widen the diffusion peak: D_0 is renormalized by an additional term proportional to the variance of the noise v .

- Novikov's theorem. Exact equations for G

Novikov's theorem provides the following identity, valid if the v are Gaussian random variables:

$$\langle w(k, t) v(k', t) \rangle = \int_0^t dt' \int dq \left\langle \frac{\delta w(k, t)}{\delta v(q, t')} \right\rangle \langle v(q, t') v(k', t) \rangle. \quad (22)$$

Such a term actually appears in equation (17), after transformation into an equation for G :

$$(\partial_t + D_0 k^2) G(k, t - t') = \delta(t - t') - \imath k \frac{\delta}{\delta \rho(k, t')} \int \frac{dq}{2\pi} \langle v(q, t) w(k - q, t) \rangle. \quad (23)$$

In the limit where $\ell_x = a \rightarrow 0$, the noise correlation is of the form: $\langle v(q, t) v(q', t') \rangle = 2\pi\sigma^2 \delta(q + q') g_t(t - t')$, with g_t peaked in $t = t'$ such that $f(t') g_t(t - t') \simeq f(t) g_t(t - t')$ for any function f . From formally integrating equation (17) between t' and t , one can express the equal-time derivative $\delta w / \delta v$ as:

$$\left. \frac{\delta w(k, t)}{\delta v(k', t')} \right|_{t'=t-0} = -\imath k w(k - k', t) \quad (24)$$

and thus obtain:

$$\begin{aligned} (\partial_t + D_0 k^2) G(k, t - t') &= \delta(t - t') - 2\pi\sigma^2 k G(k, t - t') \\ &\times \int_0^t dt' g_t(t - t') \int \frac{dq}{2\pi} (k - q). \end{aligned} \quad (25)$$

Using the shape of the function g_t , the first integral is $1/2$. The second one is a convolution integral, and its value is $\Lambda k / 2\pi + \mathcal{O}(k^2)$ (see Eq. (16)). The final differential equation for G is then, in the small- k limit, a diffusion equation with a renormalized diffusion constant:

$$D_R = D_0 + \frac{\sigma^2 \Lambda}{2}. \quad (26)$$

It is interesting to note that the model remains well defined in the limit where the “bare” diffusion constant is zero, since a non zero diffusion constant is induced by the fluctuating velocity v . This would not be true if equation (13) was interpreted with the Ito convention, where the fluctuating velocity would *not* lead to any spreading of the average density.

The most important conclusion is thus that, in the present scalar model, stresses propagate essentially vertically, even in the presence of disorder: taking $\ell \sim a$ (where $\ell_x \sim \ell_t \sim \ell$), the response at depth H to a small perturbation is confined within a distance $\propto \sqrt{D_R H}$ from the vertical. Since $D_R \simeq \ell^2/a$, $\sqrt{D_R H}$ is much less than H in the limit where $H \gg \ell^2/a$, *i.e.* when the height of the assembly of grains is much larger than the grain size.

- Exact equations for C

Exact equations can also be derived for C , following very similar calculations. From equation (17), one can deduce the corresponding one for $w(k, t)w(-k, t)$. Upon averaging, Novikov's theorem has to be used on quantities such as $\langle w(k, t)v(q, t)w(-k - q, t) \rangle$, finally leading to:

$$(\partial_t + 2D_R k^2)C(k, t) = \hat{\sigma}^2 k^2 \left[\int \frac{dq}{2\pi} C(q, t) + \rho^2 t^2 \right], \quad (27)$$

where $\hat{\sigma}^2 = (2\pi)\sigma^2$. Going to Laplace transforms in time leads to:

$$(E + 2D_R k^2)C(k, E) - C(k, t=0) = \hat{\sigma}^2 k^2 \left[\tilde{C}(E) + 2\rho^2 E^{-3} \right] \quad (28)$$

where $\tilde{C}(E) = \int \frac{dk}{2\pi} C(k, E) \equiv \int dt e^{-Et} C(x=0, t)$. This allows one to get a closed equation on $\tilde{C}(E)$:

$$\tilde{C}(E) = \int \frac{dk}{2\pi} \frac{C(k, t=0)}{E + 2D_R k^2} + \int \frac{dk}{2\pi} \frac{\hat{\sigma}^2 k^2}{E + 2D_R k^2} \left(\tilde{C}(E) + 2\rho^2 E^{-3} \right). \quad (29)$$

In the limit where $E \rightarrow 0$, the first term on the right hand side is of order $E^{-1/2}$, whereas the coefficient of $\tilde{C}(E)$ is equal to $\hat{\sigma}^2/2D_R$. This shows that one has to distinguish two cases:

- $\hat{\sigma}^2 < 2D_R$. This corresponds, for the discrete model, to the generic case where $\rho(q)$ is not the sum of two delta peaks at $q=0$ and $q=1$. The equation for $\tilde{C}(E)$ becomes, for $E \rightarrow 0$:

$$\left(1 - \frac{\hat{\sigma}^2}{2D_R} \right) \tilde{C}(E) \approx \frac{\hat{\sigma}^2}{2D_R} 2\rho^2 E^{-3}, \quad (30)$$

or $\tilde{C}(E) \sim E^{-3}$. Transforming back to real times leads to $C(x=0, t) \sim t^2$, which is consistent with the results obtained within the discrete scalar model, where the local weight is of order t , with relative fluctuations of order one. Once one knows $C(x=0, t)$, one can obtain, from equation (27), the full function $C(x, t)$. When $x \gg a$, one finds:

$$C(x, t) = t^{3/2} \mathcal{C} \left(\frac{x}{\sqrt{t}} \right), \quad (31)$$

where $\mathcal{C}(\cdot)$ is a scaling function computed explicitly in [115]. This results shows (i) that the correlations extend over distances \sqrt{t} , as expected from the diffusive nature of the model, and (ii) that $C(x \neq 0, t) \ll C(x = 0)$, meaning that asymptotically correlations between different sites vanish. The assumption that different sites become independent (which is a stronger statement) was already used above to obtain the Gamma distribution of the local weights in the scalar model. We see that this assumption is at least consistent;

- $\hat{\sigma}^2 = 2D_R$. This corresponds exactly, as shown in [115] to the critical Takayasu model where q can only take the values 0 and 1 with equal probability. In this case, a more careful analysis of the limit $E \rightarrow 0$ must be performed. Using the fact that:

$$\int \frac{dk}{2\pi} \frac{2D_R k^2}{E + 2D_R k^2} = 1 - E \int \frac{dk}{2\pi} \frac{1}{E + 2D_R k^2} \sim 1 - \sqrt{E/8D_R}, \quad (32)$$

we now find that $\tilde{C}(E) \sim E^{-7/2}$, or $C(x = 0, t) \sim t^{5/2}$. Again, this is consistent with the direct scaling analysis presented above. Extending the analysis to $x \neq 0$ now leads to:

$$C(x \neq 0, t) = t^2 \mathcal{C}_c \left(\frac{x}{\sqrt{t}} \right), \quad (33)$$

where the critical scaling function $\mathcal{C}_c(\cdot)$ can also be computed explicitly [115], and is different from $\mathcal{C}(\cdot)$. Note that the asymptotic de-correlation of different sites still takes place, since $C(x \neq 0, t) \ll C(x = 0, t)$.

• Perturbation theory

The above method gives exact results, essentially because $v(x, t)$ is short range correlated in time: $\delta w / \delta v$ is then only needed at coinciding times, where it is known, and equal to 1. This would not be true in general; furthermore Novikov's theorem requires v to be Gaussian. It is thus interesting to show how a systematic perturbation scheme can be made to work by the use of diagrams to represent equation (17). The MCA (Mode Coupling Approximation) is then a particular re-summation scheme of this set of diagrams, which was discussed in detail in [19], which sometimes provide interesting non perturbative results.

Equation (17) is multiplied on the left by the operator G_0 (see Eq. (18)), and then re-expressed as follows:

$$w(k, t) = G_0(k, t) \otimes \rho(k, t) - \imath k G_0(k, t) \otimes \int \frac{dq}{2\pi} w(q, t) v(k - q, t) \quad (34)$$

$$\begin{aligned}
\rho(k, t) &= \times & G_0(k, t) &= \text{---}\overrightarrow{\hspace{0.5cm}}\text{---} & w_0(k, t) &= \text{---}\overrightarrow{\hspace{0.5cm}}\times \\
v(k, t) &= \text{---}\overrightarrow{\hspace{0.5cm}}\text{---} & G(k, t) &= \text{---}\overrightarrow{\hspace{0.5cm}}\text{---} & w(k, t) &= \text{---}\overrightarrow{\hspace{0.5cm}}\times \\
\langle v^2 \rangle &= \text{---}\overrightarrow{\hspace{0.5cm}}\text{---}\bigcirc\text{---}\overleftarrow{\hspace{0.5cm}}\text{---} & \Sigma(k, t - t') &= \text{---}\overrightarrow{\hspace{0.5cm}}\text{---}\overset{k-q}{\bigcirc}\overset{q-k}{\text{---}\overrightarrow{\hspace{0.5cm}}\text{---}}\text{---}
\end{aligned}$$

Fig. 1. Definition of various diagrams.

\otimes Meaning a t -convolution product. This equation can be represented with diagrams as follows: as shown in Figure 1, we represent the source ρ by a cross, the “bare” propagator G_0 by a plain line and the noise v by a dashed line. The first term of equation (34), which is the noiseless solution w_0 , is then obtained as the juxtaposition of a plain line and a cross. The arrow flows against time (*i.e.* it is directed from t to $t' < t$). The juxtaposition of two objects means a t -convolution product. By definition w is represented by the juxtaposition of a bold line and a cross (this is consistent with the identification of a bold line with the full propagator G). The diagrammatic version of equation (34) is then:

$$\text{---}\overrightarrow{\hspace{0.5cm}}\times = \text{---}\overrightarrow{\hspace{0.5cm}}\times + \text{---}\overrightarrow{\hspace{0.5cm}}\overset{k-q}{\uparrow}\text{---}\overrightarrow{\hspace{0.5cm}}\overset{q}{\times} \quad (35)$$

The “vertex” stands for $-\imath k \int \frac{dq}{2\pi}$, the two emerging wave vectors being q and $k - q$ (node law). One can now iterate this equation. To second order, one obtains:

$$\text{---}\overrightarrow{\hspace{0.5cm}}\times = \text{---}\overrightarrow{\hspace{0.5cm}}\times + \text{---}\overrightarrow{\hspace{0.5cm}}\overset{\uparrow}{\text{---}}\overrightarrow{\hspace{0.5cm}}\times + \text{---}\overrightarrow{\hspace{0.5cm}}\overset{\uparrow}{\text{---}}\overset{\uparrow}{\text{---}}\overrightarrow{\hspace{0.5cm}}\times \quad (36)$$

The corresponding equation for G is obtained by taking the derivative $\delta/\delta\rho$, and averaging over the noise v . Since $\langle v \rangle = 0$, the second diagram vanishes. We represent the noise correlator by a dashed line with a centered circle (see Fig. 1), and obtain:

$$\text{---}\overrightarrow{\hspace{0.5cm}} = \text{---}\overrightarrow{\hspace{0.5cm}} + \text{---}\overrightarrow{\hspace{0.5cm}}\overset{\bigcirc}{\text{---}}\overrightarrow{\hspace{0.5cm}} \quad (37)$$

or $G = G_0 + G_0 \Sigma G_0$, where Σ is called the self-energy (see Fig. 1). Actually, one can re-sum exactly all the diagrams corresponding to $G_0 \Sigma G_0$, $G_0 \Sigma G_0 \Sigma G_0$ to obtain the Dyson equation $G = G_0 + G_0 \Sigma G$.

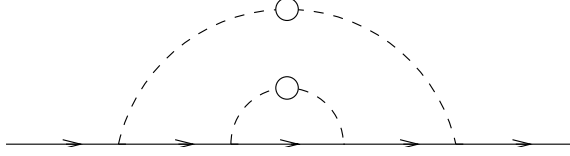


Fig. 2. Example of a diagram included in the MCA. Note that this diagram is zero if the noise is δ -correlated in time.

The MCA amounts to replacing the “bare” propagator in the diagram for Σ by the full propagator G . (Note that the MCA is of course exact to second order in perturbation theory.) We then obtain a self-consistent equation for G :

$$\Sigma_{\text{MCA}} = G_0^{-1} - G_{\text{MCA}}^{-1} = \text{diagram} \quad (38)$$

Diagrams like the one drawn in Figure 2 are now also included. The self-energy Σ_{MCA} can be easily computed, we get

$$\Sigma_{\text{MCA}}(k, t - t') = -2\pi\sigma^2 k \int \frac{dq}{2\pi} q G_{\text{MCA}}(q, t - t') g_t(t - t'). \quad (39)$$

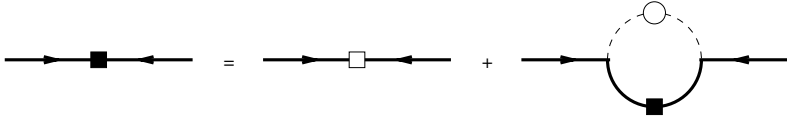
In the special case where g_t is peaked around $t = t'$, we can make the approximation $G(q, t - t') g_t(t - t') \simeq G(q, 0) g_t(t - t') = g_t(t - t')$ (since by definition $G(q, 0) = 1$). We thus get, using equation (16), $\Sigma_{\text{MCA}}(k, t - t') = -\sigma^2 \Lambda k^2 g_t(t - t')$. The expression for G_{MCA}^{-1} is thus identical to the one obtained with the exact approach, as can be seen by comparing equation (25) and $G_0^{-1} G = 1 + \Sigma G$.

Note that one can also calculate the influence of a non zero skewness ς , or kurtosis κ , which are the normalized third and fourth cumulant of the noise v . In this case, three and four dashed lines (corresponding to v) can be merged, leading to a contribution to D , of the order of $\varsigma\sigma^3$ or $\kappa\sigma^4$.

Let us turn now to the calculation of the correlation function $C(k, t) = \langle w(k, t) w(-k, t) \rangle$. The basic object which corresponds to the self-energy is now the “renormalized source” spectrum $S(k, t, t')$ defined as: $C = G \otimes S \otimes G$. S is drawn as a filled square. S_0 (empty square) is the correlation function source term which encodes the initial conditions (see below). The two first terms of the expansion are

$$\text{filled square} = \text{empty square} + \text{diagram} + \dots \quad (40)$$

Here again, we transform the perturbative expansion into a closed self-consistent equation for S by replacing G_0 and S_0 in (40) by G and S respectively. The final equation for C reads:


(41)

or, written explicitly,

$$\begin{aligned}
 C(k, t) = & \int_0^t dt' \int_0^t dt'' G(k, t - t') S_0(k, t', t'') G(-k, t - t'') + \delta^2 k^2 \int_0^t dt' \\
 & \times \int_0^t dt'' G(k, t - t') \int \frac{dq}{2\pi} C(q, t', t'') g_t(t' - t'') G(-k, t - t'').
 \end{aligned}
 \tag{42}$$

If we choose the source term to be an overload localized at $t = 0$, we get: $S_0 = \langle \rho(k, t') \rho(-k, t'') \rangle = C(k, 0) \delta(t') \delta(t'')$.

Using the fact that g_t is peaked around $t' = t''$, we again recover exactly the equation (27) above, showing again that MCA is exact in this special case.

3.3 Further results: The un-averaged response function

The *average* Green function described above is thus a Gaussian of zero mean, and of width growing as \sqrt{DRt} . However, for a *given* environment, the Green function is not Gaussian, presenting sample dependent peaks (see Fig. 3). Note however that, contrarily to what we shall find below for the tensorial case, the un-averaged Green function remains everywhere positive. Furthermore, the quantity $[x](t)$, defined as the displacement of the centroid of the weight distribution beneath a point source in a given realization:

$$[x](t) = \int_{-\infty}^{+\infty} dx' x' \frac{\delta w(x', t)}{\delta \rho(0, 0)} \tag{43}$$

typically grows with t . More precisely, one can show that:

$$\langle [x](t) \rangle = 0 \quad \text{but} \quad \langle [x]^2(t) \rangle \propto t^{1/2} \tag{44}$$

meaning that the “center” of the Green function wanders away from the origin in a sub-diffusive fashion, as $t^{1/4}$. This behaviour has actually been obtained in another context, that of a quantum particle interacting with a time dependent random environment. Physically, the q -model can indeed

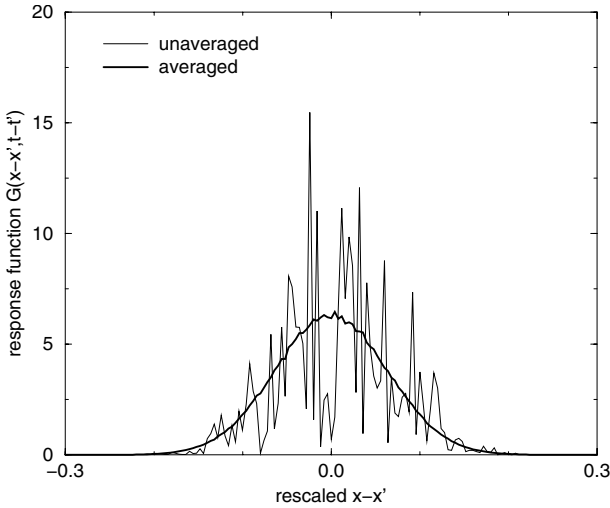


Fig. 3. Averaged (bold line) and un-averaged (thin line) response function of the scalar model, obtained numerically by simulating the q -model. One can notice how “non self averaging” is the response function, *i.e.* how different it is for a given environment as compared to the average. Note also that the un-averaged Green function is everywhere positive.

be seen as a collection of time dependent scatterers, converting in-going waves into outgoing waves with certain partition factors $q_+, q_- = 1 - q_+$, a problem equivalent to the one dimensional Schroedinger equation with a time dependent random potential (see the discussion in [47, 122]). In two dimensions (plus time), the wandering of the packet center $[x](t)$ is only logarithmic (and disappears in higher dimensions [47]).

Similarly, the participation ratio $Y_2 = \int dx \langle w^2(x, t) \rangle$ can be computed, and is found to be $\sim t^{-1/2}$, which means that the weight is not localized on a finite number of sites in this model when $t \rightarrow \infty$.

3.4 The scalar model with bias: Edwards’ picture of arches

Up to now, we have considered the mean value of v to be zero, which reflects the fact that there is no preferred direction for stress propagation. In some cases however, this may not be true. Consider for example a sandpile built from a point source: the history of the grains will certainly in-print a certain oriented “texture” to the contact network, which can be modeled, within the present scalar model, as a non zero value of $\langle v \rangle$, the sign of which depends on which side of the pile is chosen. In other words, the isotropic Edwards

assumption for the local stress transmission is expected to break down when the history of the packing explicitly breaks a symmetry.

Let us call V_0 the average value of v on the $x \geq 0$ side of the pile, and $-V_0$ on the other side. The differential equation describing propagation now reads, in the absence of disorder:

$$\partial_t w + \partial_x [V_0 \operatorname{sign}(x)w] = \rho + D_0 \partial_{xx} w. \quad (45)$$

For a constant density $\rho = \rho_0$, and for $D_0 = 0$, the weight distribution is then the following:

$$\begin{aligned} w(x, t) &= \frac{\rho_0 x}{V_0} & \text{for } 0 \leq x \leq V_0 t \\ w(x, t) &= \frac{\rho_0(ct - x)}{c - V_0} & \text{for } V_0 t \leq x \leq ct \end{aligned} \quad (46)$$

where $c = 1/\tan \phi$ (ϕ is the angle made by the slope of the pile with the horizontal x axis). For $D_0 \neq 0$, the above solution is smoothed. In any case, the local weight reaches a *minimum* around $x = 0$. Equation (45) gives a precise mathematical content to Edwards' model of arching in sandpiles [59], as the physical mechanism leading to a “dip” in the pressure distribution [128]. As discussed elsewhere [145, 146], this can be taken much further within a tensorial framework (see Sect. 5.1).

Equation (45) with noise can in fact be obtained naturally within an extended q -model, with an extra rule accounting for the fact that a grain can slide and lose contact with one of its two downward neighbour when the shear stress is too large [40]. This generically leads to arching; in the sandpile geometry and for above a certain probability of (local) sliding, the effective “velocity” V_0 becomes non zero and the weight profile (46) is recovered [40]. However, this extra sliding rule implicitly refers to the existence of shear stresses, which are absent in the scalar model, but which are crucial to obtain symmetry breaking effects modeled by a non zero V_0 (see also the discussion in Sect. 5.1). It is thus important to consider from the start the fact that stress has a tensorial, rather than scalar, nature. This is what we investigate in the following sections.

4 Static indeterminacy; elasticity and isostaticity

4.1 Elasticity and response functions

As mentioned in the introduction, the sole equilibrium equations are not sufficient to determine the stress tensor of an arbitrary material. In $d = 2$, one has two equations and three independent components of the stress tensor. In $d = 3$, there are three equations for six independent components

of σ_{ij} . In elastic materials, this indeterminacy is lifted when one adds the constraint that the stress tensor is linearly related to the strain. The most general linear relation between stresses and strains is given by:

$$\sigma_{ij} = \lambda_{ijkl} u_{kl} \quad (47)$$

where σ_{ij} denotes the components of the stress tensor, u_i is the displacement field, $u_{ij} = \frac{1}{2}(\partial_j u_i + \partial_i u_j)$ those of the strain tensor, and summation over repeated indices is implied. The four index tensor λ_{ijkl} satisfies certain symmetry conditions [89].

In order to close the problem for the stress tensor, one imposes a condition of “compatibility”, which in $d = 2$ reads:

$$\partial_z^2 u_{xx} + \partial_x^2 u_{zz} - 2\partial_x \partial_z u_{xz} = 0, \quad (48)$$

resulting simply from the fact that the tensor u_{ij} is built with the derivatives of a vector u_i . This is enough to find a closed equation for the stresses (in $d = 2$) [110]:

$$(\partial_z^4 + t\partial_x^4 + 2r\partial_x^2 \partial_z^2) \sigma_{ij} = 0 \quad (49)$$

where the two independent coefficients t and r can be expressed in terms of the components of λ_{ijkl} . *Isotropic* elasticity corresponds to $r = t = 1$.

Expanding the stresses in Fourier modes, it is easy to see that the solutions of the equations (49) are of the form

$$\sigma_{tt} = \int_{-\infty}^{+\infty} dq \sum_k a_k(q) e^{iqx + iX_k qz}, \quad (50)$$

$$\sigma_{xt} = C_{xz} - \int_{-\infty}^{+\infty} dq \sum_k a_k(q) X_k e^{iqx + iX_k qz}, \quad (51)$$

$$\sigma_{xx} = C_{xx} + \int_{-\infty}^{+\infty} dq \sum_k a_k(q) X_k^2 e^{iqx + iX_k qz}, \quad (52)$$

where C_{xx} and C_{xz} are constants. From equation (49) we see that the X_k are the roots of the following quartic equation

$$X^4 + 2rX^2 + t = 0, \quad (53)$$

which has four solutions:

$$X = \pm \sqrt{-r \pm \sqrt{r^2 - t}}. \quad (54)$$

Hence the index k runs from 1 to 4. The four functions $a_k(q)$ and the constants C_{xx} and C_{xz} must be determined by the boundary conditions. A

particularly interesting boundary condition is when one imposes a localized force at the top surface of the material. The shape of the stress *response function* to such a localized force will be of central importance in the following discussion. One can establish the existence of various “phases” in the r, t plane in terms of the shape of the response function, as obtained from the calculations presented in [110]. In that plane, the line $t = r^2$, for $r < 0$, separates the so called *hyperbolic* and the *elliptic* regions. For $t > r^2$, the above roots X_k are complex whereas for $t < r^2$ and $r > 0$ the roots X_k are purely imaginary. These two regions correspond to the *elliptic* regime, which is in fact the only accessible one in the context of classical elasticity where the coefficients r and t are constrained by the fact that the undeformed state is a minimum of the elastic energy. As shown in details in [110], the response function has a unique, broad peak of width growing linearly with depth in the region $t < r^2$ and $r > 0$, whereas the response function becomes *double peaked* in the region $r < 0$, $t > r^2$ (with a width again scaling linearly with depth). As one approaches the line $t = r^2$, the two peaks become narrower and narrower before becoming two delta-function peaks exactly on the transition line. At this point and below the transition, the system is *hyperbolic*; this limit behaviour will actually emerge naturally below in the context of granular materials.

4.2 Indeterminacy at the grain level and isostaticity

Elasticity theory can also be seen as the long-wavelength description of a network of beads and springs, for which the local equilibrium equations are fully determined at each node. When the network is disordered, the theoretical difficulty is to compute the effective elastic constants in terms of the probability distribution and correlations of the microscopic springs. The same problem arises when one wants to compute the effective conductivity, or the effective permittivity, etc. of a composite material. But in all these problems, the *microscopic* equations are sufficient to solve the problem in principle.

For an assembly of grains, this is not the case. The indeterminacy of the static equilibrium exists already at the grain level (see the simple case discussed in Sect. 1.2.2). In principle, one should describe in details the microscopic history of each contact in order to determine the precise configuration of forces within a given packing. There are however special cases where this is not the case, and where all contact forces are fully determined by the packing geometry. These situations are called isostatic, and play a special role. These equilibria are in some sense critical since the opening of one contact necessarily leads to some rearrangements. Some arguments have been put forward to suggest that an assembly of grains relaxing towards static equilibrium will most probably stop *as soon as they are stable*,

i.e., in one of these isostatic states [14]. A similar statement is actually *exact* in the context of mean-field spin-glasses, where the equilibrium states reached dynamically are marginally stable, in the sense that the spectrum of the eigenvalues λ of the Hessian (matrix of second derivatives of the energy) vanishes precisely at $\lambda = 0$. Before discussing the validity of the idea that these marginal states play a special role in granular media, let us first discuss the geometrical conditions necessary for isostaticity [125].

Consider *frictionless* grains in two dimensions. There are, per grain, two equilibrium equations since the torque is automatically zero, and one (normal) force per contact that must be determined. If N is the total number of grains and N_c the total number of contacts, the number of unknowns is N_c and the number of equations in $2N$. Therefore, one can (generically) find static solutions only if $N_c \geq 2N$. Since each contact concerns two grains, the average number of contact per grain is $n_c = 2N_c/N$ and the condition for the existence of solutions is $n_c \geq 4$. The marginal case is when $n_c = 4$, where the number of unknowns is equal to the number of equations, and corresponds to the isostatic case. The hyper-static case corresponds to a strict inequality. If the friction coefficient is non zero, then the zero-torque condition provides a third equation for each grain. If we call φ the fraction of contacts where friction is fully mobilized (*i.e.* such that $|F_T| = \mu F_N$), one has $\varphi \cdot N_c + (1 - \varphi) \cdot 2N_c$ unknowns (one per mobilized contact, two for un-mobilized contacts). The stability condition now reads $n_c(1 - \varphi/2) \geq 3$. (Note that the frictionless case corresponds to $\varphi = 1$.) In three dimensions, the same argument leads to $(3 - \varphi)n_c \geq 12$, the isostatic case corresponding to an equality. The corresponding “stability” diagram is shown in Figure 4.

4.3 Numerical simulations and Edwards’ assumption

So, are three dimensional packings of grains, obtained by letting the grains lose their kinetic energy and come to rest, generically isostatic? The only quantitative study we are aware of is that of Silbert *et al.* [125], where these authors perform Molecular Dynamics simulation of *monodisperse* grains with a specific form of contact dynamics and a certain energy dissipation coefficient at each collision. The results reported in [125] are compatible with isostaticity for frictionless spheres, $\mu = 0$. In this case, the equilibrium packings are indeed found to obey the condition $n_c = 6$, as expected from the general results of [102, 118]. However, when the friction coefficient is non zero, these authors find that the static configurations are such that (a) the fraction of fully mobilized contacts is $\varphi = 0$ and (b) the number of contacts per grain seems to saturate, in the limit of hard grains, to a value of $n_c > 4$, suggesting that the packing is not isostatic. The value of n_c appears to depend significantly on the value of the friction coefficient and the restitution coefficient; it appears from their data that smaller

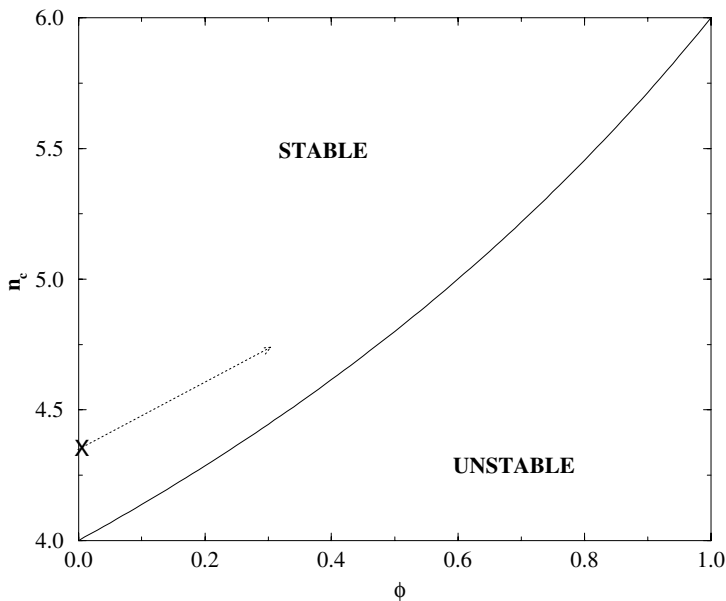


Fig. 4. Stability diagram in the plane ϕ, n_c for three dimensional assemblies. The plain line is the isostatic line that separates stable packings from unstable packings. The point $\phi = 1, n_c = 6$ corresponds to frictionless particles. The cross for $\phi = 0$ represents the numerical result of [125]; the dotted arrow is a possible path of the packing when vibrated.

restitution coefficients (*i.e.* more damping) lowers the value of n_c , perhaps down to the isostatic limit for large damping. This dependence on the details of the dynamics indicates that no universal statement about the statistics of “native” packings (*i.e.* obtained without further tapping) can be made. Again, the simplistic situation discussed in Section 1.2.2 would provide a useful benchmark.

What happens when one of these native states (possibly hyperstatic) is vibrated? Does the packing wander inside the stable regime (see Fig. 4) or remains near the isostatic boundary? Here again, it is useful to recall the results of mean field p-spin glasses, where the “vibrations” (temperature) keep the system along the ridge of marginally stable states. In this case, the reason is the exponential dominance of the number of these states over the “deeper” (more stable) ones. Therefore, even if blocked states are *a priori* equiprobable (as postulated by Edwards), the most probable situation is to observe the system in a marginal state. If this argument can be transposed to granular packings, then ideas that Edwards expressed in different

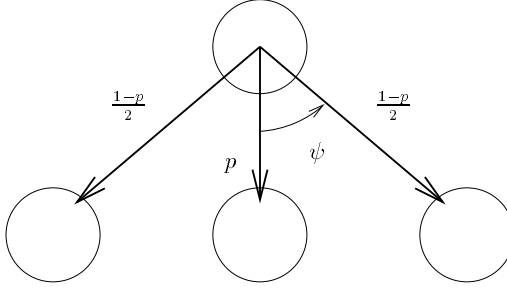


Fig. 5. Three neighbour configuration. Each grain transmits two force components to its downward neighbours. A fraction p of the vertical component is transmitted through the middle leg.

contexts (*i.e.* that blocked states are equiprobable and that only marginal (isostatic) states are important [14]) would be reconciled. It would be very interesting to compute the number of metastable states as a function of the isostatic index n_c in some (possibly artificial) model (on this point, see the attempt in [99]).

5 A stress-only approach to granular media

We now turn to the discussion of some plausible “stress-only” closure schemes for the static equilibrium of granular materials. We first start by a natural generalization of the scalar q -model to account for the vectorial nature of the forces. Then we show how the results of this “vectorial” q -model can be interpreted more generally in terms of symmetry arguments.

5.1 A vectorial q -model

It is useful to start with a simple toy model for stress propagation, which is the analogue of the scalar model presented in Section 2. We now consider the case of three downward neighbours (see Fig. 5), for a reason which will become clear below. Each grain transmits to its downward neighbours not one, but two force components: one along the vertical axis t and one along x , which we call respectively $F_t(i, j)$ and $F_x(i, j)$. For simplicity, we assume that each “leg” emerging from a given grain can only transport the force parallel to itself. This assumes that each contact is frictionless. More general transfer rules can be considered, where the forces are chosen, *à la* Edwards, randomly within the space of solutions – see *e.g.* [28, 63, 105, 131].

We assume that a fraction p of the vertical force travels through the middle leg. Correspondingly, a fraction $q_+ = (1-p)(1+\varepsilon)/2$ travels through

the right leg, and a fraction $q_- = (1 - p)(1 - \varepsilon)/2$ through the left leg, so that $p + q_+ + q_- = 1$. (Some anisotropic generalizations will be discussed below). Since the total force in these legs is oriented in the direction ψ , where ψ is the angle between grains, defined in Figure 5, the balance of the horizontal force on the grain i, j imposes a specific value for ε :

$$\varepsilon \equiv \frac{1}{(1 - p) \tan \psi} \frac{F_x(i, j)}{F_z(i, j)}. \quad (55)$$

We therefore discover a very important consequence of the existence of a shear stress F_x , which was totally absent from the scalar q -model or had to be put by hand: any non zero value of F_x necessarily leads to $q_+ \neq q_-$ and biases the propagation of F_z in the direction of F_x . This coupling between the two components of the force is at the origin of all the interesting physics discussed below.

Using the value of ε to compute the propagation of the forces from one layer to the next, we find:

$$\begin{aligned} F_x(i, j) &= \frac{1}{2} [F_x(i - 1, j - 1) + F_x(i + 1, j - 1)] \\ &\quad + \frac{1}{2} (1 - p) \tan \psi [F_t(i - 1, j - 1) - F_t(i + 1, j - 1)] \end{aligned} \quad (56)$$

$$\begin{aligned} F_t(i, j) &= w_0 + p F_t(i, j - 1) + \frac{1}{2} (1 - p) [F_t(i - 1, j - 1) + F_t(i + 1, j - 1)] \\ &\quad + \frac{1}{2 \tan \psi} [F_x(i - 1, j - 1) - F_x(i + 1, j - 1)]. \end{aligned} \quad (57)$$

Taking the continuum limit of the above equations leads to:

$$\partial_t F_t + \partial_x F_x = \rho + a \frac{1 - p}{2} \partial_{tt}^2 F_t \quad (58)$$

$$\partial_t F_x + \partial_x [c_0^2 F_t] = \frac{a}{2} \partial_{xx}^2 F_x \quad (59)$$

where $c_0^2 \equiv (1 - p) \tan^2 \psi$, a is the size of the grains, and we have kept the second order diffusion terms, which would be the only remaining term in the isotropic scalar description, and plays the role of a smoothing term for the (singular) solutions found below. Comparing equation (58) with equation (45) (with $w = F_t$), we see that the “velocity” term introduced by hand in the Edwards model is indeed a consequence of the local shear.

Eliminating (say) F_x between the above two equations leads to a *wave equation* for F_t (up to a diffusion term which becomes small in the large scale limit), where the vertical coordinate t plays the rôle of time and c_0 is the equivalent of the “speed of light”. In particular, the stress does not propagate vertically, as it does in the scalar model, but rather along two

rays, each at a *non zero angle* $\pm\varphi$ such that $c_0 = \tan \varphi$. Note that $\varphi \neq \psi$ in general (unless $p = 0$); the angle at which stress propagates has nothing to do with the underlying lattice structure and can take any value depending on the local rules for force transmission. The three-leg model was chosen to illustrate this particular point: the number of legs is irrelevant in the large scale limit, and the wave structure of the resulting equation is universal.

5.2 A constitutive relation between stress components

The above derivation can be reformulated in terms of classical continuum mechanics as follows. Considering all stress tensor components σ_{ij} , the equilibrium equation reads,

$$\partial_t \sigma_{tt} + \partial_x \sigma_{xt} = \rho \quad (60)$$

$$\partial_t \sigma_{tx} + \partial_x \sigma_{xx} = 0. \quad (61)$$

Identifying the local average of F_t with σ_{tt} and that of F_x with σ_{tx} , we see that the above equations ((58), (59)) are actually identical to ((60), (61)) provided $\sigma_{tx} = \sigma_{xt}$ (which corresponds to the absence of local torque) and, more importantly, that there exists a relation between the vertical and horizontal components of the stress tensor:

$$\sigma_{xx} = c_0^2 \sigma_{tt}. \quad (62)$$

This relation between normal stresses was postulated in [18] as the simplest “constitutive relation” among stress components, obeying the correct symmetries, that one can possibly assume. The term “constitutive relation” normally refers to a relation between stress and strain, but the model under discussion has no strain variables defined. This particular choice can be interpreted as a *local* Janssen approximation [82], in analogy with the assumption made by Janssen in 1895 in order to describe stresses in silos, where the *average* vertical stress at a given altitude is postulated to be proportional to the average horizontal stress. We return later to a more detailed discussion of this type of closure equations. In the present case, the parameter c_0^2 encodes relevant details of the local geometry of the packing (friction, shape of grains, etc.) and may thereby depend on the *construction history* of the grain assembly. Only for simple, “homogeneous” histories (such as constructing a uniform sand-bed using a sieve) will c_0^2 be everywhere constant on the mesoscopic scale. Even then, unless an ordered packing is somehow created, local fluctuations of c_0^2 will always be present. The influence of these fluctuations will be analyzed below.

5.3 Some simple situations

Using equation (62) in equations ((60), (61)) we find that these can be rewritten as:

$$\partial_u(\sigma_{xt} - c_0\sigma_{tt}) = -\frac{\rho}{2} \quad (63)$$

$$\partial_v(\sigma_{xt} + c_0\sigma_{xt}) = \frac{\rho}{2}, \quad (64)$$

where $u = x - c_0t$ and $v = x + c_0t$. This shows that in this framework, the forces are transported along the characteristics, which is what the word “force chain” usually implies [35, 61]. More precisely, the solution of equations ((60), (61)) is obtained by projecting any “initial” force (*i.e.* present at altitude $t = 0$) onto the two characteristics, and propagating and augmenting each component by an amount $(\rho/2)dt$, independently along these characteristics.

The simplest situation is that of an infinitely wide layer of sand, of depth H , with a localized (δ -function) overload at the top. The additional weight at the bottom then defines the *response function* of the wave equation, which, in two dimensions, is the sum of two δ peaks localized at $x = \pm c_0H$. These δ peaks are actually diffusively broadened by the second order terms present in equations ((58), (59)). This two-peak response function is notably different from the response function of an isotropic elastic body, for which the response function is a single hump of width proportional to the height H . However, for anisotropic elasticity, a two peak response function *can* be observed [68, 73, 110], but both peaks have a width scaling linearly with H , and not as $H^{1/2}$ for an hyperbolic equation. The question of the response function is therefore of crucial importance, and will be discussed in details below. Recent attempts to determine the response function experimentally seem to favor an elastic like response, at least for the strongly disordered systems (see Sect. 6).

Next, one can consider the sandpile geometry. For a pile at repose, the position of the free surfaces are $x = \pm cz$, where $c = \cot \phi$ with ϕ the repose angle. On these surfaces, all the stresses vanish. This boundary condition is then (for given c_0 and c) sufficient to solve for the stress field everywhere in the pile. One then finds that the vertical normal component of the stress is piecewise linear as a function of x . In particular, for $-c_0H \leq x \leq c_0H$, σ_{tt} is *constant*. Therefore, in two dimensions, this model [18] predicts a flat-topped stress profile rather than a hydrodynamic pressure hump or a dip. Such a flat top is in fact observed when building a pile from a uniform rain of grains.

For a pile created by depositing grains from above (for example by sieving sand onto a disc) it is natural to expect the free surface to be a slip plane. (This is a plane across which the stress components saturate the

Mohr-Coulomb condition – see below.) Interestingly, this provides a relation between c_0 and the friction angle ϕ , which reads: $c_0^2 = 1/(1 + 2 \tan^2 \phi)$ (note that since $c = 1/\tan \phi$, one has automatically $c > c_0$). Under these conditions one finds that the “plastic” region (where the Mohr-Coulomb condition is saturated) extends (in two dimensions) inward from the surface to encompass the outer “wings” of the pile (*i.e.* $c_0 z \leq |x| \leq cz$). This follows from the solution of the model and is not an *a priori* assumption, of the kind commonly made in elastoplastic modeling (*e.g.*, [33, 123]; see also the discussion in [104]). In three dimensions, a second closure relation is required [18], but in all cases the stress profile has a broad maximum at the center of the pile. Now, however, the Mohr-Coulomb condition is only saturated in the immediate vicinity of the free surface – the “plastic” region has zero volume in three dimensions [18, 146].

5.4 Symmetries and constitutive relations

Although above it was motivated in the context of a specific microscopic model of force transfer, the linear constitutive relation (62) can be viewed, independently of any microscopic model, as the simplest closure equation compatible with the symmetries of the problem. The latter include a *local* reflection symmetry in which $x - x_0$ is changed to $x_0 - x$ (with x_0 an arbitrary reflection plane) and also a form of “dilational” symmetry on the stress known as RSF (“radial stress field”) scaling. RSF scaling depends on the absence of any characteristic stress scale, which follows if the Young’s modulus of the grains is sufficiently much larger than any stresses arising in the granular assembly being studied. Such scaling, which requires the stress distributions beneath piles of different heights to have the same shape, is quite well confirmed in some (but not all) experiments on conical sand-piles [29, 123, 128].

Even with these two symmetries, one can consider more complicated (nonlinear) constitutive relations among stresses, which must be of the form [18]:

$$\sigma_{xx} = c_0^2 \sigma_{tt} \mathcal{F} \left(\frac{\sigma_{xt}^2}{\sigma_{tt}^2} \right). \quad (65)$$

Note that in general, such a constitutive relation violates rotational symmetry, and can only describe an anisotropic pile (for example, built from a rain of grains under gravity). The only rotationally invariant stress closure scheme must involve the two invariants of the stress tensor, namely $\text{Tr } \sigma$ and $\text{Det } \sigma$. From dimensional analysis, this relation can only be of the form:

$$\cos^2 \phi (\text{Tr } \sigma)^2 = 4 \text{Det } \sigma, \quad (66)$$

where the specific choice of the coefficient is such that we recognize the usual Mohr-Coulomb relation. Equation (66) indeed means that there exists a

choice of orthogonal axis m, n such that:

$$\left| \frac{\sigma_{nm}}{\sigma_{nn}} \right| = \tan \phi = \mu, \quad (67)$$

where μ is the internal friction coefficient. One can easily show that this relation is of the general form equation (65), for a particular form of \mathcal{F} , since equation (66) can also be rewritten such as:

$$c_0^2 \mathcal{F}(u) = \frac{1}{\cos^2 \phi} \left[\sin^2 \phi + 1 \pm 2 \sin \phi \sqrt{1 - \cot^2 \phi} u \right]. \quad (68)$$

Viewed as a constitutive equation, the Mohr-Coulomb relation defines a rigid-plastic model whose physical content is to assume that, everywhere in the material, a plane can be found across which slip failure is about to occur, hence the name “incipient failure everywhere”, (IFE), given to this model [18, 145, 146].

All closures of the form (65) lead to hyperbolic equations for stresses, although in the general case the characteristic directions of propagation (the “light rays” of the corresponding wave equation) depend on the loading and therefore vary with position.

An interesting situation arises when local reflection symmetry is broken. This is the case, for example, in sand-piles created by pouring from a point source onto a rough surface – which is the usual mode of construction. In such a pile, all grains arriving at the apex of the pile roll (in two dimensions) either to the right or to the left. The two halves of the pile therefore have different construction histories that are mirror images of each other. This violates local reflection symmetry, and in general permits constitutive equations such as:

$$\sigma_{xx} = c_0^2 \sigma_{tt} \mathcal{G} \left(\frac{\text{sign}(x) \sigma_{xt}}{\sigma_{tt}} \right). \quad (69)$$

The simplest case (found *e.g.* by expanding \mathcal{G} to first order in the shear to normal stress ratio) corresponds to a family of (quasi-) linear constitutive relations [146]:

$$\sigma_{xx} = c_0^2 \sigma_{tt} + \nu \text{sign}(x) \sigma_{xt}. \quad (70)$$

The previous, symmetrical, case has $\nu = 0$. For nonzero ν , equation (70) again leads to a wave equation, although this time *anisotropic*, in the sense that the two characteristic rays make asymmetric angles to the vertical axis. Note also that $x = 0$ is a singular line across which the directions of propagation change discontinuously.

Microscopically, $\nu \neq 0$ leads to an unequal sharing of the weight of a grain between the two characteristic rays propagating downward from it. Such a model can indeed be obtained from rules such as those in Figure 5

simply by having an asymmetric rules for partitioning the forces between the supporting grains, for example choosing two different angles ψ_+ and ψ_- . The symmetric case corresponds to $\nu = 0$ and $\nu \propto \tan \psi_+ - \tan \psi_-$. For $\nu < 0$, most of the weight travel *outwards* on the leg with the smallest opening angle; this provides, within a fully tensorial model, a mathematical description of the tendency to form arches, as developed by Edwards for the scalar case.

Solving these anisotropic wave equations for sand-piles in two dimensions one again finds for σ_{tt} a piecewise linear function, which now has a maximum at $x = 0$ when $\nu > 0$, but a minimum for $\nu < 0$, in accord with the arching picture mentioned above. If one furthermore imposes, as above, that the free surfaces are slip planes, one finds a relation between c_0^2 , ν and ϕ . One again finds the result that the material throughout the outer wings of the pile (exterior to the triangle formed by the characteristics passing through the apex) are at incipient (Mohr-Coulomb) failure.

5.5 Boundary conditions and “fragility”

All the above closure schemes lead to hyperbolic equations, which crucially differ from the elliptic equations encountered in elasticity theory when *boundary conditions* are considered. Hyperbolic equations indeed require only “half” of the boundary conditions to be specified, the other half being *determined* by “propagating” these known boundary conditions along the characteristics through the system. On the contrary, an elliptic equation (such as Laplace’s equation) requires the stress (or the displacement) on all the surfaces of the body to be specified. If one insists on applying all the boundary conditions appropriate to an elastic body, then in general no solution will exist for the hyperbolic equations that correspond to a particular choice of constitutive relation. If these boundary conditions are “incompatible” in this sense, then within an hyperbolic model, the material ceases to be in static equilibrium. This is not different from the corresponding statement for a fluid; if boundary conditions are applied that violate the conditions for static equilibrium, some motion will result. Unlike a fluid, however, for a granular medium we expect such motion to be in the form of a finite rearrangement rather than a steady flow. Such a rearrangement will change the micro-texture of the material, and thereby *alter the constitutive relation among stresses*. One expects it to do so in such a way that the new (spatially inhomogeneous) constitutive relation becomes compatible with the imposed forces.

Within this modeling approach, a granular assembly is therefore able to support some, but not all, of the surface loads that would be supportable by an elastic medium. Such models may therefore provide an interesting paradigm for the behaviour of “fragile matter” [35].

6 Experimental and numerical determination of the stress response function

The stress “response function” to a localized overload is of prime interest both from a fundamental point of view but also for many engineering applications. On large scales, the extra stresses created by a house within the soil beneath it are indeed related to this response function. Therefore, this problem has received considerable theoretical attention in the engineering community, where, as mentioned in the introduction, the granular material is often assumed to be a (possibly anisotropic) elastic material. Note that an elliptic response function corresponds to a favorable case for stability since the stresses are efficiently dispersed in space, whereas a hyperbolic response function would lead to a rather localized stress field.

In spite of its importance, the response function of granular assemblies has only very recently been measured experimentally [69, 103, 116]. Various methods were used: one is a direct quantitative measurement of the response at the bottom of a 3D packing using a local stress probe based on the deformation of a hard membrane [116], another method is based on carbon paper imprints created by a monodisperse 3D packing [103]. For 2D packing the photo-elastic response of polymeric grains was used [69] in order to evidence the inter-particle force path. This is a semi-quantitative method but it allows to visualize directly the response in the bulk as well as the topology of the path followed by the stress chains. Such an observation will be used to built the theoretical proposition exposed in the following section. These experimental efforts have lead so far to the following picture²: for strongly disordered packings (for example by considering mixtures of grains of very different sizes, or irregular grains such as natural sand), the response profile on large length scales shows a single broad peak [69, 116]. This single hump response function was also observed in numerical simulation of 2D polygonal grains packing [101].

For well ordered packings however, the two peaks structure is rather convincingly observed in two dimensions (a “ring” or three peaks in 3D) [15, 69, 103]. These hyperbolic features are also in agreement with a recent numerical simulation on (rather small) isostatic assemblies of frictionless grains [78, 138], with the work reported in [28, 63] where beads are arranged on a regular triangular lattice but where disorder is introduced by a finite friction coefficient. Similarly, two-peak response can be observed for strongly anisotropic elastic networks [73, 110].

²Note however that a purely “diffusive” response function, scaling as \sqrt{H} as predicted by the “scalar” model, was reported in [126] for a very special “brick” packing.

Obtaining a precise experimental determination of the linear response function that can be *quantitatively* compared to theoretical models is rather difficult: the perturbation must be small enough not to disrupt the packing, but also large enough to lead to a measurable signal. A very sensitive technique, based on a lock-in detection of an oscillating perturbation, has allowed one to obtain precise and reproducible results [116, 124]. One finds unambiguously that the response function $G(r, H)$ to a perturbation located at $r_0 = z_0 = 0$ is in the case of sand layers *single-peaked*, with a width growing as the height H of the layer. More precisely, the response function for different heights can be rescaled onto a unique curve by plotting $H^2 G(r, H)$ as a function of r/H . The factor H^2 is expected from force conservation: the integral of the response function over the bottom plate must be equal to the overload force F for the total force to balance. One also finds that, like for sand-piles, the pressure response profile depends on the way the granular layer was prepared – its “history”: the value of the maximum of this response is roughly twice smaller (and its width twice larger) for a dense packing than for a loose one (see Fig. 6). The quantitative shape of the experimental response function cannot be accounted for by a simple isotropic elasticity theory (see also the discussion in [147]), but in the present geometry, anisotropic elasticity leaves three extra adimensional constants that can give a large freedom to fit the data (see [110]).

Therefore, the most precise experiments on strongly disordered packings seems to favor a single peak, elastic like response, rather than a double peak response that only appears in special conditions (ordered packings, or frictionless grains). We therefore need to understand in details the rôle of randomness in hyperbolic wave equations, or in more physical terms, the large scale consequence of the fact that force chains are “scattered” by packing irregularities. Is this sufficient to convert a two peak response function into a single peak, elastic like function? This is the subject of the following sections.

7 Force chains scattering I: Weak disorder limit

7.1 A stochastic wave equation

Provided that local conservation laws (those arising from mechanical equilibrium) are obeyed, many local rules for force transmission are *a priori* compatible with the existence of contacts among rigid particles [63, 131]. Therefore, even if there is a definite mean relationship among stresses at the meso-scale, one can expect randomness in the local transmission coefficients. The simplest model for this and other sources of randomness is to introduce a randomly varying “speed of light” c_0 . This could describe the fact that, for example, the parameter p in the model of Figure 5 can vary from grain

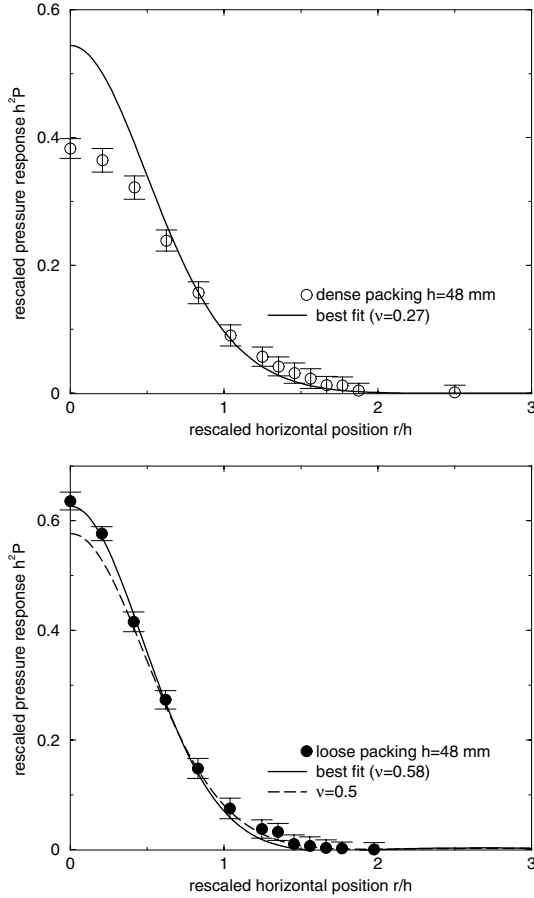


Fig. 6. Up: fit of the “dense” packing data with the standard elastic Green function. The agreement is not good at all. Down: fit of the loose packing data. The best fit value for ν exceeds the elastic bound $\nu \leq \frac{1}{2}$. From [124].

to grain. In this situation the two rays are still symmetric around the vertical direction, but with a random opening angle. The situation where the bisecting line itself is random (*i.e.* when both the above opening angles ψ_{\pm} are fluctuating) will be alluded to below.

This suggests the following stochastic wave equation for stress propagation in two dimensions:

$$\partial_{tt}\sigma_{tt} = \partial_{xx} [c_0^2(1 + v(x, t)) \sigma_{tt}] \quad (71)$$

where the random noise v is assumed to be correlated as $\langle v(x, t)v(x', t') \rangle = \sigma^2 g_x(x - x')g_t(t - t')$. The correlation lengths ℓ_x and ℓ_t are again kept finite, and of the same order of magnitude. In Fourier transform, this relation can also be written $\langle v(k, t)v(k', t') \rangle = 2\pi\sigma^2\delta(k + k')\tilde{g}_x(k)g_t(t - t')$. It turns out that the final shape of the averaged response function depends on the sign of $\tilde{g}_x(\Lambda)$. In Section 3 we implicitly made the choice $\tilde{g}_x(k) = 1$, which corresponds to: $g_x(x = 0) = 1/a$ and $g_x(x > 0) = 0$. We will keep this choice for the following calculations, but note that another form for g_x could lead to $\tilde{g}_x(\Lambda) < 0$.

In the following, σ_{tt} will be again denoted by w . After a Fourier transform along x -axis, we get, from equation (71)

$$(\partial_{tt} + c_0^2 k^2)w = \partial_t \rho - c_0^2 k^2 \int \frac{dq}{2\pi} w(q, t)v(k - q, t). \quad (72)$$

Note that the “source” term of this equation is now $\partial_t \rho$ rather than ρ itself. Therefore, if we call G the Green function (or propagator) of this equation $G = \langle \delta w / \delta \partial_t \rho \rangle$; the response function $R = \langle \delta w / \delta \rho \rangle$ of our system is now actually the time derivative of G : $R(k, t) = \partial_t G(k, t)$.

The noiseless propagator G_0 is the solution of the ordinary wave equation $(\partial_{tt} + c_0^2 k^2)G_0(k, t - t') = \delta(t - t')$ and can be easily calculated:

$$G_0(k, t) = \frac{1}{2ic_0 k} [e^{ic_0 kt} - e^{-ic_0 kt}] \theta(t) \quad (73)$$

which leads to the response function R_0

$$R_0(x, t) = \frac{1}{2} [\delta(x - c_0 t) + \delta(x + c_0 t)] \theta(t). \quad (74)$$

This last equation sums up one of the major results of the hyperbolic approach of [18, 145, 146]: in two dimensions, stress propagates along two characteristic rays. (Note that the corresponding response function in three dimensions reads $R_0(x, t) \propto (c_0^2 t^2 - x^2)^{-1/2}$ for $|x| < c_0 t$ and zero otherwise [18].) A relevant question is now to ask how these rays survive in the presence of disorder. We will show that for weak disorder, the δ -peaks acquire a finite (diffusive) width, and that the “speed of light” is renormalized to a lower value. Not surprisingly, the effect of disorder can be described by an “optical index” $n > 1$. For a strong disorder, however, we find (within a Gaussian approximation for the noise v) that the speed of light vanishes and becomes imaginary. The “propagative” nature of the stress transmission disappears and the system might behave more like an elastic body, in a sense clarified below.

7.2 Calculation of the averaged response function

One can again use Novikov's theorem in the present case if the noise is Gaussian and short range correlated in time. However, the same results are again obtained within the diagrammatic approach explained in Section 3, which can be easily transposed to the present case, and is more general. The propagator G is now represented as a line, the source $\partial_t \rho$ a cross and the vertex meaning $-c_0^2 k^2 \int \frac{dq}{2\pi}$. Within the MCA, the self-consistent equation (analogous to Eq. (38) in the scalar case) is:

$$(\partial_{tt} + c_0^2 k^2)H(k, t) = \delta(t) + \int_0^t dt' \Sigma_{\text{MCA}}(k, t')H(k, t - t') \quad (75)$$

where H is defined by $G(k, t) = H(k, t)\theta(t)$, and the self-energy Σ_{MCA} given as

$$\Sigma_{\text{MCA}}(k, t - t') = 2\pi c_0^4 \sigma^2 k^2 \int \frac{dq}{2\pi} q^2 g_t(t - t') \tilde{g}_x(k - q) H(q, t - t'). \quad (76)$$

Equation (75) can be solved using a standard Laplace transform along the t -axis (E is the Laplace variable). Using the fact that $H(k, \tau) = \tau$ in the limit where $\tau \rightarrow 0$, we find, for small k, E (corresponding to scales L such that $\ell_x, \ell_t \ll L$): $H^{-1}(k, E) = E^2 + \beta E + c_R^2 k^2$, where

$$c_R^2(k) = c_0^2 - \frac{c_0^4 \sigma^2 \Lambda^3 \ell_t}{6} \left(1 - \frac{3|k|}{2\Lambda}\right) + \mathcal{O}(k^2) \quad (77)$$

$$\beta(k) = \frac{c_0^4 \sigma^2 k^2 \Lambda^3 \ell_t^2}{9} + \mathcal{O}(k^3). \quad (78)$$

We notice here that in the limit $\ell_t \rightarrow 0$, the effect of the randomness completely disappears, as in the scalar model with the Ito convention. (Technically, this is due to the fact that $G(k, t = 0) \equiv 0$ in the present problem.) In order to calculate the inverse Laplace transform, we need to know the roots of the equation $H^{-1}(k, E) = 0$. This leads to several phases, depending on the strength of the disorder.

• The weak disorder limit

For a weak disorder, $c_R^2(k)$ is always positive. We can then define $c_R = c_R(k = 0)$. As we will show now, c_R is the shifted “cone” angle along which stress propagates asymptotically. c_R is a decreasing function of σ , meaning that the peaks of the response function get closer together as the disorder increases³. For a critical value $\sigma = \sigma_c$, c_R vanishes, and becomes imaginary for stronger disorder.

³As a technical remark, let us note that if $g_t = g_x$, the problem is symmetric in the change $x \rightarrow t$, $c^2(x, t) \rightarrow 1/c^2(x, t)$. It thus looks as if the cone should both narrow or

In the limit of large t , the propagator reads:

$$G(k, t) = \frac{1}{c_R k} \sin [c_R k t (1 + \alpha |k|)] e^{-\gamma k^2 t} \theta(t) \quad (79)$$

where the following constants have been introduced⁴:

$$\alpha = \frac{3}{4\Lambda} \left(\frac{c_0^2}{c_R^2} - 1 \right) \quad (80)$$

$$\gamma = \frac{\beta(k)}{2k^2} = \frac{\sigma^2 \Lambda^3 \ell_t^2}{18}. \quad (81)$$

From equation (79), the response function R , in the limit of small k and large t , is given by:

$$R(k, t) = \cos [c_R k t (1 + \alpha |k|)] e^{-\gamma k^2 t} \theta(t) \quad (82)$$

or in the real space,

$$R(x, t) = \frac{1}{2\sqrt{4\pi|\hat{\gamma}|(t)}} \Re \left\{ \frac{e^{-\xi_+^2/b}}{\sqrt{b}} \left[1 - \Phi \left(-\imath \frac{\xi_+}{\sqrt{b}} \right) \right] + \sqrt{b} e^{-b\xi_-^2} \left[1 - \Phi \left(-\imath \sqrt{b} \xi_- \right) \right] \right\} \quad (83)$$

where the scaling variables ξ_{\pm} , measuring distances relative to the two peaks, are defined by

$$\xi_{\pm} = \frac{x \pm c_R t}{\sqrt{4|\hat{\gamma}|t}} \quad (84)$$

and where $\hat{\gamma} = \gamma - \imath c_R \alpha$, $b = e^{\imath \arg \hat{\gamma}}$. Φ is the standard error function. Figure 7 shows R as given by expression (83). Interestingly, this propagator not only has a finite diffusive width $\propto \sqrt{t}$, but is also asymmetric around its maxima. Surprisingly, and in sharp contrast to the scalar case discussed above, the response function becomes *negative* in certain intervals (although its integral is of course equal to one because of weight conservation). This means that pushing on a given point actually reduces the downward pressure on certain points. This can be interpreted as some kind of arching: increasing the shear stress does affect the propagation of the vertical stress,

widen, depending on the arbitrary choice of x and t . There is however no contradiction with the above calculation since we assumed that v has zero mean, while $1/(1+v) - 1$ has a positive mean value, of order σ^2 .

⁴Note that the sign of α is dictated by the sign of $\tilde{g}_x(\Lambda)$.

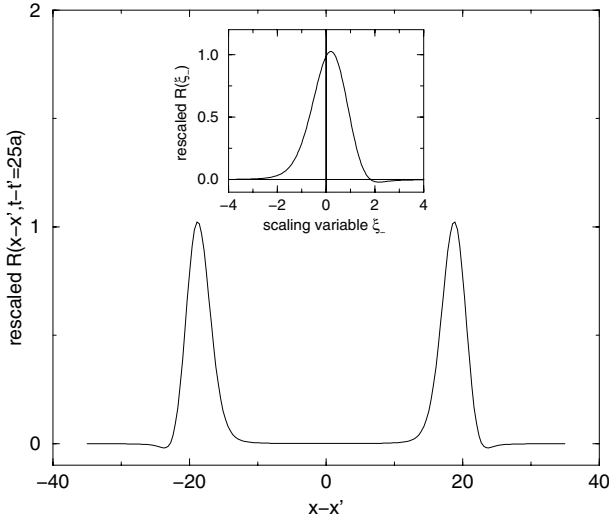


Fig. 7. Response function for weak disorder ($\sigma/\sigma_c \sim 0.32$). The two curves have been rescaled by the factor $2[4\pi|\hat{\gamma}|t]^{1/2}$. The main graph shows the general double-peaked shape of the response of the system when subjected to a peaked overload at $x = 0$, $t = 0$. The inset gives details the right-hand peak as a function of the scaling variable ξ_- . Note the asymmetry (for $\tilde{g}_x(\Lambda) > 0$), compatible with the results found in [63]. Note also that the curve becomes negative around $\xi_- = 2$.

and may indeed lead to a reduction in its local value which is redistributed elsewhere. The un-averaged response function therefore necessarily takes negative (and in fact rather large [41]) values. This is actually of crucial importance since this is the source of fundamental “fragility” of granular matter to external perturbations. Suppose indeed that as a result of the perturbation, a grain receives a negative force larger than the preexisting vertical pressure. This grain will then move and a local rearrangement of contacts will occur, inducing a variation of $c_0(x, t)$ as to reduce the cause of the instability. Thus, the stochastic wave equation implicitly demands rules similar to those introduced, *e.g.* in [40]. The present model, which is purely static, does not say what to do when a local rearrangement occurs, but certainly suggests that small perturbations should induce such rearrangements.

It is interesting to note that this response function was numerically measured in [63]; its shape is compatible with the above expression; in particular, the two peaks were found to be asymmetric with a longer “tail” extending inwards, as we obtain here. Note however that for $\tilde{g}_x(\Lambda) < 0$, the shape of the peaks is reversed: the small dips are located inside the peaks

and the longer tail extends outwards. In a more recent work [28], both the diffusive spreading and the renormalisation of the wave velocity have been observed.

- Critical disorder: The wave/diffusion transition

When the disorder is so strong that c_R just vanishes, the roots of $H^{-1}(k, E) = 0$ change nature, and so does the response function R . The two peaks of the previous expression for R merge together, while the width becomes anomalously large ($\propto t^{2/3}$). In the asymptotic, large t , regime we obtain:

$$R(k, t) = \theta(t) \cos \left[\lambda |k|^{3/2} t \right] e^{-\gamma k^2 t} \quad (85)$$

where the new constant λ is defined by $\lambda = c_0 \sqrt{3/2\Lambda}$ and $\gamma = c_0^2 \ell_t / 3$.

- Strong disorder: The pseudo-elastic regime

For larger disorder still, one finds, within the MCA (which is exact for a Gaussian, uncorrelated noise), that the renormalized value of c_0^2 , c_R^2 , becomes negative. Upon a rescaling of x as $\hat{x} = x/(ic_R)$, the effective equation on $\langle \delta \sigma_{tt} \rangle$ then becomes, on large length scales, Poisson's equation:

$$\nabla^2 \langle \delta \sigma_{tt} \rangle = \partial_t \langle \delta \rho \rangle \quad (86)$$

which means that the stress propagation becomes somewhat similar to that in an elastic body, where stresses obey an elliptic equation of similar type [89]. In particular, the cone structure of stress propagation, which is associated with the underlying, hyperbolic, wave equation finally disappears; the average response to a localized perturbation becomes a broad “bump” of width comparable to the height of the pile. However, the above transition is possibly an artifact, due to the fact that v is taken to be Gaussian, which strictly speaking is not allowed, since the local value of c_0^2 should always be positive. One can show for some other problems of the same type that a similar transition is artificially induced by the Gaussian approximation when it cannot really exist on physical grounds. We need to address the strong disorder limit with different tools in order to discuss the large scale nature of the response function in this case: this will be discussed below.

7.3 Generalized wave equations

It is tempting to generalize equations ((58), (59)) and write the most general linear equations governing the propagation of the forces which are compatible with the (local) conservation rules. These equations were first written

by de Gennes [70]:

$$\partial_t F_t + \partial_x [\eta'(x, t) F_x + \nu'(x, t) F_t] = \rho \quad (87)$$

$$\partial_t F_x + \partial_x [\eta(x, t) F_t + \nu(x, t) F_x] = 0. \quad (88)$$

Note that the terms ν, ν' break the symmetry $x \rightarrow -x$, and exist whenever the transfer rules in the three leg model are not symmetrical. Equations ((87), (88)) describe a situation where not only the opening angle of the cone can vary in space, but also its average orientation.

The same analytical techniques as above can still be used. We shall only discuss some special cases⁵:

◦ Let us first set $\nu = \nu' = 0$ and consider the case where η' is random, and η fixed (and equal to c_0^2). Taking $\eta'(x, t) = \eta'_0 (1 + v(x, t))$ with the noise v as above, one finds that the renormalized value of η' is:

$$\eta'_R = \eta'_0 \left(1 - \frac{c_0^2 \eta'_0 \sigma^2 \Lambda^3 \ell_t}{6} \right). \quad (89)$$

Now, on large length scales, one must recover the continuum equilibrium equations for the stress tensor, equations ((60), (61)). The condition of zero torque requires that the stress tensor is symmetric, and thus one must set $\eta'_R \equiv 1$, which imposes a relation between η'_0 and the amplitude of the noise σ . Note that beyond a certain value of σ , this relation can no longer be satisfied with a real η'_0 . This again means that the packing is unstable mechanically and will rearrange so as to reduce the disorder.

◦ Another interesting class of models, which one can call “ μ models”, is such that: $\eta = c_0^2, \eta' = 1$, but $\mu(x, t) = c_0 v(x, t)$ and $\mu' = 0$ or *vice versa*. These two cases yield identical results, namely, in the large t limit:

$$R(k, t) = \cos(c_0 k t) e^{-\gamma k^2 t} \theta(t) \quad (90)$$

$$R_s(k, t) = -i c_0 \sin(c_0 k t) e^{-\gamma k^2 t} \theta(t) \quad (91)$$

where $\gamma = \frac{c_0^2 \Lambda \sigma^2}{4}$. Note that in these cases, the response peaks acquire a finite diffusive width $\propto \sqrt{t}$, but the angle of the information cone is unaffected by the disorder (*i.e.* c_0 is not renormalized).

◦ Finally, there are special “symmetry” conditions where the equations can be decoupled and reduced to two “scalar” models. We will refer to this case as the “double scalar” model. This occurs when $\mu = \mu' = c_0 v_1(x, t)$ and

⁵To lowest order in perturbation theory, the case where disorder is present in the four terms η, η', ν, ν' simultaneously is very simply obtained by adding the corrections induced by each term taken individually.

$\eta' = \eta/c_0^2 = 1 + v_2(x, t)$ where v_1, v_2 are two different sets of noise. Let us define $\sigma_{\pm} = c_0 F_t \pm F_x$, $x_{\pm} = x \mp c_0 t$ and $v_{\pm} = v_1 \pm v_2$, we then obtain:

$$\partial_t \sigma_+ = c_0 \rho - c_0 \partial_{x_+} [v_+ \sigma_+] \quad (92)$$

$$\partial_t \sigma_- = c_0 \rho - c_0 \partial_{x_-} [v_- \sigma_-] \quad (93)$$

showing that σ_+ and σ_- decouple, each propagating along two rays, of “velocity” $\pm c_0$, plus a small noise v_{\pm} which, as in the scalar case, generates a nonzero diffusion constant. The response functions for σ_{tt} and σ_{xt} are thus again made of two diffusive peaks of width $\propto \sqrt{t}$, centered in $x = \pm c_0 t$. Note that by construction, this special form of disorder does not lead to negative vertical stresses.

A physically relevant question is to know how local stresses are distributed. We have seen above that within a scalar approach, an exponential-like distribution (possibly of the type $\exp -w^{\beta}$, with $\beta \geq 1$) is expected [46, 93]. One can wonder whether this exponential distribution survives within a tensorial description, and what happens for very small stresses $w \rightarrow 0$. Unfortunately, the full distribution can only be computed analytically for the “double scalar” model; but numerical results have also been obtained for the random BCC model [41] and confirm that the exponential tail holds in the strong disorder limit.

In the “double scalar” limit, the histogram of the stress distribution is obtained trivially by noting that since $\sigma_+ = w_1$ and $\sigma_- = w_2$ travel along different paths, they are independent random variables. Taking c_0 to be unity for simplicity, one thus finds:

$$P(\sigma_{tt}) = \int dw_1 \int dw_2 P^*(w_1) P^*(w_2) \delta\left(\sigma_{tt} - \frac{w_1 + w_2}{2}\right) \quad (94)$$

$$P(\sigma_{xt}) = \int dw_1 \int dw_2 P^*(w_1) P^*(w_2) \delta\left(\sigma_{xt} - \frac{w_1 - w_2}{2}\right) \quad (95)$$

where P^* is the distribution of weight pertaining to the scalar case, which, as mentioned above, depends on the specific form of the local disorder and on the discretisation procedure. In the strong disorder case which leads to equation (8) [in the case $N = 2$], we thus find that $P(\sigma_{tt})$ is still decaying exponentially (it is actually a Γ distribution of parameter $2N$), although its variance is reduced by a factor 2. For $N = 2$, one simply gets

$$P(\sigma_{tt}) = \frac{8}{3} \sigma_{tt}^3 e^{-2\sigma_{tt}} \quad (96)$$

$$P(\sigma_{xt}) = \left(|\sigma_{xt}| + \frac{1}{2}\right) e^{-2|\sigma_{xt}|}. \quad (97)$$

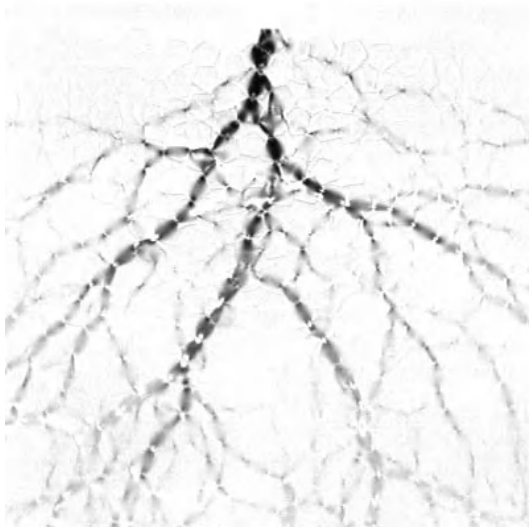


Fig. 8. Picture of the response force chains in a two-dimensional system of grains subject to a vertical force imposed at the middle of the top surface. To get this picture birefringent grains between inverse circular polarizers have been used, and the intensity difference after and before the overloading has been computed. This picture was obtained by R.P. Behringer and J. Geng.

The interest of the “double scalar” limit of the hyperbolic model is to show that the exponential tail equation (8) has indeed a certain degree of universality, and is not restricted to the scalar model.

8 Force chains scattering II: Strong disorder limit

8.1 Introduction and numerical results

From pictures of photo-elastic grains, the network of inter-particle forces propagating as a responses to a localized pressure was extracted [43, 69] (see Fig. 8). An interpretation of such a picture can be given in terms of linear force chains which tend to split upon meeting vacancies or packing defects [24].

As reviewed in the previous section, one can investigate perturbatively the role of disorder on hyperbolic equations. In this case, the two peak structure of the response function is preserved on large length scales, although the peaks are diffusively broadened. This result is in qualitative agreement with the numerical simulations [28, 63, 78]. An uncontrolled extrapolation

to strong disorder however suggests that the large scale equations might become elliptic.

In order to investigate more quantitatively the strongly disordered regime where force chains split and merge, one can study [24] the following model. If one of the force chains meets a defect (randomly distributed in space), we split it into two new ones at random angle, which then propagate until another defect (or the boundary) is reached. More precisely, a chain carrying a force f in the direction \vec{n} splits when meeting a defect into two forces f_1, f_2 in the directions \vec{n}_1, \vec{n}_2 – “ Λ process”. The two angles θ_1 and θ_2 (between \vec{n} and \vec{n}_1 and \vec{n}_2 respectively) are uniformly chosen between 0 and some maximum splitting angle θ_M . The local mechanical equilibrium imposes that the intensities f_1 and f_2 are such that $f\vec{n} = f_1\vec{n}_1 + f_2\vec{n}_2$. Sometimes, two (or more) force chains meet at the same defect – “ Y process”. In this case, we make them merge together. It is important to note that the positions of the defects are fixed before starting the computation of the forces. This idea of a frozen disorder is consistent with the experimental observation that when the local overload is added on the top of the system, the forces are transmitted along the chains originally created during the building of the packing. In other words, as long as the applied force is not too large and compatible with the pre-existing network of force chains, the geometry of the packing, and in particular the contacts between grains, remains the same (but see the discussion in Sect. 9).

With these rules, realistic force networks can be created numerically [24]. After averaging over many statistically identical samples, one can obtain stress profiles for different heights H . One finds that, as H increases, the vertical pressure response profile evolves continuously from two well defined peaks to a single broad one. It means that the hyperbolic behaviour is progressively erased by multiple scattering. The width of the single peak is found to scale like H ; the scaling function is furthermore surprisingly close to the pure elastic response of a semi-infinite two-dimensional medium. However, the numerical simulation was restricted to rather shallow (small H) samples.

8.2 A Boltzmann description of force chain splitting

In order to understand analytically the above numerical results, we write a Boltzmann equation for the probability density $P(f, \vec{n}, \vec{r})$ of finding an oriented force chain of intensity f in the direction \vec{n} around the point \vec{r} [24]. A very important point here is that force chains can be oriented in reference to the boundary conditions (see the discussion in [24, 34, 138]).

For simplicity, we first neglect the chain “merging” process which leads to a more complicated non linear Boltzmann equation (its influence is not fully understood yet and will be discussed below). We also assume that

the splitting is symmetric, *i.e.* that $\vec{n} \cdot \vec{n}_1 = \vec{n} \cdot \vec{n}_2 \equiv \cos \theta$, so that $f_1 = f_2 = f/2 \cos \theta$. Assuming a uniform density of defects, the probability distribution $P(f, \vec{n}, \vec{r})$ obeys the following general equation:

$$P(f, \vec{n}, \vec{r} + \vec{n} d\vec{r}) = \left(1 - \frac{d\vec{r}}{\lambda}\right) P(f, \vec{n}, \vec{r}) + 2 \frac{d\vec{r}}{\lambda} \int d\vec{n}' \int df' P(f', \vec{n}', \vec{r}) \Psi(\vec{n}', \vec{n}) \delta\left(f - \frac{f'}{2 \cos \theta}\right), \quad (98)$$

where λ is equal to the “mean free path” of force chains, and is of order $1/(\rho_d a^{d-1})$ in dimension d . The above equation means the following: since a chain of grains can only transport a force parallel to itself [35], the direction of the force \vec{n} also gives the local direction of the chain. Between \vec{r} and $\vec{r} + \vec{n} d\vec{r}$, the chain can either carry on undisturbed, or be scattered. The second term on the right hand side therefore gives the probability that a force chain initially in direction \vec{n}' is scattered in direction \vec{n} . This occurs with a probability $\frac{d\vec{r}}{\lambda} \Psi(\vec{n}', \vec{n})$, where Ψ is the scattering cross section, which we will assume to depend only on the scattering angle θ , for example a uniform distribution between $-\theta_M$ and $+\theta_M$. The δ -function ensures force conservation and the factor two comes from the counting of the two possible outgoing force chains. Let us now multiply equation (98) by f and integrate over f . This leads to an equation for the local average force per unit volume in the direction \vec{n} , that we will denote $F(\vec{n}, \vec{r})$. This equation reads:

$$\lambda \vec{n} \cdot \vec{\nabla}_r F(\vec{n}, \vec{r}) = -F(\vec{n}, \vec{r}) + \int d\vec{n}' \frac{F(\vec{n}', \vec{r})}{\vec{n} \cdot \vec{n}'} \Psi(\vec{n}', \vec{n}) + \frac{\lambda}{a} \vec{n} \cdot \vec{F}_0(\vec{r}), \quad (99)$$

where we have added the contribution of an external body force density $\vec{F}_0(\vec{r})$, and a is the size of a defect or of a grain. This equation is the so-called Schwarzschild-Milne equation for radiative transfer, describing the evolution of light intensity in a turbid medium [142]. We now introduce some angular averages of $F(\vec{n}, \vec{r})$ that have an immediate physical interpretation:

$$p(\vec{r}) = a \int d\Omega F(\vec{n}, \vec{r}) \quad (100)$$

$$J_\alpha(\vec{r}) = a \int d\Omega n_\alpha F(\vec{n}, \vec{r}) \quad (101)$$

$$\sigma_{\alpha\beta}(\vec{r}) = ad \int d\Omega n_\alpha n_\beta F(\vec{n}, \vec{r}), \quad (102)$$

where $\int d\Omega$ is the normalized integral over the unit sphere, that is introduced for a correct interpretation of σ (see Eq. (106) below). As will be clear from the following, \vec{J} is the local average force chain intensity per unit surface, σ

is the stress tensor. Since $\vec{n}^2 = 1$, one finds that $\text{Tr } \sigma = dp$, and therefore p is the isostatic pressure. Note that \vec{J} is not the average local force, which is always zero in equilibrium. The fact that $\vec{J} \neq \vec{0}$ comes from the possibility of *orienting* the force chains.

We now integrate over the unit sphere equation (99) after multiplying it by different powers of n_α . Using the fact that $\Psi(\vec{n}', \vec{n})$ only depends on $\vec{n} \cdot \vec{n}'$, a direct integration leads to:

$$\lambda \vec{\nabla} \cdot \vec{J} = (a_0 - 1)p, \quad (103)$$

where a_0 is called the “albedo” in the context of light scattering [142], and reads:

$$a_0 \equiv \int d\vec{n} \frac{\Psi(\vec{n}', \vec{n})}{\vec{n} \cdot \vec{n}'} \geq 1. \quad (104)$$

A second set of equations can be obtained by multiplying by n_α and integrating. Using the fact that $\int d\vec{n} \Psi(\vec{n}', \vec{n}) = 1$, it is easy to show that

$$\int d\vec{n} \vec{n} \frac{\Psi(\vec{n}', \vec{n})}{\vec{n} \cdot \vec{n}'} = \vec{n}'. \quad (105)$$

Therefore, the resulting equation is nothing but the usual mechanical equilibrium relation:

$$\nabla_\beta \sigma_{\alpha\beta} = F_{0\alpha}. \quad (106)$$

This relation in fact only reflects the local balance of forces chains. Now we multiply equation (99) by $n_\alpha n_\beta$ and again integrate. *A priori*, this introduces a new three index tensor. In order to close the equation, we now make the an assumption that is usually made in the context of light diffusion, that on large scales the force intensity becomes nearly isotropic [142]. In this case, it is justified to expand $F(\vec{n}, \vec{r})$ in angular harmonics and to keep only the first terms:

$$a F(\vec{n}, \vec{r}) = p(\vec{r}) + d\vec{n} \cdot \vec{J}(\vec{r}) + \dots \quad (107)$$

Within this expansion, we finally obtain a “constitutive” relation between $\sigma_{\alpha\beta}$ and the vector \vec{J} . We find:

$$\sigma_{\alpha\beta}|_{\alpha \neq \beta} = \frac{\lambda d^2 K_1}{\left(\frac{da_2 - a_0}{d-1} - 1\right)} (\nabla_\alpha J_\beta + \nabla_\beta J_\alpha), \quad (108)$$

and

$$\sigma_{\alpha\alpha} = \frac{\lambda d}{\left(\frac{da_2 - a_0}{d-1} - 1\right)} \left[2dK_1 \nabla_\alpha J_\alpha + \left(dK_1 - \frac{a_0 - a_2}{(d-1)(a_0 - 1)} \right) \vec{\nabla} \cdot \vec{J} \right] \quad (109)$$

with $K_1 = 1/d(2+d)$ and $a_2 = \int d\vec{n} (\vec{n} \cdot \vec{n}') \Psi(\vec{n}', \vec{n})$. Rather surprisingly, these equations have exactly the canonical form of elasticity theory, provided one identifies the vector \vec{J} with the local displacement, up to a multiplicative factor.

The above stress equations are rather non-trivial because no displacement field is introduced in the above derivation (nor in the numerical model): elastic-like equations are found in a stress-only model. The basic assumption is the existence of local force chains, which have a well defined identity over several grain sizes a , such that $a \ll \lambda$: this is the condition under which the above Boltzmann description of the force chain scattering is justified.

Since the above equations are formally identical to those of classical elasticity, one can show that $\nabla^2 p = 0$, and $\nabla^4 \vec{J} = 0$ [89]. One can therefore in principle compute the response function $G(\vec{r})$ to a localized force at $\vec{r}_0 = 0$ in the z direction, which is given by the standard (one peak) elastic Green's function. But note however that although the above equations are formally those of classical elasticity, there is one crucial difference coming from the fact that $(\sigma_{\alpha\beta})$ and \vec{J} are not independent since they are both related to the same underlying quantity $F(\vec{n}, \vec{r})$. This is a very important difference, which appears, for example in the choice of boundary conditions on \mathcal{B} that determines $P(f, \vec{n}, \vec{r})|_{\mathcal{B}}$.

8.3 The role of chain merging

We have mentioned above the fact that the numerical simulation of the full chain scattering model (including both splitting and merging) was restricted to small depths. Similarly, neglecting chain merging altogether cannot be correct on large length scales, since the number of force chains would diverge, leading to an infinite number of force chains with infinitesimal intensity. As shown in [132], the above linearized theory is in fact unstable, and chain merging play a crucial role to make the theory mathematically consistent.

On the other hand, chain merging leads to a non-linear Boltzmann equation which in the general case cannot be solved. Only special cases have, up to now, been amenable to an analytic treatment. For example, if one insists that the force chains can only take six directions a 60° degrees, with 120° degree chain splitting and chain merging, the amplitude of the force chains is constant, simply because $2 \cos 60^\circ = 1$. In this case, the full probability distribution $P(f, \vec{n}, \vec{r})$ boils down to six functions $p_n(\vec{r})$, describing the probability for a force chain to be in one of the six available directions. The result of the full analysis is that, quite surprisingly, the response function evolves back to a two-peak, hyperbolic structure on large length scales! Whether this is due to the particular structure of the model is not yet settled; preliminary results on the eight-fold model [26] suggests that

there might actually be a *transition* between a hyperbolic response for sufficiently anisotropic scattering and an elliptic response for isotropic situations (see [133] for a nice recent discussion). The existence of such a transition would perhaps, as we discuss now, allow one to reconcile the apparently contradictory experimental, numerical and theoretical results.

9 Statics of granular materials: Concluding remarks and open questions

Let us try to summarize the theoretical situation as follows. If the grains are frictionless, then packings are generically isostatic. If these packings are furthermore “sufficiently” anisotropic, then the construction of the stress everywhere in the packing can be performed by “propagating” the stress from one boundary towards the interior of the packing, as one expects for hyperbolic equations. This situation is well captured by the three-leg model introduced above, that indeed leads to hyperbolic equations on large length scales. Correspondingly, numerical simulations of the response function in *anisotropic* packings of frictionless beads indeed display the expected diffusively broadened two-peak structure, at least for the modest sizes that were simulated [78].

However, not all isostatic packings are characterized by a two-peak response function. For example, using *isotropic* isostatic packings built by Roux *et al.* [1] have found that the average response function is a single hump, qualitatively similar to the elliptic-like response observed experimentally and to the result of the chain splitting model. An example of such packings is shown in Figure 9, together with the local force chains. This picture makes it obvious that the force chains are strongly scattered, and lose their “coherence”, which makes it indeed plausible that the two-peak structure is destroyed. Again, some degree of anisotropy seems to be required to preserve hyperbolicity. Note that in the numerical determination of the response function, the applied force perturbation δf is infinitesimal and does not induce any rearrangement of the initial structure.

This remark is important since *if* rearrangements are allowed, the response has been argued in [118] to be, on general grounds, elliptic. Moreover, one expects that for any small perturbation, a sufficiently large assembly of frictionless grains *will* rearrange [44]. Therefore, the order in which the limits $H \rightarrow \infty$ and $\delta f \rightarrow 0$ are taken is physically relevant [79, 119], and one might expect that even anisotropic structures such as those studied in [78] should destabilize under a small perturbation for large enough H . It is not clear which of the limits is relevant in the experimental conditions of [116]; even if the applied force is very small and much care has been devoted to perturb as weakly as possible the packing, it might well be that these experiments are not in the infinitesimal limit.

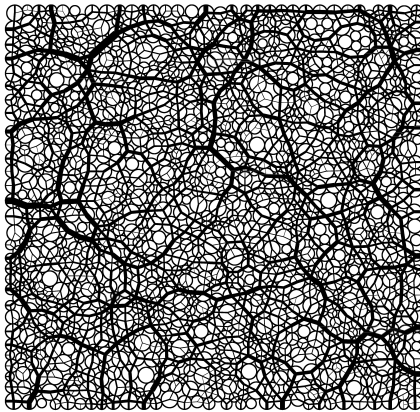


Fig. 9. Force chains in an isotropic, isostatic packing of frictionless disks. The average response function in this case has a single peak. Courtesy of Ph. Claudin.

Conversely, is isostaticity needed to obtain hyperbolicity? The numerical simulations of [28,63], where an hyperbolic response function for anisotropic ordered packing of grains with friction is observed, show that this is not the case. Similarly, the experimental determination of hyperbolic like response function in ordered lattices [69,103] shows that, as suggested by the above theoretical analysis, weak disorder does not suppress the hyperbolic nature of the force propagation. It would be extremely important, in this context, to confirm theoretically the existence of a true “hyperbolic-elliptic” phase transition in simplified models of force chain scattering.

More formal approaches have also been advocated in [2,62] to try to establish some closure relations between the components of the (coarse-grained) stress tensor starting from the equilibrium force balance at the grain level. Tkachenko and Witten [138] have insisted on the equivalence between any macroscopic linear relation between the components of the stress tensor and the existence of “floppy” modes, *i.e.* zero energy deformation modes (see also [102]). Such floppy modes can exist in certain elastic spring networks, such as a square lattice which can deform at no cost along its diagonal. One can indeed show that the large scale elasticity equations in this case are characterized by coefficients such that the marginal condition $r^2 = t$ (see Eq. (54) above) is satisfied, so that the response function becomes the sum of two delta peaks [110]. Following this line of thought, a natural conjecture is that if a system has some *extended* floppy modes, then its large scale response will be hyperbolic. Conversely, if floppy modes are all localized, then the response is locally hyperbolic, but the strong force chain scattering disrupts the long range propagation and the response

becomes elliptic like, as suggested by the force chain scattering model discussed above. We hope that these issues will be clarified in the near future; a particularly important point is to establish precisely, starting from a microscopic description à la Edwards, which kind of large scale static equation emerge and under what conditions it is hyperbolic/elliptic, and the value of the parameters entering these equations.

10 Glassy dynamics in granular media: A brief survey

10.1 *Slow compaction*

We have spent quite a long time on the static properties of granular media. The dynamics of *weakly tapped* assemblies of grains is also an extremely interesting subject, in particular in relation with the dynamics of other glassy systems, such as super-cooled liquids, colloidal glasses and foams. The most obvious experiment (with important industrial applications) is that of compaction under tapping. The basic experiment consists in studying the volume occupied by a large number of grains when the container is “tapped”, *i.e.* subject to a periodic acceleration of a certain amplitude. The packing, initially very loose, progressively compacts. However, the compaction process slows down with time, and the decay of the volume is very far from being a simple exponential. Experiments have shown that the decay of the volume towards its asymptotic value can be satisfactorily fitted by an inverse logarithm of time, or by a stretched exponential, both forms being typical of relaxation processes in glasses, where one can also study the time dependence of the volume (or of the energy) as the sample relaxes after a temperature quench. The parameters of these fits depend on the tapping amplitude – stronger tapping obviously leads to a faster compaction.

More complex experimental protocols have also been tested. For example, one can change, in the course of the experiment, the amplitude of the tapping and reveal interesting memory effects, again similar to those found in glasses and spin-glasses. The now classic experiment [108] is to start from a loose sample and increase slowly the tapping amplitude Γ , in such a way that for each tapping amplitude the density ρ appears to reach a saturation value. One finds that $\rho(\Gamma)$ increases with Γ . When Γ is reduced back to zero, the density keeps a high value, revealing a kind of irreversibility that also appears in spin-glasses under a magnetic field: when the temperature is increased the (zero field cooled) magnetization increases, but does not follow the same path on the way back. The temperature at which the two branches separate is the spin-glass transition temperature (which, if defined in this way, weakly depends on the heating/cooling rate). Similarly, there appears to be a tapping amplitude beyond which the two density branches meet. The high magnetization (field cooled) branch, as the high density

branch in the granular system, *is* reversible. As in spin-glasses, the low density branch is in fact out-of-equilibrium, but the convergence of the density (magnetization) towards its equilibrium value is much too slow to be observed.

In the first stage of another type of experiment [83], aimed at revealing “memory effects”, one taps the system with three different amplitudes – say weak, moderate and strong – during a time chosen such as to reach a certain density, identical in the three cases. In the second stage of the experiment, the tapping amplitude is then chosen to be moderate, and the density just after the amplitude “jump” is observed. If the state of the system was only described by the density, the evolution of the density after the jump should be identical for all three situations, and follow the “moderate” curve, which is taken as the reference. This is not the case: the weakly tapped system first has to *dilate* before it is able to resume its compaction, whereas the strongly tapped system compacts faster than the reference system just after the jump. This shows that the configurations reached under stronger tapping are in a sense easier to compact further. This experiment therefore indicates that some further “hidden” observables are needed to describe the large scale evolution of the system. We shall expand on this below, but want to note that a very similar effect is known in glasses as the Kovacs (or memory) effect. In this case, one prepares the system at a given temperature $T_2 < T_1$ and waits until the volume has reached the equilibrium volume at T_1 . Then one raises the temperature to T_1 . If the volume was the only relevant quantity, one should not see any further evolution since this volume is already at its equilibrium value. Again, this is not what Kovacs first observed in polymeric glasses [84]: the volume has to increase back to a maximum before decreasing again towards its equilibrium value. A similar effect was also reported in numerical simulations of spin-glasses [9] and of Lennard-Jones systems [12], and several simple models are now known to reproduce this effect (see below).

We also want to mention the very interesting experiment of d’Anna *et al.* [48], where a torsion oscillator is immersed in a vibrated granular assembly. The observable is the angle θ made by the oscillator with an arbitrary axis. The results of [48] are that (a) the angle θ performs a random walk in time: $\langle [\theta(t + \tau) - \theta(t)]^2 \rangle = D(\Gamma)\tau$ and (b) the angular diffusion constant $D(\Gamma)$ appears to vanish as the amplitude of the tapping Γ goes to zero in a way that recalls the “super-activated” Vogel-Fulcher law in glasses.

10.2 Self-inhibitory dynamics and dynamical heterogeneities

10.2.1 Non exponential relaxation

We shall call ρ^* the maximum compacity that can be reached in a tapping experiment. For $\Gamma \rightarrow 0$, this corresponds to the so-called “random close packing” configuration. [It is not entirely clear how meaningful this notion really is, but from an empirical point of view, any reasonable extrapolation of the accessible dynamics seems to converge to a density which is not the HCP density (in the case of identical spheres).] Correspondingly, we will call the difference between ρ^* and the average density ρ the “free volume” fraction, Φ . The simplest relaxation equation for Φ is obviously a rate equation:

$$\frac{d\Phi}{dt} = -\gamma\Phi. \quad (110)$$

If the decay rate γ is independent of the free-volume itself, the decay of Φ is obviously a single exponential. However, it is intuitively clear that the dynamics is self inhibitory, in the sense that it is the free volume itself that allows further compaction. Therefore, one expects that γ vanishes as $\Phi \rightarrow 0$. Assuming a power-law dependence $\gamma \sim \Phi^\beta$, with $\beta > 0$, one obtains a power-law relaxation for long times:

$$\Phi \sim (t + t_0)^{-1/\beta}. \quad (111)$$

Let us assume a simple model where particles have a volume v , and mobile holes have fixed “quantum” volume v_0 . For a particle to be able to move, we require that n^* holes meet in a volume v , such that the volume of one particle is liberated, *i.e.* $n^*v_0 = v$. If the dynamics is sufficiently chaotic, it is reasonable to assume a Poisson distribution for the holes. Therefore, the probability for a particle to move is simply Φ^{n^*} , leading to $\beta = n^*$. If the number of holes n^* needed to move one particle is large, one can approximate the long time behaviour of Φ as a logarithm:

$$\Phi \sim t^{-1/\beta} \approx \frac{1}{1 + \frac{1}{n^*} \log t}, \quad (112)$$

a form often advocated to fit the slow relaxation of the volume in glasses or granular media [108, 135] (but see also [111], where the role of convection is discussed, and [137] for a simple soluble model).

10.2.2 Dynamical heterogeneities

If one assumes that holes cannot spontaneously appear, it is clear that the dynamics is necessarily spatially heterogeneous: regions rich in holes, where dynamics is locally fast, appear only to the detriment of regions poor

in holes, where the system is jammed. This argument can be somewhat formalized to suggest that the geometry of the “fast” objects is non trivial. Call $\Phi + \phi(\vec{r}, t)$ the coarse-grained density of free volume (“holes”) around point \vec{r} at time t , such that the space average of $\phi(\vec{r}, t)$ is equal to 0. [Note that all “voids” do not necessarily contribute to the *free* volume.] Far from the boundaries of the sample where the holes can disappear, one can write a Langevin equation for $\phi(\vec{r}, t)$ which reads [51]:

$$\frac{\partial \phi}{\partial t} = D \nabla^2 \phi + \vec{\nabla} \cdot \left[\sqrt{\Phi + \phi} \vec{\xi}(t) \right], \quad (113)$$

where D is the (fast) diffusion constant of the holes, $\vec{\xi}$ is a Gaussian white noise in space and time of variance equal to D , and we have neglected the interaction between the holes. In the above equation, we have supposed that the free-volume is locally conserved. Assuming that ϕ is small leads to the result that ϕ itself is a Gaussian field with a correlation function given (in three dimensions) by⁶:

$$\langle \phi(\vec{r}, t) \phi(\vec{r}', t + \tau) \rangle = \frac{\Phi}{2} \frac{1}{(4\pi D\tau)^{3/2}} \exp \left(-\frac{(\vec{r} - \vec{r}')^2}{4D\tau} \right) \quad (\tau \geq 0). \quad (114)$$

Note that in the limit $\tau \rightarrow 0$, the field ϕ is delta-correlated in space; some short scale cut-off of the order of the grain size a would be needed to regularize this behaviour. Now, if one insists that the material particles (or grains) can only move if the local density of holes is larger than a certain threshold Φ_c , the diffusion equation for, say, the density $\rho(\vec{r}, t)$ of slow tracer particles reads (see also [94] for similar ideas):

$$\frac{\partial \rho}{\partial t} = D_0 \vec{\nabla} \cdot \left[\Theta(\Phi + \phi - \Phi_c) \vec{\nabla} \rho \right]. \quad (115)$$

Although a more careful solution of the coupled equations ((113), (115)) is required to confirm the following conclusions, a qualitative analysis of the

⁶If one considers that “holes” can be converted into voids and *vice versa*, such that ϕ is only conserved on average, the statistics of the ϕ field is altered and becomes that of an elastic membrane subject to thermal fluctuations.

problem leads to the following picture for glassy dynamics, which relates slow, self-inhibitory dynamics and dynamical heterogeneities:

- the probability that an elementary region of space is active is, for small $\Phi \ll \Phi_c$, proportional to $\exp(-C\Phi_c^2/\Phi)$, where C is a numerical coefficient. Therefore, the large scale diffusion coefficient D_R of the particles vanishes as:

$$D_R \sim D_0 \exp\left(-\frac{C\Phi_c^2}{\Phi}\right) = D_0 \exp\left(-\frac{C\Phi_c^2}{\rho^* - \rho}\right), \quad (116)$$

i.e. à la Vogel-Fulcher. This argument is actually the analogue of the classic free-volume argument leading to the Vogel-Fulcher law in glasses, and extended to granular media by Boutreux and De Gennes [27];

- the fast regions are delimited by the contour lines of a correlated Gaussian field. This has interesting consequences: for example, one expects, in the short-ranged conserved case, the active regions to be lattice animals of fractal dimension $d_f = 2$ in three dimension (and $d_f \approx 1.56$ in two dimensions). The value $d_f = 2$ turns out to be in agreement with the experimental determination of Weeks *et al.* on dense, three dimensional colloidal glasses [144]. It would be interesting to measure other geometrical characteristics of the fast clusters to confirm that these are indeed lattice animals (see *e.g.* the discussion in [88]). Interestingly, the connection between glassy dynamics and the contour lines of a dynamic random field was also suggested in [36], using rather different arguments.

It would be most interesting to make these statements more precise in the context of a specific model. Very promising steps in that directions have been made recently in dynamically constrained models [67, 117, 139].

As emphasized by Boutreux and De Gennes, a Vogel-Fulcher law such as equation (116) also leads to a logarithmic relaxation of the density. Indeed, writing:

$$\frac{d\Phi}{dt} = -\gamma_0 \exp\left(-\frac{C\Phi_c^2}{\Phi}\right) \Phi, \quad (117)$$

leads at large times to:

$$\Phi \approx \frac{C\Phi_c^2}{\log t}. \quad (118)$$

10.2.3 Another point of view: Edwards postulate

The above Vogel-Fulcher law can also be understood using Edwards' analogy with thermodynamics. Assume again that all blocked states are equiprobable. Then the states that are most likely to be observed are the most

numerous ones: this is the essence of statistical thermodynamics. Imagine for example that a container is divided by a movable piston, with grains in each compartment. The volume of the two compartments are V_1 and V_2 , with $V_1 + V_2 = V$. The Edwards entropy \mathcal{S} is the logarithm of the number of blocked states for a given overall volume. The total entropy of the container is:

$$\mathcal{S}_T = \mathcal{S}_1 + \mathcal{S}_2. \quad (119)$$

The most probable value of V_1 is such that this entropy is maximum, under the constraint $V_1 + V_2 = V$. Therefore, one has:

$$\frac{\partial \mathcal{S}_1}{\partial V_1} = \frac{\partial \mathcal{S}_2}{\partial V_2}. \quad (120)$$

In thermodynamics, this quantity (which is constant throughout the system) is equal to P/T , where P is the pressure. In the context of granular materials, $\partial \mathcal{S} / \partial V > 0$ was called the inverse compactivity by Edwards, and noted $1/X$.

A reasonable requirement for $\mathcal{S}(V)$ is that it should be proportional to the number of grains N , and only depends on the free-volume fraction Φ : $\mathcal{S}(V) = Ns(\Phi)$. One also expects that $s(\Phi)$ vanishes for $\Phi \rightarrow 0$. A possibility, suggested in [65,91], is that each grain has a number of possible positions proportional to the free-volume, which leads to $s(\Phi) = \log \Phi / v_0$, where v_0 is again a “quantum” of free-volume. Using this form for $s(\Phi)$, we finally find:

$$\frac{\partial \mathcal{S}}{\partial V} = \frac{1}{X} = \frac{N^2 v}{V^2} \frac{\partial s}{\partial \Phi} \approx \frac{\rho^{*2} v}{\Phi} \quad (\Phi \ll 1), \quad (121)$$

showing that the Edwards “temperature” X vanishes for $\Phi \rightarrow 0$ ⁷. Now, consider a small region immersed in a large container with grains, which acts as a reservoir of free volume. Exactly as in thermodynamics, one can show that the probability that a free-volume equal to v is found in this region is given by:

$$p(v) \propto \exp\left(-\frac{v}{X}\right). \quad (122)$$

The probability for a hole of the size of a grain v to appear is therefore: $p(v = v) \sim \exp(-\Phi^{*2}/\Phi)$, where $\Phi^* \equiv \rho^* v$. Assuming that the grain motion takes place when a sufficiently large hole appears, one finds that the rate of compaction has the same exponential form as above.

⁷Note the following intriguing consequence of Edwards postulate. Suppose that the two compartments contain grains of the very same material, but with different sizes (volume) v_1 and v_2 , such that $N_1 v_1 = N_2 v_2$, *i.e.* the volume fraction occupied by the grains in the two compartments is the same. The equality $X_1 = X_2$ then imposes that $\Phi_1 / \Phi_2 = v_2 / v_1$, *i.e.* that smaller grains will have a higher free volume. This conclusion holds for more general choices of the entropy $s(\Phi)$.

10.3 Granular dynamics and the trap model

The above “free-volume” ideas are interesting and certainly contain important physical ideas. However, the description of the dynamics using a single macroscopic degree of freedom (namely the average free volume density) is too naive to account for the more sophisticated “memory” experiments. Indeed, any rate equation of the form:

$$\frac{d\Phi}{dt} = -\gamma(\Phi, \Gamma)\Phi, \quad (123)$$

is unable to explain why a packing prepared under different tapping conditions (different Γ), but such as to reach the same value Φ_0 would evolve differently if tapped with the same amplitude. The same argument was used by Kovacs in the context of glasses to suggest that additional parameters are needed to fully describe a glassy state. Take the example of a one dimensional ferromagnetic Ising model that relaxes towards its equilibrium state at a temperature T . Since the system does not order, the equilibrium state is characterized by a density of domain walls (or kinks), defining a characteristic domain size, which is the distance between the kinks. The non equilibrium state can also be characterized by a density of kinks, which decays with time towards the equilibrium. However, the full description of the non equilibrium state requires the specification of the *distribution* of the domain size – only its first moment is fixed by the average density of kinks. Different initial distributions of domain sizes with the same average value do evolve differently at a given temperature. For example, if there is an initial excess probability of large domains (but such that the density of kinks is the equilibrium one), these will immediately break down, leading to a temporary increase of the density of kinks.

A simple model that encapsulates both the spatial heterogeneity and the intermittency of the dynamics, is the “trap” model. One should think of a glassy system as made of independent subsystems of a certain size ξ (see Fig. 10). Inside each of these regions, the dynamics is “coherent” in the sense that hopping between different metastable states involves all particles within a blob of size $\leq \xi$. Within each of these subunits, the dynamics can be thought of as a random walk in a rugged landscape, an idea with a long history in the context of glasses [74], and witnessing a strong recent revival in different contexts [37, 75, 85]. However, an element which often seems to be missing from the discussion is the fact that the dynamics of system *as a whole* necessarily results (for short range interactions) from the evolution in parallel of many subsystems: the dynamics of a particle in a given subregion is completely unaffected by the dynamics of far away particles. An open problem is to identify precisely the (possibly time dependent) coherence length ξ , and understand its temperature and density dependence (see [55]

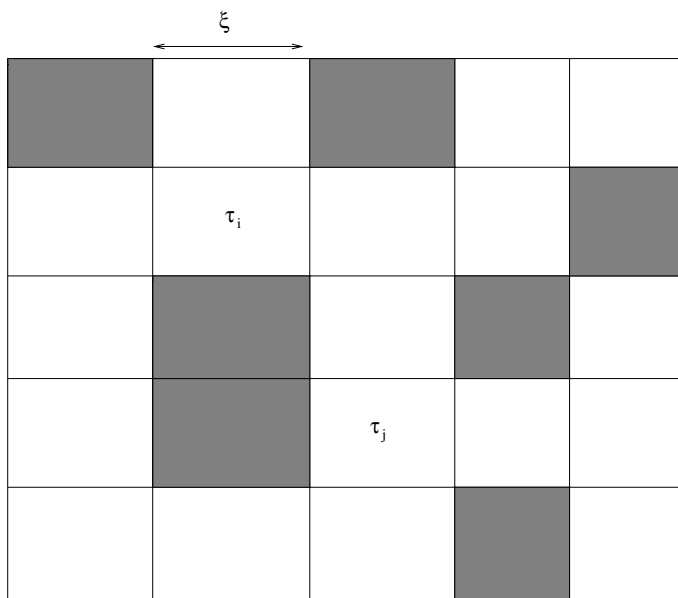


Fig. 10. Schematic view of the dynamics in glassy material. Within each “blob”, the dynamics is “coherent” in the sense that hopping between different metastable states involves all particles within a blob of size $\leq \xi$, whereas the motion of far away particles does not affect the dynamics within this blob. Within each of these subunits, the dynamics can be thought of as a random walk in a rugged landscape, with an instantaneous (random) trapping time τ_i in the i th blob. Grey regions are particularly “slow” ($\tau \gg t_w$).

for very interesting results on this aspect in the context of Lennard-Jones systems).

The dynamics of a given subsystem can be seen as a succession of hops between different metastable states, each of which blocking the dynamics for a time that depends on the local packing fraction: high densities leads to long trapping times. The state of the system at time t is described by a *probability distribution* $P(\phi, t)$, which counts the number of subsystems with a local value ϕ of the free volume. Each time a subunit unjams, we assume that it falls back into any of the blocked states with an *a priori* distribution $P_0(\phi)$, that reflects the number of states with a given packing density. The time evolution of $P(\phi, t)$ is then given by:

$$\frac{dP(\phi, t)}{dt} = -\frac{1}{\tau(\phi)}P(\phi, t) + \left\langle \frac{1}{\tau(\phi)} \right\rangle_t P_0(\phi). \quad (124)$$

This equation was introduced in [20, 58, 100] in the context of glasses, and extended to granular media by Head [77], where the free volume density ϕ plays the rôle of the energy E . This equation neglects any coupling between nearby sub-systems. This is obviously unrealistic since the free volume liberated at one point will in general help nearby volumes to unjam. A generalization of the above model that takes into account, to some extent, this coupling, can be found in [20, 76, 100].

The trap model, and its “SGR” (Soft Glassy Materials) generalisation covered in Mike Cates lectures [66, 134], exhibits a number of interesting features, such as a genuine glass transition, aging and non linear rheology. A crucial ingredient of the trap model is the possibility for the average trapping time to diverge. Taking $\tau(\phi) \sim \exp(A/\phi)$, where A is a certain constant that may depend on the tapping amplitude Γ , and $P_0(\phi) = \exp[\xi^3 s(\phi)]$ with $s(\phi) = B \log \phi$, we find that the distribution of trapping times $\Psi(\tau)$ decays very slowly, as $1/\tau(\log \tau)^a$, where $a = 2 + B\xi^3$. This means that one is always in the glassy phase of the trap model, since $\langle \tau \rangle = \infty$ ⁸. Correspondingly, one expects not only slow (logarithmic) compaction but also aging effects, such as reported in numerical simulations [107]. In the glassy phase, the trap model describes the dynamics of each subsystem as essentially *intermittent*: either the system is blocked, or it moves fast to a quite different configuration; most of the time is spent in one particularly well jammed configuration. This intermittent dynamics of glassy systems begins to have some numerical [10, 53, 54] and experimental [32, 39, 120] support. However, one should remember that if one looks at the system as a whole, the activity will be dominated by the fastest regions (which can in turn, through the coupling between nearby that we have neglected above, unlock the slow regions).

Interestingly, the trap model is able to reproduce some of the cycle effects reported above: the irreversibility in a tapping cycle [77], or the Kovacs effect [12, 143]. Variants of the trap model can also be studied, where each “trap” is decorated by the dynamics of smaller length scales [17, 23] in order to account for memory and rejuvenation effects observed in spin-glasses and other glassy systems. The Sinai model is in this family of “multi-scale” trap models [87, 90, 121], and was introduced in the context of granular media precisely to understand the memory and cycle effects [95], although the simpler “monoscale” trap model seems to be able to account for most of them. It would be very interesting to exhibit experimentally a truly “multiscale” dynamical phenomenon in granular materials. This

⁸Note that the logarithmic tail found above can be seen as an effective power-law with a time dependent effective exponent $\mu = a/\log \tau$. This suggests that the relevant coherence length after time t is such that $B\xi^3 \sim \log t$.

would have the obvious advantage over many other glassy systems that the underlying mechanism, in terms of embedded length scales, can be directly observable [23, 25].

There would be much more to say about glassy dynamics in the context of granular materials, but my lectures stopped at this point, after only quite simple ideas were expressed. Since some of the more elaborated concepts are common to spin-glass dynamics and glassy rheology, it is appropriate to refer to the lectures of Mike Cates, Leticia Cugliandolo and Giorgio Parisi in this volume, and also to [6, 11, 22, 92] for further developments.

References

- [1] A. Ayadim, Ph. Claudin and J.N. Roux, unpublished.
- [2] R.C. Ball and R. Blumenfeld, *Phys. Rev. Lett.* **88** (2002) 115505, see also [cond-mat/0301562].
- [3] A. Barrat, J. Kurchan, V. Loreto and M. Sellitto, *Phys. Rev. Lett.* **85** (2000) 5034.
- [4] A. Barrat, V. Colizza and V. Loreto, *Phys. Rev. E* **66** (2002) 011310; *Phys. Rev. E* **65** (2002) 050301.
- [5] J. Berg, S. Franz and M. Sellitto, *Euro. Phys. J. B* **26** (2002) 349.
- [6] L. Berthier, L. Cugliandolo and J.L. Iguain, *Phys. Rev.* **63** (2001) 051302.
- [7] L. Berthier and P.C.W. Holdsworth, *Europhys. Lett.* **58** (2002) 35.
- [8] L. Berthier and J.-L. Barrat, *Phys. Rev. Lett.* **89** (2002) 095702.
- [9] L. Berthier and J.-P. Bouchaud, *Phys. Rev. B* **66** (2002) 054404.
- [10] L. Berthier, *Yield stress, heterogeneities and activated processes in soft glassy materials*, Preprint [cond-mat/0209394].
- [11] L. Berthier, V. Viasnoff, O. White, V. Orlyanchik and F. Krzakala, this volume.
- [12] E. Bertin, J.P. Bouchaud, J.M. Drouffe and C. Godrèche, in preparation.
- [13] D. Blair, N. Mueggenburg, A. Marshall, H. Jaeger and S. Nagel, *Phys. Rev. E* **63** (2001) 041304.
- [14] R. Blumenfeld, S.F. Edwards and R.C. Ball, *Granular Matter and the Marginal Rigidity State*, Preprint [cond-mat/0105348].
- [15] D. Bonamy, Ph.D. Thesis, unpublished (2001).
- [16] D. Bonamy, F. Daviaud, L. Laurent, M. Bonetti and J.P. Bouchaud, *Phys. Rev. Lett.* **89** (2002) 034301.
- [17] J.-P. Bouchaud and D.S. Dean, *J. Phys. I France* **5** (1995) 265.
- [18] J.-P. Bouchaud, M.E. Cates and P. Claudin, *J. Phys. I France* **5** (1995) 639.
- [19] J.-P. Bouchaud, L. Cugliandolo, J. Kurchan and M. Mézard, *Physica A* **226** (1996) 243.
- [20] J.P. Bouchaud, A. Comtet and C. Monthus, *J. Phys. I France* **5** (1995) 1521.
- [21] J.-P. Bouchaud, P. Claudin, M.E. Cates and J.P. Wittmer, in *Physics of Dry Granular Media*, edited by H.J. Herrmann, J.P. Hovi and S. Luding, NATO ASI (1997) 97.
- [22] J.-P. Bouchaud, L. Cugliandolo, J. Kurchan and M. Mézard, in *Spin-glasses and Random Fields*, edited by A.P. Young (World Scientific, Singapore, 1998), and references therein.
- [23] J.-P. Bouchaud, in *Soft and Fragile Matter*, edited by M.E. Cates and M.R. Evans (Institut of Physics Publishing, Bristol and Philadelphia, 2000).

- [24] J.P. Bouchaud, P. Claudin, D. Levine and M. Otto, *Eur. Phys. J. E* **4** (2001) 451.
- [25] J.-P. Bouchaud, V. Dupuis, J. Hammann and E. Vincent, *Phys. Rev. B* **65** (2002) 024439.
- [26] J.P. Bouchaud, P. Claudin, M. Otto and J.E.S. Socolar, in preparation.
- [27] T. Bouteux and P.G. de Gennes, *Physica A* **244** (1997) 59.
- [28] L. Breton, E. Clément, P. Claudin and J.-D. Zucker, *Europhys. Lett.* **60** (2002) 813.
- [29] R. Brockbank, J.M. Huntley and R.C. Ball, *J. Phys. II France* **7** (1997) 1521-1532.
- [30] R.L. Brown and J.C. Richard, *Principles of Powder Mechanics* (Pergamon, New York, 1966).
- [31] J. Brujic, S.F. Edwards, I. Hopkinson and H.A. Maakse, *Characterisation of the micromechanics in a compressed emulsion system: Force distribution*, Preprint [cond-mat/0210136].
- [32] L. Buisson, L. Bellon and S. Ciliberto, *Intermittency in Aging*, Preprint [cond-mat/0210490].
- [33] F. Cantelaube and J.D. Goddard, in *Powders and Grains 97*, edited by Behringer and Jenkins (Balkema, Rotterdam, 1997), 231-234.
- [34] M.E. Cates, J.P. Wittmer, J.-P. Bouchaud and P. Claudin, *Phil. Trans. Roy. Soc. Lond. A* **356** (1998) 2535-2560.
- [35] M.E. Cates, J.P. Wittmer, J.-P. Bouchaud and P. Claudin, *Phys. Rev. Lett.* **81** (1998) 1841.
- [36] H.E. Castillo, C. Chamon, L.F. Cugliandolo, J.-L. Iguain and M.P. Kennett, *Spatially heterogeneous ages in glassy dynamics* [e-print cond-mat/0211558].
- [37] A. Cavagna, *Europhys. Lett.* **53** (2001) 490.
- [38] M. Chertkov, G. Falkovich and V. Lebedev, *Phys. Rev. Lett.* **76** (1996) 3707 and references therein.
- [39] L. Cipelletti, H. Bissig, V. Trappe, P. Ballestat and S. Mazoyer, submitted to *J. Phys. Cond. Mat.*
- [40] P. Claudin and J.-P. Bouchaud, *Phys. Rev. Lett.* **78** (1997) 231.
- [41] P. Claudin, J.-P. Bouchaud, M.E. Cates and J.P. Wittmer, *Phys. Rev. E* **57** (1998) 4441.
- [42] P. Claudin, *Ann. Phys.* **24** (1999) 1.
- [43] E. Clément, G. Reydellet, L. Vanel, D.W. Howell, J. Geng and R.P. Behringer, XIIIth Int. Cong. on Rheology, Cambridge (UK), Vol. 2 (2000) 426.
- [44] G. Combe and J.-N. Roux, *Phys. Rev. Lett.* **85** (2000) 3628.
- [45] A. Coniglio, A. Fierro and M. Nicodemi, *Probability distribution of inherent states in models of granular media and glasses* [preprint cond-mat/0206275].
- [46] S.N. Coppersmith, C.-H. Liu, S. Majumdar, O. Narayan and T.A. Witten, *Phys. Rev. E* **53** (1996) 4673.
- [47] D. Cule and Y. Shapir *Phys. Rev. B* **50** (1994) 5119.
- [48] G. D'Anna, P. Mayor, G. Gremaud, A. Barrat and V. Loreto, *Europhys. Lett.* **61** (2003) 60.
- [49] P. Dantu, *Ann. Ponts et Chaussées* **4** (1967) 144.
- [50] O. Dauchot, private communication and in preparation.
- [51] D.S. Dean, *J. Phys. A* **29** (1996) L613.
- [52] D.S. Dean and A. Lefevre, *Phys. Rev. Lett.* **86** (2001) 5639.
- [53] R. A. Denny, D. R. Reichman and J.-P. Bouchaud, *Phys. Rev. Lett.* **90** (2003) 025503.

- [54] B. Doliwa and A. Heuer, *Hopping in a Supercooled Lennard Jones liquid: Metabasins, Waiting-time distribution and Diffusion*, Preprint [cond-mat/0205283].
- [55] B. Doliwa and A. Heuer, *Energy Barriers and Activated Dynamics in a Supercooled Lennard-Jones Liquid*, Preprint [cond-mat/0209139].
- [56] J. Duran, *Sables, poudres et grains* (Eyrolles Sciences, Paris, 1997, Springer, New-York, 2001).
- [57] J. Duran and J.P. Bouchaud, *Physics of Granular Media*, *C. R. Academie des Sci. Special Issue* **3** (2002) 129.
- [58] J.C. Dyre, *Phys. Rev. Lett.* **58** (1987) 792; *Phys. Rev. B* **51** (1995) 12 276.
- [59] S.F. Edwards and R.B. Oakeshott, *Physica D* **38** (1989) 88.
- [60] S.F. Edwards and R.B.S. Oakeshott, *Physica A* **157** (1989) 1080, S.F. Edwards, in *Disorder in Condensed Matter Physics* (Oxford Science Publications, 1991).
- [61] S.F. Edwards and C.C. Mounfield, *Physica A* **226** (1996) 1, 12, 25.
- [62] S.F. Edwards and D.V. Grinev, *Phys. Rev. Lett.* **82** (1999) 5397; S.F. Edwards and D. Grinev, *Physica A* **294** (2001) 57.
- [63] C. Eloy and E. Clément, *J. Phys. I France* (1997).
- [64] D. Ertas and T. Halsey, *Phys. Rev. Lett.* **83** (1999) 5007.
- [65] M.L. Falk and J.S. Langer, *M.R.S. Bulletin* **25** (2000) 40.
- [66] S.M. Fielding, P. Sollich and M.E. Cates, *J. Rheol.* **44** (2000) 323.
- [67] J.P. Garrahan and D. Chandler, *Phys. Rev. Lett.* **89** (2002) 035704.
- [68] C. Gay and R. da Silveira [cond-mat/0208155]; R. da Silveira, G. Vidalenc and C. Gay [cond-mat/0208214].
- [69] J. Geng, D. Howell, E. Longhi, R.P. Behringer, G. Reydellet, L. Vanel, E. Clément and S. Luding, *Phys. Rev. Lett.* **87** (2001) 035506; J. Geng, G. Reydellet, E. Clément and R.P. Behringer, *Green's Function Measurements in 2D Granular Materials*, Preprint [cond-mat/0211031].
- [70] P.-G. de Gennes, Collège de France lectures, unpublished (1995).
- [71] P.-G. de Gennes, *Rev. Mod. Phys.* **71** (1999) S374.
- [72] I. Goldhirsch, in [80].
- [73] C. Goldenberg and I. Goldhirsch, *Phys. Rev. Lett.* **89** (2002) 084302.
- [74] M. Goldstein, *J. Chem. Phys.* **51** (1969) 3728.
- [75] T.S. Grigera, A. Cavagna, I. Giardina and G. Parisi, *Phys. Rev. Lett.* **88** (2002) 055502 and references therein.
- [76] D. Head, *J. Phys. A* **33** (2000) 465.
- [77] D. Head, *Phys. Rev. E* **62** (2000) 2439.
- [78] D. Head, A. Tkachenko and T. Witten, *Eur. Phys. J. E* **6** (2001) 99.
- [79] D. Head, A. Tkachenko and T. Witten, *Eur. Phys. J. E* **7** (2002) 299.
- [80] H.J. Herrmann, J.P. Hovi and S. Luding, *Physics of Dry Granular Media*, NATO ASI (1997) 25.
- [81] H.M. Jaeger, S.R. Nagel and R.P. Behringer, *Rev. Mod. Phys.* **68** (1996) 1259.
- [82] H.A. Janssen, *Z. Vert. Dt. Ing.* **39**, 1045 (1895); see also [106].
- [83] Ch. Josserand, A. Tkachenko, D.M. Mueth and H.M. Jaeger, *Phys. Rev. Lett.* **85** (2000) 3632.
- [84] A.J. Kovacs, *Adv. Polym. Sci.* **3** (1963) 394; A.J. Kovacs, *et al.*, *J. Polym. Sci.* **17** (1979) 1097.
- [85] J. Kurchan and L. Laloux, *J. Phys. A* **29** (1996) 1929.
- [86] J. Kurchan, in [92].

- [87] L. Laloux and P. Le Doussal, *Phys. Rev. E* **57** (1998) 6296.
- [88] J. Lamarcq, J.P. Bouchaud, O. Martin and M. Mézard, *Europhys. Lett.* **58** (2002) 321.
- [89] L.D. Landau and E.M. Lifshitz, *Theory of Elasticity*, 3rd Ed. (Pergamon, Oxford, 1986).
- [90] P. Le Doussal, C. Monthus and D.S. Fisher, *Phys. Rev. E* **59** (1999) 4795.
- [91] A. Lemaitre, *A dynamical approach to glassy materials*, Preprint [cond-mat/0206417].
- [92] A. Liu and S. Nagel, *Jamming and Rheology* (Taylor & Francis, 2001).
- [93] C.-H. Liu, S.R. Nagel, D.A. Scheeter, S.N. Coppersmith, S. Majumdar, O. Narayan and T.A. Witten, *Science* **269** (1995) 513.
- [94] D. Long and F. Lequeux, *Eur. Phys. J. E* **4** (2001) 371.
- [95] S. Luding, M. Nicolas and O. Pouliquen, in *Compaction of Soils, Granulates and Powders*, edited by D. Kolymbas and W. Fellin (A. A. Balkema, Rotterdam, 2000).
- [96] S. Luding, in [57].
- [97] H.A. Maakse and J. Kurchan, *Nature* **415** (2002) 614.
- [98] B. Meerson, T. Poeschel, P.V. Sasorov and T. Schwager, *Breakdown of granular hydrodynamics at a phase separation threshold*, Preprint [cond-mat/0208286].
- [99] R. Monasson and O. Pouliquen, *Physica A* **236** (1997) 395.
- [100] C. Monthus and J.-P. Bouchaud, *J. Phys. A: Math. Gen.* **29** (1996) 3847.
- [101] J.-J. Moreau, in the proceedings of the *colloque Physique et mécanique des matériaux granulaires* (Champs-sur-Marne, France, 2000), 199.
- [102] C.F. Moukarzel, *Phys. Rev. Lett.* **81** (1998) 1634; *Granular matter instability: A structural rigidity point of view*, Preprint [cond-mat/9807004].
- [103] N. Mueggenburg, H. Jaeger and S. Nagel, *Stress transmission through three dimensional ordered granular arrays* [cond-mat/0204533].
- [104] O. Narayan and S.R. Nagel, *Physica A* **264** (1999) 75.
- [105] O. Narayan, *Phys. Rev. E* **63** (2001) 10301.
- [106] R.M. Nedderman, *Statics and Kinematics of Granular Materials* (Cambridge University Press, 1992).
- [107] M. Nicodemi, A. Coniglio and H.J. Herrmann, *Phys. Rev. E* **55** (1997) 3962.
- [108] E.R. Nowak, J.B. Knight, E. Ben-Naim, H.M. Jaeger and S.R. Nagel, *Phys. Rev. E* **57** (1998) 1971.
- [109] C.S. O'Hern, S.A. Langer, A.J. Liu and S.R. Nagel, *Phys. Rev. Lett.* **86** (2001) 111.
- [110] M. Otto, J.P. Bouchaud, P. Claudin and J.E.S. Socolar, Preprint [cond-mat/0211015], to appear in *Phys. Rev. E*.
- [111] P. Philippe and D. Bideau, *Europhys. Lett.* **60** (2002) 677.
- [112] T. Poeschel and S. Luding, *Granular gases, Lecture Notes in Phys.* **564** (Springer, Berlin, 2001).
- [113] T. Poeschel, N.V. Brilliantov and T. Schwager, *Violation of Molecular Chaos in dissipative gases*, Preprint [cond-mat/0210058].
- [114] F. Radjai, D.E. Wolf, M. Jean and J.J. Moreau, *Phys. Rev. Lett.* **80** (1998) 61, and references therein.
- [115] R. Rajesh and S. Majumdar, *Phys. Rev. E* **62** (2000) 3186.
- [116] G. Reydellet and E. Clément, *Phys. Rev. Lett.* **86** (2001) 3308.
- [117] F. Ritort and P. Sollich, *Glassy dynamics of kinetically constrained models* [e-print cond-mat/0210382].

- [118] J.N. Roux, *Phys. Rev. E* **61** (2000) 6802.
- [119] J.N. Roux, *Eur. Phys. J. E* **7** (2002) 297.
- [120] E.V. Russell and N.E. Israeloff, *Nature* **408** (2000) 695.
- [121] M. Sales, J.-P. Bouchaud and F. Ritort, *J. Phys. A* **36** (2003) 665.
- [122] L. Saul, M. Kardar and N. Read, *Phys. Rev. A* **45** (1992) 8859.
- [123] S.B. Savage, in *Powders and Grains 97*, edited by Behringer and Jenkins (Balkema, Rotterdam, 1997), 185-194; see also *New Scientist* **2083** (1997) 28.
- [124] D. Serero, G. Reydellet, P. Claudin, E. Clément and D. Levine, *Eur. Phys. J. E* **6** (2001) 169.
- [125] L.E. Silbert, D. Ertas, G.S. Grest, T.C. Halsey and D. Levine, *Geometry of frictionless and frictional sphere packing*, Preprint [cond-mat/0111140] see also L.E. Silbert, D. Ertas, G.S. Grest, T.C. Halsey, D. Levine, *Granular "glass" transition*, Preprint [cond-mat/0109124].
- [126] M. da Silva and J. Rajchenbach, *Nature* **406** (2000) 70.
- [127] G. de Smedt, C. Godrèche and J.M. Luck, *Eur. Phys. J. B* **27** (2002) 363-380.
- [128] J. Smid and J. Nosvad, Proc. of 1981 Powtech Conference, *Ind. Chem. Eng. Symp.* **63** (1981) D3V 1-12.
- [129] J.H. Snoeijer and J.M.J. van Leeuwen, *Force relaxation in the q-model for granular media*, Preprint [cond-mat/0202120].
- [130] J.H. Snoeijer, M. van Hecke, E. Somfai and W. van Saarloos, *Effect of boundaries on the force distributions in granular media*, Preprint [cond-mat/0204277].
- [131] J.E.S. Socolar, *Phys. Rev. E* **60** (1999) 1999.
- [132] J.E.S. Socolar, D.G. Schaeffer and P. Claudin, *Eur. Phys. J. E* **7** (2002) 353.
- [133] J.E.S. Socolar, *Discrete models of force chain networks* [cond-mat/0212162].
- [134] P. Sollich, F. Lequeux, P. Hebraud and M.E. Cates, *Phys. Rev. Lett.* **78** (1997) 2020; S.M. Fielding, P. Sollich and M.E. Cates, *J. Rheol.* **44** (2000) 323.
- [135] L.C.E. Struik, *Physical aging in amorphous polymers and other materials* (Elsevier, Amsterdam, 1978).
- [136] H. Takayama, I. Nishikawa and H. Tasaki, *Phys. Rev. A* **37** (1988) 3110.
- [137] J. Talbot, G. Tarjus and P. Viot, *Eur. Phys. J. E* **5** (2001) 445.
- [138] V. Tkachenko and T.A. Witten, *Phys. Rev. E* **60** (1999) 687; *Phys. Rev. E* **62** (2000) 2510.
- [139] C. Toninelli, G. Biroli and D.S. Fisher, in preparation.
- [140] L. Vanel, D.W. Howell, D. Clark, R.P. Behringer and E. Clément, *Phys. Rev. E* **60** (1999) R5040.
- [141] L. Vanel, P. Claudin, J.-P. Bouchaud, M.E. Cates, E. Clément, and J.P. Wittmer, *Phys. Rev. Lett.* **84** (2000) 1439.
- [142] M.C.W. van Rossum and Th.M. Nieuwenhuizen, *Rev. Mod. Phys.* **71** (1999) 313.
- [143] V. Viasnoff and F. Lequeux, *Phys. Rev. Lett.* **89** (2002) 065701.
- [144] E.R. Weeks, J.C. Crocker, A.C. Levitt, A. Schofield and D.A. Weitz, *Science* **287** (2000) 627.
- [145] J.P. Wittmer, M.E. Cates, P. Claudin and J.-P. Bouchaud, *Nature London* **382** (1996) 336; J.P. Wittmer, P. Claudin and M.E. Cates, *J. Phys. France I* **7** (1997) 39.
- [146] J.P. Wittmer, M.E. Cates and P. Claudin, *J. Phys. I France* **7** (1997) 39.
- [147] J.P. Wittmer, A. Tanguy, J.-L. Barrat and L. Lewis, *Europhys. Lett.* **57** (2002) 423.
- [148] D.M. Wood, *Soil Behaviour and Critical State Soil Mechanics* (Cambridge University Press, Cambridge, 1990).

COURSE 5

**SUPERCOOLED LIQUIDS, THE GLASS TRANSITION,
AND COMPUTER SIMULATIONS**

W. KOB

*Laboratoire des Verres,
Université Montpellier 2,
34095 Montpellier,
France*



Contents

1	Introduction	201
2	Supercooled liquids and the glass transition: Important facts and concepts	202
3	The mode-coupling theory of the glass transition	217
3.1	The Mori-Zwanzig formalism	217
3.2	Application of the Mori-Zwanzig formalism to glass-forming systems	220
4	Computer simulations of glass-forming systems	230
5	The relaxation dynamics of glass-forming liquids as investigated by computer simulations	239
5.1	Static and dynamic properties of a simple liquid with Newtonian dynamics	239
5.2	The relaxation dynamics of a simple liquid with stochastic dynamics	250
5.3	Static and dynamic properties of a network forming liquid	255
6	Summary and perspectives	261

SUPERCOOLED LIQUIDS, THE GLASS TRANSITION, AND COMPUTER SIMULATIONS

W. Kob

1 Introduction

Although in everyday life glasses are mostly associated with pleasurable or useful things like a glass of wine or window pans, they have been, and still are, also the topic of research of an impressive number of investigations. In the last twenty years a particularly strong effort has been made to solve one of the long standing puzzles of condensed matter physics: the problem of the glass transition, *i.e.* to answer the simple question “What is a glass?”. The results of all these experimental, theoretical, and computational efforts is that today we have a much deeper understanding of the properties of glass forming systems. Nevertheless one must admit that despite the impressive activities in the field, some of the key questions are still not answered and therefore this subject is still a very active domain of research [1–4]. The goal of these lecture notes is therefore to serve as a simple introduction to the field, to familiarize the reader with some theories of the glass transition, and to discuss the results of some computer simulations that have been done to obtain a better understanding of glass-forming systems. Of course it will not be possible to present an exhaustive coverage of these different fields, since they are by now way to vast. But fortunately this is not really necessary because there exist quite a number of excellent textbooks and review articles that discuss the various aspects of glassy systems in more detail [5–23]. Thus the goal of the present text is rather to provide a relatively concise introduction to these various fields and to allow the reader to familiarize him/her-self with this rapidly evolving topic.

In the first section we hence give an introduction to the dynamics of supercooled liquids and the glass transition. The second section is devoted to discuss some of the theoretical approaches used to describe these systems. Since computer simulations are one of the important current methods to study glass-forming materials, the following section will be devoted to discuss the advantages and disadvantages of simulations of such systems.

Finally we will review some results of computer simulations of glass-forming liquids and discuss to what extent they can be used to check the validity of theoretical approaches and to increase our understanding of the static and dynamic properties of glassy materials.

2 Supercooled liquids and the glass transition: Important facts and concepts

The goal of this section is to give an introduction to some of the relevant properties of glass forming systems and to explain some of the pertinent concepts that are useful to characterize them. This overview is of course by no means exhaustive but it should nevertheless allow the reader to get familiar with these kind of systems. For a more exhaustive description we refer the reader to the additional literature mentioned in the text.

Let us consider a system in its liquid state. At sufficiently high temperatures it can be expected that the viscosity η is small, the diffusion constant D of the atoms (or more general of the constituent particles) is high, and that the typical relaxation time τ is microscopic, *i.e.* is on the order of a typical vibrational period of the system which for an atomic liquid is on the order of 0.1–1 ps (see below for a precise definition of τ). If the system is cooled below its melting temperature T_m one can anticipate it to undergo a static phase transition, *i.e.* that it crystallizes. However, in practice it is found that most liquids can be supercooled to some extent, *i.e.* it is possible to study their properties in the (metastable) supercooled regime. (More details on the lifetime of this metastable state are given below.) Many experiments as well as computer simulations have shown that the *structural* as well as the *thermodynamic* properties of supercooled liquids show only a relatively weak temperature dependence and that this dependence can often be extrapolated smoothly from the data above T_m . This is not the case for most *dynamic* properties, such as, *e.g.*, quantities like the viscosity or the diffusion constant. Instead it is found that these properties usually show a T –dependence that is much more pronounced than the one that would be expected from the one for the liquid above T_m . As a typical example for such a strong T –dependence we show in Figure 1 an Arrhenius plot of the viscosity η . From this plot we recognize that a relatively modest change in temperature (depending on the material between 20% to a factor of 3) leads to an increase of η by about 12–14 decades. Note that the data shown covers a wide range of material, including oxides such as SiO_2 , as well as molecular liquids such as toluene. A similar behavior is also found for most polymeric systems. This shows that this dramatic slowing down of the dynamics is a very general phenomenon.

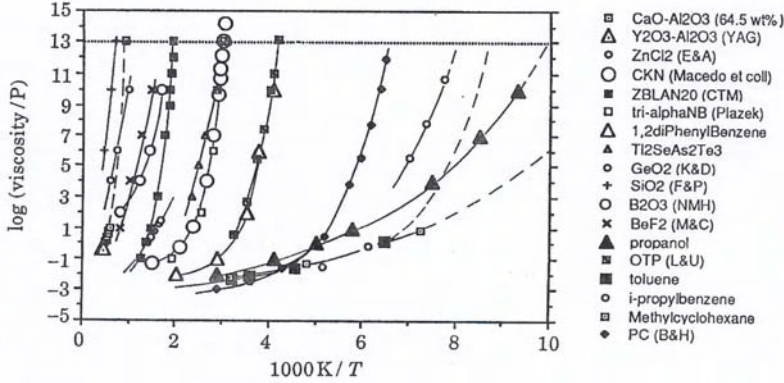


Fig. 1. Temperature dependence of the viscosity of various glass-forming materials. Reproduced from [24] with permission.

The materials shown in Figure 1 have of course characteristic temperatures (melting point, etc.) that are very different and hence the different curves spread over a wide range of temperature. It is therefore useful to make a plot in which one tries to use a reduced temperature scale. One possibility to do this, proposed first by Laughlin and Uhlmann [25], is to define a temperature T_g at which the viscosity of the system has the (somewhat arbitrary) value 10^{13} Poise ($= 10^{12}$ Pas) and to plot the viscosity as a function of T_g/T . An example of such a presentation of the data is shown in Figure 2 [26] and is commonly called “Angell-plot”. We see that in this type of plot the curves for the different materials seem to show a relatively simple pattern: there are liquids for which $\eta(T)$ is to a very good approximation just an Arrhenius law (top curves in the diagram). A prototype of such a material is SiO_2 who shows in the whole accessible temperature range this T -dependence. If one moves downwards in the diagram, one finds materials whose viscosity shows a bending at intermediate values of T_g/T . Finally the bottom curves show a quite pronounced curvature at a temperature around $T_g/T \approx 0.7$. Note that each curve can be parametrized in the form $\eta(T) = \eta_0 \exp(E(t)/k_B T)$, by definition of $E(t)$, and hence the local slope of the curves can be interpreted as a (temperature dependent) activation energy $E(t)$. Hence one concludes from the figure that there are system for which this activation energy is basically independent of temperature and others for which it increases rapidly with decreasing T . This is evidence that for the first type of systems the mechanism related to the relaxation of the liquid is independent of temperature, whereas for the latter type it depends on T . Hence Angell coined the terms “strong” and “fragile” to

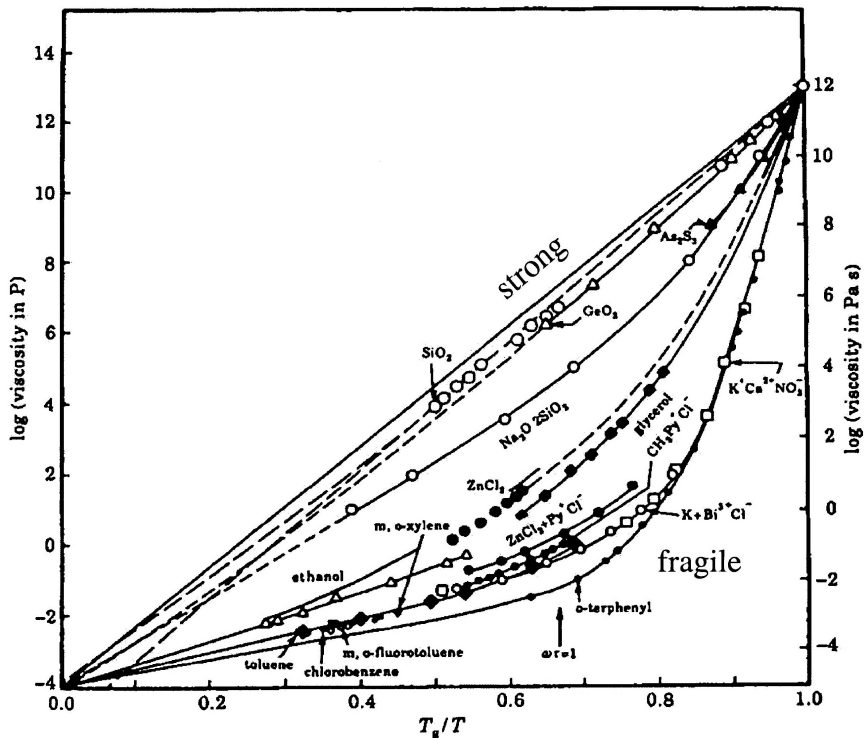


Fig. 2. Viscosity of various glass-forming liquids as a function of T_g/T , where T_g is the glass transition temperature defined *via* $\eta(T_g) = 10^{13}$ Poise. Reproduced from [24] with permission.

distinguish these two types of behaviors [26]. One possibility to characterize “fragility” in a *quantitative* way is to consider the slope of $\log(\eta(T))$ *vs.* T_g/T at T_g : large slopes correspond to fragile glass-formers and small ones to strong glass-formers. Although presently it is not very clear what distinguishes strong and fragile glass-formers on a microscopic level, it has been found empirically that there is a significant correlation between fragility and other properties of the material (T -dependence of the specific heat, time dependence of relaxation dynamics, etc.) [27]. Furthermore one observes the trend that the structure of strong glass-formers is often given by a relatively open network (*e.g.* in the case of silica by corner-shared tetrahedra) whereas the structure of fragile systems is more often compact, such as the one of a hard sphere system. Hence one can conclude that the fragility is

a quantity that does have some physical significance and later on we will come back to this point.

Starting from Figure 2 it is now possible to formulate some of the pertinent questions in the field of glass-forming materials. The first one is clearly that one wants to understand what the reason is for the dramatic slowing down of the dynamics. As mentioned above, all the structural quantities investigated so far do not show any sign of a unusual T -dependence. This is in contrast, *e.g.*, to the case of second order phase transitions where the slowing down of the dynamics upon approach to the critical point is closely related to the presence of a divergent length scale [28]. Thus for the present time it seems necessarily to look for another mechanism and in Section 3 we will discuss different theoretical approaches. Note that it is not even clear whether there is only *one* mechanism or whether there are several ones. *E.g.* it might well be that the slowing down at small and intermediate η is governed by one mechanism and that at high η a different mechanism becomes important. Such a crossover scenario might *e.g.* be used to rationalize the bending seen in the viscosity data for fragile systems.

A further important question, which is related to the first one, is the exact T -dependence of $\eta(T)$ and whether or not this dependence is the same for other typical time scales of the system, such as the diffusion constant or the relaxation time. It is found that at sufficiently high temperatures most liquids show an Arrhenius dependence. At intermediate and low temperatures the data can often, but not always!, be fitted well by the so-called Vogel-Fulcher(-Tammann)-law [29–31] which has the form

$$\eta(T) = \eta_0 \exp(A/(T - T_0)). \quad (2.1)$$

Thus this functional form predicts a T -dependence that for temperatures close to T_0 , a temperature that is usually called “Vogel-temperature”, is significantly stronger than a simple Arrhenius law. (Note that the latter corresponds to the special case $T_0 = 0$.) Although this type of fit gives a good representation of the data, there is no theoretical foundation for this Ansatz. Nevertheless it is very useful since it allows for a simple parametrization of the data with a quite good accuracy. (We point out, however, that there is experimental evidence that the Vogel-Fulcher-law does not hold exactly [32].)

For intermediate values of η , *i.e.* $10^{-1} \text{ P} \leq \eta \leq 10^2 \text{ P}$, one often finds that the data is also very well compatible with a power-law of the form:

$$\eta(T) = \eta_0 (T - T_c)^{-\gamma}. \quad (2.2)$$

This T -dependence is one of the major predictions of the so-called mode-coupling theory of the glass transition (MCT) [13,15] and in Section 3 we will discuss this theory in more detail. The value of the “critical temperature” T_c

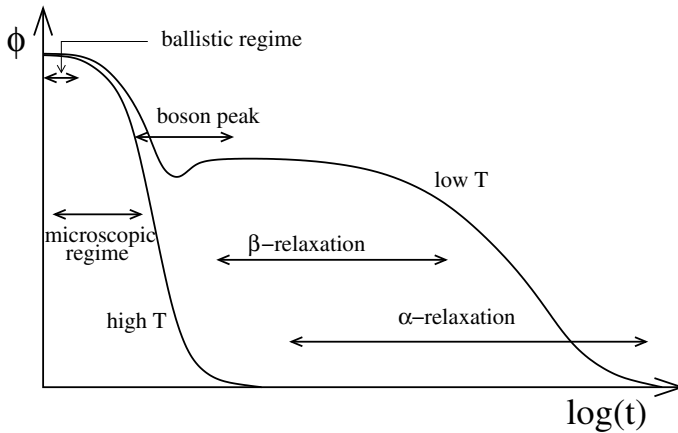


Fig. 3. Time dependence of a typical time correlation function $\Phi(t)$. The two curves correspond to a temperature that is relatively high, and a temperature in which the relaxation dynamics of the system is already very glassy.

is often found to be around 20–30% above T_g . Since equation (2.2) predicts a divergence of the viscosity at $T_c \geq T_g$ it is clear that this functional form cannot be correct for temperatures close to T_g . Below we will show however, that for temperatures that are around T_c , the theory is able to rationalize many dynamical properties of supercooled liquids.

If the Vogel-Fulcher-law given by equation (2.1) would indeed hold down to the Vogel temperature T_0 , one would have a true divergence of the viscosity at a *finite* temperature. Whether or not such a divergence really exists is one further fundamental questions in the field of glass-forming liquids. If the answer is positive it means that below T_0 the system is in an *ideal* glass state, *i.e.* it is in the global minimum of the free energy, *if one considers only amorphous states and neglects the crystal*. Note that unfortunately no experiment will be able to give an answer to this question since in practice it is not possible to equilibrate a real system at a temperature close to T_0 as can be seen as follows: every experiment last only a finite time t_{exp} and hence it will not be possible to study the equilibrium properties of the system below a temperature T_g^{exp} where T_g^{exp} is given implicitly by the relation $\tau(T_g^{\text{exp}}) = t_{\text{exp}}$. Since $\tau(T)$ will show at T_0 roughly the same divergence as $\eta(T)$ we have $T_g^{\text{exp}} > T_0$. Thus the above posed question can be answered only analytically or (at least in principle) by computer simulations (see Sect. 4).

So far we have discussed the temperature dependence of macroscopic quantities, like the viscosity. However, many experiments, such as dynamic

light scattering, inelastic neutron scattering, dielectric measurements, etc.) give also direct access to the time dependence of microscopic correlation functions, such as the density-density correlator defined in equation (3.13). Since very often the mentioned macroscopic quantities can be expressed as the time integral over such correlation functions, the latter certainly contain more information as the former. (Examples are the viscosity that is related to the integral over the stress-stress correlation function or the diffusion constant that is related to the integral over the velocity correlation function of a tagged particle [33,34].) In Figure 3 we show in a schematic way the time dependence of a typical time correlation function $\Phi(t)$ (*e.g.* the intermediate scattering function $F(q, t)$ discussed in more detail in Sects. 3 and 5). The two curves correspond to two temperatures: one at which the system is in its normal liquid state and one at which it relaxes only slowly. At the high temperature the relaxation is relatively simple: at very short times, *i.e.* at times much shorter than the typical microscopic times, the time dependence is quadratic in t . This follows directly from the Taylor expansion of the equation of motion for the particles [33,34]¹. Due to this t^2 dependence this time window is often called “ballistic regime”. For somewhat larger times the t -dependence $\Phi(t)$ is governed by the interactions between the particles and hence it is called the “microscopic regime”. (In the context of the mean squared displacement of a tagged particle, see Fig. 15, we will discuss this regime in more detail.) For even longer times, the t -dependence of $\Phi(t)$ is approximated well by an exponential function, *i.e.* the system shows a Debye-relaxation.

At low temperatures $\Phi(t)$ shows a more complex time dependence. At short times one finds again the ballistic regime that is followed by the microscopic regime. In contrast to the correlator at high temperature, $\Phi(t)$ now shows at intermediate times a plateau. The time window in which the correlator is close to this plateau is called the “ β -relaxation”. Only for times that are much longer (note the logarithmic time scale!) the correlation function decays to zero. The time window in which $\Phi(t)$ decays below the plateau is usually called the “ α -relaxation”. Note that the early part of the α -relaxation coincides with the late part of the β -relaxation. The physical meaning of the plateau is given by the so-called “cage effect”. At low temperatures each particle is surrounded by neighboring particles that form a temporary cage around it. At very short times the particles move ballistically and thus the correlation function shows a t^2 -dependence. At somewhat longer times the particles start to interact with their neighbors

¹Here we assume that this is a liquid that can be described by Newton’s equations of motion. For dissipative systems, such as colloidal particles, some of the statements have to be slightly modified.

and the correlation function enters the microscopic regime. For intermediate times the particles are trapped by their neighbors and hence the correlation function is almost constant. Only for much larger times the particles are able to leave their cage and hence the correlator starts to decay to zero. In the context of the mean-squared displacement of a tagged particle we will return to this trapped motion and will discuss it in more detail (see Fig. 15). In contrast to the case at high T , the final decay of the correlation function is not an exponential. Although the precise form is not known, it can usually be approximated well by the so-called Kohlrausch-Williams-Watts function (KWW) [35,36], often also called “stretched exponential”, which has the form

$$\Phi(t) = A \exp\left(-(t/\tau)^\beta\right). \quad (2.3)$$

Here A is an amplitude, τ can be used to define a relaxation time, and $\beta \leq 1$ is the KWW-exponent. Note that *a priori* all three parameters will depend on the observable as well as on the temperature considered. However, sometimes it is found that in a substantial temperature intervall the three parameters are independent of T . In such a case a plot of the correlator *vs.* t/τ will give a T -independent master curve and therefore one says that the system obeys the “time-temperature-superposition principle”.

The reason why a time correlation function shows at low T a non-Debye behavior, *i.e.* that $\beta < 1$, is still a matter of debate. There are two extreme scenarios [37]: the first one is that due to the disorder each particle of the system has a slightly different neighborhood. Hence also the relaxation dynamics (in particular its relaxation time) will differ from particle to particle. Therefore in this scenario, called “heterogeneous”, the stretching is due to the sum of many different Debye-laws with different relaxation times. In the second scenario, called “homogeneous”, the relaxation dynamics of the different particles is not that much influenced by the *different* surrounding disorder. Instead the (general) presence of the disorder gives rise to a non-Debye relaxation for each particle. Understanding which one of these two extreme cases are seen in a real supercooled liquid is presently still a matter of research [38–40]. But what is already quite clear is that the truth is somewhere in between.

The last time regime we mention is related to the so-called boson peak [41,42]. In many, but not all, structural glasses it is found that there exist vibrational excitations that have a frequency that is about one decade smaller than the typical vibrations in the system. The precise nature of these excitations is still a matter of debate [43–57]. Although they are usually studied in the frequency domain, where they give rise to a peak, the so-called boson peak (see Fig. 4) they also give rise to a feature in the correlation functions in the time domain, in that the latter show a small dip after the microscopic regime. For typical glass forming systems, like *e.g.*

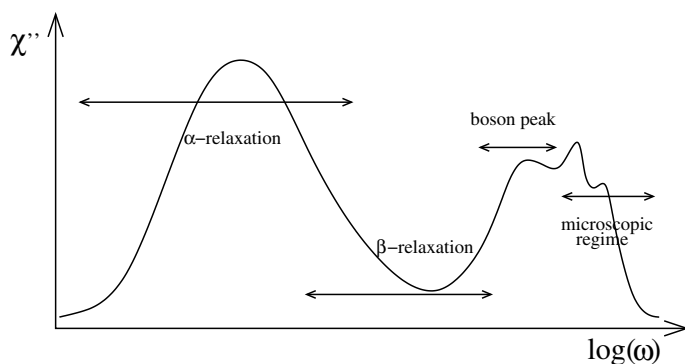


Fig. 4. Schematic plot of the frequency dependence of a typical susceptibility $\chi''(\omega)$.

silica, the location of the peak in the frequency domain is around 1 THz, which thus corresponds to a time scale of 1 ps.

The definition of the various time regimes we just gave have of course also their counterpart in the frequency domain, *i.e.* the realm of many experimental techniques (neutron- and light scattering, dielectric measurements). If one calculates the time-Fourier transform of a correlation function and multiplies its imaginary part with $\omega/2k_B T$, one obtains a frequency dependent susceptibility $\chi''(\omega)$ [33, 34]. In Figure 4 we show schematically how $\chi''(\omega)$ depends on the frequency. We recognize that in general the microscopic regime gives rise to one (or several) peaks in χ'' . The boson peak regime as well as the α -relaxation show up as distinct peaks. (Note however, that depending on how pronounced the associated excitations are, the former is sometimes only a weak shoulder on the low-frequency side of the microscopic peak(s).) Since in the time domain the α -relaxation quickly moves to larger times if T is decreased, one finds that in the frequency regime the α -peak moves rapidly to lower frequencies. In contrast to this the microscopic peaks as well as the boson peak show only a very weak dependence on temperature.

Having discussed the temperature dependence of structural and dynamical observables, where the former is weak and the latter is very strong, we now turn our attention to thermodynamic quantities. Experimentally it is found that most thermodynamic quantities, such as the pressure, specific heat, enthalpy, etc. show a very smooth and relatively mild T -dependence. (Note that we are talking about the liquid like phase, *i.e.* we are not considering non-equilibrium effects that are seen at the glass transition. These will be discussed below in the context of Fig. 7.) In view of this it is

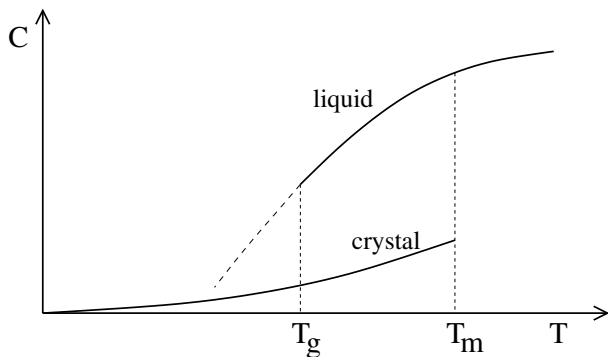


Fig. 5. Schematic plot of the temperature dependence of the specific heat of a glass-forming material in its liquid-like state and in its crystalline state.

surprising that in 1948 Kauzmann reported that the entropy of supercooled systems indicate the existence of a phase transition, or rather thermodynamic instability, at sufficiently low temperature and in the following we will review the arguments that led to this conjecture. In Figure 5 we show schematically the temperature dependence of the specific heat of a glass-forming system. Also included is the specific heat for the corresponding crystalline system. The latter curve exists only up to the melting temperature T_m and depends only weakly on T , since anharmonic effects are usually small. The specific heat of the liquid like branch is higher than the one of the crystal since the liquids is able to flow, *i.e.* there are configurational degrees of freedom (those that give rise to the relaxation/flow of the system) than are not present in the crystal. Recall that at sufficiently low temperature the typical time correlation functions of a glass-forming liquid show a separation of time scales: at short times the particles vibrate in their cage and only at much longer times they are able to leave this cage and hence allow the system to flow (see Fig. 3). Hence also the specific heat can be split up into two contribution: one that is related to the vibrational degrees of freedom and a second part that is related to the relaxation dynamics (also called “configurational degrees of freedom”). (For a more formal approach to this splitting, see [58,59].) The former is quite similar to the one in a crystal and shows also a similar temperature dependence. Hence the difference in C between a supercooled liquid and the corresponding crystal is indeed given by the configurational degrees of freedom.

Using the T –dependence of the specific heat it is possible to calculate the entropy $S(T)$ in the liquid and crystalline phase by means of a thermal

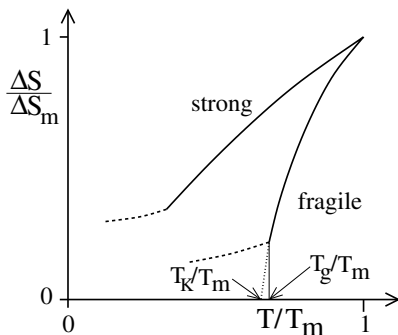


Fig. 6. Schematic plot of the temperature dependence of the normalized difference between the entropy of the liquid state and the one of the crystalline state. The solid and dashed curves correspond to the liquid state and the glass, respectively. The upper and lower curve correspond to the case of strong and fragile glass-forming material. Note that in the latter case a reasonable extrapolation of ΔS seems to vanish at a finite temperature, the so-called Kauzmann temperature.

integration, *i.e.* by using the equality

$$S_\alpha(T_m) = S_\alpha(T) + \int_T^{T_m} dT C/T \quad \alpha \in \{\text{liquid, crystal}\}. \quad (2.4)$$

With this relation it is thus possible to calculate ΔS , the difference between the entropy of a liquid and the one of the crystal. The T -dependence of this difference, normalized by its value at the melting temperature, looks schematically as drawn in Figure 6. We see that for fragile systems this difference decreases rapidly with decreasing temperature and a reasonable extrapolation (see dotted line) seems to indicate that it vanishes at a *finite* temperature T_K , the so-called Kauzmann temperature. Thus for $T < T_K$ the extrapolation predicts that the entropy of the glass is below the one of the crystal. Since in the liquid as well as in the crystal the total entropy is the sum of the entropy associated with the vibrational degrees of freedom and the entropy related to the configurational degrees of freedom, $\Delta S = 0$ implies that the configurational entropies of the glass and of the crystal are equal. This is of course a rather surprising result since the configurational entropy of the (ideal) crystal is zero, since there exists only one configuration and hence $\Delta S = 0$ implies that there exists also only one configuration for the glass. Hence for temperatures below T_K the liquid cannot flow anymore, since there is not state to go to. Thus this final state can be considered as the “ideal glass”. However, Stillinger has put forward a simple argument that

shows that *in a system with short range interactions* the existence of *one* glass state implies immediately that there are exponentially many (in the system size) and that therefore the configurational entropy of the disordered state remains always finite [60]. Thus one must conclude that sufficiently close to T_K the extrapolation shown in Figure 6 is no longer reliable and hence ΔS does not really vanish (see also [61]).

It is remarkable that the apparent vanishing of ΔS at T_K seems to be related also to the dynamics of the system in that it is found that often the value of the Vogel temperature T_0 from equation (2.1) is very close to T_K [62]. One possibility for such a connection is given by the relation proposed by Adams and Gibbs [63], who used some phenomenological arguments to argue that

$$\tau(T) = A \exp \left(\frac{B}{k_B T S_{\text{conf}}} \right), \quad (2.5)$$

where A and B are constants and S_{conf} is the configurational entropy. If one makes the Ansatz $S_{\text{conf}} \propto (T - T_K)$, equation (2.5) gives immediately the Vogel-Fulcher-law from equation (2.1) with $T_0 = T_K$.

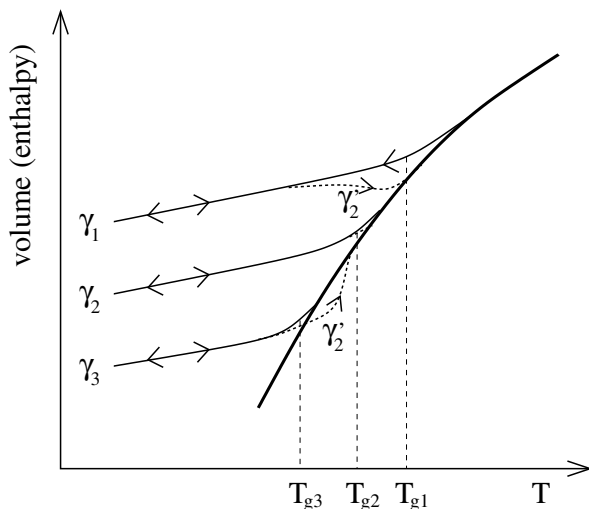


Fig. 7. Schematic plot of the temperature dependence of the volume (or enthalpy) of a glass-forming liquid that is cooled with a cooling rate γ_i (thin lines) and reheated with the heating rate γ'_2 (dotted lines). The bold solid line is the curve for equilibrium.

The results discussed so far concern the behavior of a glass-forming system in its *equilibrium* state (leaving out of course the possibility of

crystallization). However, since the typical relaxation time of the system increases rapidly with decreasing T it is not possible to equilibrate the system at arbitrarily low temperatures since the glass transition intervenes. This is explained schematically in Figure 7 where we show how the volume (or the enthalpy, or most other thermodynamic quantities) depend on temperature in a system that is subject to a quench. The bold solid curve shows the T -dependence of the volume *in equilibrium*. Let's assume that we have equilibrated the system at a high temperature and want to cool it to a lower temperature. For this we have to couple it to a heat bath and cool the system with a cooling rate γ_1 . Since the relaxation time increases with decreasing T there will exist a temperature T_{g1} below which the system is no longer able to equilibrate on the timescale $1/\gamma_1$ and hence it will fall out of equilibrium, *i.e.* it will undergo a glass transition (thin solid lines in Fig. 7). If we repeat the experiment with a cooling rate γ_2 the system will fall out of equilibrium at a temperature $T_{g2} < T_{g1}$ (see Fig. 7). Hence we see that the glass transition temperature is not a system intrinsic temperature (such as the melting temperature), since it depends on experimental parameters like the cooling rate etc. We emphasize that this dependency of T_g is not just of theoretical interest but is indeed observed in real experiments or computer simulations [64–72]. In Section 4 we will come back to this point. In addition it must be expected that T_g depends even on the quantities one considers, since different observables can have relaxation times that differ by orders of magnitude thus leading to different glass transition temperatures.

Since the glass transition temperature depends on the cooling rate, also the resulting glass will depend on γ (see discussion in context of Figs. 12 and 13). Since the glass is an out of equilibrium state, all its properties depend on time, *i.e.* it is aging [73–75]. *E.g.* this can be seen if we start to heat a glass from low to high T , as shown in Figure 7 (dotted lines). Let's start with the glass that has been produced with a cooling rate γ_1 . If we heat it with a heating rate $\gamma'_2 = \gamma_2 < \gamma_1$ it will at low T follow the cooling curve. However, for temperatures slightly below T_{g1} the system will already start to equilibrate, since the available time scale for a change in temperature is higher than the one the system had during the cooling ($\gamma_2 < \gamma_1$!). Hence the heating curve will bend downwards toward the equilibrium line. Thus we conclude that slightly below T_{g1} the properties of the system will depend on time.

If the initial glass is heated with the same rate as it has been cooled, the effect that we just mentioned is much less pronounced (see dotted curve for system γ_2). Hence the heating curve tracks very closely the cooling curve and only very closely to T_{g2} one finds a small aging effect.

If the heating is faster than the cooling, see curve γ_3 in the figure where we assume that $\gamma_3 < \gamma_2$, the system does not show pronounced aging until

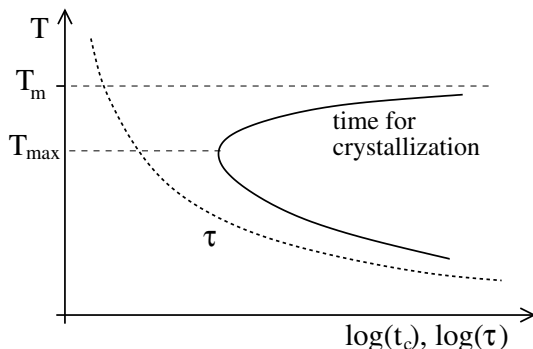


Fig. 8. Schematic plot of the temperature dependence of the time needed for a sample to crystallize (solid curve). The dashed curve shows the typical behavior of the relaxation time as a function of supercooling.

T_{g3} . Due to the “high” heating rate it will, however, not be able to start to equilibrate even if it is at a temperature slightly *above* T_{g3} , since the relaxation times are still too large. Hence it will follow a smooth extrapolation of the “glass-like” branch of the volume. Only when the system has reached a temperature close to T_{g2} the relaxation times will be short enough so that the system can equilibrate.

From this discussion it is clear that the falling out of equilibrium is an effect that depends crucially on the kinetics of the system and hence on the various time scales of the system and the experiments (cooling rate, the temperature dependence of the relaxation time and hence on the observable considered). For technical applications (manufacturing of glasses, improving the properties of glassy materials) it is important to have a good understanding of all these kinetic processes and therefore approximate schemes have been proposed already long time ago to describe them [76–79]. Although these approaches are useful to characterize the kinetics of the glass transition, they are of purely phenomenological nature and hence should not be confounded with the much more recent and advanced theories of aging [75, 80, 81] despite the fact that often the same nomenclature is used (such as “fictive temperature of the glass”). For more details on these new approaches we refer the reader to [75, 82].

Everything that we have discussed so far has been made under the hypothesis that the liquid does not crystallize even in its supercooled state. Although such an assumption is perfectly valid from a theoretical point of view, most real supercooled liquids do crystallize after some time (note that, however, there are liquids that do for all practical purposes indeed not crystallize, such as atactic polymers). In Figure 8 we plot schematically t_c , the

time needed for a liquid to crystallize as a function of its temperature. We see that if the supercooling is weak, the system can stay in this metastable state for a long time. Upon further supercooling the driving force for the nucleation and subsequent crystallization increases and hence the crystallization time decreases rapidly (note the logarithmic time axis!). However, in order to form a critical nucleus it is necessary that the particles move and as we have discussed above this dynamics slows down quickly with decreasing T (see dashed curve in the figure). Therefore at low T the nucleation rate starts to decrease and hence the time for crystallization increases again. Hence we see that there is a temperature T_{\max} at which the crystallization rate has a maximum. Depending how large this maximal rate is, it may or may not be possible to study the system experimentally around T_{\max} . Note, however, that depending on the details of the shape of the crystallization curve it might be possible to obtain an equilibrated liquid also *below* T_{\max} , *e.g.* by quenching the system sufficiently quickly and thus passing this critical temperature. We emphasize that this schematic diagram can also be obtained for real glass-forming systems (see, *e.g.* [83]) and thus it is not just of theoretical value. One important consequence of the plot is that it shows that in principle any liquid/material can be used to form a glass. The only prerequisite is that one needs an experimental setup to do a sufficiently fast quench. Finally we remark that since the curves relate temperature, time and transformation to the crystalline phase, this plot is usually called “ TTT –diagram”.

The slowing down of the relaxation dynamics that we have reviewed so far was due to a change in temperature. It is important to realize, however, that this is by no means the only possibility to slow down the dynamics of a system. Other possibilities include an increase of pressure, evaporation of a solvent in a polymeric system, increasing the density of crosslinks in polymers, etc. Although these routes to slow down the system have so far been investigated less than the temperature route, they are perfectly valid protocols to study the relaxation dynamics of glass forming systems. As we have mentioned above, the glass transition is just a kinetic phenomenon in which the time scale of the experiment becomes comparable with the relaxation time of the system. It is, however, possible to produce glasses also without ever going to high temperatures. *E.g.* one can irradiate a crystal with neutrons and the so induced radiation damage will slowly transform the sample into a glass [84]. The same is true if one compresses a crystal beyond its stability limits or if one grinds a crystalline material. Another possibility to form a glass is to deposit vapor onto a cold surface or to make a chemical reaction (sol-gel transition) [85, 86]. It has to be emphasized that glasses produced in these different ways will in general differ in their properties even if some of their macroscopic properties (density, etc.) are

the same. Strictly speaking it is therefore necessary not only to list some of the properties of a given glass to characterize the material, but also to specify its complete history of production.

Most of the systems we discussed in this section were liquids in their supercooled state. We emphasize, however, that a slow relaxation dynamics is not necessarily related to the *supercooled* state. *E.g.* for the case of SiO_2 the glass transition temperature is $T_g = 1450$ K [87] and the melting temperature is 2000 K. From Figure 2 one recognizes that at $T_g/T_m = 0.725$ the viscosity has already a value of 10^7 Poise, *i.e.* the system is already very viscous (recall that water at room temperature has a viscosity around 10^{-2} Poise!). Therefore we conclude that in order to understand the reason for the slow relaxation of a system, its supercooled state cannot be a relevant factor. For this reason one sometimes also uses the term “glassy liquids” if one wants to describe a liquid whose relaxation time is already much larger than the typical microscopic time scale. In the following we will, however, use the terms “supercooled liquids” and “glassy liquids” interchangeably.

Before we end this section we briefly summarize some of the salient features of glass-forming systems:

- presence of disorder and/or frustration (in the structure, in the interactions, ...);
- no obvious presence of long range order;
- strong dependence of the relaxation time on an external parameter (temperature, pressure, ...);
- transition to a non-ergodic phase;
- non-exponential decay of the relaxation function at low temperatures.

Of course this list is neither complete nor is it necessary that every glass-forming system has all these properties. Instead this list should give an idea what one typically finds in glass-forming systems and therefore help to answer the question asked in the Introduction: “What is a glass”. Using this “definition” one realizes that the class of glass-forming systems is very large: apart from the atomic and molecular liquids that we have considered so far, there are the huge class of polymeric systems that are of immense importance in our daily life. Of equal relevance are granular materials (sand, flour, ...) who share many properties of structural glasses at low temperatures [21, 88]. Foams and spin glasses are other systems that share many properties with glass-forming liquids. Last not least many optimization problems (folding of proteins, traveling salesman problem, “k-sat problem”) have a landscape of the cost function that is very similar to the one of the potential or free energy of more standard glassy systems and

therefore some of the ideas and concepts used in the later systems are useful in the former as well.

3 The mode-coupling theory of the glass transition

The subject of this section is the above mentioned mode-coupling theory of the glass transition. Unfortunately the derivation of all the needed equations is well beyond the scope of this article and therefore we will refer the reader to the more specialized literature (see also the review articles in [13, 15, 89–92]). Nevertheless, the predictions that MCT makes are quite simple to understand and therefore we will discuss them in the following. In addition the theory has the remarkable advantage that it makes detailed qualitative or even quantitative predictions that can be tested in experiments or in computer simulations, which is in contrast to most other theoretical approaches in this field.

The starting point of MCT is the hypothesis that all the structural properties of a glass-forming liquid are very similar to the one of the “normal”, *i.e.* high temperature, liquid. As we have seen in the previous section this assumption is well founded. The second important step in the theory is to exploit the fact that supercooled liquids show a separation of time scale, *i.e.* that there are dynamical processes, such as vibrations, that occur on a microscopic time scale and others, such as the relaxation, that are observed on a time scale that can be many orders of magnitude longer than the former one. MCT makes use of this property of glassy liquids by *i*) making the choice that the relevant slowly varying observables are given by the density distribution of the particles and *ii*) by deriving equations of motion for these slow variables. To obtain these equations of motion, the theory makes use of an *exact* formalism that is called the Zwanzig-Mori projection operator formalism [93, 94]. Since this formalism is very useful to understand the structure of the final MCT equations we will now discuss this approach in somewhat more detail.

3.1 The Mori-Zwanzig formalism

We start with a general classical N –particle system. The equation of motion for an arbitrary phase space function g is given by

$$\dot{g} = i\mathcal{L}g = \{H, g\}, \quad (3.1)$$

where \mathcal{L} and H are the Liouville operator and the Hamiltonian, respectively, and $\{.,.\}$ are the Poisson brackets. It is clear that the set of all possible phase space functions form a vector space and that one can define a scalar

product (g, h) on this space *via*

$$(g, h) = \langle \delta g^* \delta h \rangle, \quad (3.2)$$

where $\langle . \rangle$ is the usual canonical average, and $\delta g = g - \langle g \rangle$, *i.e.* is the fluctuating part of g .

Let us assume that thanks to some physical insight we have understood that the phases space variables A_n , $n = 1, \dots, k$ vary only slowly with time. In the following we will derive equations of motion for these variables that we will denote by a k -dimensional column vector \mathbf{A} . In a first step we define an operator \mathcal{P} that projects an arbitrary function g on the space spanned by the subset A_n :

$$\mathcal{P}(g) = (\mathbf{A}, g)(\mathbf{A}, \mathbf{A})^{-1} \mathbf{A} = \sum_{n,m} A_n [(A_i, A_j)]_{nm}^{-1} (A_m, g) \quad (3.3)$$

where $[(A_i, A_j)]_{nm}^{-1}$ is the n, m element of the inverse of the matrix (A_i, A_j) . Furthermore we define the projection operator $\mathcal{Q} = 1 - \mathcal{P}$. It is easily verified that \mathcal{P} and \mathcal{Q} are indeed projectors, *i.e.* that *e.g.* $\mathcal{P}^2 = \mathcal{P}$.

From equation (3.1) it follows that the time dependence of \mathbf{A} is given by $\mathbf{A}(t) = \exp(i\mathcal{L}t)\mathbf{A}$. Inserting the identity operator $\mathcal{P} + (1 - \mathcal{P})$ after the propagator $\exp(i\mathcal{L}t)$ and differentiating this equation with respect to t one finds

$$d\mathbf{A}/dt = \exp(i\mathcal{L}t)[\mathcal{P} + (1 - \mathcal{P})]i\mathcal{L}\mathbf{A} \quad (3.4)$$

$$= i\boldsymbol{\Omega} \cdot \mathbf{A}(t) + \exp(i\mathcal{L}t)(1 - \mathcal{P})i\mathcal{L}\mathbf{A}, \quad (3.5)$$

where we have introduced the so-called frequency matrix $i\boldsymbol{\Omega} = (\mathbf{A}, i\mathcal{L}\mathbf{A}) \cdot (\mathbf{A}, \mathbf{A})^{-1}$. The last term in equation (3.5) can be written as [34]

$$\exp(i\mathcal{L}t)(1 - \mathcal{P})i\mathcal{L}\mathbf{A} = \int_0^t d\tau \exp[i\mathcal{L}(t - \tau)]i\mathcal{P}\mathcal{L}\mathbf{f}(\tau) + \mathbf{f}(t) \quad (3.6)$$

where the function $\mathbf{f}(t)$ is called “fluctuating force” (see below why) and is given by

$$\mathbf{f}(t) = \exp[i(1 - \mathcal{P})\mathcal{L}t]i(1 - \mathcal{P})\mathcal{L}\mathbf{A}. \quad (3.7)$$

Note that equation (3.7) shows that the time evolution of the function \mathbf{f} from its initial value $i(1 - \mathcal{P})\mathcal{L}\mathbf{A}$ is ruled by the propagator $\exp[i(1 - \mathcal{P})\mathcal{L}t]$ instead of the usual one: $\exp[i\mathcal{L}t]$. In addition we also see immediately that due to the factor $(1 - \mathcal{P})$ we have

$$(\mathbf{A}, \mathbf{f}(t)) = 0, \quad (3.8)$$

i.e. $\mathbf{f}(t)$ is always orthogonal to \mathbf{A} .

Using in equation (3.6) the relations $\mathcal{P}\mathcal{L}\mathbf{f}(\tau) = (\mathbf{A}, \mathcal{L}\mathbf{f}(\tau)) \cdot (\mathbf{A}, \mathbf{A})^{-1} \mathbf{A}$ and $i(\mathbf{A}, \mathcal{L}\mathbf{f}(\tau)) = i((1 - \mathcal{P})\mathcal{L}\mathbf{A}, \mathbf{f}(\tau)) = -(\mathbf{f}(0), \mathbf{f}(\tau))$, we obtain for the equation of motion (3.5) the expression

$$\dot{\mathbf{A}} = i\boldsymbol{\Omega} \cdot \mathbf{A}(t) - \int_0^t d\tau \mathbf{M}(\tau) \cdot \mathbf{A}(t - \tau) + \mathbf{f}(t), \quad (3.9)$$

where we have introduced the *memory function* $\mathbf{M}(t) = (\mathbf{f}, \mathbf{f}(t)) \cdot (\mathbf{A}, \mathbf{A})^{-1}$. The equation of motion for $\mathbf{C}(t) = \langle \mathbf{A}^*(0) \mathbf{A}(t) \rangle$, the matrix of the correlation functions, is now easily obtained by multiplying equation (3.9) with \mathbf{A} :

$$\dot{\mathbf{C}}(t) = i\boldsymbol{\Omega} \cdot \mathbf{C}(t) - \int_0^t d\tau \mathbf{M}(\tau) \cdot \mathbf{C}(t - \tau). \quad (3.10)$$

Note that the third term on the right hand side of equation (3.9) does not show up in Eq. (3.10) due to equation (3.8). Equations (3.9) and (3.10) are usually called *generalized Langevin equation* and *memory equation*, respectively. Both of them are *exact* since no approximation has been made so far. The formal solution of equation (3.10) is obtained by introducing the Laplace transformed quantities

$$\widehat{\mathbf{C}}(z) = \int_0^\infty dt \exp(-zt) \mathbf{C}(t) \quad \text{and} \quad \widehat{\mathbf{M}}(z) = \int_0^\infty dt \exp(-zt) \mathbf{M}(t) \quad (3.11)$$

which give

$$\widehat{\mathbf{C}}(z) = \left[z\mathbf{I} - i\boldsymbol{\Omega} + \widehat{\mathbf{M}}(z) \right]^{-1} \cdot \widehat{\mathbf{C}}(0). \quad (3.12)$$

Here \mathbf{I} is the unit matrix. Although this solution is formally exact, it is not that useful since the time dependence of the memory function $\mathbf{M}(t)$ is very complicated. However, *if* the set \mathbf{A} of variables that we have chosen includes *all* slowly varying quantities, the memory function must either be a fast variable, or it must be possible to express it (at least approximately) as a function of the variables in \mathbf{A} , such as, *e.g.* as linear combinations of $A_i^n A_j^m$, with $n, m = 1, 2, \dots$. This coupling of the variables (modes) has given rise to the name “mode-coupling theory”. We emphasize that the Mori-Zwanzig projection operator formalism and the mode-coupling approximations are not just a technique to describe the dynamics of supercooled liquids but a method that has been widely used in all sort of situations where one is able to identify pertinent slow variables (critical phenomena, Brownian motion, etc.) [95, 96]. Whether or not this approach is successful depends of course on the situation of interest and it is in most cases difficult to tell in advance. However, it has been found that there are indeed quite a few situations in which this method works remarkably well.

3.2 Application of the Mori-Zwanzig formalism to glass-forming systems

Having discussed the general formalism that leads to mode-coupling equations, we now turn our attention back to the case of supercooled liquids. For this type of systems it has been proposed that the slow variables are $\delta\rho(\mathbf{q}, t)$, the fluctuations in the density for wave-vector \mathbf{q} , and hence the mode-coupling equations are equations of motion for the corresponding correlation functions $F(q, t)$:

$$\delta\rho(\mathbf{q}, t) = \sum_{j=1}^N \exp[i\mathbf{q} \cdot \mathbf{r}_j(t)] \quad \text{and} \quad F(q, t) = \frac{1}{N} \langle \delta\rho(\mathbf{q}, t) \delta\rho^*(\mathbf{q}, 0) \rangle. \quad (3.13)$$

(Note that here we have assumed that the system is isotropic. Hence $F(q, t)$ depends only on the modulus of \mathbf{q} .) Also important is the fluctuation in the density of a tagged particle $\delta\rho_s(\mathbf{q}, t)$ for wave-vector \mathbf{q} and its associated correlation function $F_s(q, t)$:

$$\delta\rho_s(\mathbf{q}, t) = \exp[i\mathbf{q} \cdot \mathbf{r}_j(t)] \quad \text{and} \quad F_s(q, t) = \frac{1}{N} \langle \delta\rho_s(\mathbf{q}, t) \delta\rho_s^*(\mathbf{q}, 0) \rangle. \quad (3.14)$$

(Note that due to the thermal average in the definition of $F_s(q, t)$, the correlator does not depend on the particle index j .) The space-time correlation functions $F(q, t)$ and $F_s(q, t)$ are usually called the coherent and incoherent intermediate scattering functions [33]. Apart from their theoretical importance, their significance lies in the fact that they are directly accessible in inelastic neutron scattering [33, 34, 97]. Hence obtaining a good understanding of their q and t -dependence is considered a very important task in the theory of liquids (which is not yet a solved problem).

A somewhat lengthy calculation shows that the MCT equations for $\Phi(q, t) = F(q, t)/S(q)$, where $S(q) = F(q, 0)$ is the static structure factor, are given by [13, 98]:

$$\ddot{\Phi}(q, t) + \Omega^2(q)\Phi(q, t) + \int_0^t [M^{\text{reg}}(q, t-t') + \Omega^2(q)M(q, t-t')] \dot{\Phi}(q, t') dt' = 0. \quad (3.15)$$

Thus we see that this equation does indeed have the form of the general mode-coupling equation (3.10). The value of the squared frequency $\Omega^2(q)$ follows directly from the short time expansion of the equations of motion for the particles and is given by

$$\Omega^2(q) = q^2 k_B T / (mS(q)), \quad (3.16)$$

where m is the mass of the particles. The function $M^{\text{reg}}(q, t)$, also often called the “regular part of the memory function”, governs the time dependence of $F(q, t)$ at short (*i.e.* microscopic) times, *e.g.* just after the ballistic regime. Often it is modeled by a Gaussian Ansatz [99, 100], but its precise functional form is presently not really known. Note that this part of the memory function is present also in “normal” liquids (*i.e.* liquids that are not glassy) where it governs the relaxation dynamics and thus obtaining an accurate form of the $M^{\text{reg}}(q, t)$ is a current problem of standard liquid state theory.

The long time behavior of $\Phi(q, t)$ is ruled by the memory function $M(q, t)$. Within the approximation of MCT this kernel is a quadratic function in $\Phi(q, t)$:

$$M(q, t) = \frac{1}{2(2\pi)^3} \int d\mathbf{k} V^{(2)}(q, k, |\mathbf{q} - \mathbf{k}|) \Phi(k, t) \Phi(|\mathbf{q} - \mathbf{k}|, t) \quad (3.17)$$

where the vertex $V^{(2)}$ is given by

$$V^{(2)}(q, k, |\mathbf{q} - \mathbf{k}|) = \frac{n}{q^2} S(q) S(k) S(|\mathbf{q} - \mathbf{k}|) \left(\frac{\mathbf{q}}{q} [\mathbf{k} c(k) + (\mathbf{q} - \mathbf{k}) c(|\mathbf{q} - \mathbf{k}|)] \right)^2. \quad (3.18)$$

Here $n = V/N$ is the particles density and $c(k)$ is the so-called direct correlation function that is related to the structure factor *via* $c(k) = n(1 - 1/S(q))$ [33]. Hence we see that equations ((3.15)–(3.18)) are a closed set of equations that define the time dependence of $\Phi(q, t)$ and hence of $F(q, t)$. Thus the solution of this set of equations are correlation functions that can in principle be directly compared with data from an experiment or a computer simulation.

Some remarks on these equations and their solutions:

- the form of equation (3.15) is the one of a damped harmonic oscillator with a damping that depends on time. With decreasing temperature the static structure factor becomes more peaked and hence also the vertices $V^{(2)}$ become more peaked. This means that the damping $M(q, t)$ increases, at least for certain wave-vectors, and that hence the relaxation becomes slower. Note that since the memory function depends itself on the correlators, see equation (3.17), a slowing down of the latter will increase the former, therefore leading to an even slower dynamics for $\Phi(q, t)$. This non-linear feedback effect leads to a very strong dependence of the relaxation dynamics on the structural quantities and hence gives a qualitative explanation why the relaxation times of glass-forming systems change so quickly as a function of external parameters (temperature, pressure, etc.).

- It can be shown that if the vertices are sufficiently large, the time scale at which the correlators start to decay to zero increases beyond any bound. This means that there is a critical temperature T_c (or pressure p_c) at which the correlators do not decay to zero anymore and hence at which the system undergoes a transition from an ergodic state to a non-ergodic one. Often this is called an “ideal glass transition” or the “mode-coupling transition”. Due to this ideal transition the equations are also called “ideal mode-coupling equations” and at the end of this section we will briefly discuss their generalization.
- The only input needed to solve these equations are the static quantities $S(q)$, m , n and T . In addition there is the memory function $M^{\text{reg}}(q, t)$ for the dynamics at short times. However, it can be shown that the details of $M^{\text{reg}}(q, t)$ do neither affect the existence of the MCT-transition nor the value T_c at which it occurs. Also the t -dependence of $F(q, t)$ at intermediate and long times, *i.e.* times much longer than the microscopic times, is independent of $M^{\text{reg}}(q, t)$, *apart from a system universal shift in the time scale*. Hence MCT predicts that the relaxation dynamics is completely independent of the microscopic dynamics, apart from a overall change of the time scale.
- The equations of motion discussed so far concerned only the auto-correlation function for the coherent intermediate scattering function $F(q, t)$. However, it is possible to derive also equations of motion for the incoherent function $F_s(q, t)$, defined in equation (3.14). One finds that these equations have the following form [13, 97]:

$$\ddot{F}_s(q, t) + \frac{q^2 k_B T}{m} F_s(q, t) + \int_0^t [M^{\text{reg}, s}(q, t - t') + M^s(q, t - t')] \dot{F}_s(q, t') dt' = 0. \quad (3.19)$$

Here the memory function is given by

$$M^s(q, t) = \frac{nk_B T}{(2\pi)^3 m} \int d\mathbf{q}' \left(\frac{\mathbf{k}' \cdot \mathbf{q}}{q} \right)^2 c(q') S(q') \Phi(q', t) F_s(|\mathbf{q} - \mathbf{q}'|, t). \quad (3.20)$$

Thus the memory function for the dynamics of $F_s(q, t)$ contains the normalized coherent intermediate scattering function $\Phi(q, t)$ and hence we see that in order to obtain the time dependence of $F_s(q, t)$, we need first the one for $F(q, t)$. This result is quite reasonable, since $F_s(q, t)$ describes the motion of a tagged particle in its environment (which is

disordered and time dependent). Hence it must be expected that a relevant input for the time dependence of $F_s(q, t)$ is the time dependence of the relative motion of the tagged particle with respect to its surrounding, and $F(q, t)$ provides exactly this kind of information.

- The vertices $V^{(2)}$ as given by equation (3.18) depend only on the static structure factor $S(q)$. Strictly speaking this is not quite true, since there is also an additional term that depends on the three-particle correlation function known as $c_3(\mathbf{q}, \mathbf{k})$ [33, 101, 102]. However, for *simple* liquids it has been found that this additional contribution to $V^{(2)}$ influences the quantitative predictions of the theory only very weakly [103, 104] and hence it is in most cases neglected. For the case of liquids that have a structure that is given by an open network, this is no longer true and hence these additional terms have to be taken into account [104]. In context with Figures 20 and 28 we will come back to this point.
- So far we have only discussed one-component atomic liquids. It is relatively straightforward to generalize the MCT equations also to multicomponent systems and one finds that in that case the equations of motion become matrix-equations for the partial intermediate scattering functions [103].

It is also possible to take into account the situation that two (or more) particles are permanently linked together, which opens the door to obtain a description for the translational and orientational correlation functions in molecular and polymeric systems [105–115]. The equations one obtains are, however, rather complicated and therefore difficult to solve numerically. However, if one is interested only in simple orientational correlation functions, it is possible to simplify these equations considerably and hence to treat such molecular systems also numerically [108, 109, 113, 115].

The equations ((3.15)–(3.18)) are very complicated and hence it is not surprising that no analytical solution is known. But even obtaining a qualitative understanding of these solutions is a formidable task and therefore it would be nice to have some means to simplify these equations. One possibility for doing this has been proposed in a seminal paper by Bengtzelius *et al.* [98] (see also Leutheusser [116]). By solving numerically the MCT-equations for the case of a hard sphere system, these authors found that the main contribution to the memory function $M(q, t)$ comes from wave-vectors that are close to the peak in the static structure factor. Hence they proposed to approximate $S(q)$ by a single δ -function located at this peak: $S(q) = \zeta \delta(q - q_0)$. Here ζ is the strength of the δ -function and thus is

assumed to increase with decreasing temperature. It is now found immediately that the MCT-equations simplify significantly in that they boil down to a *single* equation of the form:

$$\ddot{\phi}(t) + \Omega^2 \phi(t) + \zeta \Omega^2 \int_0^t \phi^2(t-t') \dot{\phi}(t') dt' = 0, \quad (3.21)$$

where $\phi(t) = F(q_0, t)/S(q_0)$ and we have neglected the regular part of the memory function M^{reg} , since, as discussed above, it does not influence the solution of the equations qualitatively. If one approximates the structure factor by the sum of two δ -functions, one obtains two equations of motion in which the memory function is a simple polynomial of the two correlators. The equations of motion obtained in this way are called “schematic models” and equation (3.21) is a particular example. The interest in such models lies in the fact that the generic features of their solutions are the same as the ones of the full MCT-equations. However, since they are significantly more simple than these full equations, they are very useful to obtain a general overview on the possible t -dependence of the solutions. In addition they have also been found to be very useful to discuss experimental data such as spectra of dynamical light scattering [117–120].

Before we start to discuss the generic properties of the solutions of the MCT-equations we briefly mention a very interesting connection of these equations with the time-correlation functions of spin glasses [8, 20]. From the way the MCT-equations are derived it is clear that for the case of a real liquid they are only an approximation. Since this approximation is non-perturbative (there is no small parameter), the resulting equations have often been criticized as being “uncontrolled”. Although strictly speaking this might be true for the case of real liquids, it has been found that the predictions of the theory are often so remarkably good, see [15, 90, 92] for reviews and some examples will be discussed below, that the observed agreement cannot be a mere accident. Nevertheless it would of course be comfortable if one would know systems for which the MCT-equations are exact. Surprisingly such systems do exist, as has been shown in a series of seminal papers by Kirkpatrick *et al.* [121–123]. These authors found that in certain type of mean-field spin glasses (Potts glasses and p -spin models) the equation of motion for the spin-auto-correlation function obeys exactly the MCT-equations as given by the schematic models. Thus this surprising connection between the structural glasses and spin glasses gave evidence that these two type of systems, which at a first glance have very little in common, might be much more similar than has been anticipated. In recent years a large effort has been made to test to what extend this connection holds, *i.e.*, to test whether concepts and ideas that work well for one type of system (overlap of states [124], violation of the fluctuation dissipation theorem in the glassy phase [75, 82], driving of the system, calculation of the

Kauzmann temperature [125–128], etc.) are also useful for the other type of disordered system. All these activities resulted that the field is currently still extremely active and highly interesting.

We now turn our attention to the discussion of some of the pertinent predictions of MCT. One of the most important prediction is the one already mentioned above, namely that there exists a critical temperature T_c at which the α -relaxation time of the system diverges. All the other predictions that will be presented in the following hold, strictly speaking, only very close to T_c , *i.e.* it is assumed that the parameter $\sigma = (T_c - T)/T_c$ is small. How small in practice σ has to be so that the predictions of the theory hold is presently not very clear and depends also on which prediction one considers [129, 130]. The results of experiments and computer simulations have shown, however, that often it is sufficient that $|\sigma|$ is less than 0.1–0.2, *i.e.* the predictions of the theory can be seen in a reasonable interval of T .

MCT predicts not only that the α -relaxation time diverges at T_c , but also gives the specific form of this divergence, namely a power-law:

$$\tau_x(T) = C_x(T - T_c)^{-\gamma}. \quad (3.22)$$

Here $\tau_x(T)$ denotes the α -relaxation time of a correlator that we label with x (*e.g.* this might be the relaxation time for the coherent intermediate scattering function for wave-vector q , the incoherent function, etc.). C_x is a prefactor that depends on x and whose T -dependence close to T_c can be neglected, and γ is a *system universal constant*, *i.e.* it is independent of x . Hence the implication of equation (3.22) is that all correlation functions will show a divergence of the relaxation time at the *same* temperature T_c and also the critical exponent γ will be independent of the correlator considered. (Note that by “all correlators” we mean here that the overlap of the observable of interest with $\delta\rho(\mathbf{q}, t)$ does not vanish.) One consequence of this result is that also the inverse of the diffusion constant D should show a power-law divergence, since D can be expressed as the limit $q \rightarrow 0$ of the incoherent intermediate scattering function. Hence we have:

$$D^{-1}(T) \propto \tau_x(T) = C_x(T - T_c)^{-\gamma}. \quad (3.23)$$

If the MCT equations are solved numerically, it is found that with increasing coupling (*i.e.* decreasing temperature in Eqs. ((3.15)–(3.18)), or increasing ζ in Eq. (3.21)) the time-dependence of the solution changes from a shape as given qualitatively by the high T curve shown in Figure 3 to a shape as the one of the low T curve in this figure. Thus we see that the theory is able to describe the cage effect discussed in the previous section at least qualitatively. The theory goes, however, much further in that it does not only give a qualitative description of the cage effect but predicts that in the β -relaxation regime the time dependence of all correlation functions (“all”

in the sense described above) is universal in the following sense: let $\Phi_x(t)$ be an arbitrary correlator. Then it is predicted that close to the plateau $\Phi_x(t)$ can be written as

$$\Phi_x(t) = \Phi_x^c + h_x G(t), \quad (3.24)$$

where Φ_x^c is the height of the plateau (often also called “non-ergodicity parameter”, since it gives the fraction of the memory of the initial state that still exists in the time window of the plateau), h_x is an amplitude, and $G(t)$ is a system universal function. Thus we see that the theory predicts that $\Phi_x(t) - \Phi_x^c$ is just the product of a x -dependent amplitude and a x -independent function of time. Therefore the relation given by equation (3.24) is called the “factorization property”. Furthermore the theory predicts that the function $G(t)$ has a very specific dependence on temperature in that it can be written in the form

$$G(t) = \sqrt{|\sigma|} g_{\pm}(t/t_{\sigma}), \quad \sigma = (T_c - T)/T_c, \quad (3.25)$$

where the T -independent functions g_{\pm} correspond to $T < T_c$ and $T > T_c$, respectively. The time scale t_{σ} is the location of the plateau and is predicted to show a power-law divergence of the form $t_{\sigma} = t_0 |\sigma|^{1/2a}$, where t_0 is a microscopic time scale.

The time dependence of the functions g_{\pm} can be obtained by solving (numerically) the following non-linear equations [131]:

$$\mp z^{-1} + z g_{\pm}^2(z) + i\lambda \int_0^{\infty} d\tau \exp(iz\tau) g_{\pm}^2(\tau) = 0. \quad (3.26)$$

Here the constant λ , which is also often called “exponent parameter”, can be calculated from the vertices $V^{(2)}$. Since the functions $g_{\pm}(t)$ give the time dependence of the correlation functions in the β -relaxation regime, they are called “ β -correlator”.

The solution of equation (3.26) are not known analytically but it can be shown that they have the following asymptotic form (*i.e.* very close to the plateau):

$$g_{\pm}(\hat{t}) = \hat{t}^{-a} \quad \text{for } \hat{t} \ll 1, \quad \text{i.e. } t_0 \ll t \ll t_{\sigma}. \quad (3.27)$$

This functional form is called “critical decay”. For times much larger than t_{σ} the form of $g_{-}(t)$ is given by

$$g_{-}(\hat{t}) = B \hat{t}^b \quad \text{for } \hat{t} \gg 1 \quad \text{i.e. } t_{\sigma} \ll t \ll \tau, \quad (3.28)$$

a functional form that in this context is called “von Schweidler law” [131]. The exponents a and b from equations (3.27) and (3.28) can be calculated from the exponent parameter λ from equation (3.26) *via*

$$\frac{\Gamma(1-a)^2}{\Gamma(1-2a)} = \frac{\Gamma(1+b)^2}{\Gamma(1+2b)} = \lambda, \quad (3.29)$$

where $\Gamma(x)$ is the usual Γ -function. Furthermore the theory make the interesting prediction that the exponent γ of the power-law for the α -relaxation time τ , see equation (3.22), is related to a and b by means of the relation

$$\gamma = \frac{1}{2a} + \frac{1}{2b}. \quad (3.30)$$

Hence we see that once the exponent parameter λ is known, the exponents a , b and γ are determined.

Note that according to MCT the β -relaxation is not just the cross-over regime from the microscopic dynamics to the relaxation dynamics at long times, but it is a process *of its own* (that is, however, tightly connected with the α -process). To understand what we mean by this we consider the imaginary part of a dynamical susceptibility which was shown schematically in Figure 4. In the context of that figure we have said that with decreasing temperature the α -relaxation peak moves quickly to the left, whereas the microscopic peak shows only a very weak T -dependence. Thus the existence of a minimum between the two peaks is of course trivial. The non-trivial statement of MCT is that close to the minimum $\chi''(\omega)$ is not just the sum of the low-frequency part of the microscopic peak and the high-frequency part of the α -peak, but that there is an additional intensity, the β -process that is described by the β -correlator occurring in equation (3.24).

Having discussed some of the predictions of MCT for the β -relaxation, we now turn our attention to the α -relaxation, *i.e.* the time window in which the correlators fall below the plateau. In the context of equation (3.22) we have already discussed one important property of this relaxation regime, namely that the relaxation times diverge at the same critical temperature and that also the exponent is the same. A further prediction of the theory is that the time-temperature superposition principle (TTSP), mentioned in Section 2, should hold. This means that at a temperature T the time dependence of a correlator $\Phi(t, T)$ can be written as follows:

$$\Phi(t, T) = \hat{\Phi}(t/\tau(T)), \quad (3.31)$$

where $\hat{\Phi}$ is a master function, and $\tau(T)$ is the usual α -relaxation time. (Note that if the TTSP holds, the precise definition of $\tau(T)$ is irrelevant for Eq. (3.31) to hold.)

As mentioned in Section 2, the shape of the correlators is usually approximated well by the KWW function given in equation (2.3). Although this function is not an *exact* solution of the MCT equations, it has been found that also the numerical solutions of the MCT equations are approximated very well by a KWW function. Hence it can be concluded that MCT is predicting the stretching of the time correlation function.

Before we end this section on MCT it is appropriate to make some comments to what extent this theory is applicable to real glass-forming systems. As mentioned above, the MCT equations are *exact* for certain mean-field models (see articles by Parisi and Cugliandolo in these proceedings [75, 124]). For short range systems the equations will of course only be an approximation and the real question is how good this approximation really is. Unfortunately there is presently no clear answer. There are short range spin glasses, *e.g.* the 10 state Potts model, whose static and dynamic properties are very different from the mean-field prediction, whereas in other spin glasses the mean-field prediction seems to be very reliable [132, 133]. For the case of structural glasses there is a large body of literature in which the applicability of MCT has been investigated for all sort of systems (colloids, gels, molecular glasses, network-forming glasses, polymers, etc.) and it has been found that in general the theory does a remarkably good job in explaining many dynamical features of these systems on a qualitative level, or sometimes even quantitatively (see [92] for a recent review of the experimental literature).

There are, however, also results from experiments or simulations that seem to be at odds with the predictions of the theory. A careful inspection of such findings shows that often either the theory has not been used in an appropriate way (*e.g.* because the authors have not fully understood the theory) or that only the *asymptotic* predictions of the theory have been tested. By “asymptotic predictions” we mean the following: as mentioned above, most predictions of the theory, and in particular the ones presented in this article, hold only very close to the critical point T_c . These predictions are nothing else than the mathematical properties of the solutions of the MCT equations, *i.e.* they are independent of whether or not these equations correctly describe a real system. If the parameter $\sigma = (T - T_c)/T_c$ cannot be considered as small anymore, these properties no longer hold and therefore the properties of the solutions change, and in particular they cannot be cast into simple forms as given, *e.g.*, by equations (3.27) or (3.28). Although even in such a case it is possible to make some analytical predictions [129, 130] that can be tested [134], it is in most cases simpler to make a direct comparison with the numerical solution of the MCT equations. However, this approach is quite involved and therefore not often done. But in principle it is the only systematic procedure if one really wants to find out whether or not the MCT equations give a good description of the relaxation dynamics of a real system.

Apart from the just mentioned problem on the applicability of the MCT equations, there is, however, a much more important one, namely the fact that the MCT equations, as presented here, predict a divergence of the relaxation time at a finite temperature. In Section 2 we have seen that there

is experimental evidence that there does indeed exist a *finite* temperature at which τ diverges, the Vogel temperature T_0 (see Eq. (2.1)), which is close to the Kauzmann temperature T_K in which thermodynamic quantities seem to indicate a transition (see Fig. 6). However, in experiments it is found that the divergence of τ close to T_0 is given by the Vogel-Fulcher law, equation (2.1), and not by a power-law as predicted by MCT. Thus this is evidence that one should probably not identify T_0 with T_c . Furthermore the exact calculations for the mean-field models have shown that these models do indeed have two transitions [121–123, 135, 136]. A *thermodynamic* one at a low temperature T_s and a *dynamic* one at a higher temperature T_D . (This latter transition is due to the fact that at T_D the configuration space splits up into domains that are separated by infinitely high barriers.) If we recall that the MCT equations for these spin models describe the ergodic \rightarrow non-ergodic transition at T_D , we thus are tempted to make the analogy that the Kauzmann temperature of structural glasses corresponds to the temperature T_s in spin glasses and that the T_c corresponds to the temperature T_D . Since real systems are not mean-field, the mentioned barriers that are present in the mean-field models are no longer infinite and hence there is no longer a sharp transition. Instead one can expect that close to T_c the dynamics changes from a *flow-like one*, to one in which a few particles *hop* in a cooperative way over local barriers and recent investigation on the properties of the landscape of supercooled liquids have given evidence that this is indeed the case [137–141]. Hence we come to the conclusion that the sharp transition predicted by MCT at T_c is avoided and that one finds instead only a change of the transport mechanism for the particles. Depending on the system, this change may be very pronounced, such as in colloidal suspension where close to T_c (or in that case close to the critical packing fraction of the particles) the relaxation times become macroscopically large, or only relatively mild, such as in the case of strong glass-forming liquids (silica, B_2O_3 , glycerol) where only a relatively mild change occurs [118, 142, 143].

It is of course a legitimate question to ask whether or not MCT is indeed not able to describe the relaxation dynamics also below T_c . In principle the Mori-Zwanzig formalism allows to obtain also equations of motion for that situation and the “only” thing one has to do is to take into account further slow variables [144, 145]. The result of such a calculation are equations of motion in which the memory function has a somewhat more complicated form, and these equations are usually called “generalized MCT equations” or “MCT-equations including the hopping terms” since they include the ergodicity restoring hopping terms (or at least some of these terms) (see also [146]). However, so far it has not been possible to come up with an *explicit* expression for this memory function, *i.e.* one that does not depend strongly on the approximations that one is forced to make. Therefore only

the qualitative form of this generalized memory function is known and if one wants to use these equations of motion to describe, *e.g.*, real data for $F(q, t)$, quite a few fit parameters are left [147]. Despite this difficulty it is, however, possible to make at least some predictions that should be valid independently of the functional form of the generalized memory function. The most important one is that the sharp transition at T_c no longer exists and that instead there is a cross-over from a power-law dependence above T_c to an weaker T -dependence (*e.g.* Arrhenius) below T_c . Depending on the strength of the “hopping parameters” in the generalized equations, this transition can be very sharp, or very smooth which allows to distinguish between fragile and strong glass formers. Furthermore it can be shown that despite the presence of the hopping processes, the factorization property of the β -relaxation regime still holds, although in a somewhat different form as the one given by equation (3.24) [144, 145]. Thus we see that even if our current ignorance of the exact form of the generalized MCT-equations does not allow to make a quantitative comparison between the prediction of the theory and the real data, certain qualitative checks are still possible. In the past such tests have indeed been made [148, 149] and it has been found that the theory does indeed allow to rationalize some of the dynamical properties of glass forming liquids also at temperatures below T_c .

Thus we can conclude that the theory is able to give a good description of the relaxation dynamics not only above T_c but is also a useful theory in a certain temperature range below T_c . In that sense MCT is a very valuable theoretical contribution that has helped to understand the relaxation dynamics of glass-forming liquids at intermediate temperatures². In this T -range the theory has identified the existence of a cross-over in the transport mechanism of the particles with many interesting and universal features. Nevertheless, to what extent the theory is also able to give a correct description of the relaxation dynamics of atomic liquids at temperatures at which the viscosity is much higher, is presently not really known and the focus of current research.

4 Computer simulations of glass-forming systems

As we have already mentioned in the introduction, computer simulations are one of the important tools to investigate the properties of glass-forming

²Note that in experiments of glass-forming liquids with strong or intermediate fragility it is often found that T_c is 20%–30% above T_g . For the strong glass-former silica there is evidence from simulations and experiments that T_c is even a factor of two higher than T_g [143, 149–151]. In view of these results it is therefore more appropriate to say that the theory works well at temperatures in which the viscosity has values between 10^{-1} Poise and 10^3 Poise.

systems. The goal of this section is therefore to discuss this method in some detail. However, in the following we are not going to give a general introduction to computer simulations since a much more extended coverage can be found in several excellent textbooks [152–157]. Instead we will discuss mainly some of the technical issues of such simulations that are of particular importance for glass-forming systems. But even with this restriction the field is still too vast to give a comprehensive review and therefore we will leave out almost completely important topics like the simulation of spin glasses etc. and focus instead on structural glasses.

Roughly speaking there are two broad classes of simulations: *molecular dynamics simulations* and *Monte-Carlo simulations*, and in the following we will discuss these two methods in somewhat more detail.

In a molecular dynamics (MD) simulation one tries to solve Newton's equations of motion for the system of interest and thus to obtain the trajectory of the particles in configuration space. From these trajectories many properties of the system can be directly calculated, at least in principle. The problem with MD is that the known numerical methods to solve these equations work only reliably for a time scale that is significantly smaller ($O(10^{-2})$) than the shortest typical time scale of the system, which in a liquid is given by the local motion of the particles and hence is on the order of 0.1 ps. One well known example for such an algorithm is due to Verlet and is given by:

$$\mathbf{r}_i(t+h) = \mathbf{r}_i(t) + h\mathbf{v}_i(t) + \frac{h^2}{2}\mathbf{F}_i(t) \quad (4.1)$$

$$\mathbf{v}_i(t+h) = \mathbf{v}_i(t) + \frac{h}{2}[\mathbf{F}_i(t) + \mathbf{F}_i(t+h)]. \quad (4.2)$$

Here $\mathbf{r}_i(t)$ and $\mathbf{v}_i(t)$ are the position and velocity of particle i at time t , \mathbf{F}_i is the force acting on this particle, and h is the time step which for typical liquids has to be on the order of 1 fs. In Section 2 we have seen that upon cooling the relaxation time of a glass-forming liquid increases by 12–15 decades in time. Thus if one wants to investigate this slowing down by means of a simulation it would be necessary to propagate the system by means of equation (4.2) by the same number of decades, which is currently completely impossible even for systems that are as small as 100 particles. The best one can presently do is to simulate a system with $O(1000)$ particles for $O(10^9)$ time steps, but most present day simulations cover less than 10^7 time steps since usually one has to do many independent runs to improve the statistics, to investigate different temperatures, to average (in spin glasses) over different realizations of disorder, etc., all of which together usually takes many years of single processor CPU time. Hence we recognize that one of the major problems in the simulation of glass-forming systems is the huge

time range that should be covered. Note, however, that the propagation of the system in its configuration space is so slow because the dynamics of the particles is *realistic*. Hence this type of simulations allows to calculate directly dynamical properties for the system, such as the diffusion constant, the velocity of sound, the vibrational density of states, and more. This is the main reason why MD is, despite the mentioned drawback, a very popular method to study glass-forming systems.

In a Monte Carlo simulation this drawback does, at least in principle, no longer exist. Since in this method the only rule that has to be obeyed is the one of detailed balance, *i.e.* the fact that $w(s \rightarrow s')$, the transition probabilities for the propagation of the system from an arbitrary state s to another arbitrary state s' , fulfill the relation $w(s \rightarrow s')/w(s' \rightarrow s) = \exp(-\beta[H(s') - H(s)])$, where $\beta = 1/k_B T$ and $H(s)$ is the value of the Hamiltonian at state s , a clever choice of the function $w(s \rightarrow s')$ will allow to equilibrate the system also at low temperatures. Unfortunately this is true only in principle. So far it has not been possible to find a updating scheme that allows to equilibrate an arbitrary off lattice system also at low temperatures. For certain special cases we do, however, have algorithms that allow to do this, *e.g.* systems of hard disks or binary mixtures of particles with very similar radii [158, 159]. For other models it is possible to come up with algorithms that allow at least to probe the system (in equilibrium!) at relatively low temperatures, such as, *e.g.* the parallel tempering method [160–167]. Despite this progress one is still quite far away from the ultimate goal: to have a robust algorithm that is able to equilibrate a large class of glass-forming systems (having a substantial number of particles) also at very low temperatures.

Since so far it is not possible to simulate reasonably sized systems over very large time, and since we have seen that with decreasing temperature the relaxation times of glass-forming systems increase rapidly, it is presently difficult to use computer simulations to investigate the *equilibrium* properties of such systems at low T . What does “low” mean? As mentioned above, the length of a typical run is presently around 10^7 time steps. With a step size h of a few fs, this gives a total length of 10–50 ns which corresponds to about 10^2 Poise. Using Figure 2 we thus recognize that present day simulations are just barely able to see the upturn in the $\eta(T)$ curves seen experimentally in fragile liquids.

Of course one might be tempted to circumvent this problem by making a relatively rapid quench to low temperatures, “anneal” the system for some time, and then to start to measure the properties of the system (structure, diffusion constant, relaxation dynamics, etc.). Although such an approach sounds quite reasonable, a systematic investigation of such a protocol shows that the so obtained results have very little to do with the ones of the system

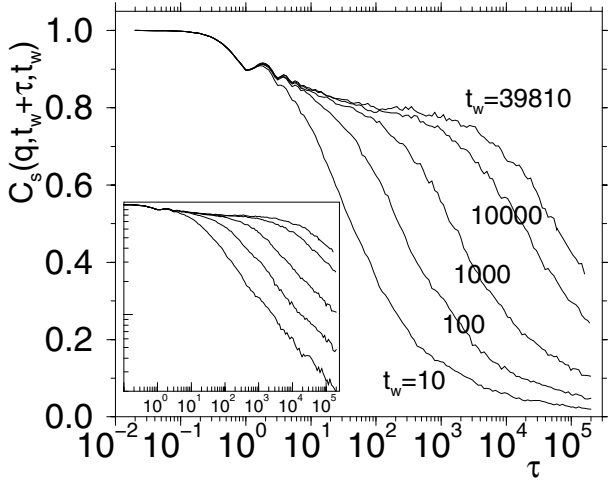


Fig. 9. Main figure: time dependence of the correlation function $C_s(q, t_w + \tau, t_w)$ defined in equation (4.4) for a binary Lennard-Jones mixture that has been quenched from a temperature $T_i = 5.0$ to a temperature $T_f = 0.4$. The different curves correspond to the stated waiting times t_w . Inset: the same data in a log-log plot showing that at long times the correlator shows a power-law dependence on time. Adapted from [168].

in *true* equilibrium and therefore should not be done. To demonstrate this one can, *e.g.*, investigate the time-dependence of the intermediate scattering function $F_s(q, t)$ (see Eq. (3.14)) after such a quench. In *equilibrium* $F_s(q, t)$ depends only on the time difference t , *i.e.*

$$F_s(q, t) = \langle \rho_s(\mathbf{q}, t) \rho_s^*(\mathbf{q}, 0) \rangle = \langle \rho_s(\mathbf{q}, t + \tau) \rho_s^*(\mathbf{q}, \tau) \rangle. \quad (4.3)$$

In the out-of-equilibrium case the second equality does no longer hold and therefore it is necessary to keep track of both time arguments t and τ , *e.g.*, we have to generalize $F_s(q, t)$ to the function

$$C_s(q, t_w + \tau, t_w) = \langle \rho_s^*(\mathbf{q}, t_w + \tau) \rho_s(\mathbf{q}, t_w) \rangle, \quad (4.4)$$

where t_w is the so-called “waiting time”, *i.e.* the time span between the start of the measurement and the time at which the system has been driven out of equilibrium. In Figure 9 we show the time dependence of a $C_s(q, t_w + \tau, t_w)$ for a binary Lennard-Jones system that at time zero has been quenched from a relatively high temperature to a low temperature [168]. The different curves correspond to different waiting times t_w . We see that, in contrast of the situation in equilibrium, the relaxation dynamics of the system depends strongly on the waiting time in that the dynamics slows down for

increasing t_w . One thus says that the system is “aging”. Although the existence of this phenomenon has been known since quite some time [73], it is only in recent years that attempts have been made to describe it by means of statistical mechanics concepts [75, 80–82, 169–176]. Note that the figure shows not only that the typical time scale for the decay of the correlation function depends on t_w , but also that the shape of the function has changed, since (see inset) it is compatible with a power-law whereas in equilibrium it can be approximated well by a KWW-function (see Sect. 2). Hence we conclude that for the investigation of the *equilibrium* dynamics of a slowly relaxing system it is most important to check carefully that one has indeed reached equilibrium. Note that experience has shown that time correlation functions are much more sensitive to out-of-equilibrium effects than static quantities. This can be understood by recalling that most static quantities show only a very weak T -dependence, whereas dynamical observables show a very strong one (see Sect. 2). Therefore in most cases it is not advisable to monitor just quantities like the energy, pressure etc. in order to check whether or not a system has reached equilibrium. Much more useful are the time correlation functions like the one defined in equation (4.4) or the function that is the analogous generalization of the mean-squared displacement.

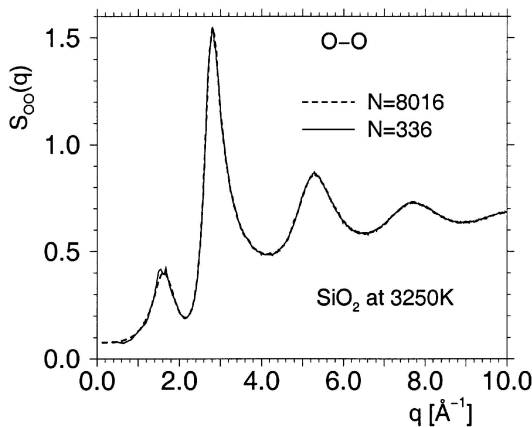


Fig. 10. Partial structure factor for the O-O correlation in amorphous SiO_2 at the density 2.36 g/cm^3 . The two curves correspond to two system sizes (box size 16.8 \AA and 48.37 \AA). It is clear that within the accuracy of the data no difference is seen.

For the case of second order phase transitions it is well known that the static as well as dynamic properties of the systems depend strongly on the size of the system [28, 157]. For the case of structural glasses such

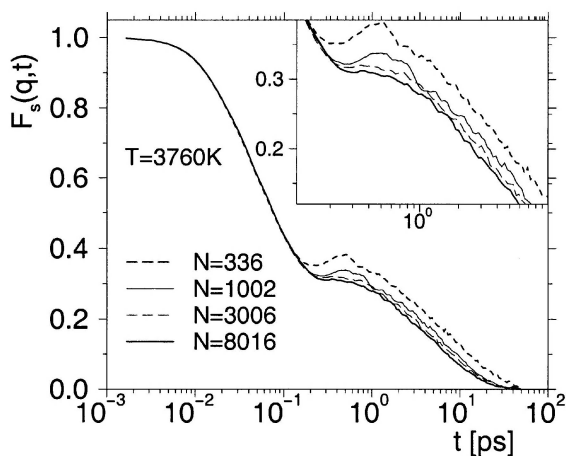


Fig. 11. Time dependence of the intermediate scattering function of SiO_2 at 3760 K. The curves correspond to different system sizes and they demonstrate that the relaxation dynamics in small systems is slower than the one in large systems. Inset: enlargement of the region close to the plateau.

dependencies are much less pronounced, although they are present. In Figure 10 we show the partial static structure factor for the O-O correlation in SiO_2 [177]. The solid and dashed curves correspond to the system sizes $N = 336$ and $N = 8016$ atoms and we see that within the accuracy of our data there is no difference between the two data sets. However, in other cases one does indeed find differences in structural properties, *e.g.* in the distribution of the angles between three neighboring particles in systems like Al-Ca-Si-O, if the system size is below a few hundred atoms [178]. Much more sensitive to system size is the relaxation dynamics. In Figure 11 we plot the intermediate scattering function for the system sizes shown in the previous figure. From this graph we recognize that the relaxation dynamics for the small system is significantly slower than the one for the larger system and that also the shape of the curves close to the plateau are not the same [179]. It has been shown that with decreasing system size and decreasing temperature this difference in the dynamics can become very pronounced in that for $N = 100$ atoms the system takes orders of magnitude longer to relax than the relaxation time for large systems [179–181]. Although the reason for this strong dependence is not understood very well it is likely related to the fact that in small systems the connectivity of the accessible configuration space is effectively smaller than in larger systems, since in the latter fluctuations in density etc. can be present that are

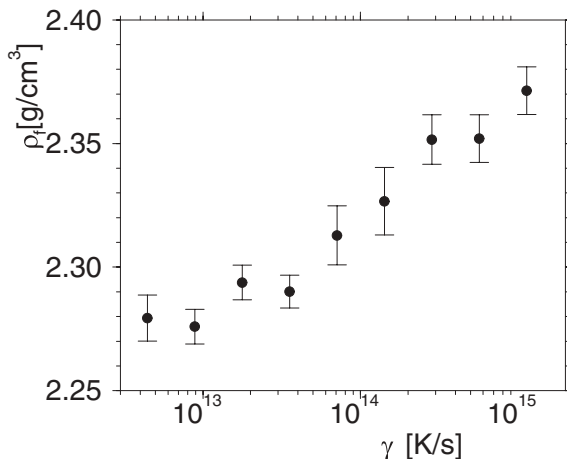


Fig. 12. Density of SiO_2 at $T = 0$ and zero pressure as a function of the cooling rate with which the glass has been produced.

strongly suppressed in the former. Note that exactly the opposite is the case for the case of spin glasses: there one finds that the smaller systems relax faster than the large ones, at least if the interaction range is not too short ranged [182–185].

As already discussed in Section 2, the glass transition is basically just a kinetic phenomenon since it occurs at that temperature at which the typical relaxation time of the system becomes comparable with the time scale of the experiment (such as the inverse of the cooling rate). This effect should not be forgotten if one uses simulations to investigate the properties of glasses, since these will in general depend quite substantially on the cooling rate. As an example we show in Figure 12 how in the case of SiO_2 the density at low temperatures depends on the cooling rate γ [71]. (Note that these quenches have been done at constant pressure.) From the figure we recognize that ρ_f does indeed depend significantly on γ and that it is far from obvious how this function should be extrapolated to the cooling rates that are typically used in a real experiment (10 K/s). The density is a quantity whose γ -dependence is relatively benign since it averages over the whole microscopic structure. More microscopic structural quantities, such as the structure factor, local coordination numbers, etc., show a even more pronounced γ -dependence [71]. Since in general it is not known how the dependence of such quantities on γ has to be extrapolated to experimental cooling rates, a comparison with experimental data becomes difficult or even impossible. (But of course many people sweep all these methodological

difficulties under the rug and go on to compare happily their results with experimental data.)

Above we have commented on the observation that structural properties of glasses are relatively insensitive to finite size effects once the system is larger than a few hundred particles. There are, however, situations where substantially larger systems are necessary. *E.g.* in recent years a significant experimental and theoretical effort has been made to understand the nature of the boson peak, mentioned in Section 2 (see Fig. 3) [43–57]. Since this peak is an excess in $g(\nu)$, the vibrational density of states, over the Debye-level, $g(\nu) \propto \nu^2$, it is reasonable to plot the density of state divided by ν^2 in order to see whether or not an excess is seen. Note that in a simulation $g(\nu)$ can be calculated from the eigenvalues of the dynamical matrix or by the time Fourier transform of the velocity-auto-correlation function [186]. In Figure 13 we show $g(\nu)/\nu^2$ as a function of the frequency ν and we do indeed see a peak at around $\nu \approx 1.5$ THz [187]. However, the plot also makes very clear that the location as well as the height of the peak depends on the size of the simulation box as well as on the cooling rate with which the glass has been produced. Also note that for a sufficiently large system $g(\nu)/\nu^2$ should show at small frequencies a plateau, the Debye-limit. The graph demonstrates however, that even a system with more than 8000 ions is not sufficiently large to show this Debye-law. Hence great care has to be taken if one starts to analyse the modes and the mechanisms that give rise to the observed peak, since it might very well be that one analyses modes that in a realistically large system are irrelevant.

Before we end this section we briefly make some general comments on the systems one simulates. Roughly speaking one can distinguish two types of simulations: in the first type one tries to obtain some general understanding of the properties of glass-forming systems that subsequently can be used to check theoretical concepts or theories (properties of the energy landscape, applicability of MCT, search for diverging length scales, etc.). In such simulations one does not really care whether or not the simulated system exists also in reality, as long as the model does not have any pathological features. Therefore one often uses very simple models such as lattice gases, Lennard-Jones fluids, spin systems on a lattice, etc. This is in contrast to the situation in which one uses a simulation to understand a particular feature of a given material. In that case it is necessary to consider models that are much more realistic since otherwise the feature of interest might even be completely absent in the simulation (*e.g.* it is not possible to study the process responsible for the light scattering mechanism by using a simple Lennard-Jones model since there are no polarization effects). The extreme limit of such a realistic calculation would of course be to solve the Schrödinger equation for the many-body problem, but of course it is clear

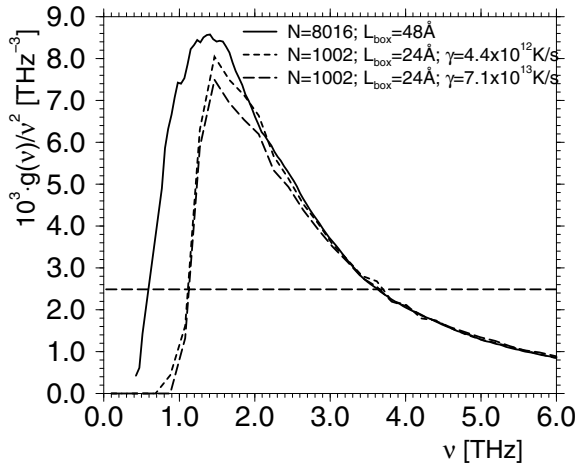


Fig. 13. Density of state of amorphous silica divided by ν^2 for two different system sizes and two different cooling rates.

that this is computationally not possible. The best thing one presently can do is to make a so-called *ab initio* calculation in which the particles obey Newton's equation of motion with a force field that is calculated directly from the wave-function of the system [188,189]. Such calculations are presently feasible for systems of $O(100)$ particles and time scales of 10 ps. As we have seen above, these sizes and time scales are for most cases insufficient and therefore one makes often the further approximation to use *effective* force field that are just the sum of a pairwise interaction potential between the particles. (Sometimes one takes into account also three-body interactions.) These potentials will depend on certain parameters (particle size, effective charges, etc.) that are obtained by fitting the potential to the results from *ab initio* calculations or to experimental data. Although the so obtained potentials might in some cases be surprisingly accurate, they are an approximation and thus it might happen that an effective potential that is reliable for one quantity, is not very realistic for another one [190]. Therefore it is very advisable to check critically to what extend the results that are predicted by a simulation with an effective potential depend on this potential. An instructive example for this can be found in [191], reproduced as Figure 1 in [192], where the authors compare the temperature dependence of the diffusion constant for different potential of SiO_2 . They found that although the structural properties of the various models are quite similar, the relaxation dynamics differs by orders of magnitude! Thus this clearly shows that it is not easy to use simulations to predict the reality.

5 The relaxation dynamics of glass-forming liquids as investigated by computer simulations

In the previous sections we have described some of the properties of glass-forming liquids. In the following we will present the results of computer simulations that have been used to investigate these properties as well as to test to what extent the mode-coupling theory of the glass transition is able to describe the relaxation dynamics of these systems. In particular we will discuss two types of systems: a binary Lennard-Jones mixture (BLJM) and silica (SiO_2). As we will see, these two systems have very different structural and dynamical properties and therefore it is of interest to see which dynamical features are nevertheless common and can be rationalized by the theory.

Although in this section we will mainly discuss the simulations of the BLJM system and silica, there is a multitude of results for other glass-forming systems, such as hard spheres, soft sphere systems, water, etc. [193–242]. It is found that many of the properties of these latter systems are qualitatively similar to either the BLJM system or to silica. Thus from this point of view we do indeed discuss the salient features of glass-forming liquids and not only the properties of two particular systems.

5.1 Static and dynamic properties of a simple liquid with Newtonian dynamics

In this section we will discuss the properties of a simple liquid in its normal and supercooled state. (Note that “simple liquid” means that the interactions are short ranged and pairwise additive [33].) Normally one-component simple liquids are not good glass-formers, since they crystallize rapidly even if they are supercooled only modestly. Therefore one usually considers binary systems since the additional disorder introduced by the different species is sufficient to prevent that the system crystallizes, at least on the time scale of present days computer simulations ($O(10^8)$ time steps). One system that seems to have very good glass-forming properties is a binary mixture of Lennard-Jones particles with interactions that were chosen to mimic the system $\text{Ni}_{80}\text{P}_{20}$ [243]. In the BLJM model we have a 80:20 mixture of particles, which in the following we will call A and B particles, that interact *via* the potential

$$V_{\alpha\beta}(r) = 4\epsilon_{\alpha\beta}[(\sigma_{\alpha\beta}/r)^{12} - (\sigma_{\alpha\beta}/r)^6] \quad \text{with} \quad \alpha, \beta \in \{\text{A}, \text{B}\}. \quad (5.1)$$

The parameters of the potential are given by $\sigma_{\text{AA}} = 1.0$, $\epsilon_{\text{AB}} = 1.5$, $\sigma_{\text{AB}} = 0.8$, $\epsilon_{\text{BB}} = 0.5$, and $\sigma_{\text{BB}} = 0.88$. Hence we use σ_{AA} and ϵ_{AA} as the unit of length and energy, respectively (setting the Boltzmann constant $k_{\text{B}} = 1$). Time will be measured in units of $(m\sigma_{\text{AA}}^2/48\epsilon_{\text{AA}})^{1/2}$, where m is the mass of the particles. The number of particles used was 1000 and the cubic

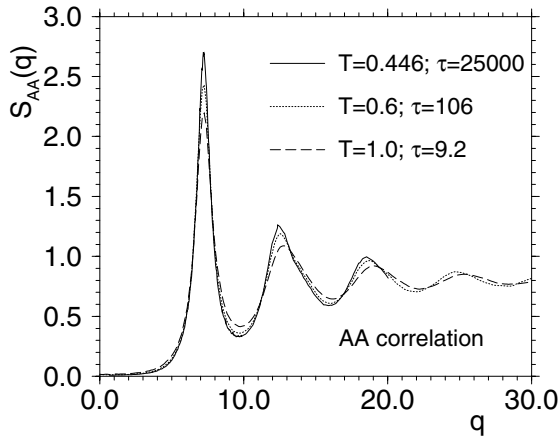


Fig. 14. Wave-vector dependence of the partial structure factor $S_{AA}(q)$ for a mixture of Lennard-Jones particles. The different curves correspond to different temperatures. Also included are the α -relaxation times τ .

simulation box had the size $(9.4)^3$. The equations of motion were integrated by means of the velocity-Verlet algorithm (Eqs. (4.1) and (4.2)) using a time step of 0.01 and 0.02 at high ($T \geq 1.0$) and low temperatures ($T < 1.0$), respectively.

In Figure 14 we show the wave-vector dependence of the static structure factor for the A particles at three different values of T [244]. (Note that in a binary system there are three partial structure factors [33].) From this graph we recognize that in the T -range considered, the structure does not change significantly. The only effect seen is that a decrease of T gives rise to peaks and minima that are more pronounced. (If the simulation would have been done at constant pressure, also the location of the peaks would show a weak T -dependence since the system expands or contracts if the temperature is changed.) Since also the two other partial structure factors do not show a more pronounced T -dependence, we conclude that this quantity is indeed rather insensitive to a change in temperature, in agreement with the comments on this in Section 2.

Although the structural and thermodynamic properties of the system show only a very mild T -dependence, the dynamic properties show a very strong one. To demonstrate this we have included in the figure also the α -relaxation time $\tau(T)$ at the three different temperatures (see below for the precise definition of $\tau(T)$). We see that in the temperature range considered this time increases by a factor of more than 10^3 , showing that the

dynamic properties of the system do indeed change much faster than the structural ones.

The relaxation time τ characterizes the dynamics only on the time scale of the α -relaxation, *i.e.* on the longest time scale of the system. In order to understand the relaxation dynamics also on the other time scales it is useful to consider time correlation functions. One important example for such a correlation function is the mean-squared displacement (MSD) of a tagged particle which is defined by

$$\langle r^2(t) \rangle = \frac{1}{N_\alpha} \sum_{i=1}^{N_\alpha} \langle |\mathbf{r}_i(t) - \mathbf{r}_i(0)|^2 \rangle. \quad (5.2)$$

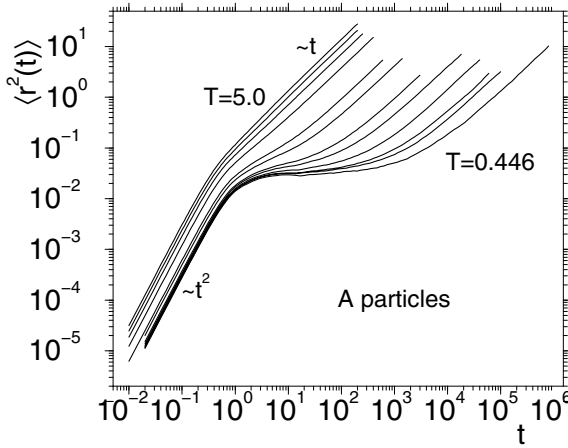


Fig. 15. Time dependence of the mean-squared displacement of the A particles for BLJM system. The curves correspond to different temperatures that are given by $T = 5.0, 4.0, 3.0, 2.0, 1.0, 0.8, 0.6, 0.55, 0.50, 0.475, 0.466$ (from left to right).

In Figure 15 we show the time dependence of $\langle r^2(t) \rangle$ for the A particles for different temperatures. Let us start the discussion of the data with the curves for high T . For short times we see that $\langle r^2(t) \rangle \propto t^2$, since we are in the ballistic regime mentioned in Section 2. Once $\langle r^2(t) \rangle$ is of the order 0.04, *i.e.* the distance is around 0.2, the time dependence changes over to a power-law with exponent 1.0, *i.e.* the system is diffusive. This change in the t -dependence is due to the collisions of the tagged particles with its neighbors that surround it at $t = 0$. Despite the presence of these neighbors the particle is still able to move away quickly from its initial position, *i.e.* $\langle r^2(t) \rangle$ increases quickly with time.

Also for low temperatures we see at early times a ballistic behavior. In contrast to the curves for high T , the mean squared displacement does at the end of this regime not cross over to the diffusive regime, but instead shows a plateau at intermediate times. This plateau is due to the cage effect mentioned in Section 2, *i.e.* the temporary trapping of the particle by its neighbors. Only for sufficiently long times the particle is able to leave this cage and once it has done so the MSD quickly crosses over to a t -dependence that corresponds to a diffusive motion. Note that the height of the plateau is around 0.03, from which it follows that the size of the cage is around 0.17, *i.e.* it is relatively small compared to the typical nearest neighbor distance which is around 1.0 [245].

The mean squared displacement gives the typical *average* distance that a tagged particles moves within a time t . It is of course also of interest to investigate the distribution of these distances. This can be done by means of the self part of the van Hove function which is defined as [33, 34]:

$$G_s^\alpha(r, t) = \frac{1}{N_\alpha} \sum_{i=1}^{N_\alpha} \langle \delta(r - |\mathbf{r}_i(t) - \mathbf{r}_i(0)|) \rangle. \quad (5.3)$$

Thus we see that $G_s^\alpha(r, t)$ is the probability that a particle of type α has moved within the time t exactly a distance r and that $\langle r^2(t) \rangle$ is just the second moment of this distribution. Furthermore we recognize that $G_s^\alpha(r, t)$ is nothing else than the space Fourier transform of the incoherent intermediate scattering function defined in equation (3.14). In Figure 16 we show $4\pi r^2 G_s^A(r, t)$ for different values of t . (The reason to plot $4\pi r^2 G_s^A(r, t)$ in-

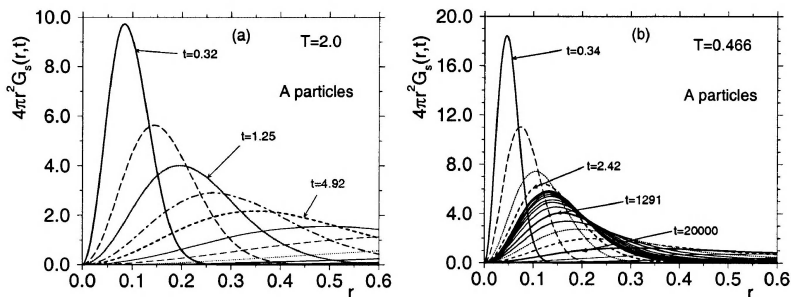


Fig. 16. r -dependence of the van Hove function for the A particles in the BLJM at a high and low temperature (panel **a**) and **b**), respectively). The curves correspond to times $t = 0.32 \times 2^n$, $n = 1, \dots$

stead of $G_s^A(r, t)$ is that it is the former that is measured in the simulation and that will enter most theoretical formula, since the system is isotropic.)

From the graph that corresponds to high T we see that at short times the van Hove function is a single peak that moves quickly to the right (its location moves $\propto t^2$). It is found that this peak is just a Gaussian distribution multiplied with $4\pi r^2$. Also for times that are longer than the duration of the ballistic regime, the curve is a Gaussian. Only now the location of the peak moves proportional to t , since the dynamics of the particles is diffusive.

For low temperatures and short times the dependence of $G_s^A(r, t)$ on t and r is similar to the one at high T . Also at very long times the function is again given by a Gaussian. For *intermediate* times we see however a very different behavior in that the curves for the lower temperature hardly depends on time. Thus we see here directly the cage effect mentioned earlier, *i.e.* that the particles are trapped by their neighbors. Note, however, that the curves still do depend on time somewhat (although only weakly). A closer inspection of the data shows that in this time window the *shape* of the curves does *not* change and that their time dependence can be written as [245]

$$G_s^\alpha(r, t) = G_s^{c,\alpha}(r) + H_\alpha(r)G(t), \quad (5.4)$$

which is nothing else than a special case of the factorization property shown in equation (3.24). Thus this is a first example that MCT is able to rationalize a non-trivial behavior for this system. Similar results have been found for the distinct part of the van Hove function [245], *i.e.* the space-time correlation function in which the second index i in equation (5.3) is replaced by another summation index j [33, 34].

The van Hove correlation function is a correlator that is very useful to understand the dynamics of the particles in *real* space. However, all scattering experiments are done in *reciprocal* space and hence it is useful to investigate also how the intermediate scattering functions, introduced in equations (3.13) and (3.14), depend on temperature, time and wave-vector. In Figure 17 we show the t -dependence of $F_s(q, t)$ for the A particles [246]. In agreement with the schematic drawing of Figure 3 we see that at high temperature the correlator decays quickly to zero and a closer inspection of the data shows that this decay is very close to the expected exponential. At low temperature we see the two-step relaxation discussed in the context of Figure 3. From this figure one clearly sees how strongly the relaxation dynamics depends on temperature. Note that the curves do *not* show a dip at intermediate times that in Figure 3 was associated with the boson-peak. The reason for this difference is that liquids that have a structure in which the particles are very closed packed do normally not have a boson-peak. Instead it is a very prominent feature in systems whose structure is given by an open network, such as, *e.g.*, silica. Finally we remark that the T - and t -dependence of $F_s(q, t)$ of the B particles as well as the one of the

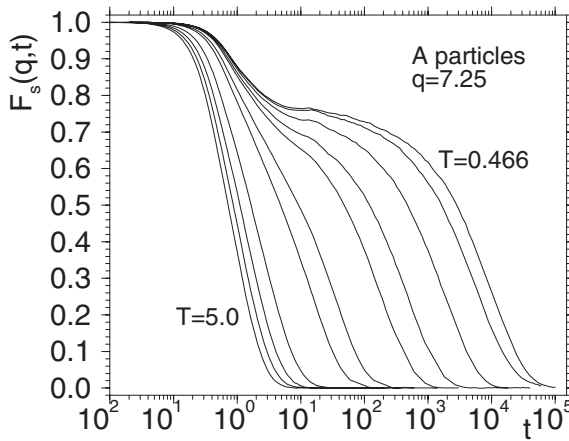


Fig. 17. Time dependence of the incoherent intermediate scattering function for different temperatures. The wave-vector corresponds to the location of the main peak in the static structure factor.

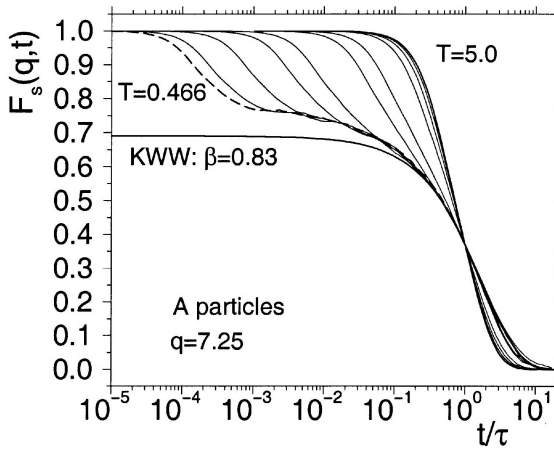


Fig. 18. Incoherent intermediate scattering function as a function of rescaled time $t/\tau(T)$ for the same correlators shown in Figure 17. Also included is a fit to the curve at the lowest T at long times with the KWW function from equation (2.3).

coherent function $F(q, t)$ look qualitatively similar to the curves shown in Figure 17 [246].

Using the time correlation functions just discussed, we can test a further prediction of MCT, the validity of the time-temperature superposition

principle (see Eq. (3.31)). For this we can define an α -relaxation time $\tau(T)$ by requiring that $F_s(q, \tau(T)) = e^{-1}$. In Figure 18 we show the correlators for the different temperatures as a function of $t/\tau(T)$. We see that we have basically two temperature regimes. At high temperatures the curves fall at long times quite well onto a master curve that is described well by an exponential. The curves at low T also fall on top of each other, but this time the master curve is a stretched exponential which is included in the figure as well. (Note that the curve for $T = 0.466$ (dashed curve) coincides so well with the KWW-function that the former cannot be seen anymore at long rescaled times.) Similar master curves are found for other correlation functions and hence we conclude that the prediction of MCT regarding the validity of the TTSP holds for the present system. We also mention that the stretching exponent β is relatively large ($\beta = 0.83$). Its value does, however, depend on the correlator considered (different wave-vector or species) and for the present system values as small as 0.5 have been found [246].

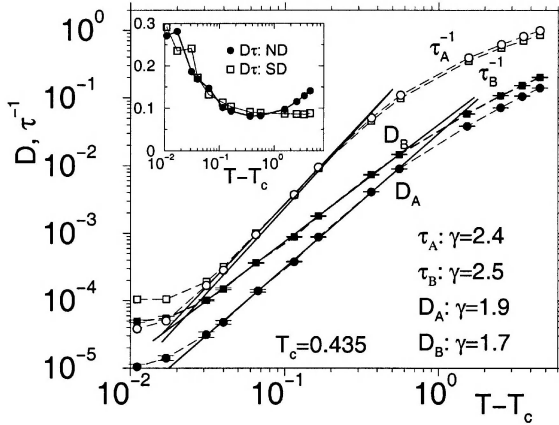


Fig. 19. Main figure: tagged particle diffusion constant D and α -relaxation time τ as a function of $T - T_c$ for the BLJM system (curves with symbols). The straight lines are fits to the data with the power-law given by equation (3.23) and γ is the exponent resulting from these fits. The inset shows the product $D\tau$ vs. $T - T_c$ for the ND (filled symbols) and the SD discussed in Section 5.2 (open symbols).

From the mean-squared displacement one obtains immediately the diffusion constant D via the Einstein relation $D = \lim_{t \rightarrow \infty} \langle r^2(t) \rangle / 6t$. From the intermediate scattering function we have determined the α -relaxation time $\tau(T)$. Thus we now can check whether the T -dependence of D and τ is indeed given by the power-law predicted by MCT (see Eq. (3.23)). That this is in fact the case is demonstrated in Figure 19 which is a log-log plot

of D and τ^{-1} vs. $T - T_c$. We see that at low, but not too low, temperatures the data does indeed fall on a straight line, *i.e.* that we have a power-law dependence. Note that we have fixed the value of T_c for all four data sets to $T_c = 0.435$, which shows that such a power-law can be seen using the *same* critical temperature, as predicted by the theory. We also note that the values of the exponents γ for the two relaxation times are very close to each other (according to MCT they should be the same) but that they differ from the one for the diffusion constant. According to equation (3.23) the product $D(T)\tau(T)$ should be a constant if one is close to T_c . In the inset of Figure 19 we show this product (filled circles) and we recognize that it does depend on T , but that this dependence is rather mild compared to the one of D or τ . (We also note that if this product is calculated for the stochastic dynamics discussed in Sect. 5.2, it is basically independent of T for high and intermediate temperatures, but shows at low T the same T -dependence as the curve for the ND, see the open symbols in the inset.) The reason for this residual T -dependence is twofold: first of all the result given by equation (3.23) holds only very close to T_c . A recent theoretical MCT calculation for a binary system has shown that if one is not extremely close to T_c the product is indeed not constant and it is likely that one reads off from the $D(T)$ and $\tau(T)$ data only an effective exponent [247]. The second reason is that very close to T_c it cannot be expected that the predictions of MCT are valid, since the hopping processes mentioned at the end of Sect. 3 will become important and modify the result given by equation (3.23). That such hopping processes are probably present at the two lowest temperatures can be seen in Figure 19 in that the data points do no longer fall on the straight line for the power-law.

Finally one wonders of course which one of the exponents γ is the correct one. Although there is unfortunately no simple answer to this question the advisable procedure to determine T_c and γ (and hence the other exponents a and b) is as follows: the exponents γ can be determined from the T -dependence of the relaxation times of various correlators as well as from the one of the diffusion constant(s). The exponents a and b (or more general the exponent parameter λ given in Eqs. (3.26) or (3.29)) can be obtained from fitting various time correlation functions (at different temperatures) in the β -regime with the β -correlator. Since all these parameters are connected in a one-to-one way to each other, one has to optimize all these fits in a global way. This approach usually allows to obtain reliable values for λ and T_c . For the present BLJM system it is found that the exponent γ should indeed be close to 2.4, *i.e.* that the values of γ as determined from D are not reliable [134, 246, 248, 249]. The reason why D is more likely of not giving the correct exponent are the mentioned hopping processes: it is sufficient that a few percent of the particles hop (leave their cage) to increase the

MSD considerably, *i.e.* these rare events can change the value of D substantially, whereas these type of events affect the average relaxation time only weakly. Hence it must be expected that very close to T_c the diffusion constant is dominated by these hopping processes that are not taken into account by the ideal version of the theory and that therefore the expected T -dependence is modified.

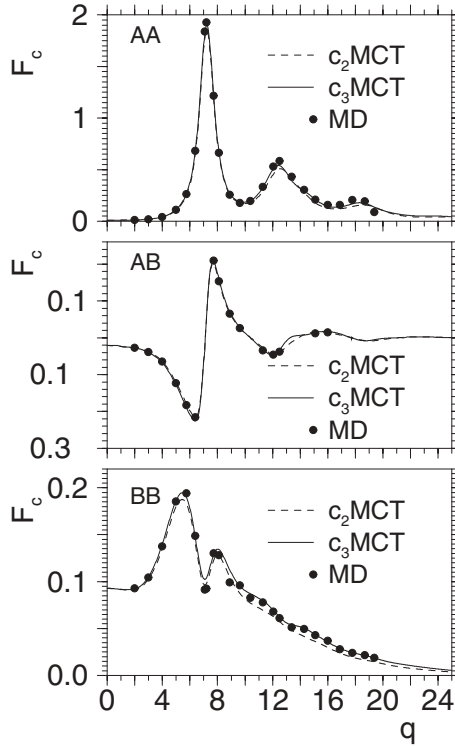


Fig. 20. Wave-vector dependence of the non-ergodicity parameter for the BLJM system. The dots are the results from the simulations and the dashed and solid lines are the predictions of MCT neglecting and including the c_3 -terms, respectively (see text for details).

All the results that we have discussed so far concern only *qualitative* tests of MCT. However, in Section 3 we have mentioned that in principle it is possible to use the theory also to do a full microscopic calculation of the relaxation dynamics, if the static quantities, such as the structure factor, are known. In the following we will show that such a calculation is indeed possible, at least for the present BLJM system.

From the simulations described above, it is also possible to obtain the wave-vector dependence of the three partial structure factors with high accuracy, *i.e.* to within 1%. From these $S_{\alpha\beta}(q)$ one can obtain the direct correlation functions, $c_{\alpha\beta}(q)$, which in turn can be used as input to calculate the vertices $V^{(2)}$ and hence the memory function (see Eqs. (3.17) and (3.18)). Hence this allows to obtain the prediction by MCT for the q and t -dependence of the intermediate scattering function that can be compared directly with the results of the simulation.

One quantity of interest for such a comparison is the non-ergodicity parameter introduced in equation (3.24), *i.e.* the height of the plateau in the β -regime. (If the correlator considered is the coherent or incoherent intermediate scattering function, this height is also known as the Debye-Waller and Lamb-Mössbauer-factor, respectively.) In Figure 20 we show the q -dependence of the non-ergodicity parameters for the three partial coherent intermediate scattering functions. The symbols are the results from the simulations [249] and the solid and dashed lines are the predictions of MCT. The dashed line corresponds to the version of the theory in which the vertices $V^{(2)}$ in equation (3.24) depend only on the structure factor, *i.e.* the contribution to $V^{(2)}$ from the three-particle correlations c_3 are neglected, whereas the solid line corresponds to the case where c_3 has been taken into account [104, 248]. (Note that the function $c_3(\mathbf{q}, \mathbf{k})$ has been determined also directly from the simulation.) From Figure 20 we recognize that these two versions of the theory give basically the same prediction for the q -dependence of the non-ergodicity parameters and hence we can conclude that for this system the effect of c_3 is very small, in agreement with the results for a system of soft spheres [250].

From the figure we also recognize that the agreement between the theoretical curve from the c_3 -MCT and the data from the simulation is excellent in that also small details are reproduced very well. We emphasize that *no* fit parameter of any kind has been used to calculate these theoretical curves. Hence we conclude that the theory is indeed able to predict highly non-trivial quantities of the relaxation dynamics with very good accuracy.

Apart from the q -dependence of the non-ergodicity parameters it is also quite simple to calculate the value of the critical exponent γ , which the theory predicts to be 2.34 [248], in very good agreement with the values 2.4–2.5 found from the simulations. Also the q -dependence of the amplitudes h occurring in equation (3.24) for the coherent and incoherent scattering function is predicted reliably. The only quantity for which a significant discrepancy between theoretical prediction and simulation is found is the critical temperature T_c for which MCT predicts a value of 0.92 whereas the value from the simulation is 0.435 [248]. Why there is such a large difference and even more puzzling why despite this large difference all the other

predictions of the theory are so accurate, is presently not well understood. It has to be mentioned, however, that this observation does not only hold for the present BLJM system but has also been found for the case of hard spheres and of soft spheres [92, 250, 251].

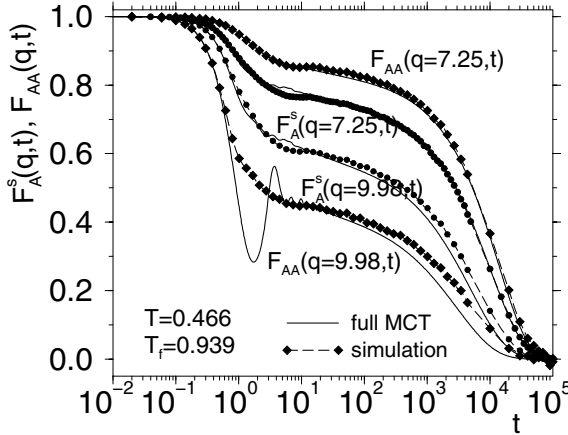


Fig. 21. Time dependence of the coherent and incoherent intermediate scattering function for the A particles. The symbols are the results of the simulation and the solid lines the prediction of MCT. The two wave-vectors correspond to the location of the first maximum and minimum in the static structure factor.

The quantitative tests of the MCT that we have presented so far concerned the dynamics on intermediate and long times, *i.e.* the time scale of the β - and α -relaxation. As we have already mentioned in Section 3, this dynamics is predicted to be independent of the microscopic dynamics (and below we will give evidence that this is indeed the case). However, if one wants to use the theory to predict the full time dependence of the correlation functions it is necessary to have also a good theory for the relaxation dynamics at *short* times, *i.e.* to know the memory function M^{reg} in equation (3.15). As already mentioned in Section 3 such a theory does presently not yet exist and therefore one has to content oneself with a phenomenological Ansatz for M^{reg} . One model that has been found to work well is given by

$$M^{\text{reg}} = \alpha(q) / \cosh(\beta(q)t), \quad (5.5)$$

where $\alpha(q)$ and $\beta(q)$ are constants that can be determined directly from sum rules over static quantities [33, 99, 100, 252]. Using this functional form of M^{reg} , the time and q -dependence of the solution of the MCT equations can be obtained numerically. The temperature dependence of these solutions enters only *via* the T -dependence of the static structure factor

and trivial kinetic factors. However, as we have mentioned above, the theory overestimates the value of the critical temperature T_c at which the system freezes ($T_c^{\text{sim}} = 0.435$ and $T_c^{\text{MCT}} = 0.92$). This means that close to T_c^{sim} the value of the vertices in the memory function are already too large. To fix this problem we have evaluated this memory function at a temperature $T_f(T)$ and have adjusted T_f such that the time scale for the α -relaxation as predicted by the theory for $F_{AA}(q, t)$ at $q = 7.25$ matched the one of the simulation at temperature T . More details on this can be found in [253, 254].

In Figure 21 we compare the time dependence of the coherent and incoherent intermediate scattering function as obtained from the simulation [246, 255] and as predicted by the theory [253, 254]. The two wave-vectors correspond to the location of the minimum and maximum in the partial structure factor for the A particles. From this figure we recognize that at intermediate and long times the agreement between theory and simulation is very good in that the height of the plateau, the time scale for the α -relaxation, as well as the shape of the α -relaxation are very similar. The main discrepancies are found for $F_{AA}(q, t)$ for the larger wave-vector in that at short times the theoretical curve shows a strong oscillation that is not present in the data from the simulation. This difference indicates that the effective damping of the correlator at short times is not described correctly, *i.e.* that for this value of q the memory function M^{reg} is too small. We emphasize, however, that this error has nothing to do with the inadequacy of the MCT but instead is related to our insufficient understanding of the dynamics of liquids at short times (see also [256]). In contrast to this the relaxation dynamics of the system at intermediate and long times is described very well by the theory since similar results as the ones shown in Figure 21 are found also for the other partial correlation functions and other wave-vector [253].

5.2 The relaxation dynamics of a simple liquid with stochastic dynamics

The results discussed in Section 5.1 concerned the static and dynamical properties of a simple liquid with *Newtonian* dynamics. However, in quite a few practical applications, such as colloids or polymers in a solvent, the microscopic dynamics is better described by a Brownian one. The goal of this subsection is therefore to investigate to what extent the microscopic dynamics influences the relaxation dynamics, and hence the slowing down of the dynamics upon cooling, in a glass-forming system.

As we have seen in the previous sections, according to mode-coupling theory a small change in structure can have a large effect on the relaxation dynamics of the system, a result that is compatible with the curves and relaxation times shown in Figure 14. Hence if we want to study the influence

of the microscopic dynamics upon the relaxation dynamics it is imperative not to change the static properties of the system. One possibility to do this is to use exactly the same interaction potential that we have used to study the dynamic properties of the BLJM system and to change only the equations of motion. One alternative to Newton's equations of motion is a Brownian dynamics in which the inertia term is neglected and instead one has a friction term as well as an external noise. However, the numerical integrators that exist for such types of equations are not very accurate and thus require a small step size [257, 258], which is of course very unpleasant for systems in which the dynamics is slow. One possibility to circumvent this problem is to use a "stochastic dynamics" (SD), in which the equations of motion are still second order, but they include also a damping and noise term [249, 258]:

$$m\ddot{\mathbf{r}}_i + \nabla_i \sum_l V_{il}(|\mathbf{r}_l - \mathbf{r}_i|) = -\zeta \dot{\mathbf{r}}_i + \eta_i(t). \quad (5.6)$$

Here V_{il} is the potential between particles i and l , $\eta_i(t)$ are Gaussian distributed random variables with zero mean, *i.e.*, $\langle \eta_i(t) \rangle = 0$, and ζ is a damping constant. The fluctuation dissipation theorem relates ζ to the second moment of η_i , and we have $\langle \eta_i(t) \cdot \eta_l(t') \rangle = 6k_B T \zeta \delta(t - t') \delta_{il}$. For the following we will use a value of ζ of 10, which is large enough that the results presented do not depend on ζ anymore (apart from a trivial shift in the time scale). More details on this simulation can be found in [134, 244]. Note that all the *static* properties of the system are completely independent of the value of ζ and that $\zeta = 0$ corresponds to the case of the Newtonian dynamics.

In Figure 22 we show the time dependence of the intermediate scattering function as obtained from the SD (solid lines). The wave-vector is 7.20, *i.e.* is the location of the maximum in the static structure factor. Although at a first glance the set of curves look quite similar to the ones found for the Newtonian dynamics (ND), see Figure 17, there are important differences. To simplify their discussion we have included in the figure also the data from the latter dynamics at certain temperatures (dashed lines). Comparing the corresponding data at the highest temperature, we see that the curve for the ND decays quicker to zero than the one for the SD and that the relaxation time τ , which can, *e.g.*, be defined again *via* $F_s(q, \tau) = e^{-1}$, is about 7 times shorter. For the lowest temperature considered, this ratio has grown to about 30. At these temperatures all curves show the plateau of the β -relaxation. However, the correlators for the ND approach this plateau very quickly whereas the ones for the SD approach it very smoothly. Thus we conclude that the way the particles explore the cage is very different. Despite these differences there are, however, also quite a few similarities in

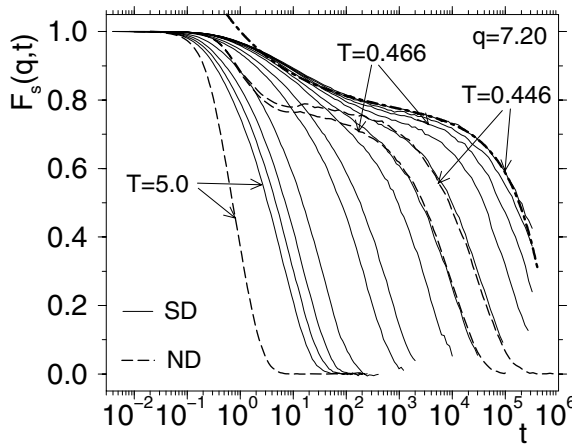


Fig. 22. Time dependence of the incoherent intermediate scattering function for the A particles. The solid lines are for the case of the stochastic dynamics at the temperatures $T = 5.0, 4.0, 3.0, 2.0, 1.0, 0.8, 0.6, 0.55, 0.5, 0.475, 0.466, 0.452$, and 0.446 . The dashed lines are for the Newtonian dynamics at $T = 5.0, 0.466$, and 0.446 . The dashed-dotted lines is a fit to the SD curve at $T = 0.446$ with the β -correlator from the MCT.

the correlators from the two types of dynamics: first of all the height of the plateau seems to be the same. This means that the size of the cage is independent of the microscopic dynamics (see also [259]). Furthermore also the shape of the correlator in the α -regime is independent of the dynamics as can be concluded from the fact that for certain temperatures the dashed and solid curves trace each other very well and the fact that at low T this shape is independent of T (see Fig. 18). These results are in agreement with the prediction of MCT since the theory does indeed predict that the relaxation dynamics at intermediate and long times is independent of the microscopic dynamics that is characterized by the memory function $M^{\text{reg}}(q, t)$ in equation (3.15).

Also included in the figure is a fit to the SD curve at the lowest temperature with the β -correlator given by equation (3.25) (dashed-dotted curve). The value of λ was fixed to 0.708 , the value that MCT predicts for this system [248] and is hence *not* a fit parameter. (We mention that in order to get reliable fits it was necessary to include also the correction to the β -correlator, which according to MCT are of the form t^{2b} [13] (see also [244, 260, 261] for more details).) The figure shows that this functional form gives a very good fit to the data for more than three decades in time,

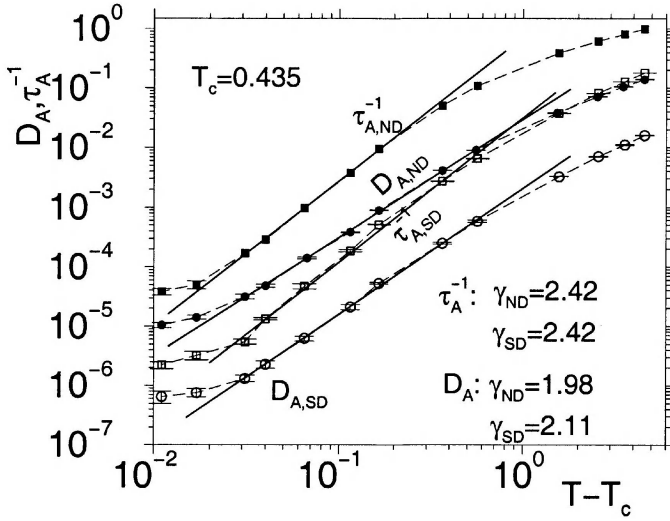


Fig. 23. Temperature dependence of the relaxation time τ as determined from the incoherent intermediate scattering function and the diffusion constant (in both cases for the A particles). The filled and open symbols correspond to the Newtonian and stochastic dynamics, respectively. The straight lines are fits with a power-law using $T_c = 0.435$ as the critical temperature. From [244].

which is strong evidence that MCT does indeed give a reliable description of the β -relaxation.

From the intermediate scattering function and the mean-squared displacement of a tagged particle one can now determine again the relaxation time $\tau(q, T)$ and a diffusion constant. According to MCT the T -dependence of these quantities should be the same as their T -dependence for the case of the ND. That this is indeed the case is shown in Figure 23 where we plot D and τ^{-1} for the two types of dynamics. The value of the critical temperature T_c has again been fixed to $T_c = 0.435$, the value we have found for the ND. The plot shows that with this value of T_c also the data for the SD are rectified for 2–3 decades in D (or τ^{-1}). Hence we conclude that the power-law given by equation (3.23) is found also for the SD. Moreover, the exponents γ , given by the slope of the straight lines, seems basically to be independent of the microscopic dynamics. In particular the values of γ as determined from $\tau(T)$ are the same within the accuracy of the data. Hence we conclude from this figure and the previous one that the whole α -process is independent of the microscopic dynamics, *apart from an overall shift in the time scale*, a result that is rather surprising. From Figure 22 we

recognize that this shift is only due to the different time dependence of the dynamics at *short* times, *i.e.* by the different choice of $M^{\text{reg}}(q, t)$. Since we have shown in Figure 21 that MCT is able to give a correct description of the relaxation dynamics at long times, we hence conclude that if we would have a reliable theory for the short time dynamics, we would be able to describe the relaxation dynamics in the whole time range and for all microscopic dynamics. (Of course this has to be restricted to the case that the microscopic dynamics is “local”, *i.e.* we do not allow, *e.g.*, *global* Monte-Carlo moves [154, 155, 157].)

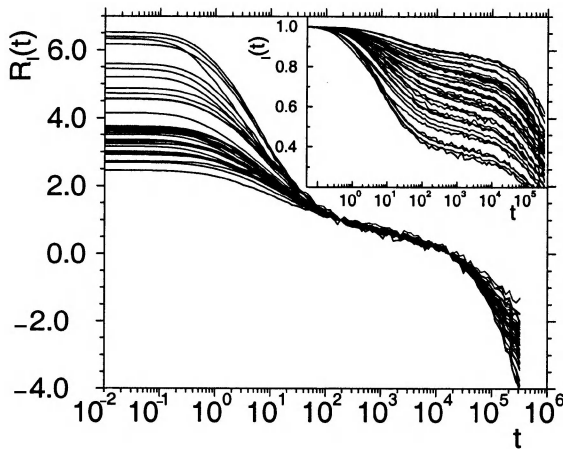


Fig. 24. Main figure: time dependence of $R_l(t)$ as defined in equation (5.7) using various correlators (see main text for details). The time dependence of these correlators are shown in the inset.

The last feature of the relaxation dynamics that we want to discuss is the factorization property given in equation (3.24). Recall that this equation says that on the time scale of the β -relaxation the shape of all time correlation function is the same. In order to check whether this is indeed true one could make fits to each of the correlation functions with the β -correlator *using the same value of λ* , as it has been done in Figure 22. Since this procedure is quite involved it is, however, more advisable to use an approach that has been proposed some time ago by Signorini *et al.* [198] and which goes as follows: let $\Phi_l(t)$ be an arbitrary correlator. From equation (3.24) it thus follows that the following ratio is independent of l :

$$R_l(t) = \frac{\Phi_l(t) - \Phi_l(t')}{\Phi_l(t'') - \Phi_l(t')}. \quad (5.7)$$

Here t' and t'' are two arbitrary times in the β -regime. If equation (3.24) does indeed hold, the time dependence of $R_l(t)$ should just be the function $G(t)$, hence be independent of l . In Figure 24 we show the time dependence of $R_l(t)$ for a total of 36 correlators, using times $t' = 200$ and $t'' = 15\,000$ [134]. These correlators include the coherent and incoherent scattering function for the A and B particles at different wave-vectors and their time dependence is shown in the inset of the figure. From this inset we recognize that the time dependence of all these correlators differs strongly in that the height of the plateaus, the stretching etc. covers a wide range of values. From the main figure we see, however, that on the time scale of the β -relaxation all these curves are indeed very similar in that the rescaling given by equation (5.7) makes them to collapse nicely onto a master curve, the shape of which is the function $G(t)$. Hence we can conclude that for this system the factorization property predicted by MCT does indeed hold.

5.3 Static and dynamic properties of a network forming liquid

In the previous two subsections we have discussed the static and dynamic properties of a *simple* liquid and have shown that this dynamics can be rationalized very well with the help of MCT. The structure of these simple liquids is quite close to the one of a close packing of hard spheres. Already in Section 2 we have mentioned, however, that the so-called strong glass-formers have a structure that is often quite open and that the T -dependence of their relaxation dynamics is, by definition, close to an Arrhenius law. Hence it is legitimate to ask whether MCT is a useful theory for these type of systems as well. The goal of this section is therefore to discuss the results of some computer simulations that have been done to address this question.

In order to make a computer simulation of a strong glass-former it is of course necessary to have an interaction model that has indeed the required properties, *i.e.* an Arrhenius dependence of the relaxation times. Fortunately silica, the paradigm of a strong glass-former, is an important material not only for fundamental science but also in technical applications as well as fields like geology. Therefore there are a multitude of potentials available that claim to give a good description of this material [6,18]. One of the potentials that does indeed seem to be quite reliable has been proposed some time ago by van Beest *et al.* (BKS) [262], and its functional form is given by

$$\phi_{\alpha\beta}(r) = \frac{q_\alpha q_\beta e^2}{r} + A_{\alpha\beta} \exp(-B_{\alpha\beta} r) - \frac{C_{\alpha\beta}}{r^6} \quad \alpha, \beta \in [\text{Si}, \text{O}], \quad (5.8)$$

where r is the distance between the ions of type α and β . The values of the constants $q_\alpha, q_\beta, A_{\alpha\beta}, B_{\alpha\beta}$, and $C_{\alpha\beta}$ can be found in [262]. Due to the

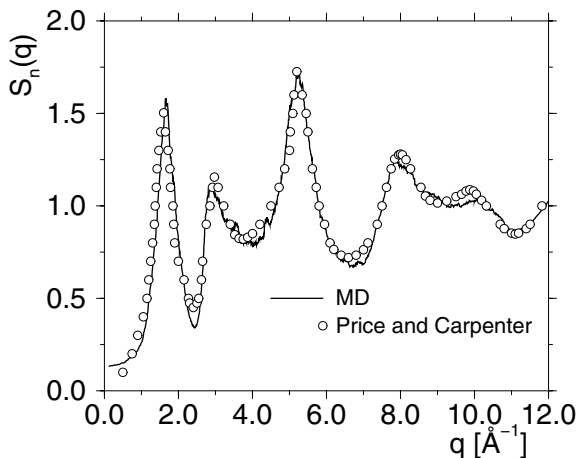


Fig. 25. Wave-vector dependence of the structure factor of SiO_2 as measured in a neutron scattering experiment. The solid line is the result of the simulation with the BKS potential and the symbols are the experimental results by Price and Carpenter [266].

presence of the Coulomb interactions it is necessary to use an Ewald summation technique to calculate the forces [154, 155], or one of the equivalent methods proposed more recently [263–265]. Therefore making a simulation of these type of systems are presently about 10 times more expensive in computer time that models with only short range interactions. As mentioned in Section 4 it is sometimes necessary to use relatively large systems in order to avoid finite size effects in the dynamics [56, 179]. Therefore the following results have been obtained for a system size of about 8000 atoms, which corresponds to a box size of around 50 Å. More information on the technical details of these simulations can be found in [143, 149].

Since we are modeling silica, *e.g.* a material that really exists in nature, it is possible to compare the results from the simulation with real experimental data (and in fact this should always be done in order to check whether the potential used is indeed reliable, *i.e.* compatible with known experimental facts). One such comparison is shown in Figure 25, where we compare $S_n(q)$, the static structure factor as measured in a neutron scattering experiment, from the simulation with real experimental data. This function can be easily calculated from the three partial structure factors $S_{\alpha\beta}(q)$ using the relation

$$S_n(q) = \frac{1}{N_{\text{Si}}b_{\text{Si}}^2 + N_{\text{O}}b_{\text{O}}^2} \sum_{\alpha,\beta} b_{\alpha}b_{\beta}S_{\alpha\beta}(q), \quad (5.9)$$

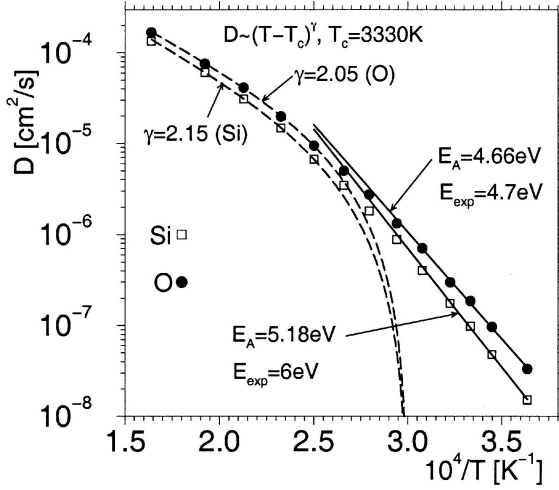


Fig. 26. Arrhenius plot of the diffusion constant for the silicon and oxygen atoms as predicted by the BKS potential. The solid straight lines at low T are fits with an Arrhenius law. The dashed lines at intermediate temperatures are fits with the power-law given by equation (3.23).

where b_α are the neutron scattering length whose experimental values can be found in the literature [267]. From the figure we see that the agreement between the experiment and the simulation is very good, which shows that the BKS potential is quite reliable³. Hence we can have some confidence that the dynamical properties as predicted by the model will not be too far off from the ones of real silica.

In Figure 26 we show the T –dependence of the diffusion constants for the Si and O atoms (which were determined using the Einstein relation) [143]. Note that the temperature scale covered is $6100 \text{ K} \geq T \geq 2750 \text{ K}$, *i.e.* the temperatures are rather high. The reason for this is that silica is a very viscous system even at high temperatures (the relaxation time at 2750 K

³A brief comment on the meaning of the various peaks: in a simple liquid, see *e.g.* Figure 14, the first main peak corresponds to the length scale of a nearest neighbor. However, for ionic systems like silica this identification is not necessarily true, since the charged atoms will induce a local ordering of the system. In the case of SiO_2 this is done in the form of tetrahedra, *i.e.* a silicon atom is surrounded by four oxygen atoms. These tetrahedra are connected *via* their corners and form an irregular open network. Thus in this system the first peak at in the structure factor (located at 1.6 \AA^{-1}) does not correspond to the nearest neighbor distance (which would be a Si-O pair) but to the distance between two neighboring tetrahedra. For even more complex systems, like $\text{Na}_2\text{O-SiO}_2$, one can have structural features at even larger length scales [56, 268–272].

is around 10 ns, see also Fig. 2) and hence it is presently not possible to equilibrate the system in a simulation at significantly lower temperature. From the figure we recognize that at low temperatures the diffusion constants show an Arrhenius dependence, as can be expected for this system (see bold solid lines). The activation energies, given in the figure, agree well with the experimental values [273, 274]. Hence we conclude that the BKS potential is indeed able to give also a satisfactory description of the relaxation dynamics of real silica.

What is surprising in the data from the simulation is that at high temperatures there is a crossover from the Arrhenius dependence of D to a weaker one, *i.e.* there is a significant bend in the curves. (Note that the viscosity and the relaxation times determined from the intermediate scattering functions shows a very similar T -dependence, hence this non-Arrhenius behavior is not a particularity of the diffusion constant.) Such a T -dependence is reminiscent to the behavior found in fragile liquids close to the critical temperature of MCT. Therefore it is reasonable to check whether the power-law predicted by the theory, see equation (3.23), can also in this case be used to rationalize the data. That this is indeed possible is demonstrated by the two dashed lines shown in the figure that represent such a power-law dependence. If one assumes that the value of T_c is the same for Si and O, the resulting critical exponents γ are indeed very close together, in agreement with the prediction of the theory. Also the α -relaxation times $\tau(T)$ show a power-law dependence and the critical temperature is the same as the one found for the diffusion constant. However, as it was already the case for the BLJM system, the value of the critical exponent γ as determined from τ is larger than the one found for D ($\gamma_\tau = 2.45$) [149].

The critical temperature T_c is found to be around 3330 K, a value that is far above the melting temperature of the system ($T_m \approx 2000$ K). Thus we see that the critical temperature of MCT has nothing to do with the system being in a supercooled state. Instead it is just a temperature at which the transport mechanism of the atoms changes, as already discussed in Section 3. Last not least we mention that Hess *et al.* have used experimental data for the viscosity to estimate T_c and have predicted a value around 3200 K [150, 151], in surprisingly good agreement with the estimate from the simulation.

That MCT is not only able to rationalize some features of the relaxation dynamics of the α -relaxation but also in the β -regime is shown in Figure 27, where we plot the functions $R_l(t)$ defined in equation (5.7). The correlators used to calculate these curves are the incoherent intermediate scattering function for Si and O at $q = 1.7, 2.2, 2.8, 4.43, 5.02$ and 5.31 \AA^{-1} , but other correlators can be included as well [275]. As it was the case of the BLJM system, we see that in the β -regime the curves fall on top of

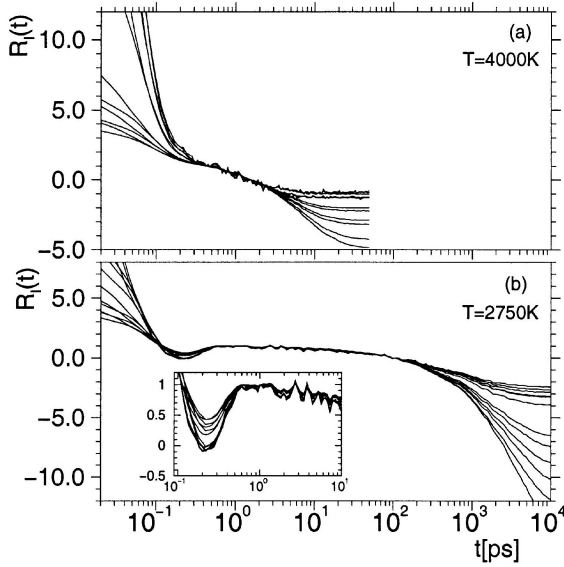


Fig. 27. Time dependence of the functions $R_l(t)$ as defined in equation (5.7) for the case of silica. The upper and lower panel corresponds to $T = 4000$ K and $T = 2750$ K, respectively. The correlators used are $F_s(q, t)$ for silicon and oxygen at $q = 1.7, 2.2, 2.8, 4.43, 5.02$ and 5.31 \AA^{-1} . The times t'' and t' are 0.4 ps and 1.6 ps for $T = 4000$ K and 1.1 ps and 106 ps for $T = 2750$ K, respectively.

each other. In agreement with the prediction of MCT, the range where a master curve is found expands if the temperature is lowered (compare the two panels). The shape of the master curve is given by the β -correlator $g_-(t)$ from which one can determine the exponent parameter λ . Using this value of λ ($= 0.713$), one can use equations (3.29) and (3.30) to calculate the theoretical value of the critical exponent γ , which turns out to be 2.35 , in very good agreement with the real value as determined from $\tau(T)$, which is around 2.45 .

As it was already the case for the BLJM system, it is important to understand also for this network-forming glass whether MCT is able to give only a qualitative description of the relaxation dynamics, or whether it is also possible to make a quantitative calculation. It is found that if one uses the expressions given by equation (3.18) for the vertex $V^{(2)}$ there is no good agreement between, *e.g.*, the wave-vector dependence of the non-ergodicity as predicted by the theory and the one found in the simulation [104, 253]. This is seen in Figure 28 where we compare the result from the simulation (circles) with the ones of MCT (dashed lines). However, we have already

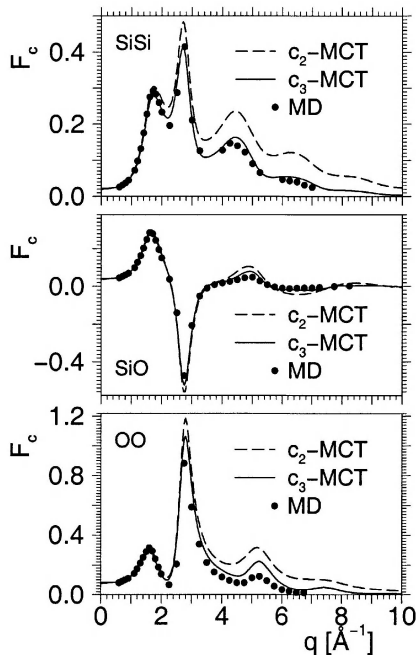


Fig. 28. Wave-vector dependence of the non-ergodicity parameter for silica. The dots are the results from the simulations and the dashed and solid lines are the predictions of MCT neglecting and including the c_3 -terms, respectively (see text for details).

mentioned in Section 3, that there are also contributions to the vertices $V^{(2)}$ that are related to the three-particles correlation function $c_3(\mathbf{q}, \mathbf{k})$. For the case of the BLJM system we have found, see Figure 20, that these contributions do not change significantly the value of the non-ergodicity parameter. For a network-forming liquid like silica this is, however, no longer the case in that there is a quite large difference between the theoretical prediction in which c_3 is neglected and the one in which c_3 is taken into account. This can be seen, *e.g.*, in Figure 28 where we have included also the curve from the MCT in which the c_3 terms are included (solid line). We find that the curve with and without these terms differ significantly in that the former is quite a bit lower than the latter one, in particular at intermediate and large wave-vectors. In addition we recognize that the inclusion of these terms lead to a much better agreement between the theory and the data of the simulation. For the case of the Si-Si correlation one can even say that the theory makes a very good prediction for this highly non-trivial

function. Hence we conclude that also for the case of silica, the prototype of a strong glass-former, the mode-coupling theory is able to rationalize not only some qualitative features of the relaxation dynamics, but also to make quantitative predictions that are surprisingly accurate.

6 Summary and perspectives

Space and time limits imposed by the (very wise!) editors, and ignorance from my side, have had the effect that many highly interesting and exciting aspects of glassy systems could not be discussed in this review. The simulations done in the context of the recent theoretical developments that seem to indicate a much closer connection between structural glasses, that have no frozen in disorder, and spin glasses, in which the disorder is quenched, could unfortunately not been mentioned. Likewise I had to leave out the discussion of the interesting and promising approach to use the language of “landscapes” (potential and free energy) to describe glassy systems, as well as the fascinating possibility that also *driven* systems (sheared, stirred, etc.) can be characterized by an effective temperature, thus suggesting a close connection between these systems and aging glasses. All these topics, and many others, will certainly be the focus of much research in the years to come.

I warmly thank Jean-Louis Barrat, Mikhail Feigelman, and Jorge Kurchan for giving me the possibility to give these lectures at the very interesting and motivating school they organized. In addition I thank all my friends and colleagues (way too many to be mentioned here) that have taught me most of the things that I have written about.

References

- [1] K.L. Ngai, *J. Non-Cryst. Solids* **131-133** (1991).
- [2] K.L. Ngai, *J. Non-Cryst. Solids* **172-174** (1994).
- [3] K.L. Ngai, *J. Non-Cryst. Solids* **235-237** (1998).
- [4] K.L. Ngai, *J. Non-Cryst. Solids* **307-310** (2002).
- [5] R.W. Douglas and S. Frank, *A History of Glassmaking* (G.T. Foulis, Henley on Thames, 1972).
- [6] C.A. Angell, J.H.R. Clarke and L.V. Woodcock, *Adv. Chem. Phys.* **48** (1981) 397.
- [7] R. Zallen, *The Physics of Amorphous Solids* (Wiley, New York, 1983).
- [8] K. Binder, A.P. Young, *Rev. Mod. Phys.* **58** (1986) 801.
- [9] J. Jäckle, *Rep. Progr. Phys.* **49** (1986) 171.
- [10] D.R. Uhlmann and N.J. Kreidl, *Glass Science and Technology: Viscosity and Relaxation*, Vol. 3 (Academic Press, Orlando, 1986).
- [11] M. Mézard, G. Parisi and M.A. Virasoro, *Spin Glass Theory and Beyond* (World Scientific, Singapore, 1987).
- [12] K.H. Fisher and J.A. Hertz, *Spin Glasses* (Cambridge University Press, Cambridge, 1991).

- [13] W. Götze, *Liquids, Freezing and the Glass Transition*, edited by J.P. Hansen, D. Levesque, J. Zinn-Justin, Les Houches. Session LI, 1989 (North-Holland, Amsterdam, 1991), 287.
- [14] J. Zarzycki, *Materials Science and Technology*, Vol. 9 (VCH Publ., Weinheim, 1991).
- [15] W. Götze and L. Sjögren, *Rep. Prog. Phys.* **55** (1992) 241.
- [16] A. Feltz, *Amorphous Inorganic Materials and Glasses* (VCH Publ., Weinheim, 1993).
- [17] U. Mohanty, *Adv. Chem. Phys.* **89** (1995) 89.
- [18] P.H. Poole, P.F. McMillan and G.H. Wolf, *Structure, Dynamics and Properties of Silicate Melts*, edited by J.F. Stebbins, P.F. McMillan and D.B. Dingwell (Mineralogical Society of America, Washington, 1995), 563.
- [19] P.G. Debenedetti, *Metastable Liquids* (Princeton University Press, Princeton, 1997).
- [20] A.P. Young, *Spin Glasses and Random Fields* (World Scientific, Singapore, 1998).
- [21] M.E. Cates and M.R. Evans, *Soft and Fragile Matter; Nonequilibrium Dynamics, Metastability and Flow*, edited by M.E. Cates and M.R. Evans (Institute of Physics, London, 2000).
- [22] P.G. Debenedetti, T.M. Truskett and C.P. Lewis, *Adv. Chem. Eng.* **28** (2001) 21
- [23] E. Donth, *The Glass Transition* (Springer, Berlin, 2001).
- [24] C.A. Angell, P.H. Poole and J. Shao, *Nuovo Cimento D* **16** (1994) 993.
- [25] W.T. Laughlin and D.R. Uhlmann, *J. Phys. Chem.* **76** (1972) 2317.
- [26] C.A. Angell, *Relaxation in Complex Systems*, edited by K.L. Ngai and G.B. Wright (US Dept. Commerce, Springfield, 1985).
- [27] R. Böhmer, K.L. Ngai, C.A. Angell and D.J. Plazek, *J. Chem. Phys.* **99** (1993) 4201.
- [28] H.E. Stanley, *Introduction to Phase Transitions and Critical Phenomena* (Oxford University Press, Oxford, 1971).
- [29] H. Vogel, *Phys. Z.* **22** (1921) 645.
- [30] G.S. Fulcher, *J. Amer. Ceram. Soc.* **8** (1925) 339.
- [31] G. Tammann and W.Z. Hesse, *Anorg. Allg. Chem.* **156** (1926) 245.
- [32] F. Stickel, E.W. Fischer and R. Richert, *J. Chem. Phys.* **102** (1995) 6251.
- [33] J.-P. Hansen and I.R. McDonald, *Theory of Simple Liquids* (Academic, London, 1986).
- [34] U. Balucani and M. Zoppi, *Dynamics of the Liquid State* (Oxford University Press, Oxford, 1994).
- [35] R. Kohlrausch, *Ann. Phys. (Leipzig)* **12** (1847) 393.
- [36] G. Williams and D.C. Watts, *Trans. Faraday Soc.* **66** (1980) 80.
- [37] R. Richert, *J. Non-Cryst. Solids* **172-174** (1994) 209.
- [38] H. Sillescu, *J. Non-Cryst. Solids* **243** (1999) 81.
- [39] M.D. Ediger, *Ann. Rev. Phys. Chem.* **51** (2000) 99.
- [40] R. Richert, *J. Phys.: Condens. Matter* **14** (2002) R703.
- [41] G. Winterling, *Phys. Rev. B* **12** (1975) 2432.
- [42] U. Buchenau, M. Prager, N. Nücker, A.J. Dianoux, N. Ahmad and W.A. Phillips, *Phys. Rev. B* **34** (1986) 5665.
- [43] P. Benassi, M. Krisch, C. Masciovecchio, V. Mazzacurati, G. Monaco, G. Ruocco, F. Sette and R. Verbeni, *Phys. Rev. Lett.* **77** (1996) 3835.

- [44] M. Foret, E. Courtens, R. Vacher and J.-B. Suck, *Phys. Rev. Lett.* **77** (1996) 3831.
- [45] S.N. Taraskin and S.R. Elliott, *Phys. Rev. B* **56** (1997) 8605.
- [46] R. Dell'Anna, G. Ruocco, M. Sampoli and G. Viliani, *Phys. Rev. Lett.* **80** (1998) 1236.
- [47] W. Schirmacher, G. Diezemann and G. Ganter, *Phys. Rev. Lett.* **81** (1998) 136.
- [48] A. Wischniewski, U. Buchenau, A.J. Dianoux, W.A. Kamitakahara and J.L. Zarestky, *Phys. Rev. B* **57** (1998) 2663.
- [49] E. Rat, M. Foret, E. Courtens, R. Vacher and M. Arai, *Phys. Rev. Lett.* **83** (1999) 1355.
- [50] A.P. Sokolov, *J. Phys.: Condens. Matter* **11** (1999) A213.
- [51] W. Götze and M.R. Mayr, *Phys. Rev. E* **61** (2000) 587.
- [52] B. Hehlen, E. Courtens, R. Vacher, A. Yamanaka, M. Kataoka and K. Inoue, *Phys. Rev. Lett.* **84** (2000) 5355.
- [53] C. Masciovecchio, A. Mermet, G. Ruocco and F. Sette, *Phys. Rev. Lett.* **85** (2000) 1266.
- [54] S.N. Taraskin and S.R. Elliott, *Phys. Rev. B* **61** (2000) 12017.
- [55] T.S. Grigera, V. Martin-Mayor, G. Parisi and P. Verrocchio, *Phys. Rev. Lett.* **87** (2001) 085502.
- [56] J. Horbach, W. Kob and K. Binder, *Eur. Phys. J. B.* **19** (2001) 531.
- [57] M. Foret, R. Vacher, E. Courtens and G. Monaco *Phys. Rev. B* **66** (2002) 024204.
- [58] J.K. Nielsen, *Phys. Rev. E* **60** (1999) 471.
- [59] P. Scheidler, W. Kob, A. Latz, J. Horbach and K. Binder, *Phys. Rev. B* **63** (2001) 104204.
- [60] F.H. Stillinger, *J. Chem. Phys.* **88** (1988) 7818.
- [61] M. Wolfgardt, J. Baschnagel, W. Paul and K. Binder, *Phys. Rev. E* **54** (1996) 1535.
- [62] R. Richert and C.A. Angell, *J. Chem. Phys.* **108** (1998) 9016.
- [63] G. Adam and J.H. Gibbs, *J. Chem. Phys.* **43** (1965) 139.
- [64] H.N. Ritland, *J. Amer. Ceram. Soc.* **37** (1954) 370.
- [65] C.Y. Yang, D.E. Sayers and M.A. Paesler, *Phys. Rev. B* **36** (1987) 8122.
- [66] C.T. Limbach and U. Gonser, *J. Non-Cryst. Solids* **106** (1988) 399.
- [67] G.P. Johari, A. Hallbrucker and E. Mayer, *J. Phys. Chem.* **93** (1989) 2648.
- [68] R. Brüning and K. Samwer, *Phys. Rev. B* **46** (1992) 11318.
- [69] R. Brüning and M. Sutton, *Phys. Rev. B* **49** (1994) 3124.
- [70] K. Vollmayr, W. Kob and K. Binder, *Europhysics Lett.* **32** (1995) 715.
- [71] K. Vollmayr, W. Kob and K. Binder, *Phys. Rev. B* **54** (1996) 15808.
- [72] C. Levelut, A. Faivre, R. Le Parc, B. Champagnon, J.-L. Hazemann, L. David, C. Rochas and J.-P. Simon, *J. Non-Cryst. Solids* **307-310** (2002) 426.
- [73] L.C.E. Struik, *Physical Aging in Amorphous Polymers and Other Materials* (Elsevier, Amsterdam, 1978).
- [74] G.B. McKenna, in *Comprehensive Polymer Science, Vol. 12, Polymer Properties*, edited by C. Booth and C. Price (Pergamon, Oxford, 1989), 311.
- [75] See article of C. F. Cugliandolo in these proceedings.
- [76] A.Q. Tool and C.G. Eichlin, *J. Opt. Soc. Amer.* **14** (1931) 276.
- [77] A.Q. Tool, *J. Amer. Ceram. Soc.* **29** (1946) 240.
- [78] O.S. Narayanaswamy, *J. Amer. Ceram. Soc.* **54** (1971) 491.
- [79] C.T. Moynihan, A.J. Eastal, M.A. DeBolt and J. Tucker, *J. Amer. Ceram. Soc.* **59** (1976) 12.

- [80] L.F. Cugliandolo and Kurchan, *Phys. Rev. Lett.* **71** (1993) 173.
- [81] J.P. Bouchaud, L.F. Cugliandolo, J. Kurchan and M. Mézard, *Physica A* **226** (1996) 243.
- [82] J.-P. Bouchaud, L.F. Cugliandolo, J. Kurchan and M. Mézard, *Spin Glasses and Random Fields*, edited by A.P. Young, (World Scientific, Singapore, 1998), 161.
- [83] D.R. Uhlmann, *J. Non-Cryst. Solids* **7** (1972) 337
- [84] See, e.g., S. Klauminzer, *Mat. Sci. Forum* **97-99** (1992) 623 and references therein.
- [85] C.Y. Brinker and G.W. Scherrer, *Sol-Gel Science* (Academic Press, San Diego, 1990).
- [86] T. Woignier and J. Phalippou, *Encyclopedia of Materials: Science and Technology* (Elsevier, Amsterdam, 2001), 3581.
- [87] R. Brückner, *J. Non-Cryst. Solids* **5** (1970) 123.
- [88] A. Metha (Ed.), *Granular Matter: An interdisciplinary approach* (Springer, Berlin, 1994).
- [89] R. Schilling, *Disorder Effects on Relaxational Processes*, edited by R. Richert and A. Blumen (Springer, Berlin, 1994), 193.
- [90] H.Z. Cummins, G. Li, W.M. Du and J. Hernandez, *Physica A* **204** (1994) 169.
- [91] Theme Issue on Relaxation Kinetics in Supercooled Liquids-Mode Coupling Theory and its Experimental Tests, edited by S. Yip, *Transport Theory and Statistical Physics* **24** (1995).
- [92] W. Götze, *J. Phys.: Condens. Matter* **10** (1999) A1.
- [93] H. Mori, *Prog. Theor. Phys.* **33** (1965) 423.
- [94] R. Zwanzig, *Lectures in Theoretical Physics*, edited by W.E. Britton, B.W. Downs and J. Downs (Wiley, New York, 1961), 135.
- [95] D. Forster, *Hydrodynamic Fluctuations, Broken Symmetry and Correlation Functions*, Benjamin (1975).
- [96] J.-L. Barrat, *Physics of Glasses*, edited by P. Jund and R. Jullien (APS, New York, 1999).
- [97] S.W. Lovesey, *Theory of Neutron Scattering from Condensed Matter* (Oxford University Press, Oxford, 1994).
- [98] U. Bengtzelius, W. Götze and A. Sjölander, *J. Phys. C* **17** (1984) 5915.
- [99] K. Tankeshwar, K.N. Pathak and S. Ranganathan, *J. Phys. C* **20** (1987) 5749.
- [100] K. Tankeshwar, K.N. Pathak and S. Ranganathan, *J. Phys. Condens. Matter* **7** (1995) 5729.
- [101] J.-L. Barrat, J.-P. Hansen and G. Pastore, *Molec. Phys.* **63** (1988) 747.
- [102] A.R. Denton and N.W. Ashcroft, *Phys. Rev. A* **39** (1989) 426.
- [103] J.-L. Barrat and A. Latz, *J. Phys.: Condens. Matter* **2** (1990) 4289.
- [104] F. Sciortino and W. Kob, *Phys. Rev. Lett.* **86** (2001) 648.
- [105] R. Schilling and T. Scheidsteger, *Phys. Rev. E* **56** (1997) 2932.
- [106] K. Kawasaki, *Physica A* **243** (1997) 25.
- [107] T. Franosch, M. Fuchs, W. Götze, M.R. Mayr and A.P. Singh, *Phys. Rev. E* **56** (1997) 5659.
- [108] S.-H. Chong and F. Hirata, *Phys. Rev. E* **57** (1998) 1691.
- [109] S.-H. Chong and F. Hirata, *Phys. Rev. E* **58** (1998) 6188.
- [110] L. Fabbian, A. Latz, R. Schilling, F. Sciortino, P. Tartaglia and C. Theis, *Phys. Rev. E* **60** (1999) 5768.
- [111] W. Götze, A.P. Singh and T. Voigtmann, *Phys. Rev. E* **61** (2000) 6934.

- [112] M. Letz, R. Schilling and A. Latz, *Phys. Rev. E* **62** (2000) 5173.
- [113] S.-H. Chong, W. Götze and M.R. Mayr, *Phys. Rev. E* **64** (2001) 011503.
- [114] T. Theenhaus, R. Schilling, A. Latz and M. Letz, *Phys. Rev. E* **64** (2001) 051505.
- [115] S.-H. Chong and W. Götze, *Phys. Rev. E* **65** (2002) 041503.
- [116] E. Leutheusser, *Phys. Rev. A* **29** (1984) 2765.
- [117] C. Alba-Simionesco and M. Krauzman, *J. Chem. Phys.* **102** (1995) 6574.
- [118] T. Franosch, W. Götze, M.R. Mayr and A.P. Singh, *Phys. Rev. E* **55** (1997) 3183.
- [119] B. Rufflé, C. Ecolivet and B. Toudic, *Europhys. Lett.* **45** (1999) 591.
- [120] W. Götze and T. Voigtmann, *Phys. Rev. E* **61** (2000) 4133.
- [121] T.R. Kirkpatrick and P.G. Wolynes, *Phys. Rev. B* **36** (1987) 8552.
- [122] T.R. Kirkpatrick and D. Thirumalai, *Phys. Rev. B* **37** (1988) 5342.
- [123] D. Thirumalai and T.R. Kirkpatrick, *Phys. Rev. B* **38** (1988) 4881.
- [124] See article of G. Parisi in these proceedings.
- [125] M. Mézard and G. Parisi, *Phys. Rev. Lett.* **82** (1999) 747.
- [126] B. Coluzzi, G. Parisi and P. Verrocchio, *Phys. Rev. Lett.* **84** (2000) 306.
- [127] M. Mézard and G. Parisi, *J. Phys.: Condens. Matter* **12** (2000) 6655.
- [128] B. Coluzzi and P. Verrocchio, *J. Chem. Phys.* **116** (2002) 3789.
- [129] T. Franosch, M. Fuchs, W. Götze, M.R. Mayr and A.P. Singh, *Phys. Rev. E* **55** (1997) 7153.
- [130] M. Fuchs, W. Götze and M.R. Mayr, *Phys. Rev. E* **58** (1998) 3384.
- [131] W. Götze, *Z. Phys. B* **60** (1985) 195.
- [132] C. Brangian, W. Kob and K. Binder, *Europhys. Lett.* **59** (2002) 546.
- [133] E. Marinari, G. Parisi, F. Ricci-Tersenghi, J.J. Ruiz-Lorenzo, *J. Phys. A: Math. Gen.* **31** (1998) 2611.
- [134] T. Gleim and W. Kob, *Eur. Phys. J. B* **13** (2000) 83.
- [135] D.J. Gross, I. Kanter and H. Sompolinsky, *Phys. Rev. Lett.* **55** (1985) 304.
- [136] T.R. Kirkpatrick and D. Thirumalai, *Transp. Theory Stat. Phys.* **24** (1995) 927.
- [137] K. Broderix, K.K. Bhattacharya, A. Cavagna, A. Zippelius and I. Giardina, *Phys. Rev. Lett.* **85** (2000) 5360.
- [138] L. Angelani, R. Di Leonardo, G. Ruocco, A. Scala and F. Sciortino, *Phys. Rev. Lett.* **85** (2000) 5356.
- [139] S. Büchner and A. Heuer, *Phys. Rev. Lett.* **84** (2000) 2168.
- [140] A. Cavagna, *Europhys. Lett.* **53** (2001) 490.
- [141] T.S. Grigera, A. Cavagna, I. Giardina and G. Parisi, *Phys. Rev. Lett.* **88** (2002) 055502.
- [142] J. Wuttke, W. Petry, G. Coddens and F. Fujara, *Phys. Rev. E* **52** (1995) 4026.
- [143] J. Horbach and W. Kob, *Phys. Rev. B* **60** (1999) 3169.
- [144] W. Götze and L. Sjögren, *Z. Phys. B* **65** (1987) 415.
- [145] W. Götze and L. Sjögren, *J. Phys. C* **21** (1988) 3407.
- [146] S.P. Das and G.F. Mazenko, *Phys. Rev. A* **34** (1986) 2265.
- [147] H.Z. Cummins, W.M. Du, M. Fuchs, W. Götze, S. Hildebrand, A. Latz, G. Li and N. J. Tao, *Phys. Rev. E* **47** (1993) 4223.
- [148] J. Baschnagel and M. Fuchs, *J. Phys.: Condens. Matter* **7** (1995) 6761.
- [149] J. Horbach and W. Kob, *Phys. Rev. E* **64** (2001) 041503.
- [150] K.-U. Hess, D.B. Dingwell and E. Rössler, *Chem. Geol.* **128** (1996) 155.
- [151] E. Rössler, K.-U. Hess and V.N. Novikov, *J. Non-Cryst. Solids* **223** (1998) 207.

- [152] M.P. Allen and D.J. Tildesley, *Computer Simulation of Liquids* (Oxford University Press, New York, 1990).
- [153] M.P. Allen and D.J. Tildesley D.J. (Eds.) *Computer Simulation in Chemical Physics* NATO ASI Series, Vol. 397 (Kluwer, Dordrecht, 1993).
- [154] D. Frenkel and B. Smit, *Understanding Molecular Simulation - From Algorithms to Applications* (Academic Press, San Diego, 1996).
- [155] K. Binder and G. Ciccotti (Eds.), *Monte Carlo and Molecular Dynamics of Condensed Matter Systems* (Italian Physical Society, Bologna, 1996).
- [156] K. Binder and D.W. Heermann, *Monte Carlo Simulation in Statistical Physics* (Springer, Berlin, 1997).
- [157] D.P. Landau and K. Binder, *A Guide to Monte Carlo Simulations in Statistical Physics* (Cambridge University Press, Cambridge, 2000).
- [158] C. Dress and W. Krauth, *J. Phys. A: Math. Gen.* **28** (1995) L597.
- [159] T.S. Grigera and G. Parisi, *Phys. Rev. E* **63** (2001) 045102.
- [160] R.H. Swendsen and J.S. Wang, *Phys. Rev. Lett.* **57** (1986) 2607.
- [161] E. Marinari and G. Parisi, *Europhys. Lett.* **19** (1992) 451.
- [162] K. Hukushima and K. Nemoto, *J. Phys. Soc. Jpn.* **65** (1996) 1604.
- [163] U.H.E. Hansmann and Y. Okamoto, *Phys. Rev. E* **56** (1997) 2228.
- [164] K. Hukushima, H. Takayama and H. Yoshino, *J. Phys. Soc. Jpn.* **67** (1998) 12.
- [165] U.H.E. Hansmann and Y. Okamoto, *Annual Rev. Comp. Phys.*, Vol. VI (World Scientific, Singapore, 1999), 179
- [166] W. Kob, C. Brangian, T. Stühn and R. Yamamoto, in *Computer Simulation Studies in Condensed Matter Physics XIII*; edited by D.P. Landau, S.P. Lewis and H.B. Schüttler (Springer, Berlin, 2000), 153.
- [167] R. Yamamoto and W. Kob, *Phys. Rev. E* **61** (2000) 5473.
- [168] W. Kob and J.-L. Barrat, *Phys. Rev. Lett.* **78** (1997) 4581.
- [169] S. Ciuchi and F. de Pasquale, *Nuclear Physics B* **300** (1988) 31.
- [170] L.F. Cugliandolo, J. Kurchan and G. Parisi, *J. Phys. I France* **4** (1994) 1641.
- [171] J.P. Bouchaud and D. S. Dean, *J. Phys. I France* **5** (1995) 265.
- [172] J. Kurchan and L. Laloux, *J. Phys. A* **29** (1996) 1929.
- [173] C. Monthus and J.-P. Bouchaud, *J. Phys. A: Math. Gen.* **29** (1996) 3847.
- [174] T.M. Nieuwenhuizen, *Phys. Rev. Lett.* **80** (1998) 5580.
- [175] A. Latz, *J. Phys. Condens. Matter* **12** (2000) 6353.
- [176] A. Latz, Preprint [cond-mat/0106086].
- [177] P. Scheidler, Diploma Thesis (Mainz University 1999).
- [178] P. Ganster, M. Benoit and W. Kob, to be published.
- [179] J. Horbach, W. Kob, K. Binder and C. A. Angell, *Phys. Rev. E* **54** (1996) R5897.
- [180] K. Kim and R. Yamamoto, *Phys. Rev. E* **61** (2000) R41.
- [181] S. Büchner and A. Heuer, *Phys. Rev. E* **60** (1999) 6507.
- [182] N.D. Mackenzie and A. P.Young, *J. Phys. C* **16** (1983) 5321.
- [183] C. Brangian, W. Kob and K. Binder, *Europhys. Lett.* **53** (2001) 756.
- [184] A. Billoire and E. Marinari, Preprint [cond-mat/0101177].
- [185] C. Brangian, W. Kob and K. Binder, *J. Phys. A: Math. Gen.* **35** (2002) 191.
- [186] M.T. Dove, *Introduction to Lattice Dynamics* (Cambridge University Press, Cambridge, 1993).
- [187] J. Horbach, W. Kob and K. Binder, *J. Phys. Chem.* **103** (1999) 4104.

- [188] R. Car and M. Parrinello, *Phys. Rev. Lett.* **55** (1985) 2471.
- [189] D. Marx and J. Hutter, p. 301-449 in *Modern methods and algorithms of quantum chemistry*, edited by J. Grotendorst (Forschungszentrum Jülich, NIC series, 2000).
- [190] M. Benoit and W. Kob, *Europhys. Lett.* **60** (2002) 269.
- [191] M. Hemmati and C.A. Angell, *Physics meets Geology*, edited by H. Aoki and R. Hemley (Cambridge Univ. Press, Cambridge, 1998).
- [192] W. Kob, *J. Phys.: Condens. Matter* **11** (1999) R85.
- [193] B. Bernu, J.-P. Hansen, Y. Hiwatari and G. Pastore, *Phys. Rev. A* **36** (1987) 4891.
- [194] H. Miyagawa, Y. Hiwatari, B. Bernu and J.-P. Hansen, *J. Chem. Phys.* **88** (1988) 3879.
- [195] G. Pastore, B. Bernu, J.-P. Hansen and Y. Hiwatari, *Phys. Rev. A* **38** (1988) 454.
- [196] J.N. Roux, J.-L. Barrat and J.-P. Hansen, *J. Phys.: Condens. Matter* **1** (1989) 7171.
- [197] J.-L. Barrat, J.-N. Roux and J.-P. Hansen, *Chem. Phys.* **149** (1990) 197.
- [198] G.F. Signorini, J.-L. Barrat and M. L. Klein, *J. Chem. Phys.* **92** (1990) 1294.
- [199] H. Miyagawa and Y. Hiwatari, *Phys. Rev. A* **44** (1991) 8278.
- [200] B.B. Laird and H.R. Schober, *Phys. Rev. Lett.* **66** (1991) 636.
- [201] P. Sindzingre and M.L. Klein, *J. Chem. Phys.* **96** (1992) 4681.
- [202] J.P. Rino, I. Ebbsjö, R.K. Kalia, A. Nakano and P. Vashishta, *Phys. Rev. B* **47** (1993) 3053.
- [203] S. Balasubramanian and K. J. Rao, *J. Phys. Chem.* **98** (1994) 10871.
- [204] L.J. Lewis and G. Wahnström, *Phys. Rev. E* **50** (1994) 3865.
- [205] J. Sarnthein, A. Pasquarello and R. Car, *Phys. Rev. Lett.* **74** (1995) 4682.
- [206] J. Baschnagel and K. Binder, *J. Phys. I France* **6** (1996) 1271.
- [207] Y. Guissani and B. Guillot, *J. Chem. Phys.* **104** (1996) 7633.
- [208] M.M. Hurley and P. Harrowell, *J. Chem. Phys.* **105** (1996) 10521.
- [209] V. Mazzacurati, G. Ruocco and M. Sampoli, *Europhys. Lett.* **34** (1996) 681.
- [210] W. Kob, C. Donati, S.J. Plimpton, S.C. Glotzer and P.H. Poole, *Phys. Rev. Lett.* **79** (1997) 2827.
- [211] F. Sciortino, P.H. Poole, U. Essmann and H.E. Stanley, *Phys. Rev. E* **55** (1997) 727.
- [212] B. Guillot and Y. Guissani, *Phys. Rev. Lett.* **78** (1997) 2401.
- [213] G. Parisi, *Phys. Rev. Lett.* **79** (1997) 3660.
- [214] J. Badro, P. Gillet and J.-L. Barrat, *Europhys. Lett.* **42** (1998) 643.
- [215] C. Bennemann, W. Paul, K. Binder and B. Dünweg, *Phys. Rev. E* **57** (1998) 843.
- [216] M. Foley, M. Wilson and P. A. Madden, *J. Chem. Phys.* **108** (1998) 9027.
- [217] S. Kämmerer, W. Kob and R. Schilling, *Phys. Rev. E* **58** (1998) 2131.
- [218] S. Kämmerer, W. Kob and R. Schilling, *Phys. Rev. E* **58** (1998) 2141.
- [219] M.C.C. Ribeiro, M. Wilson and P.A. Madden, *J. Chem. Phys.* **108** (1998) 9027.
- [220] S. Sastry, P.G. Debenedetti and F.H. Stillinger, *Nature* **393** (1998) 554.
- [221] M. Wilson and P.A. Madden, *Phys. Rev. Lett.* **80** (1998) 532.
- [222] A. van Zon and S.W. de Leeuw, *Phys. Rev. E* **58** (1998) R4100.
- [223] C. Bennemann, W. Paul, J. Baschnagel and K. Binder, *J. Phys.: Condens. Matter* **11** (1999) 2179.
- [224] L. Berthier, J.-L. Barrat and J. Kurchan, *Eur. Phys. J. B* **11** (1999) 635.
- [225] B. Böttinger and H. Teichler, *Phys. Rev. E* **59** (1999) 1948.

- [226] M. Benoit, S. Ispas, P. Jund and R. Jullien, *Eur. Phys. J. B* **13** (2000) 631.
- [227] L. Berthier, J.-L. Barrat and J. Kurchan, *Phys. Rev. E* **61** (2000) 5464.
- [228] B. Doliwa and A. Heuer, *Phys. Rev. E* **61** (2000) 6898.
- [229] P. Gallo, M. Rovere, M. A. Ricci, C. Hartnig and E. Spohr, *Europhys. Lett.* **49** (2000) 183.
- [230] S. Mossa, R. Di Leonardo, G. Ruocco and M. Sampoli, *Phys. Rev. E* **62** (2000) 612.
- [231] M. Aichele and J. Baschnagel, *Eur. Phys. J. E* **5** (2001) 229.
- [232] P. Jund, R. Jullien and I. Campbell, *Phys. Rev. E* **63** (2001) 036131.
- [233] D.J. Lacks, *Phys. Rev. Lett.* **87** (2001) 225502.
- [234] I. Saika-Voivod, F. Sciortino and P.H. Poole, *Phys. Rev. E* **63** (2001) 011202.
- [235] F.W. Starr, T.B. Schroder and S.C. Glotzer, *Phys. Rev. E* **64** (2001) 021802.
- [236] A. Mukherjee, S. Bhattacharyya and B. Bagchi, *J. Chem. Phys.* **116** (2002) 4577.
- [237] L. Berthier and J.-L. Barrat, *J. Chem. Phys.* **116** (2002) 6228.
- [238] E. La Nave, S. Mossa and F. Sciortino, *Phys. Rev. Lett.* **88** (2002) 225701.
- [239] A.M. Puertas, M. Fuchs and M.E. Cates, *Phys. Rev. Lett.* **88** (2002) 098301.
- [240] P. Scheidler, W. Kob and K. Binder, *Europhys. Lett.* **59** (2002) 701.
- [241] J. Horbach and W. Kob, *J. Phys.: Condens. Matter* **14** (2002) 9237.
- [242] K. Vollmayr-Lee, W. Kob, K. Binder and A. Zippelius, *J. Chem. Phys.* **116** (2002) 5158.
- [243] T.A. Weber and F.H. Stillinger, *Phys. Rev. B* **31** (1985) 1954.
- [244] T. Gleim, Ph.D. Thesis (Mainz University, 1999).
- [245] W. Kob and H.C. Andersen, *Phys. Rev. E* **51** (1995) 4626.
- [246] W. Kob and H.C. Andersen, *Phys. Rev. E* **52** (1995) 4134.
- [247] T. Voigtmann, to be published.
- [248] M. Nauroth and W. Kob, *Phys. Rev. E* **55** (1997) 657.
- [249] T. Gleim, W. Kob and K. Binder, *Phys. Rev. Lett.* **81** (1998) 4404.
- [250] J.-L. Barrat, W. Götze and A. Latz, *J. Phys.: Condens. Matter* **1** (1989) 7163.
- [251] W. van Megen and S.M. Underwood, *Phys. Rev. E* **49** (1994) 4206.
- [252] J.P. Boon and S. Yip, *Molecular Hydrodynamics* (Dover, New York, 1980).
- [253] M.H. Nauroth, Ph.D. Thesis (Technical University of Munich, 1999).
- [254] W. Kob, M. Nauroth and F. Sciortino, *J. Non-Cryst. Solids* **307-310** (2002) 181.
- [255] W. Kob and H.C. Andersen, *Phys. Rev. Lett.* **73** (1994) 1376.
- [256] J. Casas, D.J. González, L.E. González, M.M.G. Alemany and L.J. Gallego, *Phys. Rev. B* **62** (2000) 12095.
- [257] D.L. Ermak, *J. Chem. Phys.* **62** (1975) 4189.
- [258] W. Paul and D.Y. Yoon, *Phys. Rev. E* **52** (1995) 2076.
- [259] H. Löwen, J.-P. Hansen and J.N. Roux, *Phys. Rev. A* **44** (1991) 1169.
- [260] F. Sciortino, P. Gallo, P. Tartaglia and S.H. Chen, *Phys. Rev. E* **54** (1996) 6331.
- [261] F. Sciortino, L. Fabbian, S.H. Chen and P. Tartaglia, *Phys. Rev. E* **56** (1997) 5397.
- [262] B.W.H. van Beest, G.J. Kramer and R.A. van Santen, *Phys. Rev. Lett.* **64** (1990) 1955.
- [263] L. Greengard and V. Rokhlin, *J. Comp. Phys.* **73** (1987) 325.
- [264] D. Solvason, J. Kolafa, H.G. Petersen and J.W. Perram, *Comp. Phys. Comm.* **87** (1995) 307.
- [265] M. Deserno and C. Holm, *J. Chem. Phys.* **109** (1998) 7678.

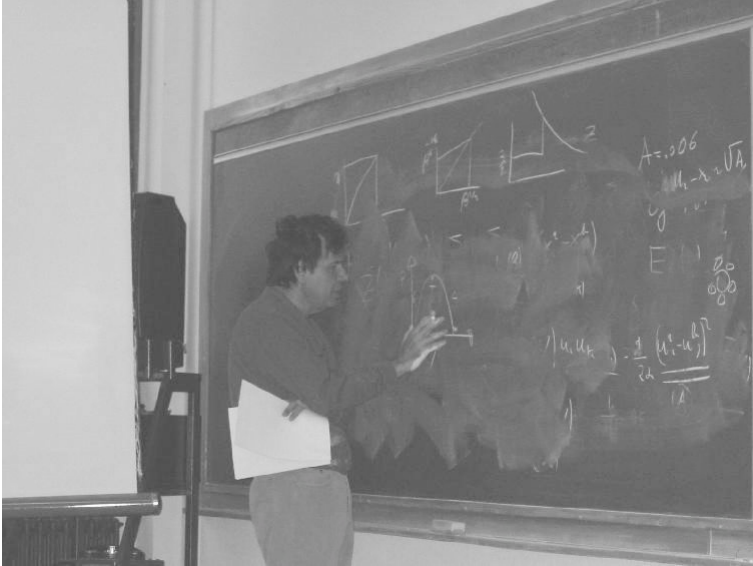
- [266] D.L. Price and J.M. Carpenter, *J. Non-Cryst. Solids* **92** (1987) 153.
- [267] S. Susman, K.J. Volin, D.G. Montague and D.L. Price, *Phys. Rev. B* **43** (1991) 11076.
- [268] J. Horbach, W. Kob and K. Binder, *Phil. Mag. B* **79** (1999) 1981.
- [269] J. Horbach, W. Kob and K. Binder, *Chem. Geol.* **174** (2001) 87.
- [270] P. Jund, W. Kob and R. Jullien, *Phys. Rev. B* **64** (2001) 134303.
- [271] J. Horbach, W. Kob and K. Binder, *Phys. Rev. Lett.* **88** (2002) 125502.
- [272] A. Meyer, H. Schober and D.B. Dingwell, *Europhys. Lett.* **59** (2002) 708.
- [273] J.C. Mikkelsen, *Appl. Phys. Lett.* **45** (1984) 1187.
- [274] G. Brébec, R. Seguin, C. Sella, J. Bevenot and J.C. Martin, *Acta Metall.* **28** (1980) 327.
- [275] W. Kob, J. Horbach and K. Binder, AIP Conference Proceedings, Vol. 469, *Slow Dynamics in Complex Systems, Tohwa University 1998* (AIP, Woodbury, 1999), 441.

COURSE 6

GLASSES, REPLICAS AND ALL THAT

G. PARISI

*Dipartimento di Fisica,
SMC and Udrml of INFN, INFN,
Università di Roma "La Sapienza",
Piazzale Aldo Moro 2, 00185 Rome,
Italy*



Contents

1	Introduction	275
1.1	General considerations	275
1.2	Glassiness, metastability and hysteresis	276
1.3	The organization of these lectures	280
2	The random energy model	281
2.1	The definition of the model	281
2.2	Equilibrium properties of the model	282
2.3	The properties of the low temperature phase	286
2.4	A careful analysis of the high temperature phase	290
2.5	The replica method	292
2.6	Dynamical properties of the model	294
3	Models with partially correlated energy	295
3.1	The definition of the models	295
3.2	The replica solution	296
3.3	The physical interpretation	300
3.4	The two susceptibilities	305
3.5	The cavity method	307
4	Complexity	310
4.1	The basic definitions	312
4.2	Computing the complexity	314
4.3	Complexity and replicas	319
4.4	A summary of the results	324
4.5	Some consideration on the free energy landscape and on the dynamics	325
4.6	Small fluctuations	328
5	Structural relations	330
5.1	Stochastic stability	330
5.2	A simple consequence of stochastic stability	333
5.3	Fluctuation dissipation relations	334
6	A short introduction to glasses	335
7	The replica approach to structural glasses: General formalism	337
7.1	The partition function	338
7.2	Molecular bound states	339
7.3	The small cage expansion	339

8	The replica approach to structural glasses: Some results	346
8.1	Three approximation schemes	346
8.2	Critical temperature and effective temperature	347
8.3	Cage size	348
8.4	Free energy, specific heat and configurational entropy	349
8.5	The missing dynamical transition	350
8.6	Lenhard-Jones binary mixtures	351
9	Discussion and perspectives	354

GLASSES, REPLICAS AND ALL THAT

G. Parisi

Abstract

In these lectures I will review the approach to glasses based on the replica formalism. Many of the physical ideas are very similar to those of older approaches. The replica approach has the advantage of describing in a unified setting both the behaviour near the dynamic transition (mode coupling transition) and near the equilibrium transition (Kauzmann transition) that is present in fragile glasses. The replica method may be used to solve simple mean field models, providing explicit examples of systems that may be studied analytically in great details and behave similarly to the experiments. Finally, using the replica formalism, it is possible to do analytic explicit computations of the properties of realistic models of glasses and the results are in reasonable agreement with numerical simulations.

1 Introduction

1.1 General considerations

In these recent years many progresses in the study of glasses have been done using the replica formalism. There are many indications that, if we would follow the evolution of a glass at a microscopical level, we would discover that at low temperatures the glass freezes in an equilibrium (or quasi equilibrium) configuration that is highly non-unique. This essential non-uniqueness of the ground state is present in many others systems where the energy landscape is highly corrugated: *e.g.* it is widely believed to be present in spin glasses, *i.e.* magnetic systems with a random mixture of ferromagnetic and antiferromagnetic interactions [1–4]. This property is responsible of the peculiar behaviour of glassy systems and, at the same time, it is the most difficult to control theoretical.

The replica approach to spin glasses was developed in the seventies and it was shown to be the most effective and sophisticated tool to study the behavior of systems characterized by the presence of many equilibrium states.

The use of the same replica techniques to study not only spin glasses, but also glasses, was not immediate because there was a strong psychological barrier to be crossed: disorder is present in the Hamiltonian for spin glasses, but it not present in the Hamiltonian for glasses and it was believed that the presence of disorder was one of the prerequisites for using the replica method. However at a certain moment it became clear that disorder in the Hamiltonian was not necessary for using the replica techniques and the study of glasses using the replica method started to develop rather fast.

In the picture glasses may freeze in many microscopically different configurations when we decrease the temperature. This statement is common to many other approaches [5, 6], however the replica approach gives us a panoplia of sophisticated physical and mathematical tools that strongly increase our ability to describe, study and compute analytically the properties of glasses.

These tools have been used to compute analytically in a detailed way the properties of toy models for the glass transition. Although theses models are very far from reality (the range of the forces is infinite) they display a very rich behaviour [7]: for example there is a soluble mean field model without quenched disorder where there is an equilibrium glass-liquid transition (Kauzmann transition [8]), a dynamical transition [9–11] (mode coupling transition [12] and, at an higher temperature, a liquid-crystal transition that cannot be seen in the dynamic of the system (starting from the liquid phase) unless we cool the system extremely slowly [13]. The existence of these soluble models is very precious to us; they provide a testing ground of new physical ideas, concepts, approximation schemes that are eventually used in more realistic cases.

The aim of these lectures is to present an introduction to the replica tools, to describe some of the technical details and to stress the physical ideas. The amount of work that has been done in the field is extremely large and here I have been forced to concentrate my attention only on a few points.

1.2 *Glassiness, metastability and hysteresis*

An essential feature of a glass system at the microscopic level is the existence of a corrugated free energy landscape. One may wonder which are the macroscopic counterparts of this property. A very important consequence is the presence of metastability in an open region of parameter space, a new and unusual phenomenon that can be experimentally studied in a carefully way.

Let us describe a non-glassy system where we have metastability. The simplest case is a system that undergoes a first order phase transition when we change a parameter. When the first order transition happens by changing

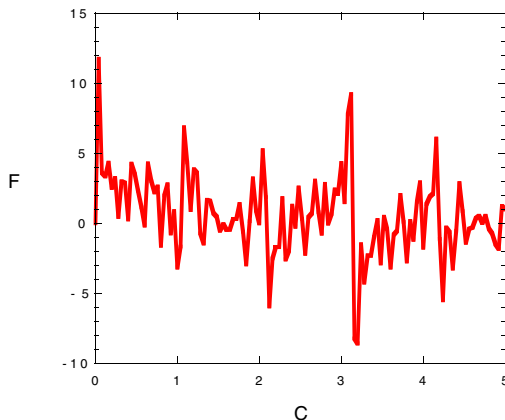


Fig. 1. An artistic view of the free energy of a system with corrugated free energy landscape as function of the configuration space.

the temperature, if we cool the systems sufficiently slowly, the high temperature phase survives also below the critical temperature up to the spinodal temperature.

In order to present a familiar example I will consider a system where the control parameter is the magnetic field h : the simplest case is the ferromagnetic Ising model. At low temperature the equilibrium magnetization $m(h)$ is given by $m(h) = m_s \text{sign}(h) + O(h)$ for small h (m_s being the spontaneous magnetization): the magnetization changes discontinuously at $h = 0$ in the low temperature phase where $m_s \neq 0$.

Let us consider a system that evolves with some kind of local dynamics. If we slowly change the magnetic field from positive to negative h , we enter in a metastable region where the magnetization is positive, and the magnetic field is negative. The system remains in this metastable state a quite large time, given by $\tau(h) \propto \exp(A/|h|^\alpha)$, where $\alpha = d - 1$ [14]. When the observation time is of order of $\tau(h)$ the system suddenly jumps into the stable state. This phenomenon is quite common: generally speaking we always enter into a metastable state when we cross a first order phase transition by changing some parameters.

If we start with the state where $m > 0$ at $h = 0$ and we add a *positive* magnetic field h at time 0, the linear response susceptibility is equal to

$$\chi_{\text{LR}} = \lim_{t \rightarrow \infty} \frac{\partial}{\partial h} m(t, h), \quad (1.1)$$

$m(t, h)$ being the magnetization at time t . Using general arguments we can

show that

$$\beta^{-1}\chi_{\text{LR}} = \lim_{h \rightarrow 0^+} \sum_i \langle \sigma(i)\sigma(0) \rangle^c \equiv \lim_{h \rightarrow 0^+} \sum_i (\langle \sigma(i)\sigma(0) \rangle - \langle \sigma(i) \rangle \langle \sigma(0) \rangle). \quad (1.2)$$

The linear response susceptibility is not equal to the equilibrium susceptibility that at h exactly equal to zero is infinite:

$$\chi_{\text{eq}} = \frac{\partial}{\partial h} \lim_{t \rightarrow \infty} m(t, h) \Big|_{h=0} \quad m_s = \frac{\partial}{\partial h} \text{sign}(h) \Big|_{h=0} = \infty. \quad (1.3)$$

Indeed

$$\chi_{\text{eq}}(h) = \chi_{\text{LR}}(h) + m_s \delta(h), \quad (1.4)$$

and the two susceptibilities χ_{eq} and χ_{LR} differs only at $h = 0$.

This is the usual stuff that is described in books [15]. We claim that in glassy systems the situation is different. For example in the case of glassy magnetic systems (*e.g.* spin glasses) there should be an open region in the space of parameters, where, if we change a parameter of the system (*e.g.* the magnetic field h) by an amount Δh , we have that $\chi_{\text{LR}} \neq \chi_{\text{eq}}$. We expect that for $|h| < h_c(T)$ we stay in the glassy phase¹.

In this region

$$\begin{aligned} \Delta m(t) &= \chi_{\text{LR}} \Delta h & \text{for } 1 \ll t \ll \tau(\Delta h), \\ \Delta m(t) &= \chi_{\text{eq}} \Delta h & \text{for } \tau(\Delta h) \ll t, \end{aligned} \quad (1.5)$$

where $\tau(\Delta h)$ may have a power like behaviour (*e.g.* $\tau(\Delta h) \propto |\Delta h|^{-4}$).

It is convenient to define the *irreversible* susceptibility by

$$\chi_{\text{eq}} = \chi_{\text{LR}} + \chi_{\text{irr}}. \quad (1.6)$$

The glassy phase is thus characterized by a non-zero value of χ_{irr} [2]. If we observe the system for a time less than $\tau(\Delta h)$, the behaviour of the system at a given point of the parameter space depends on the previous story of the system and strong hysteresis effects are present. I stress that, using the previous definitions, hysteresis and history dependence do not necessarily imply glassiness. Hysteresis may be present if the time scale for approaching equilibrium is very large (larger than the experimental time), but *finite*. Glassiness implies an equilibration time that is *arbitrarily large*. In other words hysteresis can be explained in terms of *finite* free energy barriers that may involve only a few degrees of freedom; glassiness implies

¹The function $h_c(T)$ increases when we decrease the temperature; $h_c(T)$ vanishes at the critical point.

the existence of *arbitrarily large* barriers that may arise only as a *collective* effect of many degrees of freedom.

From my point of view the aim of the theoretical study of glasses is to get a theoretical understanding of these effects and to arrive to a qualitative and quantitative control of these systems.

In these lecture I will address to various aspects of disorder systems using the replica approach. The replica formalism is a language for studying different properties of disordered systems: as any other language has some advantages and some disadvantages. The replica language has the advantage of being very compact and of putting the dirty under the carpet (thais may be also a disadvantage in some situations). In other words you can do computations in a very simple and effective manner, but sometimes it hard to understand the meaning of what are you doing. The formalism of replicas and replica symmetry breaking seems to be the most adequate to discuss from a thermodynamic point of view the situation where $\chi_{\text{irr}} \neq 0$.

The main physical problem I would like to understand is the characterization of the low temperature phase in structural glasses and in spin glasses. As you will shall see in these lectures and in Cugliandolo's lectures, the main characteristic is the presence of aging for the response [16–18]. Let us consider an aging experiment where the system is cooled at at time 0.

The response function $R(t, t_w)$ is the variation of the magnetization when we add an infinitesimal field at time t_w . Aging implies that the function $R(t, t_w)$ is not a constant in the region where t and t_w are *both* large; indeed we have

$$\begin{aligned} R(t, t_w) &= R_S \quad \text{for } t \ll t_w \\ R(t, t_w) &= R_E \quad \text{for } t \gg t_w. \end{aligned} \tag{1.7}$$

By definition $R_S = \chi_{\text{LR}}$ and the identification of R_E with χ_{eq} follows from general arguments that will discussed in Cugliandolo's lectures.

As we shall see later, replica symmetry is broken as soon $R_S \neq R_E$; we will assume that this happens in many glassy systems. This is what is experimentally seen in experiments done by humans using a value of t_w that is much shorter of their life time. These experiments are done for times that are much larger (15 or 20 order of magnitudo) that the microscopic time and many people do believe that aging in the response, *i.e.* $R_S \neq R_E$, survive in the limit where the waiting time goes to infinity.

One could also take the opposite point of view that aging is an artefact coming from doing the experiments at too short times and that aging would fades in the limits $t_w \rightarrow \infty$. This would be a quite different interpretation of the experiments; in these lecture I will stick to the hypothesis that aging is present and that R_S remains different from R_E also in the infinite time limit. Of course one could use experiments to decide which of the two hypothesis

is correct, however this must be done by extrapolating the experimental data and the discussion would be too long to be presented here: moreover, we should remember that quite often, due to practical limitations, the experiments, like the God whose siege is at Delphi, neither say nor hide, they hint.

1.3 *The organization of these lectures*

These lectures are organized as follows.

In Section 2, I will present the simplest model of a glassy system: the random energy model (REM); I will describe the analytic solution of this model using both a direct approach and the replica formalism.

In the next section I will study models with correlated disorder (*e.g.* p -spin models); the analytic solution of these models is much more complicated than that of the REM and it can be done using the replica formalism; in this framework the meaning of spontaneously broken replica symmetry is elucidated.

In Section 4, I will introduce a key concept of this (and of others) approaches: complexity (aka configurational entropy). A particular attention is given to the definition of this quantity: there is an intrinsic, albeit small, ambiguity in the value of the complexity that is present in short range model, but is absent in infinite range mean field models (if this ambiguity is neglected contradictory results may be obtained). Various methods, both analytic and numeric, are introduced to compute this fundamental quantity.

In the next section I will present some general structural properties: equilibrium stochastic stability and its dynamic extension that can be used to prove the generalized fluctuation dissipation relations that are described in more details in Cugliandolo's lectures.

In Section 6, I will present a very short introduction to the physics of structural glasses.

In the next section I will describe an analytic approach that can be used to do explicit first principles computations of the properties of glasses in the low energy phase. Different approximation techniques are illustrated.

In Section 8, I will present the results obtained using the techniques of the previous section for computing the properties of systems of interacting particles with a realistic potential. These analytic results compare in a favorable way to the numerical simulations.

Finally in the next section one finds a discussion of the open problems. Four appendices dedicated to technical problems close these lectures.

2 The random energy model

2.1 The definition of the model

The random energy model [19, 20] is the simplest model for glassy systems. It has various advantages: it is rather simple (its properties may be well understood with intuitive arguments, that may become fully rigorous) and it displays very interesting and new phenomena.

The random energy model is defined as following. There are N Ising spins (σ_i , $i = 1, N$) that may take values ± 1 ; the total number of configurations is equal to $M \equiv 2^N$: each configuration can be identified by a label s in the interval $1 - M$.

Generally speaking the Hamiltonian of the system is determined when we know all the values of the energies E_s , *i.e.* a value for each of the M configurations of the system. In many models there is an explicit expression for the energies as function of the configurations; on the contrary here the values of the E_s are random, with a probability distribution $p(E)$ that is Gaussian:

$$p(E) \propto \exp\left(-\frac{E^2}{2N}\right). \quad (2.1)$$

The energies are random uncorrelated Gaussian variables with zero average and variance equal to N .

The partition function is simply given by

$$Z_I = \sum_{s=1, M} \exp(-\beta E_s) = 2^N \int \rho_I(E) \exp(-\beta E), \quad (2.2)$$

$$\rho_I(E) \equiv 2^{-N} \sum_{s=1, M} \delta(E - E_s).$$

The values of the partition function and of the free energy density ($f_I = -\ln(Z_I)/(N\beta)$) depend on the instance I of the system, *i.e.* by all the values of the energies E_s . It can be proved that when $N \rightarrow \infty$ the dependance on I of f_I disappears with probability 1. As usual, the most likely value of f_I coincides with the average of f_I , where the average is done respect to all the possible instances of the system.

In the following I will indicate with a bar the average over the instances of the system:

$$\overline{A_I} \equiv \int d\mu(I) A(I), \quad (2.3)$$

where $\mu(I)$ is the probability distribution of the instances of the system. Using this notation we would like to compute

$$f = \overline{f_I} \quad (2.4)$$

and to prove that

$$\overline{(f_I - f)^2} \rightarrow_{N \rightarrow \infty} 0. \quad (2.5)$$

The model is enough simple to be studied in great details; exact expressions can be derived also for finite N . In the next section we will give the main results without entering too much into the details of the computation.

2.2 Equilibrium properties of the model

The first quantity that we can compute is $\overline{Z_I}$. We have immediately

$$\overline{Z_I} = \sum_s \overline{\exp(-\beta E_s)} = 2^N \exp\left(\frac{N}{2}\beta^2\right). \quad (2.6)$$

However the physically interesting quantity is $\overline{\ln(Z_I)}$, that is related to the average of the free energy:

$$-N\beta f = \overline{\ln(Z_I)}. \quad (2.7)$$

If we make to bold assumption that

$$\overline{\ln(Z_I)} = \ln(\overline{Z_I}) \quad (2.8)$$

(this approximation is usually called the annealed approximation), we find that

$$\overline{\ln(Z_I)} = N \left(\ln(2) + \frac{1}{2}\beta^2 \right). \quad (2.9)$$

Generally speaking the relation equation (2.8) is not justified. In this model it gives the correct results in the high temperature phase, but it fails in the low temperature phase. For example, as we shall see later, at low temperature we must have that the quantity

$$G = -\frac{\partial}{\partial \beta} \ln(\overline{Z_I}) = \frac{\int d\mu(I) Z_I \langle E \rangle_I}{\int d\mu(I) Z_I} \quad (2.10)$$

is different from the physically interesting quantity

$$E = -\frac{\partial}{\partial \beta} \overline{\ln(Z_I)} = \int d\mu(I) \langle E \rangle_I, \quad (2.11)$$

where $\langle E \rangle_I$ is the expectation of the energy in the instance I of the problem:

$$\langle E \rangle_I = \frac{\sum_s \exp(-\beta E_s) E_s}{\sum_s \exp(-\beta E_s)}. \quad (2.12)$$

In the computation of G we give to the different systems a weight equal to the partition function Z_I that is exponentially large (or small) and strongly fluctuates from system to system. The correct results E is obtained using the correct (flat) weight $d\mu(I)$.

One can argue (and it will be done later on in Sect. 2.4) that the previous derivation gives the correct form for the free energy in the low β region. However the previous results cannot be correct everywhere. If we identify G with E and we compute the energy density of the model using (Eq. (2.9)), we find

$$e = \beta \quad (2.13)$$

that superficially is not contradictory. However, if we use this expression for the energy to compute the entropy density, we find

$$S(\beta) = -\beta^2 \frac{\partial f(\beta)}{\partial \beta} = \ln(2) - \frac{1}{2\beta^2}. \quad (2.14)$$

This entropy density becomes negative for

$$\beta > \beta_c = \sqrt{2\ln(2)}. \quad (2.15)$$

This is a major inconsistency in a model where the configuration space is discrete and the entropy must be a non-negative quantity.

The arguments we have used in deriving equation (2.9) are not solid. We have computed the asymptotic behaviour of Z_n for positive integer n when the volume goes to infinity, but we cannot argue that the asymptotic behaviour is an analytic function of n . A simple counterexample is given by

$$\sinh(Nn) \approx \exp(N|n|). \quad (2.16)$$

The non-analyticity of the free energy density as functions of a parameter in the infinite volume limit is the essence of phase transitions. It is quite possible that at low temperatures a phase transition in n is present in the interval $0 \leq n \leq 1$, so that the extrapolation of the free energy density from $n \geq 1$ to $n = 0$ has nothing to do with the value of the free energy computed directly at $n = 0$.

There is a simple way to find the correct result [19, 20]. The probability of finding a configuration of energy in the interval $[E, E + dE]$ is given by

$$\mathcal{N}_0(E)dE, \quad (2.17)$$

where

$$\mathcal{N}_0(E) \equiv 2^N \exp\left(-\frac{E^2}{2N}\right) = \exp\left(N\left(\ln(2) - \frac{1}{2}e^2\right)\right), \quad (2.18)$$

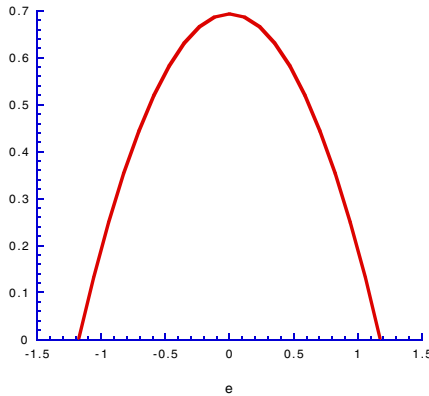


Fig. 2. The quantity $\ln(N_0(e))/N$ as function of the energy density e outside the interval the function $\mathcal{N}_0(e)$ is zero.

and $e \equiv E/N$ is the energy density. In the case of a generic system (with probability 1 when $N \rightarrow \infty$) no configurations are present in the region where $\mathcal{N}_0(E) \ll 1$, *i.e.* for

$$e^2 < e_c^2 \equiv 2\ln(2). \quad (2.19)$$

Neglecting prefactors, the average total number of configurations of energy less than e (when $e < 0$) is given by

$$\int_{-\infty}^{Ne} dE \mathcal{N}_0(E) \approx \exp \left(N \left(\ln(2) - \frac{1}{2} e^2 \right) \right). \quad (2.20)$$

This number becomes exponentially small as soon $e < e_c$, implying that for a generic system there are no configurations for $e < e_c$. We can thus write for a generic instance of the system the following relation:

$$\rho(E) \approx \mathcal{N}(E) \equiv \mathcal{N}_0(E) \theta(E_c^2 - E^2). \quad (2.21)$$

The partition function can be written as

$$\int \mathcal{N}(E) \exp(-\beta E). \quad (2.22)$$

Evaluating the integral with the saddle point method we find that in the high temperature region, *i.e.* for $\beta < \beta_c \equiv e_c^{-1}$, the internal energy density is simple given by $-\beta$. This behaviour must end somewhere because we know that the energy is bounded from below by $-e_c$. In the low temperature

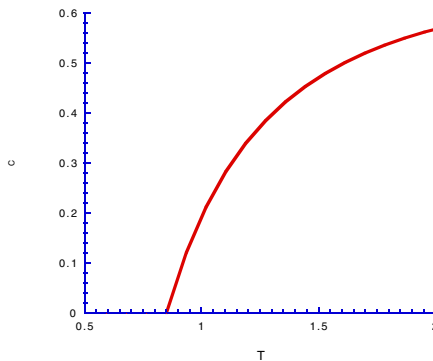


Fig. 3. The entropy density as function of the temperature.

region the integral is dominated by the boundary region $E \approx E_c$ and the energy density is exactly given by $-e_c$.

The point where the high temperature behaviour breaks down is exactly the point where the entropy becomes negative. The entropy density is positive in the high temperature region, vanishes at β_c and remains zero in the low temperature region. In the high temperature region an exponentially large number of configurations contributes to the partition function, while in the low temperature region the probability is concentrated on a finite number of configurations [20].

It is interesting to notice that in the low temperature phase the free energy is higher than the continuation from high temperature. This is the opposite of the usual situation: in conventional mean field for non-disordered systems (*e.g.* ferromagnets) the low temperature free energy is lower than the continuation from high temperature². This correspond to a jump *upward* of the specific heat when we decrease the temperature, while in the REM (and in real glasses) there is jump *downward* of the specific heat. The system has less configurations of what can be inferred from the behaviour at entropy at high temperature: some part of the predicted phase space is missing and consequently the free energy is higher than the analytic continuation of the high temperature results. This entropy crisis is the essence of the Kauzmann transition [8].

A more precise (and less hand-waving) computation can be done by

²If two branches of the free energy are present usually the relevant one has the lower free energy. We shall see later that this is not the case in glassy systems.

using the representation

$$\ln(Z) = \int_0^\infty \frac{\exp(-t) - \exp(-tZ)}{t} dt \quad (2.23)$$

and writing

$$\overline{\exp(-tZ)} = \sum_{n=0, \infty} \frac{(-tZ^n)}{n!}. \quad (2.24)$$

The quantities $\overline{Z^n}$ can be computed exactly and in this way we can also estimate the finite N corrections to the asymptotic behaviour. The details of this computation can be found in [20].

2.3 The properties of the low temperature phase

It is worthwhile to study the structure of the configurations that mostly contribute to the partition function in the lower temperature phase. The detailed computation of the finite N corrections [20] shows that in the low temperature phase the average total entropy has a value that remains finite in the limit $N \rightarrow \infty$:

$$S_T = \Gamma'(1) - \frac{\Gamma'(1-m)}{\Gamma(1-m)} \quad (2.25)$$

where the quantity m is given by

$$m = \beta_c/\beta = T/T_c. \quad (2.26)$$

The parameter m is always less the one in the whole temperature phase.

The finiteness of the total entropy implies that the probability distribution is concentrated on a finite number of configurations (see Eq. (2.38)) also in the limit $N \rightarrow \infty$. In order to study the contributions of the different configurations to the free energy, it is useful to sort the configurations with ascending energy. We relabel the configurations and we introduce new labels such that $E_k < E_i$ for $k < i$.

It is convenient to introduce the probability w_k that the system is in the configuration k ;

$$w_k \equiv \frac{\exp(-\beta E_k)}{Z}. \quad (2.27)$$

It is obvious that the w_k form a decreasing sequence and that

$$\sum_{k=1, 2^N} w_k = 1. \quad (2.28)$$

Here the probability of finding an energy E_k in the interval $[E, E + dE]$, not far from the ground state energy E_1 is given by

$$\rho(E) \approx \exp(\beta_c(E - E^*)) = \exp(\beta m(E - E^*)) \quad (2.29)$$

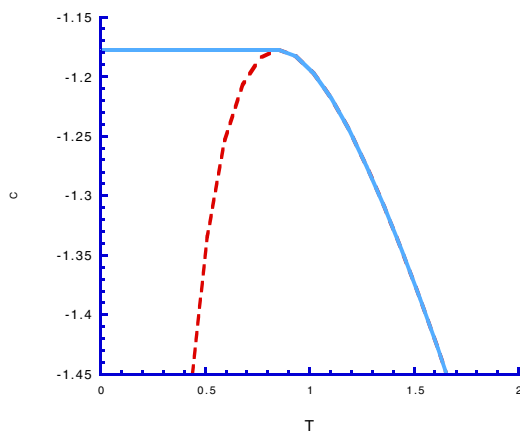


Fig. 4. The free energy density as function of the temperature and the analytic continuation of the high temperature result (dashed).

where E^* is a reference energy not far from the ground state (the parameter m controls the local exponential growth of the density of configurations). It is not difficult to prove [21] that, if we define

$$\Delta = \beta_c(E_1 - E^*), \quad (2.30)$$

the probability distribution of Δ is given by the Gumbel law:

$$P(\Delta) = \exp(\Delta - \exp(\Delta)). \quad (2.31)$$

It is somewhat more difficult³ to prove that probability of finding one of the variables w in the interval $[w, w + dw]$ is given

$$\begin{aligned} \nu(w) &= C w^{-1-m} (1-w)^{-1+m} dw, \\ C &= \frac{1}{\Gamma(m)\Gamma(1-m)} \end{aligned} \quad (2.32)$$

where the proportionality factor can be easily found using the condition

$$\int_0^1 dw \nu(w) = 1. \quad (2.33)$$

Now it is easy to compute

$$\int dw \nu(w) w^k = \frac{\Gamma(k-m)}{\Gamma(1-m)\Gamma(k)}. \quad (2.34)$$

³The proof sketched in one of the Appendices.

As particular cases we get

$$\int dw \nu(w) w^2 = 1 - m, \quad \int \nu(w) w^3 = \frac{(1 - m)(2 - m)}{2}. \quad (2.35)$$

We can check that the total entropy is given by

$$S_T = - \int dw \nu(w) w \ln(w). \quad (2.36)$$

The integral

$$\int_0^1 dw \nu(w) \quad (2.37)$$

is divergent, signaling that there are an infinite number of w 's.

A detailed computation [2, 20, 22] shows that a finite number of terms dominates the sum over k . Indeed using the explicit form of $\nu(w)$ near $w = 0$ we get that

$$\sum_{k=1, L} w_k = 1 - O(L^{-\lambda}), \quad \lambda = \frac{1 - m}{m}. \quad (2.38)$$

In this model everything is clear: in the high temperature region the number of relevant configurations is infinite (as usual) and there is a transition to a low temperature region where only few configuration dominates.

The fact that the low temperature probability distribution is dominated by a few configurations can be seen also in the following way. We introduce a distance among two configurations α and γ as

$$d^2(\alpha, \gamma) \equiv \frac{\sum_{i=1, N} (\sigma_i^\alpha - \sigma_i^\gamma)^2}{2n}. \quad (2.39)$$

We also introduce the overlap q defined as

$$q(\alpha, \gamma) \equiv \frac{\sum_{i=1, N} \sigma_i^\alpha \sigma_i^\gamma}{2N} = 1 - d^2(\alpha, \gamma). \quad (2.40)$$

The distance squared is normalized in such a way that it spans the interval 0–2. It is equal to

- 0, if the two configuration are equal ($q = 1$);
- 1, if the configuration are orthogonal ($q = 0$);
- 2, if $\sigma_i^\alpha = -\sigma_i^\gamma$ ($q = -1$).

We now consider the function $Q(d)$ and $P(q)$, *i.e.* the probability that two equilibrium configurations are at distance d or overlap q respectively. We find

- for $T > T_c$

$$Q(d) = \delta(d-1), \quad P(q) = \delta(q); \quad (2.41)$$

- for $T < T_c$

$$Q(d) = (1-A)\delta(d-1) + A\delta(d), \quad P(q) = (1-A)\delta(q) + A\delta(q-1) \quad (2.42)$$

where for each system (I) A_I is equal to $\sum_{k=1,2^N} w_k^2$. The average of A_I over the different realizations of system is equal to $1 - m$.

As soon as we enter in the low temperature region, the probability of finding two equal configurations is not zero. The transition is quite strange from the thermodynamic point of view.

- It looks like a *second* order transition because there is no latent heat. It is characterized by a jump in the specific heat (that decreases going toward low temperatures).
- It looks like a *first* order transition. There are no divergent susceptibilities coming from above or from below (in short range models this result implies that there is no divergent correlation length). Moreover the minimum value of d among two equilibrium configurations jumps discontinuously (from 1 to 0).
- If we consider a system composed by two replicas (σ^1 and σ^2) [23] and we write the Hamiltonian

$$H(\sigma^1, \sigma^2) = H(\sigma^1) + H(\sigma^2) + N\epsilon d^2(\sigma^1, \sigma^2) \quad (2.43)$$

for $\epsilon = 0$ the free energy is equal to that of the previous model (apart a factor 2) but we find a real first order thermodynamic transition, with a discontinuity in the internal energy, as soon as $\epsilon > 0$. The case $\epsilon = 0$ is thus the limiting case of a *bona fide* first order transitions.

These strange characteristics can be summarized by saying that the transition is of order one and a half, because it shares some characteristics with both the first order and the second order transitions.

It is impressive to note that the thermodynamic behaviour of real glasses near T_c is very similar to the order one and a half transition of REM. We will see later that this behaviour is also typical of the mean field approximation to glassy systems.

2.4 A careful analysis of the high temperature phase

Let us now try to justify more carefully the correctness of equation (2.8) in the high temperature phase [20].

We can firstly compute the quantity

$$Z_2 \equiv \overline{Z_I^2} = \overline{\sum_{s,s'} \exp(-\beta E_s - \beta E_{s'})}. \quad (2.44)$$

If we consider separately the terms with $s = s'$ and those with $s \neq s'$, we easily get

$$Z_2 = 2^N(2^N - 1) \exp(2A) + 2^N \exp(4A) \approx 2^{2N} \exp(2A) + 2^N \exp(4A), \quad (2.45)$$

where we have used the relation

$$\int p(E) dE \exp(m\beta E) = \exp(m^2 A), \quad (2.46)$$

with

$$A = \frac{N}{2} \beta^2. \quad (2.47)$$

In a similar way we can compute $\overline{Z_I^3}$: we neglect terms that are proportional to 2^{-N} and we separate terms with all indices equal, terms with all the indices different and terms with two indices equal and one different; finally we find that

$$Z_3 \equiv \overline{Z_I^3} \approx 2^{3N} \exp(3A) + 3 \cdot 2^{2N} \exp((4+1)A) + 2^N \exp(9A). \quad (2.48)$$

Generally speaking, using the multifactorial formula and taking the leading contribution for each term

$$Z_n \equiv \overline{Z_I^n} = \sum_l \sum_{\{m_i\}} \frac{n!}{l! \prod_{i=1}^l m_i!} 2^{lN} \exp(m_i^2 A), \quad (2.49)$$

where the constraint $\sum_{i=1}^l m_i = n$ is satisfied. The previous formula can be derived by writing

$$Z_I^n = \sum_{s_1 \dots s_n} \exp \left(\beta \sum_{a=1, n} E_{s_a} \right). \quad (2.50)$$

We now divide the n indices in l sets of size m_i and estimate the contribution from each set, that is given by

$$\overline{Z_I^{m_i}} = 2^N \exp(m_i^2 A). \quad (2.51)$$

The final results equation (2.49) is obtained by multiplying the contribution of each set and adding the a prefactor (*i.e.* $n!/(l! \prod_{i=1, l} m_i!)$) that has a combinatorial origine. It is a simple exercise to check that the previous formula reduce to the one that we have written for $n = 1, 2, 3$.

The previous formula can also written as

$$Z_n = \sum_l \sum_{\{m_i\}} \frac{n!}{l! \prod_{i=1}^l m_i!} \exp \left(N \sum_{i=1, l} G(m_i) \right) \quad (2.52)$$

where

$$G(m_i) = \ln(2) + A m_i^2. \quad (2.53)$$

For small β and for n not too large the term $l = n$ and $m_i = 1 \forall i$ is dominating: it gives that

$$Z_n \approx \exp(Nn(\ln 2 + A)). \quad (2.54)$$

We can now use the relation

$$\overline{\ln(Z)} = \lim_{n \rightarrow 0} \frac{\ln(\overline{Z^n})}{n} \quad (2.55)$$

and apply the previous formula also for non-integer n up to $n = 0$. In this way one finds that

$$\frac{\overline{\ln(Z)}}{N} = \ln 2 + A = \ln 2 + \frac{1}{2} \beta^2, \quad (2.56)$$

and therefore

$$f(\beta) = -\frac{\ln(2)}{\beta} - \frac{1}{2} \beta. \quad (2.57)$$

The same results can be obtained *manually* by writing

$$Z = 2^N - \beta \sum_s E_s + \frac{\beta^2}{2} \sum_s E_s^2 + \dots \quad (2.58)$$

This gives

$$\ln(Z) = N \ln 2 - \beta \frac{\sum_s E_s}{2^N} - \frac{1}{2} \beta^2 \left(\frac{\sum_s E_s}{2^N} \right)^2 + \frac{1}{2} \beta^2 \frac{\sum_s E_s^2}{2^N} + \dots \quad (2.59)$$

Only the first and the last term contribute in the limit $N \rightarrow \infty$ (the energies have zero average and their number is 2^N); a careful evaluation shows that the remaining terms give a vanishing contribution.

2.5 The replica method

We may wonder if the previous results in the low energy phase may be obtained by starting from equation (2.49) and by partitioning the replicas using an appropriate choice of the variables m_i that indicates the size of the different sets (or blocks).

The correct choice in the high temperature region was $m_i = 1$. An alternative choice (that is highly symmetric) is $m_i = m$. The total number of partitions l is given by n/m . This saddle point gives a contribution [2,20]

$$Z_n \approx \exp \left(N n \left(\frac{\ln(2)}{m} + m A \right) \right), \quad (2.60)$$

that correspond to

$$-\beta \bar{f} = F(m) \equiv \frac{G(m)}{m} = \frac{\ln(2)}{m} + \frac{1}{2} \beta^2 m. \quad (2.61)$$

The value of m is arbitrary. It is surprising that in the low temperature phase the correct result for the free energy is obtained by taking the maximum⁴ of $F(m)$ with respect to m , and the maximum is found in the interval 0–1 (in the high temperature phase the correct result is given $F(1)$).

This prescription can look rather strange, but we can test some consequences of this approach for other quantities. At this end we take two replicas of the same system and we compute the probability that these two configurations are the same using this approach and we compare with the known results.

Before going on we have to make a general remark. The average over the samples of the statistical averages can be simply obtained by computing the average over an ensemble of n replicas of the same system and taking

⁴If the correct results are given by the saddle point where the replicas are partitioned in equal size blocks (with $m \neq 1$) we will say that the replica is broken at one step.

the limit $n \rightarrow 0$ at the end. The precise statement is the following:

$$\begin{aligned} \overline{\langle A(\sigma) \rangle} &\equiv \overline{\left(\frac{\sum_{\sigma} A(\sigma) \exp(-\beta H(\sigma))}{\sum_{\sigma} \exp(-\beta H(\sigma))} \right)} \\ &= \lim_{n \rightarrow 0} \frac{\overline{\sum_{\sigma_1 \dots \sigma_n} A(\sigma_1) \exp(-\beta \sum_{a=1, n} H(\sigma_a))}}{\overline{\sum_{\sigma_1 \dots \sigma_n} \exp(-\beta \sum_{a=1, n} H(\sigma_a))}}. \end{aligned} \quad (2.62)$$

Indeed the last term is equal to

$$\frac{\overline{\sum_{\sigma} A(\sigma) \exp(-\beta H(\sigma)) (\sum_{\sigma} \exp(-\beta H(\sigma)))^{n-1}}}{\overline{(\sum_{\sigma} \exp(-\beta H(\sigma)))^n}}. \quad (2.63)$$

In the limit $n \rightarrow 0$ we recover the previous equation. A similar argument tells us that

$$\overline{F} = -\frac{\overline{\ln(Z)}}{\beta N} = \lim_{n \rightarrow 0} F^{(n)}, \quad (2.64)$$

where

$$F^{(n)} = -\frac{\ln(\overline{Z^n})}{\beta n N}. \quad (2.65)$$

Here to proof can be easily done by using $Z^n \approx 1 + n \ln(Z)$ and the obvious relation $\overline{1} = 1$.

We can follow the same strategy for computing quantities that depend on a pair of replicas. Let us define:

$$w^{(2)}(n) = \frac{\overline{\sum_{s_1 \dots s_n} \exp(-\beta \sum_{a=1, n} E(s_a)) \delta_{s_1, s_2}}}{\overline{\sum_{s_1 \dots s_n} \exp(-\beta \sum_{a=1, n} E(s_a))}}. \quad (2.66)$$

Also in this case we find

$$\sum_{k=1, \infty} w_k^{(2)} \equiv w^{(2)} = \lim_{n \rightarrow 0} w^{(2)}(n). \quad (2.67)$$

Indeed we can write that

$$w^{(2)}(n) = \frac{\overline{\sum_s \exp(-\beta 2E(s)) (\sum_s \exp(-\beta 2E(s)))^{n-2}}}{\overline{(\sum_s \exp(-\beta E(s)))^n}}. \quad (2.68)$$

Let us now compute $w_2(n)$ by considering the contribution of the saddle point where all the m_i are equal to m [2]. In this case $w_2(n)$ is given by the probability of finding the replicas 1 and 2 inside the same block when we average over the ways in which one can divide the n replicas into n/m

blocks of size m . The computation looks complex, but it greatly simplifies by noticing that this probability does not depend on the two replicas (1 and 2) that we are actually considering: it coincides with the probability that for a given partition, two random replicas stay in the same block. A simple computation tells us that this probability is given by

$$w_2(n) = \frac{n(m-1)}{n(n-1)}. \quad (2.69)$$

Indeed the first replica is arbitrary and the second replica is any of the remaining $m-1$ replicas of the block. The denominator is the total number of unordered pairs of replicas. In the limit $n \rightarrow 0$ we recover the correct result:

$$w_2 = 1 - m. \quad (2.70)$$

In the similar way we find

$$w_3 = \lim_{n \rightarrow 0} \frac{n(m-1)(m-2)}{n(n-1)(n-2)} = \frac{(1-m)(2-m)}{2} = \frac{\Gamma(3-m)}{\Gamma(1-m)\Gamma(3)}. \quad (2.71)$$

The computation can be trivially done for any k and from the moments we recover the distribution probability $\nu(w)$.

At this stage it is not clear why we have chosen this form of the m_i and not a different one. However it is clear from the previous computations that the choice of the m_i codes the probability distribution of the w and the situation where the logarithms of the w 's are uncorrelated identically distributed variables with an exponential distribution correspond to $m_i = m$. Different situations may correspond to different forms of the m_i , but the one that is relevant here corresponds to constants m_i . For other purposes, *i.e.* for finding finite size corrections or exponentially vanishing probabilities, different choices of the m_i are relevant [24]. It may be interesting to remark that the one that we have taken here is in some sense the maximally symmetric one if we exclude the trivial choice $m_i = 1$.

2.6 Dynamical properties of the model

The dynamical properties of the model can be easily investigated in a qualitative way. Interesting behavior is present only in the region where the value of N is large with respect to the time, but it will not be discussed here.

We consider here a single spin flip dynamics. More precisely we assume that in a microscopic time scale the system explores all the configurations that differ from the original one by a single spin flip and it moves to one of them (or remains in the original one) with probability that is proportional to $\exp(-\beta H)$. This behaviour is typical of many dynamical processes, like Glauber dynamics, Monte Carlo, heat bath.

In this dynamical process each configuration C has N nearby configurations C' to explore. The energies of the configurations C' are uncorrelated to the energy of C , so that they are of order $N^{1/2}$ in most of the case. A simple computation gives that lowest energy of the configurations C' would be of order $-(N\ln(N))^{1/2}$. The important point is that the corresponding energy density $-(\ln(N)/N)^{1/2}$ vanishes in the large N limit.

If the configuration C has an energy density e less than zero, the time needed to do a transition to a nearby configuration will be, with probability one, exponentially large. For finite times at large N a configuration of energy $e < 0$ is completely frozen. Only at times larger than $\exp(\beta e N)$ it may jump to a typical configuration of energy zero. At later times different behaviours are possible: the configuration comes back to the original configuration of energy e or, after some wandering in the region of configurations of energy density ≈ 0 , it falls in another deep minimum of energy e' . A computation of the probabilities for these different possibilities has not yet been done, although it should not be too difficult.

The conclusions of this analysis are quite simple.

- Every configuration of energy $e < 0$ is a deep local minimum of the Hamiltonian: if we flip one spin, the energy increases of a large quantity ($\approx eN$).
- If we start from a random configuration, after a time that is finite when $N \rightarrow \infty$, the system goes to a configuration whose energy is of order $-\ln(N)^{1/2}$ and stops there.
- If we start from a random configuration, only at exponentially large times the system will reach an energy density that is different from zero.

3 Models with partially correlated energy

3.1 The definition of the models

The random energy model (REM) is rather unrealistic in that it predicts that the energy is completely upset by a single spin flip. This feature can be eliminated by considering more refined models, *e.g.* the so called p -spins models [25, 26], where the energies of nearby configurations are also nearby. We could say that energy density (as function of the configurations) is not a continuous function in the REM, while it is continuous in the p -spins models, in the topology induced by the distance, equation (2.39). In this new case some of the essential properties of the REM are valid, but new features are present.

The Hamiltonian of the p -spins models depends on some control variables J , that have a Gaussian distribution and play the same role of the random energies of the REM and by the spin variables σ . For $p = 1, 2, 3$ the Hamiltonian is respectively given by

$$H_J^1(\sigma) = \sum_{i=1, N} J_i \sigma_i, \quad (3.1)$$

$$H_J^2(\sigma) = \sum_{i, k=1, N}^I J_{i, k} \sigma_i \sigma_k, \quad (3.2)$$

$$H_J^3(\sigma) = \sqrt{p!/2} \sum_{i, k, l=1, N}^I J_{i, k, l} \sigma_i \sigma_k \sigma_l,$$

where the primed sum indicates that all the indices are different and ordered. The variables J must have a variance of $(N^{(1-p)/2})$ if the system has a non-trivial thermodynamical limit. Here we will study the hard spin models [7] where $\sigma_i = \pm 1$ ⁵.

It is possible to prove by an explicit computation that, if we send first $N \rightarrow \infty$ and later $p \rightarrow \infty$, one recover the REM [25]. Indeed the energy is normalized in such a way that it remains finite when $p \rightarrow \infty$; however the differences in energy corresponding to one spin flip are of order \sqrt{p} for large p (they are order N in the REM), so that in the limit $p \rightarrow \infty$ the energies in nearby configurations become uncorrelated and the REM is recovered.

3.2 The replica solution

The main new property of the p spin model is the presence of a correlation among the energies of nearby configurations. This fact implies that if C is a typical equilibrium configuration, all the configurations that differ from it by a finite number of spin flips will differ in energy by a bounded amount, also for very large N . The equilibrium configurations are no more isolated (as in REM), but they belong to valleys: the entropy restricted to a single valley is proportional to N and it is an extensive quantity.

We can now proceed as before⁶. The computation of $Z_n = \overline{Z^n}$ can be done by introducing n replicas [2, 26]. After the Gaussian integration over

⁵A different well studied model is the spherical model [9, 11, 23], that has the same Hamiltonian: however the spins are real variables that satisfy the constraints $\sum_i \sigma_i^2 = N$. The spherical model has many features in common with the hard spin model and some computations are simpler.

⁶In this case we must use some technical tools that are also used in the study of the infinite range ferromagnetic model, described in the Appendix.

the J one gets

$$Z_n = \sum_{\Sigma} \exp \left(\frac{1}{2} N \beta^2 \sum_{a,b=1,n} Q_{a,b}(\Sigma)^p \right), \quad (3.3)$$

where Σ denotes the set of all nN σ variables and

$$Q_{a,b}(\Sigma) = N^{-1} \sum_{i=1,N} \sigma_a(i) \sigma_b(i). \quad (3.4)$$

If we introduce the Lagrange multiplier $\Lambda_{a,b}$ we find that the previous expression reduces to

$$Z_n = \int dq d\Lambda \sum_{\Sigma} \exp \left(\frac{1}{2} N \beta^2 \sum_{a,b=1,n} q_{a,b}^p + N \sum_{a,b=1,n} \Lambda_{a,b} (Q_{a,b}(\Sigma) - q_{a,b}) \right), \quad (3.5)$$

where both q and Λ are $n \times n$ symmetric matrices and the integrals dq and $d\Lambda$ runs over these matrices⁷ The sum over the spins can be done in each point independently from the other point using the relation

$$\exp \left(N \sum_{a,b=1,n} \Lambda_{a,b} (Q_{a,b}(\Sigma)) \right) = \exp \left(\sum_{i=1,N} \sum_{a,b=1,n} \Lambda_{a,b} \sigma_a(i) \sigma_b(k) \right). \quad (3.6)$$

Finally we get the result:

$$\int dq \exp \left(N \left(\frac{1}{2} \beta^2 \sum_{a,b=1,n} q_{a,b}^p + G(\Lambda) - q_{a,b} \right) \right) \quad (3.7)$$

where

$$\exp(G(\Lambda)) = \sum_{\sigma} \exp \left(\sum_{a,b=1,n} \Lambda_{a,b} \sigma_a \sigma_b \right). \quad (3.8)$$

⁷The integrals over the variables $\Lambda_{a,b}$ is along the imaginary axis and goes from $-i\infty$ to $+i\infty$.

In the limit $N \rightarrow \infty$ the previous integral is dominated by the saddle point. We have to find out the solution of the equations

$$\begin{aligned} \frac{p\beta^2 q_{a,b}^{p-1}}{2} &= \Lambda_{a,b}, \\ q_{a,b} &= \langle \sigma_a \sigma_b \rangle_\Lambda, \end{aligned} \quad (3.9)$$

where

$$\langle \sigma_c \sigma_d \rangle_\Lambda = \frac{\partial G(\Lambda)}{\partial \Lambda_{c,d}} = \frac{\sum_\sigma \exp(\sum_{a,b=1,n} \Lambda_{a,b} \sigma_a \sigma_b) \sigma_c \sigma_d}{\sum_\sigma \exp(\sum_{a,b=1,n} \Lambda_{a,b} \sigma_a \sigma_b)}. \quad (3.10)$$

The free energy density (per replica) is given by

$$f_n = \frac{-1}{-\beta n} \left(\frac{1}{2} \beta^2 \sum_{a,b=1,n} q_{a,b}^p + G(\Lambda) - \sum_{a,b=1,n} \Lambda_{a,b} q_{a,b} \right). \quad (3.11)$$

The internal energy density is given by deriving $\beta f_n(\beta)$ with respect to β . One finds:

$$E = \frac{1}{n} \beta \sum_{a,b=1,n} q_{a,b}^p. \quad (3.12)$$

In the high temperature phase we have that the only solution to the saddle equations is

$$\begin{aligned} q_{a,b} &= 0 \quad \text{for } a \neq b \\ q_{a,b} &= 1 \quad \text{for } a = b. \end{aligned} \quad (3.13)$$

The corresponding value of the internal energy is given by

$$E = -\beta. \quad (3.14)$$

Also in this model the high temperature results cannot be true for all β because it leads to a negative entropy at low temperatures.

$$\frac{\partial f}{\partial m} = \frac{\partial f}{\partial q} = 0. \quad (3.15)$$

Following the approach of the previous section we divide the n indices into sets of m indices and we put $q_{a,b} = q$ if a and b belongs to the same set and $q_{a,b} = 0$ if a and b do not belong to the same set. (Obviously $q_{a,a}$ must be equal to $\sigma^2 = 1$.) In the same way $\Lambda_{a,b} = \Lambda$, if a and b belongs to the same set, and $\Lambda_{a,b} = 0$, if a and b do not belong to the same set. Now the

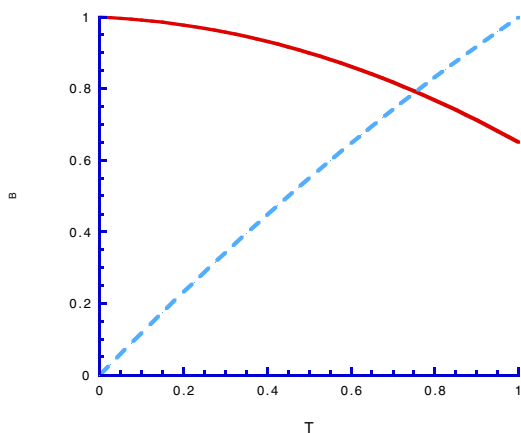


Fig. 5. The qualitative behaviour quantity q_{EA} and m (dashed line) as functions of the temperature (in units of T_c) in the p spin model for $p > 2$.

computation in equation (3.10) can be done independently for each set of m replicas. The typical quantity we have to evaluate is

$$\begin{aligned} \sum_{\sigma} \exp \left(\sum_{a,b=1,m} \frac{1}{2} \Lambda \sigma_a \sigma_b \right) &= \sum_{\sigma} \exp \left(\frac{1}{2} \Lambda \left(\sum_{a=1,m} \sigma_a \right)^2 \right) \\ &= \int d\mu(h) \exp \left(\sqrt{\Lambda} h \left(\sum_{a=1,m} \sigma_a \right) \right) = \int d\mu(h) \cosh(\sqrt{\Lambda} h)^m \end{aligned} \quad (3.16)$$

where h is a Gaussian variable with variance one:

$$d\mu(h) = (2\pi)^{-1/2} \exp(-h^2/2). \quad (3.17)$$

We finally find the equations

$$\begin{aligned} \frac{p\beta^2 q^{p-1}}{2} &= \Lambda \\ q &= \frac{\int d\mu(h) \cosh(\sqrt{\Lambda} h)^m \tanh^2(\sqrt{\Lambda} h)}{\int d\mu(h) \cosh(\sqrt{\Lambda} h)^m}. \end{aligned} \quad (3.18)$$

For each value of m we can find a solutions (or more solutions) to the previous equations and we can compute the corresponding free energy. If we use the same prescription than in the REM the correct solution is the maximum of the free energy as function of m for $0 \leq m \leq 1$. In other words we obtain a function $F(m)$ that we have to maximize. It may looks

strange to maximize the free energy, but this is what we need if the final free energy must be *higher* of the one computed in the high temperature phase, *i.e.* $F(1)$. Moreover there is a rigorous theorem, recently proved by Guerra [27], that the true free energy f satisfies the relation

$$f \geq \max_{0 \leq m \leq 1} F(m) \quad (3.19)$$

so *maximization*, and not *minimization*, of the free energy is the natural prescription in this situation [2].

In general, after having eliminated Λ the free energy can be written as function of m and q ($f(q, m)$) and the value of these two parameters satisfy the stationarity equations:

If we consider the case $p > 2$, we find that for $T < T_c$ there is a solution where the value of q at the maximum of $f(q, m)$ (that we will call q_{EA}) is different from zero. The value of q_{EA} jumps at T_c to a non-zero value. For large values of p the quantity q_{EA} (q_{EA} would be 1 in the REM) is of order $1 - \exp(-A\beta p)$, while the parameter m has the same dependence on the temperature as in the REM, *i.e.* it is equal to 1 at the critical temperature and has a linear behaviour at low temperature. When p is finite m is no more strictly linear as function of the temperature. The thermodynamical properties of the model are the same as in the REM: a discontinuity in the specific heat, with no divergent susceptibilities.

The case $p = 2$ (the Sherrington Kirkpatrick model [28] that is relevant for spin glasses) has a different behaviour especially near the critical temperature (see Fig. 6).

3.3 The physical interpretation

Also in these models for each instance I we can define the function $P_I(q)$ and compute its average over the different realization of the system. The computation goes on exactly in the same way as in the REM. For example let us consider

$$\overline{\int P_I(q)q} = \overline{\left\langle \frac{\sum_i \sigma_i^a \sigma_i^b}{N} \right\rangle} \quad (3.20)$$

where the values of the replica indices (*i.e.* a and b) do not matter, as far as they are different. In the same way as before we average over all the ways in which we can assign the two replicas to different blocks. We find

$$\overline{\int P_I(q)q} = \overline{q_{a,b}} = (1 - m)q_{EA}, \quad (3.21)$$

where $\overline{q_{a,b}}$ is the average of $q_{a,b}$ over the $n!$ permutations of the replicas.

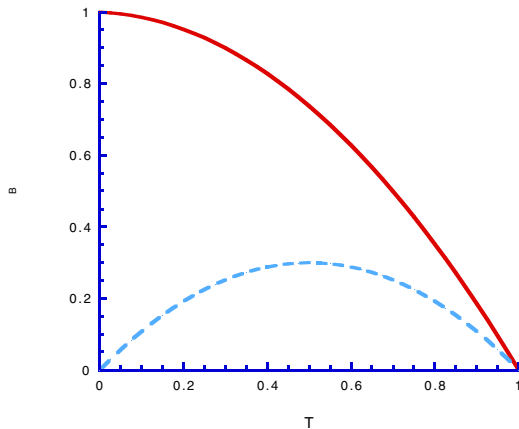


Fig. 6. The quantity q_{EA} and m (dashed line) as functions of the temperature in the p spin model (in units of T_c) for $p = 2$ (*i.e.* the SK model).

In the same way

$$\overline{P_I(q)q^s} = \overline{\left\langle \left(\frac{\sum_i \sigma_i^a \sigma_i^b}{N} \right)^s \right\rangle} = \overline{q_{a,b}^s} = (1 - m)q_{\text{EA}}^s. \quad (3.22)$$

Putting everything together one finds for the average over the different instances

$$\overline{P_I(q)} \equiv P(q) = m\delta(q) + (1 - m)\delta(q - q_{\text{EA}}). \quad (3.23)$$

One can painfully reconstruct all the probability distributions of the w 's by studying quantities like

$$\overline{\left(\int P_I(q)q \right)^2} = q_{\text{EA}}^2 \overline{\sum_k w_k^2} = \overline{q_{a,b}q_{c,d}} \quad (3.24)$$

and doing the appropriate combinatorial estimates, at the ends one finds (exactly in the same way as in the REM) that they are proportional to $\exp(-\beta F_k)$, where the F_k are distributed according to the distribution equation (2.29).

In order to develop a formalism useful to discuss the physical meaning of these results it is convenient to introduce the concept of *pure states in a finite volume* [2]. This concept is crystal clear from a physical point of view, however it can be difficult to state it in a rigorous way (*i.e.* to prove existence theorems).

We consider a system in a box of linear size L , containing a total of N spins. We partition the configuration space in regions, labeled by α , and

we define averages restricted to these regions [4, 29, 30]: these regions will correspond to our finite volume pure states or phases. It is clear that in order to produce something useful we have to impose sensible constraints on the form of these partitions. We require that the restricted averages on these regions are such that connected correlation functions are small at large distance x in a short range model (or when the points are different in an infinite range model). This condition is equivalent to the statement that the fluctuation of intensive quantities⁸ vanishes in the infinite volume limit inside a given phase.

In a ferromagnet the two regions are defined by considering the sign of the total magnetization. One region includes configurations with a positive total magnetization, the second selects negative total magnetization. There are ambiguities for those configurations that have exactly zero total magnetization, but the probability that such a configuration can occur is exponentially small at low temperature.

In order to present an interpretation of the results we assume that such decomposition exists also each instance of our problem. Therefore the *finite* volume Boltzmann-Gibbs measure can be decomposed in a sum of such finite volume pure states. The states of the system are labeled by α : we can write

$$\langle \cdot \rangle = \sum_{\alpha} w_{\alpha} \langle \cdot \rangle_{\alpha}, \quad (3.25)$$

with the normalization condition

$$\sum_{\alpha} w_{\alpha} = 1. \quad (3.26)$$

The function $P_J(q)$ for a particular sample is given by

$$P_J(q) = \sum_{\alpha, \beta} w_{\alpha} w_{\beta} \delta(q_{\alpha, \beta} - q), \quad (3.27)$$

where $q_{\alpha, \beta}$ is the overlap among two generic configurations in the states α and β .

Given two spin configurations (σ and τ) we can introduce a natural concept of distance by

$$d^2(\sigma, \tau) \equiv \frac{1}{N} \sum_{i=1}^N (\sigma_i - \tau_i)^2, \quad (3.28)$$

⁸Intensive quantities are defined in general as $b = \frac{1}{N} \sum_{i=1}^N B_i$, where the functions B_i depend only on the value of σ_i or from the value of the nearby spins.

that belongs to the interval $[0-1]$, and is zero only if the two configurations are equal. In the thermodynamical limit, *i.e.* for $N \rightarrow \infty$, the distance of two configurations is zero if the number of different spins remains finite. The percentage of different σ 's, not the absolute number, is relevant in this definition of the distance. It is also important to notice that at a given temperature β^{-1} , when N goes to infinity the number of configurations inside a state is extremely large: it is proportional to $\exp(NS(\beta))$, where $S(\beta)$ is the entropy density of the system).

We expect that finite volume pure states will enjoy the following properties that likely characterizes the finite volume pure states:

- when N is large each state includes an exponentially large number of configurations⁹;
- the distance of two different generic configurations C_α and C_γ (the first belonging to state α and the second to state γ) does not depend on the C_α and C_γ , but only on α and β . The distance $d_{\alpha,\beta}$ among the states α and β , is the distance among two generic configurations in these two states. The reader should notice that with this definition the distance of a state with itself is not zero. If we want we can define an alternative distance:

$$D_{\alpha,\beta} \equiv d_{\alpha,\beta} - \frac{1}{2}(d_{\alpha,\alpha} + d_{\beta,\beta}), \quad (3.29)$$

in such a way that the distance of a state with itself is zero ($D_{\alpha,\alpha} = 0$);

- the distance between two configurations belonging to the same state α is strictly smaller than the distance between one configuration belonging to state α and a second configuration belonging to a different state β . This last property can be written as

$$d_{\alpha,\alpha} < d_{\alpha,\beta}. \quad (3.30)$$

This property forbids to have different states such that $D_{\alpha,\beta} = 0$, and it is crucial in avoiding the possibility of doing a too fine classification¹⁰;

- the classification into states is the finest one that satisfies the three former properties.

⁹We warn the reader that in the case of a glassy system it is not possible to consider $N \rightarrow \infty$ limit of a given finite volume pure state: there could be no one to one correspondence of states at N and those at $2N$.

¹⁰For example if in a ferromagnet at high temperature we would classify the configurations into two states that we denote by e and o , depending on if the total number of positive spins is even or odd, we would have that $d_{e,e} = d_{e,o} = d_{o,o}$.

The first three conditions forbid a too fine classification, while the last condition forbids a too coarse classification.

For a given class of systems the classification into states depends on the temperature of the system. In some case it can be rigorously proven that the classification into states is possible and unique [31–33] (in these cases all the procedures we will discuss lead to the same result). In usual situations in Statistical Mechanics the classification in phases is not very rich. For usual materials, in the generic case, there is only one phase. In slightly more interesting cases there may be two states. For example, if we consider the configurations of a large number of water molecules at zero degrees, we can classify them as water or ice: here there are two states. In slightly more complex cases, if we tune carefully a few external parameters like the pressure or the magnetic field, we may have coexistence of three or more phases (a tricritical or multicritical point).

In all these cases the classification is simple and the number of states is small. On the contrary in the mean field approach to glassy systems the number of states is very large (it goes to infinity with N), and a very interesting nested classification of states is possible. We note “en passant” that this behavior implies that the Gibbs rule¹¹ is not valid for spin glasses.

The results we have obtained on the probability distribution of the overlap can be interpreted by saying that the system has many equilibrium states with weight that have the same probability distribution as a REM with the appropriate value of m such that the average value of the local magnetization squared is inside each state is just q_{EA} :

$$\frac{\sum_{i=1,N} (m_\alpha(i))^2}{N} = q_{\text{EA}}. \quad (3.31)$$

Different states have magnetization that points toward orthogonal directions:

$$\frac{\sum_{i=1,N} m_\alpha(i) m_\gamma(i)}{N} = 0 \quad (3.32)$$

if $\alpha \neq \gamma$.

The only difference with the REM is that q_{EA} is less than 1. The states in the REM are composed by a single configuration, in the p spin models local fluctuation are allowed and the states contain an exponentially number of configurations (local fluctuation are allowed) and have a non-zero entropy.

¹¹The Gibbs rule states that in order to have coexistence of n phases (n -critical point), we must tune n parameters. Here no parameters are tuned and the number of coexisting phases is infinite!

3.4 The two susceptibilities

Let us consider a model where the Hamiltonian is of the form

$$H_0(\sigma) - h \sum_i \sigma_i. \quad (3.33)$$

If the variables are interpreted as spins, h is the magnetic field. A crucial question is what happens when we change the magnetic field.

In order to simplify the analysis let us suppose that we stay in a system where, after we average on the disorder, for $i \neq k$:

$$\overline{\langle \sigma_i \sigma_k \rangle} = \overline{\langle \sigma_i \rangle \langle \sigma_k \rangle} = 0. \quad (3.34)$$

This property is valid in the p -spin models and also in simple models of spin glasses: *e.g.* in the Edwards Anderson model [1] where

$$H_0(\sigma) = \sum_{i,k} J_{i,k} \sigma_i \sigma_k, \quad (3.35)$$

where the sum over i and k runs over the nearest neighbours and the J are random variables with even probability distribution.

A simple computation [2] shows in general that the average equilibrium magnetic susceptibility is just given by

$$\chi_{\text{eq}} = \beta \int dq P(q)(1 - q). \quad (3.36)$$

Indeed

$$N\chi_{\text{eq}} = \beta \sum_{i,k=1,N} \overline{\langle \sigma_i \sigma_k \rangle - \langle \sigma_i \rangle \langle \sigma_k \rangle}. \quad (3.37)$$

The terms with $i \neq k$ do not contribute after the average over the systems (as consequence of Eq. (3.34)): the only contribution comes from the terms where $i = k$. We finally obtain

$$N\chi_{\text{eq}} = \sum_{i=1,N} \overline{(1 - \langle \sigma_i \rangle)^2} = N\beta \left(\overline{1 - \sum_{\alpha,\gamma} w_\alpha w_\gamma q_{\alpha,\gamma}} \right). \quad (3.38)$$

In p spin models using the form of the function $P(q)$ or using directly the properties of the w 's and of the q 's we find

$$\chi_{\text{eq}} = \beta(1 - (1 - m)q_{\text{EA}}) = \beta(1 - q_{\text{EA}} + mq_{\text{EA}}). \quad (3.39)$$

It is interesting to note that we can also write

$$\chi_{\text{eq}} = \beta(1 - q_{\text{EA}}) + N^{-1}\beta \sum_{\alpha,\gamma} w_\alpha w_\gamma (M_\alpha - M_\gamma)^2 \quad (3.40)$$

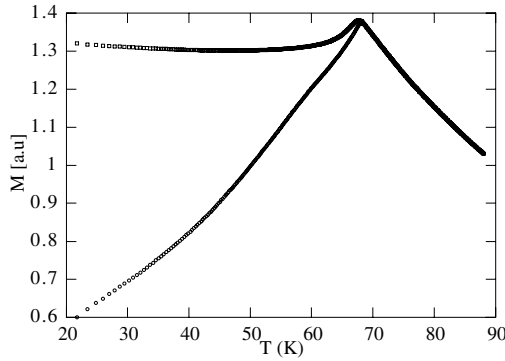


Fig. 7. The experimental results for the FC (field cooled) and the ZFC (zero field cooled) magnetisation (higher and lower curve respectively) *vs.* temperature in a spin glass sample ($\text{Cu}_{87}\text{Mn}_{13.5}$) for a very small value of the magnetic field $H = 1$ Oe (taken from [34]). For a such a low field non-linear effects can be neglected and the magnetization is proportional to the susceptibility.

where M_α is the total magnetization in the state α

$$M_\alpha = \sum_i \langle \sigma(i) \rangle_\alpha. \quad (3.41)$$

The first term (*i.e.* $\beta(1 - q_{\text{EA}})$) has a very simple interpretation: it is the susceptibility if we restrict the average inside one state and it can be this identified with χ_{LR} . The second term gives χ_{irr} :

$$\chi_{\text{irr}} = \beta \sum_{\alpha, \gamma} w_\alpha w_\gamma (q_{\text{EA}} - q_{\alpha, \gamma}) = \beta m q_{\text{EA}}, \quad (3.42)$$

where the last equality is valid in the p -spin models. In these models (for $p > 2$) χ_{irr} jumps at the critical temperature (χ remains continuous): in spin glasses ($p = 2$) q_{EA} vanishes at the critical temperature and both χ and χ_{irr} are continuous in agreement with the experimental results (Fig. 7).

The physical origin of χ_{irr} is clear. When we increase the magnetic field, the states with higher magnetization become more likely than the states with lower magnetization: this effect contributes to the increase in the magnetization. However the time to jump to a state to another state is very high (it is strictly infinite in the infinite volume limit and for infinitesimal magnetic fields where we can neglect non-linear effects are neglected): consequently the time scales relevant for χ_{LR} and χ_{eq} are widely separated.

If we look to real systems (*e.g.* spin glasses) both susceptibilities are experimentally observable.

- The first susceptibility (χ_{LR}) is what we measure if we add an very small magnetic field at low temperatures. The field should be small enough in order to neglect non-linear effects. In this situation, when we change the magnetic field, the system remains inside a given state and it is not forced to jump from a state to an other state and we measure the ZFC (zero field cooled) susceptibility, that corresponds to χ_{LR} .
- The second susceptibility (χ_{eq}) can be approximately measured by cooling the system in presence of a small field: in this case the system has the ability to chose the state that is most appropriate in presence of the applied field. This susceptibility, the so called FC (field cooled) susceptibility is nearly independent from the temperature (and on the cooling rate¹²) and corresponds to χ_{eq} .

Therefore one can identify χ_{LR} and χ_{eq} with the ZFC susceptibility and with the FC susceptibility respectively. The experimental plot of the two susceptibilities is shown in Figure 7. They are clearly equal in the high temperature phase while they differ in the low temperature phase.

The difference among the two susceptibilities is a crucial signature of replica symmetry breaking and, as far as I known, can explained only in this framework. A small change in the magnetic field pushes the system in a slightly metastable state, that may decay only with a very long time scale. This may happens only if there are many states that differs one from the other by a very small amount in free energy.

3.5 The cavity method

The cavity method is a direct approach that in principle can be used to derive in an esplicite way all the results that have been obtained with the replica method¹³. The basic idea is simple: we consider a system with N spins ($i = 1, N$) and we construct a new system with $N + 1$ spins by adding an extra spin (at $i = 0$). We impose the consistency condition that the average properties of the new spin are the same of that of the old ones [2, 35].

In order to lighten the notation I will write down the formulae only for $p = 2$, but it easy any to extend the computation to other models. The

¹²The nearly independence of the field cooled magnetization on the cooling rate can be used to argue that field cooled magnetization is near to the equilibrium one; on the contrary, if the field cooled magnetization would have been strongly dependent on the cooling rate, the statement that it correspond to the equilibrium magnetization would be quite doubtful.

¹³Not all the results have been actually derived.

Hamiltonian of the new spin is;

$$\sigma_0 \sum_{i=1,N} J_{0,i} \sigma_i. \quad (3.43)$$

If we suppose that the spins σ_i have vanishing correlations and we take care that each individual term is small, we find that

$$\begin{aligned} m'_0 &\equiv \langle \sigma_0 \rangle = \tanh(\beta h) \\ h &= \sum_{i=1,N} J_{0,i} m_i, \end{aligned} \quad (3.44)$$

where m_i denotes the magnetization of the spin σ_i *before* we add the spin 0. When the variables J are random (or the variables m_i are random), the central limit theorem implies that h is a Gaussian random variable with variance

$$\overline{h^2} = q_{\text{EA}} \equiv \frac{\sum_{i=1,N} m_i^2}{N}. \quad (3.45)$$

If we impose the condition that the average magnetization squared of the new point is equal to that of the old points, we arrive to the consistency equation:

$$q_{\text{EA}} = \overline{m_0^2} = \int d\mu_{q_{\text{EA}}}(h) \tanh^2(\beta h) \quad (3.46)$$

where $d\mu_{q_{\text{EA}}}(h)$ denotes a normalized Gaussian distribution with variance q_{EA} . It is easy to check that the increase in the total free energy of the system is

$$\Delta F(h) \equiv \frac{-\ln(\cosh(\beta h))}{\beta}. \quad (3.47)$$

In this way we have derived the replica symmetric solution that corresponds to $m = 0$.

If replica symmetry is broken the spins are uncorrelated within one states, but if we do not separate the states, we find strong correlations.

The correct computation goes as follows. We suppose that in the system with N spins we have a population of states whose total free energies F_α are distributed (when F_α is not far from a given reference value F^* that for lighten the notation we take equal to zero) as

$$\mathcal{N}_N(F_N) \propto \exp(\beta m F_N). \quad (3.48)$$

When we add the new spin, we will find a value of the field h that depends on the state α . We can now consider the conjoint probability distribution of the new free energy and of the magnetic field. We obtain

$$\mathcal{N}_{N+1}(F, h) = \int dh P_s(h) \int dF_N \mathcal{N}_N(F_N) \delta(F - F_N - \Delta F(h)) \quad (3.49)$$

where $P_s(h)$ is the probability distribution of the effective magnetic field produced on the spin at 0, for a generic state and it is still given by $d\mu_{q_{EA}}(h)$. It is crucial to take into account that the new free energy will differ from the old free energy by an energy shift that is h dependent. If we integrate over F_N and we use the explicit exponential form for $\mathcal{N}_N(F_N)$ we find that

$$\begin{aligned} \mathcal{N}_{N+1}(F, h) &\propto \exp(\beta m F) \int dh P_s(h) \exp(\beta m \Delta F(h)) \\ &\propto \exp(\beta m F) P_{N+1}(h). \end{aligned} \quad (3.50)$$

The probability distribution of the field at *fixed* value of the free energy is given by

$$P_{N+1}(h) \propto P_s(h) \exp(\beta m \Delta F(h)) = d\mu_{q_{EA}}(h) \cosh(\beta h)^m \quad (3.51)$$

and it obviously differs from $P_s(h)$ as soon as $m \neq 0$. In this way we find the consistency equation of the replica approach for q_{EA} .

A few comments are in order:

- the probability distribution of h at fixed value of the free energy of the N spins system ($P_s(h)$) is *not* the probability distribution of h at fixed value of the free energy of the $N + 1$ spins system $P_{N+1}(h)$: the two free energies differ by an h dependent additive factor and they do not have a flat distribution (as soon as $m \neq 0$). The probability distribution of h at a fixed value of the free energy of the N spins system is Gaussian, but the probability distribution of h at fixed value of the free energy of the $N + 1$ spins system is not a Gaussian;
- only in the case where $\mathcal{N}_N(F_N)$ is an exponential distribution $\mathcal{N}_{N+1}(F, h)$ factorizes into the product of an F dependent factor and an h dependent factor and the $\mathcal{N}_{N+1}(F)$ has the same form of $\mathcal{N}_N(F)$. Self-consistency can be reached only in the case of an exponential distribution for $\mathcal{N}_N(F_N)$;
- the equations do not fix the value of m . This is natural because (as we shall see later) we can write them also in the case where the free energy densities we consider are different from that of the ground state (F^* is not near to the ground state). In this case they correspond to the distribution of the free energies inside metastable states that are characterized by a different value of m than the ground state. These equations will be useful for the computation of the complexity.

It is appropriate to add a last comment. The computation we have presented relates the magnetization of a spin of the systems with $N + 1$ spins to the magnetizations of the system with N spins: they are not a closed set of

equations for a given system. However we can also write the expression of magnetization at zero as function of the magnetizations of the system with $N + 1$ spins, by computing the variations in the magnetization in a perturbative way. Let us consider the case $p = 2$ and let us denote by m the magnetization of the old system (N spins) and by m' the magnetization of the new system ($N + 1$ spins). Perturbation theory tell us that

$$m'_i \approx m_i + J_{0,i} m'_0 \frac{\partial m_i}{\partial h_i} = m_i + J_{0,i} m'_0 \beta (1 - (m'_i)^2) . \quad (3.52)$$

Using the previous formula we get the TAP equations [2, 36]:

$$m'_0 = \tanh(\beta h)$$

$$h = \sum_{i=1,N} J_{0,i} m_i \approx \sum_{i=1,N} J_{0,i} m'_i - m'_0 \sum_i J_{0,i}^2 \beta (1 - m'_i) \quad (3.53)$$

$$\approx \sum_{i=1,N} J_{0,i} m'_i - m'_0 \beta (1 - q_{\text{EA}}) \quad (3.54)$$

where $(N + 1)q_{\text{EA}} = \sum_{i=0,N} m'_i$ and we have used the fact that $\overline{J_{0,i}^2} = N^{-1}$. A detailed computation show that the free energy corresponding to a solution of the TAP equations is given by the TAP free energy.

$$F[m] = \sum_{i < k} J_{i,k} m_i m_k - N \beta \frac{(1 - q)^2}{4} - T \sum_i S(m_i), \quad (3.55)$$

where $S(m)$ is the usual single spin entropy:

$$-S(m) = \frac{1+m}{2} \ln \left(\frac{1+m}{2} \right) + \frac{1-m}{2} \ln \left(\frac{1-m}{2} \right). \quad (3.56)$$

It is important to note that the solutions of the TAP equations are also stationary points of the TAP free energy: using the relation

$$\frac{\partial q_{\text{EA}}}{\partial m_i} = 2 \frac{m_i}{N} \quad (3.57)$$

the TAP equations can be written as

$$\frac{\partial F[m]}{\partial m_i} = 0. \quad (3.58)$$

4 Complexity

It would be interesting to characterize better the free energy landscape of the models described in the previous section, especially in order to understand

the dynamics. Indeed we have already seen that in the REM the system could be trapped in metastable configurations. In models where the energies are correlated the situation is more complicated; moreover in realistic finite dimensional models there are still further subtleties.

Although the word *metastable configuration* has a strong intuitive appeal, we must define what a metastable configuration is in a more precise way. There are two different (hopefully equivalent) definitions of a metastable state or valley:

- from an equilibrium point of view a valley is a region of configuration space separated by the rest of the configuration space by free energy barriers that diverge when $N \rightarrow \infty$. More precisely the system, in order to go outside a valley by moving one spin (or one particle) at once, must cross a region where the free energy is higher than that of the valley by a factor that goes to infinity with N ;
- from the dynamic point of view a valley is a region of configuration space where the system remains for a time that goes to infinity with N ;

The rationale for assuming that the two definitions are equivalent is the following. We expect that for any reasonable dynamics where the system evolves in a continuous way (*i.e.* one spin flip at time), the system must cross a configuration of higher free energy when it goes from a valley to an other valley. The time for escaping from a valley is given by

$$\tau \simeq \tau_0 \exp(\beta \Delta F) \quad (4.1)$$

where ΔF is the free energy barrier¹⁴.

It is crucial to realize that in infinite range models valleys may have a free energy density higher than that of equilibrium states. This phenomenon is definitely not present in short range models. Two equilibrium states with infinite mean life must have the same free energy.

The proof of this statement is simple. Indeed let us suppose that the system may stay in two phases (or valleys) that we denote as A and B . If the free energy density of B is higher than that of A , the system can go from B to A in a continuous way, by forming a bubble of radius R of phase A inside phase B ¹⁵. For example, if we take a mixture of H_2 and O_2 at room

¹⁴In kinetically constrained models, where some local movements are forbidden, we can have dynamical valleys that do not correspond to valley from the equilibrium point of view.

¹⁵If the surface tension among phase A and B is finite, this happens in any short range model, for large R the volume term will dominate the free energy difference among the pure phase B and phase B with a bubble of A of radius R . This difference is thus negative at large R , its maximum will thus be finite. A finite amount of free energy is needed in order to form a seed of phase A where the spontaneous formation of phase A will start.

temperature, the probability of a spontaneous temperature fluctuation in a small region, that leads to later ignition and eventually to the explosion of the whole sample, is greater than zero (albeit quite a small number), and obviously it does not go to zero when the volume goes to infinity. This argument does not work in mean field models where in some sense surface effects are as important as volume effects (when D is large R^D , the volume, is not so different from R^{D-1} , the surface).

We have two possibilities open in positioning the predictions of mean field theory concerning the existence of real metastable states:

- we consider the presence of these metastable state with *infinite* mean life an artefact of the mean field approximation and we do not pay any attention to them;
- we notice that in the real systems there are metastable states with very large (*e.g.* much greater than one year) mean life. We consider the *infinite* time metastable states of the mean field approximation as precursors of these *finite* mean life states. We hope (with reasons) that the corrections to the mean field approximation will give a finite (but large) mean life to these states (how this can happen will be discussed in the next section).

In these notes I will explore the second possibility, that seems to be much more fruitful than the first one.

4.1 The basic definitions

Before discussing the difficulties related to the definition of the complexity in short range models, we must see the main definitions that are correct in the mean field approach.

The basic ideas are quite simple [9–11, 23, 37–40]. In principle we proceed in a way similar to the construction of equilibrium states described in Section 3.3: we partition the whole configuration space into valleys. If we call Z_α the contribution of each valley to the partition function, the corresponding free energy is given by

$$Z_\alpha = \exp(-\beta F_\alpha). \quad (4.2)$$

This definition does not give us a practical way to find the valleys. An alternative approach, that should be hopefully equivalent, is the following. In many case one can prove that the magnetization in a given valley should satisfy some equations, *e.g.* the TAP equations of the previous sections: valleys may be identified with solutions of the TAP equations and their free

energy is given by the TAP free energy¹⁶. Generally speaking in a system of N spins we can introduce a free energy functional $F[m]$ that depends on the local magnetizations $m(i)$ and on the temperature. Only in the mean field case $F[m]$ is given by the TAP free energy.

We suppose that at sufficiently low temperature the functional $F[m]$ has many local minima (*i.e.* the number of minima goes to infinity with the number (N) of spins). Exactly at zero temperature these local minima coincide with the local minima of the potential energy as function of the coordinates of the particles. Let us label then by an index α . To each of them we can associate a free energy F_α and a free energy density $f_\alpha = F_\alpha/N$. In this way the valleys are associated to local minima of the free energy functional.

In this low temperature region we suppose that the total free energy of the system can be well approximated by the sum of the contributions to the free energy of each particular local minimum. We thus find:

$$Z \equiv \exp(-\beta N f_S) = \sum_{\alpha} \exp(-\beta N f_{\alpha}). \quad (4.3)$$

When the number of minima is very high, it is convenient to introduce the function $\mathcal{N}(f, T, N)$, *i.e.* the density of minima whose free energy is near to f . With this notation we can write the previous formula as

$$Z = \int df \exp(-\beta N f) \mathcal{N}(f, T, N). \quad (4.4)$$

In the region where \mathcal{N} is exponentially large we can write

$$\mathcal{N}(f, T, N) \approx \exp(N \Sigma(f, T)), \quad (4.5)$$

where the function Σ is called the complexity or the configurational entropy (it is the contribution to the entropy coming from the existence of an exponentially large number of locally stable configurations).

The minimum (maximum) possible value of the free energy is given by $f_m(T)$ ($f_M(T)$). The relation (4.5) is valid in the region $f_m(T) < f < f_M(T)$. Outside this region we have that $\mathcal{N}(f, T) = 0$. In all cases known $\Sigma(f_m(T), T) = 0$, and the function Σ is continuous at f_m . On the contrary in mean field models it happens frequently that the function Σ is discontinuous at f_m .

For large values of N we can write

$$\exp(-N \beta f_S) \approx \int_{f_m}^{f_M} df \exp(-N(\beta f - \Sigma(f, T))). \quad (4.6)$$

¹⁶At zero temperature one could try to identify valleys with the minima of the Hamiltonian, that are called inherent structures in the glass community [6].

We can thus use the saddle point method and approximate the integral with the integrand evaluated at its maximum. We find that

$$\beta f_S = \min_f \Phi(f) \equiv \beta f^* - \Sigma(f^*, T), \quad (4.7)$$

where the potential $\Phi(f)$ (that will play a crucial role in this approach) is given by

$$\Phi(f) \equiv \beta f - \Sigma(f, T). \quad (4.8)$$

(This formula is quite similar to the well known homologous formula for the free energy, *i.e.* $\beta f = \min_E (\beta E - S(E))$, where $S(E)$ is the entropy density as function of the energy density.)

If we call f^* the value of f that minimize $\Phi(f)$. we have two possibilities:

- the minimum f^* is inside the interval and it can be found as solution of the equation $\beta = \partial \Sigma / \partial f$. In this case we have

$$\beta \Phi = \beta f^* - \Sigma^*, \quad \Sigma^* = \Sigma(f^*, T). \quad (4.9)$$

The system may stay in one of the exponentially large number of possible minima. The number of minima where is convenient for the system to stay is $\exp(N\Sigma^*)$. The entropy of the system is thus the sum of the entropy of a typical minimum and of Σ^* , *i.e.* the contribution to the entropy coming from the exponential large number of microscopical configurations;

- the minimum is at the extreme value of the range of variability of f . We have that $f^* = f_m$ and $\Phi = f_m$. In this case the contribution of the complexity to the free energy is zero. The different states that contribute the free energy have a difference in free energy density that is of order N^{-1} (a difference in total free energy of order 1). Sometimes we indicate the fact that the free energy is dominated by a few different minima by say the replica symmetry is spontaneously broken [2, 22].

From this point of view the behaviour of the system will crucially depend on the free energy landscape [41], *i.d.* the function $\Sigma(f, T)$, the distance among the minima, the height of the barriers among them...

4.2 Computing the complexity

We have seen that complexity counts the number of metastable states. It would be interesting to compute the complexity in a direct way without having to count all the metastable states (an impossible task for large N) An interesting route to the evaluation of complexity consists in introducing

new artificial couplings and to consider the behaviour of the systems in these conditions. This new approach works also in cases where the free energy functional is not known in an exact way, so that its minima cannot be computed.

The basic idea is to start from an equilibrium configuration and to explore the configuration space phase around it [38, 39]. If we can define in some way the entropy (S_v) of the valley around a given equilibrium configuration, we have that

$$S = \Sigma^* + S_v, \quad (4.10)$$

where S is the total entropy of the system and Σ^* is the equilibrium complexity.

More precisely, we study a system of N interacting variables σ_i , $i = 1, \dots, N$, with Hamiltonian $H(\sigma)$, $q(\sigma, \tau)$ is an overlap function, *i.e.* an intensive measure of similarity among the configurations σ and τ . We can consider a reference equilibrium configuration σ , that produce a fixed external potential on a replica τ . The partition function of the second system is:

$$Z(\sigma, \epsilon) = \sum_{\tau} \exp[-\beta H(\tau) + \beta \epsilon N q(\tau, \sigma)], \quad (4.11)$$

and

$$\Gamma(\epsilon) = -(N\beta)^{-1} \langle \log Z(\sigma, \epsilon) \rangle_{\sigma} \quad (4.12)$$

is the ϵ -dependent free energy ($\langle \cdot \rangle_{\sigma}$ denotes the average over the variables σ). The new term in the Hamiltonian, for ϵ sufficiently large, forces the variables τ to be near the variables σ and produces a *quenched* disorder for the variables τ . By changing the value of ϵ we can explore the phase space around a given equilibrium configuration σ . At the end we average over σ the logarithm of the σ dependent free energy.

The quantity $\Gamma(\epsilon)$ is well defined and it may be computed in also in numerical simulations. However it is interesting to evaluate it in mean field models, where analytic computations are possible. The analytic computation of $\Gamma(\epsilon)$ can be done by considering $1 + s$ replicas: the corresponding Hamiltonian is

$$H_s(\sigma) \equiv H(\sigma_1) + \sum_{a=2, s} H(\sigma_a) + \epsilon N \sum_{a=2, 1+s} q(\sigma, \sigma_a). \quad (4.13)$$

Here σ_1 plays the role of σ and the σ_a (for $a = 2, 1 + s$) are s replicas of the τ variables. The quenched limit (where there is no feedback reaction of the τ variables on the σ variables) is obtained in the limit $s \rightarrow 0$:

$$\Gamma(\epsilon) = \lim_{s \rightarrow 0} \frac{\partial}{\partial s} \ln \left(\prod_{a=1, s} \sum_{\sigma_a} \exp(-\beta H_s(\sigma)) \right). \quad (4.14)$$

In models where we have to perform the average over the instances of the problems, we have to replicate n times the s -replicated system: we have to take $n \times (1 + s)$ variables and to study simultaneously the limit $s \rightarrow 0$ and $n \rightarrow 0$. Fortunately enough, in the high temperature phase, where we are interested to the computation of the complexity, we do not need to break the replica symmetry (at least for the computation of the complexity) and we obtain the correct results already for $n = 1$.

In the following we will study the phase diagram of the model in the $\epsilon - T$ plane. Explicit computations can be found in the literature mainly for the p-spins spherical model, but the conclusions have a general validity [38,39]. At this end it is convenient to define the Legendre transform of $\Gamma(\epsilon)$, defined as

$$\begin{aligned} W(q) &= \Gamma(\epsilon(q)) - \epsilon(q)q, \\ \frac{\partial W(q)}{\partial q} &= \epsilon(q). \end{aligned} \quad (4.15)$$

The potential $W(q)$ has the meaning of the free energy with the constraint that the overlap of our configuration τ with the generic configuration σ is equal to q . As far as we are interested in studying the q -dependance of $W(q)$, we can set conventionally $W(0) = 0$.

If one computes the functions $\Gamma(\epsilon)$ and $W(q)$ in a mean field model, one typically finds that the shape of the function W is characteristic of a mean-field system undergoing a first order phase transition. At high enough temperature W is an increasing and convex function of q with a single minimum for $q = 0$. Decreasing the temperature below a value T_f , where for the first time a point q_f with $W''(q_f) = 0$ appears, the potential loses the convexity property and a phase transition can be induced by a field. A secondary minimum develops at T_D , the temperature of dynamical transition [7], signaling the presence of long-life metastable states. The height of the secondary minimum reaches the one of the primary minimum at $T = T_c$ and thermodynamic coexistence at $\epsilon = 0$ takes place. This is the usual static transition. In Figure 8 we show the shape of the potential in the various regions.

Therefore the potential $W(q)$ has usually a minimum at $q = 0$, where $W(0) = 0$. It may have a secondary minimum at $q = q_D$. We have a few different situations:

- at $T > T_D$ the potential $W(q)$ has only the minimum at $q = 0$. The quantity q_D cannot be defined and no valley with the equilibrium energy are present. This is more or less the definition of the dynamical transition temperature T_D . A more careful analysis [42] shows that for $T_D < T < T_V$ there are still valleys with energy *less* than the

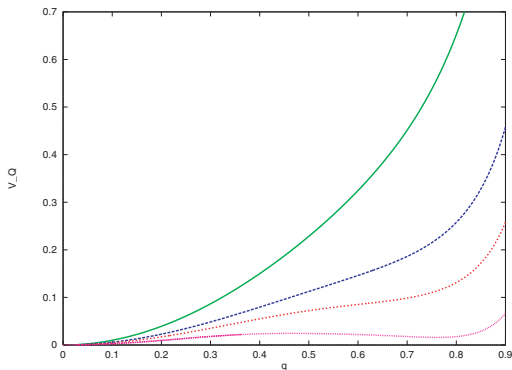


Fig. 8. Different shapes of the function W for various temperatures: the higher curves correspond to higher temperatures.

equilibrium one, but these valleys cover a so small region of phase space that they are not relevant for equilibrium physics¹⁷;

- exactly at $T = T_D$ we sit at a phase transition point where some susceptibilities are divergent. This fact implies (in short range models) that there is a divergent dynamical correlation length that is related to dynamical heterogeneities [76];
- $W(q_D) > 0$. This happens in an intermediate temperature region, above T_c , but below T_D , where we can put one replica σ at equilibrium and have the second replica τ in a valley near it. It happens that the internal energy of both the σ configuration (by construction) and of the τ configuration are equal to the equilibrium one. However the number of valley is exponentially large so that the free energy a single valley will be higher than the total free energy. One finds in this way that $W(q_D) > 0$ is given by

$$W(q_D) = \frac{\ln \mathcal{N}_e}{N} \equiv \Sigma^* \quad (4.16)$$

where \mathcal{N}_e is the average number of the valleys having the equilibrium energy [40, 44];

¹⁷In the REM limit ($p \rightarrow \infty$) the temperature T_D goes to infinity. In this limit the region $T > T_D$ does not exist. Therefore the dynamical transition is a new feature that is not present in the REM.

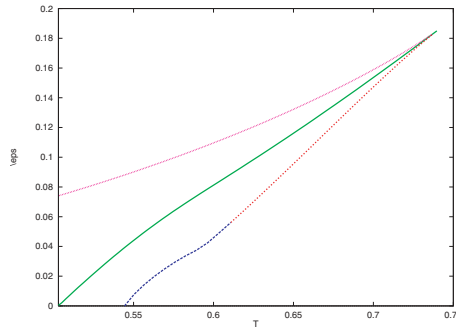


Fig. 9. Phase diagram in the $T - \epsilon$ plane. At the upper curve the low q solution disappear, at the lower curve the high q solution disappear and two locally stable solutions are present only in the region among the upper and lower curves. The middle curve the coexistence line where the two solutions have equal free energy. The coexistence line touches the axes $\epsilon = 0$ at $T = T_c$, while the lower curve touches it at $T = T_D$.

- $W(q_D) = 0$. This happens in the low temperature region, $T \leq T_c$, where we can put two replicas both at overlap 0 and at overlap q_{EA} without paying any prize in free energy. In this case $q_D = q_{EA}$.

For $T < T_D$ there is a relation (Eq. (4.10)) among the entropy inside a valley the entropy of the systems and is the configurational entropy, or complexity, that is given by the value of W at the secondary minimum. This W contribution vanishes at T_c and becomes exactly equal to zero for $T < T_c$ [7].

Although the behavior of this potential function is analogous to the one found in ordinary systems undergoing a first order phase transition the interpretation is here radically different. While in ordinary cases different minima represent qualitatively different thermodynamical states (*e.g.* gas and liquid), this is not the case here. In our problem the local minimum appears when ergodicity is broken, and the configuration space splits into an exponentially large number of components. The two minima are different manifestations of states with the same characteristics. The height of the secondary minimum, relative to the one at $q = 0$ measures the free-energy loss to keep the system near one minimum of the free energy (in configurations space). This is just T times the complexity Σ , *i.e.* the logarithm of the number of distinct valleys of the system.

The equation $\partial W(q)/\partial q = \epsilon$ may have two stable solutions (that correspond to a local minimum of $W(q) - \epsilon q$) only in the region of the $T - \epsilon$ plane shown in Figure 9. At the upper and low curves one of the two solutions

lose its stability and it disappears: these two curves are the equivalent of the spinodal lines in usual first order transition. The point where the lower curve crosses the axis $\epsilon = 0$ is the dynamical transition [39]: only at lower temperatures the two systems may remain with an high value of the overlap without having a force that keeps them together (*i.e.* $\epsilon = 0$). On the contrary the static transition is characterized by the fact that the coexistence line touches the axis $\epsilon = 0$.

General arguments tell us that the free energy is a convex function of the q , so that we the correct shape of the function W can be obtained by the Maxwell construction (see Fig. 10). In order to see the consequences of this fact on the definition of the complexity we can try to consider the function $q(\epsilon)$ for temperatures less than T_D shown in Figure 11.

As can be seen from the figures, the point where we evaluate the complexity (*i.e.* $\epsilon = 0$ and high q) is always in the metastable region for $T > T_c$ where we equilibrium complexity is non-zero. This causes an intrinsic ambiguity in the definition of complexity because the free energy is not defined with infinite precision in the metastable phase. However we can use the fact that the free energy is as C^∞ function of ϵ near the discontinuity point to extrapolate the high ϵ free energy in the metastable region. This ambiguity becomes smaller and smaller more we approach the static temperature (the amount of the extrapolation becomes smaller and smaller) and in general it is rather small unless we are very near to the dynamic phase transition. This ambiguity is not important from practical purposes; however it implies that there is no sharp, infinitely precise definition of the equilibrium complexity. If we forget this intrinsic ambiguity in the definition of the complexity we may arrive to contradictory results.

4.3 Complexity and replicas

As we have seen we can write

$$Z(\beta) = \sum_a \exp(-\beta N f_a(\beta)) = \int d\mathcal{N}(f, \beta) \exp(-\beta N f), \quad (4.17)$$

where $f_a(\beta)$ is the free energy density of the valley labeled by a at the temperature β^{-1} , and $\mathcal{N}(f, \beta)$ is the number of valleys with free energy density less than f .

We have also seen that $\mathcal{N}(f, \beta) = \exp(N\Sigma(f, \beta))$, where the configurational entropy, or complexity, $\Sigma(f, \beta)$ is positive in the region $f > f_0(\beta)$ and vanishes at $f = f_0(\beta)$. The quantity $f_0(\beta)$ is the minimum value of the free energy: $\mathcal{N}(f, \beta)$ is zero for $f < f_0(\beta)$ [39, 43, 44].

If the equation

$$\frac{\partial \Sigma}{\partial f} = \beta \quad (4.18)$$

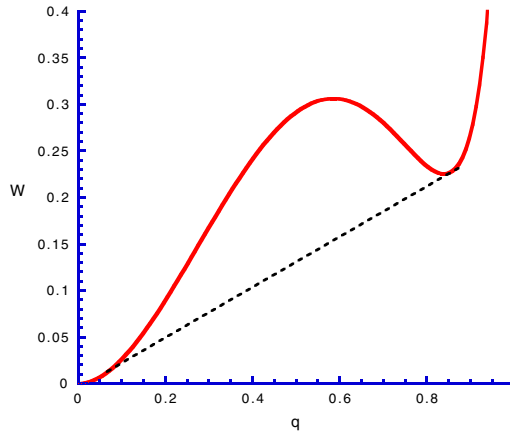


Fig. 10. The full line is the function $W(q)$ computed in the mean field approximation. The dashed line is the correct result (Maxwell construction).

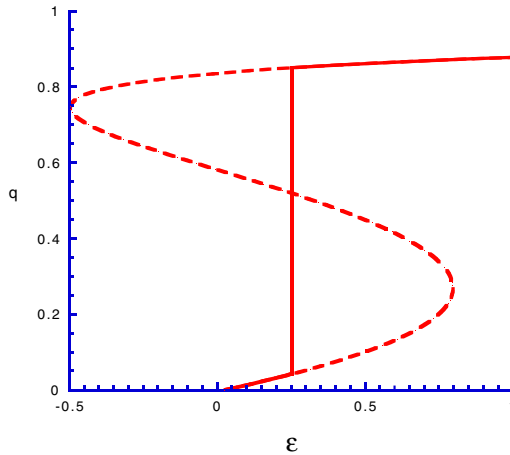


Fig. 11. The shapes of the function $q(\epsilon)$ for $T > T_c$: the full line is the correct result and the dashed line is the output of a mean field approximation.

has a solution at $f = f^*(\beta)$ (obviously this may happen only for $f^*(\beta) > f_0(\beta)$), we stay in the liquid (high temperature) phase. Here the free density is given by

$$f_{\text{eq}} = f^* - \beta^{-1} \Sigma(f^*, \beta) \quad (4.19)$$

and $\Sigma(f^*, \beta) = \Sigma^*(\beta)$.

Otherwise we stay in the glass (low temperature) phase and

$$f_{\text{eq}} = f_0(\beta). \quad (4.20)$$

In order to compute the properties in the glass phase we need to know $\Sigma(f, \beta)$: a simple strategy to compute the complexity is the following. We introduce the modified partition function

$$Z(\gamma; \beta) \equiv \exp(-N\gamma G(\gamma; \beta)) = \sum_a \exp(-\gamma N f_a(\beta)). \quad (4.21)$$

It is evident that $Z(\beta; \beta)$ is the usual partition function and $G(\beta; \beta)$ is the usual free energy. Using standard thermodynamical arguments it can be easily proven that in the limit $N \rightarrow \infty$ one has:

$$\gamma G(\gamma; \beta) = \gamma f - \Sigma(\beta, f), \quad f = \frac{\partial(\gamma G(\gamma; \beta))}{\partial \gamma}. \quad (4.22)$$

The complexity is obtained from $G(\gamma; \beta)$ in the same way as the entropy is obtained from the usual free energy [40, 43]:

$$\Sigma(\beta, f) = \frac{\partial G(\gamma; \beta)}{\partial \gamma}. \quad (4.23)$$

A few observations are in order:

- in the new formalism γ , the free energy and the complexity play respectively the same role of β , the internal energy and the entropy in the usual formalism;
- in the new formalism β only indicates the value of the temperature that is used to compute the free energy and γ controls which part of the free energy landscape is sampled;
- when $\beta \rightarrow \infty$ (at least formally) we sample the energy landscape:

$$Z(\gamma; \infty) = \sum_a \exp(-\gamma N e_a) = \int \nu(e) de \exp(-\gamma N e) \quad (4.24)$$

where e_a are the minima of the Hamiltonian and $\nu(e)$ the density of the minima of the Hamiltonian;

- the equilibrium complexity is given by $\Sigma^*(\beta) = \Sigma(\beta; \beta)$. On the other hand $\Sigma(\gamma; \infty)$ give us information on the minima of the Hamiltonian.

In principle it is possible to get the function $\Sigma(f)$ by computing directly the number of solution of the TAP equations for a given value of the free energy density. However it is simpler to obtain it by using the replica formalism and it is reassuring that one gets the same results with both methods [39, 40, 44–47].

The computation of the modified partition function $Z(\gamma; \beta)$ can be easily done in the replica formalism [39, 44]. If we consider a system with m replicas (with m integer) and we constrain them to stay in the same state we find that

$$Z(\beta, m) = \sum_a \exp(-\beta m N f_a(\beta)). \quad (4.25)$$

This expression coincide with $Z(\gamma; \beta)$ for $\gamma = m\beta$. Therefore there is a very simple way for computing $G(\gamma; \beta)$. We must consider the partition function of m replicas that are constrained to stay in the same state, *i.e.* there are at a large value of q where q is chosen in a self consistent way.

Let us firstly see how this approach works in the REM. In the REM the configurations and the states practically coincide: there is no β dependence of the complexity. The REM is defined by the property that $\Sigma(e) = e^2/2 - \ln(2)$, so that the computation of $\Sigma(e)$ using the replicas may look pointless, however it is instructive to illustrate the point.

The contribution to the partition function of m replicas coming from the region of phase space where all the m configuration are identical is given by

$$Z(\beta, m) = 2^N \exp\left(-\frac{1}{2}(\beta m)^2\right). \quad (4.26)$$

We thus get

$$\gamma G(\gamma; \beta) = \ln(2) - \frac{1}{2}\gamma^2 \quad (4.27)$$

and from the previous equation we can read back the expression for the complexity.

In the p -spin model we have to find out the partition function of a systems where all the m replicas are in the same block and are characterized by an high value of q . Here, given the value of m , we have to look for a solution q^* of the equation for q of the replica approach:

$$\frac{\partial F}{\partial q} = 0, \quad (4.28)$$

with $q^* \neq 0$, where the potential $F(q, m)$ is the replica potential introduced in the previous section. We thus find that

$$G(\beta m; \beta) = F(m, q^*). \quad (4.29)$$

The computation that we have done before for the statics contains the whole information needed to compute also the complexity and some other properties of the metastable states. Indeed we get

$$\Sigma(m) = \frac{\partial F(m, q^*)}{m} \quad (4.30)$$

and $f(m)$ can be obtained by Legendre transform or by using the relation

$$f(m) = \frac{\partial m^{-1} F(m, q^*)}{\partial m^{-1}} = F(m, q^*) - m \Sigma(m). \quad (4.31)$$

One finally finds the complexity as function of the free energy, by eliminating m .

$$\Sigma(f) = \Sigma(m(f)). \quad (4.32)$$

The dynamical temperature is the highest temperature where equation (4.28) has a solution at near $m = 1$, while the static critical temperature is the first temperature where

$$F(q(m), m)|_{m=0} = F(q(m), m)|_{m=1}. \quad (4.33)$$

The equilibrium transition temperature is given by the condition that the equilibrium complexity satisfies the condition

$$\Sigma^* \equiv \left. \frac{\partial F(m, q^*)}{\partial m} \right|_{m=1} = 0. \quad (4.34)$$

In this way we have recovered the results of one step replica symmetry breaking (together with the mysterious condition $\partial F(m)/\partial m = 0$) from general principles.

Although we have based our discussion on mean-field model, we expect that the qualitative features of the phase diagrams presented survive in finite dimension. We believe that the existence of a coexistence line, terminating in a critical point, is a constitutive feature of systems whose physics is dominated by the existence of long lived metastable states like glasses. These predictions can be submitted to numerical test in glassy model systems as like *e.g.* Lennard-Jones or hard spheres, or polymer glasses. For example the identification of the complexity Σ as the free energy difference between the stable and the metastable phases allows an other way to measure of this quantity in a simulation. Indeed the ending of the transition lines in a critical point implies that the metastable state can be reached *via* closed paths in phase diagram leaving always the system in (stable or metastable) equilibrium; the free energy difference of the two phases can be computed integrating the derivative of the free energy along such a closed path.

We have to study the shape of the function $F(m, q)$. At fixed m as function of q it may have one of the forms shown in Figure 8. Below the dynamical transition near $m = 1$ it has the shape of the lower curve Figure 8. By decreasing m the shape of this function modifies and the secondary minimum disappears. There is a temperature-dependent region of m where the equation $\partial F/\partial q = 0$ has a solution at non-zero q : in this region we can compute the complexity. It is possible that if we compute the small fluctuations in this region using the techniques of the next section we find for some values of m a not consistent result, *i.e.* negative spectrum. This phenomenon may indicate that the allowed m region is smaller than that indicated by the condition of the existence a solution to the equation $\partial F/\partial q = 0$. However it is also possible that more complex phenomena are present, that are not fully understood at the present moment.

4.4 A summary of the results

I will now summarize the results. As we have seen we can distinguish a few temperature regions.

- For $T > T_V$ the only minimum of the free energy functional is given by high temperature result: we call it the liquid minimum (in the spins models described above it has to zero magnetization).
- For $T_V > T > T_D$ there is an exponentially large number of minima [23, 42, 44]. For some values of the free energy density the complexity Σ is different from zero, however the contribution to the free energy coming from these minima is higher than the one coming from the liquid solution with zero magnetization. As discussed also in Cugliandolo's lectures the value T_D coincides with the critical temperature of the mode coupling approach and in the glass community is called T_c . The real critical temperature of the model, that we have called T_c up to now is called T_K for reasons that will be clear in the next section.
- The most interesting situation happens in the region where $T_D > T > T_c$ (or T_c becomes T_K if we use the glassy notation). In this region the free energy is still given the high temperature solution (with zero magnetization in spin models), It is extremely surprising [38, 40] that the free energy can be written also as the sum of the contribution of an exponentially large number of non-trivial minima as in equation (4.6). Although the free energy is analytic at T_D , below this temperature the the system at each given moment may stay in one of the exponentially large number of minima. The time (τ) to jump from one minimum to an other minimum is quite large and it is controlled by the height

of the barriers that separate the different minima. In the mean field approximation (*i.e.* for infinite range models) it is proportional to $\exp(AN)$ with non-zero A . In short range models at finite dimensions we expect that the barriers are finite and $\tau \approx \tau_0 \exp(\beta\Delta(T))$. The quantity $\beta\Delta(T)$ is often a large number also at the dynamical temperature [48] (*e.g.* $O(10)$) and the correlation time will become very large below T_D and for this region T_D is called the dynamical transition point. The correlation time (that should be proportional to the viscosity) should diverge at T_K . The precise form of this divergence is not well understood. It is natural to suppose that we should get divergence of the form $\exp(A/(T-T_K)^\nu)$ for an appropriate value of ν [49], whose reliable analytic computation is lacking [7, 37]. The value $\nu = 1$ (*i.e.* the Vogel Fulcher law) is suggested by the experiments.

The equilibrium complexity is different from zero (and it is a number of order 1) when the temperature is equal to T_D and it decreases when the temperature decreases and it vanishes linearly at $T = T_K$. At this temperature (the so called Kauzmann temperature) the entropy of a single minimum becomes equal to the total entropy and the contribution of the complexity to the total entropy vanishes. At an intermediate temperature T_g the correlation time becomes so large that it cannot be observed any more by humans.

- In the region where $T < T_K$ the free energy is dominated by the contribution of a few minima of the free energy having the lowest possible value. Here the free energy is no more the analytic continuation of the free energy in the fluid phase. A phase transition is present at T_K and the specific heat is discontinuous here.

4.5 Some consideration on the free energy landscape and on the dynamics

The free energy landscape is rather unusual; we present the following pictorial interpretation (Fig. 12), that is a rough simplification [50]. At a temperature near to T_D the system stays in a region of phase space that is quite flat and correspond of a minimum of the total free energy. On the contrary below T_D the phase space is similar to the one shown pictorial in Figure 12. The region of maxima and minima is separated by the region without barriers by a large nearly flat region. The minima in the region at the left are still present also when $T_f > T > T_D$, but they do not correspond to a global minimum.

At temperatures higher than T_D the system at thermal equilibrium stays in the right portion of Figure 12. When the temperature reaches T_D the

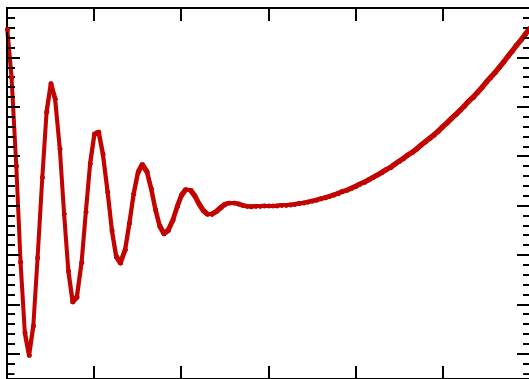


Fig. 12. The qualitative dependence of the free energy as function of the configuration space in the region relevant for the dynamical transition, *i.e.* for $T < T_D$.

system arrives in the flat region. The flatness of the potential causes a Van Hove critical slowing down that is well described by mode coupling theory [12, 18] (that is exact in the mean field approximation).

In the mean field approximation the height of the barriers separating the different minima is infinite and the temperature T_D is sharply defined as the point where the correlation time diverge. The precise meaning [39] of the dynamical temperature beyond mean field approximation has already been discussed.

Let us start from a very large system (of N particles) at high temperature and let us gradually cool it. It would like to go at equilibrium in the region with many minima. However coming from high free energy (from the right) it cannot enter in the region where are many maxima; if we wait a finite amount of time (the time to crosses the barriers diverges as $\exp(AN)$). the system remains confined in the flat region. In this case [9, 10] the so called dynamical energy,

$$E_D = \lim_{t \rightarrow \infty} \lim_{N \rightarrow \infty} E(t, N), \quad (4.35)$$

is higher than the equilibrium free energy. The situation is described in Figure 13. The difference of the static and dynamic energy is an artifact of the mean field approximation if we take literally the limit $t \rightarrow \infty$. However it correctly describes the situation on laboratory times, where metastable states are observed.

In the mean field approximation very interesting phenomena happen below T_D when the system is cooled from the high temperature phase due to the fact that the system does not really go to an equilibrium configuration but wanders in the phase space never reaching equilibrium. The phenomena

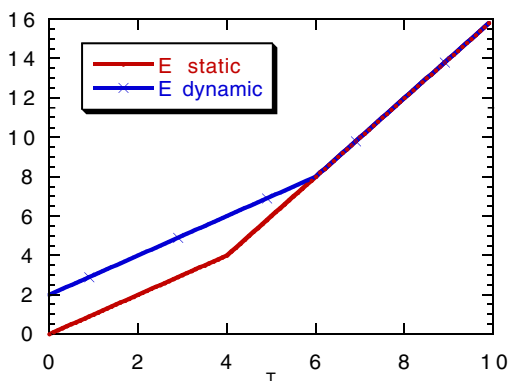


Fig. 13. The qualitative behaviour of the equilibrium energy and of the dynamical energy as function of the temperature.

are the following:

- the energy approaches equilibrium slowly when the system is cooled from an high energy configuration [9, 51]:

$$E(t, T) = E_D(T) + B(T)t^{-\lambda(T)} \quad (4.36)$$

where the exponent $\lambda(T)$ does not vanish linearly at zero temperature as happens for an activated process;

- aging is present, *i.e.* the correlation functions and the response functions in the region of large time do depend on the story of the system [10, 16, 17];
- in the region where aging is present the fluctuation dissipation theorem is no more valid. New generalized relations are satisfied [9, 10, 52–55], that replace the equilibrium fluctuation dissipation theorem.

These phenomena will be discussed in details in Cugliandolo's lectures.

It is not clear how to compute in general the quantity $E_D(T)$. There is a very simple recipe: E_D is the largest energy where $\Sigma(E) \geq 0$. According to that recipe one has to look to the smallest value of m where the equation for q has a consistent solution (as discussed in the previous section). This last condition is equivalent to impose that the spectrum of small fluctuations of the free energy (defined in the next section) has a gap. The value of E_D is characterized by the fact the one step replica broken solution is unstable at $E > E_D$ (marginal stability criterium). This marginalistic approach correctly gives E_D in the p-spin spherical model, it is not clear if it true in general [42].

4.6 Small fluctuations

We have seen that in the real world glassy systems have only one transition with divergent correlation time (at temperature T_K). However in the idealized world of mean field theories there is a second purely dynamics transition T_D at higher temperatures [7]. As it happens in many cases, slow relaxation is related to the existence of zero energy modes and this statement is true also here. This statement can be easily verified in spin models where the mode coupling theory is exact and simple computations are possible.

In spin models we concentrate our attention on the Hessian of the free energy, defined as

$$M(i, k) = \frac{\partial^2 F[m]}{\partial m(i) \partial m(k)}, \quad (4.37)$$

where $F[m]$ is the (TAP) free energy as function of the magnetization and the magnetizations do satisfy the stationarity (TAP) equations:

$$\frac{\partial F[m]}{\partial m(i)} = 0. \quad (4.38)$$

Performing the appropriate computations [56, 57] we find that the spectral density of the Hessian in these infinite range models has always a semicircular form:

$$\rho(\lambda) \propto \sqrt{(\lambda - \mu(T))(\lambda - \nu(T))}, \quad (4.39)$$

typical of random matrices [58].

- At temperatures $T > T_D$ there are no non-trivial thermodynamically relevant solutions of the equation (4.38), however the dynamics is dominated by quasi-solutions of the previous equations, *i.e.* by magnetizations such that the left hand side of the previous equation is not zero, but small [59]. The Hessian M of the quasi-solutions has negative eigenvalues and its spectrum has qualitatively the shape shown in Figure 14. These quasi stationary points of F look like saddles.
- At the dynamical transition point $T = T_D$ the quasi stationary points become real solutions of the equations (4.38). They are essentially minima: the spectrum of the Hessian is non-negative and it arrives up to zero. As it can be checked directly, the existence of these zero modes is responsible of the slowing down of the dynamics. The different minima are connected by flat regions so that the system may travel from one minimum to another [50].
- At low temperature the minima become more deep, the spectrum develops a gap as shown in Figure 14 and the minima are no more connected by flat regions. In mean field models the system would

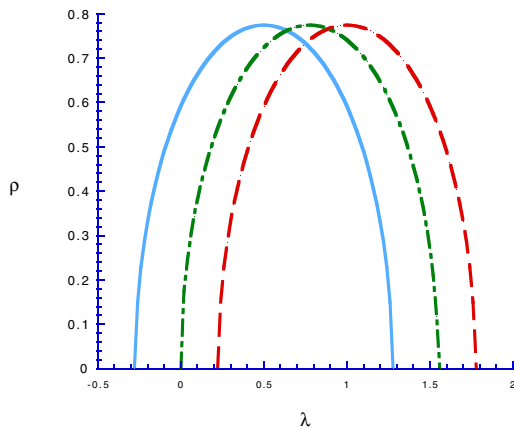


Fig. 14. The qualitative behaviour of the spectrum in mean field approximation above T_D , (full line), at T_D (dot-dashed line) and below T_D (dashed line) as function of the eigenvalue λ .

remains forever in one of these minima. If the system starts from an high temperature configuration it cannot reach these configurations.

This picture is not so intuitive because it involves the presence of saddles with many directions in which the curvature is negative, and it is practically impossible to visualize it by making a drawing in a two or a three dimensional space.

This qualitative description can be easily verified in models where the mean field approximation is exact. However, if we try to test it in finite dimensional models, we face the difficulty that the free energy functional $F[m]$ is a mythological object whose exact form is not known and consequently the eigenvalues of its Hessian cannot be computed. An alternative approach consists in studying the properties of the so called instantaneous normal modes (INM) [57,60,61] and by the saddle normal modes (SNM) [48,62–64]. For reasons of space this interesting point cannot be discussed any more the reader is invited to look to the original literatures.

These computations are particular relevant for glasses where the low temperature spectral density can be experimentally measured and one finds the famous Boson peak¹⁸. In order to explain the Boson peak one has to do realistic computations, where one has to take into account the spectrum of

¹⁸The Boson peak is defined as a bump at some small but non-zero value of the eigenvalue z of the spectral density $\rho(z)$ divided by the Debye density of states z^2 that has been observed in many material [65] and in numerical simulations [66].

phonons and this has been done or using the mode coupling formalism [67], or a microscopical approach [68].

5 Structural relations

In this section we shall define a new equilibrium order parameter function $\tilde{P}(q)$, that is connected also to fluctuation-dissipation ratio $X(q)$ (see Cugliandolo's lectures). This can be done by studying of the linear response to some special sets of perturbations of the original Hamiltonian [69]. This method has been recently used to derive interesting properties of the overlap distribution at equilibrium [70–73].

5.1 Stochastic stability

Our aim is to prove that the moments of $P(q)$ are related to the response of the system when one adds an appropriate perturbation [70]. This approach allows us to define all the relevant quantities in the case of single large system (in the infinite volume limit), while in the previous approach the function $P(q)$ was defined as the probability distribution in an ensemble of different systems, characterized by different realizations of the disorder. This difference is crucial if we consider the case (like glasses) where no disorder is present¹⁹.

In the case of spin systems an appropriate form of the long-range perturbation is given by:

$$H_p(\sigma) = \sum_{i_1, i_p=1, N}^{1, N} K_{i_1, \dots, i_p} \sigma_{i_1} \cdots \sigma_{i_p}, \quad (5.1)$$

where the couplings K_{i_1, \dots, i_p} are independent Gaussian variables with zero mean and variance $\overline{K_{i_1, \dots, i_p}^2} = 1/(2N^{p-1})$.

The Hamiltonian is

$$H_\epsilon = H_I + \epsilon H_p. \quad (5.2)$$

The canonical average of H_p verifies, for all values of ϵ , the relation

$$\overline{\langle H_p \rangle} = -\beta \epsilon N \left(1 - \int dq P_\epsilon(q) q^p \right), \quad (5.3)$$

irrespective of the specific form of H_I . Here the function $P_\epsilon(q)$ is the probability distribution of the overlap q in the presence of the perturbing term in

¹⁹In a glass we still have the possibility of averaging over the total number of particles.

the Hamiltonian; the average is done over the new couplings J at fixed H_I . The derivation, involves only an integration by parts in a finite system.

However the previous equation is strange. The function $P_\epsilon(q)|_{\epsilon=0}$ depends on the instance of the problem also in the infinite volume limit, while, for $\epsilon \neq 0$, $\langle H_p \rangle$ is a thermodynamic quantity that cannot fluctuate in the infinite volume limit when we change the instance of the system (at least for generic ϵ). A further difficulty appears when there is an additional symmetry in absence of the random perturbation that is broken by the random perturbations (*e.g.* the spin reversal symmetry for a spin system in absence of a magnetic field or the translational invariance for glasses). Therefore for a large system we may expect that

$$\tilde{P}(q) \neq P_I(q), \quad (5.4)$$

where $P_I(q)$ is the usual overlap probability distribution computed at $\epsilon = 0$, that may depend on the instance, while $\tilde{P}(q)$ is the limit $\epsilon \rightarrow 0$ of the function $P_\epsilon(q)$ (where the limit is computed outside the cross-over region, *i.e.* $\epsilon \gg N^{1/2}$) and it does not depend from the instance.

We need to understand better how the equilibrium state in the presence of the perturbation ϵH_p is related to the equilibrium state at $\epsilon = 0$. Some complications arise whenever the equilibrium expectation value of H_p is not the same for all pure phases of the unperturbed systems. Then the limit value of H_p as $\epsilon \rightarrow 0$ will be the one corresponding to the favored phases. A simple example is the Ising model in the ferromagnetic phase, where one adds a negative magnetic field term as a perturbation. Also in the vanishing field limit, the system stays in a state with negative spontaneous magnetization, while the unperturbed measure corresponds to a mixture of the positive and negative magnetization pure states.

In presence of many equilibrium states that contribute to the Gibbs-Boltzmann measure, as it happens when replica symmetry is broken, the situation is rather complex. Indeed, the stochastic perturbations that we have considered will in general reshuffle the weights of the different ergodic components in the Gibbs measure, or even change their nature, and this changes the $P(q)$ function to a different one ($\tilde{P}(q)$).

The principle of stochastic stability assumes that if consider an appropriate ensemble as for the initial random system we have that

$$P(q) \equiv \overline{P_I(q)} = \tilde{P}(q) \quad (5.5)$$

where here the bar denotes the average over the instances of the system in the appropriate ensemble.

An intuitive motivation for assuming stochastic stability is that perturbations we use are random and they are not correlated with the original Hamiltonian. So they should change the free energies of the various pure

states of the original systems by random amounts. Stochastic stability assumes in glassy systems the *distribution* of these free energies is stable under independent random increments, as has been shown in mean field (in fact this property lies at the heart of the cavity method [2]). If this is the case then the two functions $\tilde{P}(q)$ and $P(q)$ coincide. We could also say that the equality of $\tilde{P}(q)$ and $P(q)$ indicates that the systems responds to a random perturbation as a generic random system.

There are cases where stochastic stability trivially fails, *i.e.* when the original Hamiltonian has an exact symmetry, that is lifted by the perturbation. The simplest case is that of a spin glass with a Hamiltonian invariant under spin inversion. In this case $P(q) = P(-q)$, since each pure state appears with the same weight as its opposite in the unperturbed Gibbs measure. On the other hand, if we consider H_p with odd p , this symmetry is lifted. This means that in the $\epsilon \rightarrow 0$ limit only half of the states are kept. If the reshuffling of their free energies is indeed random, then we shall have $\tilde{P}(q) = 2\theta(q)P(q) \equiv \hat{P}(q)$. The same type of reasoning applies whenever the overlap q transforms according to a representation of the symmetry group of the unperturbed Hamiltonian H_0 .

If this *trivial* effect of exact symmetries is taken into account, for a large class of systems, the function $\tilde{P}(q)$ in the limit of small perturbations tends to the order parameter function $\hat{P}(q)$ of the pure system where the exact symmetries are lifted. This continuity property is called *stochastic stability*. Ordinary systems without symmetry breaking and mean-field spin glasses are examples of stochastically stable systems. In ergodic systems, the equality of \tilde{P} and \hat{P} is immediate, both functions consist in a single delta function. Thus, the problem of deriving the equality between \tilde{P} and \hat{P} , appears only when there are coexisting phases unrelated by symmetry. Unfortunately, we are not able to characterize the class of stochastically stable systems. In particular there is no rigorous proof that short-range spin glass, for which our theorem is most interesting, belong to this class. However, stochastic stability has been established rigorously in mean field problems [70, 71].

If one studies more carefully the problems, one finds that stochastic stability has far reaching consequences, *e.g.*

$$\overline{P_I(q_1)P_I(q_2)} = \frac{2}{3}P(q_1)P(q_2) + \frac{1}{3}P(q_1)\delta(q_1 - q_1). \quad (5.6)$$

These (and other) relations have been carefully numerically verified in also in numerical simulations of three dimensional spin glasses models [53] strongly suggesting the validity of stochastic stability.

5.2 A simple consequence of stochastic stability

Stochastic stability is a very powerful property, and it is the ingredient that allows to relate the properties of the low lying configurations, that dominate the Gibbs measure, to those of the configurations much higher in energy that are seen in the dynamics. This is most easily explained in the usual framework of replica-symmetry breaking, considering an approximation with only two possible values of the overlap, q_0 among different states and q_1 among the same state (*i.e.*, one-step replica-symmetry breaking). The probability of finding a state with total free energy $F_\alpha = F$ is given by $\rho(\Delta F)$, where $\Delta F = F - F_0$ and F_0 is a reference free energy the equilibrium free energy. The weight of each state is given by

$$w_\alpha \propto \exp(-\beta F_\alpha). \quad (5.7)$$

In one-step replica-symmetry breaking, the states that contribute to the Gibbs measure have nearly degenerate free energies. We have already seen the non-extensive fluctuation of their free energies, corresponding to the low ΔF regime of $\rho(\Delta F)$, is given by [25,92]

$$\rho(\Delta F) \propto \exp(\beta m \Delta F), \quad (5.8)$$

and the function $P(q)$ is given by

$$P(q) = m\delta(q - q_0) + (1 - m)\delta(q - q_1). \quad (5.9)$$

Stochastic stability forces the function $\rho(\Delta F)$ to be of the form (5.8), not only when ΔF is finite, but also in the range where ΔF is *extensive* but small (say of order ϵN). Indeed it imposes that the form of the function $\rho(\Delta F)$ remains unchanged (apart from a possible shift in F_0) when one adds a small random perturbation [69].

Let us consider the effect of a perturbation of strength ϵ on the free energy of a state, say α . The unperturbed value of the free energy is denoted by F_α . The new value of the free energy G_α is given by $G_\alpha = F_\alpha + \epsilon r_\alpha$ where r_α are identically distributed uncorrelated random numbers. Stochastic stability implies that the distribution $\rho(G)$ is the same as $\rho(F)$. Expanding to second order in ϵ we see that this implies $d\rho/dF \propto d^2\rho/dF^2$, whose only physical solution (apart the trivial one $\rho(F) = 0$, that corresponds to non-glassy systems) is given by equation (5.8)²⁰. We see that stochastic stability

²⁰The same conclusion could be obtained using the methods of reference [73] computing the sample-to-sample fluctuations of the function $P_J(q)$, that in this case, where ultrametricity is trivially satisfied, are completely determined by the knowledge of the function $P(q)$.

fixes the form of the function ρ and therefore connects in an inextricable way the low and the high free energy part of the function ρ .

This remark explain how it is possible that stochastic stability tells us something on the dynamics in the aging regime (as we shall see in the next section). In the dynamical evolution from an higher temperature initial state the difference between the total free energy at time t and the equilibrium value will be always of order N , with a prefactor going to zero when t goes to infinity. One could argue that the dynamics probes the behavior of the function $\rho(\Delta F)$ at very large argument, and should not be related to the static property that depend on the function ρ for small values of the argument. However stochastic stability forces the function $\rho(\Delta F)$ to be of the form equation (5.8), also in the range where ΔF is *extensive* but small, and this objection is no more valid.

5.3 Fluctuation dissipation relations

Let us now discuss the case of dynamics of a systems that at times 0 starts from a non-equilibrium configuration. Here the relevant quantities are the two times correlations functions and the response functions, *e.g.* the correlation defined as

$$C(t_w, t) \equiv \frac{\sum_{i=1, N} \sigma_i(t_w) \sigma_i(t)}{N}. \quad (5.10)$$

The finite-time response and correlation functions involved in the definition of the FDR are continuous functions of ϵ for $\epsilon \rightarrow 0$. It is not evident if the limit is uniform in time, *i.e.* if the infinite times and the $\epsilon \rightarrow 0$ limits do commute. The linear response regime may shrinks to zero as the time goes to infinity. This possibility shows up when the perturbations favor one phase (as discussed in the introduction). However here we consider a random perturbations and the expectations of H_p vanishes at $\epsilon = 0$: it is reasonable to assume that the linear response regime survives at very long times²¹.

If the infinite times limit and the $\epsilon \rightarrow 0$ limit do commute (this is the dynamical form of the stochastic stability), the dynamics is strongly constrained. For example, if we consider the function $X(q)$ that parametrizes the violations of the fluctuation dissipation relations in off-equilibrium experiments [9, 10], the previous assumptions imply that:

$$\tilde{P}(q) = \frac{dX}{dq}. \quad (5.11)$$

²¹Let us stress that the existence of a linear response regime uniform in time a question susceptible of experimental investigation.

The proof is simple it only involves integrations by parts. The details can be found in the original papers [69].

6 A short introduction to glasses

Glasses [74] are roughly speaking liquids that do not crystallize also at very low temperature (to be more precise: glasses also do not quasi-crystallize).

These liquids can avoid crystalization mainly for two reasons:

- the liquid does not crystallize because it is cooled very fast: the crystallisation time may become very large at low temperature (*e.g.* hard spheres at high pressure). The system should be cooled very fast at temperatures near the melting point; however if crystalization is avoided, and the temperature is low enough, (*e.g.* near the glass transition) the system may be cooled very slowly without producing crystalization;
- the liquid does not crystallize even at equilibrium. An example is a binary mixture of hard spheres with different radius: 50% type A (radius r_A , 50% type B (radius r_B), where R denotes r_B/r_A . If $.77 < R < .89$ (the bounds may be not precise), the amorphous packing is more dense than a periodic packing, distorted by defects.

Which of the two mechanism is present is irrelevant for understanding the liquid glass transition.

Other examples of glassy systems are binary mixtures: in this case we have 2 kinds of particles and the Hamiltonian of N particles is given by

$$H = \sum_{a,b=1,2} \sum_{i=1,N(a)} \sum_{k=1,N(b)} V_{a,b}(x_a(i) - x_b(k)), \quad (6.1)$$

where $a = 1, 2$; $N(a) = Nc(a)$; $\sum_{a=1,2} c(a) = 1$. In this case the values of the N concentrations c and the 3 functions $V_{a,b}(x)$ describe the model. Well studied case are:

- a power potential (non-realistic, but simple), *e.g.* $c(1) = .5$, $c(2) = .5$, $V_{a,b}(x) = R_{a,b}x^{-12}$;
- Lennard-Jones potential (more realistic), *e.g.* $c(1) = .8$, $c(2) = .2$, $V_{a,b}(x) = R_{a,b}x^{-12} - A_{a,b}x^{-6}$.

There are some choices of the parameters that are well studied such that the system does not crystallize. One has been introduced by Kob and Anderson in the L-J case [75]: it corresponds to a particular choice of the parameters R and A .

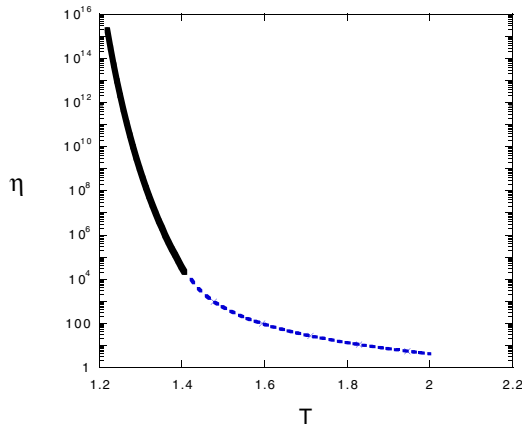


Fig. 15. The viscosity as function of the temperature according to the Vogel Fulcher law ($T_K = 1$ full line) and to the mode coupling theory ($T_K = 1.375$ dotted line).

There are many other material that are glass forming, *e.g.* short polymers, asymmetric molecules (*e.g.* OTP) ...

The behaviour of the viscosity in glass forming liquid is very interesting²². There are two regimes:

- in an high temperature region the mode coupling theory [12] is valid: it predicts $\eta \propto (T - T_d)^{-\gamma}$, where γ is *not* an universal quantity and it is $O(1)$;
- in the low temperature region by the Vogel Fulcher law [49] is satisfied: it predicts that $\eta \propto \exp(A(T - T_K)^{-1})$. Nearly tautologically fragile glasses can be defined as those glasses that have $T_K \neq 0$; strong glasses have $T_K \approx 0$.

At the glass temperature (T_g) the viscosity becomes so large that it cannot be any more measured. This happens after an increase of about 18 order of magnitude (that correspond to a microscopic time changing from 10^{-15} to 10^4 sec): the relaxation time becomes larger than the experimental time.

²²The viscosity can be defined microscopically considering a system in a box of large volume V : $T_{\mu,\nu}(t)$ is the total stress tensor at time t . We define the correlation function of the stress tensor at different times: $\langle T_{\mu,\nu}(t)T_{\rho,\sigma}(0) \rangle = VS_{\mu,\nu,\rho,\sigma}(t)$ Neglecting indices, $\eta \propto \int dt S(t) \approx \tau^{-\alpha}$, where τ is the characteristic time of the system (in a first approximation we can suppose that $\alpha = 1$).

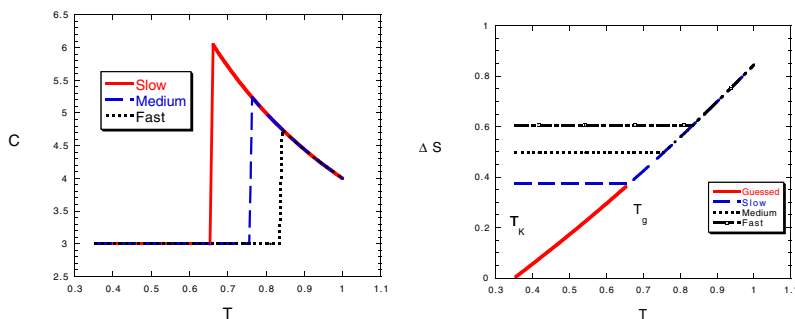


Fig. 16. The specific heat and the entropy excess ΔS for various cooling rates.

A characteristic of glasses is the dependance of the specific heat on the cooling rate. There is a (slightly rounded) discontinuity in the specific heat that it is shifted at lower temperatures when we increase the cooling time.

For systems that do crystallize if cooled too slowly, one can plot $\Delta S \equiv S(\text{liquid}) - S(\text{crystal})$ versus T in the thermalized region. One gets a very smooth curve whose extrapolation becomes negative at a finite temperature. A negative ΔS does not make sense, so there is a wide spread belief that a phase transition is present before (and quite likely near) the point where the entropy becomes negative. Such a thermodynamic transition (suggested by Kaufmann) would be characterized by a jump of the specific heat. Quite often this temperature is very similar to the temperature found by fitting the viscosity by the Volker Fulcher law and the two temperature are believed to coincide.

Usually a second order a thermodynamic phase transition induces a divergent correlation time. However the exponential dependance of the correlation time on the temperature is not so common (in conventional critical slowing down we should have a power like behaviour); an other strange property of the glass transition is the apparent absence of an equilibrium correlation length or susceptibility (linear or non-linear) that diverges when we approach the transition point²³.

7 The replica approach to structural glasses: General formalism

In this section we write down the formulas corresponding to the replica approach introduced in the previous section. We keep here to the case of simple

²³There is a dynamical correlation length that diverge at the critical temperature that is observed numerically and it is predicted theoretically [76].

glass formers consisting of N particles interacting by a pair potential $v(r)$ in a space of dimension d .

The reader may notice that in all the example that we have considered up to now a quenched disorder was present; this feature is not present in glasses, where no random quenched variables are present in the Hamiltonian. However this is not a difficulty as far as there is no need of a quenched random disorder to use the replica formalism as it is clear from the previous sections. However at the beginning it was believed that a random quenched disorder was necessary in order to use the replica approach. Only much later [13, 77–79] it was realized that the replica method could be used in translational invariant models where no disorder is present; some of these models behaves in a way very similar to real glasses: one can define both T_D and T_K and at low temperature the system crystallizes.

7.1 The partition function

The usual partition function, used *e.g.* in the liquid phase, is in three dimension

$$Z_1 \equiv \frac{1}{N!} \int \prod_{i=1}^N (d^3 x_i) e^{-\beta H}. \quad (7.1)$$

We wish to study the transition to the glass phase through the onset of an off-diagonal correlation in replica space [80, 81]. We use m replicas and introduce the Hamiltonian of the replicated system:

$$H_m = \sum_{1 \leq i < j \leq N} \sum_{a=1}^m v(x_i^a - x_j^a) + \epsilon \sum_{i=1N} \sum_{a < b=m} w(x_i^a - x_i^b) \quad (7.2)$$

where w is an attractive interaction. The precise form of w is unimportant: it should be a short range attraction respecting the replica permutation symmetry, and its strength ϵ that will be sent to zero in the end. For instance one could take

$$w(x) = \left(\frac{c^2}{x^2 + c^2} \right)^6 \quad (7.3)$$

with c is of the order of 0.2 times the typical intermolecular distance. A positive value of ϵ forces all the particles one near to the other ones. If two systems stay in the same state, the expectation value of w represents the self overlap and it very near to 1.

The partition function of the replicated system is

$$Z_m \equiv \frac{1}{N!^m} \int \prod_{i=1}^N \prod_{a=1}^m (d^3 x_i^a) e^{-\beta H_m}. \quad (7.4)$$

7.2 Molecular bound states

At low enough temperature, we expect that the particles in the different replicas may stay close to each other. The role of the attractive term w is to insure that all replicas fall into the same glass state: also for small ϵ the particles in different replicas stay at the same place, apart from some thermal fluctuations.

Thermal fluctuations are relatively small throughout the solid phase (one can see this from the Lindeman criterion) and diffusion is very small, one can identify the molecules and relabel all the particles in the various replicas in such a way that the particle j in replica a always stays close to particle j in replica b . All the other relabelings are equivalent to this one, producing a global factor $N!^{m-1}$ in the partition function.

We therefore need to study a system of molecules, each of them consisting of m atoms (one atom from each replica). It is natural to write the partition function in terms of the variables r_i that describe the centers of masses of the molecules, and the relative coordinates u_i^a , with $x_i^a = r_i + u_i^a$ and $\sum_a u_i^a = 0$:

$$Z_m = \frac{1}{N!} \int \prod_{i=1}^N (d^3 r_i) \prod_{i=1}^N \prod_{a=1}^m (d^3 u_i^a) \prod_{i=1}^N \left(m^3 \delta \left(\sum_a u_i^a \right) \right) \\ \times \exp \left(-\beta \sum_{i < j, a} v(r_i - r_j + u_i^a - u_j^a) - \beta \sum_i \sum_{a,b} W(u_i^a - u_i^b) \right). \quad (7.5)$$

7.3 The small cage expansion

In order to transform these ideas into a tool for doing explicit computations of the thermodynamic properties of a glass [81] we have to use an explicit method for computing the free energy as function of the temperature and m . As is usually the case, in the liquid phase exact analytic computations are not possible and we have to do some approximations. In this section we shall use the fact that the thermal fluctuations of the particles in the glass are small at low enough temperature: the size of the “cage” seen by each particle is therefore small, allowing for a systematic expansion. What we will be describing here are the thermal fluctuations around the minimum of the potential of each particle, in the spirit of the Einstein model for vibrations of a crystal.

We start from the replicated partition function Z_m described in molecular coordinates in (7.5). Assuming that the relative coordinates u_i^a are

small, we can expand W keeping only the quadratic term and write:

$$Z_m(\alpha) = \frac{1}{N!} \int \prod_{i=1}^N (d^3 r_i) \prod_{i=1}^N \prod_{a=1}^m (d^3 u_i^a) \prod_{i=1}^N \left(m^3 \delta \left(\sum_a u_i^a \right) \right) \\ \times \exp \left(-\beta \sum_{i < j, a} v(r_i - r_j + u_i^a - u_j^a) - \frac{1}{4\alpha} \sum_i \sum_{a,b} (u_i^a - u_i^b)^2 \right). \quad (7.6)$$

In the end we are interested in the limit $\epsilon \equiv (1/\alpha) \rightarrow 0$. We would like first to define the size A of the molecular bound state, that is also a measure of the size of the cage seen by each atom in the glass, by:

$$\frac{\partial \log Z_m}{\partial (1/\alpha)} \equiv \frac{m(1-m)}{2} dNA = -\frac{1}{4} \sum_i \sum_{a,b} \langle (u_i^a - u_i^b)^2 \rangle \quad (7.7)$$

(d is the dimension that we have taken equal to 3 and N is the number of particles). We Legendre transform the free energy $\phi(m, \alpha) = -(T/m) \log Z_m$, introducing the thermodynamic potential per particle $\psi(m, A)$:

$$\psi(m, A) = \phi(m, \alpha) - \alpha^{-1} \frac{\partial \phi(m, \alpha)}{\partial \alpha^{-1}} = \phi(m, \alpha) + Td \frac{(1-m)}{2} \frac{A}{\alpha}. \quad (7.8)$$

What we want to see is whether there exists a minimum of ψ at a finite value of A .

At low temperatures, this minimum should be at small A , and so we shall seek an expansion of ψ in powers of A . It turns out that it can be found by an expansion of ϕ in powers of α , used as an intermediate bookkeeping in order to generate the low temperature expansion.

This may look confusing since we are eventually going to send α to ∞ . However this method is nothing but a usual low temperature expansion in the presence of an infinitesimal breaking field. For instance when we compute the low temperature expansion of the magnetization in a d -dimensional Ising model in an infinitesimal positive magnetic field h , the main point is that the magnetisation is close to one. One can organise the expansion by studying first the case of a large magnetic field, performing the expansion in powers of $\exp(-2h)$, and in the end letting $h \rightarrow 0$. A little thought shows that the intermediate -large h - expansion is just a bookkeeping device to keep the leading terms in the low temperature expansion. What we do here is exactly similar, the role of h being played by $1/\alpha$.

7.3.1 Zeroth order term

We use the equivalent form:

$$Z_m(\alpha) = \frac{1}{N!} \int \prod_{i=1}^N \prod_{a=1}^m (d^3 u_i^a) \prod_i \frac{d^3 r_i}{\sqrt{\frac{2\pi\alpha}{m^2}}} \times \exp \left(-\beta \sum_{i < j, a} v(x_i^a - x_j^a) - \frac{m}{2\alpha} \sum_{i,a} (x_i^a - r_i)^2 \right). \quad (7.9)$$

In the limit $\alpha \rightarrow 0$, the identity

$$\exp \left(-\frac{m}{2\alpha} (x_i^a - r_i)^2 \right) \simeq \left(\frac{2\pi\alpha}{m} \right)^{d/2} \delta^3(x_i^a - r_i) \quad (7.10)$$

implies that:

$$Z_m^0(\alpha) = \left(\frac{2\pi\alpha}{m} \right)^{3N(m-1)/2} \frac{1}{N!} \int \prod_i d^3 r_i \exp \left(-\beta m \sum_{i < j} v(r_i - r_j) \right). \quad (7.11)$$

In this expression we recognise the integral over the r_i 's as the partition function $Z_{\text{liq}}(T^*)$ of the liquid at the effective temperature T^* , defined by

$$T^* \equiv T/m. \quad (7.12)$$

Therefore the free energy, at this leading order, can be written as:

$$\beta\phi^0(m, \alpha) = \frac{3(1-m)}{2m} \log \frac{2\pi\alpha}{m} - \frac{3}{2m} \log(m) - \frac{1}{mN} \log Z_{\text{liq}}(T^*). \quad (7.13)$$

The result is intuitive: in the limits where the particles of different replicas stay at the same point, the Hamiltonian for m replicas is just the usual one, multiplied by m .

7.3.2 First order term

In order to expand to next order of the α^{-1} expansion, we start from the representation (7.6) and expand the interaction term to quadratic order in the relative coordinates:

$$Z_m = \int \prod d^3 r_i d^3 u_i^a \prod_i \left(m^3 \delta \left(\sum_a u_i^a \right) \right) \exp \left(-\beta m \sum_{i < j} v(r_i - r_j) \right) \times \exp \left(-\frac{\beta}{2} \sum_{i < j} \sum_{a\mu\nu} (u_i^a - u_j^a)(u_i^\mu - u_j^\mu) \frac{\partial^2 v(r_i - r_j)}{\partial r^2} - \frac{1}{4\alpha} \sum_{a,b} (u_i^a - u_i^b)^2 \right).$$

(where for simplicity we have not introduced the indices μ and ν , running from 1 to d , that denote space directions). Notice that in order to carry this step, we need to assume that the interaction potential $v(r)$ is smooth enough, excluding hard cores.

After some computations one finds that the free energy to first order is equal to:

$$\beta\phi(m, \alpha) = \frac{3(m-1)}{2m} \log \frac{1}{\alpha} - \alpha\beta C + \frac{3(1-m)}{2m} \log \frac{2\pi}{m} - \frac{3}{2m} \log m - \frac{1}{mN} \log Z_{\text{liq}}(T^*) \quad (7.14)$$

where the constant C is proportional to the expectation value of the Laplacian of the potential, in the liquid phase at the temperature T^* :

$$C \equiv \frac{1}{2} \frac{1-m}{m^2} \sum_{j(\neq i)} \langle \Delta v(z_i - z_j) \rangle^*. \quad (7.15)$$

Differentiating the free energy with respect to $1/\alpha$ gives the equation for the size of the cage:

$$\beta \frac{\partial \phi}{\partial (1/\alpha)} = -\frac{(1-m)}{2m} d\alpha + \alpha^2 \beta C = -\frac{(1-m)}{2} dA. \quad (7.16)$$

Expanding this equation in perturbation theory in A we have:

$$\alpha = mA - \frac{2\beta m^3 C}{3(m-1)} A^2. \quad (7.17)$$

The Legendre transform is then easily expanded to first order in A :

$$\begin{aligned} \beta\psi(m, A) &= \beta\phi(m, \alpha) + 3 \frac{(1-m)}{2} \frac{A}{\alpha} \\ &= \frac{3(1-m)}{2m} \log(2\pi A) - \beta m A C + \frac{3(1-m)}{2m} \\ &\quad - \frac{3}{2m} \log m - \frac{1}{mN} \log Z_{\text{liq}}(T^*). \end{aligned} \quad (7.18)$$

This very simple expression gives the free energy as a function of the number of replicas, m , and the cage size A . We need to study it at $m \leq 1$, where we should maximise it with respect to A and m . The fact that we seek a maximum when $m < 1$ instead of the usual procedure of minimising the free energy is a well established fact of the replica method, appearing as soon as the number of replicas is less than 1 [2].

As a function of A , the thermodynamic potential ψ has a maximum at:

$$A = A_{\max} \equiv \frac{d(1-m)}{2\beta m^2} \frac{1}{C} = \frac{3}{\beta} \frac{1}{\int d^3r g^*(r) \Delta v(r)} \quad (7.19)$$

where g^* is the pair correlation of the liquid at the temperature T^* . A study of the potential $\psi(m, A_{\max})$, that equals $\phi(m)$, as a function of m then allows to find all the thermodynamic properties that we seek, using the formulas of the previous section. The results will be explained below in Section 8, where we shall compare the results to those of other approximations.

7.3.3 Higher orders

The systematic expansion of the thermodynamic potential ψ in powers of A can be carried out easily to higher orders. However the result involves some more detailed properties of the liquid at the effective temperature T^* . For instance at second order one needs to know not only the free energy and pair-correlation of the liquid at temperature T^* , but also the three points correlation. The results for the second order, that will be discussed in next section, will be obtained in the framework of the hypernetted chain molecular approach that is described in Appendix.

7.3.4 Harmonic resummation

One can obtain a partial resummation of the small cage expansion described above by integrating exactly over the relative vibration modes of the molecules. We shall use such a procedure here, that is a kind of harmonic expansion in the solid phase²⁴.

We work directly with $1/\alpha = 0$ and start from the replicated partition function (7.14), within the quadratic expansion of the interaction potential v in the relative coordinates u_i^a . (Clearly it is assumed that the $1/\alpha \rightarrow 0^+$ limit has been taken, and that its effect is to build up molecular bound states.) The exact integration over the Gaussian relative variables gives:

$$Z_m = \frac{m^{N3/2} \sqrt{2\pi}^{N3(m-1)}}{N!} \int \prod_{i=1}^N d^3r_i \exp \left(\beta m \sum_{i < j} v(r_i - r_j) - \frac{m-1}{2} \text{Tr} \log (\beta M) \right) \quad (7.20)$$

²⁴In some loose sense the first order in the A expansion may be compared to Einstein approximation for the specific heat and the harmonic approximation we describe he may be compared to Debye's jellium.

where the matrix M , of dimension $3N \times 3N$, is given by:

$$M_{(i\mu)(j\nu)} = \delta_{ij} \sum_k v_{\mu\nu}(r_i - r_k) - v_{\mu\nu}(r_i - r_j) \quad (7.21)$$

and $v_{\mu\nu}(r) = \partial^2 v / \partial r_\mu \partial r_\nu$. We have thus found an effective Hamiltonian for the centers of masses r_i of the molecules, that basically looks like the original problem at the effective temperature $T^* = T/m$, complicated by the contribution of vibration modes that give the “Trace Log” term. We expect that this should be a rather good approximation for the glass phase. Unfortunately, even within this approximation, it is not possible to compute the partition function exactly. The density of eigenstates of the matrix M is a rather complicated object and we have developed a simple approximation scheme in order to estimate it.

We thus proceed by using a *quenched approximation*, i.e. neglecting the feedback of vibration modes onto the centers of masses. This approximation becomes exact close to the Kauzmann temperature where $m \rightarrow 1$. The free energy is then:

$$\beta\phi(m, T) = -\frac{3}{2m} \log(m) - \frac{3(m-1)}{2m} \log(2\pi) - \frac{1}{mN} \log Z(T^*) + \frac{m-1}{2m} \langle \text{Tr} \log(\beta M) \rangle^* \quad (7.22)$$

that involves again the free energy and correlations of the liquid at the temperature T^* . Computing the spectrum of M is an interesting problem of random matrix theory, in a subtle case where the matrix elements are correlated. Some efforts have been devoted to such computations in the liquid phase where the eigenmodes are called instantaneous normal modes [60]. Here we use a simple resummation scheme that should be reasonable at high densities-low temperatures: it is described in the Appendix²⁵. Using these results we can compute the replicated free energy F_m only from the knowledge of the free energy and the pair correlation of the liquid at the effective temperature T^* . The results will be discussed in Section 8.

7.3.5 Without replicas

Up to now we have used the replica theory. Replica theory is a very powerful tool, but it has the disadvantage that many of the underlying physical hypothesis cannot be seen in a clear way. We will rederive some of the previous

²⁵If the harmonic approximation were fully consistent, all the eigenvalues of \mathcal{H} (the so called INN, Instantaneous Normal Modes [60]) should be positive. This is not the case, however the number of negative eigenvalues becomes very small at low temperature, still in the liquid phase, signaling that valleys can be approximately defined in this region.

formulae without using the replica formalism [40,43]. We only suppose that at low temperatures the phase space of the system can be approximately divided into valleys that are separated by high barriers [82–84]. In a first approximation each valley can be associated to one inherent structure [6,85], *i.e.* one minimum of the potential energy and consequently there is a one to one correspondence among the valley at two different temperatures.

Let us consider a system with N particles with Hamiltonian $H(C)$, C denoting the generic configuration of the system. If we use the approach of the previous sections, the crucial step is the computation of the generalized partition function:

$$Z(\gamma; \beta) \equiv \exp(-N\gamma G(\gamma; \beta)) = \sum_a \exp(-\gamma N f_a(\beta)). \quad (7.23)$$

Using the definition of the free energy in a valley

$$\int_{C \in \alpha} dC \exp(-\gamma H(C)) = \exp(-N\gamma f(\gamma, C)), \quad (7.24)$$

we obtain

$$\begin{aligned} Z(\gamma; \beta) &= \int dC \exp(-\gamma H(C) - N\gamma f(\beta, C) + N\gamma f(\gamma, C)) \\ &= \int dC \exp\left(-\gamma H(C) - N\gamma \hat{f}(\beta, C) + N\gamma \hat{f}(\gamma, C)\right), \end{aligned} \quad (7.25)$$

where $\hat{f}(\beta, C) = f(\beta, C) - f(\infty, C)$ and $f(\beta, C)$ is a function that is constant in each valley and it is equal to the free energy density of the valley to which the configuration C belongs.

Before entering into the computation of $\hat{f}(\beta, C)$ it is useful to make the so called *quenched approximation*, *i.e.* to make the following approximation inside the previous integral:

$$\exp(-A\hat{f}(\beta, C)) = \exp(-A\langle \hat{f}(\beta) \rangle_\gamma), \quad (7.26)$$

where $\langle \hat{f}(\beta) \rangle_\gamma$ is the expectation value of $\hat{f}(\beta, C)$ taken with the probability distribution proportional to $\exp(-\gamma H(C))$. The quenched approximation is exact if the temperature dependance of the energy of all the valleys is the same, apart from an overall shift at zero temperature. In other words we assume that the minima of the free energy have different values of the free energy but similar shapes. The quenched approximation would be certainly bad if we were using the free energy $f(\beta, C)$ at the place of $\hat{f}(\beta, C)$ because the zero temperature energy strongly varies when we change the minimum.

We finally find

$$G(\gamma; \beta) = F_L(\gamma) + \hat{f}_\gamma(\beta) - \hat{f}_\gamma(\gamma), \quad (7.27)$$

$F_L(\gamma)$ being the free energy of the liquid ($S_L(\gamma)$ and $S_\gamma(\gamma)$ are respectively the entropy of the liquid and of a valley). A simple algebra shows that

$$\Sigma(\gamma; \beta) = S_L(\gamma) - S_\gamma(\gamma) + \hat{f}'_\gamma(\gamma) - \hat{f}'_\gamma(\beta), \quad (7.28)$$

where $\hat{f}'_\gamma(\beta) = \partial \hat{f}_\gamma(\beta) / \partial \gamma$.

In the liquid phase, we find out that the configurational entropy is given by

$$\Sigma(\beta) = \Sigma(\beta; \beta) = S_L(\beta) - S_\beta(\beta). \quad (7.29)$$

The entropy of the liquid is the entropy of the typical valley plus the configurational entropy.

The thermodynamic transition is characterized by the condition

$$\Sigma(\beta_K) = 0. \quad (7.30)$$

In the glassy phase the free energy can be found by first computing the value of $\gamma(\beta)$ such that

$$\Sigma(\gamma(\beta); \beta) = 0. \quad (7.31)$$

The quantity $\gamma(\beta)$ is the inverse of the effective temperature of the valley. It is easy to show (following [40]) that the previous formulae are completely equivalent to the replica approach.

A strong simplification happens if we assume that the entropy of the valley can be evaluated in the harmonic approximation where we only keep the vibrational contributions. For a system with M degrees of freedom the harmonic entropy of the valley near to a configuration C is given by

$$S(\beta(C)) = \frac{M}{2} \ln \left(\frac{2\pi e}{\beta} \right) - \frac{1}{2} \text{Tr} (\ln(\mathcal{H}(C))), \quad (7.32)$$

where $\mathcal{H}(C)$ is an $M \times M$ Hessian matrix (*e.g.* if H depends on the coordinates x_i we have that $\mathcal{H}_{i,k} = \partial^2 H / \partial x_i \partial x_k$). The final result is just the same obtained with the replica method in the harmonic approximation if we put $m = \gamma/\beta$.

8 The replica approach to structural glasses: Some results

8.1 Three approximation schemes

We have seen up to now three approximation schemes.

- The small cage expansion has been carried out directly to first order in Section 7.3.2, and agree with the first order expansion within the molecular HNC approach.

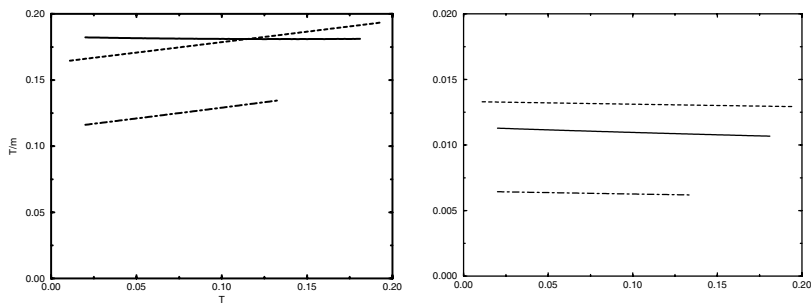


Fig. 17. The effective temperature of the molecular liquid at the transition, $T^* = T/m^*$ (left) and the quantity A/T , versus the temperature T , computed in an expansion to first order (dashed-dotted line) and second order (full line) in the cage size A , and in the harmonic resummation (dashed line).

- The second approximation scheme is the harmonic resummation method. Again we have an explicit form (9.21) for the free energy per particle $\phi(m)$ only from the knowledge of the free energy and the pair correlation of the liquid at T^* . Having this m dependance the procedure to get the thermodynamic results is entirely the same as that of the first order result.
- The third approximation scheme is obtained by the expansion of the molecular HNC free energy to second order in the cage size, as described in the Appendix.

For each of the three approximation schemes mentioned above, we need to compute the free energy and the pair correlation of the liquid in a temperature range close to the glass transition. We will first consider three dimensional soft spheres [81] interacting through a potential $v(r) = 1/r^{12}$. We work for instance at unit density, since the only relevant parameter is the combination $\Gamma = \rho T^{-1/4}$. In this case we have used the hypernetted chain approximation to get both the correlation function $g(r)$ and the free energy. Later on we will present the results for an LJ binary mixture within the harmonic approximation.

8.2 Critical temperature and effective temperature

We plot in Figure 17 the inverse of the effective temperature T^* , equal to m^*/T , versus the temperature T of the thermostat. The transition temperature is given by $T^* = T$. This gives the ideal glass transition temperature. Within the first order expansion we find $T_K \simeq .14$; the harmonic resummation gives $T_K \simeq .19$ and the second order perturbation theory is $T_K \simeq .18$.

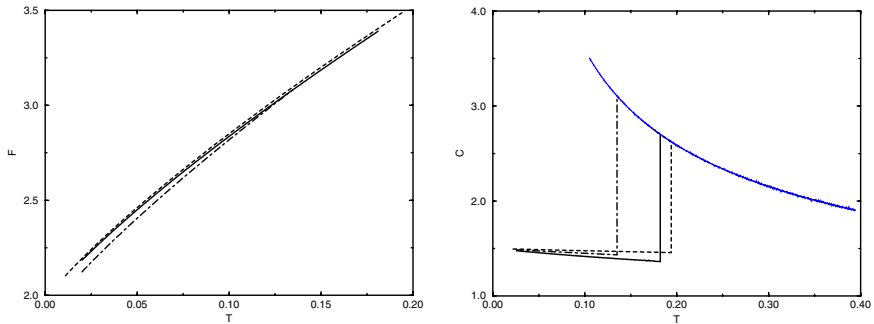


Fig. 18. The free energy (left) and the specific heat (right) *versus* the temperature, computed in an expansion to first order (dashed-dotted line) and second order (full line) in the cage size A , and in the harmonic resummation (dashed line). In the right panel the dotted line is the specific heat of the liquid.

We see that the two best methods, the second order and harmonic resummation, are in good agreement and both give a critical value of Γ around $\Gamma \simeq 1.52$. This value of Γ is in good agreement with numerical estimations of the glass transition of the soft sphere system, that range around 1.6 [86]. We also notice that the effective temperature stays relatively constant when the actual temperature varies. The effective temperature T^* (that can be experimentally observed) is always near to T_K , independently from the value of the temperature T .

8.3 Cage size

In replica space the cage size characterizes the size of the molecular bound state, in the approximation of quadratic fluctuations, as defined in (7.7). Its physical meaning is easily established: in the glass phase at low temperatures one can approximate the movement of each atom as some vibrations in a harmonic potential in the neighborhood of a local minimum of the energy. The typical square size of the displacement is given by:

$$A = \langle (r_i - \langle r_i \rangle)^2 \rangle \quad (8.1)$$

that is the physical definition of the square size. The cage size is plotted *versus* temperature in Figure 17. The cage size is nearly linear in temperature, as it would be in a T -independent quadratic confining potential. This indicates that the local confining potential has little dependance on the temperature in the whole low temperature phase.

8.4 Free energy, specific heat and configurational entropy

If we plot the free energy *versus* the temperature one would see a strong consistency between the second order term of the small cage expansion and the harmonic resummation. Both data extrapolates at zero temperature to a ground state energy of order 1.95. This is related to the typical energy of the amorphous packings of soft spheres. More precisely, if we consider all the amorphous packings of soft spheres at unit density, we can count them through the zero temperature configurational entropy. The lowest energy where one can find an exponentially large number of such packings is the ground state energy of the glassy phase that we find equal to 1.95. However we have not taken into account the existence of a crystal: therefore we must first remove all crystal like configurations, *i.e.* configurations that correspond to a crystal with some local defects. These configurations can be characterized by the presence of delta functions at the appropriate values of the momenta. This procedure of identifying crystal like solutions has been explicitly done numerically in [82].

In Figure 18 (right panel) we plot the specific heat *versus* temperature. It is basically constant and equal to $3/2$. This is the Dulong-Petit law (we have not included the kinetic energy of the particles, that would give an extra contribution of $3/2$). This result is very welcome: if we had treated the crystal at the same level of approximation as we considered here for the glass, we would have the Einstein model for which the specific heat is also given by the Dulong-Petit law. Thus the specific heat of the glass is very near to that of the crystal, has it happens experimentally. Notice that it was not obvious at all *a priori* that we would be able to get such a result from our computations. The fact of finding the Dulong-Petit law is an indication that our whole scheme of computation gives reasonable results for a solid phase.

In Figure 19 we show the configurational entropy *versus* the free energy at various temperatures, including the zero temperature case. We have included here for simplicity only the result from the harmonic resummation procedure.

We notice that the various curves corresponding to different temperatures are not far from being just shifted one from another by adding a constant to the free energy. This indicates that the main effect of temperature is to add a constant ($\approx 3/2kT$) in the energies of all amorphous packings. This correspond to the case where the vibration spectrum is approximatively state independent.

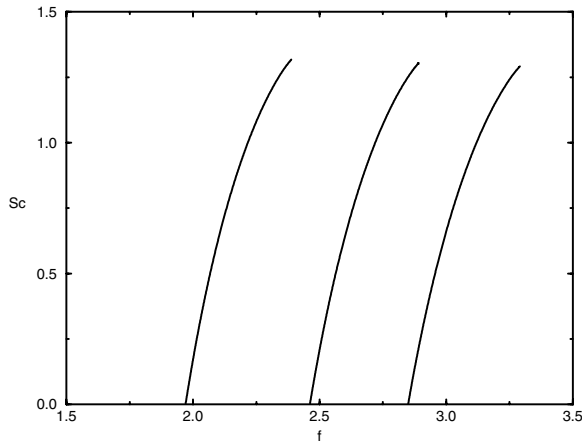


Fig. 19. The configurational entropy $\Sigma(f)$ versus the free energy, computed within the harmonic resummation, at temperatures $T = 0, .05, .1$ (from left to right).

8.5 The missing dynamical transition

We know that at the mean field level there exists a dynamical transition at a temperature T_D larger than the thermodynamic transition temperature T_K . This phase is characterized by the dynamic statement that a system will remain forever in the same valley, and its free energy is greater than the equilibrium one because it misses the contribution of the configurational entropy. This dynamic phase is just a mean field concept, that should disappear when corrections, such as activated processes, due to the short range nature of the potential, are taken into account. However if the barriers are sufficiently high, metastable states have a very large life time and they strongly affect the dynamics.

In the framework of the harmonic resummation one finds that the approximation breaks down at small but positive ϵ if the matrix of second derivatives has negative eigenvalues²⁶. From this point of view the appearance of negative eigenvalues signal the dynamic transition. Unfortunately in the chain approximation all the eigenvalues are positive at all temperatures and no dynamic phase transition can be seen: the free energy is always well defined for small ϵ : the chain approximation may be reasonable at low temperature but it is certainly not good at high temperatures. One should use a better method to compute the spectrum, giving reasonable results also at higher temperature. *E.g.* following the approach of [68] (work in this direction is in progress).

²⁶In the small cage expansion the perturbative method assumes that there is always a bound state: the breakdown of this assumption hardly be seen in a perturbative approach.

It is clear that a study of the dynamical phase transition should be done refining the tools than the one we have developed here. This is not surprising: the dynamical phase transition is present at a temperature higher than the static one and the approximations that we had used are especially good at low temperature.

8.6 Lennard-Jones binary mixtures

There other model that is interesting to consider because they do not crystallize [43,87]. Here we report the results fo is a *realistic* model for glasses, is given by a binary mixture of particles (80% large particles, 20% smaller particles) interacting *via* a Lennard-Jones potential, introduced by Kob & Andersen [75]. This Hamiltonian should mimick the behaviour of some metallic glasses and it is one of the best studied and simplest Hamiltonian that do not lead to crystalization at low temperature. We first present the data at the density $\rho = 1.2$.

The fact that the systems does not crystallizes implies that we can easily obtain information doing numerical simulations without serious difficulties [43]. Therefore one can use both an analytic or a numerical method to get information in the liquid phase. Let us start by presenting the numerical results [43]. A system of $N = 260$ particles, in a cubic box with periodic boundary conditions at density $\rho = 1.2$ has been studied *via* Monte-Carlo simulations. The entropy is obtained using the formula $S(\beta) = S(0) + \int_0^\beta d\beta' (E(\beta) - E(\beta'))$. Given an equilibrium configuration the nearest minimum of the potential is found by steepest descendent and the computation of the 780 eigenvalues of $\mathcal{H}(C)$ does not present any particular difficulty.

The results for the total entropy of the liquid and for the harmonic part are shown in Figure 20, left as function of $T^{-.4}$ (a more detailed description of the simulations can be found in [43]). The entropy of the liquid is remarkable linear when plotted *versus* $T^{-.4}$, as it happens in many cases [88].

In Figure 20, right, we show the configurational entropy as function of $T^{-.4}$. We fit it with a polynomial of second degree in $T^{-.4}$. The extrapolated configurational entropy becomes zero at a temperature $T_K = .31 \pm .04$, where the error contains systematic effects due to the extrapolation (similar conclusions have been reached in [83]).

There are many methods to compute analytically the free energy in the liquid phase that lead to integral equations for the correlation functions. Unfortunately the simple HNC dos not works well. Here I present the results [43] obtained by mixing the HNC and MSA (mean spherical approximation) closures [89]. This technique allow us to compute the internal energy in the liquid with a reasonable approximation. The computation of

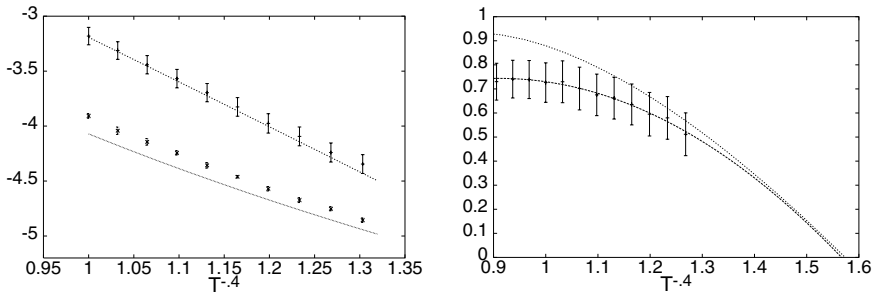


Fig. 20. Left panel: analytical entropy of the liquid (upper line) compared with the numerical one, and analytical harmonic entropy (lower line) compared with the numerical results. The horizontal axis is T^{-4} . Right panel: analytical value of the complexity (upper line) compared with the numerical one (+ points), as functions of β^4 .

the spectrum is more involved: it can be done with the same approach we used before that is described in the Appendix.

We can now put everything together [43]: the final analytic predictions for the liquid and harmonic entropy are shown in Figure 20, left. The predictions for the liquid entropy turn out to be very good, while there is a minor discrepancy for the harmonic entropy, likely due to the rather strong approximations in the analytic evaluation of the spectrum. The analytic configurational entropy is shown in Figure 20 (left). It becomes zero at $T_K = .32$, that is our analytic prediction for the thermodynamic transition.

We have in our hands all the tools to compute analytically the free energy in the low temperature case. If one computes the specific heat, one finds that the Dulong Petit law is extremely well satisfied in the low temperature region²⁷. The value of $\gamma(\beta)$ weakly depends on β : its value in the limit $\beta \rightarrow \infty$ is only about 10% higher than its value (*i.e.* β_K) at the transition temperature.

Summarizing we have found a simple method that is able to use liquid theory method in the glasses phase putting in practice the old adage *a glass is a frozen liquid*. We are able to compute with a reasonable approximation the thermodynamics and with a little more effort we can compute the static and the dynamic structure functions.

We may wonder what happens if we change the density ρ . The Kauzmann temperature should depend on ρ . A numerical estimation of the Kauzmann temperature can be done by studying the behaviour of

²⁷In the harmonic approximation the Dulong Petit law would be exact if we neglect the γ dependence of $S_\gamma(\beta)$.

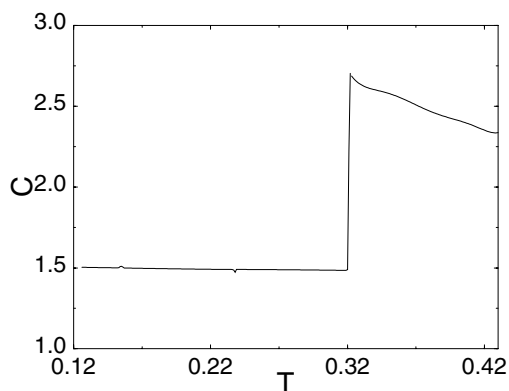


Fig. 21. The specific heat coming from the x dependent part of the Hamiltonian as a function of the temperature.

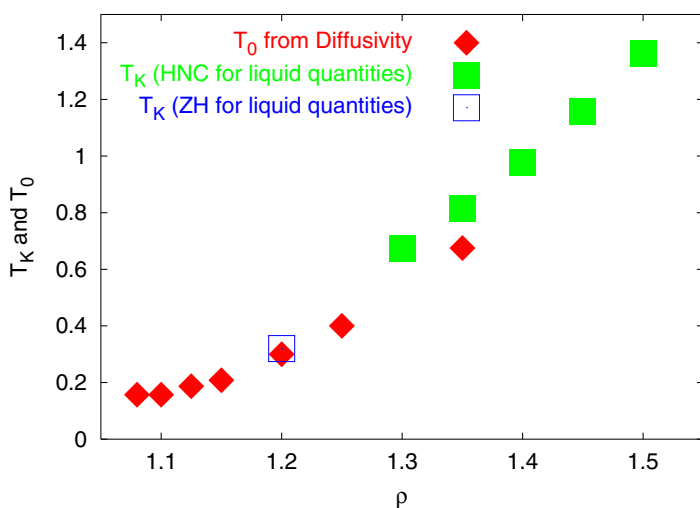


Fig. 22. The data on T_0 as function of the density ρ (T_0 should be near to T_K) obtained by Sastry [90] compared with the analytical results [91].

the diffusivity: this leads to a numerical of a temperature T_0 that would be near to T_k . The results are shown in Figure 22 together with the analytic estimates for the same model [91] that are in reasonable agreement with the numerical data.

9 Discussion and perspectives

Within the equilibrium framework, we have implemented so far our general strategy using rather crude methods. These methods should be improved, and one should perform a more careful study of the molecular liquid. The extension to the case of hard spheres seem to be particularly interesting.

There are also many other different problems that should be investigated,

- a careful numerical study of the phase diagrams for coupled replicas would be welcomed in order to test the correctness of the detailed theoretical predictions;
- it would be very interesting to demonstrate numerically that the Kauzmann transition exists beyond mean field theory and that the behaviour of the system is similar to the one we expect theoretically. Unfortunately known numerical techniques are not sufficient for thermalize a glass forming liquid at low temperature in a reasonable amount of CPU time: during the simulation the system is trapped in one of the exponentially large number of metastable states ($O(\exp(AN))$ where A is a quantity of order 1). The introduction of an appropriate lattice model, enough simple to be simulated in a very effective way, could be very useful in this respect;
- analytic and numerical method should be developed in order to compute the height of the activation barriers that should dominate the dynamics at low temperature (below the mode coupling transition);
- the analytic computation of the spectrum of the instantaneous normal modes could be strongly improved. This could be used to study the properties of the Boson peak and to find analytically the value of the mode coupling and Kauzmann temperature within the same approach;
- the analytic approach to the computation of the thermodynamic properties should be extended to the case of hard spheres;
- least, but not the last, quantum glasses are a very wide territory that should be explored theoretically with much more details.

The study of the properties at equilibrium study is to be considered as a first step before dealing the dynamics (equilibrium and off-equilibrium). A very interesting and open problem is the computation of the time dependent correlation functions (and as a by-product the viscosity) in the region above T_K and below T_c . However a better understanding of activated processes in this framework is a crucial prerequisite.

It is quite possible that in the next years we shall see progresses in some of the previously mentioned fields.

This work has been possible only by the help with many friends. I would like to thank all of them. A particular acknowledgement goes to Luca Angelani, Andrea Cavagna, Barbara Coluzzi, Leticia Cugliandolo, Silvio Franz, Irene Giardina, Tomas Grigera, Jorge Kurchan, Enzo Marinari, Victor Martin-Mayor, Marc Mézard, Federico Ricci, Felix Ritort, Juan-Jesus Ruiz-Lorenzo, Giancarlo Ruocco, Paolo Verrocchio, Miguel Virasoro and Francesco Zuliani.

Appendices

The probability distribution of the weights

We need to compute the probability distribution of the weights w that are equal to:

$$w_k \equiv \frac{\exp(-F_k)}{Z}, \quad (9.1)$$

where

$$Z = \sum_k \exp(-F_k). \quad (9.2)$$

The probability of finding an energy F_k in the interval $[F, F+dF]$, is given by

$$\rho(E) = \exp(\beta m F), \quad (9.3)$$

and the possible values of the F_k go from $-\infty$ to $+\infty$.

This computation can be done with a brute force method [92]. One assumes that the index k goes from 1 to M and the F 's belong to the interval $[-\infty, F_M]$. One finally sends M to infinity, keeping the quantity $M \exp(m F_M)$ equal to a constant (the value of the constant is irrelevant). Esplicite formulae can be written and the appropriate approximations can be done in the limit M going to infinity using the saddle point limit. The computation is not too long, but it is not too simple.

A much more clever method can be found in [93]. Here one tries to compute

$$w^{(s)} \equiv \sum_{k=1, \infty} w_k^{(s)} \quad (9.4)$$

without introducing the cutoffs M and F_M . After a few passages one finds that

$$w^{(s)} = \frac{\Gamma(s-m)}{\Gamma(s)\Gamma(1-m)}. \quad (9.5)$$

In this way we can go backward and we finally find that the probability of finding a w_k in the interval $[w, w+dw]$ is given by $\nu(w)dw$, where $\nu(w)$ is given by equation (2.32).

The mean field approach for a ferromagnet

It is interesting to see the techniques of Gaussian integration and saddle point at work in a case where we already know the result. The simplest case where this can be done is the infinite range ferromagnet [15], a model that can be exactly solved. The Hamiltonian is given by:

$$H = \frac{J}{N} \sum_{i,k=1,N} \sigma(i)\sigma(k) - h \sum_{i=1,N} \sigma(i), \quad (9.6)$$

where the sum over i, k is done over all the $N(N-1)/2$ pairs of spins. An direct computation shows that in the limit $N \rightarrow \infty$ the mean field approximation become exact and the magnetisation satisfies the mean field equation

$$m = \text{th}(\beta(Jm + h)). \quad (9.7)$$

We would like to prove this result using the saddle point method.

At this end we can rewrite the Hamiltonian as

$$H = \frac{J}{2N} \left(\sum_{i=1,N} \sigma(i) \right)^2 - h \sum_{i=1,N} \sigma(i), \quad (9.8)$$

where we have neglected and additive constant equal to $-J$, that originates from the sums of the terms with $i = k$.

The argument runs as follows. In the limit $N \rightarrow \infty$, neglecting multiplicative constants that give no contribution to the free energy density we can write that

$$Z = \sum_{\{\sigma\}} \exp(-\beta H)$$

$$\sum_{\{\sigma\}} \int dm \exp \left(-N\beta Jm^2/2 + (\beta Jm + \beta h) \sum_{i=1,N} \sigma(i) \right) = \quad (9.9)$$

$$\int dm \exp(-Nf(m)), \quad (9.10)$$

where

$$f(m) = \beta Jm^2/2 - \ln(2\text{ch}(\beta Jm + \beta h)). \quad (9.11)$$

Up to now everything was exact. The long range nature of the interaction and its homogeneity allows us to reduce the sum over N variable to an one dimensional integral. This integral can be estimated by various means. In the limit $N \rightarrow \infty$ we can use the method of the point of maximum. It gives

$$Z \approx \exp(-Nf(m^*)), \quad (9.12)$$

where m^* is the minimum of the function $f(m)$ and it is a solution of the equation

$$\frac{\partial f}{\partial m} = 0. \quad (9.13)$$

The previous equation coincide with the usual mean field equation (9.7). The correction to this result are proportional to $1/N$ (if we are not at the critical temperature) and they can be exactly computed by evaluating the corrections to the saddle point method.

The spectrum of the instantaneous normal modes

Here I would like to explain a fast method [94] for obtaining some analytic estimates on the spectrum of the matrix the matrix M , of dimension $3N \times 3N$, given by:

$$M_{(i\mu)(j\nu)} = \delta_{ij} \sum_k v_{\mu\nu}(r_i - r_k) - v_{\mu\nu}(r_i - r_j) \quad (9.14)$$

and $v_{\mu\nu}(r) = \partial^2 v / \partial r_\mu \partial r_\nu$. The fact that the diagonal terms of M do fluctuate complicate the analysis. This difficulty may be removed, if we notice that in this high density regime²⁸. There are many neighbours to each point, and thus a good approximation is to neglect the fluctuations of these diagonal terms and substitute them by their average value. We thus write:

$$\sum_k v_{\mu\nu}(r_i - r_k) \simeq \delta_{\mu\nu} \frac{1}{3} \int d^3r g^*(r) \Delta v(r) \equiv r_0. \quad (9.15)$$

In this approximation (9.15) the diagonal matrix elements are all equal and can be factorized, leading to:

$$\langle \text{Tr} \log(M) \rangle = 3N \log(r_0) + \left\langle \text{Tr} \log \left(\delta_{ij} \delta_{\mu\nu} - \frac{1}{r_0} v_{\mu\nu}(r_i - r_k) \right) \right\rangle. \quad (9.16)$$

This form lends itself to a perturbative expansion in powers of $1/r_0$ that we assume to be a *small* number. The computation of the p -th order term in

²⁸Here and in what follows, we have not written explicitly the density. We choose to work with density unity in order to simplify the formulae; however we assume that in the glassy phase the density is sufficiently high, compare to the range of the forces, that an expansion in inverse powers of the density gives the correct result. At low density the approach of [95] gives the correct results.

this expansion,

$$\mathcal{T}_p \equiv \frac{(-1)^{p-1}}{pr_0^p} \left\langle \sum_{\substack{i_1 \dots i_p \\ \mu_1 \dots \mu_p}} v_{\mu_1 \mu_2}(r_{i_1} - r_{i_2}) \dots v_{\mu_{p-1} \mu_p}(r_{i_{p-1}} - r_{i_p}) v_{\mu_p \mu_1}(r_{i_p} - r_{i_1}) \right\rangle \quad (9.17)$$

still involves the p -th order correlation functions of the liquid at T^* . We have approximated this correlation by introducing a simple *chain* approximation involving only the pair correlation. This chain approximation consists in replacing, for $p > 2$, the full correlation by a product of pair correlations. A most drastic approximation consist in selecting only those contributions that survive in the high density limit; systematic corrections can be computed following [68, 94]. Within the chain approximation, \mathcal{T}_p is approximated by:

$$\begin{aligned} \mathcal{T}_p &= \sum_{\mu_1 \dots \mu_p} \int dx_1 \dots dx_p g^*(x_1, \dots, x_p) \\ &\quad \times [v_{\mu_1 \mu_2}(x_1 - x_2) \dots v_{\mu_{p-1} \mu_p}(x_{p-1} - x_p) v_{\mu_p \mu_1}(x_p - x_1)] \\ &\simeq \sum_{\mu_1 \dots \mu_p} \int dx_1 \dots dx_p \\ &\quad \times [g^*(x_1 - x_2) v_{\mu_1 \mu_2}(x_1 - x_2)] \dots [g^*(x_p - x_1) v_{\mu_p \mu_1}(x_p - x_1)]. \end{aligned} \quad (9.18)$$

In this last form we need to compute a convolution that can be factorised through the introduction of the Fourier transform of the pair correlation function. We thus introduce the Fourier transformed functions a and b that are defined from the pair correlation $g^*(r)$ by:

$$\int d^3r g^*(r) v_{\mu\nu}(r) e^{ikr} \equiv \delta_{\mu\nu} a(k) + \left(\frac{k_\mu k_\nu}{k^2} - \frac{1}{3} \delta_{\mu\nu} \right) b(k). \quad (9.19)$$

In terms of these Fourier transforms, the p -th order term in the $1/r_0$ expansion is simply

$$\mathcal{T}_p = \int d^3k \left(a(k) + \frac{2}{3} b(k) \right)^p + (2) \int d^3k \left(a(k) - \frac{1}{3} b(k) \right)^p, \quad (9.20)$$

and the summation of the series over p is easily done and we finally find:

$$\begin{aligned} &\langle \text{Tr} \log(M) \rangle = 3 \log(r_0) \\ &+ \int d^3k \left(L_3 \left(\frac{a(k) + \frac{2}{3} b(k)}{r_0} \right) + 2 L_3 \left(\frac{a(k) - \frac{1}{3} b(k)}{r_0} \right) \right) \\ &\quad - \frac{1}{2} \int d^3r g(r) \sum_{\mu\nu} \frac{v_{\mu\nu}(r)^2}{r_0^2} \end{aligned} \quad (9.21)$$

where the function L_3 is defined as:

$$L_3(x) = \log(1-x) + x + x^2/2. \quad (9.22)$$

The hypernetted chain approximation

We derive here the form of the HNC free energy (9.32) for our molecular replicated system. One could use the standard diagrammatic method [96], but here we shall follow the “cavity” like method of Percus [97].

In the phase where the replica symmetry is broken, replicas are correlated: it is convenient to consider N molecules with coordinates $\mathbf{x}_i, i \in \{1, \dots, N\}$. Each \mathbf{x}_i stands for the coordinates of all atoms in molecule i : $\mathbf{x}_i = \{\mathbf{x}_i^a\}, a \in \{1, \dots, m\}$. The energy of the system is given by

$$H = \sum_{i < j} V(\mathbf{x}_i, \mathbf{x}_j) + \sum_i U(\mathbf{x}_i) \quad (9.23)$$

where $V(\mathbf{x}, \mathbf{y}) = \sum_a v(x^a - y^a)$, v is the intermolecular potential and the external potential $U(\mathbf{x}) = \sum_a u(x^a)$ has been introduced for future use.

We shall need the following definitions. The one molecule density is

$$\rho(\mathbf{x}) = \sum_i \left\langle \prod_a \delta(\mathbf{x}_i^a - \mathbf{x}^a) \right\rangle, \quad (9.24)$$

where the average $\langle \cdot \rangle$ is done with respect to the Boltzmann measure $\exp(-\beta H)$.

The two molecules correlation (g) is defined as:

$$\rho^{(2)}(\mathbf{x}, \mathbf{y}) = \sum_{i \neq j} \left\langle \prod_a \delta(\mathbf{x}_i^a - \mathbf{x}^a) \prod_b \delta(\mathbf{x}_j^b - \mathbf{y}^b) \right\rangle \equiv \rho(\mathbf{x})g(\mathbf{x}, \mathbf{y})\rho(\mathbf{y}) \quad (9.25)$$

where we have also defined the pair correlation function $g(\mathbf{x}, \mathbf{y})$, that goes to one at large (center of mass) distance. The connected pair correlation is:

$$h(\mathbf{x}, \mathbf{y}) \equiv g(\mathbf{x}, \mathbf{y}) - 1. \quad (9.26)$$

Functional differentiation gives:

$$\frac{\partial \rho(\mathbf{x})}{\partial(-\beta U(\mathbf{y}))} = \rho(\mathbf{x})\delta(\mathbf{x} - \mathbf{y}) + \rho(\mathbf{x})h(\mathbf{x}, \mathbf{y})\rho(\mathbf{y}). \quad (9.27)$$

One can also introduce the direct correlation function $c(\mathbf{x}, \mathbf{y})$ through:

$$\frac{\partial(-\beta U(\mathbf{x}))}{\partial \rho(\mathbf{y})} = \frac{1}{\rho(\mathbf{x})}\delta(\mathbf{x} - \mathbf{y}) - c(\mathbf{x}, \mathbf{y}). \quad (9.28)$$

The direct correlation is related to the connected pair correlation through the Ornstein-Zernike equation $c = (1 + h\rho)^{-1}h$ that reads more explicitly:

$$c(\mathbf{x}, \mathbf{y}) = h(\mathbf{x}, \mathbf{y}) + \int d\mathbf{x}_1 h(\mathbf{x}, \mathbf{x}_1) \rho(\mathbf{x}_1) h(\mathbf{x}_1, \mathbf{y}) \\ + \int d\mathbf{x}_1 d\mathbf{x}_2 h(\mathbf{x}, \mathbf{x}_1) \rho(\mathbf{x}_1) h(\mathbf{x}_1, \mathbf{x}_2) \rho(\mathbf{x}_2) h(\mathbf{x}_2, \mathbf{y}) + \dots \quad (9.29)$$

The idea of Percus is to compute the pair correlation by considering the one point density with a molecule fixed at one point. Let us consider a problem where we have added one extra molecule, fixed at a point $\mathbf{z} = \{z^1, \dots, z^m\}$. This extra molecule creates an external potential $U(\mathbf{x}) = V(\mathbf{x}, \mathbf{z})$. The one point density in the presence of this external potential, $\rho_U(\mathbf{x})$, is related to the density $\rho(\mathbf{x})$ and pair correlation $g(\mathbf{x}, \mathbf{z})$ in the absence of an external potential through the conditional probability equation:

$$\rho_U(\mathbf{x}) = \rho(\mathbf{x}) g(\mathbf{x}, \mathbf{z}). \quad (9.30)$$

The previous equations can be used to find a perturbative expansion of the logarithm of the correlation function. Doing the appropriate computations one find:

$$\log g(\mathbf{x}, \mathbf{z}) + \beta V(\mathbf{x}, \mathbf{z}) = \int d\mathbf{y} c(\mathbf{x}, \mathbf{y}) \rho(\mathbf{y}) h(\mathbf{y}, \mathbf{z}). \quad (9.31)$$

Together with the inversion relation (9.29), this defines a closed set of equations for the one and two point molecular densities that are the HNC closure. In the real word the HNC equations are not exact: there are corrections to the r.h.s.²⁹.

In a similar way one finds that the free energy in the HNC approximation is a functional of the molecular density $\rho(\mathbf{x})$ and the two point correlation $g(\mathbf{x}, \mathbf{y})$. The result is:

$$\beta\psi = \frac{1}{2m} \int d\mathbf{x} d\mathbf{y} \rho(\mathbf{x}) \rho(\mathbf{y}) [g(\mathbf{x}, \mathbf{y}) \log g(\mathbf{x}, \mathbf{y}) - g(\mathbf{x}, \mathbf{y}) + 1 \\ + \beta v(\mathbf{x}, \mathbf{y}) g(\mathbf{x}, \mathbf{y})] \\ - \frac{1}{2m} \text{Tr} \left(\log(1 + h\rho) - h\rho + \frac{1}{2} h\rho h\rho \right) + \frac{1}{m} \int d\mathbf{x} \rho(\mathbf{x}) \log \frac{\rho(\mathbf{x})}{e}. \quad (9.32)$$

²⁹The first correction is proportional to h^5 and the proof of this statement can be done most easily using a diagrammatical approach; it is remarkable that a first order computation in h may be so accurate.

In the trace term all products are *convolutions*³⁰. For instance the lowest order term in the small ρ expansion of the trace is:

$$-\frac{1}{3} \int d\mathbf{x} d\mathbf{y} d\mathbf{z} h(\mathbf{x}, \mathbf{y}) \rho(\mathbf{y}) h(\mathbf{y}, \mathbf{z}) \rho(\mathbf{z}) h(\mathbf{z}, \mathbf{x}) \rho(\mathbf{x}). \quad (9.33)$$

We would like to optimize the thermodynamic potential ψ with respect to the molecular density $\rho(\mathbf{x})$ and the two point function $g(\mathbf{x}, \mathbf{y})$. We shall work at low temperatures for which ρ should be nearly Gaussian. We thus choose an Ansatz for ρ of the type:

$$\begin{aligned} \rho(x) &= \int d^3 X \prod_{a=1}^m \left(\frac{\exp(-(x^a - X)^2/(2A))}{(2\pi A^{3/2})} \right) \\ &= \left(\frac{2\pi A}{m} \right)^{3/2} (2\pi A)^{-3/2m} \exp \left(-\frac{1}{4Am} \sum_{ab} (x^a - x^b)^2 \right) \end{aligned} \quad (9.34)$$

where the molecular density is parametrized by the single parameter A .

The ideal gas contribution (last term in (9.32)) gives:

$$\begin{aligned} \int \prod_a d^3 x^a \rho(x) \log \frac{\rho(x)}{e} &= N \left(\frac{3}{2} (1-m) \log(2\pi A) + \frac{3}{2} (1-m) \right. \\ &\quad \left. - \frac{3}{2} \log m - 1 \right). \end{aligned} \quad (9.35)$$

The interaction term is more complicated, and it can be evaluated in the small cage regime. At the end of the day one can compute the correlation function g in the limit of small cage radius A , expanding in powers of A . In this one we recover the zeroth and the first order of the A expansion that we have obtained by a direct method. In the same way after a long computation [81] we obtain the second order in A that has been used in the main text.

References

- [1] S.F. Edwards and P.W. Anderson, *J. Phys. F: Metal. Phys.* **5** (1975) 965.
- [2] M. Mézard, G. Parisi and M.A. Virasoro, *Spin glass theory and beyond* (World Scientific, Singapore, 1987).
- [3] E. Marinari, G. Parisi and J.J. Ruiz-Lorenzo, *Numerical Simulations of Spin Glass Systems* in *Spin Glasses and Random Fields*, edited by P. Young (Word Scientific, Singapore, 1997).

³⁰The trace could also be written as $\text{Tr}(L_3(-h\rho))$, where L_3 is defined in equation (9.22).

- [4] E. Marinari, G. Parisi, F. Ricci-Tersenghi, J. Ruiz-Lorenzo and F. Zuliani, *J. Stat. Phys.* **98** (2000) 973.
- [5] G. Adams and J.H. Gibbs, *J. Chem. Phys.* **43** (1965) 139; J.H. Gibbs and E.A. Di Marzio, *J. Chem. Phys.* **28** (1958) 373; M. Goldstein, *J. Chem. Phys.* **51** (1969) 3728; G. Adam and J.H. Gibbs, *J. Chem. Phys.* **57** (1972) 470.
- [6] F.H. Stillinger and T.A. Weber, *Phys. Rev. A* **25** (1982) 2408; F.H. Stillinger and T.A. Weber, *Phys. Rev. A* **28** (1983) 2408; F.H. Stillinger, *Science* **267** (1995) 1935; C.A. Angell, *Nature* **393** (1998) 521.
- [7] T.R. Kirkpatrick and D. Thirumalai, *Phys. Rev. B* **36** (1987) 5388; T.R. Kirkpatrick and P.G. Wolynes, *Phys. Rev. B* **36** (1987) 8552; R. Kirkpatrick and D. Thirumalai, *Phys. Rev. Lett.* **58** (1987) 2091; T.R. Kirkpatrick, D. Thirumalai and P.G. Wolynes, *Phys. Rev. A* **40** (1989) 1045. A review of the results of these authors and further references can be found in T.R. Kirkpatrick and D. Thirumalai, *Transp. Theor. Stat. Phys.* **24** (1995) 927.
- [8] A.W. Kauzman, *Chem. Rev.* **43** (1948) 219.
- [9] L.F. Cugliandolo and J. Kurchan, *Phys. Rev. Lett.* **71** (1993) 173; *J. Phys. A: Math. Gen.* **27** (1994) 5749.
- [10] S. Franz and M. Mézard, *Europhys. Lett.* **26** (1994) 209.
- [11] A. Crisanti, H.J. Sommers, *Z. Phys. B* **87** (1992) 341; A. Crisanti, H. Horner and H.J. Sommers, *Z. Phys. B* **92** (1993) 257.
- [12] T. Geztzi, *J. Phys. C* **16** (1983) 5805; E. Leutheusser, *Phys. Rev. A* **29** (1984) 2765; U. Bendtzelius, W. Götze and A. Sjölander, *J. Phys. C* **17** (1984) 5915; E. Leutheusser, *Phys. Rev. A* **29** (1984) 2765; T.R. Kirkpatrick, *Phys. Rev. A* **31** (1985) 939; W. Gotze and L. Sjogren, *Rep. Prog. Phys.* **55** (1992) 241; W. Gotze, *Liquid, freezing and the Glass transition*, Les Houches (1989), edited by J.P. Hansen, D. Levesque, J. Zinn-Justin (North Holland).
- [13] E. Marinari, G. Parisi and F. Ritort, *J. Phys. A (Math. Gen.)* **27** (1994) 7615; *J. Phys. A (Math. Gen.)* **27** (1994) 7647.
- [14] E.N.M. Cirillo and J.L. Lebowitz, *J. Stat. Phys.* **90** (1998) 211; and refences therein.
- [15] G. Parisi, *Statistical Field Theory* (Addison Wesley, 1988).
- [16] L.C.E. Struik, *Physical aging in amorphous polymers and other materials* (Elsevier, Houston, 1978).
- [17] J.-P. Bouchaud, *J. Phys. France* **2** (1992) 1705.
- [18] J.-P. Bouchaud, L. Cugliandolo, J. Kurchan and M. Mézard, *Physica A* **226** (1996) 243; in *Spin glasses and random fields*, edited by A.P. Young (Worlds Scientific, 1998).
- [19] N. Cabibbo, private comunication (1979).
- [20] B. Derrida, *Phys. Rev. B* **24** (1981) 2613.
- [21] J.P. Bouchaud and M. Mézard, *J. Phys. A* **30** (1997) 7997; S. Franz and G.Parisi, *Eur. Phys. J. B* **18** (2000) 485.
- [22] G. Parisi, *Field Theory, Disorder and Simulations* (World Scientific, Singapore, 1992).
- [23] J. Kurchan, G. Parisi and M.A. Virasoro, *J. Phys.* **3** (1993) 18.
- [24] M. Campellone, G. Parisi and M.A. Virasoro (in preparation).
- [25] D.J. Gross and M. Mezard, *Nucl. Phys. B* **240** (1984) 431.
- [26] E. Gardner, *Nucl. Phys. B* **257** (1985) 747.
- [27] F. Guerra, *Broken Replica Symmetry Bounds in the Mean Field Spin Glass Model* [cond-mat/0205123].
- [28] D. Sherrington and S. Kirkpatrick, *Phys. Rev. Lett.* **35** (1975) 1792.

- [29] G. Parisi, *Phys. Scr.* **35** (1987) 123.
- [30] G. Parisi, *Phil. Mag. B* **71** (1995) 471.
- [31] R. Haag and D. Kastler, *J. Math. Phys.* **5** (1964) 848.
- [32] D. Kastler and D.W. Roberts, *Comm. Math. Phys.* **3** (1965) 151.
- [33] D. Ruelle, *Statistical Mechanics* (Benjamin, Reading, 1969).
- [34] C. Djurberg, K. Jonason and P. Nordblad, *Magnetic Relaxation Phenomena in a CuMn Spin Glass* [`cond-mat/9810314`].
- [35] M. Mézard and G. Parisi, *Eur. Phys. J. B* **20** (2001) 217; *The cavity method at zero temperature* [`cond-mat/0207121` (2002)].
- [36] D.J. Thouless, P.W. Anderson and R.G. Palmer, *Phil. Mag.* **35** (1977) 593.
- [37] G. Parisi, in *The Oskar Klein Centenary*, edited by U. Lindström (World Scientific, 1995); *Il Nuovo Cimento* **16** (1994) 939.
- [38] S. Franz and G. Parisi, *J. Phys. France I* **5** (1995) 1401.
- [39] S. Franz and G. Parisi, *Phys. Rev. Lett.* **79** (1997) 2486; *Physica A* **6** (1998) 317.
- [40] E. Monasson, *Phys. Rev. Lett.* **75** (1995) 2847.
- [41] For a careful analysis of the free energy landscape see A. Cavagna, I. Giardina and G. Parisi, *J. Phys. A: Math. Gen.* **30** (1997) 7021; and references therein.
- [42] A. Barrat, R. Burioni and M. Mézard, *J. Phys. A* **29** (1996) L81; A. Barrat, S. Franz and G. Parisi, *J. Phys. A: Math. Gen.* **30** (1997) 5593.
- [43] B. Coluzzi, G. Parisi and P. Verrocchio, *Phys. Rev. Lett.* **84** (2000) 306; *J. Chem. Phys.* **112** (2000) 2933.
- [44] G. Parisi and M. Potters, *J. Phys. A: Math. Gen.* **28** (1995) 5267; *Europhys. Lett.* **32** (1995) 13.
- [45] M. Mézard, *Physica A* **265** 352 (1999).
- [46] A. Cavagna, J.P. Garrahan and I. Giardina, *J. Phys. A* **32** (1999) 711.
- [47] A. Cavagna, I. Giardina, M. Mezard and G. Parisi, *On the formal equivalence of the TAP and thermodynamic methods in the SK model* [`cond-mat/0210665`].
- [48] A. Cavagna, I. Giardina, T. Grigera and G. Parisi, *Phys. Rev. Lett.* **88** (2002) 055502.
- [49] H. Vogel, *Phys. Z* **22** (1921) 645; G.S. Fulcher, *J. Am. Ceram. Soc.* **6** (1925) 339.
- [50] J. Kurchan and L. Laloux, *J. Phys. A* **29** (1996) 1929.
- [51] B. Coluzzi and G. Parisi, *On the Approach to the Equilibrium and the Equilibrium Properties of a Glass-Forming Model* [`cond-mat/9712261`].
- [52] S. Franz and H. Rieger, *Phys. J. Stat. Phys.* **79** (1995) 749.
- [53] E. Marinari, G. Parisi, F. Ricci-Tersenghi and J.J. Ruiz-Lorenzo, *J. Phys. A: Math. Gen.* **31** (1998) 2611.
- [54] G. Parisi, *Phys. Rev. Lett.* **79** (1997) 3660.
- [55] W. Kob and J.-L. Barrat, *Phys. Rev. Lett.* (1997) **79** 3660; J.-L. Barrat and W. Kob, *Europhys. Lett.* **46** (1999) 637.
- [56] A. Cavagna, I. Giardina and G. Parisi, *Phys. Rev. B* **57** (1998) 11251.
- [57] G. Biroli, *J. Phys. Math. Gen.* **32** (1999) 8365.
- [58] M.L. Metha, *Random matrices* (Academic Press, 1991).
- [59] S. Franz and M.A. Virasoro, *J. Phys. A: Math. Gen.* **33** (2000) 891.
- [60] See for instance T. Keyes, *J. Phys. Chem. A* **101** (1997) 2921; and references therein.
- [61] S. Sastry, *Phys. Rev. Lett.* **76** (1996) 3738; F. Sciortino and P. Tartaglia, *Phys. Rev. Lett.* **78** (1997) 2385; La Nave *et al.*, *Phys. Rev. Lett.* **84** (2000) 4605.
- [62] A. Cavagna, *Europhys. Lett.* **53** (2001) 490.

- [63] L. Angelani, R. Di Leonardo, G. Ruocco, A. Scala and F. Sciortino, *Phys. Rev. Lett.* **85** (2000) 5356; K. Broderix, K.K. Bhattacharya, A. Cavagna, A. Zippelius and I. Giardina, *Phys. Rev. Lett.* **85** (2000) 5360.
- [64] A. Cavagna, I. Giardina and G. Parisi, *J. Phys. A: Math. Gen.* **34** (2001) 5317.
- [65] C. Masciovecchio *et al.*, *Phys. Rev. Lett.* **76** (1996) 3356; F. Sette *et al.*, *Science* **280** (1998) 1550; A. Matic *et al.*, *Europhys. Lett.* **54** (2001) 77; C. Masciovecchio *et al.*, *Phys. Rev. B* **55** (1997) 8049; P. Benassi *et al.*, *Phys. Rev. Lett.* **77** (1996) 3835; D. Fioretto *et al.*, *Phys. Rev. E* **59** (1999) 1470; A.P. Sokolov *et al.*, *Phys. Rev. B* **52** (1995) R9815; N.J. Tao *et al.*, *Phys. Rev. A* **44** (1991) 6665.
- [66] J. Horbach *et al.*, *Eur. Phys. J. B* **19** (2001) 531; J. Horbach *et al.*, *J. Phys. Chem. B* **103** (1999) 4104; S.N. Taraskin and S.R. Elliot, *Phys. Rev. B* **59** (1999) 8572; G. Ruocco *et al.*, *Phys. Rev. Lett.* **84** (2000) 5788.
- [67] W. Götze and M.R. Mayr, *Phys. Rev. E* **61** (2000) 587.
- [68] V. Martin-Mayor, G. Parisi and P. Verrocchio, *J. Chem. Phys.* **114** (2001) 8068; T.S. Grigera, V. Martin-Mayor, G. Parisi and P. Verrocchio, *J. Phys. A* **14** (2002) 2167-2179; *Phys. Rev. Lett.* **87** (2001) 085502.
- [69] S. Franz, M. Mézard, G. Parisi and L. Peliti, *Phys. Rev. Lett.* **81** (1998) 1758; *J. Stat. Phys.* **97** (1999) 459.
- [70] F. Guerra, *Int. J. Phys. B* **10** (1997) 1675.
- [71] M. Aizenman and P. Contucci, *J. Stat. Phys.* **92** (1998) 765.
- [72] S. Ghirlanda and F. Guerra, *J. Phys. A: Math. Gen.* **31** (1998) 9149.
- [73] G. Parisi, *On the probabilistic formulation of the replica approach to spin glasses* [cond-mat/9801081].
- [74] Reviews can be found in: C.A. Angell, *Science* **267** (1995) 1924; and P. De Benedetti, *Metastable liquids* (Princeton University Press, 1997). An introduction to the theory is: J. Jäckle, *Rep. Prog. Phys.* **49** (1986) 171.
- [75] W. Kob and H.C. Andersen, *Phys. Rev. Lett.* **73** (1994) 1376.
- [76] G. Parisi, *A divergent correlation length in off-equilibrium glasses* [cond-mat/9801034], C. Donati, S.C. Glotzer and P.H. Poole, *Phys. Rev. Lett.* **80** (1998) 4915; Franz and G. Parisi, *J. Phys.: Cond. Matt.* **12** (2000) 6335; C. Donati, S. Franz, G. Parisi and S.C. Glotzer, *Phil. Mag. B* **79** (1999) 1827.
- [77] S. Franz and J. Hertz, *Phys. Rev. Lett.* **74** (1995) 2114.
- [78] L. Cugliandolo, J. Kurchan, G. Parisi and F. Ritort, *Phys. Rev. Lett.* **74** (1995) 1012.
- [79] L. Cugliandolo, J. Kurchan, E. Monasson and G. Parisi, *Math. Gen.* **29** (1996) 1347.
- [80] M. Mezard and G. Parisi, *J. Phys. A* **29** (1996) 6515.
- [81] M. Mézard and G. Parisi, *Phys. Rev. Lett.* **82** (1998) 747; M. Mézard and G. Parisi, *J. Chem. Phys.* **111** (1999) 1076.
- [82] For example see S. Sastry, P. Debenedetti and F.H. Stillinger, *Nature* **393** (1998) 554; F. Sciortino and P. Tartaglia, *Phys. Rev. Lett.* **78** (1997) 2385; K.K. Bhattacharya, K. Broderix, R. Kree, A. Zippelius [cond-mat/9903120]; L. Angelani, G. Parisi, G. Ruocco and G. Viliani, *Phys. Rev. Lett.* **81** (1998) 4648.
- [83] W. Kob, F. Sciortino and P. Tartaglia, *Phys. Rev. Lett.* **83** (1999) 3214; W. Kob, F. Sciortino and P. Tartaglia, *Europhys. Lett.* **49** (2000) 590.
- [84] L. Angelani, G. Parisi, G. Ruocco and G. Viliani, *Phys. Rev. Lett.* **81** (1998) 4648.
- [85] G. Iori, E. Marinari and G. Parisi, *J. Phys. A Math. Gen.* **24** (1992) 5349; M. Fukugita, D. Lancaster and M.G. Mitchard, *J. Phys. Lett. A Math. Gen.* **25** (1992) L121.

- [86] B. Bernu, J.-P. Hansen, Y. Hitawari and G. Pastore, *Phys. Rev. A* **36** (1987) 4891; J.-L. Barrat, J.-N. Roux and J.-P. Hansen, *Chem. Phys.* **149** (1990) 197; J.-P. Hansen and S. Yip, *Trans. Theo. Stat. Phys.* **24** (1995) 1149.
- [87] B. Coluzzi, M. Mézard, G. Parisi and P. Verrocchio, *J. Chem. Phys.* **111** (1999) 9039.
- [88] Y. Rosenfeld and P. Tarazona, *Mol. Phys.* **95** (1998) 141.
- [89] G. Zerah and J.P. Hansen, *J. Chem. Phys.* **84** (1986) 2336.
- [90] S. Sastry, *Phys. Rev. Lett.* **85** (2000) 590.
- [91] B. Coluzzi, G. Parisi and P. Verrocchio [[cond-mat/0007144](#)].
- [92] M. Mézard, G. Parisi and M.A. Virasoro, *J. Phys. Lett.* **46** (1985) L21.
- [93] D. Ruelle, *Commun. Math. Phys.* **48** (1988) 351.
- [94] M. Mézard, G. Parisi and A. Zee, *Nuc. Phys. B* **559** (1999) 689; V. Martin-Mayor, M. Mezard, G. Parisi and P. Verrocchio, *J. Chem. Phys.* **114** (2001) 8068.
- [95] A. Cavagna, I. Giardina and G. Parisi, *Phys. Rev. Lett.* **83** (1999) 108.
- [96] See for instance J.P. Hansen and I.R. Macdonald, *Theory of simple liquids* (Academic, London, 1986); or H.N.V. Temperley, J.S. Rowlinson and G.S. Rushbrooke, *Physics of simple liquids* (NorthHolland, Amsterdam, 1968).
- [97] J.K. Percus, in *The Equilibrium Theory of Classical Fluids*, edited by H.L. Frisch, J.L. Lebowitz (New York, Benjamin, 1964).

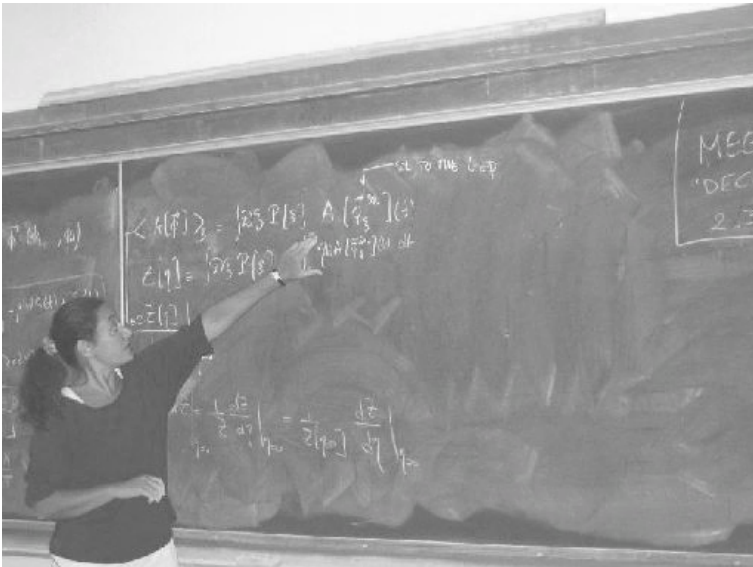
COURSE 7

DYNAMICS OF GLASSY SYSTEMS

L.F. CUGLIANDOLO

*Laboratoire de Physique Théorique,
École Normale Supérieure,
24 rue Lhomond,
75231 Paris Cedex 05, France
and*

*Laboratoire de Physique Théorique
et Hautes Énergies, Jussieu, 1er étage,
Tour 16, 4 Place Jussieu,
75252 Paris Cedex 05, France*



Contents

1	Introduction	371
2	Some physical systems out of equilibrium	374
2.1	Domain growth	374
2.2	Glasses	377
2.3	Spin-glasses	380
2.4	Quantum fluctuations	382
2.5	Rheology and granular matter	382
2.6	Elastic manifolds in random potentials	384
2.7	Aging	384
2.8	Summary	387
3	Theoretical approach	388
4	Systems in contact with environments	390
4.1	Modeling the coupled system	391
5	Observables and averages	395
5.1	Classical systems	395
5.2	Quantum problems	398
5.3	Average over disorder	399
6	Time dependent probability distributions	399
6.1	The Fokker–Planck and Kramers equations	399
6.2	Approach to equilibrium	400
6.3	Equilibrium dynamics	401
7	The fluctuation – dissipation theorem (FDT)	403
7.1	Static FDT	403
7.2	Dynamic FDT	404
7.3	Quantum FDT	404
7.4	Examples	405
8	Dynamic generating functionals	407
8.1	Classical models	407
8.2	Supersymmetry (SUSY)	409
8.3	Connection with the replica formalism	411
8.4	Quantum models	411
8.5	Average over disorder	415
9	Dynamic equations	416
9.1	A useful derivation for fully-connected models	416
9.2	Beyond fully-connected models	426
9.3	Field equations	430
9.4	The thermodynamic limit and time-scales	431
9.5	Single spin equation	431

10 Diagrammatic techniques	432
10.1 Perturbative solution	432
10.2 The mode coupling approximation (MCA)	434
10.3 MCA and disordered models	435
10.4 MCA for super-cooled liquids and glasses	438
11 Glassy dynamics: Generic results	439
11.1 The weak-ergodicity breaking scenario	439
11.2 The weak long-term memory scenario	441
11.3 Slow time-reparametrization invariant dynamics	442
11.4 Correlation scales	443
11.5 Modifications of FDT	449
12 Solution to mean-field models	455
12.1 Numerical solution	455
12.2 Solution at high temperatures	456
12.3 Solution at low- T	458
13 Modifications of FDT in physical systems	469
13.1 Domain growth	469
13.2 Structural glasses	471
13.3 Spin-glasses	472
13.4 Rheology	473
13.5 Vibrated models and granular matter	474
13.6 Driven vortex systems	474
13.7 Quantum fluctuations	475
13.8 Systems of finite size: Preasymptotic behavior	475
13.9 Critical dynamics	475
13.10 Connection with equilibrium	476
14 Effective temperatures	477
14.1 Thermodynamical tests	479
14.2 Temperature fixing by SUSY breaking	485
14.3 Fictive temperatures	485
14.4 Nonequilibrium thermodynamics	486
14.5 Statistical mechanics	486
15 Metastable states	487
15.1 Equilibrium	488
15.2 Static TAP approach	490
15.3 The TAP equations	492
15.4 Stability of, and barriers between, the TAP solutions	493
15.5 Index dependent complexity	495
15.6 Weighted sums over TAP solutions	495
15.7 Accessing metastable states with replicas	497
15.8 Dynamics and quantum systems	498

16 Conclusions	499
17 Perspectives	505
A Generalized Langevin equations	506
B The Kubo formula	509
C The response in a Langevin process	510
D Grassmann variables and supersymmetry	510
E Integrals in the aging regime	512

DYNAMICS OF GLASSY SYSTEMS

L.F. Cugliandolo

Abstract

These lecture notes can be read in two ways. The first two sections contain a review of the phenomenology of several physical systems with slow nonequilibrium dynamics. In the Conclusions we summarize the scenario for this temporal evolution derived from the solution to some solvable models (p spin and the like) that are intimately connected to the mode coupling approach (and similar ones) to supercooled liquids. At the end we list a number of open problems of great relevance in this context. These Sections can be read independently of the body of the paper where we present some of the basic analytic techniques used to study the out of equilibrium dynamics of classical and quantum models with and without disorder. We start the technical part by briefly discussing the role played by the environment and by introducing and comparing its representation in the equilibrium and dynamic treatment of classical and quantum systems. We next explain the role played by explicit quenched disorder in both approaches. Later on we focus on analytical techniques; we expand on the dynamic functional methods, and the diagrammatic expansions and resummations used to derive macroscopic equations from the microscopic dynamics. We show why the macroscopic dynamic equations for disordered models and those resulting from self-consistent approximations to non-disordered ones coincide. We review some generic properties of dynamic systems evolving out of equilibrium like the modifications of the fluctuation-dissipation theorem, generic scaling forms of the correlation functions, etc. Finally we solve a family of mean-field models. The connection between the dynamic treatment and the analysis of the free-energy landscape of these models is also presented. We use pedagogical examples all along these lectures to illustrate the properties and results.

1 Introduction

Graduate and undergraduate courses on statistical mechanics and thermodynamics are usually devoted to the theory of macroscopic systems in thermal equilibrium. In many experimental realizations, actually some of the

more interesting ones at present, the situation is, however, very different. The systems are in contact with equilibrated environments but, for one reason or another, they do not manage to equilibrate with them. The systems evolve in time in an out of equilibrium manner.

The list of systems evolving out of equilibrium is very long. The reasons for not reaching equilibrium with the environment are also varied. The most common cases are those in which the time needed to equilibrate the sample falls beyond the experimental time-window. We discuss them in the context of domain growth, phase separation and classical and quantum glassy systems. Another important cause for lack of equilibration is the action of external forces that drive the samples out of equilibrium. In this context we discuss the rheological properties of glass forming liquids and glassy materials, that are closely related to the relaxation of the same systems. The driven dynamics of granular matter is another example of this kind. Finally, we briefly touch another type of problem that has received much attention in recent years: the relaxation and weakly driven dynamics of elastic manifolds in random potentials that model magnetic domain walls in disordered materials, superconductors, Wigner crystals, etc.

A common feature among the relaxing and weakly driven examples cited above is that they evolve *very slowly*. Thus, they belong to a particular class of the full set of non-equilibrium systems. Exploiting the fact that their dynamics is slow, and other more subtle properties that we shall discuss along these notes, we can hope to develop a common theoretical description for all of them.

In these lectures we focus on the study of a family of simple models that can be adapted to mimic the above mentioned physical systems. Typically, these models are fully connected interacting spin systems or models of interacting particles in infinite dimensions. They can be seen as the equivalent of the fully connected Ising model for ferromagnetism that correctly predicts the existence of a thermodynamic transition and the nature of the two phases but fails to describe the dependence on dimensionality or the precise critical behavior. Similarly, the schematic models do not include a notion of distance inside the system. This crude approximation allows one to solve the dynamics explicitly, paying the price of losing information about the behavior in real space. Models of finite manifolds embedded in infinite dimensional spaces and under the effect of random potentials are generalizations of the schematic models that capture partial spatial information. They are also solvable analytically. Interestingly enough, one finds that these models realize several phenomenological approaches to glassy physics that have been known for long. Moreover, their dynamic macroscopic equations coincide with those arising from the self-consistent approximations used to analyze more realistic models as, for instance, the mode-coupling

approach to super-cooled liquids. Having an exact solution is very important in many respects. Firstly, it establishes the phenomenological approaches on firmer bases. Secondly, it allows one to set clear limits of validity of the self-consistent approximations to realistic models. Thirdly, being defined by interacting potentials their free-energy density is accessible to analytical studies, from which one obtains the organization of metastable states and relates it to the dynamic properties. Fourthly, many important and common features of systems evolving slowly out of equilibrium have been discovered in the analytic solution to these models. Fifthly, one is able to identify some of the missing ingredients needed for a more accurate description of real systems. Even if their treatment has been too tough to implement correctly yet, it is important to know in which direction one could try improving the analytical study. In short, they constitute a very useful “laboratory” where one identifies general trends that can be later tested numerically and experimentally in more realistic models and real materials.

Although the models on which we concentrate are simple in the sense discussed above one needs to master many analytical methods to extract all the richness of their behavior. These methods are not completely standard and are not comprehensively described in textbooks or lecture notes. For this reason, we try to present a rather complete and detailed introduction to them. We also discuss the scenario for glassy dynamics that stems out of this analysis. Finally, we mention several lines for future work that are currently being explored by several groups trying to go beyond the fully-connected and infinite dimensional models.

The lecture notes are organized as follows. In the next section we introduce the phenomenology of the physical systems we are interested in paying special attention to the dynamic properties that we later describe analytically. The rest of the lecture notes are more technical. We start by reviewing very briefly several theoretical approaches to the glassy problem in Section 3. This summary is certainly not exhaustive but it may serve as a source of references. Since in the rest of the notes we shall develop classical and quantum systems in parallel we devote Section 4 to discuss how should one model the coupling between a system and its environment in both cases. In Section 5 we set the notation and we define several useful observables for spin and particle systems. The subject of Section 6 is a brief discussion of Fokker-Planck and Kramers processes and how they describe the approach to equilibrium. In the following Section we introduce the fluctuation-dissipation theorem, valid for systems evolving in equilibrium. Once these generic properties are established it will become simpler to discuss how they are modified in a system that evolves far from equilibrium. In Section 8 we explain the functional formalism that allows one to derive a generic dynamic effective action and the dynamic equations that

we present in Section 9. We also introduce the very useful super-symmetric formulation of classical stochastic processes. In Section 10 we discuss an alternative method to obtain approximate dynamic equations. We focus on the mode-coupling (MC) approximation to show how averaging over disorder in some random models eliminates the same family of diagrams that the MC procedure neglects for non-disordered ones. The rest of the lectures are dedicated to the solution to the dynamic equations of the schematic models. We present it in as much generality as possible in Section 11. We discuss three generic results that were obtained when solving these equations without assuming equilibrium: the definition of correlation scales (Sect. 11.4), the modifications of the fluctuation-dissipation theorem (Sect. 13) and the definition of effective temperatures (Sect. 14). We also discuss how these properties appear in variations of the models that mimic the physical systems introduced in Section 2 and in finite d toy models, simulations and experiments. Finally, in Section 15 we relate the dynamic results to the organization of metastable states *via* the static and dynamic approach of Thouless *et al.* (TAP). We briefly discuss the connection between it and the studies of the potential energy landscape (Edwards measure and inherent structure approach). Finally, in Section 16 we summarize the scenario for the glass transition and glassy dynamics derived from solvable mean-field models and present some of the lines for future research in this area.

2 Some physical systems out of equilibrium

In this section we summarize the phenomenology of a number of systems with slow dynamics. We especially signal the features that we expect to capture with an analytical approach.

2.1 Domain growth

Out of equilibrium relaxational dynamics occurs, for instance, when one suddenly quenches a system with ferromagnetic interactions from its high temperature phase into its low temperature phase. When the system is in contact with a thermal bath at temperature $T > T_c$ (T_c is the Curie critical temperature) the system is disordered and the instantaneous averaged magnetization vanishes at all times. (The average refers here to a coarse graining over a region of linear size, ℓ , with $\xi \ll \ell$ and ξ the correlation length). All the one-time properties, such as the instantaneous averaged magnetization or the static magnetic susceptibility, can be computed using the Gibbs-Boltzmann distribution, P_{GB} . The system evolves in time but in a very simple manner controlled by P_{GB} . All properties of the equilibrium dynamics hold and any two-time correlation function is invariant under translations of time. Instead, if one externally and suddenly changes

T to set it below the Curie temperature, $T < T_c$, the system evolves from the very disordered initial condition *via* the growth of domains of up and down magnetic order. With simple arguments one shows that the typical linear size of the domains grows as a power of the time spent in the low temperature phase, $\mathcal{R}(t_w) = \Upsilon(T) t_w^{1/z}$ [1]. We call waiting-time, t_w , the time spent since the entrance in the low- T phase. The dynamic exponent z depends on the kind of microscopic dynamics considered, *e.g.* for non-conserved order parameter $z = 2$ while for conserved order parameter $z = 3$. All T -dependence is concentrated in the prefactor $\Upsilon(T)$. After the initial quench the system is a superposition of up and down domains and the magnetization averaged over the full system ($\ell = L$) vanishes. During coarsening domains grow. This is a *scaling regime* in which the system is statistically invariant under rescaling by the typical length $\mathcal{R}(t)$. Typically, at a time $t_{\text{REQ}} \approx L^z$ the system orders and the averaged magnetization, m , equals the magnetization of the conquering domain, say $m > 0$. *Restricted ergodicity or equilibrium within one ergodic component* holds in the sense that time and ensemble averages can be exchanged *if and only if* the time average is taken over a time window $t_{\text{REQ}} < t < t_{\text{ERG}}$ and the ensemble average is restricted to the configurations with positive magnetization. Since a rare fluctuation might lead the system to reverse from $m > 0$ to $m < 0$ another, still longer, characteristic time, t_{ERG} , appears. This time is also a function of the size of the system L and it is such that for times that are much longer than it complete ergodicity is restored. One can estimate it to be of Arrhenius type $t_{\text{ERG}} \sim \exp[cL^{d-1}/(k_B T)]$, with c a constant, d the dimension of space and cL^{d-1} the free-energy barrier to be surmounted to go from one ergodic component to the other.

The low temperature phase can also be reached with an annealing, *e.g.* by modifying the external temperature in steps of length Δt and magnitude $\Delta T < 0$ until reaching the working temperature T . Since the entrance in the low- T phase the system coarsens. If the prefactor $\Upsilon(T)$ increases with T , after a time t_w since crossing T_c a system prepared with a slow cooling rate will have much larger structures than one of the same age that has been quenched into the ordered phase. The dynamics in isothermal conditions is basically identical in both cases but the starting configuration at the final temperature T is however very different, the annealed system looking older than the quenched one. The presence or absence of cooling rate dependences as well as the effect of temperature on the low- T dynamics allow one to distinguish among different glassy system. We shall come back to this issue when discussing structural and spin glasses.

On the right panel of Figure 1 we plot the two-welled Landau free-energy density $f(m)$ against m . Transverse to the m direction there are $2^{L^d} - 1$ other directions that complete the phase space of the spin model. Note

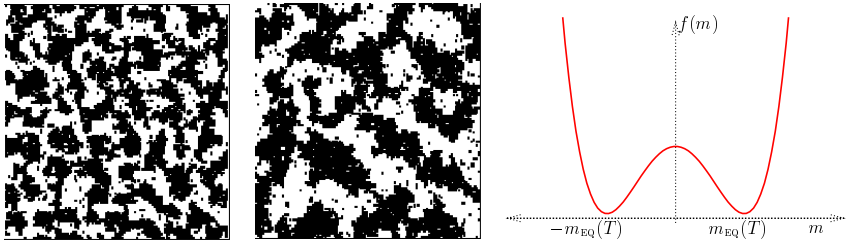


Fig. 1. Two snapshots of a 2d cut of a 3d lattice undergoing ferromagnetic domain growth with non-conserved order parameter after a quench from $T \rightarrow \infty$ to $T < T_c$ at time $t = 0$. On the left, $t_w = 10^3$ Montecarlo steps (MCs). On the right, $t_w = 10^5$ MCs. Sketch of the Landau free-energy density $f(m)$ in the low- T phase. The evolution of the system is partially described by the evolution of a point in this free-energy landscape. Just after the quench $m = 0$ and coarsening is visualized in this plot as a static point on top of the barrier. After t_{REQ} the point falls into the well around the magnetization of the conquering domain. After t_{ERG} ergodicity is restored and the point jumps the barrier *via* thermal activation [2].

that when $L \rightarrow \infty$ phase space is infinite dimensional even if real space is finite dimensional, $d < \infty$. If one wishes to view the dynamics as the wandering of a point, that represents the instantaneous configuration of the system, in the free-energy landscape, the one-dimensional plot in Figure 1 might be useful only if used carefully. The initial configuration after a quench corresponds to the top of the barrier ($m = 0$). This unstable point hides the $2^{L^d} - 1 \gg 1$, for $L \gg a$, transverse directions (a is the lattice spacing). The domain growth process takes place while the representative point sits on the top of the barrier. Falling into one well corresponds to the growth of the conquering domain. Finally, jumping over the barrier is the activated process of reversing the full system. As long as $t < t_{\text{REQ}}$ the dynamics is highly non-trivial while viewed on this plot it looks trivial, with the representative point simply sitting on the border between the two basins of attraction of the equilibrium states $m = \pm m_{\text{EQ}}$ [3].

Importantly enough, both t_{REQ} and t_{ERG} grow with L and, if the thermodynamic limit $L \rightarrow \infty$ is taken at the outset, diverging times with L cannot be reached and physical times are always smaller than t_{REQ} . The system cannot equilibrate with its environment and the non-equilibrium domain growth process goes on for ever.

2.2 Glasses

The domain growth example is very useful to visualize a non-equilibrium evolution. The mechanism behind the dynamics is clear and the growth of order can be easily identified. In other systems that undergo a non-equilibrium evolution whether there is a growing order controlling the evolution is still an open question. Glassy systems are one such example.

Understanding the glass transition and glassy dynamics is one of the greatest challenges in theoretical physics. The glassy problem can be summarized as follows [4]. Take a liquid at high temperature T_i and quench it at a constant rate, $r \equiv -\Delta T/\Delta t$. On each temperature step, the viscosity relaxes rather quickly and with a simple analysis one estimates its asymptotic value to trace a curve $\eta(T)$ that is sketched in the left panel of Figure 2 (red curve). This curve has several remarkable features. At very high temperature $\eta(T)$ very slowly grows with decreasing T . Decreasing the external temperature still the system approaches the crystallization (or melting) transition T_m . If the cooling rate r is sufficiently fast, this transition is avoided and the system enters a metastable *super-cooled liquid* phase where the viscosity grows very quickly with decreasing T . Indeed, one typically observes that when T changes by, say, 100 °C, the viscosity jumps by approximately 10 orders of magnitude. In consequence, the dynamics of the liquid slows down enormously. For several liquids the form of the $\eta(T)$ curve can be described with a Vogel-Fulcher law,

$$\eta(T) = \eta_0 \exp \left(\frac{A}{T - T_o} \right), \quad (2.1)$$

that predicts a divergence of $\eta(T)$ when $T \rightarrow T_o$. These liquids are conventionally called *fragile*. (Within the experimental precision T_o coincides with the Kauzmann temperature T_K where the extrapolation of the difference between the entropy of the liquid and the crystal vanishes.) However, this fitting procedure can be criticized for several reasons. In many cases the form of the fitting function strongly depends on the temperature window chosen for the fit. Even more important is the fact that the dynamics becomes so slow when T decreases that the time needed to equilibrate the sample goes beyond the minimal cooling rate, or the maximum time reachable in the experience. Below a temperature $T_g(> T_o)$ one can no longer equilibrate the sample. One of the most clear signatures of the absence of equilibrium below T_g is the fact that the measurement of, *e.g.*, the volume as a function of temperature, depends on the cooling rate, r , used to reach T . Moreover, T_g decreases with decreasing cooling rate. Hence, the so-called “glass transition” is not a true thermodynamic transition but a dynamic crossover from the super-cooled liquid phase, where the dynamics is slow but occurs as in equilibrium [5], to the glass phase where the system

does not manage to equilibrate with its environment. These features are schematically shown in the right panel of Figure 2. Going back to the interpretation of equation (2.1), some authors extrapolate it below T_g , where viscosity measurements are not possible, and interpret the divergence at T_0 as the signature of a true thermodynamic transition. This means that even in the limit of vanishing cooling rate one would observe a transition from the super-cooled liquid to an ideal glass phase (still metastable with respect to the crystal) at T_0 . Others prefer a scenario in which equation (2.1) has no meaning below T_g .

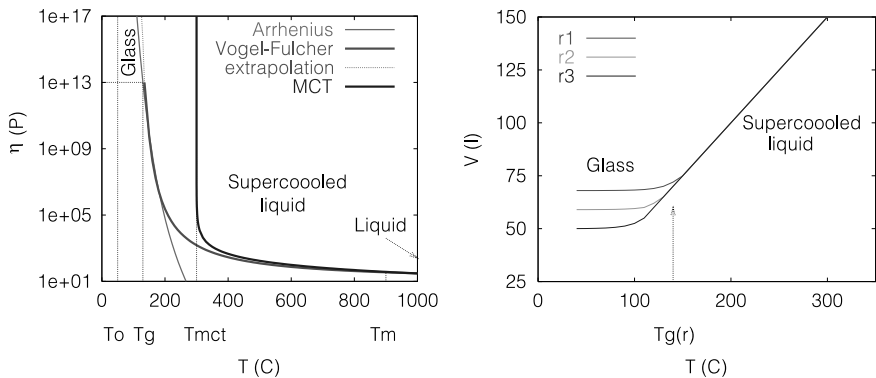


Fig. 2. Left: sketch of the viscosity against temperature approaching T_g . Rough comparison between different scaling forms. (Arrhenius: $A = 3900$ C, $\eta_0 = 10^{-6}$ P. Vogel-Fulcher: $A = 500$ C, $T_0 = 100$ C, $\eta_0 = 10$ P. MCT: $\eta = \eta_0 / (T - T_d)^\gamma$ with $T_d = 300$ C, $\gamma = 0.7$, $\eta_0 = 1700$ P.) Right: cooling rate dependence of the volume, $r1 > r2 > r3$.

In this sense, it is important to stress that the viscosity of many glass forming liquids, as the silica materials that give rise to window glass, is well fitted by an Arrhenius law

$$\eta(T) = \eta_0 \exp\left(\frac{A}{T}\right) \quad (2.2)$$

that diverges at $T \rightarrow 0$. These are the so-called *strong* glasses. It has been suggested that actually all glasses are strong since one can always fit $\eta(T)$ with an Arrhenius law if the temperature window used for the fit is close enough to T_g (as suggested in Fig. 2). This is the reason why some authors prefer a scenario in which the super-cooled liquid phase extends all the way up to $T = 0$ when an infinitely slow cooling rate is used. The curve labeled MCT in the same figure shows the prediction of the models we shall discuss in these notes (*p* spin models and mode-coupling theory). In short,

this approach predicts a dynamic transition at T_d that is typically higher than T_g , with a power law divergence of η . Albeit this and other defects, this approach is successful in many respects since it yields a satisfactory *qualitative* description of the phenomenology of super-cooled liquids and glasses.

For the purpose of our discussion the important point to stress is the fact that the liquid falls out of equilibrium at the (cooling rate dependent) temperature T_g . Indeed, even the “state” reached by the system below T_g depends on the cooling rate as seen, for instance, in measurements of volume, entropy, etc. as functions of T , see the right panel in Figure 2. The slower the cooling rate, the deeper one penetrates below the *threshold* level corresponding to $r \rightarrow \infty$. The dynamics below T_g occurs out of equilibrium since $t_{EQ} > t_{EXP}$, see the sketch in Figure 3. The properties of the system cannot be described with the use of P_{GB} and a more sophisticated analysis has to be developed.

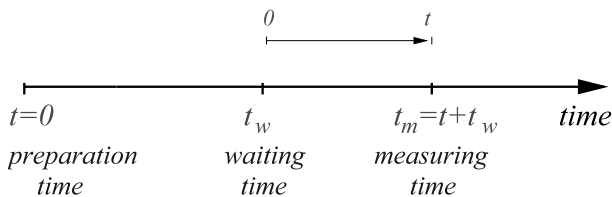


Fig. 3. Characteristic times. The waiting and measuring times are *experimental times* t_{EXP} . The equilibration time t_{EQ} can be shorter or longer than them leading to equilibrium or non-equilibrium dynamics, respectively.

The above paragraphs were devoted to the discussion of the liquid to glass transition and it implicitly assumed that the system was made of molecules in interaction. In the case of simple liquids, in which the constituents have no structure, one can describe the relevant interactions with a two body potential

$$E = \sum_{i \neq j} V(|\vec{r}_i - \vec{r}_j|). \quad (2.3)$$

Hard spheres are the simplest example of this kind where the only interactions are hard core ones that forbid the penetration of one particle by another. Adding polymers in the solution that hosts the spheres one can tune a repulsive interaction between the particles. (See Fig. 4-left below for a snapshot of one such experimental system [6].) Favorite potentials used in numerical simulations are the Lennard-Jones and soft-sphere ones

$$V(|\vec{r}_i - \vec{r}_j|) = 4\epsilon_{ij} \left[\left(\frac{\sigma_{ij}}{|\vec{r}_i - \vec{r}_j|} \right)^{12} - \left(\frac{\sigma_{ij}}{|\vec{r}_i - \vec{r}_j|} \right)^6 \right]. \quad (2.4)$$

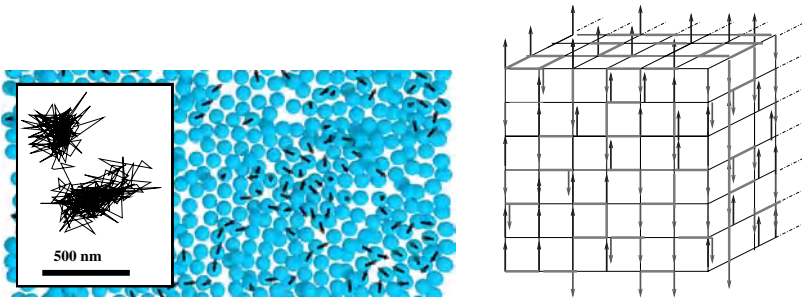


Fig. 4. Different types of glasses: on the left, a colloidal system (image taken from [6]); on the right a representation of the 3d EA spin-glass model.

To avoid crystallization one usually uses a binary system with N_A particles with mass m_A and N_B particles with mass m_B . The parameter σ_{AA} fixes the length scale, ϵ_{AA} the energy scale and m_A the mass scale. The time scale is then given by $t_0 \equiv \sqrt{m_A \sigma_{AA}^2 / \epsilon_{AA}}$. For a given density, *e.g.* $\rho = 1.2$, an adequate choice of the remaining parameters yields the expected properties of a liquid or a glass with a numerical transition at a temperature T_g where the relaxation time goes beyond the time accessible with the simulation. In the soft-sphere model one only keeps the repulsive term in the potential. Many other types of glasses are known in Nature. For instance, plastics as PVC whose mesoscopic constituents are polymers also undergo a glass transition very similar to the one described previously. Several types of interactions between the monomers that form the macromolecules are also of two-body type and they are repertoriated in the literature. The dynamics of particle systems is given by Newton's equations.

2.3 Spin-glasses

More exotic types of glasses have been studied for long. Spin-glasses have attracted the attention of experimentalists and theoreticians as a prototypical system with *quenched disorder* [7–10]. These systems are magnetic alloys in which magnetic impurities are replaced in a magnetically inert host. The impurities occupy random positions and are not displaced within the sample in experimental times. The interactions between the impurities depend on the distance between them. Since the latter are random, the interactions themselves take random values that change in sign very quickly. A number of experimental realizations exist. As in other glassy systems, spin-glasses fall out of equilibrium at a transition temperature T_g when usual cooling rate procedures are used. From experimental and numerical results near T_g complemented with standard critical analysis, it is rather generally

believed that the transition between the paramagnetic and the spin-glass phase is, in this case, a true thermodynamic transition. This is at variance with what occurs in structural and polymeric glasses. Another important difference with structural glasses and systems undergoing simple coarsening as ferromagnets is that the magnitude of cooling rate dependences is quite negligible suggesting that for spin-glasses the preferred configurations at one temperature are totally different from the ones at any other temperature. Still, slightly farther away from the transition one can no longer equilibrate the spin-glasses and observes typical non-equilibrium effects.

Edwards and Anderson proposed a simplified model for spin-glasses in which one represents the magnetic impurities with Ising spins placed on the vertices of a three dimensional cubic lattice. The random nature of the interactions are mimicked with first neighbors random interactions between the spins taken from a Gaussian (or bimodal) probability distribution with zero mean and variance $[J_{ij}^2] = \tilde{J}^2/(2z)$ where z is the connectivity of the lattice. (Hereafter we denote with square brackets the average over disorder.) The Hamiltonian is

$$H_J [\vec{S}] = - \sum_{\langle ij \rangle} J_{ij} s_i s_j \quad (2.5)$$

where the vector \vec{S} encodes the full set of spins in the sample $\vec{S} = (s_1, s_2, \dots, s_N)$ and $\langle ij \rangle$ represents nearest neighbors on the lattice. In the fully connected limit in which each spin interacts with all others the sum runs over all pair of spins and the unusual normalization of the $J_{ij}s$, $[J_{ij}^2] = \tilde{J}^2/(2N)$, ensures a correct thermodynamic limit. This is the Sherrington – Kirkpatrick (SK) model.

For many years it was common lore that the presence of explicit quenched disorder made spin-glasses intrinsically different from glasses where no quenched random forces have been identified. This belief was in part motivated by the analytical treatment used to study the *equilibrium properties* of the spin-glass phase in SK, namely, the replica trick. More recently, after a series of seminal papers by Kirkpatrick, Thirumalai & Wolynes [11], and the later solution to the non equilibrium dynamics of several glassy models [12, 13], it has been realized that the presence of quenched disorder is not that relevant. All glasses can be analyzed on the same footing. The schematic mean-field model for glasses, the p spin model, has quenched Gaussian interactions and its Hamiltonian is

$$H_J [\vec{S}] = - \sum_{\langle i_1 i_2 \dots i_p \rangle} J_{i_1 i_2 \dots i_p} s_{i_1} s_{i_2} \dots s_{i_p}. \quad (2.6)$$

($[J_{i_1 \dots i_p}] = 0$ and $[J_{i_1 \dots i_p}^2] = \tilde{J}^2 p!/(2N^{p-1})$, we henceforth set $\tilde{J} = 1$). Glauber's rule for Ising spins or Langevin equations for soft spins define the microscopic evolution.

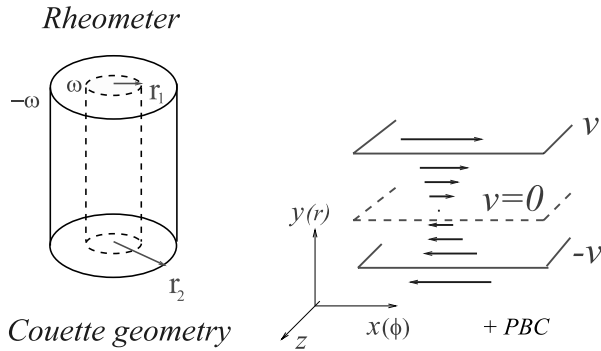


Fig. 5. Left: a Couette cell used to shear a liquid. The internal and external walls turn with opposite angular velocities and the fluid is included in between them. Right: a cut of the Couette cell. (PBC: periodic boundary conditions.)

2.4 Quantum fluctuations

Different driving dynamics slightly modify the picture just presented. Quantum glassy phases, where quantum fluctuations are at least as important as thermal activation, have been identified in a number of materials. Two such examples are the spin glass compound and the amorphous insulator studied in [14] and [15], respectively. Another interesting realization is the so-called Coulomb glass in which localized electrons interact *via* Coulomb two-body potentials and hop between localization centers [16]. In all these systems the dynamics is extremely slow and strong history dependence as well as other glassy features have been observed.

Models for magnetic compounds are constructed with $SU(2)$ spins while models for particle systems are quantized with the usual commutation relations between coordinate and momenta. In both cases the dynamics is fixed by Heisenberg equations.

2.5 Rheology and granular matter

The above examples concern systems that are not able to reach equilibrium with their environments in a reasonable time but that, let evolve on astronomical time-scales, will eventually equilibrate. Other ways of establishing non-equilibrium states with slow dynamics are possible if one externally drives the samples [17].

A dense liquid can be driven to a slow out of equilibrium stationary regime by a weak shear. A shear is an example of a force that does not derive from a potential, *i.e.* it cannot be written as $\vec{f} = -\partial V/\partial \vec{r}$. The simplest way to apply a shear on a liquid is by means of a rheometer. In

Figure 5 we show one with a Couette geometry. The shear modifies the dynamic equations for the fluid by adding an advection $\vec{v}\vec{\nabla}\rho(\vec{r}, t)$. In the planar limit $\vec{v} = \dot{\gamma}y\hat{e}_x$ where \vec{v} is the velocity of the fluid, ρ its density and $\dot{\gamma}$ the shearing rate. One mimics such a force in a spin system with a non-symmetric force, *i.e.* the force exerted by the spin i on the spin j is not equal to the force exerted by the spin j on the spin i [18, 19], *e.g.*

$$f_i = \alpha \sum_{j(\neq i)} J_{ij}s_j \quad \text{with } J_{ij} \neq J_{ji}. \quad (2.7)$$

(The motivation to define such a force comes from neural nets where the synapsis have a direction.) It is clear that this force cannot be written as the variation of a potential energy with respect to s_i , it violates detail balance, and an equilibrium measure cannot describe its effects [20].

A weak shear has a spectacular effect on the relaxation of liquids [21]. Usually, the viscosity as a function of the shear rate, $\dot{\gamma}$, has a Newtonian plateau at small $\dot{\gamma}$ that crosses over to a decreasing function that is approximately given by $\eta \approx \dot{\gamma}^{-2/3}$. Hence, by shearing the liquid one facilitates its flow and the relaxation time decreases with increasing $\dot{\gamma}$. Moreover, one introduces a shear-dependent time scale t_{SH} that plays an important role in aging experiments as discussed in Section 2.7.

Another family of materials that have captured the attention of experimentalists and theoreticians in recent years is granular matter [22]. Since the potential energy needed to displace a macroscopic grain by a distance equal to its diameter, mgd , is much larger than the characteristic thermal energy, $k_{\text{B}}T$, thermal activation is totally irrelevant for systems made of macroscopic grains. Therefore, in the absence of external driving granular matter is blocked in metastable states and there exists no statistical mechanics approach capable of describing its static behavior. Instead, when energy is pumped in in the form of shearing, vibration or tapping, transitions between the otherwise metastable states occur and granular matter slowly relaxes towards configurations with higher densities. When trying to model these systems it is also important to keep in mind that dissipation is not given by the usual Ohmic form proportional to the velocity of the grains, $-\gamma v$, but it is much more cumbersome. Glassy features such as hysteresis as a function of the amount of energy injected, slow dynamics [22], and non stationary correlations [23–25] have been exhibited.

The effect of the external drive can be described by applying time-dependent oscillatory forces, *e.g.* $f_i(\omega, t) = A\sin(\omega t)$, to each spin variable in model (2.6) [26]. One could also include complicated sources of dissipation by modifying the noise kernels obtained in Section 4 for a usual equilibrated bath.

2.6 Elastic manifolds in random potentials

The motion of a d dimensional directed elastic manifold embedded in an N dimensional space in the presence of quenched random disorder has a bearing in several areas of physics [27, 28]. (The total dimension of space is $d + N$.) The case $d = 0$ represents a particle in a random potential. With $d = 1$, $N = 2$ and an attractive punctual disorder one models, for instance, a single vortex in a dirty superconductor. When $d = 2$ and $N = 1$ one describes the dynamics of a directed interface in three dimensions. The standard model is

$$H = \int d^d x \left[\left(\vec{\nabla} \vec{\Phi}(\vec{x}) \right)^2 + V(\vec{\Phi}, \vec{x}) \right] \quad (2.8)$$

where $\vec{\Phi}(\vec{x}) = (\Phi_1, \dots, \Phi_N)(\vec{x})$ and $\vec{x} = (x_1, \dots, x_d)$ represents the transverse position of the point \vec{x} on the manifold and $V(\vec{\Phi}, \vec{x})$ is a Gaussian random potential, with zero mean and correlations $[V(\vec{\Phi}, \vec{x})V(\vec{\Phi}', \vec{x}')] = -N\nu \left[(\vec{\Phi} - \vec{\Phi}')^2 / N \right] \delta^d(\vec{x} - \vec{x}')$.

The study of these problems has been boosted by the advent of high- T_c superconductivity. Other physical systems that are modeled with similar Hamiltonians are Wigner crystals, vortex lattices, charge density waves, etc. in the presence of disorder. All these problems have an underlying periodic structure that is modified by elastic distortions, topological defects and external quenched disorder. They can be set into motion with an external force and the velocity-force characteristics has several interesting features that have been much studied. One observes a depinning transition at $T = 0$, creep dynamics when the applied force is weak and $T > 0$, hysteresis, etc. (The driven motion is achieved, for instance, by applying an external current in the case of the vortex systems and the current-voltage characteristics is monitored.) The relaxational and driven dynamics of these systems show similarities but also marked differences with that of glasses and spin-glasses that are possibly due to the existence of an ordered underlying structure.

2.7 Aging

Aging means that older systems relax in a slower manner than younger ones [29]. One defines the age of a system as the time spent in the phase under study. For instance, the age of a system that is suddenly quenched from high- T to low- T is simply t_w . The aging properties are studied by monitoring the time evolution of correlation and response functions. In the former experiments one lets the system evolve and compares its configuration at the waiting-time t_w with the one reached at the subsequent time $\tau + t_w$. In the latter one perturbs the system at t_w with, *e.g.* a dc or an ac

field, and follows the evolution of the linear response to the perturbation. In the glassy phase both correlations and responses depend on t_w in an aging manner and, within the experimentally accessible time-window, this trend does not show any tendency to stop. At temperatures that are close but above T_g one observes “interrupted aging”, that is, a dependence on the age of the system until it reaches the equilibration time ($t_w > t_{\text{EQ}}$) where the dynamics crosses over to an equilibrium one. In equilibrium correlation and response measurements are related in a system independent manner by the fluctuation-dissipation theorem (see Sect. 7). Out of equilibrium this general relation does not hold and, as we shall explain in Sections 13 and 14, important information can be extracted from its modifications.

Aging has an easy interpretation within coarsening systems. While the averaged domain size $\mathcal{R}(t_w)$ grows with t_w , its rate of increase $d_{t_w}\mathcal{R}(t_w)$ decreases, *e.g.* $d_{t_w}\mathcal{R}(t_w) \sim t_w^{1/z-1}$ in the example explained in Section 2.1. The motion of interfaces slows down as time elapses. Comparing the configuration at t_w and at a later time $\tau + t_w$, one finds a clear separation of time-scales depending on the relative value of τ with respect to t_w . If $\tau \ll \tau_0(t_w) \equiv 1/d_{t_w} \ln \mathcal{R}(t_w)$, one has $\mathcal{R}(\tau + t_w) \sim \mathcal{R}(t_w) + d_{t_w}\mathcal{R}(t_w)\tau \sim \mathcal{R}(t_w)$, and the domain walls do not move. The overlap between the configurations at t_w and $\tau + t_w$ is a sum of overlaps between domains of one and another type. (This holds when the ratio between the number of spin in the surface of the domains and in the bulk vanishes in the thermodynamic limit. Some non-standard systems have fractal scaling of the interfaces and the volume of the domains might also have a fractal dimensionality [30].) Due to thermal fluctuations within the domains, the correlation decays as in equilibrium from 1 at equal times to $m_{\text{EQ}}^2(T)$ when τ increases while still satisfying the constraint $\tau \ll \tau_0(t_w)$. For τ 's beyond this limit, the correlations decay below $m_{\text{EQ}}^2(T)$ since the interfaces move and one compares configurations with very different domain structures as shown, for instance, in the two snapshots in Figure 1.

In structural glasses, a pictorial explanation of aging is also possible imagining that each particle sees a cage made of its neighbors. When τ is short compared to a characteristic time $\tau_0(t_w)$ each particle rapidly rattles within its cage and the decorrelation is only characterized by thermal fluctuations. The correlations decay in a stationary manner from its value at equal times to a value called q_{EA} that will be defined precisely in Section 12 [in the domain growth example $q_{\text{EA}} = m_{\text{EQ}}^2(T)$]. When τ increases, the motion of the particles destroys the original cages and one sees the structural relaxation. The waiting-time dependence implies that the cages are stiffer when time evolves. The motion of a tagged particle is depicted in the left panel of Figure 4 [6]. One sees how it first rattles within a cage to later make a long displacement and start rattling within another cage.

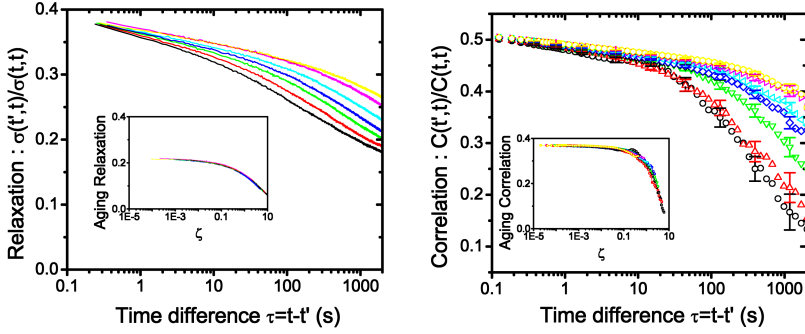


Fig. 6. Aging in the thiospinel insulator spin-glass. Decay of the thermoremanent magnetization (left) and correlations between magnetic fluctuations (right). From left to right curves for increasing waiting-times. Inset: scaling. (Curves taken from [32], see [31] and [32] for details.)

In spin-glasses no consensus as to which is the origin of aging has been reached. Still, the qualitative behavior of correlations and responses is rather close to the one in domain growth and structural glasses. In Figure 6 we show the decay of the thermoremanent magnetization (an integrated linear response) and the correlations between the fluctuations of the magnetization in a spin-glass [31,32].

Shearing may have a very strong effect on an aging system. In some cases it introduces a characteristic time t_{SH} that yields the longest relaxation time. Thus, aging is interrupted for waiting-times that are longer than t_{SH} (see Fig. 7). This effect has been known for long experimentally [21] and it has been found and explored recently within the theoretical framework that we review [33,34]. Experiments in other soft glassy materials with aging and aging interrupted by shear can be found in [35]. Some examples where the effect of shearing is not as spectacular are also known. For instance, in a phase separating mixture sheared in one direction the domains stop growing in the transverse direction while they continue to grow longitudinally (see [19] and references therein). This is a subject of intensive research.

Granular matter is usually driven with periodic forces or tapping. These perturbations pump energy into the system that is evacuated *via* friction and introduce a time-scale t_{OSC} that is simply the period of the oscillation. How these forces influence the aging properties is much less known and it is the subject of current investigations. For the moment, most of the work in this direction has been numerical [24,25] and also analytical within the kind of models we shall solve [26] (see [23] for some experimental studies).

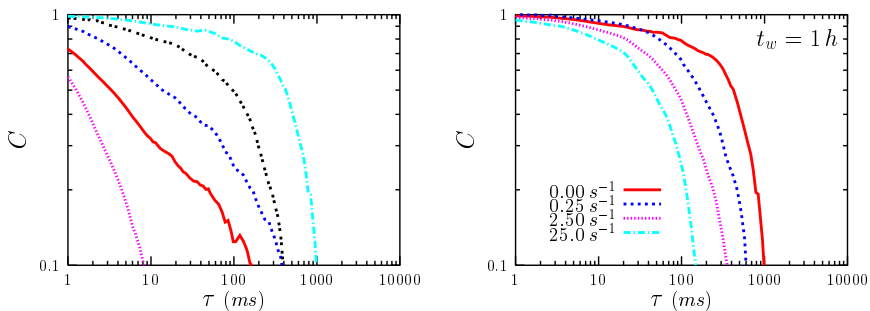


Fig. 7. Aging and interrupted aging in laponite. Decay of the correlation function in a relaxing (left) and a sheared (right) sample. In the aging case different curves correspond to increasing waiting-times from left to right, $t_w = 10, 20, 30, 40, 50$ min. (Note that the decay occurs for $\tau \ll t_w$ since the waiting-times are rather short and the sample is still very far from equilibrium; *cf.* with the results in A. Knaebel *et al.* in [35].) In the sheared case, the sample has been let wait for $t_w = 1 h$, four shear rates, $\dot{\gamma}$, with values indicated in the key were applied at this instant and the decay of the stationary correlation was recorded [44].

The aging properties of relaxing manifolds in random potentials have been found analytically [36] and numerically [37]. The experiment of Portier *et al.* [38] shows aging features in a high- T_c superconductor [39] that are also observed numerically [40,41]. However, other experimental studies using different protocols have not exhibited these properties [42]. More experiments are needed to get a better understanding of the non-equilibrium relaxation of these systems. An external electric current drives a vortex system in its transverse direction due to Lorentz forces. How the longitudinal and transverse aging properties of the system are modified in the moving phases is another problem that deserves further study [43]. The comparison between the dynamics of the moving vortex lattice, the tapped dynamics of granular matter and the sheared dynamics of dense liquids is also interesting and begins to be done.

2.8 Summary

In this section we introduced several examples of macroscopic systems that evolve with a slow non-equilibrium macroscopic dynamics. The microscopic dynamics governing the evolution of the constituents of each system is very different. For systems undergoing domain growth and classical glasses, T is the external control parameter that generates fluctuations. For glasses at very low T thermal fluctuations are almost completely irrelevant while

quantum fluctuations become important and drive the dynamics. For granular matter T is again irrelevant and the systems' relaxation is due to the external drive. In the elastic systems an underlying ordered structure is visible and may cause important differences in the macroscopic dynamics with respect to other glassy systems where no quasi order has been identified. An ubiquitous phenomenon in these slowly evolving systems out of equilibrium is (sometimes interrupted) aging or the breakdown of stationarity. Even if all these systems seem to be totally different, a common formalism to study their macroscopic dynamics is now being used and a common picture starts to develop.

In the rest of these lectures we shall explain the main technical tools needed to study simplified models for these real systems. We shall describe the main features of the out-coming scenario making contact with the phenomenology introduced in this section.

3 Theoretical approach

Besides many phenomenological descriptions of the glass transition and glassy dynamics proposed long ago, recently, several theoretical approaches have been developed. In the following we briefly describe some of the main ones.

Dynamics in the phase space

The instantaneous configuration of the full system is a point in phase space that moves as time goes on (see the right panel in Fig. 1). In a whole family of models one assumes a free-energy landscape on phase space with wells and barriers and proposes that the point evolution is given by some dynamic prescription on this space. Choosing a convenient distribution and organization of wells and barriers, aging effects are captured by such models. (An average over different systems or over different parts of the same system is implicitly assumed in order to obtain smooth results for the observables.) In “trap models”, for instance, each well has an associated trapping-time such that once the system falls in the trap it has to wait this trapping-time to escape from it. A useful choice is a Lévy distribution of trapping-times that is not bounded (this is related to assuming that the depth of wells is not bounded from below). The dynamics is such that whenever the point leaves a trap a complete “renewal” takes place in the sense that in the next time step it chooses any trap from the ensemble with equal probability. For simple probability reasons one can prove that at a time t_w after the starting time the system will be trapped in a well with life-time $\sim t_w$. This model is due to J.-P. Bouchaud and it leads to aging [45–48] (for other trap models in the glassy context see [49]).

Domain growth

A different approach most commonly used to describe the dynamics of spin-glasses assumes that the evolution is driven by the growth of domains of two (or a few) competing phases. The non-equilibrium dynamics is then very similar to ferromagnetic coarsening slowed down by the existence of disorder and/or competing interactions. To obtain concrete predictions one either uses scaling arguments that lead to the “droplet model” for spin-glasses [50] and its extension to other glassy systems or one solves exactly simple models in low dimensions, typically $d = 1$ [51, 52]. A drawback of this approach is that it has been hard to identify the growing structures in glassy systems.

Kinetic models

A third approach used to model the dynamics of glasses consists in proposing purely kinetic models with no underlying energy function. The dynamic rules are chosen so as to slow down the dynamics and lead to a dynamic arrest at some critical temperature or density. Interestingly enough tuning the nature of the constraints these models may behave as strong, fragile or may even show a fragile-to-strong crossover. They can also have non-trivial long-lasting nonequilibrium dynamics without having an underlying static transition. Several such models exist, see [51] for a collection of articles on this subject and [53].

Mean-field models

Many of the recent developments in the understanding of the similarities in the behavior of *a priori* so different systems as the ones described in Section 2 are based on the analysis of mean-field models. These models are defined by Hamiltonians with long range interactions [*e.g.* sum over all pairs of spins in Eq. (2.5)] or in infinite dimensions [*e.g.* take $N \rightarrow \infty$ in Eq. (2.8)]. Sometimes it is convenient to include quenched disordered interactions though this is not necessary.

The static properties of these models are accessible by the usual statistical mechanics analysis complemented by the less standard replica trick when disorder exists [9]. The organization of metastable states or, in other words, the full structure of the relevant Landau-type free-energy landscape, is also accessible with time-independent calculations called TAP approach in the context of spin-glass theory [56].

As for dynamics we first have to define how the microscopic variables evolve in time. In classical particle systems Newton equations determine their evolution. In quantum systems Heisenberg equations do the same.

Since in realistic situations the systems of interest are in contact with their environments we present the modelization of the coupled systems in Section 4. We show how the effect of the environment translates into noise in both cases. For classical models the elimination of the bath variables leads to Langevin equations. Non-potential forces and vibrations in classical systems are easily included by adding terms to the Langevin equations. Once the microscopic dynamics is given the techniques described in the rest of the notes allow us to solve these schematic models.

These models capture many properties of real systems. Nevertheless, their mean-field character implies many drawbacks. For example, one finds that they have sharp dynamic (with no thermodynamic anomaly) and static transitions at temperatures T_d and T_s , ($T_d > T_s$). The relationship between the dynamic solution and the organization of metastable states in the relevant free-energy landscape can be made precise and it allows us to understand the existence of these two separate transitions. In real systems, however, there is no sharp dynamic transition since T_g is actually a crossover, while T_s might not exist (recall the discussion on T_o in Sect. 2.2). In spite of this and other defects, one of the interests in these models and their solutions is that they have a great power of prediction of so far unknown effects and that they act as a source of inspiration for searching new features in the numerical and experimental study of more realistic models and systems. The rather accurate comparison to numerical simulations [57–59], and, to the extent of their availability, experiments [31,32,60–62], supports the proposal that the mechanism in these models is similar to the one responsible for the glass transition, and the glassy dynamics, in real materials. Indeed, there is growing consensus in that they provide an exaggerated realization of the actual glassy phenomenon. It is worth mentioning too that some of the features found in the mean-field models that we shall explain below have also been analysed within the other approaches mentioned above.

In the following we present the asymptotic analytic solution to this family of models. Some of the ingredients missing in their full analytic solution, that would render their description of real materials more accurate, have been identified (analysis of the dynamics in time-scales that diverge with N , description of dynamic heterogeneities, etc.). For the moment, their complete analytical treatment has proven too difficult but some recent articles report partial success and suggest interesting ways to follow up. We shall come back to these issues in the Conclusions and Perspectives.

4 Systems in contact with environments

In the typical experimental protocols discussed in Section 1 one quenches the sample and subsequently follows its evolution in time. Once arrived

at the final point in parameter space, if no external forces are applied, the system relaxes and its energy density decreases towards an asymptotic value. Hence, the system is not isolated, but in contact with an environment that acts as a source of dissipation. The system plus environment is “closed” while the system alone is “open”. The first question to answer is how to model the coupled classical and quantum system.

4.1 Modeling the coupled system

The nature of the environment, *e.g.* whether it can be modeled by a classical or a quantum ensemble, depends on the problem under study. The choice of the coupling between system and environment is determined by the symmetry properties of the system and by physical intuition. Weiss’ textbook [63] has a very complete description of this problem. We here explain the main ingredients of the modellization. The generic problem we want to study is

$$H_{\text{TOT}} = H_{\text{SYST}} + H_{\text{ENV}} + H_{\text{INT}} + H_{\text{COUNTER}}. \quad (4.1)$$

Until otherwise stated, we focus on a single particle coupled to an environment. H_{SYST} is the Hamiltonian of the isolated particle, $H_{\text{SYST}} = p^2/(2M) + V(q)$, with p and q its momentum and position. H_{ENV} is the Hamiltonian of a thermal bath that, again for simplicity, we take to be an ensemble of N independent harmonic oscillators

$$H_{\text{ENV}} = \sum_{a=1}^{N_b} \frac{\pi_a^2}{2m_a} + \frac{m_a \omega_a^2}{2} x_a^2. \quad (4.2)$$

This is indeed a very usual choice since, for example, it may represent phonons. H_{INT} is the coupling between system and environment. We restrict the following discussion to an interaction that is linear in the oscillator and particle coordinates, $H_{\text{INT}} = q \sum_{a=1}^{N_b} c_a x_a$, with c_a the coupling constants. The calculations can be easily generalized to an interaction with a more complicated dependence on the system’s coordinate, $F(q)$, that may be dictated by the symmetries of the system. We discuss the last term, H_{COUNTER} , below.

4.1.1 Statics

Classical problems

Let us first show how the static properties of a classical system are modified by its interaction with a classical thermal bath. If the coupled system is in equilibrium, it is described by a partition function given by a sum over

the combined phase space of the system and environment. Having chosen a bath of harmonic oscillators, the integration over the bath variables can be readily performed; this calculation yields the *reduced* partition function that is written as an integration over the phase space of the system only. One can easily prove that the mass of the system gets (negatively) renormalized due to the coupling to the environment [64]. Therefore one introduces the counter-term

$$H_{\text{COUNTER}} = \frac{1}{2} \sum_{a=1}^{N_b} \frac{c_a^2}{m_a \omega_a^2} q^2 \quad (4.3)$$

in such a way to eliminate the mass renormalization and to recover the partition function of the isolated system.

Quantum problems

If one includes quantum fluctuations to describe the system and environment, the situation is slightly more complex. The relevant quantity to study is the density matrix of the full system that, for instance, can be represented as a path integral on imaginary time [65]. The contribution of the environment to the effective action is quadratic and its variables can be integrated away to yield a reduced density matrix. As opposed to the classical case, the interaction with the reservoir not only induces a (negative) mass renormalization but it also generates a *retarded quadratic interaction*

$$\int_0^{\beta\hbar} d\tau \int_0^\tau d\tau' x(\tau) K(\tau - \tau') x(\tau') \quad (4.4)$$

controlled by the kernel

$$K(\tau) = \frac{2}{\pi\hbar\beta} \sum_{n=-\infty}^{\infty} \int_0^\infty d\omega \frac{I(\omega)}{\omega} \frac{\nu_n^2}{\nu_n^2 + \omega^2} \exp(i\nu_n\tau), \quad (4.5)$$

with ν_n the Matsubara frequencies, $\nu_n = 2\pi n/\hbar\beta$, n an integer in $(-\infty, \infty)$ and $I(\omega)$ the spectral density of the bath,

$$I(\omega) = \frac{\pi}{2} \sum_{a=1}^{N_b} \frac{c_a^2}{m_a \omega_a} \delta(\omega - \omega_a), \quad (4.6)$$

that is a smooth function of ω usually taken to be $I(\omega) = \gamma\omega (\omega/\omega_s)^{s-1} \times \exp(-\omega/\Lambda)$, with γ the “friction coefficient”, ω_s a constant, Λ a high frequency cut-off and s a parameter that characterizes different baths: $s = 1$ is Ohmic (and leads to the usual white noise when $\Lambda \rightarrow \infty$), $s > 1$ is super-Ohmic and $s < 1$ is sub-Ohmic. As in the classical case, one includes a counter-term to cancel the mass renormalization but the retarded interaction (4.4) cannot be eliminated.

4.1.2 Dynamics

The distinction between the effect of a reservoir on the statistic properties of a classical and a quantum system is absent from a full dynamic treatment where the coupling to the environment always leads to a *retarded* interaction. In classical problems one generally argues that the retarded interaction can be simply replaced by a local one, *i.e.* one uses white noises, if long enough time-scales are explored. In quantum problems the same simplification is not justified in general.

Classical problems

The dissipative dynamics of a classical system in contact with an environment is usually described by a phenomenological Langevin equation. If the system is simply given by a particle of mass M , whose position is denoted by q , this equation reads

$$M\ddot{q}(t) + \int_0^t dt' \gamma(t-t')\dot{q}(t') = -V'(q(t)) + \xi(t) \quad (4.7)$$

$$\langle \xi(t)\xi(t') \rangle = k_B T \gamma(t-t') \quad (4.8)$$

where $\gamma(t-t')$ is a retarded friction and $\xi(t)$ is a time-dependent Gaussian random force with zero mean and correlation given by equation (4.8). We adopt angular brackets to denote averages over the noise.

The Langevin equation was first introduced in the context of Brownian motion and later used in a variety of problems with dissipation. It can be derived from the coupled system defined in equation (4.1) [63, 66] (see Appendix A). Indeed, if one assumes that the initial coordinates and momenta of the oscillators have a canonical distribution at an inverse temperature β [shifted by the coupling to the particle $x_a(0) \rightarrow x_a(0) - c_a/(m_a\omega_a^2)q(0)$], Newton's equation for the evolution of the particle becomes equation (4.7). The random nature of the force ξ is due to the randomness in the initial values of the position and momenta of the oscillators. The use of an equilibrium measure for the distribution of the oscillators implies the invariance under time translations of the friction kernel, $\gamma(t-t')$, and its relation to the noise-noise correlation in equation (4.8). The latter is a fluctuation-dissipation theorem that holds for the bath variables (see Appendix A and Sect. 7). Different forms of $\gamma(t-t')$ can be generated by different choices of the ensemble of oscillators. Typically, the decay of $\gamma(t-t')$ occurs in a finite relaxation time, τ_ξ . When the minimum observation time is of the order of or shorter than τ_ξ one has a “colored noise”. Instead, when it is much longer than τ_ξ , any time difference satisfies $t-t' \gg \tau_\xi$ and the kernel can be approximated with a delta function $\gamma(t-t') \sim 2\gamma\delta(t-t')$, which

corresponds to a white noise. For the classical problems we shall deal with the white-noise approximation is adequate.

Once the Langevin equation has been established on a firmer ground, it can be used as a starting point to study the dynamics of more complicated classical systems in contact with classical environments. The description of the dynamics of a macroscopic system with dissipation is then given by N coupled Langevin equations with N the number of dynamic degrees of freedom. (In this case one usually couples an independent set of oscillators to each microscopic variable of the system, other choices lead to more complicated equations.) Time-dependent, $f_i(t)$, and constant non-potential forces, f_i^{NP} , as the ones applied to granular matter and in rheological measurements are simply included as part of the deterministic force. In the white noise limit

$$M\ddot{q}_i(t) + \gamma\dot{q}_i(t) = -\frac{\delta V(\vec{q})}{\delta q_i(t)} + f_i(t) + f_i^{\text{NP}} + \xi_i(t), \quad (4.9)$$

$$\langle \xi_i(t) \xi_j(t') \rangle = 2\gamma k_B T \delta_{ij} \delta(t - t'). \quad (4.10)$$

A continuous Langevin equation for classical spins is usually written replacing the hard Ising constraint $s_i = \pm 1$ by a soft one implemented with a potential term of the form $V(s_i) = u(s_i^2 - 1)^2$ with u a coupling strength that one eventually takes to infinity. The soft spins are continuous unbounded variables $s_i \in (-\infty, \infty)$ but the potential energy favors the configurations with s_i close to ± 1 . Even simpler models are constructed with spherical spins, that are also continuous variables globally constrained to satisfy $\sum_{i=1}^N s_i^2 = N$.

Quantum problems

Even if several attempts to write down quantum versions of the Langevin equation appeared in the literature, these methods remain very much model dependent and difficult to generalize [63]. A more convenient way to analyze the dynamics of a coupled system and environment with quantum fluctuations is the functional Schwinger-Keldysh formalism. We postpone the discussion of the effect of the quantum reservoir on the quantum system to Section 8 where we introduce this formalism. In short, the effect of the environment is to introduce retarded terms in the dynamic action that are similar to the ones in equation (4.4) but in real time. The white noise approximation is not acceptable and one is forced to keep the non-local in time kernels.

5 Observables and averages

As usual in statistical and quantum mechanics meaningful quantities are averaged observables. For an equilibrated system, due to ergodicity, one can either take an ensemble average or an average over a sufficiently long time-window. Out of equilibrium these do not coincide in general. In this section we define averaging procedures for classical and quantum problems out of equilibrium and we set the notation used in the rest of the notes.

5.1 Classical systems

The interaction with the environment induces fluctuations and the Langevin equation is solved in a probabilistic sense,

$$q_{\xi_k}^{\text{sol}}(t) = \mathcal{F}[(\xi_k), q_0, t]. \quad (5.1)$$

The index k labels different realizations of the thermal history, *i.e.* different realizations of the noise at each instant. q_0 is the initial condition $q_0 = q(0)$ and (ξ_k) encodes all noise values in the interval $[0, t]$. We discretize time, $t_a = a\delta$ with δ the time spacing and $a = 0, 1 \dots$. The total time is $t = \delta\mathcal{T}$. We shall be interested in the limit $\mathcal{T} \rightarrow \infty$ and $\delta \rightarrow 0$ with t fixed. Equation (5.1) means that there is a different solution for each noise history.

Any *one-time* functional of q , $A[q](t)$, must be averaged over all histories of the thermal noise to obtain a deterministic result

$$\langle A[q](t) \rangle = \lim_{\mathcal{N} \rightarrow \infty} \sum_{k=1}^{\mathcal{N}} A[q_{\xi_k}^{\text{sol}}](t) P(\xi_k) = \int \mathcal{D}\xi P(\xi) A[q_{\xi}^{\text{sol}}](t). \quad (5.2)$$

\mathcal{N} is the number of noise realizations. $P(\xi_k)$ is the probability distribution of the k th thermal history. For a Gaussian noise

$$P(\xi_k) \propto \exp \left[-\frac{1}{2k_{\text{B}}T} \sum_{ab} \xi_k(t_a) \gamma^{-1}(t_a - t_b) \xi_k(t_b) \right]. \quad (5.3)$$

The measure of the functional integral is just $\mathcal{D}\xi \equiv \prod_a d\xi(t_a)$.

Two-time functions characterize the out of equilibrium dynamics in a more detailed way and they are defined as

$$C_{AB}(t, t') \equiv \langle A[q](t) B[q](t') \rangle = \int \mathcal{D}\xi P(\xi) A[q_{\xi}^{\text{sol}}](t) B[q_{\xi}^{\text{sol}}](t'). \quad (5.4)$$

The observable $B[q]$ is measured at time t' , the observable $A[q]$ is measured at time t for each noise realization and the average is taken afterwards.

The instantaneous linear response is also a two-time function. Imagine that q represents the position of a Brownian particle that one *kicks* with a

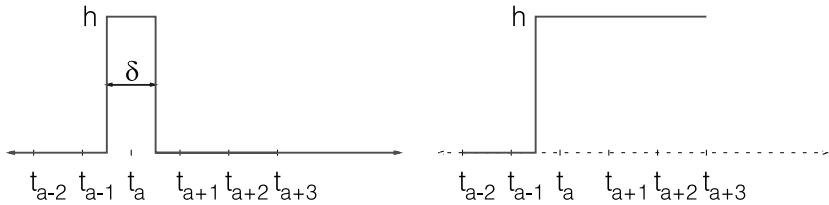


Fig. 8. Left: an instantaneous perturbation applied at t_a . Right: a step perturbation applied at t_a and held constant for all subsequent times.

weak perturbing force at time $t' = t_a$ (see Fig. 8). The subsequent position of the particle is modified by the perturbation. The linear response is given by the comparison of the perturbed dynamics with the unperturbed one, in which no force has been applied, up to linear order in the perturbation:

$$R_{AB}(t, t') \equiv \left. \frac{\delta \langle A[q] \rangle(t)}{\delta h_B(t')} \right|_{h_B=0}. \quad (5.5)$$

The subindex B indicates that the perturbation applied at t' is conjugated to the observable $B[q]$ when the Hamiltonian is modified as $H \rightarrow H - h_B B[q]$. The subindex A indicates that we examine how the observable $A[q]$ at time t reacts to the perturbation. At the end of the calculation we set $h_B = 0$ to extract the linear response. Keeping $h_B \neq 0$ yields information about the nonlinear terms in the response function. For *causal* systems the response function vanishes if $t' > t$.

In future sections we shall be interested in the integrated linear response rather than the instantaneous one. This quantity represents the linear response of the system to a *step*-like perturbation of duration $t - t'$ that starts at t' , as represented on the right panel of Figure 8:

$$\chi_{AB}(t, t') \equiv \int_{t'}^t dt'' R_{AB}(t, t''). \quad (5.6)$$

Rather often results are presented in the frequency domain. One defines the Fourier transform and its inverse

$$\tilde{A}(\omega) = \int_{-\infty}^{\infty} dt \exp(-i\omega t) A(t), \quad A(t) = \int_{-\infty}^{\infty} \frac{d\omega}{2\pi} \exp(i\omega t) \tilde{A}(\omega). \quad (5.7)$$

For a stationary process, the linear susceptibility, $\tilde{\chi}(\omega)$, is simply given by the Fourier transform of the linear response (5.5). However $R_{AB}(t, t')$ is not necessarily stationary out of equilibrium. Hence, we define two generalized

linear susceptibilities,

$$\tilde{\chi}_{AB}^{(1)}(\omega, t') \equiv \int_0^\infty d\tau \exp(-i\omega\tau) R_{AB}(t' + \tau, t'), \quad (5.8)$$

$$\tilde{\chi}_{AB}^{(2)}(\omega, t) \equiv \int_0^\infty d\tau \exp(-i\omega\tau) R_{AB}(t, t - \tau), \quad (5.9)$$

that reduce to the well-known expression for $\tilde{\chi}_{AB}(\omega)$ in a stationary system. Note that in the first line we kept the shorter time (t') fixed while in the second line we kept the longer time (t) fixed. These expressions have a real and an imaginary part that yield the in-phase ($\tilde{\chi}'$) and the out-of-phase ($\tilde{\chi}''$) susceptibilities, respectively. The integrations run over positive values of τ only due to causality.

Up to this point we have discussed the simple case in which observables only depend on time. More generally, one is interested in extending the above definitions to field theories. In the context of liquids, glasses, etc. the generic observables A and B depend on the positions and momenta of the particles. A key quantity is the density $\rho(\vec{r}, t) = \sum_{\alpha=1}^N \delta(\vec{r} - \vec{r}_\alpha)$, where \vec{r} is a d dimensional vector in real space and \vec{r}_α are the positions of the N particles in the system. From the density-density correlator $N^{-1}G(\vec{r}, t; \vec{r}', t') \equiv \langle \rho(\vec{r}' + \vec{r}, t) \rho(\vec{r}', t') \rangle$ one defines the more useful van Hove correlator $G_{\text{vh}}(\vec{r}; t, t') \equiv \int d^d r' G(\vec{r}, t; \vec{r}', t')$, that measures the probability of finding a particle i within a volume $d^d r$ around the point \vec{r} at time t given that there was a particle j at the origin at time t' . The normalization factor fixes the number of particles, $\int d^d r G_{\text{vh}}(\vec{r}, t) = N$. The density-density and van Hove correlators can be naturally separated in two contributions, a *self* and a *distinct* part. In the former, one adds over equal particles only while in the latter one adds over distinct particles. The *two-time intermediate scattering function* is constructed with the components of the real-space Fourier transform of the density at different times: $N^{-1}F(\vec{k}; t, t') \equiv \langle \rho(\vec{k}, t) \rho^*(\vec{k}, t') \rangle = \langle \rho(\vec{k}, t) \rho(-\vec{k}, t') \rangle$. When times are equal one recovers the *structure factor*, $S(\vec{k}; t) = F(\vec{k}; t, t)$ that at long times approaches a limit $S(\vec{k}; t) \rightarrow S(\vec{k})$ even for glassy systems.

The two-time intermediate scattering function is measurable via neutron scattering. Indeed, one can easily extend the proof described *e.g.* in [67] to the non-equilibrium case, to show that the cross-section per nucleus is related to the intermediate scattering function. This relation suggests to call the self and distinct correlators, *incoherent* and *coherent* ones, respectively. Many times, one defines the correlators of the local density fluctuations, $\delta\rho(\vec{r}, t) \equiv \rho(\vec{r}, t) - \langle \rho(\vec{r}, t) \rangle$. The modification of the correlations defined above follow straightforwardly. A detailed description of the properties of these correlations in an equilibrated liquid can be found in [67].

Up to now we have only discussed one-point and two-point functions. In general problems, higher order functions are not trivially related to the previous ones and bear richer information. These are *four-point functions*, $\langle A(t)B(t')C(t'')D(t'') \rangle$, or any other form of a more general type. In most of the solvable models we shall discuss below, and in most of the approximations used to analyze realistic models, higher-order functions do not appear. The reasons for their disappearance are manifold. In simplified models one can simply prove that higher order functions are exactly given in terms of one and two-point functions. In more realistic cases, higher order functions are approximated with expressions that depend on one and two-point functions only. This is done, for instance, in Gaussian approximations. However, a complete solution to a finite dimensional model should be able to predict the behavior of such higher order correlations.

5.2 Quantum problems

A quantum mechanical operator, \hat{A} , in the Heisenberg representation evolves according to

$$\hat{A}(t) = \exp\left(\frac{iHt}{\hbar}\right) \hat{A}(0) \exp\left(-\frac{iHt}{\hbar}\right). \quad (5.10)$$

Ensemble averages are defined as $\langle \hat{A}(t) \rangle \equiv \text{Tr}(\hat{A}(t)\hat{\rho}(0))/\text{Tr} \hat{\rho}(0)$, where $\hat{\rho}(0)$ is the initial density operator and the trace is defined in the usual way, $\text{Tr}[\bullet] \equiv \sum_{\alpha} \langle \psi_{\alpha} | \bullet | \psi_{\alpha} \rangle$, with $\{\psi_{\alpha}\}$ an orthonormal basis in Fock space. The normalization factor is the partition function $Z \equiv \text{Tr} \hat{\rho}(0)$. Two-time dependent correlation functions are introduced as $\langle \hat{A}(t)\hat{B}(t') \rangle \equiv Z^{-1} \text{Tr} \left(\hat{A}(t)\hat{B}(t')\hat{\rho}(0) \right)$. Clearly $\langle \hat{A}(t)\hat{B}(t') \rangle \neq \langle \hat{B}(t')\hat{A}(t) \rangle$ and one can define symmetrized and anti-symmetrized correlations:

$$C_{\{A,B\}}(t,t') = \frac{1}{2} \left\langle \hat{A}(t)\hat{B}(t') + \hat{B}(t')\hat{A}(t) \right\rangle, \quad (5.11)$$

$$C_{[A,B]}(t,t') = \frac{1}{2} \left\langle \hat{A}(t)\hat{B}(t') - \hat{B}(t')\hat{A}(t) \right\rangle, \quad (5.12)$$

respectively. The linear response and the integrated linear response are defined just as in the classical case, see equations (5.5) and (5.6). In linear response theory, in and out of equilibrium, $R_{AB}(t,t')$ and the anti-symmetrized correlation $C_{[A,B]}(t,t')$ are related by the Kubo formula [68] (see Appendix B)

$$R_{AB}(t,t') = \frac{i}{\hbar} \theta(t-t') \left\langle \left[\hat{A}(t), \hat{B}(t') \right] \right\rangle = \frac{2i}{\hbar} \theta(t-t') C_{[A,B]}(t,t'). \quad (5.13)$$

5.3 Average over disorder

Time independent *quenched* random forces and interactions exist in some of the models and systems that we study. We shall be mostly interested in quantities averaged over the distribution of disorder that we denote with square brackets $[\langle A \rangle]$.

Averaging over disorder is a delicate matter when one wishes to compute *static* properties. For instance, one has to resort to the sometimes contested replica trick [69]. We shall see in Section 8 that in a full dynamic treatment with no special initial conditions there is no need to introduce replicas and the formalism is totally free from ambiguities.

6 Time dependent probability distributions

In Section 4 we derived a Langevin equation with white noise as the microscopic dynamic equation controlling the evolution of the classical problems we shall study. In this section we prove some properties of the equilibrium dynamics of classical models with dynamics given by these equations. One can simply modify this proof for a generic Markov process, a classical problem with colored noise and a quantum model.

6.1 The Fokker–Planck and Kramers equations

The Fokker–Planck and Kramers equations are particular master equations that hold exactly for a Langevin process with white noise. The probability distribution of the thermal noise, $P(\xi)$, induces a time-dependent probability distribution of the dynamic variables q and v (or $p = v/M$):

$$P(q, v, t) = \int \mathcal{D}\xi P(\xi) \delta(q - q_{\xi}^{\text{sol}}(t)) \delta(v - v_{\xi}^{\text{sol}}(t)). \quad (6.1)$$

that satisfies the Kramers equation

$$\gamma \frac{\partial P(q, v, t)}{\partial t} = -\frac{\partial}{\partial q} (v P(q, v, t)) + \frac{\partial}{\partial v} \left[\left(v + \frac{V'(q)}{M} + \frac{\gamma k_B T}{M} \frac{\partial}{\partial v} \right) P(q, v, t) \right]. \quad (6.2)$$

For colored noises one cannot derive a simple differential equation for $P(q, v, t)$; indeed, it is clear that in these cases the stochastic process is not Markovian. The averages over thermal histories can be expressed in terms of $P(q, v, t)$, $\langle A[q, v] \rangle(t) = \int \mathcal{D}q \mathcal{D}v P(q, v, t) A[q, v]$.

When the inertial term in the Langevin equation can be dropped, $P(q, v, t)$ is replaced by an exclusive function of q , $P(q, t)$, defined as

$$P(q, t) = \int \mathcal{D}\xi P(\xi) \delta(q - q_{\xi}^{\text{sol}}(t)) \quad (6.3)$$

and determined by the Fokker-Planck equation,

$$\gamma \frac{\partial P(q, t)}{\partial t} = \frac{\partial}{\partial q} [P(q, t) V'(q)] + k_B T \frac{\partial^2}{\partial q^2} P(q, t). \quad (6.4)$$

It is very important to note that the balancing of factors on the right-hand-side (RHS) of the Fokker-Planck and the Kramers equations is a direct consequence of the equilibration of the noise (see Appendix A). This relation is known under the name of Einstein relation or fluctuation – dissipation theorem of the second kind (according to Kubo). We shall see its implications below.

6.2 Approach to equilibrium

In this section we focus, for simplicity, on the Fokker-Planck equation (6.4). In order to ensure the equilibration of the system at long times P_{GB} must be a stationary solution of the Fokker-Planck equation. Introducing $P \propto \exp(-\beta V)$ in equation (6.4) one realizes that any other ratio between the factors in front of the first and second term on the RHS of the Fokker-Planck equation would not allow for this asymptotic solution.

We still have to show that P_{GB} is the actual asymptotic solution reached by the dynamic process, $\lim_{t \rightarrow \infty} P(t) = P_{\text{GB}}$. An easy and elegant proof relies on a mapping between the Fokker-Planck and the Schrödinger equations [68]. Introducing

$$P(q, t) = \psi_0(q) p(q, t) = c e^{-\frac{\beta}{2} V(q)} p(q, t) \quad (6.5)$$

with c a positive constant, one has

$$\gamma \frac{\partial p(q, t)}{\partial t} = \left[k_B T \frac{\partial^2}{\partial q^2} - \left(-\frac{1}{2} V''(q) + \frac{\beta}{4} (V'(q))^2 \right) \right] p(q, t) = H_{\text{FP}} p(q, t). \quad (6.6)$$

This is a Schrödinger equation in imaginary time. Note however that $p(q, t)$ here is a probability density and plays the role of a wave function while in true quantum mechanics it is the modulus squared of the wave function which has a probability interpretation. If the term between square brackets grows to infinity sufficiently fast when $q \rightarrow \pm\infty$ the spectrum of the Fokker-Planck Hamiltonian H_{FP} is discrete. It is now easy to check that $\psi_0(q)$ is the ground state of H_{FP} , *i.e.* a positive definite eigenvector with eigenvalue $E_0 = 0$. We write $p(q, t) = \sum_n c_n \psi_n(q) \exp(-E_n t)$ with $\psi_n(q)$ the eigenvector associated to the eigenvalue E_n , $E_n > 0$ when $n > 0$. When $t \rightarrow \infty$ all terms vanish apart from the one with $n = 0$, $\lim_{t \rightarrow \infty} p(q, t) = c_0 \psi_0(q) = \psi_0(q)$, where we used $c_0 = \int dq \psi_0(q) p(q, 0) = \int dq P(q, 0) = 1$. This expression implies $\lim_{t \rightarrow \infty} P(q, t) = \psi_0^2(q) = c^2 \exp(-\beta V(q))$ and the

conservation of probability allows one to compute the normalization constant, $c^{-2} = \int dq \exp(-\beta V(q))$. Thus P_{GB} is indeed the asymptotic solution to the Fokker-Planck equation [68].

Note that this argument assumes that a sufficiently long t ($t > t_{\text{EQ}}$) is reached such that only the $n = 0$ term survives in the sum. This hypothesis does not hold in the asymptotic analysis for the relaxing models we analyze in the next Sections. In the low- T phase the equilibration time grows with the size of the system, $t_{\text{EQ}}(N) \rightarrow \infty$, while in the analysis we only consider times that are finite with respect to N . Moreover, when non-potential or time-dependent forces are exerted on the system, see equation (4.9), the transformation (6.5) is not sufficient to deal with their effect and equilibrium cannot be established.

Just as in usual quantum mechanics one can use an operator notation to represent the Fokker-Planck equation. Indeed, identifying $-i\partial/\partial q$ with the operator \hat{p} the usual commutation relations between momentum and coordinate are recovered. The probability distribution $P(q, t)$ is then identified with a quantum time-dependent “state” $|P(t)\rangle$. With these new names, the Fokker-Planck equation reads

$$\gamma \frac{\partial |P(t)\rangle}{\partial t} = \hat{H}_{\text{FP}} |P(t)\rangle \quad \text{with} \quad \hat{H}_{\text{FP}} = \hat{p} \left(i\hat{V}'(q) - k_{\text{B}} T \hat{p} \right). \quad (6.7)$$

$|P(t)\rangle$ is obtained from the evolution of an initial state $|P(0)\rangle$ with the operator $\exp(-\hat{H}_{\text{FP}} t)$.

6.3 Equilibrium dynamics

All average values (5.2) can be computed using $P(q, t)$ as $\langle A[q](t) \rangle = \int dq A[q] P(q, t)$. If we pursue the identification with the quantum mechanics formulation and we associate the bra $\langle -|$ to the “wave function” identical to 1 we write the average as $\langle A[q](t) \rangle = \langle -| \hat{A}[q] |P(t)\rangle$. The normalization of the probability distribution reads $\langle -|P(t)\rangle = 1$. Clearly, if the system reached equilibrium at a time t' , all averages of one-time quantities are time-independent henceforth.

Any correlation $C_{AB}(t, t')$ for two “local” functions of the variable q can be expressed as

$$\begin{aligned} C_{AB}(t, t') &= \int dq \int dq' \int dq'' A[q] T(q', t' \rightarrow q, t) B[q'] T(q'', 0 \rightarrow q', t') P(q'', 0) \\ &= \left\langle - \left| \hat{A}[q] \exp \left(-\hat{H}_{\text{FP}} (t - t') \right) \hat{B}[q] \exp \left(-\hat{H}_{\text{FP}} t' \right) \right| P(0) \right\rangle. \end{aligned} \quad (6.8)$$

In the transition probabilities, T , we included the time-dependence to clarify their meaning. In the second line we used the quantum mechanical notation.

If the time t' is longer than the equilibration time, the probability density at t' reached the equilibrium one, $\int dq'' T(q'', 0 \rightarrow q', t') P(q'', 0) = P_{\text{GB}}(q')$. Equivalently, $|P(t')\rangle = |P_{\text{GB}}\rangle$. Two properties follow immediately:

Stationarity: since the transition probability is a function of the time-difference only, $T(q, t; q', t') = T(q, q'; t - t') = \langle q | \exp(-\hat{H}_{\text{FP}}(t - t')) | q' \rangle$ the correlation is invariant under translations of time for $t' > t_{\text{EQ}}$.

Onsager relations: $\langle A[q](t) B[q](t') \rangle = \langle A[q](t') B[q](t) \rangle$ for any two observables A and B that depend only on the coordinates. Indeed,

$$\begin{aligned} \langle A(t') B(t) \rangle &= \left\langle - \left| \hat{B} e^{-\hat{H}_{\text{FP}}(t-t')} \hat{A} \right| P_{\text{GB}} \right\rangle = \left\langle P_{\text{GB}} \left| \hat{A}^\dagger \left(e^{-\hat{H}_{\text{FP}}(t-t')} \right)^\dagger \hat{B}^\dagger \right| - \right\rangle \\ &= \left\langle P_{\text{GB}} \left| \hat{A} e^{-\hat{H}_{\text{FP}}^\dagger(t-t')} \hat{B} \right| - \right\rangle \\ &= \left\langle - \left| e^{-\beta \hat{V}} \hat{A} e^{-\hat{H}_{\text{FP}}^\dagger(t-t')} \hat{B} e^{\beta \hat{V}} e^{-\beta \hat{V}} \right| - \right\rangle \\ &= \left\langle - \left| \hat{A} e^{-\beta \hat{V}} e^{-\hat{H}_{\text{FP}}^\dagger(t-t')} e^{\beta \hat{V}} \hat{B} \right| P_{\text{GB}} \right\rangle. \end{aligned} \quad (6.9)$$

The proof is completed by showing that $e^{-\beta \hat{V}} e^{-\hat{H}_{\text{FP}}^\dagger(t-t')} e^{\beta \hat{V}} = e^{-\hat{H}_{\text{FP}}(t-t')}$ for all $t - t'$ which is equivalent to $\hat{H}_{\text{FP}}^\dagger = e^{\beta \hat{V}} \hat{H}_{\text{FP}} e^{-\beta \hat{V}}$. The latter can be checked directly using the Fokker-Planck Hamiltonian. The matrix elements $\langle q | e^{-\hat{H}_{\text{FP}} \tau} | q' \rangle = T(q', t \rightarrow q, t + \tau)$ and $\langle q | e^{-\hat{H}_{\text{FP}}^\dagger \tau} | q' \rangle = T(q, t \rightarrow q', t + \tau)$ yield the transition probabilities and the first equation in this paragraph can be recast as $T(q', t \rightarrow q, t + \tau) e^{-\beta V(q')} = T(q, t \rightarrow q', t + \tau) e^{-\beta V(q)}$ which is *detailed balance*.

Similarly, one proves that the linear response $R_{AB}(t, t')$ is also stationary when $P(q', t') = P_{\text{GB}}(q')$. We represent the instantaneous infinitesimal perturbation $h(t')$ as the kick between $t_a - \delta/2$ and $t_a + \delta/2$ in Figure 8-left. The Fokker-Planck Hamiltonian in the presence of the field is $\hat{H}_{\text{FP}}^h = i\hat{p}[\hat{V}'(q) + h\hat{B}'[q] + k_B T i\hat{p}]$ while \hat{H}_{FP} is the Fokker-Planck operator in no field. The average in a field reads

$$\begin{aligned} \langle A[q] \rangle_h(t) &= \left\langle - \left| \hat{A}[q] e^{-\hat{H}_{\text{FP}}(t-t'-\frac{\delta}{2})} e^{-\hat{H}_{\text{FP}}^h[(t'+\frac{\delta}{2})-(t'-\frac{\delta}{2})]} \right. \right. \\ &\quad \left. \left. \times e^{-\hat{H}_{\text{FP}}(t'-\frac{\delta}{2})} \right| P(0) \right\rangle \end{aligned} \quad (6.10)$$

and the variation with respect to h yields

$$\begin{aligned} \frac{\Delta \langle A[q] \rangle(t)}{\Delta h_B(t')} &= \left\langle - \left| \hat{A}[q] e^{-\hat{H}_{\text{FP}}(t-t'-\frac{\delta}{2})} \left(-\delta \frac{\hat{H}_{\text{FP}}^h - \hat{H}_{\text{FP}}}{\Delta h} \right) \right. \right. \\ &\quad \left. \left. \times e^{-\hat{H}_{\text{FP}}(t'-\frac{\delta}{2})} \right| P(0) \right\rangle, \end{aligned} \quad (6.11)$$

with $\Delta h = h\delta$. The factor between parenthesis equals $(-i\hat{p}\hat{B}'[q]h\delta)/(h\delta) = -i\hat{p}\hat{B}'[q]$. Taking the limit $\delta \rightarrow 0$ and evaluating at $h = 0$ one has

$$R_{AB}(t, t') = \left\langle - \left| \hat{A}[q] \exp \left[-\hat{H}_{\text{FP}}(t - t') \right] \times \left(-i\hat{p}\hat{B}'[q] \right) \exp \left(-\hat{H}_{\text{FP}}t' \right) \right| P(0) \right\rangle. \quad (6.12)$$

From this expression one recovers several properties of the response:

Causality: The same derivation for $t' > t$ yields

$$R_{AB}(t, t') = \left\langle - \left| \left(-i\hat{p}\hat{B}'[q] \right) \exp \left[-\hat{H}_{\text{FP}}(t - t') \right] \hat{A}[q] \exp \left[-\hat{H}_{\text{FP}}t' \right] \right| P(0) \right\rangle. \quad (6.13)$$

Since $\langle -|\hat{p} = 0$, $R(t, t') = 0$ for all $t < t'$.

Stationarity: when $\exp(-\hat{H}_{\text{FP}}t') |P(0)\rangle = |P_{\text{GB}}\rangle$ one has

$$R_{AB}(t, t') = \left\langle - \left| \hat{A}[q] \exp \left[-\hat{H}_{\text{FP}}(t - t') \right] \left(-i\hat{p}\hat{B}'[q] \right) \right| P_{\text{GB}} \right\rangle = R_{AB}^{\text{ST}}(t - t'). \quad (6.14)$$

Response at equal times: $\lim_{t' \rightarrow t^-} R_{AB}(t, t') = \langle -| \hat{A}'[q] \hat{B}'[q] \times \exp[-\hat{H}_{\text{FP}}t'] |P(0)\rangle$. If $\hat{A}[q] = \hat{B}[q] = \hat{q}$ then $\hat{A}'[q] = \hat{B}'[q] = 1$ and $\lim_{t' \rightarrow t^-} R_{AB}(t, t') = \langle -|P(t')\rangle = 1$ from conservation of probability.

Fluctuation-dissipation theorem: we postpone its discussion to Section 7.2.

Onsager relations: using the relation between correlation and responses dictated by the FDT one finds that the Onsager relations must also hold between responses.

7 The fluctuation – dissipation theorem (FDT)

The fluctuation-dissipation theorem (FDT) relates the correlations of spontaneous fluctuations to the induced fluctuations in equilibrium. It is a model independent relation between the linear response and its associated correlation function that takes different forms for classical and quantum systems. The latter reduces to the former when quantum fluctuations become irrelevant. In this section we present several proofs of the FDT. When the equilibration hypothesis is not justified, this relation does not necessarily hold.

7.1 Static FDT

Many relations between correlations of fluctuations and susceptibilities are known in statistical mechanics. All these are different statements of the *static* FDT.

Take for instance a perfect gas. The fluctuations in the density $\rho = n/\tilde{V}$ where n is the number of particles within a sub volume \tilde{V} of a system with N particles and volume V , are defined as: $\sigma_\rho^2 \equiv \langle (\rho - \langle \rho \rangle)^2 \rangle$. In the thermodynamic limit $N \rightarrow \infty, V \rightarrow \infty$ with $N/V = \bar{\rho}$ fixed, these are related to the isothermal compressibility $\chi_T = -1/V \partial V / \partial P|_T$ via $\sigma_\rho^2 = (k_B T) \bar{\rho}^2 \chi_T / \tilde{V}$. This relation is a form of FDT.

For a system in equilibrium with a thermal reservoir at temperature T one has

$$\chi \equiv \left. \frac{\delta \langle A \rangle_h}{\delta h} \right|_{h=0} = \beta \langle (A - \langle A \rangle)^2 \rangle \quad (7.1)$$

for any observable A . The average $\langle \cdot \rangle_h$ is calculated with the partition function of the system in the presence of a small field coupled to A in such a way that the Hamiltonian reads $H = H_0 - hA$. For a magnetic system this equation relates the magnetic susceptibility to the magnetization fluctuations.

7.2 Dynamic FDT

There are several proofs of this theorem. Here we focus on a Fokker-Planck process. In Section 6.3 we computed R_{AB} and C_{AB} in equilibrium. Taking the derivative of equation (6.8) with respect to t' one finds

$$\begin{aligned} \frac{\partial C_{AB}(t-t')}{\partial t'} &= \left\langle - \left| \hat{A}[q] \exp \left[-\hat{H}_{\text{FP}}(t-t') \right] \left(-i\hat{p}k_B T \hat{B}'[q] \right) \right| P_{\text{GB}} \right\rangle \\ &= k_B T R_{AB}(t-t') \end{aligned} \quad (7.2)$$

for $t-t' > 0$. Note that since in equilibrium the averages of one-time quantities are constant one can replace $C_{AB}(t-t')$ by the connected correlation $C_{AB}^C(t-t') \equiv C_{AB}(t-t') - \langle A \rangle \langle B \rangle$ in the left-hand-side (LHS) and the FDT also reads $\partial_{t'} C_{AB}^C(t-t') = k_B T R_{AB}(t-t')$. In integrated form

$$\begin{aligned} k_B T \chi_{AB}(t-t_w) &= C_{AB}(t-t) - C_{AB}(t-t_w) \\ &= C_{AB}^C(t-t) - C_{AB}^C(t-t_w). \end{aligned} \quad (7.3)$$

7.3 Quantum FDT

Proofs and descriptions of the quantum FDT can be found in several textbooks [68, 70]. Here, we express it in the time-domain and in a mixed time-Fourier notation that gives us insight as to how to extend it to the case of glassy non-equilibrium dynamics.

If at time t' a quantum system has reached equilibrium the density operator $\hat{\rho}(t')$ is just the Boltzmann factor $\exp(-\beta \hat{H})/Z$. As in Section 6.3

it is then immediate to show that time-translation invariance (TTI) holds $C_{AB}(t, t') = C_{AB}(t - t')$. In addition, from the definition of $C_{AB}(t, t')$ in equation (5.11) one proves the KMS properties $C_{AB}(t, t') = C_{BA}(t', t + i\beta\hbar) = C_{BA}(-t - i\beta\hbar, -t')$. Assuming, for definiteness, that $t > 0$ it is easy to verify the following equation

$$C_{\{A,B\}}(\tau) + \frac{i\hbar}{2} R_{AB}(\tau) = C_{\{A,B\}}(\tau^*) - \frac{i\hbar}{2} R_{AB}(\tau^*), \quad (7.4)$$

where $\tau = t + i\beta\hbar/2$. This is a way to express FDT through an analytic continuation to complex times. In terms of the Fourier transformed $\tilde{C}_{AB}(\omega)$ defined in equation (5.7) the KMS properties read $\tilde{C}_{AB}(\omega) = \exp(\beta\hbar\omega) \times \tilde{C}_{BA}(-\omega)$ and lead to the following relation between Fourier transforms of symmetrized and anti-symmetrized correlations: $\tilde{C}_{[A,B]}(\omega) = \tanh(\frac{\beta\hbar\omega}{2}) \times \tilde{C}_{\{A,B\}}(\omega)$. Using now the Kubo relation (5.13) one obtains the quantum FDT

$$R_{AB}(t - t') = \frac{i}{\hbar} \int_{-\infty}^{\infty} \frac{d\omega}{\pi} \exp(-i\omega(t - t')) \tanh\left(\frac{\beta\hbar\omega}{2}\right) \tilde{C}_{\{A,B\}}(\omega), \quad (7.5)$$

$t \geq t'$. With the representation $\int_0^{\infty} dt \exp(i\omega t) = \lim_{\delta \rightarrow 0^+} i/(\omega + i\delta) = \pi\delta(\omega) + iP/\omega$,

$$\tilde{R}_{AB}(\omega) = -\frac{1}{\hbar} \lim_{\delta \rightarrow 0^+} \int_{-\infty}^{\infty} \frac{d\omega'}{\pi} \frac{1}{\omega - \omega' + i\delta} \tanh\left(\frac{\beta\hbar\omega'}{2}\right) \tilde{C}_{\{A,B\}}(\omega') \quad (7.6)$$

from which we obtain the real and imaginary relations between $\text{Im}\tilde{R}_{AB}(\omega)$, $\text{Re}\tilde{R}_{AB}(\omega)$ and $\tilde{C}_{\{A,B\}}(\omega)$. If $\beta\hbar\omega/2 \ll 1$, $\tanh(\beta\hbar\omega/2) \sim \beta\hbar\omega/2$ and equation (7.5) becomes the classical FDT, equation (7.2).

7.4 Examples

7.4.1 Harmonic oscillator and diffusion

The simplest example in which one sees the modifications of the FDT at work is a one-dimensional harmonic oscillator with no inertia coupled to a white bath. One finds

$$k_B T \frac{R(t, t')}{\partial_{t'} C(t, t')} = \left[1 + \exp\left(-\frac{2kt'}{\gamma}\right) \right]^{-1} \rightarrow \begin{cases} 1 & \text{if } k > 0 \\ \frac{1}{2} & \text{if } k = 0 \\ 0 & \text{if } k < 0 \end{cases} \quad (7.7)$$

for times $t \geq t'$ and $t' \gg \gamma/k$ with k the harmonic constant of the oscillator. Thus, when there is a confining potential and P_{GB} can be defined the FDT holds. Instead, when the potential is flat ($k = 0$) or unbounded from below ($k < 0$) no normalizable P_{GB} can be defined and the FDT is modified.

If one keeps inertia, the calculations are slightly more involved but one can carry them through to show that momenta and coordinates behave very differently [71]. Since the probability distribution of the momenta very rapidly reaches a Maxwellian for all values of k these variables equilibrate and FDT holds for them. This is the reason why the kinetic energy of a particle system serves to calibrate the external temperature. The coordinates, instead, behave as in (7.7) depending on the value of k .

7.4.2 A driven system

Take now a symmetric two-dimensional harmonic oscillator $V(x, y) = k/2(x^2 + y^2)$ and apply the non-potential force $\vec{f}(x, y) = \alpha(y, -x)$ on it. This force makes a particle turn within the potential well and one can check, by direct calculation, that the FDT does not hold.

7.4.3 No Einstein relation

If the bath is such that the Einstein relation between friction and noise correlation does not hold, the FDT for the system variables does not hold either. Again, this can be easily checked using a harmonic oscillator.

7.4.4 A complex bath

Let us couple a harmonic oscillator to a complex bath made of two parts: a white bath ($\tau_{\xi(1)} \rightarrow 0$) with friction coefficient γ_1 at temperature T_1 and a coloured bath with friction kernel $\gamma(t - t') = \gamma_2 \exp[-(t - t')/\tau_{\xi(2)}]$ kept at temperature T_2 [72]. The complex bath induces two time-scales (see Sect. 11.4 for its precise definition) in the dynamics of the oscillator: the correlation is stationary but it decays in two steps, from q_d at equal times to an “Edwards-Anderson parameter” q_{EA} for time-differences, τ , that are shorter than a characteristic time τ_0 and from q_{EA} to zero for longer τ ’s. The parameters q_d , q_{EA} and τ_0 are functions of k , the friction coefficients γ_1 and γ_2 and the two temperatures T_1 and T_2 . In Figure 9 we display the correlation decay and the parametric plot of the integrated linear response, χ , against the correlation, C , constructed using $t - t'$ as a parameter that runs from $t - t' = 0$ ($C = q_d, \chi = 0$) to $t - t' \rightarrow \infty$ ($C \rightarrow 0, \chi = \chi_{tot}$). (See Sect. 11.5.3.) The FDT predicts a linear relation between χ and C with a slope $-1/(k_B T)$ for systems equilibrated with a reservoir at temperature T . In this problem though “there is no T ” since the system is coupled to a bath with two temperatures and two time-scales. Surprisingly, one finds that the rapid decay is controlled by the temperature of the fast bath, T_1 , while the subsequent, slower, decay is controlled by the temperature of the slow bath, T_2 .

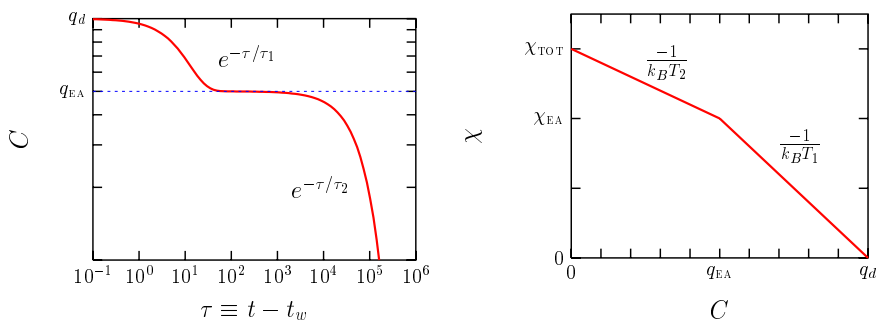


Fig. 9. Left: decay of the correlation for a harmonic oscillator coupled to a mixed bath. Right: parametric plot of the integrated linear response against the correlation.

A similar phenomenon, now self-induced, appears in glassy models. These interacting systems are coupled to an external white bath at temperature T_1 . Their dynamics is such that several time-scales, each with its own “temperature” is generated. We shall show how this arises in solvable models in Section 12 and we shall prove that the FD relation can indeed be used to define an “effective temperature” in Section 14.

8 Dynamic generating functionals

In this section we present the functional methods used to analyze the dynamics of classical [73] and quantum [74] models coupled to environments. We discuss the relation between the two approaches. The generating functionals, with their effective actions, are the adequate starting point to apply perturbation theory (when it is accepted), self-consistent approximations such as the mode-coupling approach, or even more sophisticated techniques as the functional renormalization group.

8.1 Classical models

For a classical system coupled to a classical environment, we use as a starting point a stochastic equation with an additive noise $\xi(t) = \text{EQ}(q)$. For instance, if we deal with a massive particle governed by the Langevin equation, equation (4.7), $\text{EQ}(q) = M\ddot{q} + \int_0^t dt' \gamma(t-t') \dot{q}(t') + V'(q)$.

Any averaged observable, *e.g.* $\langle A[q] \rangle(t)$ in equation (5.2), can be computed from the variation of a dynamic generating functional \mathcal{Z} with respect

to a time-dependent source η :

$$\langle A[q] \rangle(t) = \left. \frac{\delta \mathcal{Z}[\eta]}{\delta \eta(t)} \right|_{\eta(t)=0} = \frac{\delta}{\delta \eta(t)} \int \mathcal{D}\xi P[\xi] e^{\int dt' \eta(t') A[q_{\xi}^{\text{sol}}](t')} \Big|_{\eta(t)=0}. \quad (8.1)$$

Since the probability distribution $P[\xi]$ is normalized to one, $\mathcal{Z}[\eta = 0] = 1$, and the average is automatically normalized. The idea is to derive a useful expression for the generating functional \mathcal{Z} by introducing the functional identity

$$1 = \int \mathcal{D}q \, \delta(q - q_{\xi}^{\text{sol}}) = \int \mathcal{D}q \, \delta(\xi - \text{EQ}[q]) \left| \det \left(\frac{\delta \text{EQ}[q](t)}{\delta q(t')} \right) \right|. \quad (8.2)$$

In the first integral an integration and delta function is applied on each time slice and the compact notation actually represents $\int \prod_a [dq(a) \delta(q(a) - q_{\xi}^{\text{sol}}(a))]$. The second identity follows from a change of variables in the functional integral. If we focus on a time-regime with only one saddle-point solution, one can eliminate the absolute value in the determinant, and

$$\mathcal{Z}[\eta] = \int \mathcal{D}\xi \mathcal{D}q P[\xi] \delta(\xi - \text{EQ}[q]) \det \left(\frac{\delta \text{EQ}[q](t)}{\delta q(t')} \right) \exp \left(\int dt' \eta(t') A[q](t') \right). \quad (8.3)$$

This expression can be recast in a more convenient form by using the exponential representation of the delta function

$$\delta(\xi - \text{EQ}[q]) \propto \int \mathcal{D}i\hat{q} \exp \left[- \int_0^t dt' i\hat{q}(t') (\xi(t') - \text{EQ}[q](t')) \right] \quad (8.4)$$

(the constant of proportionality is numeric, a power of 2π , and irrelevant for the calculation of averages, thus we omit it), and the determinant through the introduction of a pair of fermionic variables [65]

$$\det \left(\frac{\delta \text{EQ}[q](t)}{\delta q(t')} \right) = \int \mathcal{D}\bar{\psi} \mathcal{D}\psi \exp \left[- \int_0^t dt' \int_0^t dt'' \bar{\psi}(t') \frac{\delta \text{EQ}[q](t')}{\delta q(t'')} \psi(t'') \right]. \quad (8.5)$$

Having used these identities, the generating functional becomes a functional integral over ξ , q , $i\hat{q}$, $\bar{\psi}$ and ψ . Since ξ appears in quadratic terms of the effective action only, the functional integral over ξ can be simply calculated.

We obtain

$$\begin{aligned} \mathcal{Z}[\eta, \hat{\eta}] &= \int \mathcal{D}q \mathcal{D}i\hat{q} \mathcal{D}\bar{\psi} \mathcal{D}\psi \exp(-S_{\text{EFF}}) \\ S_{\text{EFF}} &= \int_0^t dt' \int_0^t dt'' \left(-i\hat{q}(t') k_B T \theta(t' - t'') \gamma(t' - t'') i\hat{q}(t'') \right. \\ &\quad \left. + \bar{\psi}(t') \frac{\delta \text{EQ}[q](t')}{\delta q(t'')} \psi(t'') \right) \\ &\quad - \int_0^t dt' (i\hat{q}(t') \text{EQ}[q](t') - \eta(t') q(t') - \hat{\eta}(t') i\hat{q}(t')) \end{aligned} \quad (8.6)$$

where we have introduced a new source $\hat{\eta}(t)$ coupled to the auxiliary variable $i\hat{q}(t)$.

In Appendix C we prove the following very useful relations

$$R(t, t') = \langle q(t) i\hat{q}(t') \rangle \quad (8.7)$$

$$\frac{1}{2} k_B T \int_0^t dt'' (\gamma(t', t'') + \gamma(t'', t')) R(t, t'') = \langle q(t) \xi(t') \rangle. \quad (8.8)$$

Usually, the kernel $\gamma(t', t'')$ is symmetric $\gamma(t', t'') = \gamma(t'', t')$ and the latter relation simplifies. For a white noise $\gamma(t', t'') = 2\gamma\delta(t' - t'')$ and $2\gamma k_B T R(t, t') = \langle q(t) \xi(t') \rangle$.

8.2 Supersymmetry (SUSY)

In the white noise limit \mathcal{Z} in equation (8.6) can be written in a much more compact form if one introduces the super-field formulation of stochastic processes explained in [65, 76, 77], see Appendix D. One first enlarges (space)-time to include two Grassmann coordinates θ and $\bar{\theta}$, *i.e.* $t \rightarrow a = (t, \theta, \bar{\theta})$. The dynamic variable $q(t)$ and the auxiliary variable $i\hat{q}(t)$ together with the fermionic ones $\psi(t)$ and $\bar{\psi}(t)$ are encoded in a super-field,

$$\Phi(a) = q(t) + \bar{\theta}\psi(t) + \bar{\psi}(t)\theta + i\hat{q}(t)\bar{\theta}\bar{\theta}. \quad (8.9)$$

With these definitions,

$$\begin{aligned} \mathcal{Z}[\eta] &= \int d\Phi \exp \left(-\frac{1}{2} \int da \Phi(a) \left(-D_a^{(2)} \right) \Phi(a) \right. \\ &\quad \left. - \int da V[\Phi(a)] + \int da \Phi(a) \eta(a) \right) \end{aligned} \quad (8.10)$$

with $a = (t, \theta, \bar{\theta})$, $da = dt d\theta d\bar{\theta}$, and the dynamic operator $D_a^{(2)}$ defined as

$$-D_a^{(2)} = 2\gamma k_B T \frac{\partial^2}{\partial \theta \partial \bar{\theta}} + 2\gamma \theta \frac{\partial^2}{\partial \theta \partial t} - \gamma \frac{\partial}{\partial t} - M\theta \frac{\partial^3}{\partial \theta \partial t^2}. \quad (8.11)$$

If the model is spherically constrained, $-D_a^{(2)} \rightarrow -D_a^{(2)} - \mu(a)$ with $\mu(a)$ a super Lagrange multiplier introduced to enforce the constraint. The delta function $\delta(a-b)$ is defined in Appendix D and it satisfies $\int db \delta(a-b) f(b) = f(a)$. The super-symmetric notation allows one to encode in the single super correlator $Q(a, b) \equiv \langle \Phi(a) \Phi(b) \rangle$ all correlators and responses. The generalization to a system with N degrees of freedom is immediate.

Symmetries

The properties of the equilibrium dynamics, *i.e.* the invariance under time-translations, the fluctuation-dissipation theorem, etc., are consequences of the symmetries of the super-symmetric action. The non-equilibrium dynamic solution spontaneously breaks these symmetries.

For a stochastic process with a white noise the SUSY group is generated by three operators [65, 76, 77]:

$$\bar{D}' = \gamma k_B T \partial_\theta + \bar{\theta} \gamma \partial_t \quad D' = \partial_{\bar{\theta}} \quad D' \bar{D}' + \bar{D}' D = \gamma \partial_t \quad (8.12)$$

with $D'^2 = \bar{D}'^2 = 0$. We can construct an extension of this group that acts on two-point (in general n -point) functions, as

$$\begin{aligned} D'(a, b) &\equiv D'(a) + D'(b) & \bar{D}'(a, b) &\equiv \bar{D}'(a) + \bar{D}'(b) \\ [D'(a, b), \bar{D}'(a, b)]_+ &= \partial_t + \partial_{t'}. \end{aligned} \quad (8.13)$$

The meaning of the three generators can be understood when they are made to act on $Q(a, b)$. Firstly, causality plus probability conservation imply (irrespective of equilibration): $D'(a, b)Q(a, b) = 0$. This equation serves to select the non-vanishing terms in the super correlator. It imposes $\langle i\hat{q}(t)i\hat{q}(t') \rangle = 0$ and the fact that all components involving only one ψ and $\bar{\psi}$ vanish. Then

$$Q(a, b) = C(t, t') - (\bar{\theta}' - \bar{\theta}) (\theta' R(t, t') - \theta R(t', t)) \quad (8.14)$$

(the bifermionic correlator $\langle \psi(t) \bar{\psi}(t') \rangle$ equals the response $R(t, t')$). The SUSY action [the exponent in Eq. (8.10)] vanishes if evaluated on such correlators (when $\eta = \hat{\eta} = 0$). The other two generators imply

$$(\partial_t + \partial_{t'}) Q(a, b) = 0 \rightarrow \text{T TI}, \quad \bar{D}'(a, b) Q(a, b) = 0 \rightarrow \text{F DT}. \quad (8.15)$$

When is a system unable to reach equilibrium? In terms of symmetries this question can be addressed as follows. In driven system the dynamical actions break SUSY explicitly. They are externally kept far from equilibrium by the forcing. If SUSY is not explicitly broken two possibilities arise. Either the system evolves from its initial condition during an out of equilibrium transient in which neither stationarity nor FDT hold until the equilibration time t_{EQ} is reached and equilibrium establishes. In this language, SUSY is unbroken by the boundary conditions. On the contrary, if the system never achieves equilibrium the equilibration time diverges and cannot be reached in the calculation. The effect of the initial conditions is then to break SUSY [77,78] and consequently violate the equilibrium properties even for long times. SUSY is then *spontaneously broken*. The initial conditions play for SUSY the same role played in ordinary symmetry-breaking by space boundary conditions: if the symmetry is spontaneously broken their effect extends away from them, in this case for all times.

8.3 Connection with the replica formalism

The effective action in equation (8.10) is a kinetic minus a potential term $V[\Phi]$. When applying the replica trick to compute the free-energy a replicated effective potential $V[\phi^a]$ appears. A connection between the two formalisms, that is based on the similarity between the zero-dimensional replica space and the SUSY one, has been exploited. Roughly speaking, many properties of the replica overlap $Q^{ab} \equiv N^{-1} \sum_{i=1}^N \langle s_i^a s_i^b \rangle$ find a counterpart in the dynamic SUSY correlator $Q(a, b)$. For instance, a summation over a replica index, $\sum_{a=1}^n$ when $n \rightarrow 0$, translates into an integration over the supercoordinate $\int da$. For the moment, though, the connection is empirical and a formalization of the relation between the two approaches would be welcome.

8.4 Quantum models

The Schwinger-Keldysh formalism [74] allows one to analyze the real-time dynamics of a quantum system. The starting point is the time dependent density operator

$$\hat{\rho}_{\text{TOT}}(t) = e^{-\frac{i}{\hbar} \hat{H}_{\text{TOT}} t} \hat{\rho}_{\text{TOT}}(0) e^{\frac{i}{\hbar} \hat{H}_{\text{TOT}} t}. \quad (8.16)$$

Introducing identities, an element of the time-dependent density matrix reads

$$\begin{aligned} \rho(q'', x''_a; q', x'_a; t) &= \int_{-\infty}^{\infty} dQ dQ' dX_a dX'_a \left\langle q'', x''_a \left| e^{-\frac{i}{\hbar} \hat{H}_{\text{TOT}} t} \right| Q, X_a \right\rangle \\ &\times \langle Q, X_a | \hat{\rho}_{\text{TOT}}(0) | Q', X'_a \rangle \left\langle Q', X'_a \left| e^{\frac{i}{\hbar} \hat{H}_{\text{TOT}} t} \right| q', x'_a \right\rangle, \quad (8.17) \end{aligned}$$

where q is the coordinate of the particle and x_a are the coordinates of the oscillators. The first factor is the coordinate representation of the evolution operator and it can be represented as a functional integral. The third factor can also be represented in functional form. They read

$$\left\langle q'', x''_a \left| e^{-\frac{i}{\hbar} \hat{H}_{\text{TOT}} t} \right| Q, X_a \right\rangle = \int_{q^+(0)=Q}^{q^+(t)=q''} \mathcal{D}q^+(t) \int_{x_a^+(0)=X_a}^{x_a^+(t)=x''_a} \mathcal{D}x_a^+(t) e^{\frac{i}{\hbar} S_{\text{TOT}}^+} \quad (8.18)$$

$$\left\langle Q', X'_a \left| e^{\frac{i}{\hbar} \hat{H}_{\text{TOT}} t} \right| q', x'_a \right\rangle = \int_{q^-(0)=Q'}^{q^-(t)=q'} \mathcal{D}q^-(t) \int_{x_a^-(0)=X'_a}^{x_a^-(t)=x'_a} \mathcal{D}x_a^-(t) e^{-\frac{i}{\hbar} S_{\text{TOT}}^-}. \quad (8.19)$$

Interestingly enough, the evolution operator in equation (8.19) gives rise to a path integral going backwards in time, from $q^-(t) = q', x_a^-(t) = x'_a$ to $q^-(0) = Q', x_a^-(0) = X'_a$. The full time-integration can then be interpreted as being closed, going forwards from $t_0 = 0$ to t and then backwards from t to $t_0 = 0$. This motivates the name “closed time path formalism”. A doubling of degrees of freedom (q^+, q^-) appeared and it is intimately linked to the introduction of Lagrange multipliers in the functional representation of the stochastic dynamics in the classical limit.

The action S_{TOT} has the usual four contributions, from the system, the reservoir, the interaction and the counter-term. The action of the system reads

$$S_{\text{SYST}}^+[q^+(t), \eta^+(t)] = \int_0^t dt' \left[\frac{M}{2} \left(\frac{q^+(t')}{dt'} \right)^2 - V(q^+(t')) + \eta^+(t') q^+(t') \right] \quad (8.20)$$

where we have introduced a time-dependent source $\eta^+(t)$. Similarly, we introduce a source $\eta^-(t)$ in the path integral going backwards in time.

Since we are interested in the dynamics of the system under the effect of the reservoir we compute the reduced density matrix

$$\rho_{\text{RED}}(q'', q'; t) = \int_{-\infty}^{\infty} dx_a \langle q'', x_a | \hat{\rho}_{\text{TOT}}(t) | q', x_a \rangle. \quad (8.21)$$

The initial density operator $\hat{\rho}_{\text{TOT}}(0)$ has the information about the initial state of the whole system. If one assumes that the system and the bath are set in contact at $t = 0$, $\hat{\rho}_{\text{TOT}}(0)$ factorizes $\hat{\rho}_{\text{TOT}}(0) = \hat{\rho}_{\text{SYST}}(0)\hat{\rho}_{\text{ENV}}(0)$. (Other initial preparations, where the factorization does not hold, can also be considered and may be more realistic in certain cases.) If the environment is initially in equilibrium at an inverse temperature β , $\hat{\rho}_{\text{ENV}}(0) = Z_{\text{ENV}}^{-1} \exp(-\beta \hat{H}_{\text{ENV}})$. For a bath made of harmonic oscillators the dependence on the bath variables is quadratic and they can be traced away to yield:

$$\rho_{\text{RED}}(q''; q'; t) = \int_{-\infty}^{\infty} dQ \int_{-\infty}^{\infty} dQ' \int_{q^+(0)=Q}^{q^+(t)=q''} \mathcal{D}q^+ \int_{q^-(0)=Q'}^{q^-(t)=q'} \mathcal{D}q^- \\ \times e^{\frac{i}{\hbar} S_{\text{EFF}}} \langle Q | \hat{\rho}_{\text{SYST}}(0) | Q' \rangle$$

with $S_{\text{EFF}} = S_{\text{SYST}}^+ - S_{\text{SYST}}^- + S_{\text{TH}}$. The last term has been generated by the interaction with the environment and it reads

$$S_{\text{TH}} = - \int_0^t dt' \int_0^t dt'' (q^+(t') - q^-(t')) \eta(t' - t'') (q^+(t'') + q^-(t'')) \\ + i \int_0^t dt' \int_0^{t'} dt'' (q^+(t') - q^-(t')) \nu(t' - t'') (q^+(t'') - q^-(t'')). \quad (8.22)$$

The noise and dissipative kernels ν and η are given by

$$\nu(t) = \int_0^{\infty} d\omega I(\omega) \coth\left(\frac{1}{2}\beta\hbar\omega\right) \cos(\omega(t)), \quad (8.23)$$

$$\eta(t) = \theta(t) \frac{d\gamma(t)}{dt} = -\theta(t) \int_0^{\infty} d\omega I(\omega) \sin(\omega(t)). \quad (8.24)$$

In these equations, $I(\omega)$ is the spectral density of the bath, already defined in equation (4.6). γ is defined in the first identity and as we shall see below it plays the same role as the friction kernel in classical problems with colored noise.

Next, we have to choose an initial density matrix for the system. One natural choice, having in mind the quenching experiments usually performed in classical systems, is the diagonal matrix $\langle Q | \hat{\rho}_{\text{SYST}}(0) | Q' \rangle = \delta(Q - Q')$ that corresponds to a random “high-temperature” situation and that allows one to simplify considerably ρ_{RED} :

$$\rho_{\text{RED}}(q''; q'; t) = \int_{-\infty}^{\infty} dQ \int_{q^+(0)=Q}^{q^+(t)=q''} \mathcal{D}q^+(t) \int_{q^-(0)=Q}^{q^-(t)=q'} \mathcal{D}q^-(t) e^{\frac{i}{\hbar} S_{\text{EFF}}}. \quad (8.25)$$

Another representation of ρ_{RED} is obtained by renaming the variables

$$q \equiv \frac{1}{2}(q^+ + q^-) \quad i\hat{q} \equiv \frac{1}{\hbar}(q^+ - q^-). \quad (8.26)$$

and rewriting the effective action as a function of q and $i\hat{q}$. The new form is useful to establish contact with the generating functional for classical systems. The thermal part simply becomes

$$S_{\text{TH}} = - \int_0^t dt' \int_0^t dt'' \hbar i \hat{q}(t') \eta(t' - t'') 2q(t'') \\ + i \int_0^t dt' \int_0^{t'} dt'' \hbar i \hat{q}(t') \nu(t' - t'') \hbar i \hat{q}(t'')$$

as for a Langevin process in a colored noise. When $\hbar \rightarrow 0$, the full effective action approaches the classical one as can be verified by expanding in powers of \hbar , and keeping only the leading terms. If, moreover, the limit $\Lambda \rightarrow \infty$ is taken, the kernels γ and ν become proportional to δ functions and one recovers a white noise. Keeping $\hbar > 0$ the rotated version allows one to treat classical and quantum problems in parallel.

If one generalizes the above system to be one described by a field ϕ_i with $i = 1, N$ components, the symmetrized correlation function $C_{ij}(t, t') \equiv \frac{1}{2} \langle \hat{\phi}_i(t) \hat{\phi}_j(t') + \hat{\phi}_j(t') \hat{\phi}_i(t) \rangle$ (where the hats represent operators) is given by

$$C_{ij}(t, t') = \frac{\hbar^2}{2} \left[\frac{\delta^2}{\delta \eta_i^+(t) \delta \eta_j^-(t')} + \frac{\delta^2}{\delta \eta_j^+(t') \delta \eta_i^-(t)} \right] \rho_{\text{RED}} \Big|_{\eta=0} \quad (8.27)$$

$[C_{ij}(t, t') = C_{ji}(t', t)]$. Using the Kubo formula (5.13) the linear response function can be expressed in terms of the averaged commutator, $R_{ij}(t, t') = i/\hbar \theta(t - t') \langle [\hat{\phi}_i(t), \hat{\phi}_j(t')] \rangle$ and

$$R_{ij}(t, t') = \frac{\hbar}{i} \left[\frac{\delta^2}{\delta \eta_i^+(t) \delta \eta_j^+(t')} + \frac{\delta^2}{\delta \eta_j^+(t) \delta \eta_i^-(t')} \right] \rho_{\text{RED}} \Big|_{\eta=0}. \quad (8.28)$$

It is also useful to write the correlation and response in terms of the fields ϕ_i^+ , ϕ_i^- and their rotated counterparts

$$2C_{ij}(t, t') = \langle \phi_i^+(t) \phi_j^-(t') + \phi_j^+(t') \phi_i^-(t) \rangle \\ = \langle \phi_i(t) \phi_j(t') + \phi_j(t') \phi_i(t) \rangle, \quad (8.29)$$

$$R_{ij}(t, t') = \frac{i}{\hbar} \langle \phi_i^+(t) (\phi_j^+(t') - \phi_j^-(t')) \rangle = \langle \phi_i(t) i \hat{\phi}_j(t') \rangle. \quad (8.30)$$

8.5 Average over disorder

In general one is interested in the evolution of a model in which the configuration of disorder is typical. One could either attempt to solve the dynamics for one such disorder realization or one can assume that the behavior of a typical system is described by the averaged behavior over all systems, each weighted with its probability. Since the former procedure is more difficult than the latter one usually studies the dynamics averaged over disorder and computes:

$$[\langle A(t) \rangle] = \frac{\int dJ P(J) \int \mathcal{D}\phi \mathcal{D}i\hat{\phi} A[\phi, i\hat{\phi}] e^{-S_{\text{EFF}}[\phi, i\hat{\phi}]}}{\int dJ P(J) \int \mathcal{D}\phi \int \mathcal{D}i\hat{\phi} e^{-S_{\text{EFF}}[\phi, i\hat{\phi}]}}. \quad (8.31)$$

J represents here the random exchanges in equation (2.5). Similarly, one can perform an average over a random potential in a problem as the one defined in equation (2.8).

One of the advantages of using a dynamic formalism is that when the initial conditions are uncorrelated with disorder there is no need to use the replica trick to average over disorder [75]. Indeed, the classical generating functional is constructed from a path integral that is identical to 1 (and hence independent of disorder) in the absence of sources. The same holds for the quantum Schwinger-Keldysh generating functional, $\text{Tr} \hat{\rho}_{\text{RED}}(0) = 1$, since we have chosen a diagonal density matrix as the initial condition for the system. Thus,

$$[\langle A(t) \rangle] = \int dJ P(J) \int \mathcal{D}\phi \mathcal{D}i\hat{\phi} A[\phi, i\hat{\phi}] e^{-S_{\text{EFF}}[\phi, i\hat{\phi}]} \quad (8.32)$$

and these averages can be simply computed from $[\mathcal{Z}_J]$ [79].

If the initial condition *is* correlated with the random exchanges or the random potential, the situation is different. One such example is the study of the *equilibrium* dynamics of a disordered model, *i.e.* the study of the evolution of initial conditions taken from P_{GB} . In this case, the use of replicas to average $\ln \mathcal{Z}$ is unavoidable and one is forced to treat replicated dynamic correlators. For classical models this has been discussed in [80]. For quantum problems the difficulty of the calculation increases since one needs to work in a mixed real and imaginary time formalism [81]. The initial density operator is a Boltzmann factor that is represented with the Matsubara formalism while the real-time dynamics is written with the Schwinger-Keldysh approach. Mixed correlators and responses intervene in the dynamic equations.

9 Dynamic equations

In this section we present three derivations of the dynamic equations for the macroscopic order parameters that use the classical or quantum dynamic generating functionals as starting points. Each method is better adapted for different kinds of models.

9.1 A useful derivation for fully-connected models

9.1.1 Classical systems

Even if the use of the SUSY notation is not necessary to derive the dynamic equations [82], it is very useful in several aspects. Firstly, it allows to establish contact with the replicated version of the static partition function and the further study of this quantity; secondly, it is very useful as a bookkeeping tool; thirdly, it allows us to develop more sophisticated techniques amenable to derive the dynamic equations of models without fully connected interactions. For all these reasons, we preferred to introduce the SUSY formalism in Section 8.2 and use it here.

Since for classical models the use of white noises is rather generally justified we shall stick to this case. Moreover, we shall drop the inertial contribution to further simplify the presentation. We analyze here models with N variables $\vec{\phi} = (\phi_1, \dots, \phi_N)$ of the kind discussed in Section 2. In SUSY notation the dynamical generating functional after setting the sources to zero reads

$$\mathcal{Z} = \int \mathcal{D}\Phi \exp \left[- \int da \left(\frac{1}{2} \sum_i^N \Phi_i(a) \left(-D_a^{(2)} - \mu_s(a) \right) \Phi_i(a) + V[\vec{\Phi}] \right) \right] \quad (9.1)$$

with $\vec{\Phi}$ and μ_a two super-fields, the latter imposing the spherical constraint ($\mu_s(a) = \mu(t) + \text{fermionic} + \hat{\mu}(t)\theta\bar{\theta}$, $\hat{\mu}(t)$ is a Lagrange multiplier that fixes the measure of integration and $\mu(t)$ enters the Langevin equation). Soft spins with their corresponding potential energy can be studied in a similar way though their treatment is slightly more complicated. The potential energy of a rather generic fully connected disordered model can be expressed as a series expansion of the form

$$V[\Phi] = g \sum_{r \geq 0}^{\infty} F_r \sum_{i_1 < \dots < i_{r+1}} J_{i_1 \dots i_{r+1}} \Phi_{i_1} \dots \Phi_{i_{r+1}}. \quad (9.2)$$

For each r the sum is taken over all possible groups of $r+1$ spins. The fully-connected character of the model implies that there is no notion of distance or geometry. $J_{i_1 \dots i_{r+1}}$ are random interactions taken from a

Gaussian distribution with zero mean and variance $[J_{i_1 \dots i_{r+1}}^2] = (r+1)!/(2N^r)$, just as in the model in equation (2.6). Thus (9.2) is a Gaussian random potential with

$$[V(\vec{\Phi}(a))V(\vec{\Phi}(b))] = N g^2 \sum_{r \geq 0} F_r^2 \left(\frac{\vec{\Phi}(a) \cdot \vec{\Phi}(b)}{N} \right)^{r+1} = N \mathcal{V}^\bullet \left(\frac{\vec{\Phi}(a) \cdot \vec{\Phi}(b)}{N} \right). \quad (9.3)$$

The scalar product in the second member is defined as $\vec{\Phi}(a) \cdot \vec{\Phi}(b) = \sum_i \Phi_i(a) \Phi_i(b)$. The bullet means that the powers are taken locally in the super-coordinates a and b and they do not involve an operational product, see Appendix D. The term $r = 0$ corresponds to a random field linearly coupled to the spin, the term $r = 1$ is quadratic in the fields while for $r \geq 2$ we obtain higher order interactions. If $F_r = F_p \neq 0, p \geq 2$ and all other $F_r = 0$ one recovers a spherical p spin model. If two parameters are non-zero one obtains a model with two p spin terms. The model of a particle in an infinite dimensional spherical random environment correlated as in (2.8) also falls in this category if one can expand the correlator in a power series.

The disordered averaged generating functional reads

$$[\mathcal{Z}] = \int \mathcal{D}\Phi e^{-\int da \frac{1}{2} \sum_i \Phi_i(a) (-D_a^{(2)} - \mu_s(a)) \Phi_i(a) + \frac{N}{2} \int da db \mathcal{V}^\bullet \left(\frac{\vec{\Phi}(a) \cdot \vec{\Phi}(b)}{N} \right)}. \quad (9.4)$$

Introducing the order parameter $Q(a, b) = N^{-1} \sum_{i=1}^N \Phi_i(a) \Phi_i(b)$ through

$$1 \propto \int \mathcal{D}Q \mathcal{D}i\tilde{Q} e^{-\frac{1}{2} \int da db (Ni\tilde{Q}(a, b)Q(a, b) - i\tilde{Q}(a, b) \sum_{i=1}^N \Phi_i(a) \Phi_i(b))} \quad (9.5)$$

yields

$$[\mathcal{Z}] = \int \mathcal{D}\Phi \mathcal{D}Q \mathcal{D}i\tilde{Q} \exp \left[-\frac{1}{2} \int da db \left(Ni\tilde{Q}(a, b)Q(a, b) - N\mathcal{V}^\bullet(Q(a, b)) - \sum_{i=1}^N \Phi_i(a) \left(-D_a^{(2)} - \mu_s(a) \right) \delta(a - b) - i\tilde{Q}(a, b) \Phi_i(b) \right) \right]. \quad (9.6)$$

(Again we omit irrelevant normalization constants.) Note that all terms in the exponent are order N if the integrals yield finite contributions. We call the models for which this is true “mean-field” since the saddle-point evaluation of the integral when $N \rightarrow \infty$ is exact without including fluctuations. There is however a caveat in this reasoning that we discuss in Section 9.4.

The saddle-point values for the Landau fields Q are simply related to correlations of the original spins. Indeed, evaluating the generating function

in equation (9.6) with a saddle-point approximation

$$0 = \frac{\delta S}{\delta i\tilde{Q}(a, b)} \Big|_{Q_{\text{sp}}} \Rightarrow NQ_{\text{sp}}(a, b) = \sum_{i=1}^N \langle \Phi_i(a) \Phi_i(b) \rangle_{\tilde{\mathcal{Z}}[Q]}, \quad (9.7)$$

where the average on the RHS is taken with the generating functional

$$\tilde{\mathcal{Z}}[Q] \equiv \int \mathcal{D}\Phi \mathcal{D}Q \, e^{\int da db \frac{1}{2} [\sum_{i=1}^N \Phi_i(a) (-D_a^{(2)} - \mu_s(a)) \delta(a-b) \Phi_i(b) + N \mathcal{V}^\bullet(Q(a, b))]} \quad (9.8)$$

Opening up the SUSY notation equation (9.7) implies, as expected,

$$NC_{\text{sp}}(t_1, t_2) = \sum_{i=1}^N \langle q_i(t_1) q_i(t_2) \rangle_{\tilde{\mathcal{Z}}[Q]}, \quad N\hat{Q}_{\text{sp}}(t_1, t_2) = \sum_{i=1}^N \langle i\hat{q}_i(t_1) i\hat{q}_i(t_2) \rangle_{\tilde{\mathcal{Z}}[Q]},$$

$$NR_{\text{sp}}(t_1, t_2) = \sum_{i=1}^N \langle q_i(t_1) i\hat{q}_i(t_2) \rangle_{\tilde{\mathcal{Z}}[Q]}, \quad NR_{\text{sp}}^\dagger(t_1, t_2) = \sum_{i=1}^N \langle i\hat{q}_i(t_1) q_i(t_2) \rangle_{\tilde{\mathcal{Z}}[Q]}.$$

Going back to equation (9.6) we can now shift $i\tilde{Q}$, $\overline{Q} \equiv (-D_a^{(2)} - \mu(t)) \delta(a-b) - i\tilde{Q}(a, b)$, and integrate over Φ_i

$$[\mathcal{Z}] = \int \mathcal{D}Q \mathcal{D}\overline{Q} \, e^{-\frac{N}{2} \int da db [Q(a, b) \overline{Q}(a, b) + (-D_a^{(2)} - \mu(t)) \delta(a-b) Q(a, b) - \mathcal{V}^\bullet(Q(a, b))]} \\ \times e^{-\frac{N}{2} \text{Tr Ln } \overline{Q}}.$$

Using a saddle-point evaluation, we eliminate \overline{Q} , and we find $[\mathcal{Z}] = \int \mathcal{D}Q \times \exp[-NS_{\text{EFF}}(Q)]$ with

$$2S_{\text{EFF}}(Q) = \int da db \left[[-D_a^{(2)} - \mu_s(a)] \delta(a-b) Q(a, b) - \mathcal{V}^\bullet(Q(a, b)) \right] - \text{Tr Ln } Q. \quad (9.9)$$

The saddle-point equation over Q , $\delta S_{\text{EFF}}/\delta Q = 0$, yields the dynamic equation

$$\left(D_a^{(2)} + \mu(t) \right) \delta(a-b) + Q^{-1}(a, b) + \mathcal{V}^{\bullet'}(Q(a, b)) = 0, \quad (9.10)$$

that takes a more convenient form after multiplying operationally by Q :

$$\left(D_a^{(2)} + \mu(t) \right) Q(a, b) + \delta(a-b) + \int da' \Sigma(a, a') Q(a', b) = 0, \quad (9.11)$$

with the self-energy defined as

$$\Sigma(a, b) \equiv \mathcal{V}^{\bullet'}(Q(a, b)) = g^2 \sum_{r \geq 0}^{\infty} F_r^2(r+1) Q(a, b)^{\bullet r}. \quad (9.12)$$

We have recasted the saddle-point dynamic equation in the form of a Schwinger-Dyson equation. The dynamic field is here a SUSY correlator that encodes the usual correlation function, the advance and retarded linear responses and the fourth correlator (that vanishes for causal problems):

$$\begin{aligned}
\overline{G}_o^{-1}(t)R(t, t') &= \delta(t - t') + 2\gamma\hat{Q}(t, t') + \int dt'' [\Sigma(t, t'')R(t'', t') \\
&\quad + D(t, t'')\hat{Q}(t''t, t')], \\
\overline{G}_o^{-1}(t)C(t, t') &= 2\gamma k_B T R(t', t) + \int dt'' \Sigma(t, t'')C(t'', t') \\
&\quad + \int dt'' D(t, t'')R(t', t''), \\
\overline{G}_o^{-1\dagger}(t)R^\dagger(t, t') &= \delta(t - t') + \int_0^\infty dt'' \Sigma^\dagger(t'', t)R(t', t'') \\
&\quad + \int dt'' \hat{\Sigma}(t, t'')C(t'', t') + 2\hat{\mu}(t)C(t, t'), \\
\overline{G}_o^{-1\dagger}(t)\hat{Q}(t, t') &= \int dt'' \Sigma^\dagger(t, t'')\hat{Q}(t'', t') + \int dt'' \hat{\Sigma}(t, t'')R(t'', t') \\
&\quad + 2\hat{\mu}(t)R(t, t'),
\end{aligned}$$

with $\overline{G}_o^{-1}(t) \equiv M\partial_t^2 + \gamma\partial_t + \mu(t)$, $\overline{G}_o^{-1\dagger}(t) \equiv M\partial_t^2 - \gamma\partial_t + \mu(t)$, $\Sigma^\dagger(t, t') = \Sigma(t', t)$ and

$$\Sigma(t, t'') = g^2 \sum_{r \geq 0} F_r^2 (r+1) r C^{r-1}(t, t'') R(t, t''), \quad (9.13)$$

$$D(t, t'') = g^2 \sum_{r \geq 0} F_r^2 (r+1) C^r(t, t''), \quad (9.14)$$

$$\hat{\Sigma}(t, t'') = g^2 \sum_{r \geq 0} F_r^2 (r+1) r C^{r-1}(t, t'') \hat{Q}(t, t''). \quad (9.15)$$

We set to zero all fermionic correlators. We call the above integro-differential equations the Schwinger-Dyson equations for R , C , R^\dagger and \hat{Q} , respectively.

Causality can be used to simplify the four Schwinger-Dyson equations considerably. For $t' > t$ one has $R(t, t') = 0$ while for $t > t'$ one has $R(t', t) = 0$. Rewriting the equations for R and R^\dagger with these two choices of times one easily sees that $\hat{Q}(t, t') = 0$ for all t and t' (note that \hat{Q} is symmetric in t and t') and $\hat{\mu}(t) = 0$ for all t . Thus, the equation for \hat{Q} vanishes identically when causality holds. In the following we search for causal solutions and we work with their simplified version. We loose in this way the possibility of finding solutions that break causality which are related to instantons [65]. We shall come back to this point later. If we

focus on the case $t > t'$ the dynamic equations simplify to

$$\overline{G}_o^{-1}(t)R(t, t') = \int_{t'}^t dt'' \Sigma(t, t'')R(t'', t'), \quad (9.16)$$

$$\begin{aligned} \overline{G}_o^{-1}(t)C(t, t') &= \int_0^{t'} dt'' D(t, t'')R(t', t'') \\ &+ \int_0^t dt'' \Sigma(t, t'')C(t', t''). \end{aligned} \quad (9.17)$$

In their integrated form they read

$$\begin{aligned} R(t, t') &= G_o(t, t') + \int_{t'}^t dt'' \int_{t'}^{t''} dt''' \\ &\times G_o(t, t'') \Sigma(t'', t''') R(t''', t'), \end{aligned} \quad (9.18)$$

$$C(t, t') = \int_0^t dt'' \int_0^{t'} dt''' R(t, t'') D(t'', t''') R(t', t'''), \quad (9.19)$$

with the propagator given by $G_o^{-1}(t, t') \equiv \delta(t - t')\overline{G}_o^{-1}(t)$.

The equation for $\mu(t)$ can be derived from the Schwinger-Dyson equation by imposing the spherical constraint through the evaluation at $t = t'$. Multiplying operationally by G_o^{-1} one obtains

$$\begin{aligned} \mu(t) &= \int_0^t dt'' [\Sigma(t, t'')C(t, t'') + D(t, t'')R(t, t'')] \\ &+ M \int_0^t dt'' \int_0^t dt''' (\partial_t R(t, t'')) D(t'', t''') (\partial_t R(t, t''')) \\ &+ M^2 [\partial_t R(t, s) \partial_{st}^2 C(s, t) - \partial_{st}^2 R(t, s) \partial_t C(s, t')] \Big|_{s \rightarrow 0, t \rightarrow t'}. \end{aligned} \quad (9.20)$$

The last two terms are a consequence of having a kinetic term with second derivatives. It can be easily identified with minus the second-derivative of the correlation at equal times by taking the limit $t' \rightarrow t^-$ in equation (9.17). Thus

$$\mu(t) = \int_0^t dt'' [\Sigma(t, t'')C(t, t'') + D(t, t'')R(t, t'')] - M \frac{\partial^2}{\partial t^2} C(t, t') \Big|_{t' \rightarrow t^-}. \quad (9.21)$$

One way of deriving the equation for $\mu(t)$ for a Langevin process with *white noise and no inertia* goes as follows. Considering $t > t'$ in the complete Schwinger-Dyson equation for C and taking $t' \rightarrow t^-$, and considering $t < t'$ in the same equation and taking $t' \rightarrow t^+$, one finds

$$\lim_{t' \rightarrow t^-} \partial_t C(t, t') = \lim_{t' \rightarrow t^+} \partial_t C(t, t') - 2k_B T \quad (9.22)$$

where we used $R(t, t' \rightarrow t^-) = 1/\gamma$. The derivative of C has a cusp at $t = t'$. The symmetry of the correlation function about $t = t'$ implies $C(t' + \delta, t') = C(t' - \delta, t')$ and an expansion up to first order in δ implies $\lim_{t' \rightarrow t^-} \partial_t C(t, t') = -\lim_{t' \rightarrow t^+} \partial_t C(t', t)$. From equation (9.22) one has $\lim_{t' \rightarrow t^-} \partial_t C(t, t') = -k_B T$. Now, one rewrites the complete equation for C exchanging t and t' and adds this equation to the same equation in the limit $t' \rightarrow t^-$: $\gamma \lim_{t' \rightarrow t^-} (\partial_t C(t, t') + \partial_{t'} C(t, t')) = -2\mu(t) + \lim_{t' \rightarrow t^-} [\text{rhs eq. for } C + \text{rhs eq. for } C(t' \leftrightarrow t)]$. From the discussion above the LHS vanishes and the RHS implies

$$\mu(t) = k_B T + \int_0^\infty dt'' [\Sigma(t, t'')C(t, t'') + D(t, t'')R(t, t'')]. \quad (9.23)$$

For the spherical p spin model $\mu(t)$ is simply related to the energy density $\mathcal{E}(t)$. Indeed, take the Langevin equation evaluated at time t , multiply it by $s_i(t')$, sum over all sites, average over the noise and take the limit $t' \rightarrow t$. Repeat this procedure with the Langevin equation evaluated at t' and multiplying by $s_i(t)$. Adding the resulting equations and using $N^{-1} \sum_{i=1}^N \langle s_i(t) \xi_i(t') \rangle = 2\gamma k_B T R(t, t')$ (see Appendix C) we have $\mu(t) = -\lim_{t' \rightarrow t^-} \left\langle \sum_i \frac{\delta H_i(\vec{s}(t))}{\delta s_i(t)} s_i(t') \right\rangle + k_B T$ that for the spherical p spin model becomes

$$\mu(t) = -p\mathcal{E}(t) + k_B T. \quad (9.24)$$

Thanks to the mean-field character of the model the action is proportional to N and the saddle-point evaluation is exact when $N \rightarrow \infty$. For the fully connected models considered in this section the self-energy is given by a rather simple function of the interactions. In Section 9.2 we present a more powerful method that allows us to derive a similar equation for dilute (as opposed to fully connected) disordered models. For finite dimensional problems none of these procedures are exact. An effective action in terms of *local* order parameters $Q_i(a, b)$ can be written but the evaluation of the generating functional by saddle-point has to include fluctuations [83, 84].

9.1.2 Quantum models

The similarity between the effective action for classical and quantum models can be exploited to derive the dynamic equations of a quantum system in a very similar manner to what we have just done for classical models [85]. Even if the SUSY notation is not useful for quantum problems we can still use a compact notation. We first encode the variables $q, i\hat{q}$ in a vector. The quadratic terms in the action can be condensed into one term by introducing

the operator

$$\begin{aligned}\mathcal{O}p(t, t') &= \begin{pmatrix} \text{Op}^{++}(t, t') & \text{Op}^{+-}(t, t') \\ \text{Op}^{-+}(t, t') & \text{Op}^{--}(t, t') \end{pmatrix} = \left\{ \text{Op}^{\alpha\beta}(t, t') \right\}, \\ \text{Op}^{++}(t, t') &= (M\partial_t^2 + \mu^+(t)) \delta(t - t') - 2i\nu(t - t') \\ \text{Op}^{+-}(t, t') &= 2\eta(t - t') + 2i\nu(t - t') \\ \text{Op}^{-+}(t, t') &= -2\eta(t - t') + 2i\nu(t - t') \\ \text{Op}^{--}(t, t') &= -(M\partial_t^2 + z^-(t)) \delta(t - t') - 2i\nu(t - t')\end{aligned}\quad (9.25)$$

in such a way that

$$\begin{aligned}S_{\text{EFF}} [\vec{\phi}^+, \vec{\phi}^-] &= -\frac{1}{2} \int dt \int dt' \vec{\phi}^\alpha(t) \text{Op}^{\alpha\beta}(t, t') \vec{\phi}^\beta(t') \\ &\quad - \int dt V [\vec{\phi}^+] + \int dt V [\vec{\phi}^-]\end{aligned}\quad (9.26)$$

where Greek indices label $+$, $-$ and the sum convention is assumed.

Introducing the order parameter $Q^{\alpha\beta}(t, t') = N^{-1} \sum_i \phi_i^\alpha(t) \phi_i^\beta(t')$ via the identity

$$1 \propto \int \prod_{\alpha\beta} \mathcal{D}Q^{\alpha\beta} \mathcal{D}\hat{Q}^{\alpha\beta} e^{-\frac{1}{2\pi} i \hat{Q}^{\alpha\beta} (\vec{\phi}^\alpha(t) \vec{\phi}^\beta(t') - N Q^{\alpha\beta}(t, t'))}, \quad (9.27)$$

the full action can be rewritten as

$$\begin{aligned}S_{\text{EFF}} [\vec{\phi}^+, \vec{\phi}^-] &= -\frac{1}{2} \int dt \int dt' \vec{\phi}^\alpha(t) \left(\text{Op}^{\alpha\beta}(t, t') + i \hat{Q}^{\alpha\beta}(t, t') \right) \vec{\phi}^\beta(t') \\ &\quad + \frac{N}{2} \int dt \int dt' \hat{Q}^{\alpha\beta}(t, t') Q^{\alpha\beta}(t, t') + \frac{N}{2} \int dt (\mu^+(t) - \mu^-(t)) \\ &\quad + \int dt V [\vec{\phi}^+] - \int dt V [\vec{\phi}^-].\end{aligned}\quad (9.28)$$

The stationary-point values of $Q^{\alpha\beta}(t, t')$ are related to the “physical” correlations and responses defined in equations (8.29) and (8.30) as follows

$$\begin{aligned} NQ^{++}(t, t') &= \overline{\langle \vec{\phi}^+(t) \vec{\phi}^+(t') \rangle} \\ &= N \left(C(t, t') - \frac{i\hbar}{2} (R(t, t') + R(t', t)) \right), \end{aligned} \quad (9.29)$$

$$\begin{aligned} NQ^{+-}(t, t') &= \overline{\langle \vec{\phi}^+(t) \vec{\phi}^-(t') \rangle} \\ &= N \left(C(t, t') + \frac{i\hbar}{2} (R(t, t') - R(t', t)) \right), \end{aligned} \quad (9.30)$$

$$\begin{aligned} NQ^{-+}(t, t') &= \overline{\langle \vec{\phi}^-(t) \vec{\phi}^+(t') \rangle} \\ &= N \left(C(t, t') - \frac{i\hbar}{2} (R(t, t') - R(t', t)) \right), \end{aligned} \quad (9.31)$$

$$\begin{aligned} NQ^{--}(t, t') &= \overline{\langle \vec{\phi}^-(t) \vec{\phi}^-(t') \rangle} \\ &= N \left(C(t, t') + \frac{i\hbar}{2} (R(t, t') + R(t', t)) \right), \end{aligned} \quad (9.32)$$

with $NC(t, t') = \sum_i C_{ii}(t, t')$ and $NR(t, t') = \sum_i R_{ii}(t, t')$. It is easy to check that these functions satisfy the identity $Q^{++}(t, t') + Q^{--}(t, t') - Q^{+-}(t, t') - Q^{-+}(t, t') = 0$. At the classical level this identity reduces to the condition $\langle i\hat{s}(t)i\hat{s}(t') \rangle = 0$ for all pairs of times t, t' . In what follows we do not break this identity and hence do not allow for solutions that break causality.

The functional integration over $\phi_i^+(t)$ and $\phi_i^-(t)$ is now quadratic and can be performed. Symmetrizing the operator Op with respect to the greek indices and times the integral over the fields ϕ^+ and ϕ^- amounts to replacing the quadratic term in $i/\hbar S_{\text{EFF}}$ by

$$-\frac{N}{2} \int dt \int dt' \text{Tr} \log \left(\frac{i}{\hbar} \text{Op}_{\text{SYMM}}^{\alpha\beta}(t, t') + \frac{i}{\hbar} i\hat{Q}^{\alpha\beta}(t, t') \right). \quad (9.33)$$

At this stage, all terms in the action depend upon the “macroscopic” quantities $i\hat{Q}^{\alpha\beta}$, $Q^{\alpha\beta}$ and μ^α and are proportional to N . Since it is easier to write the equations in matrix notation, we encode $i\hat{Q}^{\alpha\beta}$ and $Q^{\alpha\beta}$ in two matrices

$$i\hat{\mathcal{Q}} = \begin{pmatrix} i\hat{Q}^{++} & i\hat{Q}^{+-} \\ i\hat{Q}^{-+} & i\hat{Q}^{--} \end{pmatrix} \quad \mathcal{Q} = \begin{pmatrix} Q^{++} & Q^{+-} \\ Q^{-+} & Q^{--} \end{pmatrix}$$

and we define

$$F[\mathcal{Q}](t, t') \equiv g^2 \sum_{r \geq 0} F_r^2 (r+1) \begin{pmatrix} (Q^{++}(t, t'))^r & -(Q^{+-}(t, t'))^r \\ -(Q^{-+}(t, t'))^r & (Q^{--}(t, t'))^r \end{pmatrix}, \quad (9.34)$$

the saddle-point with respect to $i\hat{Q}^{\alpha\beta}(t, t')$ yields $i\hat{Q}(t, t') = \frac{\hbar}{i}\mathcal{Q}^{-1}(t, t') - \mathcal{O}p(t, t')$. The matrix and time-operator inverse of \mathcal{Q} is denoted \mathcal{Q}^{-1} . The saddle-point equation with respect to $Q^{\alpha\beta}(t, t')$ yields $i\hat{Q}(t, t') = -\frac{i}{2\hbar}F[\mathcal{Q}](t, t')$. These saddle-point equations imply, in a compact matrix and time-operator notation,

$$\frac{i}{\hbar}\mathcal{O}p_{\text{SYMM}} \otimes \mathcal{Q} = I - \frac{1}{2\hbar^2} F[\mathcal{Q}] \otimes \mathcal{Q}, \quad (9.35)$$

where I is the identity: $I^{\alpha\beta}(t, t') = \delta^{\alpha\beta}\delta(t - t')$ and we denote with a cross the standard operational product in matrix and time (see Appendix D). The saddle-point with respect to μ^+ yields

$$i/\hbar = \left(\mathcal{O}p + i\hat{Q} \right)_{++}^{-1}(t, t) = i/\hbar Q^{++}(t, t), \quad (9.36)$$

and similarly for Q^{--} . These equations lead to the spherical constraint.

The dynamic equations for the auto-correlation and response follow from the set of equations (9.34), (9.35) and the definitions of the dynamic order parameters given in equations (9.29)–(9.32). More precisely, the equation of motion for the response function follows from the subtraction of the $++$ and $+-$ components of equation (9.35):

$$\begin{aligned} (M\partial_t^2 + \mu^+(t)) R(t, t') + 4 \int_{t'}^t dt'' \eta(t - t'') R(t'', t') &= \delta(t - t') \\ - \frac{g^2}{2i\hbar} \sum_{r \geq 0} F_r^2 (r+1) \int_0^\infty dt'' [(Q^{++}(t, t''))^r - (Q^{+-}(t, t''))^r] R(t'', t'), \end{aligned} \quad (9.37)$$

and the equation of motion for the correlation follows from the addition of the $+-$ and $-+$ components of equation (9.35):

$$\begin{aligned} \left[M\partial_t^2 + \frac{1}{2} (\mu^+(t) + \mu^-(t)) \right] C(t, t') + \frac{i}{2} (z^+(t) - z^-(t)) \hbar (R(t', t) - R(t, t')) \\ - 2\hbar \int_0^\infty dt'' \nu(t - t'') R(t', t'') + 4 \int_0^t dt'' \eta(t - t'') C(t'', t') = \\ - \frac{g^2}{2\hbar} \sum_{r \geq 0} F_r^2 (r+1) \text{Im} \int_0^\infty dt'' [(Q^{++}(t, t''))^r Q^{+-}(t'', t') \\ - (Q^{+-}(t, t''))^r Q^{--}(t'', t')] . \end{aligned} \quad (9.38)$$

Written in this way, equation (9.38) is complex. Its imaginary part yields $\mu(t) \equiv \mu^+(t) = \mu^-(t)$. Moreover, since the response is causal, products of advanced $R(t, t'')$ and retarded $R(t'', t')$ responses vanish identically for all t, t'' : $R(t, t'')R(t'', t) = 0$, $\forall t, t''$ and one can show that for any integer $k > 0$ and any constants c_1, c_2 , $[C(t, t') + c_1 R(t, t') + c_2 R(t', t)]^k = [C(t, t') + c_1 R(t, t')]^k + [C(t, t') + c_2 R(t', t)]^k - C^k(t, t')$. Using this property one has $(Q^{++}(t, t''))^r - (Q^{+-}(t, t''))^r = 2i\text{Im}[C(t, t'') - \frac{i\hbar}{2}R(t, t'')]^r$ and $\text{Im}[(Q^{++}(t, t''))^r Q^{+-}(t'', t') - (Q^{+-}(t, t''))^r Q^{--}(t'', t')] = 2C(t'', t') \times \text{Im}[C(t, t'') - \frac{i\hbar}{2}R(t, t'')]^r - \hbar R(t', t'')\text{Re}[C(t, t'') - \frac{i\hbar}{2}(R(t, t'') + R(t'', t))]^r$. We can identify the self-energy $\tilde{\Sigma}$ and the vertex \tilde{D} as

$$\Sigma(t, t') + 4\eta(t - t') \equiv \tilde{\Sigma}(t, t') \quad D(t, t') - 2\hbar\nu(t - t') \equiv \tilde{D}(t, t')$$

$$\tilde{\Sigma}(t, t') = -\frac{g^2}{\hbar} \sum_{r \geq 0} F_r^2(r+1) \text{Im}[C(t, t') - (i\hbar)/2R(t, t')]^r, \quad (9.39)$$

$$\tilde{D}(t, t') = \frac{g^2}{2} \sum_{r \geq 0} F_r^2(r+1) \text{Re}[C(t, t')$$

$$- (i\hbar)/2(R(t, t') + R(t', t))]^r. \quad (9.40)$$

Note that the total self-energy Σ and vertex D are real and have two contributions of different origin: one arises from the interaction of the system and the bath (η and ν) and one is caused by the non-linearities stemming from the average over disorder ($\tilde{\Sigma}$ and \tilde{D}).

The dynamic equations can then be written in the compact form (9.16), (9.17). It is important to realize that the self-energy $\tilde{\Sigma}(t, t')$ is proportional to the response function $R(t, t')$, which in turns implies $\tilde{\Sigma}(t, t') = \Sigma(t, t') = 0$ for $t < t'$. This means that the upper limit of integration in equations (9.16) and (9.17) is t , which renders the equations explicitly causal. There are no more independent equations for R and C . The other two equations that can be obtained from equation (9.35) are the equation for $R(t', t)$, that is equivalent to equation (9.16), and one equation that identically cancels by virtue of the identity between two-point correlators.

Real and imaginary parts of equation (9.36) and the one for Q^{--} combined with the saddle-point equation for λ imply the equal-times conditions $C(t, t) = 1$, $R(t, t) = 0$. In addition, from equation (9.37) one obtains that the first derivative of the response function is discontinuous at equal times:

$$\lim_{t' \rightarrow t^-} \partial_t R(t, t') = \frac{1}{M}, \quad \lim_{t' \rightarrow t^+} \partial_t R(t, t') = 0, \quad (9.41)$$

while from equation (9.38) one obtains that the first derivative of the correlation is continuous:

$$\lim_{t' \rightarrow t^-} \partial_t C(t, t') = \lim_{t' \rightarrow t^+} \partial_t C(t, t') = 0. \quad (9.42)$$

In conclusion, equations (9.16), (9.17) and (9.21) are the complete set of equations that determines the dynamics of the system.

9.2 Beyond fully-connected models

9.2.1 Classical models

A very useful formalism to study the *statics* of classical dilute disordered models with the replica trick has been introduced by Monasson [86] generalising the previous work of Mottishaw & de Dominicis [87]. The parallel between the static calculation using replicas and the dynamic formalism, once expressed in terms of superfields, exists also at the level of this approach. The presentation in this Section follows very closely the one in [88] where a dynamic formalism apt to analyze *dilute* disordered models was introduced.

The dilute spin-glass, or Viana-Bray model in its Ising version, is a spin model defined on a random graph with average connectivity \tilde{c} and pair random exchanges taken from the probability distribution $P(J_{ij}) = (1 - \tilde{c}/N) \delta(J_{ij}) + \tilde{c}/N [\frac{1}{2} \delta(J_{ij} - J) + \frac{1}{2} \delta(J_{ij} + J)]$. For the sake of simplicity we consider the spherical version of this model. Let us define $c(\Phi)$ as the fraction of sites with super-field Φ_i identical to a chosen value Φ

$$c(\Phi) \equiv \frac{1}{N} \sum_{i=1}^N \prod_a \delta(\Phi(a) - \Phi_i(a)), \quad (9.43)$$

for all values of the super-coordinate a . Note that $\int \mathcal{D}\Phi c(\Phi) = 1$. Similarly to what we have done when introducing $Q(a, b)$ in equation (9.5) we enforce the definition of $c(\Phi)$ in the generating functional by introducing an identity in its path integral representation: $1 \propto \int \mathcal{D}c \mathcal{D}i\hat{c} \exp[\int \mathcal{D}\Phi i\hat{c}(\Phi)(Nc(\Phi) - \sum_{i=1}^N \prod_a \delta(\Phi - \Phi_i))]$ $= \int \mathcal{D}c \mathcal{D}i\hat{c} \exp[\int \mathcal{D}\Phi N i\hat{c}(\Phi)c(\Phi) - \sum_{i=1}^N i\hat{c}(\Phi_i)]$. We obtain

$$\begin{aligned} \mathcal{Z} = & \int \mathcal{D}\Phi_i \mathcal{D}c \mathcal{D}i\hat{c} \exp \left(\int \mathcal{D}\Phi N i\hat{c}(\Phi)c(\Phi) - \sum_{i=1}^N i\hat{c}(\Phi_i) \right. \\ & \left. + \frac{N}{2} \int \mathcal{D}\Phi c(\Phi) \int da \Phi(a) (-D_a^{(2)} - \mu_s(a)) \Phi(a) - \int da V[\Phi(a)] \right). \end{aligned}$$

$V[\Phi(a)] = \sum_{ij} J_{ij} \Phi_i(a) \Phi_j(b)$. Once written in this form, the average over disorder can be simply performed and the disordered averaged generating

functional becomes $[\mathcal{Z}] = \int \mathcal{D}c \mathcal{D}i \hat{c} \mathcal{D}\Phi_i \exp(-NG)$ with

$$G = - \int d\Phi i \hat{c}(\Phi) c(\Phi) + \frac{1}{N} \sum_{i=1}^N i \hat{c}(\Phi_i) \\ + \frac{1}{2} \int d\Phi c(\Phi) \int da \Phi(a) (D_a^{(2)} + \mu_s(a)) \Phi(a) + H_{\text{EFF}}$$

and $\exp(-NH_{\text{EFF}}) = [\exp(\int da V[\Phi(a)])]$ With the notation NH_{EFF} we suggest that H_{EFF} is of order one. We shall discuss this very important issue below.

The second term in G is now the only term where the Φ_i 's appear and all of them contribute in exactly the same form. One can then replace the sum over i by a factor N times $\hat{c}(\Phi')$ and exponentiate the functional integral over the representative super-field Φ' , $\int \mathcal{D}\Phi_i \exp(-\sum_i i \hat{c}(\Phi_i)) = \exp(N \ln \int \mathcal{D}\Phi' \exp(-i \hat{c}(\Phi')))$. The saddle-point equation on $i \hat{c}$ reads $i \hat{c}(\Phi) = -\ln c(\Phi) - \ln(\int \mathcal{D}\Phi' e^{-i \hat{c}(\Phi')})$. Replacing this expression for $i \hat{c}(\Phi)$ and using the fact that $\int \mathcal{D}\Phi c(\Phi) = 1$, the generating functional averaged over disorder becomes $[\mathcal{Z}] = \int \mathcal{D}c \exp[-NS_{\text{EFF}}(c)]$ with

$$S_{\text{EFF}}(c) = \int \mathcal{D}\Phi c(\Phi) \ln c(\Phi) \\ + \frac{1}{2} \int \mathcal{D}\Phi c(\Phi) \int da \Phi(a) (D_a^{(2)} + \mu_s(a)) \Phi(a) + H_{\text{EFF}}.$$

The first term is an entropic contribution, the second term is a kinetic energy and the third one is the potential energy.

The difficulty now arises as to how to compute the effective Hamiltonian H_{EFF} . For fully connected models as the ones discussed in the previous section H_{EFF} can be calculated exactly and one recovers the dynamic equations that were already known (see below). For dilute disordered models, or models defined on a random graph, H_{EFF} is still a quantity of order one. In this sense we still call them mean-field models. This property allows us to pursue the calculation with a saddle-point approximation. H_{EFF} is determined by a set of iterative approximations. For finite dimensional models the situation worsens still since a saddle-point approximation cannot be used without taking into account the fluctuations around it.

Gaussian approximation

In this section we assume that we deal with any model such that the effective action S_{EFF} is indeed of order N . In a first step we resort to a Gaussian approximation, in which one proposes:

$$c(\Phi) = (\det Q)^{-1/2} e^{-\frac{1}{2} \int da db \Phi(a) Q^{-1}(a,b) \Phi(b)}. \quad (9.44)$$

The denominator ensures the normalization of $c(\Phi)$ and $Q(a, b)$ is correctly given by the averaged correlator: $Q(a, b) = \mathcal{N} \int \mathcal{D}\Phi \frac{1}{N} \sum_i \Phi_i(a) \Phi_i(b) \times e^{-\frac{1}{2} \int da' db' \Phi(a') Q^{-1}(a', b') \Phi(b')}$ with $\mathcal{N} = (\det Q)^{-1/2}$. After rather simple manipulations the c -dependent effective action can be expressed in terms of $Q(a, b)$, $2S_{\text{EFF}}(Q) = \text{Tr} \ln Q + \int da db \delta(a-b)(D_a^{(2)} + \mu_s(a))Q(a, b) - 2H_{\text{EFF}}(Q)$. Its variation with respect to Q yields:

$$\frac{\delta S_{\text{EFF}}(Q)}{\delta Q} = 0 = \frac{1}{2} Q^{-1}(a, b) + \frac{1}{2} (D_a^{(2)} + \mu_s(a))Q(a, b) - \frac{\delta H_{\text{EFF}}(Q)}{\delta Q(a, b)}. \quad (9.45)$$

Multiplying this equation operationally by $Q(b, a')$ (see Appendix D) the dynamic equation takes the more familiar form (9.11) with $\Sigma(a, a') = -2\delta H_{\text{EFF}}(Q)/\delta Q(a, a')$.

One example: The infinite range p spin model

The p spin spherical model is a particular case of the model in (9.2) with

$$\begin{aligned} 4H_{\text{EFF}} &= \frac{1}{N} \sum_{i_1 \dots i_p} \frac{1}{N^{p-1}} \left(\int da \Phi_{i_1}(a) \dots \Phi_{i_p}(a) \right)^2 \\ &= \int da db \left(\frac{1}{N} \sum_{i=1}^N \Phi_i(a) \Phi_i(b) \right)^p \\ &= \int \mathcal{D}\Phi'_1 \dots \mathcal{D}\Phi'_p c(\Phi'_1) \dots c(\Phi'_p) \int da db \Phi'_1(a) \Phi'_1(b) \dots \Phi'_p(a) \Phi'_p(b) \\ &= \int da db \left(\int \mathcal{D}\Phi' c(\Phi') \Phi'(a) \Phi'(b) \right)^p. \end{aligned} \quad (9.46)$$

Replacing the Gaussian *Ansatz* (9.44), H_{EFF} becomes a simple function of $Q(a, b)$:

$$H_{\text{EFF}}(Q) = \frac{1}{4} \int da db Q^{\bullet p}(a, b). \quad (9.47)$$

The full expression for the effective action $S_{\text{EFF}}(Q)$ is identical to equation (9.9). A way to prove that the Gaussian *Ansatz* (9.44) is exact for this model is to check that the *exact* equation for $c(\Phi)$ coincides with the one obtained from the Gaussian *Ansatz* and the saddle-point evaluation.

A second example: The dilute spherical spin-glass

In this case the effective Hamiltonian $H_{\text{EFF}}(c)$ reads

$$-2H_{\text{EFF}}(c) = -\tilde{c} + \tilde{c} \int \mathcal{D}\Phi \mathcal{D}\Phi' c(\Phi) c(\Phi') \cosh \left(J \int da \Phi(a) \Phi'(a) \right). \quad (9.48)$$

With the Gaussian *Ansatz*, this expression becomes

$$-2H_{\text{EFF}}(Q) = -\tilde{c} + \tilde{c}/\sqrt{\det(1 - J^2 Q^2)}. \quad (9.49)$$

The self-energy can only be expressed as a series expansion or a functional:

$$\Sigma(a, b) = \tilde{c} J^2 [Q(1 - J^2 Q)^{-1}] (a, b) = \tilde{c} J^2 \sum_{k=0}^{\infty} J^{2k} Q^{(2k+1)}(a, b). \quad (9.50)$$

Using the first expression for Σ one derives the dynamic equation

$$(\tilde{c} - 1)J^2 Q^2(a, b) + \delta(a - b) = \left(-D_a^{(2)} - \mu_s(a) \right) (Q - J^2 Q^3)(a, b). \quad (9.51)$$

Otherwise, if we use the second expression we obtain a dynamic equation involving a series. Note that this equation is much more complicated than the one for the fully connected p spin spherical model. The derivatives act on functionals of the correlator Q in this case. Moreover, the Gaussian approximation is not exact for dilute models. An iterative method can be implemented to go beyond this approximation. It was introduced in [88] but we shall not describe it here.

9.2.2 Quantum models

Once we have presented the method for the classical dynamics, its extension to a quantum system is simple. The important point to remark about the previous derivation is that the SUSY notation has been used, mostly, as a bookkeeping device. In the quantum case a SUSY formalism is not useful. Instead, it is convenient to use the formalism apt to take the classical limit, encoding the variables $(q, i\hat{q})$ in a two-component (column) *vector* $\vec{\Phi}$, and defining a (line) vector \vec{v} :

$$\vec{\Phi}_i \equiv \begin{pmatrix} q_i \\ i\hat{q}_i \end{pmatrix} \quad \vec{v} \equiv \begin{pmatrix} 1 & -\frac{i\hbar}{2} \end{pmatrix},$$

the effective action reads

$$\begin{aligned} S_{\text{EFF}} = S_{\text{KIN}} \left(\vec{v} \cdot \vec{\Phi}_i \right) - S_{\text{KIN}} \left(\vec{v}^* \cdot \vec{\Phi}_i \right) \\ + S_{\text{POT}} \left(\vec{v} \cdot \vec{\Phi}_i \right) - S_{\text{POT}} \left(\vec{v}^* \cdot \vec{\Phi}_i \right) + S_{\text{TH}} \left(\vec{\Phi}_i \right) \end{aligned} \quad (9.52)$$

with the thermal part of the action written as

$$S_{\text{TH}}(\vec{\Phi}) = \int dt \int dt' \vec{\Phi}_i^t(t) \mathcal{A}(t - t') \vec{\Phi}_i(t'). \quad (9.53)$$

Calling $a = 1, 2$ the vector indices, the notation becomes identical to the SUSY one, with a here playing the rôle of the coordinate in super-space $a = (t, \theta, \bar{\theta})$ in the classical problem. Just as in the previous section, one introduces the identity (9.43), where a is now interpreted as a vector index, to rewrite the generating functional. The analysis of the kinetic and thermal part of the effective action follows the same lines as the one presented for the classical problem.

9.3 Field equations

Once we have written the dynamic action in terms of ϕ_i and $i\hat{\phi}_i$ the “field equations” follow from exact properties of the functional integration [65]. Indeed,

$$\begin{aligned} 0 &= \int \mathcal{D}\phi \mathcal{D}i\hat{\phi} \frac{\delta}{\delta i\hat{\phi}_i(t)} e^{-S_{\text{EFF}}[\phi_i, i\hat{\phi}_i] + \int_C dt' (\eta_i(t')\phi_i(t') + \hat{\eta}_i(t')i\hat{\phi}_i(t'))} \\ &= \int \mathcal{D}\phi \mathcal{D}i\hat{\phi} \left[-\frac{\delta S_{\text{EFF}}(\phi_i, i\hat{\phi}_i)}{\delta i\hat{\phi}_i(t)} + \hat{\eta}_i(t) \right] \\ &\quad \times e^{-S_{\text{EFF}}(\phi_i, i\hat{\phi}_i) + \int_C dt' (\eta_i(t')\phi_i(t') + \hat{\eta}_i(t')i\hat{\phi}_i(t'))}. \end{aligned}$$

The subindex C in the integrals stands for “time contour” and it can describe the usual integration from the initial time to infinity for classical models or the close time path for quantum ones. Taking now the variation with respect to the source $i\hat{\eta}_j(t')$ and evaluating at $\eta = i\hat{\eta} = 0$ for all times and components we find

$$0 = \delta(t - t')\delta_{ij} - \left\langle i\hat{\phi}_j(t') \frac{\delta S_{\text{EFF}}(\phi_i, i\hat{\phi}_i)}{\delta i\hat{\phi}_i(t)} \right\rangle \quad (9.54)$$

where the brackets denote an average with the measure weighted by the dynamic action S_{EFF} . If, instead one takes the variation with respect to $\eta_j(t')$ and later evaluates at $\eta = i\hat{\eta} = 0$ one obtains:

$$\left\langle i\hat{\phi}_i(t) \frac{\delta S}{\delta \phi_j(t')} \right\rangle = 0. \quad (9.55)$$

A way to derive dynamic equations for the two-point correlators amounts to use Wick’s theorem and rewrite these averages as a sum over all possible factorizations in products of two point-functions. This is of course exact if the action is quadratic but it is only a Gaussian approximation for more general models. This kind of derivation has been mainly used in the study of the dynamics of manifolds in random potentials [89].

9.4 The thermodynamic limit and time-scales

It is very important to stress that the dynamic equations derived with the saddle-point approximation hold only when $N \rightarrow \infty$ *before* any long-time limit is taken. They describe the dynamics in finite time-scales with respect to N and they cannot capture the crossover from the non-equilibrium relaxation to the equilibrium dynamics reached in time scales that diverge with N [remember that $t_{\text{EQ}}(N)$].

Previous attempts to study the dynamics of disordered glassy systems assumed that these same equations hold for the equilibrium dynamics when N is finite and time-scales diverge with N [90]. This assumption is wrong as shown by several inconsistencies found in the solution at low temperatures: (i) the asymptotic values of one time-quantities do not necessarily coincide with the values calculated with the equilibrium distribution. (ii) The solution exhibited violates the fluctuation – dissipation theorem. These two results are not compatible with equilibrium.

In order to study the equilibrium dynamics of these models one should (i) start from random initial conditions but reach times that grow with N or (ii) impose equilibrium initial conditions. The second route has been implemented – though without solving the full dynamic problem – by Houghton *et al.* [80]. They showed that in this case one is forced to introduce the replica trick to average over disorder.

The dynamic equations here derived are correct when $N \rightarrow \infty$ at the outset. Since times are always finite with respect to N , when $t_{\text{EQ}}(N)$ diverges with N the dynamics is not forced to reach equilibrium and there is no contradiction if the solution violates the equilibrium theorems.

9.5 Single spin equation

In the limit $N \rightarrow \infty$ one can also write the full action S_{EFF} in terms of a *single* variable. This is at the expense of modifying the thermal kernel and the interaction term in a self-consistent way, through the introduction of terms arising from the non-linear interactions (the vertex and self-energy, respectively). For a classical model with white external noise the single variable equation reads

$$M\ddot{\phi}_i(t) + \gamma\dot{\phi}_i(t) + \mu(t)\phi_i(t) = \int_0^t dt'' \Sigma(t, t'') \phi_i(t'') + \rho_i(t) + \xi_i(t). \quad (9.56)$$

There are two noise sources in this equation: $\xi_i(t)$ is the original white noise while $\rho_i(t)$ is an effective (Gaussian) noise with zero mean and correlations self-consistently given by $\langle \rho_i(t)\rho_j(t') \rangle = \delta_{ij}D(t, t')$. The vertex $D(t, t')$ plays the rôle of the coloured noise correlation in a usual Langevin equation. The self-energy $\Sigma(t, t')$ appears here in the place of an “integrated friction”. A

solution of the problem can be attempted numerically using this equation and the self-consistent definitions of Σ and D .

This procedure is not particularly useful for the analysis of “polynomial” models since the transformation into a Q dependent effective action can be done exactly. It does however become useful for dealing with models whose single-spin effective action has higher order interaction terms. An example is the quantum SK model. This procedure is similar to the one used in dynamic mean-field theory [91].

Interestingly enough, as shown in Section 7.4, a rather flat harmonic oscillator coupled to a bath made of a white and a coloured part at different temperatures acquires two time-scales controlled by the two temperatures involved. We see that a similar structure might appear for the glassy system if the self-energy and vertex self-consistently arrange to act on each degree of freedom as the friction and noise-noise correlator of a complex bath. We shall see that this is indeed what happens to mean-field models. We believe that a similar mechanism arises in finite dimensional glassy models as well [72].

10 Diagrammatic techniques

In this section we first describe the perturbative solution to the Langevin process and how it is used to construct series expansions for the correlations and responses. Self-consistent approximations, such as the *mode coupling* or the *self-consistent screening*, correspond to a selection of a subset of diagrams from the full series. The connection with disordered models is demonstrated. The presentation is very close to the one in [92]. An extension to quantum problems is possible using the generating functional formalism.

10.1 Perturbative solution

Let us focus on a single scalar degree of freedom, q , with potential energy

$$V(q) = \frac{\mu(t)}{2} q^2 + \frac{g}{3!} q^3, \quad (10.1)$$

and dynamics given by the Langevin equations (4.7) and (4.8) in the white noise limit. We take the initial condition $q(t = 0) = 0$. $\mu(t)$ is a time-dependent function that we fix at the end of the derivation by requiring $C(t, t) = 1$. In vector models it is the Lagrange multiplier that self-consistently imposes a spherical constraint. Note that this potential is

not bounded from below. Setting $G_o(t, t') = [\mu(t) + \gamma\partial_t + M\partial_{t^2}]^{-1}$, a perturbative expansion for $q(t)$ in powers of the noise is easily written as

$$q(t) = (G_o \otimes \xi)(t) - \frac{g}{2} (G_o \otimes [G_o \otimes \xi \bullet G_o \otimes \xi])(t) + \dots \quad (10.2)$$

where \otimes means a time convolution, $(G_o \otimes f)(t) = \int_0^t dt' G_o(t, t') f(t')$, and \bullet is a simple product at equal times. This notation is equivalent to the one used in the SUSY formalism, see Appendix D. Causality implies $G_o(t, t') \propto \theta(t - t')$. If inertia can be neglected $G_o(t, t') = \exp\left(-\int_{t'}^t d\tau \mu(\tau)\right) \theta(t - t')$. If one keeps the second-time derivative $G_o(t, t')$ takes a more complicated form. Equation (10.2) can be graphically represented as in Figure 10. Crosses indicate noise and oriented lines indicate the bare propagator G_o . Each vertex carries a factor $g/2$. Note that the unknown q is evaluated at time t while the noises are evaluated at all previous times.

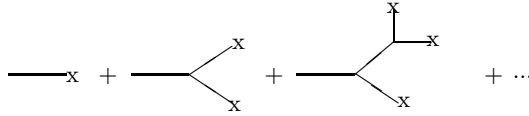


Fig. 10. Terms $O(g^0)$, $O(g^1)$ and $O(g^2)$ in the perturbative solution to the Langevin equation.

The expansion for q leads to two expansions for the correlation and response. In simple words, the former corresponds to sandwiching, *i.e.* averaging over the noise, the usual product of two series as the one in Figure 10 evaluated at different times t and t' . Due to the average over the Gaussian noise noise factors have to be taken by pairs. Let us illustrate this with a few examples.

The first term in the expansion is the result of averaging two $O(g^0)$ terms (first term in Fig. 10):

$$\begin{aligned} C_o(t, t') &= \langle (G_o \otimes \xi)(t) \bullet (G_o \otimes \xi)(t') \rangle \\ &= 2\gamma k_B T \int_0^{t'} dt'' G_o(t, t'') G_o(t', t''), \end{aligned} \quad (10.3)$$

$t \geq t'$. We depict this term and its contributions to more complicated diagrams with a single crossed line, see the first graph in Figure 11. The term $O(g)$, as well as all terms which are odd powers of g , vanishes. There are two contributions to the term $O(g^2)$. One is the result of multiplying a term $O(g^2)$ with a term $O(g^0)$ and it is a tadpole, see the second graph in Figure 11; we assume this term and all its corrections are included in the contributions from the time-dependent mass and we henceforth ignore

them. The other comes from multiplying two $O(g)$ terms, see the third graph in Figure 11.

Higher order terms are of two types: they either dress the *propagators* or they dress the *vertices*, see the last two diagrams in Figure 11. These two terms are $O(g^4)$. The first one follows from averaging two $O(g^2)$ contributions while the second one is the result of averaging an $O(g^3)$ and an $O(g)$ term. The full series yields the *exact perturbative expansion* for C .

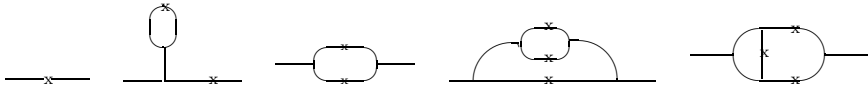


Fig. 11. From left to right: $O(g^0)$, two $O(g^2)$ and two $O(g^4)$ terms in the series for C . The next to last diagram dresses the propagator and the last term dresses the vertex. The former is kept in the MCA while the latter is neglected.

The series expansion for the response follows from the relation (8.8) in the white noise limit. In graphical terms we obtain it by multiplying the series in equation (10.2) and Figure 10 evaluated at time t by a noise evaluated at time t' and taking the average.

10.2 The mode coupling approximation (MCA)

The diagrammatic expansions for C and R can be represented analytically by introducing the kernels $\Sigma(t, t')$ and $D(t, t')$ through the Schwinger-Dyson equations (9.18) and (9.19) in their integral form. Each of them is a compact notation for a series of diagrams. These equations are exact perturbatively. However, for a generic model one cannot compute the kernels Σ and D exactly.

The mode coupling approach amounts to approximating the kernels $\Sigma(t, t')$ and $D(t, t')$ in the following way. One takes their values at $O(g^2)$ and substitutes in them the bare propagator G_0 and the bare correlation C_0 by their dressed values, *i.e.* by R and C themselves. For the model defined in equation (10.1) this yields

$$\Sigma(t, t') = g^2 C(t, t') R(t, t'), \quad (10.4)$$

$$D(t, t') = 2\gamma k_B T \delta(t - t') + \frac{g^2}{2} C^2(t, t'). \quad (10.5)$$

This approximation neglects “vertex renormalization” in the sense that all diagrams correcting the values of the lines are taken into account while all diagrams correcting the vertices are neglected. For instance, one keeps the fourth diagram in Figure 11 that represents a line correction, while leaving

aside the fifth diagram drawn in the same figure that represents a vertex correction.

The same procedure can be implemented using the SUSY representation of the dynamics. Each line represents the superfield and the super-correlator follows from the sandwich of two series for the super-field evaluated at different super-coordinates a and b .

The Schwinger-Dyson equations can be recast, after multiplying by G_o^{-1} , into the form (9.16) and (9.17) for a random potential (9.2) with only one term $r = p = 3$. Applying the MCA to the trivial (and ill-defined) model (10.1) we derived the dynamic equations for the $p = 3$ spin spherical model! On the one hand, this result is worrying since it shows that the MCA can be rather uncontrolled and it can generate glassy behavior by itself. On the other hand, since the same equations hold in the MCA of a model of interacting particles with realistic interactions, this calculation allows one to understand why the dynamic equations of the MCT for super-cooled liquids coincide with the ones of disordered spin models above T_d . In the next subsection we show how the diagrams neglected in the MCA vanish in a disordered model with a large number of components. (See also [93] for other recent discussions of the meaning and range of validity of the MCA and MCT.)

10.3 MCA and disordered models

The first to notice that the MCA for a “quadratic” dynamic equation corresponds to the exact dynamic equation of a disordered problem with a large number of components was Kraichnan [94] in the context of the Navier-Stokes equation. More recently, Franz and Hertz showed that the “schematic MCT equations of the F_p group” for super-cooled liquids are identical to those arising from a spin model with pseudo-random interactions between groups of three spins [95]. (The schematic MCT focus on a chosen wavevector).

Indeed, for the example chosen in this section, one easily demonstrates that the diagrams retained by the MCA are precisely those which survive if one modifies the initial model (10.1) and considers instead the following disordered problem [92]. First, let us upgrade q to a vector with N components or “colors” ϕ_i , where $i = 1, 2, \dots, N$. Second, let us modify the potential energy (10.1) into

$$V(\vec{\phi}) = g \sum_{i < j < k} J_{ijk} \phi_i \phi_j \phi_k \quad (10.6)$$

with couplings J_{ijk} that are independent quenched Gaussian random variables of zero mean and variance $[J_{ijk}^2]_J = 1/N^{p-1} = 1/N^2$. (p is the number

of spins in each term in V .) In the large N limit, the noise and disorder averaged correlation and response of this modified model obey equations (9.16) and (9.17) with Σ and D given by equations (10.4) and (10.5), respectively. The fact that these equations are recovered can be seen either directly on the perturbation theory, or using the functional methods given in Section 8. Since we want to stress that the diagrams neglected in the MCA vanish exactly for this model we use here the first approach.

The bare propagator is diagonal in the color indices, $G_{oij} = G_o \delta_{ij}$. The vertex is now proportional to the random exchanges J_{ijk} . The perturbative solution to the Langevin equation reads

$$\phi_i(t) = (G_o \otimes \xi_i)(t) - J_{ijk} G_o \otimes (G_o \otimes \xi_j \bullet G_o \otimes \xi_k)(t) + \dots \quad (10.7)$$

One is interested in computing the self-correlation averaged over the noise and disorder, $N^{-1} \sum_{i=1}^N [\langle \phi_i(t) \phi_i(t') \rangle]$. The latter average eliminates all terms with an odd number of couplings. Similarly, since $J_{ijk} \neq 0$ only if all indices i, j, k are different, tadpole contributions as the one in the second graph in Figure 11 vanish (the noise-noise correlation enforces that two indices in the random exchange must coincide). Finally, one can check that due to the scaling with N of the variance of the disordered interactions, vertex corrections as the one in the last graph in Figure 11 are sub-leading and vanish when $N \rightarrow \infty$. Instead, all line corrections remain finite in the thermodynamic limit. We can check this statement in the two examples shown in Figure 11 extended to include color indices. The vertex correction has four random exchanges that due to the averaging over the noise are forced to match as, e.g. $J_{ijk} J_{jlm} J_{mni} J_{kln}$ leaving 6 free-indices. Averaging over disorder one identifies the indices of two pairs of J 's, e.g. $i = l$ and $k = m$, this yields a factor $(1/N^2)^2$ and, at most, it leaves 4 color indices over which we have to sum from 1 to N (i, j, k, n). We have then an overall factor $1/N^4 \times N^4 = 1$ and this term vanishes when one normalises the correlation by N . Instead, in the line correction, after averaging over the noise, we are left with 6 free indices, e.g. $J_{ikj} J_{klm} J_{lmn} J_{inj}$, the average over the noise only imposes $k = n$ in its most convenient contribution, and the overall factor is $1/N^4 \times N^5 = N$. This term contributes to the normalised global correlation.

Interestingly enough, the equivalence between the MCA and a disordered system extends to an arbitrary *non-linear* coupling $F(q)$. Expanding F in a power series $F(q) = \sum_{r=2}^{\infty} \frac{F_r}{r!} q^r$ the MCA leads to

$$\Sigma(t, t') = g^2 \sum_{r=2}^{\infty} \frac{F_r^2}{(r-1)!} C^{r-1}(t, t') R(t, t'), \quad (10.8)$$

$$D(t, t') = 2\gamma k_B T \delta(t - t') + g^2 \sum_{r=2}^{\infty} \frac{F_r^2}{r!} C^r(t, t'). \quad (10.9)$$

[Note that for r odd, there appears an additional “tadpole” contribution in equation (10.8), which we have assumed again that it has been re-absorbed into the mass term $\mu(t)$.] The dynamic equations can also be obtained as the exact solution of the Langevin dynamics of N continuous spins ϕ_i interacting through the potential

$$V_J \left[\vec{\phi} \right] = g \sum_{r \geq 2} F_r \sum_{i_1 < \dots < i_{r+1}} J_{i_1 \dots i_{r+1}} \phi_{i_1} \dots \phi_{i_{r+1}} \quad (10.10)$$

where $J_{\alpha_1, \dots, \alpha_{r+1}}$ are quenched independent Gaussian variables with zero mean and $[(J_{\alpha_1, \dots, \alpha_{r+1}})^2] \propto N^{-r}$. Therefore the MC equations for a single dynamic variable in contact with a heat reservoir and under an arbitrary nonlinear potential $F(q)$ describe exactly a fully-connected spin-glass problem with arbitrary multi-spin interactions or a particle evolving in an N dimensional space in a quenched random potential $V[\vec{\phi}]$ with a Gaussian distribution with zero mean and variance (9.3) [89, 96]. Let us note that in order to be well defined, the model given by V must be supplemented by a constraint preventing the field ϕ_i from exploding in an unstable direction set by the coupling tensor $J_{i_1 \dots i_{r+1}}$. This problem is cured by imposing the spherical constraint $\sum_{i=1}^N \phi_i^2(t) = NC(t, t) \equiv N$.

The extension of the mapping to a space dependent $\phi(\vec{x}, t)$ (or to a multicomponent field) is straightforward. Several interesting physical examples involve an equation of the type:

$$\begin{aligned} \frac{\partial \hat{\phi}(\vec{k}, t)}{\partial t} = & -(\nu k^2 + \mu) \hat{\phi}(\vec{k}, t) \\ & - \sum_{r=2}^{\infty} \sum_{\vec{k}_1, \dots, \vec{k}_r} \frac{F_r}{r!} \mathcal{L}_r(\vec{k} | \vec{k}_1, \dots, \vec{k}_r) \hat{\phi}(\vec{k}_1, t) \dots \hat{\phi}(\vec{k}_r, t) + \xi(\vec{k}, t) \end{aligned}$$

where $\hat{\phi}(\vec{k}, t)$ is the Fourier transform of $\phi(\vec{x}, t)$, and $\xi(\vec{k}, t)$ a Gaussian noise such that $\langle \xi(\vec{k}, t) \xi(\vec{k}', t') \rangle = 2\gamma k_B T \delta(\vec{k} + \vec{k}') \delta(t - t')$. The Kardar-Parisi-Zhang (KPZ) equation [97] corresponds to $r = 2$, $\mathcal{L}_2(\vec{k} | \vec{k}_1, \vec{k}_2) = [\vec{k}_1 \cdot \vec{k}_2] \delta(\vec{k}_1 + \vec{k}_2 + \vec{k})$, while domain coarsening in the ϕ^4 theory corresponds to $r = 3$, $\mathcal{L}_3(\vec{k} | \vec{k}_1, \vec{k}_2, \vec{k}_3) = \delta(\vec{k}_1 + \vec{k}_2 + \vec{k}_3 + \vec{k})$, with a negative μ [1]. The Navier-Stokes equation is similar to the KPZ case with, however, an extra tensorial structure due to the vector character of the velocity field. The correlation and response functions now become \vec{k} dependent, $\delta^d(\vec{k} + \vec{k}') C(\vec{k}, t, t') = \langle \vec{\phi}(\vec{k}, t) \vec{\phi}(\vec{k}', t') \rangle$ and $\delta^d(\vec{k} + \vec{k}') R(\vec{k}, t, t') = \langle \partial \vec{\phi}(\vec{k}, t) / \partial \xi(\vec{k}', t') \rangle$. The generalized MC equations then read (assuming

that the structure factors are invariant under the permutation of $\vec{k}_1, \dots, \vec{k}_r$:

$$\begin{aligned} \Sigma(\vec{k}, t, t') &= g^2 \sum_{r=2}^{\infty} \frac{F_r^2}{(r-1)!} \sum_{\vec{k}_1, \dots, \vec{k}_r} \mathcal{L}_r(\vec{k}|\vec{k}_1, \dots, \vec{k}_r) \mathcal{L}_r(\vec{k}_r|\vec{k}_1, \dots, \vec{k}) \\ &\quad \times C(\vec{k}_1, t, t') \dots C(\vec{k}_{r-1}, t, t') R(\vec{k}_r, t, t') \end{aligned} \quad (10.11)$$

$$\begin{aligned} D(\vec{k}, t, t') &= 2\gamma k_B T \delta(t - t') + g^2 \sum_{r=2}^{\infty} \frac{F_r^2}{r!} \sum_{\vec{k}_1, \dots, \vec{k}_r} \left(\mathcal{L}_r(\vec{k}|\vec{k}_1, \dots, \vec{k}_r) \right)^2 \\ &\quad \times C(\vec{k}_1, t, t') \dots C(\vec{k}_r, t, t') \end{aligned} \quad (10.12)$$

where $\Sigma(\vec{k}, t, t')$ and $D(\vec{k}, t, t')$ are defined in analogy with equations (10.8) and (10.9).

10.4 MCA for super-cooled liquids and glasses

In the last 20 years the MCA has been much used in the study of super-cooled liquids. Starting from the realistic interactions between the constituents of a liquid, Götze *et al.* [98] used the MCA together with an assumption of equilibrium to derive a dynamic equation for the density-density correlator. This analysis led to the *schematic mode coupling theory* (MCT) [99] of super-cooled liquids and generalisations [100] (with no reference to wave-vector dependence) and to more sophisticated versions that include a dependence on space [98]. The difference between these models lies on the form of the kernels Σ and D . Kirkpatrick *et al.* [11] realized in the late 80 s that the schematic mode coupling equation [99] is identical to the dynamic equation for the spin-spin correlator in the disordered Potts or p spin model, building a bridge between the study of structural and spin glasses. Why these models and not SK? This will become clear when we present their dynamic and static behavior.

In this section we explained why the dynamic equation of a disordered model and the one stemming from a MCA of a model with more realistic interactions coincide: the terms neglected in the latter vanish exactly in the former. The example studied here serves also to signal the danger in using a MCA. One could conclude that a trivial model has a highly non-trivial dynamics, this being generated by the approximation itself.

In the derivation of the dynamic equations presented in this section no assumption of equilibrium was used. Therefore, these equations hold also in the low temperature phase where equilibrium is lost. It is then natural to propose that the dynamics of the p spin spherical model below T_d schematically describes the dynamics of glasses just as its dynamics above

T_d yields the schematic MCT of super-cooled liquids [13]. To go beyond the schematic theory while still keeping a single mode description (as in [100]) one simply has to consider $p_1 + p_2$ spherical disordered models. Moreover, the dynamics of a manifold in a random potential is described by dynamic equations with a \vec{k} dependence that goes beyond the single mode MCT.

Recently, Latz showed how the generic dynamic equations derived in this section can also be obtained starting from the microscopic fluid system and using the MC approximation though with no equilibration assumption [102]. Alternative derivations of mode-coupling equations are discussed in [93].

Kawasaki & Kim [103] derived the same schematic MC equation using a non-disordered quadratic Hamiltonian for densities and velocities complemented with random non-linear dynamic equations. Interestingly enough, in this case the MCT arises from a model with *trivial* statics and complex dynamics. Tuning the ratio between the number of density variables and velocity variables they even managed to include the so-called “hopping term” that softens the dynamic transition [98, 101]. It is worth noting that in Kawasaki and Kim’s model this term *is not* due to thermally activated processes but to the effect of the velocity-like variables through the complex dynamics.

11 Glassy dynamics: Generic results

Before presenting the explicit solution to the mean-field models we state some generic features of the low- T dynamics that we believe hold in general.

11.1 The weak-ergodicity breaking scenario

Figure 12-right shows a sketch of the decay of the correlation as obtained from the numerical solution to the dynamic equations for the mean-field models (see Sect. 12.1). It develops a separation of time scales in the long t' limit. It first approaches a plateau at q_{EA} in a stationary manner and it then decays below this value with an explicit waiting-time dependent form. For each waiting-time there is a sufficiently long t such that the correlation decays to zero. These properties are included in the *weak-ergodicity breaking* (WEB) scenario that states that, for $t \geq t'$, C decays in such a way that

$$\lim_{t' \rightarrow \infty} C(t, t') = q_{EA} + C_{ST}(t - t') \quad (11.1)$$

$$\lim_{t-t' \rightarrow \infty} C_{ST}(t - t') = 0 \quad \Rightarrow \quad \lim_{t-t' \rightarrow \infty} \lim_{t' \rightarrow \infty} C(t, t') = q_{EA} \quad (11.2)$$

$$\lim_{t \rightarrow \infty} C(t, t') = 0 \quad \text{at fixed } t'. \quad (11.3)$$

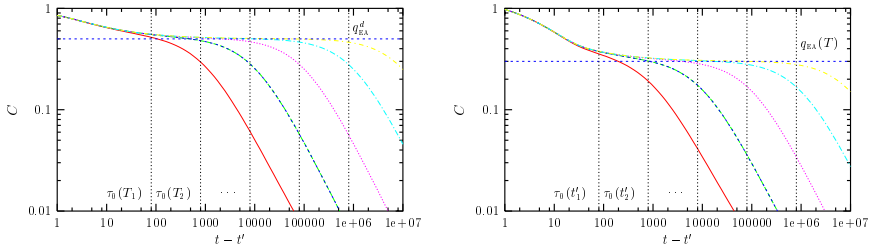


Fig. 12. Left: sketch of the decay of the stationary correlations in the high T phase close to T_d , $T_1 > T_2 > \dots$. Right: sketch of the decay of the aging correlations in the low T phase, at fixed $T < T_d$, $t'_1 < t'_2 < \dots$.

Equation (11.2) defines the Edwards-Anderson order parameter, q_{EA} . For finite t' there is a crossover between two time-scales controlled by a waiting-time dependent characteristic time $\tau_0(t')$ that is a growing function of t' whose precise form depends on the model. For large $t \geq t'$ such that $t - t'$ is small with respect to $\tau_0(t')$, the correlation function first decays from 1 to q_{EA} in a TTI manner. At longer $t - t'$ it goes further below q_{EA} to eventually reach 0 in a manner that depends both upon t and t' (the aging effect). This behavior suggests the presence of at least two time-sectors in which the dynamics is stationary and non-stationary, respectively. We shall see that the number of time-scales, or more precisely correlation scales, depends on the model.

We write C as the sum of a stationary and an aging contribution:

$$C(t, t') = C_{ST}(t - t') + C_{AG}(t, t'). \quad (11.4)$$

The matching conditions at equal times between C_{ST} and C_{AG} are $C(t, t) = 1$ implying $C_{ST}(0) + C_{AG}(t, t) = 1$ with $C_{ST}(0) = 1 - q_{EA}$ and $C_{AG}(t, t) = q_{EA}$. Together with equation (11.2) they ensure that in the two-time sector in which C_{ST} decays from $1 - q_{EA}$ to 0, C_{AG} is just a constant q_{EA} . Instead, in the two-time sector in which C_{AG} decays from q_{EA} to 0, C_{ST} vanishes identically.

The name WEB [12, 45] reflects the fact that for short time-differences the system behaves as if it were trapped in some region of phase space of “size” q_{EA} – suggesting ergodicity breaking. However, it is always able to escape this region in a time-scale $\tau_0(t')$ that depends upon its age t' . Hence, trapping is gradual and ergodicity breaking is *weak*. q_{EA} depends on temperature when $T < T_d$.

We have already described, phenomenologically, such a separation of time-scales in the decay of correlation functions when we discussed the domain growth problem and glassy dynamics in Section 2. The first term

describes in this case the fast fluctuations within domains while the second term characterises the domain growth itself. A second example where such a separation of time-scales occurs are the trap models in phase space. The first term corresponds to the dynamics within the traps while the second describes the wandering of the system from trap to trap. In glasses, the first term corresponds to the rapid rattling of each particle within its cage while the second one describes the destruction of the cages and hence the structural relaxation.

In driven models rendered stationary by a weak perturbation we also find a separation of time-scales with τ_0 increasing with weaker strengths of the perturbation. We can also propose that C and R separate in two terms, both being stationary but evolving in different time-scales.

In classical purely relaxational models governed by a Langevin equation with no inertia the correlation functions are monotonic with respect to both times t and t' , as it is easily checked numerically. Inertia introduces oscillations and the decay can be non-monotonic. The magnitude of the oscillations depends upon the relative value of the mass M with respect to the other parameters in the problem. However, for a wide choice of parameters the oscillations appear only in the stationary regime, the aging dynamics having a monotonic decay towards zero. This is relevant since it allows one to use the general properties of monotonic correlation functions proven in [104] and discussed in Section 11.4 to find the two-time scaling of $C_{AG}(t, t')$.

11.2 The weak long-term memory scenario

Regarding the response function, we propose a similar separation in two terms:

$$R(t, t') = R_{ST}(t - t') + R_{AG}(t, t') \quad (11.5)$$

with $R_{ST}(t - t') \equiv \lim_{t' \rightarrow \infty} R(t, t')$. The matching conditions close to equal times are different for a model with or without inertia. In the former case, $R(t, t) = 0$, $R(t, t^-) = 1/M$ while in the latter, using the Ito convention, $R(t, t) = 0$, $R(t, t^-) = 1/\gamma$. In both cases the equal-times condition implies $R_{ST}(0) = 0$, $R_{AG}(t, t) = 0$ while the next-to-main diagonal values yield $R_{ST}(\delta) = 1/M$, $R_{AG}(t, t - \delta) = 0$ and $R_{ST}(\delta) = 1/\gamma$, $R_{AG}(t, t - \delta) = 0$, respectively.

The response tends to zero when times get far apart, and its integral over a *finite* time-interval as well:

$$\lim_{t \rightarrow \infty} R(t, t') = 0, \quad \lim_{t \rightarrow \infty} \int_0^{t'} dt'' R(t, t'') = 0 \quad \forall \text{ fixed } t'. \quad (11.6)$$

These properties imply

$$\lim_{t-t' \rightarrow \infty} \lim_{t' \rightarrow \infty} R(t, t') = 0 \Rightarrow \lim_{t-t' \rightarrow \infty} R_{\text{ST}}(t - t') = 0, \\ \lim_{t \rightarrow \infty} R_{\text{AG}}(t, t') = 0. \quad (11.7)$$

However, the contribution of the response to the dynamic equations and to other measurable quantities is not trivial. Examining the integral of the response function over a growing time interval one finds that even if the response vanishes, it yields a contribution to the integration. Figure 15-left shows the integrated linear response (5.6). Using (11.5)

$$\chi(t, t') = \int_{t'}^t dt'' [R_{\text{ST}}(t - t'') + R_{\text{AG}}(t, t'')] = \chi_{\text{ST}}(t - t') + \chi_{\text{AG}}(t, t'). \quad (11.8)$$

If, for long enough t' , the contribution of the second term in (11.8) were negligible, $\chi(t, t')$ should be a stationary quantity. Instead, for all t' s studied and for t long enough one clearly sees a waiting-time dependence that can only come from the integration of the second term. This is a *weak long-term memory* (WLTm), the system has an “averaged” memory of its past.

When a system is in equilibrium, the response is simply related to the correlation *via* FDT. We then assume (and test on the dynamic equations) that the dynamics in the stationary regime satisfies FDT:

$$R_{\text{ST}}(\tau) = \frac{1}{k_{\text{B}}T} \frac{dC_{\text{ST}}(\tau)}{d\tau} \quad \tau \geq 0, \\ R_{\text{ST}}(\omega) = -\frac{2}{\hbar} \lim_{\epsilon \rightarrow 0^+} \int \frac{d\omega'}{2\pi} \frac{1}{\omega - \omega' + i\epsilon} \tanh\left(\frac{\beta\hbar\omega'}{2}\right) \tilde{C}_{\text{ST}}(\omega') \quad (11.9)$$

in a classical and quantum problem, respectively. One can formally prove that FDT has to hold for any generic relaxing model for short time-differences [105], see Section 11.5.4. For longer time-differences, when C_{AG} and R_{AG} vary in time while C_{ST} and R_{ST} have decayed to zero, one cannot assume the validity of FDT and, as we shall see, the equations have a solution that explicitly modifies FDT.

11.3 Slow time-reparametrization invariant dynamics

We have already mentioned that the correlations decay monotonically (only below q_{EA} if $M \neq 0$). The final insight coming from the numerical solution to the full equations is that the dynamics becomes slower and slower for fixed waiting-time and as $t - t'$ increases. In the stationary regime $\partial_{t^2}[C(t, t'), R(t, t')]$ and $\partial_{t^2}[C(t, t'), R(t, t')]$ are not negligible with respect to the terms in the RHS of equations (9.16) and (9.17). On the contrary, in

the second decay below q_{EA} , C and R decay in a much slower manner such that, $\partial_t C(t, t') \ll -\mu(t)C(t, t')$ and $\partial_{t^2} C(t, t') \ll -\mu(t)C(t, t')$ (similarly for R), and the time-derivatives can be neglected.

We choose the following strategy to solve the equations in the long t' limit where a sharp separation of time-scales can be safely assumed. First, we take advantage of the fact that one-time quantities approach a limit, as one can verify numerically, and write the asymptotic form of equation (9.23) for μ_∞ . The integrals on the RHS are approximated using the separation of C and R in two terms that vary in different time-scales that we assume are well-separated. We detail this calculation below. As regards to the equations for C and R , we proceed in two steps. On the one hand, we choose $t - t'$ short in such a way that $C > q_{\text{EA}}$ and we write the dynamic equations for C_{ST} and R_{ST} . On the other hand, we take t and t' widely separated so as $C < q_{\text{EA}}$ and we write the dynamic equations for C_{AG} and R_{AG} . In this way we double the number of unknown functions and equations but we simplify the problem enough as to make it solvable.

Once the time-derivatives are neglected and the integrals are approximated as we explain in Section 12.3.3 the aging equations become invariant under reparametrizations of time $t \rightarrow h(t)$ that transform the two-point functions as

$$C_{\text{AG}}(t, t') \rightarrow C_{\text{AG}}(h(t), h(t')), \quad R_{\text{AG}}(t, t') \rightarrow [d_{t'} h(t')] R_{\text{AG}}(h(t), h(t')). \quad (11.10)$$

This is not an exact invariance of the dynamic equations. It is only generated when dropping the time-derivatives. This invariance was first noticed by Sompolinsky [90] in his study of the equilibrium dynamics (see also [8]) and it later appeared in the nonequilibrium dynamics [12, 72, 96, 104, 106]. We shall see that this approximation forbids us to solve completely the dynamic equations, in particular, to fix the time scaling (select $h(t)$).

11.4 Correlation scales

Take three ordered times $t_3 \geq t_2 \geq t_1$. The correlations are $C(t_i, t_j) = \frac{1}{N} \sum_k \langle s_k(t_i) s_k(t_j) \rangle \equiv \cos \theta_{ji}$. The monotonicity of the decay of the correlations with respect to the longer time (keeping the shorter time fixed) and the shorter time (keeping the longer time fixed) allows us to derive general properties that strongly constrain the possible scaling forms. Indeed, one can relate any three correlation functions *via triangle relations* [104] constructed as follows. Using the fact that the decay is monotonic, one can invert the relation between correlation and times to write, for example, $t_2 = g(C(t_2, t_1), t_1)$ with $g: [0, 1] \times [0, \infty] \rightarrow [0, \infty]$. This allows us to rewrite

$C(t_3, t_1)$ as

$$C(t_3, t_1) = C(g(C(t_3, t_2), t_2), t_1) = C(g(C(t_3, t_2), g(C(t_2, t_1), t_1)), t_1). \quad (11.11)$$

We now define a real function $f(x, y)$, $f: [0, 1] \times [0, 1] \rightarrow [0, 1]$, by taking the limit $t_1 \rightarrow \infty$ while keeping the intermediate correlations fixed

$$\lim_{t_1 \rightarrow \infty} C(t_3, t_1) = f(C(t_3, t_2), C(t_2, t_1)).$$

$C(t_2, t_1)$ and $C(t_3, t_2)$ fixed

The fact that the limit exists is a reasonable working assumption. This function completely characterizes the correlations and their scales in the asymptotic limit. (Note that we defined f using the correlation between the longest time and the intermediate as the first argument.)

11.4.1 Properties

The definition of the function f , as well as the properties shown in this subsection, are model independent. The form taken by f for each model is determined by the dynamic equations.

Time reparametrization invariance. The function f is invariant under reparametrizations of time that satisfy (11.10).

Associativity. Take now four times $t_4 \geq t_3 \geq t_2 \geq t_1$. The correlation between t_4 and t_1 can be written in two ways

$$\begin{aligned} C(t_4, t_1) &= f(C(t_4, t_2), C(t_2, t_1)) = f(f(C(t_4, t_3), C(t_3, t_2)), C(t_2, t_1)), \\ C(t_4, t_1) &= f(C(t_4, t_3), C(t_3, t_1)) = f(C(t_4, t_3), f(C(t_3, t_2), C(t_2, t_1))). \end{aligned}$$

Thus f satisfies $f(f(x, y), z) = f(x, f(y, z))$, *i.e.* it is an associative function.

Identity. If one takes $t_1 = t_2$

$$C(t_3, t_1) = f(C(t_3, t_2), C(t_2, t_1)) = f(C(t_3, t_1), C(t_1, t_1)) = f(C(t_3, t_1), 1), \quad (11.12)$$

for all $C(t_3, t_1) \in [0, 1]$. Equivalently, if one takes $t_2 = t_3$

$$C(t_3, t_1) = f(C(t_3, t_2), C(t_2, t_1)) = f(C(t_3, t_3), C(t_3, t_1)) = f(1, C(t_3, t_1)), \quad (11.13)$$

for all $C(t_3, t_1) \in [0, 1]$. The correlation at equal times acts as the identity since $x = f(x, 1)$ and $y = f(1, y)$ for all $x, y \in [0, 1]$.

Zero. Taking t_3 and t_2 much larger than t_1 in such a way that $C(t_2, t_1) \sim 0$ and $C(t_3, t_1) \sim 0$ while $C(t_3, t_2) > 0$,

$$0 \sim C(t_3, t_1) = f(C(t_3, t_2), C(t_2, t_1)) \sim f(C(t_3, t_2), 0). \quad (11.14)$$

Equivalently, taking $t_3 \gg t_2$ and t_1 , then $C(t_3, t_2) \sim 0$ and $C(t_3, t_1) \sim 0$ while $C(t_2, t_1) > 0$ and one has

$$0 \sim C(t_3, t_1) = f(C(t_3, t_2), C(t_2, t_1)) \sim f(0, C(t_2, t_1)). \quad (11.15)$$

The minimum correlation acts as a zero of $f(x, y)$ since $0 = f(x, 0)$ and $0 = f(0, y)$ for all $x, y \in [0, 1]$. (This property can be easily generalised if the correlation approaches a non-zero limit.)

Bound. Given that we assume that the system drifts away in phase space, $C(t_2, t_1)$ decays as a function of t_2 for t_1 fixed, and $C(t_2, t_1)$ increases as a function of t_1 for t_2 fixed. This property implies

$$\begin{aligned} y = f(1, y) &\geq f(x, y) \quad \forall y, x < 1, \\ x = f(x, 1) &\geq f(x, y) \quad \forall x, y < 1. \end{aligned} \quad (11.16)$$

Therefore $f(x, y) \leq \min(x, y)$.

Forms for f . In [104] we proved that

$$f(x, y) = j^{-1}(j(x)j(y)) \quad \text{Isomorphic to the product} \quad (11.17)$$

$$f(x, y) = \min(x, y) \quad \text{Ultrametricity} \quad (11.18)$$

are the only possible forms that satisfy the properties of f shown above. Note that for j equal to the identity the first type of function becomes simply $f(x, y) = xy$, hence the name. It is also possible to prove that the first kind of function (11.17) is only compatible with the time scaling [104, 107]

$$C(t_2, t_1) = j^{-1}\left(\frac{h(t_2)}{h(t_1)}\right) \quad (11.19)$$

with $h(t)$ a monotonically growing function. The actual correlation can have a piecewise form. Here, instead of reproducing the proofs given in [104] we explain these statements reviewing the scaling forms found for some physical systems and in the analytic solution to mean-field models.

Examples: Domain growth

The correlation decays in two steps, see the right panel in Figure 12. For $C > q_{\text{EA}} = m_{\text{EQ}}^2$ the decay is stationary:

$$C_{21} \equiv C(t_2, t_1) = q_{\text{EA}} + C_{\text{ST}}(t_2 - t_1), \quad (11.20)$$

and it can be put in the form (11.19) using $h(t) = \exp(\ln t)$ and $j^{-1}(x) = q_{\text{EA}} + C_{\text{ST}}(x)$. Any three correlations satisfying (11.20) also verify

$t_3 - t_1 = C_{\text{ST}}^{-1}(C_{31} - q_{\text{EA}}) = t_3 - t_2 + t_2 - t_1 = C_{\text{ST}}^{-1}(C_{32} - q_{\text{EA}}) + C_{\text{ST}}^{-1}(C_{21} - q_{\text{EA}})$ that implies

$$C_{31} = C_{\text{ST}} [C_{\text{ST}}^{-1}(C_{32} - q_{\text{EA}}) + C_{\text{ST}}^{-1}(C_{21} - q_{\text{EA}})] + q_{\text{EA}}. \quad (11.21)$$

This equation is equivalent to (11.17). This means that any three correlations above q_{EA} can be related with an f that is isomorphic to the product, see (11.17), with $j_{\text{ST}}^{-1}(x) = C_{\text{ST}}(\ln x) + q_{\text{EA}}$ and $j_{\text{ST}}(x) = \exp(C_{\text{ST}}^{-1}(x - q_{\text{EA}}))$.

When the times are such that the domain walls move, the self-correlation decays below q_{EA} in an aging manner, with

$$C_{21} \equiv C(t_2, t_1) = C_{\text{AG}}(t_2, t_1) = j_{\text{AG}}^{-1} \left(\frac{\mathcal{R}(t_2)}{\mathcal{R}(t_1)} \right), \quad (11.22)$$

$j_{\text{AG}}^{-1}(1) = q_{\text{EA}}$ and $j_{\text{AG}}^{-1}(0) = 0$. It is obvious that any three correlations below q_{EA} also satisfy (11.17).

Take now $t_3 = t_2 + \tau_{32}$ with $\tau_{32} < \tau_0(t_2)$ and $C_{32} > q_{\text{EA}}$, and t_3 and t_2 sufficiently larger than t_1 ($t_3 = t_1 + \tau_{31}$ with $\tau_{31} > \tau_0(t_1)$ and $t_2 = t_1 + \tau_{21}$ with $\tau_{21} > \tau_0(t_1)$) such that $C_{31} < q_{\text{EA}}$ and $C_{32} < q_{\text{EA}}$. One has

$$\begin{aligned} C_{31} &= j_{\text{AG}}^{-1} \left(\frac{\mathcal{R}(t_3)}{\mathcal{R}(t_1)} \right) = j_{\text{AG}}^{-1} \left(\frac{\mathcal{R}(t_3)}{\mathcal{R}(t_2)} (j_{\text{AG}} \otimes j_{\text{AG}}^{-1}) \left(\frac{\mathcal{R}(t_2)}{\mathcal{R}(t_1)} \right) \right) \\ &= j_{\text{AG}}^{-1} \left(\frac{\mathcal{R}(t_3)}{\mathcal{R}(t_2)} j_{\text{AG}}(C_{21}) \right) \sim C_{21}. \end{aligned}$$

The last identity is a consequence of $\mathcal{R}(t_3)/\mathcal{R}(t_2) \sim 1$ since for a sufficiently small τ_{32} , $\mathcal{R}'(t_2)\tau_{32}/\mathcal{R}(t_2) \ll 1$.

Thus, when the times are such that two correlations, say with values a and b , are both greater than q_{EA} one explores the dynamics in the stationary regime and $f(a, b)$ is isomorphic to the product. When they are both smaller than q_{EA} one explores the dynamics in the aging coarsening regime and again $f(a, b)$ is isomorphic to the product though with a different function j . Finally, if $a > q_{\text{EA}}$ and $b < q_{\text{EA}}$, $f(a, b) = \min(a, b)$ and one finds dynamic ultrametricity.

The structure discussed in the context of the domain growth problem is indeed generic. Some special values of the correlation act as “fixed points” of $f(a, a)$, $f(a, a) = a$. A “correlation scale” spans the values of correlations comprised between two subsequent fixed points. Within a correlation scale f is isomorphic to the product. Any two correlations falling into different correlation scales are related by an ultrametric f . In the domain growth example 1, q_{EA} and 0 are fixed points that are simple to visualize physically. In more abstract models as the SK spin-glass the form of f is more involved, with a stationary scale between 1 and q_{EA} and a dense set fixed points, hence correlation scales, that fill the interval $[0, q_{\text{EA}}]$.

Scaling functions

Most solvable models, numerical data and experimental results can be described with only two correlation scales, a stationary and a slow one. Several scaling functions $h(t)$ for the slow decay have been proposed in the literature. In the following we summarize and discuss the main ones. In Figure 13 we compare the decay of the correlation from q_{EA} for three of the four laws discussed below.

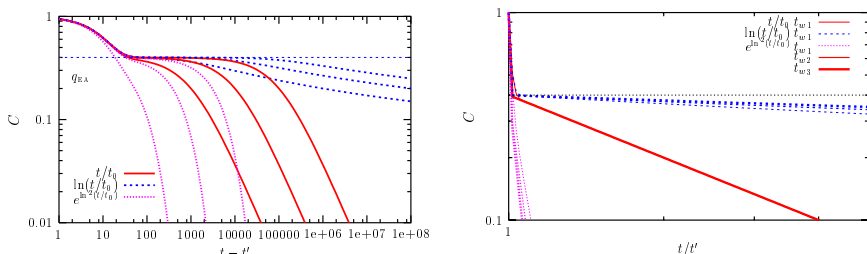


Fig. 13. Comparison between three $h(t)$ s, power law, enhanced power law and logarithm. Plot of $C(t, t') = (1 - q_{\text{EA}}) \exp(-(t - t')) + q_{\text{EA}} h(t)/h(t')$ against the time-difference $t - t'$ (on the left) and against the ratio of times t/t' (on the right) for three waiting times. Note the drift of the curves in the right panel. For the logarithmic law (sub-aging) the curves drift towards the left for increasing waiting-time. Instead, for the enhanced power law (super-aging) the curves drift to the right for increasing waiting-time. For the power law (simple aging) the scaling is perfect. In real systems the decay of the stationary part towards q_{EA} is much slower than exponential (typically power law with a small exponent) and the separation of time-scales is not so neat.

Power law: $h(t) = at^\alpha$. This is the simplest scaling also called *simple aging*. Ferromagnetic domain growth realizes this form with $\alpha = 1/2$ for non conserved dynamics and $\alpha = 1/3$ for conserved dynamics [1]. Several solvable model have simple aging, an example being the classical spherical $p = 2$ model [108, 109]. In [12] it was conjectured that a power law also characterized the aging dynamics of the fully connected p spin-model with $p \geq 3$. This was later confirmed with the algorithm of Kim & Latz [110] that allows one to reach much longer times. Aging below T_c in the simplest trap model also scales with this law [45]. The molecular dynamic simulations of Lennard-Jones mixtures show this type of scaling too. Note that for all α , C scales as a function of t_2/t_1 .

Enhanced power law: $h(t) = \exp(\ln^\alpha(t/t_0))$. This law yields the most accurate description of spin-glass experimental data. The exponent α typically takes a possibly T -dependent value about 2 [31].

Stretched exponential: $h(t) = \exp[(t/t_0)^\alpha]$. This law has been proposed to describe the slowing down of the full correlation above the critical temperature.

Logarithm: $h(t) = \ln^\alpha(t/t_0)$. In the Fisher and Huse droplet model for spin-glasses, activated dynamics is assumed and the domains are found to grow as $\mathcal{R}(t) \sim \ln(t/t_0)$. This leads to $C(t_2, t_1) \sim g(\ln(t_2/t_0)/\ln(t_1/t_0))$. However, this law does not fit the aging experimental data [31].

Dynamic ultrametricity: even though it seems mysterious at first sight there is a simple graphical construction that allows one to test it. Take two times $t_3 > t_1$ such that $C(t_3, t_1)$ equals some prescribed value, say $C(t_3, t_1) = 0.3 = C_{31}$. Plot now $C(t_3, t_2)$ against $C(t_2, t_1)$ using $t_2, t_1 \leq t_2 \leq t_3$, as a parameter. Depending on the value of C_{31} with respect to q_{EA} we find two possible plots. If $C(t_3, t_1) > q_{\text{EA}}$, for long enough t_1 , the function f becomes isomorphic to the product. Plotting then $C(t_3, t_2)$ for longer and longer t_1 , the construction approaches a limit in which $C(t_3, t_2) = j^{-1}(j(C_{31})/j(C(t_2, t_1)))$. If, instead, $C_{31} < q_{\text{EA}}$, in the long t_1 limit the construction approaches a different curve. We sketch in Figure 14 two possible outcomes of this construction. On the right, we represent a model with two correlation scales, ultrametricity holds between them and within each of them f is isomorphic to the product. On the left instead we represent a model such that dynamic ultrametricity holds for all correlations below q_{EA} . The construction approaches, in the long t_1 limit, the broken curve depicted in the sketch.

The SK spin-glass [104] and the dynamics of manifolds in an infinite dimensional embedding space in the presence of a random potential with long-range correlations [36, 96] have ultrametric decays everywhere within the aging regime. This scaling is also found in the trap model at the critical temperature [46]. Dynamic ultrametricity in finite dimensional systems has been search numerically. There is some evidence for it in the 4dEA model. In 3d instead the numerical data does not support this scaling [59, 111]. Whether this is due to the short times involved or if the asymptotic scaling is different in 3d is still an open question.

11.4.2 Definition of a characteristic time

Expanding the argument in (11.19) for $t_2 = t_1 + \tau$ with $\tau \ll t_1$ one finds, to leading order,

$$\frac{h(t_1)}{h(t_2)} = 1 - \frac{\tau}{t_c(t_1)} \quad t_c(t_1) \equiv \left(\frac{h'(t_1)}{h(t_1)} \right)^{-1}, \quad (11.23)$$

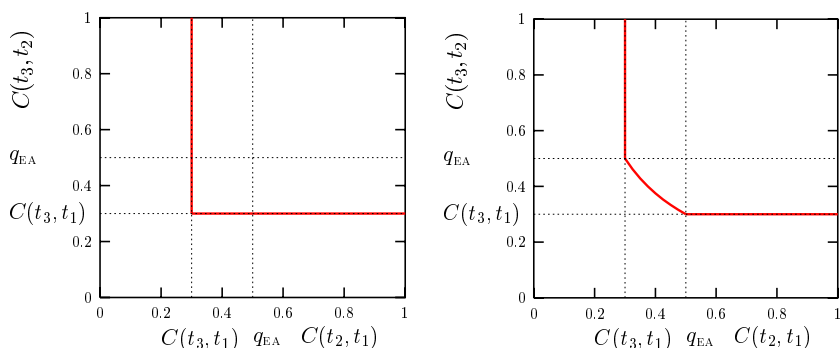


Fig. 14. Sketch of a check of ultrametricity using the parametric plot $C(t_3, t_2)$ against $C(t_2, t_1)$ for $C(t_3, t_1) = 0.3 < q_{\text{EA}}$ fixed. On the left an ultrametric model, on the right a model with two correlation scales.

with $O\left(\tau^2 \left(h'^2(t_1)/h^2(t_1) + h''(t_1)/h(t_1)\right)\right)$ corrections. The characteristic time $t_c(t_1)$ is given by

$$t_c(t_1) = \begin{cases} t_1/\alpha & \text{Power law} \\ t_1/[\alpha \ln^{\alpha-1}(t_1/t_0)] & \text{Enhanced power law} \\ t_1 (t_0/t_1)^\alpha & \text{Stretched exponential} \\ t_1 \ln(t_1/t_0) & \text{Logarithm.} \end{cases}$$

Note that $t_c(t_1)$ is defined close to the limit of equal times and (11.23) does not make sense for large τ . Rather often in the literature, the scaling variable $x = \tau/t_1^a$ has been used even for large values of τ . This scaling is incompatible with the general properties of the triangular relations recalled in Section 11.4.1 if the exponent a is larger than 1 [116]. See the right panel in Figure 13 to see the different trends of these scalings when plotted as functions of t/t' .

For the power law $t_c(t_1)$ scales just as t_1 . In the cases of the stretched exponential and the enhanced power law, $t_c(t_1)$ has a slower growth than the linear dependence iff $\alpha > 0$ in the first case and $\alpha > 1$ in the second. This behavior has been called *sub-aging*. For the logarithm $t_c(t_2)$ grows faster than linearly. This function belongs to a different class that we called *super aging* [31].

11.5 Modifications of FDT

One of the most important outcomes of the analytic solution to the mean-field glassy models [12, 104] is the need to modify the fluctuation–dissipation

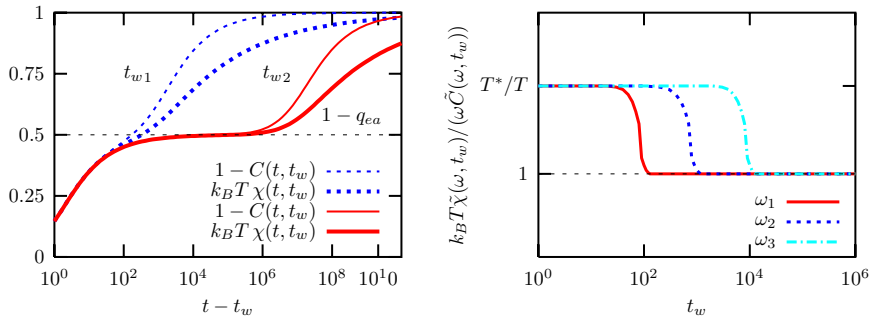


Fig. 15. Left: sketch of the modification of FDT in the time-domain. Right: sketch of the modification of FDT in the frequency domain for a glassy system, $\omega_1 > \omega_2 > \omega_3$.

relations between linear responses, $R(t, t_w)$, and their partner correlations between spontaneous fluctuations, $C(t, t_w)$, when $T < T_d$. In this subsection we discuss different ways of presenting the modification of FDT expected in rather generic systems with slow dynamics.

11.5.1 Time domain

The FDT is a linear relation between $\chi(t, t_w)$ and $C(t, t_w)$ for any pair of times (t, t_w) , see equation (7.3). In early simulations of the 3dEA model [57] as well as in the analytic solution to fully-connected disordered models a modification of this relation below T_d appeared [12]. Plotting $k_B T \chi(t, t_w)$ and $1 - C(t, t_w)$ for t_w fixed as a function of $\ln(t - t_w)$ one typically obtains the pair of curves schematically shown on the left panel of Figure 15. The two functions go together until $t - t_w$ reaches a characteristic time $\tau_0(t_w)$ and they then depart demonstrating that FDT does not hold beyond this time-scale. The characteristic time $\tau_0(t_w)$ is of the order of the time needed to reach the plateau in the correlation function (this holds asymptotically for mean-field models but it is not certain in finite dimensional systems). Summarizing

$$t - t_w < \tau_0(t_w) \quad \text{FDT holds in the fast scale,} \quad (11.24)$$

$$t - t_w > \tau_0(t_w) \quad \text{FDT is modified in the slow scale,} \quad (11.25)$$

with $\tau_0(t_w)$ an increasing function of t_w that depends on the system considered (see Fig. 12).

11.5.2 Frequency domain

As explained in Section 5.1 taking a Fourier transform with respect to the time-difference while keeping t_w fixed allows one to work in a mixed frequency-time domain. Since many experimental set-ups are prepared to apply ac-fields it is particularly important to predict the aspect FDT modification have when using these parameters. The condition $t - t_w < \tau_0(t_w)$ to explore the fast relaxation roughly translates into $\omega^{-1} < \tau_0(t_w)$, *i.e.* for a fixed waiting-time high frequencies are required. The longer the waiting time the lower the frequency one has to use to see this scale since $\tau_0(t_w)$ increases with t_w . Instead, when $t - t_w > \tau_0(t_w)$ one has $\omega^{-1} > \tau_0(t_w)$, and very low frequencies are needed to explore the slow scale. These conditions imply

$$\begin{aligned}\omega\tau_0(t_w) &> 1 && \text{FDT holds in the fast scale,} \\ \omega\tau_0(t_w) &< 1 && \text{FDT does not hold in the slow scale.}\end{aligned}\quad (11.26)$$

Reversing the argument above, if one weakly perturbs the sample with an ac-field of a fixed frequency ω_1 at a chosen time t_w , one can follow the deviation from FDT using t_w as the control parameter. This procedure yields the solid line on the right panel of Figure 15. Choosing now a lower frequency $\omega_2 (< \omega_1)$ the crossover from the slow to the fast regime occurs at a larger value of t_w . One obtains then the dotted curve on the right panel of Figure 15. So on and so forth, the smaller the frequency of the applied ac-field the longer the slow regime lasts and the longer one sees deviations from FDT. (Note that the probe does not modify the dynamics.) In the figure we chose to sketch the behavior of a system with only two-time scales, in which the FDT ratio takes two constant values separated at a single breaking point in which the correlation reaches the plateau value q_{EA} . This procedure is commonly employed experimentally, see Section 13.2 where we discuss the measurements of Grigera and Israeloff for glycerol [60].

11.5.3 Time-reparametrization invariant formulation

A more interesting way of displaying the modification of the FDT has been suggested by the analytic solution to the mean-field models discussed in Section 12.3. One of its advantages is that it allows one to classify the systems into sort of “universality classes” according to the form the FDT modification takes.

The analytic solution is such that, in the asymptotic limit in which the waiting-time t_w diverges after $N \rightarrow \infty$, the integrated linear response

approaches the limit

$$\lim_{\substack{t_w \rightarrow \infty \\ C(t, t_w) = C}} \chi(t, t_w) = \chi(C) \quad (11.27)$$

when t_w and t diverge while keeping the correlation between them fixed to C [104]. Deriving this relation with respect to the waiting time t_w , one finds that the opposite of the inverse of the slope of the curve $\chi(C)$ is a parameter that replaces temperature in the differential form of the FDT. Thus, using equation (11.27) one defines

$$k_B T_{\text{EFF}}(C) \equiv -(\chi'(C))^{-1}, \quad (11.28)$$

that can be a function of the correlation. Under certain circumstances one can show that this quantity has the properties of a temperature [112] in the sense to be described in Section 14.

One of the advantages of this formulation is that, just as in the construction of triangle relations, times have been “divided away” and the relation (11.27) is invariant under the reparametrizations of time defined in equation (11.10).

Equation (11.27) is easy to understand graphically. Let us take a waiting time t_w , say equal to 10 time units after the preparation of the system (by this we mean that the temperature of the environment has been set to T at the initial time) and trace $\chi(t, t_w)$ against $C(t, t_w)$ using t as a parameter (t varies between t_w and infinity). If we choose to work with a correlation that is normalized to one at equal times, the parametric curve starts at the point $(C(t_w, t_w) = 1, \chi(t_w, t_w) = 0)$ and it arrives at the point $(C(t \rightarrow \infty, t_w) \rightarrow \overline{C}, \chi(t \rightarrow \infty, t_w) = \overline{\chi})$. Without loss of generality we can assume that the correlation decays to zero, $\overline{C} = 0$. This first curve is traced in red in Figures 16. Now, let us choose a longer waiting time, say $t_w = 100$ time units, and reproduce this construction. One finds the green curves in Figures 16. Equation (11.27) states that if one repeats this construction for a sufficiently long waiting time, the parametric curve approaches a limit $\chi(C)$, represented by the blue curves.

When the system equilibrates with its environment, the construction approaches a straight line with slope $-1/(k_B T)$ as predicted by the FDT. This is the result shown in the left panel of Figure 16. Instead, for non-equilibrium systems evolving slowly the asymptotic limit is different, it is given by a *curve* $\chi(C)$. For solvable fully-connected models one distinguishes three families, as drawn in the right panel of Figure 16. They correspond to some systems undergoing domain growth [109] (*e.g.* the $O(N)$ model in $d = 3$ when $N \rightarrow \infty$), systems behaving like structural glasses [12, 36, 89] (*e.g.* the p -spin model) and spin-glasses [36, 89, 96, 104] (*e.g.* the SK model).

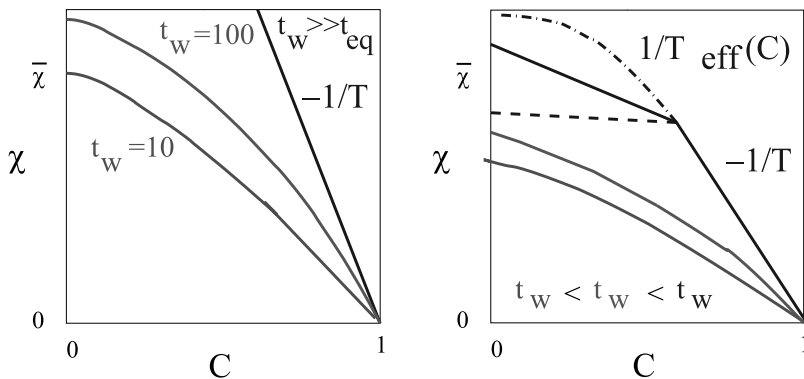


Fig. 16. The asymptotic behavior of the integrated linear response against the correlation in a parametric plot, for fixed waiting time and using t as a parameter. Left: behavior in equilibrium. Right: behavior in a slowly relaxing system out of equilibrium. See text for an explanation.

Several numerical studies in more realistic models of the three cases tend to confirm this classification [58]. However, two provisos are in order. First, one has to be very cautious about the numerical results given the very short time scales and rather small system sizes accessible in simulations [113]. Second, as shown in Section 13.1, at least one system that undergoes domain growth, the ferromagnetic chain, has a non-trivial $\chi(C)$ like the one found for the SK model.

We have already found these asymptotic $\chi(C)$ curves when we discussed the dynamics of a (flat) harmonic oscillator in contact with a complex bath made of subsystems with different characteristic times and temperatures (Sect. 7.4.4). Here we claim that the same structure arises in a glassy model coupled to a white-bath. Different values of the effective temperature are self-generated in the system.

This plot is invariant under reparametrisations of time $t \rightarrow h(t)$ acting on the two-point functions as in equations (11.10). A different choice of the functions h only changes the speed with which the $\chi(C)$ curve is traced but not its form.

11.5.4 FDT part

The formalism used in Section 7 to derive the FDT can be used to obtain a bound on FDT violations [105]. Indeed, one bounds the difference between response and variation of the correlation with the Cauchy-Schwartz

inequality leading to

$$|k_B T R(\tau + t_w, t_w) - \partial_s C(\tau + t_w, s)|_{s=t_w}| \leq c \sqrt{-d_{t_w} \mathcal{H}(t_w)} \quad (11.29)$$

where c is a constant and $\mathcal{H}(t_w) \equiv \int dq P(q, t_w) (E(q) - k_B T \ln P(q, t_w))$ is a positive definite function that monotonically decreases towards the free-energy when the system eventually equilibrates [70]. One finds a similar bound for Kramers processes and a generalization that includes the power input when time-dependent or non-potential forces are applied. For systems such that $d_{t_w} \mathcal{H}(t_w) \rightarrow 0$ sufficiently fast when $t_w \rightarrow \infty$ the bound implies that the LHS vanishes in this limit. This can be achieved in two ways: either each term is finite and the difference between them vanishes or each term tends to zero independently. The former possibility is what happens in the fast regime where FDT holds. The latter holds in the slow regime where both the response and the variation of the correlation are very small but the relation between them does not follow FDT. One derives a more useful bound by integrating (11.29) over time:

$$|k_B T \chi(\tau + t_w, t_w) - C(\tau + t_w, t_w) + C(t_w, t_w)| \leq c \int_{t_w}^{\tau+t_w} dt' \sqrt{-d_{t'} \mathcal{H}(t')}. \quad (11.30)$$

The terms in the LHS are now always finite while the value of the RHS depends on the relation between the time-difference τ and the waiting-time t_w . For sufficiently short τ such that the RHS vanishes FDT has to be satisfied in its integrated form. This result explains the existence of a common straight-line with slope $-1/(k_B T)$ in the nonequilibrium curves in Figure 16. For sufficiently long τ such that the RHS takes a finite value FDT can be violated. In this second scale a departure from the straight line of slope $-1/(k_B T)$ can occur and it is indeed what happens in systems with slow non-equilibrium dynamics, see the right panel in Figure 16. One sees how a separation of time-scales in the dynamics influences the FDT violations.

In driven systems the bound depends on the power input and only vanishes in the limit of vanishing applied forces. The FDT is not even enforced in the fast scale and deviations start as soon as C decays from 1. However, as we shall see below, the modification of FDT follow a very similar pattern to the one shown in Figure 16 with the strength of the applied force playing a similar role to the one of the waiting-time here.

11.5.5 Diffusion

In these Lectures we focus on models with a bounded self-correlation for an observable with zero average that is normalised at equal times. If the

averaged observable does not vanish but the equal-time correlation reaches a time-independent limit one can still use the simple self-correlation in the generalisations of FDT. However, in more general diffusive model with an unbounded time-dependent equal-time correlator it is more natural to compare the behaviour of the “displacement” $\Delta(t, t') \equiv C(t, t) + C(t', t') - 2C(t, t')$ (that vanishes by definition at equal times) to the linear response. In normal diffusion these are linked by $R(t, t') = 1/(2k_B T)\Delta(t, t')$. In glassy models like the massless manifold in a random potential and others this relation is modified [36, 37, 71, 163].

12 Solution to mean-field models

In this section we turn our attention to the solution to the Schwinger-Dyson equations derived in previous sections. We start by describing the simplest numerical algorithm that solves these equations and we briefly discuss the asymptotic analytic solution at high temperatures. Next we describe in quite detail the solution at low T .

12.1 Numerical solution

One can attempt a numerical solution to the set of causal integro-differential equations (9.16), (9.17) together with the equation for the Lagrange multiplier $\mu(t)$. One of the questions we would like to explore is whether they encode a non-equilibrium evolution as the one described in the Introduction and Section 2.

The correlation $C(t, t')$ and response $R(t, t')$ are two-time quantities, that is, they depend on t (which physically corresponds to the time of observation) and t' (which corresponds to the age of the system). In the simplest algorithm one discretises the two-times plane with a *uniform grid*, $t' = j\delta$ and $t = i\delta$. The correlation and response on the diagonal and the next-to-main diagonal of the two-times plane (i, j) are known, see equations (9.41) and (9.42), for all times.

The time-derivatives $\partial_t^2 C(t, t')$ and $\partial_t^2 R(t, t')$ in their discretized form are used to update the two-point functions. Due to causality, to advance one time step, the integrals only need values of C and R that are already known. This algorithm is simple and efficient but it is severely limited by the computer storage capacity. Since one has to store C and R for all previous time steps, the memory used grows as i^2 and this number becomes rather quickly prohibitive. In standard PCs one can use $i_{\text{MAX}} \sim 10^4$, get an acceptable precision for $\delta \leq 0.1$ and reach total times of the order of 10^3 .

In the quantum case the presence of non local kernels η and ν , that appear convoluted with C and R , renders the numerical solution harder. The larger the cut-off Λ , the smaller the iteration step δ we need to compute

these integrals with a good precision. The maximum total time is of the order of 10^2 in this case.

A different starting point for a numerical solution is the single variable equation (9.56). This route was followed by Eissfeller and Oppen for spin-glasses [114] and it is usually used in the so-called dynamic mean-field theory [91]. Again, this method is limited by the storage capacity.

The knowledge of the qualitative features of the solution helps one devising a more performant algorithm with a *variable two-time grid*. As we shall see from the analytic solution, C and R vary rapidly when times are near the diagonal $j = i$ and decay very slowly far from it. Kim & Latz have exploited this property and wrote such an algorithm for the spherical p spin model reaching total times of the order of 10^8 [110].

Finally, one can think of an iterative search where one starts from a trial form of C and R and uses the dynamic equations to extract the new form. One can expect to obtain the solution by repeating this procedure until the iteration converges to a fixed point. This method would allow one to look for solutions of the full set of Schwinger – Dyson equations that break causality.

The numerical solution for the causal problem, found with the simple uniform grid, has been of great help in deriving the asymptotic analytic solution. In the following we describe how this solution builds up.

12.2 Solution at high temperatures

At high temperature the system equilibrates with its environment since

$$t_{\text{EQ}}(N \rightarrow \infty, T) = \text{finite}. \quad (12.1)$$

The mere existence of an asymptotic limit implies that one-time quantities as, *e.g.*, the energy density, $\mathcal{E}(t)$, or the Lagrange multiplier, $\mu(t)$, have to approach an asymptotic limit, $\lim_{t \rightarrow \infty} \mathcal{E}(t) = \mathcal{E}_\infty$ and $\lim_{t \rightarrow \infty} \mu(t) = \mu_\infty$. In equilibrium $\mathcal{E}_\infty = \mathcal{E}_{\text{EQ}}$ and similarly for all one-time quantities. Two time-quantities, such as C and R , depend on times but only through time differences as explained in Section 6.

To solve the high T dynamics one first assumes that after a transient equilibrium is reached a solution of the form $\mu(t) \rightarrow \mu_\infty$,

$$C(t, t') \rightarrow C_{\text{ST}}(t - t'), \quad R(t, t') \rightarrow R_{\text{ST}}(t - t') \quad (12.2)$$

with R_{ST} and C_{ST} related by FDT, for long waiting-times t' and all time-differences $t - t'$, exists. These properties also apply to D and Σ that behave as a correlation and a response, respectively. This *Ansatz* should solve equations (9.16) and (9.17) when $T > T_d$, with T_d the dynamic critical temperature. In order to prove it we take t' long and we assume that we

can separate the integrals in equations (9.16) and (9.17) in a *preasymptotic* and an *asymptotic* contribution,

$$\int_0^\infty dt'' \dots \approx \int_0^{t_{\text{EQ}}} dt'' \dots + \int_{t_{\text{EQ}}}^\infty dt'' \dots \quad (12.3)$$

Next, we assume that the two-point functions decay as fast as to ensure that all preasymptotic contributions vanish, *e.g.* $\int_0^{t_{\text{EQ}}} dt'' A(t, t'')B(t', t'') \sim 0$ when t' and $t \geq t'$ are in the asymptotic regime. Using the *Ansatz* (12.2) and this assumption the integrals in the RHS of equation (9.17), for a classical problem, read

$$\begin{aligned} & \int_{t_{\text{EQ}}}^{t'} dt'' D_{\text{ST}}(t - t'') \frac{1}{k_{\text{B}}T} \frac{\partial C_{\text{ST}}(t' - t'')}{\partial t''} \\ & + \int_{t_{\text{EQ}}}^t dt'' \frac{1}{k_{\text{B}}T} \frac{\partial D_{\text{ST}}(t - t'')}{\partial t''} C_{\text{ST}}(|t'' - t'|) = \\ & \frac{1}{k_{\text{B}}T} \int_{t_{\text{EQ}}}^{t'} dt'' \frac{\partial}{\partial t''} [D_{\text{ST}}(t - t'') C_{\text{ST}}(t' - t'')] \\ & + \frac{1}{k_{\text{B}}T} \int_{t'}^t dt'' \frac{\partial D_{\text{ST}}(t - t'')}{\partial t''} C_{\text{ST}}(t'' - t'). \end{aligned}$$

The first integral in the RHS is a total derivative and it can be readily evaluated, it yields $D_{\text{ST}}(t - t')C_{\text{ST}}(0) - D_{\text{ST}}(t - t_{\text{EQ}})C_{\text{ST}}(t' - t_{\text{EQ}}) \approx D_{\text{ST}}(\tau)$ where we assumed that t and t' are well in the asymptotic regime in such a way that $C_{\text{ST}}(t' - t_{\text{EQ}}) \sim 0$, and we defined $\tau \equiv t - t'$. Integrating by parts the last integral in the RHS one finally obtains the high T equation for the correlation

$$\begin{aligned} G_{\text{o}}^{-1}(\tau)C_{\text{ST}}(\tau) &= \frac{1}{k_{\text{B}}T} D_{\text{ST}}(0)C_{\text{ST}}(\tau) \\ &\quad - \frac{1}{k_{\text{B}}T} \int_0^\tau d\tau' D_{\text{ST}}(\tau - \tau') d_{\tau'} C_{\text{ST}}(\tau') \quad (12.4) \end{aligned}$$

with $G_{\text{o}}^{-1}(\tau) = M d_{\tau^2} + \gamma d_{\tau} + \mu_{\infty}$. One can check that equation (9.16) coincides with equation (12.4) under the same assumptions. To prove this statement one has to integrate equation (9.16) with respect to t' from t_{EQ} to t' taking care of the fact that t' appears in the lower limit of the integral.

Equation (12.4) for the spherical p spin model coincides with the schematic MC equation [98, 115]. This equation has a decaying solution above a sharp critical temperature that we call $T_{\text{MCT}} = T_{\text{d}}$ where the assumptions of TTI and FDT are justified. After a short transient (eliminated

by the limit $t' \gg t_{\text{EQ}}$) the system equilibrates with its environment even if the thermodynamic limit has already been taken. At very high T the decay to zero is very fast and typical of, say, a high- T liquid. Closer to T_d , however, a very interesting structure appears. The solution takes the form sketched in the left panel in Figure 12. In a logarithmic scale one sees a two step relaxation develop with a first relatively quick decay towards a plateau at a value that we call q_{EA} and next a slower relaxation towards zero. The length of the plateau increases when temperature approaches T_d from above and it diverges at T_d . At T_d the height of the plateau, q_{EA}^d , follows from the asymptotic analysis of equation (12.4). If one loosely considers q_{EA}^d to be an order parameter, the high temperature analysis yields $q_{\text{EA}}^d > 0$ [see Eq. (12.32)] and the transition is *discontinuous*. It is important to stress that, as we shall see below, this does not mean that the model has a first order thermodynamic transition. All susceptibilities are continuous when going across T_d even though $q_{\text{EA}}^d > 0$. In the mode-coupling literature these transitions are called type B.

The details of the asymptotic analysis of the schematic MC equation and its relation with the behavior of real systems has been discussed at length in the literature (see, *e.g.* [115]). We shall not develop it here. With the purpose of future comparison with the low- T solution we just recall that the approach and departure from the plateau (*beta* relaxation) occurs with two power laws:

$$C_{\text{ST}}(\tau) \sim q_{\text{EA}}^d + c_a \tau^{-a} + \dots \quad C_{\text{ST}}(\tau) \sim q_{\text{EA}}^d - c_b \tau^b + \dots \quad (12.5)$$

given by

$$\frac{1}{k_B T_d} \frac{\Gamma^2(1+b)}{\Gamma(1+2b)} = \frac{1}{k_B T_d} \frac{\Gamma^2(1-a)}{\Gamma(1-2a)} = \frac{1}{2} \frac{\mathcal{V}'''(q_{\text{EA}}^d)}{(\mathcal{V}''(q_{\text{EA}}^d))^{3/2}}. \quad (12.6)$$

A similar analysis can be done for a quantum model.

12.3 Solution at low- T

Three families of mean-field models have been found so far. In this section we present the solution to the spherical mean-field descriptions of ferromagnetic domain growth and structural glasses in some detail. We use a generic notation that allows us to treat the classical and quantum problem simultaneously. The presentation follows [85]. By the end of this subsection we discuss the generalisation of these results to models of “spin-glass” type, models with spatial dependence and the effect of different microscopic dynamics.

The numerical solution to the dynamic equations at low T shows no evidence for an arrest in the waiting-time dependence of the decay of C

and R . In this regime of temperatures,

$$t_{\text{EQ}}(N, T < T_d) \rightarrow \infty \quad (12.7)$$

and the equations do not admit the choice of a $t' > t_{\text{EQ}}$. In order to consider the crossover towards the equilibration regime one should revisit the derivation of the dynamic equations allowing for N finite. This program has not been pursued in the literature and it remains one of the most interesting open problems in the field.

12.3.1 The Lagrange multiplier

We approximate the integral in equation (9.21) by separating its support in three intervals

$$t'': 0 \rightarrow \delta_0, \quad t': \delta_0 \rightarrow \Delta_t, \quad t'': \Delta_t \rightarrow t. \quad (12.8)$$

The first time-interval contains only finite times t'' . Hence, all correlations and responses of the form $C(t, t'')$ and $R(t, t'')$ vanish due to equations (11.3) and (11.7). In the last time-interval t'' is close to t in the sense that correlations of the kind $C(t, t'')$ are of the form $C_{\text{ST}}(t - t'') + q_{\text{EA}}$ and similarly for the responses. Finally, in the intermediate time-interval the C and R vary in the aging regime. Of course, we are sloppy in that we do not precise what are the values of δ_0 and Δ_t . The definitions of correlation scales given in Section 11.4 correct this imprecision exchanging the time limits by limits in the correlation. Within these assumptions the asymptotic value of $\mu(t)$ is given by

$$\begin{aligned} \mu_\infty = & A_\infty + q_{\text{EA}} \int_0^\infty d\tau' \Sigma_{\text{ST}}(\tau') + \tilde{D}_{q_{\text{EA}}} \int_0^\infty d\tau' R_{\text{ST}}(\tau') \\ & + \int_0^\infty d\tau' [\Sigma_{\text{ST}}(\tau') C_{\text{ST}}(\tau') + D_{\text{ST}}(\tau') R_{\text{ST}}(\tau')] + \text{Last} \end{aligned} \quad (12.9)$$

(see Appendix E). Σ and D are made of two terms, one contribution from the bath and one contribution from the interactions (see Eqs. (9.39) and (9.40)). We called Last a term that equals $-M \partial_\tau^2 C_{\text{ST}}(\tau)|_{\tau \rightarrow 0}$ in a model with inertia (classical or quantum) and simply $k_B T$ in classical models without inertia. A_∞ is the aging contribution:

$$A_\infty = \lim_{t \rightarrow \infty} \int_0^t dt'' [\Sigma_{\text{AG}}(t, t'') C_{\text{AG}}(t, t'') + D_{\text{AG}}(t, t'') R_{\text{AG}}(t, t'')]. \quad (12.10)$$

The bath does not contribute to the integrals in A_∞ when the kernels η and ν decay sufficiently fast to zero as to yield vanishing integrals. This is trivially true for a white noise. It can be a working assumption for colored

noises based on a weak limit of the strength of the coupling to the noise (see, however, [118]). More precisely, we are neglecting terms of the form $\lim_{t \rightarrow \infty} \int_0^t dt'' A(t-t'')B(t, t'')$ where A is either ν or η and B is either C_{AG} or R_{AG} . In this case

$$A_\infty = \lim_{t \rightarrow \infty} \int_0^t dt'' \left[\tilde{\Sigma}_{\text{AG}}(t, t'')C_{\text{AG}}(t, t'') + \tilde{D}_{\text{AG}}(t, t'')R_{\text{AG}}(t, t'') \right]. \quad (12.11)$$

The second and third terms in equation (12.9) come from the constant (non-zero) limit of the first decay of the correlation $q_{\text{EA}} \equiv \lim_{t-t' \rightarrow \infty} \lim_{t' \rightarrow \infty} \times C(t, t')$ and the vertex $\tilde{D}_{q_{\text{EA}}} \equiv \lim_{t-t' \rightarrow \infty} \lim_{t' \rightarrow \infty} \tilde{D}(t, t')$. For the classical spherical p spin model $\tilde{D}_{q_{\text{EA}}} = \frac{p}{2} q_{\text{EA}}^{p-1}$ and this equation also holds for its quantum extension if we use $\lim_{\tau \rightarrow \infty} R_{\text{ST}}(\tau) \ll q_{\text{EA}}$, a property of the WLTM scenario. The integral over the stationary parts can be simply performed using FDT for classical problems but it cannot in quantum problems.

12.3.2 The stationary regime

If (t, t') are such that $C(t, t') > q_{\text{EA}}$, $C(t, t') = q_{\text{EA}} + C_{\text{ST}}(t-t')$ and $R(t-t') = R_{\text{ST}}(t-t')$. The Schwinger-Dyson equation for R in this time sector reads

$$(M\partial_\tau^2 + \mu_\infty) R_{\text{ST}}(\tau) = \delta(\tau) + \int_0^\tau d\tau' \Sigma_{\text{ST}}(\tau - \tau') R_{\text{ST}}(\tau') \quad (12.12)$$

and it keeps the same form as in the high-temperature phase, apart from the fact that the constant μ_∞ has contributions from the aging regime. The Schwinger-Dyson equation for C reads

$$\begin{aligned} (M\partial_\tau^2 + \mu_\infty) (q_{\text{EA}} + C_{\text{ST}}(\tau)) = \\ A_\infty + q_{\text{EA}} \int_0^\infty d\tau' \Sigma_{\text{ST}}(\tau') + \tilde{D}_{q_{\text{EA}}} \int_0^\infty d\tau' R_{\text{ST}}(\tau') \\ + \int_{-\infty}^\infty d\tau' [\Sigma_{\text{ST}}(\tau + \tau')C_{\text{ST}}(\tau') + D_{\text{ST}}(\tau + \tau')R_{\text{ST}}(\tau')]. \end{aligned} \quad (12.13)$$

One can now Fourier-transform both equations

$$\begin{aligned} R_{\text{ST}}(\omega) &= \frac{1}{-M\omega^2 + \mu_\infty - \Sigma_{\text{ST}}(\omega)}, \quad (12.14) \\ (-M\omega^2 + \mu_\infty) C_{\text{ST}}(\omega) + \mu_\infty q_{\text{EA}} \delta(\omega) &= \left(A_\infty + q_{\text{EA}} \Sigma_{\text{ST}}(\omega) + \tilde{D}_{q_{\text{EA}}} R_{\text{ST}}(\omega) \right) \\ &\quad \times \delta(\omega) + \Sigma_{\text{ST}}(\omega) C_{\text{ST}}(\omega) + D_{\text{ST}}(\omega) \\ &\quad \times R_{\text{ST}}(-\omega). \end{aligned}$$

The formal solution to the equation for C_{ST} is

$$C_{\text{ST}}(\omega) = \left(-\mu_{\infty} q_{\text{EA}} + A_{\infty} + q_{\text{EA}} \Sigma_{\text{ST}}(\omega) + \tilde{D}_{q_{\text{EA}}} R_{\text{ST}}(\omega) \right) \times \delta(\omega) R_{\text{ST}}(\omega) + D_{\text{ST}}(\omega) |R_{\text{ST}}(\omega)|^2. \quad (12.15)$$

The first term on the RHS has an imaginary and a real part. The imaginary part vanishes identically since, due to FDT, both $\text{Im} R_{\text{ST}}(\omega)$ and $\text{Im} \Sigma_{\text{ST}}(\omega)$ are proportional to $\tanh(\beta \hbar \omega / 2)$ which is zero at $\omega = 0$ for classical and quantum problems. Concerning the real part of this first term, as we have assumed that $C_{\text{ST}}(\tau)$ goes to zero for $\tau \rightarrow \infty$, we need to impose the self-consistent condition

$$-\mu_{\infty} q_{\text{EA}} + A_{\infty} + q_{\text{EA}} \Sigma_{\text{ST}}(\omega = 0) + \tilde{D}_{q_{\text{EA}}} R_{\text{ST}}(\omega = 0) = 0. \quad (12.16)$$

This is the condition that fixes q_{EA} . We shall find it again in the next section as the matching condition between the stationary and aging regimes. The final equation for $C_{\text{ST}}(\omega)$ is

$$C_{\text{ST}}(\omega) = D_{\text{ST}}(\omega) |R_{\text{ST}}(\omega)|^2. \quad (12.17)$$

One can check that these calculations are consistent with the results from μ_{∞} . Actually, the integrals in equation for $\mu(t)$ involving the stationary parts can be evaluated with the help of the equations for R_{ST} and C_{ST} , equations (12.14) and (12.15), and yield once again equation (12.16).

Similarly to the high-temperature case one can now show that FDT for $\tilde{\Sigma}_{\text{ST}}$ and \tilde{D}_{ST} implies FDT for R_{ST} and C_{ST} . The remainder of the proof, *i.e.* to show that FDT between R_{ST} and C_{ST} implies FDT between $\tilde{\Sigma}_{\text{ST}}$ and \tilde{D}_{ST} depends only upon the form of $\tilde{\Sigma}_{\text{ST}}$ and \tilde{D}_{ST} as functions of R_{ST} and C_{ST} and is not modified from the one discussed in Section 12.2.

12.3.3 The aging regime

If we now choose the times t, t' to be well-separated so as to have $C(t, t') = C_{\text{AG}}(t, t') \leq q_{\text{EA}}$ and $R(t, t') = R_{\text{AG}}(t, t')$, the WEB and WLTM hypotheses allow us to throw the second time derivatives on the LHS. We assume that their contribution is much weaker than the one of each of the integral terms on the RHS. This is an assumption that we have to verify at the end of the calculation, once the solution for C_{AG} and R_{AG} is known. It corresponds to the over-damped limit.

Using the approximation described in Appendix E, the equation for R in the aging regime becomes

$$\begin{aligned} \mu_\infty R_{\text{AG}}(t, t') = & \tilde{\Sigma}_{\text{AG}}(t, t') \int_0^\infty d\tau' R_{\text{ST}}(\tau') + R_{\text{AG}}(t, t') \int_0^\infty d\tau' \Sigma_{\text{ST}}(\tau') \\ & + \int_{t'}^t dt'' \tilde{\Sigma}_{\text{AG}}(t, t'') R_{\text{AG}}(t'', t') \end{aligned} \quad (12.18)$$

and we call it the R_{AG} -eq. Similarly, the equation for C becomes

$$\begin{aligned} \mu_\infty C_{\text{AG}}(t, t') = & C_{\text{AG}}(t, t') \int_0^\infty d\tau' \Sigma_{\text{ST}}(\tau') + \tilde{D}_{\text{AG}}(t, t') \int_0^\infty d\tau' R_{\text{ST}}(\tau') \\ & + \int_0^t dt'' \tilde{\Sigma}_{\text{AG}}(t, t'') C_{\text{AG}}(t'', t') + \int_0^{t'} dt'' \tilde{D}_{\text{AG}}(t, t'') R_{\text{AG}}(t'', t') \end{aligned} \quad (12.19)$$

and we call it the C_{AG} -eq. In all integrals over the slow regime we neglected the contributions of the noise kernels η and ν and we approximated $\Sigma_{\text{AG}}(t, t') \sim \tilde{\Sigma}_{\text{AG}}(t, t')$ and $D_{\text{AG}}(t, t') \sim \tilde{D}_{\text{AG}}(t, t')$ (again, see [118] for a discussion on the effect of a strong bath).

12.3.4 The Edwards-Anderson parameter

The Edwards-Anderson parameter, q_{EA} , is determined self-consistently from the matching of $\lim_{t \rightarrow \infty} C_{\text{AG}}(t, t) = \lim_{t \rightarrow \infty} \lim_{t' \rightarrow \infty} C(t, t') = q_{\text{EA}}$. Taking the limit $t' \rightarrow t^-$ in the R_{AG} -eq and C_{AG} -eq one obtains

$$\mu_\infty R_{\text{AG}}(t, t) = \tilde{\Sigma}_{\text{AG}}(t, t) \int_0^\infty d\tau' R_{\text{ST}}(\tau') + R_{\text{AG}}(t, t) \int_0^\infty d\tau' \Sigma_{\text{ST}}(\tau'), \quad (12.20)$$

$$\mu_\infty q_{\text{EA}} = A_\infty + q_{\text{EA}} \int_0^\infty d\tau' \Sigma_{\text{ST}}(\tau') + \tilde{D}_{\text{AG}}(t, t) \int_0^\infty d\tau' R_{\text{ST}}(\tau'). \quad (12.21)$$

The first equation admits the solution $R_{\text{AG}}(t, t) = 0$ since $\tilde{\Sigma}_{\text{AG}}(t, t)$ is proportional to $R_{\text{AG}}(t, t)$ – see equation (9.39). This corresponds to the high-temperature solution where there is no aging regime. Here we concentrate on the other possibility. The response becomes smaller and smaller as time passes – though its integral over an infinite interval gives a finite contribution. If we neglect all terms that are proportional to $R_{\text{AG}}(t, t)$ with respect to terms that are proportional to q_{EA} , only the first term in the power expansions of $\tilde{\Sigma}$ and \tilde{D} survive and

$$\left(\tilde{\Sigma}/R \right)_{q_{\text{EA}}} \equiv \lim_{t \rightarrow \infty} \frac{\tilde{\Sigma}_{\text{AG}}(t, t)}{R_{\text{AG}}(t, t)} \quad \tilde{D}_{q_{\text{EA}}} \equiv \lim_{t \rightarrow \infty} \tilde{D}_{\text{AG}}(t, t) \quad (12.22)$$

that for the p spin model become

$$\left(\tilde{\Sigma}/R\right)_{q_{\text{EA}}} = \frac{p(p-1)}{2} q_{\text{EA}}^{p-2} \quad \tilde{D}_{q_{\text{EA}}} = \frac{p}{2} q_{\text{EA}}^{p-1}, \quad (12.23)$$

in accord with the large τ limit of the stationary values (see Sect. 12.3.2). Equations (12.20) and (12.21) become

$$\mu_{\infty} = \left(\tilde{\Sigma}/R\right)_{q_{\text{EA}}} \int_0^{\infty} d\tau' R_{\text{ST}}(\tau') + \int_0^{\infty} d\tau' \Sigma_{\text{ST}}(\tau'), \quad (12.24)$$

$$\mu_{\infty} q_{\text{EA}} = A_{\infty} + q_{\text{EA}} \int_0^{\infty} d\tau' \Sigma_{\text{ST}}(\tau') + \tilde{D}_{q_{\text{EA}}} \int_0^{\infty} d\tau' R_{\text{ST}}(\tau'). \quad (12.25)$$

The second equation is the same as the one arising from the end of the stationary regime, equation (12.16).

From equations (12.16) and (12.17) one derives

$$\int_0^{\infty} d\tau R_{\text{ST}}(\tau) = R_{\text{ST}}(\omega = 0) = \frac{1}{\mu_{\infty} - \Sigma_{\text{ST}}(\omega = 0)}, \quad (12.26)$$

and

$$1 = \left(\tilde{\Sigma}/R\right)_{q_{\text{EA}}} R_{\text{ST}}^2(\omega = 0). \quad (12.27)$$

We remind that the factor $R_{\text{ST}}^2(\omega = 0)$ can be written in terms of the stationary correlation function using FDT; therefore this is a closed equation for the correlation that determines q_{EA} . In the case of the p -spin model it reads

$$1 = \frac{p(p-1)}{2} q_{\text{EA}}^{p-2} \left(\frac{1}{\hbar} P \int_{-\infty}^{\infty} \frac{d\omega'}{\omega'} \tanh\left(\frac{\beta\hbar\omega'}{2}\right) \tilde{C}_{\text{ST}}(\omega') \right)^2. \quad (12.28)$$

In the classical case, the integral can be readily computed and the final equation for q_{EA} is

$$\frac{p(p-1)}{2} q_{\text{EA}}^{p-2} (1 - q_{\text{EA}})^2 = (k_{\text{B}}T)^2, \quad (12.29)$$

that coincides with the result for the purely relaxational dynamics [12]. For $p \geq 3$ fixed, q_{EA} is a function of temperature. Equation (12.29) can be solved graphically. The LHS has a bell shape. It vanishes at $q_{\text{EA}} = 0, 1$ and it reaches a maximum at $q_{\text{EA}}^{\text{MAX}} = (p-2)/p$. The equation has two solutions for all temperatures $(k_{\text{B}}T)^2 < (k_{\text{B}}T^{\text{MAX}})^2 = p(p-1)/2 [(p-2)/p]^{p-2} (2/p)^2$, these merge at T^{MAX} and disappear for higher T 's. The physical solution corresponds to the branch on the right of the maximum, the one that continues the solution $q_{\text{EA}} = 1$ at $T = 0$. The minimum value of q_{EA} is reached at the dynamic critical temperature $T_{\text{d}} (< T^{\text{MAX}})$, where $q_{\text{EA}}^{\text{d}} \equiv q_{\text{EA}}(T_{\text{d}}) > q_{\text{EA}}^{\text{MAX}}$.

12.3.5 Fluctuation – dissipation relation

In order to advance further we have to relate the response to the correlation. If we *assume* that

$$R_{\text{AG}}(t, t') = \frac{1}{k_{\text{B}}T^*} \frac{\partial C_{\text{AG}}(t, t')}{\partial t'}, \quad (12.30)$$

with T^* the value of an effective temperature (see Sect. 14) that is determined by equations (12.25) and (12.26) $0 = A_{\infty} - \frac{q_{\text{EA}}}{R_{\text{ST}}(\omega=0)} + \tilde{D}_{q_{\text{EA}}} R_{\text{ST}}(\omega=0)$. Using equation (12.30) and the equivalent relation between $\tilde{\Sigma}_{\text{AG}}$ and \tilde{D}_{AG} , we obtain $A_{\infty} = (k_{\text{B}}T^*)^{-1} \lim_{t \rightarrow \infty} \left(\tilde{D}_{\text{AG}}(t, t) C_{\text{AG}}(t, t) \right) = (k_{\text{B}}T^*)^{-1} q_{\text{EA}} \tilde{D}_{q_{\text{EA}}}$ and

$$\frac{1}{k_{\text{B}}T^*} = \frac{(p-2)}{q_{\text{EA}}} R_{\text{ST}}(\omega=0) = \sqrt{\frac{2(p-2)^2}{p(p-1)}} q_{\text{EA}}^{-p/2}. \quad (12.31)$$

In the classical limit $T/T^* = (p-2)(1-q_{\text{EA}})/q_{\text{EA}}$ and the result in [12] is recovered. Note that both in the classical and quantum case, $T^* \rightarrow \infty$ if $p=2$. Since the case $p=2$ is formally connected to ferromagnetic domain growth in $d=3$ (in the mean-field approximation) there is no memory neither in the classical nor in the quantum domain growth.

The *Ansatz* in equation (12.30) solves classical *and* quantum aging equations. The modification of the FDT in this regime became thus classical even when quantum fluctuations exist. This is an interesting sort of decoherent effect that will become clearer when we shall discuss the interpretation of this results in terms of effective temperatures.

Using equation (12.30) for all values of C below q_{EA} we assumed that there is only one aging correlation scale in the problem. Interestingly enough, one can do a more general analysis using the formalism described in Section 11.4 and find that the dynamic equations force the solution to have only one aging correlation scale [78].

12.3.6 Discontinuous classical transition

The classical dynamic critical point ($T_{\text{d}}, \hbar=0$) can arise either when $q_{\text{EA}} \rightarrow 0$ or when $T^* \rightarrow T$. For the p spin model, using equations (12.29) and (12.31) the latter holds and [12]

$$(k_{\text{B}}T_{\text{d}})^2 = \frac{p(p-2)^{p-2}}{2(p-1)^{p-1}} \quad q_{\text{EA}}^{\text{d}} = \frac{p-2}{p-1}. \quad (12.32)$$

The transition is *discontinuous* since the order parameter q_{EA} jumps at T_{d} . However, it is still of *second order* thermodynamically since there are no thermodynamic discontinuities, all susceptibilities being continuous

across T_d . For instance,

$$\lim_{t \gg t_w} \chi(t, t_w) = \frac{1}{k_B T} (1 - q_{EA}) + \frac{1}{k_B T^*} q_{EA} \rightarrow \frac{1}{k_B T} \quad \text{when } T \rightarrow T^* \text{ at } T_d. \quad (12.33)$$

The dynamic transition occurs at a value T_d that is higher than the static transition temperature T_s . The latter is fixed as the temperature where replica symmetry breaking occurs (using the standard prescription to fix the parameters in the Parisi *Ansatz* to compute the free-energy density) [166]. This feature is an explicit realisation of the discussion on T_g and T_0 in Section 2. They are sharp in this model.

12.3.7 The classical threshold level

The asymptotic energy density reads $\mathcal{E}_\infty = -\frac{1}{p} \int_0^\infty dt'' [\Sigma(t, t'') C(t, t'') + D(t, t'') R(t, t'')]$ where we used equation (9.24). Replacing the solution found above we obtain

$$\mathcal{E}_\infty = -\frac{1}{2} \left[\frac{1}{k_B T} (1 - q_{EA}^p) + \frac{1}{k_B T^*} q_{EA}^p \right] \equiv \mathcal{E}_{TH}. \quad (12.34)$$

If one compares this expression with the equilibrium energy density, found studying the partition function [166], one discovers that [12]

$$\mathcal{E}_\infty = \mathcal{E}_{TH} > \mathcal{E}_{EQ}. \quad (12.35)$$

Thus, the non-equilibrium dynamics does not approach the equilibrium level asymptotically but it reaches a *threshold* level that is extensively higher than equilibrium (note that the inequality (12.35) holds for the energy density). The name *threshold* is motivated by a similarity with *percolation* (in phase space) that we shall discuss in Section 15 [12].

12.3.8 Two p models

In Section 12.3.4 we took the limit $t' \rightarrow t^-$, or equivalently, $C_{AG} \rightarrow q_{EA}^-$ in the equations for the slow part of the response and the correlation and this lead us to equations (12.27) and (12.31) for q_{EA} and T^* . Let us now take subsequent variations of this equation with respect to the correlation and evaluate them in the same limit. It is easy to see that if we neglect the contributions from the integral between t' and t , assuming that the integrands are analytic in this limit, we get new equations linking T^* and q_{EA} that, for generic models, are not compatible. Indeed, as we shall see below, the pure spherical p spin model is the only one for which the solution is given by an analytic function $j^{-1}(x)$ when $x \rightarrow 1^-$.

The way out of this contradiction is to propose that the correlation approaches the plateau at q_{EA} with a power law decay and that it departs from it with another non-trivial power law [36, 89]:

$$C_{\text{ST}}(t - t') = (1 - q_{\text{EA}}) + c_a^{(1)}(t - t')^{-a} + c_a^{(2)}(t - t')^{-2a} + \dots \quad (12.36)$$

$$C_{\text{AG}}(t, t') = q_{\text{EA}} - c_b^{(1)} \left(1 - \frac{h(t')}{h(t)}\right)^b - c_b^{(2)} \left(1 - \frac{h(t')}{h(t)}\right)^{2b} + \dots \quad (12.37)$$

with $c_a^{(i)}$ and $c_b^{(i)}$ constants. If the exponent b is smaller than one, the integrals generated by taking derivatives with respect to C_{AG} do not vanish when $t' \rightarrow t^-$. The expansion of the stationary and aging equations around q_{EA} fix the exponents a and b . One finds [89]

$$\frac{1}{k_{\text{B}}T^*} \frac{(\Gamma(1+b))^2}{\Gamma(1+2b)} = \frac{1}{k_{\text{B}}T} \frac{(\Gamma(1-a))^2}{\Gamma(1-2a)} = \frac{1}{2} \frac{\mathcal{V}'''(q_{\text{EA}})}{(\mathcal{V}''(q_{\text{EA}}))^{3/2}} \quad (12.38)$$

that are to be confronted to equations (12.5) and (12.6) for the high T behavior. We recall that $\mathcal{V}(C)$ is the correlation of the random potential. Importantly enough, the exponents a and b are now T -dependent and they are related *via* an equation in which T^* enters.

Classical spherical p spin model

Since $\mathcal{V}(C) = C^p/2$ using equations (12.27) and (12.31) to fix T^* and q_{EA} one finds $(\Gamma(1+b))^2/\Gamma(1+2b) = 1/2$ and $b = 1$ for all $T < T_{\text{d}}$. The exponent a interpolates between $a = 1/2$ at $T \rightarrow 0$ and $a = 1$ at $T \rightarrow T_{\text{d}}$ since $(\Gamma(1-a))^2/\Gamma(1-2a) = T/(2T^*)$.

Classical mixed $p_1 + p_2$ spherical spin model

For adequate choices of the coefficients in $\mathcal{V}(C) = a_1/2C^{p_1} + a_2/2C^{p_2}$ (see Sect. 12.3.9) one finds T -dependent exponents $a(T)$ and $b(T)$.

Ultrametric limit

It is interesting to notice that $(\Gamma(1+b))^2/\Gamma(1+2b)$ is bounded by one. Thus, equation (12.38) constrains the random potentials for which a solution with only two correlation scales exists. For a particle in a power-law correlated random potential one sees that the transition towards an ultrametric-like solution arrives when the potential goes from short-range to long-range correlated [89]. To our knowledge this has not been found in a static calculation. An interpretation of the exponents a and b , and this consequence, in terms of the properties of the TAP free-energy landscape is not known either.

12.3.9 SK model and similar

A different family of models, to which the SK model belongs, are solved by an ultrametric *Ansatz*, $C_{31} = f(C_{32}, C_{21})$, for all correlations below q_{EA} . The $\chi(C)$ plot yields a non-trivial curve (instead of a straight line) for $C \in [0, q_{\text{EA}}]$. The transition is continuous $q_{\text{EA}}^{\text{d}} = 0$. These models are called type A in the MCT literature.

Indeed, for a generic disordered model with random potential correlated as in equation (9.3), one finds that the solution is ultrametric if and only if [89]

$$\frac{\mathcal{V}'''(C)}{\mathcal{V}'''(q_{\text{EA}})} \left(\frac{\mathcal{V}''(q_{\text{EA}})}{\mathcal{V}''(C)} \right)^{3/2} < 1. \quad (12.39)$$

This bound constrains, for instance, the values of the coefficients in a polynomial random potential for which the dynamic solution is ultrametric. The FDT is modified with a C dependent factor given by $T/T_{\text{EFF}}(C) = q_{\text{EA}} \mathcal{V}'''(C) \sqrt{\mathcal{V}''(q_{\text{EA}})} / (4(\mathcal{V}''(C))^{3/2})$.

12.3.10 Mode dependence

The models we solved so far have no spatial dependence. The manifold problem (2.8) has an internal structure that leads to a mode-dependence. This model has been solved for generic potential correlations [36]. We summarize the outcome without presenting its detailed derivation. All modes are slaved to one in the sense that one has to solve for the dynamics of one of them and the mode-dependence follows from an algebraic equation. The value of the effective temperature does not depend on the mode. The mathematical reason for this is the slaved structure of the equations. The physical reason is that all interacting observables evolving in the same time-scale have to partially equilibrate and acquire the same effective temperature (see Sect. 14). The height of the plateau, q_{EA} , is a k dependent quantity. The approach to it and departure from it also depends on k but only *via* the prefactors; the exponents a and b , see equations (12.36) and (12.37), are the same for all modes.

Mode-coupling equations including a wave-vector dependence have been derived by Latz using the Mori-Zwanzig formalism; the structure of the solution to these equations shares the properties just described [102].

12.3.11 Quantum fluctuations

The simplest effect of quantum fluctuations is to introduce oscillations in the first step of relaxation. These disappear at long enough time-differences and they are totally suppressed from the second decay, that superficially looks classical [85, 106].

The Edwards-Anderson parameter q_{EA} depends upon T and \hbar . As expected, quantum fluctuations introduce further fluctuations in the stationary regime and they decrease the value of q_{EA} , $q_{\text{EA}}(T, \hbar \neq 0) < q_{\text{EA}}(T, \hbar \rightarrow 0)$.

The modification of FDT in the quantum model is of a rather simple kind: R_{AG} and C_{AG} are related as in the classical limit. For the quantum extension of the p spin model there are two correlation scales, one with the temperature of the environment, T , the other with another value of the effective temperature, T^* , that depends on T , \hbar and the characteristics of the environment. This is a kind of decoherent effect.

As regards to the transition from the glassy to the liquid or paramagnetic phase, an interesting effect appears. Keeping all other parameters fixed, the plane $(T, \Gamma \equiv \hbar^2/(JM))$ is separated in these two phases by a line that joins the classical dynamic critical point $(T_d, \Gamma = 0)$ and the quantum dynamic critical point $(T = 0, \Gamma_d)$. Close to the classical dynamic critical point the transition is discontinuous but of second order thermodynamically until it reaches a tricritical point where it changes character to being of first order. This behavior is reminiscent of what has been reported for the quantum spin-glass studied in [14].

A still more dramatic effect of quantum mechanics is related to the very strong role played by the quantum environment on the dynamics of a quantum system. Indeed, the location of the transition line depends very strongly on the type of quantum bath considered and on the strength of the coupling between system and environment [118].

12.3.12 Driven dynamics

The effect of non potential forces can be mimicked with a force as the one in (2.7) [18, 19] where the strength of the force, α , is analogous to the shear stress σ . For strengths that are not too strong, the dynamics presents a separation of time scales with a fast approach to the plateau and a slow escape from it that is now, however, also stationary. Indeed, after a characteristic time t_{SH} the full dynamics becomes stationary though the system is still far from equilibrium. One defines a structural relaxation time, τ_α , as the time needed to reach, say, a correlation equal to a half. One relates the structural relaxation to the viscosity *via* $\eta \equiv \int dt C(t)$. The scaling of η with the shear rate $\dot{\gamma} \equiv \sigma/\eta$ has been successfully confronted to the behavior in rheological experiments in super-cooled liquids and glasses [19]. In terms of the general scalings discussed in Section 11.4, the correlations are characterised by two different functions j , one for the fast decay towards the plateau and another for the slow decay from the plateau, while the functions $h(t)$ are simple exponentials.

Interestingly enough, from the study of FDT violations above (though close to) and below T_d , when the forcing is weak, one extracts a still

well-defined slope of the $\chi(C)$ plot when C evolves in the slow scale [18, 19, 121]. This means that an effective temperature can also be identified for these systems kept explicitly out of equilibrium (see also [171]).

Oscillatory forces, as the ones used to perturb granular matter, have a different effect. Aging is not stopped in a finite region of the phase diagram (T -strength of the force-frequency of the force) [26]. An effective temperature can still be defined as the slope of the $\chi(C)$ plot drawn using stroboscopic time, with a point per oscillatory cycle.

13 Modifications of FDT in physical systems

In this section we discuss the realizations of the modifications of FDT in each of the physical systems presented in Section 2.

The asymptotic curves in Figure 16 have a rather peculiar form. They are linear with slope $-1/(k_B T)$ when the correlation decreases from 1 to the plateau value q_{EA} . After this breaking point, when the correlation decays towards zero, the curve is non-trivial, taking the three forms described in Section 11.5.3 for ferromagnetic domain-growth (in $d > d_c$), structural glasses and spin-glasses. The separation between these two parts is sharp when the dynamics has a sharp separation of time-scales. In Section 11.5.4 we gave a formal explanation for the existence of the first scale where FDT holds for any relaxing system. Here and in the two next subsections we give more intuitive arguments for the validity of FDT in the fast regime in the context of the physical systems discussed in the Introduction.

For the sake of comparison we show in Figure 18 the form of the $\chi(C)$ plot for a p spin model adapted to mimic a structural glass (the original model), a sheared liquid or glass, vibrated granular matter and a quantum glass.

13.1 Domain growth

The separation of time-scales is easy to visualize in the case of a system undergoing domain growth. If the two times t and t_w are not very different, the domain walls do not move between t and t_w and the dynamics consists of spin flips within the domains due to thermal fluctuations. This dynamics is identical to the equilibrium dynamics since the system can be thought of as being a patchwork of independent equilibrated finite systems of linear size $\mathcal{R}(t_w)$. It is then natural that the FDT holds in this time scale. On the contrary, if t grows in such a way that τ becomes of the order of $\mathcal{R}(t_w)$, the domains grow and the non-equilibrium dynamics takes place. The motion of the domain walls in the presence of an external perturbing random field introduced to measure the staggered response is due to two competing factors: on the one hand, the system tends to diminish the curvature of the

interfaces due to surface tension, on the other hand the random field tends to pin the domain walls in convenient places. The full response of the walls is approximately [119]

$$\chi_I(\tau + t_w, t_w) \approx \rho(\tau + t_w) \chi_s(\tau + t_w, t_w) \approx \mathcal{R}^{-1}(\tau + t_w) \chi_s(\tau + t_w, t_w) \quad (13.1)$$

where $\rho(\tau + t_w)$ is the density of interfaces and $\chi_s(\tau + t_w, t_w)$ is the integrated response of a single wall. The contribution of a single interface depends on dimensionality and, for a ferromagnetic Ising model with first neighbor interactions and non-conserved order parameter it has been estimated to be

$$\chi_s(\tau + t_w, t_w) = t^{-\alpha} \quad \text{with} \quad \alpha = \begin{cases} (3-d)/4 & d < 3 \\ 0 & d > 3 \end{cases}$$

and $0.33 + 0.066 \ln \tau$ in $d = 3$ [119]. Thus, below the critical dimension $d_c = 3$ the response of a single interface *grows* indefinitely with the time-difference. The same trend though with a different value of d_c and with slightly different exponents has been obtained for a continuous spin model. Still, for all $d > 1$, ρ decays sufficiently fast as to compensate the growth of χ_s , χ_I vanishes and the integrated linear response function gets stuck at the value reached at the end of the stationary time scale, $\chi_{\text{EQ}} = (k_B T)^{-1} (1 - m_{\text{EQ}}^2)$. In the slow regime the parametric plot is then given by a flat straight line with vanishing slope, see the dashed line in the right panel of Figure 16. Instead, the case $d = 1$ behaves in a totally different way: $\rho(\tau + t_w)$ still decays as $(\tau + t_w)^{-1/2}$ while χ_s grows as $\tau^{1/2}$, thus, in the regime of times such that τ/t_w is finite the interfaces do contribute to the integrated response and the $\chi(C)$ curve is non-trivial. As explained in [119] these results can be easily interpreted as follows. When $d > d_c$ the curvature driven mechanism dominates and the interface response decreases with ρ . When $d < d_c$ instead this mechanism is weakened while the field driven motion, and consequently the single interface response, becomes more important. In the limit $d = 1$ the curvature driven mechanism disappears, χ_s compensates exactly the decay in ρ and χ_I is non-trivial [119].

Besides the qualitative arguments just presented, the ferromagnetic Ising chain is completely solvable and very instructive [48, 120, 169]. The transition occurs at $K = J/(k_B T) \rightarrow \infty$ and this limit can be reached either by letting $T \rightarrow 0$ or $J \rightarrow \infty$. The latter is better adapted to compute the integrated linear response and one finds

$$\chi(C) = \frac{\sqrt{2}}{\pi} \arctan \left[\sqrt{2} \cot \left(\frac{\pi}{2} C \right) \right]. \quad (13.2)$$

The fast regime is eliminated for this choice of parameters and the full $\chi(C)$ curve is given by this equation. This model is a concrete example of

a system undergoing domain growth that has a non-trivial $\chi(C)$. For finite J (or finite T) the equilibration time is finite and, for $t_w \geq t_{\text{EQ}}$ the trivial $\chi(C) = 1/(k_B T)$ must be reached. However, for fixed $t_w \leq t_{\text{EQ}}$ one still finds a very rich structure: the master curve $\chi(C)$ corresponding to $J \rightarrow \infty$ is followed from $C(t_w, t_w) = 1$ down to $C_{\text{EQ}} = C(t_{\text{EQ}}, t_w)$. For longer time-differences, $\tau + t_w > t_{\text{EQ}}$ the system equilibrates and $\chi(C)$ departs from the master curve and approaches the point $(0, 1/(k_B T))$. The point of departure C_{EQ} depends on J and t_w . For fixed t_w , C_{EQ} increases with increasing J ; for fixed J , C_{EQ} increases with increasing t_w . Corberi *et al.* also argued that even if the form of C and R depend on the microscopic dynamics, the $\chi(C)$ curve should be universal.

Note an unexpected feature of this result: when $J \rightarrow \infty$, even if the correlation and response vary in a single time-scale with a simple aging scaling, the $\chi(C)$ relation is a continuous function. This property poses some problems for the interpretation of the slope of the $\chi(C)$ plot as an effective temperature (see Sect. 14) as well as the relation between statics and dynamics discussed in Section 13.10. It would be interesting to identify the generic origin of these “contradictions”.

For some time it has been argued that systems undergoing domain growth cannot have a non-trivial $\chi(C)$. This example, even though in $d = 1$, demonstrates that this is not true. It would be extremely interesting to construct a coarsening model in higher dimensions with a non-trivial contribution to the integrated response coming from the interfaces in such a way that $\chi(C)$ be non-trivial.

13.2 Structural glasses

For glassy systems, where no such growth of order has been identified yet, the form of the FDT modification is different from the one found for domain growth. These systems still show a separation of time-scales in the sense that the correlation decays in two sharply separated steps as suggested by numerical studies. The asymptotic parametric curve has the form of the solid line in Figure 16. One can argue in terms of cage motion to get an intuitive interpretation of why FDT holds in the fast correlation scale. Indeed, in this correlation-scale the time-difference $t - t_w$ is so short that each particle moves within a rather “solid” cage formed by its neighbors. Loosely speaking, the cages act as a confining potential on each particle. The rapid motion is again due to thermal fluctuations and the dynamics is like the one expected in equilibrium: it is then no surprise that FDT holds. For the moment there is no easy interpretation for the form of the second part of the parametric curve. Why does it have a non-zero constant slope or, equivalently, a single finite value of the effective temperature? This

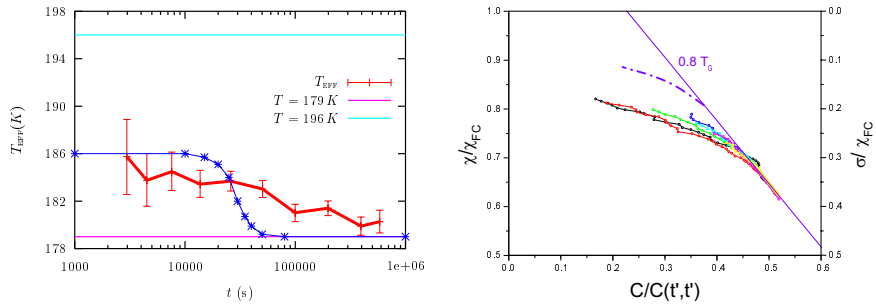


Fig. 17. Left: the waiting-time evolution of the effective temperature of glycerol [60]. Right: the parametric $\chi(C)$ plot for thiospinel, an insulator spin-glass [32].

result was obtained using fully-connected models and it was later checked numerically in a number of more realistic glassy models [58].

Two sets of experiments using laponite [61] and glycerol [60] have investigated the modifications of FDT in glasses. The former is explained in [61]. In the latter Grigera & Israeloff [60] monitored the time-evolution of the FD ratio for glycerol at $T = 179.8$ K, the glass transition being at $T_g = 196$ K. The measurements were done at fixed frequency $\omega = 7.7$ Hz and the results presented in the manner described in Section 11.5.2. For a perfect time-scale separation the curve should have a step-like form as sketched in the right panel of Figure 15 and also included with line-points in Figure 17. The experience shows that the FD ratio evolves very slowly from T^* to T with a very long transient between one and the other. Measurements at lower frequencies should yield a more sharp separation between the two steps.

13.3 Spin-glasses

The parametric curve for the fully-connected SK model for spin-glasses is given by the curve with a varying slope in the right panel of Figure 16. This result corresponds to having a succession of temporal scales each one with an effective temperature, $T_{\text{EFF}}(C)$. The question as to whether this behavior also applies to the finite dimensional case remains open. The only results available for the moment and, most probably, for a long while are numerical and experimental. For the time-scales explored, the parametric curves obtained have a very mild curvature. In order to decide beyond doubt if the asymptotic plot is curved it is necessary to perform a very careful analysis of the times and sizes explored (see [113]).

Very recently Herisson and Ocio studied the evolution of the correlations in the magnetization fluctuations (noise) and the thermoremanent magnetization (integrated response) of thiospinel, an insulator spin-glass [32]. Their

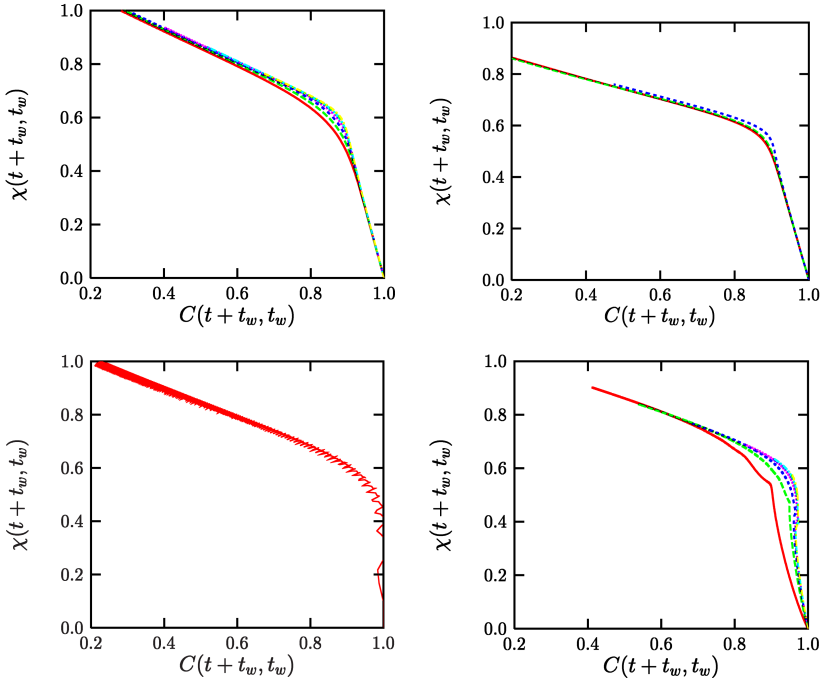


Fig. 18. The parametric $\chi(C)$ plot for the p -spin model: relaxational dynamics (upper left panel) [12], with asymmetric interactions (upper right panel) [18], under the effect of an oscillatory field (lower left panel) [26] and with quantum fluctuations (lower right panel) [85]. The different curves on each panel correspond to different waiting-times.

aim was to obtain the parametric curve $\chi(C)$. In the right panel of Figure 17 we show their results. It is important to note that even the experimental data is very far away from the expected nonequilibrium asymptote that is estimated to be given by the dotted-dashed curve in the figure. (For more details on this experiment see [32].)

13.4 Rheology

In Section 2 we have already explained that a non potential external force might stop aging. When the strength of this force is small, the separation of time-scales is still present but the dynamics becomes stationary. This fact makes the dynamics much simpler when observed in the time domain but it still captures some of the interesting features of non-equilibrium. For instance, the correlation function of a super-cooled liquid under homogeneous

shear approaches a non-equilibrium stationary state and the parametric construction of Figure 16 yields the same results where the waiting-time dependence is replaced by a shearing rate dependence. Thus, the red curve corresponds to a rather strong shearing rate, the green curve to a shearing rate of intermediate magnitude and the blue curves to the limit of vanishing shearing rate depending on the underlying system studied. These results were first obtained by solving the dynamics of a fully-connected model with non-symmetric interactions as the one introduced in equations (2.7) and (4.9) [18, 34]. The numerical study of Lennard-Jones mixtures under uniform shear performed by Berthier and J.-L. Barrat completed the study of this framework [121] (see also [171] and [19]).

In Section 14 we present the interpretation of the modification of FDT in terms of self-generated effective temperatures. Let us use this language here to explain these results and motivate further studies in other systems with different microscopic dynamics. Within the effective temperature interpretation, we see that $T_{\text{EFF}}(C) > T$ control the slow relation. In slightly more technical terms, the correlation scales in which the time derivatives of the correlation are negligible with respect to the correlation itself evolve according to a temperature that is given by the modification of the FDT relation. This fact suggests that the effective temperatures should appear in systems in which the microscopic dynamics is not necessarily thermal but in which a separation of time-scales rapid-slow is self-generated as time passes.

13.5 Vibrated models and granular matter

In fact, a similar modification to FDT has also been observed for glassy models driven by a time-dependent oscillatory force that mimics the perturbations used to move granular matter [26]. In this case, since the perturbation introduces its own characteristic time $t_c \propto 1/\omega$ it is more convenient to present the data using stroboscopic time, *i.e.* using a single point for each cycle. Modifications of FDT in models for granular matter were studied in [25, 122, 123].

13.6 Driven vortex systems

The effective temperature has also been observed in the transverse motion of a drive vortex system [43]. Very interestingly, T_{EFF} shares many quantitative properties with the “shaking temperature” of Koshelev & Vinokur [172].

13.7 Quantum fluctuations

Even more spectacular are the results for glassy models in which quantum fluctuations are important and keep a separation of fast-slow time-scales [85, 106]. The fast scale is fully controlled by the quantum dynamics and the FDT takes the complicated quantum form described in Section 7. In the slow scale though the quantum FDT is no longer valid and it is replaced by a modified classical form in which the deviations from the classical FDT depend on the strength of quantum fluctuations. The dynamics in the slow scale superficially looks classical. This result was found in the solution to mean-field models (quantum extensions of the p spin and SK, fully connected $SU(N)$). It is important to notice that Montecarlo simulations of quantum problems in real-time are not possible.

13.8 Systems of finite size: Preasymptotic behavior

The previous discussion shows that the correlation scales (time-scales) play a very important role in the global behavior of the systems. For relaxational systems we argued that the asymptotic parametric curve appears in the limit $\lim_{t_w \rightarrow \infty} \lim_{N \rightarrow \infty}$. The thermodynamic limit that is taken first ensures that the equilibration time, t_{EQ} , diverges and cannot be reached by the waiting-time. For a systems of finite size, $N < +\infty$, the equilibration time is a function of N . In consequence, the limit curve $\chi(C)$ has a lifetime that is bounded by t_{EQ} . When the waiting-time becomes of the same order of magnitude as t_{EQ} , the curve $\chi(C)$ starts changing to approach the equilibrium asymptote, the straight line of slope $-1/(k_B T)$. The way in which the approach to equilibrium is achieved is not known in general. It is a very difficult problem even for fully-connected models and there is little hope to solve a problem in sufficient detail as to be able to determine all the crossovers. This might be possible for the $O(N)$ model of ferromagnetic growth or for the spherical SK disordered model. Crisanti & Ritort [159] analysed the crossover to equilibrium in the p spin model with numerical simulations.

13.9 Critical dynamics

Godrèche and Luck studied the coarsening dynamics of ferromagnetic models quenched to the critical point T_c . Spatial correlations develop in the system but only up to a length scale that grows as $(\tau + t_w)^{1/z_c}$ with z_c the dynamic critical exponent. The equilibrium magnetization, m_{EQ} , and, hence, q_{EA} , vanish. Still, the dynamics is highly non-trivial. For finite though long t_w a stationary regime for $\tau \ll t_w$ and an *interrupted aging* regime for $t_0 \ll t_w \approx \tau + t_w$ can be identified even if they are not clearly

separated by a plateau in the correlation at a finite q_{EA} . In the former regime, the correlation and response are stationary and satisfy FDT. In the latter

$$C(t, t_w) \approx t_w^{-2\beta/\nu z_c} F_C\left(\frac{t}{t_w}\right), \quad \chi(t, t_w) \approx t_w^{-2\beta/\nu z_c} F_\chi\left(\frac{t}{t_w}\right), \quad (13.3)$$

with β and ν the usual static critical exponents and F_C and F_χ two scaling functions. As t_w increases the stationary regime arrives up to lower values of C and when t_w grows to infinity the full decay is stationary as in equilibrium. Since the interrupted aging part of C and R decay only algebraically with t_w the $\chi(C)$ plot for finite though long t_w is very rich with a non-trivial functional form. Similar results were obtained for the critical dynamics of the XY model [124].

13.10 Connection with equilibrium

The relation

$$-T \frac{d^2 \chi(C)}{dC^2} \Big|_{C=q} = \lim_{h \rightarrow 0} P_h(q), \quad (13.4)$$

between the static and non-equilibrium dynamic properties of slowly decaying systems, where $\chi(C)$ is the non-equilibrium relation between integrated response and correlation function as defined in equation (11.27) and $P_h(q)$ is the probability distribution of overlaps¹ in the perturbed Gibbs state, became apparent from the analytic solution to some mean-field models.

This relation holds in the exact solution to the SK model [104] and the problem of a finite dimensional manifold embedded in an infinite dimensional space in the presence of a random potential with long-range correlations [36, 96]. It is not verified in the exact solution to the p spin model and the manifold in a random potential with short range correlations. The reason for this discrepancy is that for the latter models the dynamics in the $t_w \rightarrow \infty$ $N \rightarrow \infty$ limit approaches the threshold and not equilibrium. More precisely, all generalized susceptibilities, and in particular the energy density, approach a limit $\lim_{t_w \rightarrow \infty N \rightarrow \infty} \chi^{\text{GEN}}(t_w) = \chi_{\text{TH}}^{\text{GEN}} \neq \chi_{\text{EQ}}^{\text{GEN}}$. In all cases the dynamics occurs in a region of phase space that is different from the one sampled in equilibrium and, for p spin models and the like it has different statistical properties. For the former models, even if still the region of phase space explored by the dynamics is different from the one corresponding to the equilibrium states, its statistical properties can be thought to be somehow equivalent, since $\lim_{t_w \rightarrow \infty N \rightarrow \infty} \chi^{\text{GEN}}(t_w) = \chi_{\text{TH}}^{\text{GEN}} = \chi_{\text{EQ}}^{\text{GEN}}$, and the relation (13.4) holds.

¹The overlaps are given by the correlation between two equilibrated configurations.

More recently, Franz, Mézard, Parisi and Peliti proposed that the connection (13.4) goes beyond mean-field and applies to finite d systems in which all dynamic susceptibilities converge to their equilibrium values, linking in this way the (easy to measure) non-equilibrium dynamics properties of realistic models to the (hard to measure) equilibrium properties of the same models. Since a threshold level as the one found for the p spin model cannot subsist for ever in finite d , they argued that the validity of equation (13.4) should be rather generic.

Several comments are in order. Corberi *et al.* showed that there is a non-trivial nonequilibrium dynamic $\chi(C)$ that does not satisfy equation (13.4) in one dimensional coarsening systems where the interface response does not vanish asymptotically (see Sect. 13.1). Even if the hypothesis of convergence of the generalized susceptibilities is not verified in this model, it provides a very simple example where the relation (13.4) does not hold. It might be possible to extend this result to domain growth in $d > 1$ with an interface geometry such that the domain wall response does not vanish asymptotically. This problem deserves further study.

Based on numerical simulations, Marinari *et al.* claimed [125] that the relation (13.4) is verified in the 3dEA. As pointed out by Berthier, Holdsworth and Sellitto in the context of the XY model [124] and by A. Barrat & Berthier [113] in the context of the 2d and 3d EA models, one has to be extremely careful when extrapolating the numerical results obtained for finite waiting-time out of equilibrium and finite size in equilibrium. Indeed, these authors showed that one can tune the finite waiting-time and the finite size to have a relation like (13.4) well before the asymptotic limits are reached and even in the trivial phase of the XY and 2dEA models.

Finally, it is worth stressing that a non-trivial $\chi(C)$ has been found in explicitly out of equilibrium situations for which equilibrium is trivial as, for instance, in rheological measurements of super-cooled liquids or in the long-time dynamics of super-cooled liquids before equilibration is reached. Indeed, non-trivial $\chi(C)$ curves have been found above the putative T_g in Lennard-Jones systems and at finite T in models for which $T_g = 0$ like the kinetically constrained lattice models [53, 54].

In conclusion, a better determination of which are the conditions under which (13.4) holds is necessary.

14 Effective temperatures

Temperature has remained an ill-defined concept until the development of thermodynamics and statistical mechanics. Evidently, the fact that a quantity, called temperature, must characterize the sensation of coldness or

warmth has been known since the old times. However, temperature was usually confused with heat.

The thermodynamics is an empirical theory based on four postulates that has been developed to determine some properties of the macroscopic objects without knowing the details of their constituents and interactions. After t_{EQ} , an isolated and finite system reaches an equilibrium macroscopic state that can be characterized by a small number of parameters, the state variables. Temperature is one of these parameters. The first law states that energy is conserved in an isolated system after having established the equivalence between heat and work. The zeroth law states that if two systems are in thermal equilibrium with a third, then they are also in equilibrium between them. The temperature is determined by an auxiliary measurement. One sets a thermometer in contact with the system, waits until thermal equilibrium is established and then determines the temperature by calibrating the reading of the thermometer. If one repeats this procedure with a second system, equilibrated with the first one, the first law ensures that the thermometer will itself be in equilibrium with the second system and, consequently, its reading will yield the same temperature. Hence, all systems in thermal equilibrium among them are at the same temperature.

The statistical mechanics establishes a bridge between the mechanical description of the microscopic constituents of the system and its macroscopic behavior. It yields a precise sense to the concept of temperature. To illustrate this statement, let us take an isolated system in the microcanonical ensemble with volume V and internal energy U . The entropy of the system is defined as $S(U) = k_B \ln \Omega(U)$ with $\Omega(E)dE$ the number of accessible states with mean energy between E and $E + dE$. The microcanonical definition of temperature is given by $1/(k_B T) \equiv \partial S(E)/\partial E$, evaluated at $E = U$. The development of statistical mechanics allows one to show that this definition is equivalent to the thermodynamic one. One can equally find it with the canonical and grandcanonical formalisms.

The previous paragraphs describe the behavior of systems in thermal equilibrium. What can one say about the systems that evolve out of equilibrium? Can one define a temperature for them? Or is it at least possible for a subclass of nonequilibrium systems? If this holds true, can one use this definition as a first step towards the development of a thermodynamics and a statistical mechanics for systems far from equilibrium?

Hohenberg and Shraiman discussed the possibility of defining a temperature for certain systems out of equilibrium [126] using the modification of FDR. In reference [112] we critically studied the definition of such an *effective temperature*, T_{EFF} , we insisted on the need to reach a regime with slow dynamics (related to small entropy production) to be able to define such a “state variable” and we demonstrated the importance of analyzing

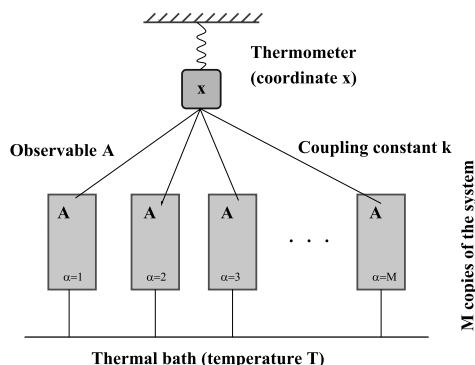


Fig. 19. Coupling between a thermometer and the observable A of the system.

it in separated time-scales. In this section we show in which sense the expected properties of a temperature are satisfied by T_{EFF} and we display some numerical tests.

14.1 Thermodynamical tests

14.1.1 How to measure a temperature

In normal conditions, the temperature of an object is measured by coupling it to a thermometer during a sufficiently long time interval such that all heat exchanges between thermometer and system take place and the whole system equilibrates.

Let us call $t = 0$ the instant when thermometer and system are set in contact. For simplicity, we choose to describe the thermometer with a single variable x . In order to have a statistical measure of the object's temperature [72, 127] we couple the thermometer to M independent copies of the system. Each system is characterized by a variable $\vec{\phi}_\alpha$, $\alpha = 1, \dots, M$. The energy of the total system is

$$E_{\text{TOT}} = m \frac{\dot{x}^2}{2} + V(x) + \sum_{\alpha=1}^M E(\vec{\phi}_\alpha) - \frac{k}{\sqrt{M}} x \sum_{\alpha=1}^M A[\vec{\phi}_\alpha],$$

with $V(x)$ the potential energy of the isolated thermometer and $E(\vec{\phi}_\alpha)$ the one of the α th isolated system. Note the similarity between this coupled model, the treatment of system+environment done in Section 4, and the discussion on the harmonic oscillator coupled to a complex bath in Section 7.4.4. For a given value of M , the last term acts as an infinitesimal field kx/\sqrt{M} that is coupled to the observable $A[\vec{\phi}]$ of each copy. The

equation of motion of the thermometer reads

$$m\ddot{x}(t) = -\frac{\partial V(x)}{\partial x(t)} - \frac{k}{\sqrt{M}} \sum_{\alpha=1}^M A[\vec{\phi}^\alpha](t). \quad (14.1)$$

Again for simplicity we choose an observable A with vanishing mean $\langle A[\vec{\phi}] \rangle_{k=0} = 0$ where the angular brackets represent the average over different histories of the system (see Sect. 5.1) or the average over different systems, *i.e.* $\langle f \rangle = 1/M \sum_{\alpha=1}^M f_\alpha$. When the averaged observable does not vanish we use the difference between the observable and its average as the fundamental quantity. The index $k=0$ indicates that the average is taken in the absence of the thermometer. We denote $\langle \quad \rangle_k$ the average in the presence of the thermometer. Equation (14.1) can be rewritten as

$$m\ddot{x}(t) = -\frac{\partial V(x)}{\partial x(t)} + k^2 \int_0^t ds R(t,s)x(s) + \rho(t) \quad (14.2)$$

with $R(t,s)$ the linear response of the observable $A(\vec{\phi})$ to the change in energy $E_{\text{TOT}} \rightarrow E_{\text{TOT}} - k/\sqrt{M} x A(\vec{\phi})$ performed at time s . The force $\rho(t)$ is a sum of M independent random variables and due to the central limit theorem, it becomes a Gaussian variable with vanishing average and variance

$$\langle \rho(t)\rho(s) \rangle_k = k^2 C(t,s) = k^2 \left\langle A[\vec{\phi}](t) A[\vec{\phi}](s) \right\rangle_{k=0} \quad (14.3)$$

for large M at first order in k . Thus, the evolution of the thermometer is determined by a Langevin-like equation [*cf.* Eq. (4.7)] with a correlated noise $\rho(t)$ and a retarded friction generated by the coupling to the systems. For a generic system out of equilibrium there is no relation between R and C . For the problems we are interested in there is one. Next we explore the consequences of the modification of FDT for the reading of the thermometer.

If the systems are equilibrated with their environments FDT holds and it ensures that R is related to C by $R(t,s) = 1/(k_B T) \partial_s C(t,s) \theta(t-s)$, with T the temperature of the thermal bath. The thermometer is then coupled to an equilibrated colored bath and it will eventually reach equilibrium with it. The reading of the thermometer is defined from the value of its asymptotic internal energy and it has to be calibrated from the characteristics of the thermometer that, of course, must be known before starting the measurement. If one takes a simple harmonic oscillator as a thermometer, one proves that the internal energy approaches $k_B T$. This is the result expected from equipartition since the oscillator has only two degrees of freedom (position and momentum).

Imagine now that the systems are glassy of the type discussed in Section 12. If one studies a system with two correlation scales such that

$$R(t, s) = \begin{cases} R_{\text{ST}}(t-s) & \text{if } t-s \ll s \\ \frac{1}{t} R_{\text{AG}}\left(\frac{s}{t}\right) & \text{if } \frac{s}{t} = O(1) \end{cases} \quad C(t, s) = \begin{cases} C_{\text{ST}}(t-s) & \text{if } t-s \ll s \\ C_{\text{AG}}\left(\frac{s}{t}\right) & \text{if } \frac{s}{t} = O(1) \end{cases}$$

$$R_{\text{ST}}(t-s) = \frac{1}{k_{\text{B}}T} \partial_s C_{\text{ST}}(t-s), \quad R_{\text{AG}}\left(\frac{s}{t}\right) = \frac{t}{k_{\text{B}}T^*} \partial_s C_{\text{AG}}\left(\frac{s}{t}\right)$$

with T the temperature of the thermal bath and T^* a different value read from the modified FDT relation. The reading of the thermometer, or its asymptotic internal energy density, is found to be [112]

$$E_{\text{THERM}} = \frac{\omega_0 \tilde{C}(\omega_0, t_w)}{\tilde{\chi}''(\omega_0, t_w)} \quad (14.4)$$

where ω_0 is the characteristic frequency of the thermometer, $\tilde{C}(\omega_0, t_w)$ is the Fourier transform of the correlation function with respect to the time-difference and $\tilde{\chi}''(\omega_0, t_w)$ is the out of phase susceptibility defined in equation (5.8).

If the characteristic frequency ω_0 is very high, the thermometer evaluates the evolution during the first step of the relaxation $t-s \ll s$, one finds $E_{\text{THERM}} = k_{\text{B}}T$ and one identifies T with the temperature of the system. Instead, if the characteristic frequency is very low, the thermometer examines the behavior of the system in the long time scales, $s/t = O(1)$ in the example, one finds $E_{\text{THERM}} = k_{\text{B}}T^*$ and one identifies T^* as the temperature of the system.

One can easily generalize this discussion to a problem with many correlation scales, each with a different value of the effective temperature. In order to measure them it is sufficient to tune the characteristic frequency of the oscillator to the desired scale.

A concrete realization of this measurement corresponds to a generalization of the Brownian motion experience of Perrin in which one follows the evolution of a tracer immersed in the fluid. If the latter is equilibrated at temperature T , after a short equilibration period, each component of the averaged kinetic energy of the tracer approaches $k_{\text{B}}T/2$. Instead, if the fluid evolves out of equilibrium, one can choose the mass of the particle (that plays the role of the characteristic frequency in the previous discussion) in order to examine the rapid dynamics, or the slow dynamics. The tracer acquires an averaged kinetic energy $E_{\text{KIN}} = k_{\text{B}}T^*/2$ with T^* the value

of the effective temperature in the time scale explored. Berthier & J.-L. Barrat [121] performed this measurement in a numerical experiment using a dense liquid modeled as in equation (2.4) under homogeneous shearing in contact with a thermal bath at temperature T as a fluid. They chose a Lennard-Jones particle as a tracer with mass m_{TR} . The left panel shows the asymptotic value of the transverse component of the averaged kinetic energy (transverse to the shearing rate direction) as a function of the mass of the tracer. One clearly sees how the effective temperature $T^* = m_{\text{TR}}\langle v_z^2 \rangle / k_B$ interpolates between the value T at small masses and the value $T^* > T$ for large masses. The trend can be easily understood. A very light tracer easily reacts to the quick bombardment of the particles in the fluid and it feels the temperature of the bath *via* the rapid scale of relaxation. A heavy tracer instead can only move *via* large rearrangements of the fluid and these correspond to the slow part of the relaxation. The transition between the two values is very smooth and it occurs over several orders of magnitude in the mass. The consistency of the explanation, *i.e.* the relation between T^* and the FDT relation, will become explicit in Section 14.1.2.

A complementary discussion on thermometric measurement of T_{EFF} and, in particular, of the effect of not having well-separated time-scales, appeared in [41, 128].

14.1.2 Zeroth law

A temperature, even if it is defined out of equilibrium, should control the direction of heat flows and the partial equilibration between observables in interaction. (Two observables interact if and only if the crossed linear response $R_{AB}(t, t')$, as defined in Eq. (5.5), does not vanish.)

With a pair of observables A and B one constructs two self and two cross correlations and responses. In each correlation scale the FDT relation is modified by a constant factor with which one constructs the effective temperature. If the notion of an effective temperature is correct, two interacting observables that evolve in the same time-scale should acquire the same value of T_{EFF} . The equilibration between different observables is well defined only in the limit of small heat, or energy, exchanges. This limit is achieved in a free relaxing system when the waiting time becomes very long or in a driven system rendered stationary when the nonconservative force vanishes. It is only possible for observables evolving in the same time-scale (note that even a single observable can have several values of the effective temperature when examined on different time-scales). We call *partial equilibrations* those arriving in the same time-scale. In contrast, if the two observables A and B do not interact they should evolve in different time-scales.

The property of partial equilibration has been proven analytically for the fully connected models solved in Section 12 [112] and, later, for all

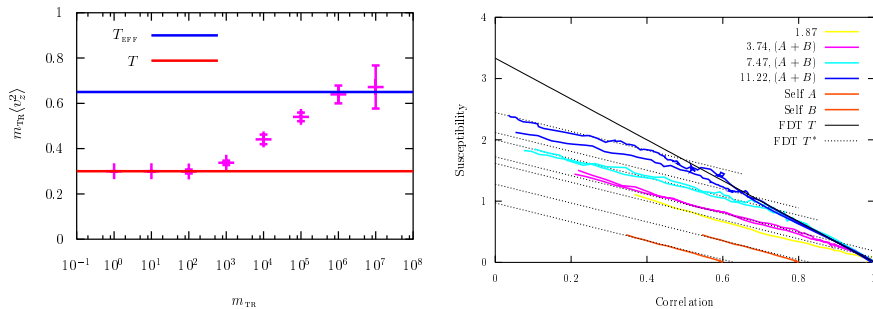


Fig. 20. A Lennard-Jones liquid with two types of particles, A and B , in its liquid phase under homogeneous shear. Left: the asymptotic value of the transverse component of the averaged kinetic energy of the tracer particle normalized by k_B , $T_{\text{EFF}} = m_{\text{TR}} \langle v_z^2 \rangle / k_B$, against its mass. Right: parametric plot between the linear response integrated over a time-interval of length $t - t_w$, $\chi(k; t - t_w)$, and the incoherent scattering function $C(k; t - t_w)$. The four first curves correspond to $k = 1.87, 3.74, 7.47, 11.22$. The self-displacement is also shown. The equilibrium straight line of slope $-1/(k_B T)$ is represented by a black line while the black dotted parallel straight lines have slopes $-1/(k_B T^*)$. From reference [121].

perturbative approximation of more realistic models under the assumption of there being a slow dynamics with a sharp separation of time-scales [72, 130]. It can be seen numerically as follows. Take, *e.g.*, two p spin models with different exchange strengths, \tilde{J}_1 and \tilde{J}_2 in contact with the same thermal bath at temperature T and couple them linearly with a term $\alpha \sum_{i=1}^N s_i \sigma_i$ where s_i and σ_i are the dynamic variables of each system and α is the coupling constant. (Other couplings are, of course, possible.) When $\alpha = 0$ the two systems evolve independently and their T_{EFF} 's in the aging scale take different values. If we now let the coupled system ($\alpha > 0$) evolve it will reach an asymptotic limit (roughly when the energy of the full system decays very slowly). In this limit we trace the FDT parametric plots for the two self and cross C and R 's. We observe that if $\alpha < \alpha_c$ the cross responses vanish and the effective temperatures still take different values in the aging scales that are now forced to evolve with different scalings. Instead, if $\alpha > \alpha_c$, the cross responses do not vanish, the two systems lock and T_{EFF} in the aging scale acquires the same value for both self and cross FD relations. Note that for the manifold, all modes have the same value of the effective temperature in the same correlation scale. This is achieved internally and it means that all modes are in interaction.

Partial equilibrations have been tested numerically by Berthier & J.-L. Barrat [121] in the dense homogeneously sheared liquid discussed in

Section 14.1.1 (in the relaxational case they were studied by Kob & J.-L. Barrat in [58]). The relevant correlators for this system are the wave vector dependent incoherent scattering functions and their associated responses. Berthier and Barrat measured these two-time functions for the same and different species and several values of the wave vector. Figure 20 shows the parametric FDT plots. All the curves have a broken line form with a first part with slope $-1/(k_B T)$ and a second part with a *common* slope $-1/(k_B T^*)$. The value T^* is identical to the result found monitoring the kinetic energy of the tracer (see Sect. 14.1.1) demonstrating that the scenario is consistent. Note that in this case we cannot tune the coupling between different wave vectors as we did when we externally coupled the two p spin model. The fact that T_{EFF} in the slow scale is the same for all wave vectors studied shows that they interact. This is also seen from the fact that the cross responses do not vanish.

A different example is given by coupled oscillator models with parallel or sequential Montecarlo dynamics do and do not partially equilibrate, respectively [129]. In the latter case the thermal conductivity is very small and one is in situation in which, effectively, $\alpha < \alpha_c$.

Intriguingly, the fact that each time-scale has its own effective temperature has been shown to fail in two models. These are the trap model [48] and the 1d Ising chain at $T = 0$ [48, 119, 120] when special perturbations are applied. In both cases one can construct observables that evolve in the same time-scale but have different values of the effective temperatures. In the first case, the failure might be ascribed to the fact that the model does not have an equilibrium state. This is not the case in the second model though. The origin of the failure might then be related to having used special observables, see the discussion in [48]. Still another pathology was already signaled for this problem: the global correlation and response decay in a single time-scale but the asymptotic $\chi(C)$ is a curve contradicting the notion of a correlation-scale dependent effective temperature. It is quite plausible that this problem is also related to the failure of the relation between dynamics and statics discussed in Section 13.10. A good understanding of the conditions under which this property holds is still lacking. Experiments in laponite show some mismatch between the value of T_{EFF} found with mechanical and electrical measurements. The reason for this is unclear [61].

One can also verify that the heat exchanges go from the higher values of T_{EFF} to lower ones. However, it is still not clear why one can have a partial equilibration to a *higher* value of T_{EFF} than those of the two independent observables, as it has been obtained analytically for some solvable fully-connected models.

14.1.3 Auxiliary thermal baths

A supplementary verification of the thermodynamic character of the effective temperature comes from the study of the action of complex thermal baths on the dynamics of simple systems, as discussed in Section 14.1.3, or glassy systems.

We found that an arbitrarily weak auxiliary bath with $\gamma(0)$ small has an important effect provided it is sufficiently slow and its temperature is within the range of values of the effective temperatures of the slow dynamics. The (slow) time dependence of all C and R 's are affected by a time rescaling $t \rightarrow K(t)$. This is such that the time-scale which has an effective temperature equal to the temperature of the auxiliary bath, say T_1 , is locked to the time-scale of the bath. In particular, if we couple an aging system with a bi-valued $T_{\text{EFF}} = (T, T^*)$ to a composite stationary bath with two time scales, $\tau_1 \rightarrow 0$ and $\tau_2 > 0$ and two temperatures T and T_2 , respectively, we find that the system becomes stationary if $T_2 > T^*$, and is hardly affected if $T_2 < T^*$. More generally, an aging system with multiple effective temperatures, $T_{\text{EFF}}(C)$, becomes partially stationary for all the time-scales with $T_2 > T_{\text{EFF}}(C)$, but still ages for time-scales with $T_2 < T_{\text{EFF}}(C)$. We found this behavior in Montecarlo simulations of the 3dEA model [130].

14.2 Temperature fixing by SUSY breaking

For any model one can derive a set of integro-differential equations that couple all two-point functions. These admit a representation in terms of the super-correlator $Q(a, b)$. In the asymptotic limit in which we neglect the time-derivatives, these equations are invariant under any change of supercoordinates, a , that have unit superjacobian [161]. Fixing the time-reparametrisation (the function $h(t)$ in each correlation scale) and the value of the effective temperature corresponds to breaking this large symmetry group to a subgroup [130].

14.3 Fictive temperatures

“Fictive temperatures” are phenomenological concepts that have been used to describe experimental data [131] (see also [132]). The basic idea has been to claim that, when crossing T_g , the system remembers its equilibrium configuration before the quench and it remains effectively at a higher temperature T_f . Several refined prescriptions to extract time and preparation dependences of T_f have been proposed. The relation between T_{EFF} and T_f has been discussed in [112]. Here we simply stress that even if the same basic idea can be used to interpret T_{EFF} , the latter has the properties of a thermodynamic temperature while this is not obvious for T_f .

14.4 Nonequilibrium thermodynamics

Once equipped with a *bonafide* effective temperature the natural next step is to try to construct a thermodynamics for such systems out of equilibrium. This has been proposed by Nieuwenhuizen [133] based on two previous results: (1) similar constructions done using the fictive temperatures by Tool, Moynihan and others [131]. (2) the relation between the dynamics and the TAP approach that we shall discuss in Section 15. The idea is to define generalized thermodynamic potentials in which T_{EFF} intervenes as a supplementary parameter (one can also include other state variables as an effective pressure, etc.). For the fully connected models these potentials have a precise meaning based on the TAP analysis (Sect. 15). Their validity for more realistic models is still an open problem.

14.5 Statistical mechanics

Edwards measure

In the 80 s Edwards proposed that the stationary properties of dense granular matter under a weak forcing can be determined with a *flat* distribution of the blocked configurations, *i.e.* those in which no grain is able to move, at the chosen density [134]. Note that this is possible in granular matter since the external temperature is irrelevant. Following this “microcanonical” approach the logarithm of the number of blocked configurations at constant density defines an entropy from which one obtains a compactivity by simple derivation with respect to the density. Extending this prescription one can define an Edwards’ temperature for soft systems by considering blocked configurations at fixed energy and computing $1/(k_B T_{\text{EDW}}) = \partial S_{\text{EDW}}(E)/\partial E$.

Edwards’ temperature can be calculated explicitly for the fully connected models at zero external temperature (again using techniques discussed in Sect. 15). Surprisingly, one finds that its actual value coincides with the value taken by T_{EFF} defined from the modification of FDT in a purely dynamic calculation. This result has boosted the study of solvable models in low dimensionalities analytically and more realistic systems numerically to check if the coincidence goes beyond the fully-connected case. Until now, several models where Edwards’ distribution yield very good results have been exhibited [122, 135] while some others where it fails have also been shown (*e.g.* the random field Ising model [122]). In the latter cases one finds a well-defined T_{EFF} while Edwards’ measure fails to give the correct results. The result of including additional constraints on the configurations counted have also been analysed and naturally improve the results derived from Edwards’ measure. This area of research is very active and more work is necessary to determine the limits of validity of Edwards’ proposal.

The definition of Edwards' measure is unambiguous since it is a zero temperature entity based on the study of minima of the potential energy. An extension to finite T necessitates the analysis of a free-energy landscape. This can be done analytically for fully-connected models as explained in Section 15. In finite d cases for which one is forced to use numerical techniques it is not, however, obvious how to define, let alone compute, the entropy $\Sigma(\beta, f)$.

Inherent structures

The *inherent structure* approach of Stillinger & Weber [136] has been recently revisited and extended to study dynamic properties of glass formers and glasses [137]. The original approach, even if static, is close to the ideas of Edwards. At the static level it consists in dividing the partition function in inherent structures, or pockets of configurations around minima of the *potential energy*, and transforming the sum into sums over minima and the configurations associated to them. In order to connect with the dynamics, one computes the entropy of the inherent structures and then derives an inherent structure temperature with a similar prescription to the one of Edwards. The sampling of the inherent structures numerically is a non-trivial issue.

A critical analysis of the applicability of this approach at finite temperatures has been presented by Biroli & Monasson [142] who stressed the need of analyzing the free-energy, instead of the potential energy, at finite T . They also compared with the TAP analysis discussed in Section 15. Having said this, the use of the inherent structure approach has been rather successful when confronted to T_{EFF} [137].

15 Metastable states

The aim of the TAP approach is to define and study a free-energy density as a function of the relevant order parameters [56]. Its stationary points are the (stable and unstable) metastable states. For a fully connected Ising magnet the TAP free-energy density simply depends on the averaged global magnetization and, below T_c , has the form drawn on the right panel of Figure 1. The vanishing global magnetization is not a good order parameter for disordered spin systems and one is forced to introduce all local ones. The approach can be extended to describe classical and quantum systems in and out of equilibrium [143, 144]. Under different names similar approaches appear in other branches of condensed matter physics. The *density functional theory* of the inhomogeneous electron gas in solids or the *dynamic mean-field theory* of strongly correlated electrons are very similar in spirit to the TAP approach [91].

The clearest way of deriving the TAP free-energy density for disordered models is based on two ingredients: one identifies an adequate perturbative expansion, and one Legendre transforms the standard free-energy density with respect to a well-chosen set of parameters. When these two choices are correctly done, only a finite number of terms in the expansion do not vanish for typical configurations of disorder for infinite dimensional models. In finite d one can attempt a large d expansion [146].

For spin-glasses at low- T the TAP free-energy density has an infinite number of stationary points. The TAP approach gives us access to the complete organization of metastable states of any type of stability (minima, saddles of all types, maxima). In particular, this has been analysed in great detail for the p spin model and the like since we expect it to mimic what occurs in real glassy systems though in an exaggerated manner.

In the following we first derive the TAP free-energy density for a generic spin model with Ising or spherical variables. Next we summarize the consequences of this approach for the p spin spherical model. We also briefly explain how the number of metastable states is computed and how this depends on the parameters in the model. We explain how the approach is generalized to deal with dynamic properties. This full set of results gives us a complementary view of the non-equilibrium dynamics and serves as the basis for an image of the dynamics of finite d glassy models.

15.1 Equilibrium

Before describing the TAP approach let us summarize the equilibrium behavior of the mean-field models as derived from the analysis of its disordered averaged free-energy density $-\beta[f]_J = [\ln Z]_J/N$ with the replica trick. Again the three classes, ferromagnetic-like ($p = 2$), glassy-like ($p \geq 3$) [166] and spins-glass-like (SK) [9] models have different characteristics.

For the spherical p spin model with $p \geq 3$ [166] the standard Parisi *Ansatz* [69] yields a static transition at T_s from a paramagnetic phase where a *replica symmetric Ansatz* solves the problem to a glassy phase where a *one step replica symmetry breaking Ansatz* is needed. At low T 's, the breaking point parameter, x , and the Edwards-Anderson order parameter, $q_{\text{EA}} \equiv N^{-1} \sum_i [\langle s_i \rangle^2]$, in the Parisi matrix are fixed by requiring that the free-energy density be a maximum. This yields a static transition temperature, T_s , given by the set of equations $T_s = y \sqrt{p/(2y)} (1 - y)^{p/2-1}$ and $2/p = -2y(1 - y + \ln y)/(1 - y)^2$. One can check that $T_s < T_d$. The static transition is discontinuous in the sense that q_{EA} jumps at T_s but it is of second order thermodynamically since all susceptibilities are continuous across T_s . The equilibrium energy density at $T = 0$ is given by the implicit equation $\sqrt{2y/p} = [-\mathcal{E}(T = 0) - \sqrt{-\mathcal{E}^2(T = 0) - \mathcal{E}_{\text{TH}}^2}]/(p - 1)$. One checks that $\mathcal{E}_{\text{EQ}} < \mathcal{E}_{\infty} = \mathcal{E}_{\text{TH}}$.

A modified prescription to determine the breaking point, x , in the one step *Ansatz* yields different results. If instead of extremizing with respect to x one requires that the solution be *marginally stable* by setting the *replicon eigenvalue* of the matrix of quadratic fluctuations [174] to zero, leads to a different solution with a dynamic meaning. (All other eigenvalues are positive.) Namely, one finds a transition from the paramagnetic to the glassy phase at a higher temperature that coincides with the dynamic critical temperature found with a purely dynamic calculation, T_d . Moreover, q_{EA} coincides with the dynamic one and the breaking point x yields the ratio T/T_{EFF} . Consequently, all one-time quantities as the asymptotic energy density and generalized susceptibilities coincide with the ones found dynamically (e.g. $\mathcal{E} = \mathcal{E}_{TH}$). The fact that with the condition of marginal stability we access the region of phase space reached dynamically is due to the fact that with both we search for the path of flat direction formed by the threshold level, as explained below.

When $p = 2$ instead [108], the replica solution below T_s is *replica symmetric* with a non-vanishing q_{EA} and marginally stable. The static transition is continuous, dynamic and static transition temperatures coincide, $T_s = T_d$, and $x = T/T_{EFF} = 0$ [109]. The gap between the threshold and the equilibrium level collapses and the static energy density is the value reached dynamically, $\mathcal{E}_{EQ} = \mathcal{E}_{\infty}$. Still, the nonequilibrium dynamics does not stop in finite times with respect to N .

For SK the equilibrium calculation needs a *full replica symmetry breaking solution* [9]. This can be interpreted as being equivalent to having a sequence of correlation scales in the nonequilibrium dynamics. The static transition is continuous, the static and dynamics q_{EA} are identical, the relation in (13.4) holds and all one-time quantities coincide with the equilibrium values. The static solution is also marginally stable.

From these three paragraphs one observes that the structure of the static and dynamic solution of purely potential mean-field problems is indeed very similar. One can propose a “dictionary”

$$\begin{aligned} \text{RS} &\Leftrightarrow 2 \text{ corr. scales, the aging one with } T_{EFF} = T^* \rightarrow \infty \\ 1 \text{ step RSB} &\Leftrightarrow 2 \text{ corr. scales, the aging one with } T_{EFF} = T^* < +\infty \\ \text{full RSB} &\Leftrightarrow \infty \text{ corr. scales, the aging ones with } T_{EFF}(C) < +\infty \end{aligned}$$

while remembering that the replica solution that describes the statistical properties of the region of phase space reached dynamically has to be determined using the condition of marginal stability – and not equilibrium. This connection between replicas and dynamics has been extensively exploited to use the replica trick as a substitute for dynamics. In fact, partial information about dynamics as the dynamic critical temperature, the value of T_{EFF} , etc. is thus obtained. One has to keep in mind though that many

aspects of the dynamics go beyond static calculations. Features like the existence of an effective temperature have been shown in models with trivial statics [53, 54] or above the dynamic transition when non-potential or time-dependent forces are included [19, 26].

15.2 Static TAP approach

In the introduction to this section we announced that two choices facilitate the derivation of the TAP free-energy density. In order to use a good perturbative expansion we weight a part of the original Hamiltonian with a parameter α . For the p spin model we simply propose

$$H(\alpha, \vec{s}) = \alpha \sum_{i_1 < \dots < i_p} J_{i_1, \dots, i_p} s_{i_1} \dots s_{i_p}. \quad (15.5)$$

In other models we weight the higher order interactions with α without modifying the quadratic terms. The idea is to expand in powers of α and set $\alpha = 1$ at the end of the calculations to recover the original model [145, 146].

The second important step in the derivation is the choice of the order parameters to use in the Legendre transform of the free-energy density. For spin models these are the averaged local magnetizations m_i and a global spin constraint l . The Legendre transform reads

$$-\beta\Gamma(\beta, \alpha; m_i, l; h_i, \lambda) = \ln \text{Tr}_{S_i} e^{-\beta H(\alpha, \vec{s}) - \sum_{i=1}^N h_i (s_i - m_i) - \frac{\lambda}{2} \sum_{i=1}^N (s_i^2 - l)}. \quad (15.6)$$

The trace represents a sum over all configurations of the spins, *e.g.* $\text{Tr}_{S_i} = \prod_{i=1}^N \sum_{s_i = \pm 1}$ for Ising and $\text{Tr}_{S_i} = \int_{-\infty}^{\infty} \prod_{i=1}^N ds_i$ for spherical variables. Requiring stationarity with respect to the Langrange multipliers h_i and λ one obtains

$$m_i \equiv \langle s_i \rangle \quad \text{and} \quad l \equiv \frac{1}{N} \sum_{i=1}^N \langle s_i^2 \rangle, \quad (15.7)$$

for all values of α . The angular brackets indicate the statistical average over the spins using the full Boltzmann weight in (15.6). Since the RHSS depend on h_i and λ these equations can be inverted to yield $h_i(\beta, \alpha; m_i, l)$ and $\lambda(\beta, \alpha; m_i, l)$. that one substitutes in (15.6) to write Γ as a function of $(\beta, \alpha; m_i, l)$. Henceforth we drop the parameter dependence and simply note Γ . The introduction of the parameter α allows us to express $-\beta\Gamma$ as a power series in α :

$$-\beta\Gamma = \sum_{n=0}^{\infty} \left. \frac{\partial^n (-\beta\Gamma)}{\partial \alpha^n} \right|_{\alpha=0} \frac{\alpha^n}{n!}. \quad (15.8)$$

For the p spin model and the like this is equivalent to a high T expansion. In other cases it is an expansion around an “equivalent” free theory. Interestingly enough only a finite number of terms contribute to the series for fully connected models. For finite dimensional cases a truncated series yields an approximation around mean-field.

The zero-th order term depends on the nature of the spins considered:

$$\begin{aligned} -\beta\Gamma^{\text{ISING}} &= -\sum_{i=1}^N \left[\frac{1+m_i}{2} \ln \left(\frac{1+m_i}{2} \right) + \frac{1-m_i}{2} \ln \left(\frac{1-m_i}{2} \right) \right], \\ -\beta\Gamma^{\text{SPH}} &= \frac{N}{2} \ln \left(1 - \frac{1}{N} \sum_{i=1}^N m_i^2 \right). \end{aligned}$$

These are the entropies of N independent Ising or spherical spins constrained to have local magnetizations m_i . The first order term is proportional to

$$\begin{aligned} \left. \frac{\partial(-\beta\Gamma)}{\partial\alpha} \right|_{\alpha=0} &= \sum_{i_1 \leq \dots \leq i_p} J_{i_1 \dots i_p} \langle s_{i_1} \dots s_{i_p} \rangle_{\alpha=0} - \sum_{i=1}^N \left. \frac{\partial h_i}{\partial\alpha} \right|_{\alpha=0} \langle s_i - m_i \rangle_{\alpha=0} \\ &\quad - \sum_{i=1}^N \left. \frac{\partial\lambda}{\partial\alpha} \right|_{\alpha=0} \sum_{i=1}^N \langle s_i^2 - l \rangle_{\alpha=0} = \sum_{i_1 \leq \dots \leq i_p} J_{i_1 \dots i_p} m_{i_1} \dots m_{i_p}. \quad (15.9) \end{aligned}$$

In the first equality, the last two terms on the RHS vanish due to equations (15.7). The average in the first term factorizes since it has to be taken with the free-action ($\alpha = 0$). The quadratic term in the expansion is proportional to

$$\left. \frac{\partial^2(-\beta\Gamma)}{\partial\alpha^2} \right|_{\alpha=0} = \left\langle \left(\sum_{i_1 \dots i_p} Y_{i_1 \dots i_p} \right)^2 \right\rangle_{\alpha=0}^c \quad (15.10)$$

with $Y_{i_1 \dots i_p} = J_{i_1 \dots i_p} s_{i_1} \dots s_{i_p} - (s_{i_1} - m_{i_1})m_{i_2} \dots m_{i_p} - \dots - m_{i_1} \dots m_{i_{p-1}} \times (s_{i_p} - m_{i_p})$. This term has been computed using the following identities. First, the variation of $-\beta\Gamma$ in equation (15.6) with respect to m_i and l yields $h_i = \frac{\partial(-\beta\Gamma)}{\partial m_i}$ and $\lambda = \frac{2}{N} \frac{\partial(-\beta\Gamma)}{\partial l}$. Taking the variation with respect to α and evaluating at $\alpha = 0$ one has

$$\left. \frac{\partial h_i}{\partial\alpha} \right|_{\alpha=0} = \left. \frac{\partial^2(-\beta\Gamma)}{\partial m_i \partial\alpha} \right|_{\alpha=0}, \quad \left. \frac{\partial\lambda}{\partial\alpha} \right|_{\alpha=0} = \frac{2}{N} \left. \frac{\partial^2(-\beta\Gamma)}{\partial l \partial\alpha} \right|_{\alpha=0}. \quad (15.11)$$

Now, the contributions $O(N)$ are proportional to J_{i_1, \dots, i_P}^2 and these can be estimated by replacing its value by $p!/(2N^{p-1})$ since $J_{i_1, \dots, i_p} \sim \sqrt{p!/(2N^{p-1})}$. As done for the first order term we factorize the thermal averages evaluated at $\alpha = 0$ and

$$\left. \frac{\partial(-\beta\Gamma^{\text{ISING}})}{\partial\alpha^2} \right|_{\alpha=0} = 2N (1 - q_{\text{EA}}^p - p(q_{\text{EA}}^{p-1} - q_{\text{EA}}^p)) \quad (15.12)$$

$$\left. \frac{\partial(-\beta\Gamma^{\text{SPH}})}{\partial\alpha^2} \right|_{\alpha=0} = \frac{\beta^2}{2} N (l^p - q_{\text{EA}}^p - p(lq_{\text{EA}}^{p-1} - q_{\text{EA}}^p)) \quad (15.13)$$

where we introduced the overlap or (static) Edwards-Anderson parameter,

$$q_{\text{EA}} \equiv \frac{1}{N} \sum_{i=1}^N m_i^2. \quad (15.14)$$

Higher order terms in the series expansion are sub-leading in N and do not contribute in the thermodynamic limit. Thus, for these mean-field models the TAP free-energy density is made of three terms: the zero-th order has an entropic origin, the first order is the interaction term in the mean-field approximation which is exact for fully connected models, and the second order is the reaction or Onsager term.

15.3 The TAP equations

The variation of the TAP free-energy density, $-\beta\Gamma$, with respect to m_i (and l for the spherical model) yields the TAP equations. For the spherical model one finds [147]

$$\frac{m_i}{(1 - q_{\text{EA}})} = \beta p \sum_{(i_2 \leq \dots \leq i_p) \neq i} J_{i, i_2, \dots, i_p} m_{i_2} \dots m_{i_p} - \frac{\beta^2 p(p-1)}{2} q_{\text{EA}}^{p-2} (1 - q_{\text{EA}}) m_i \quad (15.15)$$

$$\lambda = \frac{1}{1 - q_{\text{EA}}} + \frac{p\beta^2}{2} (1 - q_{\text{EA}}^{p-1}). \quad (15.16)$$

The study of these equations is simplified by defining the angular variables $\sigma_i \equiv m_i/\sqrt{q_{\text{EA}}}$ that verify the spherical constraint $\sum_i \sigma_i^2 \equiv 1$. Multiplying equations (15.15) by σ_i and summing over i we rewrite them in terms of the zero-temperature energy density $\mathcal{E} \equiv -\frac{1}{N} \sum_{i_1 < \dots < i_p} J_{i_1, \dots, i_p} \sigma_{i_1} \dots \sigma_{i_p}$:

$$\mathcal{E} \sigma_i = - \sum_{i_2 < \dots < i_p} J_{i, i_2, \dots, i_p} \sigma_{i_2} \dots \sigma_{i_p}. \quad (15.17)$$

The overlap q_{EA} is related to \mathcal{E} by

$$\beta p \mathcal{E} = -\frac{1}{q_{\text{EA}}^{(p-2)/2}(1-q_{\text{EA}})} \left[1 + \beta^2 \frac{p(p-1)}{2} (1-q_{\text{EA}})^2 q_{\text{EA}}^{p-2} \right]. \quad (15.18)$$

Equation (15.17) does not depend on T while (15.18) does. The multiplicity of solutions at a given \mathcal{E} is entirely determined by equation (15.17), see Section 15.5. The existence or not of these solutions has to be tested with equation (15.18). The remaining equation (15.16) fixes λ .

Conveniently rewritten equation (15.18) is quadratic and yields

$$q_{\text{EA}}^{(p-2)/2}(1-q_{\text{EA}}) = \frac{k_{\text{B}}T}{p-1} \left[-\mathcal{E} \pm \sqrt{\mathcal{E}^2 - \mathcal{E}_{\text{TH}}^2} \right] \quad \text{with} \quad \mathcal{E}_{\text{TH}} \equiv -\sqrt{\frac{2(p-1)}{p}}. \quad (15.19)$$

This equation admits a real solution only if $\mathcal{E} < \mathcal{E}_{\text{TH}}$, the *threshold* energy density at $T = 0$. The minus (plus) sign corresponds to a minimum (maximum) of the free-energy. The physical q_{EA} is then associated to the minus sign. With this choice, q_{EA} takes its maximum value on the threshold and then monotonically decreases until reaching its minimum value on the equilibrium level, $q(\mathcal{E}_{\text{TH}}) \geq q_{\text{EA}}(\mathcal{E}) \geq q_{\text{EA}}(\mathcal{E}_{\text{EQ}})$.

For fixed β and \mathcal{E} the LHS in equation (15.19) has a bell shape form. When $T \rightarrow 0$, $q_{\text{EA}} \rightarrow 1$ and $\beta(1-q_{\text{EA}})$ is finite. The maximum is located at $q_{\text{EA}}^* = (p-2)/p$ and it has a height $2/p \left((p-2)/p \right)^{(p-2)/2}$. Each solution at $T = 0$ that corresponds to a given \mathcal{E} can be followed to finite T until it disappears at $T^*(\mathcal{E})$ when the LHS reaches the maximum. One can check that the TAP solutions do not merge nor bifurcate as a function of T . Then at any temperature T we label the TAP solutions with their associated zero temperature energy density \mathcal{E} .

Plugging \mathcal{E}_{TH} in equation (15.18) we find that the overlap q_{EA} is given by the equation

$$\frac{p(p-1)}{2} q_{\text{TH}}^{p-2} (1-q_{\text{TH}})^2 = (k_{\text{B}}T)^2. \quad (15.20)$$

The threshold energy density \mathcal{E}_{TH} and the overlap q_{TH} coincide with the asymptotic value of the dynamic energy density and the Edwards-Anderson parameter at $T = 0$, respectively. Thus, the nonequilibrium dynamics approaches asymptotically the threshold level.

15.4 Stability of, and barriers between, the TAP solutions

The spectrum of the free-energy Hessian around a stationary point of the TAP free-energy is a shifted semi-circle. The lowest eigenvalue λ_{MIN} is greater than zero for sub-threshold free-energy densities (or zero-temperature energy density). This means that for $\mathcal{E} < \mathcal{E}_{\text{TH}}$ typical stationary states are

minima. Instead, near the threshold λ_{MIN} drops to zero as [12]

$$\lambda_{\text{MIN}}(f, T) \sim \frac{p}{q_{\text{TH}}} (f_{\text{TH}} - f) \quad (15.21)$$

and the stationary states on the threshold are typically marginal in the sense that they have many flat directions.

Even if the connection between dynamics and the static TAP free-energy landscape is not obvious *a priori*, it has been proposed and used in several works [11, 12]. The formalism in Section 15.8 and [143] settles it on a firm ground. If one imagines that the dynamics can be viewed as the displacement of a representative point in the free-energy landscape, not only the organization minima, saddles and maxima has to be known but also how do the barriers between these stationary points scale with N . Few results about barriers exist and, in short, they are the following. The barriers between threshold states vanish when $N \rightarrow \infty$ [3, 148] and there is no sharp separation between them. This has been proven by analyzing the constrained complexity, related to the number of threshold states that have an overlap \tilde{q} with a chosen one ($\tilde{q} \equiv N^{-1} \sum_{i=1}^N \sigma_i \tau_i$ where $\vec{\sigma}$ and $\vec{\tau}$ are the two configurations). This complexity decreases with increasing values of \tilde{q} and it vanishes as a power law at $\tilde{q} = q_{\text{TH}}$. This means that one can find threshold states that are as similar as required to the chosen one. The threshold level is then a series of flat connected channels. The non-equilibrium dynamics starting from random (typical) initial conditions approaches this level asymptotically and it never stops since the system drifts in a slower and slower manner as time evolves following these flat directions [12]. On the other hand, the barriers between equilibrium and metastable states have been estimated to be $O(N)$ [147, 148]. One can guess that the barriers between sub-threshold TAP states also scale with N . For finite N the dynamics should penetrate below the threshold and proceed by thermal activation. An Arrhenius-like time will then be needed to descend from one level to the next. Naturally one should see another kind of separation of time-scales develop. Simulations of the p spin model for finite N confirm the existence of metastable states below the threshold. This is most clearly seen following the evolution of the energy density of the model weakly perturbed with a non-potential force. One sees periods of trapping in which the energy-density is fixed to a given value and periods in which the system escapes the confining state and surfs above the threshold until being trapped in a new state [18, 19, 26] (see also [159] for a numerical study of the finite N p -spin model with pure relaxational dynamics).

15.5 Index dependent complexity

At low T 's the number of stationary points is exponential in N . This suggests to define the *complexity* $\Sigma_J(\mathcal{E})$:

$$\Sigma_J(\mathcal{E}) \equiv \lim_{N \rightarrow \infty} N^{-1} \ln \mathcal{N}_J(\mathcal{E}), \quad (15.22)$$

where $\mathcal{N}_J(\mathcal{E})$ is the number of solutions with energy density \mathcal{E} . Actually, one can refine the study by grouping the stationary points of the TAP free-energy density into classes according to the number of unstable directions. Thus, minima are saddles of index 0, saddles with a single unstable direction have index 1 and so on and so forth. The complexity of each kind of saddle is $\Sigma_{Jk}(\mathcal{E}) \equiv \lim_{N \rightarrow \infty} N^{-1} \ln \mathcal{N}_{Jk}(\mathcal{E})$, where k denotes the index of the considered saddles. For the spherical p spin model, their average over disorder, $\Sigma_k \equiv [\Sigma_{Jk}]$, are ordered in such a way that [149]

$$\begin{aligned} \Sigma_0(\mathcal{E}) &> \Sigma_1(\mathcal{E}) > \Sigma_2(\mathcal{E}) > \dots & \text{for all } \mathcal{E} < \mathcal{E}_{\text{TH}} \\ \Sigma_0(\mathcal{E}) &= \Sigma_1(\mathcal{E}) = \Sigma_2(\mathcal{E}) = \dots & \text{if } \mathcal{E} = \mathcal{E}_{\text{TH}}. \end{aligned}$$

Thus, when $\mathcal{E} < \mathcal{E}_{\text{TH}}$ minima are exponentially dominant in number with respect to all other saddle points. Moreover, one proves that the complexities vanish at a k -dependent value of \mathcal{E} . The complexity of minima is the last one to disappear at \mathcal{E}_{EQ} .

15.6 Weighted sums over TAP solutions

The thermodynamics at different T is determined by the partition function, \mathcal{Z}_J . De Dominicis & Young [150] showed that the equilibrium results obtained with the replica trick or the cavity method are recovered from the TAP approach when one writes \mathcal{Z}_J as a weighted sum over the TAP stationary states.

Indeed, if one divides phase space into pockets of configurations that surround the stationary points of the TAP free-energy one can carry out the statistical sum on each sector of phase space:

$$\mathcal{Z}_J = \sum_{\vec{s}} \exp(-\beta H_J(\vec{s})) = \sum_{\alpha} \sum_{\vec{s}^{\alpha}} \exp(-\beta H_J(\vec{s}^{\alpha})) \quad (15.23)$$

where the index α labels the TAP solutions and $\sum_{\vec{s}^{\alpha}}$ represents a restricted sum over the configurations that belong to the pocket associated to the solution α . In order to make this separation precise one needs to assume that the barriers separating the pockets diverge in such a way to avoid ambiguities when associating a configuration to a TAP solution. The restricted sum is related to the free-energy of the TAP solution $\exp(-\beta F_J(\vec{m}^{\alpha})) =$

$\sum_{\vec{s}^\alpha} \exp(-\beta H_J(\vec{s}^\alpha))$ and the partition function becomes $\mathcal{Z}_J = \sum_{\alpha} \exp[-\beta F_J(\vec{m}^\alpha)]$. Thus, any statistical average can be computed using the weight $\exp[-\beta F_J(\vec{m}^\alpha)]/\mathcal{Z}_J$. The sum over solutions can be replaced by an integral over free-energies if one introduces their degeneracy $\mathcal{N}_J(\beta, f)$ and their associated complexity, $\Sigma_J(\beta, f) = N^{-1} \ln \mathcal{N}_J(\beta, f)$, with $f \equiv F/N$,

$$\mathcal{Z}_J = \int df \exp[-N(\beta f - \Sigma_J(\beta, f))]. \quad (15.24)$$

Since the complexity is a self-averaging quantity we then write $\Sigma_J(\beta, f) = \Sigma(\beta, f)$. When $N \rightarrow \infty$ the integral is dominated by the solutions that minimize the generalized free-energy, $\beta f - \Sigma(\beta, f)$. This is achieved either by $f = f_{\min}$ with $\Sigma(\beta, f_{\min}) = 0$ or by states that do not have the minimum free-energy if their complexity is finite, in which case [138]

$$\beta = \left. \frac{\partial \Sigma(\beta, f)}{\partial f} \right|_{f^*} \Rightarrow \mathcal{Z}_J \sim \exp[-N(\beta f^* - \Sigma(\beta, f^*))]. \quad (15.25)$$

Minima of the generalized free-energy density with higher ($f > f^*$) or lower ($f < f^*$) free-energy density are metastable.

From the analysis of the partition function one distinguishes three temperature regimes [11, 138]:

$$\text{Above the dynamic transition } T > T_d = \sqrt{\frac{p(p-2)^{p-1}}{2(p-1)^{p-1}}}$$

The paramagnetic or liquid solutions $m_i = 0$, $\forall i$, dominate the partition sum, $\mathcal{Z} \sim \exp(-\beta f^{\text{PM}})$. States with $m_i \neq 0$ exist in this range of temperatures but they do not dominate the sum.

$$\text{Between the static and dynamic transitions } T_s < T < T_d$$

The paramagnetic state is fractured into an exponential in N number of non-trivial TAP solutions with $m_i \neq 0$. Their free-energy density and the partition sum are given by equation (15.25). Each of these states has a rather high free-energy that is counterbalanced by the entropic contribution. Besides the states that dominate the partition sum, a very large number of other metastable states, with higher and lower free-energy density, also exist but are thermodynamically irrelevant. It turns out that f^* coincides with the extrapolation of f^{PM} from $T > T_d$ to this temperature region even if the paramagnetic solution does not exist. Note that in this temperature regime the standard replica calculation fails since it tells us that the equilibrium state is the simple paramagnet. Refinements on this method are able to extract more precise information about the non-trivial states contributing to equilibrium [148].

Below the static transition $T < T_s$

An infinite though not exponential in N number of states with the minimum free-energy density dominate the sum. The complexity $\Sigma(\beta, f)$ vanishes and this is associated to an entropy crisis. This is similar to the argument used by Kauzmann to justify the existence of a dynamic crossover at $T_g > T_s$ since, otherwise, the projection of the difference between the liquid and the crystal entropy would vanish at T_K . In this sense, this model realizes the Kauzmann paradox at T_s .

15.7 Accessing metastable states with replicas

The replica trick can be improved to access the non-trivial metastable states existent between T_s and T_d [138, 139, 168] using a “pinning-field” or a “cloning method”. Let us sketch how the latter works. Consider x copies or clones of the systems coupled by an attractive, infinitesimal (but extensive) interaction. The free energy for the system of x clones reads:

$$f_{Jx} = \lim_{N \rightarrow \infty} \frac{-1}{\beta N} \ln \mathcal{Z}_{Jx} = \lim_{N \rightarrow \infty} \frac{-1}{\beta N} \ln \int df \exp[-N(\beta x f - \Sigma(\beta, f))] \quad (15.26)$$

using the formalism described in the previous subsection. On the other hand, the free-energy density of the x clones can also be computed with the replica approach:

$$f_{Jx} = \lim_{N \rightarrow \infty} \frac{-1}{\beta N} [\ln \mathcal{Z}_{Jx}] = \lim_{N \rightarrow \infty, n \rightarrow 0} \frac{-1}{\beta N n} \ln [\mathcal{Z}_{Jx}^n] \quad (15.27)$$

where we used the fact that the free-energy density is self-averaging. Since the attractive coupling between the x clones is infinitesimal, the computation of the RHS of equation (15.27) reduces to the calculation of $\lim_{n' \rightarrow 0} (x/n') \ln [\mathcal{Z}_{Jx}^{n'}]$, where the replica symmetry between the n groups of x -replicas ($n' = nx$) is *explicitly* broken. When the system is in the replica symmetric phase ($T_s < T$), the problem becomes one where one has to study one-step replica symmetry breaking solutions non-optimized with respect to x :

$$- \lim_{N \rightarrow \infty} \frac{1}{\beta N} \ln \int df \exp[-N(\beta x f - \Sigma(\beta, f))] = x \text{ Extr}_{q_{\text{EA}}} f_{\text{REP}}(q_{\text{EA}}; \beta, x), \quad (15.28)$$

where f_{REP} is the free-energy-density computed by using replicas, q_{EA} is the Edwards-Anderson parameter and x is the breakpoint or the size of the blocks in the replica matrix. (For simplicity we consider that the inter-state overlap q_0 equals zero [9].) Since the integral on the LHS of equation (15.28) is dominated by a saddle point contribution, one finds that, for a given T ,

fixing the value of x one selects the states with a given free-energy-density F . The relationship between f and x reads

$$\beta^* \equiv \beta x = \frac{\partial \Sigma(\beta, f)}{\partial f}. \quad (15.29)$$

Note that within this framework one does not optimize with respect to x . Instead, x is a free parameter and, by changing the value of x , one selects different groups of metastable states. Inversely, choosing a value of the free-energy density one determines an “effective temperature” $T^* \equiv T/x$. This value coincides, indeed, with the dynamic result for T_{EFF} in the aging scale when $f = f_{\text{TH}}$. Otherwise, it gives a free-energy level dependent effective temperature. If one pursues the empirical relation between this parameter and the dynamic effective temperature this result means that when the system evolves in sufficiently long time-scales as to penetrate below the threshold it takes different values of T_{EFF} depending on the deepness it reached.

Mézard and Parisi generalised this approach to search for a Kauzmann critical temperature ($T_K = T_s$) and characterise the thermodynamic properties of the glassy phase below T_s in finite d interacting particle systems. The mean-field nature of the approach has been stressed by Thalmann [141] who showed that there is no lower critical dimension.

15.8 Dynamics and quantum systems

The derivation of the TAP equations presented in Section 15.2 can be generalized to treat other problems as the real-time dynamics [143] of the same models or their quantum extensions [144]. Again, the procedure can be made easy if one correctly chooses the perturbative expansion and the order parameters. To study the real-time dynamics of the classical problem one is forced to Legendre transform with respect to the time-dependent local magnetization, the two-time correlation and the response [143]. The presentation is further simplified when one uses the SUSY notation introduced in Section 8.2 that renders the dynamic formalism very close to the static one. For quantum problems in equilibrium one uses the Matsubara representation of the partition function and then Legendre transforms with respect to the imaginary-time correlation as well as the local magnetizations [144]. In order to derive TAP equations for a quantum problem in real-time one should use the Schwinger-Keldysh formalism.

The derivation and study of dynamic TAP equations justifies the interpretation of the asymptotic non-equilibrium dynamics in terms of the local properties of the TAP free-energy density landscape. Biroli [143] showed that the dynamics in the TAP free-energy landscape is in general non-Markovian due to the presence of memory terms in the dynamic TAP equations. In

the very long-time limit and for random initial conditions the contribution of these terms vanishes and one proves that the dynamics is a relaxation following flat directions in the TAP free-energy landscape (the *threshold*) as proposed in [3, 12].

16 Conclusions

We discussed the behaviour of a family of disordered models that yield a mean-field description of the glass transition and dynamics of super-cooled liquids and glasses. The relevance of these models to describe structural glasses was signaled and explained by Kirkpatrick, Thirumalai and Wolynes in the 80s [11]. Their nonequilibrium dynamics and hence the connection with other systems far from equilibrium started to develop more recently [12].

In short, their behaviour is the following. The dynamic transition arises when the partition function starts being dominated by an exponentially large number of metastable states yielding a finite complexity. The static transition instead is due to an entropy crisis, *i.e.* it occurs when the complexity vanishes and the number of states is no longer exponential in N , just as in the Adams-Gibbs-di Marzio scenario [176]. These transitions mimic, in a mean-field way, the crossover to the glassy phase at T_g and the putative static transition at T_o (or T_K) of fragile glasses, see Figure 2-left [11].

The equilibrium dynamics close and above T_d coincides with the one obtained with the mode-coupling approach [11]. It describes the relaxation of super-cooled liquids and it contains its most distinctive feature of having a two step decorrelation. The first step is ascribed to the motion of particles within the cages made by their neighbours while the second one is the structural relaxation related to the destruction of the cages.

Below T_d the equilibration time diverges with the size of the system and the models do not equilibrate any longer with their environments (unless one considers times that grow with the size of the system) [12]. This is very similar to the situation encountered in real systems below T_g . The experimental time-window is restricted and one is not able to equilibrate the samples any longer below T_g . Aging effects as shown in Figure 7 are captured. The correlations still decay to zero but they do in a waiting-time dependent manner. Their decay also occurs in two steps separated by a temperature-dependent plateau at a value related to the size of the cages. One can interpret their stiffness as increasing with the age of the system given that the beginning of the structural relaxation is delayed and slowed down for longer waiting-times.

The nonequilibrium dynamics below T_d approaches a threshold level of flat directions in phase space and it never goes below this level in finite times

with respect to the size of the system [12]. The aging dynamics corresponds to the slow drift of the point representing the system in the slightly tilted set of channels that form the threshold. The motion that is transverse to the channels is related to thermal fluctuations and the first stationary step of the relaxation towards q_{EA} , that characterises then the transverse “size” of the channel. The longitudinal motion along the channels is related to the structural relaxation. The tilt is proportional to the magnitude of the time-derivatives and these become less and less important as time passes. In more generality one interprets the long but finite time nonequilibrium dynamics following saddles that are the borders between basins of attraction of more stable states in phase space [3].

For times that scale with the size of the system, N , the sharp dynamic transition is avoided, the system penetrates below the threshold *via* activation and it approaches equilibrium in much longer time-scales. Metastable states below the threshold are typically minima [147, 149] (the fact that they are local minima can be checked studying the dynamics with initial conditions set to be in one of them [18, 139, 156]). This structure allows one to describe the cooling rate effects described in Figure 2-right. For large but finite N and sufficiently slow cooling rate, the system penetrates below the threshold *via* activation when this is facilitated by T , *i.e.* when passing near T_d . To which level it manages to arrive (roughly speaking to which of the curves in the figure) depends on how long it stays close to T_d . The slower the cooling rate the lower level the system reaches with the ideal “equilibrium” glass corresponding to an infinitely slow cooling [157].

The region of phase space reached asymptotically in the thermodynamic limit is the threshold of flat directions. The replica analysis of the partition function gives an alternative way of determining its statistical properties. Indeed, by evaluating the partition function on a marginally stable saddle-point in replica space one selects the threshold “states”. Dynamic information such as the value of q_{EA} is thus obtained with a pseudo-static calculation. Other facts as, for instance, the scaling of the correlation are not accessible in this way.

One of the hallmarks of the glassy nonequilibrium dynamics is the modification of the relation between correlations and responses, namely, the fluctuation-dissipation theorem. In mean-field models for structural glasses one finds that the integrated linear response is in linear relation with the associated correlation with a proportionality constant that takes the equilibrium value $1/(k_B T)$ when the correlation is above the plateau and it takes a different value $1/(k_B T^*)$ when it goes below the plateau [12]. This behaviour has been found in a number of finite dimensional glassy models numerically [53–55, 58].

The behavior just described corresponds to a family of mean-field disordered models to which the p spin models with $p \geq 3$ and the Potts glass belong. Other two families exist and they are related to ferromagnetic domain growth and spin-glasses. Two representative models are the spherical p spin model with $p = 2$ and the SK model, respectively. They are characterised by different scalings of the correlations in the aging regime and by different forms of the modification of FDT. The classification in families according to the nonequilibrium behaviour has a static counterpart given by the structure of replica symmetry breaking in the low- T phase, see Section 15.1.

The modification of FDT allows one to define an observable and correlation-scale dependent effective temperature [112]. Fast observables like the kinetic energy are equilibrated with the environment and the effective temperature equals the thermal bath temperature for them. Other observables though show different values of the effective temperature depending on the time-scales on which one investigates them. The effective temperature has a thermodynamical meaning even if defined out of equilibrium. In particular, it can be directly read with a thermometer coupled to the desired observable and a zero-th law holds for interacting observables that evolve in the same time-scale. As one should have expected the effective temperature shares some of the qualitative features of the phenomenological fictive temperatures [131]. For instance, a system that is quenched from high temperatures has effective temperatures that take higher values than the temperature of the bath, etc. At the mean-field level, when $N \rightarrow \infty$, it is history independent but one expects it to depend on the preparation of the sample for finite size and finite dimensional systems. (This is in close relation to the discussion above on cooling rate effects.) There is still no precise determination of which are the necessary conditions a nonequilibrium system has to fulfill to ensure the existence of well-behaved effective temperatures. A clear condition is the need to reach a dynamic regime in which the dynamics is slow and heat exchanges are weak.

Once the effective temperature has been identified one interprets the behaviour in the low T phase as follows: the system adjusts to a situation in which each observable sees two baths, one is the white external one and the one characterising the fast motion of the particles, the other is coloured and at a different temperature T^* . The latter is generated by the interactions. In more complex systems – as mean-field spin-glasses – the asymptotic regime might be multithermalised with several time-scales each with its own value of the effective temperature. These results, first derived explicitly for p spin fully-connected models [112] actually hold for any resummation of the perturbative approach that keeps an infinite subset of diagrams (the MCA being one such example). The structure of time-scales and values of the

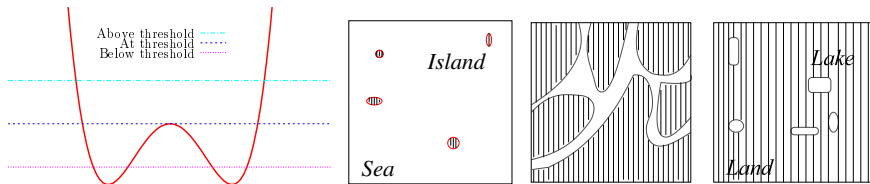


Fig. 21. Left: a 1d simplified sketch of the free-energy density. Three top views of the free-energy landscape: above, at and below the threshold.

effective temperature is related to the breaking of supersymmetry down to a residual group [130].

The structure of the free-energy landscape can be computed exactly for mean-field models in general, and for the spherical p spin model in particular [12, 147–149, 170]. We expect its main features to be reproduced – at least in a smoothen way – in real glassy systems. The free-energy landscape at fixed and low T has a structure as the one roughly sketched in Figure 21. A pictorial image of the aging process can be quite helpful to understand it. Imagine that one fills phase space with water whose level reaches a free-energy density value, say, f . At high levels of the water, *i.e.* for high free-energy densities, the landscape has only some few isolated stationary states. Looking at the landscape from above one only sees some maxima that are represented as islands in the second panel in the figure. Lowering the water level the islands grow in size and some of them merge: land bridges develop. Lowering still the water level, it eventually reaches a threshold, that corresponds to $f = f_{\text{Th}}$, where land percolates. One is left with a labyrinthic path of water as drawn schematically in the third panel that represents a top view of the landscape. This level is “marginal” since the bottom of the water channels is almost completely flat. Draining water from the system the “connectivity” of paths is reduced until the water level goes below the threshold, $f < f_{\text{Th}}$, where minima dominate. In the fourth panel we represent them as lakes immersed in land. Lowering the water level one sees the sizes of the lakes diminish and some of them dry. These minima exist until the lowest level, $f = f_{\text{Eq}}$. A “gap” in free-energy density separates the threshold and the equilibrium levels.

This picture allows us to give a natural interpretation of the nonequilibrium dynamics following a quench. Initially, the system is in a configuration typical of high- T , thus, its initial “free-energy density” is very high. This corresponds to a high level of water that fills the landscape. As time passes, water abandons the landscape in such a way that the quantity of water progressively diminishes lowering its level. The system’s configuration can be associated to a ship and its evolution to the displacements of the ship

sailing on the water. Initially, the water level is very high and the ship can move very rapidly far away from its initial position. It only sees some very few isolated islands that it simply avoids along its motion and the dynamics is very fast. As time passes the water level goes down. Roughly speaking we can associate the speed of drainage with the magnitude of the rate of change of the energy-density. When it approaches the threshold the available path becomes a series of rivers forming a very intricate network. The ship can still follow this network without remaining trapped in any confining region. Its motion, however, gets slower and slower. In finite times with respect to N the water level does not go below the threshold. But for longer times that scale with N it does. When such long times are attained the ship remains trapped in lakes. For still longer times the higher lakes dry and, if the ship got trapped in one of them it must be transported through the land to reach other lakes at lower levels. This action represents an activated process. Part of this image was introduced by Sibani and Hoffmann, and Campbell, phenomenologically [151]. The p spin-models and the like realise it explicitly. All quantitative features of the landscape here described with words have been, or in principle can be, calculated analytically. The use of this image has been ultimately justified by the dynamic TAP approach of Biroli [143].

The value taken by the effective temperature is in direct relationship with the structure of the free-energy landscape. Indeed, again for p -spin model and the like, it has been shown analytically that the asymptotic value T^* reached for long but finite times with respect to N is given by $\beta^* = \partial \Sigma(\beta, f) / \partial f|_{f_{\text{th}}}$, with Σ the complexity [138]. For even longer times such that the system penetrates below the threshold one expects the effective temperature to take different values related to the complexity at lower free-energy density levels. The Edwards-Anderson parameter, q_{EA} , also changes since $q_{\text{EA}}(f)$. In the longest time-scale such that equilibrium is reached q_{EA} equals the equilibrium value also obtained with a replica calculation using the standard maximization prescription to determine the breaking point parameter x . This result is intimately related to Edwards' flat measure for granular matter [33, 134] and also to the more recent use of a flat measure over inherent structures [136] to describe the nonequilibrium dynamics of glasses [137, 159, 160]. Note that these, being defined using the *potential energy-density* landscape, are valid only at zero temperature (see, e.g. [142]). However, extensive numerical checks recently performed suggest that the approach, even if not obviously correct at finite T , yields a very good approximation [137].

Within this picture two distinct regimes would appear in the low- T isothermal dynamics of real systems: a mean-field-like one when the system approaches a pseudo-threshold of flat directions in phase space and a

slower activated regime in which the system jumps over barriers to relax its excess energy density and very slowly progress towards equilibrium. How and if the aging properties in the first and second regime resemble is a very interesting open problem.

The existence of a threshold plays a fundamental role in explaining several features of many experimental observations in such diverse systems as driven granular matter, the rheological properties of complex liquids and glasses, etc. Just to cite two examples, trapping and Reynolds dilatancy effects in granular matter [26, 33] as well as the existence of a static yield stress and thixotropic behaviour in some rheological experiments [19] can be interpreted in terms of threshold and subthreshold states. These features support the claim that this free-energy structure exists in real physical systems. Moreover, maybe not surprisingly, this structure also appears in optimisation problems such as XOR-SAT and K-SAT that can be mapped to dilute p -spin models at zero temperature. In this context the control parameter is the number of requirements over the number of variables, α , and the static transition, α_s , is related to the sat-unsat transition while the dynamic transition, $\alpha_d < \alpha_s$ corresponds to the value where some greedy algorithms fail to find the existing solutions [152].

All these arguments can be adapted to include quantum fluctuations. The statics is studied with the Matsubara replicated partition function [173], metastability with an extension of the TAP approach [144] and the real-time dynamics with the Schwinger-Keldysh formalism [85, 106]. The picture that arises is very similar to the one above with some intriguing new ingredients as the emergence of truly first order transitions close to the quantum critical point [173, 175], highly non-trivial effects due to the quantum environments [144], a waiting-time dependent quantum-to-classical crossover in the dynamic scaling, etc.

The models we studied in these notes have quenched random interactions. Real glassy systems of the structural type do not. One may wonder if this is an important deficiency of the approach or if similar results can be obtained for models with no disorder. A large variety of models of mean-field type, or defined on large d spaces, with no explicit quenched disorder and having the same phenomenology have been introduced in recent years [140, 165]. Finite d models with similar, eventually interrupted, dynamic behaviour have also been exhibited [53–55]. Their existence supports the belief that the scenario here summarized goes beyond simple modelling. Indeed, it is at the basis of several conjectures for the behaviour of other nonequilibrium systems with slow dynamics that have been later checked numerically. It has also motivated several experimental investigations in a variety of systems.

17 Perspectives

We would like to end these notes by mentioning some of the directions for future development in this area. Within the “mean-field” approach there remain at least two important open technical problems to complete their analytic solution:

Matching. Having approximated the dynamic equations as explained in the text we are not able to determine the complete scaling form of correlations and responses. In models like the p spin spherical we cannot fix the scaling function $h(t)$. Going beyond the asymptotic solution requires to solve the matching of the solution at short time-differences with the one at long time-differences. This is a very tough mathematical problem.

Dynamics at infinite time-scales. In order to penetrate below the threshold in p spin spherical models and approach equilibrium one has to consider times that grow with N and include instanton solutions to describe the activated dynamics below T_d . This will smoothen the dynamic transition and convert it into a crossover. It will also possibly allow the mode-coupling and similar approaches to yield more accurate quantitative predictions.

Even though the models we discussed are mean-field we believe that the general picture developed holds beyond this limit. Some numerical and experimental tests support this belief. Still, one would like to justify this claim theoretically. Some of the lines of research that are now being followed with this aim are:

Dynamics of dilute disordered models. These are disordered spin models on random graphs. Even if still mean-field they include some spatial fluctuations that one can study numerically and analytically [88, 153]. Moreover, their relation to optimisation problems make them interesting *per se*.

Dynamic heterogeneities. Supposedly these are nanoscale regions in supercooled liquids and glasses that are very important in determining the glass transition and the dynamics. They have been studied numerically and experimentally so far and one would like to have a theoretical model including and describing them. A step in this direction was followed in [84] where a sigma-model-like description for the spin-glass problem was introduced. This lead to proposing that the distribution of the coarse-grained local correlations and responses should be constrained to follow the global relation $\chi(C)$; this proposal was checked numerically in [117] for the 3dEA and studies on other disordered models are underway. The study of these distributions in real glasses as well as the development of a complete analytical description are problems that deserve further study.

Dynamic functional renormalisation group (FRG). It would be very interesting to extend the FRG to attack nonequilibrium situations with aging dynamics.

FD relations for finite d systems. Many questions about the form of the relations between global responses and correlations in real systems can be raised. Do all systems undergoing domain growth in $d > 1$ have two-time scales with the slower one characterised by $T^* \rightarrow \infty$? Can a situation as the one found for the SK model be realised, *i.e.* does any real system have an effective temperature with more than two values (T and T^*)?

Relations between statics and dynamics. A link between the nonequilibrium FD relations and Parisi's $P(q)$ was found in some mean-field models (note that it does not hold for models with a threshold as the p spin). It was then argued that it should hold in finite d systems under certain assumptions [154]. The long-lasting debate about the nature of the spin-glass phase has now been rephrased in nonequilibrium terms, the question now being what is the form of the asymptotic $\chi(C)$ plot. Recent experiments address this problem [32]. Analytical results for finite d models are yet not available.

Thermodynamics and statistical mechanics out of equilibrium. From a more generic viewpoint, the development of a thermodynamics and statistical mechanics for models that evolve slowly out of equilibrium is a very important issue. Some progress in both directions has been made recently. One should try to establish these proposals in a less phenomenological way.

All these problems are challenging and very interesting. Many more could be added to this short list. We can expect to see progress in this very active area of research in the near future.

The author specially thanks J. Kurchan for his collaboration on this and other subjects, and G. Semerjian for very useful discussions and the careful correction of the manuscript. LFC is ICTP research scientist, acknowledges financial support from the Guggenheim Foundation and the ACI "Algorithms d'optimisation et systèmes désordonnés quantiques" and thanks the Universities of Buenos Aires and La Plata (Argentina) and Harvard University for hospitality during the preparation of these notes.

A Generalized Langevin equations

In this Appendix we derive a generalized Langevin equation starting from time-reversal microscopic equations for the motion of the system *and* the constituents of the bath. We use the simplest image of a thermal bath that is given by an ensemble of harmonic oscillators with masses m_α and frequencies ω_α , $\alpha = 1, \dots, N$ and, for simplicity, we consider a system made of a single particle with mass M . We consider the one-dimensional case to simplify the notation. The generalization to more complex systems and/or

to more complicated baths and higher dimensions is straightforward [155]. We call q, p and x_α, p_α , $\alpha = 1, \dots, N$ the positions and momenta of the particle and oscillators, respectively. The Hamiltonian of the total system is of the form (4.1),

$$H = \frac{p^2}{2M} + V(q) + \frac{1}{2} \sum_{\alpha=1}^N \frac{c_\alpha^2}{m_\alpha \omega_\alpha^2} q^2 + \sum_{\alpha=1}^N \frac{p_\alpha^2}{2m_\alpha} + \frac{1}{2} \sum_{\alpha=1}^N m_\alpha \omega_\alpha^2 x_\alpha^2 - \sum_{\alpha=1}^N c_\alpha q x_\alpha.$$

All these terms have been discussed in Section 4.1.1. Hamilton's equations for the particle are

$$\dot{q}(t) = \frac{p(t)}{M}, \quad \dot{p}(t) = -\frac{\partial V(q)}{\partial q(t)} - \sum_{\alpha=1}^N \frac{c_\alpha^2}{m_\alpha \omega_\alpha^2} q(t) + \sum_{\alpha=1}^N c_\alpha x_\alpha(t), \quad (\text{A.1})$$

while the dynamic equations for each member of the environment read

$$\dot{x}_\alpha(t) = \frac{p_\alpha(t)}{m_\alpha}, \quad \dot{p}_\alpha(t) = -m_\alpha \omega_\alpha^2 x_\alpha(t) + c_\alpha q(t), \quad (\text{A.2})$$

showing that they are all forced massive harmonic oscillators. These equations are readily solved yielding

$$x_\alpha(t) = x_\alpha(0) \cos(\omega_\alpha t) + \frac{p_\alpha(0)}{m_\alpha \omega_\alpha} \sin(\omega_\alpha t) + \frac{c_\alpha}{m_\alpha \omega_\alpha} \int_0^t dt' \sin(\omega_\alpha(t-t')) q(t') \quad (\text{A.3})$$

with $x_\alpha(0)$ and $p_\alpha(0)$ the initial coordinate and position at time $t = 0$ when the particle has been set in contact with the bath. The replacement of this expression in the last term on the RHS of equation (A.1), implies

$$\dot{p}(t) = -\frac{\partial V(q)}{\partial q(t)} + \eta(t) - \int_0^t dt' \gamma(t-t') \dot{q}(t') - \sum_{\alpha=1}^N \frac{c_\alpha^2}{m_\alpha \omega_\alpha^2} \cos(\omega_\alpha t) q(0), \quad (\text{A.4})$$

with the kernel γ given by

$$\gamma(t-t') = \sum_{\alpha=1}^N \frac{c_\alpha^2}{m_\alpha \omega_\alpha^2} \cos(\omega_\alpha(t-t')), \quad (\text{A.5})$$

and the time-dependent force η given by

$$\eta(t) = \sum_{\alpha=1}^N \frac{c_{\alpha}}{m_{\alpha}\omega_{\alpha}} p_{\alpha}(0) \sin(\omega_{\alpha}t) + \sum_{\alpha=1}^N c_{\alpha} x_{\alpha}(0) \cos(\omega_{\alpha}t). \quad (\text{A.6})$$

Usually, the environments are made of ensembles of *equilibrated* entities at a chosen temperature T . Then, $\{p_{\alpha}(0), x_{\alpha}(0)\}$ are initially distributed according to

$$P(\{p_{\alpha}(0), x_{\alpha}(0)\}) = \frac{\exp(-\beta H_{\text{ENV}}[\{p_{\alpha}(0), x_{\alpha}(0)\}])}{\int \prod_{\alpha=1}^N dp_{\alpha}(0) dx_{\alpha}(0) \exp(-\beta H_{\text{ENV}}[\{p_{\alpha}(0), x_{\alpha}(0)\}])}. \quad (\text{A.7})$$

It is convenient to assume that the equilibrium distribution is shifted with respect to the coupling to the particle at the initial time; this allows one to eliminate the last term in equation (A.4). As when including the counter-term, we choose

$$H_{\text{ENV}} = \sum_{\alpha} \left[\frac{m_{\alpha}\omega_{\alpha}^2}{2} \left(x_{\alpha} - \frac{c_{\alpha}}{m_{\alpha}\omega_{\alpha}^2} q(0) \right)^2 \frac{p_{\alpha}^2}{2m_{\alpha}} \right]. \quad (\text{A.8})$$

Defining a new noise $\xi(t) = \eta(t) - \sum_{\alpha=1}^N \frac{c_{\alpha}^2}{m_{\alpha}\omega_{\alpha}^2} \cos(\omega_{\alpha}t) q(0)$, it is a Gaussian random variable with

$$\langle \xi(t) \rangle = 0 \quad \text{for all times}, \quad (\text{A.9})$$

$$\langle \xi(t)\xi(t') \rangle = k_{\text{B}}T \gamma(t-t') \quad (\text{A.10})$$

and the Langevin equation simplifies to

$$\dot{p}(t) = -\frac{\partial V(q)}{\partial q(t)} + \xi(t) - \int_0^t dt' \gamma(t-t') \dot{q}(t'). \quad (\text{A.11})$$

A random force with non-vanishing correlations on a finite support is usually called a *colored noise*.

Interestingly enough, $\gamma(t-t')$ and the noise-noise correlation are proportional, with a constant of proportionality of value $k_{\text{B}}T$. This is a generalized form of the fluctuation-dissipation relation, and it applies to the environment. In this derivation it is clear that it is a consequence of having assumed the equilibration of the bath.

The third term on the RHS of equation (A.11) represents a rather complicated friction force. Its value at time t depends explicitly on the history of the particle at times $0 \leq t' \leq t$. The memory kernel $\gamma(t-t')$ plays the rôle of a retarded friction function. This term makes equation (A.11) non-Markovian.

Different choices of the environment are possible by selecting different ensembles of harmonic oscillators. The simplest choice, that leads to an approximate Markovian equation, is to consider identical oscillators coupled to the particle *via* the coupling constants $\pm c/\sqrt{N}$ but having a non-trivial distribution of frequencies, that in the limit $N \rightarrow \infty$, can be treated as continuous. This allows one to introduce the spectral density $I(\omega)$ and rewrite the kernel γ as

$$\gamma(t-t') = \frac{c^2}{m} \int_0^\infty d\omega I(\omega) \frac{\cos(\omega(t-t'))}{\omega^2}. \quad (\text{A.12})$$

For a Debye distribution of frequencies

$$I(\omega) = \frac{3\omega^2}{\omega_D^3} \theta(\omega_D - \omega) \quad \text{one has} \quad \gamma(t-t') = \frac{3c^2}{m\omega_D^2} \frac{\sin(\omega_D(t-t'))}{\omega_D(t-t')}. \quad (\text{A.13})$$

If ω_D is sufficiently large, γ can be approximated by a delta function, $\gamma(t-t') = 2\gamma\delta(t-t')$ with $\gamma = 3c^2\pi/(2m\omega_D^2)$, and equation (A.4) becomes Markovian.

Different environments are characterized by different choices of the spectral density $I(\omega)$ at small ω . For example, one has an Ohmic ($s = 1$), sub-Ohmic ($s < 1$) or super-Ohmic ($s > 1$) bath if $I(\omega) \sim \omega^s$ for $\omega \sim 0$.

B The Kubo formula

The Kubo formula relates the linear response to the asymmetric correlation of a quantum process. It holds at the level of the linear response even if the system is out of equilibrium. The linear response reads

$$\begin{aligned} R_{AB}(t, t') &= \frac{\delta}{\delta h_B(t')} \left[\frac{1}{Z(h_B)} \text{Tr} \left(\hat{U}_t(h_B) \hat{A}(0) \hat{U}_t^{-1}(h_B) \hat{\rho}(0) \right) \right] \Big|_{h_B=0} \\ &= -\frac{1}{Z^2(h_B)} \frac{\delta Z(h_B)}{\delta h_B(t')} \text{Tr} \left[\hat{U}_t(h_B) \hat{A}(0) \hat{U}_t^{-1}(h_B) \hat{\rho}(0) \right] \Big|_{h_B=0} \\ &+ \frac{1}{Z(0)} \text{Tr} \left[\left(\frac{\delta \hat{U}_t(h_B)}{\delta h_B} \hat{A}(0) \hat{U}_t^{-1}(h_B) + \hat{U}_t(h_B) \hat{A}(0) \frac{\delta \hat{U}_t^{-1}(h_B)}{\delta h_B} \right) \hat{\rho} \right] \Big|_{h_B=0} \end{aligned}$$

where $U_t(h_B)$ is the evolution operator, $U_t(h_B) \exp[i/\hbar \hat{H} \delta]$ for all infinitesimal time intervals except from the one going from $t' - \delta/2$ to $t' + \delta/2$ where it takes the form $U_t(h_B) \exp[i/\hbar (\hat{H} - h_B \hat{B})]$. See the left-panel in Figure 8 for a graphical representation of a kick-like perturbation. $t \geq t'$. Calculating

the variations explicitly, and using $\langle \hat{A}(t) \rangle = 0$, we have

$$\begin{aligned} R_{AB}(t, t') &= \frac{1}{Z(0)} \text{Tr} \left[\frac{i}{\hbar} \left(-B(t') U_t(0) A(0) U_t^{-1}(0) \right. \right. \\ &\quad \left. \left. + U_t(0) A(0) B(t') U_t^{-1}(0) \right) \hat{\rho} \right] \Big|_{h_B=0} \\ &= \frac{i}{\hbar} \langle [A(t), B(t')] \rangle. \end{aligned} \quad (\text{B.1})$$

C The response in a Langevin process

By definition the linear response is given by

$$\begin{aligned} \frac{\delta \langle q(t) \rangle_h}{\delta h(t')} \Big|_{h=0} &= \frac{\delta}{\delta h(t')} \int \mathcal{D}q \mathcal{D}i\hat{q} \mathcal{D}\bar{\psi} \mathcal{D}\psi q(t) \\ &\quad \times \exp \left(-S_{\text{EFF}} + \int dt'' i\hat{q}(t'') h(t'') \right) \Big|_{h=0} \end{aligned}$$

with S_{EFF} defined in equation (8.6) and evaluated at vanishing sources. The RHS immediately leads to $R(t, t') = \langle q(t) i\hat{q}(t') \rangle$, *i.e.* equation (8.7).

The proof of the relation (8.8) is slightly more involved. The correlation between coordinate and noise can be obtained from the variation with respect to $\lambda(t, t')$ of the generating functional (8.3) once the identities (8.4) and (8.5) have been used and the source

$$\int dt'' dt''' \lambda(t'', t''') q(t'') \xi(t''') \quad (\text{C.1})$$

has been added. Integrating over the noise and keeping only the linear terms in λ in the effective action since all others will vanish when setting $\lambda = 0$

$$\begin{aligned} \text{Linear terms} &= \frac{k_B T}{2} \int dt_1 dt_2 dt_3 dt_4 [\lambda(t_1, t_2) q(t_1) \gamma(t_2, t_3) i\hat{q}(t_4) \delta(t_4 - t_3) \\ &\quad + i\hat{q}(t_1) \delta(t_1 - t_2) \gamma(t_2, t_3) \lambda(t_4, t_3) q(t_4)]. \end{aligned} \quad (\text{C.2})$$

The variation with respect to $\lambda(t, t')$ yields $(k_B T)/2 \int dt'' [\gamma(t'', t'') + \gamma(t'', t')] \langle q(t) i\hat{q}(t') \rangle = \langle q(t) \xi(t') \rangle$.

D Grassmann variables and supersymmetry

Grassmann variables anticommute $\theta^2 = \bar{\theta}^2 = [\theta, \bar{\theta}]_+ = 0$. The integration rules are $\int d\theta = \int d\bar{\theta} = 0$ and $\int d\theta \theta = \int d\bar{\theta} \bar{\theta} = 1$ while the derivation is such that $\partial_\theta = \int d\theta$ and $\partial_{\bar{\theta}} = \int d\bar{\theta}$.

In the supersymmetric formalism used in Section 8 one enlarges the usual “bosonic” space to include two conjugate Grassmann variables θ and $\bar{\theta}$: $t \rightarrow a = (t, \theta, \bar{\theta})$. A “superfield” and its “supercorrelator” are then defined as

$$\Phi(a) \equiv q(t) + \psi(t)\bar{\theta} + \bar{\psi}(t)\theta + i\hat{q}(t)\bar{\theta}\theta, \quad Q(a, b) \equiv \langle \Phi(a)\Phi(b) \rangle, \quad (\text{D.1})$$

$b = (t', \theta, \bar{\theta}')$. The latter encodes the usual correlations $\langle q(t)q(t') \rangle$, $\langle q(t)i\hat{q}(t') \rangle$, $\langle i\hat{q}(t)q(t') \rangle$, $\langle i\hat{q}(t)i\hat{q}(t') \rangle$, as well as “fermionic” correlators $\langle q(t)\psi(t') \rangle$, $\langle \bar{\psi}(t)i\hat{q}(t') \rangle$, $\langle \bar{\psi}(t)\psi(t') \rangle$, etc. The solutions we construct and study are such that all correlators that involve only one fermionic variable ψ and $\bar{\psi}$ vanish. We are then left with the usual four purely bosonic correlators and the fermion bilinears. One proves that the latter equal the linear response. If, moreover, we only consider causal solutions, $\hat{Q}(t, t') \equiv \langle i\hat{q}(t)i\hat{q}(t') \rangle = 0$ and

$$Q(a, b) = C(t, t') - (\bar{\theta}' - \bar{\theta})(\theta' R(t, t') - \theta R(t', t)). \quad (\text{D.2})$$

Convolutions, or operational products, and Hadamard, or simple products, are defined as

$$\begin{aligned} Q_1(a, b) \otimes Q_2(b, c) &= \int db Q_1(a, b) Q_2(b, c), \\ Q_1(a, b) \bullet Q_2(a, b) &= Q_1(a, b) Q_2(a, b), \end{aligned} \quad (\text{D.3})$$

respectively, with $db \equiv dt d\bar{\theta} d\theta$.

For correlators of the causal form (D.2), the convolution and the Hadamard product respect the structure of the correlator. Indeed, the result of the convolution is again of the form (D.2) with

$$\begin{aligned} C_{\text{CONV}}(t, t'') &= \int dt' [C_1(t, t') R_2(t'', t') + R_1(t, t') C_2(t', t'')], \\ R_{\text{CONV}}(t, t'') &= \int dt' R_1(t, t') R_2(t', t''), \end{aligned} \quad (\text{D.4})$$

and the result of the Hadamard product is also of the form (D.2) with

$$\begin{aligned} C_{\text{HAD}}(t, t') &= C_1(t, t') C_2(t, t'), \\ R_{\text{HAD}}(t, t') &= C_1(t, t') R_2(t, t') + C_2(t, t') R_1(t, t'). \end{aligned} \quad (\text{D.5})$$

The Dirac delta function is defined as $\delta(a - b) = \delta(t - t')(\bar{\theta} - \bar{\theta}')(\theta - \theta')$.

E Integrals in the aging regime

Integrals of the form

$$I_1(t) \equiv \int_0^t dt'' A(t, t'') B(t, t'') \quad (\text{E.1})$$

appear, for example, in the equation for $\mu(t)$. We separate the integration time-interval as in equation (12.8). If δ is chosen to be a finite time, $A(t, t'')$ and $B(t, t'')$ in the first interval can be approximated by $A(t, 0)$ that vanishes when $t \rightarrow \infty$. Since the integration interval is finite, this term can be neglected. In the second interval the functions vary in the aging regime and in the third interval they vary in the stationary regime. Thus

$$I_1(t) \sim \int_{\delta}^{\Delta_t} dt'' A_{\text{AG}}(t, t'') B_{\text{AG}}(t, t'') + \int_{\Delta_t}^t dt'' \left[\left(A_{\text{ST}}(t - t'') \right. \right. \\ \left. \left. + \lim_{t-t'' \rightarrow \infty} \lim_{t'' \rightarrow \infty} A(t, t'') \right) \left(B_{\text{ST}}(t - t'') + \lim_{t-t'' \rightarrow \infty} \lim_{t'' \rightarrow \infty} B(t, t'') \right) \right].$$

We assume that this separation is sharp and that we can neglect the corrections associated to mixing of the three regimes. In the third term we replaced A and B in terms of A_{ST} , B_{ST} . We can now replace the lower limit of the first integral by 0 and its upper limit by t . In addition, assuming that B is proportional to the response,

$$\lim_{t-t'' \rightarrow \infty} \lim_{t'' \rightarrow \infty} B(t, t'') = 0, \quad (\text{E.2})$$

and that A is a function of the correlation such that

$$\lim_{t-t'' \rightarrow \infty} \lim_{t'' \rightarrow \infty} A(t, t'') = A_{q_{\text{EA}}} \quad (\text{E.3})$$

we have

$$I_1(t) \sim \int_0^t dt'' A_{\text{AG}}(t, t'') B_{\text{AG}}(t, t'') + A_{q_{\text{EA}}} \int_0^{\infty} d\tau' B_{\text{ST}}(\tau') \\ + \int_0^{\infty} d\tau' A_{\text{ST}}(\tau') B_{\text{ST}}(\tau')$$

where the upper limit tending to infinity is $t - \Delta_t \rightarrow \infty$.

Another type of integrals is: $I_2(t, t') \equiv \int_{t'}^t dt'' A(t, t'') B(t'', t')$. In particular, if $B = 1$, $A(t, t'') = R(t, t'')$, $t' = 0$ and $t \rightarrow \infty$, this integrals yields the static susceptibility. If instead, t' is long and t too we have the type of integral appearing in the equation for the response. Let us assume

that t and t' are far apart; we start by dividing the time interval in three subintervals

$$\int_{t'}^t = \int_{t'}^{\Delta_{t'}} + \int_{\Delta_{t'}}^{\Delta_t} + \int_{\Delta_t}^t \quad (\text{E.4})$$

and by approximating the functions A and B assuming that they have a two-step decay as the one in Sections 11.1 and 11.2:

$$\begin{aligned} I_2(t, t') \sim & \int_{t'}^{\Delta_{t'}} dt'' A_{\text{AG}}(t, t'') B(t'' - t') + \int_{\Delta_{t'}}^{\Delta_t} dt'' A_{\text{AG}}(t, t'') B_{\text{AG}}(t'', t') \\ & + \int_{\Delta_t}^t dt'' A(t - t'') B_{\text{AG}}(t'', t'). \end{aligned} \quad (\text{E.5})$$

In the first term $B(t - t'')$ can be replaced by $B(t - t'') = \lim_{t-t'' \rightarrow \infty} \times \lim_{t'' \rightarrow \infty} B(t, t'') + B_{\text{ST}}(t - t'')$. The same applies to A in the last term. All functions vary fast in the stationary regime but very slowly in the aging regime. The next assumption is that functions in the aging regime that are convoluted with functions in the stationary regime, can be considered to be constant and taken out of the integrals. That is to say

$$\begin{aligned} I_2(t, t') \sim & A_{\text{AG}}(t, t') \int_{t'}^{\Delta_{t'}} dt'' B(t'' - t') + \int_{\Delta_{t'}}^{\Delta_t} dt'' A_{\text{AG}}(t, t'') B_{\text{AG}}(t'', t') \\ & + B_{\text{AG}}(t, t') \int_{\Delta_t}^t dt'' A(t - t'') \\ \sim & A_{\text{AG}}(t, t') \int_0^\infty d\tau' B(\tau') + \int_{t'}^t dt'' A_{\text{AG}}(t, t'') B_{\text{AG}}(t'', t') \\ & + B_{\text{AG}}(t, t') \int_0^\infty d\tau' A(\tau'), \end{aligned} \quad (\text{E.6})$$

where we used $t - \Delta_t \rightarrow \infty$ and $\Delta_{t'} - t' \rightarrow \infty$. When this integral appears in the equation for the response, $A(\tau')$ and $B(\tau')$ are proportional to the response function since one is the response itself and the other is the self-energy. Using FDT the integrals in the first and third term can be computed in the classical limit or they can be expressed as functions of the correlation in the quantum case. The second term instead depends exclusively on the aging dynamic sector.

All other integrals can be evaluated, in the large-time limit, in a similar way.

References

- [1] A.J. Bray, *Adv. Phys.* **43** (1994) 357.
- [2] See, e.g. D.S. Fisher, *Physica A* **263** (1999) 222.
- [3] J. Kurchan and L. Laloux, *J. Phys. A* **29** (1996) 1929.
- [4] Many review articles describe the phenomenology of super-cooled liquids and glasses. See, e.g. M.D. Ediger, C.A. Angell and S.R. Nagel, *J. Phys. Chem.* **100** (1996) 13200. P.G. Debenedetti and F.R. Stillinger, *Nature* **410** (2001) 259. W. Kob in this volume.
- [5] One can think as the super-cooled liquid as a metastable state in the usual sense: its properties can be computed using a restricted partition function and, in particular, the dynamics is stationary and satisfies FDT even if the system is not equilibrated in its true most favorable state – the crystal. The glass, instead, is also metastable but of a different kind: one cannot describe all its properties with a stationary probability distribution.
- [6] E. Weeks and D. Weitz, *Phys. Rev. Lett.* **89** (2002) 095704. <http://www.physics.emory.edu/faculty/weeks/>
- [7] K. Binder and A.P. Young, *Rev. Mod. Phys.* **58** (1986) 801. K. Fischer and J. Hertz, *Spin-glasses* (Cambridge Univ. Press., Cambridge, 1991).
- [8] V. Dotsenko, M.V. Feigel'man and L.B. Ioffe, *Spin-glasses and related problems*, Soviet Scientific Review, 15, Harwood, 1990. S.L. Ginzburg, *Sov. Phys. JETP* **63** (1986) 439.
- [9] M. Mézard, G. Parisi and M.A. Virasoro, *Spin-glasses and beyond* (World Scientific, Singapore, 1987).
- [10] H. Kawamura and M.S. Li, *Phys. Rev. Lett.* **87** (2001) 187204. H. Kawamura, [`cond-mat/0210012`] and references therein [`cond-mat/0212591`].
- [11] T.R. Kirkpatrick and D. Thirumalai, *Phys. Rev. Lett.* **58** (1987) 2091; *Phys. Rev. B* **36** (1987) 5388. T.R. Kirkpatrick and P. Wolynes, *Phys. Rev. B* **36** (1987) 8552.
- [12] L.F. Cugliandolo and J. Kurchan, *Phys. Rev. Lett.* **71** (1993) 173.
- [13] For a review see J.-P. Bouchaud, L.F. Cugliandolo, J. Kurchan and M. Mézard, in *Spin glasses and random fields*, A.P. Young ed. (World Scientific, 1998).
- [14] W. Wu *et al.*, *Phys. Rev. Lett.* **67** (1991) 2076. W. Wu *et al.*, *Phys. Rev. Lett.* **71** (1993) 1919. T.F. Rosenbaum, *J. Phys. C* **8** (1996) 9759. E. Courtens, *J. Phys. Lett. (Paris)* **43** (1982) L199; *Phys. Rev. Lett.* **52** (1984) 69. E. Matsushita and T. Matsubara, *Prog. Theor. Phys.* **71** (1984) 235. R. Pirc, B. Tadic and R. Blinc, *Z. Phys. B* **61** (1985) 69; *Phys. Rev. B* **36** (1987) 8607.
- [15] S. Rogge, D. Natelson and D.D. Osheroff, *Phys. Rev. Lett.* **76** (1996) 3136. S. Rogge, D. Natelson, B. Tigner and D.D. Osheroff, *Phys. Rev. Lett.* **78** (1997) 11256. D. Natelson, D. Rosenberg and D.D. Osheroff, *Phys. Rev. Lett.* **80** (1998) 4689.
- [16] A. Vaknin, Z. Ovadyahu, M. Pollak, *Phys. Rev. Lett.* **84** (2000) 3402. Z. Ovadyahu, in this volume.
- [17] M. Cates, in this volume. A. Adjari, in this volume.
- [18] L.F. Cugliandolo, J. Kurchan, P. Le Doussal and L. Peliti, *Phys. Rev. Lett.* **78** (1997) 350. See also H. Horner, *Z. Phys. B* **57** (1984) 29; *ibid.*, 39.
- [19] L. Berthier, Ph.D. Thesis, ENS-Lyon, France, 2001 and [`cond-mat/0209394`].
- [20] R. Graham, *Springer Tracts Modern Phys.* **66** (Springer, Berlin, 1973).
- [21] J.D. Ferry, *Viscoelastic properties of polymers* (Wiley, New York, 1980). R.G. Larson, *The structure of rheology of complex fluids* (Oxford Univ. Press, Oxford, 1990).

- [22] H.-M. Jaeger, S.R. Nagel and R.P. Behringer, *Rev. Mod. Phys.* **68** (1996) 1259. J.-P. Bouchaud, in this volume.
- [23] C. Josserand, A. Tkachenko, D.M. Mueth and H.M. Jaeger, *Phys. Rev. Lett.* **85** (2000) 3632. J. Török, S. Krishnamurthy, J. Kertész and S. Roux [`cond-mat/0003070`]. F. Restagno, C. Ursini, H. Gayvallet, E. Charlaix [`cond-mat/0209210`].
- [24] M. Sellitto, *Eur. J. Phys. B* **4** (1998) 135. M. Nicodemi, *Phys. Rev. Lett.* **82** (1999) 3734. M. Nicodemi and A. Coniglio, *Phys. Rev. Lett.* **82** (1999) 916. A. Barrat and V. Loreto, *J. Phys. A* **33** (2000) 4401. M. Sellitto and J.J. Arenzon, *Phys. Rev. E* **62** (2000) 7793. J. Talbot, G. Tarjus and P. Viot, *Eur. J. E* **5** (2001) 495. M. Sellitto, *Phys. Rev. E* (2001) 060301R. J. Berg and A. Mehta, *Adv. Compl. Syst.* **4** (2001) 309.
- [25] A. Barrat, V. Colizza and V. Loreto [`cond-mat/0205285`].
- [26] L. Berthier, L.F. Cugliandolo and J.L. Iguain, *Phys. Rev.* **63** (2001) 051302.
- [27] G. Blatter *et al.*, *Rev. Mod. Phys.* **66** (1994) 1125. T. Giamarchi and P. Le Doussal, *Statics and dynamics of disordered elastic systems* in “Spin-glasses and random fields”, ed. A.P. Young (World Scientific, Singapore, 1998). T. Nattermann and S. Scheidl, *Adv. Phys.* **49** (2000) 607.
- [28] T. Giamarchi [`cond-mat/0205099`].
- [29] L.C.E. Struick, *Physical aging in amorphous polymers and other materials* (Elsevier, Houston, 1976).
- [30] The geometrical properties of low-energy excitations in spin-glasses are the subject of present debate. See, *e.g.* J. Houdayer, F. Krzakala and O.C. Martin, *Eur. J. Phys. B* **18** (2000) 467. F. Krzakala, Ph.D. Thesis Univ. Paris Sud, France, 2002. M. Palassini and A.P. Young, *Phys. Rev. Lett.* **85** (2000) 3017. J. Lamarcq *et al.* *Eur. Lett.* **58** (2002) 321. The geometrical properties of growing objects has been discussed in H. Yoshino, K. Hukushima and H. Takayama [`cond-mat/0202110`] and [`cond-mat/0203267`]. H. Castillo *et al.* (in preparation).
- [31] The aging properties in spin-glasses are reviewed in E. Vincent *et al.* *Slow dynamics and aging in glassy systems*, in Sitges 1996, ed. M. Rubí (Springer-Verlag, Berlin, 1997). P. Nordblad and P. Svendlidh, *Experiments on spin-glasses in Spin-glasses and random fields*, ed. A.P. Young (World Scientific, Singapore, 1998).
- [32] D. Herisson and M. Ocio, *Phys. Rev. Lett.* **88** (2002) 257202. D. Herisson, Ph.D. Thesis, Univ. Paris Sud, France, 2002. M. Ocio, in this volume.
- [33] J. Kurchan, *Rheology and how to stop aging*, in “Jamming and rheology: constrained dynamics in microscopic and macroscopic scales”, ITP, Santa Barbara, 1997, ed. S.F. Edwards *et al.*
- [34] L. Berthier, J.-L. Barrat and J. Kurchan, *Phys. Rev. E* **61** (2000) 5464.
- [35] L. Bellon, S. Ciliberto and C. Laroche, *Europhys. Lett.* **51** (2000) 551. A. Knaebel, M. Bellour, J.-P. Munch, V. Viasnoff, F. Lequeux and J.L. Harden, *Europhys. Lett.* **52** (2000) 73. M. Cloitre, R. Borrega and L. Leibler, *Phys. Rev. Lett.* **85** (2000) 4819. L. Cipelletti, S. Manley, R.C. Ball and D.A. Weitz, *Phys. Rev. Lett.* **84** (2000) 2275. C. Derec, A. Ajdari, G. Ducouret, F. Lequeux, C.R. Acad. Sci. (Paris) *IV-PHYS* **1** (2000) 1115. C. Derec, A. Ajdari, F. Lequeux, *Eur. Phys. J E* **4** (2001) 355; I. Cipelletti, H. Bissig, V. Trappe, P. Ballesta and S. Mazoyer, *J. Phys. C* **15** (2003) 5257; H. Bissig, V. Trappe, S. Romer and L. Cipelletti [`cond-mat/0301265`].
- [36] L.F. Cugliandolo, J. Kurchan and P. Le Doussal, *Phys. Rev. Lett.* **76** (1996) 2390.
- [37] A. Barrat, *Phys. Rev. E* **57** (1998) 3629. H. Yoshino, *Phys. Rev. Lett.* **81** (1998) 1493.
- [38] F. Portier *et al.* [`cond-mat/01`]. F. Portier, Ph.D. Thesis, Univ. Paris-Sud, France (2002).

- [39] See also the measurements in S.O. Valenzuela and V. Bekeris, *Phys. Rev. Lett.* **84** (2000) 4200, *ibid.* **86** (2001) 504.
- [40] R. Exartier and L.F. Cugliandolo, *Phys. Rev. B* **66** (2002) 012517.
- [41] R. Exartier, Ph.D. Thesis, Paris VI, France (2001).
- [42] C. Simon, private communication.
- [43] A.B. Kolton, R. Exartier, L.F. Cugliandolo, D. Domínguez and N. Grönbech-Jensen [`cond-mat/0206042`]. A.B. Kolton, Ph.D. Thesis (Univ. Decuyo, Argentina, 2003).
- [44] D. Bonn, S. Tanase, B. Abou, H. Tanaka and J. Meunier, *Phys. Rev. Lett.* **89** (2002) 015701; V. Viasnoff and F. Lequeux, *Phys. Rev. Lett.* **89** (2002) 065701; and V. Viasnoff, Ph.D. Thesis (Paris VI, 2003).
- [45] J.-P. Bouchaud, *J. Phys. I (France)* **2** (1992) 1705. J.P. Bouchaud and D.S. Dean, *J. Phys. I (France)* **5** (1995) 265. C. Monthus and J.-P. Bouchaud, *J. Phys. A* **29** (1996) 3847. B. Rinn, P. Maas and J.-P. Bouchaud, *Phys. Rev. Lett.* **84** (2000) 5403; G.B. Arous, A. Bovier and V. Gayrard, *Phys. Rev. Lett.* **88** (2002) 087201.
- [46] E. Bertin and J.-P. Bouchaud, *J. Phys. A* **35** (2002) 3039.
- [47] M. Sasaki and K. Nemoto, *J. Phys. Soc. Jpn.* **68** (1999) 1148.
- [48] S. Fielding and P. Sollich [`cond-mat/0107627`] [`cond-mat/0209645`]. S. Fielding, P. Sollich and P. Mayer [`cond-mat/0111241`], *J. Phys. C*. S. Fielding, Ph.D. Thesis Univ. Edinburgh UK (2000).
- [49] M.V. Feigel'man and V.M. Vinokur, *J. Phys. France* **49** (1988) 1731; J. Dyre, *Phys. Rev. Lett.* **58** (1987) 792; *Phys. Rev. B* **51** (1995) 12276.
- [50] W.L. Mc Millan, *J. Phys. C* **17** (1984) 3179; *Phys. Rev. B* **31** (1985) 340. A.J. Bray and M.A. Moore, *J. Phys. C* **17** (1984) L463 and in *Heidelberg Colloquium in Glassy Dynamics, Lecture Notes in Physics* **275**, ed. J.L. van Hemmen and I. Morgenstern (Springer, Berlin, 1988). G. Koper and H.J. Hilhorst, *J. Phys. (France)* **49** (1988) 429. D.S. Fisher and D. Huse, *Phys. Rev. B* **38** (1988) 373.
- [51] See the articles in *Glassy behaviour in kinetically constrained models*, ed. F. Ritort and P. Sollich, Barcelona 2002, *J. Phys. C* **14** (2002) 1381 and references therein.
- [52] J.D. Shore, M. Holtzer and J.P. Sethna, *Phys. Rev. B* **46** (1992) 11376.
- [53] J. Kurchan, L. Peliti and M. Sellitto, *Europhys. Lett.* **39** (1997) 365.
- [54] J.-P. Garrahan and M.E.J. Newman, *Phys. Rev. E* **62** (2000) 7670. D.S. Sherrington, L. Davison, A. Buhot and J.P. Garrahan, *J. Phys. C* **14** (2002) 1673. A. Buhot and J.P. Garrahan, *Phys. Rev. E* **64** (2002) 021505, *J. Phys. C* **14** (2002) 1499, *Phys. Rev. Lett.* **88** (2002) 225702.
- [55] G. Biroli and M. Mézard, *Phys. Rev. Lett.* **88** (2002) 225702. A. Lipowski, *J. Phys. A* **30** (1997) 7365. A. Lipowski and D.A. Johnston, *Phys. Rev. E* **61** (2000) 6375. M. Weigt and A.K. Hartmann [`cond-mat/0210054`].
- [56] D.J. Thouless, P.W. Anderson and R.G. Palmer, *Phil. Mag.* **35** (1977) 593.
- [57] J.-O. Andersson, J. Mattson and P. Svedlindh, *Phys. Rev. B* **46** (1992) 8297.
- [58] An incomplete list of references where the nonequilibrium evolution of different glassy systems has been studied numerically is the following. Spin models: H. Rieger, Annual reviews of computational physics II, 295 (World Scientific, Singapore, 1995). Spin-glasses: S. Franz and H. Rieger, *J. Stat. Phys.* **79** (1995) 749. E. Marinari *et al.*, *J. Phys. A* **31** (1998) 2611. J. Kisker, L. Santen, M. Schreckenberg and H. Rieger, *Phys. Rev. B* **53** (1996) 6418. H. Rieger, *Physica A* **224** (1996) 267. Particle models with Lennard-Jones interactions: G. Parisi, *Phys. Rev. Lett.* **79** (1997) 3660. W. Kob and J.-L. Barrat, *Phys. Rev. Lett.* **78** (1997) 4581; *Eur. Phys. J B* **13** (2000) 319. J.-L. Barrat and W. Kob, *Europhys. Lett.* **46** (1999) 637. R. di Leonardo *et al.*, *Phys. Rev. Lett.* (2000) **84** 6054. Models for silica glasses: H. Wahlen and H. Rieger, *J. Phys. Soc. Jpn.* **69** Suppl. A 242 (2000). Frustrated

- lattice gases: A. Fierro, A. de Candia and A. Coniglio, *Phys. Rev. E* **62** (2002) 7715. M. Sellitto, *Eur. J. B* **4** (1998) 135. J.J. Arenzon, F. Ricci-Tersenghi and D.A. Stariolo, *Phys. Rev. E* **62** (2000) 5978. F. Ricci-Tersenghi, D.A. Stariolo and J.J. Arenzon, *Phys. Rev. Lett.* **84** (2000) 4473. Oscillator models: L.L. Bonilla, F.G. Padilla and F. Ritort, *Physica A* **25** (1998) 315. Spin models with dipolar interactions: J. Toloza, F. Tamarit and S.A. Cannas, *Phys. Rev. B* **48** (1998) R8885.
- [59] M. Picco, F. Ricci-Tersenghi and F. Ritort, *Eur. Phys. J B* **21** (2001) 211.
- [60] T. Grigera and N. Israeloff, *Phys. Rev. Lett.* **83** (2000) 5083.
- [61] L. Bellon, S. Ciliberto and C. Laroche, *Europhys. Lett.* **53** (1999) 5038. S. Ciliberto in this volume.
- [62] L.F. Cugliandolo, D.R. Gempel, J. Kurchan and E. Vincent, *Europhys. Lett.* **48** (1999) 699.
- [63] U. Weiss, *Quantum dissipative systems*, Ser. mod. Cond. Matt. Phys. **10** (World Scientific, Singapore, 1999).
- [64] Note that the sign of the mass term generated by the coupling to the environment is negative. If strong enough, it may render unstable an initially stable potential well. One way to avoid this problem is to introduce the counterterm. One could also think that the coupling to the bath must be very weak and that the last term must vanish by itself (say, all $c_a \rightarrow 0$). However, this might be problematic when dealing with the stochastic dynamics since a very weak coupling to the bath implies also a very slow relaxation. It is then conventional to include the counterterm to cancel the mass renormalization.
- [65] J. Zinn-Justin, “*Quantum Field Theory and Critical Phenomena*” (Clarendon Press, Oxford, 1989).
- [66] R. Zwanzig, *J. Stat. Phys.* **9** (1973) 215.
- [67] J.-P. Hansen and A. Mac Donald, *Theory of simple liquids* (Academic Press, New York, 1976).
- [68] G. Parisi, *Statistical Field Theory*, Frontiers in Physics, Lecture Notes Series (Addison-Wesley, 1988).
- [69] G. Parisi, in this volume.
- [70] R. Kubo, M. Toda and N. Hashitume, *Statistical Physics II: Non-equilibrium Statistical Mechanics* (Springer Verlag, Berlin, 1992).
- [71] N. Pottier and A. Mauger, *Physica A* **282** (2000) 77, *ibid.* **291** (2001) 327. N. Pottier [cond-mat/0205307].
- [72] L.F. Cugliandolo and J. Kurchan [cond-mat/9911086], Frontiers in magnetism, *J. Phys. Soc. Jpn., Physica A* **263** (1999) 242.
- [73] C.P. Martin, E. Siggia and H.A. Rose, *Phys. Rev. A* **8** (1973) 423, H.K. Janssen, *Z. Phys. B* **23** (1976) 377 and *Dynamics of critical phenomena and related topics, Lecture notes in physics* **104**, ed. C.P. Enz (Springer Verlag, Berlin, 1979).
- [74] J. Schwinger, *J. Math. Phys.* **2** (1961) 407. L.V. Keldysh, *Zh. Eksp. Teor. Fiz.* **47** (1964) 1515, *Sov. Phys. JETP* **20** (1965) 235. P. Danielewicz, *Ann. Phys.* **152** (1984) 239.
- [75] C. de Dominicis, *Phys. Rev. B* **18** (1978) 4913.
- [76] E. Gozzi, *Phys. Rev. D* **30** (1984) 1218.
- [77] J. Kurchan, *J. Phys. I France* **1** (1992) 1333.
- [78] L.F. Cugliandolo and J. Kurchan, *Phil. Mag. B* **71** (1995) 50.
- [79] Note that the nonequilibrium correlation and response functions are self-averaging.
- [80] A. Houghton, S. Jain and A.P. Young, *Phys. Rev. B* **28** (1983) 2630.

- [81] L.F. Cugliandolo, D.R. Grempel and C.A. da Silva Santos, unpublished.
- [82] H. Sompolinsky and A. Zippelius, *Phys. Rev. Lett.* **45** (1981) 359, *Phys. Rev. B* **25** (1982) 274.
- [83] H. Sompolinsky and A. Zippelius, *Phys. Rev. Lett.* **50** (1983) 1297.
- [84] C. Chamon, M.P. Kennett, H. Castillo and L.F. Cugliandolo [cond-mat/0109150], *Phys. Rev. Lett.* **89** (2002) 217201.
- [85] L.F. Cugliandolo and G. Lozano, *Phys. Rev. Lett.* **80** (1998) 4979; *Phys. Rev. B* **59** (1999) 915.
- [86] R. Monasson, *J. Phys. A* **31** (1998) 513.
- [87] C. de Dominicis and P. Mottishaw, *J. Phys. A* **20** (1987) L1267, *ibid.*, L365.
- [88] G. Semerjian and L.F. Cugliandolo [cond-mat/0204613].
- [89] L.F. Cugliandolo and P. Le Doussal, *Phys. Rev. E* **53** (1996) 152.
- [90] H. Sompolinsky, *Phys. Rev. Lett.* **47** (1981) 935.
- [91] A. Georges, *Exact functionals, effective actions and (dynamical) mean-field theories: some remarks* in Windsor (2001). A. Georges, G. Kotliar, W. Krauth and M.J. Rozenberg, *Rev. Mod. Phys.* **68** (1996) 13.
- [92] J.-P. Bouchaud, L.F. Cugliandolo, J. Kurchan and M. Mézard, *Physica A* **226** (1996) 243.
- [93] K. Kawasaki, Recent Res. Devel. *Stat. Phys.* **1** (2001) 41. K. Kawasaki and B.-S. Kim [cond-mat/0110536]. E. Zaccarelli *et al.*, *Europhys. Lett.* **55** (2001) 157. E. Zaccarelli, Ph.D. Thesis, Dublin 2000. J.-L. Barrat, *Mode coupling theories*, in Cargèse Summer School *Glass physics* (1999).
- [94] R. Kraichnan, *J. Fluid. Mech.* **7** (1961) 124.
- [95] S. Franz and J. Hertz, *Phys. Rev. Lett.* **74** (1995) 2114.
- [96] S. Franz and M. Mézard, *Europhys. Lett.* **26** (1994) 209 (1994); *Physica A* **209** (1994) 48.
- [97] T. Halpin-Healey and Y.C. Zhang, *Phys. Rep.* **254** (1995) 217.
- [98] For reviews, see W. Götze, in *Liquids, freezing and glass transition*, Les Houches 1989, J.P. Hansen, D. Levesque, J. Zinn-Justin Eds., North Holland. W. Götze, L. Sjögren, *Rep. Prog. Phys.* **55** (1992) 241. W. Götze, *J. Phys. C* **11** (1999) A1.
- [99] E. Leutheusser, *Phys. Rev. A* **29** (1984) 2765.
- [100] U. Bengtzelius, W. Götze and A. Sjölander, *J. Phys. C* **17** (1984) 5915.
- [101] W. Götze and T. Voigtmann [cond-mat/0001188].
- [102] A. Latz, *J. Phys. C* **12** (2000) 6353 [cond-mat/9911025] [cond-mat/0106068]
- [103] K. Kawasaki and B.-S. Kim, *Phys. Rev. Lett.* **86** (2001) 3582.
- [104] L.F. Cugliandolo and J. Kurchan, *J. Phys. A* **27** (1994) 5749.
- [105] L.F. Cugliandolo, D.S. Dean and J. Kurchan, *Phys. Rev. Lett.* **79** (1997) 2168.
- [106] M.P. Kennett and C. Chamon, *Phys. Rev. Lett.* **86** (2001) 1622. M.P. Kennett, C. Chamon and Y. Ye, *Phys. Rev. B* **64** (2001) 224408. M.P. Kennett, Ph.D. Thesis Princeton Univ. 2002. G. Biroli and O. Parcollet, *Phys. Rev. B* **65** (2002) 094414. H. Westfahl Jr., J. Schmalian and P.G. Wolynes [cond-mat/0202099].
- [107] M. Hazewinkel, *Formal groups and applications* (Academic Press, New York, 1978).
- [108] J.M. Kosterlitz, D.J. Thouless and R.C. Jones, *Phys. Rev. Lett.* **36** (1976) 1217.
- [109] P. Shukla and S. Singh, *J. Phys. C* **14** (1981) L81. S. Ciuchi and F. de Pasquale, *Nucl. Phys.* **B300** [FS22], 31 (1988). L.F. Cugliandolo and D.S. Dean, *J. Phys. A* **28** (1995) 4213; *ibid.* L453 (1995); W. Zippold, R. Kuehn and H. Horner, *Eur. J. Phys. B* **13** (2000) 531; G. Ben Arous, A. Dembo and A. Guionnet, *Prob. Th. Rel. Fields* **120** (2001) 1.

- [110] B. Kim and A. Latz, *Europhys. Lett.* **53** (2001) 660. H. Horner, unpublished.
- [111] S. Franz and F. Ricci-Tersenghi, *Phys. Rev. E* **61** (2000) 1121. L. Berthier, J.-L. Barrat and J. Kurchan, *Phys. Rev. E* **63** (2001) 016105. D.A. Stariolo, *Europhys. Lett.* **55** (2001) 726.
- [112] L.F. Cugliandolo, J. Kurchan and L. Peliti, *Phys. Rev. E* **55** (1997) 3898.
- [113] A. Barrat and L. Berthier, *Phys. Rev. Lett.* **87** (2001) 087204.
- [114] H. Eissfeller and M. Oppen, *Phys. Rev. Lett.* **68** (1992) 2094.
- [115] W. Kob, in this volume.
- [116] J. Kurchan, *Phys. Rev. E* **66** (2002) 017101.
- [117] H. Castillo, C. Chamon, L.F. Cugliandolo and M.P. Kennett, *Phys. Rev. Lett.* **88** (2002) 237201; H. Castillo, C. Chamon, L.F. Cugliandolo, J.L. Iguain and M.P. Kennett [*cond-mat/0211558*].
- [118] L.F. Cugliandolo, D.R. Gempel, G. Lozano, H. Lozza and C.A. da Silva Santos, *Phys. Rev. B* **66** (2002) 014444.
- [119] F. Corberi, E. Lippiello and M. Zannetti, *Phys. Rev. E* **63** (2001) 061506, *Eur. Phys. J B* **24** (2000) 359.
- [120] C. Godrèche and J.-M. Luck, *J. Phys. A* **33** (2000) 1151; and *J. Phys. A* **33** (2000) 9141; E. Lippiello and M. Zannetti, *Phys. Rev. E* **61** (2000) 3369. F. Corberi, C. Castellano, E. Lippiello and M. Zannetti, *Phys. Rev. E* (to appear). P. Mayer, L. Berthier, J.P. Garrahan and P. Sollich [*cond-mat/0301493*].
- [121] L. Berthier and J.-L. Barrat, *Phys. Rev. Lett.* **89** (2002) 095702, *J. Chem. Phys.* **116** (2002) 6228.
- [122] A. Barrat, J. Kurchan, V. Loretto and M. Sellitto, *Phys. Rev. Lett.* **85** (2000) 5034.
- [123] H. Maske and J. Kurchan, *Nature* **415** (2002) 614.
- [124] L. Berthier, P. Holdsworth and M. Sellitto, *J. Phys. A* **34** (2001) 1805.
- [125] E. Marinari, G. Parisi, F. Ricci-Tersenghi and J.J. Ruiz-Lorenzo, *J. Phys. A* **31** (1998) 2611.
- [126] P. Hohenberg and B. Shraiman, *Physica D* **37** (1989) 109.
- [127] J.-L. Barrat, private communication.
- [128] R. Exartier and L. Peliti, *Eur. Phys. J. B* **16** (2000) 119.
- [129] A. Garriga and F. Ritort, *Eur. Phys. J. B* **20** (2000) 105, *ibid.* **21** (2001) 115.
- [130] L.F. Cugliandolo and J. Kurchan, *Physica A* **263** (1999) 242.
- [131] A.Q. Tool, *J. Am. Ceram. Soc.* **29** (1946) 240. R. Gardon and O.S. Narayanaswamy, *J. Am. Ceram. Soc.* **53** (1970) 380. O.S. Narayanaswamy, *J. Am. Ceram. Soc.* **54** (1971) 491. C.T. Moynihan *et al.*, *J. Am. Ceram. Soc.* **59** (1976) 12. G.W. Scherer, *J. Am. Ceram. Soc.* **67** (1984) 504. J. Jäckle, *Rep. Prog. Phys.* **49** (1986) 171. G.W. Scherer, *J. Non-Cryst. Solids* **123** (1990) 75.
- [132] S.F. Edwards, in *Disorder in condensed matter physics* (Oxford Science Pub., 1991).
- [133] T.M. Nieuwenhuizen, *Phys. Rev. Lett.* **80** (1998) 5580; *Phys. Rev. E* **61** (2000) 267.
- [134] S.F. Edwards in *Disorder in condensed matter physics* Oxford Science Publications, 1991 and in *Granular matter: an interdisciplinary approach*, ed. A. Mehta (Springer-Verlag, New York, 1994).
- [135] J.J. Brey, A. Prados and B. Sánchez-Rey, *Phys. Rev. E* **60** 5685. A. Fierro, M. Nicodemi and A. Coniglio [*cond-mat/01-7134*]. J. Berg and A. Mehta [*cond-mat/0108225*]. A. Lefevre and D.S. Dean, *Phys. Rev. Lett.* **86** (2001) 5631, *J. Phys. A* **34** (2001) L213 [*cond-mat/0111331*]. J. Berg, S. Franz and M. Sellitto, *Eur. Phys. J. B* **26** (2002) 349.

- [136] F.H. Stillinger and T.A. Weber, *Phys. Rev. A* **25** (1982) 978; *Science* **225** (1984) 983. S. Sastry, P.G. Debenedetti and F.H. Stillinger, *Nature* **393** (1998) 554. S. Sastry, *Nature* **409** (2001) 164.
- [137] W. Kob, J.-L. Barrat, F. Sciortino and P. Tartaglia [`cond-mat/9910476`]. W. Kob, F. Sciortino and P. Tartaglia, *Phys. Rev. Lett.* **83** (1999) 3214. P. de Gregorio *et al.* [`cond-mat/0111018`]. C. Donati, F. Sciortino and P. Tartaglia, *Phys. Rev. Lett.* **85** (2000) 1464. F. Sciortino and P. Tartaglia, *Phys. Rev. Lett.* **86** (2001) 107. R. Di Leonardo, L. Angelani, G. Parisi, G. Ruocco, A. Scala and F. Sciortino [`cond-mat/0106214`]. S. Mossa, E. La Nave, P. Tartaglia and F. Sciortino [`cond-mat/0209181`].
- [138] R. Monasson, *Phys. Rev. Lett.* **75** (1995) 2847.
- [139] S. Franz and G. Parisi, *J. Phys. I France* **5** (1995) 1401.
- [140] M. Mézard and G. Parisi, *Phys. Rev. Lett.* **82** (1998) 747; *J. Phys. C* **11** (1999) A157.
- [141] F. Thalmann, *J. Chem. Phys.* **116** (2002) 3378.
- [142] G. Biroli and R. Monasson, *Europhys. Lett.* **50** (2000) 155.
- [143] G. Biroli, *J. Phys. A* **32** (1999) 8365.
- [144] G. Biroli and L.F. Cugliandolo, *Phys. Rev. B* **64** (2001) 014206.
- [145] T. Plefka, *J. Phys. A* **15** (1982) 1971.
- [146] A. Georges and J.S. Yedidia, *J. Phys. A* **24** (1991) 2173.
- [147] J. Kurchan, G. Parisi and M.A. Virasoro, *J. Phys. France I* **3** (1993) 1819.
- [148] A. Cavagna, I. Giardina and G. Parisi, *J. Phys. A* **30** (1997) 7021.
- [149] A. Cavagna, I. Giardina and G. Parisi, *Phys. Rev. B* **57** (1998) 11251.
- [150] C. de Dominicis and A.P. Young, *J. Phys. A* **16** (1983) 2063.
- [151] P. Sibani, *Phys. Rev. B* **35** (1987) 8572. K.H. Hoffmann and P. Sibani, *Z. Phys. B* **80** (1990) 429; I.A. Campbell, *J. Phys. Lett. Paris* **46** (1985) 1159.
- [152] O.C. Martin, R. Monasson and R. Zecchina, *Theor. Comp. Sc.* **265** (2001) 3. F. Ricci-Tersenghi, M. Weigt and R. Zecchina, *Phys. Rev. E* **63** (2001) 026702. S. Franz, M. Leone, F. Ricci-Tersenghi and R. Zecchina, *Phys. Rev. Lett.* **87** (2001) 127209; G. Semerjian and R. Monasson [`cond-mat/0301272`].
- [153] A. Barrat and R. Zecchina, *Phys. Rev. E* **59** (1999) R1299. A. Montanari and F. Ricci-Tersenghi [`cond-mat/0207416`].
- [154] S. Franz, M. Mézard, G. Parisi and L. Peliti, *Phys. Rev. Lett.* **81** (1998) 1758; *J. Stat. Phys.* **97** (1999) 459.
- [155] R.P. Feynman and F.L. Vernon, Jr., *Ann. Phys.* **24** (1963) 114.
- [156] D. Thirumalai and T.R. Kirkpatrick, *Phys. Rev. B* **38** (1988) 4881. A. Barrat, R. Burioni and M. Mézard, *J. Phys. A* **29** (1996) L81.
- [157] Note that many glass formers have a crystalline structure that corresponds to most convenient equilibrium configuration. How much does the crystal influence the behaviour or the glass is an interesting still unanswered question, see the discussion in [158].
- [158] T.S. Grigera and N.E. Israeloff, *Phil. Mag. B* **82** (2002) 313. A. Cavagna, I. Giardina and T.S. Grigera [`cond-mat/0207165`].
- [159] A. Crisanti and F. Ritort, *Europhys. Lett.* **52** (2000) 640; *Physica A* **280** (2000) 155.
- [160] A. Cavagna, *Europhys. Lett.* **53** (2001) 490. K. Broderix, K.K. Bhattacharya, A. Cavagna, A. Zippelius and I. Giardina, *AIP Conf. Proc.* **553** (2001) 23.
- [161] S. Franz and J. Kurchan, *Europhys. Lett.* **20** (1992) 197.

- [162] D.S. Fisher, P. Le Doussal and C. Monthus, *Phys. Rev. Lett.* **80** (1998) 3539; *Phys. Rev. E* **64** (2001) 066107.
- [163] L. Laloux and P. Le Doussal, *Phys. Rev. E* **57** (1998) 6296.
- [164] A.V. Lopatin and L.B. Ioffe, *Phys. Rev. B* **60** (1999) 6412; *Phys. Rev. Lett.* **84** (2002) 4208.
- [165] J.P. Bouchaud and M. Mézard, *J. Phys. I (France)* **4** (1994) 1109. E. Marinari, G. Parisi and F. Ritort, *J. Phys.* **A27** (1994) 7615; *J. Phys.* **A27** (1994) 7647. L.F. Cugliandolo, J. Kurchan, G. Parisi and F. Ritort, *Phys. Rev. Lett.* **74** (1995) 1012. P. Chandra, L.B. Ioffe and D. Sherrington, *Phys. Rev. Lett.* **75** (1996) 713. P. Chandra, M.V. Feigel'man, L.B. Ioffe and D.M. Kagan, *Phys. Rev. B* **56** (1997) 11553; G. Franzese and A. Coniglio, *Phys. Rev. E* **58** (1998) 2753; *Phys. Rev. E* **59** (1999) 6409; *Phil. Mag. B* **79** (1999) 1807; A. Fierro, G. Franzese, A. Decandia and A. Coniglio, *Phys. Rev. E* **59** (1999) 60.
- [166] A. Crisanti and H.-J. Sommers, *Z. Phys. B* **87** (1992) 341.
- [167] A.J. Leggett, S. Chakravarty, A.T. Dorsey, M.P. A. Fisher, A. Garg and W. Zwermer, *Rev. Mod. Phys.* **59** (1987) 1.
- [168] T.R. Kirkpatrick and D. Thirumalai, *Phys. Rev. B* **36** (1987) 5388.
- [169] C. Godrèche and J.-M. Luck, *J. Phys. A* **33** (2000) 9141. M. Henkel, M. Piemling, C. Godrèche and J.-M. Luck, *Phys. Rev. Lett.* **87** (2001) 265701. A. Picone and M. Henkel, *J. Phys. A* **35** (2002) 5572. M. Henkel [hep-th/0205256]. P. Calabrese and A. Gambassi, *Phys. Rev. E* **65** (2002) 066120 [cond-mat/0207452] [cond-mat/0207487].
- [170] A. Cavagna, I. Giardina and G. Parisi [cond-mat/9702069].
- [171] I.K. Ono, C.S. O'Hern, D.J. Durian, S.A. Langer, A.J. Liu and S.R. Nagel, *Phys. Rev. Lett.* **89** (2002) 095703. L. Angelani, G. Ruocco, F. Sciortino, P. Tartaglia and F. Zamponi [cond-mat/0205182] and F. Zamponi, tesi di Laurea, Univ. di Roma I, 2001. F. Corberi, G. Gonnella, E. Lippiello and M. Zannetti [cond-mat/0210464, cond-mat/0205627].
- [172] A.E. Koshelev and V.M. Vinokur, *Phys. Rev. Lett.* **73** (1994) 3580. I. Aranson, A.E. Koshelev and V.M. Vinokur, *Phys. Rev. B* **56** (1997) 5136.
- [173] L.F. Cugliandolo, D.R. Grempel and C.A. da Silva Santos, *Phys. Rev. Lett.* **85** (2000) 2589; *Phys. Rev. B* **64** (2001) 014402.
- [174] A.J. Bray and M.A. Moore, *J. Phys. C* **12** (1979) L441.
- [175] T.M. Nieuwenhuizen and F. Ritort, *Physica A* **250** (1996) 89.
- [176] J.H. Gibbs and E.A. di Marzio, *J. Chem. Phys.* **28** (1958) 373. G. Adams and J.H. Gibbs, *J. Chem. Phys.* **43** (1965) 139.

COURSE 8

**EQUILIBRIUM STATES AND DYNAMICS
OF EQUILIBRATION: GENERAL ISSUES
AND OPEN QUESTIONS**

D.S. FISHER

*Lyman Laboratory of Physics, Harvard
University, Cambridge, MA 02138,
USA*



Contents

1	Introduction	525
2	Equilibrium states	526
2.1	Infinite system ground states	527
2.2	Positive temperature states	532
2.3	Number of equilibrium states?	533
3	Dynamics and barriers	535
3.1	Domain coarsening	536
3.2	Dynamics and local equilibrium	539
4	Spin glasses	541
4.1	Scaling scenario	543
4.2	Observation of many states?	547
5	Non-random systems: True glasses	549

EQUILIBRIUM STATES AND DYNAMICS OF EQUILIBRATION: GENERAL ISSUES AND OPEN QUESTIONS

D.S. Fisher

Abstract

Equilibrium states and the dynamics of equilibration are reviewed with emphasis on general issues and open questions. Macroscopic systems with quenched randomness, including random field magnets and spin glasses, are the primary focus. Structural glasses are discussed briefly at the end for contrast and to frame questions. For spin glasses, specific questions are raised about whether infinitely many equilibrium states could arise and how these might be manifested in experiments.

1 Introduction

The sluggish dynamics that characterize glassy systems, both those with quenched randomness such as spin glasses, and those that must generate their own randomness such as structural glasses, intrinsically involve the evolution of spatial structures and correlations. Unfortunately, because of the daunting obstacles to describing and understanding these phenomena, much of the theoretical work makes little or no explicit reference to heterogeneous spatial correlations or their dynamical evolution. Mean field theories [1], including mode-coupling theories [2], only involve spatial structures in some kind of averaged manner, and theories that invoke “free energy landscapes” [3] or “hierarchies of barriers” [4] often do so without interpretation of what these mean in terms of the actual local degrees of freedom. Furthermore, even in the situations in which the system is *trying* to equilibrate, as is frequently studied, the nature of the correlations that could, or should, develop have been beyond the scope of most theoretical approaches.

In contrast, work on the static equilibrium properties of glassy systems, in particular spin glasses, often focusses on large but finite systems that are in *full* equilibrium [5]. Yet the relevance, even in principle, of such

considerations to large experimental samples is not often questioned. For example, does it even make sense to weight different thermodynamic states in the partition function by their total free energy? Indeed, are free energy differences of order T – as needed for two states to both contribute to the canonical partition sum – even meaningful? Even if these considerations would play a role in perfect equilibrium, what aspects of this or other equilibrium physics are important when a large sample has equilibrated for a very long time but still not fully?

In this lecture, we will focus first on questions of equilibrium in infinite systems, then address the crucial issue: how do systems with short range interactions approach equilibrium? What can we infer about the long time aspects of spatial correlations and their evolution from knowledge of equilibria of infinite – or very large – systems? As we shall see, much can be learned from a simple notion: local properties of slowly equilibrating large systems are related to equilibrium properties of small sub-systems with some sort of random boundary conditions that reflect the state of the rest of the system.

For definiteness, we will focus on model problems with quenched randomness because these, in addition their intrinsic interest, have been the source of much of the confusion on these matters. At the end, we will comment briefly on related issues in the context of other glassy systems, in particular that of structural glasses.

2 Equilibrium states

Any physicist can tell one what the “ground state” of a system is: the state – in a classical system simply the configuration – with the lowest energy. Yet even most statistical physicists need to give some thought before answering the followup question: what do you mean by the “lowest energy” in an infinite system for which all the states have infinite energy? A discourse on limits of ground states of large finite systems is likely to follow. But how does one know whether such a limit exists? And if it does, is the resulting limiting ground state unique or does it depend on how the limit is taken?

At some point an experimentalist listening in is likely to – or at least should! – interrupt: what does any of this talk of “limits”, “infinite systems”, or even precisely defined “ground states” have to do with real experiments on macroscopic systems? Even a large sample is not infinite. Furthermore, the sample is not completely isolated from its environment, so that the Hamiltonian can vary slightly with time and is unlikely to be well defined at the level one would need for the discussion between the theorists to make sense. Many external perturbations – including graduate students walking around the lab – can cause changes much larger than $k_B T$.

And – now that it has been brought in – what about the effects of non-zero temperature? If a first course in statistical mechanics is remembered, questions about the appropriate *ensemble* should be raised: even at zero temperature the equivalence between the canonical and grand-canonical ensembles (*e.g.*, if the sample is connected to wires for measuring, electrons can flow in and out) is only valid for free energies *per unit volume*; the free energies themselves are, in a real sense, ill-defined to accuracies better than of order the square root of the volume.

In light of this, an outsider to the field would be surprised to learn that an overwhelming majority of the theoretical papers on spin glasses – and a considerable fraction of the experimental ones – have been based on analyses of properties of the infinite range Sherrington-Kirkpatrick model which focus on aspects of large systems that depend on free energy differences of order $k_B T$ between macroscopically different states [12]. Although such considerations were clearly valuable at early stages of the field (and this body of work has had highly productive spin-offs in other fields, notably neural networks and optimization problems), at this point, it is essential to shift the focus: both for spin glasses and more generally for macroscopic statistical mechanical systems one should endeavor to articulate the *right* set of questions.

2.1 Infinite system ground states

Although we are interested in the dynamics, we must first try to understand towards what equilibrium state or states an undisturbed system strives. As glassy phenomena occur at low temperatures, we initially focus on zero temperature.

With the worries discussed above in mind, we first ask again the basic question: what is a ground state of an infinite classical system? The simplest answer is an entirely physical one: a ground state is a configuration whose energy cannot be lowered by *any finite* change. This definition has, as we shall see, the virtue that it can be extended in natural ways to help understand “metastable” configurations and the concomitant slow dynamics. [It is convenient to restrict consideration to systems with no exact degeneracies other than those implied by symmetry: when there are degeneracies, a ground “state” will consist of the set of all configurations that can be reached from another configuration in the same ground state set by finite changes that do not alter the energy: in such cases, which we will not discuss here, ground states will have non-zero entropy.]

Any specific infinite-system ground state, which we denote by α , can alternatively be defined as a limit of finite system ground states [6]: if we know the ground state already, one can consider a sequence of nested boxes $\{\mathcal{B}_j\}$, centered on the origin – or any other chosen point – with the

ground state outside of each box giving a natural set of boundary conditions, $\partial\mathcal{B}_j^\alpha$ on the box. The limit of such boundary conditions will force the configuration of any finite region to correspond to the infinite system ground state: for large enough j the boxes will contain the finite region. The limit of the sequence of finite system ground states with the appropriate boundary conditions thus trivially gives back the original infinite system ground state, α .

But is the infinite system ground state unique? How can one define, even in principle, the full set of infinite system ground states? The limiting process described above provides a natural route [6, 7]. Define a set of boundary conditions, $\partial\mathcal{B}_j^{\Gamma_j}$ on the sequence of boxes. This will yield a sequence of finite-subsystem states Γ_j . If this sequence of states approaches a limit, the limit will be an infinite system ground state, γ . The essence of this is as follows: for any finite change of γ that one might consider, there will be some J such that the considered change will lie inside all the boxes, \mathcal{B}_j with $j \geq J$ (indeed, the change will be far from the box boundaries for large j). The configuration in the region of the considered change will also be independent of j for $j \geq J$; this follows from the existence of the limit. By construction, the energy cannot be lowered by any changes within any of the boxes. Thus the same is true of the considered change in the infinite system ground state. As this holds for any finite change considered, the limiting state satisfies the conditions for an infinite system ground state. [Strictly speaking, if there are continuous degrees of freedom, the states in the interior of the boxes can depend slightly on j , but for large j these will be arbitrarily close to the infinite system state.]

Nitpickers – who should be encouraged in this field! – might ask whether a limit, and thus *any* infinite system ground state, is guaranteed to exist: the answer is yes, provided the space of possible states is defined appropriately. The appropriate *compact* space is defined in terms of the set of all correlation functions among variables in all finite regions of the system [6, 7]. Many – or in some of the cases of interest, most – sequences of boundary conditions will not yield a limit. However one or more *subsequences* of any sequence *must* yield limits, a consequence of the compactness of the space of states. And many different sequences will yield the same limit. The *set of all possible limits* is the set of infinite system ground states.

At this point, some examples should be helpful.

Non-random Ising models

For a ferromagnetic Ising model with no external field, limits of sequences of boundary conditions in which, for example, a majority of the boundary spins are constrained to be up will yield the *up* ground state: $S_x = +1$ for all sites x . Similarly, a majority of down boundary spins will yield the *down* state. These states could also be obtained by applying positive or

negative boundary *fields* to the box which mimic the effects of the exchange interactions with the spins outside of the box. Are the *up* and *down* states the only ground states? What will happen with free boundary conditions?

Free boundary conditions yield a *mixed state* which is a 50–50 mixture of the *up* and *down* states in the sense, applicable at positive as well as zero temperature, that all the correlation functions, \mathcal{C} , will be

$$\mathcal{C}^{\text{mixed}} = \frac{1}{2}\mathcal{C}^{\text{up}} + \frac{1}{2}\mathcal{C}^{\text{down}}. \quad (2.1)$$

Linear combinations of the *up* and *down*, with different weights are also possible. *Pure states*, such as the *up* and *down* states, cannot be decomposed into linear combinations of other states [6]. At the level of ground states, one can immediately see that such mixed states are different beasts than pure states: the two configurations that make them up *cannot* be reached from one another by flipping any finite collection of spins. Thus it is reasonable to exclude such mixed states from consideration: they will in any case not play a role in experiments on macroscopic systems any more than macroscopic linear superpositions of states such as Schroedinger’s $\frac{1}{\sqrt{2}}|\psi^{\text{alive}}\rangle + \frac{1}{\sqrt{2}}|\psi^{\text{dead}}\rangle$ “cat” states do in quantum mechanics. As in the quantum case, mixed states are extremely susceptible to environmental perturbations: for the classical ground states, any perturbation that breaks the symmetry will convert a mixed state to one of its pure state constituents. In the case of free boundary conditions, or more generally in the absence of any intentional symmetry breaking perturbations, mixed states reflect ignorance of which of the two pure states the system is in; in this sense they are analogous to mixed states in quantum mechanics that are incoherent superpositions of states usually described in terms of a density matrix.

Do ferromagnetic Ising models also have other *pure* states? Perhaps surprisingly, the answer is “yes”. If a sequence of boxes symmetrically centered on the origin is used with positive field boundary conditions on the left half and negative on the right half, a *domain wall state* will result. This consists of +1 spins in the left half of the system and −1 in the right half. [It is not a mixed state as correlations between pairs of spins on opposite sides of the domain wall are different than those in the *up* and *down* states and cannot be expressed as a linear combination of these.] There exists an infinite set of such domain wall states which differ only in the location and/or orientation of the wall. Yet sequences of random or other non-special boundary conditions will not have a subsequences that produce any of these states; they are thus rather special. Furthermore, states with two or more parallel domain walls *cannot* be constructed: as soon as the boundaries of a box are far enough away, the energy can be lowered by eliminating both walls in the bulk of the box leaving only walls near the boundaries; in the

large box limit these walls will be arbitrarily far away from the origin or any other fixed point of interest.

The domain wall states of ferromagnetic Ising models do, in a well-defined sense, have higher energy than the *up* and *down* states: if the energy of, for example, the *up* and a domain wall state are compared in any chosen finite region, the latter will always have higher energy. Thus for this situation, it is reasonable to consider only the former as a ground state. But, as we shall see, in random systems the comparison between the energies of two states can be inconclusive, and we cannot rely on being able to further discriminate by such regional comparisons.

Random field Ising models

A far more interesting and instructive example is provided by ferromagnetic Ising models in weak random magnetic fields. The model Hamiltonian is

$$\mathcal{H} = - \sum_{(x,y)} J S_x S_y - \sum_x h_x S_x \quad (2.2)$$

with positive exchange J coupling nearest neighbor pairs, (x, y) , and the $\{h_x\}$ independent random fields drawn from a continuous distribution with variance h^2 that is symmetric under $h_x \rightarrow -h_x$. This *ensemble of Hamiltonians* has no global symmetries but it has a *statistical symmetry* under $\{S_x\} \rightarrow \{-S_x\}$ as the corresponding system with each h_x replaced by $-h_x$ is equally probable. The ensemble also has statistical translational invariance.

In dimension, d , greater than two, weak random fields, $h \ll J$, do not destroy the long range ferromagnetic order at low temperatures [8]. Thus we expect that there will be two ground states which we again call *up* and *down*. But these ground states will not be trivial: because of rare regions in which there are anomalously many negative random fields, some spins will point down even in the *up* ground state. Likewise, in the *down* ground state spins in different rare regions in which there are anomalously many positive random fields will point up. These two ground states are thus *not* related by symmetry. Nevertheless, the *up* and *down* states are *statistically similar*: the statistics of their correlations over many samples or over a large volume are related by symmetry.

How can the ground states of a random-field Ising model be obtained from sequences of boundary conditions? As for the non-random ferromagnet, one sequence that gives each is trivial: strong positive fields on the boundary spins in each box for the *up* state, and negative on the boundary spins for the *down* state.

What will happen with free boundary conditions? In contrast to the non-random system, the ground states on a generic sequence of boxes with free boundary conditions will *not* approach a limit! The reason for this is

simple: in a box of volume V , the total strength of the random fields will be of order \sqrt{V} and have a definite, albeit random, sign. Crudely, therefore, we expect the finite size ground state to be that corresponding to the overall sign of the cumulative random fields in the box. In actuality, this is not quite right because of the small fraction of spins that will be aligned by local fields independent of boundary conditions [9]: for small h this will renormalize the cumulative random fields by sample-dependent random amounts that are typically small. Although these renormalizations can change the overall sign of the effective total random field, the naive estimate is correct: the *up* and *down* states restricted to a volume V of the system will differ in energy by a random amount of order $h\sqrt{V}$ for small h . We can thus not answer the question which ground state of the infinite system has lower energy! In a large but finite system with free boundary conditions, which of the two states is preferred is not a matter of indifference, as it was for the non-random case, but is determined by the sample specific details of the random fields.

In a sequence of boxes with free or random boundary conditions, the ground states will vary from mostly up to mostly down, with changes typically occurring every factor or two or so in volume [9]. If a *subsequence* of boxes is chosen *a posteriori* by selecting, for the sample of interest, only those boxes whose ground state magnetization is, say, positive, then the *up* state will be obtained. But it is important to note that such a sequence of boxes which yields a limiting ground state with free boundary conditions *cannot* be chosen independently of the random fields in the specific sample.

As in the non-random ferromagnet, one can also try to construct domain wall states in random field Ising systems. But here an important extra consideration enters: in three dimensions, domain walls in random systems are not flat but roughened by the randomness [10]. A domain wall locally minimizes the combination of the exchange and the random-field energies: this causes deformations away from flat thereby adding to the exchange energy but decreasing the random field energy by more than enough to compensate. Since the deviation from flat grows without bound as the size of the domain wall grows, one cannot guarantee that manipulating a domain wall far away will force it to pass near the origin (or any other predetermined position). Thus a sequence of half-positive half-negative boundary conditions on larger and larger boxes will generally lead to a domain wall that passes further and further from the origin. In the middle region of the box, the ground state will thus coincide with either the *up* or the *down* state depending on which side of the origin the wall passes for that particular box in the specific sample. Such split boundary conditions will thus not lead to a limiting ground state; rather, distinct subsequences will lead to each of the *up* and *down* states. Although strictly speaking domain wall states are thus

not distinct infinite system ground states, the fact that large finite systems can have ground states with a domain wall passing through their deep interior will play a role in the dynamical approach to equilibrium. [Note that in four or more dimensions domain walls can be flat and true domain wall states analogous to those in non-random Ising magnets do exist in infinite systems for small h .]

2.2 Positive temperature states

We have so far considered only ground states, finding that subtleties arise in thinking carefully about ground states in infinite systems. One might expect that the effects of thermal fluctuations would make matters far more complicated: there is no obvious generalization of the notion of stability of infinite system ground states to finite changes even if, as is essential at positive temperatures, one considers *free energies*. Yet the definition of infinite system “states” in terms of limits of states of nested series of finite boxes with a sequence of boundary conditions extends naturally to non-zero temperature [7]. Perhaps surprisingly, other than some extra subtleties associated with defining the space in which the states converge, temperature does not introduce many extra complications as far as equilibrium static properties. For our purposes, the main additional feature is one that already occurs in non-random Ising magnets: mixed states caused by fluctuating domain walls.

In non-random three dimensional Ising ferromagnets, there is typically a range of temperatures below the ordering temperature in which domain walls thermally roughen rather than being flat and pinned to the lattice as they are at low temperatures. If split boundary conditions that would give rise to a domain wall state at zero temperature are used in the regime in which the domain walls are rough, the limiting state is no longer a pure state: it is a mixed state consisting of a linear superposition of the *up* and *down* states. The underlying reason for this is very physical: with its roughness diverging on long length scales, in a large system the imposed domain wall will almost always be far from the origin – or any other fixed region – and thus the correlations will be those of one of the two pure states. The degree of mixing reflects the fraction of the time that the domain wall is on either side of the origin.

For ferromagnets, it is trivial to choose sequences of boundary conditions that will give one or the other of the pure states. But what happens in a random system such as a spin glass when boundary conditions that are not tailored to the particular sample are used? It is tempting to think, following the Parisi analysis of the Sherrington-Kirkpatrick model of spin glasses [5, 12], in terms of some set of approximate infinite system “states” being present in a very large system with weights proportional to their

Boltzmann factors $\exp(-F_\alpha/T)$ determined by their free energies $\{F_\alpha\}$. But how are these free energies defined? In particular how can they be defined unambiguously with an accuracy of order T , when the typical contribution due to entropy of a single degree of freedom near the boundary is of this order? Indeed, as argued above, mixed states such as those in the Parisi solution are not physically relevant for experiments on macroscopic systems: they are better thought of as reflections of ones ignorance of which pure state the system is in. Conversely, as we have seen for the case of random field Ising magnets, states whose free energy in a large volume are greater, by any natural definition, than that of another state by much more than T – e.g. of order \sqrt{V} – can nevertheless be important.

But the free energy difference between infinite system states cannot be *too* large: the *free energy density* of all of the equilibrium states must be the same. Indeed, the contribution to the free energies of equilibrium states from within a large box cannot differ from one another by more than some multiple of the box's surface area as this is the maximum amount by which boundary conditions can alter the free energy of the box. If two states differed in free energy in any region by more than of order the surface area of the region, the putative larger free energy state could decrease its free energy by replacing its central region by the other state, with a cost of no more than the area of the surface over which the two states were patched together. This physical process is the basis for the nucleation of the lower free energy state after supercooling through a first order transition.

For static correlations in low temperature phases, finite temperature states can usually be considered as approximate ground states of a coarse-grained effective Hamiltonian that takes into account the effects of the small scale fluctuations which give rise to entropic contributions to the free energy. This will be a good description of many of the properties of the system at long length scales provided the phase is controlled, in a renormalization group (RG) sense, by a (stable) zero-temperature fixed point [11]. Exceptions to this are low temperature phases, of which the Kosterlitz-Thouless phase of the two dimensional XY model is the best known example, that are controlled by a line of positive temperature fixed points with temperature exactly *marginal*.

2.3 Number of equilibrium states?

The suggestion that there might be an infinite number of pure states in spin glasses and perhaps in other random systems has deservedly attracted a great deal of attention [12]. But what does it mean? As we have seen, even non-random ferromagnets have an infinite number of domain wall states at low temperatures in three dimensions. Presumably something different is envisioned. The most interesting possibility would be an infinite number of

states that differed from each other in a manner similar to the *up* and *down* states of random field Ising models: although these are *statistically similar*, consideration of almost any large region of the system will reveal that these states are distinct and *not* related by symmetry [13]. Such pairs of states have been termed *incongruent*. In contrast, domain wall states are very similar to either the *up* or the *down* state over most of the system, differing substantially only near the domain wall: a lower dimensional region which occupies a negligible fraction of the volume [14].

How many different infinite-system states could exist in a large sub-volume of the system? More precisely, with a given appropriately defined tolerance ϵ , how many infinite system states can be distinguished in a typical large cube of size L^d ? The fact that the state in the interior of the cube is only linked to the state far away *via* the boundary of the cube (we are assuming the interactions are short-range), implies that the number of states, $N_S(L, \epsilon)$, that are distinguishable in the cube is bounded by

$$N_S(L, \epsilon) \leq e^{C(\epsilon)L^{d-1}} \quad (2.3)$$

with C an ϵ dependent coefficient [7]. This simple bound has important consequences: it immediately implies that the logarithm of the number of states cannot be extensive. If, for example, 2^d cubes of size L^d are put together to form a $(2L)^d$ cube, the number of states distinguishable in the larger cube is much less than the naive estimate obtained by enumerating all possible combinations of the states restricted to the smaller cubes: this is a consequence of the states in one region being correlated with those in all other regions. As we shall see, these restrictions on the growth of the number of possible states with the length scale on which boundary conditions or other constraints are imposed, has significant consequences for the dynamics of equilibration.

Another consequence of (2.3), concerns the contribution to the entropy of the multiplicity of states: even if it could be arranged so that all the infinite-system states distinguishable in a large volume appeared with non-negligible Boltzmann weights, the additional contribution to the entropy would be at most of order the surface area and thus similar to other forms of the boundary condition dependent entropy.

A cautionary note is in order for those with experience of infinite-range models or Bethe lattices (also called Cayley trees) as representatives of the high dimensional limit of short range models. Bethe lattices have finite surface to volume ratio independent of their size, thus the number of possible boundary conditions – in fact the number of possible states – is exponentially large in the *volume* (the number of sites) [16]. Concomitantly, the free energy density of each of these infinite system states need *not* be the same.

Problems also occur in mean-field p-spin models [17]: the enormous number of “states” found in these models is likewise unphysical.

Returning to physical models, we must ask: for finite dimensional systems with short range interactions, are there tighter bounds than (2.3) on the number of distinguishable states in finite regions? One can construct [15] examples in dimensions $d > 3$ for which the number of ϵ -distinguishable statistically similar incongruent states is of order

$$N_S(L, \epsilon) \sim e^{C(\epsilon)L^\sigma} \quad (2.4)$$

with

$$\sigma = d - 3. \quad (2.5)$$

If one can find examples with $d - \sigma < 3$, a seemingly minor improvement, this might lead to the intriguing possibility of short-range models with an infinite number of incongruent states in three dimensions. With power-law interactions that decay as $1/r^3$ – as dipole and RKKY interactions do – three dimensional examples, albeit artificial ones, can probably be constructed.

3 Dynamics and barriers

The discussion so far has focussed on the equilibrium properties of large or infinite systems. We now turn to the primary question: what actually matters for macroscopic systems on experimentally accessible time scales? Are the equilibrium states relevant? If so, in what way and what aspects of them? In systems with a multiplicity of equilibrium states – especially incongruent states – how will these be manifested?

We start with some basic observations. Strictly speaking, neither phase transitions nor multiple equilibrium states can occur in finite systems at non-zero temperature: any singularities in the free energy will be rounded out by finite size effects. Yet the basic tenet of statistical mechanics is that sufficient time is available for exploration of all of phase space; for large systems, long times are needed; for infinite systems, infinitely long times. We are thus faced with an apparent quandary: infinite systems are needed to have more than one state, yet infinite times are needed to achieve this. We must thus, from the beginning, consider notions of local equilibrium and separation of time scales.

Let us first consider the establishment of equilibrium in well understood contexts. In practice, it is often a reasonable approximation to speak of an equilibration time, τ_{eq} , that characterizes the approach to asymptotic equilibrium for a particular finite size sample. This equilibration time will, of course, depend on the thermodynamic variables, in particular the temperature as well as the sample size and shape.

At high temperatures when equilibrium correlations are short-range, equilibration is essentially local and hence independent of sample size for large systems – at least in the absence of conservation laws. If diffusion plays a role, then the relaxation takes longer, usually $\tau_{\text{eq}} \sim DL^2$, with D a diffusion coefficient and L the sample diameter. But with a conserved quantity, each region of the system can rapidly reach a local equilibrium associated with the local value of the conserved quantity (or quantities) and the longer time scale behavior can be considered in terms of nearly-equilibrium coarse-grained properties.

3.1 Domain coarsening

At low temperatures in a phase in which there is more than one equilibrium state, the dynamics is very different than in high temperature phases. For example, in a non-random Ising ferromagnet, the evolution towards equilibrium from a disordered initial configuration will be quite slow because of the necessity to establish a single state – either *up* or *down* – over the whole system: long range order takes a long time to establish. If the order parameter is not conserved, simple arguments involving the dynamics of domain walls lead to $\tau_{\text{eq}}^{\text{S}} \sim L^2$ with a coefficient that involves the interfacial tension, σ , and the mobility of domain walls [18]; we use the superscript “S” for “single state”. The process involved in establishment of a single state is near to local equilibrium at long times: large regions of the system will be either approximately in the *up* state, in the *down* state, or, for the small fraction of the system near the domain walls, approximately in an equilibrium state with a domain wall – even if such a state does not, because of fluctuations, strictly exist in an infinite system.

Although a large sample will reach one of the two equilibrium states in $\tau_{\text{eq}}^{\text{S}}$, is this actually the asymptotic equilibration time? What happens to a large ferromagnetic sample that has reached (or was started in) the *up* state in zero magnetic field? In particular, how long will it take to fluctuate to the *down* state? Again domain walls control the behavior: in order to get from the *up* to the *down* state, a domain wall must be created and pass across the whole sample. As the free energy of such a domain wall configuration is larger than that of the *up* or *down* states by of order L^{d-1} , this process involves a large activation barrier. The equilibration time for full equilibrium will thus be of order $\tau_{\text{eq}}^{\text{F}} \sim \exp(\sigma CL^{d-1}/T)$ with σ the interfacial free energy per unit area – the surface tension –, C a shape dependent order-unity coefficient and the “F” superscript denoting “full” equilibrium. On time scales between $\tau_{\text{eq}}^{\text{S}}$ and $\tau_{\text{eq}}^{\text{F}}$, the sample will effectively be in one of the two equilibrium pure states. There is thus a strong separation of time scales. Only on the much longer time scale will fluctuations between the two pure states occur and time-averaged correlations approximate those of the

equilibrium mixed state. But whether or not there are *actual* (rather than “virtual”) fluctuations between *up* and *down* will be very sensitive to small perturbations: in particular any symmetry breaking energies substantially larger than T .

In general, with short range interactions in a d -dimensional system, the longest time scale for equilibration will grow no more rapidly than exponentially in the cross sectional area, as it does in the Ising ferromagnetic phase. More important for most purposes is the time scale, $\tau(L)$, for establishing local equilibrium in a region of size L : again, we expect this will satisfy $\tau(L) \leq \exp(KL^{d-1}/T)$. For pure systems, such as simple Ising ferromagnets, local equilibrium can often be established much faster, but this is not always the case.

In three-dimensional non-random Ising magnets below the roughening temperature of the domain walls – more precisely, below the temperature, if it exists, at which the equilibrium shape of a droplet of the minority phase becomes fully faceted – domain wall motion will involve nucleation and growth of steps on the flat faceted domain walls [19]. This gives rise to much slower coarsening than with continuum walls: $\tau(L) \sim \exp(\mu L/T)$ with μ proportional to the free energy per unit length of the steps. On shorter time scales, the local correlations will be similar to those of the equilibrium states in the presence of a domain wall or domain wall bend; for systems in which this slow dynamics occurs, there exist, in addition to the states with a single flat domain wall, equilibrium states with a domain-wall that has a sharp bend along a line. These bent-wall states correspond to two of the facets and the edge joining them on fully faceted crystal-like droplets of the minority phase.

In systems with quenched randomness, the dynamics in ordered phases is typically much slower than in non-random systems with the same basic phases. For example, in the ferromagnetic phase of random field Ising magnets, domain walls between the *up* and *down* phases will prefer some locations over others because of favorable variations of the random fields in their vicinity. This will cause the walls to deviate from flatness by of order L^ζ over sections of scale L [10]. The *roughness exponent* ζ is $\frac{2}{3}$ in three dimensions; thus although large angles are possible on small scales, the fact that $\zeta < 1$ means that the domain walls will deviate from flat by only small angles on large length scales. The random landscape makes it necessary for domain walls to overcome barriers in order to move; this decreases their mobility dramatically. The resulting time scale to get rid of domain walls out to scale L is

$$\ln \tau(L) \sim L^\psi \quad (3.1)$$

with $\psi = 1$. We have given $\ln \tau(L)$ here rather than writing $\tau(L) \sim \exp(KL^\psi)$ because (in contrast to the faceted case above) there is

randomness in the coefficient, K . This crucial aspect of the dynamics arises from the underlying random nature of barriers; as a consequence, the actual $\tau(L)$ – in contrast to its logarithm – will vary enormously from one region to another [20]. The exponent ψ characterizes the *typical* barrier heights, B , that need to be overcome to eliminate domain walls closer to each other, or with radii of curvature smaller than, scale L :

$$B \sim L^\psi. \quad (3.2)$$

Note that the value of $\psi = 1$ implies that these barriers are less than both σL^{d-1} , the barrier for flipping a sample of diameter L from the *up* to the *down* state, and $hL^{\frac{d}{2}}$, the typical difference in free energy between the *up* and *down* states in a region of size L .

The balance between the interfacial and random field energies that gives rise to the barrier-height exponent ψ and to the $L^{\frac{2}{3}}$ roughness of a section of domain wall, is subtle; it was the subject of a great deal of controversy in the '70s and '80s closely related to the question of whether a ferromagnetic phase can exist in three dimensional random field systems [21]. As we consider less well understood systems, it is worth remembering that careful scaling arguments and phenomenological renormalization group considerations proved to be far more reliable routes to the truth for random field magnets than a panoply of formal – and sometimes elegant – techniques, including field theoretic, supersymmetric and replica methods.

The slow growth of domains in the ordered phase of random field magnets is not special to these systems: *any* amount of exchange randomness in an Ising magnet will also give rise to characteristic times for domain growth that grow exponentially with the length scale, albeit with a smaller exponent ψ [18, 20]. This occurs even though the equilibrium properties of the ordered phase are scarcely affected by the randomness: it is only the dynamics – and the concomitant difficulties in reaching equilibrium – that are strikingly affected by the randomness.

The high barriers that need to be surmounted to make large scale rearrangements in random systems lead naturally to notions of metastability on a broad spectrum of time scales. The largest barriers that can be surmounted in a time t by thermal activation have height $B_t \approx T \ln(t/t_0)$; for long times, this is only weakly sensitive to the microscopic time scale t_0 . In ordered phases, or more generally at low temperatures, one can often consider coarse-grained aspects of finite temperature states as “ground states” of an effective coarse-grained Hamiltonian. This effective Hamiltonian is really a free energy functional that includes the effects of small scale fluctuations. For this to make sense, the length scale of the coarse graining must be large enough that there is little entropy in longer scale fluctuations [22]. Provided this coarse-graining scale is smaller than the

dominant length scale of processes of interest, one can still consider thermal fluctuation effects on larger scales: in particular activation over large free energy barriers. Metastable states in a given “epoch” – a range of $\log t$ – can then be loosely defined as configurations of the coarse-grained Hamiltonian whose free energy cannot be lowered by any processes with barrier lower than $B_t = T \ln(t/t_0)$. In the limit of low temperature, this notion becomes sharper and sharper; of course for practical purposes it becomes useless for the collective phenomena of interest as the relevant barriers no longer involve large scale processes even at the longest accessible time scales.

It is important to contrast the behavior of metastability in random systems with that of the better known phenomena that occur near to conventional first order phase transitions. In the latter, there is usually *one* characteristic process – some form of nucleation – that can take the system out of its metastable “state”; associated with this, there is one characteristic time scale, albeit a strongly temperature dependent one. In random systems with a spectrum of barriers, there will, in contrast, be metastability on any macroscopic time scale: most processes will either be much faster, and hence in local equilibrium, or much slower, and hence out of equilibrium. A hallmark of this is that only a small fraction of the system will show substantial evolution on any given long time scale, and this evolution will be spatially localized.

3.2 Dynamics and local equilibrium

A typical experiment on a glassy systems involves cooling into a low temperature phase and then allowing the system to equilibrate for some waiting time, t_w . Although in practice the dynamics along the cooling path often matters, it is instructive to consider an ideal infinitely rapid quench from the disordered phase to a fixed temperature in the low temperature phase.

We first consider a simple random system, such as a random Ising ferromagnet, that has a discrete set of equilibrium states in the low temperature phase. The equilibration will then generally involve coarsening dynamics of domain walls separating the various states. After time t_w domains will have grown until the typical domain wall spacings and radii of curvature are of order

$$L_w \sim [\ln(t_w/t_0)]^{\frac{1}{\psi}} \quad (3.3)$$

with ψ depending on the type of randomness, and t_0 a “microscopic” time which may include the effects of activation on the smallest scale processes, and/or critical slowing down at temperatures near to a phase transition. Within one domain, the correlations averaged over times long compared to t_0 but short compared with t_w will be characteristic of one of the equilibrium states of the system. Near the domain walls, the free energy density and

the correlations will differ from those of the equilibrium states, but over time scales short compared to t_w , they will be similar to the equilibrium correlations near a domain wall that is imposed by boundary conditions in a finite system. But the appropriate size of such an analogous finite system is roughly equivalent to the characteristic length, ℓ_w , over which the domain walls temporarily pinned by the randomness are in local equilibrium; this is much less than the domain size: $\ell_w \sim L_w^{\frac{1}{2-\zeta}} \ll L_w$ with $\zeta < 1$ the roughness exponent of the walls [20]. [The existence of these two length scales and the strong inequality between them is a consequence of the irrelevance, in the renormalization group sense, of randomness at the ordered fixed point that controls the low temperature phase.]

From the above picture, we see that on time scales shorter than the waiting time, properties of the various regions of a non-equilibrium macroscopic system can be understood, at least roughly, in terms of *equilibrium* properties of small systems of appropriate sizes. As the time waited for equilibration grows, the appropriate sizes for comparison also grow – albeit sometimes in non-trivial ways. This picture of the development of correlations as equilibrium is gradually approached connects naturally to the earlier discussion of equilibrium states in terms of sequences of finite systems with length-scale-dependent boundary conditions.

The length-scale, L_w , represents the maximum distance over which information about the state of one region of a system can be communicated in the time t_w . In particular, if we focus on one region of diameter L_w – call it the central region – the regions to its left and to its right will influence it *incoherently*. Each of these regions will reflect the initial conditions, the dynamical evolution, and the character of the states in its own region – in particular which equilibrium state or states demarcated by domain walls it resembles – but *not* any of these aspects of regions further than L_w or so away. Thus as far as the inner parts of the central region are concerned, the left and right regions will act as if they are statistically independent. At least crudely, we can thus approximate the non-equilibrium effects of neighboring regions by boundary conditions along each of the edges of the central region that *locally* reflect the equilibrium correlations of *one* of the equilibrium states in the neighboring regions. The incoherence between the neighboring regions implies that which equilibrium state is reflected locally should vary randomly every L_w or so around the boundary of the central region.

If the boundary conditions on the central region result in a domain wall crossing it, the behavior will be more complicated because of the second length scale, ℓ_w , described above. For the domain walls to correctly represent the likely configurations in which they will be pinned on time scales of order t_w , the boundary conditions that force the domain walls must be imposed on regions of size ℓ_w . This is because it takes much longer for

sections of domain walls of scale L to approach their asymptotic large scale roughness than it does for them to become less rough than L – the latter being all that is needed for the domain wall spacing and radii of curvature to become of order L_w .

Up to these caveats associated with the two length scales that characterize the evolution towards equilibrium, the equilibrium correlations of a given region with boundary conditions chosen as above should *statistically* be a good approximation to the correlations in the same region of the non-equilibrium system. More precisely, if many quench-and-wait experiments with the same t_w are done and the *same* region examined in each, we expect the statistical properties to be similar to those obtained from equilibrium properties of this particular region with an appropriately chosen ensemble of boundary conditions reflecting properties of it and neighboring regions. Note, however, that if the number of equilibrium states realizable in a finite subsystem does grow exponentially with its size, as in (2.4), there may well be two or more length scales involved in the effects of boundary conditions and the results will be subtle [15].

One of the main points of this lecture is the generalization of the basic observation: the properties of macroscopic systems that are equilibrated for a long time, t_w . that is not enough for full equilibration, will be *locally* similar to equilibrium properties of small systems with *some* ensemble of boundary conditions. Furthermore, the appropriate sizes of the corresponding small systems will grow with t_w at least as fast as $(\ln t_w)^{\frac{1}{d-1}}$ [note that ℓ_w above satisfies this]. Thus the almost-steady states of large systems that cannot fully equilibrate should be described in terms of a patchwork of regions that closely correspond to equilibrium pure states of the infinite system. The appropriate pure states are defined in as limits of sequences of boundary conditions [7]; these all have the *same* free energy density, but their overall free energies – so crucial in the replica-symmetry-breaking framework [5] – play no role whatsoever.

4 Spin glasses

The term “spin glass” is used rather loosely for a host of magnetic alloys and theoretical models that combine *frustration* among the exchange interactions with randomness that is sufficiently strong to destroy any ferromagnetic or antiferromagnetic order. The simplest class of models are Ising spin glasses with Hamiltonian

$$\mathcal{H} = - \sum_{(x,y)} J_{xy} S_x S_y \quad (4.1)$$

with the $\{J_{xy}\}$ random exchange interactions drawn from some distribution. Such models have been extensively studied for almost three decades. They have engendered many exciting ideas – particularly the possibility of a multitude of equilibrium states – as well as a great deal of controversy.

Yet more than two decades after the first suggestions that the ordered phase of spin glasses might be characterized by the existence of infinitely many pure states [23], there is still no consistent scenario for how this might occur in finite-dimensional systems. Such a scenario would need to include explicitly spatial correlations between the different states as well as whether and how the many states are manifested in finite size systems. Ideally, it would also yield useful information about slowly equilibrating large systems. Many workers in the field would probably disagree with the above sentences and argue that it is sufficient to focus on equilibrium properties of large systems with free (or periodic) boundary conditions – in particular quantities like overlaps between replicas [5]. But the general considerations outlined above should, at the very least, be taken into account in comparing theory with experiment. Indeed, the random field Ising model provides an example of the perils of ignoring the general notions of equilibrium states and how they are manifested in finite systems: if only a collection of large samples with free boundary conditions were considered, each random field Ising sample would appear to have only *one* state – one, but not both, of the *up* and *down* states that surely exist in three dimensions!

At this point, there is no convincing argument that spin-glass models in finite dimensions cannot have a multiplicity of pure states unrelated by symmetry – indeed, they probably can. But we must distinguish between Edwards-Anderson (EA) spin glasses, general spin-glass models, and actual experimental systems. The first, and best studied, of these has a special *statistical gauge symmetry*: with the $\{J_{xy}\}$ drawn *independently* from a distribution that is symmetric under $J \Leftrightarrow -J$. This results in a perfect balance between ferro- and antiferro-magnetic tendencies and provides a powerful tool to aid theoretical analysis. Although the evidence that some deviations from this statistical symmetry or from perfect independence do not change the universal aspects of the low temperature phase, other changes can surely do so. Whether any or all spin glass systems are in the same class as EA models, in the the class of models with correlations among the $\{J_{xy}\}$ that are believed to have many states [15], or in some other class, is highly uncertain and clearly an important question.

For both pedagogical and historical reasons we focus primarily on EA spin-glass models.

4.1 *Scaling scenario*

At present the only *consistent* scenario for the behavior of finite-dimensional Edwards-Anderson spin glasses is one based on scaling and “droplet” arguments [24, 25]. This scenario, which is certainly the simplest possible, involves only one pair of states – related by the global spin-inversion symmetry – at any given temperature. Nevertheless, it has rich phenomenology and yields a range of qualitative and semi-quantitative predictions that have been born out by experiments [26]. For purposes of the more general discussion, we outline a few of the primary features of this theory [24, 25].

At fixed temperature in the ordered phase, as there is a unique pair of infinite system equilibrium states, we can describe near-equilibrium configurations as a network of domain walls separating regions whose local correlations – particularly the local magnetizations of individual spins – are similar to those of one of these states, from regions similar to the other – the spin reversed – state. Although this sounds superficially similar to the unfrustrated ferromagnets discussed above, there are crucial differences. Instead of tending towards being flat on large scales, the domain walls in spin glasses will be *fractal* with surface area scaling with their length scale as L^{d_s} with the fractal dimension $d - 1 < d_s < d$. The possibility that $d_s = d$, so that the walls fill a finite fraction of the system, has sometimes been confused with the question of the existence of many pure states [27], but these are not related. As explained earlier, different pure states are induced in a region by different sets of *sample-specific* boundary conditions; the differences between them can be characterized by a *collection* of domain walls. In contrast, a single region-spanning domain wall can be induced by merely changing the sign of half the boundary spins. Thus many incongruent pure states could in principle occur even if $d_s < d$; indeed, two incongruent states do occur in just this way in the random field Ising model. An argument against single spin-glass domain walls being space filling is given in [24].

The large area of domain walls is closely related to the lack of an interfacial tension: looking at a section of wall that is small compared to the scale on which it is forced (by either boundary conditions or non-equilibrium effects) one cannot tell whether or not there is a wall present at all! (Unless, of course, one knows the actual pure states.) The excess free energy of a scale L section of domain wall is of order L^θ with θ the fundamental scaling exponent for energies in the ordered phase. As θ is necessarily small

$$\theta \leq \frac{d-1}{2}, \quad (4.2)$$

the excess free energy per unit area of a wall is typically of order $L^{\theta-d_s}$ which is negligible for large L . Indeed, some sections of the wall will actually lower the free energy locally: it is only the overall constraint that walls be either

closed or extend out to the boundaries that prevent such negative-energy wall segments from forming spontaneously and modifying the equilibrium states.

The exponent θ plays a crucial role in the finite temperature properties of spin glasses. If θ is positive, large scale excitations – reversal of a connected collection of spins from one of the ground states – typically cost a lot of energy and are thus unlikely to be thermally excited. This implies that the low temperature behavior is governed by the same RG fixed point that controls the ground states; the RG eigenvalue of temperature is simply $-\theta$. If θ is negative, on the other hand, then there are large scale excitations in any region that cost little energy. These will be thermally excited and destroy the broken symmetry of the ground states: at any positive temperature there will then be a unique equilibrium state which is disordered. In the marginal case $\theta = 0$, one needs to know more information, in particular whether there might be logarithmic length-scale dependence of excitation and domain wall energies which could stabilize the low temperature phase [as occurs for one dimensional Ising ferromagnets with $1/r^2$ interactions [28]].

We now turn to consideration of finite subregions of an infinite system. In particular, consider pulling some region – a “box” – out of a specific infinite sample and exploring the properties of the box as boundary conditions on it are varied. Some of the results within the droplet scenario can be guessed by analogy with random ferromagnets. One specific boundary condition – the one that correctly reflects the preferences of the rest of the system – will give the corresponding infinite-system equilibrium state in the whole of the box. The spin reversal of this boundary condition will give the other state.

Attempts to force a domain wall through the box by split boundary conditions will, because of the extreme roughness of the domain walls, almost always result in the imposed domain wall missing the center – or any other predetermined point deep in the interior – by a distance that is typically some fraction of the box size. This is a consequence of the domain walls not being space filling. Nevertheless, generic boundary conditions will give rise to a dense network of domain walls near the edges of the box. This network will gradually thin out towards the interior of the box with typically no wall, one wall, or a only a few walls, passing through the middle part – say the middle 3^{-d} th fraction – of its volume. In two dimensions, this has been shown convincingly in [29]; in three dimensions, for which only small sample sizes can be studied, it is still controversial [30].

Free boundary conditions, which some advocate using and might seem most natural, behave rather like generic random boundary conditions. But because of relaxation near the boundary that does not take into account

compromises between interactions among spins inside and outside the box, free boundary conditions will generally give rise to finite box states that have lower free energy (by of order the surface area) than the infinite system states restricted to the box. These have, however, no relevance for the properties of systems much larger than the box being considered: regions near to either free or inappropriately fixed boundaries will not be characteristic of the bulk.

The dynamics in the two-state picture of spin glasses is also superficially similar to that of random ferromagnets, but again there are crucial differences. For a domain wall between the two equilibrium states to move – or to disappear if it bounds a closed region – typically requires that it pass through some configurations whose excess free energy is much larger than that of a minimal domain wall free energy. For positive θ , the barriers that must be overcome will grow with length scale as

$$B \sim L^\psi \quad (4.3)$$

with the exponent ψ in the range

$$\theta \leq \psi \leq d - 1. \quad (4.4)$$

For three dimensional spin glasses, for which estimates of θ are in the range of 0.2 [31], these inequalities allow for an order of magnitude uncertainty in the value of ψ and concomitantly a great deal of uncertainty in the maximum length scales at which local equilibrium can be achieved, the subject to which we now turn.

In the ordered phase of a spin glass with a unique pair of states, equilibration will proceed, as for ferromagnets, by coarsening of a patchwork of domains of the two equilibrium states. The typical distance between domain walls a long time t_w after a quench into the ordered phase will be

$$\ell_w \sim [\ln(t_w/t_0)]^{\frac{1}{\psi}}. \quad (4.5)$$

But, to reiterate: the domain walls are fractal and have no free energy density; local measurements will be unable to confirm or deny the existence of a domain wall passing through a region. Statistically, except for the slight excess free energy density and the slow evolution towards equilibrium, it will be hard to tell from local measurements how far apart the non-equilibrium domain walls are or even whether they are present at all. Yet local measurements *can* – and we hope in the near future will – test far better than macroscopic measurements the predictions of the scaling theory. Furthermore, if competing predictions are forthcoming, local measurements could distinguish the two state picture from possible scenarios with many states.

Since the presence of domain walls cannot be established in a single experiment, what is needed are multiple repetitions of experiments with the same thermodynamic conditions and history. Local probes that are sensitive to scales smaller than those on which local equilibrium can be established could be used to scan the *same* region of the sample in each repeat of the experiment and look for differences and similarities between the runs. Ideally, if the net magnetization in small enough regions can be measured and averaged over times short compared to the waiting time but long compared to typical fluctuations on the scales of the probe, one could look for similarities between two runs over regions of the sample. In principle, this should enable *relative* domain walls between different runs to be located: these are the boundaries between regions that are similar in the two runs and regions that are similar except for an overall sign change of the local magnetizations. But even if a local probe is not sensitive to the signs of the spins, equilibrium regions will have signatures. For example, the spectrum of dynamic fluctuations of the local magnetization will vary from region to region [32]. Although within a domain such a local signature will be independent of which of the two states the region resembles, *relative* domain walls between two runs could be located by mapping the (in principle fractal) regions in which the local signatures differ. In the next sub-section, we consider how the behavior might differ if there are many, rather than only two, pure states.

Unfortunately, there is a great deal of uncertainty in the length scales involved in the low temperature phase of spin glasses [33]. The logarithmic factor in (4.5) depends both on the macroscopic time scale of the experiment and on the effective microscopic time scale t_0 . If the latter is long because of low temperatures or proximity to the critical temperature – it is hard to avoid at least one of these being a factor! – this will limit the ratio of the length scale of the domain network to the appropriate “microscopic” scale: either the critical correlation length $\xi(T)$ (which diverges at T_c with a concomitant rapid divergence of t_0) or the scale of the limiting processes at low temperatures. With t_0 in the range from a picosecond to a millisecond and t_w of a megasecond (a fortnight), $\ln(t_w/t_0)$ varies from about twenty to forty. But the uncertainty in ψ means that this translates into ℓ_w/ξ anywhere from as small as five to macroscopic: clearly one needs a better estimate!

Some features of the two-state spin glass dynamics are simpler than those of random ferromagnets with which they share logarithmic growth of domain sizes with time. This is a consequence of the dominance of randomness at all scales in spin-glasses – the ordered phase is governed by a random zero-temperature fixed point – and the concomitant fractal domain walls. In particular, there will only be one characteristic length scale in spin glass

coarsening rather than the two – ℓ_w and L_w – of random ferromagnets. Furthermore, on any given long time scale – even a factor of two in t_w – the evolution of the order in spin glasses will primarily take place in only a small fraction of the system. Because of the breadth of the distribution of barrier heights at long length scales, on macroscopic time scales almost all barriers will either be substantially smaller than B_{t_w} , and thus already surmounted, or substantially larger than B_{t_w} and thus insurmountable. This strong local metastability contrasts with the relatively uniform evolution of the domain wall network in random ferromagnets. It is also the root cause of the ageing phenomena that are seen in so many glassy systems [36].

Many of the most interesting features of the spin glass phase are associated with the hypersensitivity of the equilibrium states to changes of temperature [34]. This phenomenon – sometimes rather misleadingly called “chaos” – implies that equilibration at one temperature does not help much for equilibration at a substantially different temperature: the latter evolution must be considered in terms of the network of domains of the states at the new temperature. On scales longer than an *overlap length* which depends inversely on the temperature difference, the equilibrium states at the second temperature will consist of a random sponge of the states at the first temperature. We will not go into these issues here, except to note that the existence of hypersensitivity to temperature changes relies on very weak assumptions: recent claims in the literature that “chaos” with temperature does not occur in the Sherrington-Kirkpatrick model [35] cannot be carried over to finite range systems; this will apply even if there are many equilibrium states in both.

4.2 Observation of many states?

If a real spin-glass (whether EA-like or not) exhibited many pure states, how might these be observed? From the discussion of the droplet/scaling scenario, it is clear that one should focus on correlations on length scales small enough that local equilibrium can be established. But how do we know that local equilibrium will occur at all if there are many states? Fortunately, the necessity for all equilibrium states to have the same free energy density implies that there must be evolution towards some kind of local equilibrium. Quite generally, the minimal rate of growth of the scale over which such equilibrium will be established is $\ell_w \sim (\ln t_w)^{\frac{1}{\psi}}$ with $\psi \leq d - 1$, allowing for the possibility of several different scales with the *shortest* – hence lower case ℓ – defining this ψ . This bound on ψ follows from the observation that all combinations of spin flips in a region can be accomplished in the time it takes to pass a (maximum-energy) domain wall across it: *i.e.* in time less than $\exp(KL^{d-1}/T)$. After a time of this order, we expect that the free

energy density of the region will only differ from that in equilibrium by at worst terms of order the surface to volume ratio: $\sim 1/\ell_w$

In a locally equilibrated region of volume $v_w \sim \ell_w^d$, the number of different “states” can grow no more rapidly than the number of possible boundary conditions: *i.e.* exponentially in the surface area [7]. Although our understanding of possible scenarios is sufficiently poor that the nature of evolution towards equilibrium is far from clear, the simplest expectation is that the number of distinguishable states in a region will grow more slowly than the upper bound, probably as the number of infinite system states that can be differentiated in v_w : $N_S \leq \exp(C\ell_w^\sigma)$ with $\sigma \leq d - 1$ [14]. In any case, the number of possible states will be far less than the total number of configurations in the region which grows as $\exp[\overline{C}v_w]$. Thus *equilibration must develop spatial correlations*.

The simplest scenario is that the correlations in locally equilibrated regions will be similar to those of one of the equilibrium states in the region. But which state this is will depend on the particular stochastic initial conditions and history as well as the influence of neighboring regions. As neighboring regions of size greater than ℓ_w will evolve roughly independently, they will typically make incompatible choices of states. These conflicts must be resolved as ℓ_w grows. This conflict resolution will result in changes of the states within at least some of the regions that were already locally-equilibrated. If many quench-and-wait experiments are performed, one should see many different outcomes for the correlations in the same region. But even if the requisite long time scales and a reasonable range of ℓ_w can be achieved, it will be difficult to distinguish this type of subtle behavior from a system with only two pure states: in the latter there will be a multiplicity of non-equilibrium metastable “states” in regions that have not yet equilibrated. In order to even attempt to distinguish these, it is necessary to develop scenarios with many states to the point at which predictions that go beyond the general considerations outlined here become possible. This should be a key goal of future research in on spin glasses.

As applying uniform magnetic fields can be instructive in spin-glasses, we note that the presence or absence of a phase transition in Ising spin-glasses in a non-zero magnetic field is related to whether or not non-symmetry related states exist in zero-field: if there are indeed only a pair of states in zero field, then the droplet scenario prediction that a magnetic field destroys the spin glass phase is almost certainly correct. But if there are many states in zero field, the possibility is opened up, but by no means assured, of a phase transition and many states in non-zero field as occurs for the Sherrington-Kirkpatrick model.

5 Non-random systems: True glasses

The fundamental difference between random systems with “glassy” dynamics and structural glasses is the origin of the wide separation of time scales between various processes that is observed in both: is this preordained or must it be established by the system itself? In spin glasses and random field magnets the *Hamiltonian* controlling the dynamical degrees of freedom is explicitly random, this *quenched randomness* having been established by non-equilibrium processes that are completely frozen on experimental time scales at the temperatures of interest for the magnetic degrees of freedom. In true glasses, in contrast, the Hamiltonian is *not* explicitly random: the structural randomness must be generated by the dynamics [37]. A natural exception to this is the behavior at temperatures far below the glass temperature; for this the frozen structural configuration acts like quenched randomness [38]. But the low temperature properties, while undoubtedly interesting, do not involve the basic issues of structural glasses. The far more fundamental questions concern *formation* of the glass itself; for these, assuming quenched randomness – as is sometimes done [17] – is rather cheating!

It is usually asserted that glass forming materials would like to be crystalline solids and are only constrained from being so by the dynamics. But need this always be the case? Or are there materials – or at least models – whose *equilibrium* phase in some range of temperature has static structural correlations that are glass-like: non-uniform, aperiodic, positional correlations that persist for infinite times? At this point, aside from quasicrystals, which exhibit Bragg peaks although they are not strictly periodic, the answer to this question is not known. Indeed, rather surprisingly, it has received remarkably little attention.

Aperiodic ground states are known to exist for some lattice and continuum models with finite range interactions and can be “generic” in the sense that small changes of the interactions preserve the aperiodicity of the ground states [39]. Much of the work in this field, in particular that by Radin and collaborators, has been in terms of tiling models: generalizations of the well-known Penrose tilings that form quasicrystals under constraints on their positioning. These constraints can be thought of as arising from a Hamiltonian for interactions among the tiles that is minimized only by the arrangements satisfying the constraints [39]. Like their quasiperiodic counterparts, the known aperiodic ground states do have regularities, just not enough to make them periodic or even, in some cases, to exhibit any preferred orientations in their spatially averaged correlations.

Intriguing questions that are only starting to be addressed involve the positive temperature behavior of models with aperiodic ground states [40]. Can these have a low temperature phase in which the translational

symmetry is broken but the correlations are aperiodic? If so, what are the conditions for such a – dare one call it a true glass? – phase to exist? What is the nature of transitions into such phases? One possibility might be a sequence of periodic phases with larger and larger unit cells leading to an aperiodic phase either at some positive temperature, or perhaps only at zero temperature.

Whether or not aperiodic phases can exist at positive temperature, the dynamics of such systems are certainly well worth exploring. How their subtle correlations develop with time may provide useful hints for understanding the development of spatial correlations in real glasses. For lattice models with discrete degrees of freedom but aperiodic ground states, the concepts of domain walls and their motion are likely to be useful. More generally, motion of other types of defects [41] – and perhaps associated barriers – may well play a role given that the ground states consist of large regions that are very similar to one another [39].

One of the clear lessons from this lecture should be that for real glasses as well as models spatial correlations *must* develop: the primary questions are their nature and the maximum lengths over which some form of local equilibrium – perhaps in a restricted part of phase space that excludes crystallinity – can be established on experimental time scales [42]. Does the length scale, analogous to ℓ_w , grow logarithmically in time – perhaps only as $\sqrt{\ln t_w}$ in three dimensions – or faster? Are there several characteristic lengths? How many different local configurations can exist in regions of size ℓ_w ?

Of course, it is entirely possible that all of the physics of glass forming materials takes place on length scales that are only two or three molecular diameters. If this is the case, there is presumably little reason to expect any universality. But surely it is worth considering the more interesting alternative, especially in fragile glasses for which the crossover from fast to slow dynamics happens over such a narrow range of temperature [37].

Whatever understanding I might have of these subjects is due in large part to stimulating interactions with numerous colleagues over the past twenty years; to all of these, I am most grateful. But one in particular I have collaborated with on many of the problems discussed here: to David Huse exceptional thanks are due. Most of the recent work, particularly on possibilities of many states, is in collaboration with Olivia White to whom I am also indebted. Much of this research was supported by the National Science Foundation Materials Theory Program.

References

[Note] *There is a great deal of literature on many of the topics discussed in this lecture. The references cited are mostly either recent articles or reviews in which other references can be found, or particularly relevant original articles.*

- [1] E.g. L.F. Cugliandolo, J. Kurchan, R. Monasson, *et al.*, *J. Phys. A-Math. Gen.* **29** (1996) 1347.
- [2] W. Gotze and L. Sjogren, *Transp. Theory Stat. Phys.* **24** (1995) 801; J.P. Bouchaud, L. Cugliandolo, J. Kurchan, *et al.*, *Physica A* **29** (1996) 243, and references therein.
- [3] H. Frauenfelder, A.R. Bishop, A. Garcia, *et al.*, *Physica D* **107** (1996) 13; For a criticism of some of the applicability of some of these concepts: D.S. Fisher, *Physica D* **107** (1997) 204.
- [4] A.T. Ogielski and D.L. Stein, *Phys. Rev. Lett.* **55** (1985) 1634; E. Bertin and J.-P. Bouchaud, *J. Phys. A-Math. Gen.* **35** (2002) 3039.
- [5] For a recent review, see E. Marinari, G. Parisi, F. Ricci-Tersenghi, J.J. Ruiz-Lorenzo and F. Zuliani, *J. Stat. Phys.* **98** (2000) 973.
- [6] D. Ruelle, *Statistical Mechanics: Rigorous Results* (W.A. Benjamin, Reading, MA, 1969).
- [7] For an extended exposition see C.M. Newman and D.L. Stein, *J. Stat. Phys.* **106** (2002) 213; for some of the specific issues: C.M. Newman and D.L. Stein, *Phys. Rev. E* **55** (1997) 5194; C.M. Newman and D.L. Stein, *Commun. Math. Phys.* **224** (2001) 205.
- [8] J.Z. Imbrie *Commun. Math. Phys.* **8** (1985) 145; J. Bricmont and A. Kupiainen, *Commun. Math. Phys.* **116** (1988) 539.
- [9] For figures and references see: A.A. Middleton and D.S. Fisher, *Phys. Rev. B* **65** (2002) 134411.
- [10] J. Villain, *Phys. Rev. Lett.* **52** (1984) 1543.
- [11] For discussion of zero-temperature fixed points in random systems see, *e.g.* [9, 10, 20, 24].
- [12] M. Mezard, G. Parisi and M.A. Virasoro, *Spin glass theory and beyond* (World Scientific, 1987), and references therein.
- [13] D.A. Huse and D.S. Fisher, *J. Phys. A Lett.* **20** (1987) L997.
- [14] C.M. Newman and D.L. Stein, *J. Stat. Phys.* **82** (1996) 1113; C.M. Newman and D.L. Stein, *Phys. Rev. E* **6302** (2001) 016101.
- [15] O. White and D.S. Fisher, unpublished.
- [16] J.T. Chayes, L. Chayes, J.P. Sethna and D.J. Thouless, *Commun. Math. Phys.* **106** (1986) 41; J.M. Carlson, J.T. Chayes, L. Chayes, J.P. Sethna and D.J. Thouless, *J. Appl. Phys.* **63** (1988) 4001; M. Mezard and G. Parisi, *Eur. Phys. J. B* **20** (2001) 217.
- [17] T.R. Kirkpatrick and D. Thirumalai, *Phys. Rev. B* **36** (1987) 5388; A. Cavagna, I. Giardina and G. Parisi, *J. Phys. A-Math. Gen.* **30** (1997) 7021.
- [18] For a review, see: A.J. Bray, *Adv. Phys.* **43** (1994) 357; and for more recent references, see, *e.g.* M.R. Evans, *J. Phys. Cond. Matt.* **14** (2002) 1397.
- [19] J.D. Shore and J.P. Sethna, *Phys. Rev. B* **43** (1991) 3782.
- [20] For lecture notes and reviews, see, *e.g.* D.S. Fisher, *Low temperature phases, ordering and dynamics in random media*, edited by T. Riste and D. Sherrington, *Proceedings of NATO Advanced Study Institute on Phase Transitions and Relaxation in Systems with Competing Energy Scales* (Kluwer, Amsterdam, 1993); J.P. Bouchaud, L.F. Cugliandolo, J. Kurchan and M. Mezard, *Out of equilibrium dynamics in spin-glasses and other glassy systems*, edited by A.P. Young, *Spin glasses and random fields* (World Scientific Singapore, 1998).

- [21] D.S. Fisher, *Phys. Rev. Lett.* **56** (1986) 1964.
- [22] Coarse graining in random systems, especially spin-glasses, is very subtle. For a given (long) length scale, L , of interest, coarse-graining out to a scale that can grow as a subdominant power of L may be needed; see, *e.g.* [24].
- [23] G. Parisi, *Phys. Rev. Lett.* **43** (1979) 1754; M. Mezard, G. Parisi, N. Sourlas, G. Toulouse and M. Virasoro, *Nature Spin-Glass Phase* **52** (1984) 1156.
- [24] D.S. Fisher and D.A. Huse, *Phys. Rev. B* **38** (1988) 386.
- [25] D.S. Fisher and D.A. Huse, *Phys. Rev. B* **38** (1988) 373; for a recent discussion of aging and related issues: L. Berthier and J.-P. Bouchaud, *Phys. Rev. B* **66** (2002) 054404.
- [26] T. Jonsson, K. Jonason, P. Jonsson and P. Nordblad, *Phys. Rev. B* **59** (1999) 8770, and references therein; J. Mattsson, T. Jonsson, P. Nordblad, H.A. Katori and A. Ito, *Phys. Rev. Lett.* **74** (1995) 4305; E. Vincent, V. Dupuis, M. Alba, *et al.*, *Europhys. Lett.* **50** (2000) 674; K. Jonason, E. Vincent, J. Hammann, *et al.*, *Phys. Rev. Lett.* **81** (1998) 3243; J.P. Bouchaud, E. Vincent and J. Hammann, *J. Phys. I France* **4** (1994) 139; P.E. Jonsson, H. Yoshino and P. Nordblad, *Phys. Rev. Lett.* **89** (2002) 097201; R. Mathieu, P.E. Jonsson, P. Nordblad, H.A. Katori and A. Ito, *Phys. Rev. B* **65** (2002) 012411; L. Berthier and J.-P. Bouchaud, *Comment on "Symmetrical temperature-chaos effect with positive and negative temperature shifts in a spin glass"* (2002) [cond-mat/0209165].
- [27] See, *e.g.* [5]. This and various other confusions are cleared up in [7].
- [28] M. Aizenman, J.T. Chayes, L. Chayes, *et al.*, *J. Stat. Phys.* **50** (1988) 1. Some of the properties that appear in "replica symmetry breaking" are closely related to those of systems in which θ is exactly zero so that there is a low temperature phase governed by a non-trivial fixed line. The $1/r^2$ Ising chain is not really an example of this: the excitation energies grow as $\ln L$.
- [29] A.A. Middleton, *Phys. Rev. Lett.* **83** (1999) 1672.
- [30] F. Krzakala and O.C. Martin, *Phys. Rev. Lett.* **85** (2000) 3013; M. Palassini and A.P. Young, *ibid* (2000) 3017.
- [31] A.K. Hartmann and A.P. Young, *Phys. Rev. B* **64** (2001); and references therein.
- [32] M.B. Weissman, *Rev. Mod. Phys.* **65** (1993) 829.
- [33] J.-P. Bouchaud, V. Dupuis, J. Hammann and E. Vincent, *Phys. Rev. B* **65** (2002); C. Djurberg, J. Mattsson, P. Nordblad, *et al.*, *J. Magn. Magn. Mater.* **140** (1995) 1721.
- [34] D.S. Fisher and D.A. Huse, *Phys. Rev. Lett.* **56** (1986) 1601; A.J. Bray and M.A. Moore, *Phys. Rev. Lett.* **58** (1987) 57.
- [35] R. Mulet, A. Pagnani and G. Parisi, *Phys. Rev. B* **63** (2001) 184438.
- [36] On aging phenomena, see, *e.g.*, lectures in this volume by L. Cugliandolo and J.-P. Bouchaud.
- [37] For a review of phenomena see: C.A. Angell and M. Goldstein, *Dynamic aspects of structural change in liquids and glasses* (N.Y. Acad. Sci., New York, 1986); and for recent theory see articles in: *J. Phys. Cond. Matt.* **12** (1999) 6295.
- [38] For recent work see, *e.g.*: D. Natelson, D. Rosenberg and D.D. Osheroff, *Phys. Rev. Lett.* **80** (1998) 4689; S. Rogge, D. Natelson and D.D. Osheroff, *Phys. Rev. Lett.* **76** (1996) 3136; and references therein.
- [39] See, *e.g.*: C. Radin, *J. Phys. A-Math. Gen.* **22** (1989) 317; C. Radin, *Ann. Math.* **139** (1994) 661; D. Berend and C. Radin, *Commun. Math. Phys.* **152** (1993) 215 (1993).
- [40] T.A. Weber, G.H. Fredrickson and F.H. Stillinger, *Phys. Rev. B* **34** (1986) 7641; L. Leuzzi and G. Parisi, *J. Phys. A-Math. Gen.* **33** (2000) 4215.

- [41] F. Ritort and P. Sollich, *Glassy dynamics of kinetically constrained models* (2002) [[cond-mat/0210382](#)]; and references therein.
- [42] Recent papers that discuss length scales in glasses include: C. Donati, S. Franz, S.C. Glotzer, *et al.*, *J. Non-Cryst. Lids* **307** (2002) 215; C. Donati, S.C. Glotzer, P.H. Poole, W. Kob and S.J. Plimpton. *Phys. Rev. E* **60** (1999) 3107; U. Tracht, M. Wilhem, A. Heuer, *et al.*, *Phys. Rev. Lett.* **81** (1998) 2727.

COURSE 9

EXPERIMENTAL ANALYSIS OF AGING

S. CILIBERTO

*École Normale Supérieure de Lyon,
Laboratoire de Physique,
CNRS UMR 5672 du 46 allée d'Italie,
69364 Lyon Cedex 07,
France*



Contents

1	Introduction	557
2	Aging, memory and rejuvenation	558
2.1	Aging range: A simple quench experiment	558
2.2	Memory and rejuvenation	562
2.3	Discussion on the memory effect	573
3	Effective temperature of an aging material	575
3.1	The X-ray scattering experiment	577
3.2	Supercooled liquid experiment	579
3.3	Gel electric properties	580
3.4	Polycarbonate dielectric properties	586
3.5	Rheological measurements	595
3.6	Discussion and conclusions on the effective temperature	600
4	General conclusions	601

EXPERIMENTAL ANALYSIS OF AGING

S. Ciliberto

Abstract

Several experimental aspects of the aging dynamics are discussed. We first introduce the general features of aging. We then describe several experimental procedures, based on the response function, which have been useful to study memory and rejuvenation effects in various materials. A comparison of the results obtained in the different materials is done. The experimental analysis of the violation of the Fluctuation-Dissipation Theorem (FDT) in aging materials is presented. We describe several experiments where the violation has been studied in some details. The amplitude, the persistence time and the observable dependence of the violation observed in the experiments are analyzed. The relevance of these experimental results for recent models of aging is discussed.

1 Introduction

Many physical systems in nature are not in thermodynamic equilibrium because they present very slow relaxation processes. A typical example of this phenomenon is the aging of glassy materials: when they are quenched from above their glass transition temperature T_g to a temperature $T < T_g$, any response function of these systems depends on the aging time t_w spent at T . For example, the dielectric and elastic constants of polymers continue to evolve several years after the quench [1]. The magnetic susceptibility of spin-glasses depends on the time spent at low temperature [2]. Another example of aging is given by colloidal-glasses, whose properties evolve during the sol-gel transition which may last a few days [3]. An important feature of aging materials is the dependence of their physical properties on the thermal history of the sample. Indeed experimental procedures, based on multiple cycles of cooling, heating and waiting times, have shown the existence of two spectacular effects: memory and rejuvenation. Specifically, aging materials present a rejuvenation for any negative temperature perturbation and

at the same time during heating they remind the stops at fixed temperature done during cooling (see for example [4, 5] and references therein). In the first part of this lecture we will describe these two effects and the experimental procedures used to characterize them. These procedures have been extremely useful to fix several constraints for the phenomenological models [6, 7] and thus they merit to be described in some details.

In the second part of the lecture we will address another important problem of the aging dynamics. Indeed glasses are out of equilibrium systems and usual thermodynamics does not necessarily apply. However, as the time evolution is slow, some concepts of the classical approach may be useful for understanding the glass aging properties. A widely studied question, is how the temperature of these systems can be defined. One possible answer comes from the study of the deviation to the Fluctuation Dissipation Theorem (FDT) in an out of equilibrium system (for a review see [9, 10] and Cugliandolo lecture in these proceedings). In this lecture we will describe a series of experiments where this question is analyzed in some details on real material. The implications of these experimental results on the model of aging are finally discussed.

2 Aging, memory and rejuvenation

The aging of glassy materials is a widely studied phenomenon [1, 2] which is experimentally analyzed by measuring as a function of time the dielectric susceptibility, the elastic constants, the density and the thermal properties of the materials. In the next subsection we will give an example of the aging of the dielectric constant of plexiglass (PMMA), which is a polymer glass with $T_g = 388$ K [12]. We will show first the aging properties and then, in the next sections the memory effects in the same material.

2.1 Aging range: A simple quench experiment

To determine the dielectric constant, we measure the complex impedance of a capacitor whose dielectric is the PMMA sample. In our experiment a disk of PMMA of diameter 10 cm and thickness 0.3 mm is inserted between the plates of a capacitor whose vacuum capacitance is $C_0 = 230$ pF (see Fig. 1 for details). The capacitor is inside an oven whose temperature T may be changed from 300 K to 500 K. The temperature stability is within 0.1 K. The maximum heating and cooling rate $|R| = |dT/dt|$ is about 180 K/h. We checked that the temperature difference between the two capacitor plates is always smaller than 1 K both during the heating and the cooling cycles.

The capacitor is a component of the feedback loop of a precision voltage amplifier whose input is connected to a signal generator. We obtain the real and imaginary part of the capacitor impedance by measuring the response

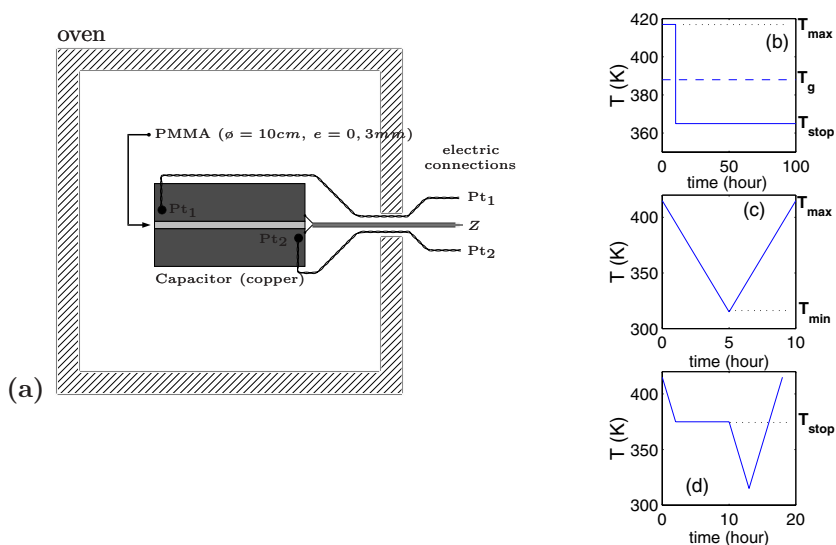


Fig. 1. a) Experimental set-up for PMMA. PMMA is the dielectric of a capacitor whose vacuum capacitance is $C_0 = 230$ pF. This impedance Z is inside an oven which controls the temperature and acts like an electrical screen. The dielectric temperature is measured by two platinum probes (Pt). **b–d) Typical thermal cycles applied to the sample.** **b)** Temperature quench from above to below T_g . **c)** Temperature ramp at constant cooling and heating rates. **d)** Cooling stop for 10 h at T_{stop} .

of the amplifier to a sinusoidal input signal. This apparatus allows us to measure the real and imaginary part of the dielectric constant $\epsilon = \epsilon_1 + i \epsilon_2$ as a function of temperature T , frequency f and time t . Relative variations of ϵ smaller than 10^{-3} can be measured in all the frequency range used in this experiment, *i.e.* $0.1 \text{ Hz} < f < 100 \text{ Hz}$. The following discussion will focus only on ϵ_1 (thus we will omit subscript 1), for which we have the best accuracy, but the behaviour of ϵ_2 leads to the same conclusions.

The measurement is performed in the following way. We first initialize the PMMA history by heating the sample at a temperature $T_{\text{max}} > T_g$. In this case the applied thermal cycle is that shown in Figure 1b. The sample is left at $T_{\text{max}} = 415$ K for a few hours, so that equilibrium can be assumed for the initial condition. The temperature is rapidly decreased at $R = -180$ K/h to a temperature $T_{\text{stop}} < T_g$, where it is regulated by the oven. The zero of the aging time is taken at the instant, during the quench, when the sample temperature is equal to T_g . Typical aging curves of ϵ as a function of time are shown in Figure 2, for different T_{stop} at $f = 1$ Hz and

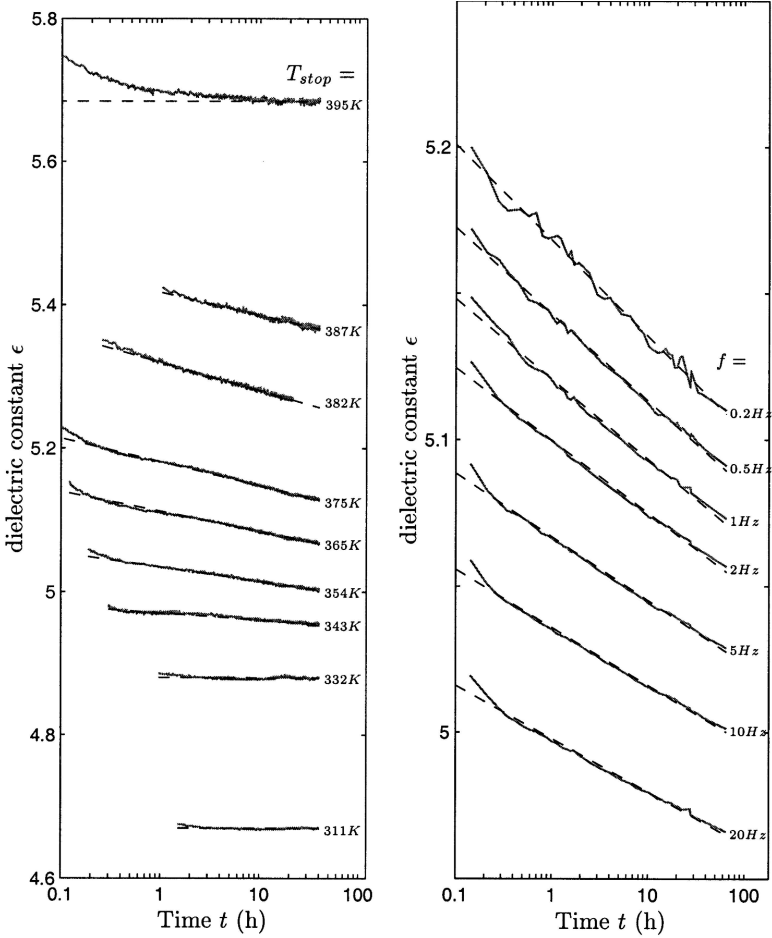


Fig. 2. Dependence on t of ϵ after a quench. **a)** Aging measured at $f = 1$ Hz after a quench at various T_{stop} . **b)** Aging measured after a quench at $T_{\text{stop}} = 365$ K at various f . A logarithmic fit in time of all these curves is accurate as soon as temperature is stabilized, except for $T_{\text{stop}} = 395$ K $> T_g$.

different f at $T_{\text{stop}} = 365$ K. We clearly notice a logarithmic dependence on time of the dielectric constant as soon as the temperature is stabilized, in all the temperature and frequency range we have explored. However the aging curve depends on T_{stop} and f : the sample properties evolve faster when T_{stop} is close to T_g and f is small.

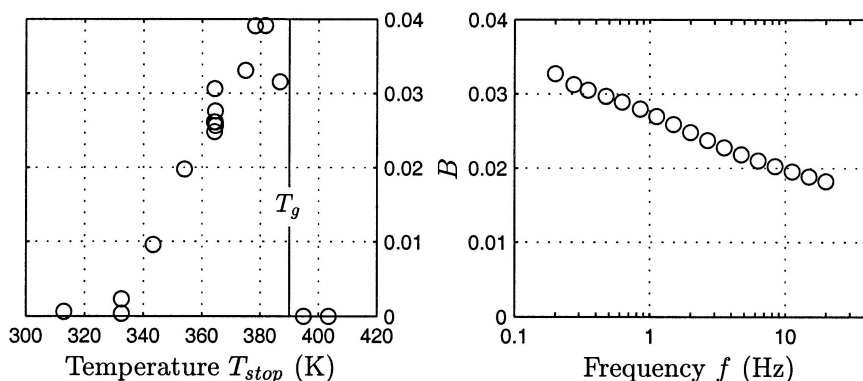


Fig. 3. a) Dependence on T_{stop} of B at $f = 1$ Hz, where B is the parameter of the logarithmic fit of the dielectric constant $\epsilon(T_{\text{stop}}, t, f) = A(T_{\text{stop}}, f) - B(T_{\text{stop}}, f) \log(t/1h)$ after a quench at T_{stop} . **b)** Dependence on f of B at $T_{\text{stop}} = 365$ K.

Specifically one can write $\epsilon(T_{\text{stop}}, t, f) = A(T_{\text{stop}}, f) - B(T_{\text{stop}}, f) \log(t/t_o)$ with $t_o = 1$ h. Here A is the value of ϵ at $t = t_o$. It is found that A and B are functions of T_{stop} and of the frequency f at which the dielectric constant is measured. Note that as A and B depend also weakly on the cooling rate R , we always use $R = -180$ K/h in these experiments. The values of B , measured at $f = 1$ Hz, are plotted in Figure 3a as a function of T_{stop} . B is an increasing function of T_{stop} till a temperature T_m close to T_g , but goes down to 0 if $T_{\text{stop}} > T_g$. Indeed for a quench temperature larger than T_g the sample can reach a thermodynamic equilibrium, so no aging is observed but only a relaxation of ϵ toward its stationary value. The long time behaviour is stationary and B goes to 0.

The values of B , measured at $T_{\text{stop}} = 365$ K, are plotted in Figure 3b as a function of f . B is a slowly increasing function for $f \rightarrow 0$. Indeed aging is smaller at high frequencies than at low frequencies (a theoretical justification of such a behaviour can be found for example in [9]).

These curves determine the region where to work. In our dielectric measurement aging can be accurately observed between 335 K and $T_g = 388$ K. We will probe $f = 0.1$ Hz and $f = 1$ Hz where aging effects are the largest in our frequency range.

2.2 Memory and rejuvenation

2.2.1 Historical background

In spite of the interesting experimental [4, 13–23] and theoretical progress [2, 9, 25], done in the last years, the physical mechanisms of aging are not yet fully understood. In fact on the basis of available experimental data it is very difficult to distinguish which is the most suitable theoretical approach for describing the aging processes of different materials. In order to give more insight into this problem several experimental procedures have been proposed and applied to the study of the aging of various materials, such as spin-glasses (SG) [4, 13, 16, 21–23], orientational glasses (OG) [14, 17], polymers [1, 18, 20, 26, 45] and supercooled liquids (SL) [15].

The very well known Kovacs [26] experiment was probably among the first in showing that the state of a glass is strongly determined by its thermal history. In the Kovacs experiment the material is submitted to the following temperature cycle sketched in the insert of Figure 4a. The material is rapidly quenched from the liquid at a temperature T_0 to the glass phase at a temperature T_1 at which the volume of the glass is V_1 . The material is maintained at T_1 for about 100 h. Because of aging the volume of the material decreases as a function of time going from V_1 to V_2 , as shown in Figure 4a. Then the material is rapidly heated at a temperature T_2 at which V_2 is the equilibrium volume. One could think that no appreciable evolution appears as a function of time. Instead the time evolution of the sample volume at temperature T_2 , sketched in Figure 4b, is quite different. The volume first increases, reaches a maximum and then decreases to reach again the value V_2 . As shown in Figure 4b, the amplitude of the maximum depends of course on T_1 and on the waiting time at T_1 . Figure 4a points out the difference between the time evolution of the volume after a quench from T_0 to T_2 and after the aging at T_1 . Another example of history dependent effect is that induced by the aging at low temperature, known as prepeak in polymer literature [18]. Such an aging does not produce important changes in the enthalpy. However when increasing temperature, a peak in the curve of the heat capacity *versus* temperature is observed at a temperature close to T_g .

Other procedures were proposed for spin glasses and applied to other materials. Among these procedures we may recall the applications of small temperature perturbations to a sample during the aging time [13–15, 45]. One of the main results of these experiments is that the time spent at low enough temperature does not contribute to the aging behaviour at the higher temperature. In order to have a better understanding of the free energy landscape of SG and OG, a very smart protocol has been proposed [4] and used in several experiments [4, 16, 17]. This protocol, which is

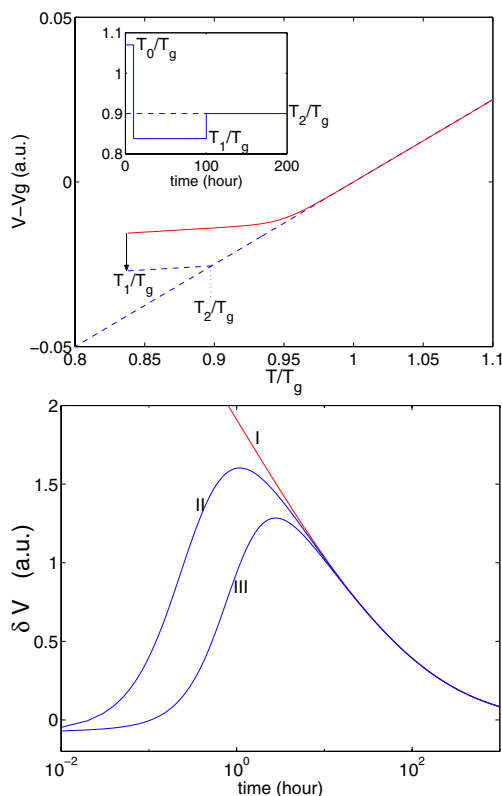


Fig. 4. Kovacs's experiment. **a)** Volume of a sample *versus* temperature during a quench from a temperature $T_0 > T_g$ to a temperature $T_1 < T_g$. The sample is aged about 100 h at T_1 and volume decreases from V_1 to V_2 . The temperature is then changed to T_2 at which V_2 is the equilibrium volume. In the insert we sketch the sample temperature as a function of time. **b)** Time evolution of $\delta V = V - V_2$ when the sample is directly quenched from T_0 to T_2 (curve I) and when the temperature is changed from T_1 to T_2 (curves II and III) for two different T_1 . The amplitude of the peak increases by increasing the difference $T_2 - T_1$.

characterized by a temporary cooling stop, has revealed that in SG and in OG the low temperature state is independent of the complete cooling history (*Rejuvenation*) but that these materials keep the memory of all the aging history (*Memory effect*) [4]. In the next section we describe in some details the application of a procedure to the aging of PMMA.

As we already mentioned, several kinds [18,26] of “memory effects” for polymers have been described in literature. The most famous one is that

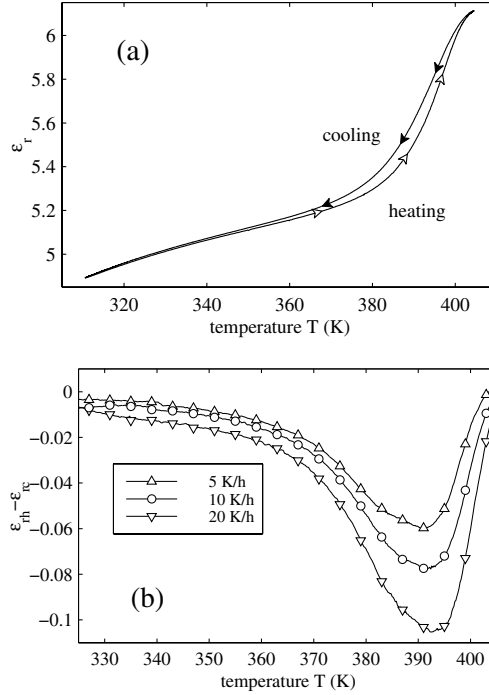


Fig. 5. a) Evolution of ϵ_r at $f = 0.1$ Hz as a function of T . Reference curve obtained with $|R| = 20$ K/h. **b) Hysteresis of the reference curve** (difference between the heating and cooling curves $\epsilon_{rh} - \epsilon_{rc}$) for 3 different $|R|$: 5 K/h (Δ), 10 K/h (\circ) and 20 K/h (∇).

of Kovacs [26]. However the thermal cycles used in these experiments are quite different from those proposed in [4]. Thus it is interesting to check how polymers behave when they are submitted to this new thermal procedure, which can give new insight on the aging of these materials. Moreover, the use of the same protocols makes the comparison between different kinds of glasses easier.

2.2.2 Memory experiment on PMMA

We describe experiments following the protocol first proposed in [4]: a temporary stop is done during the cooling of the sample, and its consequence on the dielectric constant behaviour are studied. The measurement is performed in the following way: the PMMA history is first reinitialized by heating the sample at a temperature $T_{\max} > T_g$ and leaving it at $T_{\max} = 415$ K

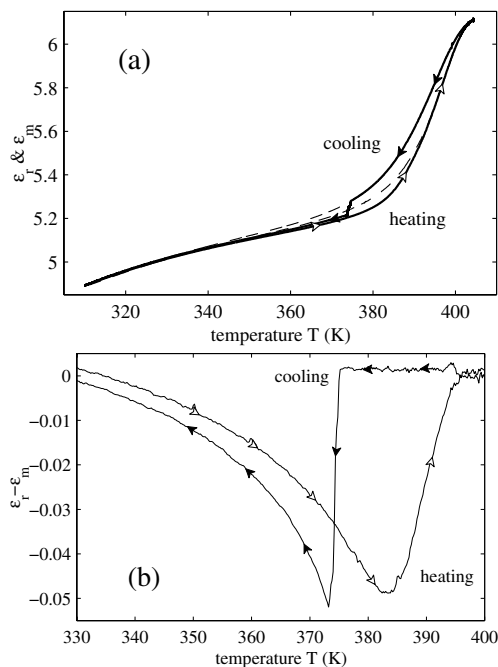


Fig. 6. Memory effect. **a)** Evolution of ϵ at $f = 0.1$ Hz as a function of T . The dashed line corresponds to the reference curve (ϵ_r) of Figure 5a. The solid bold line corresponds to a different cooling procedure: the sample is cooled, at $R = -20$ K/h, from T_{\max} to $T_{\text{stop}} = 374$ K, where cooling is stopped for 10 h. Afterwards the sample is cooled at the same R till T_{\min} and then heated again at $R = 20$ K/h till T_{\max} . **b)** Difference between the evolution of ϵ_r and ϵ_m . Downward filled arrows correspond to cooling ($\epsilon_{mc} - \epsilon_{rc}$) and upward empty arrows to heating ($\epsilon_{mh} - \epsilon_{rh}$).

for a few hours. Then it is slowly cooled from T_{\max} to a temperature $T_{\min} = 313$ K at the constant rate R and heated back to T_{\max} at the same $|R|$. The dependence of ϵ on T obtained by cooling and heating the sample at a constant $|R|$ (temperature time evolution of Fig. 1c, is called the reference curve ϵ_r).

As an example of reference curve we plot in Figure 5a ϵ_r , measured at 0.1 Hz and at $|R| = 20$ K/h. We see that ϵ_r presents a hysteresis between the cooling and the heating in the interval $350 \text{ K} < T < 405 \text{ K}$. This hysteresis depends on the cooling and heating rates. Indeed, in Figure 5b, the difference between the heating curve (ϵ_{rh}) and the cooling curve (ϵ_{rc}) is plotted as a function of T for different $|R|$. The faster we change

temperature, the bigger hysteresis we get. Furthermore the temperature of the hysteresis maximum is a few degrees above T_g , specifically at $T \approx 392$ K. The temperature of this maximum gets closer to T_g when the rate is decreased. We neglect for the moment the rate dependence of the hysteresis and we consider as reference curve the one, plotted in Figure 5a, which has been obtained at $f = 0.1$ Hz and at $|R| = 20$ K/h. The evolution of ϵ can be quite different from ϵ_r if we use the temperature cycle proposed in [4] and shown in Figure 1d. After a cooling at $R = -20$ K/h from T_{\max} to $T_{\text{stop}} = 374$ K the sample is maintained at T_{stop} for 10 h. After this time interval the sample is cooled again, at the same R , down to T_{\min} . Once the sample temperature reaches T_{\min} the sample is heated again at $R = 20$ K/h up to T_{\max} . The dependence of ϵ as a function of T , obtained when the sample is submitted to this temperature cycle with the cooling stop at T_{stop} , is called the memory curve ϵ_m . In Figure 6a, ϵ_m (solid line), measured at $f = 0.1$ Hz, is plotted as a function of T . The dashed line corresponds to the reference curve of Figure 5a. We notice that ϵ_m relaxes downwards when cooling is stopped at T_{stop} : this corresponds to the vertical line in Figure 6a where ϵ_m departs from ϵ_r . When cooling is resumed ϵ_m merges into ϵ_r for $T < 340$ K. The aging at T_{stop} has not influenced the result at low temperature. This effect has been called *rejuvenation* in recent papers [22].

During the heating period the system reminds the aging at T_{stop} (cooling stop) and for $340 \text{ K} < T < 395$ K the evolution of ϵ_m is quite different from ϵ_r . In order to clearly see this effect we divide ϵ_m in the cooling part ϵ_{mc} and the heating part ϵ_{mh} . In Figure 6b we plot the difference between ϵ_m and ϵ_r . Downward filled arrows correspond to cooling ($\epsilon_{mc} - \epsilon_r$) and empty upward arrows to heating ($\epsilon_{mh} - \epsilon_r$). The difference between the evolutions corresponding to different cooling procedures is now quite clear. The system reminds its previous aging history when it is reheated from T_{\min} . The amplitude of the memory corresponds well to the amplitude of the aging at T_{stop} but the temperature of the maximum is shifted a few degrees above T_{stop} . In Figure 7 we show that this temperature shift is independent of T_{stop} for temperatures where aging can be measured in a reasonable time (above 335 K). In contrast the amplitude of the downward relaxation at T_{stop} is a decreasing function of T_{stop} , as expected from the first section measurements: no aging can be measured at $T_{\text{stop}} < 335$ K (see Fig. 3a).

This memory effect seems to be permanent because it does not depend on the waiting time at T_{\min} . Indeed we performed several experiments in which we waited till 24 h at T_{\min} , before restarting heating, without noticing any change in the heating cycle. In contrast the amplitude and the position of the memory effect depend on R and on the measuring frequency. As expected from the measurements of Section 2.1, the higher is the frequency,

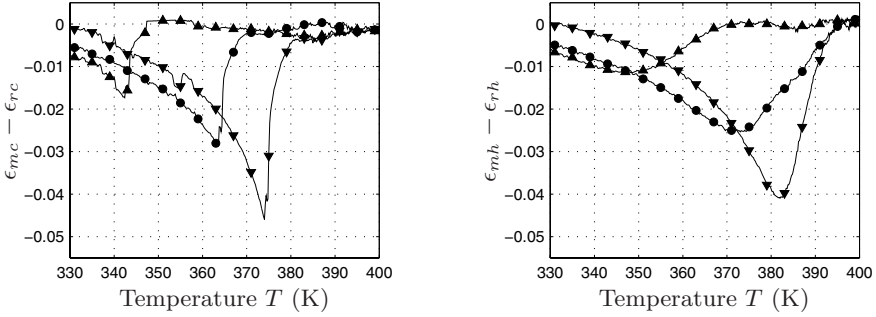


Fig. 7. Dependence on T_{stop} . Difference between ϵ_r and ϵ_m for 3 different cooling stops measured at $f = 0.1$ Hz for $|R| = 10$ K/h and $t_{\text{stop}} = 10$ h. **a)** Writing memory (cooling): $\epsilon_{mc} - \epsilon_{rc}$ with $T_{\text{stop}} = 344$ K (\blacktriangle), 364 K (\bullet) and 374 K (\blacktriangledown). **b)** Reading memory (heating): $\epsilon_{mh} - \epsilon_{rh}$ (same symbols as in **a**)).

the smaller is the downward relaxation, so the smaller is the memory effect. Furthermore the faster is the rate $|R|$, the larger is the downward relaxation of the dielectric constant during the cooling stop. As the amplitude of the memory effect is equal to that of the relaxation, we just expect the memory effect to increase with $|R|$. But as we can see in Figure 8, the temperature positions of the maxima are rate dependent too: the larger is $|R|$, the farther the temperature of the maximum is shifted above the aging temperature T_{stop} . The cooling rate is not the only control parameter of the memory effect, the heating rate is relevant too.

2.2.3 Advanced memory experiments

In this section we apply to the PMMA sample more complicated temperature histories (inspired from spins glasses experiments [4,21]): what happens if we try to read a memory twice? If we make two cooling stops?

2.2.4 Deleting memory

In this experiment, we show that a memory can be read only one single time: reading a memory effect also deletes it. This experiment is inspired from similar ones done in spin glasses [21]. First we follow the classic procedure described in the previous section: during the cooling ramp at $R = -20$ K/h, a temporary stop is done for $t_{\text{stop}} = 20$ h at $T_{\text{stop}} = 345$ K, and then heating the sample from T_{min} with the same $|R|$. In Figure 9a we plot the difference between the heating branches of ϵ_m and ϵ_r measured at $f = 0.1$ Hz. The departure from the reference curve above T_{stop} when lowering temperature is due to a smooth cutting of cooling, but this imperfection has no detectable

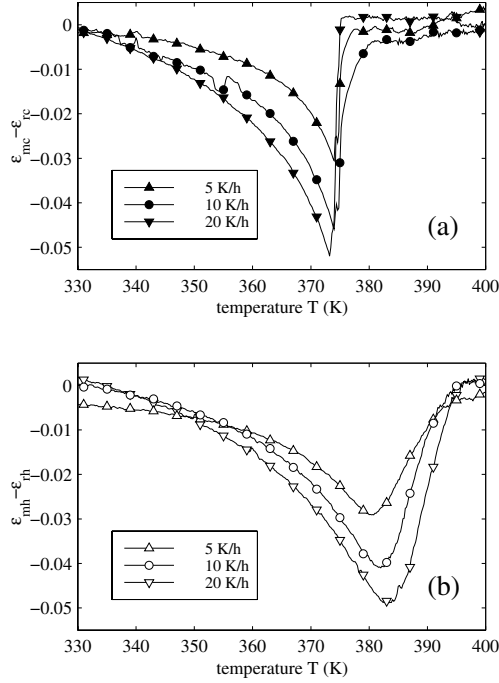


Fig. 8. Dependence on the cooling and heating rate. Difference between ϵ_r and ϵ_m (aging at $T_{\text{stop}} = 374$ K for 10 h) measured at $f = 0.1$ Hz for 3 $|R|$. **a)** Writing memory (cooling): $\epsilon_{mc} - \epsilon_{rc}$ at 5 K/h (\blacktriangle), 10 K/h (\bullet) and 20 K/h (\blacktriangledown). **b)** Reading memory (heating): $\epsilon_{mh} - \epsilon_{rh}$ at 5 K/h (\triangle), 10 K/h (\circ) and 20 K/h (\triangledown).

effect on the heating curve. We can follow the memory of the cooling stop at T_{stop} , and when the memory curve almost merges the reference one, for $T_i = 368$ K, we quickly stop heating and resume cooling at $R = -20$ K/h. Notice that this inversion temperature T_i is smaller than T_g , which means that the sample has not been reinitialized. When T_{min} is reached again, we make a classic heating at $R = +20$ K/h (see the temperature history of the sample in the inset of Fig. 9a).

This second heating curve is really different from the first one: there are no tracks of the cooling stop at $T_{\text{stop}} = 345$ K, but something like the memory of a stop around 370 K. What we see now is in fact only the memory of the stop at T_i : as the sample stays a few minutes around T_i (the time needed to inverse R to $-R$), it ages a little at T_i and we find a memory of this event. This can be checked in Figure 9b, where we only show the memory of the inversion at the same temperature T_i , without the

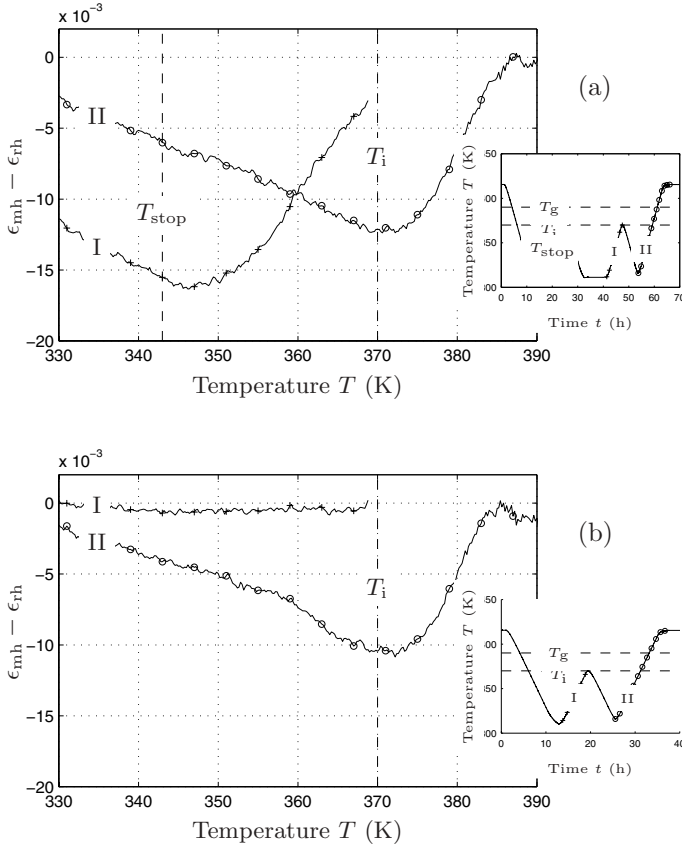


Fig. 9. Deleting a memory by reading it. a) Difference between heating curves ϵ_{rh} and ϵ_{mh} after the temperature history shown in the inset: after a classic reading the memory of a 20 h stop at $T_{stop} = 345$ K with $|R| = 20$ K/h and $f = 0.1$ Hz (+), the sample is cooled again when the temperature reaches $T_i < T_g$. The second reading (o) is very different since no tracks of T_{stop} is found but a sort of memory of the inversion temperature T_i . This can be checked on b), where we only test the memory of the inversion. The difference between the second heating curves (o) $\epsilon_{mh} - \epsilon_{rh}$ is exactly the same for both temperature histories. Heating the sample up to T_i reinitializes the lower temperature behaviour, even though $T_i < T_g$.

first memory. The curves corresponding to the second heating are exactly the same for the two experiments, showing that the first heating deletes all information about temperatures lower than T_i , even though $T_i < T_g$.

2.2.5 Double memory

More insight on the properties of the memory effects can be obtained by submitting the sample to a more complex cooling procedure consisting of two cooling stops. This procedure, which has been called the double memory effect, has been carried out successfully in spin glasses [4] where it has been observed that if two stops are done during cooling, the heating curve will present a memory effect for both stops. The difficulty that arise when trying to reproduce this experiment in PMMA is the narrowness of the aging range: when cooling the sample under T_{stop} , ϵ_m rejoins the reference curve only for temperatures where aging almost vanishes. It is therefore difficult to record two well distinct cooling stops. This is illustrated in Figure 10, where $T_{\text{stop1}} = 375$ K and $T_{\text{stop2}} = 345$ K: ϵ_m has not completely merged into ϵ_r when we stop cooling for the second time.

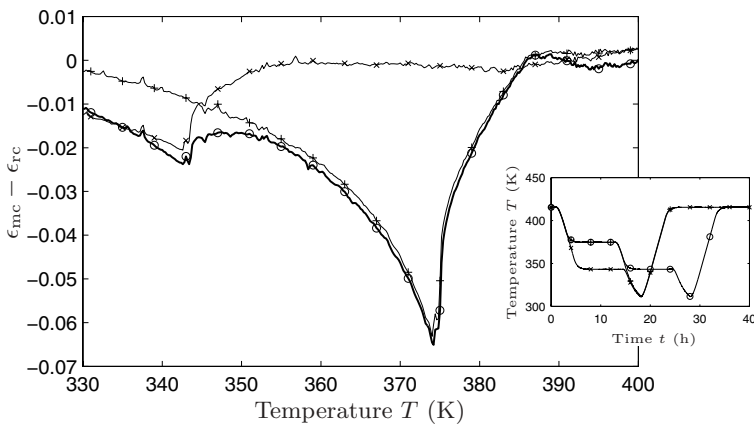


Fig. 10. Double memory recording. Difference between cooling curves ϵ_{mc} and ϵ_{rc} during the temperature history shown in the inset, for $|R| = 20$ K/h, and $f = 0.1$ Hz: one 10 h stop at $T_{\text{stop1}} = 375$ K (+), one 10 h stop at $T_{\text{stop2}} = 345$ K (x), and two 10 h stops at $T_{\text{stop1}} = 375$ K and $T_{\text{stop2}} = 345$ K (o). The low temperature state is independent of high temperature history: aging during 10 h at T_{stop2} produces the same relaxation, whatever happened before at higher temperatures.

The double memory experiments allow us to point out another important property of PMMA aging: when temperature is lowered after the first stop, the system not only recover the same value of ϵ , but also the same aging properties. Indeed, a 10 h stop at 345 K produces the same downward relaxation of ϵ , whatever the previous history is. The low temperature state is thus completely uninfluenced by the high temperature history.

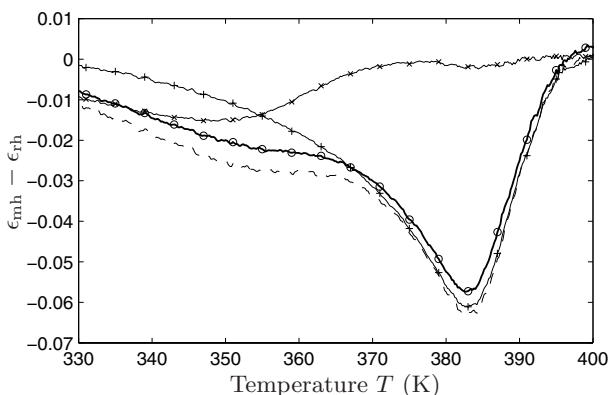


Fig. 11. Double memory reading. Difference between heating curves ϵ_{mh} and ϵ_{rh} corresponding to the cooling curves of Figure 10: reading of a single stop at $T_{stop1} = 375$ K (+) and $T_{stop2} = 345$ K (x), reading of a double stop at T_{stop1} and T_{stop2} (o). The dashed line is the sum of the two single stop curves, it is a very good approximation of the double memory reading. Memory effects thus appear only additive in this case, where T_{stop1} and T_{stop2} are sufficiently far from each other.

If we now heat the sample after the two cooling stops, we obtain the bolt curve of Figure 11. If the memory of T_{stop1} is obvious, the lower temperature stop at T_{stop2} must be hidden in the first part of the curve. In order to check the presence of the memory effect of the second stop, let us suppose that this effect is just additive, that is the memory of a double stop is just the sum of the memory of both individual stops if their temperature is sufficiently different. So we plot with a dashed line in Figure 11 the sum of the single memories of T_{stop1} and T_{stop2} . Within errors bars, the two curves are the same, so we conclude that even if the memory effects overlap in the narrow aging range of PMMA, double memory experiments also work in this polymer.

2.2.6 Direct comparison with the memory effects in spin-glasses

In the previous section we have described the behaviour of a PMMA sample submitted to the same temperature cycle used to study memory and rejuvenation effects in various kinds of spin glasses and in orientational glasses. Our dielectric measurements clearly show the presence of rejuvenation and memory in PMMA. However these effects are less strong in PMMA than in spin-glasses. In order to stress this difference we consider the results of an experiment performed by Dupuis, on a spin glass $\text{CdCr}_{1.7}\text{In}_{0.3}\text{S}_4$ with

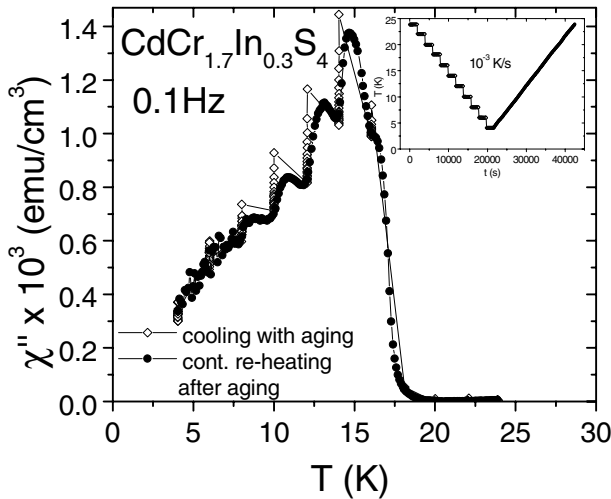


Fig. 12. Memory and rejuvenation in a spin glass. Multiple memories on the magnetic susceptibility, measured at 0.1 Hz, of a spin glass. The sample has been cooled by successive stops (see insert for the temperature history) and heated at constant rate. At each cooling stop the sample ages (downward relaxation). During heating the sample remembers all the cooling stops [23] (see text for details).

$T_g \simeq 17$ K [23,24]. One of the main results of this experiment is shown in Figure 12, which has been kindly given to us by Vincent. The temperature cycle applied to the sample is sketched in the insert. The sample is heated at 25 K and then cooled by steps of 2 K till 3 K. It is then heated again at a constant rate till 25 K. Between two successive cooling steps the temperature is kept constant for 2000 s. During this temperature cycle the magnetic susceptibility is measured at a frequency of 0.1 Hz. The imaginary part χ'' of the magnetic susceptibility is plotted in Figure 12 as a function of temperature. The open symbols correspond to cooling and the filled symbols to heating. The isothermal aging is observed on the downward relaxation at each temperature plateau. At the same time we see that a cooling step produces an upward jump of χ'' and a restart of aging: this is the rejuvenation effect. When the sample is heated again, χ'' presents minima exactly at the temperatures where the sample was aged during the cooling: this is the memory effect.

Comparing Figure 12 with the results on PMMA, described in the previous section, we immediately notice that there are analogies but very important differences. We clearly see that the SG has no hysteresis and the

memory effect occurs at the same temperature of the cooling stops. Most importantly multiple stops are quite well remembered by the SG, whereas are weakly seen in PMMA.

2.3 Discussion on the memory effect

As we already mentioned in Section 2.2.1 the observation of a memory of the thermal history in polymers is not new and various thermal protocols have been used to show this effect. The thermal protocol described in Section 2.2 of this lecture is the same used to study aging phenomena in SG and OG. Thus the application to a polymer glass of the same procedure used in OG and SG allows us to address the question of the universality of the memory and rejuvenation phenomena in different materials. This is a very important point in order to understand whether the same theoretical approach can be used to describe aging phenomena in different materials.

Let us summarize the main results of these low frequency dielectric measurements on PMMA:

- a) the reference curve ϵ_r , obtained at constant cooling and heating rate $|R|$ is hysteretic. This hysteresis is maximum a few degrees above T_g ;
- b) the hysteresis of ϵ_r increases with $|R|$;
- c) writing memory: a cooling stop produces a downward relaxation of ϵ_m . The amplitude of this downward relaxation depends on T_{stop} and it decreases for decreasing T_{stop} . It almost disappears for $T_{\text{stop}} < 335$ K.
- d) when cooling is resumed ϵ goes back to the cooling branch of the reference curve. This suggests that the low temperature state is independent on the cooling history;
- e) reading memory: upon reheating ϵ_m reminds the aging history and the cooling stop (*Memory*). The maximum of the memory effect is obtained a few degrees above T_{stop} ;
- f) the memory effect does not depend on the waiting time at low temperature but it depends both on the cooling and heating rates. The memory effect increases with $|R|$;
- g) double memory effects are observed with more difficulty in PMMA than in SG. The difference comes from the fact that aging effects are reduced when temperature is lowered. However a careful analysis of experimental data allows us to show the existence of double memory effects in PMMA;

- h) the memory effect is deleted by a reading, even if the temperature remains smaller than T_g .

It is interesting to discuss the analogies and the differences between this experiment and similar ones performed on SG [4,16,22,23] and on OG [17]. It turns out that, neglecting the hysteresis of the reference curve of PMMA and of OG, the behaviour of these materials is quite similar to that of SG. A strong rate dependence has been observed in Ising spin-glasses too [22]. During the heating period PMMA, SG and OG remember their aging history, although the precise way, in which history is remembered, is material dependent. Furthermore in these materials the low temperature state is independent on the cooling history. One can estimate the temperature range δT where the material response is different from that of the reference curve because of the cooling stop. It turns out that the ratio $\delta T/T_G$ is roughly the same in PMMA, in SG and in OG, specifically $\delta T/T_G \simeq 0.2$. The important difference between SG and PMMA is in the dependence on T_{stop} of the amplitude of the downward relaxation: it is strong in PMMA and weak in SG (compare Fig. 12 with Figs. 10, 11).

Our results seem to indicate that memory and rejuvenation phenomena in the aging process may be described by models based on a hierarchical free energy landscape, whose barriers grow when temperature is lowered [4,13]. However the dependence of the memory effect on $|R|$ and the independence on the waiting time at T_{min} mean that, at least for PMMA, the free energy landscape has to depend not only on temperature but also on $|R|$. Many models [6, 7, 9, 13, 27] and numerical simulations [38, 40] do not take into account this dependence because they consider just a static temperature after a quench. In contrast point f) indicates that the cooling history is relevant too.

These difficulties can be avoided if one considers models based on a slow domain growth and domain walls reconformations in the pinning field created by disorder (see for example [25] and references therein). These models imply the existence of a hierarchy of length scales l with a characteristic time $\tau \propto l^z$. Recent numerical simulations [28] show that this is an important ingredient in order to have memory/rejuvenation effects. However one of the drawbacks of such a model is that memory is recovered only if the time spent at low temperature is short enough [25]. This effect does not seem to be true for PMMA and other materials at least on reasonable laboratory time scales.

As a conclusion the “memory” and rejuvenation effects seem to be two universal features of aging whereas the hysteresis is present in PMMA and in OG but not in all kinds of spin glasses. It would be interesting to know whether these effects are observed in other polymers and in supercooled liquids. These measurements show that many features of aging seem to be

“universal” in several materials and that models based on spin glasses may be useful to describe aging in polymeric materials.

3 Effective temperature of an aging material

The experimental procedures described in the previous section have been extremely useful to fix several constraints for the phenomenological models [6, 7], but these procedures are mainly based on the study of the response of the system to an external perturbation. Therefore they are unable to give informations on the system dynamics. Therefore, from an experimental point of view, it is extremely important to study not only the response of the system but also its thermal fluctuations. The analysis of thermal fluctuations is related also to another important aspect of aging dynamics, that is the definition of the temperature. Recent theories [11, 30] based on the description of spin glasses by a mean field approach proposed to extend the concept of temperature using a Fluctuation Dissipation Relation (FDR) which generalizes the Fluctuation Dissipation Theorem (FDT) for a weakly out of equilibrium system (for a review see [9–11]).

In order to understand this generalization, we recall the main consequences of FDT in a system which is in thermodynamic equilibrium. We consider an observable V of such a system and its conjugate variables q . The response function $\chi_{Vq}(\omega)$, at frequency $f = \omega/2\pi$, describes the variation $\delta V(\omega)$ of V induced by a perturbation $\delta q(\omega)$ of q , that is $\chi_{Vq}(\omega) = \delta V(\omega)/\delta q(\omega)$. FDT relates the fluctuation spectral density of V to the response function χ_{Vq} and the temperature T of the system:

$$S(\omega) = \frac{2k_B T}{\pi\omega} \text{Im} [\chi_{Vq}(\omega)] \quad (3.1)$$

where $S(\omega) = \langle |V(\omega)|^2 \rangle$ is the fluctuation spectral density of V , k_B is the Boltzmann constant, $\text{Im} [\chi_{Vq}(\omega)]$ is the imaginary part of $\chi_{Vq}(\omega)$. Textbook examples of FDR are Nyquist’s formula relating the voltage noise to the electrical resistance and the Einstein’s relation for Brownian motion relating the particle diffusion coefficient to the fluid viscosity [31].

When the system is not in equilibrium FDT, that is equation (3.1), may fail. For example violations, of about a factor of 2, of equation (3.1) have been observed in the density fluctuations of polymers in the glassy phase [32]. The first to propose that the study of the FDT violations are relevant for glassy systems was Sompolinsky [33]. This idea, which was generalized in the context of weak turbulence [34], has been reconsidered by Cugliandolo & Kurchan [11, 30] and successively tested in many analytical and numerical models of glass dynamics [10, 35–41] and in a few experiments.

Let us briefly recall the main and general findings of these models, which are very well described in this proceedings in the Cugliandolo lecture [11].

Because of the slow dependence on t_w of the response functions, it has been proposed to use an FDR which generalizes equation (3.1) and which can be used to define an effective temperature $T_{\text{eff}}(\omega, t_w)$ of the system [10, 11]:

$$T_{\text{eff}}(\omega, t_w) = \frac{S(\omega, t_w) \pi \omega}{\text{Im} [\chi_{Vq}(\omega, t_w)] 2k_B}. \quad (3.2)$$

In the time domain the effective temperature is usually defined by means of correlation functions $C(t, t_w)$ (Fourier transform of $S(\omega, t_w)$) and integrated response $R(t, t_w)$ (Fourier transform of $\chi_{Vq}(\omega, t_w)$) [11]:

$$T_{\text{eff}}(t, t_w) = \frac{-C(t, t_w) + C(t_w, t_w)}{k_B R(t, t_w)}. \quad (3.3)$$

It is clear that if equation (3.1) is satisfied $T_{\text{eff}} = T$, otherwise T_{eff} turns out to be a decreasing function of t_w and ω . The physical meaning of equation (3.2) is that there is a time scale (for example t_w), which allows one to separate the fast processes from the slow ones. In other words the low frequency modes, such that $\omega t_w < 1$, relax towards the equilibrium value much slower than the high frequency ones which rapidly relax to the temperature of the thermal bath. Therefore it is conceivable that the slow frequency modes keep memory of higher temperatures for a long time and for this reason their temperature should be higher than that of the high frequency ones. This striking behavior has been observed in several models of aging [10, 35–41]. Further analytical and numerical studies of simple models show that equation (3.2) is a good definition of temperature in the thermodynamic sense [10, 11]. In spite of the large amount of theoretical studies there are only a few experiments where FDR is studied in aging materials. The experimental analysis of the dependence of $T_{\text{eff}}(\omega, t_w)$ on ω and t_w is very useful to distinguish among different models of aging because the FDT violations are model dependent [10, 35–41]. Furthermore the direct analysis of the noise signal allows one to understand if the dynamics is either intermittent or continuous in time. this is another important characteristic of the aging models. Let us consider for example the trap model [6] which is based on a phase space description. Its basic ingredient is an activation process and aging is associated to the fact that deeper and deeper valleys are reached as the system evolves [8]. The dynamics in this model has to be intermittent because either nothing moves or there is a jump between two traps. This contrasts, for example, with mean field dynamics which is continuous in time [30]. This is not the only difference because in the trap model T_{eff} depends on the observable whereas it is observable independent in mean field model [8, 42].

FDT violations in aging materials have been measured just in a few experiments [44–49]. In the next sections we will first describe the X-ray

experiment where the violation of FDT have been first observed and we will describe the reasons why these measurements are not sufficient to test FDR. We then briefly analyze another experiment [44] where FDR has been studied in some details. This is a single frequency experiment and thus T_{eff} is not completely characterized. For this reason we summarize the main results of two experiments where the FDT violation has been studied in the dielectric measurements of a gel [45, 46], during the sol-gel transition, and of a polymer, after a quench. In both cases the effective temperature defined using equation (3.2) is huge and the persistent time of the violation is extremely long. We have therefore analyzed directly the time evolution of the noise signal in both experiments and we find a strongly intermittent behaviour in both materials. In this lecture we will describe the main results of this analysis and we want also to point out the common features observed in the slow relaxation dynamics of these two materials.

In the case of the gel we want to address another important question. Specifically we have analyzed whether T_{eff} does depend on the couple of conjugated variables used in the measure of FDR. This is actually another important information because this dependence of T_{eff} on the observables is not the same in all the models [11, 42].

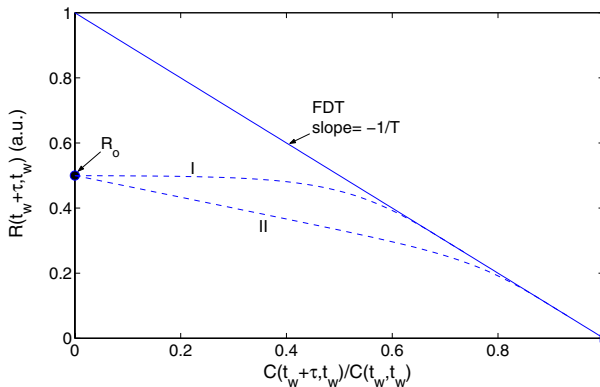


Fig. 13. X-ray experiment. Schematic drawing of the response *versus* correlation. The response is in this case the isothermal compressibility and the correlation is given by the density fluctuations. The continuous straight line of slope $1/T$ is the prediction of FDT in this plot. See text for more details.

3.1 The X-ray scattering experiment

The violation of the FDT in aging polymers was already pointed out by Wendorff & Fisher [32]. Indeed in a X-ray scattering experiment, the

intensity $I(0)$ of scattered X-rays at small angles is related to the density fluctuations $\delta\rho$:

$$\frac{\langle\delta\rho^2\rangle}{\rho^2} \propto I(o). \quad (3.4)$$

From FDT one finds:

$$\langle\delta\rho^2\rangle = \frac{K_B T \rho^2 \chi_T}{V} \quad (3.5)$$

where χ_T is the isothermal compressibility of the polymer under study. They separately measured χ_T by standard techniques and $\langle\delta\rho^2\rangle$ by X-ray scattering. Weandorf and Fisher found that equation (3.5) was satisfied by standard liquids, whereas a violation between 2.5 and 5 of equation (3.5) was observed for various polymers. Although this measurement is a strong indication that FDT is violated in an aging polymer, it is not very useful to know the behaviour of $T_{\text{eff}}(t, t_w)$ and to compare it with theoretical models. Indeed to compare with theory one has to consider the equation [11]:

$$-C(t_w + \tau, t_w) + C(t_w, t_w) = K_B T_{\text{eff}}(t, t_w) R(t_w + \tau, t_w). \quad (3.6)$$

In order to construct $T_{\text{eff}}(t, t_w)$ one has to measure, as a function of t_w and τ , both the correlation $-C(t_w + \tau, t_w)$ of the density fluctuations and the integrated response $R(t_w + \tau, t_w)$, that is the isothermal compressibility. Equation (3.5) is just the limit for $\tau \rightarrow \infty$ of equation (3.6), that is $\lim_{\tau \rightarrow \infty} C(t_w + \tau, t_w) = 0$ and $\lim_{\tau \rightarrow \infty} R(t_w + \tau, t_w) = R_o$. Thus only two points are available on the plane $(C(t_w + \tau, t_w), R(t_w + \tau, t_w))$, specifically the point $(C(t_w, t_w), 0)$, obtained from the measure of $\langle\delta\rho^2\rangle = C(t_w, t_w)$, and the point $(0, R_o)$ where R_o is the response (isothermal compressibility) measured at large τ and t_w . As it is shown in Figure 13 these two points are not enough to determine $T_{\text{eff}}(t, t_w)$. In this figure the solid line has slope $1/T$ and corresponds to the FDT. In the figure R_o is certainly smaller than the value predicted by FDT and thus there is a violation. However the curves I and II indicates that several possibilities exist to make the connections between the measured R_o and $C(t_w, t_w)$ measured by the X-ray scattering. For example curves I and II correspond to an infinite T_{eff} and to $T_{\text{eff}} \simeq 3 T$ respectively.

The main conclusion of this discussion is that the experiment of Wendorf & Fisher [32] is certainly useful to point out that a violation of FDT exists in polymers, but this is not enough to determine T_{eff} and more experiment are needed in order to understand FDR in more details. In the next sections we will describe several experiments whose aim is just that of studying FDR in several materials and with different techniques.

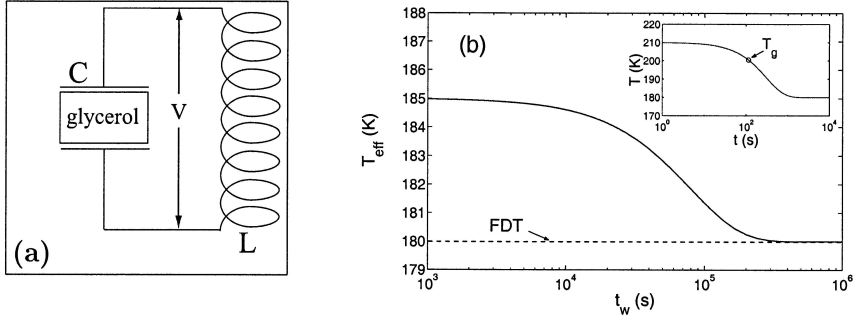


Fig. 14. Experiment on supercooled fluids. a) Electrical circuit used to measure the FDT violation in Glycerol b) T_{eff} , measured at 7 Hz, *versus* time, after a quench from 220 K to 180 K. The sample thermal history is sketched in the inset. See text for more details.

3.2 Supercooled liquid experiment

This experiment has been performed by Grigera & Israeloff [44] by realizing an experiment first proposed in [10]. The idea is in some way that of measuring the temperature an electric harmonic oscillator, composed by a perfect inductance L and a capacitor C whose dielectric is just an aging material. As the dielectric constant is complex then $C = C' + iC''$. In the experiment of [44] the dielectric is just Glycerol which is a liquid with $T_g = 196$ K. The schematic diagram of the circuit is drawn in Figure 14. The electrical impedance of this circuit is:

$$Z(\omega) = \frac{i \omega L}{1 - \omega^2 C' L + i \omega^2 C'' L}. \quad (3.7)$$

The FDR for an electrical impedance $Z(\omega)$ is given by a generalization of the Nyquist formula:

$$S_V(\omega, t_w) = \frac{2k_B T_{\text{eff}}(\omega, t_w)}{\pi} \text{Re}[Z(\omega, t_w)] \quad (3.8)$$

where $S_V(\omega, t_w)$ is the spectrum of the voltage thermal fluctuations measured on the impedance. For the circuit of Figure 14a, equation (3.8) becomes:

$$S_V(\omega, t_w) = \frac{2k_B T_{\text{eff}}(\omega, t_w) \omega^3 L^2 C''}{\pi [(1 - \omega^2 L C')^2 + \omega^4 L^2 C''^2]}. \quad (3.9)$$

The idea of this experimental configuration is very smart because from the single measure of $S_V(\omega, t_w)$ one can extract simultaneously the value of T_{eff}

and C . Indeed, if L is known, the resonance frequency is $\omega_0 = 1/\sqrt{LC'}$, the resonance width is proportional to C'' and the amplitude at resonance is proportional to T_{eff} . Except for several experimental details this is the technique used to study FDR in glycerol [44]. In the experiment of [44] the resonance frequency is 7 Hz. The glycerol sample is heated at 210 K and quenched at 180 K in about 10^3 s (see inset of Fig. 14b). The zero of t_w is taken when the temperature is equal to T_g . The main result of the experiment of [44] is that $T_{\text{eff}}(\omega_0, t_w)$ evolves as sketched in Figure 14b. In spite of the fact that, at $t_w = 1000$ s the sample temperature is already at the thermal bath temperature, we see that FDT is violated and the violation lasts for a time which is much larger than $1/\omega_0$. It finally relaxes to 180 K after 10^5 s.

The drawback of this interesting experiment is that one has access only to $T_{\text{eff}}(\omega_0, t_w)$, that is to the value of the effective temperature at resonance. Therefore there is no idea on how the effective temperature evolves as a function of ω at different t_w . The experiments described in the next sections analyze this problem.

3.3 Gel electric properties

FDR, equation (3.1), is studied during the colloidal glass formation in Laponite RD [50], a synthetic clay consisting of discoid charged particles. It disperses rapidly in water and solidifies even for very low mass fraction. Physical properties of this preparation evolves for a long time, even after the sol-gel transition, and have shown many similarities with standard glass aging [3, 51]. Recent experiments [51] have proved that the structure function of Laponite at low concentration (less than 3% mass fraction) is close to that of a glass. As in our experiment the Laponite concentration is low, we call the solid like Laponite solution either a colloidal glass or simply a glass.

3.3.1 The experimental apparatus

The Laponite [50] solution is used as a conductive liquid between the two golden coated electrodes of a cell (see Fig. 1). It is prepared in a clean N_2 atmosphere to avoid CO_2 and O_2 contamination, which perturbs the electrical measurements. Laponite particles are dissolved at a concentration of 2.5% mass fraction in pure water under vigorous stirring during 300 s. To avoid the existence of any initial structure in the sol, we pass the solution through a $1\text{ }\mu\text{m}$ filter when filling our cell. This instant defines the origin of the aging time t_w (the filling of the cell takes roughly two minutes, which can be considered the maximum inaccuracy of t_w). The sample is then sealed so that no pollution or evaporation of the solvent can occur. At

this concentration, the light scattering experiments show that Laponite [50] structure functions are still evolving 500 h after the preparation [3]. We only study the beginning of this glass formation process.

The two electrodes of the cell are connected to our measurement system, where we alternately record the cell electrical impedance $Z(t_w, \omega)$ and the voltage noise density $S_Z(t_w, \omega)$ (see Fig. 15). Taking into account that in this configuration $\text{Im}[\chi_{Vq}(t_w, \omega)] = \omega \text{Re}[Z(t_w, \omega)]$, one obtains from equation (3.2) that the effective temperature of the Laponite solution as a function of the aging time and frequency is:

$$T_{\text{eff}}(t_w, \omega) = \frac{\pi S_Z(t_w, \omega)}{2k_B} \text{Re}[Z(t_w, \omega)] \quad (3.10)$$

which, as already mentioned in Section 3.2 (Eq. (3.8)) is an extension of the Nyquist formula.

The electrical impedance of the sample is the sum of 2 effects: the bulk is purely conductive, the ions of the solution follow the forcing field, whereas the interfaces between the solution and the electrodes give mainly a capacitive effect due to the presence of the Debye layer [52]. This behavior has been validated using a four-electrode potentiostatic technique [53] to make sure that the capacitive effect is only due to the surface. In order to test only bulk properties, the geometry of the cell is tuned to push the surface contribution to low frequencies. Specifically the cell is composed by two large reservoirs in contact with the electrodes which have an area of 25 cm². The reservoirs are connected by a rigid tube (see Fig. 15) whose section and length give the main contribution to the bulk electrical resistance. Thus by changing the sizes of the tube the bulk resistance can be changed from 300 Ω to 100 K Ω . We checked that the dynamics of the system does not depend on the value of the bulk resistance. For a bulk resistance of about 10⁵ Ω the cutoff frequency of the equivalent R-C circuit (composed by the series of the Debye layers plus the bulk resistance) is about 0.02 Hz. In other words above this frequency the imaginary part of the cell impedance is about zero.

3.3.2 FDR measurements

In Figure 16a, we plot the real part of the impedance as a function of the frequency f , for a typical experiment and two different times. The time evolution of the resistance of one of our sample is plotted in Figure 16b: it is still decaying in a non trivial way after 24 h, showing that the sample has not reached any equilibrium yet. This aging is consistent with that observed in light scattering experiments [3].

As the dissipative part of the impedance $\text{Re}(Z)$ is weakly time and frequency dependent, one would expect from the Nyquist formula that so does

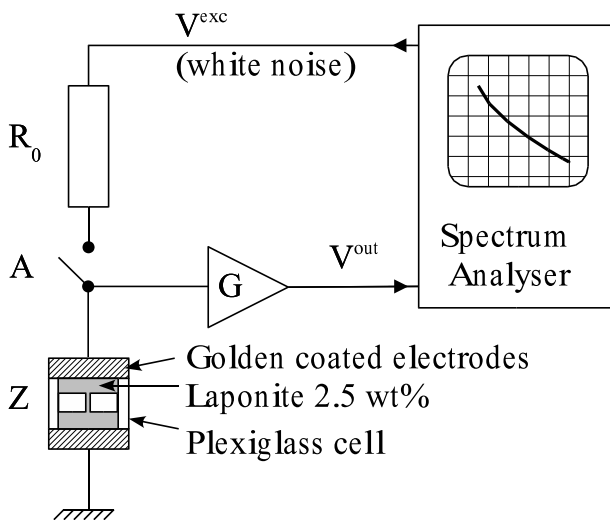


Fig. 15. Laponite experimental set-up. The impedance under test Z is a cell filled with a 2.5wt% Laponite sol. The electrodes of the cell are golden coated to avoid oxidation. One of the two electrodes is grounded whereas the other is connected to the entrance of a low noise voltage amplifier characterized by a voltage amplification G . With a spectrum analyzer, we alternately record the frequency response $FR(\omega) = \langle V^{\text{out}}/V^{\text{exc}} \rangle$ (switch A closed) and the spectrum $S(\omega) = \langle |V^{\text{out}}|^2 \rangle$ (switch A opened). The input voltage V^{exc} is a white noise excitation, thus from $FR(\omega)$ we derive the impedance $Z(\omega)$ as a function of ω , that is $Z(\omega) = R_0/(G/FR(\omega) - 1)$; whereas from $S(\omega)$, we can estimate the voltage noise of Z , specifically $S_Z(\omega) = [S(\omega) - S_a(\omega)]/G^2$ where $S_a(\omega)$ is the noise spectral density of the amplifier.

the voltage noise density S_Z . But as shown in Figure 17, FDT must be strongly violated for the lowest frequencies and earliest times of our experiment: S_Z changes by several orders of magnitude between highest values and the high frequency tail¹. This violation is clearly illustrated by the behavior of the effective temperature in Figure 18². For long times and

¹This low frequency noise cannot be confused with the standard $1/f$ noise observed in many electronic devices. We recall that the $1/f$ appears only when an external current produced by an external potential goes through the device. In our cell no external potential is applied.

²The usual representation of the effective temperature in simulations is the slope of the response *versus* correlation plot, but it is not suited for our experimental data: the system being almost only dissipative, the response function is close to a delta distribution, thus FDT is only one point in this representation.

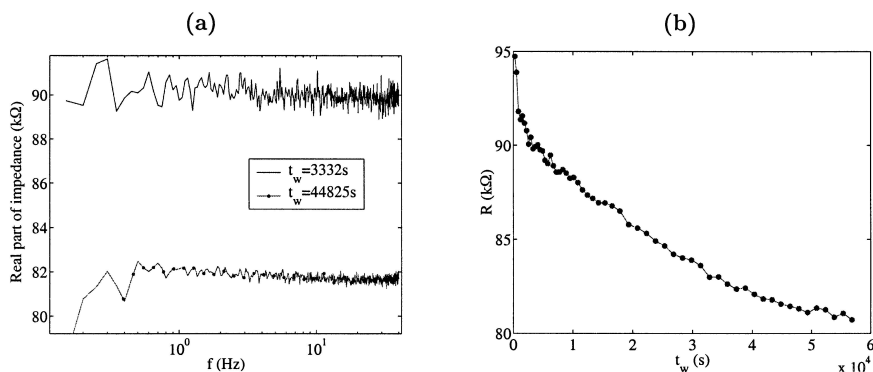


Fig. 16. Laponite response function. a) Frequency dependence of a sample impedance for 2 different aging times: continuous line $t_w = 3332$ s; (●) $t_w = 44825$ s. b) Time evolution of the resistance. This long time evolution is the signature of the aging of the sol. In spite of the decreasing mobility of Laponite particles in solution during the gelation, the electrical conductivity increases.

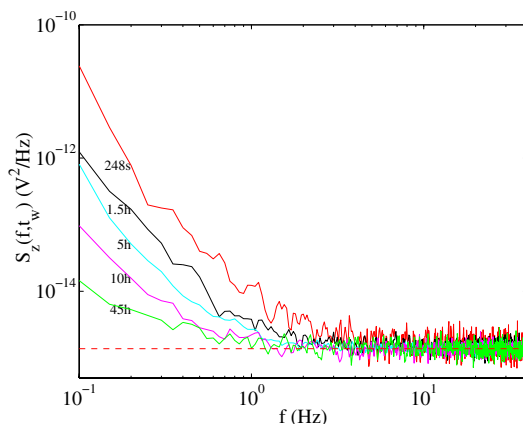


Fig. 17. Voltage fluctuations for Laponite. Voltage noise density of one sample for different aging times. The horizontal dashed line is the FDT prediction.

high frequencies, the FDT holds and the measured temperature is the room one (300 K); whereas for early times T_{eff} climbs up to 3×10^3 K at 1 Hz. Moreover, T_{eff} could be even larger for lower frequencies and lower aging times: indeed, we found in all the tested samples no evidence of a saturation of this effective temperature in our measurement range. In order to be sure that the observed violation is not due to an artifact of the experimental

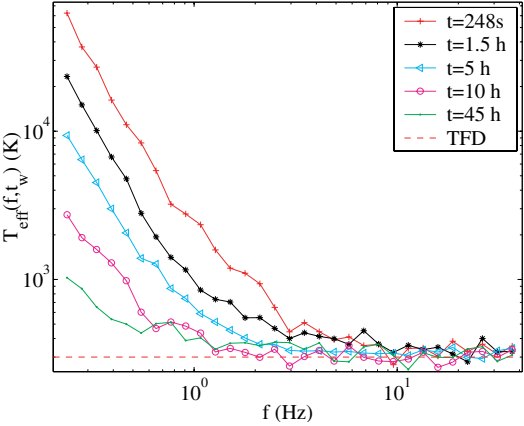


Fig. 18. Effective temperature of Laponite. Effective temperature as a function of frequency for different aging times. As S_Z in Figure 17, T_{eff} strongly increases and reaches huge values for low frequencies and short aging times.

procedure, we filled the cell with an electrolyte solution with pH close to that of the Laponite sol such that the electrical impedance of the cell was the same. Specifically we filled the cell with NaOH solution in water at a concentration of $10^{-3} \text{ mol.l}^{-1}$. The results of the measurements of T_{eff} are shown in Figure 19 at two different times after the sample preparation. In this case we did not observe any violation of FDT at any time.

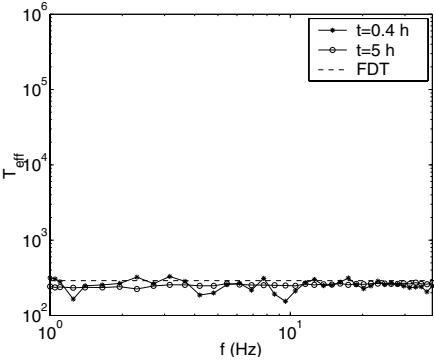


Fig. 19. Effective temperature of an NaOH solution in water. The effective temperature is plotted as a function of frequency for two different times after the preparation. This solution has a pH close to that of the Laponite, and no violation is observed in this case for any aging time.

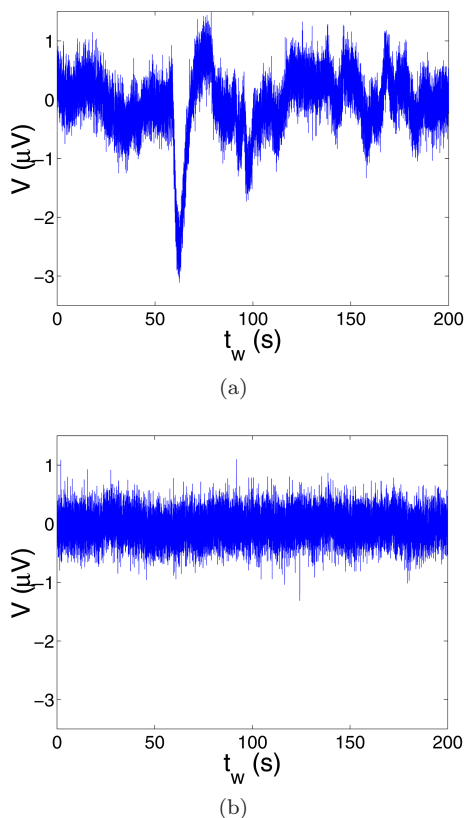


Fig. 20. Voltage noise signal in Laponite. **a)** Noise signal, 2 h after the Laponite preparation, when FDT is violated. **b)** Typical noise signal when FDT is not violated.

3.3.3 Statistical analysis of the noise

In order to understand such a behavior we have directly analyzed the noise voltage across the Laponite cell. This test can be safely done in our experimental apparatus because the amplifier noise is negligible with respect to the thermal noise of the Laponite cell even when FDT is satisfied. In Figure 20a we plot a typical signal measured 2 h after the gel preparation when the FDT is strongly violated. The signal plotted in Figure 20b has been measured when the system is relaxed and FDT is satisfied in all the frequency range. By comparing the two signals we immediately realize that there are very important differences. The signal in Figure 20a is interrupted by bursts of very large amplitude which are responsible for the increasing

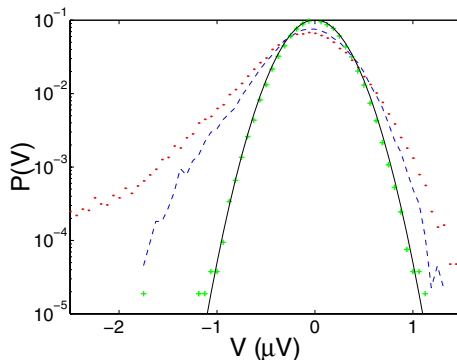


Fig. 21. PDF of the voltage noise in Laponite. Typical PDF of the noise signal at different times after preparation, with from top to bottom: (...) $t_w = 1$ h, (--) $t_w = 2$ h, (+) $t_w = 50$ h. The continuous line is obtained from the FDT prediction.

of the noise in the low frequency spectra (see Fig. 17). The relaxation time of the bursts has no particular meaning, because it corresponds just to the characteristic time of the filter used to eliminate the very low frequency trends. As time goes on, the amplitude of the bursts reduces and the time between two consecutive bursts becomes longer and longer. Finally they disappear as can be seen in the signal of Figure 20b recorded after 50 h when the system satisfies FDT. The evolution of the intermittent properties of the noise can be characterized by studying the probability density function (PDF) of the signal as a function of time. To compute the PDF, the time series are divided in several time windows and the PDF are computed in each of these windows. Afterwards the results of several experiments are averaged. The PDF computed at different times are plotted in Figure 21. We see that at short t_w the PDF presents very high tails which slowly disappear at longer t_w . Finally a Gaussian shape is recovered at $t_w = 16$ h. This kind of evolution of the PDF clearly indicates that the signal is very intermittent at the very beginning and it relaxes to the Gaussian noise at very long times.

The comparison of these results with aging models will be done in the conclusions. We prefer to describe now another experiment in a completely different material.

3.4 Polycarbonate dielectric properties

In order to give more insight into the problem of the violation of FDT and of the intermittent behavior discussed in the previous section we have done

wide band (20 mHz–100 Hz) measurements of the dielectric susceptibility and of the polarization noise in a polymer glass: polycarbonate. We present in this lecture several results which show a strong violation of the FDT when this material is quenched from the molten state to below its glass-transition temperature. The effective temperature defined by equation (3.2) slowly relaxes towards the bath temperature. The violation is observed even at $\omega t_w \gg 1$ and it may last for more than 3 h for $f > 1$ Hz.

3.4.1 The experimental apparatus

The polymer used in this investigation is Makrofol DE 1-1 C, a bisphenol A polycarbonate, with $T_g \simeq 419$ K, produced by Bayer in form of foils. We have chosen this material because it has a wide temperature range of strong aging [1]. This polymer is totally amorphous: there is no evidence of crystallinity [54]. Nevertheless, the internal structure of polycarbonate changes and relaxes as a result of a change in the chain conformation by molecular motions [1, 55, 56]. Many studies of the dielectric susceptibility of this material exist, but no one had an interest on the problem of noise measurements.

In our experiment polycarbonate is used as the dielectric of a capacitor. The capacitor is composed by 14 cylindrical capacitors in parallel in order to reduce the resistance of the sample and to increase its capacity. Each capacitor is made of two aluminum electrodes, 12 μm thick, and by a disk of polycarbonate of diameter 12 cm and thickness 125 μm . The experimental set-up is shown in Figure 22a. The 14 capacitors are sandwiched together and put inside two thick aluminum plates which contain an air circulation used to regulate the sample temperature. This mechanical design of the capacitor is very stable and gives very reproducible results even after many temperature quenches. The capacitor is inside two Faraday screens to insulate it from external noise. The temperature of the sample is controlled within a few percent. Fast quench of about 50 K/min are obtained by injecting Nitrogen vapor in the air circulation of the aluminum plates. The electrical impedance of the capacitor is $Z(\omega, t_w) = R/(1 + i\omega R C)$, where C is the capacitance and R is a parallel resistance which accounts for the complex dielectric susceptibility. It is measured using a Novocontrol Dielectric Analyzer. The noise spectrum of this impedance $S_Z(\omega, t_w)$ is:

$$S_Z(f, t_w) = 4 k_B T_{\text{eff}}(f, t_w) \text{Re}[Z(\omega, t_w)] = \frac{4 k_B T_{\text{eff}}(f, t_w) R}{1 + (\omega R C)^2} \quad (3.11)$$

where T_{eff} is the effective temperature of the sample. In order to measure $S_Z(f, t_w)$, we have made a differential amplifier based on selected low noise JFET(2N6453 InterFET Corporation), whose input has been polarized by a resistance $R_i = 4$ G Ω . Above 2 Hz, the input voltage noise of this amplifier

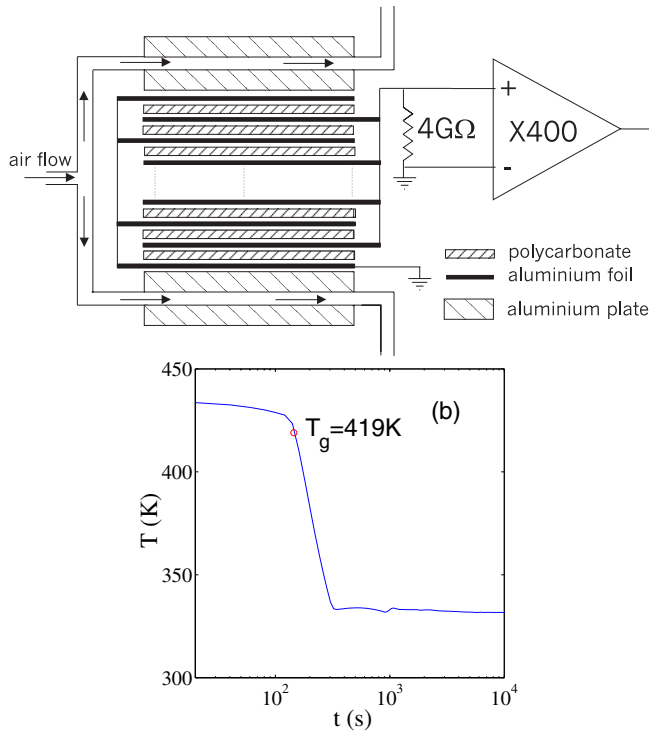


Fig. 22. a) Polycarbonate experimental set-up. b) typical temperature quench: from $T_i = 433$ K to $T_f = 333$ K, the origin of t_w is at $T = T_g$.

is $5 \text{ nV}/\sqrt{\text{Hz}}$ and the input current noise is about $1 \text{ fA}/\sqrt{\text{Hz}}$. The output signal of the amplifier is analyzed either by an HP3562A dynamic signal analyzer or directly acquired by a NI4462 card. It is easy to show that the measured spectrum at the amplifier input is:

$$S_V(f, t_w) = \frac{4k_B R R_i (T_{\text{eff}}(f, t_w) R_i + T_R R + S_\xi(f) R R_i)}{(R + R_i)^2 + (\omega R R_i C)^2} + S_\eta(f) \quad (3.12)$$

where T_R is the temperature of R_i and S_η and S_ξ are respectively the voltage and the current noise spectrum of the amplifier. In order to reach the desired statistical accuracy of $S_V(f, t_w)$, we averaged the results of many experiments. In each of these experiments the sample is first heated to $T_i = 433$ K. It is maintained at this temperature for 4 h in order to reinitialize its thermal history. Then it is quenched from T_i to $T_f = 333$ K in about 2 min. A typical thermal history of the quench is shown in Figure 22b. The reproducibility of the capacitor impedance, during this thermal cycle

is always better than 1%. The origin of aging time t_w is the instant when the capacitor temperature is at $T_g \simeq 419$ K, which of course may depend on the cooling rate. However adjustment of T_g of a few degrees will shift the time axis by at most 30 s, without affecting our results.

3.4.2 FDR measurements

In Figure 23a and b, we plot the measured values of R and C as a function of f at T_i and at T_f for $t_w \geq 200$ s. We see that lowering temperature R increases and C decreases. At T_f aging is small and extremely slow. Thus for $t_w > 200$ s the impedance can be considered constant without affecting our results. From the data plotted in Figures 23a and 23b one finds that $R = 10^{10}(1 \pm 0.05) f^{-1.05 \pm 0.01} \Omega$ and $C = (21.5 \pm 0.05)nF$. In Figure 23a we also plot the total resistance at the amplifier input which is the parallel of the capacitor impedance with R_i . We see that at T_f the input impedance of the amplifier is negligible for $f > 10$ Hz, whereas it has to be taken into account at slower frequencies.

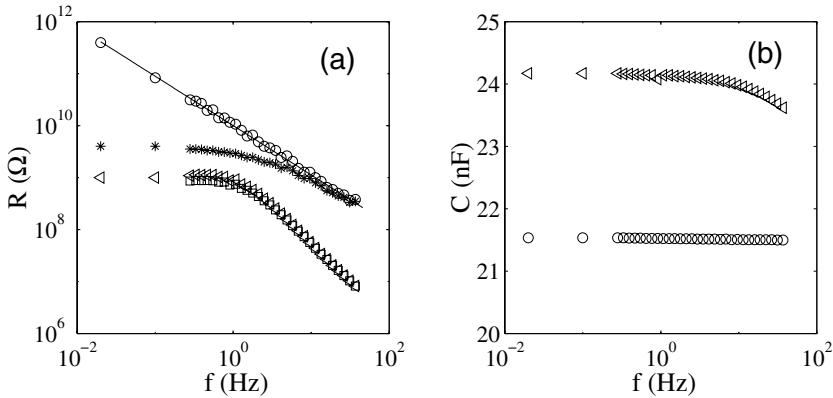


Fig. 23. Polycarbonate response function. **a)** Polycarbonate resistance R as a function of frequency measured at $T_i = 433$ K (\triangleleft) and at $T_f = 333$ K (\circ). The effect of the $4G \Omega$ input resistance is also shown at $T = 433$ K (\square) and at $T = 333$ K ($*$). **b)** Polycarbonate capacitance *versus* frequency measured at $T_i = 433$ K (\triangleleft) and at $T_f = 333$ K (\circ).

Figure 24a represents the evolution of $S_V(f, t_w)$ after a quench. Each spectrum is obtained as an average in a time window starting at t_w . The time window increases with t_w so to reduce error for large t_w . Then the results of 7 quenches have been averaged. At the longest time ($t_w = 1$ day) the equilibrium FDT prediction (continuous line) is quite well satisfied. We clearly see that FDT is strongly violated for all frequencies at short times.

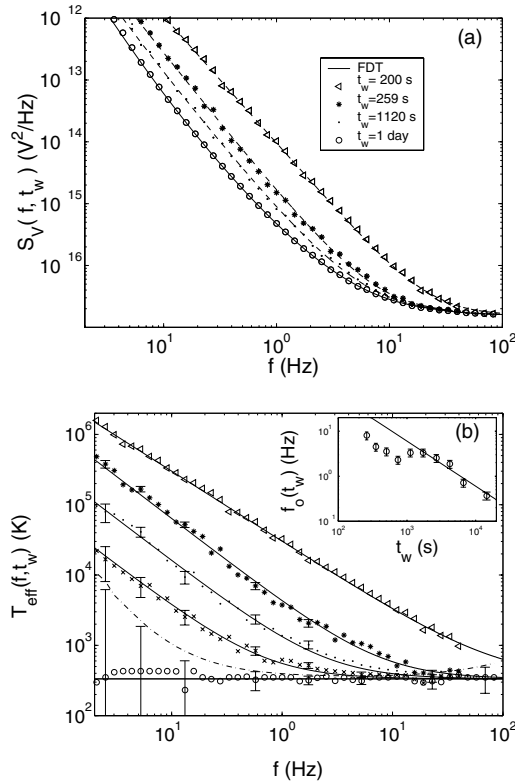


Fig. 24. Voltage noise and effective temperature in polycarbonate. **a)** Noise power spectral density $S_V(f, t_w)$ measured at $T_f = 333$ K and different t_w . The spectra are the average over seven quenches. The continuous line is the FDT prediction. Dashed lines are the fit obtained using equations (3.12) and (3.13) (see text for details). **b)** Effective temperature *vs.* frequency at $T_f = 333$ K for different aging times: (\triangleleft) $t_w = 200$ s, ($*$) $t_w = 260$ s, (\bullet) $t_w = 2580$ s, (\times) $t_w = 6542$ s, (\circ) $t_w = 1$ day. The continuous lines are the fits obtained using equation (3.13). The horizontal straight line is the FDT prediction. The dot dashed line corresponds to the limit where the FDT violation can be detected. In the inset the frequency $f_0(t_w)$, defined in equation (3.13), is plotted as a function of t_w . The continuous line is not a fit, but it corresponds to $f_0(t_w) \propto 1/t_w$.

Then high frequencies relax on the FDT, but there is a persistence of the violation for lower frequencies. The amount of the violation can be estimated by the best fit of $T_{\text{eff}}(f, t_w)$ in equation (3.12) where all other parameters are known. We started at very large t_w when the system is relaxed and $T_{\text{eff}} = T$

for all frequencies. Inserting the values in equation (3.12) and using the S_V measured at $t_w = 1$ day we find $T_{\text{eff}} \simeq 333$ K, within error bars for all frequencies (see Fig. 24b). At short t_w data show that $T_{\text{eff}}(f, t_w) \simeq T_f$ for f larger than a cutoff frequency $f_0(t_w)$ which is a function of t_w . In contrast, for $f < f_0(t_w)$ we find that T_{eff} is: $T_{\text{eff}}(f, t_w) \propto f^{-A(t_w)}$, with $A(t_w) \simeq 1$. This frequency dependence of $T_{\text{eff}}(f, t_w)$ is quite well approximated by

$$T_{\text{eff}}(f, t_w) = T_f \left[1 + \left(\frac{f}{f_0(t_w)} \right)^{-A(t_w)} \right] \quad (3.13)$$

where $A(t_w)$ and $f_0(t_w)$ are the fitting parameters. We find that $1 < A(t_w) < 1.2$ for all the data set. Furthermore for $t_w \geq 250$, it is enough to keep $A(t_w) = 1.2$ to fit the data within error bars. For $t_w < 250$ s we fixed $A(t) = 1$. Thus the only free parameter in equation (3.13) is $f_0(t_w)$. The continuous lines in Figure 24a are the best fits of S_V found inserting equation (3.13) in equation (3.12).

In Figure 24b we plot the estimated $T_{\text{eff}}(f, t_w)$ as a function of frequency at different t_w . We see that just after the quench $T_{\text{eff}}(f, t_w)$ is much larger than T_f in all the frequency interval. High frequencies rapidly decay towards the FDT prediction whereas at the smallest frequencies $T_{\text{eff}} \simeq 10^5$ K. Moreover we notice that low frequencies decay more slowly than high frequencies and that the evolution of $T_{\text{eff}}(f, t_w)$ towards the equilibrium value is very slow. From the data of Figure 24b and equation (3.13), it is easy to see that $T_{\text{eff}}(f, t_w)$ can be superposed onto a master curve by plotting them as a function of $f/f_0(t_w)$. The function $f_0(t_w)$ is a decreasing function of t_w , but the dependence is not a simple one, as it can be seen in the inset of Figure 24b. The continuous straight line is not fit, it represents $f_0(t_w) \propto 1/t_w$ which seems a reasonable approximation for these data. For $t_w > 10^4$ s we find the $f_0 < 1$ Hz. Thus we cannot follow the evolution of T_{eff} anymore because the contribution of the experimental noise on S_V is too big, as it is shown in figure 24b by the increasing of the error bars for $t_w = 1$ day and $f < 0.1$ Hz.

Before discussing these experimental results we want to compare them to the single frequency experiment performed on glycerol (Sect. 3.2) [44]. In this experiment, T_{eff} has been measured only at 7 Hz. Thus we studied how $T_{\text{eff}}(7 \text{ Hz}, t_w)$ depends on t_w at 7 Hz in our experiment. The time evolution of $T_{\text{eff}}(7 \text{ Hz}, t_w)$ is plotted as a function of t_w in Figure 25a. The time evolution of $T_{\text{eff}}(2 \text{ Hz}, t_w)$ is also plotted just to show the large temperature difference between two frequencies. Let us consider the evolution at 7 Hz only. As in the experiment described in Section 3.2 [44], we confirm the fact that the violation is observed even if $\omega t_w \gg 1$, which is in contrast with theoretical predictions. The biggest violation is for short times after the quench where the effective temperature is surprisingly huge: around

800 K at 7 Hz and $t_w = 300$ s. In the experiment on glycerol the first data reported are for $t_w > 1000$ s. Thus if we consider only data at $t_w > 1000$ s in Figure 25a we see that our results are close to those of [44]. Indeed at $t_w = 1000$ s we find in our experiment $(T_{\text{eff}} - T_f)/(T_g - T_f) \simeq 2.4$. The glycerol data give $(T_{\text{eff}} - T_f)/(T_g - T_f) \simeq 1$. Thus the relative violations of FDT at 7 Hz are very close in glycerol and polycarbonate. However it would be interesting to check whether at shorter times and at lower frequencies large T_{eff} could be observed in glycerol too.

In order to compare with theoretical predictions [10, 30] and recent spin glass experiment [47] we may plot the integrated response $R(t, t_w)$ as a function of the correlation $C(t, t_w)$. The latter is obtained inserting measured $T_{\text{eff}}(f, t_w)$ in equation (3.11) and by Fourier transforming this equation. $R(t, t_w)$ can be computed by Fourier transforming $\text{Real}[Z(\omega, t_w)]$. FDR now takes the form [10, 11]:

$$-C(t, t_w) + C(t_w, t_w) = k_B T_{\text{eff}}(t, t_w) R(t, t_w). \quad (3.14)$$

In the inset of Figure 25b, we see that for $t_w > 300$ s the shape of the decay of $C(t_w, t)$ remains essentially the same. Indeed data for different t_w can be scaled onto a single master curve by plotting $C(t_w, t)$ as a function $(t - t_w)/t_0(t_w)$, where $t_0(t_w)$ is an increasing function of t_w : approximately $t_0(t_w) \propto 1/f_0(t_w)$ for $t_w > 200$ s. The self-similarity of correlation functions, found on our dielectric data, is a characteristic of the universal picture of aging [9, 10, 36, 37, 57], which has been also observed in spin-glass experiment [47] and in the structure function of the dynamic light scattering of colloidal gels [58]. Thus our results confirm that this picture of aging applies also to the polymer dielectric measurements. To further investigate this aging, we plot, in Figure 25b, $R(t, t_w)$ as a function $(-C(t, t_w) + C(t_w, t_w))/k_B$ at different t_w . The slope of this graph gives $1/T_{\text{eff}}$. The symbols correspond to the data whereas the dashed line are obtained by inserting the best fit of T_{eff} in equation (3.13), in equation (3.11). We clearly see that data at small $C(t, t_w)$ asymptotically converge to an horizontal straight line, which means that the system has an infinite temperature. At short time, large $C(t, t_w)$, FDT prediction is recovered (continuous straight line of slope $1/T_f$). This result is quite different to what has been observed in recent experiments on spin glasses where $T_{\text{eff}} \simeq 5T_g$ has been measured [47]. In contrast infinite T_{eff} has been observed during the sol gel transition [45] and in numerical simulation of domain growth phenomena [38].

3.4.3 Statistical analysis of the noise in Polycarbonate

In order to understand the origin of such large deviations in our experiment we have analyzed the noise signal. We find that the signal is characterized by

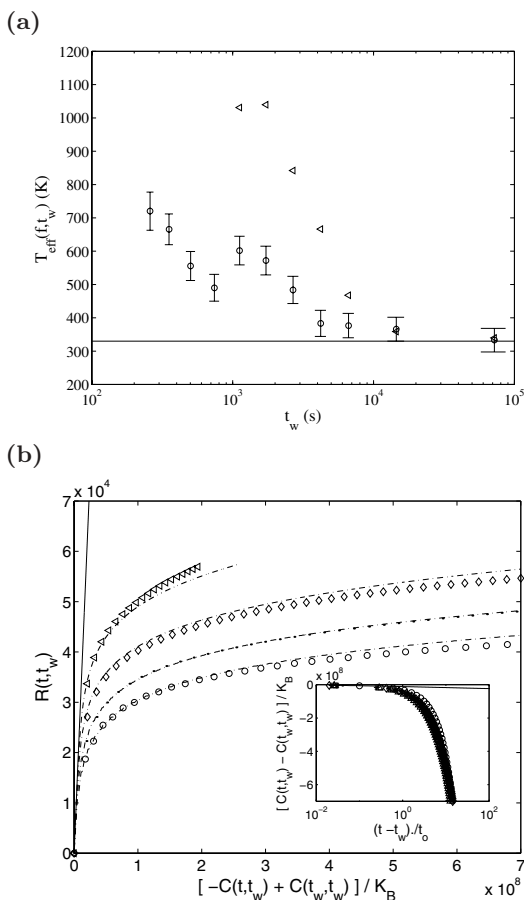


Fig. 25. Violation of FDT in polycarbonate. **a)** Effective temperature at 7 Hz (\circ) and 2 Hz (\triangleleft) measured as a function of t_w at $T_f = 333$ K. **b)** Plot of the integrated response $R(t, t_w)$ as a function of $-C(t, t_w) + C(t_w, t_w)$ at different t_w . Symbols correspond to the data: (\circ) $t_w = 256$ s, (\bullet) $t_w = 353$ s, (\diamond) $t_w = 4200$ s, (\triangleleft) $t_w = 6542$ s. The dashed lines are obtained from the best fits (see text for details). In the inset $C(t, t_w) - C(t_w, t_w)$ is plotted as a function of time for several $t_w = 250$ s; 353 s; 503 s; 1120 s; 1624 s; 2583 s; 4200 s. The correlation functions have been superposed by scaling $t - t_w$ by a characteristic time $t_0(t_w)$ which is an increasing function of t_w .

large intermittent events which produce low frequency spectra proportional to $f^{-\alpha}$ with $\alpha \simeq 2$. Two typical signals recorded at $1500 \text{ s} < t_w < 1900 \text{ s}$ and $t_w > 75\,000 \text{ s}$ are plotted in Figure 26. We clearly see that in the signal

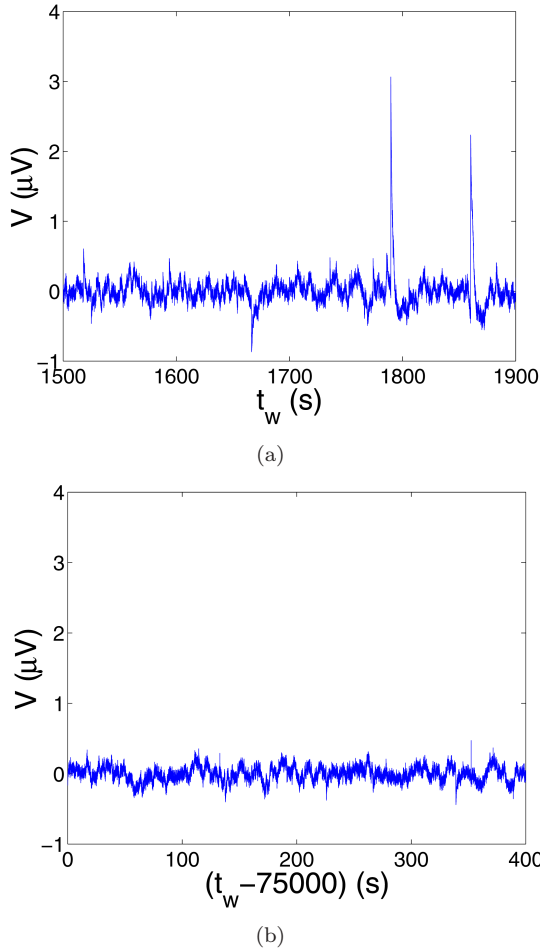


Fig. 26. Voltage noise signal in polycarbonate. Typical noise signal of polycarbonate measured at $1500 \text{ s} < t_w < 1900 \text{ s}$ **a**) and $t_w > 75\,000 \text{ s}$ **b**).

recorded at $1500 \text{ s} < t_w < 1900 \text{ s}$ there are very large bursts which are on the origin of the frequency spectra discussed in the previous section. In contrast in the signal (Fig. 26b), which was recorded at $t_w > 75\,000 \text{ s}$ when FDT is not violated, the bursts are totally disappeared.

As for Laponite we have studied the PDF of the signal as a function of t_w for polycarbonate. The results are shown in Figure 27. We clearly see that the PDF, measured at small t_w , has very high tails which becomes smaller and smaller at large t_w . Finally the Gaussian profile is recovered after 24 h.

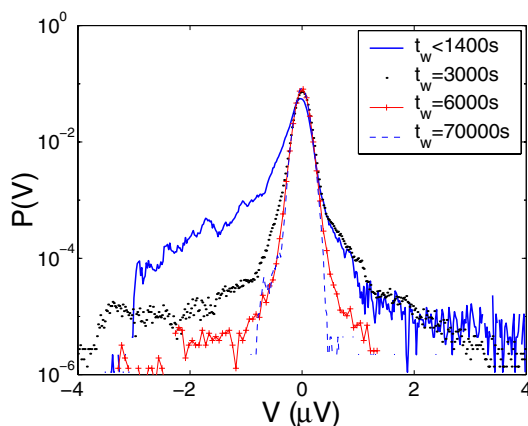


Fig. 27. PDF of voltage noise in polycarbonate. Typical PDF of the noise signal of polycarbonate measured at various t_w .

This strongly intermittent dynamics is reminiscent of the intermittence observed in the local measurements of polymer dielectric properties [59] and in the slow relaxation dynamics of a colloidal gel [60].

3.5 Rheological measurements

In the previous section we have shown that the FDR is strongly violated by the electrical properties of Laponite. We want to understand whether a violation can be observed in the measurements of other physical properties. Of course there are no reasons to assume that T_{eff} is the same for all the variables [42, 43] but the differences and the analogies found in the evolution of T_{eff} obtained by the measurements of several variables may give new insight on aging theories and on the coupling of the different variables in an aging material. Therefore we performed rheological measurements on Laponite and we checked FDR in these measurements.

3.5.1 Experimental apparatus

To achieve this result we built a new rheometer which is sensitive to thermal fluctuations. The principle of the rheological measurement is a standard one and is illustrated in Figure 28. We describe here only the main features, more details can be found in [62, 63]. A rotor of diameter 12 mm is inserted in a cylindrical cell. The gap of 1 mm between the rotor surface and the cell is filled with the fluid under study. The rotor is suspended by two steel wires. On the top of the rotor we fixed an optical prism. This

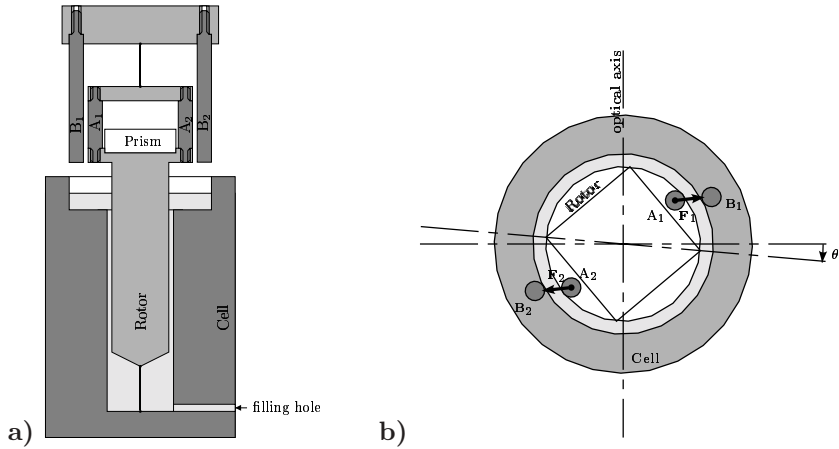


Fig. 28. Rheometer. Vertical **a)** and horizontal **b)** cross section of the rheometer. The torque is applied through the electrostatic interaction of electrodes $A_{1,2}$ and $B_{1,2}$ when the voltage V_c is applied to this capacitor.

prism is part of a Nomarski interferometer [64] which is used to measure the rotation angle θ of the rotor. The sensitivity of this system is better than 10^{-10} rad/ $\sqrt{\text{Hz}}$ corresponding to a torque on the rotor of about 10^{-13} N m/ $\sqrt{\text{Hz}}$. An external torque Γ_{ext} can be applied to the rotor by using the electrostatic interaction of a capacitor (see Fig. 28). One of the two electrodes of the capacitor is fixed on the rotor whereas the other is fixed on the cell walls. When a voltage difference V_c is applied on this capacitor the attractive force between these two electrodes produces a torque on the rotor which is equilibrated by the stiffness of the steel wires.

Let us consider the simple case of a Newtonian fluid of viscosity η . The response of this torsion pendulum in Fourier space is

$$\chi_{\theta\Gamma_{\text{ext}}} = \frac{\delta\theta}{\Gamma_{\text{ext}}} = \frac{1}{(k - J\omega^2) - i\alpha\eta\omega} \quad (3.15)$$

where J is the rotor inertia moment, k the steel wires stiffness and α is a geometric factor.

In the experiment we have access to two quantities: the angular position θ of the rotor, and the voltage V_c driving the torque. Γ_{ext} being quadratic in V_c , we add a constant offset to it in order to linearise this relation. For small displacements, the response function $\chi_{\theta\Gamma_{\text{ext}}}$ is then simply proportional to $\chi_{\theta V_c}$. The missing constant can be found by performing a inertial calibration of the response: the real part of $1/\chi_{\theta\Gamma_{\text{ext}}}$ is a parabola

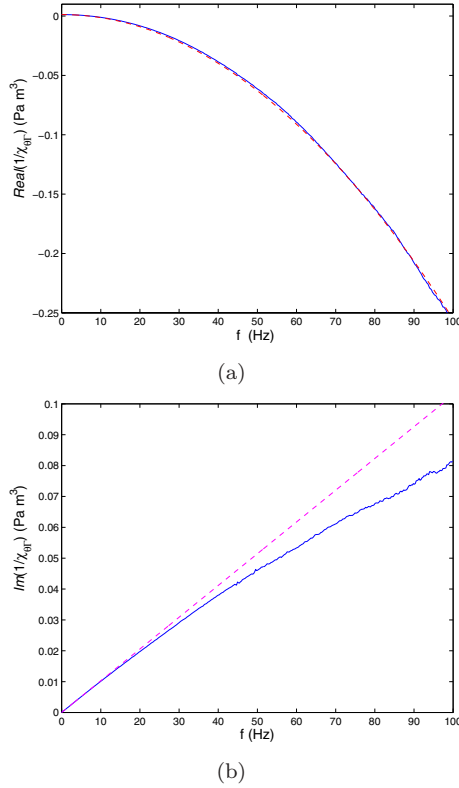


Fig. 29. Response of the rheometer to a white noise excitation. The real **a)** and imaginary **b)** part of $1/\chi_{\theta\Gamma_{\text{ext}}}$ are plotted as a function of frequency. The rheometer is filled with a viscous oil with $\eta = 2$ Pas. The dashed curve in **a)** corresponds to a quadratic fit of the data, and allows inertial calibration of the measurement (see text for details). The dashed line in **b)** is a linear fit of low frequency data, it is consistent with a newtonian behaviour of the fluid.

whose quadratic coefficient is the rotor inertia moment J . J is known with a good precision, and thus can be used to calibrate the measurement.

This rheometer has been tested using a silicon oil with $\eta = 2$ Pas. We first measure the response by using a white noise voltage excitation for V_c with an amplitude corresponding to a torque $\Gamma_{\text{ext}} \simeq 10^{-10}$ N m/ $\sqrt{\text{Hz}}$. The real and imaginary part of $1/\chi_{\theta\Gamma_{\text{ext}}}$ are plotted as a function of frequency in Figures 29a and b respectively. We see that in agreement with equation (3.15) the real part of $1/\chi_{\theta\Gamma_{\text{ext}}}$ is very well fitted by a parabola whereas the imaginary part is linear for small f . The deviation of the data

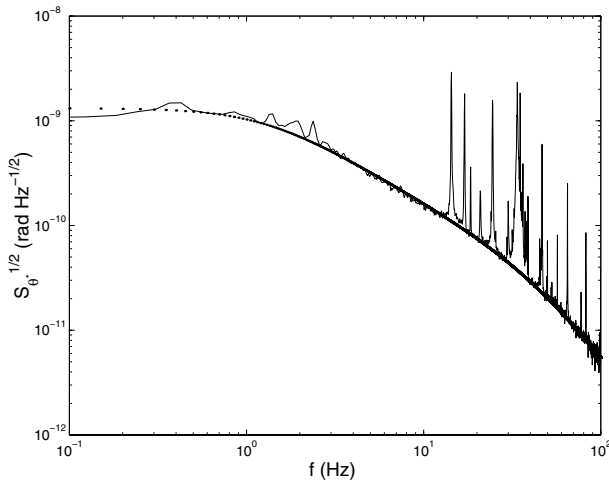


Fig. 30. Spectrum of the thermal fluctuations of θ . The rheometer is filled with the same oil used to measure the response reported in Figure 29. The continuous line is the result of the measurement whereas the dashed line is computed inserting in equation (3.16) the measured response of the rheometer and $T = 300$ K.

from the linear behaviour is due to the non-newtonian character of the silicon oil at higher frequencies. Once the response is known one can set the external torque to zero and measure S_θ , the spectrum of the thermal fluctuations of θ . In this case the fluctuation dissipation relation is:

$$S_\theta = \frac{4k_B T}{\omega} \text{Im}(\chi_{\theta\Gamma_{\text{ext}}}). \quad (3.16)$$

By inserting the measured $\chi_{\theta\Gamma_{\text{ext}}}$ in equation (3.16), we get an estimation of the fluctuation spectrum S_θ . The comparison between this computed S_θ and the measured one is done in Figure 30. Except for the existence of the peaks due to environmental noise the agreement is quite good. Thus the rheometer has enough sensitivity to verify FDR in viscous fluids.

3.5.2 FDR on the rheology of Laponite

We have studied the rheological properties of Laponite at 3% mass concentration in water. Laponite has been prepared in the way described in Section 2 for electrical measurements and the rheometer is mounted inside a container filled with a clean Nitrogen atmosphere. Moreover, a thin oil layer on top of the Laponite solution ensures no evaporation can occur. We

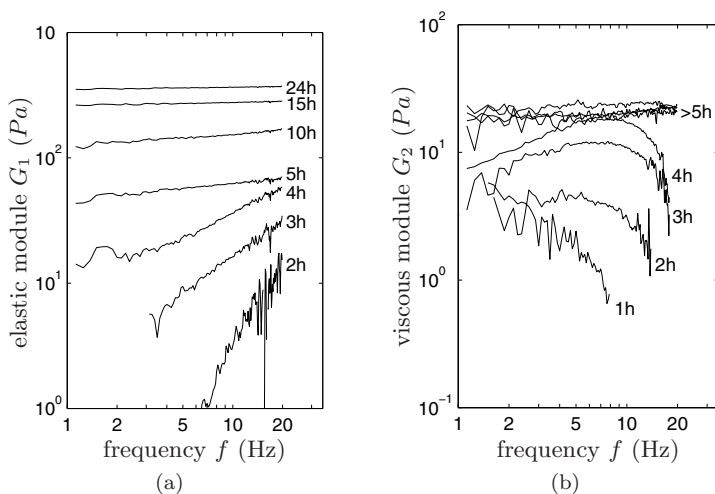


Fig. 31. Aging of the viscoelastic module of Laponite at a 3% mass concentration in water. The real **a)** and imaginary **b)** part of the viscoelastic module are plotted as a function of frequency.

first measure the response at different times t_w after the preparation. The measured elastic and viscous modules of Laponite are plotted as a function of frequency in Figure 31a and b respectively. We clearly see that at short t_w the liquid like solution has only viscous response. As time goes on an elastic modulus appears and the viscosity grows of about one order of magnitude. After 24 h the solution has a solid like aspect with a viscoelastic response. The measurement the thermal fluctuation spectrum S_θ averaged on the first hour of the aging processes of Laponite is plotted in Figure 32. The peak at 1.5 Hz has no physical meaning and is due to a mechanical resonance of the table. Whereas the resonance at 7 Hz is the resonant frequency of the torsion pendulum of the rheometer. The measure is compared to the prediction of the fluctuation dissipation theorem by inserting in equation (3.16) the measured values of the Laponite viscous response and $T = 300$ K. We also inserted in equation (3.16) the effective temperature obtained by the electrical measurements averaged on the first hour. We clearly see that in the case of rheological measurements no violation of FDR can be detected within experimental errors. If a violation exists, it is much smaller than that observed in the electric measurements.

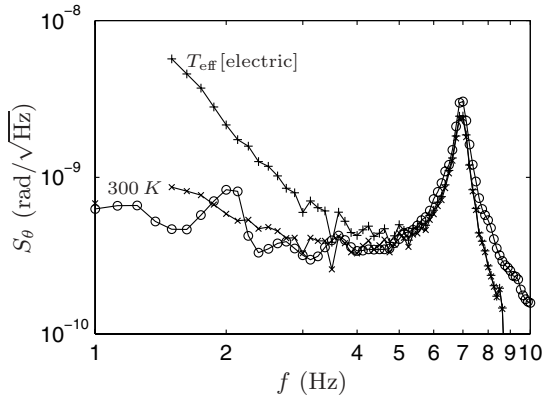


Fig. 32. Thermal fluctuation spectrum of the rheometer filled with Laponite. The line with \circ is the the result of the measurement. The line with \times is the FDT prediction for $T = 300$ K. The line with $+$ is obtained from equation (3.16) by inserting in T the values of T_{eff} estimated from electric measurements.

3.6 Discussion and conclusions on the effective temperature

Let us resume the main results of the experiments described in the previous sections. We have seen that dielectric measurements of Laponite, during the sol-gel transition, and of polycarbonate, after a temperature quench, show a strong violation of FDT. The effective temperature defined by equation (3.2) is huge at small t_w and slowly relaxes towards the bath temperature. In contrast to theoretical predictions the violation is observed even at $\omega t_w \ll 1$ and it may last for more than 3 h for $f > 1$ Hz. We have than investigated the behaviour of the noise signals and we have shown that the huge T_{eff} is produced by very large intermittent bursts which are at the origin of the low frequency power law decay of noise spectra. Furthermore we have also shown that for both materials the statistic of this event is strongly non Gaussian when FDT is violated and slowly relaxes to a Gaussian one at very long t_w . Thus these two very different materials have a very similar relaxation dynamics, characterized by a strong intermittency. This strongly intermittent dynamics is reminiscent of the intermittence observed in the local measurements of polymer dielectric properties [59]. Furthermore recent measurements done, using Time Resolved Correlation in Diffusing wave spectroscopy, have shown a strong intermittency in the slow relaxation dynamics of a colloidal gel [60]. This kind of behaviour can indeed be interpreted on the basis of the trap model [6, 42], which predicts non trivial violation of FDT associated to an intermittent dynamics. The

system evolves in deeper and deeper valleys on the energy landscape. The dynamics is fundamentally intermittent because either nothing moves or there is a jump between two traps. In our case these jumps could explain the presence in the dielectric voltage noise of very large and rare peaks with a slow relaxation after the jump. Clearly answer to this question can be given by a detailed study of the statistics of the time intervals between large peaks. This work is in progress.

However it is important to point out that intermittent dynamics and very large T_{eff} are not observed in all the systems. Indeed spin-glass experiments [47, 48] have a behaviour, which, at least for temperatures close to T_g , is coherent to mean field predictions. Instead on the basis of the available experimental data nothing can be said about the supercooled liquid dynamics, because, as we have seen in Section 3.2, only single frequency measurements have been done on these materials.

Another important point that we have discussed is the dependence of T_{eff} on the observable. In Section 3.3 we have studied this problem by measuring FDR of the rheological properties of Laponite. These measurements show that, within experimental errors, either there is no violation of FDT or this violation is certainly much smaller than that observed in the dielectric measurements. The reasons of this difference between electrical and mechanical measurements are unclear and much work is necessary to give new insight on these problems. However it is important to stress that this difference is coherent with trap models, which predict not only an intermittent dynamics, but also an observable dependent T_{eff} [42].

4 General conclusions

The purpose of this lecture was that of discussing several experimental approaches which are useful to characterize the aging dynamics. In the first part we have discussed methods based on the analysis of the response functions, showing the existence of very spectacular effects such as memory and rejuvenation. However we have seen that, although these two effects are extremely useful to fix constraints for the models of aging, the informations extracted by these techniques are not enough to make a distinction among the different models. For this reason in the second part of the lecture we have discussed the measurement of the FDR for different materials and observables. As the FDR is strongly model dependent, the association of thermal noise and response measurements is extremely useful to give new insight on the aging dynamics.

As we have already mentioned many questions are still open. For example it will be very useful to clarify whether the intermittent dynamics is always associated with an observable dependent T_{eff} . Further, it will

be important to understand whether the intermittency observed on global variables is related to local rearrangement inside the sample. Much work is needed in order to answer to these questions.

L. Bellon and L. Buisson are thanked for extremely useful and productive collaboration. We acknowledge valuable discussion with J.L. Barrat, L. Berthier, J.P. Bouchaud and J. Kurchan. We also thank E. Vincent for having send us Figure 12.

References

- [1] L.C. Struik, *Physical aging in amorphous polymers and other materials* (Elsevier, Amsterdam, 1978).
- [2] *Spin Glasses and Random Fields*, edited by A.P. Young, Series on Directions in Condensed Matter Physics, Vol. 12 (World Scientific, Singapore, 1998).
- [3] M. Kroon, G.H. Wegdam and R. Sprik, *Phys. Rev. E* **54** (1996) 1.
- [4] K. Jonason, E. Vincent, J. Hammann and J.P. Bouchaud, *Phys. Rev. Lett.* **81** (1998) 3243.
- [5] L. Bellon, S. Ciliberto and C. Laroche, *Eur. Phys. J. B* **25** (2002) 223.
- [6] J.P. Bouchaud and D.S. Dean, *J. Phys. I France* **5** (1995) 265.
- [7] D.S. Fisher and D.A. Huse, *Phys. Rev. Lett.* **56** (1986) 1601; D.S. Fisher and D.A. Huse, *Phys. Rev. B* **38** (1988) 373.
- [8] E. Bertin and J.P. Bouchaud, *J. Phys. A Math. Gen.* **35** (2002) 3039. Also in [cond-mat/0112187].
- [9] J.P. Bouchaud, L.F. Cugliandolo, J. Kurchan and M. Mézard, *Out of equilibrium dynamics in Spin Glasses and other glassy systems*, in *Spin Glasses and Random Fields*, edited by A.P. Young (World Scientific, Singapore, 1998). Also in [cond-mat/9702070].
- [10] L. Cugliandolo, J. Kurchan and L. Peliti, *Phys. Rev. E* **55** (1997) 3898.
- [11] L. Cugliandolo, these proceedings.
- [12] N.G. McCrum, B.E. Read and G. Williams, *Anelastic and Dielectric Effects in Polymeric Solids* (Dover, 1991).
- [13] M. Lederman, R. Orbach, J.M. Hammann, M. Ocio and E. Vincent, *Phys. Rev. B* **44** (1991) 7403; E. Vincent, J.P. Bouchaud, J. Hammann and F. Lefloch, *Phil. Mag. B* **71** (1995) 489.
- [14] F. Alberici, P. Doussineau and A. Levelut, *Europhys. Lett.* **39** (1997) 329.
- [15] R.L. Leheny and S.R. Nagel, *Phys. Rev. B* **57** (1998) 5154.
- [16] T. Jonsson, K. Jonason and P. Nordblad, *Phys. Rev. B* **59** (1999) 9402.
- [17] P. Doussineau, T. Lacerda-Aroso and A. Levelut, *Europhys. Lett.* **46** (1999) 401.
- [18] E. Muzeau, G. Vigier, R. Vassoille and J. Perez, *Polymer* **36** (1995) 611.
- [19] L. Bellon, S. Ciliberto and C. Laroche, *Temperature cycling during the aging o a polymer glass*. Also in [cond-mat/9905160].
- [20] L. Bellon, C. Laroche and S. Ciliberto, *Europhys. Lett.* **51** (2000) 551.
- [21] K. Jonason, P. Nordblad, E. Vincent, J. Hammann and J.-P. Bouchaud, *Eur. Phys. J. B* **13** (2000) 99.
- [22] V. Dupuis, E. Vincent, J.P. Bouchaud, J. Hammann, A. Ito and H. Aruga Katori, *Phys. Rev. B* **64** (2001) 174204. Also in [cond-mat/0104399].

- [23] V. Dupuis, *Dynamique Lente des Systèmes magnétiques Désordonnés*, Ph.D. Thesis (Université de Paris XI, Orsay, 2002).
- [24] J.P. Bouchaud, V. Dupuis, J. Hamman and E. Vincent, *Phys. Rev. B* **65** (2002) 024439.
- [25] J.P. Bouchaud, *Aging in glassy systems: New experiments, simple models and open questions*, in *Soft and Fragile Matter: Nonequilibrium Dynamics, Metastability and Flow*, edited by M.E. Cates and M.R. Evans (IOP Publishing, Bristol and Philadelphia, 2000), 285-304. Also in [cond-mat/9910387].
- [26] A. Kovacs, *J. Polym. Sci.* **30** (1958) 131.
- [27] A.J. Bray and M.A. Moore, *Phys. Rev. Lett.* **58** (1987) 57.
- [28] L. Berthier and P.C. Holdsworth, *Europhys. Lett.* **58** (2002) 35. Also in [cond-mat/0109169v1].
- [29] E. Vincent, J. Hammann, M. Ocio, J.P. Bouchaud and L.F. Cugliandolo, in *Complex Behavior of Glassy systems* (Springer Verlag), *Lecture Notes in Phys.* **492**, edited by M. Rubi (1997) 184. Also in [cond-mat/9607224].
- [30] L. Cugliandolo and J. Kurchan, *Phys. Rev. Lett.* **71** (1993) 173.
- [31] S.R. de Groot and P. Mazur, *Non equilibrium thermodynamics* (Dover, 1984).
- [32] J.H. Wendorff and E.W. Fischer, *Kolloid-Z. u. Z. Polymere* **251** (1973) 876.
- [33] H. Sompolinsky, *Phys. Rev. Lett.* **47** (1981) 935.
- [34] P. Hohenberg and Shraiman, *Physica D* **37** (1989) 109.
- [35] G. Parisi, *Phys. Rev. Lett.* **79** (1997) 3660.
- [36] W. Kob and J.L. Barrat, *Phys. Rev. Lett.* **78** (1997) 4581.
- [37] J.L. Barrat and W. Kob, *Europhys. Lett.* **46** (1999) 637.
- [38] A. Barrat, *Phys. Rev. E* **57** (1998) 3629.
- [39] M. Sellitto, *Eur. Phys. J. B* **4** (1998) 135.
- [40] E. Marinari, G. Parisi, F. Ricci-Tersenghi and J.J. Ruiz-Lorenzo, *J. Phys. A Math. Gen.* **31** (1998) 2611.
- [41] L. Berthier, J.L. Barrat and J. Kurchan, *Phys. Rev. E* **61** (2000) 5464.
- [42] S. Fielding and P. Sollich, *Phys. Rev. Lett.* **88** (2002) 50603-1.
- [43] A. Perez-Madrid, D. Reguera and J.M. Rubi, *Origin of the Violation of the Fluctuation-Dissipation Theorem in Systems with Activated Dynamics*. Also in [cond-mat/0210089].
- [44] T.S. Grigera and N. Israeloff, *Phys. Rev. Lett.* **83** (1999) 5038.
- [45] L. Bellon, S. Ciliberto and C. Laroche, *Europhys. Lett.* **53** (2001) 511.
- [46] L. Bellon and S. Ciliberto, *Physica D* **168** (2002) 325.
- [47] D. Herrisson and M. Ocio, *Phys. Rev. Lett.* **88** (2002) 257702. Also in [cond-mat/0112378].
- [48] M. Ocio, these proceedings.
- [49] L. Buisson, L. Bellon and S. Ciliberto, *J. Phys.: Cond. Matt.* (2003).
- [50] Laponite RD is a registered trademark of Laporte Absorbents, P.O. Box 2, Cheshire, UK.
- [51] D. Bonn, H. Tanaka, G. Wegdam, H. Kellay and J. Meunier, *Europhys. Lett.* **45** (1999) 52; D. Bonn, H. Kellay, H. Tanaka, G. Wegdam and J. Meunier, *Langmuir* **15** (1999) 7534.
- [52] R. Hunter, *The foundation of colloid science* (Oxford Science Publications, 1989).
- [53] J. Koryta, L. Dvorak and L. Kavan, *Principles of Electrochemistry*, 2nd Ed. (Wiley, 1993).

- [54] C.G. Robertson and G.L. Wilkes, *Macromolecules* **33** (2000) 3954.
- [55] L. Saviot, E. Duval, J.F. Jal and A.J. Dianoux, *Eur. Phys. J. B* **17** (2000) 661.
- [56] R. Quinson, *Caractérisation et modélisation de la déformation non élastique des polymères amorphes à l'état solide*, Ph.D. Thesis (INSA, 1998).
- [57] L. Berthier and J.P. Bouchaud, *Phys. Rev. B*. Also in [cond-mat/0202069v1].
- [58] L. Cipelletti, S. Manley, R.C. Ball and D.A. Weitz, *Phys. Rev. Lett.* **84** (2000) 2275.
- [59] E. Vidal Russel and N.E. Israeloff, *Nature* **408** (2000) 695.
- [60] L. Cipelletti, H. Bissig, V. Trappe, P. Ballestat and S. Mazoyer, submitted *J. Phys: Cond. Matt.*
- [61] *Light Scattering by Liquid Surfaces and Complementary Techniques*, edited by D. Langevin (Dekker, New York, 1992).
- [62] L. Bellon, *Viellissement des systèmes vitreux et rapport fluctuation-dissipation*, Ph.D. Thesis (ENS de Lyon, 2001).
- [63] L. Bellon, L. Buisson, S. Ciliberto and F. Vittoz, *Rev. Sci. Instrum.* **73** (2002) 3286.
- [64] G. Nomarski, *J. Phys. Radium* **16** (1955) 110.

COURSE 10

**FLUCTUATION DISSIPATION RELATION
IN A NON-STATIONARY SYSTEM: EXPERIMENTAL
INVESTIGATION IN A SPIN GLASS**

M. OCIO

*DSM, Service de Physique de l'État
Condensé, CEA Saclay,
91191 Gif-sur-Yvette, France*



Contents

1	Introduction	607
2	Theoretical background	608
3	Experimental	609
3.1	Measurement of magnetic fluctuations	609
3.2	Principle of measurement: An absolute thermometer	611
3.3	Experimental results	614
4	Discussion	616
5	Conclusion	620

FLUCTUATION DISSIPATION RELATION IN A NON-STATIONARY SYSTEM: EXPERIMENTAL INVESTIGATION IN A SPIN GLASS

M. Ocio¹ and D. Hérisson¹

Abstract

We present the first experimental determination of the time autocorrelation of magnetization $C(t', t)$ in the aging regime of a spin glass, and its quantitative comparison with the corresponding response, the relaxation of magnetization $\sigma(t', t)$. These measurements were performed in a new experimental setup equivalent to an absolute thermometer. Clearly, we observe a non-linear fluctuation dissipation relation between σ and C : at large C (short observation times $t - t'$) fluctuation dissipation theorem is obeyed, while in the aging regime (small correlation and large $t - t'$), the fluctuation dissipation relation is driven by an effective temperature higher than the bath temperature. According to theoretical predictions on mean field models, and lately on short range ones, in the limit of large waiting times t' , the $\sigma(C)$ relation in the aging regime is temperature independent for a given system. A scaling procedure allows us to extrapolate to the limit of long waiting times by separating stationary and non-stationary contributions in both σ and C , and to check the validity of these predictions.

1 Introduction

About 15 years ago, the first experiments on free “thermodynamic” magnetic fluctuations were performed on a spin glass system [1]. At that time, the purpose of the experiment was to measure the so called “ $1/f$ ” noise one could expect in these systems with large distribution of relaxation times. Data analysis was performed by classical FFT methods, and within the frequency range of the first experiments, it was found that the power spectrum was stable and related by fluctuation dissipation theorem (FDT) [2]

¹Service de Physique de l’État Condensé, CEA Saclay, 91191 Gif-sur-Yvette, France

to the out-of-phase susceptibility [3,4]. At the same period, the strong non-stationarity of spin glasses was experimentally detected [5] and related later to equivalent properties of glassy polymers already investigated long time before [6,7]. Very soon too, the non-stationarity of the very low frequency magnetic noise power spectrum was detected [3], showing that the behavior of these systems is quite different when looking on different timescales. The non-stationarity of spin glasses, the so-called “aging” was the subject of intensive experimental studies [8]. Meanwhile, the theoretical community was mainly preoccupied on the solution of the problem of the Gibbs equilibrium state. Unfortunately for experimentalists, the only solvable model of a spin glass was the Sherrington-Kirkpatrick (SK) mean field model – which has a rather loose relation with a real spin glass –, but the output was finally the concept of hierarchical ultrametric phase space organization derived by Parisi *et al.* [9]. Despite its esoteric nature, this concept was a very powerful qualitative tool, making understandable most of the far from intuitive manifestations of non-stationarity in spin glasses, what is known now as “rejuvenation” and “memory” effects [10].

For experimentalists working on magnetic noise, the problem was challenging: could it be possible to insert FDT, the masterpiece of statistical physics, into a more general relation valid in non-ergodic systems? Spin glasses are globally non-stationary, they are non-ergodic. Still, in specific timescale conditions, FDT is obeyed. If one looks at two-time dependent quantities, like the response to a field perturbation, non-stationarity is manifest. But if one looks at one-time dependent ones, like the free energy, or the field-cooled magnetization, there are remarkably stable. In particular, the energy seems to reach very quickly an essentially stationary value and experimentally, its variations are undetectable. If it is possible to find fluctuation dissipation relations valid in non-ergodic systems, obviously spin glasses are good candidates for an experimental investigation.

2 Theoretical background

In its basic form, FDT reads $R(t' - t') = \beta \partial C(t - t') / \partial t'$, where $R(t, t')$ is the impulse response of an observable to its conjugate field, $C(t', t)$ is the time autocorrelation of the observable and $\beta = 1/k_B T$. Actually, FDT is intimately linked to the thermodynamic definition of the temperature. In non-stationary systems, FDT is not expected to hold. A quite general relation can be written as $R(t', t) = \beta X(t', t) \partial C(t', t) / \partial t'$ (Note that now t and t' are referred to the “birth” of the system, *i.e.* the instant where, by the variation of some control parameter – temperature, concentration – it enters in its glassy state.) FDT corresponds to $X = 1$. Determination of X , the fluctuation dissipation ratio (FDR), or of an

“effective temperature” $T_{\text{eff}} = T/X$, was the aim of many recent theoretical studies, following the seminal works of Cugliandolo and Kurchan [11, 12]. In mean field models, a generalization of FDT was predicted on the basis of the “weak ergodicity breaking” scenario [13]. It was conjectured that, in the asymptotic limit of large times, when stationary and non-stationary timescales are well separated, the FDR would depend on time only through the correlation function: $X(t', t) = X(C(t', t))$ for t' (and $t > t'$) $\rightarrow \infty$. The dependence of X on C would reflect the level of thermalization within different timescales [14]. The integrated form of the FD relation would become $\chi(t', t) = \beta \int_{C(t', t)}^{C(t, t)} X(C) dC$ (susceptibility function) and $\sigma(t', t) = \beta \int_0^{C(t', t)} X(C) dC$ (relaxation function). The equilibrium limit of $\chi(t', t)$ would read $\chi_{\text{eq}} = \beta \int_0^{C(t, t)} X(C) dC = \beta(1 - \int_0^1 C(X) dX)$ (in the simplest Ising case with $C(t, t) = 1$), formally equivalent to the Gibbs equilibrium susceptibility in the Parisi replica symmetry solution for the SK model [15], with $C \Leftrightarrow q$ (overlap between pure states) and $X \Leftrightarrow x$ (repartition of overlap). Within PaT hypothesis [16], it was shown that in the non-stationary regime, *i.e.* for $C < q_{\text{EA}}$, the $\chi(C)$ curve is temperature independent, and thus unique for a given system. Theoretical works, analytical [17] (with the constraint of stochastic stability) and numerical [18] (with the problem of size effects) were done in order to confirm the above properties in short range models. FDT links linearly the relaxation function $\sigma(t', t)$ – as well as the susceptibility function $\chi(t', t)$ – to the autocorrelation function: for instance, $\sigma(t', t) = \beta C(t', t)$. Non-equilibrium properties can be characterized and classified by the deviations from this relation.

3 Experimental

3.1 Measurement of magnetic fluctuations

Measurement of magnetic fluctuations is conceptually the simplest experiment one could imagine. The sample, of cylindrical shape, is inserted into a pick-up (PU) coil connected by a twisted pair to the input coil of a SQUID (Fig. 1a); all the circuit is made of superconducting (SC) wire. The system is contained in a ^4He cryogenic setup allowing temperature regulation above 4.2 K. Moments fluctuations in the sample induce a fluctuating flux in the PU. From flux conservation in the SC circuit, this fluctuating flux generates a fluctuating current proportional to the flux in the circuit, and thus the SQUID delivers an output voltage proportional to the fluctuating flux. The enormous difficulty lies in the extreme weakness of the amplitude of the magnetic fluctuation in the sample: in our case, it corresponds to the response of the sample to a field about 10^{-7} G. As it is quite impossible to suppress the ambient field at such a level, the solution is twofold. First to

reduce it at a level of order 1 mG and stabilize it as best as possible: this is obtained by isolation and shielding procedures which will not be developed further here. Second, to use a gradiometric PU coil: a third order gradiometer as used in our experiment suppresses the effect of the field up to second order and all even orders. In our experimental setup, the result of the above precautions is that the proper noise power spectrum of the system without sample allows time analysis of the magnetic fluctuations signal over up to 2000 s with more than 20 dB of signal/noise ratio.

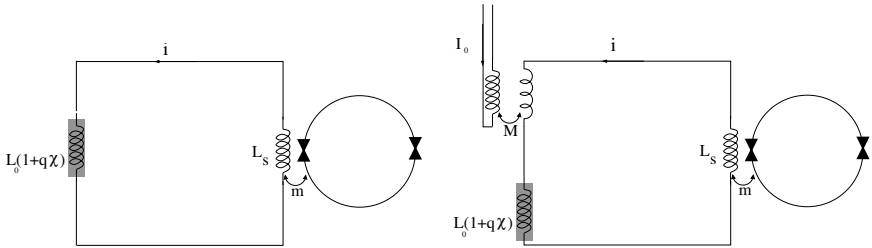


Fig. 1. a) (Left): basic SQUID circuit for magnetic fluctuations measurement. **b)** (Right): circuit allowing fluctuation and response measurements (absolute thermometer).

In a non-stationary system, the time autocorrelation of magnetic fluctuations must be determined as an ensemble average over a large number of equivalent records of the fluctuations signal, each one initiated by a quench from above T_g (“birth” of the system). Moreover, we want to compare *quantitatively* correlation and relaxation data. The relaxation function (TRM relaxation) is measured by cooling the sample at time zero from above T_g to the working temperature in a small field, turning off the field at time t' and recording the magnetization signal at further times t (in this experiment, it is implicitly assumed that the field cooled susceptibility χ_{FC} is equivalent to the dynamical limit of $\chi(t', t)$ for $(t - t')/t' \rightarrow \infty$; despite some approximative experimental evidences, this equivalence is of course questionable). In general, this measurement is done in a classical magnetometer with an homogeneous field, and a quantitative comparison with correlation results is quite impossible since the coupling factors of the sample to the measuring systems are driven by two quite different relevant field geometries. Therefore, we have developed a new setup allowing measurement of both fluctuation and response in exactly the same relevant field configuration. Fundamentally, the system is an FDR “black box”, or in other words, it works as an absolute thermometer.

3.2 Principle of measurement: An absolute thermometer

Let's consider a magnetic sample inserted into a PU coil. By the so called reciprocity theorem, a moment \mathbf{m}_i at position \mathbf{r}_i induces in the coil a flux $\delta\Phi = \mathbf{m}_i \mathbf{h}_i$ where \mathbf{h}_i is the field one unit of current flowing in the coil would produce at \mathbf{r}_i . Therefore, the flux in the coil due to the sample is given by:

$$\Phi = \sum_i \sum_{\mu} m_i^{\mu} h_i^{\mu} \quad (3.1)$$

where μ indexes the spin components: $\mu = \{x, y, z\}$ for Heisenberg spins, $\mu = \{z\}$ for Ising ones, etc. We suppose that the medium is homogeneous, the fluctuations components are statistically independent and their spatial correlations are much smaller than the scale of the PU: $\langle m_i^{\mu}(t') m_j^{\nu}(t) \rangle = \langle m(t') m(t) \rangle \delta_{ij} \delta_{\mu\nu}$. Then, the flux autocorrelation is given by:

$$\langle \Phi(t') \Phi(t) \rangle = \sum_{\mu} \sum_i h_i^{\mu 2} \langle m(t') m(t) \rangle = QC(t', t). \quad (3.2)$$

The flux autocorrelation in the PU is thus the one site moment autocorrelation per degree of freedom $C(t', t)$, multiplied by the coupling factor Q determined by the geometries of the PU field and of the sample.

On the other hand, the impulse response function of one moment in the sample is given by

$$R_{ij}^{\mu\nu}(t', t) = \frac{\partial m_j^{\nu}}{\partial h_i^{\mu}} = R(t', t) \delta_{ij} \delta_{\mu\nu} \quad (3.3)$$

where $R(t', t)$ is the averaged one site response function of the sample. if a current I is injected in the coil, the flux on it due to the polarization of the sample reads

$$\Phi(t) = \sum_i \sum_{\mu} h_i^{\mu 2} \int^t R(t', t) I(t') dt'. \quad (3.4)$$

Thus, the response function of the flux due to the sample in the PU circuit is

$$R_{\Phi}(t', t) = QR(t', t). \quad (3.5)$$

The same coupling factor $Q = \sum_i \sum_{\mu} h_i^{\mu 2}$ determines the values of correlation and response of the flux due to the sample.

Note that the term h is the value of the internal field into the sample, due to a unit of current flowing in the coil. Therefore, Q corresponds to the same demagnetizing field conditions in both measurements. Actually, Q is time dependent, since the internal field is $h_{\text{int}} = h_0 \mu(t', t)$ where $\mu(t', t)$ is

the time dependent sample permeability, but the important point is that $Q(t', t)$ is exactly the same in both experiments.

The above derivation is done in the context of a magnetic system, showing that the measured quantities represent those used in theoretical works. Incidentally, equivalent derivation could be done for any system with magnetic response, for instance the eddy currents in a conductor, with the same result: coupling factors are the same in fluctuations and response.

The basic measurement circuit is depicted in Figure 1b. A small coil coupled to an excitation winding with mutual inductance M is inserted in the PU circuit. The total flux impulse response of the circuit to the current $i(t')$ flowing on it is

$$R_L(t', t) = \sum L \delta(t - t') + Q(t', t) R(t', t) \quad (3.6)$$

where $\sum L$ is the total self inductance of the circuit. Flux conservation in the (SC) PU circuit leads to

$$\Phi_{\text{exc}}(t) + \int_{-\infty}^t R_L(t', t) i(t') dt' = 0 \quad (3.7)$$

where $\Phi_{\text{exc}}(t) = MI(t)$ is obtained by injecting a current $I(t)$ in the excitation winding. The conjugate variable of the circuit current i is the flux Φ_{exc} injected by the excitation coil.

The properties of the system are easy to derive in the case of an ergodic sample. By time translational invariance, equation (3.7) can be transformed into the frequency regime as $\tilde{\Phi}_{\text{exc}}(\omega) + \tilde{R}_L(\omega) \tilde{i}(\omega) = 0$ where \tilde{x} represents the Fourier transform of x , leading to the current response function to flux excitation

$$\tilde{R}_i(\omega) = -\frac{1}{\tilde{R}_L(\omega)} = -\frac{\sum L + \tilde{Q}(\omega) \otimes \tilde{R}^*(\omega)}{\tilde{R}_L(\omega) \tilde{R}_L^*(\omega)}. \quad (3.8)$$

Since $\tilde{Q}(\omega)$ is a real quantity,

$$\Im \tilde{R}_i(\omega) = \frac{\tilde{Q}(\omega) \otimes \Im \tilde{R}(\omega)}{\tilde{R}_L(\omega) \tilde{R}_L^*(\omega)}. \quad (3.9)$$

The ergodic sample obeys FDT,

$$\tilde{C}(\omega) \equiv S(\omega) = \frac{2k_B T}{\pi \omega} \Im \tilde{R}(\omega) \quad (3.10)$$

where $S(\omega)$ is the magnetic fluctuations power spectrum. Thus, by using equation (3.9), one finds the circuit current noise power spectrum

$$S_i(\omega) = \frac{\tilde{Q}(\omega) \otimes \tilde{S}(\omega)}{\tilde{R}_L(\omega) \tilde{R}_L^*(\omega)} = \frac{2k_B T}{\pi \omega} \Im \tilde{R}_i(\omega). \quad (3.11)$$

Thus, fluctuations and response of the circuit current obey FDT relation. Translation into the time domain follows classically: $\sigma_i(t - t') = \frac{1}{k_B T} C_i(t - t')$.

The SQUID gain is $G = V_S/i$. Thus, if a current $I(t) = I_0(1 - \theta(t))$ is injected in the excitation coil, the relaxation of the SQUID output voltage is related to its fluctuations autocorrelation function by

$$V_S(t) = \frac{MI_0}{G} \frac{1}{k_B T} \langle V_S(0)V_S(t) \rangle. \quad (3.12)$$

The system is an absolute thermometer since, by measuring both the response voltage to an excitation current step and the autocorrelation of the voltage free fluctuations, it allows a determination of the temperature whose precision (once a sample with large signal is chosen) depends only on the precision of the determination of the experimental parameters I_0 , G and M .

In the case of a non-stationary sample, things are of course more complex. Nevertheless, it is possible to analyze the case of a system with only one timescale (or correlation scale) in the large t' limit. In that case, $X(C) = X_1 < 1$ for $C < q_{EA}$, and the time can be re-parametrized [8] such that $R(t', t) \equiv R(\lambda(t') - \lambda(t'))$ and $C(t', t) \equiv C(\lambda(t') - \lambda(t'))$ yielding

$$\begin{aligned} \chi(\lambda - \lambda') &= \beta X_1 \int_{C(\lambda - \lambda')}^{q_{EA}} dC + \beta q_{EA} \\ &= \beta(1 + X_1)q_{EA} - \beta X_1 C(\lambda - \lambda'). \end{aligned} \quad (3.13)$$

Therefore, time translational invariance is recovered “in λ ”. The behavior of the thermometer can be analyzed in the same way than in the ergodic case, showing that the measured response will vary linearly as a function of the measured correlation with slope $\frac{MI_0}{G} X_1 \beta$. According to mean field predictions [12], this could be true within any timescale in a multi timescale system.

The main drawback of the elementary measuring circuit depicted above is that the response to an excitation step involves the instantaneous response of the total self inductance of the circuit (first term in the R.H.S of Eq. (3.6)). In our case, both the susceptibility of the sample and the coupling factor Q are weak. The quantity to be measured, – the second term in the R.H.S of equation (3.6) –, represents few percent of the first one. Thus, a bridge configuration depicted in Figure 2a has been adopted. Now, the main branch involving the sample is balanced by an equivalent one without sample. This second branch is excited oppositely, in such a way that when the sample is extracted from the PU, there is no response of the SQUID to an excitation step. When the sample is placed into the PU, the response of the SQUID is determined only by the response of the sample. Nevertheless, now, the

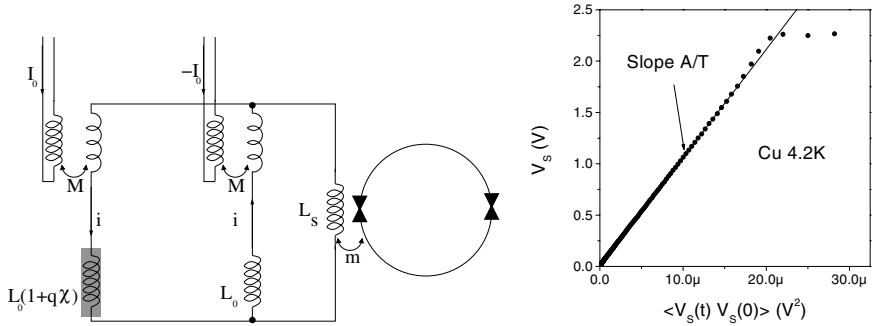


Fig. 2. a) (Left): balanced configuration circuit. **b)** (Right): σ vs. C plot obtained with the copper sample.

loop coupling of the sample to the SQUID involves different self inductance terms in both measurements, and one gets:

$$V_S(t) = \frac{MI_0}{G} \frac{L_0}{L_0 + 2L_S} \frac{1}{k_B T} \langle V_S(0)V_S(t) \rangle \quad (3.14)$$

where L_0 and L_S are the self inductances of the PU and of the SQUID input respectively, and the effect of the sample has been neglected in the value of L_0 . This adds sources of error on the calibration since self inductances are difficult to determine precisely. Thus the thermometer was calibrated by using a perfect ergodic system, a cylinder of pure copper with very high conductivity ($\rho_{300\text{ K}}/\rho_{4.2\text{ K}} > 1000$). At 4.2 K (^4He boiling temperature at normal pressure) the SQUID signal fluctuations autocorrelation was determined by standard FFT algorithms, and the relaxation after an excitation step was recorded. The result is depicted in Figure 2b where relaxation data are plotted *versus* correlation ones. Except for the few points at the shortest times (where the effect of the filters in the current excitation circuit is apparent), the relation between both measured quantities is linear with slope A/T , where $A = \frac{MI_0}{k_B G} \frac{L_0}{L_0 + 2L_S}$ is the *sample independent* calibration factor which can be determined since the temperature is known. From the knowledge of the numerical value of A , the experimental FDT slope is known *exactly* at any temperature and for any sample.

3.3 Experimental results

The FD relation was investigated in the insulating thiospinel spin glass $\text{CdCr}_{1.7}\text{In}_{0.3}\text{S}_4$. The pure Cr compound is a ferromagnet where the Cr^{3+} ions have ferromagnetic interactions between nearest neighbors, and antiferromagnetic ones between next nearest neighbors. Substitution of Cr by In

introduces disorder and frustration since it favours the antiferromagnetic interactions. The compound enters a spin glass phase below a transition temperature $T_g = 16.7$ K [19]. Just above T_g , the susceptibility is Curie-Weiss like, with a Curie constant corresponding to ferromagnetic clusters of about 50 spins, and a small antiferromagnetic interaction between clusters ($\theta = -22$ K). This clustering complicates the analysis of the experimental results as will be shown below, but it is the reason of the large susceptibility and fluctuations amplitude, allowing good noise measurements which would be impossible in a canonical metallic spin glass in the present state of the experimental possibilities. Extensive investigations of the aging properties of the magnetic response were performed in this compound: aging of TRM relaxation [20] and of the out-of-phase susceptibility [21], effect of the temperature variations [22]. On it, the first (and probably the only) systematic measurement of the aging of the magnetic noise power spectrum in a spin glass was performed by collecting an ensemble average of noise power at 10^{-2} Hz. This allowed a *qualitative* comparison with the results of out-of-phase susceptibility aging at the same frequency, showing that, in the *quasi-stationary regime* ($\omega t \gg 1$), FDT was approximately valid [21].

In the spin glass sample, $\langle V_S(t')V_S(t) \rangle$ and $V_S(t', t)$ were measured after quench from an annealing temperature $T \simeq 1.2T_g$ to working temperatures $T = 0.6T_g$, $0.8T_g$ and $0.9T_g$. In the relaxation experiments, the excitation current was such that the field in the sample was less than 1 mG. The cooling procedure was the following: first slow cooling from the annealing temperature to 3 K above working temperature, and then fast quench to the working temperature. This procedure was chosen in order to reduce the perturbation of the cryogenic bath – which would lead to SQUID instabilities –, while keeping a definition of the time zero (“birth” time) within less than 10 s error.

The autocorrelation was determined from an ensemble average of up to 350 records of the fluctuation signal after quench, with length up to 12000 s. To improve the averaging convergence, the ensemble averages were computed from short time averages of the signal at t' and t in each record. The best compromise allowing a good average convergence, still being compatible with non-stationarity was $\delta t' \leq t'/20$ and $\delta t \leq (t - t')/10$. As there is an arbitrary offset on the SQUID signal (due to the SQUID itself, as well as to the effect of the residual field on the sample), the connected correlation was computed:

$$C_V(t', t) = \langle (V_S(t') - \langle V_S(t') \rangle) (V_S(t) - \langle V_S(t) \rangle) \rangle. \quad (3.15)$$

Nevertheless, the above procedure cannot suppress a random offset in the results, due to fluctuating modes of period longer than 2000 s. These modes involve not only the fluctuating signal of the sample but also uncontrolled

long timescale drifts of the measurement setup. As it is impossible to disentangle both contributions, the correlation data have been normalized by taking as the origin the value of $\langle V_S^2(t') \rangle$. Due to the elementary measurement time constant, this term corresponds to an average over $t - t'$ about 10^{-2} s *i.e.* a range of $(t - t')/t'$ corresponding to the stationary regime where all C curves must merge. This amounts to shifting all the data by a common unknown offset C_0 . The result at $T = 0.8T_g$ is shown in Figure 3a (right sided scale), as a function of $t - t'$. Residual oscillations – and large error bars – at lowest t' reveal the limit of efficiency of the averaging procedure. In comparison with the above, the measurement of relaxation data is very easy. The relaxation curves at $0.8T_g$ are plotted in Figure 3b. In both results, the curves merge at small $t - t'$, meaning that they do not depend on t' (stationary regime). At $t - t' \gg t'$, they strongly depend on t' , the slower decay corresponding to the longer t' : the curves follow roughly a $(t - t')/t'$ scaling in the aging regime. Yet at this stage, a point can be stressed: the experimental waiting times t' are not long enough for timescales separation since it is apparent on the curves that the non-stationary regime begins while the stationary relaxation has not ended.

4 Discussion

Experimental results can be represented on a $\sigma(C)$ plot (plot of $\sigma(C)$ for each t' , using t as parameter) following the ideas of Cugliandolo and Kurchan. The inset in Figure 4 displays the results at 0.8 K plotted in experimental units. A clear linear range appears at large correlation (small $t - t'$). In the figure, the FDT slope, *computed from the value of the calibration factor A* is represented by the full straight line. The data display the FDT slope with less than 3% error in the sector of large correlation corresponding to a reduced correlation $\tilde{C} \geq 0.47$ (see below for the definition of \tilde{C}). Now, the correlation offset must be suppressed. As correlation zero is unreachable in experimental times, suppression of the offset could be obtained from the knowledge of $C(t, t)$ (square of the moment of the elementary fluctuator). Unfortunately, due to clustering, $C(t, t)$ depends on temperature and cannot be determined by the high temperature susceptibility. To obtain an evaluation of $C(t, t)$, an *ansatz* inspired by the properties of the canonical compounds like 1% Cu:Mn [23] was used. In these compounds with negligible clustering, the field cooled (FC) susceptibility is Curie like above T_g and temperature independent below T_g , in agreement with the PaT hypothesis, yielding $C(t, t) = T_g \chi_{FC}(T)$. The *ansatz* consists in using a generalization of this relation with the condition that a smooth dependence of $C(t, t; T)$ must result. This is obtained by using for T_g a slightly different value $T_g^* = 17.2$ K. Then, writing $C(t, t; T) = 17.2 \chi_{FC}(T)$, $C(t, t; T)$ can

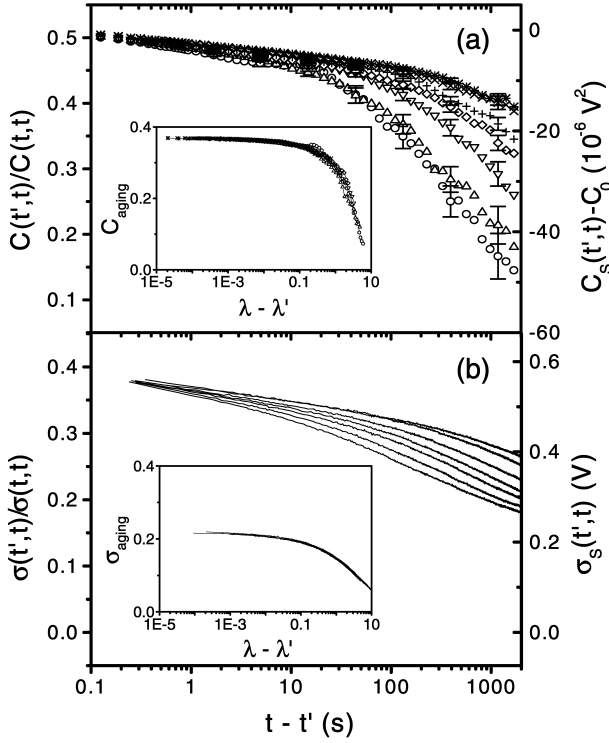


Fig. 3. **a)** Correlation and **b)** relaxation measured at 0.8 K. In the insets, scaling of the non-stationary contributions.

be obtained and suppression of the offset can be performed using the $\sigma(C)$ plot by the following procedure. One plots the normalized susceptibility function $\tilde{\chi}(t', t) = 1 - \tilde{\sigma}(t', t)$ where $\tilde{\sigma}(t', t) = V_S(t', t)/V_S(t, t)$ (note that $V_S(t, t)$ is the FC (initial) value of the relaxation SQUID signal), *versus* normalized autocorrelation $\tilde{C}(t', t) - \tilde{C}_0 = (C_S(t', t) - C_0)/C_S(t, t; T)$ where $C_S(t', t) = \langle V_S(t')V_S(t) \rangle$. In this graph, the FDT line has slope $-T^*/T$ and crosses the \tilde{C} axis at $\tilde{C} = 1$. The result is shown in Figure 4 for all investigated temperatures. It is of course based on a rough *ansatz* on $C(t, t; T)$ which needs further justifications, but the resulting uncertainty concerns only the position of the zero on the \tilde{C} axis, and not the shape and slope of the curves. With decreasing \tilde{C} (increasing $t - t' \geq t'$), the data points depart from the FDT line. Despite the scatter of the data, a t' dependence in the non-FDT regime is clear: the data at small t' depart the FDT line at larger values of \tilde{C} . This is the consequence of the non-separation of the timescales in the range of the experimentally accessible values of t' . Even

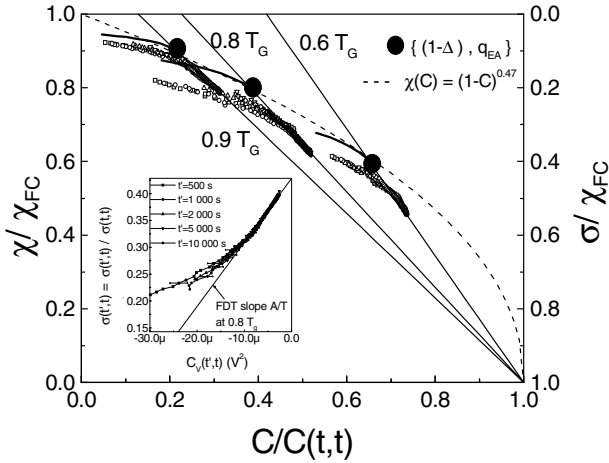


Fig. 4. $\tilde{\chi}$ vs. \tilde{C} plots at $0.6, 0.8$ and $0.9T_g$. In the inset, σ vs. C plot of the data at $0.8T_g$ in experimental units.

if the long t' limit for $\tilde{\chi}(\tilde{C})$ does exist, it is not reached in the results of Figure 4b and a t' dependence of the $\tilde{\chi}(\tilde{C})$ curves is expected.

Further insight would result of the separation of stationary and non-stationary contributions in the data. In the “weak ergodicity breaking” scenario, the relaxation and correlation can be written as the sum of two parts, a stationary one and a non-stationary one [8]. For instance:

$$\tilde{C}(t', t) = (1 - q_{EA})\mathcal{F}_{\text{stat}}(t - t') + q_{EA}\mathcal{F}_{\text{aging}}(t', t) \quad (4.1)$$

where $\mathcal{F}_{\text{aging}}(t', t)$ is a function obeying roughly $'(t - t)/t'$ scaling. This additive formulation is valid in the limit of large t' where both timescales are separated but is questionable otherwise. Indeed, it would lead, in case of very long tail in the stationary correlation, to a stationary regime *after* the end of the non-stationary one. More probably, in the mixed timescales regime, both contributions are more intricate than a simple addition. A first step to take it into account is to adopt a multiplicative formulation. For instance:

$$\tilde{C}(t', t) = ((1 - q_{EA})\mathcal{F}_{\text{stat}}(t - t') + q_{EA})\mathcal{F}_{\text{aging}}(t', t). \quad (4.2)$$

Note that for very large t' such that $\mathcal{F}_{\text{stat}}(t') \rightarrow 0$, one recovers equation (4.1). During the last decade, a form of scaling was used successfully to analyze aging relaxation. Inspired by the old work of Struik [7] on glassy polymers, this scaling corresponds in fact to one timescale time

re-parametrization [8]. Applied to equation (4.2) for $\tilde{\sigma}$, it leads to:

$$\tilde{\sigma}(t', t) = ((1 - \Delta)(1 + (t - t')/t_0)^{-\alpha} + \Delta)\varphi(\lambda(t) - \lambda(t')) \quad (4.3)$$

where t_0 is an elementary time of order 10^{-10} s, φ is a scaling function of an effective time $\lambda(t) = t^{1-\mu}/(1-\mu)$ depending on the subaging coefficient $\mu < 1$, and α can be determined with good precision from the stationary power spectrum of fluctuations $S(\omega) \propto \omega^{\alpha-1}$. The inset in Figure 3b displays the scaling of the aging part of the relaxation curves at $0.8T_g$, with $\alpha = 0.06$, $\Delta = 0.225$ and $\mu = 0.84$. As shown in the inset of Figure 3a, the scaling works rather well on the autocorrelation data with the same exponents, but now, q_{EA} replaces Δ ($q_{EA} = 0.4$). If granted, the scaling would allow an artificial separation of the timescales, by separating stationary and non-stationary contributions. The smoothed curves $\tilde{\chi}_{aging}(\tilde{C}_{aging})$ are plotted in Figure 4 at each temperature, as well as the couples $((1 - \Delta), q_{EA})$. On the basis of the PaT hypothesis, in the mean field SK model, the $\chi(C)$ curve is temperature independent, and can be described by $\chi = (1 - C)^{0.5}$, at least for large correlations [24]. At small correlation it is assumed to follow a behavior like $1 - \chi \propto C^2$, insuring that $X(C) \equiv x(q)$ has zero slope at the origin, or in other words that there is no peak of the distribution $P(q)$ at $q = 0$. It has been shown recently by numerical simulations that in short range models, a generalized relation like $\chi = A(1 - C)^B$ with $B < 1$ is more adequate [18]. Rather remarkably, in Figure 4, the couples $((1 - \Delta), q_{EA})$, as well as the beginning of the $\tilde{\chi}(C)$ curves (short times) are well described by $\tilde{\chi}(\tilde{C}) = (1 - \tilde{C})^{0.47}$ (dashed curve in the figure). This apparent conformity with the mean field model prediction is rather astonishing for a real material, and moreover it is contradictory with the very small exponent of the stationary relaxation $\alpha \leq 0.1$, while the mean field prediction is $\alpha = 0.5$. At large times, (small correlation) the $\tilde{\chi}(\tilde{C})$ data curves separate from the theoretical one, tending to a smaller slope, and they point to values smaller than 1 on the $\tilde{\chi}$ axis. An experimental bias cannot be excluded *a priori*, but it can be remarked that this is contradictory with the fact that the effect is the largest at the highest temperature, *i.e.* when the amplitude of fluctuations is the largest and the perturbation of the measuring system by the quench is the smallest. On the other hand, it can be noted that the general trend of the results is not coherent with a one timescale interpretation, but rather with multiple timescales one. In that case, one can expect that the $\tilde{\chi}(\tilde{C})$ curves tend to zero derivative at the origin, which is the tendency in the results. To summarize, even if a temperature independent behavior seems to be approached by the data in Figure 4b, they are dependent on rather questionable hypothesis and does not allow a conclusive statement: i) the ansatz used to determine $C(t', t:T)$ can be not realistic enough and needs further justifications; ii) the one timescale scaling used to separate

stationary and non-stationary contributions seems not valid in the range of times of the experiments.

5 Conclusion

As in any first trial of a new and difficult kind of experiment, the ensemble of results presented here gives a limited and ambiguous view on the physical reality, and opens more questions than it proposes answers. Nevertheless, at long last, it is now proven that it is possible to determine experimentally the time autocorrelation of the magnetic fluctuations in the aging regime of a spin glass. The task of the experiment was also to compare *quantitatively* fluctuations autocorrelation and relaxation. This was made possible by reconsidering in detail the experimental principles: the physical problem being fundamentally connected with the thermodynamic definition of the temperature, the experimental setup might be understood as an absolute thermometer.

Due to the non-canonical nature of the insulating compound investigated here, the interpretation of the results and the comparison with the recent theoretical predictions needed the use of hypothesis which are far for being justified at the theoretical level. In particular, the *ansatz* used to determine $C(t, t; T)$ is rather rough; an experimental determination, by neutron diffraction techniques for instance, is needed for a more rigorous interpretation of the data.

Nevertheless, we believe that this work opens a new and powerful experimental way in the general effort towards a generalization of the fluctuation theorem in real non-stationary systems.

References

- [1] M. Ocio, H. Bouchiat and P. Monod, *J. Phys. Lett.* **46** (1985) L647-L652.
- [2] H.B. Callen and T.A. Welton, *Phys. Rev.* **83** (1951) 34-40; R. Kubo, *J. Phys. Soc. Jpn.* **12** (1957) 570-586.
- [3] M. Ocio, H. Bouchiat and P. Monod, *J. M. M. M.* **54-57** (1986) 11-16.
- [4] P. Réfrégier, M. Ocio and H. Bouchiat, *Europhys. Lett.* **3** (1987) 503-510.
- [5] L. Lundgren, P. Svedlindh, P. Nordblad and O. Beckman, *Phys. Rev. Lett.* **51** (1983) 911-914.
- [6] M. Ocio, M. Alba and J. Hammann, *J. Phys. Lett.* (1985) L1101-1107.
- [7] L.C.E. Struik, *Physical ageing in amorphous polymers and materials* (Elsevier Scientific Publ., Houston, Tex., 1978).
- [8] For a review, see E. Vincent, J. Hammann, M. Ocio, J.P. Bouchaud and L.F. Cugliandolo, *Complex behavior of glassy systems* (Springer Verlag), *Lecture Notes in Phys.* **492**, edited by M. Rubi (1997) 184-219.
- [9] For a review, see M. Mézard, G. Parisi and M.A. Virasoro, *Spin glass theory and beyond* (World Scientific), *Lecture Notes in Phys.* **9** (1987).

- [10] V. Dupuis, E. Vincent, J.P. Bouchaud, J. Hammann, A. Ito and H. Aruga Katori, *Phys. Rev. B* **64** (2001) 174204 1-7.
- [11] L.F. Cugliandolo and J. Kurchan, *Phys. Rev. Lett.* **71** (1993) 173-176.
- [12] L.F. Cugliandolo and J. Kurchan, *J. Phys. A* **27** (1994) 5749-5772.
- [13] J.P. Bouchaud, *J. Phys. France I* **2** (1992) 1705-1713.
- [14] L.F. Cugliandolo, J. Kurchan and L. Peliti, *Phys. Rev. A* **55** (1997) 3898-3914.
- [15] G. Parisi, *J. Phys. A* **13** (1980) 115-121.
- [16] G. Parisi and G. Toulouse, *J. Phys. Lett.* **41** (1980) L361-L364.
- [17] S. Franz, M. Mézard, G. Parisi and L. Peliti, *Phys. Rev. Lett.* **81** (1998) 17581761.
- [18] E. Marinari, G. Parisi, F. Ricci-Tersenghi and J. Ruiz-Lorenzo, *J. Phys. A* **33** (2000) 2373-2382.
- [19] E. Vincent and J. Hammann, *J. Phys. C* **20** (1987) 2659-2671.
- [20] M. Alba, J. Hammann, M. Ocio, P. Réfrégier and H. Bouchiat, *J. Appl. Phys.* **61** (1987) 2683-2688.
- [21] P. Réfrégier, M. Ocio, J. Hammann and E. Vincent, *J. Appl. Phys.* **63** (1988) 4343-4345.
- [22] P. Réfrégier, E. Vincent, J. Hammann and M. Ocio, *J. Phys.* **48** (1987) 1533-1539.
- [23] S. Nagata, P.H. Keesom and H.R. Harrison, *Phys. Rev. B* **19** (1979) 1633-1638.
- [24] E. Marinari, G. Parisi, F. Ricci-Tersenghi and J. Ruiz-Lorenzo, *J. Phys. A* **31** (1998) 2611-2620.

COURSE 11

**NON-EQUILIBRIUM DYNAMICS AND AGING
IN THE ELECTRON GLASS**

Z. OVADYAHU

*The Racah Institute of Physics,
The Hebrew University,
Jerusalem 91904, Israel*



Contents

1	Introduction	625
2	The characteristics of the electron-glass	626
2.1	The field effect technique	626
2.2	Preliminary results	627
2.3	Basic features of the electron-glass	631
3	The role of the electron–electron interaction	637
3.1	Experimental evidence for the role of interactions	637
3.2	The Coulomb gap	643
3.3	Theoretical treatment of relaxation in the presence of interactions	644
4	Concluding remarks	646

NON-EQUILIBRIUM DYNAMICS AND AGING IN THE ELECTRON GLASS

Z. Ovadyahu

1 Introduction

In these notes, we review the experimental evidence for the existence of a relatively new type of a glassy system – Electron-Glass. You are all familiar with another type of an electronic glass – Spin-Glass, which is arguably the best studied glassy system. The non-ergodic effects in spin glasses are revealed in the magnetic properties of the material. In electron glasses, these effects are observable in the transport properties of the system such as its electrical conductivity. The existence of this type of glass has been anticipated theoretically years ago. Anderson has discussed the freeze-out of electrons in disordered electronic systems in his lecture notes presented at Les Houches in 1978, and Mott and Davis used the term Fermi-Glass as synonymous with an Anderson insulator in their classic textbook [1]. The term “electron-glass” was first coined by Lee *et al.* [2] to describe a system where the combination of disorder and inter-electron interaction will lead to a glassy arrangement of the electronic charge in a degenerate Fermi gas.

In the concluding remarks of their paper, Lee, Rice, and Davies stated:

“This glass state may also appear in the dependence of the electrical conductivity on the sample’s history, with difference between samples cooled in an electric field and without”. As we shall see, these predictions are indeed borne out by experiments performed on a number of disordered electronic systems with regard to both, history and memory of applied electric field. In addition, these systems exhibit some other non-ergodic effects, such as slow relaxation and aging that are characteristic of glasses.

In the first part of this seminar, we shall describe the main techniques used in these measurements, and the main features that are observed. These are slow relaxation from an excited state, aging and other memory effects. These will establish the existence of the electron glass. The second part will focus on the physics underlying the observed phenomena, namely, what are the reasons for the freeze-out of the charge degree of freedom in these systems and in particular, what is responsible for the observed sluggish energy-relaxation processes.

2 The characteristics of the electron-glass

2.1 The field effect technique

We start by first describing the experimental technique that exposed the glassy nature of a disordered electronic system. This technique, called Field-Effect (FE), is simple. The conductance G of a sample, usually a thin film of a metal or semiconductor, is measured as function of a potential difference applied between it and a nearby metallic object called a “gate”. The gate is separated for the sample by an insulating material (spacer) such that the final arrangement is essentially a capacitor. Changing the gate voltage V_g then adds or depletes charge from the sample. This will naturally lead to a change in G from which one can estimate the carrier concentration n in the sample. This, in fact, is the principle of operation of the FE transistor, which is a basic element in many current electronic devices. The contacts to the sample, which are used to measure its conductance, are traditionally called “source” and “drain”, terms that are borrowed from the “transistor-world” where these two objects are built differently. In samples made for FE studies, however, the source and drain can be usually interchanged, as they are identical in all respects.

The FE technique is routinely used to study properties of semiconductors and metals. In particular, it can yield information on the energy dependence of the density of states $\frac{dn}{d\mu}(\varepsilon)$ near the Fermi-energy E_F .

Few years ago, Ben-Chorin *et al.* [3] found a surprising result when they applied the FE technique to the study of Anderson insulating indium-oxide films. An Anderson insulator is a degenerate Fermi gas – just like a metal, and just like a metal, it has a finite density of states near E_F . It differs from a metal in that its diffusivity D vanishes at the absolute zero of temperature. This happens when the static disorder in the system exceeds a threshold value and the electronic states become localized [4]. Namely, the amplitude of the wave functions is appreciable only over a certain point in space and it decays exponentially away from it. The characteristic decay length of the amplitude ξ is called the localization length. This length gets smaller with increased disorder and diverges at the metal-insulator transition.

In what way does an Anderson insulator differ from a “textbook” insulator like diamond?

The conductivity of a system is generally given by the Einstein relation: $\sigma = e^2 \frac{dn}{d\mu} D$. Here $\frac{dn}{d\mu}$ is the thermodynamic density of states and D is the diffusion constant. To qualify as an insulator σ has to vanish as T goes to zero. For that to happen either $\frac{dn}{d\mu} = 0$ or $D = 0$ (or both). A textbook insulator like Si, Ge, or NaCl has $\sigma = 0$ by virtue of $\frac{dn}{d\mu} = 0$. In an Anderson-insulator, $\frac{dn}{d\mu}$ is expected to be finite and in this regard, it differs

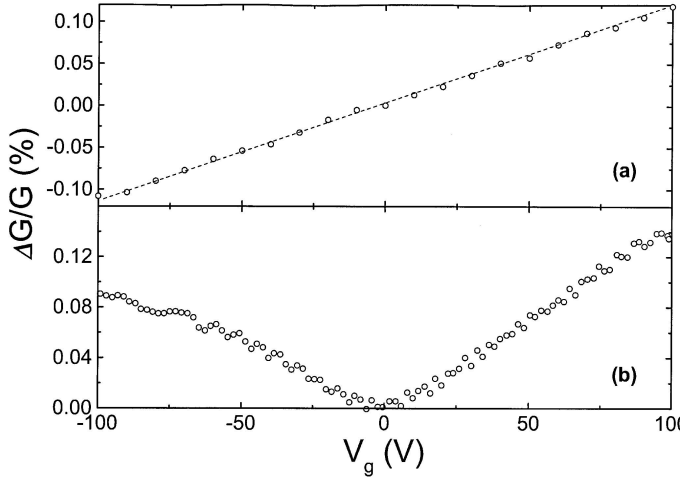


Fig. 1. The fractional change of conductance $\Delta G/G$ versus gate-voltage V_g measured at $T = 4.11$ K. The samples in **a)** and **b)** are 200 Å thick amorphous indium-oxide film deposited on 100 μm glass substrate. Gold film deposited on the back side acts as the gate. The sample in **a)** has $R_s = 40\text{k}\Omega$, the sample in **b)** has $R_s = 15\text{M}\Omega$.

qualitatively from the band-insulator. This difference should be evident in the FE experiment; to get charge into a band insulator V_g has to exceed some constant times the energy gap while for an Anderson insulator there ought to be no such threshold.

2.2 Preliminary results

The surprising result found by Ben-Chorin *et al.* is shown in Figure 1. Normally, adding charge to the sample leads to an increase of G while depleting it from charge results in diminished conductance. This means that ΔG will be an anti-symmetric function of V_g . This is indeed what is observed for the sample in Figure 1a, and for all other samples with lower degrees of disorder (as judged by the value of the resistivity or the sheet-resistance R_s at a given temperature).

The FE in Figure 1b however, is quite different; G appears to increase when V_g is changed from a specific value ($V_g = 0$ in this case) for *both* gate-voltage polarities! In other words, $\Delta G(V_g)$ acquires a component that is symmetric around $V_g = 0$. This immediately raises the question;

What is special about this value of the gate voltage?

Perhaps we can get a hint from another case where a similarly “special” situation is known to occur in conductance measurements.

A symmetrical change of conductance is expected as a function of a magnetic field H . Indeed, $G(H)$ is compelled to be symmetric with respect to $H = 0$ due to the Onsager relation [5] which mandates $G(H) = G(-H)$. This means that $H = 0$ is indeed “special” and the fundamental reason for that is that a zero field differs from any finite H because a magnetic field breaks time reversal symmetry. The point I wish to make here is that changing V_g also results in broken time reversal symmetry albeit in a different sense. It is not as fundamental as the effect of H but it is quite basic by its own right; when V_g is changed, charge flows into (or out of) the sample through the “source” and “drain”. The system then gets out of equilibrium, and once a system is out of equilibrium things change in time in a one-sided fashion – time reversal symmetry is broken.

This of course is always true. It ought also to have occurred in the sample shown in Figure 1a (and for that matter, in any other FE experiment), but usually it does not, why? Well, the out-of-equilibrium signature in ordinary cases simply does not last long enough for us to take notice. The sample shown in Figure 1b however is not ordinary. It turns out that upon increasing the disorder (going from sample in figure 1a to the sample in Fig. 1b) the system became glassy, and glasses, as you know, have some amazing properties. Perhaps the most familiar is that, once driven out of equilibrium they take their time reaching equilibrium again.

This is the first and foremost reason for the appearance of the anomalous FE exhibited in Figure 1b. It can be immediately illustrated that this anomaly is a non-equilibrium effect: Figure 2 demonstrates that the magnitude of the symmetrical $G(V_g)$ depends on the rate at which V_g is swept. The slower the rate is, the smaller is the magnitude of the anomalous cusp, and in the limit of very long sweep-time the resulting FE approaches the equilibrium, anti-symmetric $G(V_g)$. It can also be seen that each trace is composed of a “normal”, anti-symmetric FE (which has the same slope for all sweeps), and an anomalous, rate-dependent cusp-like dip.

The second element that is involved in this non-equilibrium phenomenon is that the equilibrium mobility of the system is at a local minimum. This is a general property inherent to the hopping regime [3]. Electronic transport in an Anderson insulator involves hops between localized states. Each such event is a quantum mechanical tunneling from a site i to site j that are separated by r_{ij} from one another, and having in general different energies ε_i and ε_j respectively. The transition probability $i \rightarrow j$ is controlled by two factors [6]; The first is the Boltzmann factor $\exp[-\frac{(\varepsilon_j - \varepsilon_i)}{kT}]$ accounting for the energy difference between the sites, and the other is $\exp[-\frac{2r_{ij}}{\xi}]$ due

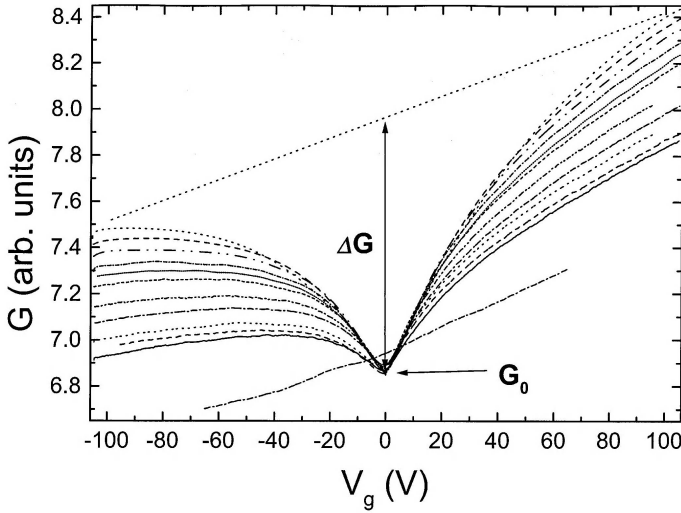


Fig. 2. The FE for a typical sample using different sweep-rates; 50, 25, 12, 6, 3, 1.5, 0.5, 0.2, 0.1, 0.05, 0.02 Volts/second (top to bottom respectively). The $G(V_g)$ trace plotted over the range $V_g = -65$ V to $V_g = 65$ V (dotted-dash curve) took over 36 h to accomplish. Note that even for this extremely slow sweep-rate $G(V_g = 0)$ still exceeds the “equilibrium-conductance” G_0 . The straight dotted-line on top is a construct used to estimate the magnitude of the excess conductance ΔG (shown here for the 50 Volts/seconds scan. Evidently, lines drawn for other scan-rates are all parallel).

to the overlap between site i and j (assuming $r_{ij} > \xi$ which is the usual situation at sufficiently low temperatures).

In equilibrium such transitions require a source of energy which is usually supplied by the phonons *i.e.*, temperature T . As T goes to zero the probability of transitions then vanishes exponentially and with it the diffusivity (and the conductivity). At any finite T the diffusivity is finite but typically small. Obviously, any source of excess energy that is coupled to the electrons would assist the hopping process and enhance conductivity. We shall see examples for that later on.

Suppose now that the system is driven out of equilibrium, which means that the occupation of states differs from the Fermi-Dirac distribution. In this case, some states below E_F that in equilibrium are occupied will be empty, and empty states above E_F will be occupied. Thus, transitions that in the equilibrium are Pauli-excluded become possible in the out-of-equilibrium state resulting in an enhanced mobility.

We have now a heuristic explanation of the anomalous cusp. The mobility increases when V_g is swept away from $V_g = 0$ because the system is taken out of equilibrium. The accompanying anti-symmetric part of the FE reflects the change of the conductance associated with the change in the carrier concentration. The fact that G increases even when charge is depleted from the system simply means that the increase in mobility in this case overpowers the decrease due to the decrease in carrier concentration. Such a situation is likely to occur in systems where n is large since the slope of the normal part of $G(V_g)$ is relatively small. Indeed, the anomalous cusp in FE studies has so far been observed in amorphous and crystalline indium-oxide films [3], granular Pb [7], granular Au [8], and granular Al films [9]. These systems are quite different in many respects. The two features that are common to all of them are that they are Anderson insulators, and they have high carrier concentration. To save space, we show here results for the indium-oxide system only. Also, all reported measurements are performed at $T \simeq 4$ K and all samples are in the strongly-localized regime having R_s in the range $5M\Omega$ to $10G\Omega$.

Now, what about the special role of $V_g = 0$? On the logic presented above the special role of $V_g = 0$ is just a consequence of the fact that $V_g = 0$ happens to be the “equilibrium-point”—the sample was cooled and equilibrated under this value of the gate voltage thus $V_g = 0$ is the point at which the system is at a local minimum.

This conjecture is amenable to a simple experimental test: if we now cool the sample, and equilibrate it with another value of V_g we expect the cusp to appear at this gate voltage. Results of such an experiment are shown in Figure 3. The sample is cooled to the measuring temperature with a voltage $V_g^o \neq 0$ held at the gate, and is allowed to equilibrate for several hours. Then, a $G(V_g)$ trace is taken by sweeping V_g across a voltage range straddling V_g^o . The resulting $G(V_g)$ now exhibits a local minimum centered at V_g^o , thus confirming our conjecture. Moreover, at the end of this initial sweep, a new gate voltage, V_g^n (differing from V_g^o by typically few volts), is applied and maintained at the gate between subsequent V_g sweeps that are taken consecutively at latter times (measured from the moment V_g^n was first applied). Each such sweep reveals *two* minima; one at V_g^o (with magnitude A_1) which fades away with time, and the other at V_g^n (with magnitude A_2) whose magnitude increases with time. For obvious reasons this experiment is referred to as the “two-dip-experiment” (TDE).

A useful aspect that can be studied with the TDE is the dependence of the characteristic relaxation time τ on various parameters of the system. Monitoring the TDE pattern amounts to studying the dynamics of the “forming” of a cusp at a newly imposed V_g^n and the “healing” of an “old” cusp at V_g^o . A characteristic-time may be defined as the time at

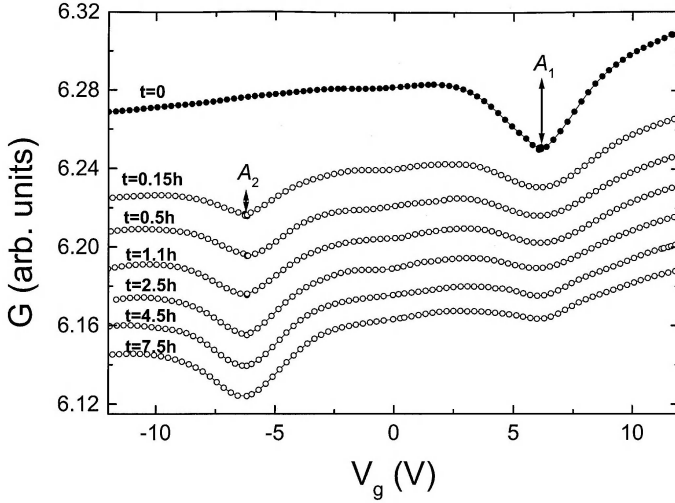


Fig. 3. A typical two-dip-experiment (TDE). Initially, the sample was cooled and equilibrated holding $V_g = 6$ V. After taking the first $G(V_g)$ trace (labeled $t = 0$), V_g was set at -6 V and subsequent sweeps taken at later times (as labeled on each trace). The arrows indicate the amplitudes of the dips. The gate-to-sample spacing in this sample is $0.5 \mu\text{m}$ hence the relatively smaller range of V_g . Traces are shifted for clarity.

which the amplitude of the cusp at V_g^n just equals the amplitude of the cusp at V_g^o (cf., Fig. 4). This τ is easily obtained by interpolation between $G(V_g)$ scans taken at different times, it is experimentally well-defined, and it is fairly independent of the particular relaxation law.

The existence of the “old” minimum, which the system “remembers” even after many hours after a new gate voltage was imposed (Fig. 3), is an intriguing characteristic of the electron glass. A somewhat analogous feature has been observed in spin glasses as well as in several structural glasses [10]. Before discussing the meaning of this peculiar memory effect let’s review some of the other glassy features this system exhibits.

2.3 Basic features of the electron-glass

Figure 5 shows the change of the conductance *versus* time after a sample has been quenched from 120 K to 4 K. Note that the lattice temperature has already reached the bath temperature (as attested by the lack of time dependence of a Ge-thermometer anchored to the sample stage) while the conductance continues to change for a very long time. The relaxation of

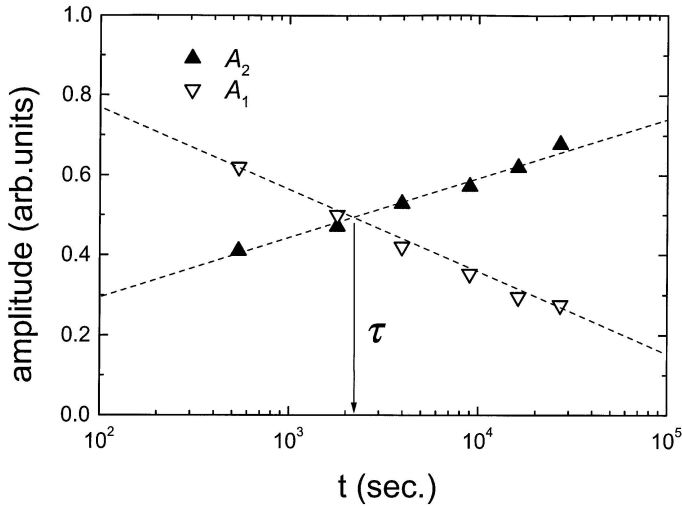


Fig. 4. The temporal dependence of the “old” and “new” dip-amplitudes (A_1 and A_2 respectively, illustrated in Fig. 3), and the empirical definition of a characteristic relaxation time τ .

the conductance appears to be logarithmic over at least five decades in time (Fig. 6). This is the analog of the “free-volume” reduction with time of a polymer glass after cool-quench [11], which also shows logarithmic dependence.

2.3.1 Slow relaxation

Being an electronic system, relaxation in the electron-glass can be measured after exciting it out of equilibrium in many more ways than in other glasses. For example, energy may be easily pumped into the electronic system by:

- changing the gate voltage;
- exposing the sample to a burst of light;
- biasing the source-drain with a sufficiently large electric field.

In all these cases, the conductance of the system increases in response to the excitation since, as explained above, excess energy imparted to the electrons enhances their mobility. Then, upon removal of the exciting agent, there is a slow relaxation of G towards its equilibrium value as illustrated in Figure 7. The common feature in these experiments is the sample was allowed to equilibrate prior to exciting it for a time much longer than over

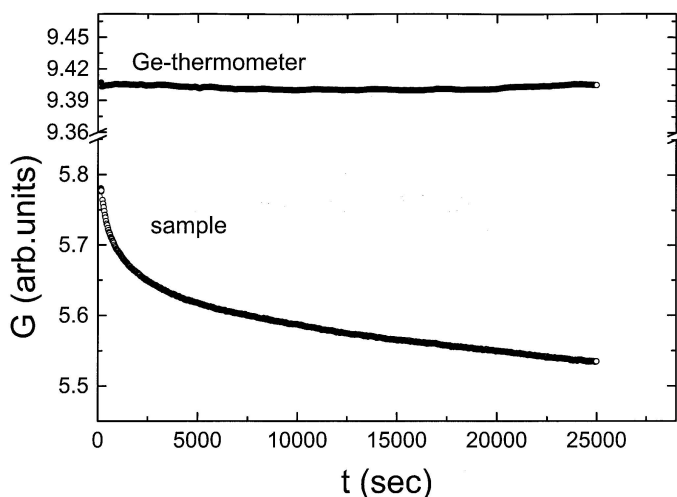


Fig. 5. Conductance *versus* time for a typical sample that was quench-cooled from 120 K to 4 K in 20 s (lower curve). The upper curve shows the simultaneous behavior of a Ge-thermometer.

which relaxation was eventually recorded. And in all these cases the relaxation law of the excess conductance ΔG was purely logarithmic, *i.e.*, $\Delta G(t) = -\log(t)$. Such a relaxation law that has no time scale is typical to many glassy systems.

2.3.2 Aging

When the time over which relaxation is monitored exceeds the equilibration time in a previous state, another property, commonly found in glasses, is observed: the relaxation-law depends on the time the system has spent under external conditions that differ from those during the relaxation that follows the removal of the exciting agent. This peculiar property of the glass is one of the aspects of “aging”, a term used to describe the fact that the relaxation law depends on the sample history. A typical aging experiment involves the following procedure. The system is allowed to equilibrate under a set of external conditions $\{X_i^o\}$ that control some macroscopic response function P . Then, $\{X_i^o\}$ is changed to $\{X_i^n\}$ for a waiting-time t_w during which $P[\{X_i^o\}]$ evolves towards $P[\{X_i^n\}]$. Finally, the “old” conditions $\{X_i^o\}$ are restored, and the response P is monitored *versus* time t starting from the moment $\{X_i^o\}$ are re-established. In a glassy system it is commonly found that $P(t)$ reflects t_w (as well as $\{X_i^o\}, \{X_i^n\}$). Namely, $P(t)$ is in general a function of both t and t_w .

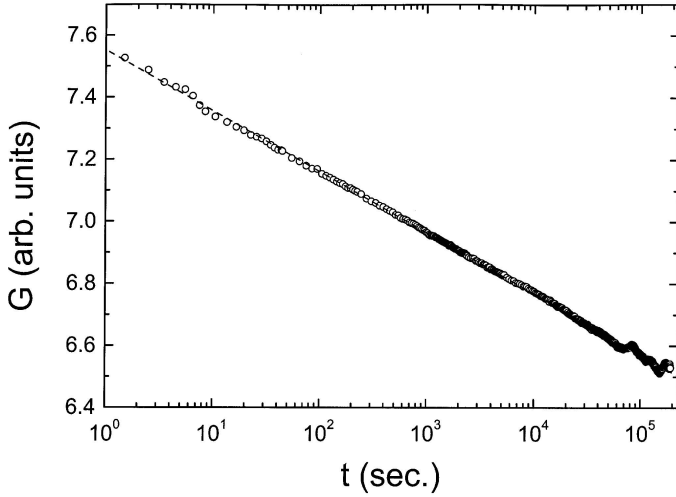


Fig. 6. Conductance *versus* time for a sample quench-cooled from 90 K to 4 K in 12 s. Note the logarithmic dependence of the excess conductance.

A special case of aging is when $P(t, t_w) = P\left(\frac{t}{t_w}\right)$. Such a behavior of the relaxation, so called “simple-aging” [12], has been recently observed in Anderson-localized indium-oxide films [13]. In these experiments $\{X_i\}$ was the carrier concentration n (controlled *via* a gate voltage), and the response P was the electronic conductance G . The aging experiment proceeded in this case as follows. The sample is cooled to the measurement temperature T_m with a voltage V_g^o held at the gate, and is allowed to equilibrate for at least 15 h. Next, still holding V_g^o fixed, one starts monitoring both the conductance G and the gate voltage V_g as function of time to obtain a baseline conductance $G_o(V_g^o, T_m)$. This typically takes 5 min. Then, the gate voltage is switched to V_g^n and is maintained there for a certain “waiting-time” t_w . Finally, the gate voltage is switched back to V_g^o and $G(t)$ is measured from this time onward. A specific experimental run is shown in Figure 8. In the following we focus on the behavior of $\Delta G(t) = G(t) - G_o$ for $t \geq 0$ (taking $t = 0$ as the time when V_g re-attains the original value V_g^o). Note that the quantities $G(t \geq 0)$ and G_o that determine $\Delta G(t)$ are measured under the *same* external conditions. This ensures that the relaxation of the conductance embodied in $\Delta G(t \geq 0)$ excludes spurious contributions such as the equilibrium (anti-symmetric) field-effect.

The behavior of $\Delta G(t \geq 0)$ for a given sample depends on several parameters. These are t_w , T_m , and $\delta V_g = |V_g^n - V_g^o|$. The most important one turns out to be the waiting-time t_w . Results for $\Delta G(t, t_w)$ at constant

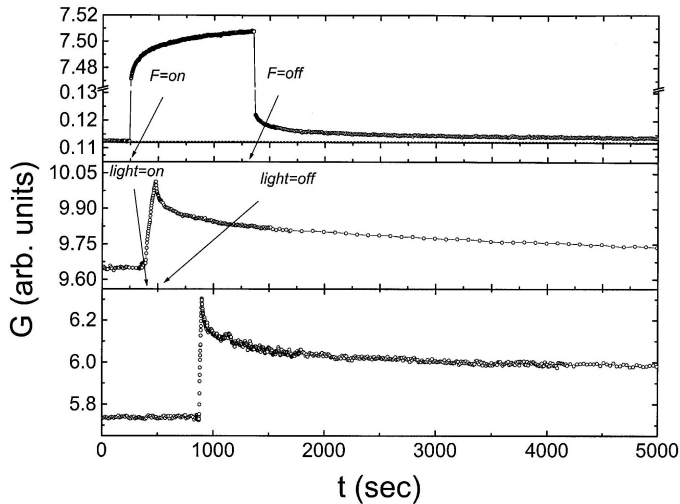


Fig. 7. Various ways to excite the electron-glass and observe slow relaxation of the conductance. Bottom graph: by changing the gate voltage – at $t \approx 900$ s V_g is changed from -50 V (at which the sample was equilibrated) to 50 V (which is held at this value for $t \geq 900$ s). Middle graph: by exposing the sample to an infra-red light source during the time marked by the arrows. Top graph: By biasing the sample with a large electric field F applied between the source and drain during the time shown. Note the large increase of G resulting from the application of F , and the slow relaxation of G after F is reduced.

T_m and δV_g are shown in Figure 9. The top graph shows $\Delta G(t)$ for 4 different t_w 's and illustrates that the waiting time significantly affects both the magnitude and shape of the relaxation. The main result is that when the relaxation data are plotted as $\Delta G\left(\frac{t}{t_w}\right)$ all curves collapse onto a single curve (bottom graph of Fig. 9). It is emphasized that this scaling *does not involve any parameter*. The only parameter used in this procedure is t_w which has in fact been *measured*. No re-scaling of the amplitude can make the $\Delta G(t)$ curves to collapse – this is accomplished entirely by normalizing the time scale by the measured waiting time.

Note that the relaxation law in this case differs qualitatively from the “free” relaxation studied in Figures 6 and 7 in that it has a characteristic time scale – the waiting time. This means that the system “remembers” how long it was allowed to (partially) equilibrate under different conditions.

Let's summarize what we have seen so far.

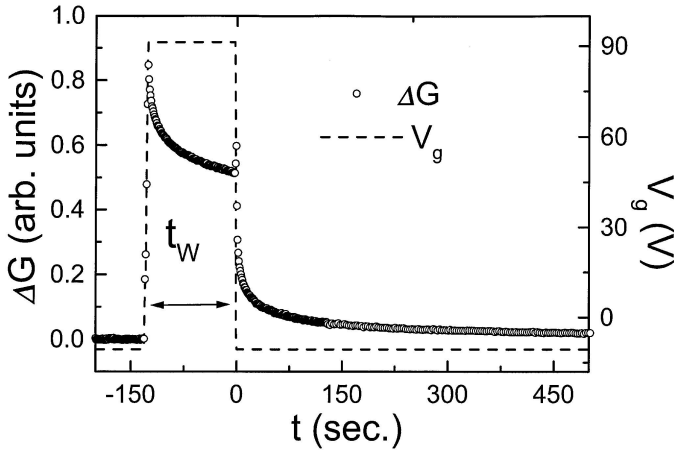


Fig. 8. Basic procedure used in the aging experiment. ΔG is the excess conductance (measured relative to the equilibrium G) monitored as function of time while V_g is switched from its “old” value to a “new” value (where it is held for t_w) and back. $t = 0$ is the time at which V_g attained its “old” (equilibrium) value.

Electronic transport in Anderson localized systems exhibit pronounced non-equilibrium effects that are analogous to well-known features of glasses. These include:

- an anomalous, time-dependent field effect characterized by a cusp-like dip in $G(V_g)$ centered around the cool-down gate voltage;
- slow conductance relaxation from an excited state that persists for many hours;
- two types of memories; Memory of the gate voltage under which the system was equilibrated, and memory of the time the system spent at a previous state (aging).

Two questions need now to be addressed. The first is what is the reason for the sluggish response of the electrons, and the second is what is the source of memory in this system. In the following, we discuss a set of experiments that seem to suggest that the answer for both questions is associated with the interactions between the electrons.

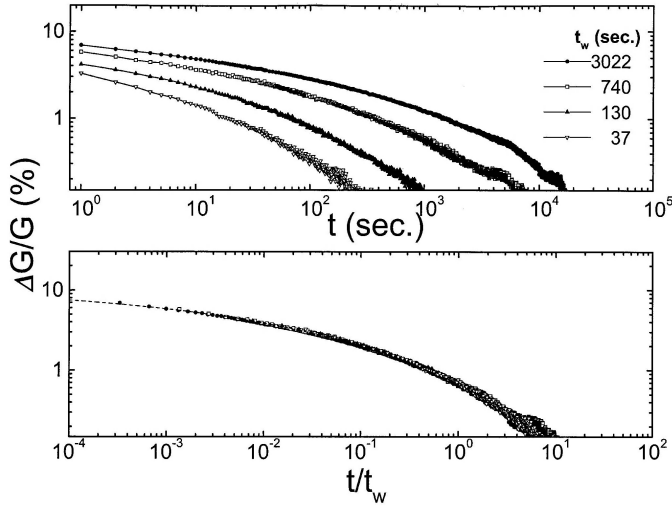


Fig. 9. The excess conductance *versus* time for $t \geq 0$ (see Fig. 8) using four different values of t_w . Upper graph: as function of t . Lower graph: same data plotted as function of the normalized time (see text).

3 The role of the electron–electron interaction

3.1 Experimental evidence for the role of interactions

The TDE has established that the electron glass retains a memory of the cusp in $G(V_g)$ at the “old” gate voltage under which it was equilibrated (Fig. 3). We now show that this “memory cusp” may be completely erased once the energy inserted to the system exceeds a certain value. This may be done, for example, by exposing the sample to a burst of IR light source (Fig. 10) or by biasing the source-drain with a large enough electric field (Fig. 11). In either case, the system loses the memory of the “old” position of the gate voltage once the IR intensity or the applied source-drain field exceeds a certain value. Not surprisingly, it turns out that when this happens, the aging phenomena are gone, and the relaxation of the conductance following these excitations reverts to the “history-independent”, logarithmic form.

Naturally, it is of interest to find out what is the energy that must be supplied to erase the memory from the system. The following experiments suggest that this energy is associated with the typical width of the FE cusp (from which an energy scale can be estimated).

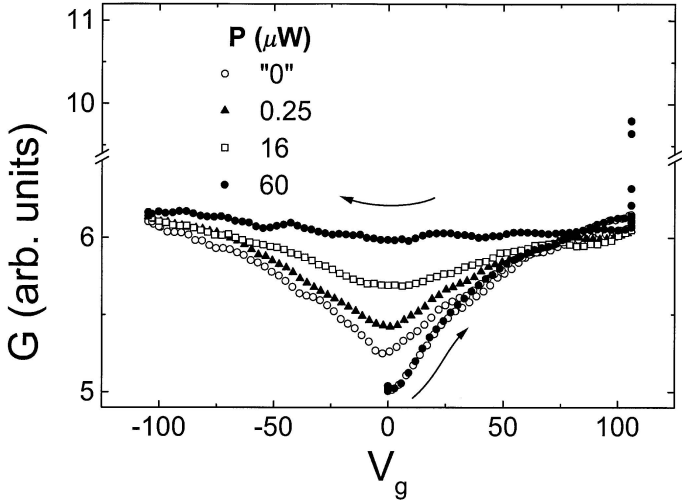


Fig. 10. Field effect traces measured after a brief exposure to IR radiation with various power levels P . Each trace starts by sweeping V_g from zero to $V_g = 106$ V (as indicated by the lower arrow) and held there for $t = 20$ s, and during 5 of these seconds the sample is exposed to IR radiation with the indicated power P). Then, V_g is swept back to -106 V (as indicated by the upper arrow).

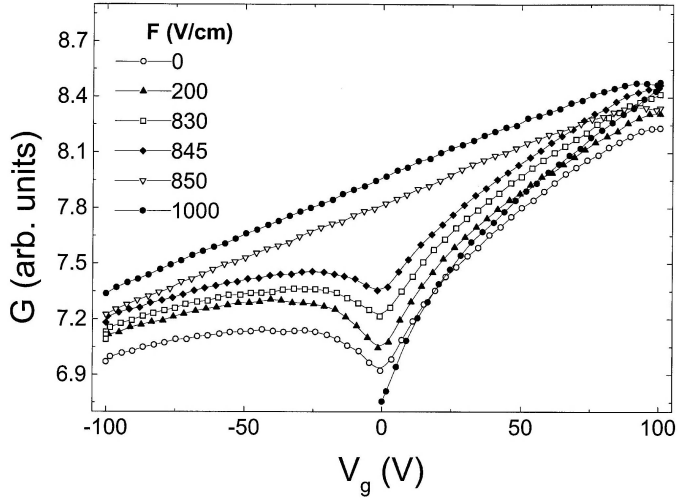


Fig. 11. Same as in Figure 10 except that instead of exposure to IR, a large source-drain electric field F is now applied for 5 of the total 20 s the sample spends at $V_g = 106$ V.

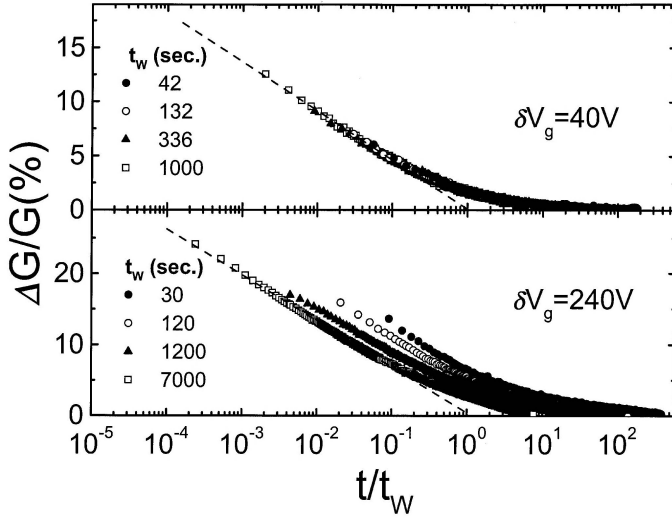


Fig. 12. The fractional change of conductance $\Delta G/G$, measured during an “aging” experiment after V_g^n is switched back to V_g^o . Data are shown for two series of experiments on the same sample employing different δV_g ’s. $V_g^o = 0$ V; $V_g^n = 40$ V and $V_g^o = -120$ V; $V_g^n = 120$ V for the top and bottom graph respectively.

In the measurements exhibited in Figure 12, we describe the outcome of the aging experiment, using the same procedure as before, while using two different sets of V_{go} and V_{gn} on the same sample. A near-perfect collapse of the data occurs when $\delta V_g = |V_g^n - V_g^o|$ is small (upper graph in Fig. 12) while when δV_g exceeds a certain value the curves begin to fall apart (lower graph). Figure 13 shows the TDE corresponding to the very same conditions. Focusing on the memory-cusp observed after V_g is first returned from V_g^n to V_g^o one can observe that it is relatively weaker for the case of the larger δV_g . Namely, the fact that δV_g is large degrades the memory in the system. This degradation prevents the curves from collapsing when δV_g is large enough. From Figure 13 it is seen that this occurs when the two dips are well separated. This suggests that the characteristic energy needed to destroy the correlations responsible for the system memory is the typical width of the anomalous FE cusp.

These experiments then call attention to the FE cusp and in particular, to its characteristic width. It turns out that the width Γ is independent of the way the measurement is performed. Namely, the shape of the cusp in the $G(V_g)$ scans does not depend on the scan-rate, the temperature, the static disorder, or a magnetic field (measured up to $H = 20$ T). All these factors do

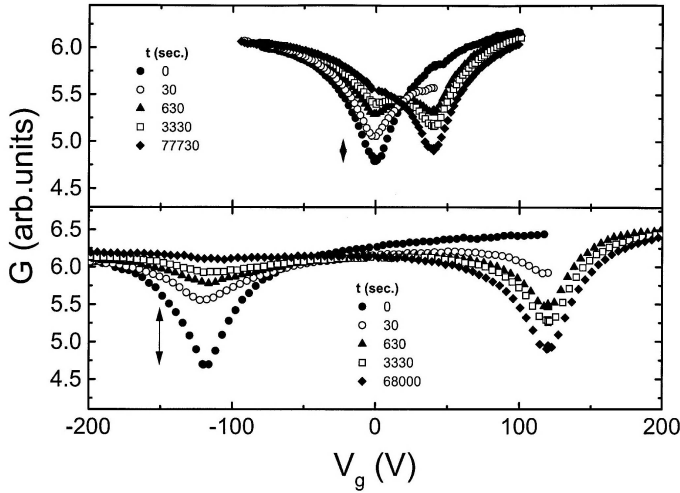


Fig. 13. $G(V_g)$ traces measured during two TDE performed on the same sample (and the same δV_g 's) as in Figure 12. Note that upon sweeping V_g back from V_g^n to V_g^o there is a larger loss of the “old” dip-amplitude in the bottom graph (quantified by the length of the arrows). It was confirmed that this difference is due to the larger δV_g rather than to difference in the sweep-time by adjusting the sweep rates such that the sweep time from V_g^n to V_g^o (or back) is the same.

affect the *magnitude* of the cusp but they have no effect on its *shape* (except for temperature smearing). On the other hand, the cusp width changes quite significantly with the carrier concentration n as shown in Figure 14. The data shown in the figure was taken on a series of amorphous indium-oxide films prepared by e-gun evaporation of 99.999% pure In_2O_3 as described elsewhere [14], and, by a judicious choice of evaporation-rate/partial- O_2 -pressure, the carrier-concentration n (estimated from Hall-effect measurements at room temperature) of the films was varied to produce samples with different n in the range 10^{19} – 10^{22} cm^{-3} . The samples had lateral dimensions of 0.5×0.5 mm^2 and thickness of 200 ± 20 Å. The degree of disorder for a specific composition was deliberately fine-tuned by thermal annealing in such a way that at $T = 4$ K all samples had similar sheet-resistance R_S (typically, $R_S \approx 5$ MΩ). As mentioned earlier, all data reported here were taken at this convenient temperature. Figure 15 compares the FE taken for two of these samples having different n 's, and illustrates the experimental definition of Γ .

Figure 14 shows that Γ depends on the carrier concentration in a systematic way – the higher n is the wider is the cusp. Even more dramatic is

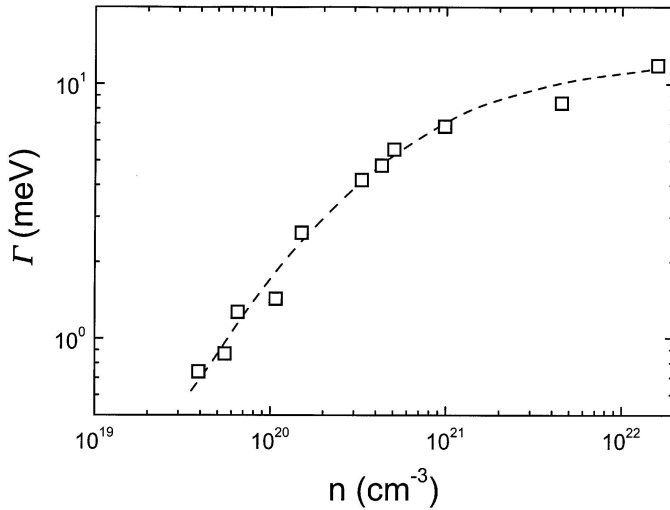


Fig. 14. The dependence of the $G(V_g)$ dip-width Γ on the carrier concentration n in a series of amorphous indium-oxide films. See Figure 15 for the experimental definition of Γ . The dashed line is a guide for the eye.

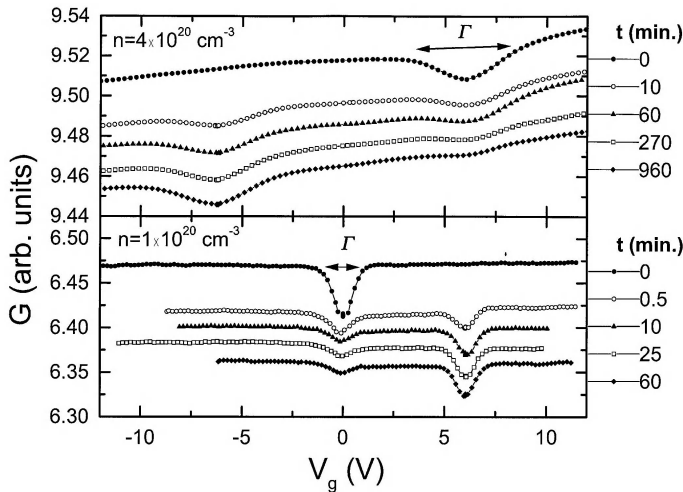


Fig. 15. TDE on two typical amorphous indium-oxide samples with different n 's illustrating the way Γ is estimated from the data. Note the larger Γ for the sample in the top graph, as well as the longer time it takes to equalize the "old" and "new" dip-amplitudes for this sample. Traces are shifted for clarity.

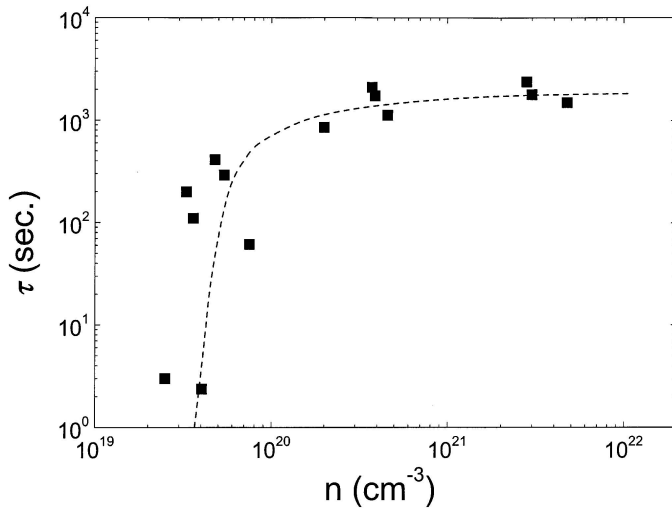


Fig. 16. The dependence of τ (defined by the procedure illustrated in Fig. 4) on the carrier concentration n in a series of amorphous indium-oxide films.

the dependence of τ on n in these series of samples. This is illustrated in Figure 16 for the same series of samples where τ was defined by the TDE as explained above (*cf.*, Figs. 3 and 4). Note that all these samples have essentially the same conductance, which means that the basic transition rates that determine G should be similar. Likewise, as far as the measuring circuit is concerned, these samples are nearly identical. The reason for the vastly different relaxation times must therefore be associated with the different n . One can rule out the possibility that, given similar G , samples with larger n have larger disorder, and this leads to slower dynamics: increasing the disorder in a sample (say, R_s is changed from $5M\Omega$ to $50G\Omega$) while keeping n fixed increases τ by typically 20–25%. This effect is much smaller than the three orders of magnitude change of τ caused by varying n over the range shown. We are forced then to look for another explanation.

A natural explanation of these results is that they reflect the role played by the inter-particle interactions. Indeed, increasing n means that the electrons are packed closer, and since the interaction strength usually diminishes with the inter-particle separation, we expect that interactions will be more conspicuous for larger n . That the contribution of interactions becomes more important with increased density is the rule in most many-body problems, as *e.g.*, in gases – the more dilute a gas is the closer it is to being “ideal”. An exception to this rule is the case of the metal. Due to the peculiar property of screening the interactions in a metal are less important

when n is large. A fundamental difference between a metal and an Anderson insulator is the lack of screening in the latter, which restores the “normal” dependence of the interactions on the carrier concentration.

3.2 The Coulomb gap

These considerations lead us to discuss the role of interactions in the transport properties of Anderson insulators. This is a formidable problem, and despite intensive research over more than three decades, our understanding of these issues is at best rudimentary. It is not even clear, whether interactions enhance or diminish the conductivity. There is however one issue that seems to be indisputable – the interactions modify the single-particle density-of states (DOS). This has been predicted on general grounds by Pollak in 1970 [15]. Five years later, Efros and Shklovskii [16] used for concreteness the long-ranged Coulomb interaction to show that the DOS of the localized system must vanish at the chemical potential, namely, $N(\varepsilon) = 0$ when $\varepsilon = 0$.

The existence of this so called Coulomb-gap has been confirmed by computer simulations [2]. The detailed way $N(\varepsilon)$ depends on ε and on the parameters of the system is somewhat different, depending on the specific assumptions and algorithms used in the simulations. Nevertheless, several features are commonly found in all such simulations:

- 1 the Coulomb-gap is “soft” – $N(\varepsilon)$ vanishes only for $\varepsilon = 0$, and it increases monotonically for $|\varepsilon| > 0$;
- 2 the characteristic width of this anomaly (the range of energy over which $N(\varepsilon)$ falls below the non-interacting value), increases with the carrier-concentration n (or with the thermodynamic density of states $\frac{\partial n}{\partial \mu}$);
- 3 the Coulomb-gap is anchored to the chemical potential. This feature is shared by a group of phenomena, called “Fermi-edge-singularities” that are characterized by an anomaly in the DOS centered at E_F . Examples are the Kondo effect, the BCS-gap in a superconductor, and the Altshuler-Aronov cusp in the DOS of a disordered metal [17]. All these DOS anomalies result from some underlying interaction. When a new chemical potential is imposed (say by changing the carrier concentration), a specific modulation in the DOS begins to form at the new “would-be” chemical potential. At the same time, the anomaly originally centered at the “old” chemical potential fades away. Both processes take a finite time to accomplish, although the question of how long it takes is rarely asked [18].

It is interesting to note that the anomalous cusp in our $G(V_g)$ experiments show qualitatively all these features. In particular, Γ increases with n (Fig. 14), and point 3 above describes a scenario that is reminiscent of the evolution of the TDE (Fig. 3). Namely, the appearance of a cusp-like dip centered at a specific gate-voltage that was imposed and held on the system for a certain time. The simplest way we can understand such a feature is if electron-electron interactions are involved. Note that upon setting a particular V_g , say V_g^o the system will eventually establish the corresponding chemical potential. In the presence of interactions (and disorder), a dip in $N(\varepsilon = V_g^o)$ will be created and once V_g is moved to another value, say, V_g^n a similar modulation will start to build up at $N(\varepsilon = V_g^n)$ while the one around V_g^o will fade away with time. It seems plausible to assume that the modulation in $N(\varepsilon)$ translates into an energy dependent G . This seems a natural way to explain the occurrence of the dips in $G(V_g)$. We are not aware of any explanation for this memory effect without the assumption of interactions being involved.

The details of how $N(\varepsilon)$ relates to G are by no means well understood. In fact, the picture described above has some basic difficulties that should be stressed. First, the Coulomb-gap is a *single-particle* DOS which strictly speaking, is a property that affects a measurement done on a time scale faster than any relaxation in the system *e.g.*, as in tunneling or photo-emission experiments. The cusp in $G(V_g)$ is a signature in the conductance, which is measured under “mixed-conditions”; on one hand it is carried on time scale evidently shorter than *some* relaxation processes. On the other hand, the sweep rate of V_g is never fast enough to exclude *all* relaxation processes (some of them may occur on the scale of inverse phonon frequencies, *i.e.*, $\approx 10^{-12}$ s). Therefore $G(V_g)$ cannot faithfully monitor the single-particle DOS although it might conceivably reflect some of its characteristics such as its shape, and typical width. Secondly, the Efros-Shklovskii’s Coulomb gap is a classical model and does not take into account quantum and spin effects, while both may be important in the real system [19].

3.3 Theoretical treatment of relaxation in the presence of interactions

The possible relevance of the Coulomb-gap to the time evolution of the anomalous cusp in the FE has been recently considered by Clare Yu [20]. She has used a simplified version of the Efros-Shklovskii model to calculate how long it takes the Coulomb gap to form. Interestingly, her results (*cf.*, Fig. 1 in Ref. [20]) bear a considerable resemblance to the time-evolution of the cusp in the FE experiments shown in Figure 17. In particular, the time scale in the calculations is quite comparable to the experimentally observed values.

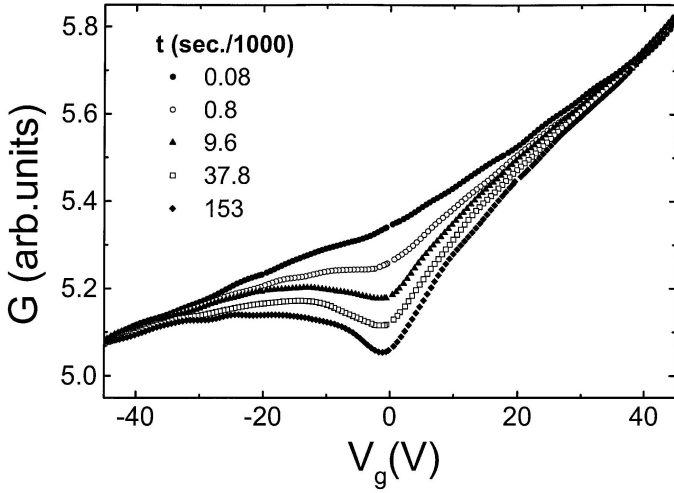


Fig. 17. $G(V_g)$ traces taken at various times t after the sample was quench-cooled from 100 K to 4.1 K. This cooling-cycle procedure was repeated for each trace using different values of t as indicated. Compare with Figure 1 in reference [20].

A different approach to the question of how interactions affect energy relaxation in Anderson insulators was taken by Pérez-Garrido *et al.* [21]. These authors performed Monte-Carlo simulations of the energy relaxation for a localized system using three different scenarios: Coulomb-interaction, short-range-interaction, and no-interaction between the electrons. For the interacting cases, they argued that the non-equilibrium properties of these systems are affected by dynamic correlations in the motion of electrons. This in turn requires knowledge of the low-lying states and energies of the system, which they obtained as a first stage of the calculations. Then, the Monte-Carlo simulation proceeded by letting the computer select the fastest route for the system to dissipate energy *via* transitions involving these many-particle states. In all three types of conditions, they found an initial (power-law) slow-relaxation up to a maximal time t_x . For longer times ($t \geq t_x$) the relaxation became faster (presumably ergodic). The important finding is that for any given set of parameters (disorder, system-size, and temperature), t_x was largest for the case of Coulomb-interaction, and smallest for the non-interacting system. In all cases, t_x was found to increase with the system-size, which was rather limited ($\leq 10 \times 10 \times 10$ sites). Yet, even for such small systems the simulations yielded t_x of the order of *days* for the Coulomb-interacting case thus confirming that relaxation times as long as experimentally observed are quite feasible when

long-ranged interactions are present. For the non-interacting system t_x was many orders of smaller. These results clearly demonstrate the dramatic role that interaction could play in slowing down energy relaxation.

The question is what are the constraints imposed by the interactions that hinder energy relaxation processes. A possible answer for this question may be found in the computer work performed by Baranovskii *et al.* [22]. These authors found that the “true” ground state of an interacting system could not be reached by just single-particle transitions. Rather, the system energy, after being initially reduced by fast single-particle transitions, “hangs” at a state (termed “pseudo-ground-state”) having higher energy than the equilibrium state (and thus exhibiting higher conductance). Further reduction in energy presumably must involve correlated, many-particle transitions. The latter are exponentially rare events and this leads to a sluggish, ever-slowing process.

Such considerations suggest that in the limit of a dilute system relaxation would become much faster. This is indeed observed in our experiments (Fig. 16) as a sharp drop in τ below a certain value of n . This may be understood as follows. The unscreened Coulomb interaction has no characteristic spatial scale but its magnitude does go down with the inter-particle separation r . Electrons that are separated by $r > L$ with L given by $\frac{e^2}{\kappa L} \approx \frac{\hbar^2}{2m^*\xi^2}$ are essentially uncorrelated. Here ξ is the localization length, κ is the dielectric constant of the medium, and m^* is the effective mass. The physical reason is that once the disorder energy $\frac{\hbar^2}{2m^*\xi^2}$ exceeds the Coulomb repulsion $\frac{e^2}{\kappa L}$ the electrons distribution is controlled by the random potential of the ions (*i.e.*, disorder) rather than by the long-range Coulomb interaction. The condition for being in the dilute phase is thus: $n_c L^3 \approx 1$ namely $n_c^{\frac{1}{3}} \approx \frac{\kappa \hbar^2}{2m^* e^2 \xi^2}$. Note that this condition depends only weakly on disorder because $\kappa = \kappa(\xi)$ and near the metal insulator transition [23] $\kappa \propto \xi^2$. Taking $\kappa \approx 10$, $m^* \approx 10^{-27}$ gm, and $\xi \approx 10$ Å as typical values one gets $n_c \approx 10^{19}$ cm $^{-3}$ which is in good agreement with our findings (Fig. 16).

Obviously, a more realistic model needs to be developed to treat this problem. Nevertheless, it is clear even from our crude picture that a long τ is favored by high-density systems such as indium-oxide and granular metals and less expected in lightly doped semiconductors. This may be the reason why non-ergodic effects of the kind described here have not yet been observed in impurity-band systems.

4 Concluding remarks

We have reviewed some of the experimental evidence for non-ergodic effects in the transport properties of Anderson insulators. These effects are

restricted to the strongly localized phase of the metal-insulator transition and they are absent in the diffusive regime. In other words, the glassy phase is a property of the Anderson insulator, which means that the glass transition coincides with the metal-insulator transition. In three dimensions this transition is believed to occur at a critical amount of disorder. Therefore, the first condition for the existence of the electron-glass is a sufficiently strong disorder.

The role of temperature in this transition is less clear. The magnitudes of the non-equilibrium effects described here are considerably weakened by raising the temperature. For example, the amplitude A of the anomalous cusp in the FE depends on temperature as [24] $A = \exp[-\frac{T}{T^*}]$. Although such a functional dependence does suggest a characteristic temperature (*i.e.*, T^*), it is clearly not the usual glass-temperature as defined in other, more familiar glassy systems. In particular, the characteristic relaxation time τ does not show any tendency to diverge at or below T^* . In fact, τ seems to be essentially T -independent over a wide temperature range [13], which is quite unlike the behavior of A . This may suggest that motion in phase-space of the electron-glass is controlled by topological rather than energy considerations. That would be the case if the relevant barriers are crossed by quantum tunneling rather than by thermal activation. These peculiar aspects of the electron-glass need obviously further experimental and theoretical investigation.

These lecture notes are based on a series of studies performed in collaboration with Michael Pollak. The author acknowledges illuminating discussions with A. Vaknin, and V. Orlyanchik. The research has been supported by grants administered by the US-Israel Binational Science Foundation, and the German-Israel Science Foundation.

References

- [1] N.F. Mott and E.A. Davis, *Electronic Processes in Non-Crystalline Materials* (Clarendon Press, Oxford, 1979).
- [2] J.H. Davies, P.A. Lee and T.M. Rice, *Phys. Rev. Lett.* **49** (1982) 758.
- [3] M. Ben-Chorin, Z. Ovadyahu and M. Pollak, *Phys. Rev. B* **48** (1993) 15025.
- [4] P.W. Anderson, *Phys. Rev.* **109** (1958) 1492.
- [5] N.W. Ashcroft and N.D. Mermin, *Solid-State Physics* (Holt, Rinehart and Winston, 1976) 262.
- [6] A. Miller and E. Abrahams, *Phys. Rev.* **120** (1970) 745.
- [7] G. Martinez-Arizala, D.E. Grupp, C. Christiansen, *et al.*, *Phys. Rev. Lett.* **78** (1997) 1130.
- [8] C.J. Adkins, J.D. Benjamin, J.M.D. Thomas, *et al.*, *J. Phys. C* **17** (1984) 4633.
- [9] T. Grenet (private communication).
- [10] S. Rogge, D. Natelson and D.D. Osheroff, *Phys. Rev. Lett.* **76** (1996), 268.
- [11] L.C.E. Struik, *Physical aging in amorphous polymers and other materials* (Elsevier, Amsterdam, 1978); L.M. Hodge, *Sci.* **267** (1995) 1945.

- [12] A. Conoglio and M. Nicodemi, *Phys. Rev. E* **59** (1999) 2812.
- [13] A. Vaknin, Z. Ovadyahu and M. Pollak, *Phys. Rev. Lett.* **84** (2000) 3402.
- [14] Z. Ovadyahu, *J. Phys. C: Solid State Phys.* **19** (1986) 5187; O. Cohen and Z. Ovadyahu, *Phys. Rev. B* **50** (1994) 10442.
- [15] M. Pollak, *Discuss. Faraday Soc.* **50** (1970) 13.
- [16] A.L. Efros and B.I. Shklovskii, *J. Phys. C* **8** (1975) L49.
- [17] B.L. Altshuler and A.G. Aronov, *Zh. Eksp. Theor. Fiz.* **77** (1979) 2028 [*Sov. Phys. JETP* **50** (1979) 968]; Y. Imry and Z. Ovadyahu, *Phys. Rev. Lett.* **49** (1982) 841.
- [18] Y. Meir, P. Nordlander and M. Pustilnik, *Phys. Rev. Lett.* **83** (1999) 808.
- [19] A. Vaknin, Z. Ovadyahu and M. Pollak, *Phys. Rev. Lett.* **81** (1998) 669.
- [20] C. C. Yu, *Phys. Rev. Lett.* **82** (1999) 4074.
- [21] A. Pérez-Garrido, M. Ortuño, A. Díaz-Sánchez and E. Cuevas, *Phys. Rev. B* **59** (1998) 5238.
- [22] S.D. Baranovskii, A.L. Efros, B.L. Gelmont and B.I. Shklovskii, *J. Phys. C Solid State Phys.* **12** (1979) 1023; E.I. Levin, V.L. Nguyen, B.I. Shklovskii and A.L. Efros, *Zh. Eksp. Theor. Fiz.* **92** (1987) 1499 [*Sov. Phys. JETP* **68** (1989) 1081].
- [23] Y. Imry and Y. Gefen, *Phil. Mag. B* **50** (1984) 203.
- [24] A. Vaknin Z. Ovadyahu and M. Pollak, *Europhys. Lett.* **42** (1998) 307.

COURSE 12

**PROTEINS: STRUCTURAL, THERMODYNAMIC
AND KINETIC ASPECTS**

A.V. FINKELSTEIN

*Institute of Protein Research, Russian
Academy of Sciences,
142290 Pushchino, Moscow Region,
Russia*



Contents

1	Introduction	651
2	Overview of protein architectures and discussion of physical background of their natural selection	651
2.1	Protein structures	651
2.2	Physical selection of protein structures	656
3	Thermodynamic aspects of protein folding	670
3.1	Reversible denaturation of protein structures	670
3.2	What do denatured proteins look like?	673
3.3	Why denaturation of a globular protein is the first-order phase transition	677
3.4	“Gap” in energy spectrum: The main characteristic that distinguishes protein chains from random polymers	681
4	Kinetic aspects of protein folding	685
4.1	Protein folding <i>in vivo</i>	685
4.2	Protein folding <i>in vitro</i> (in the test-tube)	685
4.3	Theory of protein folding rates and solution of the Levinthal paradox	692

PROTEINS: STRUCTURAL, THERMODYNAMIC AND KINETIC ASPECTS

A.V. Finkelstein

1 Introduction

Proteins are molecular machines, building blocks, and arms of a living cell. Enormous variety of protein functions is based on their high specificity for the treated molecules that resembles the key-and-lock relationship. This specificity requires a definite, stable and rather rigid spatial structure of the operating protein.

Protein is a heteropolymer with unique (for each protein) sequence of links. In an “operating” protein its chain is folded in a strictly specified (“*native*”) structure. In the late 1950s, Perutz and Kendrew solved the first structures of protein crystals and demonstrated highly intricate protein spatial structures [1,2]. Later, the identity (to small fluctuations) of structures of various proteins in a crystal and in solution was demonstrated by NMR spectroscopy [3].

Protein physics is grounded on three fundamental experimental facts: (i) many proteins have well defined three-dimensional structures [1–3]; (ii) many protein chains are capable of self-organization, *i.e.*, they form their native structures spontaneously in appropriate environment [4,5], and (iii) the native state of many proteins is separated from the unfolded state of the chain by the “all-or-none” phase transition [6]. The latter ensures robustness of protein action.

The aim of these lectures is to overview modern understanding of physical principles of arrangement and self-organization of protein structures.

2 Overview of protein architectures and discussion of physical background of their natural selection

2.1 Protein structures

Before considering protein physics, it is not out of place to remind to physical audience what the proteins are and how do they look like.

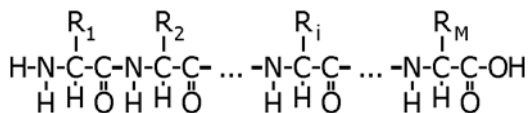


Fig. 1. Chemical structure of protein chain: regular backbone with various side groups.



Fig. 2. A piece of amino acid sequence of protein chain. The residues with hydrophobic (non-polar) side chains are indicated with shaded boxes. The residues with polar (hydrophilic) side chains are not shaded; those of them which have positive or negative charges at normal pH (pH7) are marked by + or -. The size of a box is proportional to the amino acid volume.

Proteins are built up by amino acids that are linked into a *peptide chain* (this was found by Fischer at the beginning of the 20th century). The chain consists of a chemically regular backbone (“main chain”) from which various side chains (R_1, R_2, \dots, R_M) project (Fig. 1).

In the early 1950s Sanger showed that the *primary structure*, *i.e.*, the sequence R_1, R_2, \dots, R_M of amino acid residues in protein chain is unique for each protein (Fig. 2). The “residue” (Fig. 3) is the portion of a free amino acid that remained after polymerization. There are 20 main natural amino acid residues; their position in the protein chain is gene-encoded.

Three-dimensional (3D) structures of protein chains are maintained, first of all, by hydrogen bonds and hydrophobic interactions, as well as by electrostatic and van der Waals forces [7]. Side chains of the 20 natural amino acids are different with respect to these interactions (Fig. 2); therefore, different sequences stabilize different 3D structures. However, the main chain of nearly all natural amino acids has NH and CO groups (Fig. 1) that can form similar hydrogen bonds, and this leads to formation of regular *secondary structures* of polypeptide chains [8,9] (α -helices and β -sheets being the most important of them); large pieces of these secondary structures (Fig. 4) play a key role in protein architectures [10,11].

Proteins “live” under various environmental conditions leaving an obvious mark on their structures. The less water is around, the more valuable the hydrogen bonds are. These bonds reinforce the regular, periodic 3D structures of protein backbone, and thus, the less water is around, the more regular the stable protein structure ought to be.

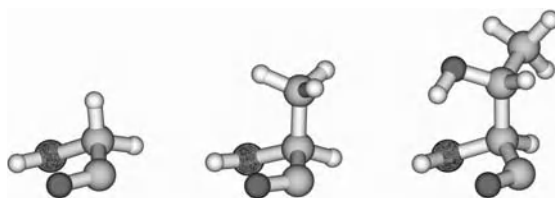


Fig. 3. Some of the amino acid residues. The backbone (HN-CH-CO) is at the bottom, the side chain looks up. From left to right: glycine (Gly), which has no side group (it consists of only a single H atom: this is the only mirror-symmetric natural amino acid); alanine (Ala), whose side chain consists of CH_3 group (like all other natural amino acids with side groups, Ala can have two dissymmetric forms that differ in the direction of the side group relative to the backbone; only one of these forms, the “L” form shown in the figure, is used in proteins); threonine (Thr), whose side chain consists of HO-CH-CH_3 group. All amino acids have rotational degrees of freedom in the backbone; large side-groups, like Thr, have rotational degrees of freedom in the side chain as well. H-atoms are shown in white, C-atoms in light-gray, N-atoms in dark-gray, O-atoms in black.

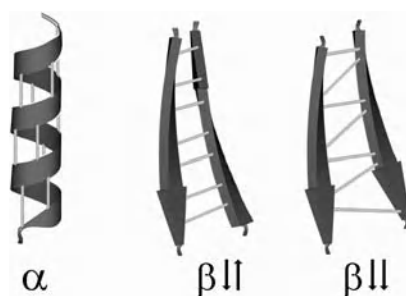


Fig. 4. The secondary structures of protein chains: α -helix and two kinds of β -sheets composed of extended (antiparallel or parallel) β -strands. Strips and arrows trace the backbone; side groups are not drawn. Light lines indicate the backbone-backbone hydrogen bonds.

Roughly, according to their “environmental conditions” and general structure, proteins can be divided into three large groups (Fig. 5).

- 1) Fibrous proteins form vast aggregates; their structure is usually highly hydrogen-bonded, highly regular and maintained mainly by interactions between different polypeptide chains.
- 2) Membrane proteins “live” in a water-lacking membranes (although partly project into water). Their intramembrane portions are highly

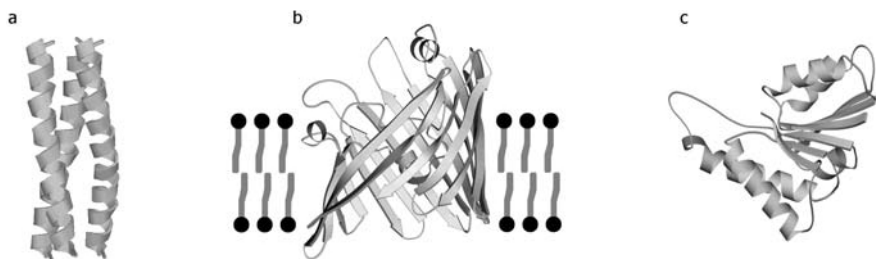


Fig. 5. Typical shapes of proteins. Secondary structures are outlined schematically, side chains are not shown for the sake of simplicity. **a)** A aggregate of fibrous proteins (a fragment); **b)** membrane protein (lipids, with polar heads and non-polar tails, are shown only schematically); **c)** water-soluble globular protein.

regular (like fibrous proteins) and highly hydrogen-bonded, but restricted in size by the membrane thickness (30–40 Å).

- 3) Water-soluble (living in water) globular proteins are less regular (especially the small ones). Their structure is maintained by interactions of the chain with itself and sometimes with various other molecules (co-factors). Typical size of the globule is 30–50 Å.

Lastly, small or hydrophobic group-poor polypeptides can have no fixed structure but obtain it by interacting with other molecules (all the above mentioned well-structured proteins also loose their unique structures under “denaturing”, *i.e.*, structure-destroying conditions).

The above classification is certainly extremely rough. Some proteins may comprise a fibrous “tail” and a globular “head” (like myosin, for example), or a membrane and a globular part, and so on.

To date we know $\sim 10^6$ protein sequences and $\sim 10^4$ three-dimensional (3D) protein structures. Most of known 3D structures belong to water-soluble globular proteins: they are easily isolated as separate molecules and then studied by X-ray in crystals and by NMR in solution. As to membrane and fibrous proteins, their solved 3D structures are few.

For similar experimental reasons, protein folding is also better studied for water-soluble globular proteins.

That is why, when speaking about “protein structure” and “protein structure formation” one often actually means regularities shown for water-soluble globular proteins only. This must be kept in mind when reading books and papers.

Following this tradition, I will also concentrate on water-soluble globular proteins. Moreover, I will concentrate on relatively small “single-domain”

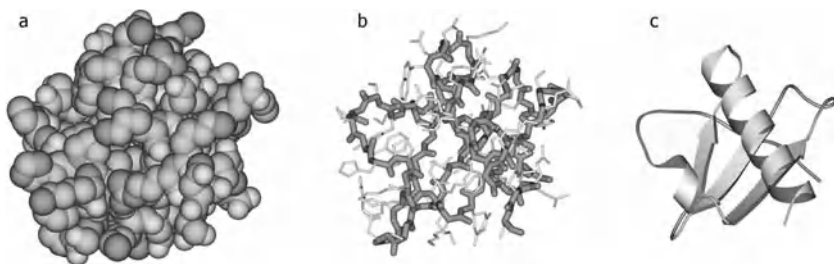


Fig. 6. The structure of a small globular protein, interleukine 8, shown as a space-filling atomic model **a**), as a wire model with the backbone outlined by dark line **b**), and as a ribbon diagram that outlines secondary structures **c**). This and the other drawings of protein structures is done using their PDB [12] coordinates and the MOLSCRIPT [13] program.

proteins that form one compact protein globule. Larger globular proteins consist of a few sub-globules, or “domains”.

Protein architectures, especially those of water-soluble globular proteins, are complex and of great diversity, unlike the universal double helix of DNA. Nevertheless, certain “standard” motifs are detected in proteins as well. In small or medium-size proteins, they envelop the entire globule; in larger globular proteins, they envelop their compact domains rather than a whole molecule.

Let us consider a small globular protein more attentively. Although Figure 5 seemingly shows that there is an ample empty space in the interior of the protein, and can create an impression that the protein is “soft”, this is not true. Protein is hard: its chain is packed tightly, atoms against atoms (Fig. 6a). The space-filling representation is inconvenient, though, for studying protein anatomy, its skeleton, its interior; these can be seen using the wire model with “transparent” atoms and a clearly seen pathway of the protein chain (Fig. 6b).

The space-filling model (Fig. 6a) gives no idea even of the polymeric nature of protein; it only shows the surface of a globule. This model, as well as the detailed wire model shown in Figure 6b, is useful for studying protein function: it is physico-chemical and geometrical properties of the surface that determine specificity of the protein activity, whereas the protein skeleton (Fig. 6c) is responsible for creation and maintenance of this surface.

The accumulated experience shows that comparison and classification of protein structures are to be based on the arrangement of secondary structures forming a skeleton of the protein (see Figs. 5 and 6c where the side chain atoms are stripped off and secondary structure elements stand out). Therefore, these simplified pictures are widely used.

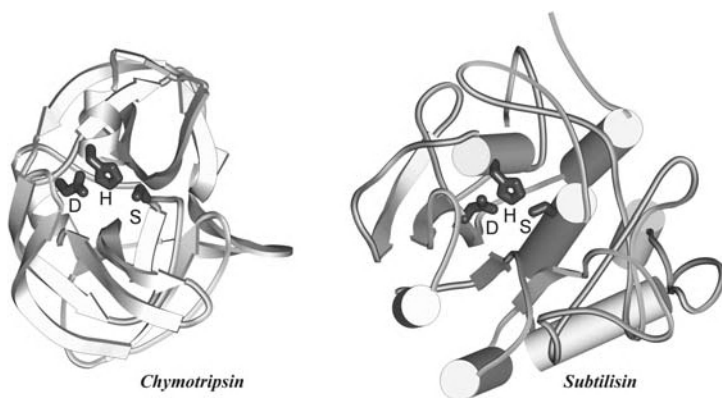


Fig. 7. Two proteins structurally different but almost identical in function (serine proteases): chymotrypsin, formed by two β -structural domains, and subtilisin, a single-domain protein formed by β -structure and many α -helices (cylinders), some of which pertain to the active site. In spite of very different chain folds, their catalytic sites comprise the same key residues similarly positioned in space: Ser195 (S), His57 (H) and Asp102 (D) in chymotrypsin and Ser221 (S), His64 (H) and Asp32 (D) in subtilisin.

Active (*e.g.*, catalytic) site usually occupies only a small part of the protein (Fig. 7). Therefore, it is not a surprise that proteins with similar functions (and similar active sites) sometimes have completely different architectures (Fig. 7), while many proteins with completely different functions often share a common folding pattern (Fig. 8).

Thus, as shown by a many examples (see [10,11]), the protein function and its folding pattern are not tightly connected. It seems that the main task of the bulk of the protein chain is to be hard and provide a solid foundation for the active site.

However, many protein architectures contain inherent cavities that are often used by active sites, since a molecule coming into the cavity is surrounded by many amino acid residues of the protein (Fig. 9), which can be used to create various active sites, no matter what function they perform. Another typical position of the active site is an interface of domains (see chymotrypsin in Fig. 7).

2.2 Physical selection of protein structures

Now we will discuss general rules established for 3D folds of globular proteins and physical reasons that may underlie the empirical observations.

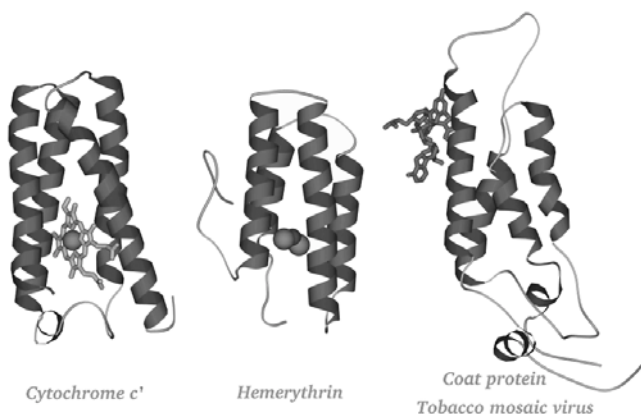


Fig. 8. Three proteins similar in overall architecture (comprising four α -helices each), but different in function (cytochrome, electron carrier; hemerythrin, oxygen carrier; and virus coat protein, which binds RNA and the other coat proteins). Protein chain is shown as a ribbon; co-factors are shown as follows: wire models, heme (in cytochrome) and RNA fragment (in coat protein); gray balls, iron ions (in the heme of cytochrome and in hemerythrin); the black ball is an iron-bound oxygen (in hemerythrin).

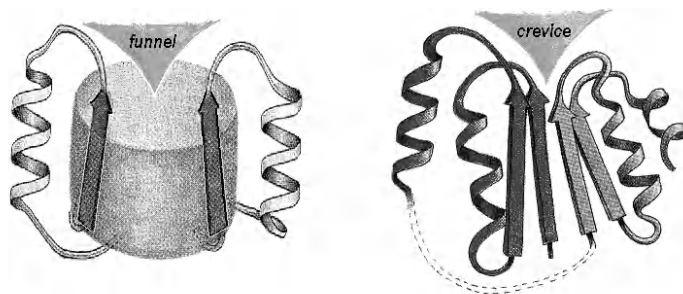


Fig. 9. Typical locations of the active sites: **a**) in the “funnel” on the axis of the “TIM barrel” proteins (see Fig. 10), and **b**) in the crevice formed by drawn apart loops in the “Rossmann fold” (see subtilisin in Fig. 7). Adapted from [10].

It has been shown that majority of 3D protein folds fit a limited set of folding patterns [14–18], though many proteins, very similar in their folds, seem to have no common ancestry or function. This observation forms a basis of modern classifications of protein folds [19–21] that give their convenient survey (Fig. 10).

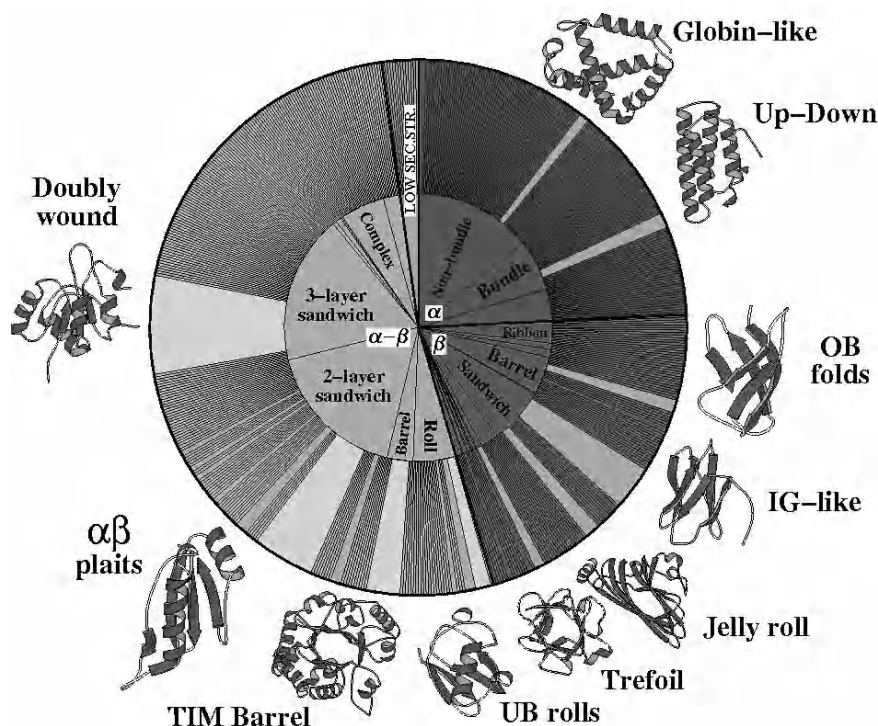


Fig. 10. “Catherine plot” showing the distribution protein folds amongst different structural classes (“ α ”, “ β ”, etc.), different architectures within the classes (“Non-bundle”, etc.) and different folding patterns within architectures (“Globin-like”, etc.). The sector width is proportional to the fold’s occurrence. The drawings of the most popular folds show their frameworks built of α -helices and β -strands. Adapted from [21].

To answer the questions: what are the remarkable features of the “common” folding patterns, found in functionally and phylogenetically different proteins? – we shall analyze stability advantages and disadvantages of different folds. This “thermodynamic” approach is justified by that the same 3D protein structures can be obtained by quite different processes: *in vivo* (during the biosynthesis), and *in vitro*, when the protein refolds in the test-tube from a completely unordered and unfolded state (see below). This means that a detailed sequence of actions does not play a crucial role in protein folding.

Let us start with a simple question – why are the most common folding patterns based on the secondary structures? The answer is that the

secondary structures can form the stable elements of the fold since they involve the most powerful non-covalent interactions existing in protein chains, the hydrogen bonds, which fix many degrees of freedom of the chain. And a stable fold must generally consist of stable elements!

This does not mean, though, that there are no folds without secondary structures. However, the protein chains, having these rare folds, are also “unusual” as a rule: *e.g.*, they contain a great many of Cys residues, whose side chains can form covalent disulfide bonds, and S-S bonds between these residues stabilize these folds.

Let us go further and consider the typical packings of secondary structures (also called “protein architectures”). Figure 10 shows that the secondary structure segments form the frameworks of protein globules; that the α -helices and β -strands typically go from one side of the globule to another; that they are arranged in layers (flat, twisted or even cylindrical); and that the irregular connections do not come inside the globule. Let us figure out why the stability of a globule requires all this.

All these features of the protein globule are due to the H-bonds, which cost a lot, and therefore all, or almost all of them, must be saturated in any stable protein structure. The donors and acceptors of H-bond are present in the backbone of any amino acid residue. They can be saturated with the bonds either with water, or between themselves. In the latter case the secondary structures (α or β) are formed. The backbone of the chain forming a secondary structure does not make further H-bonds and becomes hydrophobic, while it is hydrophilic in the regions where the secondary structure is absent. Therefore only the backbone formed secondary structures can avoid water environment. These structures stick together, form the framework of protein and screen from water its hydrophobic core, made of the non-polar side chains, mainly outgoing of these structures. On the other hand, the elements with “free” (*i.e.*, saturated with water) hydrogen bond donors and acceptors (loops, edges of β -sheets, ends of α -helices) must remain at the surface and contact to water.

The α -helices, with the H-bonds inside them, and the β -sheets, with the H-bonds between β -strands (Fig. 4) cannot be mixed within the same layer. Otherwise, the potential H-bonds at the β -sheet edge will “wall” the helix: they will be lost; the globule will have a considerable (in the terms of energy) “structural defect” and will not be stable.

In principle, one could suggest a sequence, where some specially positioned polar side chains will heal the lost hydrogen bonds of the loop or the β -edge, involved in the middle of a globule. Or to suggest a sequence, which compensates these lost bonds with some powerful interactions, *e.g.*, with the covalent (Cys-Cys) or co-ordinate (through the metal ion) bonds.

In principle, this seems to be possible. But these sequences will be *very special, i.e., very rare*.

And, may be, this is the reason: may be, the “common” protein folds are created by the “normal” (*i.e.*, not too strongly selected) sequences, while the “special” (*i.e.*, very strongly selected) sequences are just rare?

We will come to this point once and once again, considering the other peculiarities of typical protein folds.

A vast majority of protein domains can be represented as two-, three- or (rarely) four-layer packings. Globules with more than four layers are extremely rare, – and, in principle, it is clear why [18]. Too large globules would contain too many residues screened from water [22], which means – for a 1:1 ratio of polar and non-polar side chains, typical of proteins – that many polar side groups will loose their H-bonds with water. This is very unfavorable energetically, and such a protein could not be stable.

Therefore, for the sake of stability, large compact globules of a “normal” amino acid composition must be divided into sub-globules called domains (which we indeed see in large proteins).

Figures 9 and 10 show one more peculiar feature of the common folding patterns: namely, that β -sheets are often surrounded by α -helices (while the opposite is extremely rare).

This phenomenon can be explained from the same point of view (“usual” *vs.* “rare” sequences). Let us compare the pair of β -strands, situated in the middle of the globule, with the α -helix, also situated in the middle (Fig. 11). The lengths of these segments are dictated by the globule’s diameter, which is large in a large globule. α -helix includes twice more residues than β -strand of the same length. If we fix the chain positions for two β -strands or for the α -helix, the fully hydrophobic segments (necessary, for the sake of stability, for both these structures, and including equal number of residues) will have the same odds to occur (see legend to Fig. 11). However, the fully hydrophobic sequence aimed for the internal helix consists of one continuous piece, while the sequence aimed for the pair of internal β -stands consists of two fully hydrophobic pieces. These two pieces can have much more positions in the chain than the single piece. Therefore, there are much more sequences compatible with two internal β -strands than with one internal α -helix.

In the other words, among random sequences there are much more of those, which can stabilize a fold with two internal β -strands, than those, which can stabilize a fold with a single internal α -helix.

And this advantage of odds (estimated from random sequences!) is exactly that what we see in protein folds. Thus, we see that a consideration of that what can be more readily formed by random sequences can help to understand the folds of real globular proteins. It seems that though the

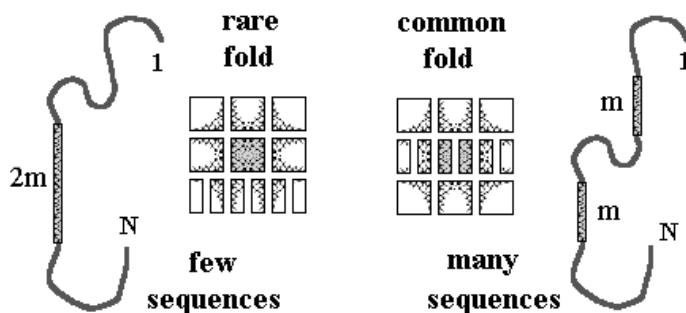


Fig. 11. Multilayer folds; a schematic view from the ends of α -helices (squares) and β -strands (rectangles). The probability of occurrence of one long entirely hydrophobic sequence of $2m$ residues (for α -helix) in a given chain position is small ($\sim p^{2m}$, where $p \approx 1/2$ is the average fraction of non-polar residues in protein chains), but it is equal to the probability of occurrence of two twice shorter hydrophobic blocks (for two β -strands) in two given chain positions [$\sim (p^m) \times (p^m) = p^{2m}$]. However, one block can be placed in the N -residue chain in only $\approx N$ different ways, while two blocks can be positioned in $\approx N^2/2$ different ways. Therefore, if $Np^{2m} \ll 1$, which is always the case for a large N (since $m \approx N^{1/3}$), much more sequences are compatible with two internal β -strands than with one internal α -helix.

proteins are certainly the products of natural selection, this selection has much more space to operate when the fold is compatible with many sequences, and much less when it is compatible with only a few.

Of course, it may seem strange to speak about proteins coded by naturally selected genes and to borrow the arguments from the random sequences. However, let us look at proteins. Statistical analysis shows that amino acid sequences of globular proteins, and we are now speaking about them, look almost “random” [23], – in the sense that they have neither blocks, typical of membrane proteins, nor repeats, typical of fibrous proteins (Fig. 12). The distribution of secondary structures over the chains of globular proteins also looks almost “random”, compatible with a random clustering of the non-polar groups making the hydrophobic surfaces of these structures [18]. And what does this mean, – “to look like a random chain”? This means to look like *most* of the chains. Thus, speaking on structures that can be formed by random sequences, we actually consider the structures compatible with many various sequences. And, up to now, we have obtained something reasonable!

- 3) the usual connection of parallel β -strands is the right-handed (see Fig. 14) connection, *i.e.*, all the connections have the same handedness and therefore, taken together, form the super-helices.

The first peculiarity is already clear to us. That is, we understand why the layered construction of the secondary structure packing is energetically favorable, and why the loops in the core (the “structural defects!”) are energetically unfavorable. If we want to understand the other peculiarities following the same line of the fold shape confrontation with its stability (and, further, with the number of the fold-stabilizing sequences), we have to ask: what is energetically wrong with the crossed loops? and with the left-handed connections?

Indeed, what is energetically wrong with the crossed loops (Fig. 14a)? When we say “crossed”, we do not mean that one loop runs into another, we only mean that one loop covers the other! Covers, clasps to the core, – and screens its polar backbone from water: *i.e.*, the covered loop loses some of its hydrogen bonds with water. And we will again need a “special” sequence to heal the lost bonds and to maintain the stability of the globule with the crossed loops.

However, here we must feel ourselves embarrassed. Indeed, the loop covered by another one loses only one, may be two hydrogen bonds, – much less, than a loop piercing the entire globule, which has been discussed earlier. The lost one-two hydrogen bonds cost only three-five kilocalories per mole [18]. This is much less than the total energy of interactions within the globule, amounting to hundreds of kilocalories (according to protein melting data [24]). Moreover, this is much less than the usual margin of stability of the native globule (*i.e.*, the free energy difference between the folded and unfolded protein under physiological conditions), which, according to the same experiments, amounts to about 10 kcal/mol. Then, why does an “energy defect” of only 3–5 kcal/mol virtually exclude the crossing of loops in the native protein globules? And one more question: why the upper loop cannot make an additional bend (dotted line in Fig. 14a) and thus avoid covering and screening of the lower loop from water? May be, this is prevented by a limited loop elasticity? [A simple calculation [18] shows that such a bend of a polypeptide chain will cost a few (again a few!) kcal/mol].

Let us postpone these questions and discuss why the left-handed connection is worse than the right-handed connection (Fig. 14b).

The stability criterion again allows pointing out the “better” of these two dissymmetric connections. The basis is hidden in the dissymmetry of all (except for Gly, see Fig. 3) natural amino acids. As a result, the right-handed (looking along the strands) twist of the β -sheet is usually more stable (and is much more often occurs in proteins) than the left-handed twist or the absence of twist [25].

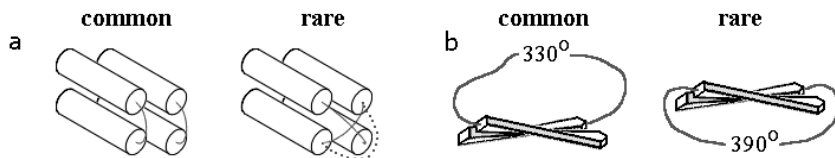


Fig. 14. Rare and common elements of protein folding patterns. **a)** The overlapping (as well as bypassing) loops, connecting the secondary structures, are relatively very rare in proteins. **b)** The left-handed connection of parallel β -strands is rare in proteins, while their right-handed connection is common.

The right-handed twist makes the angle between two adjacent strands close to -30° [25]. Therefore, the turn of the loop connecting the parallel β -strands is close to $360^\circ - 30^\circ = 330^\circ$ for the right-handed connection of strands, and to $360^\circ + 30^\circ = 390^\circ$ for the left-handed connection (Fig. 14b). As a result of limited loop elasticity the right-handed turn (of 330°) costs a few (again a few!) kcal/mol less than the left-handed turn (of 390°) [18].

Thus, the left-handed connection has (on the average over sequences) a “stability defect”, and just this type of connection is rare in proteins.

Here, however, anybody who knows polymer physics must stop me and say: “Polymer elasticity is *not* an energetic, but rather an entropic effect! That is, the more bent chain has the same energy, but much less possible conformations than the less bent chain! Thus, you are speaking on the fluctuating loop, *not* about the loop in the protein globule, where the loop is fixed, and its entropy is zeroing in any case! Then, what is the “defect” you are talking about? May be, it can concern the flexible semi-folded folding intermediates. But how can it concern the fixed, solid protein structures?”.

My answer will be: “You are right when saying that the more bent loop has fewer possible conformations than the less bent loop, and you are right that in any case only one conformation, the most stable one, will be fixed and observed in protein. But I can show that this means that the more bent loop can be stabilized (in the *folded* protein!) by fewer sequences than the less bent loop”.

Indeed, a randomly taken sequence can make the most stable (of all the chain structures) either *one of* the few conformations corresponding to the left-handed way of connection, or *one of* the many conformations corresponding to the right-handed connection. Besides, of course, all these left- and the right-handed connections of β -strands can be unstable against the multitude of the other chain conformations (*e.g.*, of those without any β -strands), and the latter certainly is the most probable for a random sequence. However, if we have to choose only between the left- and the right-handed folds: which of them has the greater odds to occur in the stable folded protein?

If the loop elasticity is a purely entropic effect, each *separate* conformation with the right-handed connection is neither better nor worse than each *separate* conformation with the left-handed connection – assuming that each of these conformations have an equal compactness, secondary structure content, etc. However, there are *much more* right-handed (less bent) conformations than the left-handed ones, and the odds are that the majority will win [26–28].

Actually, we have a kind of a lottery, where a toss of the coin is done by the random sequences. Each lottery ticket (each particular possible conformation) has equal chance to win the prize (*i.e.*, to be the most stable 3D structure of a sequence). The “right-handed fold” has many lottery tickets (many possible conformations) in this lottery, and the “left-handed fold” has only a few. Which of them, the “right” or the “left”, will win, if any? Probably, the one who has more tickets! And the probability to win is proportional to the number of “tickets”, *i.e.* of the possible conformations.

In the other words: the wider is the set of *possible* conformations, the more often a randomly taken sequence can find its most stable structure in this set.

Just this is seen in globular proteins: here the less restricted right-handed connection (with the wider set of possible conformation) is the rule and the left-handed connection (with the more narrow set of possible conformations, *i.e.*, with an “entropic defect” of a separately taken loop) is an exception. (The most striking exception is presented by “left-handed β -helices” having non-twisted β -sheets of very short strands, unusual *left* connections between them, – and *unusual quasi-periodic sequences*.)

A ≈ 3 kcal/mol (at room temperature) defect in elastic free energy of the separately taken left-handed connection results from its “entropic defect” that corresponds to ~ 100 time decrease in the number of possible loop conformations, and this results in that the “left” connection can be stabilized by ~ 100 times lesser sequences than the “right” one.

The same consideration concerns the additional bend of the loop in Figure 14a. Here we also have an “entropic defect”.

However, we still have to explain the “energetic defects”. In particular, we have to explain why the overlap of loops is virtually forbidden in proteins by only a ≈ 3 kcal/mol loss in the *energy* of the loop screened from water by another one. The question is why such a great structural effect is done by only the 3 kcal/mol energy loss, – against the background of much greater *total energy* of the protein? Although, we can already expect that even a small “energy defect” leads to a significant loss in the number of the fold-stabilizing sequences.

The other statistical rules known for protein structures show the same: high-free-energy structural details are rare, while low-free-energy details

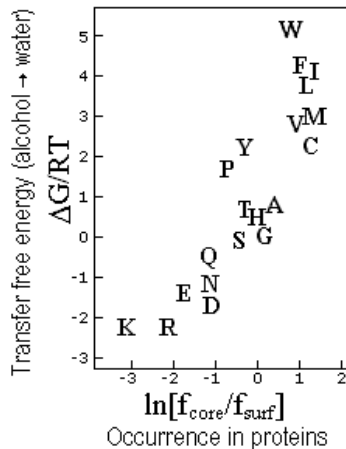


Fig. 15. Correlation between the experimental transfer free energy ΔG and the occurrence of amino acid residues inside and outside protein globules [29]. $f_{\text{surf}} = N_{\text{surf}}/\Sigma N_{\text{surf}}$ is the observed frequency of a residue at the surface (N_{surf} being the number of surface residues of a given type); f_{core} is the observed frequency of a residue in the protein interior; $RT = 0.6$ kcal/mol at 300 K. Amino acid names are given in one-letter code (A = Ala, etc.).

are usual. But here we have greater statistics and can withdraw some quantitative estimates, not only the qualitative ones.

For example, the distribution of amino acid residues between the core and the surface of proteins (Fig. 15) is tightly connected [29] with the hydrophobicity of the residues, experimentally measured as the free energy (ΔG) of their transfer from octanol (modeling the protein interior) to water. The slope of the dependence (when ΔG is expressed in RT units at room temperature T) is roughly 1.5. Thus, the observed statistics can be approximately presented as

$$\text{OCCURRENCE} \sim \exp(-\text{FREE_ENERGY}/RT_C), \quad (2.1)$$

where T_C is some “conformational temperature” [30] close to 400 K, and R is the gas constant.

We see that such protein statistics outwardly looks like the Boltzmann statistics. Pohl was the first to point this similarity in 1971 for statistics of amino acid rotamers [30]. Then the same has been shown for statistics of secondary structures, ion pairs, cavities, etc. (for further discussion and references see [11, 28]). This empirical relationship is never perfect, but is so common that it is even used to estimate the strength of interactions.

However, it should be stressed that *only* the exponential form of the protein structure statistics look like Boltzmann statistics. Their physical sense is *absolutely different*.

The Boltzmann statistics originates from that the particles move from one position to another, and spend more time there, where their energy is lower [31]. On the contrary, the amino acid residues are fixed and do not wander, say, from the protein interior to the surface. For example, Leu72 of myoglobin is *always* inside the native globule. And if the statistics say that 80% of all the Leu is inside protein and 20% is outside, – this does not mean that each Leu spends 80% of time inside and 20% outside. This only means that some selection has fixed 80% of Leu residues inside and 20% outside.

Let us now see how the mutation of a residue in a given position can change the number of the fold-stabilizing sequences. How will this number be changed, for example, by the Leu \rightarrow Ser mutation inside the protein? Let us put aside the difference in the Leu and Ser volumes and shapes and consider only their hydrophobicity. Leu is more hydrophobic than Ser. When Leu is inside, the protein fold is more stable against unfolding than the same fold with Ser inside. This means that the sequences which can stabilize a fold with Ser inside can also stabilize the fold with Leu inside, – but the fold will Leu inside will be, *in addition*, stabilized by some sequences which cannot stabilize the fold with Ser inside.

What will this increase in the number of fold-stabilizing sequences be? Let us consider this problem in a formal, but general and simple way.

The native (observed) structure is stable if its free energy is below that of the unfolded chain and of all the other globular folds; *i.e.*, if it is below some energy threshold (independent on the native fold itself). Let us assume, for simplicity, that “our” fold competes only with the unfolded state, and that the internal residues of the fold are completely screened from water, while the external residues, as well as all residues of the unfolded protein are completely exposed to water (for more accurate and detailed theory, see [27, 28]; it is based on the Random Energy Model (REM) [32]).

Let $\Delta\varepsilon + \Delta F$ be the free energy difference between the given chain fold and the unfolded state of the chain. Here $\Delta\varepsilon$ is the free energy difference for the concerned element (including the element’s interaction with the surrounding; *e.g.*, the Leu’s free energy in the core minus its free energy in the unfolded chain), and ΔF is the “given fold – unfolded chain” free energy difference for the remaining chain. The fold is stable against unfolding when $\Delta F + \Delta\varepsilon < 0$, but it worthwhile to consider the stability requirement in a form

$$\Delta F + \Delta\varepsilon < -G, \quad (2.2)$$

where $-G \leq 0$ is some small “stability threshold” that may be necessary

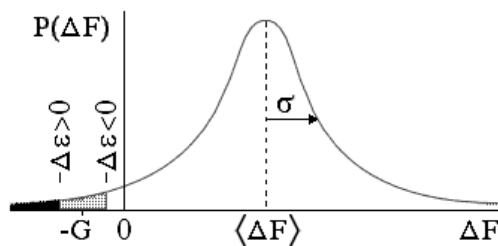


Fig. 16. Typical (Gaussian) form of distribution of the free energy value ΔF over the random sequences. $-G \leq 0$ is the “stability threshold” of protein structure. The blackened region meets the fold stability requirement ($\Delta F < -\Delta\varepsilon - G$) at $\Delta\varepsilon > 0$, the “black + gray” region meets this requirement at $\Delta\varepsilon < 0$. The second region is greater, that is, more random sequences make the given fold stable when the free energy of the element of interest ($\Delta\varepsilon$) is below zero than when it is above zero.

(see the next chapters) for functioning and rapid folding of the protein. Thus,

$$\Delta F < -\Delta\varepsilon - G. \quad (2.3)$$

The values ΔF и $\Delta\varepsilon$ depend on the amino acid sequence. Let us consider all those sequences which preserve the $\Delta\varepsilon$ value [*e.g.*, all sequences with Leu (or Ser) in the given chain point; for the core positions, $\Delta\varepsilon \approx -2$ kcal/mol for Leu (and ≈ 0 for Ser), while for the surface positions $\Delta\varepsilon = 0$]. The value ΔF will change with the sequence. The probability that $\Delta F < -\Delta\varepsilon - G$ is

$$P^*(\Delta F < -\Delta\varepsilon - G) = \int_{-\infty}^{-\Delta\varepsilon - G} P(\Delta F) d(\Delta F), \quad (2.4)$$

where $P(\Delta F)$ is the probability of the given ΔF value for a randomly taken sequence.

The ΔF value is composed of many independent terms. Therefore (according to the Central Limit Theorem and REM), $P(\Delta F)$ has a simple Gaussian (Fig. 16) form:

$$P(\Delta F) = (2\pi\sigma^2)^{-1/2} \exp \left[-(\langle \Delta F \rangle - \Delta F)^2 / 2\sigma^2 \right]. \quad (2.5)$$

Here $\langle \Delta F \rangle$ is the mean (averaged over all the sequences) value of ΔF , and σ is the root-mean-square deviation of ΔF from $\langle \Delta F \rangle$.

Actually, the only important (for us) feature of $P(\Delta F)$ is its exponential growth with ΔF at the low ΔF values, where $P(\Delta F)$ is small. This concerns, in particular, the region where ΔF is close to 0 (the “margin of stability”), since $P(\Delta F)$ must still be very small here, – otherwise a random

sequence would have a significant chance to stabilize exactly the concerned fold, which is absurd (why – namely this fold from the multitude of all folds?). Thus, $\langle \Delta F \rangle \gg \sigma$. The value $(\langle \Delta F \rangle - \Delta F)^2 \approx \langle \Delta F \rangle^2 - 2\langle \Delta F \rangle \Delta F$ when ΔF is close to 0; here $P(\Delta F) \approx \{(2\pi\sigma^2)^{-1/2} \exp[-\langle \Delta F \rangle^2/2\sigma^2]\} \times \exp[\Delta F \langle \Delta F \rangle / \sigma^2]$, and

$$P^*(\Delta F < -\Delta\varepsilon - G) = \int_{-\infty}^{-\Delta\varepsilon - G} P(\Delta F) d(\Delta F) \\ \simeq \text{const} \times \exp \left[-\frac{\Delta\varepsilon + G}{\sigma^2 / \langle \Delta F \rangle} \right]. \quad (2.6)$$

The const [equal to $\{(2\pi\sigma^2)^{-1/2} \exp[-\langle \Delta F \rangle^2/2\sigma^2]\} \times (\sigma^2 / \langle \Delta F \rangle)]$ is not interesting for us, while the really important term $\exp[-(\Delta\varepsilon + G)/(\sigma^2 / \langle \Delta F \rangle)]$ demonstrates the following [26–28]:

- 1) the term $\exp[-\Delta\varepsilon/(\sigma^2 / \langle \Delta F \rangle)]$ demonstrates that the element's free energy $\Delta\varepsilon$ has an exponential (Boltzmann-like!) impact on the number of the fold-stabilizing sequences (this concerns the “energy defect” of any kind);
- 2) the term $\exp[-G/(\sigma^2 / \langle \Delta F \rangle)]$ demonstrates the decrease in the number of the fold-stabilizing sequences with the increase of the required fold's stability. It suggests that stability of most of proteins should be close the minimally required stability threshold G ;
- 3) the value $RT_C = \sigma^2 / \langle \Delta F \rangle$ plays the same role in the statistics of stable protein folds as the value RT in the Boltzmann statistics. However, T_C is “the temperature of selection” *in the protein sequence space*, – rather than the usual temperature of the surrounding 3D space.

It is noteworthy that T_C is *not* proportional to the size of the protein: since both the dispersion (σ^2) and the average ($\langle \Delta F \rangle$) of the random value ΔF are proportional to the number of terms summarized in ΔF , the ratio $\sigma^2 / \langle \Delta F \rangle$ does not depend on this number. This shows that the “defect's” free energy $\Delta\varepsilon$ must be compared (to estimate its impact on the occurrence) *not* with the total protein energy, but rather with $\sigma^2 / \langle \Delta F \rangle$, which is something like the energy of *one* residue in the native protein. This suggests that T_C must be connected with the protein melting temperature. And indeed, a more detailed analysis has shown [28] that T_C is rather close to (though does not coincides with) the protein heat melting temperature, which has been the subject of intensive theoretical studies [33–35].

Thus, we now understand that the fold's “structural defect” can be caused either by the low entropy or by the high energy of any of its separately

taken structural element, and why “defects” of only a few kcal/mol can rule out (not completely, but usually) many “rare” protein folds.

It is noteworthy that the effect caused by the additional energy defect’s energy $\Delta\varepsilon > 0$ can be caused also a “defect of variety”, *i.e.*, by the decrease in the dispersion σ^2 of interactions within the fold (*e.g.*, by the decreased number of interactions within a given fold [26–28]). However, such peculiarities are not so easily visualized in protein structures as the above described energy and entropy defects.

The obtained understanding of the physical selection of protein structures has been achieved when we posed a simple question: “what is the fraction of sequences that is able to stabilize a fold with a given feature?” Each stable element of the fold increases this fraction, while the unstable one decreases it exponentially. It seems that the natural globular proteins follow this “multitude” [28] (or “designability”, as it usually called now [36–38]) principle: the more sequences can stabilize the fold, the more often it is met in nature.

Thus, the “physical selection” forms the background at which the biological selection has to operate.

3 Thermodynamic aspects of protein folding

3.1 Reversible denaturation of protein structures

Earlier we considered stability of fixed, “solid” protein structures. However, depending on ambient conditions, the most stable state of a protein molecule may be not solid but molten or even unfolded. Then the protein denatures and loses its native, “working” 3D structure.

Usually protein denaturation is observed *in vitro*, caused by an abnormal temperature or denaturant (like urea, H^+ or OH^-). However, decay of the “solid” protein structure and its subsequent refolding can occur also in a living cell, *e.g.*, in trans-membrane transport of proteins.

Denaturation and renaturation of the water-soluble globular proteins is best studied, and, as earlier, I will speak about them only.

It is well established that denaturation of small proteins is a cooperative transition with a simultaneous abrupt change of many (though sometimes not all) characteristics of the molecule (Fig. 17a). The S-shaped experimental curves and the narrow transition regions suggest that the transition embraces many amino acid residues. Moreover, protein denaturation occurs as an “all-or-none” transition [6, 24] (Fig. 17b).

The latter means that the transition embraces the molecule as a whole, and that only the initial (native) and the final (denatured) states amount to visible quantities, while “semi-denatured” states are unstable and practically absent. [Though, of course, they do exist to a very small quantity,

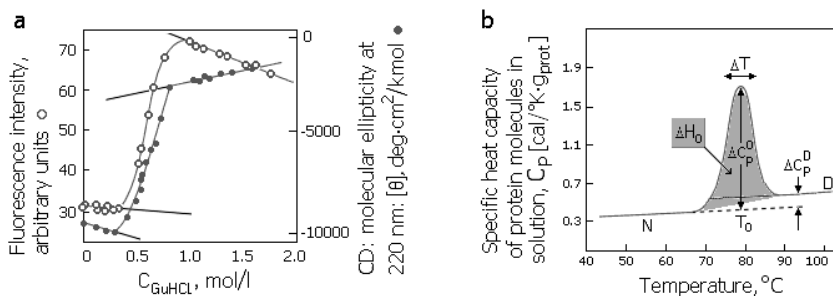


Fig. 17. Protein denaturation. **a)** Abrupt change of compactness (observed by fluorescence) and secondary structure content (observed by circular dichroism (CD) at 220 nm) of phosphoglycerate kinase denaturated with increased concentration of guanidine dihydrochloride (GuHCl). Adapted from [39]. **b)** Calorimetric study of the lysozyme heat denaturation. The position of the heat capacity (C_p) peak determines transition temperature T_0 , the peak width gives the transition width ΔT , the area under the peak gives the heat ΔH absorbed by the protein sample. The values ΔT , $\Delta H \times \text{protein's mol. weight}$ and T_0 satisfy to equations (3.1) indicating that the denaturation occurs as an “all-or-none” transition. The increased heat capacity (ΔC_p) of the denatured protein (D) originates mainly from the enlarged (as compared with the native state N) interface between non-polar groups and water in the D state. Adapted from [6].

since a native molecule cannot come to its denatured state without passing the intermediate forms, and their presence has a crucial effect on kinetics of the transition, which we will discuss in the next chapter.]

In other words, the “all-or-none” transition is a microscopic analog of the first-order phase transitions in macroscopic systems (*e.g.*, crystal melting). However, unlike the true phase transitions, the “all-or-none” transitions in proteins have a non-zero temperature width, since this transition embraces a microscopic system. I want to specify that the “all-or-none” denaturation actually concerns small proteins and to separate domains of large proteins, while denaturation of a large protein is a sum of denaturations of its domains [24, 40].

To prove that melting is an “all-or-none” transition, one has to compare (1) “effective latent heat” of transition calculated from its width (*i.e.*, the amount of heat consumed by one independent melting unit) with (2) “calorimetric heat” of this transition, *i.e.*, the amount of heat consumed by one melting protein molecule.

The latter is $\Delta H_0/N$, where ΔH_0 is the heat consumed by all N protein molecules contained in the calorimeter ($N = m/M$, where m is the total mass of the protein in the test-tube, and M is the protein molecular mass).

The latent heat of a melting unit is calculated as $\Delta H = 4RT_0^2/\Delta T$, where ΔT is the transition width. This van't Hoff equation follows from the model where the “melting unit” can be in two states, *e.g.*, “solid” and “molten”, with the enthalpy difference ΔH and the entropy difference ΔS per a unite, so that $P_{\text{solid}} = 1/\{\exp[-(\Delta H - T\Delta S)/RT] + 1\}$ is the solid state probability, the molten state probability $P_{\text{molten}} = 1 - P_{\text{solid}}$, while $T_0 = \Delta H/\Delta S$ is the mid-transition temperature. If

$$\Delta H_0/N = 4RT_0^2/\Delta T, \quad (3.1)$$

then the *whole* protein is one melting unit, and its melting is an “all-or-none” transition. This is the van't Hoff criterion for existence of the “all-or-none” transition. If $\Delta H_0/N > 4RT_0^2/\Delta T$, this means that the “melting unit” is smaller than the whole protein, *i.e.*, that it melts in parts. If $\Delta H_0/N < 4RT_0^2/\Delta T$, this means that the “melting unit” is greater than the protein, *i.e.*, that this “unit” consists of several protein molecules.

Is a denatured protein able to *renature* and to restore its native structure? That is, is the denaturation reversible?

Yes, it is. This is known since Anfinsen's experiments of 1960's [4]: a protein can renature if it is not too large and has not been subjected to substantial chemical modifications after the *in vivo* folding (and if the protein solution is sufficiently diluted to avoid aggregation). In this case, a “mild” (without chemical decay) destruction of the protein's native structure (by temperature, denaturant, etc.) is reversible, and the native structure spontaneously restores after environmental conditions have become normal.

The reversibility of protein denaturation is very important: it shows that the entire information necessary to build up the protein structure is contained in its amino acid sequence and that the protein structure itself (to be more exact, the structure of a not too modified and not too large protein) is thermodynamically stable. This allows using thermodynamics to study and describe de- and renaturation transitions.

Heat denaturation of proteins is usually accompanied by a large heat effect, ~ 1 kcal per mole of amino acid residues.

Protein melting, *i.e.*, the decay of its structure due to elevated temperature, looks natural; however, a “cold” denaturation of proteins also exists at abnormally low temperatures (Fig. 18). It is observed not for all proteins, though, since water in the test-tube is usually first to freeze.

The cold denaturation of proteins has been also shown to be a reversible “all-or-none” transition.

It occurs due to abnormal temperature dependence of hydrophobic forces [42], which drastically decrease with the decreasing temperature. As a result, the native structure stability (*i.e.*, the free energy difference between the native and the denatured state) has its maximum at about room temperature, and starts to decrease at low temperatures.

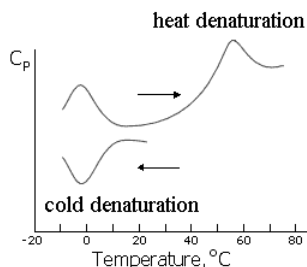


Fig. 18. Reversible “cold” denaturation of protein (apomyoglobin) at an abnormally low temperature (the lower curve; the arrow shows that temperature decreases during the experiment). The upper curve shows renaturation of the cold-denatured protein (the left heat capacity peak) with increasing temperature, as well as its subsequent melting (the right peak) at high temperature. Adapted from [41].

Paradoxically, there is some similarity between denaturation of proteins and water boiling. As you know, there are two ways to boil water: either to increase temperature or to decrease pressure. Hydrophobic pressure (condensing the protein globule) significantly decreases at low temperatures, and the protein begins to “boil”. By the way, it really “boils”: the protein chain unfolds completely, and its volume grows many-fold after the cold denaturation, while the heat denaturation usually only “melts” the protein, and its volume increases only slightly.

3.2 What do denatured proteins look like?

Numerous *thermodynamic* experiments have shown that there are no cooperative transitions within the denatured state of a protein molecule. Therefore, it was initially assumed that the denatured protein is always a very loose random coil (as it is in a “very good” solvent like concentrated solution of urea [43]).

However, *structural* studies of denatured proteins reported on some large-scale rearrangements within the denatured state, that is, on some stable “intermediates” between the completely unfolded coil and the native state of proteins (Figs. 19, 20).

This contradictory picture of protein denaturation was clarified only by using a bunch of methods. Measurements of protein solution viscosity informed about the hydrodynamic volume of protein molecules; far UV CD spectra (circular dichroism in the far ultraviolet region) informed on their secondary structure; near UV CD spectra informed on asymmetry, that is, on ordering of the environment of aromatic side chains; infrared

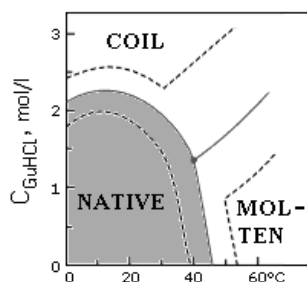


Fig. 19. Phase diagram of conformational states of lysozyme at pH 1.7 in GuHCl solution at various temperatures: the solid NATIVE state, the completely unfolded COIL, and a more compact temperature-denatured state (MOLTEN). The solid line corresponds to the mid-transition, the dashed lines outline the transition zones (from the proportion $\approx 9:1$ in favor of one state to $\approx 1:9$ in favor of another). One can see that the COIL – MOLTEN transition is much wider than the others. Adapted from [44].

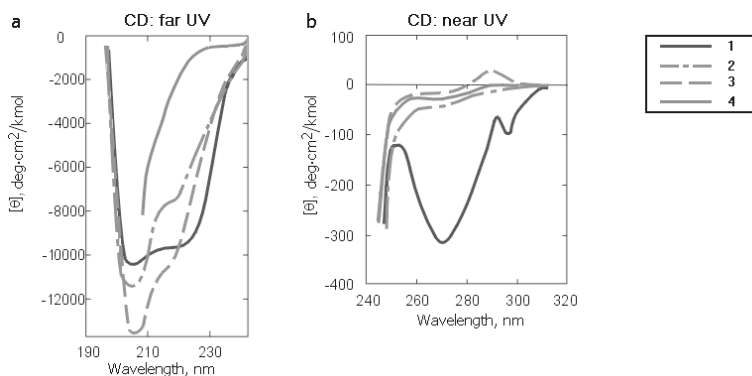


Fig. 20. CD spectra in the near **a)** and far **b)** ultraviolet regions for α -lactalbumin in the native (1), heat-denatured (2), acid-denatured (3) and denaturant-unfolded (4) forms. Far-UV CD spectra are significantly changed only by unfolding (see curve 4). Near-UV CD spectra are always changed by denaturation (see curve 1). Adapted from [45].

spectroscopy, NMR, measurements of protein activity, etc., as well as theoretical considerations also elucidate many important details.

It became clear that, apart from activity, only two protein properties *always* abruptly change during denaturation. These are: (1) ordering of the environment of aromatic side chains observed by near UV CD (Fig. 20b) and by NMR, and (2) rigidity of globular structure followed (using NMR)

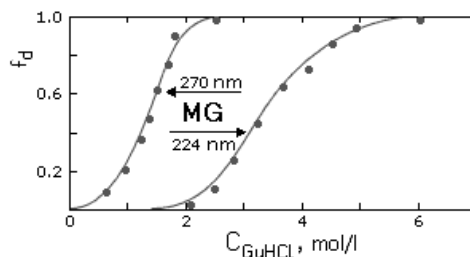


Fig. 21. Relative changes of α -lactalbumin CD in the near (270 nm) and far (224 nm) UV regions at increasing denaturant (CuHCl) concentrations. $f_d = 0$ concerns the signal from the native structure, $f_d = 1$ concerns the signal from the completely denatured molecule. The “intermediate state” (the “molten globule”, **MG**) exists between the first and the second transitions, at $C_{\text{GuHCl}} = 2$ mol/l. Adapted from [46].

by exchange of hydrogens of the protein’s polar groups for deuteriums of water, and by acceleration of the protein chain digestion.

On the other hand, the ordering of protein main chain (*i.e.*, its secondary structure), the volume of protein molecule, and the density of its hydrophobic core can be virtually preserved in some cases and strongly changed in others, depending on denaturation conditions (Fig. 20a).

Protein chain looks like a random coil in a “very good” solvent like concentrated solution of urea or GuHCl; then its volume is proportional to the chain length in the power $3/2$ or close to $3/2$.

However, in poor solvent the volume of denatured globule is proportional to the chain length and is often only a little larger than the volume of the native protein. Thus, the above studies have revealed a universal, or rather, nearly universal intermediate of protein unfolding and folding, which is now known as the “molten globule” (Figs. 21, 22).

On the face of it, the molten globule properties are contradictory. Its secondary structure is usually developed nearly as that of the native protein. On the other hand, the molted globule (like the completely unfolded protein) has nearly no ordering of side chains, which is so typical of the native protein. However, some portion of the side chain native contacts evidently remains in the molten globule; NMR shows that this concerns aromatic rather than to aliphatic side chains. The molten globule is a little less compact than the native protein (as the hydrodynamic volume measurements report), and its core is virtually as compact as that of the native protein (as the “middle-angle” X-ray scattering reports); on the other hand, a rather high rate of hydrogen exchange shows that at least separate solvent molecules easily penetrate into the globule [47,48]. To some extent, these contradictions may

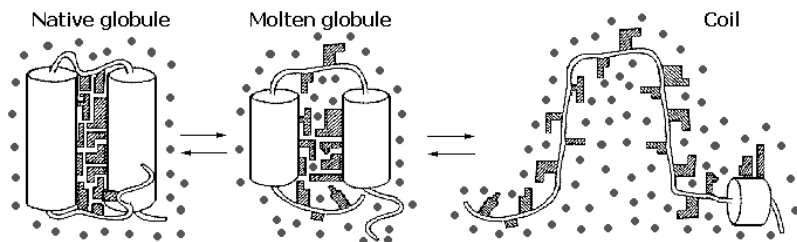


Fig. 22. Schematic model of the molten protein globule [47–50] in comparison to the native protein and the coil. For simplicity, the protein is shown to consist of only two helices and irregular loops. The backbone is covered with numerous side chains (dashed). Reinforced by H-bonds, the secondary structures are stable until the globule is “dissolved” by a solvent. Usually, waters are unable to do this without a strong denaturant. In the molten globule, side chains lose their close packing, but acquire the free movements, *i.e.*, they lose energy but gain entropy. The waters (●) come into pores of the molten globule (that appear when the close packing is lost), but, until the denaturant is not too strong, cause no further decay of the globule; a stronger denaturant converts the globule into the coil.

be conciliated by assumption that the molten globule has a relatively dense, native-like core and more loose loops. However, the assumption that the molten globule has the completely native core and the completely unfolded loops is in a clear contradiction with experiment, and specifically with the absence of the ordered environment of aromatic side chains in the molten globule observed by the near UV CD and by the NMR spectroscopy.

For very many (though not for all) proteins, the “molten globule” arises at a moderate denaturing impact upon the native protein, and decays (turns into a random coil) only under the impact of a concentrated denaturant. The molten globule-like state often occurs after temperature denaturation (“melting”), and this melting has been always observed to be the “all-or-none” transition. The molten globule usually does not undergo cooperative melting with increasing temperature (see Fig. 19), but its unfolding caused by a strong denaturant looks like a cooperative S-shaped transition (Fig. 21).

However, some proteins (especially small ones) unfold directly into a coil without the mediating molten globule state; and many other proteins are converted into the molten globule by some denaturing agents (*e.g.*, by temperature or by acid), while other agents (*e.g.*, urea) directly convert them into a coil. In all these cases, though, the decay of the native state is the “all-or-none”, *i.e.*, the first order phase transition [47].

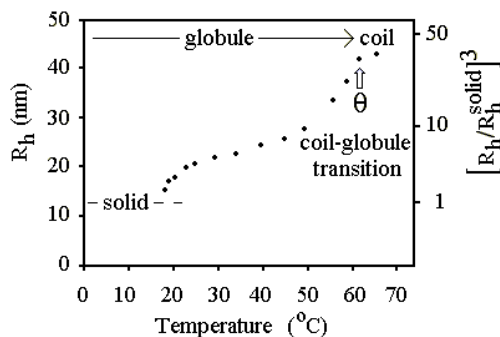


Fig. 23. Hydrodynamic radius R_h vs. temperature for poly(methyl-metacrylate) chains (M.W. = 6.5×10^6 Dalton). The “ θ -point”, *i.e.*, the globule-to-coil transition corresponds to 61 °C. The globule exists below 61 °C, the coil above 61 °C. Dashed line: the computed radius of the solid polymer. Adapted from [52].

3.3 Why denaturation of a globular protein is the first-order phase transition

It is really astonishing that denaturation of protein occurs as a usual sharp first-order phase transition: protein is a highly heterogeneous system (where, nevertheless, each atom sits at its own place), and heterogeneity is known to slur over the phase transitions in usual molecular systems.

Understanding of protein denaturation has been hampered by that that the globule-to-coil transition in “normal” synthetic polymers (that had been initially supposed to be an analog of denaturation) is quite different from the first-order phase transition like melting or sublimation, while protein denaturation turned out to be similar just to melting or sublimation of a solid.

Experiments show (Fig. 23) that conversion into a coil goes without any phase separation or abrupt jump in the polymer’s density (*i.e.*, without the first order transition) and occurs only when the polymer globule is rather swollen; besides, the theory [51] suggests that the main difference between the globular and coil phases is the difference not in density, but rather in the scale of fluctuations (small in the globule, large in the coil).

Strictly speaking, the polymer theory states that an abrupt transition of the dense globule into the loose coil, though possible in principle, occurs only under hardly obtainable requirement, *e.g.*, when the chain monomers are repulsed in pairs but attracted to one another when the simultaneously interacting particles are many. This requires a very special construction of the chain monomers. Usual polymers do not have such a construction of their links, but the protein chains have, as we will see soon.

It is not out of place to mention that a “usual” crystal melting also cannot explain protein denaturation: proteins have no periodic crystal lattice, while the lattice is the main that distinguishes a crystal from liquid, and the origin of crystal melting is just a decay of this lattice.

To understand protein denaturation, one has to explain why there exist two equally stable phases of the protein chain (which is impossible for usual polymers), and why they are separated by a free energy barrier (which is necessary for the “all-or-none” transition) [49, 50]. That is, one has to explain why the protein globule cannot decay by gradual swelling, like usual polymer globules do.

In doing so, one has to take into account the main peculiarities of proteins (those which differ them from usual polymers): that each protein has one chain fold distinguished by its peculiar stability; that flexible side groups are attached to a more rigid backbone of the protein chain; and that the native protein is packed as tightly as a molecular crystal.

Side groups of protein chains are capable of rotational isomerization, *i.e.*, jumps from one allowed conformation to another. Each jump requires some vacant volume around the jumping side chain; but the native protein fold is distinguished by a tight packing (contributing to a peculiar stability of this fold) that excludes these jumps. Besides, the side chains are bound to the rigid backbone, which is especially rigid inside the globule where the chain forms α - and β -structures that are necessary to involve the backbone into the dense globule (Figs. 6, 24). These structures are stable at least until the solvent penetrates into the globule (that requires approximately the same free volume as the jumps of side groups).

One can consider two scenarios of protein denaturation: a uniform and a non-uniform swelling of the native globule. The latter is accompanied with creation a boundary between the more and less expanded parts of the globule, and the increased free energy of this boundary (*i.e.*, the surface tension) creates a free energy barrier separating the native and the denatured phases. Thus, the “non-uniform” scenario is incompatible with a gradual swelling; however, as we will see later, it is of crucial importance for kinetics of protein unfolding and folding.

A uniform swelling can be gradual, in principle. However, we shall see that a uniform expansion also cannot avoid a necessity to overcome a free energy barrier. When a globule expands, each of the rigid secondary structures has to move as a whole (at least at the beginning of the globule’s uniform expansion), with the entire forest of side chains attached.

Therefore, uniform expansion of the closely packed globule through movement of α - and β -structures creates approximately equal free spaces near each side chain, and these spaces are either insufficient for isomerization of each of the side chains (when the globule’s expansion is too small),

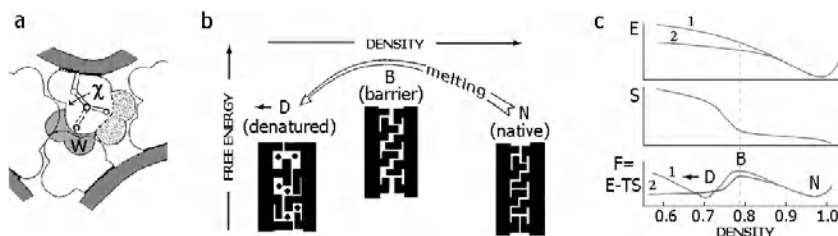


Fig. 24. a) A sketch of the side chain packing. Only a small piece of the globule is shown. The dashed region W corresponds to an alternative rotamer of the side chain (χ being its rotational angle); this rotamer is forbidden by close packing. Its appearance requires additional vacant volume for W of at least 30 \AA^3 (i.e., the volume of a methyl group), or $\approx 1/5$ of the average amino acid volume. Nearly the same volume is required for H_2O penetration in the core. **b)** Origin of the free-energy barrier between the native and any denatured state of the protein. The “barrier” state **B** arises at a small expansion of the native, closely packed state **N**. The pores formed in the state **B** *already* cause a great increase in the van der Waals energy, but *yet* allow neither side chain liberation nor penetration of the solvent (\bullet) inside the protein; the latter requires a strong solvent that causes a further swelling of the globule’s denatured state **D**. **c)** The density dependence of the globule’s energy *E* (computed from van der Waals interactions) in a poor (line 1) and strong (line 2) solvent, of its entropy *S* computed from side chain and backbone movements (both are prohibited when the globule’s density is high; the backbone movements are at least partly hindered also in the swollen globule), and of the resulting free energy *F* at the temperatures of the native state – molten globule (line 1) and the native state – coil (line 2) transitions. Adapted from [49,50].

or sufficient for isomerization of many of them at once. This means that liberation of the side chains (as well as solvent penetration) does not occur gradually but only at once, when the globule’s expansion crosses some threshold, the “barrier” (Fig. 24). These two events can make a less dense state of the protein chain as stable as its native state, but only after the critical density has been passed.

Thus, a small (“pre-barrier”) expansion of the native globule *always* increases its free energy: it *already* increases the globule’s energy but does not increase its entropy because the small expansion does not *yet* liberate the rotational isomerization of the side chains. On the contrary, a large (“post-barrier”) expansion liberates the rotational isomerization and leads (at sufficiently high temperature) to decreasing free energy (see legend to Fig. 24). As a result, protein denaturation does not occur gradually but as a jump over the free energy barrier, in accordance with the “all-or-none” principle.

Thus, the protein tolerates, without a change, modification of ambient conditions up to a certain limit, and then melts altogether, like a solid body. This resistance and hardness of protein, in turn, provides reliability of its biological functioning.

Prior to the molten globule state discovery, protein denaturation was usually considered as a complete decay of protein structure, *i.e.*, as a transition to the coil. After this discovery, it became clear that the denatured protein can be rather dense as well as loose depending on the solvent's strength and hydrophobicity of the protein chain. The pores in the molten globule (*i.e.*, the vacant spaces necessary for the side chain movements, see Figs. 22, 24) are "wet", *i.e.*, they are occupied by the solvent because a water molecule inside the protein is still better than a vacuum. Experimentally, the "wetness" of the molten globule is proved by the absence of a visible increase in the protein partial volume after denaturation of any kind [53].

When the solvent is poorly attracted by the protein core (consisting mainly of hydrophobic groups, although including some polar backbone atoms too), it only occupies the pores that already exist in the molten core to ensure side chain movements, but it does not create new pores and does not expand the globule (like water does not expand a sponge, although occupies its pores). Then the denatured protein remains in the wet molten globule state. Its compactness is maintained by residual hydrophobic interactions.

However, if the residual hydrophobic interactions are weak, *i.e.*, if the solvent is strongly attracted by the protein chain, the solvent starts to expand the pores, and the globule starts to swell.

The greater the attraction between the solvent and the protein chain, and the smaller the attraction within the chain, the greater the swelling: up to transition to the random coil.

Figure 19 shows that the coil arises directly from the native state if the temperature is low, *i.e.*, when the role of the entropy of side chain liberation is not crucial, and the main denaturation effect is produced by the solvent (recall also the cold denaturation); and at a higher temperature the coil can arise rather after the swelling of the molten globule.

It seems [50] that the molten globule swelling and its transition to the coil can be described by the conventional theory of globule-coil transitions [51], *i.e.*, that it can proceed without any jump in density.

However, at least for one protein (carbonic anhydrase) it has been shown that the molten globule is separated from the more swollen ("pre-molten") globule by an "all-or-none" transition [54] (which may concern, though, only the decay of a large β -sheet of carbonic anhydrase, which is of an "all-or-none" type in synthetic polypeptides [55]). Only the further unfolding

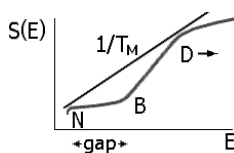


Fig. 25. Entropy S on energy E dependence for the expanding protein globule (for the case of a poor solvent). The melting temperature T_M corresponds to a tangent (whose slope $1/T \equiv [dS(E)/dE]$) that touches the high- and the low-energy parts of the concave $S(E)$ curve simultaneously.

of the “pre-molten” globule of carbonic anhydrase seems to be a gradual transition into the coil.

I have to conclude that the nature of the molten globule to the coil transition (that may or may not pass *via* a “pre-molten” state) is yet to be understood, that is, a more accurate physical theory of this phenomenon is needed.

3.4 “Gap” in energy spectrum: The main characteristic that distinguishes protein chains from random polymers

It is instructive to consider the above described melting of native protein structures using energy spectra of protein globules.

Having plotted the protein entropy S and energy E as functions of protein density (Fig. 24c), we can plot the S -on- E dependence (Fig. 25). Since $S(E)$ is proportional to the logarithm of the number of structures with energy E , we can grasp a typical appearance of the density of the protein energy spectrum. We see that the “all-or-none” transition results from an “energy gap” between the low-energy native fold and the region where the energy spectrum density starts a rapid growth with the energy.

Thus, the only one peculiarity, the gap in the energy spectrum between the native fold and the most of others, is responsible for both main features that distinguish protein globules from the ones formed by homopolymers and random heteropolymers: (i) the existence of a definite 3D structure and (ii) its “all-or-none” rather than a gradual decay.

It is noteworthy that although most of random sequences do not produce any visible energy gap, such a gap is produced by a little but very important fraction them.

Investigation of randomness or, better to say, quasi-randomness of protein sequences and structures has been pioneered by Bresler and Talmud [22], Poroikov *et al.* [23] and Ptitsyn [57].

Investigation of energy spectra of random and quasi-random heteropolymers has been started in pioneer works of Bryngelson and Wolynes [33, 56, 58], Garel and Orland [59] and Shakhnovich and Gutin [34, 60]. The idea was to apply statistical description of energy spectra developed to random systems like spin glasses [32, 61] to heteropolymers and protein chains.

Bryngelson and Wolynes postulated [33] that the main peculiarity of proteins is an enhanced correlation of energies of various interactions in the native fold of its chain. As for the random heteropolymers, it has been proven [34] that their energy spectra are well described by the random energy model of Derrida [32], which is the simplest model describing a large class of systems with random Hamiltonians. According to the random energy model, a typical freezing of the random system looks like a vitrifying, since, almost always, the energy spectrum density of the random system gradually increases with energy. However, the same model predicts that *some small part* of the random systems has a considerable energy gap between their lowest-energy structure and the region where the energy spectrum density starts a continuous growth with the energy (Fig. 26).

Two peculiar temperatures are determined by such energy spectra. These are the melting temperature T_M and the vitrifying temperature T_C (see legend to Fig. 26). A typical random heteropolymers does not have the “energy gap” (or rather, this gap is negligible, about kT_C); it has only the vitrifying transition at $T = T_C$. On the contrary, the lowest-energy fold of protein chain freezes (by an “all-or-none” transition) at $T_M > T_C$ (T_C being the same for random and protein sequences equal in amino acid content).

It can be shown [27, 35] that the difference between T_M and T_C values depends on the gap width ΔE as

$$T_M - T_C = (2\Delta E T_C / C_C)^{1/2} \quad (3.2)$$

when the gap is comparatively narrow ($\Delta E \ll T_C C_C$; still, it is assumed that $\Delta E \gg kT_C$). Here $C_C = -[T_C^2(d^2S(E)/dE^2)]^{-1}$ is the heat capacity corresponding to the continuous spectrum at $T \rightarrow T_C$ from the above; it is proportional to the number of residues in the chain. Under the same condition $\Delta E \ll T_C C_C$, the latent heat of protein melting is

$$E_{\text{MELT}} = (2\Delta E T_C C_C)^{1/2} \quad (3.3)$$

i.e., it is much larger than the gap ΔE itself.

This means that the “all-or-none” protein melting needs only a moderately large energy gap between the lowest-energy fold and the bulk of the others: the gap width ΔE should be large as compared with kT_C , but it is not required to be proportional to the number of residues in the chain.

The energy gap is a privilege of selected, “protein-suitable” chains only. Only such chains allow a unique stable fold, and this fold is both formed

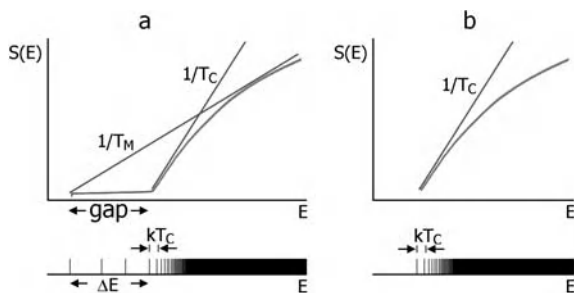


Fig. 26. Tentative dependence of the entropy S on the energy E for the protein chain **a)** and for a random heteropolymer **b)**. Typical energy spectra are shown below. Each spectrum line (only a few of them are shown) corresponds to one chain conformation (more precisely, to one energy minimum in the conformational space). The right, high-energy part of each spectrum has plenty of such lines, and they merge into a virtually continuous spectrum. The tangent touching the lower part of the $S(E)$ curve (in **a**), to the right of the gap) determines the temperature T_C of chain vitrifying (the same temperature, by the way, appears in statistics of protein structures, see [26–28]). The main peculiarity of the spectrum of protein (the “selected” heteropolymer) is a large energy gap (width $\Delta E \gg kT_C$) between the lowest-energy fold and other “misfolded” structures. The energies of only a few structures get into this “gap”; typically, they are somewhat disordered or nearly folded variants of the lowest-energy fold. They play no role in thermodynamics of the chain but are important for kinetics of its folding (as we will see later on). The tangent touching (in **a**)) the lowest-energy fold and the high-energy part of the $S(E)$ curve determines the melting temperature T_M (the temperature of co-existence of the lowest-energy structure and a multitude of high-energy ones). Since the slope of this tangent is less than that of the former one, $T_M > T_C$. This means that cooling of the “protein” (a chain with a large energy gap $\Delta E \gg kT_C$) leads to “all-or-none” freezing of its lowest-energy structure prior to vitrifying of the chain, that is, prior to freezing of misfolded structures corresponding to the right side of the gap. A typical random heteropolymer (a chain having no “gap”), on the contrary, has only a vitrifying transition.

and protected against gradual softening by the “all-or-none” transition. It seems that the natural selection picks up such sequences because of their unique capability of forming solid protein globules with fixed 3D structures: only among them it can find those capable of reliable functioning in the organism.

In principle, one could obtain all three main parameters (T_C , C_C , ΔE) of the above described protein model from the three experimental values ($T_M = T_0$, ΔC_p , ΔH) shown in Figure 19. Unfortunately, this estimate

will be not reliable: a large part of ΔC_p is due to the temperature shift of individual energy lines (*i.e.*, to the increased heat capacity of hydrophobic side chains exposed to the water in the denatured state) rather than to the shift of this state along the spectrum, which is only taken into account by the above described REM-based model of protein melting.

However, one can estimate the $\Delta E/kT_C$ value from quite different experiments. Using the REM-based model of proteins, the fraction of random heteropolymers with the energy gap of a given width ΔE can be estimated [27, 62] as

$$\text{FRACTION}(\Delta E) \sim \exp(-\Delta E/kT_C) \quad (3.4)$$

(*cf.* Eq. (2.6)). This fraction is rather small when $\Delta E \gg kT_C$, which is reasonable: protein creation is not at all easy. Though, this fraction is not negligible: if $\Delta E \sim 20kT_C$ (which is far enough to create a reliable barrier between the native fold and its competitors), this fraction amounts to $\sim 10^{-9}$.

Modern experimental methods in molecular biology (for example, the phage display method [63, 64]) are already able to select such a small fraction of polypeptides provided they can acquire some structure and become capable of strong binding to something. Therefore, it is no wonder that some recent experiments with random polypeptides proved to be able to produce the “protein-like” molecules [65–67]. The success of these experiments helps us to estimate the $\Delta E/kT_C$ value as $\sim 20kT_C$.

It is noteworthy that the same REM-based model of proteins predicts that it is much harder to produce a chain that can stabilize two (or more) different folds. That is, the gap ΔE that separates *two* folds from their competitors occurs in $\sim \exp(-2\Delta E/kT_C)$ of “random” chains only. In other words, to make a chain with one native fold is a wonder, to make a chain with two native fold is a squared wonder, with three a cubed wonder, and so on... Therefore, it is no surprise that there are almost no proteins having alternative native structures (“almost”, because there is at least one protein of this kind: serpin, which passes from its active to inactive fold in about an hour without any association or chemical change of the molecules).

The energy gap is fundamental for protein physics. It is this gap that provides the reliability of protein’s biological functioning: without it, the protein would not be able to tolerate a change of ambient conditions without changing its fold. You will see that the gap is necessary for rapid and reliable folding of protein structure (and it is quite possible that this determines the appropriate ΔE value). Therefore, an experimental estimate of this gap would be most interesting. Alas, this is not done yet, – and measuring this gap is a challenge to protein physics.

4 Kinetic aspects of protein folding

4.1 Protein folding *in vivo*

In a living cell, protein is synthesized by a ribosome that makes a protein chain (whose sequence is encoded by *mRNA*) residue by residue, from its N- to C-end, and not quite uniformly: there are temporary rests of the synthesis at the “rare” codons (they correspond to *tRNAs* which are rare in the cell, and these codons are rare in the cell’s *mRNAs*, too). It is assumed that the pauses may correspond to the boundaries of structural domains that can help a quiet maturation of the domain structures. The biosynthesis takes about a minute and yielding of a “ready” folded protein lasts as long: the experiment does not see any difference [68, 69].

Some enzymes, like prolyl-peptide- or disulfide-isomerases accelerate *in vivo* folding. They catalyze slow, if unaided, $\text{trans} \leftrightarrow \text{cis}$ conversions of prolines and formation (and decay) of S-S bonds.

Protein chain folds under the protection of special proteins, chaperons. These are the cell’s trouble-shooters that fight the aggregation, since, in a cell, folding takes place in a highly crowded molecular environment. There is no reason to assume, though, that anything other than the amino acid sequence determines protein conformation in the cell [70, 71].

It looks as though the biosynthetic machinery (ribosomes + chaperons + ...), besides of chemical synthesis of the protein chain, serve only as a kind of incubator, which does not determine the protein structure (at least if the protein is not very large) but rather provides “hothouse” conditions for its maturation, – just like a usual incubator helps a nestling to develop but does not determine what will be developed, a chicken or a duckling.

Unfortunately, it is difficult to follow the *in vivo* folding of a nascent protein chain against the background of the huge ribosome. It is known, though, that the first synthesized domains of multi-domain proteins are able to fold before the biosynthesis of the whole chain is completed [68, 71]; but there is virtually no data of this kind for single-domain proteins.

Therefore, most of experiments on protein folding are done *in vitro*.

As above, I will consider mostly the single-domain water-soluble globular proteins which are studied much better than the others.

4.2 Protein folding *in vitro* (in the test-tube)

In about 1960, a remarkable discovery was made: it was shown that a globular protein is capable of spontaneous folding *in vitro* [4]. If protein chain has not been heavily chemically modified after the initial (*in vivo*) folding, then the protein gently (without chain damaging) unfolded by temperature,

denaturant, etc., spontaneously “renatures”, *i.e.*, restores its activity and structure after solvent “normalization”. True, the effective renaturation requires a careful selection of experimental conditions; otherwise, aggregation can prevent the protein from folding.

Furthermore, it was demonstrated [5] that the protein chain synthesized chemically, without any cell or ribosome, and placed in the proper ambient conditions, folds into a biologically active protein.

The phenomenon of spontaneous folding of protein native structures allows us to detach, at least to a first approximation, the study of protein folding physics from the study of protein biosynthesis.

Protein folding *in vitro* is the most simple (and therefore, the most interesting for a physicist) case of pure *self*-organization: here nothing “biological” (but for the sequence!) helps protein chain to fold.

4.2.1 The Levinthal paradox

The ability of proteins (and RNA) to fold spontaneously immediately raised a fundamental problem that has come to be known as the Levinthal paradox [72]. It reads as follows.

On the one hand, the same native state is achieved by various folding processes: *in vivo* on the ribosome, *in vivo* after translocation through the membrane, *in vitro* after denaturation with various agents. The existence of the spontaneous and correct folding of chemically synthesized protein chains suggests that the native state is thermodynamically the most stable state under the “biological” conditions.

On the other hand, a chain has zillions of possible conformations (at least 2^{100} for a 100-residue chain, since at least two conformations are possible for each residue), and the protein can “feel” the right stable structure only if it is achieved exactly, since even a 1 Å deviation can strongly increase the chain energy in the closely packed globule. Thus, the chain needs at least $\sim 2^{100}$ picoseconds, or $\sim 10^{10}$ years to sample all possible conformations in its search for the most stable fold.

Then, how can the chain find its most stable structure within a “biological” time (minutes)?

The paradox is that, on the one hand, the achievement of the same (native) state by a variety of processes is (in physics) a clear-cut evidence of its stability. On the other hand, Levinthal’s estimate shows that the protein simply does not have enough time to prove that the native structure is the most stable among all possible structures!

Then, how does the protein choose its native structure among zillions of others, asked Levinthal, and answered: it seems that there exists a specific folding pathway, and the native fold is simply the end of this pathway rather than the most stable chain fold. Should this pathway be narrow, only a small

part of the conformational space would be sampled, and the paradox would be avoided. In other words, Levinthal suggested that the native protein structure is under kinetic rather than under thermodynamic control, *i.e.*, that it corresponds not to the global but rather to the easily accessible free energy minimum.

4.2.2 Folding pathways and folding intermediates

The question as to whether the protein structure is under kinetic or thermodynamic control is not a purely speculative question. It is raised again and again when one faces practical problems of protein physics and engineering. For example: when trying to predict protein structure from its sequence, what have we to look for? The most stable or the most rapidly folding structure? When designing a *de novo* protein, what have we to do? To maximize stability of the desired fold or to create a rapid pathway to this fold?

A discussion on protein folding mechanisms started immediately after discovery of the spontaneous folding. It seems that the first proposed hypothesis was that by Phillips who suggested that the folding nucleus is formed by the N-end of the nascent protein chain, and the remaining part of the chain wraps around it [73]. This appealing hypothesis is present in some works up to now. However, it has been refuted experimentally, as far as single-domain proteins are concerned. The elegant works by Goldenberg and Creighton have shown that the N-terminus has no special role in the *in vitro* folding: it is possible to glue the ends of the chain of a small protein with a peptide bond, and it folds into the correct 3D structure, nevertheless [74]. Moreover, it is possible to cut this circular chain so that to make a new N-end at the former middle of the chain; and it folds, nevertheless, to the former native structure. Nowadays, protein engineering routinely produces circularly permuted proteins.

In an effort to solve the folding problem, Ptitsyn proposed a model of stepwise protein folding [75] (Fig. 27). Later given the name “framework model”, this hypothesis stimulated investigation of folding intermediates. It postulated a stepwise involvement of different interactions in the protein structure formation, stressed the importance of rapidly folded α -helices and β -hairpins at the initial folding steps, gluing of these helices and hairpins into a native-like globule, and the final crystallization of the structure within this globule at the last step of folding.

The cornerstone of this concept was then hypothetical and now well known folding intermediate, the “molten globule”, which was later discovered and studied first as the equilibrium state of a “weakly denatured” protein [76, 77] and then as a kinetic folding intermediate [78].

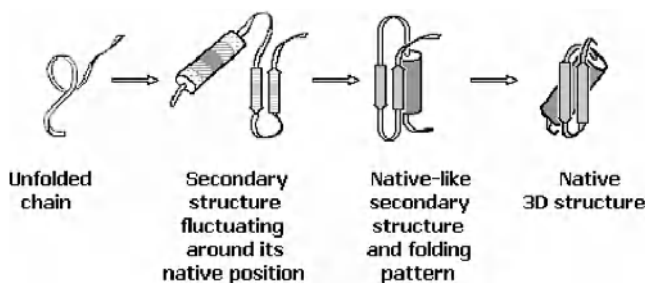


Fig. 27. Framework model of stepwise folding [75]. The secondary structures are shown as cylinders (α -helices) and arrows (β -strands). Both predicted intermediates have been already observed; the first is now known as the “pre-molten globule” and the other as the “molten globule” [47].

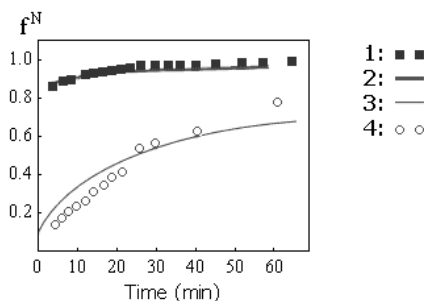


Fig. 28. Kinetics of recovery of a “degree of nativity” (f^N) in the process of carbonic anhydrase B renaturation [78]. Transition of the protein from its fully unfolded state (existing at 5.45 M GuHCl concentration) to the native state (at 0.97 M GuHCl) is followed by intrinsic viscosity (1), by ellipticity at 222 nm (2) and at 270 nm (3), and by enzymatic activity (4).

Figure 28 shows that different properties of the native protein have two quite different rates of restoring, which is an evidence for accumulation of some “intermediate” state of the protein molecule (as shown, the molten globule [78]) at the beginning of the folding process.

The molten globule is an early folding intermediate in the *in vitro* folding of many proteins at physiological conditions [47, 79, 80]. It takes a few milliseconds to form, while the complete restoration of native properties of a 100–300 residue chain can take seconds for some proteins and hours for others. Thus, the rate-limiting folding step concerns formation of the native “solid” protein from the molten globule rather than formation of the molten globule from the coil.

The molten globule is not the only intermediate observed in protein folding. The “pre-molten” globule (that also fits the “framework model”) was observed to precede the molten globule formation. This intermediate was discovered with the use ultra-fast (sub-millisecond) measuring techniques. In addition, the proteins with disulfide bonds allow trapping various intermediates indicative of the order of S-S bond formation, etc.

The “kinetic control” hypothesis initiated very intensive studies of folding intermediates. Actually, it was clear almost from the very beginning that the metastable intermediates are not obligatory for folding (since the protein can fold also near the point of equilibrium between the native and denatured states, where the transition is of the “all-or-none” type, which excludes any metastable intermediates). The idea was, though, that the intermediates, if trapped, would help to trace the folding pathway, like intermediates in a complicated (bio)chemical reaction trace its pathway. This was, as it is now called, “chemical logic”. However, this logic worked only in part when it came to the protein folding. The intermediates (like molten globules) were found for many proteins, but the main question as to how the protein chain can rapidly find its native structure among zillions of alternatives remained unanswered.

4.2.3 “Two-state” protein folding

Recent progress in the understanding of protein folding [81, 82] has been achieved just by investigation of those proteins, which fold without “unnecessary complications” (previously widely used to trace the folding pathway): without accumulation of any intermediates at the folding pathways, without *cis-trans* proline isomerization, and without S-S bond formation. The folding (and the unfolding) kinetics looks very simple in this case: all the properties of the native (or denatured) protein are restored synchronically (in the contrast to Fig. 28), following the single-exponential kinetics [83]. For some proteins, this simplicity is observed in a wide range of conditions, including the zone of the reversible thermodynamic transition between two phases (the native and the denatured state); for others, only in the transition zone (Fig. 29). Thus, the universal features of folding (and unfolding) can be observed just in the transition zone, while the moving off this zone towards the “biological” conditions reveals individualities of various proteins (which are the “unnecessary complications”, when we try to understand the basics of protein folding).

The above statement looks, in a sense, paradoxical. Indeed, what can we get from investigation of folding (or unfolding) in the transition zone, where we cannot accumulate any transition intermediates? The answer is: just here we can most readily, though indirectly observe the folding transition state (TS), whose stability (or, more exactly, instability) determines the

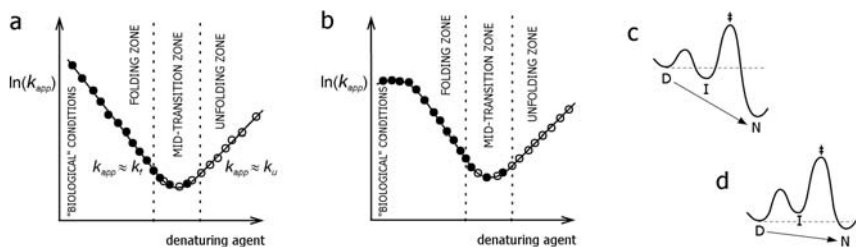


Fig. 29. Typical appearance of a chevron plot presenting the apparent rate of the folding/unfolding process (k_{app}) vs. the denaturant concentration (or the temperature). The closed circles correspond to folding occurring when the protein comes from the denaturing to renaturing medium. The open circles correspond to unfolding that occurs when the protein is transferred from the native to denaturing conditions. Note that circles of both kinds overlap at mid-transition. **a)** Typical plot for a protein having the two-state folding throughout the whole range of experimental conditions. For the two-state folding, $k_{app} = k_f + k_u$, where k_f is the folding rate and k_u is the unfolding rate: thus, $k_{app} \approx k_f$ in the folding zone (where $k_f \gg k_u$), $k_{app} \approx k_u$ in the unfolding zone (where $k_f \ll k_u$) and $k_f \approx k_u \approx k_{app}/2$ at the mid-transition [86]. **b)** Typical plot for the “multi-state” folding protein: it has the two-state folding only close to the mid-transition (*i.e.*, the point of thermodynamic equilibrium between the native and denatured states), but not at the “biological” conditions where a multi-state folding occurs. **c, d)** Free energy changes along the pathway of the “multi-state” protein folding at “biological” conditions **c)** and close to the mid-transition **d)**.

folding (and unfolding) rate [80–85]. The TS corresponds to the free energy maximum on the folding/unfolding pathway, – or, better to say, to the free energy saddle point on the network of these pathways. The folded part of TS is called “folding nucleus”.

4.2.4 Folding nucleus

“Folding nucleus” plays a key role in protein folding: its instability determines the folding and unfolding rates. So far, there is only one, very difficult experimental method to identify the folding nuclei in proteins: to find residues whose mutations affect the folding rate by changing the TS stability as strongly as that of the native protein [86, 87] (Figs. 30, 31).

The participation of a residue in the folding nucleus is expressed by the residue’s ϕ value. ϕ is defined as $\Delta \ln k_f / \Delta \ln K$, where k_f is the folding rate constant, $K = k_f / k_u$ is the folding-unfolding equilibrium constant, and Δ means the mutation-induced shift of the corresponding value. According to the model of a native-like folding nucleus [86, 87], $\phi = 1$ means that

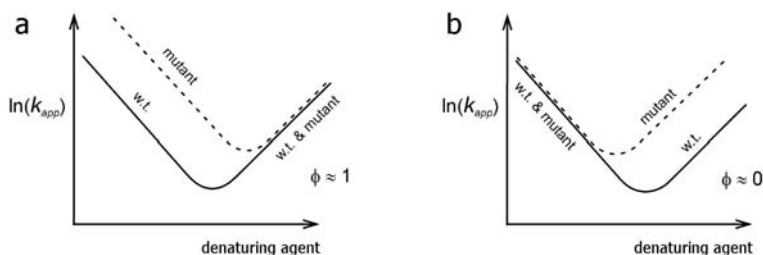


Fig. 30. Folding nucleus identification using site-directed mutations (a scheme). **a)** Mutation of a residue, having its native environment and conformation (*i.e.*, its native interactions) already in the transition state TS, changes the mutant's folding rate rather than its unfolding rate. Such a residue is in the nucleus. **b)** Mutation of a residue, which does not belong to the nucleus, *i.e.*, remains in the denatured state in the TS, has the opposite effect.

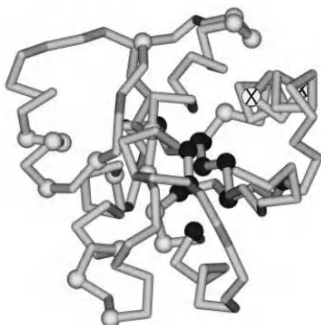


Fig. 31. Experimentally outlined folding nucleus for CheY protein [88]. The experimentally studied residues are shown as beads against the background of the native chain fold. The residues forming the folding nucleus are shown in black. Usually, the nucleus is shifted to the surface and does not coincide (though partially overlaps) with the protein's hydrophobic core. The gray beads indicate the residues that are not involved in the nucleus. The crossed beads show two residues that are difficult for interpretation since their $\Delta \ln K$ values are close to zero.

the residue has its native conformation and environment already in the transition state (*i.e.*, that this residue is in the folding nucleus), while $\phi = 0$ means that the residue remains unfolded in the TS. The values $\phi \approx 0.5$ are ambiguous: either the residue is at the surface of the nucleus, or it is in one of the alternative nuclei, belonging to different folding pathways. It is noteworthy that the values $\phi < 0$ and $\phi > 1$ (which would be inconsistent with the model of a native-like folding nucleus) are extremely rare and never concerns a residue with a reliable measured $\Delta \ln K$.

It has been shown that proteins with different sequences but similar 3D structures often have similar folding nuclei [89–91]. However, there are many exceptions [92]. It has been shown also that circular permutation, changing the protein topology, sometimes changes [93, 94] and sometimes does not change [95] the transition state.

4.3 Theory of protein folding rates and solution of the Levinthal paradox

All experimental data we discussed, though exciting, cannot answer the main question as to how a protein manages to find its native, apparently the most stable structure among zillions of others within those minutes or seconds that are assigned for its folding.

The difficulty of this problem is that it cannot be solved in direct experiment. Indeed, suppose that the protein has some structure that is more stable than the native one but folds very slowly. How can we find it if the protein does not do so itself? Shall we wait for $\sim 10^{10}$ years?

However, is there a real contradiction between “the most stable” and the “rapidly folding” structure? Maybe, the stable structure *automatically* forms a focus for the “rapid” folding pathways, and therefore it is *automatically* capable of fast folding?

Before considering *kinetic* aspects of protein folding, let us recall some basic facts concerning protein *thermodynamics* (I will talk about single-domain proteins only). This will help us to understand what chains and what folding conditions we have to consider. The facts are as follows:

- 1) protein folding-unfolding is a reversible “all-or-none” transition: only the native and denatured states of the chain are present (close to the denaturation point) in a visible quantity, while the others are virtually absent. Such a transition requires the amino acid sequence that provides a large energy gap between the native and the other folds;
- 2) the denatured state, at least that of small proteins unfolded by a strong denaturant, is often the random coil;
- 3) even under physiological conditions the native state of a protein is only by a few kcal/mol more stable than its unfolded state (and these states have equal stability at mid-transition, naturally).

Thus, to solve the “Levinthal paradox” and to show that the most stable chain fold can be found within a reasonable time, we could, to a first approximation, consider only the rate of the “all-or-none” transition between the coil and the most stable structure. And we may consider only the case when the most stable fold is close to thermodynamic equilibrium with the

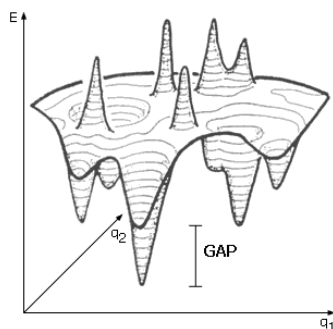


Fig. 32. Schematic representation of the bumpy energy landscape of a protein chain. Only two coordinates (q_1 and q_2) can be shown in the drawing, while the protein chain conformation is determined by hundreds of coordinates. A wide energy gap between the global and other energy minima is necessary to provide the “all-or-none” type of decay of the stable protein structure. This, in turn, makes the protein function specific: the protein either works or not, like a bulb.

coil, all other forms of the chain being unstable close to the “all-or-none” transition midpoint. Here the analysis is the simplest: it must not account for accumulating intermediates. True, the maximal folding rate is achieved when the native fold is much more stable than the coil (Fig. 29), and then the observable intermediates often arise. But let us consider the situation when the folding is not the fastest but the simplest.

Since the “all-or-none” transition requires a large energy gap between the most stable structure and the other ones (Figs. 26, 32), *we will assume that the considered amino acid sequence provides such a gap.*

I am going to show you that the “gap condition” provides a rapid folding pathway to the global energy minimum, to estimate the rate of folding, and to prove that the most stable structure of a normal size domain can fold within seconds or minutes [96].

To prove that the most stable chain structure is capable of rapid folding, it is sufficient to prove that at least one rapid folding pathway leads to this structure. Additional pathways can only accelerate the folding since the rates of parallel reactions are additive. [One can imagine water leaking from a full to an empty pool through cracks in the wall between them: when the cracks cannot absorb all the water, each additional crack accelerates filling of the empty pool. And, by definition of the “all-or-none” transition, all semi- and mis-folded forms together are too unstable to absorb a significant fraction of the folding chains and trap them.]

A rapid pathway must include not too many steps, and, first of all, it must not require overcoming of a too high free energy barrier.

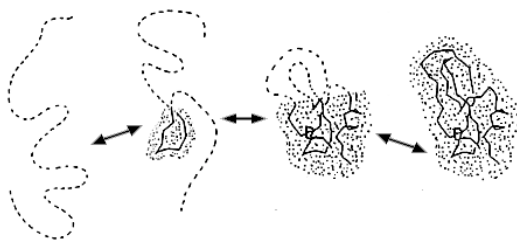


Fig. 33. Sequential folding (and unfolding) pathway. The folded part (dotted) is native-like. The bold line shows the backbone fixed in this part; the fixed side chains are not shown for the sake of simplicity (the volume that they occupy is dotted). The dashed line shows the unfolded chain.

An L -residue chain can attain its lowest-energy fold in L steps, each adding one fixed residue to the growing structure (Fig. 33). If the free energy went downhill along the entire pathway, a 100-residue chain would fold in ~ 100 – 1000 ns, since the growth of a structure (*e.g.*, an α -helix) by one residue is known to take a few nanoseconds [97]. Protein folding takes much more than $1\ \mu\text{s}$ only because of the free energy barrier, since most of the folding time is spent on climbing up this barrier and falling back, rather than on moving along the folding pathway.

According to the conventional transition state theory [98], the time of the process is estimated as

$$\text{TIME} \sim \tau \times \exp(+\Delta F^\# / RT). \quad (4.1)$$

Here τ is the time of one step ($\sim \text{ns}$ for adding a residue to protein structure [97]), and $\Delta F^\#$ the free energy barrier height.

Our main question is: how high is the free energy barrier $\Delta F^\#$ on the pathway leading to the lowest-energy structure?

If the fold-stabilizing contacts start to arise only when the chain comes very close to its final structure (that is, if the chain has to lose almost all its entropy *before* the energy starts to decrease), the initial free energy increase would form a very high free energy barrier (proportional to the *total* chain entropy lost). The Levinthal paradox claiming that the lowest-energy fold cannot be found within any reasonable time, since this involves exhaustive sampling of all chain conformations, originates exactly from this picture (loss of the entire entropy *before* the energy gain).

However, this paradox can be avoided if there is a folding pathway where the entropy decrease is immediately or nearly immediately covered by the energy decrease (as in the usual first order phase transitions).

Let us consider a *sequential* (Fig. 33) folding pathway. At each step of this process, one residue leaves the coil and takes its final position in the

lowest-energy 3D structure. This pathway looks a bit artificial, but it is exactly the pathway of unfolding of the lowest-energy structure, went in the opposite direction. The detailed balance law [99] reads that direct and reverse reactions must follow the same pathway(s) under the same conditions (and we already agreed to consider the mid-point of the folding-unfolding equilibrium). The advantage of considered folding scenario is that it obviously exists (though the others are also not excluded); second, it allows us to consider only those residue-residue contacts which exist in the native protein [100].

Since, in the equilibrium point, the free energies of the native and the unfolded phases are equal, the additional free energy $\Delta F^\#$ of the nucleus is due only to the boundary between the native and the unfolded phases. If the boundary goes across the globule (Fig. 33), it includes not more than $\approx L^{2/3}$ out of L residues of the chain. The energy of this boundary can be estimated as $\approx 0.25\varepsilon L^{2/3}$ [96], where ε is the protein denaturation energy per residue. The latter has been experimentally estimated as ≈ 1 kcal/mol, or $\approx 2RT$ at the room temperature [24]. Besides, depending on the protein topology and the boundary position, the surface of the nucleus may be or may be not covered by the unfolded closed loops, whose entropy adds to the conventional surface energy of the boundary. This term does not exceed $RTL^{2/3}$ [96].

Thus, the free energy barrier for folding (and unfolding) in the mid-transition can be estimated as

$$\Delta F^\# = (1 \pm 0.5)RT L^{2/3} \quad (4.2)$$

$\Delta F^\#$ is $1.5L^{2/3}RT$, when the boundary is densely covered by loops, and $0.5L^{2/3}RT$, when the boundary is free of them [96]. Since a characteristic time of rearrangement of one residue τ is ≈ 10 ns [97], it takes up to ~ 10 ns $\times \exp(1.5L^{2/3})$ to overcome the free energy barrier of nucleation in the first case, and only ~ 10 ns $\times \exp(0.5L^{2/3})$ in the second. This range is exactly consistent with the observed times of protein folding near the mid-transition (Fig. 34). It has been also estimated that knotting of a 100–300-residue chain can increase this time a few times at most [101].

The reason for the obtained “non-Levinthal” estimate of achievement of the lowest-energy structure,

$$\text{TIME} \sim \exp \left[(1 \pm 0.5)L^{2/3} \right] \text{ nanoseconds}, \quad (4.3)$$

is that the entropy decrease is almost immediately compensated for by the energy gain along the sequential folding pathway [105], and the free energy barrier occurs owing to the surface effects only.

nuclei [110], can be obtained from analysis of the networks of folding pathways (or rather, the networks of pathways of unfolding of native protein structures).

It should be noted [111] that a hierarchic scheme of protein folding [72, 73, 75, 112], as well as many simplified “protein folding funnel” models [113, 114] do not solve the Levinthal paradox since they cannot provide a *simultaneous* explanation for all the above discussed major features observed for protein folding: (i) folding within non-astronomical time, (ii) the fact that the same native structure can be achieved at very different conditions (including the thermodynamic mid-transition) and with very different folding rates, and (iii) co-existence, in a visible quantity, of only the native and unfolded molecules during folding of moderate size (single-domain) proteins near the thermodynamic mid-transition between the native and denatured states.

On the contrary, a nucleation mechanism can account for all these major features simultaneously and thus resolves the Levinthal paradox.

The obtained results show, in accordance with experiment, that the most stable fold of a 100-residue protein must be normally found out within minutes even near the thermodynamic mid-transition. They explain also why the very large protein should consist of the separately folding domains (“foldons”): otherwise, the chains of more than ~ 300 residues would fold too slowly.

Besides, the considered theory [96] suggests that the folding nucleus is large and includes, roughly, a half of the protein, which is consistent with nearly equal slopes of two chevron plot limbs (see Fig. 27).

So far, we only considered the folding rate close to the mid-transition, where only one (the “native”) fold competes with the coil, and all other globular forms, even taken together, are unstable.

If we come to environment that stabilizes the native protein fold, it stabilizes the other globular structures as well. At first, this only increases the folding rate (see the rise of the left chevron limb from the mid-transition in Fig. 29), since the folding nucleus also is stabilized, and the competing with the native fold misfolded structures are still unstable (relative to the initial unfolded state) due to the energy gap between them and the native fold (Fig. 35a). Since the nucleus embraces, roughly, half of the protein, the decrease in the native state free energy by ΔG decreases the free energy of the nucleus by $\approx \Delta G/2$ and thus multiplies the folding rate by $\sim \exp(-\Delta G/2RT)$.

However, the acceleration proceeds up to a certain limit only: the maximal folding rate is achieved when the “misfolded” states become as stable as the unfolded state, *i.e.*, when the folding intermediates arise (see the plateau at the top of the left chevron limb in Fig. 29b). The further

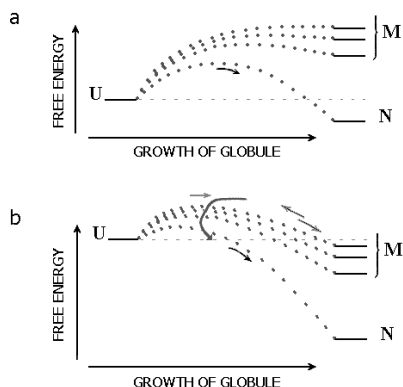


Fig. 35. Folding under conditions when **a)** the most stable fold N is only a little more stable than the unfolded chain U , and **b)** when N is much more stable than U . The mis- or semi-folded structures are shown by numerous lines M . Being less stable than U in the case **a)**, these structures are more stable than U in the case **b)**. Dotted lines schematically show the free energy changes along the folding pathways leading to different structures; their maxima correspond to the transition states on these pathways. Adapted from [96].

increase in stability of the folded states leads to a rapid misfolding followed by a relatively slow conversion into the native state (Fig. 35b).

Actually, all this resembles crystallization (where a kind of the Levinthal paradox also exists, since the decrease in the number of configurations during the crystallization is really huge): at the freezing temperature, a perfect large monocrystal (the lowest-energy structure) arises, although extremely slowly. As the temperature is a bit decreased, the monocrystal grows faster; and a further temperature decrease leads to a rapid formation of the multitude of chips rather than of a perfect large monocrystal.

Therefore, it is not out of place now to compare the above given theory of protein folding rates with a conventional theory developed for the first order phase transitions [99]. According to this theory, the time necessary to initiate the first order phase transition in a given point of space accords to equation (4.1), where the transition state free energy $\Delta F^\#$ is estimated as follows.

The free energy of the growing droplet (or chip) has a form

$$\Delta F(n) = \Delta\mu n + Bn^{2/3}, \quad (4.4)$$

where n is the number of particles in the droplet of the nascent phase, $\Delta\mu$ is the difference of chemical potentials between the nascent and the initial phases (thus, $\Delta\mu < 0$ if the new phase arises, while $\Delta\mu = 0$ corresponds the

phase equilibrium), and $B > 0$ is proportional to the additional free energy of one particle at the droplet's surface. Estimating the maximal ΔF value from $d(\Delta F)/dn = 0$, we have

$$\Delta F^\# = (4/27)B^3/(\Delta\mu)^2, \quad (4.5)$$

while the size of the critical nucleus is $n^\# = (8/27)B^3/(-\Delta\mu)^3$.

Let L be the number of particles in the smallest stable droplet, whose free energy $\Delta F(L) = 0$. Then $L = B^3/(-\Delta\mu)^3$, and we can express the $-\Delta\mu$ value as a function of L :

$$-\Delta\mu = B/L^{1/3}. \quad (4.6)$$

Then we see that the transition state free energy on the pathway to the smallest stable droplet depends on the size L of this droplet as

$$\Delta F^\# = (4/27)BL^{2/3}, \quad (4.7)$$

i.e., it has the same scaling with L as the free energy of the protein folding transition state (see Eq. (4.2)). This stresses a resemblance of protein folding and the first order phase transitions once again. The only difference is that protein is so small that the free energy difference between its two phases (native and denatured) is always about a few kT , while the total free energy difference of two macroscopic phases is always huge as compared with kT (though, close to mid-transition, it is very small as compared with kT , if calculated per particle).

Now, it is worthwhile to consider protein folding in a case when two (or more) protein structures instead of one are separated from others with a large energy gap. In this case the structure with the lower folding barrier is the first to fold, but, if it is even a little less stable than another one, it will later undergo a slow (see Fig. 35) transition to this another structure. This transition is similar to the polymorphous transition in crystals (recall the “tin disease”, *i.e.*, transition of white tin into gray tin). The “polymorphous” proteins must be rare, though, as it is suggested by discussion at the end of Chapter 3. However, such a slow transition is known at least for one protein, serpin. Besides, prions (recall the “mad cow disease”) undergo similar, extremely slow transition coupled with association of the transformed (infected) prion globules.

The existence of polymorphous transitions in proteins again shows a resemblance of protein folding and the first order phase transitions.

The above given scheme of entropy-by-energy compensation along the folding pathway and the conclusion that it can solve the Levinthal paradox are applicable to formation of the native protein structure not only from the coil but also from the molten globule or from another intermediate.

However, for these scenarios, all the estimates would be much more cumbersome, while these processes do not show (experimentally) any drastic advantage in the folding rate. Therefore, I will not go beyond the simplest case of the coil-to-native globule transition.

Actually, protein folding differs from interconversions of small molecules only by the following: 1) a particular protein structure is the result of many weak interactions; 2) a large change in conformational entropy occurs; 3) the native and denatured phases are separated during the folding. And it differs from first order phase transitions like crystallization mainly by a microscopic size of the protein and, to a lesser extent, by heterogeneity of monomers beaded at the protein chain.

I am grateful to D.S. Rykunov, O.V. Galzitskaya, D.N. Ivankov, N.S. Bogatyreva and S.A. Garbyzinskii for their kind assistance in preparation of these lectures. The work was supported by the Russian Foundation for Basic Research and by an International Research Scholar's Award from the Howard Hughes Medical Institute.

References

- [1] J.C. Kendrew, G. Bodo, H.M. Dintzis, *et al.*, *Nature* **181** (1958) 662.
- [2] M.F. Perutz, M.G. Rossmann, A.F. Cullis, *et al.*, *Nature* **185** (1960) 416.
- [3] K. Wüthrich, *NMR of proteins and nucleic acids* (John Wiley & Sons, N.Y., 1986).
- [4] C.B. Anfinsen, E. Haber, M. Sela and F.H. White, *Proc. Natl. Acad. Sci. USA* **47** (1961) 1309.
- [5] B. Gutte and R.B. Merrifield, *J. Amer. Chem. Soc.* **91** (1969) 501.
- [6] P.L. Privalov and N.N. Khechinashvili, *J. Mol. Biol.* **86** (1974) 665.
- [7] L. Pauling, *General chemistry* (W.H. Freeman & Co., N.Y., 1970).
- [8] L. Pauling, R.B. Corey and H.R. Branson, *Proc. Natl. Acad. Sci. USA* **37** (1951) 205.
- [9] L. Pauling and R.B. Corey, *Proc. Natl. Acad. Sci. USA* **37** (1951) 729.
- [10] C. Branden and J. Tooze, *Introduction to Protein Structure* (Garland Publ., Inc., N.Y. – London, 1991).
- [11] A.V. Finkelstein and O.B. Ptitsyn, *Protein Physics. A Course of Lectures* (Academic Press, An Imprint of Elsevier Science, Amsterdam – Boston – London – N.Y. – Oxford – Paris – San Diego – San Francisco – Singapore – Sydney – Tokyo, 2002).
- [12] F.C. Bernstein, T.F. Koetzle, E.F. Meyer Jr., *et al.*, *J. Mol. Biol.* **112** (1977) 535.
- [13] P.J. Kraelis, *J. Appl. Cryst.* **24** (1991) 946.
- [14] M. Levitt and C. Chothia, *Nature* **261** (1976) 552.
- [15] J.S. Richardson, *Nature* **268** (1977) 495.
- [16] J.S. Richardson, *Adv. Prot. Chem.* **34** (1981) 167.
- [17] O.B. Ptitsyn and A.V. Finkelstein, *Quart. Rev. Biophys.* **13** (1980) 339.
- [18] A.V. Finkelstein and O.B. Ptitsyn, *Progr. Biophys. Mol. Biol.* **50** (1987) 171.
- [19] L. Holm, C. Ouzonis, C. Sander, G. Tuparev and G. Vriend, *Protein Sci.* **1** (1993) 1691.

- [20] A.G. Murzin, S.E. Brenner, T. Hubbard and C. Chothia, *J. Mol. Biol.* **247** (1995) 536.
- [21] C.A. Orengo, A.D. Michie, S. Jones, *et al.*, *Structure* **5** (1997) 1093.
- [22] C.E. Bresler and D.L. Talmud, *Doklady AN SSSR* **47** (1944) 326; *ibid.*, 367.
- [23] V.V. Poroikov, N.G. Esipova and V.G. Tumanyan, *Biofizika* **21** (1976) 397.
- [24] P.L. Privalov, *Adv. Protein Chem.* **33** (1979) 167.
- [25] C. Chothia, *J. Mol. Biol.* **75** (1973) 295.
- [26] A.V. Finkelstein, A.M. Gutin and A.Ya. Badretdinov, *FEBS Lett.* **325** (1993) 23.
- [27] A.V. Finkelstein, A.M. Gutin and A.Ya. Badretdinov, *Subcellular Biochem.* **24**, *Proteins: Structure, Function and Protein Engineering*, edited by B.B. Biswas and S. Roy (Plenum Press, 1995) 1.
- [28] A.V. Finkelstein, A.Ya. Badretdinov and A.M. Gutin, *Proteins* **23** (1995) 142.
- [29] S. Miller, J. Janin, A.M. Lesk and C. Chothia, *J. Mol. Biol.* **196** (1984) 641.
- [30] F.M. Pohl, *Nature New Biol.* **23** (1971) 277.
- [31] L.D. Landau and E.M. Lifshitz, *Statistical Phys.* (Pergamon, London, 1959).
- [32] B. Derrida, *Phys. Rev. B* **24** (1981) 2613.
- [33] J.B. Bryngelson and P.G. Wolynes, *Proc. Natl. Acad. Sci. USA* **84** (1987) 7524.
- [34] E.E. Shakhnovich and A.M. Gutin, *Biophys. Chem.* **34** (1989) 187.
- [35] R.A. Goldstein, Z.A. Luthey-Schulten and P.G. Wolynes, *Proc. Natl. Acad. Sci. USA* **89** (1992) 4918; *ibid.*, 9029.
- [36] S. Govindarajan and R.A. Goldstein, *Proc. Natl. Acad. Sci. USA* **93** (1996) 3341.
- [37] H. Li, R. Helling, C. Tang and N. Wingreen, *Science* **273** (1996) 666.
- [38] R. Mélin, H. Li, N.S. Wingreen and C. Tang, *J. Chem. Phys.* **110** (1999) 1252.
- [39] H. Nojima, A. Ikai, T. Oshima and H. Noda, *J. Mol. Biol.* **116** (1977) 429.
- [40] P.L. Privalov, *Adv. Protein Chem.* **35** (1982) 1.
- [41] Yu.V. Griko, P.L. Privalov, S.Yu. Venyaminov and V.P. Kutysenko, *J. Mol. Biol.* **202** (1988) 127.
- [42] J.F. Brandts and L. Hunt, *J. Am. Chem. Soc.* **89** (1967) 4826.
- [43] T.E. Creighton, *Proteins*, 2-nd Ed. (W.H. Freeman & Co., N.Y., 1991).
- [44] C. Tanford, *Adv. Prot. Chem.* **23** (1968) 121.
- [45] D.A. Dolgikh, L.V. Abaturon, I.A. Bolotina, *et al.*, *Eur. Biophys. J.* **13** (1985) 109.
- [46] W. Pfeil, V.E. Bychkova and O.B. Ptitsyn, *FEBS Lett.* **198** (1986) 287.
- [47] O.B. Ptitsyn, *Adv. Protein Chem.* **47** (1995) 83.
- [48] C.M. Dobson, *Curr. Biol.* **4** (1994) 636.
- [49] E.I. Shakhnovich and A.V. Finkelstein, *Biopolymer* **28** (1989) 1667.
- [50] A.V. Finkelstein and E.I. Shakhnovich, *Biopolymers* **28** (1989) 1681.
- [51] I.M. Lifshitz, A.Yu. Grosberg and A.R. Khokhlov, *Rev. Mod. Phys.* **50** (1979) 683.
- [52] N. Kayaman, E.E. Guerel, B.M. Baysal, F. Karasz, *Macromolecules* **32** (1999) 8399.
- [53] P.I. Bendsko, W.A. Pfeil, P.L. Privalov and E.I. Tiktopulo, *Biophys. Chem.* **29** (1988) 301.
- [54] V.N. Uversky, G.V. Semisotnov, R.H. Pain and O.B. Ptitsyn, *FEBS Lett.* **314** (1992) 89.
- [55] V.G. Adonts, T.M. Birshtein, A.M. Elyashevich, A.M. Skvortsov, *Biopolymers* **15** (1976) 1037.
- [56] J.D. Bryngelson and P.G. Wolynes, *J. Phys. Chem.* **93** (1989) 6902.

- [57] O.B. Ptitsyn, *Conformation in Biology*, edited by R. Srinivasan, R.M. Sarma (Academic Press, N.Y., 1983), 49.
- [58] J. D. Bryngelson and P. G. Wolynes, *Biopolymers* **30** (1990) 177.
- [59] T. Garel and H. Orland, *Europhys. Lett.* **6** (1988) 307; *ibid.*, 597.
- [60] E.I. Shakhnovich and A.M. Gutin, *Nature* **346** (1990) 773.
- [61] K. Binder and A.P. Young, *Rev. Mod. Phys.* **58** (1986) 801.
- [62] A. Šali, E.I. Shakhnovich and M. Karplus, *J. Mol. Biol.* **235** (1994) 1614.
- [63] T. Clackson, H.R. Hoogenboom, A.D. Griffiths and G. Winter, *Nature* **352** (1991) 624.
- [64] H. Gu, Q. Yi, S.T. Bray, *et al.*, *Protein Sci.* **4** (1995) 1108.
- [65] C. Cheadle, Y. Ivashchenko, V. South, *et al.*, *J. Biol. Chem.* **269** (1994) 24034.
- [66] N.C. Wrighton, F.X. Farrell, R. Chang, *et al.*, *Science* **273** (1996) 458.
- [67] P. Minard, M. Scalley-Kim, A. Watters and D. Baker, *Protein Sci.* **10** (2001) 129.
- [68] L. Stryer, *Biochemistry*, 4th Ed. (W.H. Freeman & Co., N.Y., 1995).
- [69] V.A. Kolb, E.V. Makeev and A.S. Spirin, *EMBO J.* **13** (1994) 3631.
- [70] R.J. Ellis and F.U. Hartl, *Curr. Opin. Struct. Biol.* **9** (1999) 102.
- [71] B. Hardesty, T. Tsalkova and G. Kramer, *Curr. Opin. Struct. Biol.* **9** (1999) 111.
- [72] C. Levinthal, *J. Chim. Phys. Chim. Biol.* **65** (1968) 44.
- [73] D.C. Phillips, *Sci. Am.* **215** (1966) 78.
- [74] D.P. Goldenberg and T.E. Creighton, *J. Mol. Biol.* **165** (1983) 407; *ibid.*, **179** (1984) 527.
- [75] O.B. Ptitsyn, *Doklady AN SSSR* **210** (1973) 1213.
- [76] K. Kuwajima and S. Sugai, *Biophys. Chem.* **8** (1978) 247.
- [77] D.A. Dolgikh, R.I. Gilmanshin, E.V. Brazhnikov, *et al.*, *FEBS Lett.* **136** (1981) 311.
- [78] D.A. Dolgikh, A.P. Kolomiets, I.A. Bolotina and O.B. Ptitsyn, *FEBS Lett.* **164** (1984) 88.
- [79] J.H. Dyson and P.E. Wright, *Ann. Rev. Phys. Chem.* **47** (1996) 369.
- [80] S.E. Jackson, *Fold. Des.* **3** (1998) R81.
- [81] A.R. Fersht, *Curr. Opin. Struct. Biol.* **5** (1995) 79.
- [82] C.M. Dobson and M. Karplus, *Curr. Opin. Struct. Biol.* **9** (1999) 92.
- [83] B.B. Kragelund, C.V. Robinson, J. Knudsen, C.M. Dobson and F.M. Poulsen, *Biochemistry* **34** (1995) 7217.
- [84] S.-I. Segawa and M. Sugihara, *Biopolymers* **23** (1984) 2473.
- [85] R. Fersht, *Curr. Opin. Struct. Biol.* **7** (1997) 3.
- [86] A. Matouscheck, J.T. Kellis Jr., L. Serrano, M. Bycroft and A.R. Fersht, *Nature* **346** (1990) 440.
- [87] A. Matouscheck, J.T. Kellis Jr., L. Serrano and A.R. Fersht, *Nature* **340** (1989) 122.
- [88] E. López-Hernández and L. Serrano, *Fold. Des.* **1** (1996) 43.
- [89] J.C. Martinez and L. Serrano, *Nat. Struct. Biol.* **6** (1999) 1010.
- [90] D.S. Riddle, V.P. Grantcharova, J.V. Santiago, *et al.*, *Nat. Struct. Biol.* **6** (1999) 1016.
- [91] D. Perl, C. Welker, T. Schindler, *et al.*, *Nat. Struct. Biol.* **5** (1998) 229.
- [92] E. Steensma and C.P.M. van Mierlo, *J. Mol. Biol.* **282** (1998) 653.
- [93] A.R. Viguera, L. Serrano and M. Wilmanns, *Nat. Struct. Biol.* **3** (1996) 874.

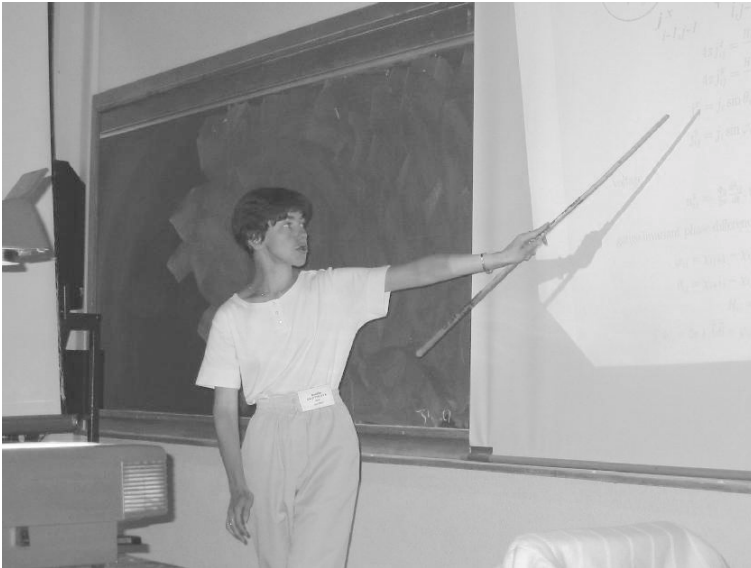
- [94] M.O. Lindberg, J. Tangrot, D.E. Otzen, *et al.*, *J. Mol. Biol.* **314** (2001) 891.
- [95] D.E. Otzen and A.R. Fersht, *Biochemistry* **37** (1998) 8139.
- [96] A.V. Finkelstein and A.Ya. Badretdinov, *Fold. Des.* **2** (1997) 115.
- [97] R. Zana, *Biopolymers* **14** (1975) 2425.
- [98] J.W. Moore and R.G. Pearson, *Kinetics and Mechanism* (J. Wiley, N.Y., 1981).
- [99] E.M. Lifshiz and L.P. Pitaevskii, *Physical Kinetics* (Pergamon, London, 1981).
- [100] N. Gö, *Int. J. Pept. Prot. Res.* **7** (1975) 313.
- [101] A.V. Finkelstein and A.Ya. Badretdinov, *Fold. Des.* **3** (1998) 67.
- [102] P.A. Thompson, W.A. Eaton and J. Hofrichter, *Biochemistry* **36** (1997) 9200.
- [103] V. Muñoz, P.A. Thompson, J. Hofrichter and W.A. Eaton, *Nature* **390** (1997) 196.
- [104] O.V. Galzitskaya, D.N. Ivankov and A.V. Finkelstein, *FEBS Lett.* **489** (2001) 113.
- [105] N. Gö, *Ann. Rev. Biophys. Bioeng.* **12** (1983) 183.
- [106] D. Thirumalai, *J. Phys. France* **5** (1995) 1457.
- [107] A.M. Gutin, V.I. Abkevich and E.I. Shakhnovich, *Phys. Rev. Lett.* **77** (1996) 5433.
- [108] K.V. Plaxco, K.T. Simons and D. Baker, *J. Mol. Biol.* **277** (1998) 985.
- [109] D.N. Ivankov and A.V. Finkelstein, *Biochemistry* **40** (2001) 9957.
- [110] O.V. Galzitskaya and A.V. Finkelstein, *Proc. Natl Acad. Sci. USA* **96** (1999) 11299.
- [111] N.S. Bogatyreva and A.V. Finkelstein, *Protein Eng.* **14** (2001) 521.
- [112] R.L. Baldwin and G.D. Rose, *Trends Biochem. Sci.* **24** (1999) 26; *ibid.*, 77.
- [113] H.S. Chan and K.A. Dill, *Proteins* **30** (1998) 2.
- [114] D.J. Bicut and A. Szabo, *Protein Sci.* **9** (2000) 452.

COURSE 13

SELF-ORGANIZED CRITICALITY IN GRANULAR SUPERCONDUCTORS

N.E. SAVITSKAYA

*Petersburg Nuclear Physics Institute,
Gatchina, Russia*



Contents

1	Introduction	707
2	1D multijunction SQUID with random location of the junctions	708
3	Single-junction SQUID	710
4	1D sandpile model	712
5	The simplified model of 1D multijunction SQUID	713
6	Computer simulation results	715
7	Conclusions	717

SELF-ORGANIZED CRITICALITY IN GRANULAR SUPERCONDUCTORS

S.L. Ginzburg¹ and N.E. Savitskaya¹

Abstract

We study the critical state of a one-dimensional granular superconductor (multijunction SQUID with random arrangement of junctions) in an increasing magnetic field. We show that the system under consideration demonstrates the self-organized behavior.

1 Introduction

During the recent years considerable interest has been paid to the magnetic properties of granular superconductors [1–4]. The properties of such systems are similar to those for “hard” type-II superconductors.

The essential feature of conventional type-II superconductor is the existence of two critical magnetic field values. An external magnetic field can penetrate inside the superconductor and form a lattice of vortices if its intensity lies between these two critical values. In this case, there are only microscopic supercurrents in the system. An attempt to pass a transport current through the sample leads to the motion of vortices and, as a result, to energy dissipation. In order to obtain the macroscopic supercurrent, it is necessary to stop the vortex motion by means of artificial or natural defects that are named as pinning centers. Such type-II superconductors with pinning centers are called “hard” type-II superconductors. In such systems the phenomenon of critical state can be observed [5].

It was demonstrated in a number of theoretical works [1–4] that granular superconductors due to their discreteness can also pin vortices and reach

This work is supported by the Russian Foundation for Basic Research (projects Nos. 02-02-16979, 02-02-06687), the Scientific Council “Superconductivity” (contract No. 40.012.1.1.11.46), the State programs “Investigations of collective and quantum effects in condensed matter” and “Quantum Macrophysics”. N.S. would like to thank “Science support foundation” (Grant for Talented Young Researches).

¹Petersburg Nuclear Physics Institute.

the critical state. The possibility of creating of the critical state depends strongly on the parameter $V \sim j_c a^3 / \Phi_0$ (a is the grain size, j_c is the critical current density in the intergranular junctions, and Φ_0 is the magnetic flux quantum). For $V \gg 1$ the granular system has a large number of metastable states. This feature is typical for the so called self-organized systems [6].

The concept of self-organized criticality (SOC) was proposed by Bak *et al.* in order to explain a behavior of many-body systems consisting of a large number of interacting elements [6], for instance, stock markets, animal populations, human brains and so on. The common amazing feature of these various systems is that the interaction between the elements makes any small external perturbation to propagate through the whole system and leads to a chain reaction and, as a result, to the energy dissipation. In addition, it was observed that the main output energetic characteristic of such systems has a power-law distribution.

According to the main principles of the SOC-concept, there is a number of giant dissipative dynamical systems which are able to accumulate small external perturbations. Under their action these systems naturally evolve into the critical state, which is self-reproducing and can persist without fine-tuning of external parameters. This state is an ensemble of various metastable states. The critical system never comes to a stable state but migrates from one metastable state to another by means of dynamical processes ("avalanches"). Avalanches may be small or large but all of them are initiated by small local perturbations. Such a critical state is called a self-organized one and a mathematical criterion of self-organization is a power-law behavior of probability density of avalanche sizes. A simple mathematical model for this type of behavior was proposed by P. Bak, C. Tang, and K. Wiesenfeld [6] (sandpile or BTW model) with many modifications subsequently introduced [7–9].

The aim of this lecture is to demonstrate that the critical state of a granular superconductor can be self-organized. This paper shows an unusual picture of the critical state in superconductors. In addition, the physical nature of granular systems introduces a series of new properties into the theory of self-organization. Our approach allows to study self-organization under conditions which have never been considered in previous models.

2 1D multijunction SQUID with random location of the junctions

The simplest example of granular superconductor is a one-dimensional multijunction SQUID that can be described as two superconducting layers that are infinitely long in the y direction and connected by Josephson junctions (Fig. 1). The junctions with size l are placed along the x axis, and the distance between the i th and $(i + 1)$ th junctions is a random variable b_i .

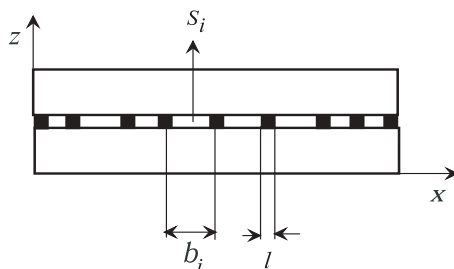


Fig. 1. The (x, z) section of one-dimensional disordered multijunction SQUID.

The system is placed into a slowly increasing magnetic field H_{ext} aligned along the y axis.

The variations of the external field H_{ext} induce the currents described by Maxwell equations:

$$4\pi j_i = \frac{H_i - H_{i-1}}{l} \quad (2.1)$$

where j_i is the current density for i th junction, H_i is the magnetic field in i th cell formed by two nearest junctions, the cells are numbered by neighboring left junction, l is the size of the junction.

Using the resistive model of Josephson junction [10], we can write the current density j_i as:

$$j_i = j_c \sin \varphi_i + \frac{\Phi_0}{2\pi\rho} \frac{d\varphi_i}{dt}, \quad (2.2)$$

where φ_i is the gauge-invariant phase differences at (i) th junction, j_c is the critical current density, ρ is the junction resistivity per unit surface, Φ_0 is the magnetic flux quantum.

Magnetic field and magnetic flux Φ_i through the cell are given by:

$$H_i = \frac{\Phi_i}{S_i}, \quad \frac{2\pi}{\Phi_0} \Phi_i = \varphi_{i+1} - \varphi_i \quad (2.3)$$

where S_i is the area of i th cell.

Substituting (2.2) and (2.3) in (2.1) we obtain the following equations for gauge-invariant phase differences:

$$\begin{aligned} V \sin \varphi_i + \tau \frac{\partial \varphi_i}{\partial t} &= J_i(\varphi_{i+1} - \varphi_i) + J_{i-1}(\varphi_{i-1} - \varphi_i); \quad i \neq 1, N; \\ V \sin \varphi_1 + \tau \frac{\partial \varphi_1}{\partial t} &= J_1(\varphi_2 - \varphi_1) - 2\pi h_{\text{ext}} \\ V \sin \varphi_N + \tau \frac{\partial \varphi_N}{\partial t} &= J_{N-1}(\varphi_{N-1} - \varphi_N) + 2\pi h_{\text{ext}}, \end{aligned} \quad (2.4)$$

with $V = \frac{16\pi^2 a l \lambda_L j_c}{\Phi_0}$, $\tau = \frac{8\pi a l \lambda_L}{\rho}$, $J_i = \frac{a}{b_i}$, $h_{\text{ext}} = \frac{2\lambda_L a}{\Phi_0} H_{\text{ext}}$, $a = \langle b_i \rangle$, where N is a number of junctions, λ_L is the London penetration depth.

The dimensionless parameter V is the main one for the system under consideration. Physically it determines the maximum flux difference in the neighboring cells. The coefficients J_i are related to inductances of the corresponding cells and depend on their areas. They characterize the orderliness of the system. If the system is regular, the coefficients J_i are identical and can be normalized to be equal to unity.

Due to its discrete structure, the multijunction SQUID is able to pin magnetic flux and reach the critical state. This critical state is a self-reproduced one. It means that after any external perturbation leading to the energy dissipation the critical state restores itself [4]. The magnetic properties of the system under consideration strongly depend on the value of the parameter V . In order to demonstrate this dependence, let us consider magnetic properties of a single element of granular system.

3 Single-junction SQUID

The single-junction SQUID is a superconducting cylinder with a Josephson junction inserted in. According to reference [10], this system is described by

$$V \sin \varphi + \tau \frac{\partial \varphi}{\partial t} = -\varphi + 2\pi F_{\text{ext}}, \quad (3.1)$$

where the gauge-invariant phase difference φ is proportional to the internal magnetic flux Φ

$$\varphi = \frac{2\pi}{\Phi_0} \Phi, \quad (3.2)$$

$F_{\text{ext}} = \frac{\Phi_{\text{ext}}}{\Phi_0}$ describes external perturbations, $\Phi_{\text{ext}} = H_{\text{ext}} S$ with S being the area of the SQUID ring, $\tau = \frac{4\pi l S}{\rho}$, $V = \frac{8\pi^2 l S}{\Phi_0} j_c$.

Considering the stable states of the SQUID, we can see that for small values of V , the internal magnetic flux Φ is approximately proportional to Φ_{ext} . In this case, the average supercurrent in the SQUID is equal to zero. For larger values of V this dependence changes and becomes multivalued for $V > 1$ (Fig. 2). For $V \gg 1$ the average supercurrent flowing through the junction is positive. It means that for $V \gg 1$ the SQUID becomes a pinning center and can accumulate a large number of magnetic flux quanta. From Figure 2 it is seen that for $V \gg 1$ the SQUID has a large number of metastable states for the same value of the external magnetic field.

The difference in properties of a single element for $V < 1$ and $V > 1$ results in two types of the critical profiles of magnetic field for large granular systems. If V is small, the field profiles consist of peaks with practically the same heights. Every peak corresponds to a single magnetic vortex occupying

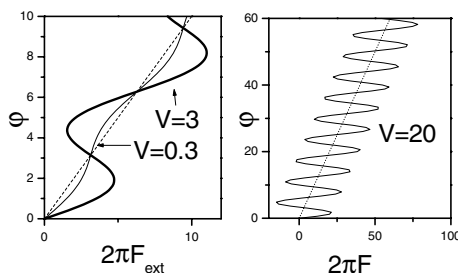


Fig. 2. The dependence of the internal magnetic flux on F_{ext} in the single-junction SQUID for different values of V .

some cells and containing one quantum of magnetic flux. This state is often referred to as vortex state. For large values of V every cell acts as a pinning center, the profile has a maximum field at the center of the sample and has pyramid-like shape [1, 4]. This state is called the Bean-like critical state.

For $V \gg 1$, the dynamical properties of a single-junction SQUID are also quite intriguing [10]. The equation (3.1) can be rewritten in the following form:

$$z = -\varphi/2\pi + F_{\text{ext}}, \quad z = z_c \sin \varphi + \frac{\tau}{2\pi} \frac{\partial \varphi}{\partial t}, \quad (3.3)$$

where z is the dimensionless current with z_c being its critical value. If the current z flowing through the junction is less than z_c , the SQUID is a superconducting ring and the phase difference is constant. If the current exceeds the critical value, the system “looses” its superconductivity and the phase slowly changes during the period T then “slides” by 2π . At this moment one flux quantum penetrates into the system, the current decreases and superconductivity reappears. As the external magnetic field increases, the process repeats itself. In this case the phase difference can be approximated by a step function:

$$\varphi \approx 2\pi p + \frac{\pi}{2}, \quad (3.4)$$

where p is an integer. We can introduce in our system the discrete time $t_k = kT$ and write the following equations for phase dynamics:

$$\varphi(k+1) = \varphi_k + 2\pi\theta[z(k) - z_c], \quad (3.5)$$

θ -function points that the phase difference changes by 2π if the current z exceeds the critical value z_c .

According to (3.3) and (3.2) at the moment of phase “sliding” the dimensionless current and internal magnetic flux $f = \Phi/\Phi_0$ change following

the algorithm:

$$z \rightarrow z - 1; f \rightarrow f + 1 \quad (3.6)$$

Thus, for $V \gg 1$, the SQUID is a threshold element.

The granular superconductor with $V \gg 1$ is a dynamical system consisting of threshold elements. This system has a large number of metastable states and can reach a self-reproducing critical state. This situation is typical for self-organized systems.

4 1D sandpile model

One of the most popular model for self-organized criticality is the one-dimensional sandpile model proposed in reference [6] and studied in detail in references [8] and [9]. This model is considered as a one-dimensional lattice of N sites with a positive variable h_i ($i = 1, \dots, N - 1$) defined for each cell and called a “height of pile”. The cells are numbered by the neighboring left site. Another variable is a “slope of pile” z_i . It is associated with each lattice site $z_i = h_i - h_{i-1}$ ($i = 1, \dots, N$). The dynamics of this system consists of two kinds of steps. The first kind is addition:

$$h_i \rightarrow h_i + \delta h, \quad (4.1)$$

where $i = 1, \dots, N - 1$ is a randomly chosen cell. The second kind is toppling:

$$\begin{aligned} \text{if } z_i > z_c \text{ then } h_i &\rightarrow h_i - 1 \\ h_{i-1} &\rightarrow h_{i-1} + 1. \end{aligned} \quad (4.2)$$

The boundary conditions can be chosen as follows:

$$z_0 = 0, h_N = 0. \quad (4.3)$$

Repeating the procedure (4.1), we build the pile until the slope in any site exceeds the critical value z_c . At this moment the toppling (4.2) occurs and an avalanche begins. When the dynamics stops, we perturb the system again according to the addition rule (4.1), etc.

The avalanche size is defined as the total number of topplings during the avalanche process:

$$S_n = \sum_{t_{\text{bn}}}^{t_{\text{en}}} \sum_{i=1}^{i=N} \theta(z_i - z_c), \quad (4.4)$$

where t_{bn} and t_{en} are the initial and final moments of the n th avalanche, respectively.

As was shown in reference [9], this model exhibits the self-organized behavior for $\delta h = 1/2$. Note that in the case of $\delta h = 1$ or if the grains

are added to the boundary site the system has only one metastable critical state.

The sandpile model and its modifications are the main objects for theoretical investigations of SOC. Despite the self-organized behavior is observed for a wide range of dynamical systems, the problem of finding a physical system with self-organization available for experimental investigations remains still actual. Granular superconductors can become convenient objects for experimental studies of SOC.

5 The simplified model of 1D multijunction SQUID

In the case of $V \gg 1$ the dynamics of multijunction SQUID can be described not only by differential equation (2.4) but also by the simplified model that is an analogue of the 1D sandpile model [13].

The main variables for the 1D sandpile model are the slope of pile that is associated with lattice site and the height that is defined for every cell. For 1D multijunction SQUID we have three main quantities: dimensionless current $z_i = \frac{8\pi\lambda_L a l}{\Phi_0} j_i$, dimensionless magnetic field $h_i = \frac{2\lambda_L a}{\Phi_0} H_i$ and dimensionless magnetic flux $f_i = \Phi_i / \Phi_0$.

According to Maxwell equation (2.1) for dimensionless junction current z_i , ($i \neq 1, N$) we have the following expression:

$$z_i = h_i - h_{i-1}. \quad (5.1)$$

Comparing this equations with the algorithm for the 1D sandpile model we see that the dimensionless current z_i is an analogue of a pile slope associated with i th site and the dimensionless magnetic field h_i is an analogue of a height of pile associated with i th cell.

It was shown earlier that for $V \gg 1$ phase differences can be approximated by the step function (3.4) and the discrete time $t_k = kT$ can be introduced. Hence we have the following equation for phase difference φ_i :

$$\varphi_i(k+1) - \varphi_i(k) = 2\pi(\theta[z_i - z_c] - \theta[-z_i - z_c]); \quad (5.2)$$

with $z_c = V/2\pi = \frac{8\pi\lambda_L a l}{\Phi_0} j_c$.

Substituting this equation in equation (2.3) we obtain the system of maps for f_i that can be rewritten as a following algorithm:

$$\begin{array}{ll} \text{perturbation rules} & f_0 = f_N = h_{\text{ext}} \rightarrow h_{\text{ext}} + \Delta h_{\text{ext}} \\ \text{toppling rules} & \\ \quad \text{if } z_i > z_c \text{ then} & \begin{array}{l} f_i \rightarrow f_i - 1 \\ f_{i-1} \rightarrow f_{i-1} + 1 \end{array} \\ \quad \text{if } z_i < -z_c \text{ then} & \begin{array}{l} f_i \rightarrow f_i + 1 \\ f_{i-1} \rightarrow f_{i-1} - 1 \end{array} \end{array} \quad (5.3)$$

where for the dimensionless currents we have:

$$\begin{aligned} z_i &= h_i - h_{i-1}, \quad i \neq 1, N \\ h_i &= \frac{2\lambda_L a}{\Phi_0} H_i = J_i f_i, \quad i \neq 0, N \end{aligned} \quad (5.4)$$

$z_N = h_{\text{ext}} - h_{N-1}$, $h_0 = f_0$, $h_N = f_N$ on the boundary.

Note, that the pile height is not the magnetic flux f_i but the dimensionless magnetic field h_i (Eq. (5.1)). Because $h_i = J_i f_i$, the algorithm for h_i can be written as

$$\begin{aligned} \text{perturbation rules} \quad h_0 = h_N = h_{\text{ext}} &\rightarrow h_{\text{ext}} + \Delta h_{\text{ext}} \\ \text{toppling rules} \\ \text{if } z_i > z_c \text{ then} & \quad h_i \rightarrow h_i - J_i \\ & \quad h_{i-1} \rightarrow h_{i-1} + J_{i-1} \\ \text{if } z_i < -z_c \text{ then} & \quad h_i \rightarrow h_i + J_i \\ & \quad h_{i-1} \rightarrow h_{i-1} - J_{i-1}. \end{aligned} \quad (5.5)$$

This algorithm is similar to that for the one-dimensional sandpile (4.1) and (4.2). But there are differences producing qualitatively different behavior.

First, we see from equation (2.4), and algorithm (5.5) that the system is perturbed by external magnetic field H_{ext} . The perturbations are applied not to randomly chosen cell [6], [9] but to the boundaries of the system, *i.e.* it is deterministic.

Next, this model also takes into account that in real SQUIDS the increasing magnetic field induces both positive and negative currents. As a result, there is a second (negative) critical value for z in algorithms. The system has closed boundary conditions and the total current is conserved. However, the closed boundary conditions do not prevent the appearance of self-organization because the positive and negative currents can annihilate. The annihilation process effectively substitutes the current outflow which takes place in open systems [14].

Finally, in our consideration, the coefficients J_i are random, whereas in references [6] and [9] they are equal to unity. The introduction of random J_i leads to non-conservation of the total magnetic field expressed by the variable $h = \sum_{i=1}^{i=N-1} h_i$. This fact arises naturally from physical principles that require only conservation of the total magnetic flux in the system. As may be seen from equation (5.3), only one flux quantum migrates from one cell to another but, due to the differences in cell areas, the magnetic field in cells changes by different values. It may also be seen that there is an integer number of flux quanta in each cell. This situation is illustrated by Figure 3.

The constructed algorithm (5.5) can be referred to as *a sandpile model with intrinsic spatial randomness*.

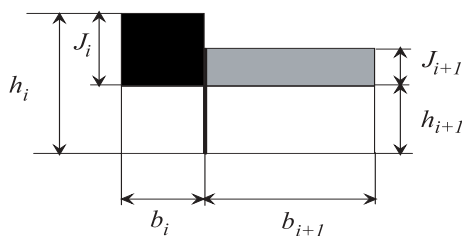


Fig. 3. Migration of the one quantum of magnetic flux in the simplified model of 1D multijunction SQUID. The magnetic fields in cells change by different values because of differences of cell sizes. But the equality $b_i J_i = b_{i+1} J_{i+1}$ holds.

6 Computer simulation results

We have studied the original system of equation (2.4) and the corresponding sandpile model (5.5) by computer simulations for the system size $N = 129$. For equation (2.4) we used the Euler integration scheme with $dt = 0.01$, $V = 40$, $\tau = 1$. For the algorithm (5.5) we take $z_c = 6.33$. The simulation proceeded similarly to other simulations of SOC-systems.

Before starting, a set of random values J_i was chosen, which were unchanged during the simulation process. Beginning from the state $\varphi_i = 0$ or $z_i = h_i = 0$, the system was perturbed by increasing the external field h_{ext} by unity that is $h_{\text{ext}} \rightarrow h_{\text{ext}} + 1$. After this perturbation the system is allowed to relax to the next metastable state. We take that the system reaches a metastable state if $z_i < z_c$ or $\frac{d\varphi_i}{dt} < 10^{-7}$ for every site. During the relaxation process the value of h_{ext} does not change. When the dynamics stops and the system reaches the next metastable state, we perturb it again by increasing h_{ext} , the relaxation process is repeated and so on.

After the transition process, the systems described by equation (2.4) and algorithm (5.5) reach the critical state that is an ensemble of metastable states. The distribution of z_i for the sandpile model is shown in Figure 4. The distribution of h_i in the positive subsystem is similar to the height distribution in the BTW model (Fig. 4). The junction with $i = 65$ plays the role of an open boundary for each of subsystems. An avalanche triggered by the perturbation leads the system to the next metastable state. The structure of this state remains the same but the values of h_i and z_i are slightly changed. We have the same picture for the original system (2.4), as well.

In framework of the simplified model (5.5) for every avalanche we calculated the quantity W_n that is a measure of the total number of topplings

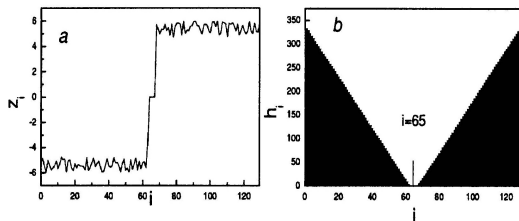


Fig. 4. Distribution of z_i and h_i in one of metastable states for the sandpile model with intrinsic spatial randomness with dispersion of J_i from 1 to 1.5.

(an avalanche size in the sandpile model):

$$W_n = \frac{1}{M} \sum_{k=k_{\text{bn}}}^{k=k_{\text{en}}} \sum_{i=M+2}^N (\theta[z_i(k) - z_c(k)]), \quad (6.1)$$

where $M = \frac{N-1}{2}$, k_{bn} and k_{en} are the initial and the final moment of the n th avalanche, respectively.

According to equation (3.5) a similar quantity can be derived for evolution of the the systems of equation (2.4):

$$u_n = \frac{\Phi_0}{2\pi M} \sum_{i=M+2}^N (\varphi_i(t_{\text{en}})) - \varphi_i(t_{\text{bn}})), \quad (6.2)$$

where t_{bn} and t_{en} denote the initial and the final moments of the n -th avalanche. Note that this quantity has a clear physical meaning. It is an integral voltage over the positive part of the system during the avalanche time. This fact was discussed in detail in references [11] and [15].

We consider our systems for several sets of J_i with a different scatter. For every set we calculate the probability densities $\rho(W)$ and $\rho(u/\Phi_0)$. The resulting dependencies are shown in Figure 5. From these figures we see that the results for the sandpile model with intrinsic randomness (algorithm (5.5)) and for the original system (Eq. (2.4)) coincide.

Figure 5a shows the probability densities for the case where all J_i are equal to unity, *i.e.*, the situation is the same as considered in reference [6]. In this case, no self-organization is observed in both systems and they return to the same metastable state after every perturbation. All avalanches have the same size $W_0 \approx 32.5$ and the probability density has the form of a δ -function. Figure 5b illustrates the case where the J_i values are randomly chosen in the interval from 1 to 1.01. One can see that in this case there are also avalanches with sizes different from W_0 but they are small in number.

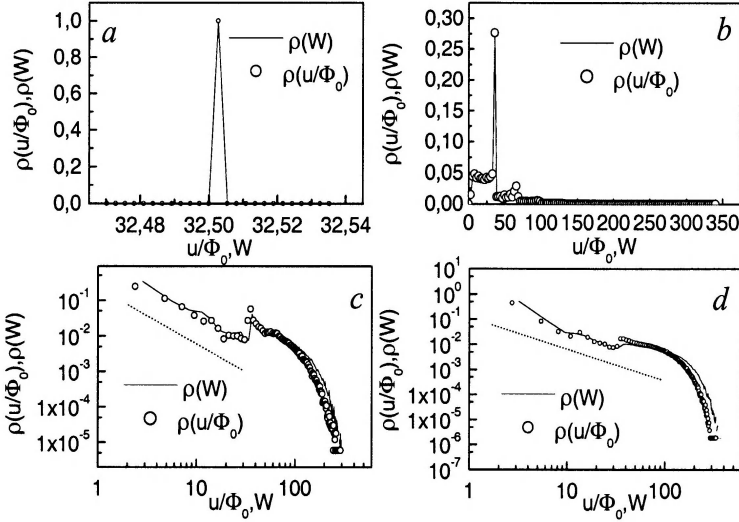


Fig. 5. Probability density $\rho(u/\Phi_0)$ and $\rho(W)$ for different dispersions of inter-junction distances: **a)** all J_i are the same and equal to 1; **b)** J_i are scattered from 1 to 1.01; **c)** J_i are scattered from 1 to 1.2, straight line has a slope $\alpha = -1.62$; **d)** J_i are scattered from 1 to 1.4, straight line has slope $\alpha = -1.2$.

As the dispersion of J_i increases, the probability density becomes more and more different from that for the case shown in Figure 5a, although the peak at u_0/Φ_0 is still seen (Fig. 5c). This peak disappears for the dispersion in the range from 1 to 1.4 and the probability density becomes a power function with an exponent close to unity (Fig. 5d). This consideration shows that, due to an increase in scatter of the coefficients J_i , the self-organization arises in the systems without dispersion of initial conditions and under a fully deterministic perturbation.

7 Conclusions

We have demonstrated that the critical state of granular superconductors can be self-organized. Avalanches manifest themselves as pulses of voltage. The integral value of the voltage plays the role of the avalanche size. Self-organized criticality can be experimentally observed in granular superconductors as a power-law behavior of the probability density of the voltage. This result is important because it shows that granular superconductors can serve as a convenient objects for experimental investigations of SOC. The

external conditions that we have considered are the simplest for the experimental realization.

We have also presented a new model of a self-organized system based on real physical equations. This model demonstrates a self-organized behavior in the cases when no self-organization is predicted by the earlier models. An intrinsic spatial randomness introduced into the presented model allows to obtain self-organization in the one-dimensional case and under a fully deterministic perturbation.

References

- [1] T. Wolf and A. Majhofer, *Phys. Rev. B* **47** (1993) 5383.
- [2] A. Majhofer, T. Wolf and W. Dieterich, *Phys. Rev. B* **44** (1991) 9634.
- [3] D.-X. Chen, J.J. Moreno and A. Hernando, *Phys. Rev. B* **53** (1996) 6579.
- [4] D.-X. Chen, A. Sanchez and A. Hernando, *Phys. Rev. B* **50** (1994) 13735.
- [5] P.G. de Gennes, *Superconductivity of Metals and Alloys* (Addison-Wesley, Redwood City, CA, 1989).
- [6] P. Bak, C. Tang and K. Wiesenfeld, *Phys. Rev. Lett.* **59** (1987) 381.
- [7] D. Dhar, *Phys. Rev. Lett.* **64** (1990) 1613.
- [8] S.T.R. Pinho, C.P.C. Prado and S.R. Salinas, *Phys. Rev. E* **55** (1997) 2159.
- [9] L. Kadanoff, S.R. Nagel, L. Wu and S.-M. Zhou, *Phys. Rev. A* **39** (1989) 6524.
- [10] K.K. Likharev, *Dynamics of Josephson Junctions and Circuits* (Gordon and Breach, New York, 1986).
- [11] S.L. Ginzburg, *JETP* **79** (1994) 334.
- [12] S.L. Ginzburg, M.A. Pustovoi and N.E. Savitskaya, *Phys. Rev. E* **57** (1998) 1319.
- [13] S.L. Ginzburg and N.E. Savitskaya, *JETP Lett.* **69** (1999) 133.
- [14] S.L. Ginzburg and N.E. Savitskaya, *JETP Lett.* **68** (1998) 719.
- [15] S.L. Ginzburg and N.E. Savitskaya, *JETP* **90** (2000) 202.

COURSE 14

HIKING THROUGH GLASSY PHASES: PHYSICS BEYOND AGING

L. BERTHIER¹, V. VIASNOFF², O. WHITE³,
V. ORLYANCHIK⁴ AND F. KRZAKALA⁵

¹ *Theoretical Physics, 1 Keble Road,
Oxford OX1 3NP, UK*

² *LPM, ESPCI, 10 rue Vauquelin,
75005 Paris, France*

³ *Jefferson Laboratories, Harvard
University, Cambridge, MA 02140,
USA*

⁴ *The Racah Institute of Physics, The
Hebrew University, Jerusalem 91904,
Israel*

⁵ *LPTMS, Bât. 100, Université
Paris-Sud, 91406 Orsay, France*



Contents

1	Introduction	721
2	Experimental facts	723
2.1	Rejuvenation	723
2.2	Overaging and underaging	724
2.3	Memory effect of the first kind, or “Kovacs effect”	725
2.4	Memory effect of the second kind	726
2.5	Need for a generic and robust phenomenology	726
3	Two mean-field theoretical approaches	727
3.1	Trap and multi-trap models	727
3.2	Infinite-range models	727
4	Spatial approaches	728
4.1	Domain growth	728
4.2	A minimal phenomenology	729
4.3	Back to experiments	730
4.4	Droplets and chaos in spin glasses	732
4.5	Surfing on a critical line	734
5	Two experiments	735
5.1	Anderson insulator	735
5.2	Colloidal suspension	737
6	Conclusion	739

HIKING THROUGH GLASSY PHASES: PHYSICS BEYOND AGING

L. Berthier, V. Viasnoff, O. White, V. Orlyanchik and F. Krzakala

Abstract

Experiments performed on a wide range of glassy materials display many interesting phenomena, such as aging behavior. In recent years, a large body of experiments probed this nonequilibrium glassy dynamics through elaborate protocols, in which external parameters are shifted, or cycled in the course of the experiment. We review here these protocols, as well as experimental and numerical results. Then, we critically discuss various theoretical approaches put forward in this context. Emphasis is put more on the generality of the phenomena than on a specific system. Experiments are also suggested.

1 Introduction

In this summer school, we were given many examples of glassy systems, glassy dynamics, and glass transitions, even though a proper definition of the word “glassy” was not really provided. However, all glassy materials share the property that their relaxation times are extremely large compared to the time scale of a typical experiment, at least in a part of their phase diagram. For practical purposes, they are thus out of equilibrium, meaning that in principle the whole sample history is relevant to a description of their physical properties. This paper is dedicated to the study of some specific histories applied to various glassy materials.

As physicists, we want to study the simplest histories that allow for an understanding of all the relevant mechanisms at work. Hopefully, an understanding of simple protocols will also allow for prediction or calculation of the behavior resulting from increasingly elaborate procedures.

Over the last decades, the experiment most often performed has been the *simple aging* experiment, see Figure 1. The system is quenched from a non-glassy part of the phase diagram, E , into the glassy phase, A . The system relaxation time is so large that all its physical properties continue to evolve

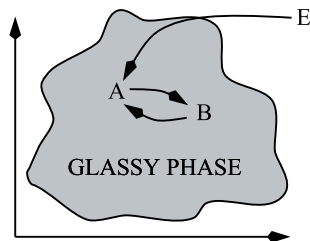


Fig. 1. Schematic view of the phase diagram of a glassy material. The relaxation time of the system in the shaded area is too large for the system to equilibrate on an experimental time scale. The arrows depict simple aging ($E \rightarrow A$), shifts ($E \rightarrow A \rightarrow B$), or cycling ($E \rightarrow A \rightarrow B \rightarrow A$) experiments. We do not label the axis, since the paper deals with an Anderson insulator, a colloidal suspension, a spin glass model, and a ferromagnet at criticality.

slowly with time (aging). This phenomenon has been known for a long time in the field of structural glasses [1] before its rediscovery in the field of spin glasses [2]. Interestingly, aging is observed in a still increasing number of experimental systems such as soft materials (like pastes [3], colloidal suspensions [4], or clays [5]), dipolar glasses [6], disordered ferromagnets [7] and ferroelectrics [8], granular matter [9], superconductors [10], etc. Loss of stationarity is best illustrated by the study of two-time quantities. One typically computes the correlation between times t and w , $C(t, w)$, or the response of the system at time t to a perturbation applied at w , or equivalently the time evolution of a susceptibility at frequency ω , $\chi(\omega, t)$. In most common experimental regimes, two-time quantities scale as $C(t, w) \sim \mathcal{F}_C(t/w)$, $\chi(\omega, t) \sim \mathcal{F}_\chi(\omega t)$, where $\mathcal{F}_*(x)$ denotes a scaling function. This scaling indicates that after a time t the only relevant time scale in the system is the time t itself.

In order to probe the dynamics of the glassy phase in greater detail, more elaborate and systematic experimental protocols have been performed [11], in which some external parameters are shifted, or cycled, during the experiment, see Figure 1. Such experiments reveal spectacular new phenomena, such as rejuvenation and memory effects. Such new effects must be accounted for by any theory of aging, possibly allowing for discrimination between different theoretical approaches to glasses and aging phenomena. In addition, more detailed experiments may allow for discrimination between different families of glassy systems, and thus may help theoreticians refine their description of specific glassy systems. A large number of recent experimental papers are dedicated to such experiments, on a wide variety of systems, making the subject a very active one. By contrast, these protocols

are barely mentioned in the classic theoretical review in the field [12] and it is one of this paper’s purpose to fill this little gap.

In the first part of the paper we review briefly the basic experimental facts. Next we discuss two mean-field theoretic approaches to the problem. We then formulate the rudiments of a simple, but fairly robust, phenomenology in terms of length scales which grow with time and discuss realizations of this scenario. Last, we show that a nice account of both recent experiments performed on an Anderson insulator and on a colloidal suspension can be given in terms of such growing length scales.

2 Experimental facts

In this section, we present the main experimental facts observed when the protocols of Figure 1 are actually performed. This will allow us also to define precisely the vocabulary used throughout the paper. We use our own data to describe these phenomena, but emphasize that a similar phenomenology has been observed in many different systems. Such experiments were first performed on spin glasses (rejuvenation and memory effects [11, 13–15]) and polymer glasses (mechanical rejuvenation [16] and Kovacs effect [1, 17, 18]) in temperature shift or cycling experiments. Thus, we adopt “temperature” as a control parameter, but also discuss the case of other control parameters. The degree to which different such external parameters are equivalent is a completely open question. It was recently asked in the present context [19], as a part of a more general research line [20, 21]. Here, we take a pragmatic approach and elaborate on experimental similarities. Sections 2.1–2.3 deal with effects encountered in shift experiments, while Section 2.4 deals with cycling experiments.

2.1 Rejuvenation

First consider a shift experiment, see Figure 1. The system is quenched at initial time $t = 0$ from a high temperature to a temperature T_A in the glassy phase. For $0 < t < t_A$, the temperature is kept constant. Up to this point, this is a simple aging experiment, manifested by the slow evolution of physical quantities. Such typical slow evolution is shown in the left part of Figure 2 where a quantity analogous to a magnetic susceptibility at given frequency is computed in the numerical simulation of a microscopic spin glass model [22].

At $t = t_A$, the temperature is shifted to T_B . As seen in Figure 2, aging is restarted by a negative shift ($T_A > T_B$) in the sense that the resulting curve is similar to that obtained in a direct quench to T_B . This restart of the dynamics is called *rejuvenation effect* because the time t_A spent at T_A – the sample “age” – seems to have no influence on the dynamics following

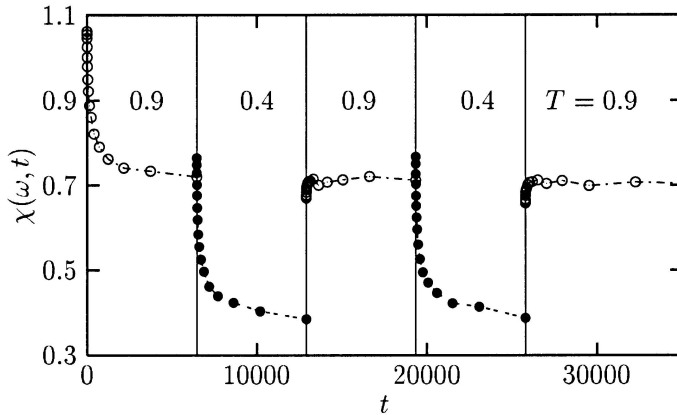


Fig. 2. A temperature cycling experiment performed numerically in a spin glass model. The system is quenched at $t = 0$ in the spin glass phase, $T_A < 1.0$. It ages at the temperature $T_A = 0.9$ as demonstrated by the time evolution of a quantity analogous to a magnetic susceptibility. The temperature is then shifted at $t_A = 6450$ to $T_B = 0.4$ where rejuvenation takes place. At $t_B = 12900$, the temperature is shifted back to $T_A = 0.9$, demonstrating, after a very short transient, the memory effect. A second cycle is then performed.

the shift. The same effect is obtained if $T_B > T_A$. We note also that the term “rejuvenation” was first employed to describe the effect of large stresses on the aging of polymers [1, 16].

2.2 Overaging and underaging

Obviously, if $T_B = T_A$, no rejuvenation takes place, meaning that in order for rejuvenation to be observed in a shift experiment, $|T_A - T_B|$ must be “large enough”. For small or intermediate $|T_A - T_B|$, a phenomenon recently called *overaging* is observed [19], when $T_A > T_B$. This is illustrated in Figure 3 (up), where results obtained with a polymer are presented [23]. In this figure, two-time linear response to a stress step (creep compliance) after a shift from T_A to T_B is compared to that obtained in a simple aging experiment at T_B with the same aging time. The response after the shift is slower than that obtained in the simple aging experiment, and the system looks “older”, or “overaged”. Similarly, an *underaging* would be obtained if $T_A < T_B$.

These effects were also observed experimentally in a colloidal suspension submitted to a transient oscillatory shear [19], as well as in temperature

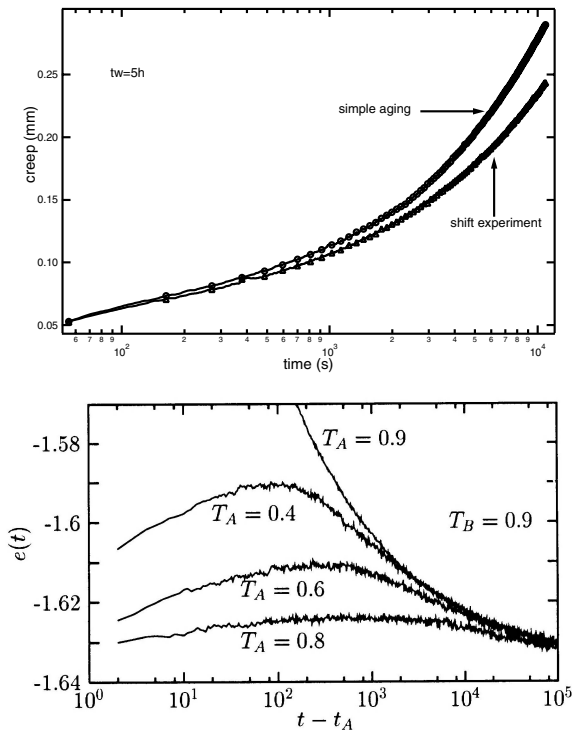


Fig. 3. Up: overaging observed in a shift experiment with $T_B < T_A$. The creep compliance of a polymer after the shift (triangles) is compared to the curve obtained in a simple aging experiment at T_B (circles) and the same aging time, $t_A = 5$ h. The long-time response is clearly slower after the shift. Down: Kovacs effect observed in a shift experiment with $T_B > T_A$. The energy density of a spin glass model recorded after the shift exhibits a typical nonmonotonic behavior.

shift protocols in experimental [11,14] and numerical [22,24] studies of spin glasses.

2.3 Memory effect of the first kind, or “Kovacs effect”

A *memory effect* takes place in the shift protocol when $T_B > T_A$. It was first observed by Kovacs in polymers [17]. To distinguish it from a second memory effect (see below), this effect was called *Kovacs effect* in [25]. Kovacs measured the specific volume, $V(t)$, of the polymer during the experiment, but other physical quantities (index of refraction, energy density, ...) can be investigated. The effect is particularly striking when t_A is chosen so

that $V(t_A) = V_{\text{eq}}(T_B)$, which means that immediately after the quench, the volume has already reached its equilibrium value at the new temperature. Hence, a naive expectation would be that $V(t > t_A) = \text{const} = V_{\text{eq}}(T_B)$. Instead Kovacs observed a nonmonotonic variation of the volume showing that the system has some *memory* of its state at the initial temperature. This experiment is reproduced in Figure 3 using the energy density of a microscopic spin glass model in a numerical simulation [22]. Similar results have been obtained in supercooled liquids [26], granular materials [9], foams [27] or dipolar glasses [6].

2.4 Memory effect of the second kind

Let us describe the continuation of the experiment shown in Figure 2. At time $t_B > t_A$, T is shifted back to its initial value T_A . After a very short transient, $\chi(\omega, t)$ resumes its evolution as if there had been no aging at T_B . The system has a *memory* of the first stage, despite the strong rejuvenation observed in the intermediate stage of the cycle. Simultaneous observation of rejuvenation and memory is spectacularly demonstrated in the “dip experiment” [15]. The protocol is essentially a cycling experiment in which the temperature is decreased at a fixed, finite rate (instead of at an infinite rate as in an idealized cycle). The ramp from high temperature stops at T_A , where the temperature is kept constant a time t_A after which cooling is resumed. In this context rejuvenation means that the further evolution of the system is almost the same with or without the stop at T_A . The temperature is then raised back at a constant rate. Memory means that near T_A , the system “remembers” its stop [15, 28] and behaves differently from a system not held at T_A . However, this experiment is less simple to analyze theoretically because it mixes cooling rate effects with rejuvenation and memory. For this reason, we stick to cycles in what follows.

2.5 Need for a generic and robust phenomenology

This quick experimental review shows that a number of effects are both highly non-trivial as well as generically observed in a wide range of materials, suggesting that these phenomena are intrinsic to nonequilibrium glassy dynamics. This has two immediate consequences. (1) Any phenomenological theory of aging must account for these effects in addition to the results of simple aging experiments. (2) The phenomenology should be based upon general considerations, which themselves proscribe the range of experimental systems to which the theory applies. Ideally this would be the large range of quite different experimental systems in which glassy dynamics is observed.

3 Two mean-field theoretical approaches

As reviewed in [12], theoretical approaches to aging phenomena can be classified in three large families. We analyze two mean-field ones in this subsection in view of the above experimental facts.

3.1 Trap and multi-trap models

A first approach, made popular through the “trap model” formulated in [29], considers the dynamics from the point of view of phase space and describes the dynamics of a point particle evolving through a given energy landscape. The reduction of a many-body system to a one-particle problem classifies this approach in the mean-field family. The “complexity” stems from an assumed large distribution for the free energy of the metastable states, typically chosen to be exponential, $\rho(E) \sim \exp(-E/T_g)$. If one further assumes that energy barriers are related to the free energy of the states, one gets the distribution of trapping times $\rho(\tau) \sim \tau^{-(1+T/T_g)}$, the first moment of which diverges for $T < T_g$. The absence of a mean trapping time then results in the typical t/w scaling of two-time quantities. Obtaining this scaling in a one-body problem is a remarkable result. The crucial drawback of the approach is, obviously, the lack of a precise interpretation of what “traps” are.

To account for the effects described above, the model was phenomenologically extended to multi-trap models [30], each level having its own glass temperature T_g . The phenomenology of cycles is straightforward. When the temperature is lowered, new levels of the hierarchy start to age (rejuvenation effect), while higher levels are completely frozen and unaffected by the stay at low temperature (memory). This “hierarchical phase space picture” has often been invoked by the Saclay group to interpret experiments on spin glasses [14]. Furthermore, numerical simulations of concrete realizations of multi-trap models confirm that this picture satisfactorily reproduces the experiments [31]. As a similar realization of this picture, the Sinai model was recently studied in this context [32].

3.2 Infinite-range models

A more microscopic approach can also be used to describe aging [12]. The aim is to solve exactly the dynamics starting from the Hamiltonian of a glassy system. This ambitious program has been successful for systems with infinite-range interactions. They are thus mean-field realizations of realistic systems. Simple aging experiments can be accounted for, as described in detail in Cugliandolo’s lectures [33]. These solvable models have proved

to be extremely rich, but by construction they are incomplete descriptions since real space is completely ignored.

Two families of models have emerged. Schematically, the first has the phenomenology of structural glasses – an example is the p -spin model – and typically exhibits t/w scalings [34]. The second family is closer to spin glasses – the prototype being the Sherrington-Kirkpatrick model. The behavior of the latter in simple aging experiments is quite involved, since it displays “dynamic ultrametricity” [35]. Without giving the details [33], this implies a complex scaling of two-time functions, with the presence of a continuous hierarchy of diverging time scales. When submitted to shifts and cycles, this second family (but not the first one) was shown to exhibit rejuvenation and memory asymptotically [36]. It would be useful to have simulations of these models in order to go beyond the asymptotic analysis of [36] and to get some comparison to experiment. Within this approach, the glassy effects of the previous section are explained through the existence of a hierarchy of time scales.

However, as honestly noted in the conclusion of [36], a strong drawback is that the dynamic ultrametricity on which the whole interpretation relies is incompatible with experiments. Obviously this weakens the general validity of these results.

4 Spatial approaches

4.1 Domain growth

A third family of models describing slow dynamics focuses directly on spatial aspects [12]. Simple aging experiments are explained with reference to a characteristic length scale, $\ell(t)$, which grows with time. The physical content of $\ell(t)$ is that on scales smaller than ℓ the system appears equilibrated while on larger scales it does not.

A pure Ising ferromagnet quenched from its paramagnetic to its ferromagnetic phase provides a simple example of coarsening dynamics. In the low temperature phase, the ferromagnet has two equilibrium states, with magnetizations $+$ and $-$. As time passes, spatial domains of these equilibrium phases develop and coarsen, with a typical associated length scale $\ell(t)$. This domain growth is driven by surface tension of domain walls. The dynamic scaling hypothesis is that the only length scale involved in this process is the domain size $\ell(t)$ itself. In a pure ferromagnet, the growth law is temperature independent [37], $\ell(t) \sim t^{1/2}$, and this leads to t/w scaling of two-time correlators.

This phenomenology does not provide for the rejuvenation and memory effects discussed above and indeed such effects are not observed in ferromagnets. For instance, consider rejuvenation. Thermal reequilibration

within the domains is quasi-instantaneous since thermal fluctuations in the ferromagnetic phase are short-range, of typical size $\xi_{\text{eq}}(T) \ll \ell(t)$. Also, since lowering temperature during domain growth leaves the growth rate unchanged, after a temperature cycle $T_A \rightarrow T_B \rightarrow T_A$, there cannot be regions initially equilibrated at T_A that remain unchanged during the cycle.

However, coarsening in a disordered system cannot be analogous to that in a pure system [38]. Coarsened domains will no longer be simple convex objects with energy decreasing monotonically with curvature. This can be seen readily by considering a ferromagnet with some added impurities. Walls separating $+$ and $-$ domains will tend to avoid unusually strong bonds and will tend to be pinned at unusually weak bonds. In such a disordered system, domain growth will be slower than it is in a pure ferromagnet. In the case of high disorder, domain growth is likely activated, leading to a characteristic domain size $\ell(t) \sim (\ln t)^p$ [39]. Secondly, in important contrast to pure systems, renormalization of a disordered system's Hamiltonian yields statistically similar Hamiltonians. In particular this means that we should not expect that the equilibrium states in the low temperature phase of a disordered system at temperatures T_A and T_B are related in any simple way. A simple example is given by the effective interaction between two spins on the opposite vertices of a square. Just as the sign of the effective interaction between these two spins can change with a perturbation in bond strength, so too can it change with a perturbation in temperature [40].

4.2 A minimal phenomenology

These differences stated, one can ask whether there is a phenomenological coarsening theory for aging in glassy materials analogous to that in systems like pure ferromagnets. We formulate such a “minimal” phenomenology in terms of a growing length scale. It must contain the following features.

- (i) *Existence of a growing coherence length ℓ .* This coherence length has the same physical content as described above: objects smaller than ℓ are quasi-equilibrated while larger objects still retain their nonequilibrium initial conditions. A more precise definition of the “objects” is not necessary at this point. For clarity we will draw compact domains in our cartoons. Furthermore, the coherence length must grow slowly with time so that equilibrium domains of size ℓ remain fixed on time scales associated with objects smaller than ℓ . This first assumption is very natural for some systems, *e.g.*, disordered ferromagnets. Yet for other systems it is very non-trivial. For instance, no typical length scale has been invoked yet to explain the aging of supercooled liquids or colloidal suspensions.

- (ii) *Sensitivity of equilibrium on all length scales.* Obviously, the specific equilibrium state of the system depends upon the particular values of the control parameters, but sensitivity is required in order to provide for the rejuvenation effects. Of course, even a simple two-level system has to readapt its Boltzmann weights upon a temperature change [41]. There remains to be understood what “levels” are in a realistic system, and how those evolve with temperature. In fact as discussed above, sensitivity of the equilibrium state to control parameter values is a natural consequence of a renormalization procedure in a disordered system. Note that there are nevertheless questions outstanding. In particular, which if any glassy systems can be described in terms of a glassy phase fixed point? And even if some can be, is the sort of “chaos” that one gets automatically in fact responsible for the observed rejuvenation and memory phenomena in glassy materials? We will return to these points shortly.
- (iii) *Separation of length scales.* The length at which a system is equilibrated after a given wait time depends strongly on external parameters. Memory effects are a consequence of such dependence. This is very natural for the thermally activated domain growth expected in disordered systems [42]:

$$t(\ell, T, \dots) \sim t_0 \exp\left(\frac{E(\ell, T, \dots)}{k_B T}\right), \quad (4.1)$$

where t is the time needed to equilibrate the length scale ℓ , t_0 a microscopic time scale, and $E(\ell, T, \dots)$ an activation energy that in principle can depend on the coherence length itself and on temperature. The dots stand for possible control parameters in addition to T . If $E(\ell) \propto \ell/T$, the growth law is logarithmic and “super-Arrhenius”: $\ell \propto T^2 \ln(t/t_0)$. If instead barriers grow logarithmically, $E = k_B T_0 \ln \ell$, one gets a T -dependent power law growth, $\ell \sim t^{T/T_0}$. In either case, thermal activation (Eq. (4.1)) implies that the range of length scales “active” in a given time window depends strongly on T and, more generally, on other external parameters in systems with glassy dynamics [41, 42].

4.3 Back to experiments

Consider the cycling experiment $E \rightarrow A \rightarrow B \rightarrow A$ of Figure 1. Again we write the control parameter as a temperature T . The three above assumptions lead to the cartoon of Figure 4 which we now explain.

For times $0 < t < t_A$, this is a simple aging experiment at T_A . Feature (i) entails that the system equilibrates up to a growing coherence length,

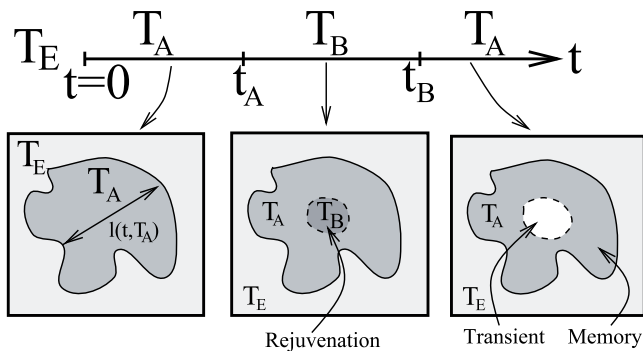


Fig. 4. Cartoon suggested by the considerations of Section 4.2 for a temperature cycling experiment. The related effects are discussed in Section 4.3.

$\ell(t, T_A)$, leading to a $\ell(t, T_A)/\ell(w, T_A)$ scaling of two-time functions. This is the usual domain growth picture of aging. Small length scales, $\ell_s < \ell(t, T_A)$, with characteristic times $t_s \ll t$ have reached equilibrium at T_A , while big ones, $\ell_b > \ell(t, T_A)$ with characteristic times $t_b \gg t$ still retain their initial nonequilibrium state at T_E , see Figure 4.

Then the temperature is shifted to $T_B < T_A$ at time t_A with $|T_A - T_B|$ “large”. Feature (ii) entails that all length scales, $\ell \leq \ell(t_A, T_A)$, must adapt to the new temperature T_B . This occurs through the growth of a new coherence length, $\ell(t - t_A, T_B)$, as shown by a dashed line in Figure 4. Aging is thus restarted from scratch and *rejuvenation due to the reequilibration of small length scales* is observed.

At time t_B , the system is shifted back to A . Due to (iii), $T_B < T_A$ implies a much slower growth of ℓ during the intermediate stage. Hence, for $t_B - t_A \approx t_A$, as is often the case in experiments, one has $\ell(t_B - t_A, T_B) < \ell(t_A, T_A)$ and the behavior for $t > t_B$ is due to three types of length scales. Small length scales, $\ell < \ell(t_B - t_A, T_B)$, have to reequilibrate at T_A . Intermediate lengths, $\ell(t_B - t_A, T_B) < \ell < \ell(t_A, T_A)$, are already equilibrated at T_A . *It is in these length scales that the memory resides.* Large lengths, $\ell(t_A, T_A) < \ell$, still have to equilibrate at T_A . Hence, after a short transient of duration τ given by $\ell(\tau, T_A) \sim \ell(t_B - t_A, T_B) < \ell(t_A, T_A)$, aging proceeds as the continuation of the first stage. Note that under the assumption of activated dynamics, simple inequality of length scales corresponds to a large degree of inequality in terms of time scales.

If one chooses instead $T_B > T_A$, the essential situation should be unchanged, provided that the condition $\ell(t_B - t_A, T_B) < \ell(t_A, T_A)$ is fulfilled, see Figure 4. This property is called “symmetrical effect” in the field of spin glasses [11]. Note, however, that this condition on the lengths is extremely

difficult to satisfy due to feature (iii). Therefore, in most experiments with $T_B > T_A$ the equilibrated length grown at T_B is larger than that grown at T_A . All memory is subsequently erased, resulting in an apparent asymmetry between positive and negative cycles.

Let us finally turn to Kovacs' experiments. Two types of length scales must be distinguished in order to understand this effect. Small scales, $\ell < \ell(t_A, T_A)$, are equilibrated at T_A but must adapt to a new, *higher*, temperature T_B . Large lengths, $\ell(t_A, T_A) < \ell$, in contrast, are still in their nonequilibrium high temperature initial state and must adapt to a *smaller* temperature T_B . If the energy density $e(t)$ is computed, as in Figure 3 (down), small length scales contribute to increase $e(t)$, while large length scales contribute to decrease $e(t)$. This accounts in simple terms for the Kovacs effect.

Schematic discussions based on (i, ii), and (iii) like that above allow for qualitative prediction of the outcome of given experimental protocols. However, while (i, ii) and (iii) are natural features for a phenomenological theory of coarsening in a glassy system, in the above they are put in by hand. Consequently we now discuss models that explicitly realize these properties.

4.4 Droplets and chaos in spin glasses

The scaling, or droplet, model of spin glasses [43, 44] possesses these three features and provides quantitative, experimentally testable predictions. These predictions are clearest in the case of Ising spin glasses, which we discuss here. At a given temperature in the spin glass phase, the assumptions made by the scaling picture resemble those made in the case of pure ferromagnetic systems, but differ due to the disorder in a spin glass.

The initial assumption of the droplet model is that Ising spin glasses have two equilibrium states, related by spin flip symmetry. Spin glass dynamics are then described in terms of "droplets", low lying excitations about these states [44]. Because of disorder, the boundaries of low lying excitations wander in order to take advantage of bonds not satisfied in the ground state and to avoid satisfied bonds that are particularly strong. Thus droplets are expected to be non-convex with fractal surface of dimension $d_f > d - 1$, where d is the space dimensionality. The droplet model assumes that the energy of larger droplets is, on average, larger than that of smaller ones and hence that the spin glass phase is not destroyed by arbitrarily large, arbitrarily low energy, excitations. In particular, it makes the scaling ansatz that the average free energies of these low lying excitations scales with their size, $F_\ell \sim \Upsilon(T)\ell^\theta$, $\theta > 0$. As a result of disorder, $\theta < (d - 1)/2$, and the distribution of F_ℓ is expected to be broad, with weight down to zero for all ℓ . Further the droplet model assumes that dynamics is activated and makes the

second scaling assumption that activation barriers scale with droplet size, $B_\ell \sim \Delta(T)\ell^\psi$ where the distribution of B_ℓ also has weight down to zero. Stiffness moduli $\Upsilon(T)$ and $\Delta(T)$ go to zero at the critical temperature T_c as $(1 - T/T_c)^{-\nu\psi}$, where ν is the standard exponent.

Feature (i) given above follows immediately from the assumptions of the scaling picture. Aging proceeds by equilibration of droplets in increasingly larger equilibrium domains of size $\ell(t, T) \sim (\frac{T}{\Delta(T)} \ln t)^{1/\psi}$. Feature (iii) also follows immediately both from activated dynamics and from the temperature dependent stiffness coefficients. Thus the droplet picture predicts simple aging behavior as well as memory effects, at least under certain experimental conditions.

The dynamics provided by the droplet model of spin glasses differs importantly from the dynamics of a pure ferromagnet in the role of temperature change [44]. A spin glass at $0 < T < T_c$ is indeed described in terms of a renormalized Hamiltonian with a renormalized ground state. However, as mentioned above, this renormalized finite temperature Hamiltonian is only statistically similar to the zero temperature Hamiltonian. Hence the equilibrium states and droplet excitations thereof at various temperatures are not related to one another in any simple way. In fact, a straightforward statistical argument [44, 45] provides an overlap length associated with a small temperature change from T to $T + \Delta T$, given by $\ell_o(T, \Delta T) \propto |\Delta T|^{-\zeta}$ where $\zeta = \frac{2}{d_t - 2\theta}$. The equilibrium state at T is unchanged on scales $\ell \ll \ell_o(T, \Delta T)$ but altered significantly on scales $\ell \gg \ell_o(T, \Delta T)$. This “temperature chaos” realizes feature (ii) and predicts rejuvenation when $\ell_o(T, \Delta T)$ is sufficiently small compared to $\ell(t, T)$ [46].

Remark that the droplet picture makes certain reasonable, but as yet unverified, assumptions. It assumes that there are equilibrium states with reference to which low lying excitations can be defined, even as equilibrium domains are growing. Such assumptions are still a matter for debate [47]. Furthermore, the properties of these excitations are given by reasonable but assumed scaling laws. For work examining the validity these assumptions see [48].

Even if the assumptions made in the droplet model are valid, it is not clear whether this model is sufficient to explain observed rejuvenation and memory effects. In order for it to do so, the overlap length $\ell_o(\Delta T)$ must be small enough to affect observations corresponding to experimental length scales. We note that the characterization of $\ell_o(\Delta T)$ in spin glasses is still a very active topic at the theoretical level [49]. A cautious conclusion is that, if ℓ_o exists, it certainly is too large to be observed in numerical simulations of systems like spin glasses. However, because F_ℓ and B_ℓ are both broadly distributed, the droplet model anticipates that in rare regions, reorganization with change of temperature will take place even on unusually small length

scales and experimentally viable time scales. If such anomalous reorganization is common enough, rejuvenation and memory may still be accounted for by the droplet model even if the characteristic overlap length $\ell_o(\Delta T)$ itself is not readily obtainable in experimental wait times [50]. The distribution of length scales about the overlap length $\ell_o(\Delta T)$ certainly requires further theoretical investigation.

On an experimental level, rejuvenation effects do not constitute a proof of temperature chaos. They are simply consistent with its existence. In fact, in the simulational study of [22] it is argued that a rejuvenation effect is observed in a regime in which no chaotic effect of the kind described above can be detected [51]. Hence, it is worth considering other mechanisms that might provide for rejuvenation and memory effects.

4.5 *Surfing on a critical line*

Another mechanism has recently been invoked to account for rejuvenation effects, while retaining the simplicity of the domain growth approach [25]. We showed in Section 4.1 that the absence of rejuvenation in standard coarsening comes from the short-range character of thermal fluctuations. Since the inequality $\xi_{\text{eq}}(T) \ll \ell(t)$ prevents rejuvenation, the idea of [25] is simply to consider opposite situations where $\ell(t) \ll \xi_{\text{eq}}(T)$. Away from critical points, $\xi_{\text{eq}}(T)$ is usually small. The suggestion is hence to “surf on a critical line” [52] where $\xi_{\text{eq}}(T) = \infty$.

A simple aging experiments corresponds then to a quench to a critical point. In this case, the coherence length is equal to the dynamic correlation length $\ell(t) = \xi(t) \sim t^{1/z_c}$, where z_c is the dynamic critical exponent. Aging is thus nothing but the successive equilibration of the critical fluctuations. Similarities between this situation and aging in glassy materials were noted [53].

When the temperature is shifted, all the critical fluctuations have to adapt to a new critical point with a new set of critical exponents. This is the origin of the rejuvenation effect in this context. It is now obvious that all the discussion of Section 4.3 applies, with the dictionary “objects” = “critical fluctuations” and “coherence length” = “dynamic correlation length”. The mechanism for rejuvenation is subtly different from temperature chaos, even taken close to the critical point [54]. Here, all length scales are always reshuffled without any “overlap length” [22, 25].

The XY model is a microscopic realization of this picture. It undergoes, in two dimensions, a Kosterlitz-Thouless transition from a standard paramagnetic state to a non-magnetized state with power-law correlations. It presents then a “line of critical points”, with a continuous variation of the critical exponents with temperature. As a consequence, the 2D XY model exhibits aging, rejuvenation, memory and Kovacs effects [25]. The example

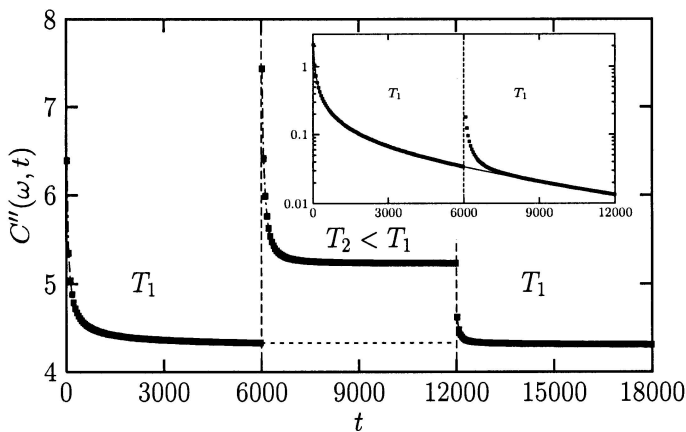


Fig. 5. Fourier transform of the spin autocorrelation function of the 2D XY model computed analytically in a temperature cycling experiment.

of a temperature cycle, where rejuvenation and memory are present, is given in Figure 5. Note that property (ii) is not naturally present in the model, since $\ell(t) = \sqrt{\rho(T)t}$ where $\rho(T)$ is the (renormalized) spin wave stiffness. To build Figure 5, $\rho(T)$ was arbitrarily, but not unreasonably, chosen to ensure the separation of length scales, $\rho(T_A) = 20\rho(T_B)$.

This analogy raises the question: are glassy systems critical? A possible answer is yes they are, in which case they should have in common a line of critical points below the glass transition, in analogy with the 2D XY model. A microscopic mechanism giving rise to such a behavior in, say, spin glasses, is lacking. Another is no; but they do experimentally behave as if there is a critical line. The second, more pragmatic solution requires that $\ell(t)$ is never decoupled from $\xi_{\text{eq}}(T)$, even when the latter is finite. One might argue this if the excitations on length scales exceeding $\xi_{\text{eq}}(T)$ are dominated by activation, and hence give exponentially increasing times for $\ell(t) \geq \xi_{\text{eq}}$. These conditions may make it virtually impossible to enter the regime $\ell(t) > \xi_{\text{eq}}(T)$. Slow evolution in the crossover region could result in effective critical behavior with continuous evolution of the exponents. This is at least fully consistent with results in spin glasses [22].

5 Two experiments

5.1 Anderson insulator

We mention the Anderson insulator, or “electron glass”, in this paper since its experimental properties were discussed at length in this school by

Ovadyahu [55,56]. Hence, we do not present the system and directly discuss the results. Also, we only focus here on one of the many measurements performed on this system, and refer to [56] for more details. Our aims are (1) to rephrase the “aging experiment” described by Ovadyahu in the present context; (2) to show that the phenomenology of Section 4.2 might be useful to interpret the data.

The electron glass is first prepared in its “glassy phase”. This corresponds to a given low temperature and a gate voltage $V = V_A$, used as the “control parameter” [55]. This corresponds then to a “simple aging experiment”. Aging manifests itself through a logarithmic time evolution of the conductance G , used as a probe of the dynamics. Presumably, two-time functions would display in this regime interesting scaling behaviors, but no such measurements have been performed yet.

After a very large time, typically days, G is almost constant. The gate voltage is then shifted to V_B during a time t_w . Experiments show that G restarts to evolve in a logarithmic way. This corresponds to a “rejuvenation effect”, since the days already spent in the glassy phase are apparently forgotten. In a third stage of the experiment, V is shifted back to its initial value V_A . The experiments show that, after a time of order t_w , G reaches its initial value again. This is analogous to what we called the “transient”, followed by the “memory effect of the second kind”. Furthermore, experiments have shown that during the third stage of the experiment (“transient” and “memory”) the conductance satisfies the scaling law $G = \mathcal{G}(t/t_w)$ where t is the time counted from the beginning of the third stage [55, 56]. This behavior was called “aging” in [56], because of the t/t_w scaling, although the experiment is in fact a complete cycle in terms of V .

Can one go beyond words and analogies? If the similarity between these experiments and standard temperature cycling experiments is assumed, then the cartoon of Figure 4 can be used. The t/t_w scaling of the conductance tells that the duration of the “transient” has the same magnitude as the duration of the second stage. This means that there is almost no separation of time scales in the electron glass for this range of gate voltages, as noted in [56]. Building further on analogies, one can reproduce this experiment using the 2D XY model. Stay first a very long (infinite) time at temperature T_A , then do a shift of duration t_w at T_B and come back at T_A at time $t = 0$. In this case, one can compute the time dependence of the spin autocorrelation function between times t and 0, noted $C_{t_w}(t, 0)$, as a function of the duration of the shift t_w . One finds, dropping irrelevant

factors and using the notations of Section 4.5:

$$C_{t_w}(t, 0) = C_{\text{eq}}(t) \left(\frac{1}{\ell_{T_A}(t)} \right)^{\frac{\eta_B - \eta_A}{2}} \left(\frac{\left(2\ell_{T_B}^2(t_w) + \ell_{T_A}^2(t) \right)^2}{4\ell_{T_B}^2(t_w) \left(\ell_{T_A}^2(t) + \ell_{T_B}^2(t_w) \right)} \right)^{\frac{\eta_B - \eta_A}{4}}, \quad (5.1)$$

where $C_{\text{eq}}(t)$ is the equilibrium correlation function obtained when $t_w = 0$ (no shift at all) and η_A and η_B are the usual critical exponents at temperatures T_A and T_B . The second and third term of the right hand side respectively account for the “transient” and the “memory”. For $\ell_{T_A}(t) \ll \ell_{T_B}(t_w)$, the transient term is dominant and aging is observed through a power law decay. When $\ell_{T_A}(t) \gg \ell_{T_B}(t_w)$, both terms combine to restore equilibrium, accounting for the memory. Interestingly, the crossover time scale t_c is given by

$$\ell_{T_A}(t_c) \sim \ell_{T_B}(t_w). \quad (5.2)$$

No separation of length scales amounts thus to $t_c \sim t_w$ as is observed in the electron glass. Deviations from t/t_w , as observed at higher gate voltages V [55], could be tentatively related *via* equation (4.1) to a decrease of an activation energy at high V . This effect could be more systematically investigated using equations (4.1) and (5.2).

5.2 Colloidal suspension

Overaging was introduced in Section 2. It is reproduced in Figure 6 showing a multiple light scattering experiment on a colloidal suspension [19]. Two interesting points in this experiment are (1) the control parameter is an external oscillatory shear strain, as opposed to temperature in “standard” shift experiments; (2) no obvious coherence length is known to grow during the aging of colloids. Therefore, such experiments could possibly be used to characterize length scales in colloidal glasses.

In this context, “simple aging experiments” consist in a “quench” from a shear strain of very large amplitude (typically more than 20%) mimicking a “high temperature”. Standard t/w scalings have been observed in many similar soft glassy materials [3–5, 19]. It is thus natural to start and investigate more complex protocols, in the spirit of shifts and cycles [19, 57, 58]. A first possibility is to quench first towards a small, but finite, shear strain during a time t_w , after which the shear is completely stopped. One can then compare the results with a temperature shift experiment, $T_E \rightarrow T_A \rightarrow T_B < T_A$, which are more commonly performed.

In spin glasses, in agreement with the phenomenology developed above, the following results are known. We already discussed the case of large $\Delta T = T_A - T_B$: rejuvenation is observed [13]. For very small ΔT , the

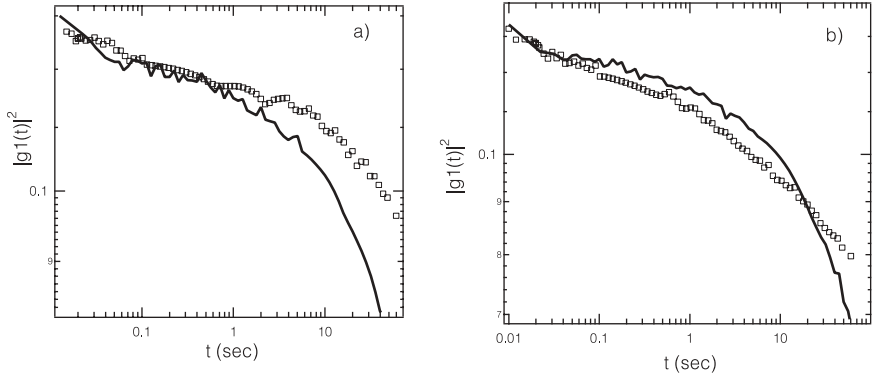


Fig. 6. Overaging in a colloidal suspension. The data show two-time intensity correlation functions obtained with a multiple scattering technique. Full lines refer to a simple aging experiment, squares to a “strain-shift” experiment with an intermediate strain of 5.9%. **a)** $w = 163$ s. Overaging is observed as in Figure 3. **b)** $w = 100$ s. The strain difference is strong enough to partially rejuvenate the system (square curve below the full line at short times while overaging is still observed at long times). This is the “intermediate” shift described in the text where both rejuvenation and overaging are mixed.

relaxation of the system after the shift has the same shape as in a direct quench to T_B , but with an “effective age” $t_w^{\text{eff}} > t_w$ [14]. Indeed, a small ΔT means that the objects growing at T_A will be almost unchanged at T_B (no rejuvenation). However, due the property (iii), the time spent at higher temperature is more efficient in growing the coherence length. Hence, the relaxation is slower after the shift, the system looking “older” or “overaged”. This is observed in the colloidal suspension in a “strain-shift” experiment, see Figure 6a. More quantitatively, the effective age t_w^{eff} can be estimated in terms of the coherence length as [22, 24, 41]

$$\ell(t_w^{\text{eff}}, T_B) \sim \ell(t_w, T_A). \quad (5.3)$$

Repeating this protocol for various (t_w, T_A, T_B) gives thus quantitative informations on the growth law of the coherence length [22, 41, 59]. Furthermore, equation (4.1) shows that this protocol allows a quantitative study of the energy barriers encountered by the system during its nonequilibrium dynamics [41].

For intermediate ΔT , of course, the result will be a combination of rejuvenation and overaging. This has been observed in spin glasses [14, 22, 24] and in polymers [23]. That this is the case in the colloidal suspension with oscillatory strain as a control parameter is demonstrated in Figure 6b.

Again, systematic studies using equations (4.1) and (5.3) could possibly lead to a quantitative characterization of a coherence length in this and other systems.

6 Conclusion

This paper is the result of a discussion group organized during this summer school. It has become a kind of a review of what glassy dynamics looks like, as encountered in experiments performed on different materials using diverse control parameters. Although first observed in spin and structural glasses, it now is clear that these spectacular effects are quite generic. This points towards the necessity of having a simple interpretation of these phenomena and we have used the concept of a coherence length to develop one. Note that all the theoretical interpretations discussed in this paper rely on a some sort of hierarchical picture: hierarchy of traps levels, of time scales in infinite-range glass models, of length scales in spatial approaches. We have focused on the latter because we think it gives greater physical insight. We note, however, that definition, characterization and measurement of a coherence length is still largely an open problem for most of the systems discussed here! In this respect, we mentioned several times that the experimental protocols discussed in this paper and their interpretation, for instance equations (5.2) and (5.3), constitute a promising starting point for progress on the crucial problem of length scales in glassy materials.

We would like to express our gratitude to the organizers for giving us the opportunity to appear in these proceedings. We also acknowledge discussions and collaborations with G. Biroli, J.-P. Bouchaud, D. Fisher, P. Holdsworth, R. da Silveira, H. Yoshino and P. Young.

References

- [1] L.C.E. Struik, *Physical aging in amorphous polymers and other materials* (Elsevier, Amsterdam, 1978).
- [2] L. Lundgren, P. Svedlindh, P. Nordblad and O. Beckman, *Phys. Rev. Lett.* **51** (1983) 911.
- [3] M. Cloitre, R. Borrega and L. Leibler, *Phys. Rev. Lett.* **85** (2000) 4819.
- [4] L. Cipelletti, S. Manley, R.C. Ball and D.A. Weitz, *Phys. Rev. Lett.* **84** (2000) 2275; C. Dérec, A. Ajdari, G. Ducouret and F. Lequeux, *C. R. Acad. Sci. Paris IV* **1** (2000) 1115.

- [5] M. Kroon, G. Wegdam and R. Sprik, *Phys. Rev. E* **54** (1996) 1; D. Bonn, H. Tanaka, G. Wegdam, H. Kellay and J. Meunier, *Europhys. Lett.* **45** (1999) 52; A. Knaebel, M. Bellour, J.-P. Munch, V. Viasnoff, F. Lequeux and J.L. Harden, *Europhys. Lett.* **52** (2000) 73.
- [6] F. Alberici-Kious, J.-P. Bouchaud, L.F. Cugliandolo, P. Doussineau and A. Levelut, *Phys. Rev. Lett.* **81** (1998) 4987.
- [7] E. Vincent, V. Dupuis, J. Hammann and J.-P. Bouchaud, *Europhys. Lett.* **50** (2000) 674.
- [8] E.V. Colla, L.K. Chao, M.B. Weissman and D.D. Viehland, *Phys. Rev. Lett.* **85** (2000) 3033.
- [9] J.B. Knight, C.G. Fandrich, C.N. Lau, H.M. Jaeger and S.R. Nagel, *Phys. Rev. E* **51** (1995) 3957; C. Jossierand, A. Tkachenko, D.M. Mueth and H.M. Jaeger, *Phys. Rev. Lett.* **85** (2000) 3632; M. Nicolas, P. Duru and O. Pouliquen, *Eur. Phys. J. E* **3** (2000) 309; P. Philippe and D. Bideau, *Europhys. Lett.* **60** (2002) 677.
- [10] C. Rossel, Y. Maeno and I. Morgenstern, *Phys. Rev. Lett.* **62** (1989) 681; E.L. Papadoulou and P. Nordblad, *Eur. Phys. J. B* **22** (2001) 187.
- [11] E. Vincent, J. Hamman, M. Ocio, J.-P. Bouchaud and L.F. Cugliandolo, in *Complex behavior of glassy systems*, edited by M. Rubi (Springer Verlag, Berlin, 1997); P. Nordblad and P. Svendlidh, in *Spin glasses and random fields*, edited by A.P. Young (World Scientific, Singapore, 1998).
- [12] J.-P. Bouchaud, L.F. Cugliandolo, J. Kurchan and M. Mézard, in *Spin glasses and random fields*, edited by A.P. Young (World Scientific, Singapore, 1998).
- [13] P. Réfrégier, E. Vincent, J. Hammann and M. Ocio, *J. Phys. France* **48** (1987) 1533.
- [14] J. Hammann, M. Lederman, M. Ocio, R. Orbach and E. Vincent, *Physica A* **185** (1992) 278.
- [15] K. Jonason, E. Vincent, J. Hammann, J.-P. Bouchaud and P. Nordblad, *Phys. Rev. Lett.* **81** (1998) 3243.
- [16] G.B. McKenna and A.J. Kovacs, *Polym. Eng. Sci.* **24** (1984) 1131.
- [17] A.J. Kovacs, *Adv. Polym. Sci.* **3** (1963) 394; A.J. Kovacs, *et al.*, *J. Polym. Sci.* **17** (1979) 1097.
- [18] C.A. Angell, K.L. Ngai, G.B. McKenna, P.F. McMillan, and S.W. Martin, *J. Appl. Phys.* **88** (2000) 3113.
- [19] V. Viasnoff and F. Lequeux, *Phys. Rev. Lett.* **89** (2002) 065701.
- [20] A.J. Liu and S.R. Nagel, *Nature* **396** (1998) 21.
- [21] M.E. Cates, this volume.
- [22] L. Berthier and J.-P. Bouchaud, *Phys. Rev. B* **66** (2002) 054404.
- [23] V. Viasnoff (unpublished).
- [24] T. Komori, H. Yoshino, and H. Takayama, *J. Phys. Soc. Jpn. Suppl. A* **69** (2000) 228.
- [25] L. Berthier and P.C.W. Holdsworth, *Europhys. Lett.* **58** (2002) 35.
- [26] R.L. Leheny and S.R. Nagel, *Phys. Rev. B* **57** (1998) 5154.
- [27] R. Höhler, S. Cohen-Addad and A. Asnacios, *Europhys. Lett.* **48** (1999) 93.
- [28] L. Bellon, S. Ciliberto, C. Laroche, *Europhys. Lett.* **51** (2000) 551; *Eur. Phys. J. B* **25** (2002) 223.
- [29] J.-P. Bouchaud, *J. Phys. I France* **2** (1992) 1705.
- [30] J.-P. Bouchaud and D.S. Dean, *J. Phys. I France* **5** (1995) 265.
- [31] M. Sasaki and K. Nemoto, *J. Phys. Soc. Jpn.* **69** (2000) 2283.
- [32] M. Sales, J.-P. Bouchaud and F. Ritort, Preprint [cond-mat/0207273].

- [33] L.F. Cugliandolo, this volume, Preprint [[cond-mat/0210312](#)].
- [34] L.F. Cugliandolo and J. Kurchan, *Phys. Rev. Lett.* **71** (1993) 173.
- [35] L.F. Cugliandolo and J. Kurchan, *J. Phys. A* **27** (1994) 5749.
- [36] L.F. Cugliandolo and J. Kurchan, *Phys. Rev. B* **60** (1999) 922.
- [37] A.J. Bray, *Adv. Phys.* **43** (1994) 357.
- [38] G. Grinstein and S.K. Ma, *Phys. Rev. B* **28** (1983) 2588; G. Grinstein and J.F. Fernandez, *Phys. Rev. B* **29** (1984) 6389; D.A. Huse and C. Henley, *Phys. Rev. Lett.* **54** (1985) 2708; D.S. Fisher and A.A. Middleton, *Phys. Rev. B* **65** (2002) 134411.
- [39] T. Nattermann, in *Spin glasses and random fields*, edited by A.P. Young (World Scientific, Singapore, 1998).
- [40] S. Miyashita and E. Vincent, *Eur. Phys. J. B* **22** (2001) 203.
- [41] J.-P. Bouchaud, V. Dupuis, J. Hammann and E. Vincent, *Phys. Rev. B* **65** (2001) 024439.
- [42] J.-P. Bouchaud, in *Soft and fragile matter: Nonequilibrium dynamics, metastability and flow*, edited by M.E. Cates and M.R. Evans (Institute of Physics Publishing, Bristol, 2000).
- [43] A.J. Bray and M.A. Moore, *J. Phys. C* **17** (1984) L463; and in *Heidelberg Colloquium on Glassy Dynamics, Lectures Notes in Phys.* **275**, edited by J.L. van Hemmen and I. Morgenstern (Springer, Berlin, 1987).
- [44] D.S. Fisher and D.A. Huse, *Phys. Rev. Lett.* **56** (1986) 1601; *Phys. Rev. B* **38** (1988) 373; *ibid.* **38** (1988) 386.
- [45] A.J. Bray and M.A. Moore, *Phys. Rev. Lett.* **58** (1987) 57.
- [46] H. Yoshino, A. Lemaître and J.-P. Bouchaud, *Eur. Phys. J. B* **20** (2001) 367.
- [47] D.A. Huse and D.S. Fisher, *J. Phys. A* **20** (1987) L997; D.S. Fisher and D.A. Huse, *J. Phys. A* **20** (1987) L1005; C.M. Newman and D.L. Stein, *Phys. Rev. B* **46** (1992) 973; *Phys. Rev. Lett.* **72** (1994), 2286; *ibid.* **76** (1996) 515; *ibid.* **76** (1996) 4821; *ibid.* **84** (2000) 3966; *Phys. Rev. E* **55** (1997) 5194; *ibid.* **57** (1998) 1356; *ibid.* **63** (2001) 160101; A.A. Middleton, *Phys. Rev. Lett.* **83** (1999) 1672; E. Marinari, G. Parisi, F. Ricci-Tersenghi, J. Ruiz-Lorenzo and F. Zuliani, *J. Stat. Phys.* **98** (2000) 973; D.S. Fisher, this volume; F. Krzakala and O.C. Martin, *Phys. Rev. Lett.* **85** (2000) 3017; M. Palassini and A.P. Young, *Phys. Rev. Lett.* **85** (2000) 3017.
- [48] J. Lamacq, J.-P. Bouchaud, O.C. Martin and M. Mézard, *Europhys. Lett.* **58** (2002) 321; A.A. Middleton, *Phys. Rev. B* **63** (2001) 060202; J. Houdayer, F. Krzakala and O.C. Martin, *Eur. Phys. J. B* **18** (2000) 467.
- [49] T. Aspelmeier, A.J. Bray and M.A. Moore, *Phys. Rev. Lett.* **89** (2002) 197202; T. Rizzo and A. Crisanti, Preprint [[cond-mat/0209333](#)]; M. Sales and H. Yoshino, *Phys. Rev. E* **65** (2002) 066131; D.A. Huse and L.F. Ko, *Phys. Rev. B* **56** (1997) 14597; F. Krzakala and O.C. Martin, *Eur. Phys. J. B* **28** (2002) 199.
- [50] P.E. Jönsson, H. Yoshino and P. Nordblad, *Phys. Rev. Lett.* **90** (2003) 059702.
- [51] L. Berthier and J.-P. Bouchaud, *Phys. Rev. Lett.* **90** (2003) 059701.
- [52] Although “surfing on glassy phases” would have been a possible title for this paper, we believe that “hiking” is better suited in the context of a summer school taking place so close to the Alps and the “Mer de Glace”.
- [53] C. Godrèche and J.-M. Luck, *J. Phys. A* **33** (2000) 9141; L. Berthier, P.C.W. Holdsworth and M. Sellitto, *J. Phys. A* **34** (2001) 1805.
- [54] M. Nifle and H.J. Hilhorst, *Phys. Rev. Lett.* **68** (1992) 2992.
- [55] Z. Ovadyahu, this volume.

- [56] A. Vaknin, Z. Ovadyahu and M. Pollak, *Phys. Rev. Lett.* **84** (2000) 3402; *Phys. Rev. B* **65** (2002) 134208; V. Orlyanchik, A. Vaknin, Z. Ovadyahu, M. Pollak, *Phys. Stat. Sol.* **230** (2002) 61.
- [57] V. Viasnoff, S. Jurine and F. Lequeux, *Farad. Discuss.* **123** (2002), XXX, Preprint [`cond-mat/0210636`].
- [58] F. Ozon, T. Narita, A. Knaebel, G. Debregeas, P. Hebraud and J.-P. Munch, Preprint [`cond-mat/0210554`].
- [59] V. Dupuis, E. Vincent, J.-P. Bouchaud, J. Hammann, A. Ito and H.A. Katori, *Phys. Rev. B* **64** (2001) 174204.

COURSE 15

KINETICALLY CONSTRAINED MODELS AND DRIVEN SYSTEMS WITH SLOW DYNAMICS

M. CLINCY¹, H.S. BOND² AND S. WHITELAM¹

¹ *School of Physics, Univ. of
Edinburgh, King's Buildings,
Edinburgh EH9 3JZ, UK*

² *Chemistry Dept. Univ. of
California, Berkeley, CA 94720, USA*



Contents

1	Introduction and overview	745
2	The Fredrickson-Andersen model	747
3	The Kob-Andersen model	749
4	The <i>ABC</i> model	751
5	Conclusions and outlook	752

KINETICALLY CONSTRAINED MODELS AND DRIVEN SYSTEMS WITH SLOW DYNAMICS

M. Clincy, H.S. Bond and S. Whitelam

Abstract

Three lattice models which exhibit slow dynamics are reviewed, namely the kinetically-constrained Fredrickson- Andersen and Kob-Andersen models, and the ABC model which is a driven system exhibiting anomalously slow coarsening. All three are defined by local dynamical rules. We discuss the differences arising between particle-conserving and non-conserving dynamics, and examine the origin of the slow relaxation for each model. In addition we present some recent work in this field.

1 Introduction and overview

Systems far from equilibrium have been of long-standing interest. They exhibit a rich variety of collective behaviour, and in contrast to equilibrium phenomena no unified framework for their description exists. Of particular interest are non-equilibrium systems exhibiting slow dynamics and, frequently, coarsening. Many different approaches to modelling these systems have been proposed. Possible starting points include a Hamiltonian description, as in the case of p -spin models (L. Cugliandolo) and spin glasses, a constitutive equation as for rheological problems (M.E. Cates), or an equation of motion as in the case of Mode Coupling Theory (W. Kob, all this volume).

In contrast, the kinetically constrained models and driven systems presented in this article are defined exclusively by their local dynamics. All are defined on lattices, and their behaviour is solely determined by exchange rules between neighbouring sites. Despite the local nature of these rules, interesting collective behaviour such as slow coarsening and phase separation can emerge.

Generally, the dynamics is imposed by starting from an initial configuration (usually corresponding to some higher temperature prior to a quench)

and updating the system at each time step by picking a site on the lattice at random, comparing it to its neighbours, and applying a prescribed set of rules. This procedure is relatively easy to implement, making these models ideal candidates for study *via* Monte-Carlo methods. In addition, there exist various methods of tackling them analytically.

The hope with these simple models is that if non-equilibrium universality classes exist then they might play a role similar to the Ising model in equilibrium physics; namely, a “toy” model capturing many of the essential features of more complex processes.

Before discussing the models in detail we will first present a short overview and highlight some of their similarities and differences. There are essentially two different types of dynamics possible, depending on whether or not the rules conserve the number of particles (for a simple model in which both types of rules are present – *i.e.* particle-conserving spin exchanges and non-particle-conserving spin flips – see Z. Racz’s lecture this volume). In addition, these models may be defined in different dimensions and for a varying number of particle types.

The next two sections are devoted to kinetically constrained models, namely the Fredrickson-Andersen (FA) model [1] (Sect. 2) and the Kob-Andersen (KA) model [2] (Sect. 3). In order to achieve a critical slowing down, the dynamical processes are impeded by some constraint imposed “by hand” on the microscopic dynamics, which prevents certain transitions from occurring. The first model has non-conserving dynamics whereas for the latter the total number of particles is constant. In contrast to these constrained models, the slowing down in the driven ABC model described in Section 4 is self-generated [3]. Its dynamics also preserves the number of particles. Note that all of the models are defined with periodic boundary conditions.

The FA model is defined on a lattice (originally 2d) for two types of particles denoted as “up” and “down” spins. A field is applied such that the down spins (relaxed) are favoured over the up spins (excited). In the 1d FA model, in contrast to the 1d Ising model, spins are only able to flip if either one (or both) of their neighbours is excited. The spin itself is then said to be “facilitated”. If this constraint is fulfilled, up spins can relax with a rate 1, whereas down spins can become excited with a rate $\epsilon \equiv \exp(-1/T)$ (chosen to enforce detailed balance). Because of this constraint, the FA model exhibits a coarsening process and a dynamical arrest.

It is clear that the dynamics is spatially symmetric, and hence the 1d FA model is also known as the Symmetrically Constrained Ising Chain (SCIC).

A variation of this model in one dimension is the Asymmetrically Constrained Ising Chain (ACIC) in which the constraint states that a spin is only facilitated if its *right* neighbour is excited. One might already

suspect that this stronger constraint will slow the dynamics even further. It has indeed been shown [4] that the SCIC relaxes with an Arrhenius law like a strong glass whereas the dynamics in the ACIC obeys a Bässler law, resembling a fragile glass, and so these simple models can exhibit non-trivial scaling laws like those observed in glasses. Since the ABC model defined below also displays anomalous coarsening, it has been suggested there might be some connections between the ACIC and this driven system [5].

Section 3 is devoted to the KA model which was originally defined in three dimensions, but has also been recently studied in 2d. To our knowledge, no 1d equivalent has been defined. Despite its dynamics being conserved, its constraints are quite similar to the FA model if the “up” and “down” spins are mapped onto occupied and empty lattice sites. The essential dynamical rule of the KA model is that a particle can only hop to an empty neighbouring lattice site if it has fewer than m neighbours in the initial state before a jump (where m depends on dimension). This rule mimics an attractive potential between neighbouring sites. The dynamics here depends crucially on the initial particle concentration.

A different approach is taken in Section 4 with the *ABC* model [3]. It is also a one-dimensional model with conserving dynamics, yet for three species denoted as A , B and C particles. The rules are such that it is preferable for B to be to the right of A , for C to be to the right of B and for A to be to the right of C , so that a randomly chosen pair of AB (BC or CA) transforms into BA (CB or AC) with rate $q < 1$ and back with rate 1 with *no* constraints imposed. Starting from a random configuration, these rules define a coarsening process into a fully phase separated state which is anomalously slow.

In the following three sections we will describe these models in more detail and give some overview over current research in this field.

2 The Fredrickson-Andersen model

A liquid near the glass transition often exhibits a critical slowing down of its characteristic relaxation time, and, in contrast to a conventional phase transition, fails to develop long-range order. This “dynamical glass transition” can be viewed as arising through an increasing cooperativity of local processes (such as molecular translations and rotations) with decreasing temperature, and this cooperativity can be represented by a system possessing dynamical constraints. Such constraints must be included “by hand”, being independent of the statics of the system and so not appearing in the Hamiltonian. Palmer *et al.* [6] introduced the concept of a hierarchy of constrained dynamics in which different degrees of freedom relax in serial, and they demonstrated that a broad spectrum of characteristic times can

emerge naturally from this idea. An alternative approach was pioneered by Fredrickson & Anderson [1], who introduced the n -spin facilitated kinetic Ising model in which the slow cooperative relaxation of a system of Ising spins was achieved by stipulating that a given spin could flip only if at least n of its nearest neighbours are pointing against an external field. It is a one-dimensional version of this simple model that we consider. See [7] for recent analytical and numerical results pertaining to this model.

It may be possible to replace the dynamical constraints modifying this noninteracting system by a system exhibiting “normal” dynamics but possessing interactions. One possible strategy, followed here, is to try and remove the dynamical constraints at the expense of introducing a nontrivial metric in the space of configurations.

Starting from a Monte-Carlo description of a system, it is possible to write down a Fokker-Planck equation and so give a different interpretation of the dynamical constraint. For convenience we consider a one-dimensional chain of spins $x_i(t)$ whose values are continuous and unrestricted. We let the system’s Hamiltonian be noninteracting and quadratic, $H = J \sum_i x_i^2$, and we define a facilitation function $f_i(x_{i-1}, x_{i+1})$ that represents the effect of spin i ’s nearest neighbours on its dynamics. The functional form of f_i must be such that it is small when the system’s energy is small. “Facilitated Metropolis” Monte-Carlo dynamics are implemented by quenching the system from an initial distribution, generating random spin flips r_i , and accepting the change $x_i(t + \delta t) = x_i(t) + r_i$ with a probability $\min(f_i, f_i \exp(-\beta \delta E))$, where $\delta E \equiv H(t + \delta t) - H(t)$ is the energy change following the flip. The evolution of the discrete FA model corresponds to the diffusion of isolated defects with timescale $\approx \exp(1/T)$, typical of a strong glass: numerical studies indicate that the continuous system exhibits a similar timescale.

The Monte-Carlo dynamics corresponds to a master equation

$$\begin{aligned} \tau \partial_t P(\mathbf{x}; t) = & \sum_i \int P(\dots, x_i + r_i, \dots; t) W(x_i + r_i | x_i) \\ & - \sum_i \int P(\dots, x_i, \dots; t) W(x_i | x_i + r_i), \end{aligned} \quad (2.1)$$

where the integrals are over all spinflips r_i , and the transition probabilities per unit time W are chosen *via* the facilitated Metropolis prescription, as defined above. Since ordinary Metropolis dynamics satisfy detailed balance, and our only modification has been to multiply both rates by the same factor f_i , the presence of the kinetic constraint has no effect on the equilibrium solutions of the model. It is this distinction – that the dynamics depends on the rates W , but the statics only on their ratio – that ensures no violation of detailed balance takes place in the presence of the kinetic constraint.

In the limit of a constant, infinitesimal spin flip Δ we obtain the diffusive Fokker-Planck equation

$$\tau \frac{\partial}{\partial t} P(\mathbf{x}; t) = \frac{1}{2} \frac{\partial}{\partial x_\mu} \left(-4Jf_\mu x_\mu P(\mathbf{x}; t) + \Omega f_\mu \frac{\partial}{\partial x_\mu} P(\mathbf{x}; t) \right), \quad (2.2)$$

where the various constants have been absorbed into the parameter Ω . We note that the Fokker-Planck equation on a general manifold reads

$$\frac{\partial}{\partial s} \rho(\mathbf{r}_s, s | \mathbf{r}_t, t) = \left(-\frac{\partial}{\partial r_s^\mu} A^\mu(\mathbf{r}_s, s) + \frac{1}{2} \frac{\partial^2}{\partial r_s^\mu \partial r_s^\nu} G^{\mu\nu}(\mathbf{r}_s, s) \right) \rho(\mathbf{r}_s, s | \mathbf{r}_t, t), \quad (2.3)$$

and so we can interpret the result as describing the (driven) diffusion of a particle on a manifold with inverse metric $G^{\mu\nu} = f_\mu \delta^{\mu\nu}$. Studies of this problem are ongoing.

3 The Kob-Andersen model

The Kob-Andersen model [2] is a model defined on a lattice of 2 or greater dimensions. Each site is assigned a value of either -1 (for an empty lattice site) or 1 (for a site containing a particle). The number of particles on the lattice at all times is conserved, and all configurations in the model are equally likely. A move is attempted as follows. First, a particle is randomly chosen. One of its 2d nearest neighbors is then picked at random. The particle is allowed to move if and only if the following three conditions are met.

- The particle can only move to an empty site;
- The particle can only move if at least a certain fraction of its nearest neighbors are unoccupied. This fraction is usually taken to be one half;
- The move must obey detailed balance.

Thus, a particle is only allowed to move when it is surrounded by a sufficient number of free lattice sites. This mimics the behavior of glassy fluids, where rearrangement in the liquid is blocked when a “cage” is formed around a particular section in that material. As can be expected, the addition of the dynamic constraint leads to a dramatic slowing down of relaxation times in the Kob-Andersen model as the concentration of particles increases.

The dynamics of this model have been studied previously, particularly in 3 dimensions. The diffusion constant apparently vanishes at a particle

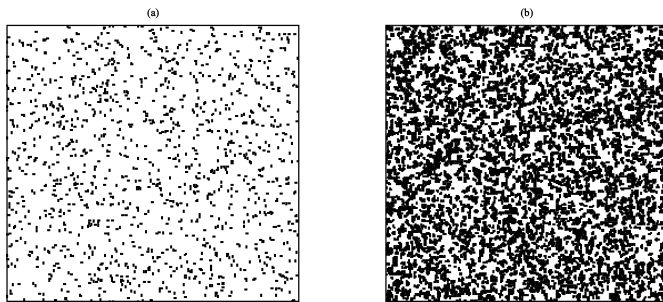


Fig. 1. d_i for **a)** $\tau = 5.0$ lattice sweeps and **b)** $\tau = 100.0$ at a concentration of 0.65 in a 2d Kob-Andersen model.

concentration lower than one, and correlation functions and relaxation behavior have been previously examined. Unlike the studies of other models mentioned in this work, this focuses on understanding the dynamical behavior of the Kob-Andersen model in equilibrium. It is important to note that since all configurations are equally likely in equilibrium, there is no static correlation between any two particles.

A different method of studying dynamics has been introduced elsewhere [8]. This method introduces the “dynamic heterogeneity field”, d_i , as follows:

$$d_i(\tau) = \left| \frac{1}{\tau} \sum_{t=1}^{t+\tau} s_i(t) \right|^2. \quad (3.1)$$

The summation above is performed not over lattice sites but over some coarse-graining time τ . It can be thought of as a measure of how quickly the value of lattice site i changes over the time τ . Suppose that some lattice site i changes very quickly over the summation time. Its value fluctuates from -1 to 1 and back. When the summation in (3.1) is performed, cancellation occurs and d_i is found to be very close to zero. On the other hand, for some site i which remains essentially unchanged over time τ , d_i will be close to one. Thus, essential information about dynamics can be captured by coarse-graining the lattice over time.

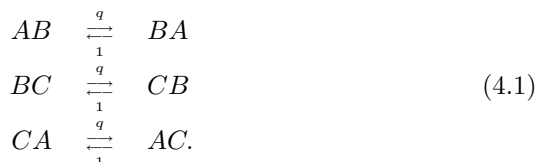
Although d_i is indexed by the spatial position of the lattice site, it is important to note that it depends explicitly on τ . If τ is chosen to be 0, no coarse graining takes place, and d_i is 1 for every lattice site. On the other hand, if τ tends to infinity, d_i will tend towards a uniform value across the lattice and again provides no useful information. Intermediate values are far more interesting.

The importance of the choice of τ can be seen in Figure 1. For a short coarse-graining time, very little structure can be seen in d_i . As the time increases, however, a significant difference can be seen. Because all configurations in the Kob-Andersen model are equally likely, there is no spatial correlation between particles whatsoever. A choice of τ which is sufficiently long makes it clear, however, that spatial correlation exists in the dynamics of the Kob-Andersen model.

Studying the spatial structure of the dynamics is hoped to elucidate the dynamical transition exhibited by these models.

4 The *ABC* model

The *ABC* model is defined on a 1d ring with L lattice sites. Each site is occupied by one of three types of particles denoted as A , B or C . They exhibit hard-core interaction, *i.e.* only one particle per site is allowed. Each time step, neighboring sites on the ring are chosen at random and the configuration is updated according to the following rules:



Applying these rules leads to the particles diffusing asymmetrically around the ring. Note that periodic boundary conditions are implied and the dynamics conserves the number of particles.

This model has been extensively studied in [3] by analytical and numerical means. We will summarise the main results here. Starting from an initially random configuration, the system will coarsen into a strongly phase separated state for any $q < 1$. Thus the system exhibits long-range order, even though the dynamics is strictly local. For $q = 1$ particles of all species have equivalent dynamics which results in a steady state in which no configuration is preferred and the steady state of the system is disordered.

To understand the coarsening dynamics, note that when $q < 1$ domain walls of the type BA , CB and AC are unstable to interchanges leading to AB , BC and CA respectively. This results in the diffusion of *e.g.* A particles to the left in a B domain and to the right in a C domain. Thus the system arrives at a metastable configuration of the form $A_1 B_1 C_1 A_2 B_2 C_2 \dots$ (X_i denotes a domain of X particles, where $X = A, B, C$), and a slow coarsening process, involving the elimination of the smallest domains, ensues. For example, the time it takes an A particle to traverse a B domain of length l is of order q^l . Thus the elimination of domains of size l occurs at a rate of

order q^{-l} which results in the typical domain size growing as $l \sim \ln t$. This growth law which is slower than any power of t is referred to as anomalous coarsening [5]. Ultimately the coarsening process results in a strongly phase separated state comprising three pure domains.

In the special case of equal particle numbers $N_A = N_B = N_C = L/3$ one can show that the ground state obeys detailed balance with respect to a long-range asymmetric energy function \mathcal{H} . A configuration of the system is specified by the set of indicator variables $\{X_i\} = \{A_i, B_i, C_i\}$ which take values 1 or 0 according to whether site i is occupied by the relevant particle. For example $A_i = 1$ if site i is occupied by an A particle. Clearly, $A_i + B_i + C_i = 1$. With these indicator variables the energy function may be written as:

$$\mathcal{H}(\{X_i\}) = \sum_{i=1}^L \sum_{k=1}^{L-1} \left(1 - \frac{k}{L}\right) (C_i B_{i+k} + A_i C_{i+k} + B_i A_{i+k}) - (L/3)^2. \quad (4.2)$$

Note that the asymmetric interaction between sites i and $i+k$ decays as $(1-k/L)$. Due to the infinite range of this interaction, this energy function is superextensive and scales quadratically with system size L .

The width of the domain walls in the phase separated state is of order $1/|\ln q|$ [3]. So for $q \rightarrow 1$ the size of the domain walls diverges and the system will be in a homogeneous disordered state. Moreover we expect a scaling regime to occur when the width of the domain walls is of the order of the domain lengths $L/3$ *i.e.*

$$\frac{1}{|\ln q|} \sim O(L) \quad (4.3)$$

so that the scaling regime is given by

$$q = \exp\left(-\frac{\beta}{L}\right). \quad (4.4)$$

Under the scaling (4.4) the control parameter is now β instead of q .

One question of interest is how the system approaches the disordered limit $q = 1$, *i.e.* $\beta = 0$: it could be a singular point or there could be phase transition for finite β . We find that in the above scaling limit an order-disorder transition occurs at a finite temperature for which the critical exponents can be determined numerically [9].

5 Conclusions and outlook

We have presented three simple lattice models which show slow relaxational dynamics. In the FA and the KA models this slowing is achieved by imposing kinetic constraints. The FA model is a non-equilibrium spin flip

model in which glassy Arrhenius behaviour is observed. In Section 2 we presented one possible approach of mapping these ad hoc constraints onto a more “normal” dynamics by introducing a nontrivial metric in the space of configurations.

In contrast, the KA model is an equilibrium model with a conserved number of particles. Although this means that slow relaxation of the particle configurations as a collective phenomenon does not appear as a function of time, but as a function of the initial concentration of particles, we showed in Section 3 that local variables show interesting temporal features.

The ABC model presented in Section 4 is not kinetically constrained, but driven by local dynamics such that slow relaxation is self-generated. Under certain conditions this model obeys detailed balance with respect to a long-range energy function in its phase separated ground state. In this case it is possible to study an order-disorder transition and numerically calculate critical exponents.

We would like to conclude by pointing out that the list of models presented here is, of course, by no means exhaustive. We have restricted ourselves to models with hard-core interaction on square lattices with periodic boundary conditions.

A class of models with open boundaries which have a crucial effect on the dynamics are the Asymmetric Simple Exclusion Processes (ASEP) [10–14] or 1d sandpile models as the one introduced by Bak *et al.* [15, 16]. The latter also does not have hard core interactions and shows self-organised criticality (see Savitskaya, Racz, this volume). Further models in which the numbers of particles per site is not restricted to one are *e.g.* the Zero Range Process [17] and Urn Models [18].

Interesting features have also been observed in models with different geometries such as triangular lattices [19].

It is, furthermore, possible to study one-dimensional systems with hard-core particles in continuum. One example is the Asymmetric Random Average Process (ARAP) [20, 21] which can be connected to the q -model [22] (for a review of the q -model see J.-P. Bouchaud’s lecture, this volume).

MC would like to thank the Gottlieb Daimler – und Karl Benz – Stiftung as well as EPSRC for financial support. SW would like to thank EPSRC for financial support.

This material is based upon work supported under a National Science Foundation Graduate Research Fellowship. Any opinions, findings, conclusions or recommendations expressed in this publication are those of the author(s) and do not necessarily reflect the views of the National Science Foundation.

We thank C. Toninelli for fruitful discussions.

References

- [1] G.H. Fredrickson and H.C. Andersen, *Phys. Rev. Lett.* **53** (1984) 1244.
- [2] W. Kob and H.C. Andersen, *Phys. Rev. E* **48** (1996) 4364.
- [3] M.R. Evans, Y. Kafri, H.M. Koduvely and D. Mukamel, *Phys. Rev. E* **58** (1998) 2764.
- [4] A. Buhot and J.P. Garrahan, *Phys. Rev. E* **64** (2001) 021505.
- [5] M.R. Evans, *J. Phys. Cond. Matt.* **14** (2002) 1397.
- [6] R.A. Palmer, D.L. Stein, E. Abrahams, P.W. Anderson, *et al.*, *Phys. Rev. Lett.* **53** (1984) 958.
- [7] M. Schulz and S. Trimper, *J. Stat. Phys.* **94** (1999) 173.
- [8] J.P. Garrahan and D. Chandler, *Phys. Rev. Lett.* **89** (2002) 035704.
- [9] M. Clincy, B. Derrida and M.R. Evans (2002) [[cond-mat/0209674](#)].
- [10] J. Krug, *Phys. Rev. Lett.* **67** (1991) 1882.
- [11] B. Derrida, M.R. Evans, V. Hakim and V. Pasquier, *J. Phys. A* **26** (1993) 1493.
- [12] G. Schütz and E. Domany, *J. Stat. Phys.* **72** (1993) 277.
- [13] T. Sasamoto, *J. Phys. A* **32** (1999) 7109.
- [14] R.A. Blythe, M.R. Evans, F. Colaiori and F.H.L. Essler, *J. Phys. A* **33** (2000) 2313.
- [15] P. Bak, C. Tang and K. Wiesenfeld, *Phys. Rev. Lett.* **59** (1987) 381; P. Bak, C. Tang and K. Wiesenfeld, *Phys. Rev. A* **38** (1988) 364.
- [16] L. Kadanoff, S.R. Nagel, L. Wu and S.-m. Zhou, *Phys. Rev. A* **39** (1989) 6524.
- [17] See, *e.g.*, F. Spitzer, *Advances in Math.* **5** (1970) 246; M.R. Evans, *Braz. J. Phys.* **30** (2000) 42.
- [18] For a review of various urn models, see C. Godrèche and J.M. Luck, *J. Phys. Cond. Matt.* **14** (2002) 1601.
- [19] M.E.J. Newman and C. Moore *Phys. Rev. E* **60** (1999) 5068.
- [20] J. Krug and J. García, *J. Stat. Phys.* **99** (2000) 31.
- [21] R. Rajesh and S.N. Majumdar, *J. Stat. Phys.* **99** (2000) 943.
- [22] S.N. Coppersmith, C.-h. Liu, S. Majumdar, O. Narayan and T.A. Witten, *Phys. Rev. E* **53** (1996) 46.

COURSE 16

DYNAMIC TRANSITIONS IN THERMAL AND ATHERMAL SYSTEMS

C.B. HOLMES¹, J.H. SNOEIJER² AND TH. VOIGTMANN³

¹ *School of Physics,
University of Edinburgh,
JCMB, King's Buildings, Mayfield
Road,
Edinburgh EH9 3JZ, UK*

² *Instituut Lorentz, Univ. Leiden,
Postbus 9506, 2300 RA Leiden,
The Netherlands*

³ *Physik-Department,
James-Franck-Str.,
TU München, 85748 Garching,
Germany*



Contents

1	Introduction	757
2	Universal behavior of the force distribution?	758
3	Colloidal glasses and gels	760
4	Jamming transitions	762
5	Conclusion	764

DYNAMIC TRANSITIONS IN THERMAL AND ATHERMAL SYSTEMS

C.B. Holmes, J.H. Snoeijer and Th. Voigtmann

Abstract

Dynamic transitions from a fluid to a solid-like state occur in a wide variety of physical systems. In this article, we discuss the notion that universal physics might lie behind transitions which, at first, appear rather different. We highlight some features which appear to be common to various transitions, as well as looking at those aspects which differ.

1 Introduction

Equilibrium phase transitions are now rather well understood and classified. One knows about their peculiarities and, most importantly, about their universal features. Much less is known about non-equilibrium phase transitions (see the lectures by Rácz in this issue [1]), or purely dynamic transitions. Among the latter are phenomena such as the (ideal) glass transition, gelation in attractive colloidal systems, and jamming transitions under an external force, each of which is a transition from an ergodic fluid to a nonergodic, amorphous solid. These are regarded as *dynamic* transitions since the dynamics are drastically different on either side of the transition, whilst no thermodynamic quantity has been found to diverge at to the transition (as would be the case for standard thermodynamical phase transitions). In particular, it is difficult to tell from looking at a single snapshot of the system whether it is on the fluid or the solid side of the transition. However, in Section 2, we discuss a static quantity which, it has been speculated, may show a characteristic change at such a transition.

These “glassy” phenomena occur in a wide variety of systems, including molecular systems, colloids, or granular media; many examples have been provided in this school. The ubiquity of these phenomena, and the similarities between them, provoked Liu and Nagel [2] to pose the question of whether a unifying framework for these fluid-solid transitions may exist. In

other words, are all these transitions just different facets of the same universal physics, or do the names “glass transition”, “gelation” and “jamming” really refer to fundamentally different phenomena? At first sight, their idea may seem far-fetched: can the physics of a pile of sand really be related to that of window glass? But there are certain features of these systems which appear analogous. For instance, the densification of granular materials upon vibrating the sample is somewhat similar to that of glasses upon varying the temperature (see [3] and references therein).

Colloids appear to be suitable systems in which to further examine the proposed unification: these systems have already proven to be a suitable testing ground for theories of the glass transition, as we shall see below. In addition, they allow us to make a connection to granular matter by increasing particle size until Brownian motion is insignificant. For colloidal systems, the conjecture is that by altering either inverse density (expressed as the inverse volume fraction of the colloidal particles, $1/\phi$), the strength of the interparticle attraction (in this context usually measured by $k_B T/U$ where U is the attractive well depth), or applied external stress, one encounters transitions from fluid to amorphous solid states that are, in some respect, equivalent. By lowering any of the mentioned parameters, the system undergoes dynamic arrest and ends up in what Liu and Nagel called the “jammed” state (see Fig. 1). Experimental evidence for such universality has been found in the $(\phi, k_B T/U)$ plane of such a diagram [4, 5]. Note that in what follows, we refer to the arrested state as a “glassy” one, and restrict the word jamming to describe a fluid-solid transition which occurs due to applied stress.

In this article, we discuss the idea of a unifying phase diagram, focussing upon colloidal and granular systems. In the following section, we address the conjecture that the force distribution displays a “universal” change when crossing the transition boundary. In Section 3 we discuss to what extent theory may provide a unifying framework for the $k_B T/U - 1/\phi$ plane; we then investigate the effect of applied stress in Section 4, and finish with some conclusions.

2 Universal behavior of the force distribution?

The glass transition is considered to be a purely dynamic transition, since static quantities undergo little change across the transition [6]. However, recent numerical simulations and experiments suggest that the distribution of forces $P(f)$ is one static property which *does* display a characteristic change at the glass transition. Before discussing this feature in detail, let us consider why the force distribution might be of relevance.

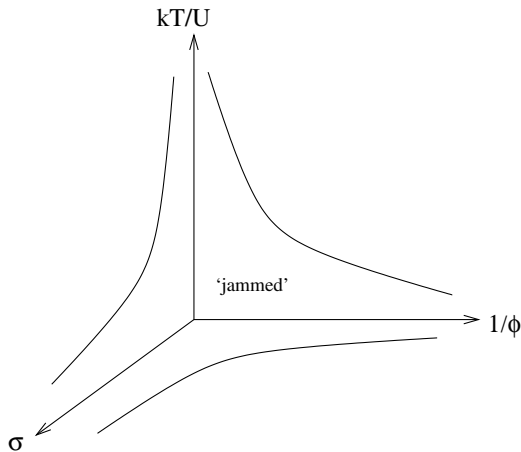


Fig. 1. A “jamming phase diagram” in which the axes are the inverse volume fraction ($1/\phi$), a measure of inverse attraction strength ($k_B T/U$), and some external load such as a shear stress (σ). In this figure, the relevant parameters are altered slightly from that of the original proposal, in order to study colloids [4]. Note that different systems may require their own choice of axes – for example in granulars, both T and U are effectively zero.

The force distribution is not a conventional object in the context of glass transitions. However, it is simply a different way of representing the pair distribution function $g(r)$, since $P(f)df \sim r^2 g(r)dr$ (for smooth potentials in three dimensions). One reason to consider the force distribution is that for steep repulsive potentials, $P(f)$ is much more sensitive than $g(r)$ to configurational changes at small length scales. Another reason is that particles have been observed to organize themselves into complicated *force networks*. These structures are able to sustain large loads (see also Sect. 4) and might be related to the dynamic arrest [7]. Force networks have been investigated, both experimentally and theoretically, in particular for granular materials (see Bouchaud in this issue [8]). In these studies one generically finds distributions which decay exponentially for large forces; the small force behavior is less clear, as will be discussed at the end of this section.

Since static granulars are glassy (in the general sense), one may ponder the relevance of the exponential tail of the force distribution. Is this found in other glassy systems? The answer to this is yes. However, it is also found in other systems which are *not* glassy. For example, they are observed for Lennard-Jones systems, both in the liquid and the glassy state [9]. Also, one can make a simple argument which suggests an (almost) exponential tail in $P(f)$ for Lennard-Jones systems, with no reference to glassiness [9].

These factors suggest that the exponential tail is irrelevant as regards the transition to a disordered solid.

However, there is a second feature of the force distribution which may be of more relevance. In simulations of foams, supercooled liquids and granular materials, $P(f)$ has been observed to develop a small peak around the average force [9, 10] as the system becomes glassy. It is intriguing that this feature occurs in these rather different glassy systems. This might point towards commonality of the underlying physics. The microscopic origin for this change of $P(f)$ is currently not well understood, but Liu *et al.* speculate that it is related to the emergence of a percolating force network [9].

Some of these features have also been found experimentally in granulars. In the so-called carbon paper experiments [11], $P(f)$ is again found to have a small peak around the average force. In these experiments, one extracts the forces between the container wall and the adjacent particles from imprints on carbon paper. It is not clear, however, that these forces display the same statistics as those in the bulk: indeed, a recent study reveals that the particle-wall force statistics can differ substantially from $P(f)$ in the bulk [12].

It appears then, that the observed behavior of the force distribution provides an interesting perspective on the dynamic fluid–solid transition. In particular, it appears to be a good candidate for a static quantity which marks the transition. At this moment, however, there is still a lack of microscopic understanding of the change in $P(f)$: even for granular materials, where $P(f)$ has been studied extensively, the small force behavior is not well-understood. Intriguing as the observations are, without a microscopic understanding of the peak’s origin, it is difficult to argue persuasively about the relevance of the peak to glassiness.

3 Colloidal glasses and gels

The glass transition in hard-spheres (HS) provides us with a paradigm for the colloidal glass transition. The dynamic arrest of HS from the metastable fluid into an amorphous solid has been well studied experimentally [13]. Computer simulation studies suggest that aspects of this transition are not so different from those in many molecular fluids ([14] and references therein). This is in agreement with the common approach in which hard spheres serve as a model system for many simple liquids.

Thus one argues that the excluded volume effect is key to understanding the glass transition, *i.e.* the transition is of mainly entropic origin, and that the so-called cage effect is the dominant physical mechanism driving the transition. If one considers any particle in the fluid, its motion is hindered due to a cage formed by its neighbours. Due to a low overall compressibility,

it is unlikely that the particle will escape from this cage through a spontaneous density fluctuation. Instead, all particles have to move cooperatively, *i.e.* one of the caging particles has to make way, which can only happen if one of its neighbours moves, and so forth.

In the framework of statistical mechanics, a mode-coupling theory of the (ideal) glass transition (MCT) has been worked out by Götze and co-workers [15–17]. In this microscopic approach, the cage effect is expressed through a set of self-consistent equations of motion for the density correlation functions, which exhibit a nonlinear feedback. The MCT compares well to experimental data in many cases [17], although there are undeniably flaws [6]. For a short introduction to MCT, we refer the reader to [18].

One characteristic of the dynamics close to a glass transition is a two step relaxation process, involving two distinct timescales which, upon approaching the transition, diverge according to power laws. This has been demonstrated for hard-sphere colloids in the experiments by van Meegen *et al.* [19]. Another way to investigate the dynamics of the glass state is to study the mean-squared displacement of a tagged particle. In the glass, this quantity never reaches a long-time diffusive limit but instead levels off onto some plateau that is directly connected with the particle's localization length and thus a measure of the cage size. In typical hard-sphere like glasses, the localization length is about 10% of the particle diameter. Once a particle is able to move substantially more than some fraction of its own diameter, the frozen structure melts.

So far in this section, we have considered the transition to a non-ergodic solid state (the *glass*) which occurs in a system of HS if the density is made sufficiently large. Let us continue by considering the effect of adding to the HS repulsion some short-ranged attraction. (This can be realised experimentally through colloid-polymer mixtures [20], which are an effective one-component attractive system of colloidal particles.) If the attraction is sufficiently strong, one can find a transition to a non-ergodic amorphous solid state at low particle densities. This state is known as the *gel*.

The effect of such an attraction on the MCT transition have been discussed recently [21–23]. Perhaps surprisingly, the theory seems to be able to capture the physics of the low-density nonergodicity transition, although this statement must be qualified. Gelation is a complicated transition: the loss of ergodicity is accompanied by other phenomena, such as aggregation into clusters and percolation; the latter are not described by MCT, although extensions are being worked on [24]. Despite this qualification, MCT captures some physical aspects found in real gels: again, the dynamics shows a two-step relaxation process similar to the one close to the glass transition [5, 25], albeit governed by different exponents.

At the gel transition, particles are more localised than at the glass transition. Basically, one finds localization lengths to be of the order of the potential range, which is typically smaller than the localization length found at the glass transition. This is just one of the theoretical predictions pointing to a difference of the glassy state and the gel. These differences arise because in the gel, it is “bonding”, *i.e.* the attractive interaction, instead of the excluded volume repulsion that is responsible for the arrest.

Perhaps the most interesting prediction MCT makes for transitions in the $(1/\phi, U/k_B T)$ plane concerns the “intermediate” region of attractive systems with higher density. For sufficiently short attraction ranges, MCT predicts that the glass and the gel transition lines do not cross over smoothly. Rather, a “line-crossing phenomenon” occurs [23], whereby the glass transition line terminates upon meeting the gel transition line, and the latter continues into the glass region until it stops at an endpoint (see Fig. 2). In other words, there appears a so-called glass-glass transition (or glass-gel in the terminology of this paper), both sides of which can be joined by a smooth path in the glass state avoiding the transition. Within MCT, the endpoint corresponds to a so-called higher order (compared to the standard glass transition) singularity. Its hallmarks are the appearance of new dynamic phenomena, most notably logarithmic decay laws instead of the common power-law scenario [26]. These predictions have stimulated a number of experimental [27, 28] and computer-simulation [29, 30] studies, indicating that indeed the line-crossing phenomenon can be found.

The appearance of this line-crossing phenomenon indicates that there is an interplay of two distinct physical mechanisms, *viz.*: caging *vs.* bonding, one relevant for the glass transition, the other for gelation. From this point of view, the two transitions are different. However, at larger attraction ranges, the endpoint merges into the glass transition line, making the glass-glass transition disappear. In this case, the two mechanisms cross over smoothly, and one can argue that there is some universality in the transition.

Despite some open questions regarding the applicability of MCT, it appears that the topology of the diagram proposed by Liu and Nagel may be more complicated than first envisaged. On the other hand, the idea gains credence, in that the description of both the glass and the gel transitions within the theory suggests a degree of commonality in the underlying physics.

4 Jamming transitions

In the previous section, we considered the relationship between (seemingly) different fluid–solid transitions without considering the effect of applied stress. However, there is always some stress on the system due to the

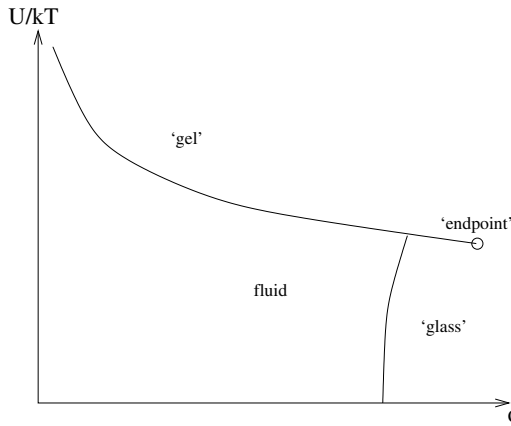


Fig. 2. Schematic view of the glass/gel state diagram as predicted by mode-coupling theory for sufficiently small ranges of the interparticle attraction. The gel transition line continues as a glass-glass transition line into the glassy state and terminates at a higher-order singularity endpoint.

isotropic pressure. This quantity either fixes the density, or is irrelevant (in colloids, due to an incompressible solvent). Therefore, any effect of the pressure is acknowledged by defining the density. In what follows, the stresses referred to do not, unless otherwise stated, include the isotropic pressure.

Anisotropic stresses are capable of fluidising a glassy state, as discussed elsewhere in this volume [31]. However, they are also capable of taking a concentrated system *into* a solid state [7]. An example of such a situation is a bucket of sand: this is certainly a solid in one sense, since one can stand upon the sand, and it will happily support the added weight – the response is, to a good approximation, that of a solid. However, this solidity is due solely to the presence of gravity – under this (body) force, the sand adopts a structure which is able to support the weight of those grains at a greater height. When we then stand upon the sand, we impose a load which is essentially the same as that which *jammed* the system in the first place. In contrast, when the bucket is tilted, the sand flows like a liquid because the imposed load acts in a different direction (in the reference frame of the bucket) – no structure exists to support this load. This property, that a macroscopic applied load in one direction may be statically supported, whilst a small applied load in a different direction causes flow, has been termed *fragility* [7]. These properties will obviously tend to complicate any phase diagram, should such an idea have any validity.

Having established that applied stresses may lead to solidity, we are able (at least conceptually) to split glassy solids into two types: those whose existence does, or does not, depend upon the presence of an applied stress (other than the isotropic pressure). This makes distinct the cases of a transition which occurs simply because a system is too crowded; and that of a system which becomes solid upon application of some anisotropic stress. This initial separation of transitions into two types serves to distinguish between what is commonly thought of as a glass transition and what we call a *jamming* transition. The question which one would like to address then, is whether these two cases are actually two sides of the same coin.

As mentioned earlier, colloids appear a suitable system to test such an idea. However, whether colloids may truly be jammed into a solid by an applied stress is presently unresolved. Upon strongly shearing a concentrated colloid, the system undergoes *discontinuous shear thickening*, meaning that at some value of the applied shear rate, the shear stress jumps to a much larger value [32,33]. The nature of this shear thickened state is unclear. One group does report a transition in which a liquid suspension is transformed into a solid upon shearing [34], but the particles in this case are too large for Brownian motion to be significant. This raises the question of whether or not a statically jammed state is possible in the presence of significant Brownian motion. Also, it would be interesting to ascertain whether model systems (such as hard spheres) may undergo such a transition.

From a theoretical viewpoint, much work is needed before we have a real understanding of jamming transitions and the relationship with the glass transition. Recent microscopic models appear to capture much of the physics of fluidisation by shear [35,36], but so far jamming has only been captured in phenomenological models [37]. Interestingly, a recent model [38] showed that an MCT-like theory of the glass transition could be modified (albeit in a phenomenological way) in order to describe jamming. In view of a unifying description, this could provide a theoretical connection, adding weight to the idea of a common nonergodicity transition. Whilst we are far from a full understanding of the jamming transition (and in particular its relation to the glass transition), the questions at least are becoming clear: therefore we may be optimistic about our future understanding of this area.

5 Conclusion

The idea that similar physics underlies transitions to a “glassy” state, regardless of the system under consideration, and regardless of the parameter being altered, is rather appealing to physicists. If the idea is correct, it unites a wide range of situations. However, resolving this issue provides great challenges – this is not surprising, given that we are

considering athermal, macroscopic situations (such as granular materials) alongside the thermodynamic, microscopic world (atomic and molecular systems), *via* an intermediate stage (colloids). In this article we have tried to highlight some of the issues pertinent to the problem, concentrating on colloidal and granular systems.

Perhaps the best understood piece of the jigsaw is the relationship between the (conventional) glass transition and the gel transition. Besides experimental evidence, it appears that mode-coupling theory may provide a theoretical description of both of these transitions. This does not mean, however, that these transitions are “the same”. Mode-coupling theory is a rather general tool, even in the specific form with which we are concerned. The feedback which appears in the theory can come about in different ways. For example, one distinguishes the repulsion-driven caging feedback of the HS glass from the attraction-driven feedback of the low density gel. Therefore, these two states are inescapably different (as are a liquid and a gas), but yet there is surely a rather strong connection between the two.

Perhaps the biggest challenge is to clarify the relationship between jamming and the other transitions. Experiments suggest that a dense colloidal fluid can be driven *into* an arrested state by increasing the applied stress. It is a challenge for theorists to provide a microscopic description of such a transition, and for experimentalists to further investigate the nature of the transition. An intuitive picture associated with jamming is provided by the concept of force-chains, which can emerge under large stresses. This may be closely related to the conjectured universal behaviour of the force distribution at the transition. However, as long as there is no microscopic understanding of this behaviour, this remains a rather controversial issue.

Finally the question of terminology remains. At present there is little consistency in different authors’ use of the various terms. Liu and Nagel used the term jamming as the generic term for a dynamic transition to an amorphous solid. However, we reserve jamming to mean a transition under applied (anisotropic) stress (otherwise there is no specific name for a stress-driven transition). We leave it to the reader to decide upon a common name for the glassy state, perhaps depending upon how firmly one believes glasses, gels and jammed states to represent equivalent physical situations.

Financial support from the Scottish International Education Trust, EPSRC and Unilever (CBH); from the Deutsche Forschungsgemeinschaft, DFG grant Go.154/12-1 (TV); and from the FOM foundation (JHS) is gratefully acknowledged.

References

- [1] Z. Rácz, in this issue.
- [2] A.J. Liu and S.R. Nagel, *Nature* **396** (1998) 21.

- [3] S.R. Nagel, in *Soft and Fragile Matter: Nonequilibrium Dynamics, Metastability and Flow*, edited by M.E. Cates and M.R. Evans (IOP Publishing, Bristol, 2000), scottish Universities Summer School in Physics 53.
- [4] V. Trappe, V. Prasad, L. Cipelletti, P.N. Segrè and D.A. Weitz, *Nature* **411** (2001) 772.
- [5] P.N. Segrè, V. Prasad, A.B. Schofield and D.A. Weitz, *Phys. Rev. Lett.* **86** (2001) 6042.
- [6] W. Kob, in this issue.
- [7] M.E. Cates, J.P. Wittmer, J.-P. Bouchaud and P. Claudin, *Phys. Rev. Lett.* **81** (1998) 1841.
- [8] J.P. Bouchaud, in this issue.
- [9] C.S. O'Hern, S.A. Langer, A.J. Liu and S.R. Nagel, *Phys. Rev. Lett.* **86** (2001) 111.
- [10] L.E. Silbert, D. Ertas, G.S. Grest, T.C. Halsey and D. Levine, *Phys. Rev. E* **65** (2002) 051307.
- [11] D.M. Mueth, H.M. Jaeger and S.R. Nagel, *Phys. Rev. E* **57** (1998) 3164.
- [12] J.H. Snoeijer, M. van Hecke, E. Somfai and W. van Saarloos [*cond-mat/0204277*].
- [13] P.N. Pusey and W. van Meegen, *Nature* **320** (1986) 340.
- [14] W. Kob, *J. Phys. Cond. Matt.* **11** (1999) R85.
- [15] U. Bengtzelius, W. Götze and A. Sjölander, *J. Phys. C* **17** (1984) 5915.
- [16] W. Götze, in *Liquids, Freezing and Glass Transition*, edited by J.-P. Hansen, D. Levesque and J. Zinn-Justin (Noth-Holland, Amsterdam, 1991), 287–503, les Houches Summer School LI (1989).
- [17] W. Götze, *J. Phys. Cond. Matt.* **11** (1999) A1.
- [18] W. Götze, *Cond. Matt. Phys.* **1** (1998) 1.
- [19] W. van Meegen and S.M. Underwood, *J. Phys. Cond. Matt.* **6** (1994) A181.
- [20] S. Asakura and F. Oosawa, *J. Polym. Sci.* **33** (1954) 183.
- [21] L. Fabbian, W. Götze, F. Sciortino, P. Tartaglia and F. Thiery, *Phys. Rev. E* **59** (1999) R1347.
- [22] J. Bergenholtz and M. Fuchs, *Phys. Rev. E* **59** (1999) 5706.
- [23] K. Dawson, G. Foffi, M. Fuchs, W. Götze, F. Sciortino, M. Sperl, P. Tartaglia and Th. Voigtmann, *Phys. Rev. E* **63** (2001) 011401.
- [24] K. Kroy *et al.*, to be published.
- [25] H. Verduin and J.K.G. Dhont, *J. Colloid Interface Sci.* **172** (1995) 425.
- [26] W. Götze and M. Sperl, *Phys. Rev. E* **66** (2002) 011405.
- [27] K.N. Pham, A.M. Puertas, J. Bergenholtz, *et al.*, *Science* **296** (2002) 104.
- [28] T. Eckert and E. Bartsch, *Phys. Rev. Lett.* **89** (2002) 125701.
- [29] A.M. Puertas, M. Fuchs and M.E. Cates, *Phys. Rev. Lett.* **88** (2002) 098301.
- [30] E. Zaccarelli, G. Foffi, K.A. Dawson, S.V. Buldyrev, F. Sciortino and P. Tartaglia, *Phys. Rev. E* **66** (2002) 041402.
- [31] M.E. Cates, in this issue.
- [32] W.J. Frith, P. d'Haene, R. Buscall and J. Mewis, *J. Rheol.* **40** (1996) 531.
- [33] J. Bender and N.J. Wagner, *J. Rheol.* **40** (1996) 899.
- [34] E. Bertrand, J. Bibette and V. Schmitt, *Phys. Rev. E* **66** (2002) 060401(R).
- [35] L. Berthier, J.-L. Barrat and J. Kurchan, *Phys. Rev. E* **61** (2000) 5464.
- [36] M. Fuchs and M.E. Cates, *Faraday Discuss.* **123** (2003).
- [37] D.A. Head, A. Ajdari and M.E. Cates, *Phys. Rev. E* **64** (2001) 061509.
- [38] C.B. Holmes, M. Fuchs and M.E. Cates [*cond-mat/0210321*].